D 2022

U.PORTO
FEUP FACULDADE DE ENGENHARIA
UNIVERSIDADE DO PORTO

SEISMIC RISK REDUCTION OF REINFORCED CONCRETE BUILDINGS RETROFITTED WITH STEEL BRACES

RODRIGO ESMERIZ FALCÃO MOREIRA

TESE DE DOUTORAMENTO APRESENTADA
À FACULDADE DE ENGENHARIA DA UNIVERSIDADE DO PORTO EM
ENGENHARIA CIVIL – RAMO DE ESPECIALIZAÇÃO EM ESTRUTURAS

U.PORTO

FEUP FACULDADE DE ENGENHARIA
UNIVERSIDADE DO PORTO

SEISMIC RISK REDUCTION OF REINFORCED CONCRETE BUILDINGS RETROFITTED WITH STEEL BRACES

RODRIGO ESMERIZ FALCÃO MOREIRA

A thesis submitted to the Faculty of Engineering of the University of Porto, in partial fulfilment of the requirements for the degree of Doctor of Philosophy in Earthquake and Structural Engineering.

Supervisors:

José Miguel de Freitas Castro, Associate Professor (FEUP)

Humberto Salazar Amorim Varum, Full Professor (FEUP)

Mário António Lage Alves Marques, Researcher (CONSTRUCT)

DOCTORAL PROGRAM IN CIVIL ENGINEERING, 2022

FACULTY OF ENGINEERING, UNIVERSITY OF PORTO

Ph.D. Thesis – Doctoral Program in Civil Engineering (PRODEC)

© Rodrigo Esmeriz Falcão Moreira & FEUP, 2022

To my daughter, may this small contribution help make the World a safer place for her.

"Thousands of people live in older homes that can and should be seismically strengthened… An earthquake can throw an entire frame off the foundation and turn a house into a heap of rubble. The good news is that this is probably preventable."

Los Angeles Times editorial, March 21st, 1994

ACKNOWLEDGEMENTS

For many years, the writing of this thesis was an ambition that kept being postponed due to several professional (and some personal) challenges. Somehow, the time never seemed to be right. Then some things happened, and the time finally came. Now that it's done, I almost feel tempted to say I never thought it would take this long. But (deep down) I always knew it would. At this juncture, it is only fair to address a few words to the people that contributed the most (in different ways) to the success of this long work journey. The lines below are dedicated to you.

First of all, to my advisors, I would like to thank for accepting to supervise this work. In particular, to Professor Miguel Castro, I want to thank for persuading me (for so long) to apply for a Ph.D. grant and thus commit to this journey. On this matter, I also want to thank Professor Rui Faria, who constantly challenged me (right from my undergraduate degree) by saying what a shame and waste it would be not to do it. For believing in me – and for your friendship – thank you.

To my colleagues and friends at FEUP – Aires Colaço, Alexandre Pinto, Ana Ramos, André Furtado, Araliya Mosleh, Cássio Gaspar, Cláudio Horas, Janine Figueiredo, Rachel Martini, Sérgio Pereira – I would like to thank for the motivation and support, the long conversations, and the good times spent together (at least until we got hit by the CoViD-19 pandemic). Thank you for keeping my spirit young, but at the same time never letting me forget "how old" I really am (true friendship is indeed a wonderful thing!). I hope we can keep in touch in years to come.

To my colleagues in the Department of Civil Engineering at the School of Engineering of the Polytechnic of Porto (ISEP-IPP), I would like to thank for the encouragement and for always trying to create the best possible conditions for me during periods when work was more intense. Also, to Professor Maria João Viamonte, Dean of ISEP-IPP, and Professor Ana Almeida, Head of the Scientific Council, I want to thank for the constant support and appreciation. I'm proud to be a part of our school.

To my associates at GROUNDMOTION – Earthquake & Structural Engineering International, I want to thank for taking care of business while I was away. For your trust, loyalty, friendship, and support, I am in your debt. I would specially like to thank Emanuel Correia, who so many times helped me regain perspective when I was in too deep (your natural talent for structural engineering never cesses to impress me), and Ruben Pereira, for taking the time to adapt and develop some of the figures and drawings in this document. Last but not least, I would like to thank Hugo Rocha for… well, for everything. I look forward to overcoming many more challenges with all of you.

To Neil Raymond Mason, my old friend, and all-time English Professor, I would like to thank for my proficiency in English. We have known each other for more than 30 years and, even though it's been long since I have sat in one of your classrooms, never have I stopped learning from you (a nice way of saying you never miss the chance to correct me when I slip). We have always spoken (or written) to each other in English, which has helped me to live up to your high standards. If we keep doing this for the next 30 years, I just might get to be as good as Sir Humphrey Appleby (in BBC's *Yes Minister,* who used to wield the English language like a scalpel in the hands of a gifted surgeon). Thank you so much, Neil, for everything.

To my parents, I want to thank for the opportunity to accomplish this. Growing up, you taught me that everybody at home had a job, and mine was studying. You provided all the best opportunities for me to do so. Thank you, Father, for setting such an impressive example for me. I can only hope to live up to your name. And thank you, Mother, for always demanding me to do so well and better than those around me. Even though I'm over 40 years-old now, you still haven't stopped "breathing down my neck" when it comes to getting my work done. I must say that there were times when the pressure to meet the high standards set by both was almost overwhelming, but I have no doubt it has laid the foundation for the man I am now. I hope to have made you proud.

To Ana, I want to thank for being by my side during the last few years. You have endured the ups and downs of this work journey, always supporting me, and never complaining. Your music makes everything better, your ever positive attitude towards life is inspiring, and your embrace always provides me with peace when I need it. I hope you can find it in your heart to forgive me for my bad temper and for the endless working hours. Maybe now we can take all those trips you have been planning for so long. We will have the rest of our lives to do it.

Finally, the acknowledgements would not be complete without mentioning Dr. Romain Ribeiro de Sousa, who played such an important role in the final part of this work. I came to you for advice when I was drowning in a sea of numerical results, you listened to my concerns, and said: "Don't worry, I will help you with that.". I will never be able to thank you enough. My special thanks also to Professor Xavier Romão, who so many times helped to clear my doubts. Surprisingly, you always seemed to know exactly what I was going to ask… How do you do that?

If by any chance I have forgotten to mention someone, I apologize. Or maybe there is just no need for names. You know who you are. Thank you.

Rodrigo Falcão Moreira

January 1st, 2022

Acknowledgments due for financial support:

- Portuguese Foundation for Science and Technology (FCT) – individual Ph.D. grant (SFRH/BD/103473/2014);
- Project "SMARTER – Seismic urban risk assessment in Iberia and Maghreb" (PT-DZ/0002/2015);
- Project "MitRisk – Framework for seismic risk reduction resorting to cost-effective retrofitting solutions" (PTDC/ECI-EST/31865/2017 – POCI/01/0145/FEDER/031865, funded by FEDER funds through COMPETE2020 – *Programa Operacional Competitividade e Internacionalização* (POCI), and by national funds (PIDDAC) through FCT/MCTES).

ABSTRACT

During a violent earthquake, the damage and collapse of buildings, infrastructures, and other equipment – not the earthquake by itself – are responsible for the most extensive human and economic losses. This means that the so-called seismic catastrophes are not exactly natural, but in fact mainly caused by man-made surroundings. Fortunately, it also means that, while seismic hazard is determined by Nature, the vulnerability and exposure of the built environment are humanly determined parameters that, as such, can be controlled and reduced. It is therefore essential that research in earthquake engineering is also directed towards assessing the vulnerability of the existing building stock and the development of retrofitting techniques, so that the effects of future seismic events (human casualties and economic losses) can be mitigated.

The final purpose of this study is to contribute to the reduction of the seismic risk to which the Portuguese RC building stock is exposed. As the worldwide experience from past and present seismic activity shows that non-ductile RC frame buildings are (by far) one of the most vulnerable, these pose a large threat to human life and property in future earthquakes. Within this context, motivated by the known benefits of using steel braces to reinforce RC frame buildings, as well as by the fact that in Portugal there are almost no application examples, the first objective of this thesis is to improve knowledge on the seismic behaviour of such retrofitted structures, directly considering the main characteristics of the building classes that exist in the country. Afterwards, given the limitations of conventional seismic design methodologies when applied to hybrid RC-steel systems, the second objective is to propose a displacement-based design procedure, applicable to steel X-brace retrofitting systems for RC frame buildings, and demonstrate it is robust enough to be applied systematically by practitioners involved in such matters.

As background, a general overview of several topics involved in the seismic assessment and retrofitting of existing RC buildings is provided. A review of past studies on seismic risk in mainland Portugal and on the characterization of the Portuguese RC building stock, along with a discussion of the typical causes of damage and failure, are also included. The nonlinear modelling of RC frames under cyclic loading is addressed, as well as the applicable analysis methods. The current codes and guidelines are reviewed, with special emphasis on the methodology defined by EC8-3 (2005), the common practice among structural design professionals, and the simplified methods introduced by the LNEC Report 81/2019 (Sousa *et al,* 2019). Finally, the available steel-based retrofitting techniques for RC frames are reviewed, as well as the most relevant past studies on the seismic behaviour and design of RC buildings retrofitted with steel X-braces.

KEYWORDS: Seismic assessment and retrofitting of existing RC buildings; Concentric steel braces; Displacement-based design; Seismic risk reduction.

RESUMO

Durante um evento sísmico violento, os danos e colapsos de edifícios, infraestruturas, e outros equipamentos – não o sismo *per se* – são responsáveis pelas perdas humanas e económicas mais extensas. Isto significa que as chamadas "catástrofes sísmicas" não são propriamente naturais, mas na realidade essencialmente causadas por envolventes criadas pelo Homem. Felizmente, isto também significa que, embora a perigosidade sísmica seja determinada pela Natureza, a vulnerabilidade e exposição do ambiente construído são parâmetros humanamente determinados que, como tal, podem ser controlados e reduzidos. Por conseguinte, é essencial que a investigação em Engenharia Sísmica seja também orientada para a avaliação da vulnerabilidade do parque edificado, assim como para o desenvolvimento de técnicas de reforço estrutural, para que os efeitos de eventos sísmicos futuros (baixas humanas e perdas económicas) possam ser mitigados.

O objetivo final deste estudo é contribuir para a redução do risco sísmico a que está exposto o parque edificado de betão armado (BA) em Portugal. Mostrando a experiência mundial, adquirida em eventos sísmicos passados e recentes, que os edifícios não-dúcteis em betão armado são (de longe) dos mais vulneráveis, estes representam uma grande ameaça para a vida e propriedade humanas em eventos sísmicos futuros. Neste contexto, motivado pelos conhecidos benefícios da utilização de contraventamentos metálicos para reforçar edifícios de BA, bem como pelo facto de em Portugal quase não existirem exemplos de aplicação, o primeiro objetivo desta tese é melhorar o conhecimento sobre o comportamento de tais estruturas reforçadas, considerando diretamente as principais características das classes de edifícios que existem no país. Em seguida, dadas as limitações das metodologias convencionais de dimensionamento sísmico quando aplicadas a sistemas híbridos aço-betão, o segundo objetivo é propor um processo de dimensionamento baseado em deslocamentos, aplicável a sistemas de reforço constituídos por contraventamentos em X para edifícios de BA, e demonstrar que é suficientemente robusto para ser aplicado sistematicamente por profissionais envolvidos nestas matérias.

Como base, é oferecida uma visão geral sobre vários tópicos relacionados com a avaliação de segurança e reforço sísmico de edifícios de BA. Uma revisão de estudos anteriores sobre risco sísmico em Portugal Continental e sobre a caracterização do seu parque edificado de BA, assim como uma discussão sobre causas típicas de colapso, estão também incluídas. A modelação não-linear de pórticos de BA sujeitos a carregamento cíclico é abordada, bem como os métodos de análise aplicáveis. Os regulamentos e orientações atuais são revistos, com especial ênfase na metodologia definida pelo EC8-3 (2005), naquilo que é a prática comum entre profissionais, e nos métodos simplificados introduzidos pelo Relatório LNEC 81/2019 (Sousa *et al,* 2019). Finalmente, são revistas as técnicas de reforço com estrutura metálica disponíveis para edifícios de BA, bem como os estudos anteriores mais relevantes sobre comportamento sísmico e dimensionamento de edifícios de BA reforçados com contraventamentos em X.

PALAVRAS-CHAVE: Avaliação de segurança e reforço de edifícios existentes de BA; Contraventamentos metálicos concêntricos; Dimensionamento baseado em deslocamentos; Redução do risco sísmico.

TABLE OF CONTENTS

CHAPTER 1 – INTRODUCTION

1.1. GENERAL OVERVIEW AND MOTIVATION 1.1

1.2. SCOPE AND OBJECTIVES 1.6

1.3. THESIS OUTLINE 1.7

CHAPTER 2 – LITERATURE REVIEW

2.1. INTRODUCTION 2.1

2.2. EXISTING STUDIES ON SEISMIC RISK IN PORTUGAL 2.3

2.3. CHARACTERIZATION OF THE PORTUGUESE RC BUILDING STOCK 2.9

2.3.1. Geometric properties 2.10

2.3.2. Material properties 2.13

2.3.3. Limitations of the study 2.15

2.4. TYPICAL CAUSES OF DAMAGE AND FAILURE OF NON-DUCTILE RC BUILDINGS 2.15

2.5. NONLINEAR MODELLING OF RC FRAMED STRUCTURES 2.18

2.5.1. Models for beam-column elements 2.19

2.5.2. Finite element formulations for distributed plasticity models 2.27

2.5.3. Material models for RC members under cyclic loading 2.29

2.5.4. Masonry infills 2.38

2.6. NONLINEAR ANALYSIS METHODS 2.46

2.6.1. Nonlinear static analysis 2.47

2.6.2. Adaptive nonlinear static analysis 2.49

2.6.3. Nonlinear dynamic analysis 2.50

2.7. SEISMIC ASSESSMENT OF EXISTING RC BUILDINGS 2.53

2.7.1. Methodology according to EC8-3 ..... 2.54

2.7.2. Seismic demand definition 2.70

2.7.3. Common practice among structural design professionals 2.81

2.7.4. Simplified methods introduced by LNEC Report 81/2019 ..... 2.82

2.8. TECHNIQUES USING STEEL ELEMENTS FOR THE SEISMIC RETROFITTING OF RC BUILDINGS 2.88

2.8.1. Retrofitting approaches and strategies 2.89

2.8.2. Traditional retrofitting techniques 2.92
2.8.3. Innovative retrofitting techniques 2.98
2.9. SEISMIC BEHAVIOUR OF RC BUILDINGS RETROFITTED WITH CONCENTRIC STEEL BRACES 2.104
2.9.1. Behaviour of steel braces 2.105
2.9.2. Behaviour of RC members 2.107
2.9.3. Interaction between steel braces and RC members 2.108
2.10. METHODOLOGIES FOR THE SEISMIC DESIGN OF CONCENTRIC STEEL-BRACE RETROFITTING SYSTEMS 2.110
2.10.1. Force-based design 2.111
2.10.2. Displacement-based design 2.116
2.11. CONCLUDING REMARKS 2.124

CHAPTER 3 – AN APPLICATION OF THE EC8-3 SEISMIC SAFETY ASSESSMENT PROCEDURE

3.1. INTRODUCTION 3.1
3.2. CASE STUDY CHARACTERIZATION 3.2
3.2.1. Geometry and section detailing 3.2
3.2.2. Masonry infill walls 3.6
3.2.3. Material properties 3.7
3.2.4. Vertical loads 3.10
3.2.5. Earthquake input used in the PsD tests 3.11
3.2.6. Experimental results 3.13
3.3. NUMERICAL MODELLING AND STRUCTURAL ANALYSIS 3.22
3.3.1. Modelling options 3.23
3.3.2. Structural analysis results 3.35
3.4. SEISMIC ASSESSMENT PROCEDURE 3.45
3.4.1. Seismic demand definition 3.45
3.4.2. Member capacities computation 3.51
3.4.3. Performance evaluation 3.54
3.5. CONCLUDING REMARKS 3.61

CHAPTER 4 – ON THE APPLICABILITY OF CONVENTIONAL SEISMIC DESIGN METHODOLOGIES TO HYBRID RC-STEEL SYSTEMS

4.1. INTRODUCTION 4.1

4.2. THE *Q*-FACTOR APPROACH IN EC8-3 ..... 4.2
4.3. APPLICATION TO A RETROFITTING CASE STUDY 4.3
4.3.1. Structural characterization 4.4
4.3.2. Design of the retrofitting system 4.5
4.3.3. RC member safety checks 4.6
4.4. EVALUATION OF THE DESIGNED RETROFITTING SYSTEM 4.8
4.4.1. Nonlinear modelling 4.9
4.4.2. Seismic demand definition 4.13
4.4.3. Member capacities computation 4.14
4.4.4. Performance evaluation 4.16
4.4.5. Discussion 4.17
4.5. CONCLUDING REMARKS 4.21

CHAPTER 5 – A NEW DISPLACEMENT-BASED DESIGN PROCEDURE FOR THE RETROFITTING OF RC BUILDINGS WITH STEEL BRACES

5.1. INTRODUCTION 5.1
5.2. BASES OF THE PROCEDURE 5.2
5.3. STEPS OF THE PROCEDURE 5.3
5.3.1. Primary data compilation 5.3
5.3.2. Design process 5.4
5.3.3. Validation process 5.10
5.4. CASE STUDY APPLICATION 5.11
5.4.1. Design procedure 5.11
5.4.2. Validation 5.17
5.4.3. Discussion 5.19
5.5. CONCLUDING REMARKS 5.21

CHAPTER 6 – VALIDATION AND CALIBRATION OF THE PROPOSED DESIGN PROCEDURE

6.1. INTRODUCTION 6.1
6.2. SAMPLE DEFINITION 6.2
6.3. NUMERICAL MODELLING 6.3
6.4. SEISMIC ASSESSMENT 6.5

6.4.1. Modal periods 6.5
6.4.2. Seismic demand definition 6.5
6.4.3. Member capacities computation 6.8
6.4.4. Performance evaluation 6.9
6.4.5. Discussion 6.9
6.5. SEISMIC RETROFITTING 6.10
6.5.1. Conceptual design 6.10
6.5.2. Design procedure 6.12
6.5.3. Validation 6.15
6.5.4. Discussion 6.16
6.6. CONCLUDING REMARKS 6.19

CHAPTER 7 – ON THE EVOLUTION OF THE SEISMIC RISK OF THE STUDIED SAMPLE OF STRUCTURES

7.1. INTRODUCTION 7.1
7.2. FRAMEWORK OF THE STUDY 7.2
7.3. FRAGILITY ANALYSIS 7.3
7.3.1. Selection of ground motion records 7.3
7.3.2. Definition of limit states 7.4
7.3.3. Fragility curves 7.5
7.3.4. Discussion 7.8
7.4. RISK ANALYSIS 7.9
7.4.1. Hazard model 7.9
7.4.2. Exposure model 7.11
7.4.3. Vulnerability model 7.12
7.4.4. Risk assessment 7.13
7.4.5. Discussion 7.15
7.5. CONCLUDING REMARKS 7.17

CHAPTER 8 – CLOSURE

8.1. CONCLUSIONS 8.1
8.2. RECOMMENDATIONS FOR FUTURE DEVELOPMENTS 8.4

REFERENCES

APPENDICES (1 TO 7)

APPENDIX 1 – PRE-CODE RC BUILDINGS – DESIGN DRAWINGS

APPENDIX 2 – PRE-CODE RC BUILDINGS – MEMBER CAPACITIES

APPENDIX 3 – PRE-CODE RC BUILDINGS – PERFORMANCE EVALUATION

APPENDIX 4 – RETROFITTED BUILDINGS – DESIGN DRAWINGS

APPENDIX 5 – RETROFITTED BUILDINGS – DESIGN PROCEDURE

APPENDIX 6 – RETROFITTED BUILDINGS – PERFORMANCE EVALUATION

APPENDIX 7 – GROUND MOTION RECORD SETS

CHAPTER 1

INTRODUCTION

1.1. GENERAL OVERVIEW AND MOTIVATION

For thousands of years, theories have been proposed for the origin of earthquakes. In ancient Greece earthquakes were associated with "winds and tidal waves" deep inside the Earth. From then, the study of the seismic phenomenon (seismology) has evolved immensely. However, it was not until the development of the plate tectonics theory, in the 20th century, that a rational explanation was obtained and generally accepted by the scientific community. Nonetheless (and unfortunately) this improved knowledge about earthquake formation mechanisms, associated with the laws of propagation for seismic waves, has not yet allowed for the prediction of potentially destructive events, thus leading to the public's general conception that "earthquakes are natural catastrophes against which little or nothing can be done". Fortunately, this is inaccurate.

During a violent earthquake, the damage and collapse of buildings, infrastructures, and other equipment – not the earthquake by itself – are responsible for the most extensive human and economic losses. This means that the so-called seismic catastrophes are not exactly natural, but in fact mainly caused by man-made surroundings. The observation made by Nick Ambraseys in 1968 on the fact that *"earthquakes don't kill people, buildings do"* contributed to clarify this confusion between the seismic phenomenon and its consequences. It will remain as valid today as it was then if modern earthquake resistant design practices are not considered (Bilham, 2006). Fortunately, it also means that, while seismic hazard is determined by Nature, the vulnerability and exposure of the built environment are humanly determined parameters that, as such, can be controlled and reduced.

In order to give a general perspective about the several impacts caused by these events, Figure 1.1 (below) shows a comparison between the estimated economic losses, the number of affected people, and the number of casualties associated to: (i) four significant earthquakes; (ii) the 2010 Australian floods; (iii) the Chernobyl nuclear accident. The extent of the areas devastated by these six events is also presented and helps complete this overview. The compiled data demonstrate how earthquakes can be far more deadly than other disasters, and how the value of the immediate economic losses can also be considerably large (Romão *et al,* 2014a).

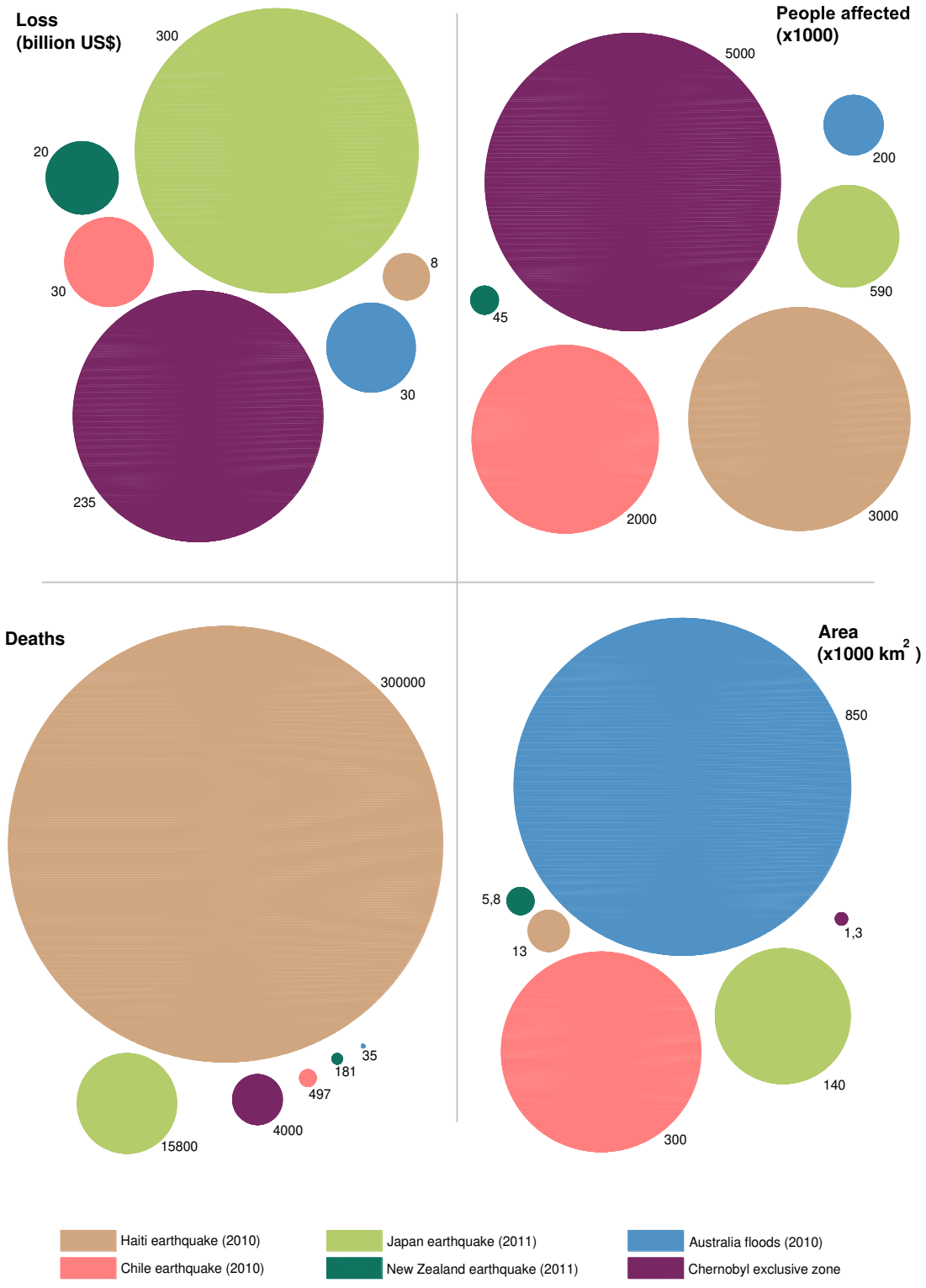

Figure 1.1 – Comparison between the estimated economic losses, number of affected people, number of casualties and extent of devastated areas due to: (i) four significant earthquakes; (ii) the 2010 Australian floods; (iii) the Chernobyl nuclear accident (Romão *et al*, 2014a)

Another aspect to be noticed from Figure 1.1 is how earthquake events in different locations led to significantly different effects in terms of economic losses, casualties, and damages. The Christchurch earthquake in New Zealand (2011, M_S = 6.3), for instance, claimed 181 lives and caused 20 billion USD of economic losses, while the Port au Prince earthquake in Haiti (2010, M_W = 7.0) claimed a much higher number of lives (300.000) but led to less than half the economic losses (8 billion USD). On the other hand, the Concepción earthquake in Chile (2010, M_W = 8.8) caused less deaths (497) than those due to the Haiti earthquake, but the associated economic losses were approximately 4 times higher (30 billion USD). This reveals how different conditions, in terms of vulnerability and exposure of the built environment, can influence the final statistics of a major earthquake in terms of the resulting damage and death.

The main factor influencing the number of human casualties and injuries is the existence of man-made structures and infrastructures lacking appropriate seismic design that will, as such, inevitably exhibit inadequate structural behaviour (Romão, 2012). The importance of this factor can be clearly observed when comparing the number of fatalities of the Haiti and Chile earthquakes in 2010. The severe death toll in Haiti has been largely attributed to the lack of adequate earthquake resistant design practice and to the poor quality of a large part of the building stock (ARUP, 2010; Eberhard *et al*, 2010; Romão, 2012). On the other hand, the low number of deaths in Chile (compared to the number of affected people) can be seen as a consequence of the relatively good performance of the affected structures (Elnashai *et al*, 2010; Kato *el al*, 2010; Rojas *et al*, 2010; Romão, 2012). This is a direct consequence of the earthquake resistant codes and standards adopted in that country. Similar analyses have been made for the outcomes of the New Zealand earthquake in 2011 (Chouw *et al*, 2011; Clifton *et al*, 2011; EERI, 2011), as well as for others that have occurred in highly populated zones, leading to similar findings and conclusions.

Other recent earthquakes (e.g., Nidri, Greece, 2015; Amatrice, Italy, 2016; Umbria / Marche, Italy, 2016) have painfully reminded us that Europe's existing building stock also suffers from the above-described vulnerability. Despite the data indicating that recent structures (i.e., designed according to modern earthquake resistant codes) have been able to reduce the threat to human life, the distribution of seismic risk is still far from being uniform (Romão, 2012). In fact, the majority of buildings constructed before 1980 in Europe's earthquake prone areas are considered deficient in terms of seismic resistance. Regarding building typology, reinforced concrete (RC) is the most common construction material, which poses a large threat to human life and property in future earthquakes as the worldwide experience, from past and present seismic activity, shows that non-ductile RC frame buildings are (by far) one of the most vulnerable. For instance, most of the existing RC buildings in Portugal were designed and built before the overall implementation of the (still current but with known expiration date) national code for earthquake resistant structures (RSA, 1983), hence being prepared to withstand only gravity and wind loads. Their distribution according to decade of construction is shown in Figure 1.2, indicating the relation with the implementation dates of the national earthquake resistant codes, and the estimated stock percentages lacking the appropriate lateral resistance to withstand a violent seismic event.

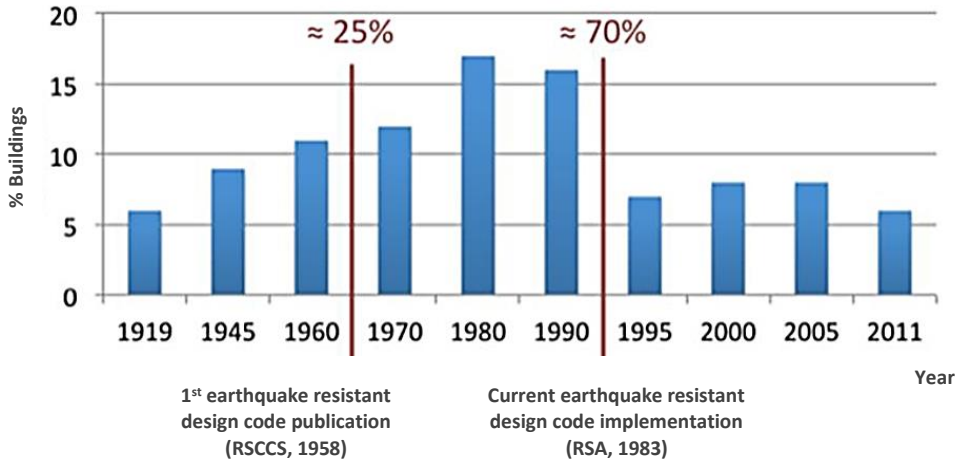

Figure 1.2 – Evolution of the construction of RC buildings in Portugal and relationship with the introduction of earthquake resistant design codes (adapted from Sousa *et al*, 2017b)

Even though the threat of severe earthquakes is today approximately the same as it was 100 years ago, the potential for related major catastrophes has grown alarmingly over this period due to the significant increase in population and urbanisation in seismically active regions. Therefore, research in earthquake engineering (EE) must continue to focus on the seismic performance evaluation of the existing building stock, despite the progressively increasing reduction of the modern buildings' vulnerability with the evolution of seismic design codes. The development of new retrofitting techniques also represents a key issue in the effort to mitigate the effects of future earthquakes and, consequently, reduce both human casualties and economic losses. In the United States, for instance, millions of dollars are spent every year with the purpose of saving lives and money.

In pursue of the above-referred goals, the past twenty-five years have witnessed the development of the performance-based earthquake engineering (PBEE) philosophy, which is a conceptual framework that involves the design, assessment, and construction of engineering structures. The fundamental principles which are inherent to PBEE seek to improve the quantification of the behaviour of those exposed to earthquake loading, in order to predict their performance with sufficient confidence (Krawinkler, 1997; Romão, 2012). The research lines promoted by this framework, in particular towards the development of seismic risk assessment and reduction methodologies, have also led to significant advances in the use of probabilistic approaches in EE. Extensive information about this topic can be found in the works of Marques (2011), Romão (2012), and others.

During the above-referred period, a significant number of codes and standards specifically addressing the seismic assessment of existing buildings began to be drafted in several countries, for instance, in the USA: ATC 40 (1996); FEMA 273 (1997); FEMA 274 (1997); FEMA 310 (1998); FEMA 356 (2000); ASCE 31-03 (2003); ASCE 41-06 (2007); ATC 63 (2009); in Japan: BRI (2001a); BRI (2001b); in Italy: OPCM 3274 (2003); OPCM 3431 (2005); NTC (2008); in New Zealand: NZSEE (2006). In the particular context of Europe, Eurocode 8 – Part 3 (EC8-3, 2005) was specifically developed to address this matter. Most of these documents include chapters on modelling techniques, structural analysis, and verification procedures, the latter usually being more complex than those applicable to the design of new

structures. Hence, such procedures should be thoroughly validated in practice, to determine if any modifications are required. Franchin *et al* (2010) have stated that EC8-3 (2005), for instance, should be seen as experimental and will most likely undergo further progress in the near future, based on the results of applications and studies regarding the involved methodologies. However, the current number of critical discussions addressing its key issues is still scarce (e.g., Pinto and Franchin, 2008; Franchin *et al*, 2010; Jalayer *et al*, 2011; Romão *et al*, 2012; Pinto and Franchin, 2014; Manfredi and Masi, 2017). Therefore, there is an obvious need for further studies concerning the provisions of the codes and standards specifically developed to address the seismic assessment and retrofitting of existing buildings.

The development of innovative, more effective, and economically attractive retrofitting techniques, as well as of the associated design methodologies, is also an issue under the scope of the PBEE framework. While providing new buildings with the required seismic resistance is nowadays a straightforward matter, retrofitting existing ones may involve considerable costs – including those of disrupting use – and poses specific problems. Techniques such as bonding and/or jacketing with composite materials or modifying the structural system by adding RC shear walls have been successfully adopted in the past to retrofit RC framed buildings. However, in the past three decades, several authors (e.g., Maheri and Sahebi, 1997; Youssef *et al,* 2007; Eskandari *et al,* 2017) have demonstrated the benefits of using steel braces in RC frames. This technique was applied for the first time as a retrofitting measure in 1978, to strengthen an earthquake-damaged building in Japan (Kawamata and Masaaki, 1980), despite having been used in new constructions years before (e.g., John Hancock Center, Chicago, USA, 1969). Architectural flexibility, reduced weight and impact on foundations, ease and speed of construction, and the ability to choose systems that are more ductile, can be referred as the main advantages over, for instance, global strengthening based on the inclusion of RC shear walls (Eskandari *et al,* 2017). Unfortunately, application examples of this kind of solution in Portugal are almost inexistent, mainly due to the lack of codes and standards providing information about the detailed design of strengthening interventions at the storey or global levels. Further development and improvement of the EC8-3 (2005) provisions on this matter are hence necessary.

Seismic design is currently codified by structural codes and standards of practice using the so-called "force-based design" (FBD). This is mainly due to historical reasons and related to how design is carried out for other actions such as dead and live loads (Priestley *et al,* 2007). This procedure involves the consideration of a behaviour factor (q-factor) as a simple mean to account for the nonlinear behaviour of the structure while performing linear static analysis. However, in structures designed according to old seismic codes (or even non-seismic codes), the uncertainties about the nonlinear behaviour are relevant (for instance, the location and ductility capacity of the potentially inelastic regions are not fully known). It is therefore very difficult to establish a direct correlation between the real internal forces that develop in structural members during the seismic excitation and those experienced by an equivalent indefinitely elastic structure. Moreover, when steel braces are added to RC structures, the improvement in the seismic behaviour does not seem to be proportional to the corresponding increase in lateral strength. This has led several authors (e.g., Mpampatsikos *et al,* 2008) to suggest that a q-factor based design process might not be an efficient approach to obtain retrofitted structures with good seismic performance.

An alternative to the traditional FBD methods is given by modern displacement-based design (DBD) procedures. Unlike the former, whose main purpose is collapse prevention, the latter seek to ensure that pre-determined damage levels are not exceeded when a structure is subjected to a set of seismic intensity scenarios (Priestley *et al,* 2007). Their application has been progressively increasing in the past ten years (Villani *et al,* 2010; Macedo and Castro, 2012; Malekpour *et al,* 2013; Valente and Milani, 2017) and many advantages have been pointed out regarding the force-based counterpart. A study conducted by Sousa and Castro (2012) adopted this new design philosophy and applied it to the seismic retrofitting of RC frames using steel braces, in an attempt to explicitly consider the interaction between the two structural systems. Even though the scope of the study was limited due to the reduced number of designed structures, the obtained results clearly confirm the advantages of the DBD procedure over the traditional methodologies. Therefore, this research line should be followed and expanded with the main objective of developing, validating, and calibrating robust DBD methods that may contribute for the mitigation of the above-referred lack of codes and standards addressing the design of such seismic retrofitting techniques.

1.2. SCOPE AND OBJECTIVES

The final purpose of this study is to contribute to the reduction of the seismic risk to which the Portuguese RC building stock is exposed. Earthquake engineering experts, policy makers, and public in general agree on this being a matter of high priority. In 2010, the Portuguese Parliament issued a recommendation to the Government emphasizing the need to take urgent action towards this objective. Unfortunately, despite the growing number of conferences, workshops and seminars dedicated to the topic, public authorities did not do much. Only in the second half of 2019 did the Government publish legal diplomas defining the terms and conditions applicable to the refurbishment of existing buildings (Decree-Law 95/2019 of July 18th), defining the situations that require a seismic vulnerability assessment report and/or a seismic retrofitting design project (Ordinance 302/2019 of September 12th), and enforcing the use of the Eurocodes in structural design projects (Normative Dispatch 21/2019 of September 17th). However small, this was an important step towards the change that is necessary for this matter to be adequately addressed.

Motivated by the above-referred benefits of using steel braces to reinforce RC framed buildings, as well as by the fact that in Portugal there are almost no application examples, the first objective of this thesis is to improve knowledge on the seismic behaviour of such retrofitted structures, directly considering the main characteristics of the building classes that exist in the country. A preliminary analysis is thus required to identify which would benefit the most from this type of global retrofitting technique. For this matter, the results produced by the PRISE research project (PTDC/ECM-EST/3062/2012) are reviewed, namely the classification of the Portuguese RC building stock according to year of construction, number of storeys, and seismic design criteria. During this preliminary stage, the EC8-3 (2005) seismic assessment methodology is also reviewed, along with the recommendations of several authors concerning issues that require further research. Within this context, the initial chapters of this thesis include contributions: (i) to the calibration of nonlinear analytical models that adequately reproduce the behaviour of older-type RC buildings and can, therefore, be extensively used

in the seismic assessment of such structures; (ii) to a better interpretation of the assessment results provided by the EC8-3 (2005) procedure, highlighting the influence that the infill walls might have on the overall outcome of the process; (iii) to help practitioners become more aware of the likely error associated with the several adjustments that have to be introduced in conventional seismic code provisions (i.e., FBD procedures), in order to try to apply them to such hybrid RC-steel systems. These contributions are supported not only by analytical results, but also (in part) by the experimental results of the ICONS research programme (Pinto *et al,* 2002; Varum, 2003; and others), which is thought to be a further advantage.

The second objective of this thesis is to propose a DBD methodology applicable to steel X-brace retrofitting systems for RC framed buildings. This methodology, which follows up on the above-referred study by Sousa and Castro (2012), consists of a performance-based approach relying on deformation control for different levels of seismic intensity, and explicitly considers the interaction between both structural systems, namely the influence of the steel braces' resistance on the RC elements' deformation capacity. To demonstrate that it is robust enough to be applied systematically by practitioners, the developed procedure is extensively validated and calibrated according to the performance requirements defined by EC8-3 (2005). As a conclusion to this stage, a study is presented on the evolution of the seismic risk of the chosen sample of structures, combining information about their structural fragility with the seismic hazard of the locations in question. The proposed DBD methodology thus contributes to mitigate the above-referred lack of guidance for the seismic retrofitting of RC structures using steel braces and could eventually be considered as an input to a future version of Eurocode 8. As for the performed seismic risk study, its results provide important inputs to the ongoing research project MitRisk (POCI/01/0145/FEDER/031865), which focus on the development of a cost-benefit analysis platform, meant to support the development of retrofitting plans, focused on the most vulnerable types of buildings out of the Portuguese building stock.

1.3. THESIS OUTLINE

Within the above-described scope and in pursue of the above-referred objectives, this thesis is organized in eight chapters (including this one). A short description of their contents is given below, as well the author's perspective of how this work might influence the interested reader to further pursue the research lines that may be derived from it:

- Chapter 2, *Literature review*, provides a general overview of several topics involved in the seismic assessment and retrofitting of existing RC buildings. A review of past studies on seismic risk in mainland Portugal and on the characterization of the Portuguese RC building stock, along with a discussion of the typical causes of damage and failure, are also included. The nonlinear modelling of RC frames under cyclic loading is addressed, as well as the applicable analysis methods. The current codes and guidelines are reviewed, with special emphasis on the methodology defined by EC8-3 (2005), the common practice among structural design professionals, and the simplified methods introduced by the LNEC Report 81/2019 (Sousa *et al,* 2019). The final part of the chapter is dedicated to the available steel-based retrofitting

techniques for RC frames, as well as to the review of past studies on the seismic behaviour and design of RC buildings retrofitted with steel X-braces.

- Chapter 3, *An application of the EC8-3 seismic safety assessment procedure*, examines the seismic behaviour of an older-type RC framed structure, with and without considering the effect of its masonry infill walls. The options considered during the development of the numerical models of the bare and infilled frames are discussed in light of the state-of-the-art provisions presented in Chapter 2, and their validation is carried out based on the experimental results of the above-referred ICONS research programme. The seismic assessment of the structure is then performed according to the provisions of EC8-3 (2005), running nonlinear static and dynamic analyses, and conclusions are drawn from the obtained results. In particular, local results are compared with the damage observed during the experimental tests, and the influence of the infill walls is discussed regarding the overall conclusions of the seismic assessment process.
- Chapter 4, *On the applicability of conventional seismic design methodologies to hybrid RC-steel systems*, initially reviews the *q*-factor based EC8-3 (2005) seismic assessment procedure, and afterwards presents a case-study application intended to analyse and discuss the difficulties a practitioner will face when defining and assessing the efficiency of a steel-brace retrofitting system for a RC framed structure within the framework of EC8-1 (2004). The performance of the obtained retrofitted structure is then evaluated using the same nonlinear methods of analysis presented in Chapter 3. The obtained results are discussed in light of the EC8-3 (2005) performance requirements, and conclusions are drawn about the adequacy of the FBD methodology (and associated behaviour factors) to such situations.
- Chapter 5, *A new displacement-based design procedure for the retrofitting of RC buildings with steel braces*, presents a design methodology aimed at obtaining retrofitted structures with better and more predictable seismic performance. The bases of the method are described, as well as the required input parameters. Afterwards, an application example is carried out for the same RC building studied in Chapters 3 and 4, and the advantages over the traditional design process are discussed.
- Chapter 6, *Validation and calibration of the proposed design procedure*, demonstrates that the design methodology proposed in Chapter 5 is robust enough to be systematically applied to the retrofitting of Portuguese RC framed buildings that were built before the publication of the national seismic code (RSA, 1983). A sample of ten structures, with different numbers of spans and storeys, is put through the EC8-3 (2005) assessment process, considering four seismic hazard scenarios of growing intensity. For those deemed unsafe, retrofitting systems are designed according to the methodology proposed in Chapter 5. The assessment process is then carried out for the retrofitted structures, and conclusions are drawn from the obtained results, concerning the effectiveness of the design method and its calibration according to the EC8-3 (2005) performance requirements.
- Chapter 7, *On the evolution of the seismic risk of the studied sample of structures*, conducts a seismic risk study of the structures that were retrofitted in Chapter 6. Combining information about structural fragility with the seismic hazard of the locations in question, the evolution of

seismic risk is analysed, between the original conditions and those created by the retrofitting systems designed with the methodology proposed in Chapter 5. From the obtained results, inputs are provided for the above-referred research project MitRisk.

- Chapter 8, *Closure*, summarizes the main conclusions of the previous chapters, and provides recommendations for the future development of some of the research lines that may be derived from the findings of this work.

Overall, this thesis aims at providing the reader with a reasonable amount of information about the main topics involved in the seismic assessment of existing RC buildings, and their retrofitting using steel elements. Given the importance of the matter for public safety, and the clear lack of confidence that most Portuguese designers still show towards these procedures, the author hopes that at least some steps towards the necessary change can be taken from here.

CHAPTER 1 – INTRODUCTION

1.1. GENERAL OVERVIEW AND MOTIVATION 1.1

1.2. SCOPE AND OBJECTIVES 1.6

1.3. THESIS OUTLINE 1.7

CHAPTER 2

LITERATURE REVIEW

2.1. INTRODUCTION

In geological (plate tectonics) terms, Portugal is located at the southwest part of the Eurasian plate, near where the African and North American plates meet. Consequently, it may experience offshore seismic events, with large to very large magnitude, and onshore events with moderate to large magnitude (Moreira, 1989). The mainland seismicity pattern is characterized by the occurrence of small to moderate magnitude earthquakes and by non-frequent high impact earthquakes (Sousa and Campos Costa, 2016). Nonetheless, Portugal has its past marked by the occurrence of very destructive earthquakes. The All Saints' Day Lisbon earthquake (1755, $M_{w,est}$ = 8.7) is the most referred event, due to the massive destruction and death toll it caused. More than 50% of the building stock is estimated to have been heavily damaged or destroyed and approximately 10% of the population perished. 154 years later, a moderate event struck the village of Benavente in the district of Santarém (1909, M_w = 6.0), causing 46 casualties and heavy damages to more than 3000 dwellings (Choffat, 1912). More recently, a strong offshore event occurred (1969, M_w = 7.3) which, despite the registered low ground motion, still caused widespread damage in the southern part of the country, particularly on old masonry structures. This was the last strong earthquake to occur in mainland Portugal.

RC buildings represent about 50% of the total building stock in the country and serve 60% of the population, according to the 2011 Census Survey (http://censos.ine.pt/). At that time and within this building class, 49% of the buildings had not been designed according to the current national seismic design code (RSA, 1983), which puts approximately 3.1 million people living at homes that might not be able to withstand the effects of a moderate seismic event. Therefore, information about the year of construction is critical for a structure's classification concerning the seismic design level. The number of storeys is also an important distinctive factor. According to the 2011 Census Survey, more than 95% of the RC building stock in Portugal has less than 5 storeys. Within this interval, most buildings have 2 storeys (42%), followed by 1-storey buildings (28%) while 3- and 4-storey buildings represent the remaining part (about 15% each). Figure 2.1 shows a summary of the RC building stock considering the above-referred parameters and its spatial distribution throughout mainland Portugal. The terms "PreCode", "MidCode" and "PostCode" refer, respectively, to buildings constructed during the

following time periods: (i) before the publication of the first earthquake resistant design code RSCCS (1958), (ii) between 1958 and the publication of RSA (1983) and (iii) after 1983.

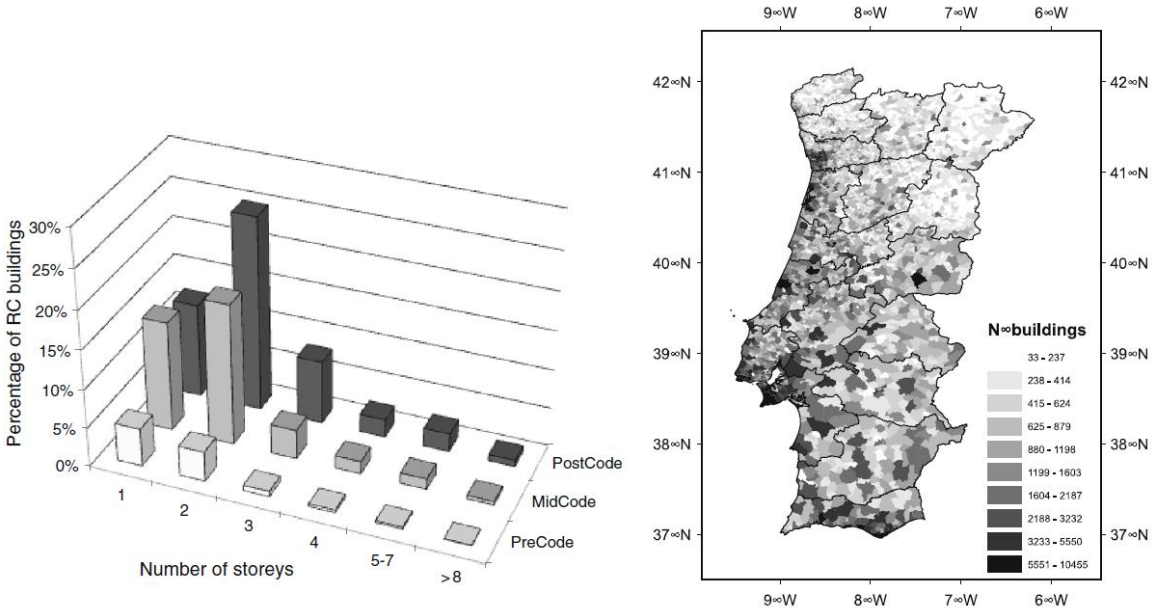

Figure 2.1 – Percentage of RC buildings according to year of construction and number of storeys (left) and spatial distribution throughout mainland Portugal (right), according to the 2011 Census Survey (Silva *et al*, 2015b)

Seismic vulnerability can be defined as the likelihood of a structural member to suffer loss due to the effects of an earthquake (Silva, 2013). The magnitude of losses during a seismic event is critically influenced by the vulnerability of the exposed elements, as discussed in Chapter 1 (refer in particular to comments on Figure 1.1). As such, a vulnerability model which can provide the probabilistic distribution of loss ratio as a function of a set of ground motion parameters, is a fundamental tool to perform earthquake loss estimation and seismic risk assessment (Silva *et al*, 2015b). The former process can play an important role in the sustainable development of a given region, providing local authorities (and other decision makers) with the necessary information for the creation of risk mitigation actions, such as: strategic urban plans, building retrofitting campaigns, post-disaster emergency plans, etc. Different methodologies can be applied to evaluate the vulnerability of exposed elements (Calvi *et al*, 2006), for instance: (1) empirical methods that use post-earthquake damage data to derive fragility functions (e.g. Rota *et al*, 2008); (2) simplified approaches, where a set of structural parameters is employed to derive a vulnerability index, which is then used to plot a curve relating levels of damage with a set of intensity measure levels (e.g. Lagomarsino and Giovinazzi, 2006) or (3) analytical methodologies that rely on numerical models to simulate the seismic performance of structures for increasing ground motion levels (e.g. Vamvatsikos and Cornell, 2002; Freeman, 2004; Rossetto and Elnashai, 2005). Analytical methods have the obvious advantage of not depending on the availability of post-earthquake damage data but need to be carefully applied and handled. This matter is thoroughly discussed in the following sections.

The assessment of seismic risk is thus based on the combination of three components: (i) a probabilistic seismic hazard model; (ii) a set of vulnerability functions as described above and (iii) an exposure model defining the spatial distribution of the exposed elements (Figure 2.2).

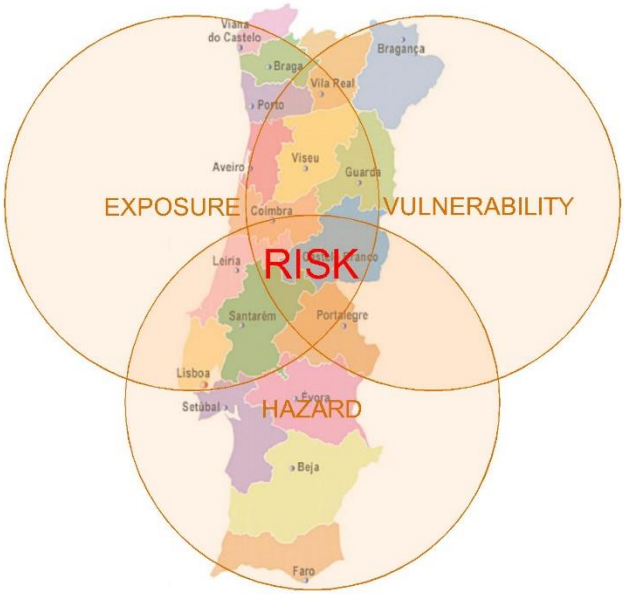

Figure 2.2 – Components involved in the evaluation of the country's seismic risk

As previously referred, high impact seismic events in Portugal have a high return period, hence the seismic hazard in the territory has been evaluated as moderate by several authors (e.g., Sousa and Campos Costa, 2009; Silva *et al*, 2015a; Woessner *et al*, 2015). However, in similar countries, this degree of hazard has caused considerable economic and human losses (Barata, 2005). It should be kept in mind that more than half of the country's building stock is comprised of masonry structures, which is a typology that is usually more vulnerable to earthquakes and, as such, at significant risk even when only subjected to moderate events (Vicente *et al*, 2010). According to a scenario loss assessment performed by Sousa (2006), if the above-referred historical seismic episodes were to occur again, large economic and human losses would still be observed. This stresses the need for a reliable and comprehensive evaluation of the seismic risk in Portugal, as well as for strategic development of risk mitigation measures (Silva *et al*, 2015a).

2.2. EXISTING STUDIES ON SEISMIC RISK IN PORTUGAL

An updated, reliable, and comprehensive evaluation of the seismic hazard and risk in Portugal is a fundamental tool for the definition and implementation of measures that will help reduce potential losses due to future earthquakes. Several studies have contributed for this matter, some of them international, covering part or all the territory of mainland Portugal, and others on a regional or local scale (Silva *et al*, 2015a).

On a global level, the Global Seismic Hazard Assessment Program (GSHAP) (Giardini, 1999) was one of the first initiatives towards understanding seismic hazard. Started in 1992, its main objective was the definition of seismic hazard models for different regions in the world. The program was concluded in 1999 with the publication of the first global hazard map of peak ground acceleration (PGA) for a 475-yrp. More recently, another global initiative was founded, covering not only seismic hazard but also seismic risk assessment. The denominated *Global Earthquake Model* (GEM) (www.global-quakemodel.org) involves experts from around the world and aims to develop new datasets, models, and tools for the referred purposes. GEM has already developed an opensource platform for the calculation of seismic hazard and risk, the *OpenQuake* engine (Silva *et al*, 2014a), which is available online at https://platform.openquake.org/.

On the European level, three initiatives are worth mentioning, each focusing on individual components of seismic risk: (1) SHARE project (2009-2013) (www.share-eu.org); (2) SYNER-G project (2009-2013) (www.vce.at/SYNER-G) and (3) NERA project (2010-2014) (www.nera-eu.org). SHARE was founded with the target of creating a homogeneous seismic hazard model for Europe and, through a set of ground motion prediction equations compatible with the European tectonic environment, has produced a European seismic hazard map. SYNER-G focused on the structural fragility of buildings, infrastructures and networks and proposed a unified methodology for the evaluation of their physical and socio-economic systemic vulnerability. NERA promoted the sharing of information and collaboration of several institutions involved in seismic risk assessment. One of its outputs was the inventory and classification of the European building stock and the development of an exposure model covering all European countries.

On a narrower geographic scope inside Europe, two more projects can be mentioned: (4) RISK-EU project (2001-2004) (Mouroux and Le Brun, 2006) and (5) LESSLOSS (2004-2007) (Calvi and Pinho, 2004). Both initiatives evaluated the seismic hazard and structural vulnerability of several European cities (including Lisbon) and employed the obtained results to calculate the seismic risk. Regarding the Iberian Peninsula, a probabilistic seismic hazard assessment was conducted by Pelaez and Casado (2002), through an approach combining zonified (area sources) and non-zonified (smoothed seismicity) probabilistic methodologies. As a result, PGA hazard maps were produced for 100-, 475- and 975-yrp.

Concerning mainland Portugal, the first comprehensive seismic hazard assessment study was carried out by Oliveira *et al* (1997). Later, in the scope of the draft of the National Annex for EC8-1 (2004), additional studies were performed, resulting in the development of a seismic hazard map for moderate magnitude events at short distance and large magnitude events at long distance (Oliveira *et al*, 1999). A few years after that, Sousa (2006) performed a seismic risk assessment study, applying the hazard model developed by Sousa (1996), several simplified methodologies for the building vulnerability assessment and a detailed exposure model based on the data of the 2001 Building Census Survey. Human and economic loss maps were calculated for several return periods, as well as loss maps for two deterministic seismic events, equivalent to the historical earthquakes of Lisbon in 1755 and Benavente in 1909. Finally, Vilanova and Fonseca (2007) carried out a study that contributed for the creation of a national PGA hazard map for a probability of exceedance of 10% in 50 years. A logic tree approach was considered by the authors to characterize the various epistemic uncertainties in hazard

modelling, such as seismic sources characterization, selection of ground motion prediction equations, earthquake catalogues and methodologies to derive the magnitude-frequency relationship parameters.

Recently, Silva *et al* (2015a) used the information contained in the above referred studies, together with the data from the 2011 Building Census Survey, to compile the input models required to perform an updated evaluation of the seismic hazard and risk in mainland Portugal. Moreover, this study introduced the following innovations in the process, listed by the authors:

- Application of the most recent probabilistic seismic hazard assessment (PSHA) for Portugal, including state-of-the-art ground motion prediction equations;
- A logic tree approach to characterize the epistemic uncertainty from various sources, such as seismic zonation, earthquake catalogue, magnitude-frequency distribution derivation methodology, ground motion prediction equations, site conditions;
- Two simplified methodologies to include the amplification due to varying soil conditions;
- A new vulnerability model based on an analytical approach for the RC building stock, which takes into consideration the seismic zonation;
- Uncertainty in the distribution of loss ratio in the vulnerability model;
- An exposure model based on the latest Building Census Survey (2011);
- A higher spatial re-distribution of the assets in the exposure model using population data from the LandScan™ dataset;
- Probabilistic maps of economic loss for the mean as well as the 16^{th} and 84^{th} percentiles;
- Loss disaggregation according to the various building typologies.

The study provided an up-to-date identification of the regions that are more vulnerable to earthquakes, as well as the expected losses for a probability of exceedance of 10% in 50 years (equivalent to a 475-yrp, commonly used as the reference for seismic design purposes) and their disaggregation according to building typology. The open-source software *OpenQuake*, developed within the GEM initiative as previously referred, was used to obtain these results. The full description of the undergone process to obtain the input models for *OpenQuake* can be found in Silva *et al* (2015a). The obtained seismic hazard maps are shown in Figure 2.3. Some significant differences regarding the hazard map of the design code RSA (1983) were revealed by this study, especially around the Lower Tagus Valley and in the south (Algarve). It is noteworthy that the spatial distribution of the hazard and the range of PGA obtained by Silva *et al* (2015a) agree with the results proposed by Vilanova and Fonseca (2007), despite the different ground motion prediction equations scheme considered. A new seismic zonation has been proposed for Portugal by Campos Costa *et al* (2008), within the scope of the nationally determined parameters (NDP) of EC8-1 (2004). Two types of seismic action are defined: (1) Type 1, characterizing large magnitude events at long distance and (2) Type 2, characterizing moderate magnitude events at short distance (identical to what is structured in RSA (1983), but the Type 1 action here described corresponds to the Type 2 action in RSA (1983)). Considering this new zonation and the distribution of PGA associated with each type of seismic action, the results obtained by Silva *et al* (2015a) are close to the Type 2 seismic action, except for the Lower Tagus Valley region for which the attained seismic hazard is higher.

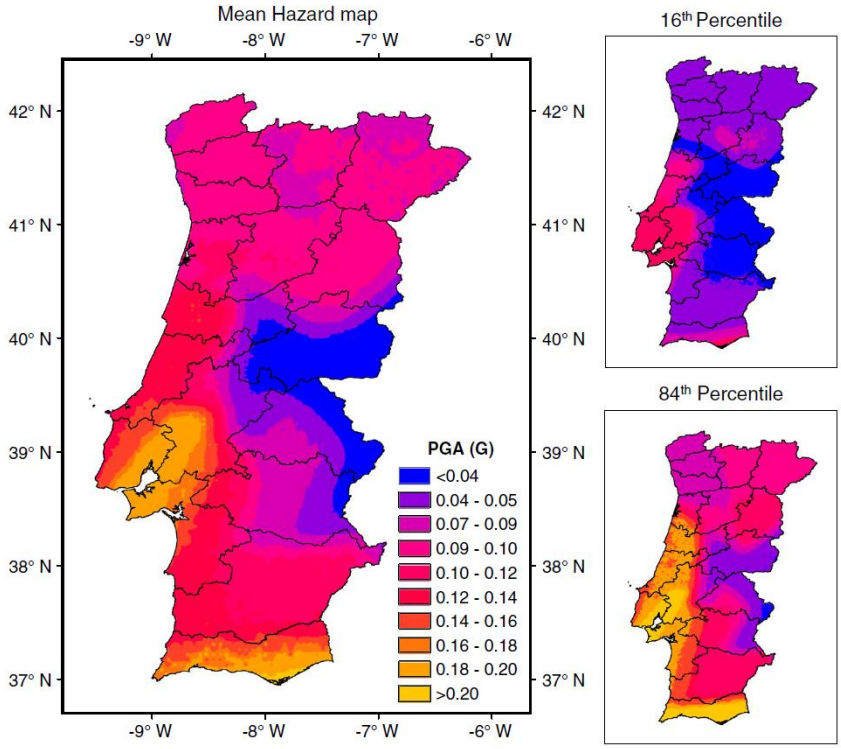

Figure 2.3 – Mean seismic hazard map and 16th and 84th percentile maps in PGA (*g*) for rock, for a probability of exceedance of 10% in 50 years (475-yrp) (Silva *et al*, 2015a)

In terms of seismic risk, Silva *et al* (2015a) concluded the estimated economic losses in mainland Portugal to be mostly concentrated in the western region and the south (Algarve). In the region above the Lower Tagus Valley, despite the decrease in the seismic hazard, significant economic losses are still expected due to the existence of a large amount of weak masonry buildings. Moreover, these buildings are founded on soft soils, which can amplify the spectral acceleration by a factor of 1.5 for short periods and 2.0 for longer periods (Stewart *et al*, 2012). The mean aggregated economic loss for the 475-yrp has been estimated as 47.2 ± 6.6 billion Euro. Figure 2.4 shows the obtained mean loss map for the grid-based exposure model, along with the 16th and 84th percentile results.

The disaggregation of the economic losses according to the building typology indicated a high percentage of loss for low rise masonry typologies and pre-code RC buildings. The overall percentage of loss was estimated as 15.7% of the whole building stock, which represents about 31.8% of the Portuguese gross domestic product (GDP) of 2011 (Silva *et al*, 2015a). Therefore, being the most seismically vulnerable, these are the typologies for which strengthening / retrofitting should be focused on. The work of Campos Costa *et al* (2009) demonstrated that, by carrying out selective retrofitting interventions in the Metropolitan Area of Lisbon building stock, the economic risk could be reduced by 36% for all return periods. Other authors have also performed seismic risk studies for this regional area (e.g., Mendes-Victor *et al*, 1994; SNPC, 2001; Oliveira *et al*, 2005). More studies can be mentioned on a regional or local level. For the province of Algarve: Oliveira (2004); Sousa *et al* (2010). For downtown city of Coimbra: Vicente *et al* (2010). For the vulnerability assessment of the old city of

Seixal: Ferreira *et al* (2013). For further information on the most relevant studies carried out in the last decades regarding risk reduction in Portugal, a summary can be found in Oliveira (2013).

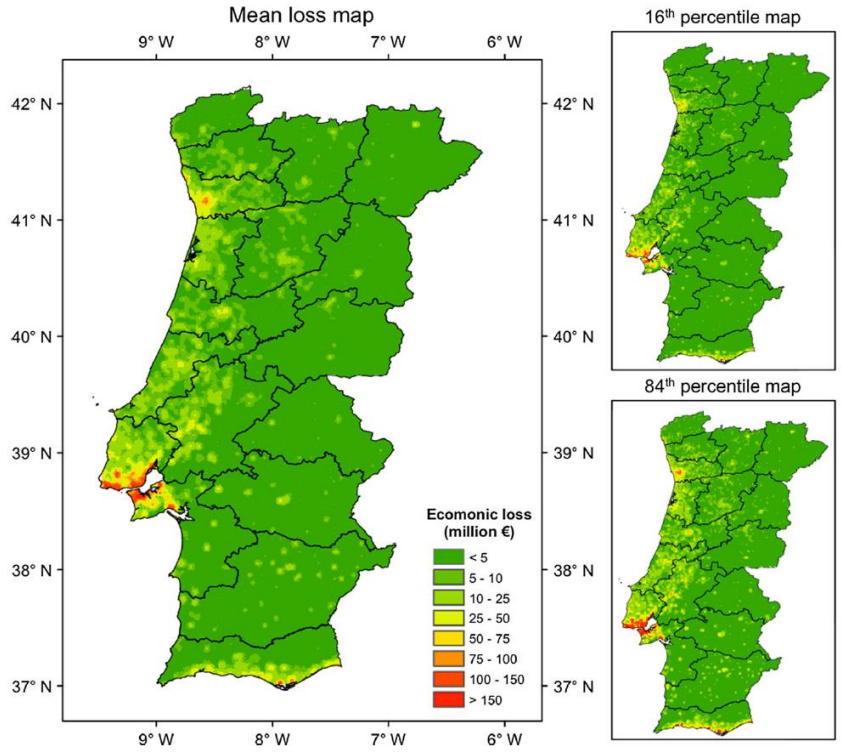

Figure 2.4 – Economic loss map, for a probability of exceedance of 10% in 50 years (475-yrp), considering the grid-based exposure model (Silva *et al*, 2015a)

Concerning fragility and vulnerability, such functions are widely recognized as fundamental tools for the seismic risk assessment of buildings. However, the vulnerability of the Portuguese building stock has not been the target of much investigation in recent years. Carvalho *et al* (2002) derived several sets of fragility functions for each existing building typology in the country, based on the simplified approach proposed by FEMA and NIBS (1999). Soon after that, Oliveira *et al* (2005) characterized the physical vulnerability of the Portuguese building stock, applying two different methodologies: (1) using the vulnerability curves developed by Coburn and Spence (2002), in terms of macroseismic intensity and (2) calculating vulnerability indexes for each building typology and, by combining them with the formulae proposed by Lagomarsino and Geovinazzi (2006), estimating mean damage curves, also in terms of macroseismic intensity.

The importance and contributions of the fragility model proposed by Carvalho *et al* (2002) are well recognized, having already been employed by Campos Costa *et al* (2009) in a seismic risk assessment study for Portugal. However, due to some limitations of the underlying FEMA and NIBS (1999) simplified approach, Silva *et al* (2015b) recently proposed a new fragility / vulnerability model for Portugal. The limitations referred by the authors were the following: (i) the use of spectral ordinates for the inelastic period (thus a specific period for each level of ground motion) complicates the seismic

risk methodology and does not allow the direct use of commonly available ground motion prediction equations to compute the ground motion at the location of the assets; (ii) the design parameters used in the construction of the capacity curves (strength coefficient, over-strength factor, elastic period and ductility factor) are specifically calibrated for structures typically found in the United States; (iii) the shape of the simplified capacity curves fails to account for the decrease in the base shear capacity due to P-Delta effects and (iv) in the case of the RC building typologies, the influence of eventual masonry infill panels is neglected.

The study performed by Silva *et al* (2015b) focused only on the vulnerability of RC buildings, hence covering about 50% of the total building stock in the country according to the previously referred 2011 Census Survey. Due to the lack of post-earthquake damage data for this type of buildings in Portugal, an analytical methodology was adopted to obtain the fragility and vulnerability functions for each building typology. A large set of moment resisting frames (one hundred per building typology) was randomly generated (Monte Carlo simulation based on probabilistic distributions for the frames' geometric and material properties – see sub-section 2.3) to represent the RC building stock and each generated frame was subjected to one hundred ground motion records using nonlinear dynamic analyses. For each analysis, the maximum global drift and inter-storey drift were the used parameters to allocate each frame in a damage state, according to a five-level damage scale: (i) none; (ii) slight; (iii) moderate; (iv) extensive and (v) collapse. The respective fragility functions (i.e., probability of exceeding the defined damage states for a given level of ground motion) were then obtained and combined with a consequence model (i.e., fraction of loss for each damage state) to produce the desired vulnerability functions (i.e., probability of loss for a given level of ground motion). Figure 2.5 shows the proposed mean vulnerability functions (and associated 10% and 90% percentiles), for the global drift and inter-storey drift damage criteria, according to six pre-defined RC building typologies (see sub-section 2.5 for details). An increase in the probability of loss is noticeable for pre-code (PC) buildings, regardless of the number of storeys. The full discussion of the obtained results and conclusions can be found in Silva *et al* (2015b).

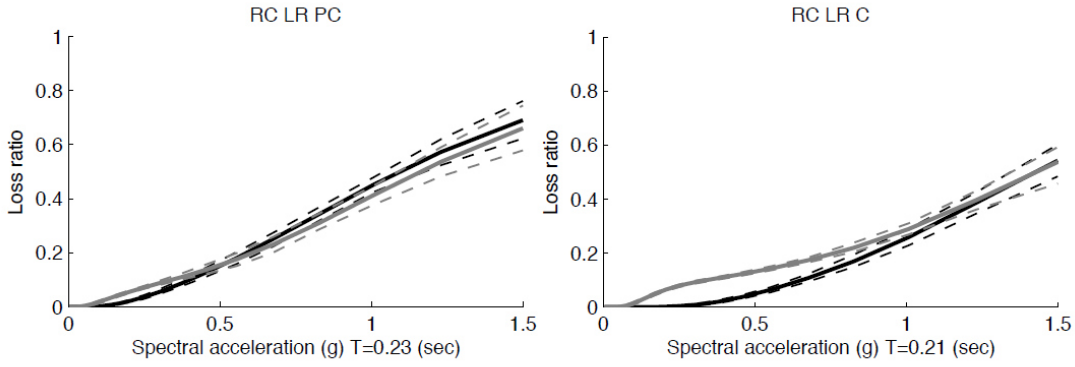

Figure 2.5 (1/2) – Vulnerability model for RC framed buildings in Portugal, assuming a global drift (black) and an inter-storey drift (grey) damage criterium. PC: pre-code (before RSA, 1983); C: post-code (after RSA, 1983); LR: low-rise (up to 3 storeys); MR: mid-rise (4 to 6 storeys); HR: high-rise (7+ storeys) (adapted from Silva *et al*, 2015b)

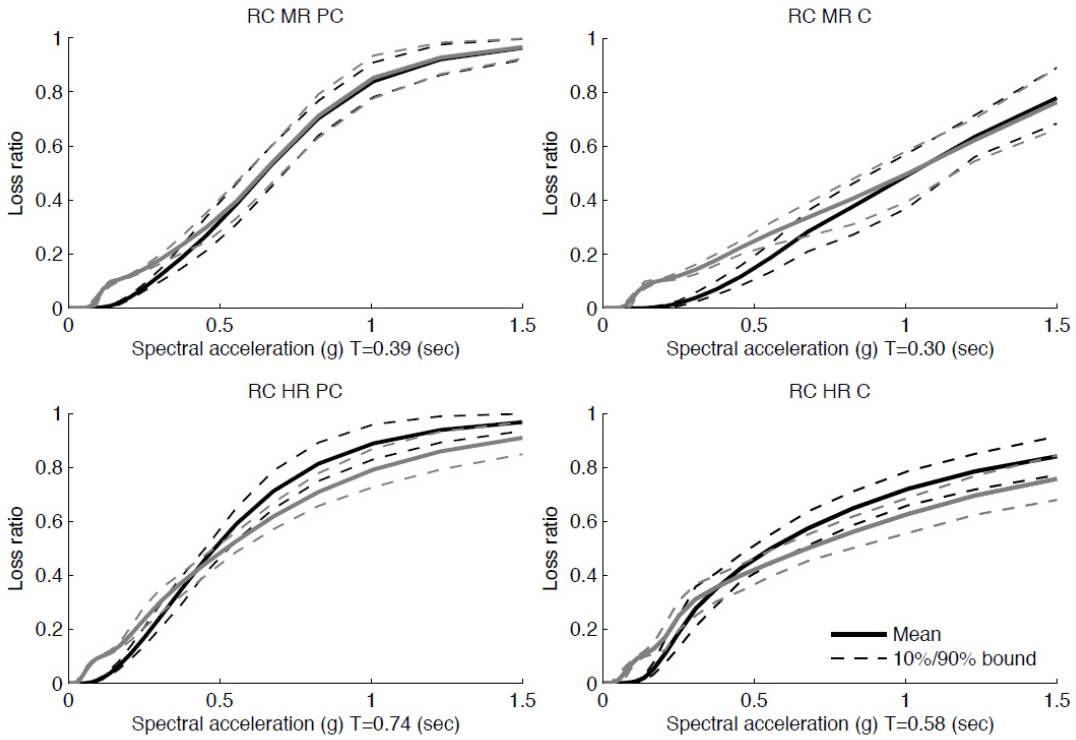

Figure 2.5 (2/2) – Vulnerability model for RC framed buildings in Portugal, assuming a global drift (black) and an inter-storey drift (grey) damage criterium. PC: pre-code (before RSA, 1983); C: post-code (after RSA, 1983); LR: low-rise (up to 3 storeys); MR: mid-rise (4 to 6 storeys); HR: high-rise (7+ storeys) (adapted from Silva *et al*, 2015b)

When applying analytical approaches to derive sets of vulnerability functions, there are four main components that can strongly affect the results: (i) structural modelling options; (ii) damage state criteria; (iii) method of selection of the ground motion records and (iv) consequence model used to convert fragility curves in vulnerability curves. Silva *et al* (2015b) discuss extensively the various assumptions and main results of the performed study for each of these components, in order to evaluate the impact of the chosen methodology on the resulting capacity, fragility and vulnerability outputs. It is noteworthy that, despite the existence of several studies evaluating the impact of alternative methodologies on the seismic response of buildings, research is scarcer on the effect of such choices on the computation of fragility and vulnerability functions. For further discussion on this matter, readers are referred to the work of Silva *et al* (2014b) in which the computational effort and numerical stability provided by each approach are also evaluated and conclusions are drawn regarding the balance between accuracy and complexity.

2.3. Characterization of the Portuguese RC building stock

Census surveys have been carried out in Portugal since 1864, with a 10-year periodicity, although information about the building portfolio was only introduced after 1970. In 2011, a total of 3544389 residential buildings were reported, housing 5878756 dwellings. Amongst the attributes considered in the Building Census Survey, the year of construction (or seismic design philosophy and practice) and

the number of storeys were used by Silva (2013) as the base for the proposed classification of the RC building stock. Six typologies were considered. RC buildings constructed (hence, designed) before the publication of RSA (1983) were categorized as pre-code (PC), whilst the ones built after were termed post-code (C). Regarding the number of storeys, buildings up to three storeys were categorized as low-rise (LR), between four and six storeys as mid-rise (MR) and with seven or more storeys as high-rise (HR). A summary of the RC building stock following these parameters is shown in Figure 2.6. More recently, the previously referred research project PRISE (http://prise.fe.up.pt/) followed the same methodology and extended this classification to portal steel framed industrial building facilities.

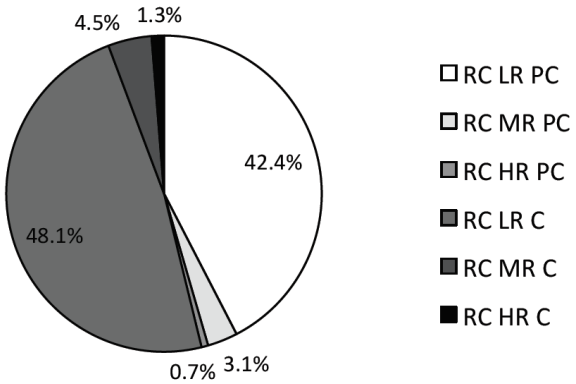

Figure 2.6 – Percentile distribution of residential RC buildings in Portugal according to seismic design philosophy and practice (PC/ C) and number of storeys (LR/ MR/ HR) (adapted from Silva, 2013)

Concerning the geometric and material properties associated with the defined building typologies, Silva (2013) analysed data on a large number of real buildings located in different parts of the country, as previously referred, with the purpose of capturing the variability associated to the structural design and construction practices followed in each region. Hundreds of drawings and design specifications on RC buildings with a moment-resisting frame as the structural system were thoroughly analysed, as well as available results from on-site tests performed on existing buildings that suffered structural interventions. The results of this study are reviewed in the following sub-sections.

2.3.1. Geometric properties

For each of the analysed buildings, the main structural frames (concerning lateral loads resistance) were taken as representative to measure the following set of geometric parameters: ground story and upper storeys heights; column widths and depths; beam lengths, widths, and depths; slab thicknesses. The data for the referred parameters were then disaggregated according to the six building typologies, to assess if some geometric properties were directly related to the date of construction and / or number of storeys and, as such, should be considered separately from the data associated with the other typologies.

Concerning the approach to the modelling of each geometric property, the work of Silva (2013) was based on a similar study performed by Bal *et al* (2008) for the Turkish building stock. Several

probabilistic distributions (Normal, Lognormal, Exponential, Gamma, Beta and Weibull) were considered, and the associated statistical parameters were derived applying the maximum likelihood approach. Each distribution was then evaluated in terms of the best-fit (i.e., size of the residue between the reference and the modelled data) and goodness-of-fit (i.e., capability of providing a satisfactory fit for a given level of significance). For the latter, the Chi-square test was used with levels of significance of 1%, 5% and 10%. The detailed description of the undergone study, as well as considerations about the obtained results can be found in Silva *et al* (2015b). Therefore, only the final results are summarized herein, for the purposes of fully characterizing the Portuguese RC building stock and organizing the data for the development of numerical models in the present work.

2.3.1.1. Inter-storey height

The architectural design of residential buildings in Portugal usually shows larger ceiling heights at the ground storey than at the upper storeys. This is because such spaces are frequently used for commercial purposes, which require more space for the installation of electrical, mechanical, and plumbing equipment. Hence, the data on the ground storey and regular storey heights was retrieved by Silva (2013) from the collected blueprints, thoroughly analysed and organised according to the defined building typologies. No significant differences were observed in the statistics when disaggregating the data according to the date of construction or number of storeys, therefore, in the end, all the data was considered together when estimating the respective distributions.

The ground storey height was found to follow a lognormal distribution, with a mean value of 3.21 *m* and a coefficient of variation of 13%, whilst the regular (upper) storey height was modelled with a normal distribution with a mean value of 2.88 *m* and a coefficient of variation of 7%. In terms of goodness-of-fit, both distributions passed the Chi-square test for a significance level of 1%. The correlation between the two heights was estimated equal to 0.24, therefore deemed to be insignificant. Thus, these two parameters can be sampled independently when generating synthetic frames to conduct numerical analyses. Table 2.1 summarizes the full statistics for the inter-storey height.

Table 2.1 – Probabilistic distribution of inter-storey height for all RC buildings (adapted from Silva, 2013)

Height	Number of buildings	Probabilistic distribution	Mean [m]	Coefficient of variation	Chi-square test
Ground storey	200	Lognormal	3.21	13%	1%
Regular storey	200	Normal	2.88	7%	1%

2.3.1.2. Column properties

The two dimensions of the columns' cross-sections (depth and width) were analysed separately in order to detect different behaviours towards the influence of the number of storeys and date of construction. Concerning the depth, it was found (as expected) to have a strong dependence on the number of storeys and date of construction. Table 2.2 summarizes the statistics for the column depth.

The symbol "NS" means that the Chi-square test could not be satisfied. Concerning column width, no relevant discrepancies were verified between pre-code buildings with a distinct number of storeys, whereas for post-code buildings the cross-section width increased with the number of storeys. The results for this parameter are summarized in Table 2.3.

Table 2.2 – Probabilistic distribution of column depth for each RC building typology (adapted from Silva, 2013)

Building typology		Number of buildings	Probabilistic distribution	Mean [m]	Coefficient of variation	Min [m]	Max [m]	Chi-square test
Pre-code	Low-rise	33	Lognormal	0.28	15%	0.20	0.44	NS
	Mid-rise	43	Normal	0.36	23%	0.24	0.55	10%
	High-rise	20	Lognormal	0.57	40%	0.28	1.00	10%
Post-code	Low-rise	38	Normal	0.38	20%	0.26	0.60	10%
	Mid-rise	48	Lognormal	0.43	20%	0.28	0.70	5%
	High-rise	18	Lognormal	0.51	36%	0.30	0.95	10%

Table 2.3 – Probabilistic distribution of column width for each RC building typology (adapted from Silva, 2013)

Building typology		Number of buildings	Probabilistic distribution	Mean [m]	Coefficient of variation	Min [m]	Max [m]	Chi-square test
Pre-code		96	Lognormal	0.27	16%	0.20	0.53	NS
Post-code	Low-rise	38	Normal	0.25	11%	0.20	0.30	1%
	Mid-rise	48	Normal	0.27	13%	0.20	0.37	1%
	High-rise	18	Lognormal	0.31	23%	0.21	0.53	NS

2.3.1.3. Beam properties

Three parameters were investigated concerning beams: length, width, and depth. Regarding the first two, the disaggregation of the data according to the date of construction and number of storeys revealed no significant differences. Table 2.4 summarizes the statistics for the beam length and width. The beam depth, however, exhibited a different behaviour. A relevant discrepancy was observed in the statistics when comparing the results for buildings constructed before and after the publication of RSA (1983). Thus, the data was separated, and Table 2.5 summarizes the calculated statistics for the beam depth. Regarding its dependence on the number of storeys, as expected no significant differences were found.

The correlation between the beam geometric parameters was investigated, as the calculation of the depth was expected to be directly related to the associated length. For the pre-code buildings, a correlation of 0.53 was estimated while for the post-code buildings, a larger correlation of 0.76 was observed. The employment of an adequate correlation factor during the generation of synthetic RC frames (using a Monte Carlo sampling approach, for instance) for the purpose of conducting numerical analyses is fundamental to ensure that unrealistic structural elements are not created (e.g., long beams with reduced section depth). The scatter between the beam depths and the respective beam lengths, for the analysed buildings, can be found in the work of Silva (2013).

Table 2.4 – Probabilistic distribution of beam length and width for all RC buildings (adapted from Silva, 2013)

Beam parameter	Number of buildings	Probabilistic distribution	Mean [m]	Coefficient of variation	Chi-square test
Length	200	Lognormal	4.37	11%	5%
Width	200	Lognormal	0.27	16%	NS

Table 2.5 – Probabilistic distribution of beam depth for pre-code and post-code RC buildings (adapted from Silva, 2013)

Building typology	Number of buildings	Probabilistic distribution	Mean [m]	Coefficient of variation	Chi-square test
Pre-code	96	Normal	0.44	22%	1%
Post-code	104	Lognormal	0.50	18%	NS

2.3.1.4. Slab thickness

Concerning the type of solution, the floors of the Portuguese residential RC buildings are mostly composed of pre-cast lightweight composite slabs. However, for larger spans (more recent), cast-in-place thick slab or flat slab (no beams) solutions are also found. The main parameter defining the weight of the floor is the slab thickness, so this was investigated based on the collected blueprints and design specifications. The number of storeys was found to have no significant influence on this parameter, whereas a clear difference was found comparing the results for buildings constructed before and after the publication of RSA (1983). Again, the data was disaggregated based on the date of construction and Table 2.6 summarizes the obtained results.

Table 2.6 – Probabilistic distribution of slab thickness for pre-code and post-code RC buildings (adapted from Silva, 2013)

Building typology	Number of buildings	Probabilistic distribution	Mean [m]	Coefficient of variation	Chi-square test
Pre-code	96	Lognormal	0.17	19%	1%
Post-code	104	Weibull	0.25	18%	NS

2.3.2. Material properties

Silva (2013) tried to investigate the probabilistic distributions of the mechanical properties of the concrete and steel reinforcement used to construct the Portuguese residential RC buildings. Ideally, a large number of random buildings should have been selected for this study, and field tests should have been carried out to determine properties such as the concrete compressive strength or the steel rebars yielding and ultimate strengths. However, this would have required a considerable amount of human and economic resources, so different approaches had to be considered to carry on. The following sub-sections summarize the adopted strategies and the obtained results.

2.3.2.1. Concrete properties

The study was based on the data available from tests on buildings that had been subjected to structural retrofitting / rehabilitation or demolition, provided by the public and private institutions that had

performed such tests. Most of the data was composed of results of laboratory destructive compression tests, performed on concrete specimens removed (drilled) from the columns and / or beams of the intervened buildings. The experimental results from core drilling tests in 76 buildings, located mainly in the centre and north of Portugal, were used to determine the concrete compressive strength statistics. However, the disaggregation of the data based on the date of construction or the concrete's design resistance class was not possible due to confidentiality issues regarding the access to such additional information. Table 2.7 summarizes the derived statistics regarding the concrete compressive strength. The large coefficient of variation exhibited by the scatter of results is most likely due to the fact that the samples were taken from buildings constructed in very different time periods, meaning that several resistance classes and different design codes might have been involved. In fact, in the work of Bal *et al* (2008), which employed a similar process to estimate the probabilistic distribution of this parameter, a similar coefficient of variation (51%) was obtained.

Table 2.7 – Probabilistic distribution of concrete compressive strength for all RC buildings (adapted from Silva, 2013)

Material parameter	Number of buildings	Probabilistic distribution	Mean [MPa]	Coefficient of variation	Chi-square test
Concrete compressive strength	76	Gamma	23.79	49%	10%

2.3.2.2. Steel properties

Concerning steel reinforcement properties, no results were available for the above-referred sample of buildings, since only concrete specimens were tested. Therefore, the work of Silva (2013) investigated and employed the results from previous studies (e.g., Pipa, 1993; Fernandes *et al*, 2011; Rodrigues *et al*, 2012). Most of the buildings in Portugal were designed using steel ribbed bars with nominal strength of 400 or 500 *MPa*. A smaller fraction of buildings mainly constructed until the 1970's, employed plain bars with lower resistance. In the work of Pipa (1993), several material parameters (yielding and ultimate strength and strain) of A400 and A500 steel classes were analysed using experimental results from a sample with about 700 specimens, coming from many European producers (e.g., Italy, Portugal, Spain). Each parameter was assumed to follow a Normal distribution and the mean and standard deviation were computed for the whole sample. The probabilistic distribution of the yielding strength, however, was estimated considering only the steel bars produced in Portugal. The statistics proposed by Pipa (1993) for this parameter are presented in Table 2.8. In the work of Fernandes *et al* (2011) and Rodrigues *et al* (2012), results within the range proposed by Pipa (1993) were obtained for the yielding strength, although based on a smaller sample of steel bars.

Silva (2013) concluded, from the evaluation of the technical specifications of the sample of RC buildings constructed after the publication of RSA (1983), that both steel classes were used with the same frequency. For buildings prior to the publication of this code, the use of steel class A230 was also found. However, as no statistical study seems to exist for Portugal regarding the material properties of this steel class, Silva (2013) adopted the mean yielding strength of 344.3 *MPa* proposed by Carvalho and Coelho (2001) for European and Mediterranean buildings. A coefficient of variation of 20% was

adopted, leading to a characteristic yielding strength (5% fractile) of 230 *MPa*, equal to the nominal strength of steel class A230. These statistics are in agreement with the work of Akyuz and Uyan (1992) for Turkey, in which more than 200 steel samples (class S220) were evaluated, leading to a mean yielding strength of 371 *MPa*, with a coefficient of variation of 24%. Concerning the frequency of use of each steel class in buildings constructed before the publication of RSA (1983), Silva (2013) proposed a relative weight of 0.50 for steel class A400 and an equal relative weight of 0.25 for steel classes A230 and A500.

Table 2.8 – Probabilistic distribution of the yield strength of steel produced in Portugal (Pipa, 1993)

Steel class	Size of sample	Mean yield strength [MPa]	Standard deviation [MPa]	Coefficient of variation
A400	84	495	22	4.4%
A500	51	589	30	5.1%

2.3.3. Limitations of the study

The results of the statistical study presented above constitute a useful contribution for research in the field of seismic vulnerability assessment of the RC building stock in Portugal. However, the following limitations should be kept in mind when using these results, as referred by the author of the study (Silva, 2013):

- The number of failed Chi-square tests suggests that the size of the analysed sample of RC buildings needs to be further increased;
- The obtained results were based on the observation of drawings and technical specifications, which might differ from what was actually built;
- The investigated RC building population was composed exclusively by regular moment frame structures and, therefore, the influence of stiff elements like elevator shafts, staircases or other shear walls was neglected.

2.4. TYPICAL CAUSES OF DAMAGE AND FAILURE OF NON-DUCTILE RC BUILDINGS

As previously referred in Chapter 1, RC framed structures were the most commonly used solution for building construction in southern Europe until the late 1970's and most are deficient in terms of seismic resistance (Varum, 2003). Therefore, seismic rehabilitation efforts for buildings belonging to that period should be focused on this structural typology. Concerning more recently constructed buildings, despite the current rather strict seismic code requirements, several examples are still found with inadequate balance of stiffness, strength and ductility between members, connections and supports. The major sources of seismic weakness in buildings can be grouped in four main categories, as suggested by Tankut and Ersoy (1998) and Sasani *et al* (1999):

i. Design deficiencies (e.g., insufficient lateral stiffness and strength, horizontal and vertical irregularities, soft-storeys, short columns, weak-column strong-beam mechanisms, critical torsional response, inadequate spacing between adjacent structures, etc.);

ii. Detailing deficiencies (e.g., insufficient confinement, insufficient and improper anchorage of the longitudinal reinforcement at the joints and footings, inexistence or inadequate beam-column joint reinforcement, lack of adequate amount and detailing of the longitudinal and transverse reinforcement along the beams and columns, inadequate lap-splice in column longitudinal reinforcement, etc.);
iii. Construction deficiencies (e.g., poor workmanship, poor quality concrete, disrespect for the design and detailing specifications, etc.);
iv. Deterioration and structural modifications.

These categories, however, should not be looked at separately, as design, detailing and construction are directly related (Varum, 2003). For instance, if a member's detailing is too complex, good workmanship might be difficult to achieve. In fact, some reinforcement details may work on paper and in laboratory specimens, effectively bringing improvements to seismic behaviour, but be too complex to execute on site (Bertero, 1982). Economy issues may also pose an obstacle. A list of the most common causes of damage and failure of RC buildings can be found in the work of Varum (2003), as well as an extensive description of each cause of damage together with various photographic examples. The following are referred in the text:

(1) Stirrups/ hoops, confinement, and ductility;
(2) Bond, anchorage, lap-spices, and bond splitting;
(3) Inadequate shear capacity and failure;
(4) Inadequate flexural capacity and failure;
(5) Inadequate shear strength of the joints;
(6) Influence of the infill masonry on the seismic behaviour of frames;
(7) Vertical and horizontal irregularities;
(8) Higher modes effect;
(9) Strong beam-weak column mechanism;
(10) Structural deficiencies due to architectural requirements.

Ductility can be defined as the ability of a material, structural component, or entire structure to sustain inelastic deformations after its initial yield, without any significant reduction in yield strength or risk of collapse, having a decisive effect on the energy dissipation capacity of a building (Varum, 2003). Shear behaviour is typically non-ductile, while flexural behaviour can be made ductile by the designer. However, designers in general are more concerned about strength than ductility, as the former appears to be more important to static vertical loading in everyday design. On the other hand, as earthquakes happen from time to time, the importance of ductility in preventing structural collapse during such events is gradually being realized (the principle of ductility in earthquake engineering was only fully understood a few decades ago). Nonetheless, a large number of older buildings and their structural elements are non-ductile, which represents a serious risk to the safety of the populations occupying such dwellings.

Shear failure is one of the most frequent during earthquakes, mostly because the typical gravity and wind design loads usually lead to design shear forces that are significantly lower than those that may be developed in a column during a seismic episode. Moreover, shear demand is better controlled by

capacity design procedures, a relatively new principle that still hasn't had the time to become common practice among designers. The standard design procedure considers a global seismic force reduction factor (the q-factor, as previously referred in Chapter 1) that affects equally flexural (ductile behaviour) and shear (brittle behaviour) forces. Consequently, the shear capacity is reached soon after yielding starts, therefore precluding energy dissipation (Varum, 2003).

Structural configuration plays an important role in a building's seismic behaviour. Several authors (e.g., Bento and Azevedo, 2000) have argued that a large number of the structural collapses related, to some extent, to configuration problems or wrong conceptual design. The most serious problem of this type in earthquake engineering are the so-called "soft-storeys", even though it is a well-known structural misconception, frequently addressed in earthquake reconnaissance literature. This is probably because, most of the times, architectural reasons are behind such situations (e.g., absence of infills and larger column height at the ground storey for commercial purposes). These irregular structural systems are highly vulnerable, as the excessive inter-storey drift at a soft-storey level leads to a concentration of damage, thus rapidly compromising structural safety. Moreover, this high level of horizontal deformation potentiates the effects of geometric non-linearity, which might not have been carefully controlled during structural design. Another frequently ignored conceptual problem is the inadequate separation between adjacent structures that might interact when under the effect of an earthquake. Local column damage might occur due to pounding of the roof of a shorter building against the columns of a taller one (Moehle and Mahin, 1991). Examples of this phenomenon have been referenced during the 1985 Mexico earthquake, for instance.

In order to create a stable energy dissipating mechanism, a hierarchic formation of plastic hinges should be enforced by design (Bento and Lopes, 2000). Hence, modern seismic design codes recommend the weak-beam strong-column mechanism to localize damage and control the global and inter-storey drifts. Accordingly, the strength of the columns at any joint must be greater than that of the beams. However, as existing RC framed structures were constructed before the implementation of current design codes, they were designed without having this concept in attention. Furthermore, even today it is sometimes difficult to enforce such code prescriptions due to architectural requirements. Unfortunately, the importance of this prescription has been confirmed by the collapse and / or severe damage of many structures, due to the development of strong beam-weak column mechanisms during recent earthquakes.

Moehle and Mahin (1991) have stated that a properly selected structural system tends to be relatively forgiving towards lapses in structural analysis, detail, and construction. However, extra attention regarding analysis, detail and construction is not likely to significantly improve the performance of a poorly conceived structural system. The satisfaction of architectural requirements is seldom to blame for a designer's option for taking the path of ill structural conception, with severe consequences in terms of a building's seismic vulnerability. Complex structural systems that introduce uncertainties in the analysis and detailing or that rely on non-redundant load paths will lead to unanticipated and potentially undesirable structural behaviour. Simple, regular, and compact building layouts, incorporating a continuous and redundant lateral force resisting system, on the other hand, are a

guarantee of solid structural performance and, as such, should be enforced whenever the seismic hazard is relevant (Varum, 2003).

2.5. NONLINEAR MODELLING OF RC FRAMED STRUCTURES

Even though seismic design is usually done using elastic analysis, it is generally accepted that most building structures will experience significant inelastic deformations when subjected to medium-high intensity earthquakes. Modern performance-based design methods require ways to determine the realistic behaviour of structures under such conditions. Enabled by advancements in computing technologies and available test data, nonlinear analysis provides the means for calculating structural response beyond the elastic range, including strength and stiffness deterioration associated with inelastic material behaviour and large displacements. As such, it can play an important role in the design and assessment of new and existing buildings (Deierlein *et al*, 2010).

The constant progress of computational tools over the years has allowed for the gradual evolution of nonlinear modelling, putting a wide range of alternatives at the designer's disposal. However, each alternative poses different difficulties, related not only with performing nonlinear analyses but also with their dependency on both the chosen nonlinear structural models and the adopted computer programs. The work of Bianchi *et al* (2011), for instance, demonstrated modern software packages to be able to accurately reproduce experimental seismic tests, carried out on a simple bridge column, by means of numerical dynamic analyses. However, the results also revealed a high dispersion, sometimes obtained with the same software package. These deviations demonstrate the above-referred difficulties as well as the impact that different modelling decisions can produce in the overall results (Sousa *et al*, 2011).

Several authors (e.g., Kunnath and Erduran, 2008; Sousa *et al*, 2011) have recognized that the seismic response of a structure, obtained through numerical simulation, is highly dependent on the applied computational tools, calculation assumptions and introduced approximations in the modelling process. Today it is thus still important to run several sensitivity analyses that help determine the relative importance of each modelling option in the computed response, therefore assessing the robustness of the obtained results. In the future, the improved understanding of material behaviour, the growing performance of the existing element models and the increasing development of computational methods may turn nonlinear analysis into a generalized tool. However, for the time being, it is recommended that only experienced designers use these procedures, assuming they are aware of the associated difficulties and keep a critical stance towards the results of the analyses (Carvalho *et al*, 2013).

The following sub-sections review the work of several authors (e.g., Calabrese *et al*, 2010; Carvalho *et al*, 2013; Galanis and Moehle, 2015) on some modelling issues, which have proved to be crucial in the seismic assessment of existing RC structures. The nonlinear models for frame elements, their cross-section discretization and the applicable finite element formulations are addressed, as well as the available (most representative) material models for the behaviour of concrete and steel under cyclic loading (e.g., Menegotto and Pinto, 1973; Mander *et al*, 1988).

2.5.1. Models for beam-column elements

Nonlinear models for frame structures can be divided in two categories (Figure 2.7): (i) distributed plasticity models, where the inelastic behaviour of the whole element is modelled to automatically compute the spread of plasticity along its length and (ii) concentrated plasticity models, where the inelastic behaviour is lumped at the critical sections (sections that are subjected to multiple excursions into the inelastic range, often followed by their gradual mechanical degradation caused by the cycles of loading and unloading), corrected by a fixed parameter that assumes an ideal plasticity distribution (Carvalho *et al*, 2013).

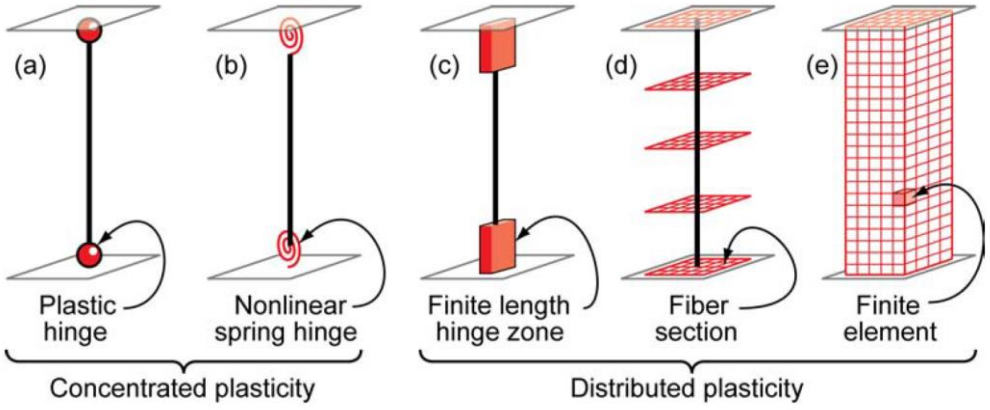

Figure 2.7 – Idealized models of beam-column elements (Deierlein *et al*, 2010)

Even though concentrated plasticity formulations have been used in earthquake engineering applications since the 1960's, distributed plasticity elements are becoming widely employed in standard professional practice. Their advantages in relation to the simpler concentrated plasticity models, as well as a description of their historical evolution and discussion of existing limitations, can be found in the work of Fragiadakis and Papadrakakis (2008). In particular, distributed plasticity elements do not require calibration of empirical response parameters against the response of an actual or ideal frame element under idealized loading conditions, in opposition to concentrated plasticity models. This is an important advantage for designers with less modelling experience because all that is required is to introduce the geometrical and material characteristics of structural members, i.e., standard engineering parameters. The definition of nonlinear zones, lengths, and the estimation of characteristics for the moment-curvature diagrams at the critical sections (considering the axial force and the time degradation) on concentrated plasticity models require from the analyst a high level of knowledge and expertise (Sousa *et al*, 2011).

The flexural behaviour of a beam-column element's cross-sections is usually modelled according to two possible approaches: (i) the definition of hysteretic rules, which are calibrated to assess element stiffness, ductility, and energy dissipation (Stojadinovic and Thewalt, 1996) or (ii) a fibre model, where a uniaxial model of each fibre material is directly computed (Taucer *et al*, 1991). However, while in the

former the two directions of bending must be considered separately and no axial force interaction is considered during the analysis (the average axial force due to gravity loads is computed), the latter approach does not have such limitations. Fibre modelling consists of a discretization of the element's cross-section into a finite number of axial springs (fibres) acting in parallel, by considering the Euler-Bernoulli beam theory (Carvalho *et al*, 2013). Each fibre follows a material uniaxial inelastic behaviour (Figures 2.8 and 2.9) and the section stiffness is computed based on the tangent stiffness of each fibre material, on its area of influence and on its coordinates within the cross-section. In a distributed plasticity model, a finite number of cross-sections is usually computed throughout the element to more accurately consider the spreading of inelasticity along its length. The sectional stress-strain state is then obtained through the integration of the nonlinear uniaxial stress-strain response of the individual fibres in which the section has been subdivided.

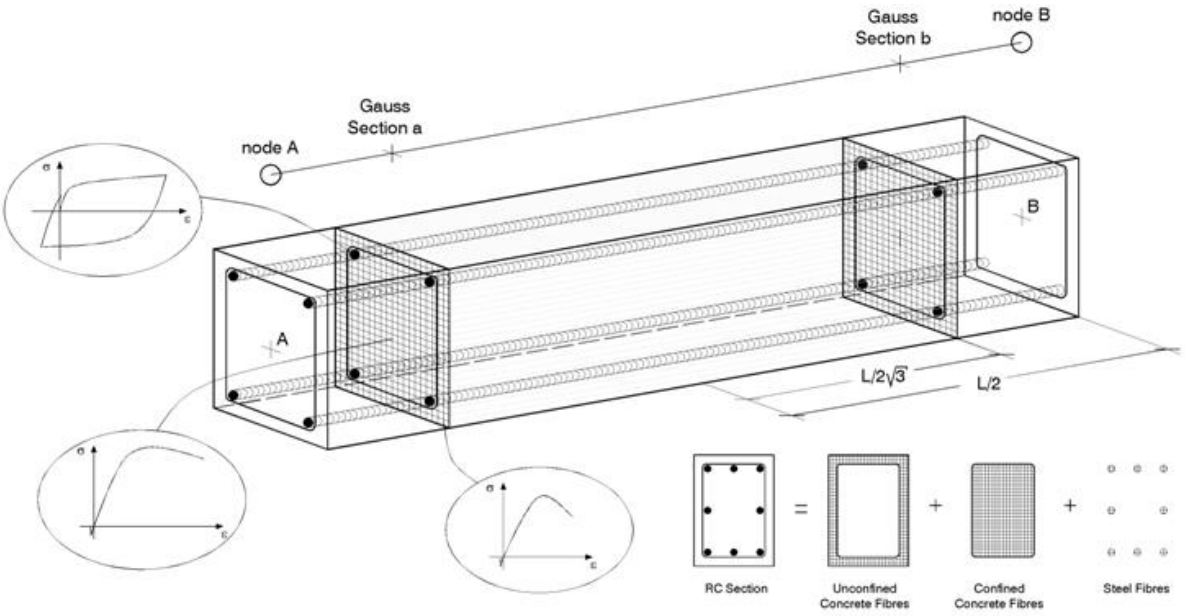

Figure 2.8 – Discretization of a typical RC cross-section (Seismosoft, 2018)

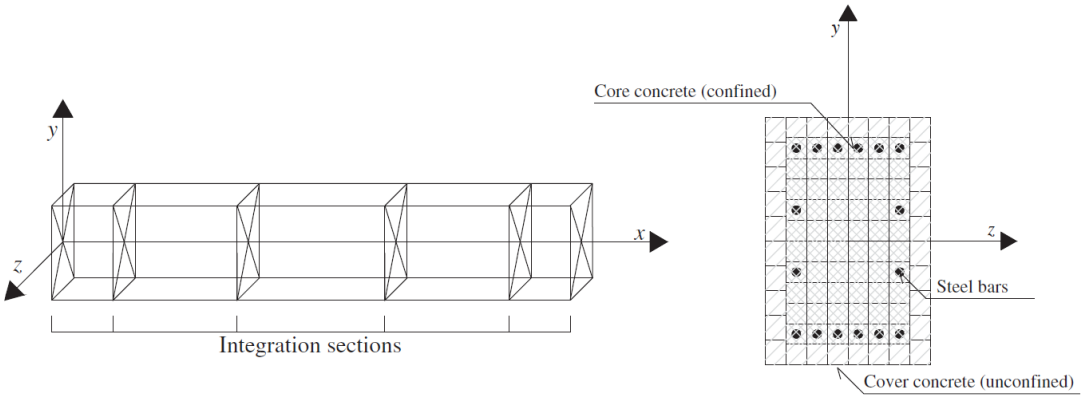

Figure 2.9 – Example of controlling sections along the element and section fibre discretization (Calabrese *et al*, 2010)

Fibre modelling has inarguable assets (Calabrese *et al*, 2010): no requirement of a prior moment-curvature analysis of members; no need to introduce any element hysteretic response (as it is implicitly defined by the material constitutive models); direct modelling of axial load-bending moment interaction (both on strength and stiffness); straightforward representation of biaxial loading; interaction between flexural strength in orthogonal directions. However, even though distributed plasticity formulations model stress and strain variations in more detail (through the section and along the member), important local behaviours such as strength degradation due to local buckling of rebars or the nonlinear interaction between bending and shear are difficult to capture without very sophisticated and numerically intensive models. Concentrated plasticity formulations, on the other hand, may be better suited to capture the nonlinear degrading response of members through calibration using member test data on phenomenological moment-rotation and hysteresis curves (Deierlein *et al*, 2010). When selecting a nonlinear model, it is thus important to understand: (i) the expected behaviour; (ii) the assumptions and (iii) the approximations introduced by each model type. To analyse small test examples using different models and software platforms is also helpful to evaluate specific behavioural effects and, as such, gain knowledge and confidence to carry out more complex analyses.

Field evidence of the behaviour during earthquakes of existing non-ductile RC buildings, as well as experimental tests, demonstrate that such structures experience shear failure, failure at beam-column joints and phenomena such as slippage of rebars (especially when plain steel is used) and strain penetration (SP) (O'Reilly and Sullivan, 2017). Therefore, hypotheses like the nonlinear structural response not being affected by shear failures (a requirement of modern capacity design standards) are rather optimistic for such cases. Appropriate models that consider the mentioned phenomena should thus be used, explicitly considering two sources of nonlinearity in the analyses: (i) inelastic flexure and (ii) inelastic shear and shear-induced axial failure (Galanis and Moehle, 2015). Unfortunately, shear models are currently under development and their applicability to complex systems is still far from being straightforward because current software packages do not provide for a smooth transition between these two failure modes. To consider phenomena like SP and slippage of rebars with acceptable accuracy can also be difficult, depending on the adopted modelling options, but to disregard them might not be acceptable at all.

Slippage of rebars causes rigid body rotations that can significantly increase the flexibility of RC columns (Figure 2.10). According to Sritharan *et al* (2000) and Sezen and Moehle (2004), the total lateral displacement of RC members built with ribbed rebars can be increased up to 40% due to SP effects. In the case of older-type RC structures built with plain rebars, the consideration of these effects can become even more critical – experimental tests conducted on both RC columns (Verderame *et al,* 2008) and beam-column joints (Melo *et al,* 2011) revealed that this mechanism may contribute to nearly 90% of the overall member deformation at failure. Because the explicit simulation of the interface between the rebars and the surrounding concrete is not a straightforward task when considering beam-column elements featuring lumped or distributed plasticity, the inclusion of bond-slip effects in such models has been essentially achieved through the employment of simplified formulations based on empirical relations – for a detailed review of the reference numerical models (explicit and implicit) that do take SP effects into account, readers are referred to the work of Sousa

(2015). However, some important limitations were identified by Sousa (2015) when evaluating the impact of those simplified modelling approaches on the finite element simulation results and, consequently, on the prediction of engineering demand parameters (EDP's).

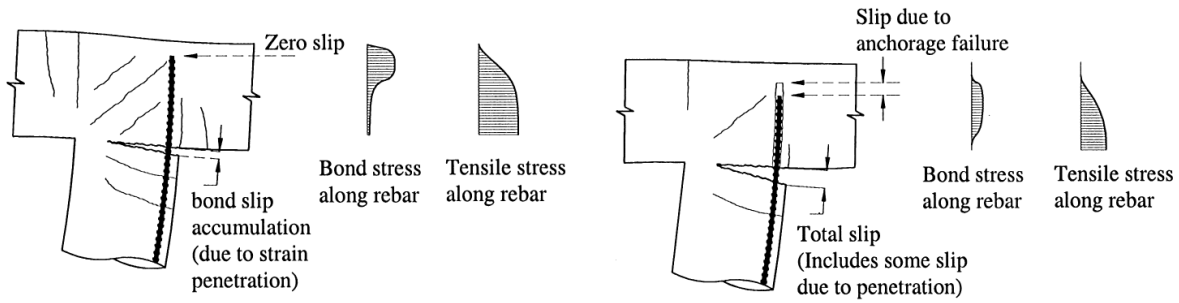

Figure 2.10 – Behaviour of anchorage regions with adequate (left) and limited (right) embedment length (adapted from Sritharan *et al*, 2000)

With the purpose of overcoming the foregoing limitations (without employing advanced bond-slip models within detailed 3D finite element formulations – an approach which is computationally too heavy for most practical seismic analysis of RC framed structures), Sousa *et al* (2017a) proposed a novel bond-slip model for RC structures that simulates the member-end deformations associated with SP effects. The model, which in its final form is implemented as a "zero-length" element, was developed to be compatible with any general fibre-based frame analysis software. A schematic representation of the model's components is shown in Figure 2.11. In summary, the element response is determined from cross-sectional fibre integration, where at each rebar the anchorage mechanism is explicitly modelled through a series of virtual integration points (IP's) distributed along the anchorage length. The analysis is carried out by an algorithm that enforces both equilibrium and compatibility at every IP, making use of a state-of-the-art bond stress-slip cyclic constitutive relation applicable to a wide variety of anchorage conditions. Therefore, features such as the expected failure mode (pull-out or splitting) or parameters such as the concrete strength, embedment length, cyclic degradation, amplitude of steel strains, rebar type (plain or ribbed), transverse pressure, level of confinement and bond conditions can be explicitly modelled (Sousa, 2015). The developed link element was implemented by Sousa (2015) in the well-known software platform *SeismoStruct* (Seismosoft, 2018) and its performance was assessed against several experimental tests, showing encouraging numerical stability and accuracy while retaining appreciable computational efficiency.

More recently, Caruso *et al* (2018) provided indications regarding the use of a simplified bond-slip model when analysing SP effects in old RC walls built with plain rebars. Three wall specimens were numerically modelled using software platform *OpenSees* (McKenna *et al,* 2000), considering a distributed plasticity model with fibre discretization. SP effects were firstly determined considering the bond-slip model proposed by Sousa *et al* (2017a). Afterwards, the obtained results served as basis for a calibration procedure carried out to establish reference reduction values for the reinforcing steel's Young's modulus and maximum stress. This type of approach, involving the modification of the

reinforcing steel's constitutive law, has been proposed in the past by Varum (2003) and Fernandes *et al* (2007), but at the time lacked clear application guidance and calibration to adjust the required parameters to different element typologies and anchorage conditions. The results obtained by Caruso *et al* (2018) now allow for the definition of indicative values that can be used to reduce the rebars' Young's modulus and maximum strength, in order to account for SP effects implicitly in numerical analyses in a very expedite manner. For a full description of this study's scope, limitations and results, readers are referred to the full research paper.

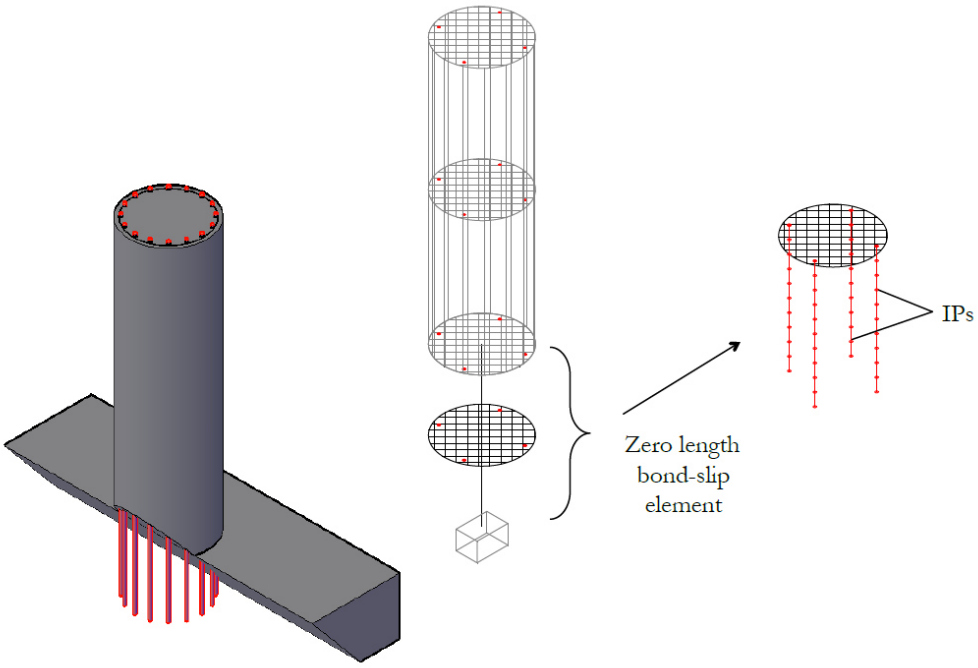

Figure 2.11 – Schematic representation of the different components of the bond-slip model proposed by Sousa *et al* (2017a) (Sousa *et al*, 2017a)

Concerning the nonlinear modelling of shear effects, it remains a significant challenge, typically handled by neglecting them altogether (Guner and Vecchio, 2011). However, as previously referred, many existing buildings in Europe possess column members that are prone to shear failure. One of the most infamous cases in RC framed structures during past seismic events occurred at the "San Salvatore Hospital" in L'Aquila, Italy. The shear failure of three columns along with the out-of-plane failure of masonry infills resulted in the evacuation of the hospital, which would have been otherwise critical in providing medical aid following the earthquake (O'Reilly and Sullivan, 2017). The incorporation of shear response is thus an important aspect of modelling non-ductile columns, as significant strength and stiffness degradation may follow flexural yielding. Despite this, currently used in practice software platforms (e.g., *SAP2000* (CSI, 2016)) typically neglect these mechanisms by default. The parameters required to model shear response are indeed challenging and usually approximated by empirical equations that are limited to the database on which they have been based, but not to consider it can

lead designers to grossly inaccurate and unsafe seismic performance assessment of older-type RC buildings. The development and implementation of analytical models which can simulate the cyclic behaviour of non-ductile RC columns, while remaining computationally efficient for large-scale applications, is consequently a topic of very active research. Several proposals have been published in the past recent years, as well as some comparative studies pointing out advantages and shortcomings between approaches. However, at this stage, there is still no consensus on which of the available models is the most efficient (Amirsardari, 2018).

Elwood (2004) proposed a model that represented (at the time) a key advancement in uniaxial material models defining shear response. Unlike prior models which were only capable of capturing failure if the column's shear strength was less than its flexural strength (Figure 2.12), this model is also capable of detecting failure due to the exceedance of the column's shear drift capacity (defined at a displacement on which the column's shear strength decreases by 20%). Hence, it made possible to capture shear failures which occur after flexural yielding as a result of the column's shear capacity decreasing with the increase of inelastic deformations (Figure 2.13). Flexural response is simulated using fibre section elements while an elastic spring element is used for shear response. Once the shear strength or deformation capacity is exceeded, the lateral strength of the shear spring is enforced to decrease (in-cycle strength deterioration) to simulate the shear failure mechanism (i.e., the shear spring backbone curve is redefined to include a user-defined degrading shear slope and a residual force). This model is implemented in software platform *OpenSees* and is known as the *Limit State Material* model. It does, however, have some limitations: Elwood (2004) explains that convergence issues may occur if the beam-column element experiences flexural degradation prior to shear failure, on account of multiple solutions being possible.

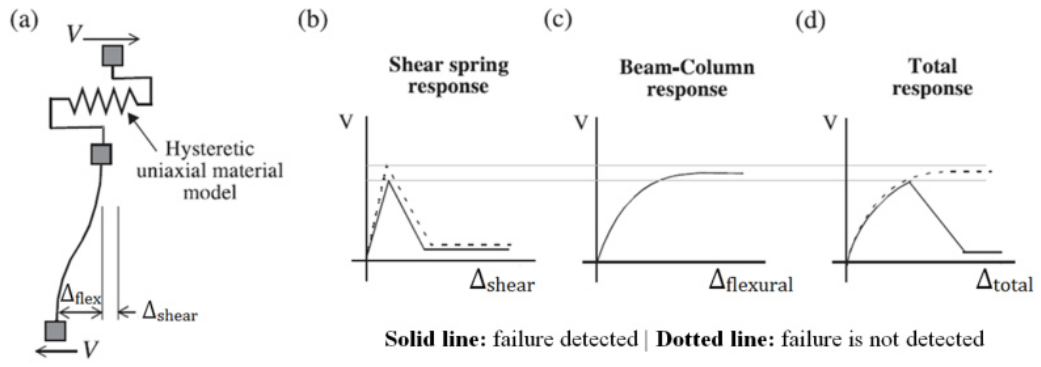

Figure 2.12 – Material model capturing shear failure when the column's shear strength is less than its flexural strength (adapted from Elwood, 2004)

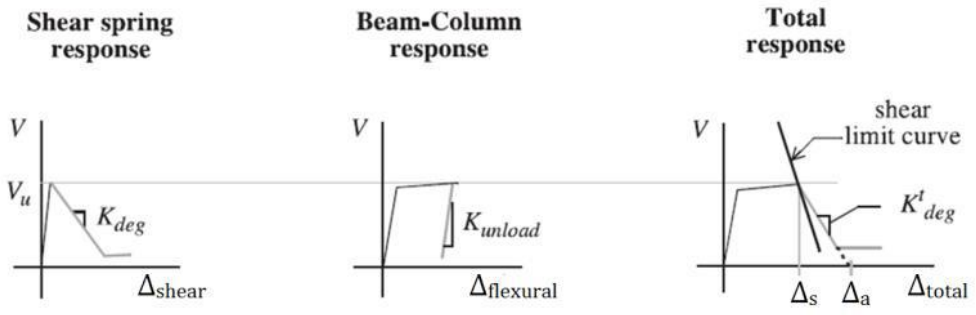

Figure 2.13 – Material model capturing shear failure due to the exceedance of the column's shear drift capacity (adapted from Elwood, 2004)

LeBorgne (2012) took up the work conducted by Elwood (2004) and proposed a new uniaxial material model that overcame some of the limitations of the *Limit State Material* model. An alternative rotation-based shear spring element was proposed based on shaking table tests of non-ductile RC columns (Ghannoum and Moehle, 2012a, 2012b) – the obtained results showed that shear failure occurred when the maximum inelastic rotation reached a critical value, indicating that shear failure could be more accurately represented by using rotational-based shear spring elements than by using lateral drift-based shear spring elements. Additional fibre section elements were added to the model in the plastic hinge regions (plastic hinge length D_c assumed to be equal to the column's cross-section depth) to prevent strain localization issues (see next sub-section), along with fibre section-based zero-length elements to simulate bond-slip response. Pinching and cyclic strength deterioration were also incorporated in the model. The member configuration as presented in LeBorgne (2012) is illustrated in Figure 2.14, as well as the nonlinear material model governing the behaviour of the shear spring element. This model is also implemented in software platform *OpenSees,* under the designation *Pinching Limit State Material*.

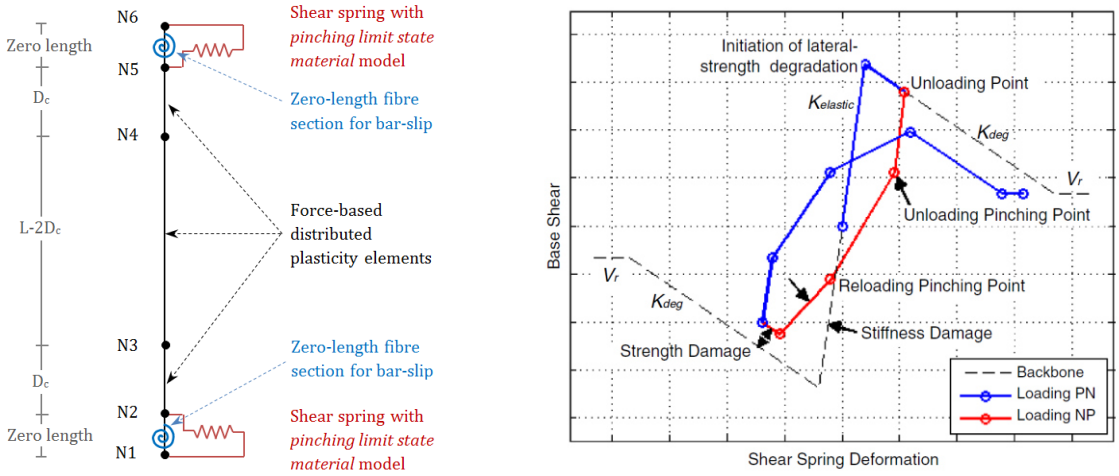

Figure 2.14 – Analytical representation of the beam-column member (left) and nonlinear material model governing the behaviour of the shear spring element (right) (adapted from LeBorgne, 2012)

To effectively estimate the parameters required to define lateral deformation limits and hence the shear spring response, several authors (e.g., Elwood and Moehle, 2003; LeBorgne, 2012; LeBorgne and Ghannoum, 2014; Wibowo *et al,* 2014; Wilson *et al,* 2015) have proposed empirical equations based on different databases of experimental test results obtained with flexure-shear and shear governed columns. A review of these models can be found in the work of Amirsardari (2018), as well as a comparison between the results provided by each. The definition of the critical points of the backbone curve varies between models, but the most typical are represented in Figure 2.15. Deformation at shear failure Δ_s is defined in Elwood and Moehle (2003), Wibowo *et al* (2014) and Wilson *et al* (2015) as the displacement at which the shear resistance drops below 80% of the maximum recorded shear force – this is the conventional method of defining lateral strength failure. On the other hand, in LeBorgne (2012) and LeBorgne and Ghannoum (2014) the deformation limit at shear failure is based on the total rotation limit θ_f allowed in the plastic hinge region and it corresponds to the deformation at which the maximum shear force was recorded (Δ_u). The deformation limit at axial failure Δ_a is defined in Elwood and Moehle (2003) as the displacement at which load failure was observed in the experiment – this approximately corresponds to the displacement at which the shear resistance dropped to zero. LeBorgne (2012) and LeBorgne and Ghannoum (2014) do not provide this deformation limit directly – rather, the shear displacement Δ_r corresponding to the difference between the displacements at which ultimate shear force and residual lateral strength were observed in the experiment is provided. Lastly, Wibowo *et al* (2014) and Wilson *et al* (2015) define the deformation limit at axial failure as the displacement at which the shear resistance drops below 50% of the maximum applied shear force ($\Delta_{a\ 50\%}$).

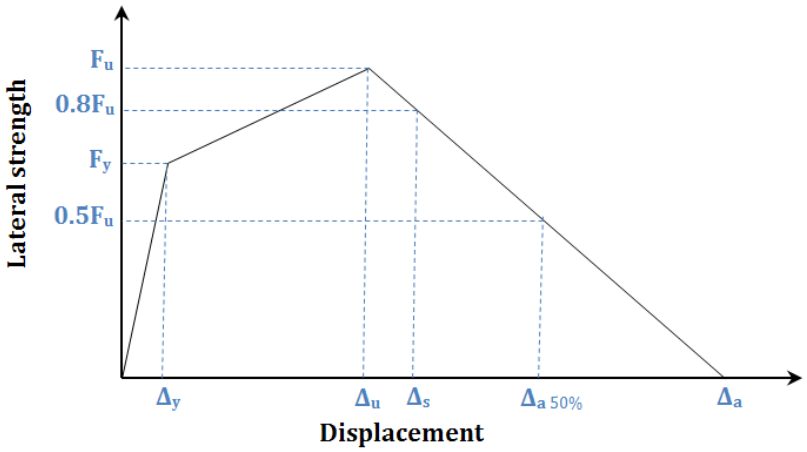

Figure 2.15 – Definition of critical points for the lateral strength-displacement response of non-ductile columns (adapted from Amirsardari, 2018)

Shoraka and Elwood (2013) proposed improvements to the work of Elwood (2004) using the concepts introduced in the ASFI method (a displacement-based analysis method proposed by Mostafaei *et al* (2009) to predict the point of shear failure while approximately accounting for axial-shear-flexural

interaction in the column response). The proposed model is based on physical mechanics rather than empirical relations and deemed to be capable of representing with acceptable accuracy the flexural, shear and bar-slip response in columns baring different failure modes. The onset of shear failure is defined as the state when large diagonal shear cracks develop and the column response reaches peak shear resistance, immediately followed by a state where increasing drifts are associated with strength degradation (a definition slightly different from that used by Elwood (2004)). To simulate the pre-peak shear behaviour, a simplified piece-wise linear model representing the nonlinear response from the Modified Compression Field Theory (Vecchio, 1990) is used. To predict the point of shear failure, the ASFI method is modified to monitor local shear deformations across the plastic hinge region of the column. Finally, a shear-friction model is used to represent the degrading slope of the lateral force-deformation response after shear failure. For details on the implementation and validation of this macro-model, the interested reader is referred to the original research paper.

The scientific work referred and summarized in this sub-section is a valuable source of information for researchers and practitioners that need to select a nonlinear model for performance-based earthquake engineering. However, several comparative studies have also been published recently and can serve as further reference for that purpose. For instance: Galanis *et al* (2016) performed shaking table tests on 12 frames with ductile and non-ductile RC columns, ran computer simulations using two different analytical models representing inelastic flexural and shear behaviours, and evaluated their accuracy based on the previously obtained experimental results; O'Reilly and Sullivan (2017) discussed modelling techniques which account for the strength and stiffness degradation of non-ductile RC members, and highlighted the benefits of using such techniques instead of the more traditional approaches; Salgado and Guner (2018) evaluated the performance of three numerical models with varying computational demand levels, used experimental results to assess the accuracy of the calculated responses, presented an overview of the performance-based modelling processes, and analysed the critical points for minimizing the computational demand without losing calculation accuracy.

2.5.2. Finite element formulations for distributed plasticity models

Two different finite element (FE) formulations can be used to implement distributed inelasticity frame elements: the classical displacement-based (DB) formulation (e.g., Hellesland and Scordelis, 1981; Mari and Scordelis, 1984) and the more recent force-based (FB) formulation (e.g., Spacone *et al*, 1996; Neuenhofer and Filippou, 1997). The DB formulation is based on the element stiffness – the displacement field is imposed using shape functions corresponding, for instance, to a linear variation of curvature along the element and forces on elements are then found by energy considerations. On the other hand, the FB formulation is built on the element's flexibility – the force field is imposed through a linear moment variation within each element and displacements are then obtained by work equivalence balance.

If linear elastic material behaviour is considered, these two approaches (obviously) produce the same results, provided that only nodal forces act on the element. However, in case of material inelasticity, imposing a displacement field (DB formulation) does not allow to capture the real deformed shape

because the curvature field will typically be highly nonlinear. Each structural member (beam or column) must then be discretized, for the computation of nodal forces / displacements, so that the assumption of a linear curvature field inside each sub-domain becomes acceptable (typically four to five elements per structural member will suffice). The FB formulation, on the other hand, is always exact because it does not depend on the assumed sectional constitutive behaviour. Each structural member can thus be modelled with a single element, allowing a one-to-one correspondence between both. The element's displacement field is not restrained in any way and the discrete number of control sections that is considered along the element for numerical integration introduces the only approximation. A minimum number of three integration sections is required to avoid under-integration. However, such an option will generally not simulate the spread of inelasticity in an acceptable way. The suggested minimum number of IP's is then four, although five to seven can typically be used. Concerning the numerical integration scheme, the Gauss-Lobatto quadrature is recommended, as it controls the end sections of the element which are privileged locations for seismic inelastic response (Calabrese *et al*, 2010; Sousa, 2015).

For a hardening type of sectional constitutive behaviour, both FB and DB elements produce an objective response at the global (force-displacement) and local (moment-curvature) levels (i.e., the computed output converges to a unique solution as the level of discretization increases), whereas the results are non-objective in the case of a softening sectional law. This numerical issue, commonly known as *strain localization* (or simply *localization*), was firstly discussed by Zeris and Mahin (1988) for DB elements, while Coleman and Spacone (2001a) studied it for FB elements. Formally, it corresponds to the loss of ellipticity of the governing differential equations, resulting in the loss of uniqueness of the mathematical solution. The initial boundary-value problem thus becomes mathematically ill-posed, and the numerical solution becomes mesh-dependent. This issue can be particularly relevant in the case of RC frame members under strong lateral loading, as an increase in the axial load ratio may induce shift from hardening to softening sectional response. The need for regularization techniques that help maintain post-peak objectivity while producing results that are consistent and of physical value is thus evident.

Regularization techniques were first applied to DB elements (the original formulation of the Finite Element Method) and typically require a user-defined parameter specifying the physical dimension of the region into which curvatures localize (Coleman and Spacone, 2001b; Légeron and Paultre, 2005; Papaioannou *et al,* 2005). In earthquake engineering, the latter corresponds to the expected length of the plastic hinge. To avoid the common confusion with formulas for the *equivalent* plastic hinge length (a fictitious quantity that is in principle only applicable to plastic hinge analysis), some authors (e.g., Almeida *et al,* 2014) have explicitly adopted the term *real* plastic hinge length. The average verification of equilibrium in DB formulations poses various difficulties in the interpretation of the fibre-based element behaviour. In particular, it becomes impossible to predict *a priori* if localization will take place in the most strained IP (Calabrese *et al,* 2010) or simultaneously in both IP's of the element (Almeida *et al,* 2014), which is probably the most common case. Consequently, it is not possible to know in advance, i.e., before running structural analysis, if the appropriate regularization technique should imply setting the length of the element as the expected length of the plastic hinge or rather twice that value (Sousa, 2015).

The first regularization method for FB elements was suggested by Coleman and Spacone (2001a). The proposed technique modified the material stress-strain behaviour to maintain a constant energy release after strain-softening initiates and was originally applied to the Kent and Park concrete model (Kent and Park, 1971). However, due to its time-consuming two-stage application, other proposals followed (e.g., Scott and Fenves, 2006; Addessi and Ciampi, 2007), based on *ad hoc* integration schemes and the observation that, unlike DB approaches, the post-peak accumulation of curvatures in FB elements is bound to happen at the most strained IP. Such proposals, therefore, scale the integration weights at the element's ends to match the value of the expected plastic hinge length. The method developed by Scott and Fenves (2006), for instance, confines material nonlinearity to the element's ends over specified plastic hinge lengths, maintains the correct numerical solution for linear curvature distributions and ensures objective response at the section, element, and structural levels. It is based on a modified Gauss-Radau quadrature, to overcome the difficulties that arise with Gauss-Lobatto integration for strain-softening behaviour. Plastic rotations are hence defined in a consistent manner and directly related to plastic curvature through the specified plastic hinge lengths. This procedure is available in software platform *OpenSees,* under the designation *Beam with Hinges,* and constitutes a straightforward way of incorporating a physically meaningful plastic hinge length in the simulation of the strain-softening response of RC framed structures using FB beam-column elements.

On the downside, the main problem with regularization methods for FB elements is that they may simulate an unrealistically flexible response when (objective) strain-hardening constitutive behaviour occurs (Sousa, 2015). To tackle this issue, a new quadrature rule was advanced by Scott and Hamutçuoglu (2008), which includes two additional IP's at the extremities. More recently, a versatile adaptive integration scheme was proposed by Almeida *et al* (2012), which ensures high numerical accuracy in the pre-peak phase and a regularized response in the post-peak branch. The interested reader is referred to the original research papers for full details on these recent proposals.

2.5.3. Material models for RC members under cyclic loading

The monotonic behaviour of concrete and steel has been observed for a long time, with the associated analytical models focusing mainly on reproducing the adequate stiffness and strength at any strain level, as well as on the effects of different confinement arrangements. However, the development of methodologies for the seismic analysis and design of RC structures (along with adequate details for the reinforcement layout) requires understanding how members behave under cyclic loading. Authors like Kent and Park (1971), Menegotto and Pinto (1973), Scott *et al* (1982), Mander *et al* (1988) or Martinez-Rueda and Elnashai (1997) have thus dedicated attention to the development of reliable steel and concrete models for such loading conditions. Nonetheless, despite the numerous models available in literature, Mander's concrete model (Mander *et al,* 1988) and Menegotto-Pinto's steel model (Menegotto and Pinto, 1973) prevail as two of the most commonly adopted in the nonlinear analysis of RC structures. The effect that the selection of different material models might have on the computed structural response has been addressed in recent studies (e.g., Yazgan and Dazio, 2011b; Blandon, 2012; Sousa, 2015), showing that (in particular) an inadequate choice of the steel model will have significant impact on the computed maximum and residual displacements.

Aside from material characteristics, the seismic behaviour of RC members is also influenced by the joint interaction between steel and concrete. Regions where plastic hinges are expected to develop should be carefully detailed for ductility to ensure that, for instance, moment redistribution can occur. One of the most important design requirements for ductility is the provision of enough transverse reinforcement, as it ensures adequate confinement of the compressed concrete core, avoids buckling of the longitudinal rebars and prevents shear failure (Mander *et al*, 1988). Good confinement of the compressed core is essential to ensure that columns have enough plastic rotation capacity to maintain flexural strength at high curvatures. In general, the higher the axial load, the greater the amount of confining reinforcement to achieve ductile performance, because the depth of the neutral axis increases with the axial load, making the flexural capacity of the column more dependent on the contribution of the concrete compressive stress distribution.

The selection of the appropriate material models and corresponding parameters is hence of the utmost importance for the development of numerical models that can predict the seismic behaviour of RC structures with various arrangements of longitudinal and transverse reinforcement. The uniaxial stress-strain relations for both concrete and the steel affect cross-sectional response at each of the element's integration points and constitute the primary source of material nonlinearity. The following sub-sections summarize the work of some of the above-referred authors on these issues.

2.5.3.1. Steel constitutive laws

Cyclic loading induces changes in the monotonic behaviour of steel. During the first load cycle, the loading branch is identical. After yielding, the unloading branch starts from a straight line with a slope equal to the initial Young modulus, becoming nonlinear before the stress reaches the original yielding limit, with no presence of a yielding plateau. The phenomenon, referred to as the *Bauschinger effect,* depends on the history of displacements applied to the specimen (Guedes, 1997; Appleton, 2013). This nonlinear behaviour repeats itself during the following load cycles, as shown in Figure 2.16.

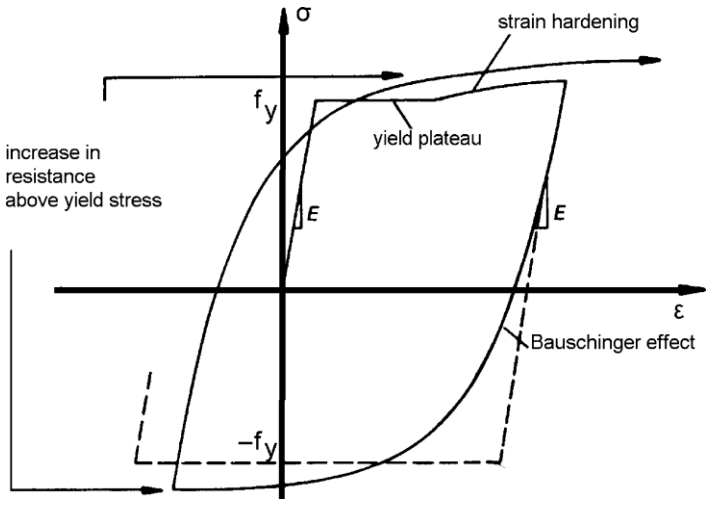

Figure 2.16 – Cyclic stress-strain behaviour of reinforcement steel bars, without buckling effect (Fardis, 2009)

Steel bars exhibit linear elastic behaviour before yielding, therefore no hysteretic effect with energy dissipation occurs. After yielding, response curves obtained from experimental cyclic tests show a strong hysteretic effect with significant energy dissipation. However, this type of hysteretic behaviour is only possible if steel bars do not experience buckling during the compression stages, otherwise both ductility and the maximum load capacity will be compromised. The buckling of the longitudinal reinforcement bars is, in fact, the main factor for the degradation of the load capacity of RC members under cyclic loading. The presence of adequate amounts of transverse reinforcement is critical to prevent this from happening, as stated before.

Concerning the deformation capacity of RC members, two characteristics of steel bars stand out as the most influent: (i) the ultimate strain ε_{su} and (ii) the ratio between the ultimate stress and the yielding stress f_u/f_y (Appleton, 2013). The ultimate strain ε_{su} may determine, in some situations, the maximum curvature ϕ_u that a cross-section can develop and, consequently, the curvature ductility factor $\mu_\phi = \phi_u/\phi_y$, where ϕ_y is the cross-section's yielding curvature (Figure 2.17). The f_u/f_y ratio represents the steel's strain hardening and influences the length l_p of the plastic hinge at the member's end (Figure 2.18). The larger this length is, the higher the rotation θ_u of the plastic hinge will be and, consequently, the higher the member's rotational ductility factor $\mu_\theta = \theta_u/\theta_y$ will become. Some design standards (e.g., EC2-1-1, 2004) impose lower limits for the characteristic value ε_{uk} of ε_{su}, as well as boundaries for the characteristic value f_{uk}/f_{yk} of the f_u/f_y ratio. The lower boundary assures that ductile RC members have adequate deformation capacity while the upper boundary controls the maximum bending moments that may develop on plastic hinges. Additionally, an upper limit for the maximum value of the steel's yielding stress is also imposed: $f_{yk\,0.95} \leq 1.25 \cdot f_{yk}$, where f_{yk} is the steel's characteristic yielding stress.

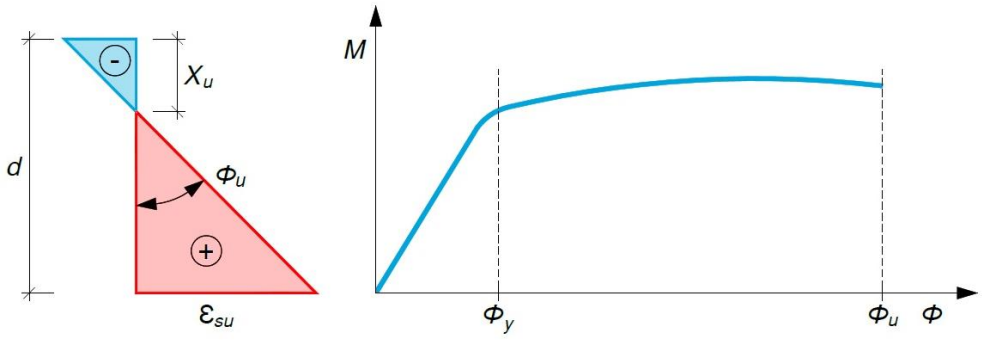

$$\phi_u = \frac{\varepsilon_{su}}{d - x_u} \qquad \mu_\phi = \frac{\phi_u}{\phi_y}$$

Figure 2.17 – Maximum curvature and curvature ductility factor (adapted from Appleton, 2013)

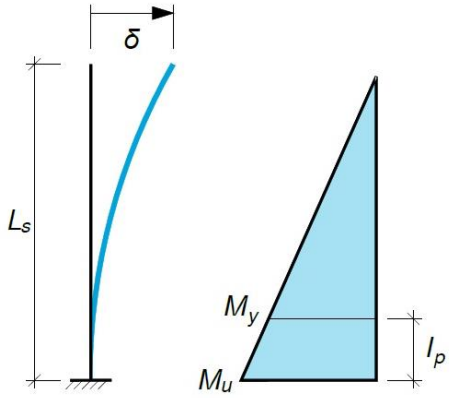

$$l_p = L_s \cdot \left(1 - \frac{M_y}{M_u}\right) = L_s \cdot \left(1 - \frac{f_y}{f_u}\right)$$

Figure 2.18 – Plastic hinge length (adapted from Appleton, 2013)

The Ramberg-Osgood relations (1943) used by Kent and Park (1973) and the Menegotto and Pinto (1973) model are two examples of nonlinear modelling of the cyclic behaviour of steel that automatically consider the characteristic softening of the curves in the reloading branches, as described above. The Menegotto and Pinto (1973) model (Figure 2.19) supports an algebraic explicit stress-strain law, based on experimental tests on bars under cyclic loading and has been included in several studies for its simplicity and efficiency (Varum, 2003). The Bauschinger effect is accounted for through two parameters ($A1$ and $A2$) that adjust the shape of the transition curves. It was initially programmed by Yassin (1994), coupled with the isotropic hardening rules proposed by Filippou *et al* (1983). It is particularly recommended for the modelling of RC structures under complex loading histories, where significant load reversals might occur. Although it was initially developed with ribbed rebars in mind, with the correct calibration it can also be employed for the modelling of smooth rebars, as often found in existing RC structures (Prota *et al*, 2009). More information and full details about its explicit formulation can be found in Guedes (1997).

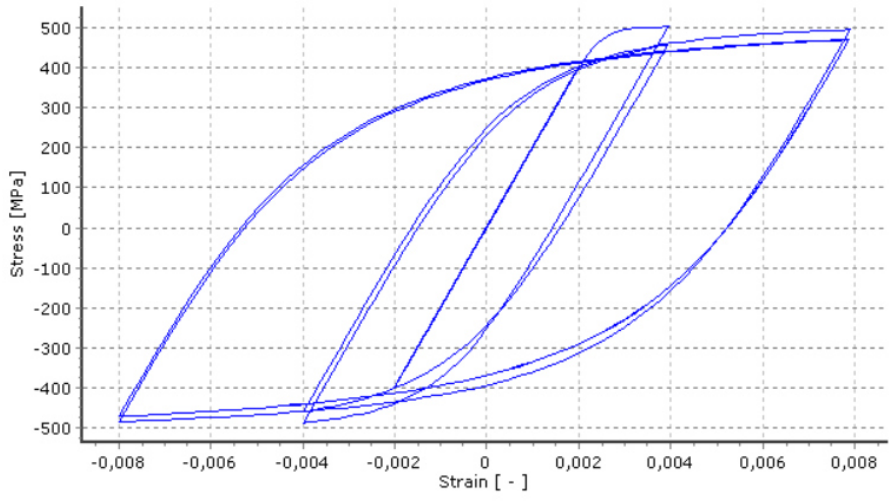

Figure 2.19 – Menegotto-Pinto (1973) steel model (Seismosoft, 2018)

Several nonlinear analysis software platforms focused on earthquake engineering problems (e.g., *SeismoStruct*) have implemented the Menegotto-Pinto (1973) steel model in their codes. The definition of the following model-calibrating parameters is required for the mechanical behaviour of steel to be fully described:

- Modulus of elasticity (initial elastic stiffness) E_s
- Yield stress f_y
- Strain hardening parameter μ
- Transition curve initial shape parameter R_0
- Transition curve shape calibrating coefficients $A1$ and $A2$
- Isotropic hardening calibrating coefficients $A3$ and $A4$
- Fracture/ buckling strain
- Steel specific weight γ_s (7850 *kg/m*^{3})

The strain hardening parameter μ represents the ratio between the post-yield stiffness E_{sp} and the initial elastic stiffness E_s of steel. The former is defined as $E_{sp} = \left[\left(f_u - f_y\right)/\left(\varepsilon_u - f_y/E_s\right)\right]$, where f_u and ε_u represent the ultimate stress and strain capacity of steel, respectively. The transition curve initial shape parameter R_0 is the initial (first loading cycle) value of the parameter R, that controls the shape of the transition curve between initial and post-yield stiffness. This is necessary to accurately represent Bauschinger effects and pinching of the hysteretic loops. The transition curve shape calibrating coefficients $A1$ and $A2$ are used to calibrate the changes that must be applied to parameter R_0 in order to obtain the updated transition curve shape parameter R_n. The isotropic hardening calibrating coefficients $A3$ and $A4$ are used to define the degree to which isotropic hardening is introduced in the stress-strain cyclic response characteristics of steel. Finally, the fracture/ buckling strain is the strain at which fracture or buckling of rebars in RC sections occurs. This value should be set with care, even using an infinitely large value when no fracture / buckling modelling is desired.

Regarding the other steel models available in the literature, reference should be made to the simple bilinear uniaxial rebar model and to the Monti-Nuti (1992) steel model. The former neglects the Bauschinger effect, hence overestimating the energy dissipation and its abrupt pre-to-post yield stiffness change often proves to be numerically more challenging for the analyses than when the Menegotto-Pinto (1973) model is employed (Sousa, 2015). The latter uses the Menegotto-Pinto (1973) stress-strain relation coupled with the buckling rules proposed by Monti and Nuti (1992). It accounts for the longitudinal rebars slenderness ratio (s/d_b) in their response when undergoing large inelastic deformations (s is the specified tie spacing and d_b is the longitudinal rebar diameter). Furthermore, to overcome stability issues associated with small strain reversals, the updated model incorporates the improvements introduced by Fragiadakis *et al* (2008). This study, along with others (e.g., Bae *et al,* 2005; Cosenza and Prota, 2006) indicate that buckling in longitudinal rebars is mainly dependent on the slenderness of the rebars, the stiffness and the rigidity of the hoops, the strain hardening of steel and is favoured for slenderness ratios greater than around 5.

2.5.3.2. Concrete constitutive laws

The parameter that most affects the maximum concrete strength and corresponding strain is the confining reinforcement. Figure 2.20 illustrates the schematic axial stress vs. strain response curve of a concrete specimen under increasing axial deformation. In compression, a parabolic curve is assumed from the initial unloaded stage up to the peak stress value, with initial tangent modulus equal to the concrete Young modulus. After an almost linear region up to around half the compression strength, micro-cracking induces pronounced nonlinear behaviour with strong degradation of stiffness. A straight line describes the softening branch, and its evolution depends mainly on the concrete's degree of confinement (i.e., on the transverse steel ratio and spacing between transverse steel bars). Under tension, a bilinear curve is adopted. From zero to the maximum tensile strength, the model presents a linear elastic behaviour with slope equal to the initial compression Young modulus. The second branch, also described by a straight line, expresses the post-peak softening behaviour accounting for tension stiffening effects (i.e., the ability of intact concrete between adjacent cracks to carry out tensile stresses) (Guedes, 1997; Varum, 2003).

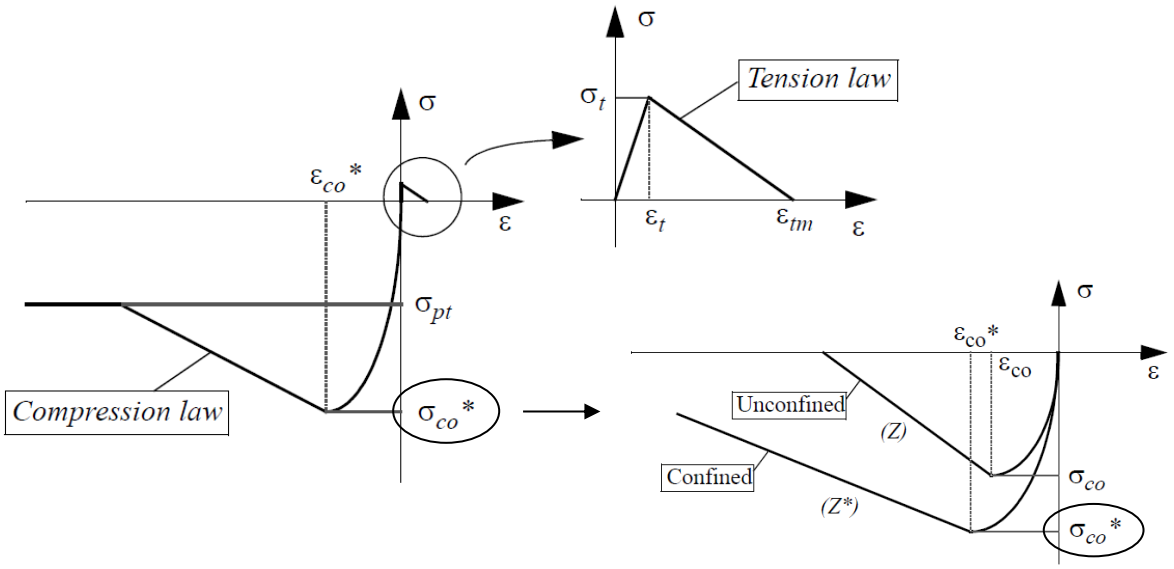

Figure 2.20 – Concrete response curves for monotonic loading and confinement effect (adapted from Guedes, 1997)

The schematic behaviour of concrete under compressive cyclic loading is represented in Figure 2.21, together with the envelope curve. Experimental results show that the latter can be considered unique and identical to the monotonic loading curve (Castellani *et al*, 1993). Unloading reflects the stiffness degradation due to concrete damage and the reloading curve, from zero or tensile stresses, tends to the envelope showing some strength degradation. The energy dissipated by the material (i.e., the area enclosed by unloading-reloading hysteresis loops) is small when compared to that of steel under cyclic loading. The intersection point between the unloading and the reloading curves defines the common points line: stresses above this line produce additional plastic strains while internal cycles below this line correspond to stable loops (Guedes, 1997).

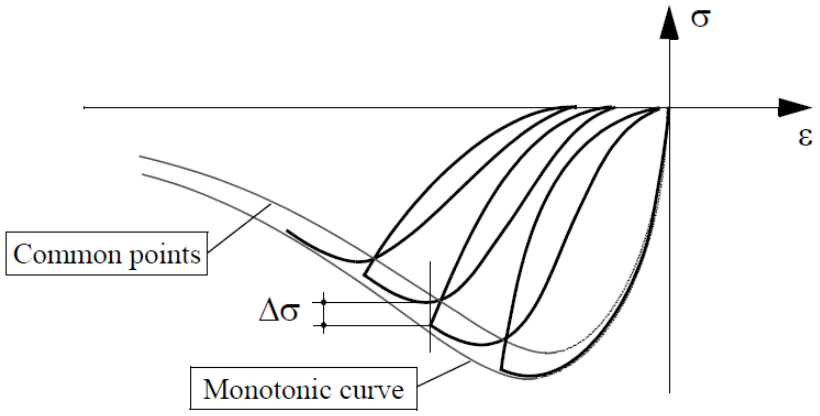

Figure 2.21 – Concrete response under compressive cyclic loading (Guedes, 1997)

Due to the progressive concrete's stiffness and strength degradation, the ductility of RC members becomes compromised. For instance, Figure 2.22 shows the failure of a RC column during the 1994 Northridge earthquake, due to lack of ductility in the plastic hinge region. The concrete's deformation capacity was insufficient to withstand the deformation imposed by the earthquake, which led to the crushing of the concrete core. (Appleton, 2013). If good confinement of the compressed concrete core is provided, significant increase in both strength and ductility can be achieved, as stated before. Figure 2.20 (above) shows that the post-peak confined curve presents not only a lower strength-decreasing ratio but also residual strength for important strains (Guedes, 1997). According to Park and Paulay (1975), this is due to the coupling between the confinement effect provided by the transverse reinforcement and the interlocking effect of the aggregates. The results of a series of compression loading tests on RC specimens described by Hoshikuma *et al* (1995) illustrate all these phenomena quite well.

Figure 2.22 – Failure of a RC column due to lack of ductility (Appleton, 2013)

The confinement effect provided by the transverse reinforcement is associated to the restriction of the lateral expansion of the concrete specimen when subjected to axial compression stresses (Poisson's effect). The effectively confined concrete corresponds to the region located inside the transverse reinforcement bars. The cover concrete is unconfined and will eventually become ineffective and spall after the compressive strength is attained (Figure 2.23). Analytical formulae and detailed description of confined concrete behaviour models can be found in EC2-1-1 (2004), Model Code 2010 (fib, 2013) and Appleton (2013).

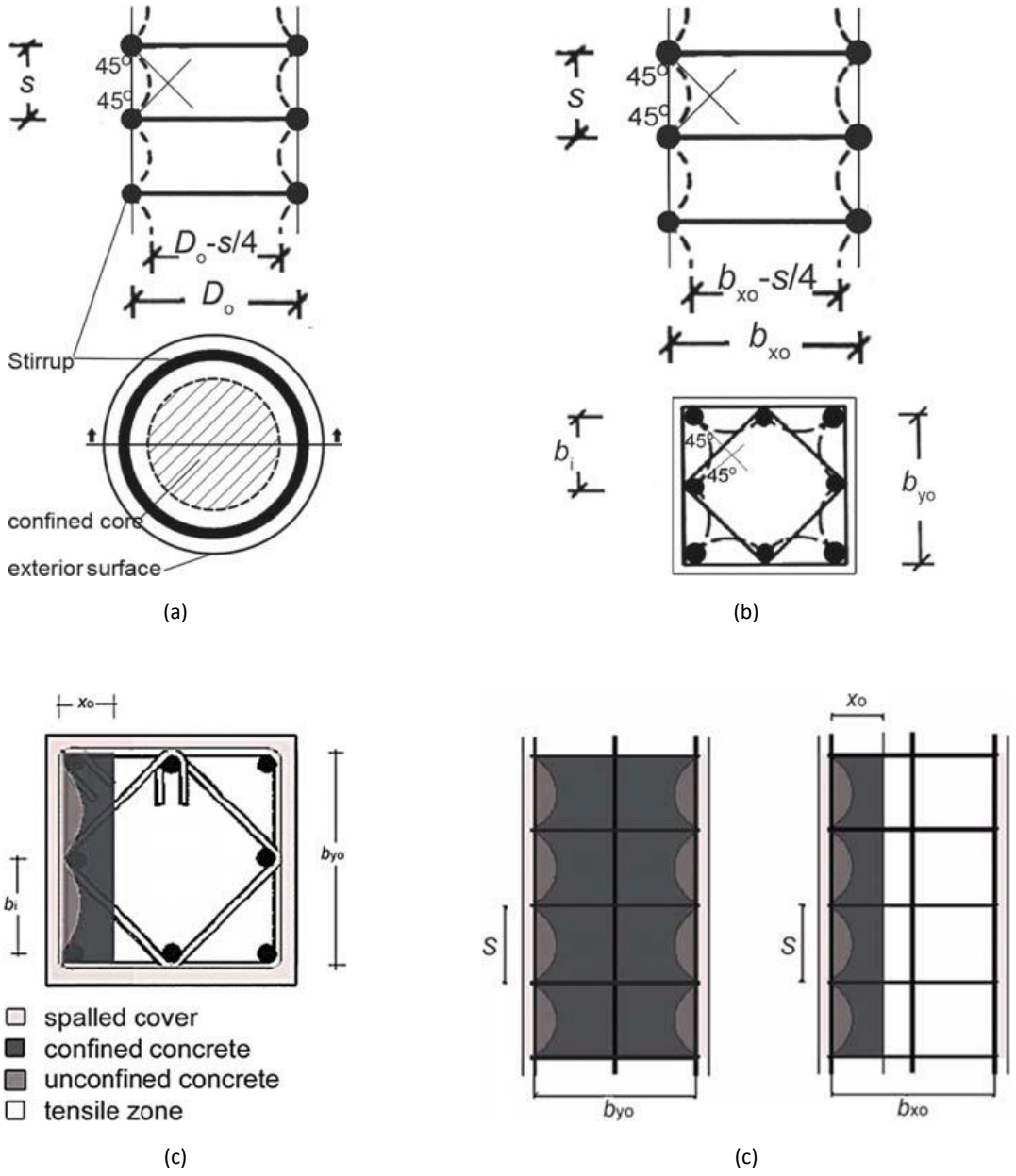

Figure 2.23 – Confined and unconfined parts over the cross-section and along a member with: (a) circular section and circular hoops or (b) square section and multiple ties; (c) confinement effectiveness in the compression zone of the confined core of a member in flexure (adapted from Fardis, 2009)

Several constitutive relations featuring different confinement models are known to describe well the cyclic behaviour of concrete, for instance: (i) Mander *et al* (1988); (ii) Madas and Elnashai (1992); (iii) Kappos and Konstantinidis (1999). The Mander *et al* (1988) model (Figure 2.24) is a uniaxial nonlinear constant confinement model, initially programmed by Madas (1993), that follows the constitutive relationship proposed by Mander *et al* (1988) combined with specific cyclic rules proposed by Martinez-Rueda and Elnashai (1997). The confinement effects provided by the transverse reinforcement are incorporated through the rules proposed by Mander *et al* (1988), whereby constant confining pressure is assumed throughout the entire stress-strain range.

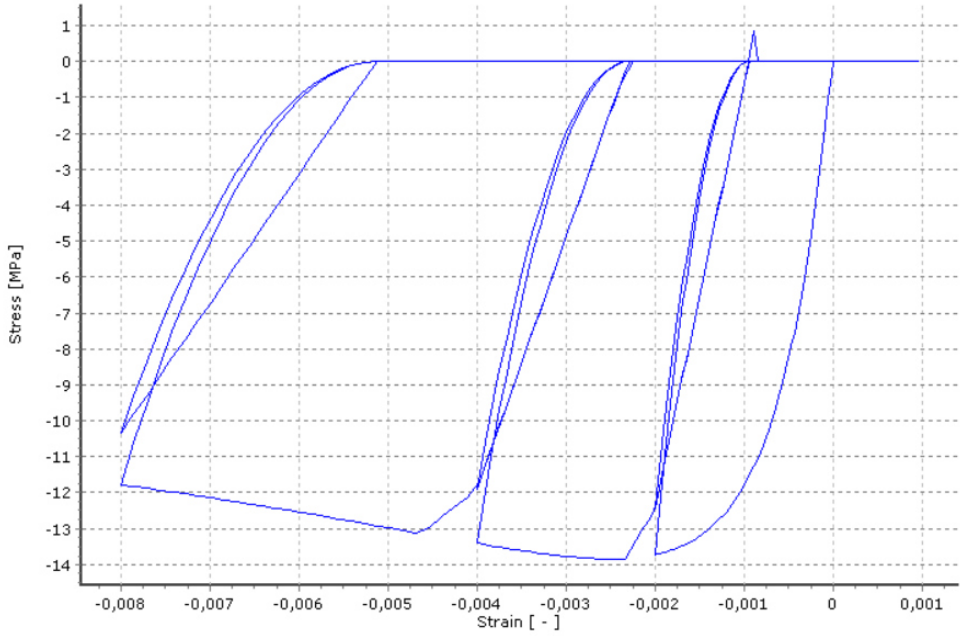

Figure 2.24 – Mander *et al* (1988) concrete model (Seismosoft, 2018)

Following the same constitutive relation assumed by Mander *et al* (1988), the model proposed by Madas and Elnashai (1992) considers a confinement factor that varies during the analysis. This coefficient depends on the cross-sectional properties of the elements (cross-section dimensions, mechanical characteristics, and transverse reinforcement details) and on the axial load at each step of the analysis. Later, Kappos and Konstantinidis (1999) observed that, despite the maximum strength of confined concrete being well predicted by most of the confinement models, higher dispersion between the different stress-strain relations was observed beyond the peak stress. Accordingly, they proposed an alternative constitutive model, calibrated for high-strength concrete, following the relation proposed by Nagashima *et al* (1992) and incorporating the confinement effects through the modified Sheikh and Uzumeri (1982) factor (i.e., the so-called *confinement effectiveness factor*). Contrarily to the Madas and Elnashai (1992) model, the one proposed by Kappos and Konstantinidis (1999) assumes constant confinement throughout the entire stress-strain range, in a similar way as the Mander *et al* (1988) model.

The Mander *et al* (1988) concrete model has been implemented in several nonlinear analysis software platforms focused on earthquake engineering problems (e.g., *SeismoStruct*). For the mechanical behaviour of concrete to be fully described, the definition of the following model-calibrating parameters is required:

- Compressive strength (cylinder 100×200 *mm*) f_c
- Tensile strength f_t
- Modulus of elasticity (initial elastic stiffness) E_c
- Strain at unconfined peak compressive stress ε_c
- Specific weight γ_c (2450 *kg/m³*)

Regarding the definition of the concrete's tensile strength f_t, two options are usually considered: (i) to neglect it ($f_t = 0$) or (ii) to define $f_t = 0.75 \cdot \sqrt{f_c}$, as proposed by Priestley *et al* (1996) for members under flexure. In the latter case, the tensile stress is assumed to increase linearly with strain up until the defined tensile strength is reached, followed by an abrupt loss of tensile resistance.

2.5.4. Masonry infills

Infill panels are commonly used in RC buildings as interior partitions and external walls. Consequently, they are normally treated as non-structural elements and expected to develop no significant interaction with the main structural system. However, while this hypothesis might stand for static loads, it will not be valid for earthquake loads. In the latter case, infill panels are known to develop strong interaction with the bounding RC frames, therefore contributing significantly to the lateral stiffness and overstrength of the structure but also (on the downside) reducing its global ductility and inducing additional shear forces on column members that can cause them to experience brittle shear failure mechanisms (as frequently observed in past earthquakes). Figure 2.25 shows an example of capacity curves for bare and infilled frames. While the referred increment in strength and stiffness is evident at the initial stage, it is also clear the sudden deterioration of the infill panels' capacity (less ductile than the RC frames) and consequent drop in the total base shear values to ones close to those of the bare frames.

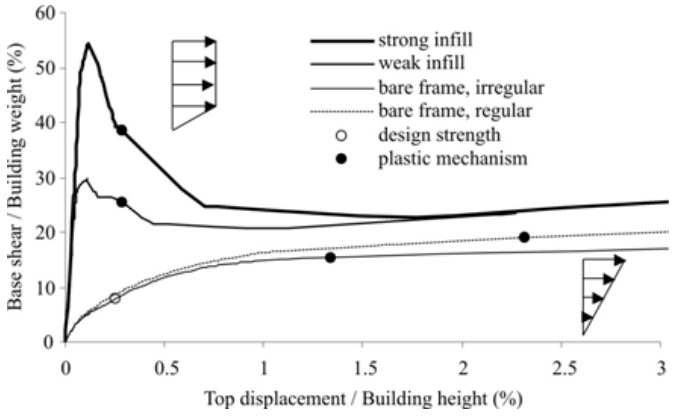

Figure 2.25 – Force-displacement curves for bare and infilled frames (adapted from Fajfar and Dolšek, 2008)

Field experience and scientific research have thus demonstrated the beneficial contribution of infill walls to the overall seismic performance of RC buildings, especially when the latter exhibit limited lateral resistance and provided that the seismic demand does not exceed the deformation capacity of the former. Through their in-plane horizontal stiffness and strength, infill walls decrease storey drift demands and increase storey lateral force, respectively, while significantly contributing to the global energy dissipation capacity (Smyrou, 2006). However, other authors (e.g., Masi, 2003; Tanganelli *et al,* 2011) have identified situations which may lead to the deterioration of the overall seismic performance of infilled RC buildings. For instance: (i) the interruption of infill walls in height may lead to the formation of soft-storeys and (ii) an irregular in plan distribution of infill walls may generate torsional structural response to the translational horizontal components of the seismic action. It seems thus clear that, as argued by Kappos and Ellul (2000), the only feasible way to account for the positive and negative effects of infill walls is to directly include them in the analytical models used for seismic design and assessment purposes.

Several attempts have been made to realistically describe the behaviour of infill walls, including the potential failure modes as observed in experimental tests (i.e., shear cracking; compression failure; flexural cracking). Different modelling techniques have thus been proposed, which can be divided into two main categories in terms of simulation approach: (i) fundamental or micro-models and (ii) simplified or macro-models (Smyrou *et al,* 2011). The plane finite elements and the equivalent truss models are the typical examples of the first and second categories, respectively. Micro-models can simulate structural behaviour with detail (e.g., large displacements; rotation and sliding between blocks; automatic detection of new contacts during calculations), provided that adequate constitutive models are used. However, they are computationally intensive and difficult to apply to the analysis of large structures due to the amount of information that is required. On the other hand, macro-models exhibit obvious advantages in terms of computational simplicity and efficiency. Their formulation is based on a physically reasonable representation of the behaviour of the infilled frame. They can describe the overall response but often do not capture local phenomena appearing between the infill panels and the surrounding RC frame. However, they represent a good compromise between accurate representation and numerical efficiency (O'Reilly, 2016).

A detailed review of the existing proposals for modelling the seismic response of infilled frames is beyond the scope of this work. Readers are referred to the work of Crisafulli *et al* (2000) for a thorough review of the most relevant publications on this matter, as well as to the following (more recent) works: Kakaletsis and Karayannis (2008), on the influence of openings on infill walls; Sassun *et al* (2015), on the in-plane behaviour of infill walls; Furtado *et al* (2016), on the out-of-plane behaviour of infill walls. However, due to the relevance of this matter for the performance-based seismic assessment of existing RC buildings, the following sub-sections summarize a modelling approach that can be adopted within software platforms *SeismoStruct* or *Opensees*. The described model is capable of accounting for the local effects in the surrounding frame, due to the presence of the infill panel, without a significant increase in the complexity of the analysis. Further details on the implementation of this modelling approach can be found in Smyrou *et al* (2011) and O'Reilly (2016).

2.5.4.1. Equivalent strut approach

The equivalent strut approach represents the strut action of the infill wall through the introduction of diagonal compression-only struts. Crisafulli *et al* (2000) studied the influence of the three strut models shown in Figure 2.26 on the structural response of infilled frames, focusing on the stiffness of the structure and the actions induced in the surrounding frame. The obtained results were compared to those of a more refined finite element model of the case study structure. The effects on the bending moment and shear force induced in the columns were then examined in detail to provide insight into which approach provided the most accurate representation of the frame-infill interaction.

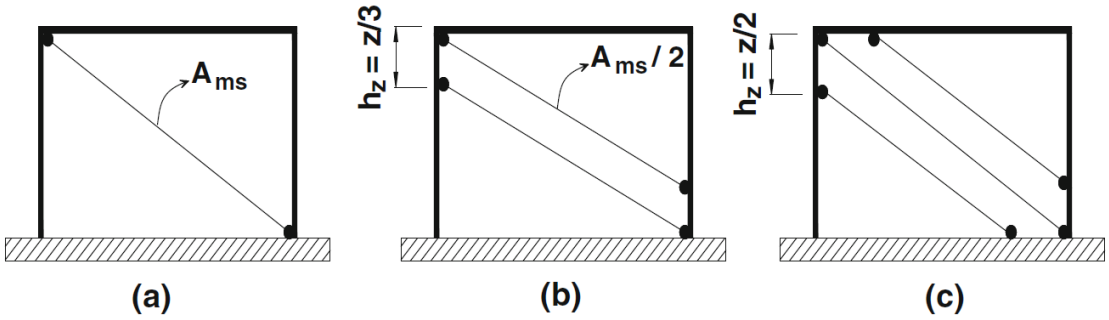

Figure 2.26 – Possible strut models: (a) single-strut; (b) double-strut; (c) triple-strut (Crisafulli, 1997)

The three models behaved similarly in terms of lateral stiffness, leading to the conclusion that (as recently confirmed by Celarec and Dolšek (2013) and others) the single-strut model constitutes a good enough tool for the prediction of the overall response of the infilled frame, offering adequate estimations of lateral stiffness and axial forces induced in frame members. However, regarding the bending moments and shear forces induced in the surrounding frame, these were underestimated by the single-strut model. On the other hand, the double- and triple-strut models provided accurate enough estimates on these parameters, with the double-strut model having the advantage of being less complex to implement. The latter was adopted by Crisafulli (1997) within his proposal of an advanced nonlinear cyclic model for masonry panels, offering the possibility of modelling the material with different levels of accuracy, according to the amount of available information. A summary of this proposal is presented in the next sub-section.

Strut models have been adopted during the last twenty years in studies analysing the influence of masonry infills on the seismic response of RC frames. For instance, Dolšek and Fajfar (2008) applied the single-strut modelling approach, while Celarec and Dolšek (2013) used the double-strut model and Jeon *et al* (2015) the triple-strut model. However, no consensus has been reached as to which approach is the most realistic since it depends on what the analyst requires and whether the layout of elements accurately represents the actual conditions of the infills (O'Reilly, 2016). While it may seem that the triple-strut modelling approach represents the best option to capture the complete behaviour of the infills, Celarec and Dolšek (2013) believe that a double-strut approach will suffice since the actual connectivity and contact between the top of an infill wall and the underside of the upper beam is

typically quite weak. Moreover, the forces induced on the surrounding beam elements need not be modelled with such precision since most of the problems that have been observed in past earthquakes are related to the interaction of infill walls with column members.

2.5.4.2. Element formulation

The nonlinear cyclic model for masonry panels developed by Crisafulli (1997), featuring a double-strut modelling approach, is capable of providing good insight on frame-infill interaction effects at reasonable modelling and computational costs (Smyrou *et al,* 2011). As illustrated in Figure 2.27, the proposed nonlinear element is defined by two components: (i) compression / tension struts; (ii) shear springs. Each panel is thus represented by four axial struts and two shear springs: each diagonal direction features two parallel struts to account for axial forces and deformation across two opposite corners, and one shear spring to account for bed-joint resistance and sliding forces. As the shear spring acts solely across the diagonal that is under compression, its "activation" depends on the deformation of the panel. Moreover, four internal nodes are employed to account for the actual points of contact between the frame and the infill panel (i.e., to account for the width and height of the columns and beams, respectively), whilst four dummy nodes are introduced to account for the contact length between the frame and the infill panel.

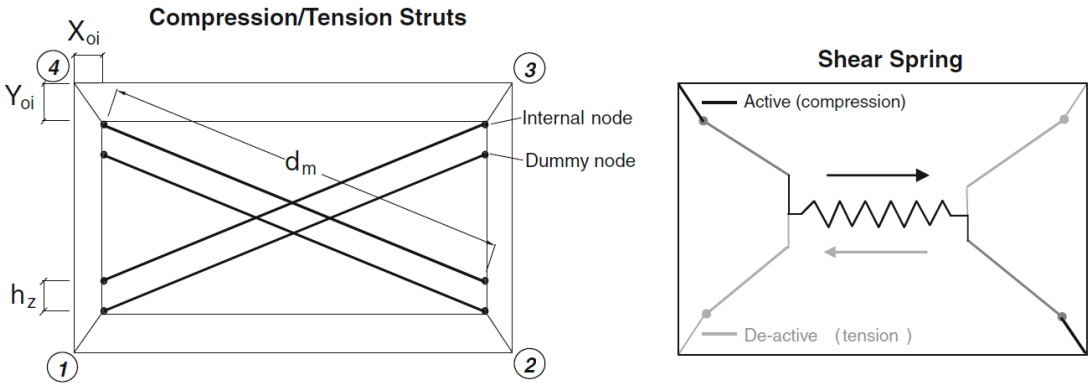

Figure 2.27 – Infill panel model (Crisafulli and Carr, 2007)

The total stiffness of the element is distributed proportionally between the shear spring (K_S) and the struts (K_A), according to the following expressions:

$$K_S = \gamma_s \cdot \frac{A_{ms} \cdot E_m}{d_m} \cdot (\cos\theta)^2 \tag{2.1}$$

$$K_A = (1 - \gamma_s) \cdot \frac{A_{ms} \cdot E_m}{2 \cdot d_m} \tag{2.2}$$

where γ_s is the percentage of the total stiffness assigned to the shear spring, E_m is the masonry's elastic modulus, A_{ms} is the area of the struts, d_m and θ are the length and the inclination, respectively, of the diagonal of the infill panel. The stiffness matrix and coordinates transformation procedure are obtained from equilibrium and compatibility of forces and displacements, respectively. All the internal forces must be transformed to the exterior four nodes, where the infill panel element is connected to the frame. Forces and displacements obtained in the dummy nodes must first be transferred to the adjacent internal nodes and then to the external nodes. The transformation of the forces and displacements obtained with the shear spring is simpler because only the step from the internal to the external nodes needs to be carried out. For further numerical details on these procedures, readers are referred to Crisafulli and Carr (2007). Readers are also reminded that this model is not capable of modelling potential plastic hinges developing in the columns, even though the effect of the strut's eccentricity is considered. If it is important to model the development of plastic hinges in the length of the columns, a different strut configuration must be implemented.

Besides the four corner nodes, the following model-calibrating parameters need to be defined in order to fully characterize the proposed nonlinear element (Smyrou *et al,* 2011):

- Hysteretic relationship for the compression/tension struts;
- Hysteretic relationship for the shear spring;
- Infill panel thickness (t), which may be simply considered equal to the thickness of the bricks;
- Strut area 1 (A_1), defined as the product of the panel's thickness by the equivalent width of the strut (b_w), normally varying between 10 and 40% of the diagonal of the infill panel (d_m) as concluded by several authors based on experimental data (e.g., Crisafulli *et al,* 2000);
- Strut area 2 (A_2), taken as a percentage of A_1 and which tries to account for the fact that, due to cracking of the infill panel, the contact length between the frame and the infill decreases as the lateral and (consequently) axial displacement increase, thus affecting the area of the equivalent strut (see Crisafulli, 1997);
- Equivalent contact length (h_z), taken as a percentage of the panel's height, effectively yielding the distance between the internal and dummy nodes, as to consider the contact length z between the frame and the infill panel, as defined by Stafford Smith (1966) – for suggestions of values, refer to (e.g.) Crisafulli *et al* (2000);
- Horizontal and vertical offsets (X_{oi} and Y_{oi}), taken as a percentage of the horizontal and vertical dimensions of the panel, representing the reduction of the latter due to the depth of the frame members (in practical terms, these parameters provide the distance between the external corner and the internal nodes);
- Proportion of stiffness assigned to shear (γ_s), representing the proportion of the panel stiffness that should be assigned to the shear spring (values ranging between 0.50 and 0.75 are suggested by Crisafulli *et al* (2000)).

The hysteretic relationships (for compression/tension struts and shear springs) that must be supplied to the panel model are briefly discussed in the following sub-section. The approach of Crisafulli *et al* (2000) is referred, as well as that of Decanini *et al* (2004) in conjunction with the modifications proposed by Sassun *et al* (2015).

2.5.4.3. Hysteretic relationships

The compression/tension cyclic relationship proposed by Crisafulli (1997) is based on results that were previously published by other authors. It features the effects of small inner cycles, tension softening and tension stiffening, besides the compression envelope and associated loading, unloading and reloading rules (Smyrou *et al,* 2011). Figure 2.28 illustrates the proposed model.

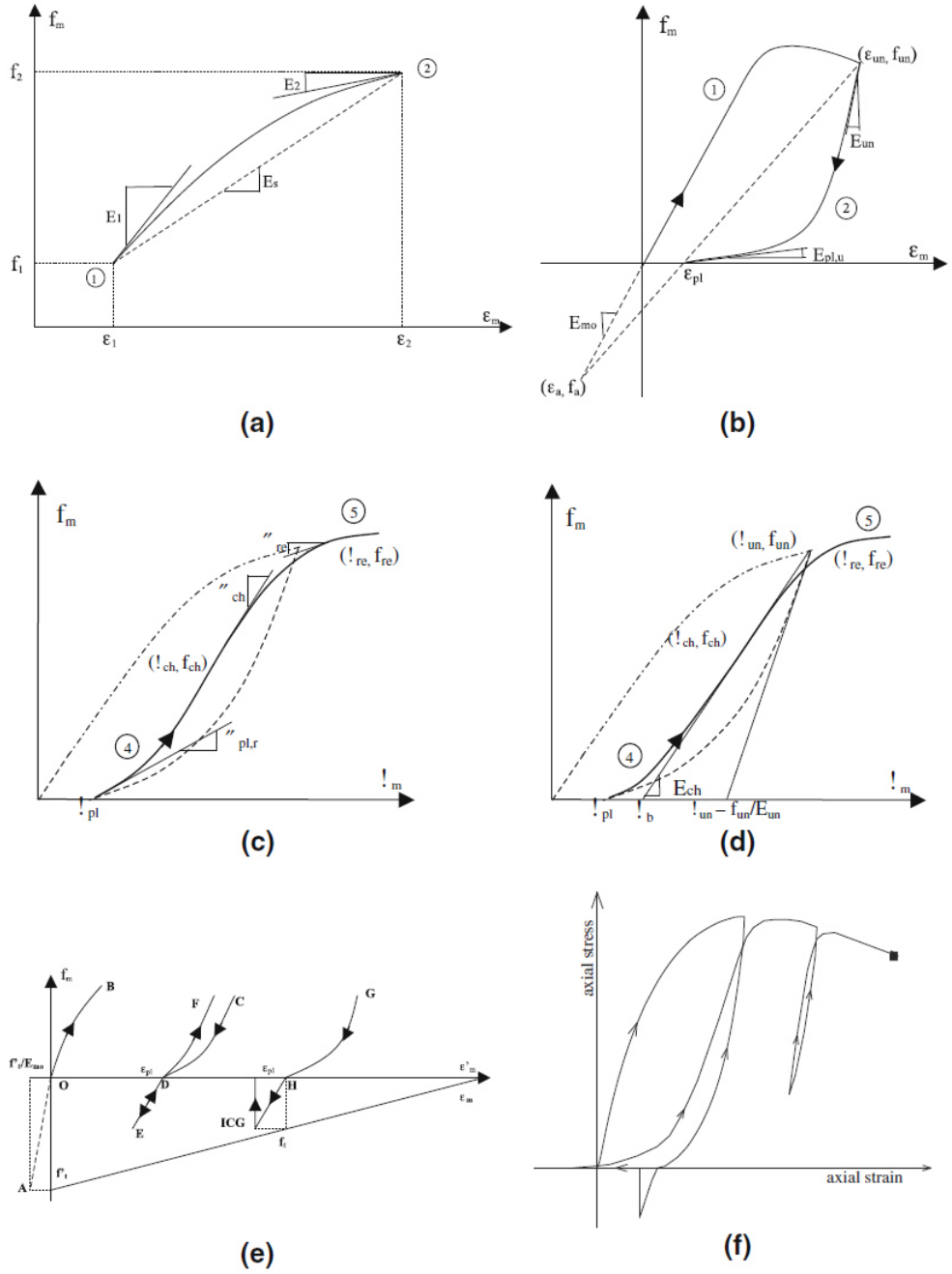

Figure 2.28 – Compression/tension cyclic relationship: (a) unloading and reloading; (b) stress-strain curves for unloading; (c) parameters associated with reloading; (d) definition of change point for unloading; (e) rule for tensile behaviour; (f) masonry strut hysteretic response (Crisafulli, 1997)

The definition of six mechanical parameters is required to characterize the model: (i) initial Young modulus E_m; (ii) compressive strength $f_{m\theta}$; (iii) tensile strength f_t; (iv) strain at maximum stress ε_m; (v) ultimate strain ε_{ult}; (vi) closing strain ε_{cl}. Comments and recommendations concerning value ranges can be found in Crisafulli (1997) and Smyrou *et al* (2011). Additionally, nine empirical factors, exclusively associated with the cyclic rules, need to be defined within the model. These empirical parameters come as a natural consequence of the infill panels' complex behaviour (explanations about their meaning and recommended value ranges are given in Crisafulli (1997)). However, a sensitivity study carried out by Smyrou (2006) indicates that only three parameters play relevant roles in the energy dissipation capacity of the infill panel (i.e., the remaining parameters are not expected to have a major impact if changed from the proposed default values).

Concerning the cyclic shear relationship, Crisafulli (1997) proposed that shear strength is computed independently of the failure mechanism (shear friction failure; diagonal tension failure; compression failure) being developed within the infill panel. This is a typical pragmatic approach, combining two shear resistance mechanisms (bond strength and friction resistance between the mortar joints and the bricks), which effectively means that shear strength can be expressed as the sum of the initial shear bond strength τ_0 with the product of the friction coefficient μ by the absolute value of the normal compressive force in the direction perpendicular to the bed joints. However, in order to fully characterize the response curve depicted in Figure 2.29, two more parameters need to be defined: maximum shear strength τ_{max} and reduction shear factor α_s. Explanations and recommendations about these four parameters can be found in Crisafulli (1997). It should be noted, though, that the actual hysteretic response may differ from the one shown in Figure 2.29, in which the normal stress is assumed to remain constant, since in reality the latter undergoes changes as the infill panel deforms in shear (Smyrou *et al,* 2011).

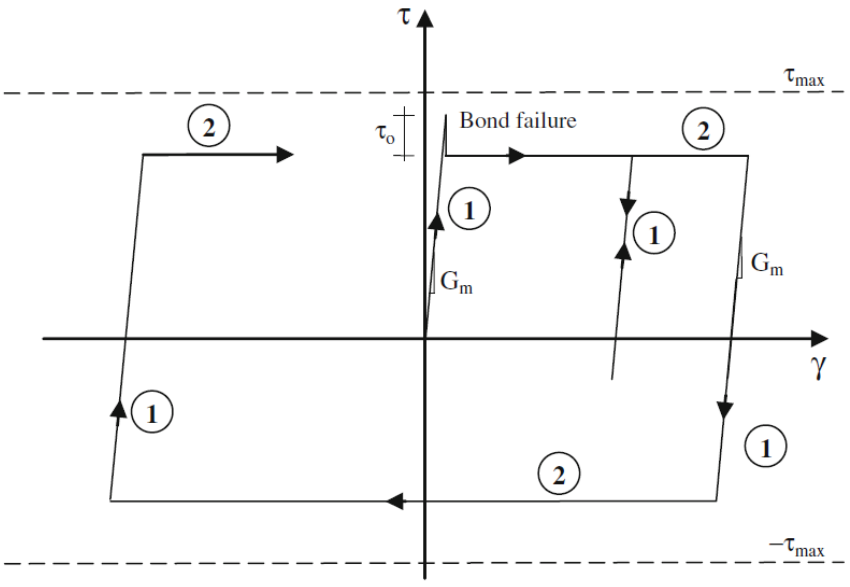

Figure 2.29 – Shear cyclic relationship (Crisafulli, 1997)

An alternative implementation of the infill's hysteresis can be found in O'Reilly (2016). The backbone curve is computed using the approach of Decanini *et al* (2004) in conjunction with the modifications proposed by Sassun *et al* (2015). This offers the advantage of being a simple model that considers different failure mechanisms, in addition to defining storey drift values (at each limit state) according to experimentally measured values provided by numerous test specimens. However, the consideration of openings such as doors or windows was not considered, neither was the out-of-plane failure of the infill panels. The various terms of the backbone curve are illustrated in Figure 2.30. For a further description of this implementation, readers are referred to O'Reilly (2016).

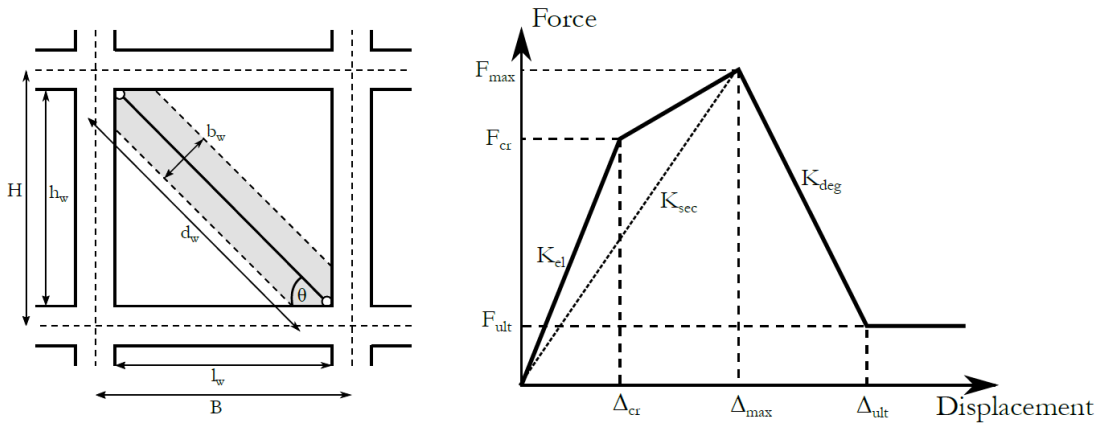

Figure 2.30 – Illustration of the infill's backbone definition (O'Reilly, 2016)

2.5.4.4. Modelling of openings

The presence of openings in masonry panels constitutes an important uncertainty in the evaluation of the behaviour of infilled frames and significant work has been devoted, since the 1950's, to the investigation of the influence that different configurations (in terms of size and location) might have on strength and stiffness (Smyrou *et al,* 2011). Unfortunately, though understandably, the large number of involved variables and uncertainties has not yet allowed for an agreement to be reached on this topic and, consequently, has led to various conclusions and recommendations. Engineering judgement and experience, coupled with a thorough consult of the most recent applicable literature, must therefore be used to decide on how to consider the presence of openings on the panels of the infilled structure under analysis.

As an expedite recommendation, Smyrou *et al* (2011) suggest reducing the above referred value of the strut area A_1 (hence, the panel's stiffness) in proportion to the area of the opening in relation to that of the panel. As shown by Smyrou (2006), good response predictions might be obtained by reducing the value of A_1 between 30 to 50%, if the area of the opening does not exceed 15 to 30% of that of the panel. Concerning the strength of the infill panel, Smyrou *et al* (2011) suggest that, in absence of good evidence, no change in its value should be introduced for opening areas up until 30% of the area of the infill panel.

2.6. NONLINEAR ANALYSIS METHODS

As referred in Chapter 1, according to current codes the seismic design methodology of new buildings is force-based, working with linear-elastic analysis combined with damped elastic response spectra (for seismic demand definition) and behaviour factors accounting (mainly) for ductility and energy dissipation capacity. On the contrary, the methodology for the seismic assessment of existing buildings is fully displacement-based. The underlying reason is practical: force-based approaches entail capacity-demand comparisons in terms of internal forces, with no direct evaluation of the members' deformations. However, because the seismic action is not a set of given forces to be resisted by the structure (unlike gravity or wind actions), but in fact a given dynamic displacement input to be accommodated, the parameter which is important for a member's seismic performance (including failure) is not the force but its deformation capacity (Priestley *et al*, 2007; Fardis, 2009).

The main objective of any nonlinear analysis method within a displacement-based seismic assessment framework is, hence, the calculation of deformation demands in structural members. Codes and standards concerning this matter (e.g., EC8-3, 2005) allow the following options: (i) nonlinear static (pushover) analysis and (ii) nonlinear dynamic (time-history) analysis. The latter is, at present time, the most accurate approach to evaluate a structure's seismic response. Nonetheless, some drawbacks exist, such as: the necessary time to run the required calculations; the need for the selection of a set of real or synthetic accelerograms, along with an adequate scaling technique (to be able to consider different intensities); the possible variability in structural response due to inherent properties of the selected ground motions; etc. (Sousa *et al*, 2011). On the other hand, nonlinear static analysis represents a simplified approach to evaluate the behaviour of a structure under the effect of an increasing monotonic lateral load. Although limited in its ability to capture transient dynamic behaviour with cyclic loading and degradation, it provides a convenient and fairly reliable method for structures whose dynamic response is governed by first-mode sway motions. Even when not appropriate for a complete performance evaluation, nonlinear static analysis can be an effective tool to investigate aspects of the analysis model and the nonlinear response that are difficult to perceive with nonlinear dynamic analysis. For instance, it can be useful to: (i) debug the analysis model; (ii) improve understanding of the yielding mechanisms and deformation demands and (iii) test alternative design parameters and their effect on the response (Deierlein *et al*, 2010).

Despite being considered a suitable approach to regular structures, limitations have been pointed out about nonlinear static analysis concerning its application to irregular ones. Consequently, several authors (e.g., Fajfar *et al*, 2005a; Bhatt, 2012) have proposed improvements to existing nonlinear static procedures (NSP's) that, directly or indirectly, try to deal with the particularities of the response of irregular buildings, namely torsional effects. Studies performed by Bento *et al* (2010) and Pinho *et al* (2013) indicate that some of the more advanced NSP's provide results that are, in general, closer to those provided by nonlinear dynamic analysis. However, as the complexity of the analysed structures increases (i.e., higher torsional effects and / or influence of higher order vibration modes), the correlation between the two approaches decreases.

It is thus fundamental to fully understand the advantages and limitations of each analysis method, along with those of the before discussed modelling options, in order to adequately control the

obtained seismic response for the structure under evaluation. The limited scrutiny to which some of the most recent (however promising) may yet have been subjected to should also be taken into account before considering their generalized application. The following sections review the main characteristics of each of the referred nonlinear analysis methods, along with the necessary steps to apply them to a seismic assessment problem.

2.6.1. Nonlinear static analysis

Nonlinear static analysis (commonly called "pushover" analysis) is essentially the extension into the nonlinear regime of the lateral force procedure of static analysis (Fardis, 2009). A system of lateral loads is applied at the masses' levels of the structural model, and monotonically increased to simulate the dynamic inertia forces due to the horizontal component of the seismic action (the vertical component is not addressed). This procedure is carried out under constant vertical loads so as to capture the effects of gravity-induced forces and *P-Δ* effects on component yielding and post-peak response. As the lateral loads are increased, the analyst can follow the gradual formation of plastic hinges and the evolution of the plastic mechanism and damage as a function of the magnitude of the imposed lateral loads and of the resulting displacements (Deierlein *et al*, 2010).

This method was initially developed for 2D analyses, even though it is frequently applied to 3D structural models. Nonetheless, even in that situation, the lateral loading simulates inertia forces due to a single horizontal seismic action component. According to EC8-1 (2004), when applying pushover analysis to buildings, two distinct lateral load patterns should be considered at the location of the masses in the model (F_i is the force at the frame level i):

i. A "modal" pattern, proportional to the lateral forces' distribution consistent with the 1st vibration mode shape, in the horizontal direction for which the analysis is being carried out, given by:

$$F_i = \lambda \cdot m_i \cdot \phi_i \tag{2.3}$$

ii. An "uniform" pattern, based on lateral forces that are proportional to mass, regardless of elevation (uniform response acceleration), given by:

$$F_i = \lambda \cdot m_i \tag{2.4}$$

where λ is the load factor, m_i is the modal mass and ϕ_i is the modal coordinate corresponding to the 1st vibration mode shape. The most unfavourable result obtained with the two load patterns should be used when extracting conclusions. It should be noted that, unless the structure is symmetric about an axis at right angles to the considered component of the seismic action, the analysis should be carried out for both senses (positive and negative) of each load pattern.

Unfortunately, conventional pushover analysis is unable to account for the effects that progressive stiffness degradation (typical of strong earthquake loading) has on the characteristics of the dynamic response of structures, thus on the pattern of the applied equivalent static loads. The fixed nature of

the applied loads distribution ignores the potential redistribution of forces during an actual dynamic response, which pushover analysis tries to reproduce. Consequently, the resulting changes in the modal characteristics of the structure (typically period elongation) and consequent variation in the dynamic response amplification are not accounted for. This might introduce non-negligible inaccuracies, particularly in those cases where the influence of the higher modes is (or becomes) significant. Such effects can only be accounted for by means of more sophisticated versions of pushover analysis (e.g., Antoniou and Pinho, 2004), that do not use a fixed pattern of applied lateral loads but instead "adapt" it to the evolution of nonlinearity. However, this increase in accuracy is at the expense of the most attractive feature of pushover analysis, namely its simplicity. For the case of low-rise regular buildings, whose dynamic response is dominated by the fundamental sway mode of vibration, conventional pushover analysis will suffice. For taller, slender, or irregular buildings, where several vibration modes will affect the dynamic behaviour, it will be less suitable (Fardis, 2009; Deierlein *et al*, 2010).

The result of the pushover analysis of a building is usually presented in the form of a nonlinear force-displacement curve (Figure 2.31), representing the variation of the total shear force resistance in the considered horizontal direction (base shear) with the displacement response of a node located on the top of the structural model. This curve is commonly referred to as "capacity curve" and the top node is usually referred to as "control node". According to EC8-1 (2004), the capacity curve should be plotted for values of the control displacement ranging between zero and the value corresponding to 150% of the so-called "target displacement", which represents the displacement demand that the earthquake ground motions would impose on the structure. For further analyses and overall building performance evaluation purposes, the capacity curve can be simplified considering idealised sloping branches of elastic, post-yield hardening and softening (degrading) behaviour.

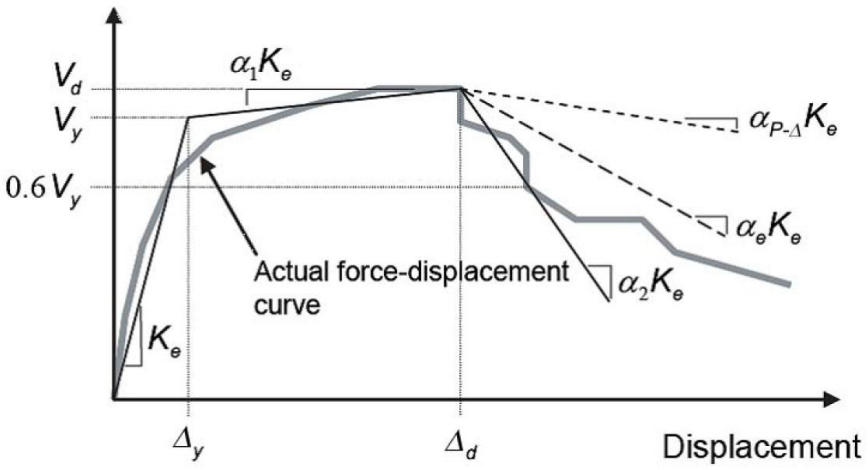

Figure 2.31 – Force-displacement pushover curve and idealised linear branches (Deierlein *et al*, 2010)

2.6.2. Adaptive nonlinear static analysis

Several attempts have been made to overcome the limitations of conventional pushover analysis regarding torsional, higher-mode, and stiffness degradation effects (e.g., Paret *et al*, 1996; Bracci *et al*, 1997; Gupta and Kunnath, 2000; Chopra and Goel, 2002). A new enhanced adaptive pushover procedure, firstly proposed by Elnashai (2000), was further developed and tested by Antoniou *et al* (2002). The suggested procedure is "adaptive" in the sense that the lateral load distribution is constantly updated during the analysis. Like this, the structural stiffness at different deformation levels is considered in the evaluation of the new forces, the system degradation and period elongation can be accounted for, and the change of the inertia loads during dynamic analysis for different deformation levels may be successfully modelled.

The method is multi-modal, thus explicitly accounting for higher-mode effects, with the possibility to include (or not) spectral amplification of the different modes. This requires the consideration of a site-specific (usually code-based) spectrum in the definition of the new load patterns. As an alternative, a particular seismic record can be used to derive the spectral coordinates. If spectral amplification is not considered, the force distribution will still be updated at every step (or only at predefined steps, to reduce the computational effort) but only according to the modal properties of the structure. The full details of this methodology are described in the work of Antoniou and Pinho (2004a), along with the results of the validation and efficiency assessment procedure that was carried out using a series of framed systems with different configurations and heights. Several ground motions with different dynamic characteristics were considered and the obtained results were compared with those of conventional pushover and nonlinear dynamic analyses.

The conclusions show that the proposed adaptive static procedure yielded results very close to those obtained with the more sophisticated nonlinear dynamic analyses and was able to capture response characteristics that also only detailed dynamic methods could predict. Overall, the method is expected to perform better than any pushover procedure with a fixed force pattern, providing an efficient and stable analysis option for the performance evaluation of structural systems under seismic loading. The basic steps of the proposed methodology are summarized below (Antoniou *et al*, 2002):

(1) At each step, prior to the application of any additional load, perform eigenvalue analysis considering the stiffness state at the end of the previous load step and calculate the periods and eigenvectors of the system;
(2) Based on the obtained modal shapes and the participation factors, the patterns of storey forces are determined separately for each mode. If a spectral shape is considered, the corresponding for each mode of vibration is also considered in the computation of force pattern;
(3) The lateral load profiles of the modes are combined using either the Square Root of the Sum of Squares (SRSS) or the Complete Quadratic Combination (CQC) method. Since only the relative values of storey forces are of interest (the absolute values are determined by the load factor λ and the nominal loads), the horizontal loads are normalized with respect to the total value;

(4) Update (increase) the load factor λ. The forces applied at each storey are evaluated as the product of the updated load factor, the nominal load at that storey and the storey forces obtained above (note that, normally, the nominal loads at all the storeys should be equal because the effect of the different mass values is accounted for by the eigenvalue procedure). If incremental scaling is applied, only the load increment is updated, and then added to the load at the previous step;
(5) Apply the new calculated forces to the model and solve the system of equations to obtain the structural response at the new equilibrium state;
(6) Calculate the updated tangent stiffness matrix of the structure and return to step 1 of the algorithm, for the next iteration of the adaptive pushover analysis.

The described methodology is (obviously) force based. Nonetheless, both non-adaptive and adaptive pushover analyses can be carried out by monotonically applying a set of lateral displacements to the structure, rather than forces. A detailed description of such a procedure can be found in the work of Antoniou and Pinho (2004b), where the integrity of the analysis algorithm is verified through an extensive comparative study involving the static and dynamic nonlinear analysis of twelve RC buildings subjected to four different acceleration records. The study shows that the approach can provide much improved response predictions, throughout the entire deformation range, in comparison to those obtained by the force-based methods. Plus, the proposed algorithm proved to be numerically stable, even in the highly inelastic region, whereas the additional modelling and computational effort is negligible. The method is therefore shown to constitute an appealing displacement-based tool for structural assessment, fully in line with the modern performance-oriented trends in the field of earthquake engineering.

2.6.3. Nonlinear dynamic analysis

Nonlinear dynamic analysis was developed in the 1970's as a method for research, code-calibration or special applications, but has since then gained its place in engineering practice. Its main application, currently and most likely in the near future, is for the seismic assessment of existing structures, for which it is considered to be the most accurate approach, especially when strong ground shaking is involved (Fardis, 2009). This is due to the fact that the most adequate way of representing the seismic action, without neglecting important motion properties such as shape and energetic content, is through accelerograms registered during a real seismic event. Nonetheless, due to the inherent variability in earthquake ground motions, the consideration of more than one record is required for the calculation of statistically robust values of the demand parameters for a given seismic intensity or earthquake scenario.

Input ground motions should be selected and scaled so as to accurately represent the specific hazard of interest. The applicable American standard ASCE 7 (ASCE, 2010), for instance, refers that the ground motions should reflect the characteristics of the dominant earthquake source at the building site, such as fault mechanism, distance to the fault, site conditions and characteristic earthquake magnitude. Moreover, several studies (e.g., Baker and Cornell, 2006) have shown that the shape of the ground motion's response spectra is also an important factor for the choice and scaling of records, particularly

for higher intensity motions. Detailed information on the definition of the target hazard spectra, type of source and number of ground motions to be considered during analysis can be found in EC8-1 (2004), ASCE 7 (ASCE, 2010) and further applicable literature. Nonetheless, a brief review on such matters is presented further ahead.

Concerning the modelling of damping effects, it is important to maintain consistency across methods (i.e., linear vs. nonlinear analysis), as well as with the elastic response spectra to which the input ground motions should comply (normally code-defined and associated with a viscous damping ratio of 5% of critical). Therefore, nonlinear dynamic analysis should have a built-in 5% viscous damping ratio, which is considered to include all sources of damping up to member yielding (i.e., in the linear range). After member yielding, hysteretic damping should be reflected by the nonlinear force-deformation laws describing the post-yield behaviour of members under cyclic loading. Hence, only the effects of other non-modelled energy dissipation mechanisms (such as claddings, partitions, foundations, and soil, etc.) need to be added as viscous damping (Fardis, 2009). However, the definition of the appropriate amount of viscous damping to be considered in the nonlinear range remains a complex subject and difficult to generalize. More information on this issue can be found in the work of Fardis (2009), Deierlein *et al* (2010), Sousa (2015) and Chopra and McKenna (2016). The work of Sousa (2015), for instance, includes a summary of several studies dedicated to the quantification of damping in existing structures and identification of correlations with structural parameters.

The dynamic response of the structure is calculated for the input ground motions through the direct integration of the well-known nonlinear equations of motion (2.5):

$$[M] \cdot \{\ddot{u}(t)\} + [C] \cdot \{\dot{u}(t)\} + [K(t)] \cdot \{u(t)\} = -[M] \cdot \{1\} \cdot \ddot{u}_G(t) \tag{2.5}$$

where $[M]$ is the mass matrix (usually diagonal, with lumped masses at the nodes), $[C]$ is the damping matrix, $[K(t)]$ is the nonlinear stiffness matrix, $\{u(t)\}$ is the vector of nodal degrees of freedom (DoF's) relative to the ground and $\ddot{u}_G(t)$ is the ground acceleration time-history in the considered direction. The response-history data can then be obtained for the pertinent structural demand parameters. For convenience of the numerical integration, the damping matrix $[C]$ is typically (e.g., Clough and Penzien, 1993; Chopra, 2001) determined as a linear combination (2.6) of the mass and stiffness matrixes (Rayleigh damping formulation):

$$[C] = \alpha_M \cdot [M] + \alpha_K \cdot [K] \tag{2.6}$$

where the proportionality factors α_M and α_K are chosen to provide the defined percentage ξ_0 of critical damping at two specific periods of vibration. At a circular frequency ω, Rayleigh damping gives a viscous damping ratio ξ equal to:

$$\xi = \frac{1}{2} \cdot \left(\frac{\alpha_M}{\omega} + \alpha_K \cdot \omega\right) \tag{2.7}$$

To achieve damping ratio values that are as close as possible to the target value $\xi = \xi_0$ within the predominant frequency range of the response, ξ should then be made equal to ξ_0 at two circular frequencies ω_1 and ω_2 straddling that range, solving for α_M and α_K to get:

$$\xi = \frac{\xi_0}{\omega_1 + \omega_2} \cdot \left(\frac{\omega_1 \cdot \omega_2}{\omega} + \omega \right) \tag{2.7a}$$

For analysis under a single component of the seismic action, a possible choice for ω_1 is the circular frequency of the mode with the highest modal base shear in the elastic range. The value of ω_2 may be set as two or three times ω_1, bracketing the range of the 1st and 2nd modes in the considered direction (Chopra, 2001; Fardis, 2009). It should be noted, however, that the Rayleigh formulation was originally developed in the context of linear-elastic dynamic analysis, where the stiffness matrix $[K]$ is constant and the vibration modes are uniquely calculated. For nonlinear analysis, where member stiffnesses are changing and unique vibration modes do not exist, the application of the method has implementation issues, as discussed by Priestley and Grant (2005), Hall (2006), Charney and McNamara (2008) and others. For instance, Priestley and Grant (2005) suggested the use of stiffness-proportional damping (SPD) rather than Rayleigh's after demonstrating that, if a given structure is insensitive to rigid body motion, mass-proportional damping (MPD) will generate unrealistic energy dissipation. The stiffness-proportional damping approach was then further subdivided in initial stiffness- (ISPD) and tangent stiffness-proportional damping (TSPD), the latter being shown as possibly the soundest option for common structures (further details in Sousa, 2015). The proportionality factor α_K for this approach is typically computed (though not exclusively) using Equation (2.8).

$$\alpha_K = \frac{2 \cdot \xi_0}{\omega_1} \tag{2.8}$$

Numerical instabilities in nonlinear response-history analyses are not rare (especially when the number of DoF's is very large and analyses are carried out for many ground motions). Special attention should therefore be paid to the choice of the numerical integration scheme. Usually the time-step Δt for the numerical integration is chosen the same as the discretisation interval of the ground acceleration $\ddot{u}_G(t)$ (typically 0.01 s) or one-half of it. Only implicit integration schemes, which are unconditionally stable for linear systems, are appropriate for such a long Δt. Hence, two widely used schemes, both unconditionally stable for linear systems, are recommended (Chopra, 2001):

- Newmark's average acceleration method (Newmark, 1959);
- Wilson's θ method (Wilson and Penzien, 1972).

In Newmark's average acceleration method (obtained with $\gamma = 0.50$ and $\beta = 0.25$), $\ddot{u}$ is taken constant within the interval $[t, t + \Delta t]$ while the Wilson-θ method considers it to vary linearly within the interval $[t,\ t + \theta \cdot \Delta t]$. The value of parameter θ is usually taken between 1.37 and 1.42. More information about each method's detailed formulations as well as compared numerical examples can be found in Chopra (2001). It should be kept in mind, however, that despite providing bounded

solutions regardless of the adopted time-step, there are always computational errors inherent to any numerical solution. The error of a given numerical method is usually measured in terms of amplitude decay and period elongation / shortening of the response motion and is associated with the ratio between time-step Δt and the structure's relevant period of vibration T (Sousa, 2015). A traditional rule of thumb suggests that Δt equal or lower than $0.1 \cdot T$ and 0.02 seconds is generally enough to produce reasonably accurate results, ensuring at the same time a smooth transition between analysis steps (Chopra, 2001). Nonetheless, the consideration of a reduced time-step for large structures can lead to unreasonable analysis time without visible improvements in terms of accuracy.

As nonlinear dynamic analysis involves fewer assumptions than nonlinear static methods, fewer limitations are associated to it. Global displacement demands are determined in the course of the analysis and, unlike in static procedures, it is possible to carry out the direct comparison of the demand quantities with the acceptance criteria. Torsional, 3D and higher mode effects are fully accounted for, as well as the concurrent application of two (or three) seismic action components. Moreover, nonlinear dynamic analysis provides estimates not only of peak deformations (which are important for the overall safety and integrity of the structure) but of residual ones as well, which are the most meaningful measure of damage and, as such, very important for performance-based design or assessment (Fardis, 2009). It should be noted, however, that the accuracy of the obtained results depends on the details of the analysis model and of how faithfully it captures the significant behavioural effects of the structure. It should also be noted that, despite the referred advantages, some important drawbacks can be pointed out, especially if the application within the context of a typical design office is to be considered (Fardis, 2009; Deierlein *et al*, 2010; Sousa *et al*, 2011):

- Most practitioners are not familiarized with such sophisticated methods, lacking the knowledge to fully understand all the involved phenomena, and hence set all the input values to correctly describe them;
- Direct integration methods demand considerable computation effort and are very time-consuming, especially in the case of multi-storey and/ or highly irregular buildings;
- The need to consider more than one acceleration record, for the calculation of statistically robust values of the structure's demand parameters for a given seismic intensity, implies more analysis time and the processing of large sets of results;
- Record selection and scaling for time-history analysis is also a matter that is not usually known to most practitioners, posing additional difficulties;
- Results obtained with nonlinear dynamic analysis are highly dependent on the modelling options, such as the hysteretic relations considered for the involved materials, hence requiring detailed calibration.

2.7. SEISMIC ASSESSMENT OF EXISTING RC BUILDINGS

Several methodologies to assess the seismic safety of structures are currently being used, ranging from the more complex and general to those simpler and easier to apply. The latter usually involve more assumptions and simplifications, in opposition with the more general methodologies that try to reproduce reality as close as possible. Modern probabilistic methods deal explicitly with any

probability distribution of the seismic action, evaluating its effects using nonlinear dynamic analysis and defining structural capacities through probability distribution functions, in order to evaluate the probability of collapse of the structure under analysis (Delgado *et al*, 2010). However, the existence of many different approaches (namely within seismic codes of different countries) suggests that no consensus has yet been achieved, which means that margin still exists for the improvement of current procedures.

The European EC8-3 (2005), the American Standard ASCE 41-13 (2014) and the New Zealand NZSEE guidelines (NZSEE, 2006) represent three of the very few international documents that have followed the state-of-the-art of the analytical seismic assessment of buildings, incorporating the recent concepts of capacity design, performance levels and acceptance criteria. Nonetheless, the associated assessment procedures follow conceptually different approaches, as previously referred. Because a significant part of the present research is anchored on the application of EC8-3 (2005), the following sub-sections will only address its contents (and shortcomings). For further discussion about the application of EC8-3 (2005) and other seismic assessment codes and guidelines, a comparative review of the current procedures can be found in the work of Pinto and Franchin (2008), Mola and Negro (2009) and others.

2.7.1. Methodology according to EC8-3

Among all the Eurocodes, EC8-3 (2005) is the only standard that discusses the safety of existing structures. It contains procedures for the evaluation of the seismic performance of existing buildings as well as for the design of some (very few) structural strengthening solutions. The main body of the document (incorporating corrigendum March 2010) is composed by (only) 25 pages, complemented by three informative annexes composed by 55 pages in total. Each annex is dedicated to a different type of building, concerning its constitutive material (reinforced concrete, steel, or masonry) and essentially provides information on the definition of capacity models. The proposed methodology considers a performance-based approach to determine a structure's level of safety. In fact, most of the described assessment procedures enforce a displacement- or deformation-based approach while restricting the use of classical force-based methods to only a few situations. The global sequence of steps is summarized below:

(1) Performance requirements definition:
   - Limit state of Near Collapse (NC)
   - Limit state of Significant Damage (SD)
   - Limit state of Damage Limitation (DL)

(2) Knowledge Level definition (treatment of uncertainty):
   - KL1: Limited knowledge
   - KL2: Normal knowledge
   - KL3: Full knowledge

(3) Structural analysis method selection:
   - Lateral force analysis (linear)
   - Multi-modal response spectrum analysis (linear)

- Nonlinear static (pushover) analysis
- Nonlinear dynamic (time-history) analysis
- *q*-factor approach

(4) Safety verifications:

- Ductile mechanisms: Chord rotation demand-to-capacity (*D/C*) ratios
- Brittle mechanisms: Shear force demand-to-capacity (*D/C*) ratios

The concepts involved in each step will be discussed in the following sub-sections. Even though it is not absolutely clear, this methodology seems to indicate that a building is to be deemed safe according to a given limit state (LS) only when the seismic demands on all individual structural members do not exceed the corresponding capacities. It should, however, be discussed if it is reasonable to enforce such a strict condition at all times, under pain of obtaining an overly pessimistic scenario after performing the seismic assessment of a stock of existing buildings. Moreover, the scope of EC8-3 (2005) is to provide information on how to perform seismic assessment, while it does not refer anything about when the procedure should be carried out (i.e., when it is mandatory to perform the assessment of a building). Additionally, even when the procedure is carried out, the final decision (retrofit vs. "do nothing") depends mostly on economic issues alongside with the will of individuals (buildings owners) and/ or governments.

2.7.1.1. Performance requirements and compliance criteria

Damage and loss collection in post-earthquake scenarios have shown that, in many cases, buildings that were not compliant with modern design code rules did not necessarily perform unacceptably and, as such, did not require any significant repair measures (Mola and Negro, 2009). Hence, the objective of seismic safety assessment should not be to attempt to upgrade a building in order for it to comply with current design code provisions (the cost would most likely be prohibitive) but to ensure defined levels of damage to prevent collapse during a ground motion with given probability of exceedance (Araújo and Castro, 2017). The evaluation criteria in current codes and guidelines are thus expressed in terms of performance objectives, characterized by inter-storey drift limits, chord rotations, element ductility and element damage indices, paired with different levels of seismic hazard. In the particular case of EC8-3 (2005), the fundamental performance requirements refer to the state of damage in the structure, defined through the three above-referred limit states (LS), each characterized as follows:

- LS of Near Collapse (NC): the structure is heavily damaged, with low residual lateral strength and stiffness, although vertical elements are still capable of sustaining vertical loads; most non-structural components have collapsed; large permanent drifts are present; the structure is near collapse and will probably not survive another earthquake, even a moderate intensity one;
- LS of Significant Damage (SD): the structure is significantly damaged, with some residual lateral strength and stiffness; vertical elements are capable of sustaining vertical loads; non-structural components are damaged, although partitions and infills have not failed out-of-plane; moderate permanent drifts are present; the structure can sustain after-shocks of moderate intensity; the structure is likely to be uneconomic to repair;

- LS of Damage Limitation (DL): the structure is only lightly damaged; structural elements do not exhibit significant yielding and retain their strength and stiffness properties; non-structural components, such as partitions and infills, may show distributed cracking; damage can be economically repaired; permanent drifts are negligible; no structural repair measures are necessary.

It should be noted that the definition of limit state of Near Collapse (NC) given in EC8-3 (2005) is closer to the actual collapse of a building than the one given in EC8-1 (2004) and corresponds to the fullest exploitation of the deformation capacity of the structural members. The limit state associated with the "no collapse" requirement in EC8-1 (2004) is roughly equivalent to the one defined herein as limit state of Significant Damage (SD). The appropriate levels of protection are achieved by selecting, for each limit state, a return period (yrp) for the seismic action. These return periods are defined in accordance with the protection levels normally considered for ordinary new buildings and, unless stated otherwise in the country's National Annex, the values of 2475, 475 and 225 years for the NC, SD, and DL limit states, respectively, are proposed (probabilities of exceedance of 2%, 10% and 20% in 50 years, respectively). Moreover, it is the National Authorities' decision whether all three limit states shall be checked, or two or just one of them.

The draft version of the EC8-3 (2005) Portuguese National Annex (NA) refers that the limit states to be verified depend on the importance class of the building (see EC8-1 (2004): 4.2.5). For buildings belonging to importance classes III or IV, all the above-referred limit states (NC, SD, and DL) need to be verified; for buildings belonging to importance class II, only the limit state of SD needs to be verified; for importance class I, no verifications are mandatory. Concerning the return periods associated with each limit state, the values of 975, 308 and 73 years for the NC, SD, and DL limit states, respectively, are defined (probabilities of exceedance of 5%, 15% and 50% in 50 years, respectively). The values of the reference peak ground acceleration on type A ground a_{gR} to be adopted for each limit state are obtained multiplying the values of a_{gR} indicated in Table NA.I of the EC8-1 (2004) Portuguese National Annex (corresponding to a 475-yrp) by the coefficients indicated in Table 2.9.

Table 2.9 – Coefficients for the calculation of a_{gR} for the application of the EC8-3 (2005) seismic assessment methodology (adapted from EC8-3 (2005): Portuguese NA (draft version))

Limit state (LS)	Type 1 spectrum	Type 2 spectrum	
		Mainland	The Azores
Near collapse (NC)	1.62	1.33	1.22
Significant damage (SD)	0.75	0.84	0.89
Damage limitation (DL)	0.29	0.47	0.55

Compliance with the requirements of non-exceedance of the three limit states is achieved by adoption of the seismic action, method of analysis, verification and detailing procedures contained in EC8-3 (2005), as appropriate for the different structural materials within its scope. However, as previously

mentioned, the compliance criteria appear to be overly restrictive as they seem to indicate that safety checks must be satisfied for all individual primary members (very few existing buildings would pass the test). Driven by the apparent inconsistency of this member-oriented approach, several studies were carried out (e.g., Pinto and Franchin, 2008; Romão *et al*, 2014) in order to evaluate the code's effectiveness in terms of safety and economy criteria. Those studies pointed out that code provisions make no distinction between primary elements in terms of their importance in the integrity of the whole structure (i.e., every member has the same importance). A structure is deemed unsafe if a single member does not comply with the given LS, even if all others are far from the corresponding limit. Similarly, a structure may be deemed safe if the D/C ratios of all members for a given LS are high but just below 1.0. Furthermore, no recommendations on how to perform a cost-benefit analysis of a retrofitting solution are included in EC8-3 (2005). This led to the conclusion that the limit state approach, as it is, still needs to be improved in order to provide more effective criteria for the seismic assessment and retrofitting of existing buildings.

2.7.1.2. Treatment of uncertainty and confidence factors

The amount and quality of the information about the structural properties of an existing building may vary a lot, depending on the variety of sources and processes used to obtain it. This input data may be obtained through available documentation specific to the building, field investigations and (in most cases) in-situ and / or laboratory measurements and tests. While documentation on the building may not be accurate, field surveys and in-situ testing involve measurement errors (however well developed the techniques may be) and the results may lead to a considerable degree of uncertainty (Romão, 2012). Therefore, there is always some degree of incompleteness in the knowledge about relevant structural characteristics associated with the process of assessing the seismic safety of existing buildings.

EC8-3 (2005) tries to cover this issue through the definition of different Knowledge Levels (KL), related to the amount and quality of the usable information, and the use of a single factor – the Confidence Factor (CF) – that deals with all types of uncertainties. Three different levels of knowledge are defined: Limited (KL1), Normal (KL2) and Full (KL3). The factors determining the appropriate KL are the following:

i. Geometry: the geometrical properties of the structural system and of such non-structural elements (e.g., masonry infill panels) as may affect structural response;
ii. Details: including the amount and detailing of reinforcement in RC structures, connections between steel members, the connection of floor diaphragms to the lateral resisting structure, the bond and mortar jointing of masonry and the nature of any reinforcing elements in masonry;
iii. Materials: the mechanical properties of the constituent materials.

The value of CF depends on the chosen KL. The values of 1.35, 1.20 and 1.00 are suggested for KL1, KL2 and KL3, respectively, unless stated otherwise in a country's National Annex. It is noteworthy that, for a predefined KL, the CF remains the same for all limit states. This factor plays a somehow similar role

to that of a partial safety factor in the safety verifications stage, as it will be seen ahead on this chapter. Besides defining the value of CF to be adopted, the level of knowledge determines the admissible types of analysis methods that can be employed in the assessment procedure (see Table 2.10). Some controversial features about KL's and the CF have, however, been recognized by some authors (e.g., Romão *et al*, 2008; Franchin *et al*, 2010).

Table 2.10 – Knowledge levels (KL) and corresponding methods of analysis (LF: Lateral Force procedure; MRS: Modal Response Spectrum analysis) and Confidence Factors (CF) (adapted from EC8-3, 2005)

Knowledge Level	Geometry	Details	Materials	Analysis	CF
KL1	From original outline construction drawings with sample **visual** survey *or* from **full** survey.	Simulated design in accordance with relevant practice *and* from **limited** in-situ inspection.	Default values in accordance with standards of the time of construction *and* from **limited** in-situ testing.	LF MRS	1.35
KL2		From incomplete original detailed construction drawings with **limited** in-situ inspection *or* from **extended** in-situ inspection.	From original design specifications with **limited** in-situ testing *or* from **extended** in-situ testing.	All	1.20
KL3		From original detailed construction drawings with **limited** in-situ inspection *or* from **comprehensive** in-situ inspection.	From original test reports with **limited** in-situ testing *or* from **comprehensive** in-situ testing.	All	1.00

Franchin *et al* (2010) questioned the ability of the CF approach to consider all the uncertainties related with the available knowledge and tested its soundness by running probabilistic analyses. The procedure was applied to three RC framed structures of increasing size, employing nonlinear static and dynamic analysis methods, and considering all three KL's. The study concluded that the CF depends on more factors than those referred in EC8-3 (2005), namely the analysis method / modelling options and the structural type (size, regularity, constitutive material, load-resisting system, etc.). Additionally, it was referred that the so-called Full Knowledge (KL3) does not actually correspond to a state of perfect knowledge about the structure, hence it should be penalized with a CF value larger than 1.00. As a result, the author suggested that the present state of development of the code should be improved on this matter.

Romão *et al* (2010a) compared the EC8-3 (2005) deterministic approach with a probabilistic approach for the three LS's, the three KL's (i.e., considering the corresponding three CF's), different analysis methods and two verification stages (ductile and brittle mechanisms). Among their conclusions, it was emphasized that the CF does in fact depend on the LS, a fact that EC8-3 (2005) ignores. Significant differences were observed for both the verification methods tested, displacement- and force-based, with the latter revealing itself to be less sensitive. An alternative approach to the CF was hence proposed, similar to the one included in ASCE 41-13 (2014), by enforcing its application to the overall resistance of structural members instead of to the material strength. Several advantages were pointed out to this approach regarding its ability to capture different behaviour and strength degradation effects according to the expected mechanisms for each LS.

Concerning material strength, EC8-3 (2005) prescribes the use of mean values of properties, divided by the CF for the appropriate KL, within the analysis model and when calculating member capacities that are to be compared with demands for safety verifications. Regarding this procedure, Franchin *et al* (2010) argued that the averaging operation produces in general a structure that is stronger than the reference one. Hence, on average, the assessment results will converge to a state that is illusorily safer than the actual one. This fact is schematically shown in Figure 2.32. For the chosen structure (a chain), the actual strength is equal to that of its weakest link. By measuring the strength of only two links (e.g., KL1 in Figure 2.32), one finds two out of five values and attributes their average strength to all links, resulting in an estimated strength that is larger than the actual one (of course in such a structure one would always have to use the smallest one, but here the chain serves only for illustration purposes). The procedure is thus labeled as generally unconservative, leading on average to underestimating the demand-to-capacity ratio of the structure.

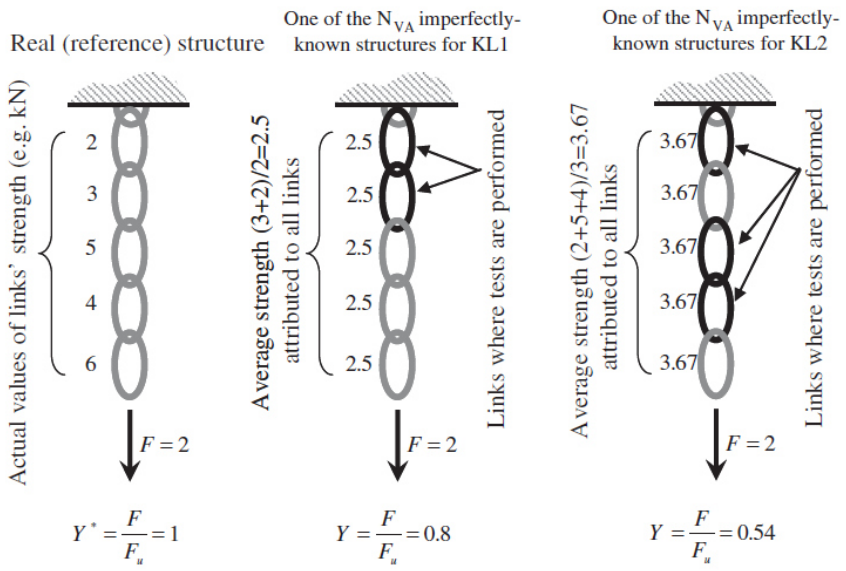

Figure 2.32 – Effect of averaging on increasing the assessed safety – the number of tests increases with KL – F_u is the average strength and N_{VA} is the number of different states of imperfect knowledge on the reference structure (adapted from Franchin *et al*, 2010)

2.7.1.3. Allowed structural analysis methods

The accuracy of the method of analysis to be employed in the assessment process of an existing building is a matter of crucial importance. An excessively conservative method may lead to unnecessary and expensive interventions, while an overly optimistic one may leave the building exposed to an excessive risk. On this matter, EC8-3 (2005) offers five different (previously referred) options that are, in general terms, the same as defined in paragraph 4.3.3 of EC8-1 (2004) for the design of new structures. For a chosen performance requirement, the effects of the seismic action (combined with the other permanent and variable loads) may thus be evaluated by means of linear or nonlinear methods of analysis, depending on the characteristics of the structure in question and the choice of the analyst. Besides the obvious differences, the available methods involve different levels of complexity, accuracy, and computational effort, as well as requirements for specialized knowledge in the field.

Concerning linear methods, EC8-3 (2005) defines an applicability condition that aims to evaluate the regularity of the structure in quantitative terms. This condition states that the ratio ρ_i between demand D_i and the corresponding capacity C_i must be sufficiently uniform across the ductile primary resisting elements of the structure with $\rho_i \geq 1$, where plastic hinges are expected to form. The ratio ρ_{max}/ρ_{min} must not exceed a value in the range between 2 and 3 (2.5 is the recommended value unless stated otherwise in a country's National Annex). The assumption underlying the method is that if the structure goes into the inelastic range with an approximately uniform distribution of inelastic demands (expressed in terms of the *D/C* ratios), the structural response in terms of displacements is acceptably accurate. However, case-study applications have shown that, in practice, it is not to be expected that many existing buildings can satisfy such a strict condition, the consequence of which is that nonlinear methods of analysis will be likely employed in the vast majority of cases (Pinto and Franchin, 2008; Romão *et al*, 2010a; Kappos, 2013).

The application of the *q*-factor approach (a linear static design method with reduced input seismic action) is also bound to strict conditions. EC8-3 (2005) proposes a default value of q = 1.5 for RC structures, not being in general worth attempting to justify analytically the use of larger values unless the ductility properties of the building can be easily and properly documented. With such a small value, this method becomes too conservative in most (if not in all) cases and, as such, should only find application in the case of buildings with apparent overcapacity and / or located in low seismicity regions (Pinto and Franchin, 2008). It should be recalled that this approach is prescribed by EC8-1 (2004) as the basic design method and usually referred to as the most conservative. However (and unfortunately), due to its simplicity and popularity for the design of new structures, practitioners are more likely to resort to it than to more complex nonlinear procedures when involved in situations requiring the seismic assessment and strengthening of existing RC buildings.

Regarding structural modelling, EC8-3 (2005) states that all provisions of section 4.3.1 of EC8-1 (2004) should be applied without modifications. In particular, the stiffness of members should be simulated according to paragraphs 4.3.1 (6) and 4.3.1 (7). The former states that the stiffness of the load bearing elements should be evaluated considering the effect of cracking, corresponding to the initial yielding of the reinforcement. The latter states that, unless a more accurate analysis of the cracked elements

is performed, the elastic flexural and shear stiffness properties of RC elements may be taken equal to one-half (50%) of the corresponding stiffness of uncracked elements. On the other hand, EC8-3 (2005) refers in paragraph A.3.2.4 (5) of Annex A that, for the LS of DL and when verifications are carried out in terms of deformations, the stiffness of each element should be taken equal to the mean value of the yielding stiffness at the two ends of the element (this issue will be discussed ahead). Therefore, contrast seems to exist between the provisions of EC8-1 (2004) and EC8-3 (2005), a situation that may lead to some confusion.

The 50% gross stiffness simplification is widely used and generally accepted for the design of new structures, but it is difficult to justify for the assessment of existing ones. In fact, one of the assumptions of the assessment procedure is that such information can be obtained from in-situ tests and / or surveys. Moreover, several studies have mentioned that special attention should be taken in the modelling of the stiffness, especially for members that are prone to early cracking (Pinto and Franchin, 2008). Mpampatsikos *et al* (2008) evaluated two different approximations for members' stiffness in linear analysis: (i) the mean actual secant stiffness at yielding (EI_{eff}) and (ii) the 50% gross stiffness ($0.5 \cdot EI_{gross}$). The conclusions were that the consideration of EI_{eff} generally overestimated the ductile response, while considering $0.5 \cdot EI_{gross}$ underestimated the ductile response and led to unconservative results. In terms of the response of brittle elements, the results did not present significant variations between hypothesis, leading to the conclusion that the consideration of $0.5 \cdot EI_{gross}$ is an adequate one.

2.7.1.4. Performance evaluation and capacity models

The final step of the EC8-3 (2005) seismic performance assessment methodology corresponds to the safety verification stage, where the conformity of each structural mechanism is checked according to procedures that depend on the nature of the members' mechanisms (ductile or brittle) and the adopted method of analysis (linear or nonlinear). Given the important role of the member's chord rotation demand in this methodology, its quantification according to EC8-3 (2005) is examined herein, along with a review of the alternative formulations proposed in the work of Mpampatsikos *et al* (2008) and Romão *et al* (2010b). A review of the capacity models proposed in Annex A of EC8-3 (2005) then follows, for both ductile and brittle mechanisms and the applicable LS's.

When nonlinear methods of analysis are used, demands D_i on both ductile and brittle mechanisms are directly obtained from the results of the analysis (carried out using mean values of mechanical properties). The demand on ductile mechanisms is given by the chord rotation at members' ends (i.e., the angle between the tangent to a member's axis at the yielding end and the chord connecting that end with the point of contraflexure), while on brittle mechanisms it is given by the shear force at the same locations. On the other hand (when linear analysis is used), the action effects on ductile and brittle mechanisms must be evaluated differently, according to a capacity design philosophy aimed to check the occurrence of undesirable failure mechanisms (Romão, 2012). Demand on ductile mechanisms is obtained in the same way as if nonlinear analysis had been carried out, but on brittle mechanisms it must be obtained by means of equilibrium conditions, considering the actions transmitted by the relevant ductile components. These actions are those from the analysis if the ductile

element satisfies the condition $\rho_i \leq 1$ (i.e., if the element remains below yielding), but should be taken equal to the capacity of the element (evaluated with mean values of material properties) multiplied by the appropriate CF, if $\rho_i > 1$.

As stated above, the chord rotation θ at a member's end section is defined as the angle between the chord connecting the considered end section to the point where the bending moment demand *M* is null and the tangent to the member's axis at the same end section (Figure 2.33). As the bending moment demand *M* is proportional to the curvature ϕ, the section at which *M* = 0 corresponds to the member's point of contraflexure. Hence, each member can be seen as composed by two cantilevers, fixed at the end sections and spanning up to the referred point of contraflexure, the position of which is defined in EC8-3 (2005) by the so-called "shear span" L_S, as given by Expression (2.9):

$$L_S = \frac{M}{V} \tag{2.9}$$

where *M* and *V* are the bending moment and shear demands, respectively, at the considered end section (sections 1 or 2 in Figure 2.33).

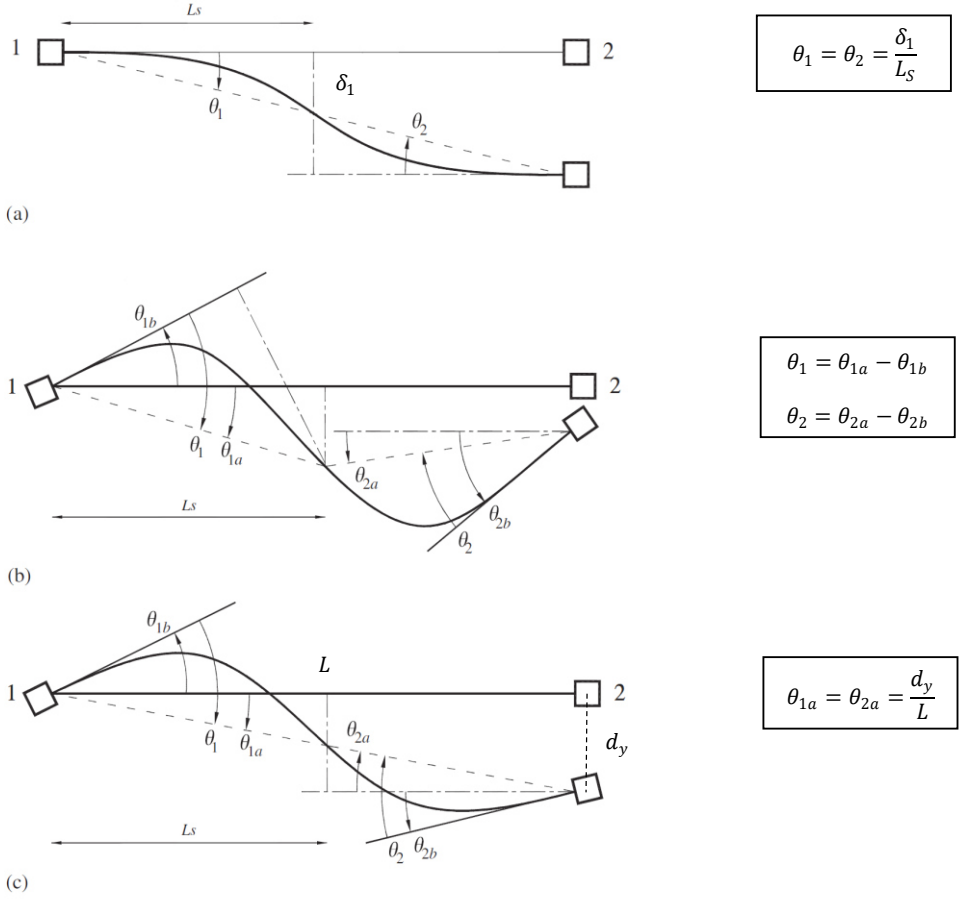

Figure 2.33 – Examples of chord rotation definition (adapted from Romão *et al*, 2010b)

Figure 2.33(a) represents a member with only transversal displacements at its ends, i.e., the simplified interpretation of the deformation of a column, where the chord rotations θ_1 and θ_2 are easily determined. In the more general case of Figure 2.33(b), where both the rotation and the transversal deformation of the member's ends are present, θ_1 and θ_2 are determined computing the difference between the contribution of the deflections at L_S in relation to the initial member configuration (θ_{1a} and θ_{2a}) and the nodal rotations (θ_{1b} and θ_{2b}), considering clockwise rotations to be positive. Figure 2.33(c) presents an additional example that will be addressed ahead, in which θ_{1a} is considered equal to θ_{2a} and given by the member's drift ratio. It should be noted, however, that L_S will only coincide with the point of contraflexure if the member under analysis is not subjected to any transversal loading, e.g., a typical frame column (Romão *et al*, 2010b). In the case of beams, which are usually also under the effect of gravity loading, the approximation introduced by Expression (2.9) will only produce acceptable results if the influence of such loading is small when compared to that of the earthquake loading. In situations where such influence is significant, two points of contraflexure may occur within the member length (instead of only one), raising questions on how to proceed. Further difficulties may arise in cases where there is no point of contraflexure within the member span, a situation typically found in columns and in short beams (Figure 2.34(a), (b) and (c), respectively). Under such conditions, the quantification of chord rotations following the EC8-3 (2005) procedure (i.e., where L_S is based on the *M/V* ratio) is difficult to enforce and may lead to inadequate results.

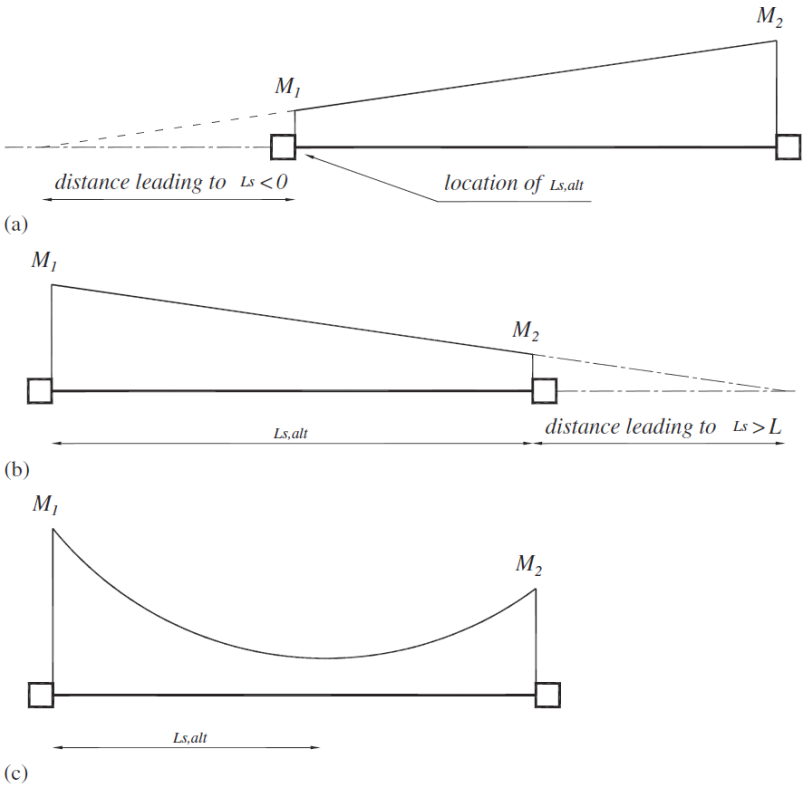

Figure 2.34 – Examples of moment diagrams causing difficulties in the chord rotation evaluation – an alternative definition for L_S is necessary to address such cases (adapted from Romão *et al*, 2010b)

The adequate evaluation of the chord rotation demand can thus be seen to depend on a suitable definition for the shear span L_S. Several alternative approaches aiming to overcome the referred difficulties can be found in the work of Romão *et al* (2010b), as well as an extensive assessment of their effectiveness and recommendations for their practical use. Some of the proposed methods define alternative interpretations for the value of the shear span L_S, enabling the application of the above-described procedure in the presence of the referred difficulties. Others define alternative chord rotation evaluation methods that do not require the quantification of L_S. From the latter, the *approximate geometrical method that considers member drift and nodal rotations for beams and columns (AGM-DR)* is recommended by the authors, since it exhibited the best overall performance in columns and beams during the study. The AGM-DR is adapted from the displacement-deformation relationship under large displacements proposed in Filippou and Fenves (2004) for frame elements and has the advantage of being straightforward to compute after running pushover or dynamic analyses (post-processing stage), provided the nodal displacements are stored at each step. Figure 2.33(c) helps to understand the approximations introduced by this method, as it shows a particular chord rotation example in which $\theta_{1a} = \theta_{2a}$. Under that assumption, those components of the chord rotation can be obtained without evaluating L_S by:

$$\theta_{1a} = \theta_{2a} = \frac{d_y}{L} \tag{2.10}$$

where d_y represents the relative transversal displacement of sections 1 and 2, neglecting the contribution of the axial deformation of the member (Filippou and Fenves, 2004). Assuming these approximations for θ_{1a} and θ_{2a}, the chord rotation demands can be calculated without further difficulties by the following expressions, where θ_{1b} and θ_{2b} represent the nodal rotations at sections 1 and 2, as previously referred (see Figure 2.33(b)).

$$\theta_1 = \theta_{1a} - \theta_{1b} \tag{2.11}$$

$$\theta_2 = \theta_{2a} - \theta_{2b} \tag{2.12}$$

Once the demands D_i have been evaluated, the respective capacity values C_i are required to perform the safety verifications (in terms of *D/C* ratios, as previously referred) for both ductile and brittle mechanisms. Annex A of EC8-3 (2005) contains specific information on capacity models for the assessment and strengthening (when necessary) of existing RC buildings (only a few models for strengthening are included, though, with relatively scarce information). However, prior to calculating the capacity values C_i of each structural member for the different LS's involved in the analysis of a specific building, several aspects should be carefully examined in order to define the appropriate KL (hence, the CF), as previously discussed. Ductile mechanisms can then be checked in terms of deformations, with the respective capacity values C_i computed using mean values of mechanical properties divided by the CF. On the other hand, brittle mechanisms should be checked in terms of

strength, with the respective capacity values C_i computed using mean values of mechanical properties divided by both the usual partial safety factor and by the CF (Romão *et al*, 2010a). The expressions given in Annex A of EC8-3 (2005) are reviewed below in detail. The associated classification of RC structural members / mechanisms is the following:

i. Ductile: beams, columns, and walls under flexure, with or without axial force;
ii. Brittle: shear mechanism of beams, columns, walls, and joints.

Ductile capacities are defined in terms of the admissible NC, SD, and DL member chord rotations, while brittle capacities are characterized by the admissible NC shear force. For the quantification of the NC total chord rotation capacity (elastic plus inelastic part) θ_{NC}, the following empirical expression is proposed (Panagiotakos and Fardis, 2001):

$$\theta_{NC} = \frac{1}{\gamma_{el}} \cdot 0.016 \cdot 0.3^{\upsilon} \cdot \left[\frac{\max(0.01;\omega')}{\max(0.01;\omega)} \cdot f_c\right]^{0.225} \cdot \left[\min\left(9;\frac{L_S}{h}\right)\right]^{0.35} \cdot 25^{\left(\alpha \cdot \rho_{sx} \cdot \frac{f_{yw}}{f_c}\right)} \cdot 1.25^{100 \cdot \rho_d} \quad (2.13)$$

where γ_{el} is equal to 1.5 for primary seismic elements and to 1.0 for secondary ones, $\upsilon = N/(b \cdot h \cdot f_c)$ is the normalized axial force (N is the axial force, positive for compression, b is the width of the compression zone, h is the depth of the cross-section, f_c is the estimated value of the concrete compressive strength in *MPa*), ω and ω' are the mechanical reinforcement ratios of the tension and compression, respectively, longitudinal reinforcement, L_S is the moment-to-shear ratio at the end section (as previously defined in Expression (2.9)), $\rho_{sx} = A_{sx}/(b_w \cdot s_h)$ is the ratio of transverse steel area A_{sx} parallel to the direction x of loading (s_h is the stirrup spacing and b_w is the shear web width), f_{yw} is the estimated value of the stirrup yield strength in *MPa,* ρ_d is the steel ratio of diagonal reinforcement (if any) in each diagonal direction and α is the confinement effectiveness ratio as given in the following expression:

$$\alpha = \left(1 - \frac{s_h}{2 \cdot b_0}\right) \cdot \left(1 - \frac{s_h}{2 \cdot h_0}\right) \cdot \left(1 - \frac{\sum b_i^2}{6 \cdot h_0 \cdot b_0}\right) \quad (2.14)$$

where b_0 and h_0 are the dimensions of the confined concrete core to the centreline of the hoop and b_i is the centreline spacing of longitudinal bars (indexed by *i*) laterally restrained by a stirrup corner or a cross-tie along the perimeter of the cross-section. The value of the plastic part of the NC chord rotation capacity θ_{NC}^{pl} may be calculated from the following expressions:

$$\theta_{NC}^{pl} = \frac{1}{\gamma_{el}} \cdot 0.0145 \cdot 0.25^{\upsilon} \cdot \left[\frac{\max(0.01;\omega')}{\max(0.01;\omega)}\right]^{0.3} \cdot f_c^{0.2} \cdot \left[\min\left(9;\frac{L_S}{h}\right)\right]^{0.35} \cdot 25^{\left(\alpha \cdot \rho_{sx} \cdot \frac{f_{yw}}{f_c}\right)} \cdot 1.275^{100 \cdot \rho_d} \quad (2.15)$$

$$\theta_{NC}^{pl} = \theta_{NC} - \theta_y \quad (2.15a)$$

where γ_{el} is equal to 1.8 for primary seismic elements and to 1.0 for secondary ones, θ_y should be calculated according to expressions (2.16) given below and all other variables are defined as for Expression (2.13). If expressions (2.13) and (2.15) are applied to members without detailing for earthquake resistance, the obtained values should be divided by 1.2. Additional corrective factors are available in Annex A of EC8-3 (2005) to consider the existence of reinforcement lap splices at the ends of the members and / or the use of smooth (plain) longitudinal bars. The SD chord rotation capacity θ_{SD} is assumed to be $3/4$ of the ultimate chord rotation capacity θ_{NC}. For the quantification of the DL chord rotation capacity θ_{DL}, the following (equivalent) expressions are proposed (for this LS, the corresponding capacity is given by the chord rotation at yielding θ_y):

$$\theta_{DL} = \theta_y = \phi_y \cdot \frac{L_S + \alpha_v \cdot z}{3} + 0.0014 \cdot \left(1 + 1.5 \cdot \frac{h}{L_S}\right) + \frac{\varepsilon_{sy}}{d - d'} \cdot \frac{d_{bL} \cdot f_y}{6 \cdot \sqrt{f_c}} \quad (2.16a)$$

$$\theta_{DL} = \theta_y = \phi_y \cdot \frac{L_S + \alpha_v \cdot z}{3} + 0.0014 \cdot \left(1 + 1.5 \cdot \frac{h}{L_S}\right) + \phi_y \cdot \frac{d_{bL} \cdot f_y}{8 \cdot \sqrt{f_c}} \quad (2.16b)$$

where the first term accounts for the flexural contribution, the second one represents the contribution of the shear deformation and the third one accounts for the anchorage slip of longitudinal bars. ϕ_y is the yield curvature of the end section, $\alpha_v \cdot z$ is the tension shift of the bending moment diagram, as defined in EC2-1-1 (2004), z is the length of the internal lever arm (taken equal to $d - d'$, where d and d' are the depths of the tension and compression reinforcement, respectively), d_{bL} is the mean diameter of the tension reinforcement, f_y is the estimated value of the longitudinal reinforcement yield strength in *MPa* and $\varepsilon_{sy} = f_y / E_s$. If shear cracking is expected to precede flexural yielding at the end section (i.e. when the yield moment at the end section, M_y, exceeds the product of L_S times the shear resistance of the member taken without shear reinforcement, $V_{Rd,c}$, according to EC2-1-1, 2004), then $\alpha_v = 1$; otherwise $\alpha_v = 0$. Finally, if the longitudinal reinforcement of a member is asymmetric, all these chord rotation capacities need to be computed for both bending signs.

Concerning the evaluation of the yield curvature ϕ_y, this can be done theoretically (considering either the permanent axial load due only to gravity loads or the variable axial load due to the seismic load combination) but the process to do so is complex and laborious. However, available experimental results (Priestley, 2003) showed that ϕ_y is essentially sensitive to the cross-section's depth h and to the yielding strain of the longitudinal tensile steel ε_{sy}. Other parameters (such as the amount of longitudinal reinforcement, the $\sigma - \varepsilon$ law of concrete or the amount of axial load) do not influence much the value of ϕ_y, though they affect the value of the yield moment M_y and, therefore, the secant stiffness at yielding. A set of empirical expressions ((2.17) to (2.19)) was then proposed by Priestley (2003) for the simplified computation of ϕ_y, while Biskinis (2006) later proposed an alternative expression ((2.20)), valid for both columns and beams. Mpampatsikos *et al* (2008) tested the results yielded by these expressions on several case study structures against those given by the theoretical approach and deemed them as acceptable.

(Priestley, 2003) for rectangular beams: $\phi_y = 1.87 \cdot \frac{\varepsilon_{sy}}{h}$ (2.17)

(Priestley, 2003) for T-section beams: $\phi_y = 1.7 \cdot \frac{\varepsilon_{sy}}{h}$ (2.18)

(Priestley, 2003) for columns: $\phi_y = 2.1 \cdot \frac{\varepsilon_{sy}}{h}$ (2.19)

(Biskinis, 2006) for columns and beams: $\phi_y = 1.75 \cdot \frac{\varepsilon_{sy}}{h}$ (2.20)

Concerning the calculation of demands for the LS of DL, Annex A of EC8-3 (2005) states that, unless the used calculation model is a fully nonlinear one, deformation demands should be obtained with a numerical model where the stiffness of members is simulated as the average effective (secant-to-yield) stiffness K_{eff} given by:

$$K_{eff} = \frac{1}{4} \cdot \left(\frac{M_{y,1}^{+}}{3 \cdot \theta_{y,1}^{+}} \cdot L_{S,1}^{+} + \frac{M_{y,1}^{-}}{3 \cdot \theta_{y,1}^{-}} \cdot L_{S,1}^{-} + \frac{M_{y,2}^{+}}{3 \cdot \theta_{y,2}^{+}} \cdot L_{S,2}^{+} + \frac{M_{y,2}^{-}}{3 \cdot \theta_{y,2}^{-}} \cdot L_{S,2}^{-} \right) \quad (2.21)$$

where the indexes 1 and 2 refer to the two end sections of the member and the apexes + and – refer to positive and negative bending, respectively. In this calculation, L_S may be taken to be equal to half the member's length. In columns, the consideration of K_{eff} according to Expression (2.21) presents no difficulties, assuming that top and bottom reinforcement are equal in both end sections and considering that the axial load N necessary for the computation of M_y can be set to the value associated with gravity loads only (Mpampatsikos *et al*, 2008). On the other hand, the application of Expression (2.21) to beams may lead to inadequate structural behaviour results, given that the top and bottom reinforcement of an end section may be different. The corresponding values of M_y and θ_y can lead to considerably different values of positive and negative bending secant-to-yield stiffnesses that may even be excessively low to adequately represent the behaviour of the member. Hence, this matter should be handled with caution.

Lastly on the quantification of ductile capacities, Annex A of EC8-3 (2005) offers an alternative expression for the quantification of the NC total chord rotation capacity θ_{NC}, based on theoretical assumptions, that divides the overall curvature into two contributions: (i) elastic curvature, which grows linearly from zero at the free end of the equivalent cantilever to ϕ_y at the fixed end of the equivalent cantilever; (ii) plastic curvature ($\phi_u - \phi_y$), constant over a length L_{pl}, called "plastic hinge length". Consequently, the ultimate chord rotation capacity is evaluated as the sum of an elastic part, due to the elastic curvature, plus a plastic part, due to the constant plastic curvature developed over the plastic hinge length. However, this complex and long to be applied theoretical formulation is expected to yield results close to those given by the above-described empirical expressions, since the code allows the use of both approaches indifferently. The complete details on this formulation will not be developed further here but can be found in the work of Mpampatsikos *et al* (2008).

For the quantification of the admissible shear force, Annex A of EC8-3 (2005) considers the effects of both cyclic loading and inelastic response by decreasing the shear strength with the increase of the cyclic inelastic deformations. As the chord rotation is considered the most meaningful deformation quantity at the member's level, the NC shear force capacity V_{NC} is assumed a function of the plastic part of the chord rotation ductility demand $\theta_{dem}^{pl} = \theta_{dem} - \theta_y$. The following expression is proposed (Fardis and Biskinis, 2003):

$$V_{NC} = \frac{1}{\gamma_{el}} \cdot \left[\frac{h-x}{2 \cdot L_S} \cdot \min(N; 0.55 \cdot A_c \cdot f_c) + \left(1 - 0.05 \cdot \min\left(5; \mu_\Delta^{pl}\right)\right) \cdot \right. \\ \left. \cdot \left(0.16 \cdot \max(0.5; 100 \cdot \rho_{tot}) \cdot \left(1 - 0.16 \cdot \min\left(5; \frac{L_S}{h}\right)\right) \cdot \sqrt{f_c} \cdot A_c + V_w\right)\right] \quad (2.22)$$

where γ_{el} is equal to 1.15 for primary seismic elements and to 1.0 for secondary ones, x is the compression zone depth, N is the compressive axial force (positive, equal to zero for tension), $A_c = b_w \cdot d$ is the cross-section area (b_w is the width of the rectangular web and d is the structural depth), $\mu_\Delta^{pl} = \left(\theta_{dem} - \theta_y\right)/\theta_y$ is the ratio between the plastic part of the chord rotation demand and the yield chord rotation, ρ_{tot} is the total longitudinal reinforcement ratio and V_w is the contribution of transverse reinforcement to shear resistance given by:

$$V_w = \rho_w \cdot b_w \cdot z \cdot f_{yw} \quad (2.23)$$

where ρ_w is the transverse reinforcement ratio and z is the previously defined length of the internal lever arm. For the computation of Expression (2.22), N should be taken as the member's compressive axial force under gravity loads, as suggested by Mpampatsikos *et al* (2008) and the term $(h - x)$, representing the distance between the member's compression centres, should be assumed equal to $2 \cdot h/3$, as suggested by Romão *et al* (2010a). Even though shear failure is considered a brittle mechanism, the underlying idea of Expression (2.22) is that two distinct types of failure may occur (Mpampatsikos *et al*, 2008):

i. "Brittle shear" – ultimate shear failure occurs before flexural yielding, at relatively low deformations, associated with a large drop in lateral load resistance. Numerically, this happens when the shear force $V_y = M_y/L_S$ corresponding to the flexural yielding is higher than the elastic shear resistance $V_{NC,0}$ (determined according to Expression (2.22) with $\mu_\Delta^{pl} = 0$);
ii. "Ductile shear" – members may first yield in flexure but at the end fail showing strong and clear shear effects, like wide inclined cracks, while the peak force resistance experiences a gradual drop with cycling. V_y is smaller than $V_{NC,0}$ but higher than the inelastic shear resistance V_{NC} computed through Expression (2.22).

Expression (2.22) can be applied to beams or slender columns, but it should be noticed that it refers only to diagonal tension failure. If in a concrete column the shear span ratio L_S/h at the end section with the maximum of the two end moments is less or equal to 2.0, its shear strength V_{NC} should not

be taken greater than the value $V_{NC,max}$ corresponding to the failure by web crushing along the diagonal of the column after flexural yielding. The following empirical expression is proposed for the computation of $V_{NC,max}$:

$$V_{NC,max} = \frac{{}^{4}/_{7} \cdot \left(1 - 0.02 \cdot \min\left(5; \mu_{\Delta}^{pl}\right)\right)}{\gamma_{el}} \cdot \left(1 + 1.35 \cdot \frac{N}{A_c \cdot f_c}\right) \cdot \left(1 + 0.45 \cdot (100 \cdot \rho_{tot})\right) \cdot \cdot \left(\sqrt{\min(40; f_c)} \cdot b_w \cdot z \cdot \sin(2 \cdot \delta)\right) \quad (2.24)$$

where $\delta = \arctan(h/(2 \cdot L_S))$ is the angle between the diagonal strut and the axis of the column and all other variables are as defined as for Expression (2.22). Lastly on the quantification of brittle capacities, the shear capacity values obtained with expressions (2.22) and (2.24) should be compared with those determined in accordance with the provisions of EC2-1-1 (2004). The minimum value should then be used in the seismic assessment of the structure under analysis.

The above presented capacity models of both ductile and brittle mechanisms can be seen to be a function not only of the geometrical and mechanical properties of the structural members, but also of demand-related parameters. This consideration is important for existing structures, especially for those lacking relevant earthquake-design provisions, because no failure modes can be excluded *a-priori,* neither degradation effects may be disregarded (not the case for new structures because up-to-date seismic design codes include provisions that guarantee the location and type of the failure mechanisms, protecting them from brittle failures or unforeseen collapse modes). Thus, capacity values may change from one analysis to the other, making this approach computationally intensive and time-consuming. Mpampatsikos *et al* (2008), however, investigated the possibility of simplifying the procedure by attempting to eliminate the referred demand-capacity coupling. Some of the proposed simplifications were already referred along the above-written text but, nonetheless, the full set is summarized here below:

- to consider constant the axial force N on columns, by using the value obtained from gravity loads, instead of considering a more relevant value that varies during the analysis;
- to compute the yield curvature ϕ_y with the empirical expressions proposed by Priestley (2003) or Biskinis (2006) instead of considering its theoretical evaluation procedure;
- to consider the shear span L_S constant and equal to half the member's length instead of the varying moment-to-shear ratio at the end section.

Based on the results of the conducted sensitivity analyses, the authors deemed the proposed approximations capable of yielding results with acceptable accuracy. The computation of the capacities of both ductile and brittle mechanisms for the LS's of NC, SD and DL can thus be carried out more swiftly, as the only calculation parameter that remains depending on demand is $\mu_{\Delta}^{pl} = \left(\theta_{dem} - \theta_y\right)/\theta_y$ in Expression (2.22). However, Romão *et al* (2010b) conducted a similar study and did not validate the general use of $L_S = L/2$ as proposed by Mpampatsikos *et al* (2008). Despite the acceptable (conservative) results obtained for the shear capacity model, the study indicates that L_S should be computed for an adequate application of the deformation capacity models. Nonetheless,

since the evolution of θ_{NC} according to Expression (2.13) may lead to inconsistent results for small values of L_S, the validity of the obtained results in this domain should be examined.

2.7.2. Seismic demand definition

Depending on the selected analysis method, the effective seismic demand needs to be defined in different ways. In structural design codes (e.g., EC8-1, 2004), the most common representation of the seismic action is through the response spectrum of an elastic single degree of freedom (SDOF) oscillator with a viscous damping ratio of 5% of critical. Hence, in order to maintain coherence across analysis methods (an important matter, as seen before), any alternative representation should conform on average with the 5% damped elastic response spectrum representing the seismic hazard scenario under consideration (Deierlein *et al*, 2010).

When nonlinear static analysis is selected, the seismic demand is usually characterized by a set of target displacements, defined for each peak ground acceleration (PGA) value and for each of the considered force or displacement patterns (e.g., modal or uniform). These displacements can be determined through simplified methods, usually referred to as Nonlinear Static Procedures (NSP's), which combine the pushover analysis of a relatively simple mathematical model with the response spectrum approach (Sousa *et al,* 2012). In general terms, the capacity curve of the multi-degree of freedom (MDOF) structure is transformed into an equivalent SDOF curve to allow the superimposition with a response spectrum. The seismic performance is then estimated, for the LS of interest, by "intersecting" the capacity curve of the structure with the reduced response spectrum, based on its inherent energy dissipation. EC8-3 (2005) recommends one specific NSP, but several other (more sophisticated) proposals are available in the applicable literature and recourse to such methods is explicitly allowed by the note in paragraph 4.4.4.5 (2). Some of the most popular options are briefly addressed in the following sub-section. Further information on these methods and a comparison of their performance on several case studies can be found in the work of Sousa *et al* (2011), Bhatt and Bento (2012), and others.

On the other hand, if nonlinear dynamic analysis is to be performed, acceleration records (time-histories) of the ground motion are necessary to evaluate the structural demands. These record sets may be obtained either from real earthquake events or artificially simulated, although preference is given to the former since they contain a realistic variety of frequency content, intensity, and duration (Fardis, 2009; Araújo *et al*, 2016). Design codes establish criteria for the selection and scaling of the chosen record set according to the defined target spectrum, as well as recommend the minimum number of records that should compose each set. EC8-1 (2004), for instance, imposes a minimum of three ground motion records. However, at least seven need to be considered so that the mean response of a given parameter can be taken as a valid result. Otherwise, the maximum response for that parameter, obtained among all within the set, should be considered. Nonetheless, this issue is still far from being consensual within the scientific community and, as such, will be further discussed in sub-section 2.7.2.2.

2.7.2.1. Target displacement computation for nonlinear static analysis

NSP's for seismic analysis were firstly introduced by Freeman *et al* (1975) with the development of the "Capacity Spectrum Method" (CSM). This method advocates a force-based non-adaptive conventional pushover using a first mode proportional load pattern, and graphically compares the global force-displacement (V vs. Δ_R) capacity curve of a structure with an earthquake response spectrum. In order for the capacity curve to be directly comparable to the demand spectrum plotted in acceleration-displacement response spectrum (ADRS) format, it is converted to the same set of spectral coordinates (S_a vs. S_d), using the dynamic characteristics of the first mode to represent the structure as an equivalent linear SDOF oscillator. In this format, period can be represented as radial lines emanating from the origin and increasing clockwise. Figure 2.35 shows the graphical representation of the CSM as presented in the FEMA 440 (2005) guidelines for NSP's. To find the so-called "structural performance point" (PP), one must determine a spectral displacement along the capacity curve, which is consistent with the seismic demand. As such, the PP must simultaneously lie: (i) on the capacity spectrum curve, in order to represent the structure at a given displacement and (ii) on a spectral demand curve, reduced from the 5% damped elastic spectrum in order to represent the nonlinear demand at the same displacement (i.e., on a higher damped response spectrum that takes into account the hysteretic nonlinear response of the structure).

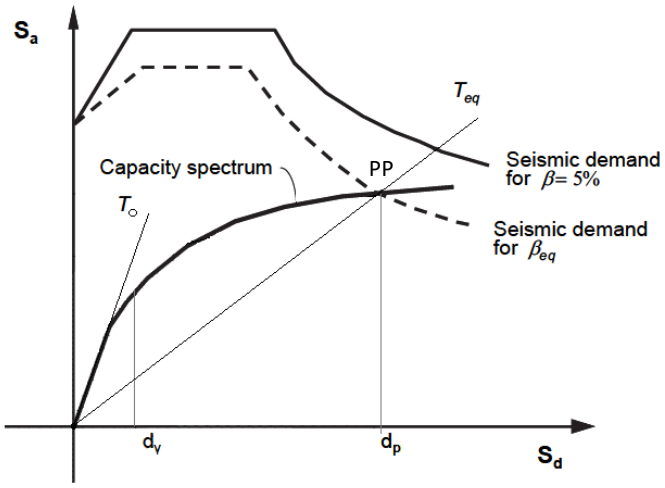

Figure 2.35 – Capacity Spectrum Method of equivalent linearization (adapted from FEMA 440, 2005)

The basic assumption in equivalent linearization (an approximate technique for solving nonlinear differential equations) is that the maximum deformation of a nonlinear SDOF system can be approximated from that of an equivalent linear elastic SDOF system, with period and damping ratio larger than the initial values of those for the nonlinear system. These are commonly referred to as equivalent period (T_{eq}) and equivalent damping ratio (β_{eq}), respectively. The equivalent period is computed as a function of the nonlinear system's initial period of vibration T_0 and maximum displacement ductility ratio μ_Δ, the latter being defined as the ratio of the maximum displacement d_p to the yield displacement d_y. Similarly, the equivalent damping ratio is computed as a function of the

nonlinear system's initial elastic viscous damping ratio β (e.g., 5%) and maximum displacement ductility ratio μ_Δ. The main differences among the many equivalent linear methods that are available in the literature stem primarily from the functions used to compute T_{eq} and β_{eq}. However, a common property is that all require prior knowledge of μ_Δ, which is not initially known when assessing an existing structure. Consequently, an iterative or graphical procedure is required in order to determine the above-referred structural performance point PP. The first step is the conversion of the V vs. Δ_R capacity curve to the S_a vs. S_d capacity spectrum, which is carried out based on the dynamic characteristics of the first vibration mode, as previously referred. The following expressions apply (Freeman, 1998; FEMA 440, 2005):

$$S_a = \frac{V}{g \cdot \sum m_i} \cdot \frac{1}{\alpha_1} \tag{2.25}$$

$$S_d = \frac{1}{PF1} \cdot \frac{\Delta_R}{\phi_{R,1}} \tag{2.26}$$

$$\alpha_1 = \frac{1}{\sum m_i} \cdot \frac{(\sum m_i \cdot \phi_{i,1})^2}{\sum m_i \cdot {\phi_{i,1}}^2} \tag{2.27}$$

$$PF1 = \frac{\sum m_i \cdot \phi_{i,1}}{\sum m_i \cdot {\phi_{i,1}}^2} \tag{2.28}$$

where V and Δ_R are, respectively, the base shear force and top displacement of the MDOF system; m_i is the mass of the i^{th} storey; $\phi_{i,1}$ and $\phi_{R,1}$ are, respectively, the amplitude of the first mode at level i and at top level; α_1 and $PF1$ are, respectively, the modal mass coefficient and the modal participation factor for the first mode; S_a and S_d are, respectively, the spectral acceleration and the spectral displacement of the equivalent SDOF system. The effective modal mass $m_e = \alpha_1 \cdot \sum m_i$ of the latter can also be expressed as the following ratio:

$$m_e = \frac{(\sum m_i \cdot \phi_{i,1})^2}{\sum m_i \cdot {\phi_{i,1}}^2} = \frac{{L_n}^2}{M_n} \tag{2.29}$$

where L_n and M_n are, respectively, the modal excitation factor and the generalised modal mass for the first mode. Finally, the secant period T at each point along the S_a vs. S_d capacity spectrum can be calculated by Expression (2.30).

$$T = 2 \cdot \pi \cdot \sqrt{\frac{S_d}{S_a \cdot g}} \tag{2.30}$$

Once the capacity spectrum has been obtained, the demand spectrum should then be plotted in ADRS format for several levels of damping. For any point of the acceleration response spectrum (given a damping ratio), the corresponding spectral displacement can be computed through Expression (2.31), which is no more than a rearrangement of Expression (2.30). The 5% damped spectrum generally represents the demand while the structure is still responding within its linear-elastic range. The higher damped spectra (each obtained for a different level of β_{eq}) are used to represent inelastic response spectra that account for the hysteretic nonlinear response of the structure when subjected to the earthquake ground motion.

$$S_d = \frac{1}{4 \cdot \pi^2} \cdot S_a \cdot g \cdot T^2 \tag{2.31}$$

As stated before, the equivalent damping β_{eq} associated with each of the higher damped spectra is computed as a function of the elastic viscous damping β and expected value of the structure's displacement ductility μ_Δ (see Expression (2.32) below, where β_{hyst} represents the hysteretic damping). The concept of equivalent viscous damping (EVD) was first proposed by Jacobsen (1930) to obtain approximate solutions for the steady forced vibration of damped SDOF systems, with linear force-displacement relationships but with damping forces proportional to the n^{th} power of the velocity of motion, when subjected to sinusoidal forces. Years later, the same author extended the concept of EVD to yielding SDOF systems (Jacobsen, 1960). Since then, many methods have been proposed in the literature. The approach adopted by Priestley *et al* (2007), for instance, is to use values of EVD that have been calibrated for different hysteresis rules to give the same peak displacements as the hysteretic response, using inelastic time-history analysis. For a full discussion of the development of methods relating EVD to ductility, the interested reader is referred to Dwairi *et al* (2007).

$$\beta_{eq} = \beta + \beta_{hyst}\,(\mu_\Delta) \tag{2.32}$$

Having both the capacity spectrum and the demand spectra defined with the same set of spectral coordinates, they can now be plotted together. For this purpose, it is useful to approximate an equivalent bilinear capacity spectrum representation that establishes an effective yield point ($\mu_\Delta = 1$) and an effective peak inelastic limit ($\mu_\Delta = d_{max}/d_y$, where d_{max} represents the inelastic limit of the pushover analysis). If the elastic limit of the capacity curve does not reach the 5% damped demand spectrum, the elastic demand exceeds the elastic capacity, and the structure will displace into the inelastic range. If the inelastic branch of the capacity curve can extend through the envelope of the demand spectra, the building survives the earthquake (Freeman, 1998). The performance point PP (and corresponding target displacement d_p) representing the inelastic response of the equivalent SDOF system is defined by the intersection of the capacity curve with the appropriately damped demand spectrum (i.e., the demand spectrum associated with the equivalent damping ratio β_{eq} given by the displacement ductility ratio $\mu_\Delta = d_p/d_y$).

One of the attributes that makes the CSM appealing is its intuitive nature. It is relatively straightforward to think of an earthquake as presenting a demand on a structure and the structure as possessing a certain capacity to resist this demand. When capacity and maximum demand are equal, the system is considered in a state of "equilibrium" that defines the expected performance of the structure (FEMA 440, 2005). The use of effective or equivalent linear parameters is also appealing from an intuitive point of view. First, it seems reasonable that the period of a structure lengthens as the latter loses stiffness. Second, it seems logical that inelastic behaviour and damage produce increased damping (hence, reduction of the seismic demand for increasing displacement). Moreover, the graphical representation provides a clear picture on how a building responds to earthquake ground motion, making it a powerful tool to evaluate how various retrofitting techniques, such as adding stiffness, strength, or damping, will impact its response capacity (ATC-40, 1996).

An alternative NSP was later proposed by Fajfar and Fischinger (1988): the "N2 method", which is currently recommended by EC8-3 (2005). Although originally devised for planar, single mode dominated structures, this method was later adapted (Fajfar *et al,* 2005) in order to account for the plan asymmetry of buildings (usually referred to as the "Extended N2 method"). Same as the CSM, it uses a force-based non-adaptive conventional pushover to estimate the V vs. Δ_R capacity curve of the structure and then estimates its performance, for a given seismic hazard, using an elastic response spectrum. According to EC8-3 (2005), by referring to EC8-1 (2004), a least two lateral load patterns should be used: (i) first mode proportional and (ii) uniform. The computation of the target displacement for the MDOF system then requires the transformation of its capacity curve into an idealized elastic-perfectly plastic curve, based on the equal energy assumption between both curves. However, this transformation should be applied to the capacity curve of an equivalent SDOF oscillator (a mathematical option that relates very well to the definition of seismic demand in terms of spectral quantities, as discussed above). A key feature for this transformation is the plastic mechanism point, that EC8-3 (2005) defines as the point of the capacity curve that corresponds to the formation of the plastic mechanism of the structure (Fardis, 2009; Romão, 2012) (Figure 2.36).

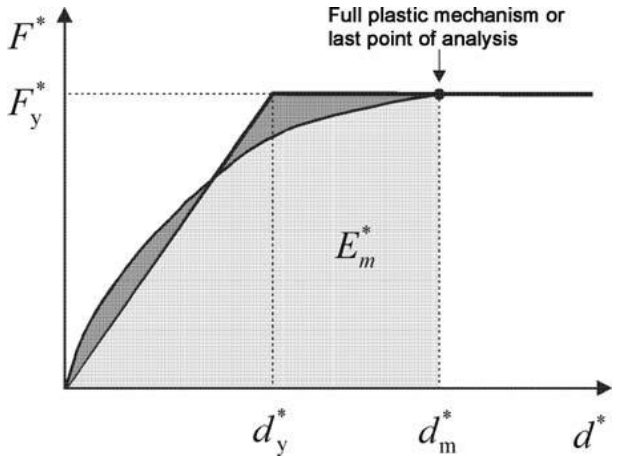

Figure 2.36 – Elastic-perfectly plastic idealization of the capacity curve of the equivalent SDOF system (EC8-1, 2004)

As referred by Romão *et al* (2010a), EC8-3 (2005) does not discuss further the definition of "plastic mechanism" or the criteria driving its definition (e.g., a global demand parameter, such as the maximum inter-storey drift; a local demand parameter, such as a maximum ductility demand in a member; a combination of local demand parameters, such as the formation of a given number of plastic hinges). In some cases, depending on the numerical modelling assumptions, it is possible to define visually that the plastic mechanism occurs when the capacity curve tends to become horizontal. However, this approximation may reveal itself impossible or inadequate in situations where, for instance, the structure is significantly sensitive to second order effects. Some engineering judgement is thus required to define this point, mainly because the N2 method yields target displacements that are sensitive to this initial definition. In order to deal with this difficulty, EC8-1 (2004) proposes an (optional) iterative procedure which can compute the same target displacements irrespective of the initially defined plastic mechanism point. Therefore, by applying this procedure, the initial guess becomes irrelevant, even when points corresponding to elastic behaviour of the structure are selected (Romão, 2012). The steps of both procedures are summarized below, according to what is described in Annex B of EC8-1 (2004):

(1) Transformation to an equivalent SDOF system:

$$m^* = \sum m_i \cdot \phi_i = \sum \bar{F}_i \tag{2.33}$$

$$\Gamma = \frac{m^*}{\sum m_i \cdot \phi_i^2} = \frac{\sum \bar{F}_i}{\sum \left(\frac{\bar{F}_i^2}{m_i}\right)} \tag{2.34}$$

$$F^* = \frac{F_b}{\Gamma} \tag{2.35}$$

$$d^* = \frac{d_n}{\Gamma} \tag{2.36}$$

where m^* is the mass of the equivalent SDOF system; m_i is the mass of the i^{th} storey; ϕ_i are the normalized displacements ($\phi_n = 1$, where n is the control node); $\bar{F}_i$ are the normalized lateral forces; Γ is the transformation factor; F^* and d^* are, respectively, the force and displacement of the equivalent SDOF system; F_b and d_n are, respectively, the base shear force and the control node displacement of the MDOF system;

(2) Determination of the idealized elastic-perfectly plastic force-displacement relationship:

$$d_y{}^* = 2 \cdot \left(d_m{}^* - \frac{E_m{}^*}{F_y{}^*}\right) \tag{2.37}$$

where $d_y{}^*$ and $d_m{}^*$ are, respectively, the yield displacement and the displacement at the formation of the plastic mechanism of the idealized SDOF system; $F_y{}^*$ is the base shear force at the formation of the plastic mechanism of the idealized SDOF system and $E_m{}^*$ is the actual

deformation energy up to the formation of the plastic mechanism – the initial stiffness K^* of the idealized system is determined in such a way that the areas under the actual and the idealized force-deformation curves are equal (see Figure 2.36);

(3) Determination of the period of the idealized equivalent SDOF system:

$$T^* = 2\pi \cdot \sqrt{\frac{m^* \cdot {d_y}^*}{{F_y}^*}} = 2\pi \cdot \sqrt{\frac{m^*}{K^*}} \tag{2.38}$$

where T^* is the period of the idealized equivalent SDOF system;

(4) Determination of the target displacement for the equivalent SDOF system:

$${d_{et}}^* = S_e(T^*) \cdot \left[\frac{T^*}{2\pi}\right]^2 \tag{2.39}$$

where ${d_{et}}^*$ is the target displacement of the structure with period T^* and unlimited elastic behaviour and $S_e(T^*)$ is the elastic acceleration response spectrum at period T^*; for the determination of the target displacement ${d_t}^*$, different expressions (given below) must be used depending on the structure being in the short or in the medium and long period ranges; the transition (corner) period T_C between the short and medium period ranges is defined in paragraph 3.2.2.2 of EC8-1 (2004);

a) $T^* < T_C$ (short period range):

If ${F_y}^*/m^* \geq S_e(T^*)$, the response is elastic and thus

$${d_t}^* = {d_{et}}^* \tag{2.40}$$

If ${F_y}^*/m^* < S_e(T^*)$, the response is nonlinear and

$${d_t}^* = \frac{{d_{et}}^*}{q_u} \cdot \left(1 + (q_u - 1) \cdot \frac{T_C}{T^*}\right) \geq {d_{et}}^* \quad \wedge \quad {d_t}^* \leq 3 \cdot {d_{et}}^* \tag{2.41}$$

$$q_u = \frac{S_e(T^*) \cdot m^*}{{F_y}^*} \tag{2.42}$$

where q_u is the ratio between the accelerations in the structure with unlimited elastic behaviour $S_e(T^*)$ and in the structure with limited strength ${F_y}^*/m^*$.

b) $T^* \geq T_C$ (medium and long period range):

$$d_t{}^* = d_{et}{}^* \tag{2.43}$$

(5) Determination of the target displacement of the MDOF system:

$$d_t = \Gamma \cdot d_t{}^* \tag{2.44}$$

where d_t is the target displacement of the MDOF system, corresponding to the displacement of the control node;

(6) Iterative procedure (optional):
If the target displacement $d_t{}^*$ determined in step 4 is much different than the displacement $d_m{}^*$ (see Figure 2.36) used in step 2 for the determination of the idealized elastic-perfectly plastic force-displacement relationship, an iterative procedure may be applied in which steps 2 to 4 are repeated by using $d_t{}^*$ (and the corresponding $F_y{}^*$), instead of $d_m{}^*$, in step 2. The procedure is then repeated until the desired tolerance between steps is achieved.

Concerning the determination of the target displacement for the equivalent SDOF system (step 4), the relation between different quantities can be visualized in Figure 2.37. The plots shown are in ADRS format, similarly to what is done in the CSM. Hence, period T^* is represented by the radial line emanating from the origin of the coordinate system to the point at the elastic response spectrum defined by coordinates $d_{et}{}^*$ and $S_e(T^*)$. This method considers the so-called "equal displacement approximation" – which states that the displacement of the inelastic system is the same as that of the equivalent system with elastic stiffness and unlimited strength – combined with a correction for the short period range. It is worth referring that the chosen target displacement should be the higher value obtained from the two pushover curves computed with the modal proportional and uniform load patterns, as required by EC8-1 (2004).

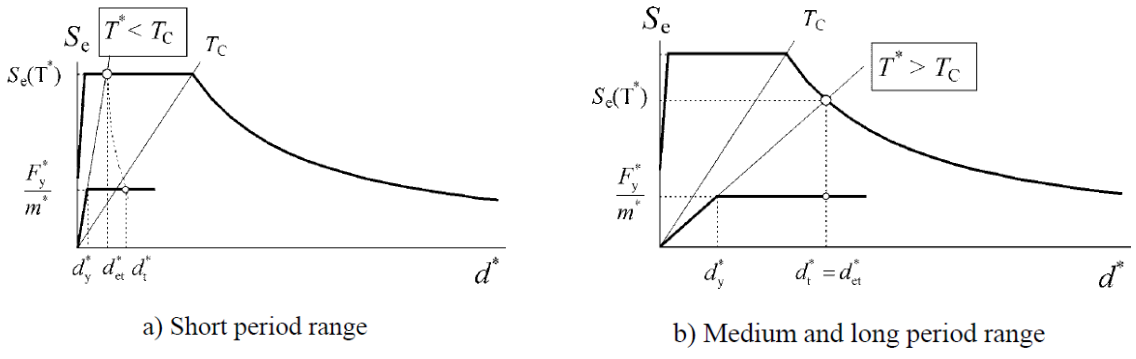

Figure 2.37 – Determination of the target displacement for the equivalent SDOF system (adapted from EC8-1, 2004)

For structures responding mainly in the first mode, conventional NSP's have proven to be a reliable option to estimate inelastic demands. However, when assessing 3D buildings that are irregular in plan, such methods are not able to provide completely reliable results. Demands on upper levels tend to be underestimated in mid- to high-rise structures (when compared to those provided by more sophisticated nonlinear dynamic analysis), which suggests an increasing relevance in the effect of the higher modes (Kunnath and Kalkan, 2004). To overcome this issue, several authors developed and proposed innovative procedures, such as the "Modal Pushover Analysis" (MPA) (Chopra and Goel, 2002; 2004), the "Adaptive Capacity Spectrum Method" (ACSM) (Casarotti and Pinho, 2007; Pinho *et al,* 2008) or the "Extended ACSM" (Bhatt, 2012), besides the previously referred "Extended N2 method", among others. A detailed discussion on the performance of these more sophisticated methods is beyond the scope of this document. Nonetheless, a short summary of their main characteristics is given below.

The MPA is essentially a nonlinear version of the Response Spectrum Analysis (RSA). Thus, it consists in running pushover analyses considering lateral load patterns proportional to the deformed shape of the most relevant dynamic modes of the structure. The total seismic response is then obtained combining individual mode responses according to an appropriate modal combination rule (e.g., SRSS or CQC). The Extended N2 method follows the same principles of the original method but conjugates the results from both nonlinear static analysis and elastic response spectrum analysis. The main difference consists in considering a set of torsional correction factors that are intended to "amplify" the torsional response obtained with pushover analysis. The ACSM is based on the concepts of the CSM but, instead of employing an invariant load pattern, it uses a displacement-based adaptive pushover (DAP) (see sub-section 2.6.2.). In its extended version, it combines the main philosophy followed by the ACSM with the contribution of torsional correction factors, similarly to the extended version of the N2 method. Conclusions on the comparative performance of these methods have been published by some authors. Readers are referred, for instance, to the works of Bhatt and Bento (2012) and Pinho *et al* (2013).

Finally, it is worth referring that the results obtained with NSP's should be conservative (i.e., close but never lower) in comparison to those obtained with nonlinear dynamic analysis, in order never to underestimate the structural response of the buildings under evaluation. The innovative procedures that incorporate torsional coefficients, such as the ones referred above, generally comply with this requirement. However, due to the increased complexity, one could say that their application seems to be too laborious and demanding for what is to be expected of an NSP. For instance, Baros and Anagnostopoulos (2008) stated that, despite sophisticated extensions of NSP´s to unsymmetrical buildings may be possible, it must be recalled that such methods were introduced as simple tools for checking potential weaknesses of new seismic designs and capacities of existing structures. Therefore, refining them to a degree that may not be justified by the underlying assumptions and making them more difficult to apply than nonlinear dynamic analysis itself is certainly not justified and ultimately defeats the purpose of using such procedures.

2.7.2.2. Selection of accelerograms for nonlinear dynamic analysis

Several scientific studies focusing on the influence of ground motion records on the structural response of buildings have concluded the latter to be highly dependent on the type of the former (i.e., artificial, real, or simulated), as well as on the methods used for their selection and scaling. This variability is recognized by current seismic codes which, by imposing a minimum number of records to be selected and scaled, aim at providing realistic estimates of mean seismic demands (Bradley, 2011; Araújo *et al*, 2016). Records should be selected according to the expected seismological characteristics (i.e., magnitude, source-to-site distance, rupture mechanism and soil profile) of the events that are more likely to hit the structure. This pre-selection is expected to provide unbiased mean seismic demand estimates, although results from several studies have shown no consensus (e.g., Krawinkler *et al*, 2003; Iervolino and Cornell, 2005). The amplitude of the applied scale factors and how it may change the intensity measures of the selected ground motion records, when compared to those expected for the considered seismic hazard scenario, has also been found to be a source of bias induced in the mean structural responses (Bradley, 2013). But again, no definitive conclusions on this issue were yet obtained within the scientific community. In addition to defining the minimum number of ground motion records to be used, EC8-1 (2004) specifies the following conditions concerning their selection and scaling for the demand-based assessment of buildings (see Figure 2.38):

i. The mean of the zero-period spectral response acceleration values calculated from the individual time-histories should not be smaller than the value of $a_g \cdot S$ for the site under study, being a_g the design ground acceleration on rock and S the soil parameter;
ii. In the range of periods between $0.20 \cdot T_1$ and $2.0 \cdot T_1$, where T_1 is the fundamental period of the structure in the direction where the record will be applied, no value of the mean 5% damping elastic spectrum, calculated from all time-histories, should be less than 90% of the corresponding value of the 5% damping elastic response spectrum.

Concerning the most adequate type of records, Iervolino *et al* (2008) referred that it appears to be easier to meet such conditions using artificial spectral-matching records or by numerically altering real recorded ones in order to reduce the spectral mismatch of the time series (see e.g., work by Hancock *et al*, 2006).

The above-referred lack of consensus on this matter is behind the different approaches proposed by other seismic codes, like the American Standard ASCE 41-13 (2014) or the New Zealand Standard NZS 1170.5 (2004) (Araújo *et al*, 2016). However, further improvement of such methods is required in order to tackle several important deficiencies that have been identified by recent studies (e.g., Beyer and Bommer, 2007; Sextos *et al*, 2011; Araújo and Castro, 2017). The fact that the seismic response variability is addressed in a deterministic manner is, by itself, a controversial issue. As pointed out by Bradley (2011), it is not clear what the likelihood is of the maximum of three seismic responses, or the mean of seven or more, to be below the "true" mean seismic response. Moreover, no explicit guidance is given on how the mean seismic response is affected by the number of records or by the mismatch between the spectra of the individual records and the target spectrum. Additionally, no reference is made to the fact that some engineering demand parameters are significantly more sensitive than others to the input ground motions (Krawinkler *et al*, 2003).

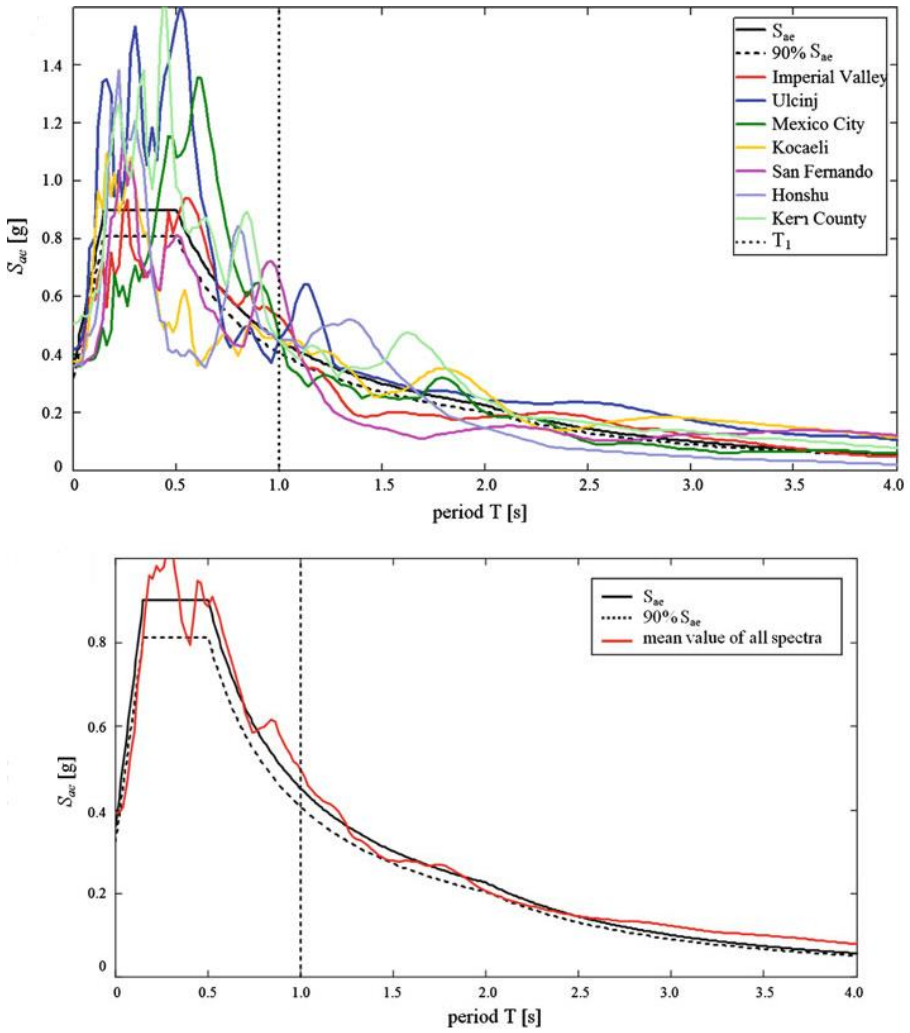

Figure 2.38 – (a) Acceleration response spectra of seven selected and scaled real earthquakes together with the elastic target spectrum and its 90% value; (b) mean value of all spectra (adapted from Causevic and Mitrovic, 2011)

Proposals of alternative procedures for the selection and scaling of ground motion records for the code-based design and assessment of buildings can be found in the works of Bradley (2011) and Araújo *et al* (2016), among others. Bradley (2011) proposed a probability-based approach for estimating deterministic design seismic demands with constant and known likelihood (16%) of being below the "true" mean value, regardless of the number of records and the variability associated with the input ground motions. On the other hand, Araújo *et al* (2016) studied the advantage of including a simple and expeditious additional criterion in the selection of each individual record by limiting to ± 50% the spectral mismatch relative to the target spectrum. This proposal was based on previous findings by Lucco and Bazzurro (2007) and Hancock *et al* (2008), who demonstrated that both the required number of records and the bias systematically decrease when records with a spectral shape similar to that of the target spectrum are adopted and additional constraints of the selection and scaling of the records are considered.

2.7.3. Common practice among structural design professionals

Past earthquakes have seriously tested the seismic performance of the existing RC building stock of many different countries, revealing not only the high vulnerability of pre-code buildings (Silva *et al,* 2015b), but also (and critically) the lack of guidance to designers in the assessment, repair and strengthening processes. For instance, the work of Searer *et al* (2008; 2011) has alarmingly demonstrated a clear distrust and lack of confidence of American practitioners in their seismic assessment and strengthening code ASCE 41-13 (2014). A similar survey conducted recently by Araújo and Castro (2017) among Portuguese practitioners showed that, although half of the respondents had previously dealt with a seismic safety assessment problem, only 8% used EC8-3 (2005), 37% used EC8-1 (2004) and the vast majority still applied the former national code RSA (1983) (which defines seismic actions in combination with EC2-1-1 (2004) or other design and detailing national codes). Among the reasons for not applying EC8-3 (2005), 35% of the participants admitted to being unaware of its existence, while 36% consider it too complex to be applied in everyday practice. Concerning the use of nonlinear static and dynamic procedures, the survey results revealed that half of the respondents are not familiar with such procedures and only 12% have applied them in practice.

It is therefore clear that, when involved in situations requiring the seismic assessment and strengthening of existing RC buildings, practitioners commonly resort to: (i) linear elastic analysis procedures; (ii) codes that prescribe general design and detailing rules, and (iii) seismic codes oriented towards the design of new buildings. Such practices, however, because they are conceptually different from those prescribed in the assessment and strengthening codes, ignore several of the associated and previously referred specific matters (Castro *et al,* 2017), as they:

i. do not recognize the level of knowledge of the structural condition of the existing building;
ii. rely on safety factors that only account for the uncertainty in the properties of materials produced under controlled quality specifications, which may or may not reflect those of existing buildings;
iii. imply the pre-selection of a ductility class (e.g., seismic design to EC8-1 (2004)), which is associated with a behaviour factor that has been derived for new buildings with known and controlled dissipative mechanisms;
iv. are based on the q-factor approach and rely on linear methods of analysis, which may not provide an accurate enough prediction of the most probable failure mechanism of the existing building;
v. do not consider specific seismic detailing that assures the achievement of acceptable levels of ductility at the member or joint level (when EC2-1-1 (2004) or other design and detailing national codes are adopted in combination with national standards that define seismic actions).

The latter point is critical when strengthening techniques are applied to columns with the purpose of avoiding the formation of possible soft-storey mechanisms, hence relying on beams to control the performance of the existing building. While EC8-3 (2005) establishes acceptance criteria at member level, controlling deformation demands in ductile members and strength in brittle members, EC8-1 (2004) establishes global criteria (e.g., control of second-order effects) that might imply significant

lateral strength and stiffness requirements for the structure (Peres and Castro, 2010). These global criteria can easily lead to over-strengthened and more expensive solutions. Concerning the use of the Portuguese code RSA (1983), which may be taken as representative of other seismic codes in use since the 80's, it does not refer to any serviceability verifications and the return period associated with the defined seismic action is twice the one considered in EC8-1 (2004). Finally, it should be kept in mind that the seismic assessment of existing buildings can only be performed employing linear analysis if the applicability criterion prescribed by EC8-3 (2005) (see sub-section 2.7.1.3. above) is verified, and the weak beam-strong column condition, prescribed by EC8-1 (2004), is guaranteed. Otherwise, nonlinear analysis methods must be employed.

2.7.4. Simplified methods introduced by LNEC Report 81/2019

Following the publication of recent legal diplomas by the Portuguese Government – (i) Decree-Law 95/2019 of July 18th, defining the terms and conditions applicable to the refurbishment of existing buildings; (ii) Ordinance 302/2019 of September 12th, defining the situations that require a seismic vulnerability assessment report and/or a seismic retrofitting design project; (iii) Normative Dispatch 21/2019 of September 17th, enforcing the use of the Eurocodes in structural design projects – the National Laboratory for Civil Engineering (LNEC) released Report 81/2019 (Sousa *et al,* 2019) with the purpose of defining alternative procedures that, while not intending to replace the applicable codes and standards, allow for the expedite seismic assessment (when compared to the EC8-3 (2005) reference methodology) of a significant sub-class of buildings. However, given the importance of fully understanding the conditions under which these simplified procedures may be applied, those will be discussed herein along with the proposed workflows.

Sousa *et al* (2019) refer to the possible approaches to the seismic assessment of RC buildings as "Methods I, II, II, and IV", progressing with the involved accuracy and complexity. Methods I and II are the two proposed simplified procedures. Method III corresponds to the EC8-3 (2005) methodology, discussed in sub-section 2.7.1., and is taken as reference for comparison. Method IV is the most complex approach, involving explicit probabilistic analyses, thus allowing for the quantification of seismic performance levels with increased accuracy and detail, namely regarding the expected levels of damage and operationality for different intensities of the seismic demand. Due to the significant complexity of the analyses involved in Method IV, the application of the latter is only recommended / justified for buildings of high importance for the public safety (e.g., schools, hospitals, powerplants, fire stations). Figure 2.39 shows the flowchart proposed by Sousa *et al* (2019) for deciding which of these methods to apply. The choice depends on the following building characteristics, some of them evaluated according to the applicable provisions of EC8-1 (2004):

- Importance class;
- Number of storeys above ground;
- Implantation area;
- Structural regularity;
- Dynamic interaction with adjacent buildings;
- Local geotechnical conditions.

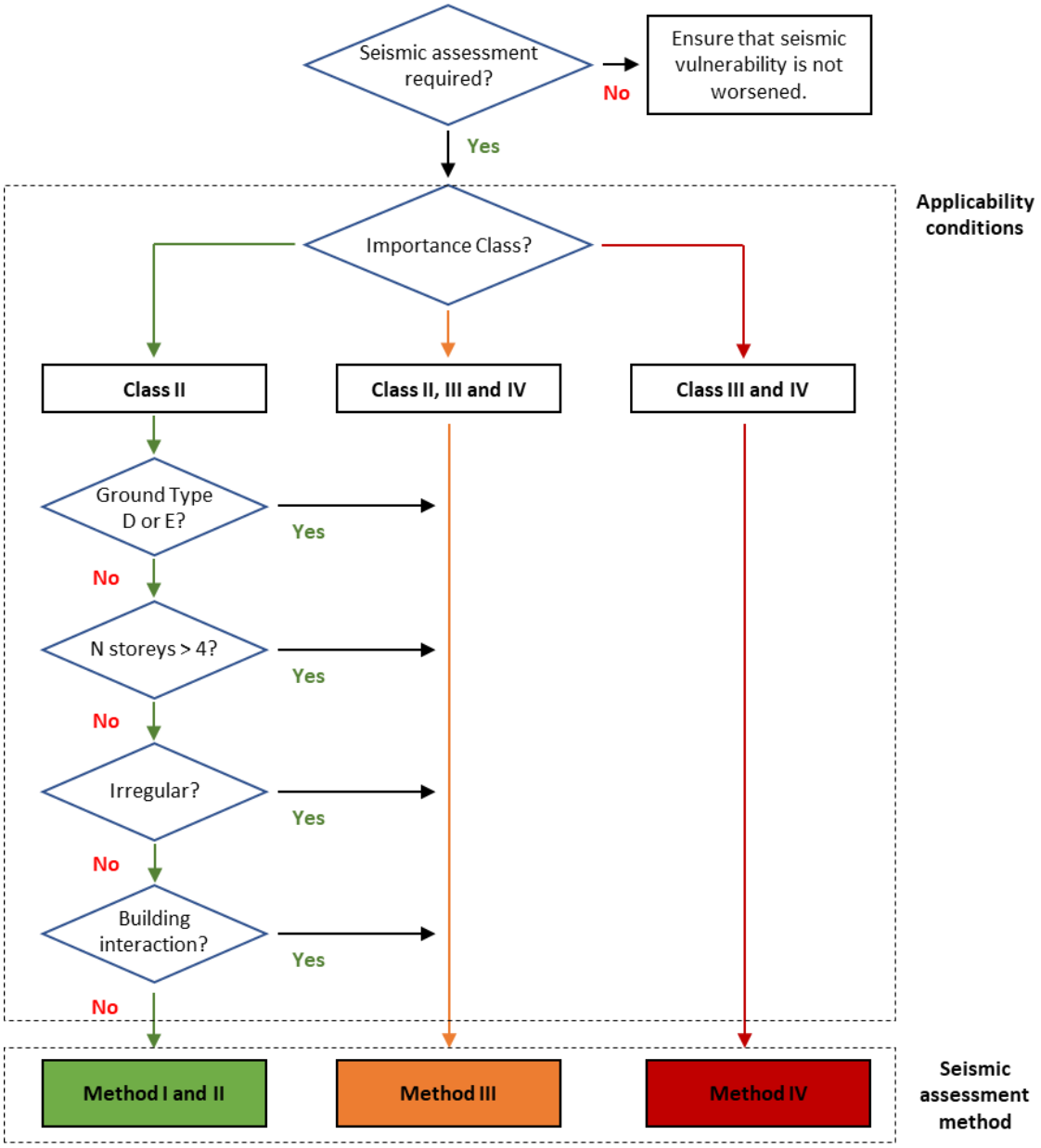

Figure 2.39 – Flowchart for the choice of the seismic assessment method (adapted from Sousa *et al,* 2019)

A building's importance class is evaluated according to Table 2.11, which reproduces the contents of Table 4.3 in EC8-1 (2004). The underlying criteria are the importance for the public safety and likely loss of lives in case of collapse, all in the event of an earthquake. Structural regularity (plan and elevation) is evaluated according to the requirements of clause 4.2.3 in EC8-1 (2004), with the exception of residential buildings with only one or two storeys, which are considered to be robust enough not to have to fulfil these conditions. The criterium concerning the dynamic interaction with adjacent buildings does not apply if the in-between space allows for a minimum lateral displacement equal to 2.2% of the height of the lowest building. In opposite cases, Methods I and II are generally not applicable (see Sousa *et al* (2019) for the few exceptions). Concerning the local geotechnical conditions, the applicability of Methods I and II is limited to buildings founded on ground types A, B

and C as defined by Table 3.1 in EC8-1 (2004). Buildings on softer ground types require more complex assessment methods and, eventually, additional studies to evaluate potential vulnerabilities induced by local ground conditions in the event of an earthquake. Finally, the application of Methods I and II is restricted to buildings with four or less storeys above ground, with a maximum floor implantation area of 400 m^2 per storey. This restriction intends to ensure that these simplified procedures are not applied to structures whose dynamic behaviour could be significantly influenced by the effect of higher order vibration modes.

Table 2.11 – Importance classes for buildings (adapted from EC8-1, 2004)

Importance Class	Buildings
I	Buildings of minor importance for public safety (e.g., agricultural buildings, etc.).
II	Ordinary buildings, not belonging in the other categories.
III	Buildings whose seismic resistance is of importance in view of the consequences associated with a collapse (e.g., schools, assembly halls, cultural institutions, etc.).
IV	Buildings whose integrity during earthquakes is of vital importance for civil protection (e.g., hospitals, fire stations, powerplants, etc.).

Unlike the more complex methods (III and IV), Methods I and II do not require the development of numerical analysis models. The seismic assessment process is based only on the area of the cross-sections of the vertical structural members of the building under analysis, eventually complemented by data about their longitudinal and transversal reinforcement details. However, only the continuous vertical elements (i.e., with no interruptions from foundation to the top floor) should be considered when calculating the building's seismic resistance and, within those, no short columns are allowed due to the high potential for collapse in the event of an earthquake. In order to evaluate whether a column should be considered as short, the ratio between its length L and the height of its cross-section h is compared to the limit values shown in Figure 2.40. If such structural elements are identified, then a more complex seismic assessment method will have to be carried out.

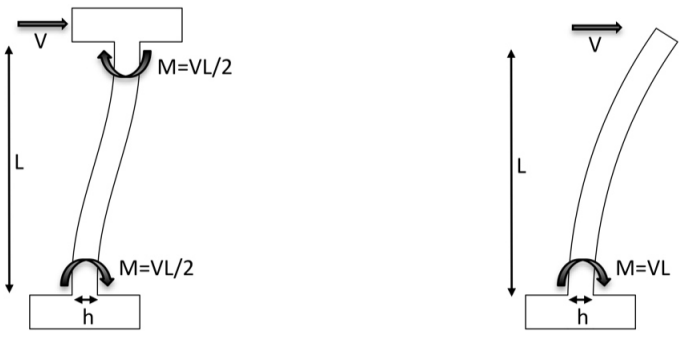

$\frac{L}{h} \leq 5.0$ $\frac{L}{h} \leq 2.5$

Figure 2.40 – Limit values for which a column should be considered as short (adapted from Sousa *et al,* 2019)

According to Method II, an existing building can be deemed safe for the applicable seismic demand if the rule defined by Expression (2.45) is verified, for the two main horizontal directions (XX and YY) at every storey j:

$$CS_{C,j} \geq CS_{E,j} = \eta_j \cdot CS_E \tag{2.45}$$

where $CS_{C,j}$ is a seismic coefficient – defined below by Expression (2.46) – that represents the capacity of storey j, $CS_{E,j}$ is the required seismic coefficient for that storey, CS_E is the required global seismic coefficient – given in Table 2.12 according to seismic zone, number of storeys and type of foundation ground (GT) – and η_j is factor defined in Table 2.13 for each storey j.

Table 2.12 – Values for the required global seismic coefficient CS_E (adapted from Sousa *et al,* 2019)

Seismic Zone (*)	1 storey			2 storeys			3 storeys			4 storeys		
	GT A	GT B	GT C	GT A	GT B	GT C	GT A	GT B	GT C	GT A	GT B	GT C
1.1	0.26	0.37	0.45	0.24	0.32	0.39	0.22	0.29	0.35	0.22	0.27	0.32
1.2	0.19	0.28	0.35	0.18	0.25	0.31	0.17	0.23	0.28	0.16	0.22	0.26
1.3	0.12	0.19	0.24	0.12	0.18	0.22	0.11	0.17	0.20	0.11	0.16	0.19
1.4	0.06	0.11	0.14	0.07	0.10	0.13	0.06	0.10	0.12	0.06	0.09	0.12
1.5	0.02	0.05	0.06	0.03	0.05	0.06	0.03	0.05	0.06	0.03	0.05	0.06
1.6	0.01	0.02	0.02	0.01	0.02	0.03	0.01	0.02	0.03	0.01	0.02	0.03
2.1	0.14	0.22	0.26	0.12	0.16	0.19	0.10	0.13	0.15	0.08	0.10	0.12
2.2	0.09	0.15	0.19	0.08	0.12	0.15	0.06	0.10	0.12	0.05	0.07	0.09
2.3	0.05	0.09	0.12	0.05	0.08	0.10	0.04	0.07	0.08	0.04	0.05	0.07
2.4	0.02	0.04	0.06	0.02	0.04	0.06	0.02	0.03	0.05	0.01	0.03	0.04
2.5	0.01	0.02	0.03	0.01	0.02	0.04	0.01	0.02	0.03	0.01	0.02	0.02

(*) according to EC8-1 (2004): Portuguese NA

Table 2.13 – Values for factor η_j (adapted from Sousa *et al,* 2019)

	Number of storeys			
Storey	**4**	**3**	**2**	**1**
4	0.40	-	-	-
3	0.70	0.50	-	-
2	0.90	0.83	0.67	-
1	1.00	1.00	1.00	1.00

The building's seismic capacity is evaluated considering that its structural members can develop both ductile and brittle collapse mechanisms (same as in Method III). Hence, the seismic coefficient $CS_{C,j}$ is defined by Expression (2.46) as the ratio between the storey's resistance towards horizontal forces $V_{H,j}$ and the building's total weight W_E (given by the code combination of vertical (dead and live) static loads for the seismic design situation):

$$CS_{C,j} = \frac{V_{H,j}}{W_E} = \frac{\sum_{i=1}^{n} \min\left(V_{F,i}\,;\, V_{C,i}\right)}{W_E} \tag{2.46}$$

where $V_{F,i}$ and $V_{C,i}$ are, respectively, the flexural and shear capacities of each column i of a given storey j with a total number n of columns. For the quantification of those capacities, the following expressions are proposed:

$$V_{F,i} = 1.24 \cdot \left(\frac{b_i \cdot {h_i}^2 \cdot \rho_{l,i} \cdot f_{yl}}{L_{v,i}} \right)^{0.73} \tag{2.47}$$

$$V_{C,i} = 0.87 \cdot A_{c,i} \cdot \left\{ \tau_c \cdot \left[1 - 0.16 \cdot \min\left(5; \frac{L_{v,i}}{h_i}\right) \right] + \rho_{w,i} \cdot f_{yw,i} \right\} \tag{2.48}$$

where b_i and h_i are the dimensions of the cross-section, that are respectively perpendicular and parallel to the direction of loading, $\rho_{l,i} = A_{sl,i}/(b_i \cdot h_i)$ is the longitudinal reinforcement ratio ($A_{sl,i}$ is the total longitudinal reinforcement area), $f_{y,l}$ is the estimated value of the longitudinal reinforcement yield strength, $L_{v,i}$ is the shear span (considered equal to half the column's length for fixed ends conditions, and to its full length for cantilever members), $A_{c,i} = b_i \cdot h_i$ is the cross-section area, τ_c is the equivalent shear strength for brittle collapse mechanisms, taken equal to 0.24 *MPa*, $\rho_{w,i} = A_{sw,i}/(b_i \cdot s_h)$ is the ratio of transversal steel area $A_{sw,i}$ parallel to the direction of loading (s_h is the stirrup spacing), and $f_{yw,i}$ is the estimated value of the transversal reinforcement yield strength, divided by a safety factor equal to 1.55 (which comes from considering the steel's partial safety factor γ_s = 1.15 combined with a Confidence Factor CF = 1.35).

About Method I, it renders the seismic assessment process even swifter to carry out as it requires no information about the structural members' reinforcement details. Instead, a storey's seismic capacity is defined in terms of the percentage of floor area $A_{PC,j}$ occupied by columns. Expression (2.49a) defines the rule that needs to be verified at every storey j for the building to be deemed safe under the applicable seismic demand.

$$A_{PC,j} \geq A_{PE,j} \tag{2.49a}$$

$$A_{PE,j} = \eta_j \cdot A_{PE} \tag{2.49b}$$

The percentage $A_{PC,j}$ is obtained by adding up the cross-section areas of all the columns on storey j and dividing the result by the corresponding floor's area. This parameter represents the actual seismic capacity of storey j, to be compared to its required capacity given by parameter $A_{PE,j}$ as defined by Expression (2.49b). In the latter, A_{PE} is the required global seismic capacity – given in Table 2.14 according to seismic zone, number of storeys and type of foundation ground (GT) – and η_j is a factor for each storey j, previously defined and given in Table 2.13. Unlike Method II, this procedure does not consider two main horizontal directions, rather defining globally the seismic safety of a building composed by several storeys.

Table 2.14 – Required columns' cross-section area percentages A_{PE} (adapted from Sousa *et al,* 2019)

Seismic Zone (*)	1 storey			2 storeys			3 storeys			4 storeys		
	GT A	GT B	GT C	GT A	GT B	GT C	GT A	GT B	GT C	GT A	GT B	GT C
1.1	0.9	1.2	1.5	1.6	2.1	2.6	2.2	2.9	3.5	2.9	3.6	4.3
1.2	0.6	0.9	1.2	1.2	1.7	2.0	1.7	2.3	2.8	2.2	2.9	3.5
1.3	0.4	0.6	0.8	0.8	1.2	1.5	1.1	1.6	2.0	1.5	2.1	2.5
1.4	0.2	0.3	0.5	0.4	0.7	0.9	0.6	1.0	1.2	0.8	1.3	1.6
1.5	0.1	0.2	0.2	0.2	0.3	0.4	0.3	0.5	0.6	0.4	0.6	0.8
1.6	0.1	0.1	0.1	0.1	0.1	0.2	0.1	0.2	0.3	0.1	0.3	0.4
2.1	0.5	0.7	0.9	0.8	1.1	1.3	1.0	1.3	1.5	1.0	1.3	1.6
2.2	0.3	0.5	0.6	0.5	0.8	1.0	0.6	0.9	1.2	0.7	1.0	1.2
2.3	0.2	0.3	0.4	0.3	0.5	0.7	0.4	0.7	0.8	0.5	0.7	0.9
2.4	0.1	0.1	0.2	0.1	0.3	0.4	0.2	0.3	0.5	0.2	0.4	0.5
2.5	0.1	0.1	0.1	0.1	0.2	0.2	0.1	0.2	0.3	0.1	0.2	0.3

(*) according to EC8-1 (2004): Portuguese NA

Despite the simplicity of the methods proposed by Sousa *et al* (2019), they are supported by the results of explicit probabilistic analyses applied to the seismic assessment of a sample of structures chosen to be representative of a relevant fraction of the Portuguese RC building stock. The modelling and analysis of those buildings, using nonlinear static analysis models, allowed for a relation between seismic coefficient and structural reliability for different intensities of the seismic demand that characterizes the Portuguese Territory. The same sample of buildings was also assessed from the standpoint of EC8-3 (2005), for the purpose of establishing a compatible level of reliability. Those results were taken as reference for the proposed methods' calibration, allowing for the definition of performance levels according to seismic zone, local ground conditions and number of storeys. Finally, the accuracy of the methods was assessed through more than forty-thousand numerical simulations, involving variations of the building's characteristics as well as of the seismic demand's intensity. The conclusions were: (i) in 86.0% (Method II) and 78.4% (Method I) of the cases, the obtained results led to the same assessment conclusions as those of the EC8-3 (2005) procedure, and (ii) from the other cases, only in 5.4% (Method II) and 0.2% (Method I) of them were the results less conservative than those provided by the reference procedure.

A verification example consisting of an existing 4-storey RC building is included in LNEC Report 81/2019 (Sousa *et al,* 2019), for the purpose of illustrating the efficiency of the proposed methods, as well as of demonstrating the coherence and conservative tendency of the provided results when compared to those of the EC8-3 (2005) reference method. The author believes this to be an important and valuable contribution for practitioners to be able to perform, simply and quickly, the seismic assessment of small to medium regular RC buildings but cannot stress enough the importance of not applying such simplified procedures outside their scope. The criteria that must be fulfilled in order for the buildings under analysis to be eligible for such approaches were objectively defined by Sousa *et al* (2019), as previously referred, and should be verified before anything else.

2.8. TECHNIQUES USING STEEL ELEMENTS FOR THE SEISMIC RETROFITTING OF RC BUILDINGS

Seismic retrofitting can be defined as the upgrading of the properties of a structural system, or some of its structural members, in order to obtain an improved performance level during futures earthquakes (Wyllie, 1983; Varum, 2003). The need to retrofit or not a specific building and the scope and targets of the intervention (in terms of deficiencies to be corrected) will normally be the result of a seismic safety assessment process (Fardis, 2009). The few available codes and guidelines that specifically address this issue are relatively recent and were referred in the previous section. They introduce new performance-based concepts that (most of the times) imply the use of advanced and complex nonlinear methods of analysis and are still unknown to many practitioners, as demonstrated by the study conducted by Araújo and Castro (2017). Consequently, most designers resort to structural codes that were developed for the purpose of designing new structures and rely on their engineering judgement to perform the assessment and retrofitting of existing ones. However, and as stated before, such practices are conceptually different from those followed by the above-referred assessment and strengthening codes and should be implemented with caution as they ignore several specific important matters (Castro *et al*, 2017).

Many techniques and design strategies have been investigated and adopted in the past to retrofit existing RC buildings, such as bonding and / or jacketing with composite materials, using special devices, modifying the structural system by adding RC shear walls, adding steel elements and sub-systems, etc. Among this wide range of upgrading options, the use of steel elements offers a diversity of applications and might be considered as a rational alternative to other strengthening techniques due to their ease of design and detailing and cleaner, less intrusive, and disruptive implementation (Castro *et al*, 2017). Several studies and research initiatives have been conducted in the past with the purpose of investigating the performance of RC buildings subjected to such strengthening techniques (e.g., Varum, 2003; D'Aniello, 2007; Sousa and Castro, 2012; Varum *et al*, 2013; RFCS, 2013). A recent study by Furtado *et al* (2015) concerning a typical existing Portuguese RC building showed that they can be very efficient. A steel bracing system with energy dissipation devices was demonstrated to be as efficient as the concrete jacketing of RC columns or adding RC shear walls, while costing four times less and around 10% of the property value of the building. These conclusions strongly support the idea that the addition of steel elements is highly worth considering by practitioners when devising seismic retrofitting solutions for existing RC buildings.

Unfortunately, even the most recent versions of codes dealing with the seismic assessment and strengthening of buildings, such as EC8-3 (2005), reveal some inconsistencies in the assessment procedures (see e.g., Pinto, 2005; Franchin *et al*, 2010; Romão *et al*, 2010b; Romão *et al*, 2010a; Romão *et al*, 2012; Araújo and Castro, 2016) and provide scarce information regarding the detailed design of the strengthening techniques (see e.g., Romão and Penna, 2017). For instance, in the case of RC buildings, EC8-3 (2005) only provides guidance for the strengthening of members using jacketing approaches and no further references exist regarding strengthening interventions at the storey or global levels. Further development and improvement of the EC8-3 (2005) provisions on this matter are hence necessary to assist practitioners in the design of such retrofitting solutions. Concerning the existing guidelines, FEMA 547 (2006) is one of the very few documents that provide thorough guidance

to practitioners in terms of the most common structural deficiencies found in RC buildings (Castro *et al*, 2017). Strengthening techniques are proposed for each structural deficiency and comments on execution, cost, disruption, and proprietary concerns are included. However, despite the pertinence of associating general strengthening techniques with specific building weaknesses, it should be kept in mind that the effectiveness of each retrofitting solution is case dependent and varies with the level of seismic hazard (Asteris *et al*, 2014).

2.8.1. Retrofitting approaches and strategies

The target of retrofitting a building is to ensure that all its relevant elements fulfil the general verification inequality $E_d \leq R_d$, where E_d refers to demands and R_d to capacities, for all the required performance levels under the corresponding seismic action (Fardis, 2009). This may be achieved through one of the following strategies, or even by combining them:

i. Reducing seismic demand on members and structure as whole (global modification);
ii. Increasing member capacities (local modification).

The difference between strategies is well illustrated comparing the before- and after-retrofitting capacity curves of the structure under analysis, together with the corresponding target displacements for the relevant seismic action (Figure 2.41). In the first approach, global modifications are made to the structural system so that displacement demands on structural members become lower than the corresponding deformation capacities. Common techniques include adding structural walls, steel braces or base isolators. No local strengthening of members is thus normally required, provided that the designed modifications do not impair their resistance to gravity loads (e.g., due to increased axial force). The second approach involves local modification of isolated weak components of the structural system, with the purpose of increasing their deformation capacities to levels which are compatible with the required limit states. Common techniques include adding concrete, steel, or fibre reinforced polymer composite (FRPC) jackets (Fardis, 1998; Moehle, 2000).

(a)

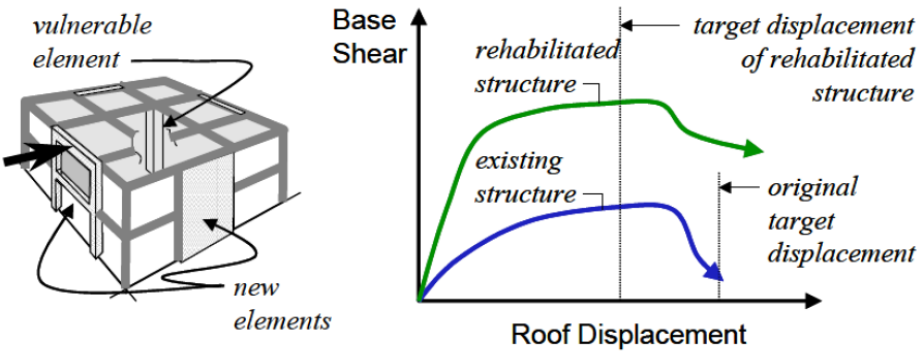

Figure 2.41 (a) – Effect of global modifications to the structural system (adapted from Moehle, 2000)

(b)

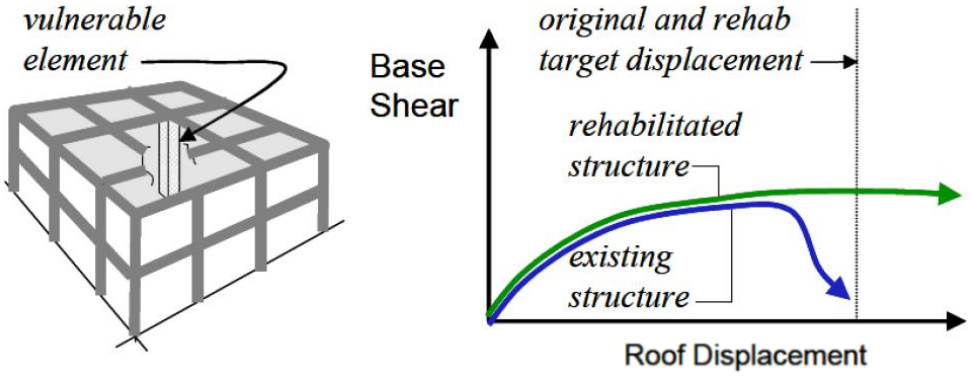

Figure 2.41 (b) – Effect of local modifications to the structural system (adapted from Moehle, 2000)

Each retrofitting technique will have its own advantages and drawbacks, scope and limitations of use and fit better in one of the above-referred strategies. The following groups of techniques can be defined (Castro *et al,* 2017):

i. Local strengthening measures;
ii. Removal or reduction of irregularities and structural discontinuities;
iii. Global structural stiffening and reinforcement measures;
iv. Mass reduction measures.

The choice of one or more of the above for a given building is influenced by general factors such as the locally available materials and technologies, cost considerations, the disruption of use it entails and the duration of the works, as well as architectural, functional and aesthetics considerations or restrictions (Fardis, 2009). Furthermore, it depends on the structural deficiencies revealed by the building's seismic assessment. An overview of the most common structural deficiencies and subsequent retrofitting techniques is presented in Table 2.15. The general code prescriptions according to which the design of the chosen solution(s) should be performed are also included (see last column of Table 2.15).

Observing the relations between structural deficiencies and retrofitting techniques given in Table 2.15 and making the association with the two previously referred retrofitting strategies, some conclusions may be drawn. For instance, retrofitting strategy no. 1 will most likely be more cost-effective in the cases where a general deficiency exists in the building, as it will reduce seismic demands throughout structural members. On the other hand, if there are capacity deficiencies in just a few scattered members, it will probably be more cost-effective to focus only on them and upgrade their capacities with strategy no. 2. Concerning the code verifications, as no lateral stiffness and / or strength requirements are explicitly defined in EC8-3 (2005), Castro *et al* (2017) suggest the adoption of EC8-1 (2004) criteria regarding the inter-storey drift limits (to control non-structural damage at the serviceability limit state) and the assessment of second-order effects. Similarly, in the cases where the capacity of columns is increased, leaving it up to the beams to govern the seismic response of the

existing building (e.g., when eliminating a soft-storey mechanism), the verification of the weak beam-strong column condition (EC8-1 (2004): 4.4.2.3) is suggested. However, as each retrofitting intervention is a special case with more than one appropriate solution, the generalisation of rules is neither possible nor advisable (Fardis, 2009). Therefore, these considerations should be taken as general (not absolute) guidelines to follow, depending on the outcome of the seismic safety assessment process.

Table 2.15 – Common structural deficiencies, retrofitting techniques and code-based compliance criteria (adapted from Castro *et al*, 2017)

Structural deficiencies	Retrofitting technique	Code-based compliance criteria
▪ Lack of member or joint ductility under seismic conditions; ▪ Lack of local and/ or global strength and stiffness; ▪ Insufficient in-plane wall shear strength or flexural capacity; ▪ Insufficient reinforcement.	▪ Selective local strengthening at member level; ▪ Addition of new dissipative elements to provide stable failure mechanisms or increase lateral stiffness and strength; ▪ Reduction of seismic demand by removing upper storeys or adding seismic isolation or supplemental damping; ▪ Removal of the components that create short columns.	▪ Verify local deformation and strength capacities by fulfilling the general safety inequality ($E_d \leq R_d$) for all limit states; ▪ Skip ductility verifications if sufficient reinforcement and detailing is provided according to EC8-1 (2004); ▪ Include and control second-order effects in structural analysis (e.g., EC8-1 (2004) and EC2-1-1 (2004)); ▪ Control inter-storey drifts at the serviceability limit state according to EC8-1 (2004); ▪ Verify the weak beam-strong column condition as proposed in EC8-1 (2004); ▪ Consider the EC8-1 (2004) structural regularity criteria for good practice; ▪ Verify the EC8-3 (2005) linear analysis applicability criterion.
▪ Structural irregularity in plan and in elevation; ▪ Presence of a weak storey; ▪ Change in failure mechanism (e.g., development of a soft storey) due to the collapse of non-structural components (e.g., coupled infill walls).	▪ Addition of strength and stiffness at storey levels to achieve vertical regularity in demands; ▪ To ensure diaphragm effect and sufficient connection between elements to guarantee the load path; ▪ Creation of new expansion joints to transform a single irregular building into various regular ones; ▪ Addition of new balancing elements to reduce torsional effects; ▪ Uncoupling of infill walls or conversion to structural walls.	

Finally, it should be kept in mind that no retrofitting intervention, regardless of its type and extent, should in any way impair the safety or capacity of any part of the building. As such, the designer must make sure that: (i) upgrading the flexural capacity of an element does not make it critical in shear; (ii)

strengthening of a beam does not shift plastic hinging to columns and (iii) consequences of discontinuing the retrofitting in elevation are tolerable. Both the existing and the retrofitted structures should be carefully checked in terms of safe transfer of inertia forces, from the masses (where they originate) to the lateral-load-resisting elements and from there to the foundations. The safety of the connections within the floor systems, between the floors and the lateral-load-resisting elements and between existing and new components, should also be verified.

2.8.2. Traditional retrofitting techniques

In general, the purpose of locally strengthening RC members should be to correct their inadequate shear, flexural and axial compression capacities, as well as any irregular plastic hinge confinement and lap splice (fib, 2003). However, this will be a cost-effective solution when only a reduced number of members in a structure are deficient, as previously referred. On the other hand, global interventions can be considered cost-effective when disruption of occupancy and damage to partitions, architectural finishings and other non-structural components are of concern (Fardis, 2009). Current assessment codes, such as EC8-3 (2005), do not explicitly address this issue, limiting the level of damage only to the structural components. However, past earthquakes have shown that non-structural losses (e.g., businesses interruption, content losses, etc.) often overcome structural losses. A recent study conducted by Araújo *et al* (2015) on the potential for property losses of the Portuguese industrial steel buildings stock has also offered an interesting perspective over this matter. The following sub-sections summarize the features of the most common retrofitting techniques using steel elements.

2.8.2.1. Local capacity upgrading using steel plates

A common technique for retrofitting RC beams consists of using bonded external steel plates applied to the soffit of the existing member. Ease of application, limited disruption and low price of the involved materials make it a rational choice for the improvement of ductile flexural capacity. However, several previous studies (e.g., Oehlers, 1992; Leung, 2001; Aykac *et al*, 2013) have shown that, if not properly designed, such strengthening technique is highly prone to premature plate peeling failure before the development of the members' full flexural capacities, due to diagonal shear and vertical flexural cracking at the plates' end locations. With the purpose of providing further recommendations concerning this technique, Aykac *et al* (2013) have recently conducted an extensive experimental test campaign on several RC beams strengthened with soffit steel plates anchored with the help of bolts or side plates (collars) with different heights. The bottom plate was epoxy-bonded to the beam in every specimen. Figure 2.42 (a) presents the layout of some of these specimens, for illustrative purposes. A discussion of the several design aspects involved in these variant solutions as well as the obtained conclusions and practice recommendations can be found in the referred study's report and in the work of Castro *et al* (2017).

Another usual technique for RC beams, when the issue is to improve their strength and shear capacity, is the use of bolted side-plates (see Figure 2.42 (b)). Contrarily to bonding external plates to the soffit of the beams, this technique has the advantage of not requiring the removal of infill walls, which makes

it a logical approach when minimizing disruption. The strengthening mechanism relies on the slip between the RC beam and the steel plates, which mobilizes the anchor bolts and transfers forces to the steel plates. However, significant differential deformation between the steel plates and the RC beam can still occur, particularly when plastic hinging initiates (Siu and Su, 2010). This partial interaction depends on the strength of the bolts and plates and controls the most probable failure mechanisms, hence its effect in the composite behaviour of the beam should be accurately accounted for to obtain a safe design. Su *et al* (2010) studied the behaviour of the four arrangements shown in Figure 2.42 (b) (where SB, SP, WB and WP stand for "strong bolts", "strong plates", "weak bolts" and "weak plates", respectively) and concluded that three failure mechanisms may develop: (i) a concrete-controlled mechanism; (ii) a bolt-controlled mechanism and (iii) a plate-controlled mechanism. Further conclusions and recommendations about the design and use of this technique may be found in the referred study's report and in the work of Castro *et al* (2017).

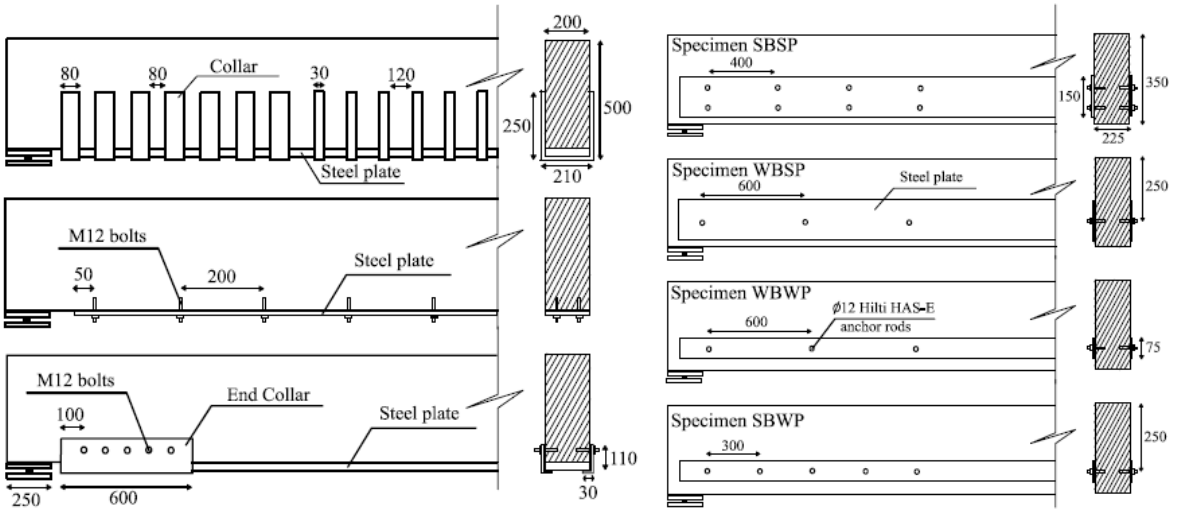

(a) [mm] (b) [mm]

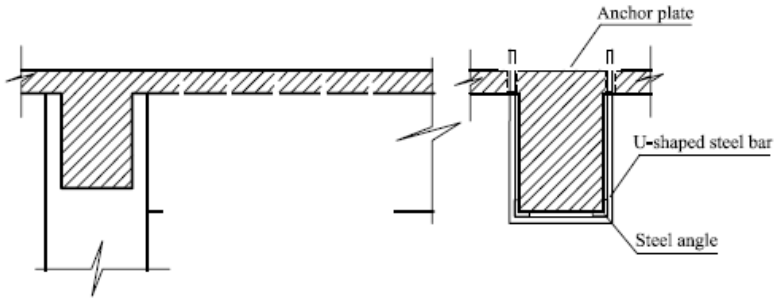

(c) [mm]

Figure 2.42 – Strengthening of RC beams by means of: (a) bonded steel plates; (b) bolted side plates and (c) U-shaped bars welded to steel angles (adapted from Aykac *et al* (2013); Su *et al* (2010) and P100-3/2008 (2009), respectively)

Still regarding the strengthening of RC beams, the Romanian code P100-3/2008 (2009) proposes a simple technique that consists of applying steel angles, along the bottom corners of the RC beam's cross-section, welded to U-shaped steel bars which should be anchored to the slab with the help of an anchor plate (see Figure 2.42 (c)). More information about the design and detailing of this technique may be found in P100-3/2008 (2009), which is in fact one of the very few normative documents that provide guidance and detailing in terms of strengthening of existing members.

Concerning the strengthening of RC columns, steel jacketing is the most rational and widely adopted solution (see Figure 2.43). Although being more expensive than concrete jacketing, this technique is simple, familiar to the industry and readily available (Fardis, 2009; Castro *et al*, 2017). As briefly described in EC8-3 (2005), it consists of caging RC columns with four corner steel angles, to which continuous steel plates or discrete steel strips are welded. Alternatively, thin-walled steel jackets may be used. This solution is particularly relevant for the case of circular columns, for which it consists of semi-circular halves fitting closely around the column and field-welded along two vertical seems. This strengthening technique tries to create additional confinement to that already provided by transverse reinforcement, as well as to increase the member's shear capacity and correct deficient lap-splices (Aboutaha *et al*, 1996). Moreover, the improved confinement may equally enhance the member's lateral deformation capacity, as well as restrain rebars from buckling. The corner steel angles may also provide an effective increase of longitudinal reinforcement (Montuori and Piluso, 2009). Conclusions about the various parameters that influence the effectiveness of steel jacketing can be found in the several experimental studies performed at the Technical University of Valencia (e.g., Adam *et al*, 2008; Giménez *et al*, 2009; Garzón-Roca *et al*, 2011) and in the work of Castro *et al* (2017). From the normative side, EC8-3 (2005) provides guidance for quantifying the increase in the member's shear capacity and for the detailing of regions where deficient lap-splices exist. The above-referred Romanian code P100-3/2008 (2009) also provides details on this technique.

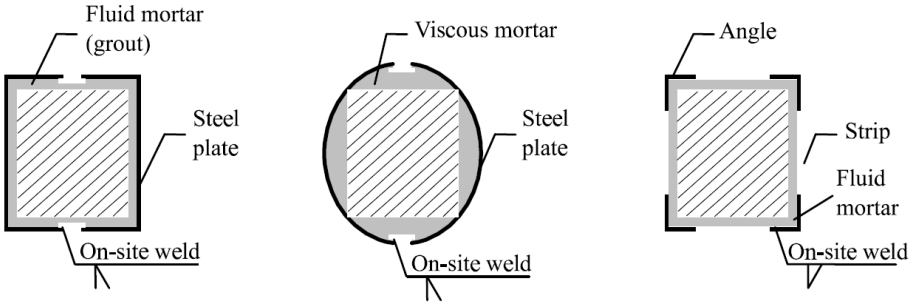

Figure 2.43 – Strengthening of RC columns by means of thin-walled jackets or caging strips welded to four corner angles (adapted from P100-3/2008, 2009)

Finally, other strengthening techniques for RC columns have been investigated with the aim of minimizing some of the shortcomings of the above-described solutions. For more information, readers are referred to the work of Said and Nehdi (2008), Wang and Su (2013) and others.

2.8.2.2. Global reduction of demands using concentric steel braces

The adding of steel braces to existing RC buildings is a commonly adopted technique for increasing lateral stiffness and strength, of a specific storey or of the overall structure. It was applied for the first time as a retrofitting measure to strengthen an earthquake-damaged building in Japan in 1978 (Kawamata and Masaaki, 1980), despite having been used years before in new constructions (e.g., John Hancock Center, Chicago, USA, 1969). Shortly after, Del Valle (1980) reported a 12-storey RC building in Mexico City, retrofitted after a small earthquake revealed seismic deficiencies. The intervention included bracing the perimeter frames, in the weak direction of the structure, as well as strengthening of the slabs and foundations. It was completed in 10 months, at approximately 20% of the replacement cost of the building and with minimum disturbance to its users. This structure would come to perform very well during the devastating 1985 Mexico City earthquake (M_W = 8.0), unlike many surrounding buildings (Badoux and Jirsa, 1990). The benefits of this technique have been demonstrated by several other authors (e.g., Maheri and Sahebi, 1997; Youssef *et al,* 2007; Eskandari *et al,* 2017) during the past three decades. Architectural flexibility, reduced weight and impact on foundations, ease and speed of construction and the ability to choose systems that are more ductile can be considered as the main advantages in comparison with, for instance, global strengthening based on the inclusion of RC shear walls (Eskandari *et al*, 2017).

Steel bracing systems typically consist of concentric X-diagonal, V or inverted-V braces, falling into two main categories (Maheri *et al,* 2003): (i) external braces and (ii) internal braces. In the external systems, steel elements are attached to the exterior frames of the building (Figure 2.44). Architectural concerns and difficulties in providing appropriate connections between the steel braces and the RC frames are two of the shortcomings of this method, making it rather unpopular. On the other hand, internal systems incorporate steel elements inside the individual bays of the RC frames (Figure 2.45). This method has the advantage of not interfering with the exterior architectural design of the building but can be more disruptive of the interior layout of spaces. However, it is one of the most effective systems to improve the seismic performance of existing RC frames (Rahimi and Maheri, 2018).

Figure 2.44 – Seismic retrofitting of existing RC buildings with external steel braces (located in California, USA and Tokyo, Japan, respectively) (adapted from Sousa, 2010)

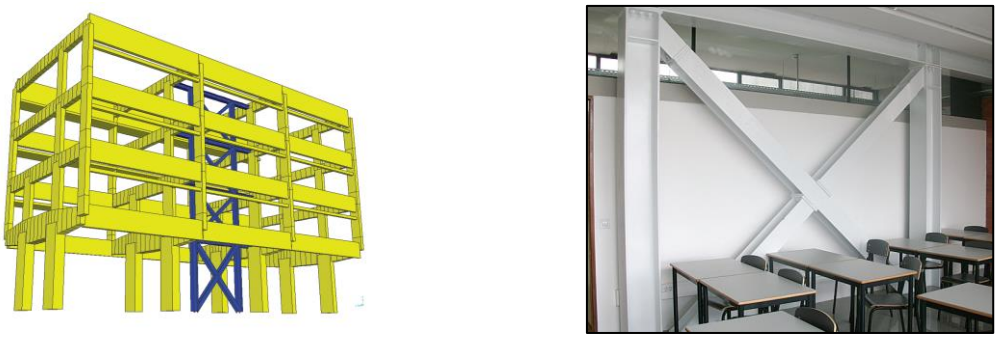

(a) (b)

Figure 2.45 – Seismic retrofitting of an existing RC building with internal steel braces: (a) numerical model and (b) view of one of the upper floors (located in Lisbon, Portugal) (adapted from Proença and Sousa Gago, 2011)

The effect of the retrofitting on the flow of forces through the structure should be as simple as possible, to avoid load concentration or potentially weak zones. An appropriate definition of the braces' layout is thus important. It may seem adequate to brace as many bays as possible, hence uniformly distributing the increase in strength and stiffness. However, it is often preferable not to brace the end bays due to two main reasons (Badoux and Jirsa, 1990): (i) these may be shorter than intermediate bays, making brace geometry difficult, and (ii) a typical interior column will resist overturning forces better than an exterior one. Figures 2.46 and 2.47 show some configurations and patterns for bracing systems, as proposed by Badoux and Jirsa (1990). More recently, Faella *et al* (2014) published a refreshing study on this topic, inspired by a practical retrofitting project of a RC school building located in the neighbourhood of L'Aquila, Italy.

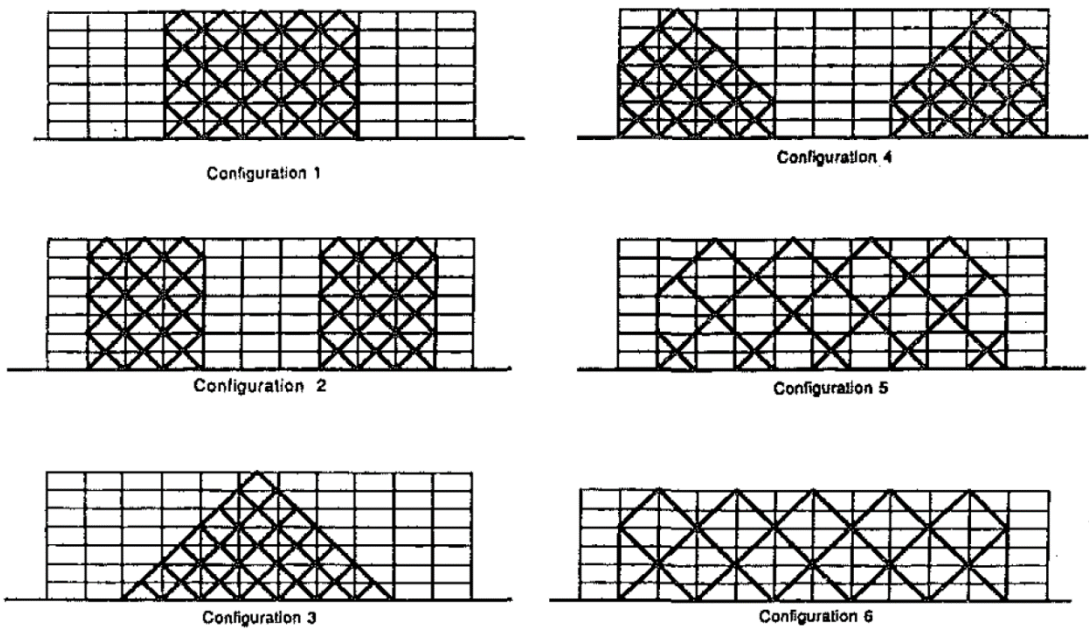

Figure 2.46 – Possible steel brace configurations (Badoux and Jirsa, 1990)

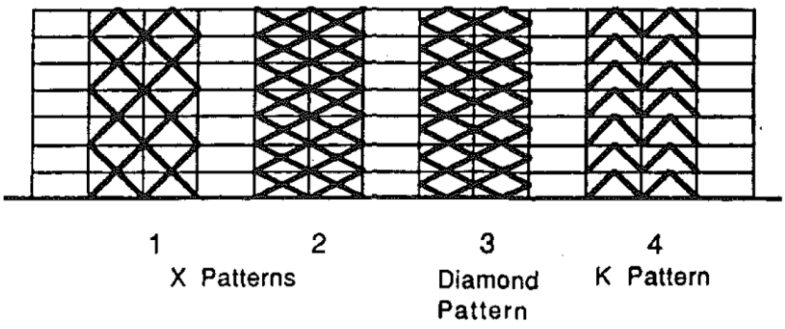

Figure 2.47 – Steel brace patterns (Badoux and Jirsa, 1990)

The transfer of forces between the steel braces and the RC frames plays a fundamental role on the success of this retrofitting technique and has thus been the focus of extensive research in the past. For instance, Massumi and Tasnimi (2008) experimentally tested five types of connections between the RC joint and the gusset plate located at the end of the brace, and came to the following conclusions: (i) braces simply bolted at the end of columns (specimen BF12 on Figure 2.48 (b)) exhibit significant cyclic strength deterioration and do not allow the new system to achieve its maximum potential strength capacity; (ii) bolted connections to both column and beam ends (specimen BF11 on Figure 2.48 (b)) were seen to provide good results (and similar to those found by Youssef *et al* (2007)); (iii) connections based on caging the column end without any bonding adhesive (specimen BF21 on Figure 2.48 (b)) were seen to be prone to slippage – thus not being able to transfer effectively the forces between the braces and the existing structure – and should be avoided; (iv) higher strength capacities and energy dissipation were obtained when epoxy-bonded jacketing solutions were adopted (specimen BF22 on Figure 2.48 (b)). A comprehensive discussion on the design of this type of connections can be found in Maheri and Hadjipour (2003) and in Maheri and Yazdani (2016a; 2016b), with indications that some can be successfully designed by combining the current guidelines and provisions set by codes of practice for brace-steel frame connections with those for base plate-RC member connections.

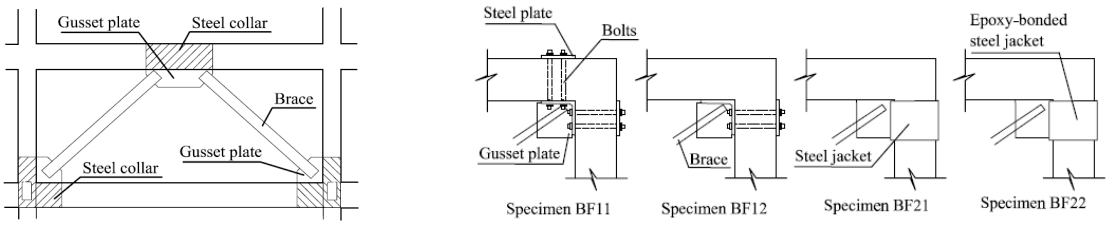

(a) (b)

Figure 2.48 – Strengthening of existing RC frames: (a) schematic representation of a possible steel bracing system and (b) types of local connections to existing elements (adapted from P100-3/2008 (2009) and Massumi and Tasnimi (2008), respectively)

Connecting the steel braces directly to the RC frames has the advantage of being slightly intrusive and easy to execute, therefore inexpensive. Nevertheless, the resistance of these local connections might be insufficient when very high lateral forces are involved. A common alternative is to install the diagonal braces within a steel frame (i.e., beams and columns) firmly attached to the surrounding concrete members (FEMA 547, 2006; Fardis, 2009). The connection is usually done using epoxy-grouted post-installed fasteners, as shown in Figure 2.49. Other techniques to attach the new steel elements to the existing RC frames have been studied by Ishimura *et al* (2012), wherein existing procedures to design this type of strengthening intervention have been equally assessed and validated. However, this tends to be a laborious, therefore expensive, solution to execute. Another shortcoming of this alternative is that interpreting the dynamic behaviour of the retrofitted structure is sometimes challenging, due to the interaction between the steel and RC frames. It should also be referred that the installation of new braced frames within the existing RC structure might be preferable when a single storey is to be strengthened, since continuity of the solution is not possible along the height of the building (FEMA 547, 2006). Otherwise, the new braced frames should be placed alongside the existing RC frames or externally at the façades of the building. Some connection details regarding these situations can be found in the previously referred Romanian code P100-3/2008 (2009).

Figure 2.49 – Connection of new steel elements to the existing RC frame using epoxy-grouted post-installed fasteners (adapted from Varum, 2003)

2.8.3. Innovative retrofitting techniques

Even though concentric steel bracing systems provide a satisfactory enhancement of the seismic performance of existing non-ductile RC buildings, they can exhibit a somehow complex behaviour at times, triggered by local and global instability phenomena. To overcome this from both the structural and economic points of view, innovative strengthening techniques that incorporate energy dissipation devices (e.g., friction, viscoelastic, or metallic dampers) have been developed (D'Aniello, 2007). These innovative solutions have the advantage of reducing demands in the original structure by concentrating the energy dissipation on devices that can be easily replaced after the occurrence of an earthquake (Castro *et al,* 2017). The following sub-sections present the features of some of these innovative solutions by reviewing the outcomes from the experimental campaign carried out by the University of Naples "Federico II" group within the ILVA-IDEM project (Della Corte *et al,* 2008; D'Aniello *et al,* 2008; Mazzolani, 2008; Mazzolani *et al,* 2009; De Matteis *et al,* 2009 and Della Corte *et al,* 2014).

The ILVA-IDEM project represented a unique research opportunity to conduct full-scale testing of various strengthening techniques, implemented in a real two-storey RC building that had been condemned.

2.8.3.1. Eccentric braces

Strengthening systems using eccentric braces (EB's) are typically composed by an inverted Y-shaped assembly, wherein a dissipative link is attached to the existing RC slab or beam (Mazzolani, 2008; Mazzolani *et al,* 2009), as shown in Figure 2.50 (a) and (b). The size of the cross-section and length of the link are the fundamental parameters for the design of EB's because they determine the shear plastic strength of the storey and the stiffness of the bracing system, respectively. Three eccentric bracing solutions were investigated in the ILVA-IDEM project by designing the link according to different criteria.

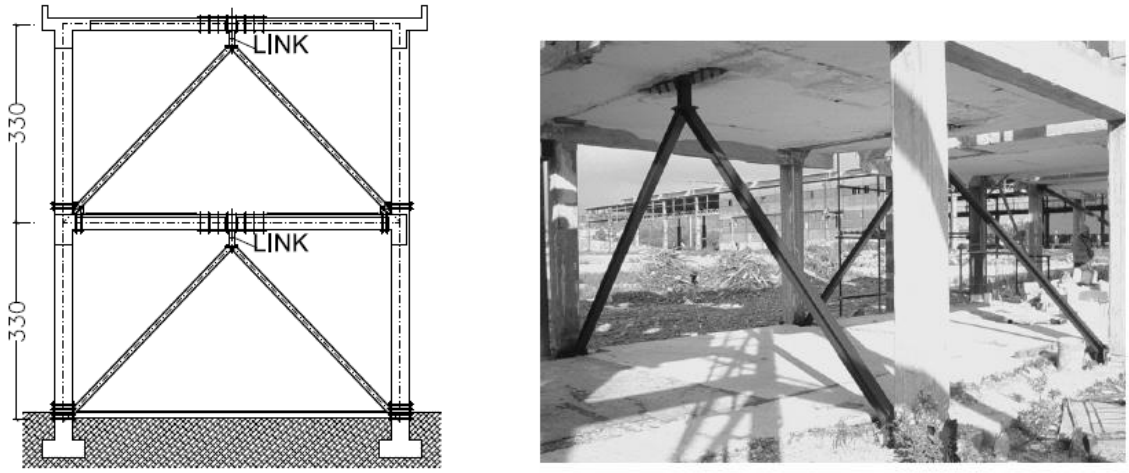

(a) (b)

Figure 2.50 – Strengthening with EB's of the existing RC building studied in the ILVA-IDEM project: (a) the adopted solution and (b) the strengthened building (adapted from Mazzolani *et al,* 2009)

In the first case, the braces were designed according to EC8-1 (2004) but no capacity design criteria were applied. The shear strength capacity was estimated based on the first-yielding definition provided by Popov and Engelhardt (1988) and the link length was defined to satisfy the conditions of being the shortest and of achieving the maximum inelastic link shear rotation with the formation of the first plastic hinge in the existing building. Concerning the verification of the serviceability limit state, the inter-storey drift limit imposed by EC8-1 (2004) was considered (D'Aniello, 2007). An end-plate bolted connection between the link and the slab was adopted, whereas the braces were connected to the RC frame using gusset plates bolted to the beam-column joint (Figure 2.51). In the second case, capacity design principles were applied to the design of the link end-plate connection, leading to an increase in the plate's thickness. Finally, in the third case the link was designed to increase the system's ductility

by forcing the plastic deformations to be confined within the links. A steel built-up section without web-stiffener was designed so that the shear strength of connections would be two times greater than the average yield strength of the links. This solution was influenced by the need to increase the steel grade of the bolts.

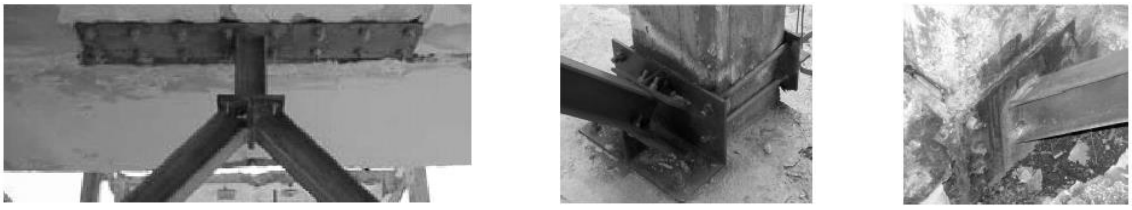

(a) (b) (c)

Figure 2.51 – Details of the strengthening with EB's of the existing RC building studied in the ILVA-IDEM project: (a) link to slab connection; (b) brace to RC column joint and (c) brace to RC column base connection (adapted from Mazzolani *et al,* 2009)

The following conclusions were drawn from the obtained experimental results (Mazzolani, 2008; Mazzolani *et al,* 2009): (i) the three tested eccentric bracing systems were seen to provide promising results, substantially increasing the lateral stiffness and strength of the existing RC building; (ii) although the link designed under capacity design principles led to the highest increase in the lateral strength of the system, it failed suddenly due to shear failure of the bolts connecting the link to the braces; in turn, the most dissipative built-up link provided the best performance enhancement both in terms of increasing the system's lateral stiffness and strength and of the energy dissipation capacity; (iii) the link's shear over-strength was found to play a critical role on the overall strength of the system and to be significantly larger than previously expected. Recently, Della Corte *et al* (2013) demonstrated that the link shear over-strength mostly depends on the combined effect between tensile axial forces (developing due to axial deformation restraints and nonlinear geometrical effects) and the link's geometrical properties, namely the ratios between the flange and web areas and between link length and cross-section depth (Castro *et al,* 2017).

2.8.3.2. Buckling-restrained braces

Buckling-restrained braces (BRB's) consist of a core axial load-bearing steel element, subdivided into a central yielding part and two non-yielding segments at the core ends, involved by a casing buckling-restraining element intended to prevent global brace buckling and restrain higher-mode core buckling (Della Corte *et al,* 2014). Preventing the overall buckling phenomena is an advantage because it allows to design BRB's for yielding at low inter-storey drift levels, anticipating dissipative action, and providing substantial and stable energy dissipation capacity to existing RC buildings (Castro *et al,* 2017). Two types of BRB's have been extensively investigated in the scientific literature, differing mainly in the adopted casing, namely: (i) unbounded braces, in which the restraining tube is filled with either

concrete or mortar and an unbounding layer is added to the contact surface between the core and the filling concrete, in order to allow the core to freely slide inside the casing element and expand when in compression (Lin *et al,* 2015) and (ii) all-steel braces, which typically consist of two or more restraining tubes placed in direct contact with the yielding steel core. Relative deformations between members need to be allowed, so an air gap between the brace and the restraining tube exists in both types of device (Della Corte *et al,* 2014). All-steel BRB's have the advantage of being lighter than unbounded braces and can be detailed to be detachable, making inspection and maintenance operations easier (Castro *et al,* 2017). Further details on the seismic design of BRB's can be found in Takeuchi *et al* (2013), Lin *et al* (2015) and NIST (2015).

Figure 2.52 (a) and (b) show the overall arrangement of the BRB system implemented in the ILVA-IDEM project RC building. The braces were connected to the RC beam-column joints using bolted connections (Figure 2.52 (c)). Two solutions were investigated in the test campaign: (i) two buckling-restraining rectangular steel tubes in contact with an internal core element and a couple of internal plates welded to the tube walls to complete the restraining action (Figure 2.52 (d)) and (ii) a core tapered in a more gradual manner, thus reducing the buckling length of the end portion of the core, to provide extra flexural stiffness for out-of-plane buckling strength and to allow full axial yielding of the core element (Figure 2.52 (e)). The latter system was conceived to be fully detachable by joining the two buckling-restraining tubes together using bolted stiffened elements (Figure 2.52 (f)).

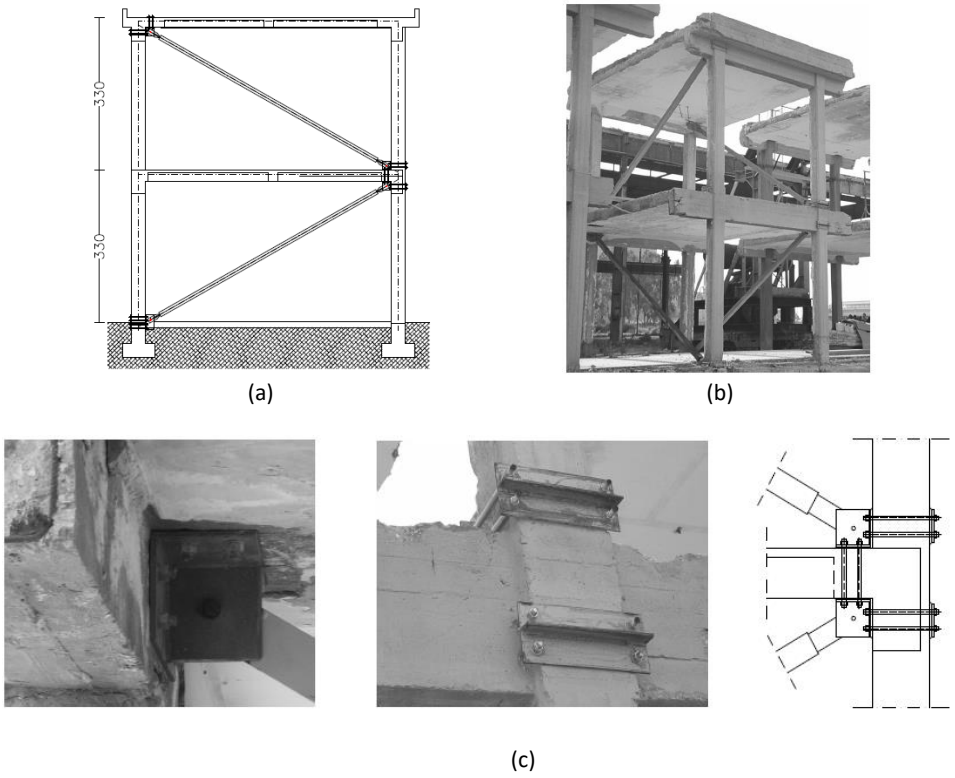

Figure 2.52 (1/2) – Strengthening with BRB's of the existing RC building studied in the ILVA-IDEM project: (a) adopted solution; (b) the strengthened building; (c) brace to RC beam-column joint (adapted from Della Corte *et al,* 2014)

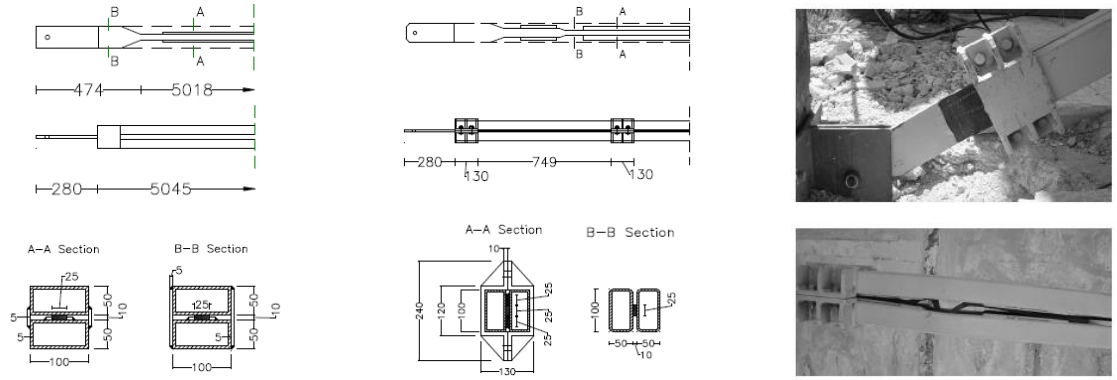

(d) (e) (f)

Figure 2.52 (2/2) – Strengthening with BRB's of the existing RC building studied in the ILVA-IDEM project: (d) un-detachable all-steel BRB tested; (e-f) detachable all-steel BRB tested (adapted from Della Corte *et al,* 2014)

The following conclusions were drawn by Mazzolani (2008), Mazzolani *et al* (2009) and Della Corte *et al* (2014) from the results of the test campaign: (i) the available theoretical models were seen to provide adequate design and performance control of BRB's; (ii) BRB's with a core tapered more sharply were seen to be more susceptible to local buckling at brace ends, producing strong flexural deformation and failure of the closing plates (although ensuring the expected increase in the lateral stiffness and strength of the existing building, this type of BRB was characterised by a rather limited ductility capacity); (iii) detachable BRB's with a core tapered in a more gradual manner were seen to provide not only the expected lateral stiffness and strengthening of the existing RC frame, but also a substantial increase in its deformation capacity (around two times that of the bare RC structure) – however, local buckling of one end-plate was still observed, even satisfying capacity design criteria, which resulted from strong local geometrical imperfections and a flexible end-restraint; (iv) the brace-to-RC joint connections were seen to influence the loading / unloading stiffness of the system, even though it was not possible to derive a general conclusion since these effects depend on the adopted technique to drill the holes required to fill in the mortar on site. Besides the conclusions from the ILVA-IDEM project, further design recommendations for BRB systems have been provided within research project "Steelretro" (RFCS, 2013) and can be found in its report.

2.8.3.3. Metal shear panels

Strengthening systems using metal shear panels (MSP's) offer a rational and innovative solution as they combine significant strength, stiffness and ductility enhancements with limited weight, low erection costs and space constraints. However, deeper attention and further research about this technique is still required (De Matteis *et al,* 2009).

MSP's typically consist of a series of steel plates, located around a certain service area or within perimetric frames, with the aim of creating a stiffening core capable of resisting horizontal demands (Castro *et al,* 2017). They are essentially divided into two main categories: (i) compact shear panels

and (ii) slender shear panels. The former tries to dissipate the energy input by the ground motion through the development of a pure shear-resisting mechanism. In such case, shear buckling should be avoided using low yield strength steel or pure aluminium materials, properly endowed with flexural stiffeners (De Matteis *et al,* 2009). On the other hand, slender shear panels are made of thin steel plates connected to the members of a surrounding steel frame, by means of welded or bolted connections, aiming at improving the strength and stiffness of the original structure. This type of MSP's is expected to buckle under elastic regime, activating a tension field mechanism characterized by diagonal (i.e., parallel to the principal stresses direction) tensile bands at the web, that transfers the lateral shear forces. This mechanism produces a hysteretic behaviour that is characterized by a pronounced pinching effect (Mazzolani, 2008; De Matteis *et al,* 2009). A design procedure that relies on the participation of the original RC building in addition to that of the MSP's to resist external horizontal actions has been proposed by De Matteis *et al* (2009). Extensive numerical analysis on the behaviour of slender MSP's has also been conducted by Formisano *et al* (2007). In opposition, if the strengthening system is to be designed as a dual system, attention must be paid to the assessment of the capacity of the original RC frame to accommodate the forces resulting from the tension field mechanism that develops within the MSP's.

According to RFCS (2013), load transfer beams can be a favourable solution to transfer forces to parts of the structure with sufficient capacity. This solution was adopted in the ILVA-IDEM project, as shown in Figure 2.53 (a). DX56D grade steel panels (Figure 2.53 (b)) and EN AW 1050 A grade aluminium alloy panels (Figure 2.53 (c)) were tested. The performance of the RC building was significantly improved by both solutions (Mazzolani, 2008; De Matteis *et al,* 2009), although the dissipative behaviour provided by the aluminium panels was more satisfactory. Both cases relied on a dual system, in which a combined plastic mechanism characterized by hinging at the RC beam-column joints and plastic deformation of the tensioned diagonals of the MSP's was developed (Figure 2.53 (b) and (c)).

(a) (b) (c)

Figure 2.53 – Strengthening with MSP's of the existing RC building studied in the ILVA-IDEM project: (a) the strengthened building; (b-c) plastic mechanisms developed in the steel and aluminium panels, respectively (Mazzolani, 2008)

2.9. SEISMIC BEHAVIOUR OF RC BUILDINGS RETROFITTED WITH CONCENTRIC STEEL BRACES

Sub-section 2.8.2.2. has already addressed this retrofitting technique, pointing out its benefits regarding the improvement of the seismic performance of existing RC frame buildings and summarizing the associated design topics, along with brief references to several of the experimental and analytical studies conducted over the last years. In detail, Abou-Elfath and Ghobarah (2000) numerically simulated the behaviour of low-rise RC frames, before and after retrofitting with direct steel bracing, while Maheri *et al* (2003) conducted experimental tests on scaled RC frames, retrofitted with X- and knee-braces, and demonstrated the efficiency of X-braces when increased capacity and stiffness were required and that of knee-braces when improved ductility was of concern. Later, Youssef *et al* (2007) conducted a new experimental study on RC frames retrofitted with concentric steel braces and reported similar conclusions. Concerning the interaction between steel braces and RC members, an extensive discussion can be found in Massumi and Absalan (2013) and Faella *et al* (2014), the latter pointing out the implications of choosing different brace configurations. More recently, TahamouliRoudsari *et al* (2017) conducted a new experimental study to investigate the effect of different types of steel braces on the behavioural properties of RC members, while Rahimi and Maheri (2018) numerically simulated the effects that X-brace retrofitting systems have on the performance of RC columns. On the topic of the connection between steel braces and RC frame, experimental programs were conducted by Maheri and Hadjipour (2003), Massumi and Tasnimi (2008) and Maheri and Ghaffarzadeh (2008). Applying to the test specimens the Uniform Force Method (UFM) design provisions for steel brace-steel frame connections, they showed that: (i) connections and elements were strong enough to withstand the involved forces, and (ii) brace failure preceded that of connection elements. More recently, Maheri and Yazdani (2016a; 2016b) carried out an extensive numerical investigation and proposed several guidelines for the design of the components of steel brace-RC frame connections.

Due to the relatively high stiffness supplied by the steel braces, this retrofitting technique is very effective in limiting lateral deformation. For this matter, steel braces and RC frame can be considered as coupled independent systems, each with its own lateral strength and stiffness (Badoux and Jirsa, 1990; Di Sarno and Manfredi, 2009). Some authors believe that, under the earthquake's ground motion, the bracing system should absorb and dissipate a large amount of hysteretic energy, while the RC frame supports only vertical loads and responds elastically to the seismic demand. However, Sousa and Castro (2012) have showed that allowing the existing building to undergo inelastic deformations may have advantages from both the economical and structural stand points. The bracing system can compensate for inadequate RC frame strength and/or stiffness but should not change the original frame's failure mode. Over increasing the capacity of the braces may increase too much the axial forces on the RC columns, which might lead to an excessive reduction of their deformation capacity or (in some cases) to their premature failure. This important effect was first referred by Pincheira and Jirsa (1995) and recently discussed again by Rahimi and Maheri (2018; 2020). In order to provide further insight into the seismic behaviour of these hybrid RC-steel systems, the following sub-sections address in detail the behaviour of the two independent structural systems that coexist in a retrofitted RC building, as well as the interaction between them.

2.9.1. Behaviour of steel braces

The response of a concentrically braced frame (CBF) is typically dominated by the behaviour of its bracing members. During a strong earthquake, the latter are subjected to large inelastic deformations in cyclic tension beyond yield, and compression into the post-buckling range. The hysteretic axial load (P) response of an unrestrained steel brace against its axial deformation (δ) is schematically shown in Figure 2.54. In compression, its elastic behaviour is defined by linear branch [*OA*], until the buckling load P_u is reached. A plastic hinge then develops at the most stressed cross-section (at mid-span), until a kinematic mechanism is formed (point *B*). The brace's post-buckling behaviour is then represented by equilibrium curve [*BC*], leading to a gradual capacity reduction. On reversing the load, elastic unloading occurs (branch [*CD*]). When the brace is completely unloaded, a residual plastic axial deformation remains, which is related to the residual mid-span deflection. The following branches represent the straightening process of the brace member in tension. The behaviour is elastic along branch [*DE*], with point *E* corresponding to the development of a new kinematic mechanism due to yielding of the mid-span cross-section, now under tension combined with bending. Along the mechanism's curve [*EF*], the brace becomes more and more straightened (while the mid-span bending moment reduces), until a new yielding condition is attained in pure tension (point *F*) when it has become completely straightened. Subsequent loading in compression results in buckling at loads lower than the initial strength, due to the residual deflections, the increase in length and the Bauschinger effect. Moreover, due to the accumulated permanent elongation, tensile yielding occurs at axial deformations that increase with each loading cycle (Elghazouli, 2003; Longo *et al,* 2008).

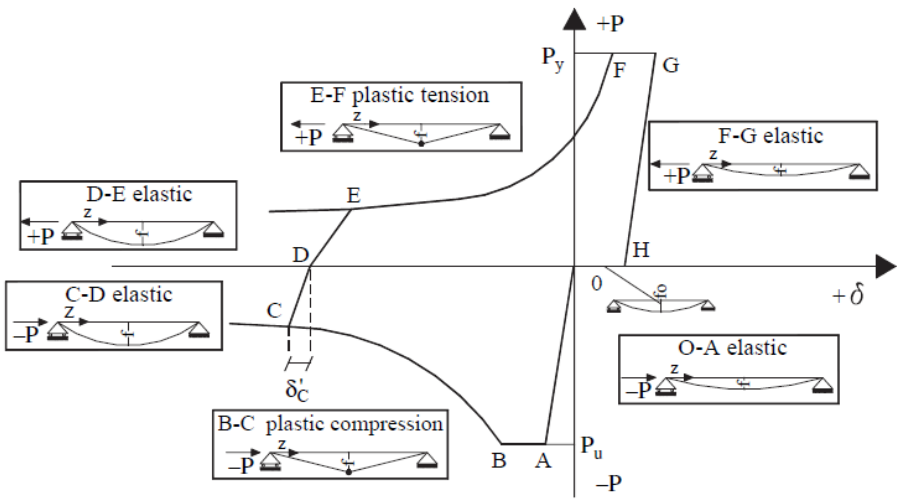

Figure 2.54 – Axial cyclic response of an unrestrained steel brace (adapted from Longo *et al,* 2008)

The nominal capacity in tension is given by the product of the cross-sectional area A by the steel's nominal yield strength f_y. However, the actual capacity of the member in tension may be considerably higher due to several factors: (i) the actual yield strength of steel can exceed the nominal value by up to 20% or more; (ii) strain hardening may lead to an increase of the tension force between 5% and 10%

on average (depending on the ductility demand in tension); (iii) the higher strain rate under actual seismic conditions may also lead to an additional increase in the yield strength, when compared to the nominal value. These factors are recognised by most seismic codes – including EC8-1 (2004) – usually through the provision of an enhancement coefficient. Realistically, whenever the maximum tensile brace force needs to be considered in the analyses, material partial safety factors γ_{Mi} should not be applied and an allowance for the actual yield strength of steel needs to be included (Tremblay, 2002; Elghazouli, 2003; Longo *et al,* 2008).

In compression, the overall buckling load depends on the slenderness of the brace member, which is represented in EC3-1-1 (2005) by its non-dimensional slenderness $\bar{\lambda}$. For non-slender cross-sections, the latter is defined by Expression (2.50), where N_{cr} is the theoretical elastic (Euler) buckling load and the other parameters have been defined above. Combined with the appropriate buckling curve – based on the type of cross-section and axis of buckling – it determines the reduction factor χ that allows for the calculation of the buckling resistance N_b as a percentage of the member's nominal capacity in tension (Expression (2.51)). The value of N_b normally provides a conservative assessment of the minimum buckling resistance under monotonic loading, with the possibility of the actual buckling strength being up to 10% - 15% higher. On the other hand, under cyclic loading there is a characteristic reduction of the buckling strength after one or two cycles. These effects may be accounted for through the application of enhancement and/or reduction factors. It is also important to evaluate the post-buckling resistance N_{pb} of the brace, as it has direct impact over the forces that develop in other frame members (e.g., columns). EC8-1 (2004) recommends a value of $N_{pb} = 0.3 \cdot N_b$, which is a typical relation of good agreement with experimental results, for values of $\bar{\lambda}$ within the range of interest for practical design (Elghazouli, 2003; Longo *et al,* 2008).

$$\bar{\lambda} = \sqrt{\frac{A \cdot f_y}{N_{cr}}} \tag{2.50}$$

$$N_b = \chi \cdot A \cdot \frac{f_y}{\gamma_{M1}} \tag{2.51}$$

Seismic codes normally impose limits to brace members' slenderness, in order to ensure satisfactory hysteretic behaviour. For instance, according to EC8-1 (2004), the non-dimensional slenderness $\bar{\lambda}$ should be limited to $1.3 < \bar{\lambda} \leq 2.0$. The upper limit prevents early elastic buckling and the consequent accumulation of plasticity, which would result in severely pinched hysteretic loops and low energy dissipation. On the other hand, the lower limit is adopted so that, during the pre-buckling stage (when both compression and tension braces are active), the frame's columns are not overloaded beyond the action effects at the ultimate stage. These limits have considerable influence on the design of brace members and direct effect on the performance of the overall structure. However, in strict terms, these code provisions apply to concentric-braced steel frames, therefore not being mandatory for the design of steel-braced RC structures, although serving as a possible reference for it.

2.9.2. Behaviour of RC members

The level of axial load plays an important role in the behaviour of RC members subjected to combined bending and shear. Given a cross-section, the calculated values of axial load N and bending moment M, for a particular combination of strains ε_c and ε_y on the top and bottom faces of the section, can be plotted as a point on a diagram such as the one shown in Figure 2.55. By repeating calculations for several other combinations of strains, the so-called "feasible region" of $N - M$ pairs is defined. The boundary of the latter is usually called the "failure envelope" or "interaction curve". Pairs of N and M that lie outside this boundary cannot be applied to the cross-section under analysis, i.e., such loading conditions will cause the cross-section to fail (Collins and Mitchell, 1997). It is well known that the maximum flexural capacity occurs when a moderate level of compression is present. However, for high levels of compression or in tension conditions, it renders substantially decreased. The shear capacity is influenced in similar way, benefiting from the presence of axial compression but being significantly reduced under the effect of tension forces.

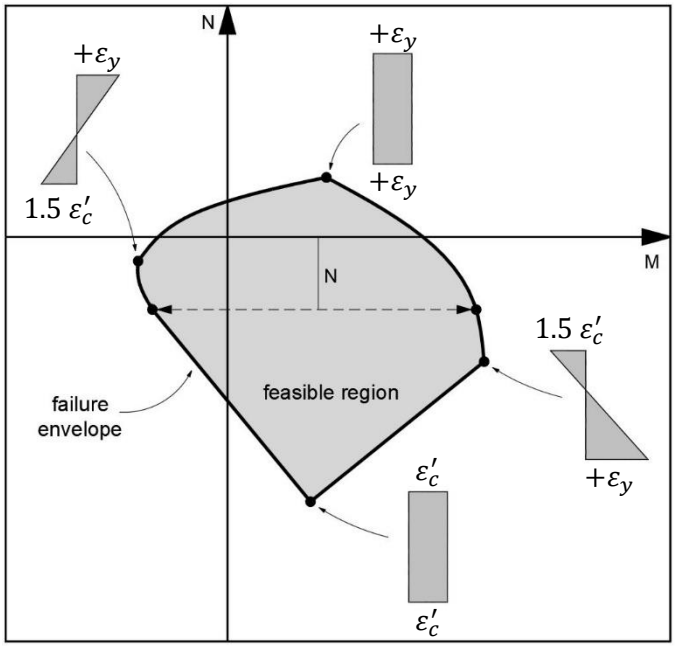

Figure 2.55 – Axial load-bending moment interaction diagram of a RC member (adapted from Collins and Mitchell, 1997)

Besides evaluating the effect on the bending and shear capacities of RC members, attention should also be given to the impact of the level of axial load on their deformation capacity. Figure 2.56 illustrates this effect by plotting the moment-curvature ($M - \phi$) diagram of a given cross-section for different levels of axial load N (negative for compression). The above referred beneficial effect of compression over the flexural capacity of the cross-section can also be observed therein but, on the other hand, it is seen to reduce its curvature capacity. Therefore, a loss of ductility is to be expected in RC members with increasing compression levels, which might lead to premature failure under earthquake loading if not conveniently controlled.

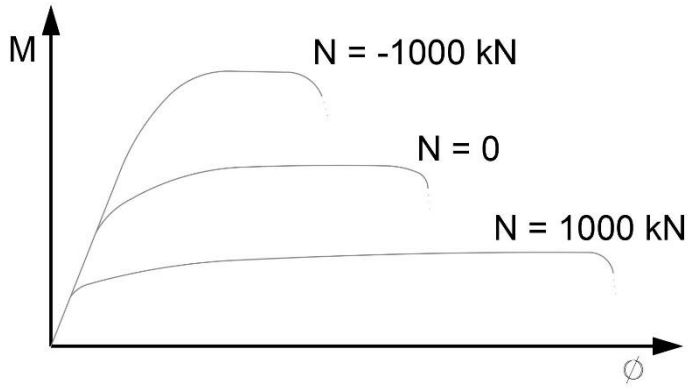

Figure 2.56 – Influence of axial load on moment-curvature response (adapted from Collins and Mitchell, 1997)

When steel braces are added to an existing RC frame, the load paths through which lateral forces are transferred change considerably, as does the distribution of demands on the frame's structural members (Rahimi and Maheri, 2018; 2020). Therefore, when evaluating the effectiveness of this retrofitting technique, it is important not to overlook side-effects – as the ones described above – on the behaviour of the affected RC members (particularly those on columns). For instance, the study by Pincheira and Jirsa (1995) concluded that satisfactory performance was obtained only for bracing schemes that controlled inter-storey drifts to levels that did not cause significant damage to the original RC members. However, for medium- and high-rise buildings, the level of axial forces induced by the steel braces would adversely affect the lateral strength of those members or, in some cases, exceed their axial capacity (tension or compression). Consequently, localized strengthening of columns on braced bays was recommended to ensure the adequate performance of bracing systems designed for such buildings. More recently, Rahimi and Maheri (2018; 2020) conducted an updated numerical study, using nonlinear dynamic analysis models, and examined possible complications of retrofitting older-type RC frames with steel X-bracing systems, in terms of columns shear and axial force, as well as of low cycle fatigue life. The obtained conclusions were in good agreement with those of Pincheira and Jirsa (1995), i.e., the retrofitting was beneficial in almost every aspect to the performance of the columns of low-rise RC frames, whereas for medium- and high-rise frames local strengthening of the columns attached to the bracing system (e.g., using steel, RC or FRP jacketing) should simultaneously be undertaken.

2.9.3. Interaction between steel braces and RC members

The global deformed shape of a single-bay, two storey, steel-braced RC frame under lateral loading is illustrated in Figure 2.57 (b). Braces under tension are shown in blue, while those in compression are shown in red. This shape can be expressed as a combination of shear force distortion (Fig. 2.57 (c)) and overturning moment rotation (Fig. 2.57 (d)). Due to the latter, the columns on the right are in compression, while those on the left experience tension. This causes the axial forces on the braces to have opposite signs to those on the shear force distortion component. However, as the forces induced by the acting shear force are typically higher than those induced by the overturning moment, the

resulting signs of the forces on the braces are those shown in Figure 2.57 (b). The path of forces on the frame's RC members can thus be deducted, as shown in Figure 2.58. By analysing the sign of the vertical force components, one concludes that it does not change in each side of the frame. This means that the columns on the right suffer an increment in compression equal to the sum of the vertical components of the forces acting on the braces, while the columns on the left experience the same force value, but now in tension. The magnitude of the induced forces depends on the slenderness of the braces and needs to be carefully controlled, as referred in the previous sub-section.

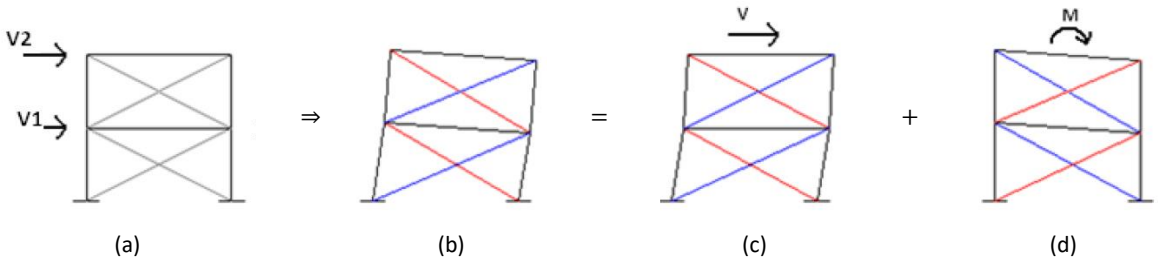

Figure 2.57 – Deformation of a hybrid RC-steel system: (a) undeformed frame with applied lateral loading; (b) deformation due to applied lateral loading; (c) frame distortion due to shear force; (d) frame rotation due to overturning moment (adapted from Sousa, 2010)

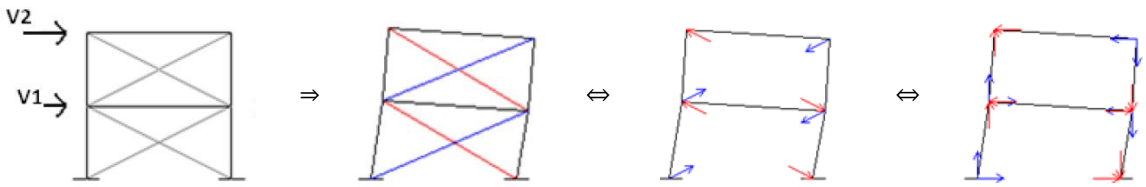

Figure 2.58 – Path of forces in a hybrid RC-steel system under lateral loading (adapted from Sousa, 2010)

Adding steel braces to an existing RC building causes an overall increment to its lateral strength and stiffness, as previously referred. Figure 2.59 below shows (in green) what could be the capacity curve of the above-shown steel-braced RC frame. The contributions of the two independent systems (RC frame in blue and steel braces in red) for the global base shear are also shown. The plot concerning the RC frame is no more than its original capacity curve (i.e., before retrofitting), whereas the one concerning the steel braces represents the evolution of the sum of the horizontal components of the forces acting on the braces located at the first storey. By adding these two isolated contributions (in purple), one obtains a very good approximation to the response of the retrofitted structure. This corroborates the previously referred theory about a hybrid RC-steel system being seen as two coupled independent systems, each with its own lateral strength and stiffness (Badoux and Jirsa, 1990; Di Sarno and Manfredi, 2009), and demonstrates that the increment of base shear produced by the retrofitting system depends solely on the braces at the first storey.

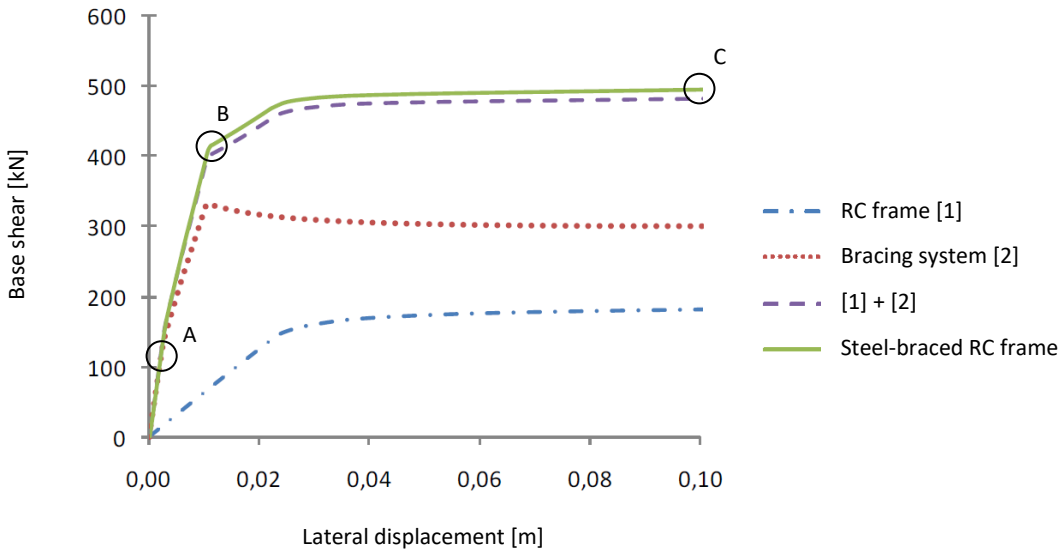

Figure 2.59 – Contribution of each structural system for the global base shear of the retrofitted structure (adapted from Torres Queirós *et al,* 2009)

A closer look at Figure 2.59 reveals particular points on the capacity curve of the steel-braced RC frame (A, B and C), which are relevant to the analysis of its seismic behaviour in light of the modern performance-based earthquake engineering (PBEE) approach. Point A marks the moment when the compressed brace reaches its buckling load. This happens at a relatively low level of base shear, due to the high slenderness of the braces when compared to that of the RC members. A gradual reduction of lateral stiffness then occurs until point B, which marks the moment when the tensioned brace reaches its maximum capacity. From that point on, a significant stiffness reduction occurs, along with the corresponding increase in the lateral displacement's profile. The ultimate capacity of the retrofitted structure is then attained (point C) for a level of base shear close to that which caused the yielding of the tensioned brace. From this analysis, three main ideas should remain: (i) except for the unlikely case in which very stiff steel braces are combined with weak RC columns, the first significant yielding of the structure is expected to occur with the buckling of the compressed braces; (ii) the lateral displacement corresponding to the global yielding of the structure can be reasonably well predicted by relating it to the lateral displacement of the tensioned braces; (iii) the ultimate displacement of the structure is governed by the RC columns, which again stresses the need to relate their deformation capacity with the level of axial load induced by the bracing system.

2.10. METHODOLOGIES FOR THE SEISMIC DESIGN OF CONCENTRIC STEEL-BRACE RETROFITTING SYSTEMS

Seismic design is currently codified by structural codes and standards of practice using the so-called "force-based design" (FBD). This is mainly due to historical reasons and related to how design is carried out for other actions such as dead and live loads (Priestley *et al,* 2007). This procedure involves the consideration of a behaviour factor (q-factor) as a simple mean to account for the nonlinear behaviour of the structure while performing linear static analysis. However, in structures designed according to

old seismic codes (or even non-seismic codes), the uncertainties about the nonlinear behaviour are relevant, making it very difficult to define a direct correlation between the real internal forces that develop in structural members during the seismic excitation, and those experienced by an equivalent indefinitely elastic structure. Moreover, the improvement in the seismic behaviour of a RC structure retrofitted with steel braces does not seem to be proportional to the corresponding increase in lateral strength, which has led several authors (e.g., Mpampatsikos *et al,* 2008) to suggest that the *q*-factor based design process might not be an efficient approach to obtain retrofitted structures with good seismic performance.

Alternative to the traditional FBD methods is given by the modern displacement-based design (DBD) procedures. Unlike the former, whose main purpose is collapse prevention, the latter seek to ensure that pre-determined damage levels are not exceeded when a structure is subjected to a set of seismic intensity scenarios (Priestley *et al,* 2007). Their application has been progressively increasing in the past years (Villani *et al,* 2010; Macedo and Castro, 2012; Sullivan, 2013) and several advantages have been pointed out regarding their force-based counterpart. The possibility to take explicit consideration of the interaction between both structural systems (RC frame and steel braces), namely the influence of the steel braces' resistance on the deformation capacity of RC columns, seems to be the upper hand for the design of this kind of retrofitting systems.

The discussion about the advantages and disadvantages of the above-referred design approaches is still wide and ongoing. Hence, both are addressed in the following sub-sections. The FBD methodology is first reviewed, followed by a discussion of the few existing studies that resulted in proposals for the *q*-factors to be applied in the design of RC buildings strengthened with steel braces. Afterwards, the fundamentals of the DBD procedure are reviewed and its advantages, when compared to traditional design methodologies, are discussed.

2.10.1. Force-based design

In simple terms, FBD involves the calculation of a seismic base shear force F_b, which is a function of the structure's global mass and fundamental period, of the applicable (usually code-based) response acceleration spectrum, and of the considered *q*-factor. This base shear force is then applied to the structure as a set of equivalent static lateral forces, adequately distributed along its height (typically according to the fundamental vibration mode shape). Figure 2.60 shows the shape of the elastic response acceleration spectrum according to EC8-1 (2004). For the quantification of F_b, Expression (2.52) can be used, provided that the structure's seismic response is not significantly affected by the contributions of higher order vibration modes, in each principal direction. In the referred expression, T_1 is the structure's fundamental period for lateral motion in the considered direction, $S_d(T_1)$ is the ordinate of the design acceleration spectrum at period T_1, m is the structure's total mass above the foundation (or above the top of a rigid basement), and λ is an effective modal mass-related factor ($\lambda = 0.85$ when $T_1 \leq 2 \cdot T_C$ and the structure has more than two storeys; $\lambda = 1.0$ otherwise). Lastly, the ordinates of the design acceleration spectrum are obtained from those of the elastic spectrum by scaling them down using the applicable *q*-factor.

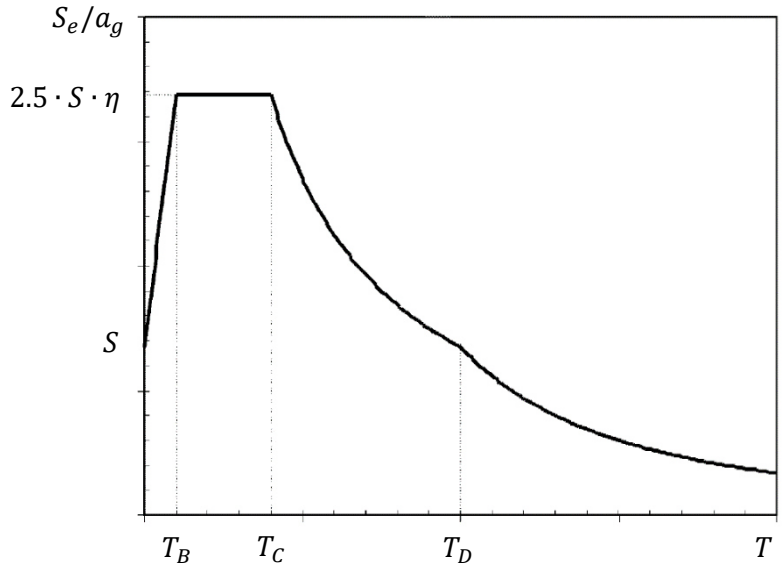

Figure 2.60 – Shape of the elastic response acceleration spectrum (EC8-1, 2004)

$$F_b = S_d(T_1) \cdot m \cdot \lambda \tag{2.52}$$

Once the equivalent static lateral forces have been applied to the structure, member capacity checks are then carried out, along with some simple lateral deformation checks. It is generally accepted that damage can be related to material strains and the latter to maximum response displacements, but not to response accelerations. As such, the design procedure would be expected to emphasize the importance of estimating the peak displacement response in inelastic systems, which is still a matter characterized by some uncertainty. The most common approach is the so-called "equal displacement approximation", which states that the displacement of the inelastic system is the same as that of the equivalent system with elastic stiffness and unlimited strength. The design displacement $\Delta_{max,duct}$ can thus be estimated by Expression (2.53), where $S_e(T_1)$ is the ordinate of the elastic acceleration spectrum at period T_1. The principle underlying the equal displacement approximation is illustrated in Figure 2.61. However, as this approach is known to be non-conservative for short period structures (i.e., $T_1 < T_C$), some national codes (e.g., Central and South America; some Asian countries) apply the so-called "equal energy approximation" when determining peak displacements. This assumption equates the energy absorbed by the inelastic system, on a monotonic displacement to peak response, to the energy absorbed by the equivalent elastic system with the same initial stiffness. The peak displacement can thus be estimated by Expression (2.54).

$$\Delta_{max,duct} = \Delta_{max,elastic} = \frac{{T_1}^2}{4 \cdot \pi^2} \cdot S_e(T_1) \tag{2.53}$$

$$\Delta_{max,duct} = \Delta_{max,elastic} \cdot \left(\frac{q^2+1}{2 \cdot q}\right) = \frac{{T_1}^2}{4 \cdot \pi^2} \cdot S_e(T_1) \cdot \left(\frac{q^2+1}{2 \cdot q}\right) \tag{2.54}$$

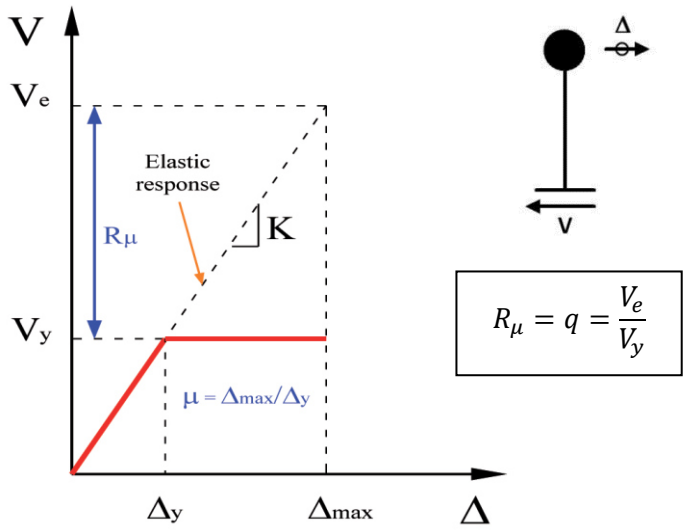

Figure 2.61 – Idealized response of a SDOF system: equal displacement approximation (adapted from Carrillo *et al,* 2014)

Although it might seem simple to determine which rule yields the best approximation (e.g., by running nonlinear dynamic analysis tests), Priestley (2003) referred that all are correct at some part of the period range of structural response, and all are wrong at other periods. This can be explained using typical displacement spectra, as those shown in Figure 2.62, where the influence of inelastic response is represented by an effective period's lengthening, and hysteretic damping is represented as equivalent viscous damping. For short period structures, the increase in displacement response due to period elongation is less than the decrease resulting from increased damping; for medium period structures, the two effects almost balance each other; for long period structures, the period's elongation does not cause significant increase in displacement, but the effect of the increased damping is to reduce the overall displacement response; lastly, for very long period structures, the displacement is equal to the ground's displacement and independent of period and/or damping ratio.

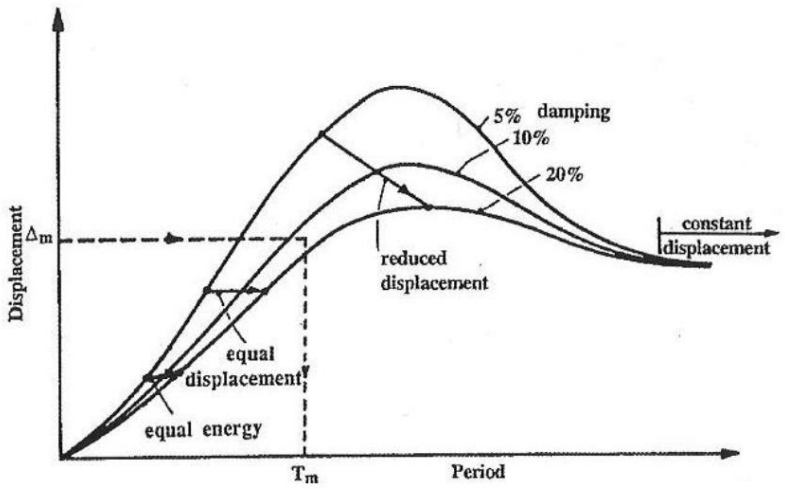

Figure 2.62 – Displacement spectra for different levels of damping (Priestley, 2003)

The relevance of the q-factor in the context of seismic FBD methodologies is evident in the above-referred principles. Its value depends on the plastic deformation and energy dissipation capacities of the structure, globally, and of its members, individually. Several recommendations regarding which value to adopt can be found in EC8-1 (2004), depending on the structure's material, typology, and ductility class. In Figure 2.61 (above), for a structure expected to observe a pre-defined displacement ductility demand $\mu = \Delta_{max}/\Delta_y$, the q-factor is defined as the ratio between the strength of the equivalent elastic system with the same initial stiffness, V_e, and the actual design strength V_y of the inelastic system. However, this is valid for a SDOF system with stable hysteretic behaviour. In the case of real MDOF systems, the q-factor should be defined while taking the structure's pushover curve into due consideration. Figure 2.63 shows the typical lateral response curve of a ductile frame structure, where V_{el} represents the base shear if it were to respond elastically, V_y represents the ductile structure's maximum base shear, V_{1y} represents the base shear when the first plastic hinge develops, and V_d represents the design base shear. The horizontal axis refers to the horizontal displacement Δ of the control node on the last floor. In agreement with the evolution of the described capacity curve, the associated q-factor can be defined by Expression (2.55).

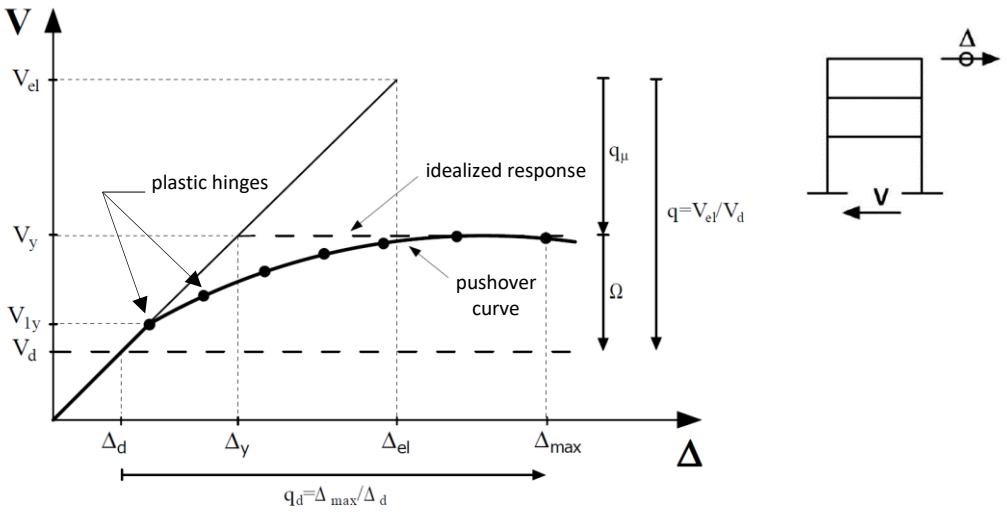

Figure 2.63 – Behaviour factor definition for MDOF systems (adapted from Villani *et al,* 2009)

$$q = \frac{V_{el}}{V_d} = \frac{V_{el}}{V_y} \cdot \frac{V_y}{V_d} = q_\mu \cdot \Omega \tag{2.55}$$

The above defined terms $q_\mu = V_{el}/V_y$ and $\Omega = V_y/V_d$ represent, respectively, the ductility and overstrength components of the q-factor. The force ductility factor q_μ is directly related with the structure's energy dissipation level, while the overstrength ratio Ω represents all its sources of overstrength, such as plastic redistribution capacity, strain hardening, difference between real and design material strengths, and others. Figure 2.63 also quantifies the displacements amplification factor $q_d = \Delta_{max}/\Delta_d$, which relates the structure's maximum inelastic displacement with its elastic

displacement when subjected to the design base shear V_d. However, if one considers the previously referred equal displacement approximation ($\Delta_{max} = \Delta_{el}$), then q_d can be taken equal to the *q*-factor as defined by Expression (2.55), provided that the structure's fundamental period T_1 is higher than the corner period T_C of the design acceleration spectrum.

As the recommendations found in EC8-1 (2004) concerning the choice of a *q*-factor are not easily applied to the design of hybrid RC-steel systems, the main goal of the studies performed in the past (e.g., Maheri and Akbari, 2003; Torres Queirós *et al,* 2009; TahamouliRoudsari *et al,* 2017) was to investigate the applicability of the FBD methodology to steel-braced RC structures, and to propose adequate values for the behaviour factors (q or R) to be adopted. Maheri and Akbari (2003) performed numerical tests on RC buildings, with four, eight, and twelve storeys, changing the braces' layout in such a way that they would carry different percentages of the total base shear. The tests were conducted using X- and knee braces. The obtained results seemed to indicate the number of storeys as the predominant variable influencing the behaviour factor R, when compared to the type of braces or shared percentage of base shear. However, the latter was also deemed to play an important role, which was expected since the strength of the braces governs both the yielding and the ultimate capacity (hence, the ductility level) of the retrofitted structure, as previously referred. Table 2.16 shows the values proposed by Maheri and Akbari (2003) for the behaviour factor R, depending on the ductility demand $\mu = \Delta_{max}/\Delta_y$. Further considerations about the obtained results can be found in the original research paper, its reading being strongly recommended as the straightforward application of the proposed factors is far from consensual.

Table 2.16 – Tentative values of behaviour factor R for steel-braced RC frames (Maheri and Akbari, 2003)

	$\mu = 2$	$\mu = 3$	$\mu = 4$	$\mu = 5$
R	5.0	7.0	9.0	12.0

Torres Queirós *et al* (2009) also conducted numerical tests on RC frames, with one and three storeys, considering three different X-brace retrofitting systems. The steel braces were selected according to their non-dimensional slenderness $\bar{\lambda}$, as defined by EC3-1-1 (2005). The study confirmed that, in general, as the strength of the bracing system increased, the *q*-factor decreased. There was an exception, however, in the one-storey frame, probably because the additional axial load induced by the steel braces in the RC columns was low enough not to significantly reduce the lateral deformation capacity of the latter. Another relevant conclusion was that the *q*-factor value almost doubled from the one-storey to the three-storey frame. However, the most interesting value obtained during the study was $q = 0.7$, for the one-storey frame retrofitted with the strongest brace system. This value indicates that the ultimate capacity of the retrofitted structure was higher than the elastic seismic demand and that, as such, it would respond elastically to the design earthquake. Table 2.17 shows the values proposed by Torres Queirós *et al* (2009) for the *q*-factor, depending on the number of storeys and robustness of the bracing system. A direct relation with the conclusions presented by Maheri and Akbari (2003) seems difficult to establish.

Table 2.17 – Tentative values of *q*-factor for steel-braced RC frames (Torres Queirós *et al,* 2009)

	Number of storeys	$\bar{\lambda}$		
		2.5	**2.0**	**1.5**
q	**1**	1.4	1.6	0.7
	3	3.0	2.7	1.5

Lastly, TahamouliRoudsari *et al* (2017) conducted experimental tests on scaled (1:3) RC frames, with one storey and one bay, considering different brace types such as the concentric X, knee, chevron, eccentric, and chevron with vertical link. All the frames were subjected to cyclic loading and their hysteresis load-displacement diagrams were plotted. Strength, stiffness, crack expansion, ductility, energy dissipation and strength reduction factor (R) were assessed. The obtained results indicate that, from the ductility and strength reduction factor standpoints, the eccentric braces deliver the best performance. However, from the stiffness, strength, and cracking control standpoints, the X-braces have the upper hand. Moreover, at the final moment of loading, the frame with the eccentric braces had sustained the most damage to the RC members. Table 2.18 shows the values recommended by TahamouliRoudsari *et al* (2017) for the strength reduction factor R of retrofitted frames, depending on the chosen brace type (again, it seems difficult to establish a relation with the results of the above referred studies). Even though the X-braces earned the recommendation for the lowest R-factor (being the system that most reduced energy dissipation and ductility), the increase in stiffness and strength, the cracking pattern, and the failure type of the retrofitted structure were much better than those of the other samples. Therefore, this is considered to be a good indicator of the related potential for suitable seismic performance. For further conclusions of this study, the interested reader is referred to the original research paper.

Table 2.16 – Tentative values of behaviour factor R for steel-braced RC frames (TahamouliRoudsari *et al,* 2017)

	X	Knee	Chevron	Eccentric	V. link
R	3.0	5.0	5.0	7.0	5.0

2.10.2. Displacement-based design

The previous sub-section analysed the FBD of structures subjected to earthquakes. Among other details, it discussed how member deformations are indirectly addressed, via the *q*-factor, at the end of the design process. In the event that code-specified displacement limits are exceeded, a revision of the structural members' stiffness is required. This constitutes an attempt to upgrade the traditional force-based approach, with a displacement check, to ensure that acceptable performance levels are achieved during the design earthquake. However, Priestley *et al* (2007) argue that the resulting protection against damage – provided to different structures under a given seismic intensity – is non-uniform, which seems to be philosophically incompatible with the uniform-risk seismic intensity incorporated in most design codes. Moreover, performance criteria are still not directly addressed at the initial stage of design, i.e., emphasis continues to be on strength control.

Priestley *et al* (2007) further argue that a fundamental problem with FBD, particularly when applied to RC or masonry structures, lies in the estimates of initial stiffness required to determine the distribution of design forces between structural members. A common assumption is 50% of the stiffness of uncracked elements (widely used for the design of new structures, as previously referred), though some design codes specify values that depend on member type and level of axial force. Evidently, the assumed value has significant influence on the design seismic forces – for instance, considering the response spectrum depicted in Figure 2.60 (above) in the period range between T_C and T_D, a 40% reduction of the design seismic force is obtained when assuming 35% instead of 100% of the gross stiffness – but that is not the main issue. Regardless of the value, the assumption of constant member stiffness implies that the yield curvature is directly proportional to flexural strength, as shown in Figure 2.64 (a). However, detailed analyses and experimental evidence (the interested reader is referred to Priestley *et al,* 2007) essentially show that, given a cross-section, stiffness is proportional to strength, and yield curvature is independent of strength, as shown in Figure 2.64 (b). This interdependency of strength and stiffness makes it impossible to perform an accurate analysis of either the elastic vibration periods, or of the elastic distribution of required strength throughout the structure, until member strengths have been determined. Since the latter are the end-product of FBD, the consequence is that an iterative process must be carried out for an adequate elastic characterization of the structure to be obtained. Although this is a simple process, it is rarely performed by designers. Nonetheless, it does not solve the additional problems associated with initial stiffness representation, which are briefly addressed below.

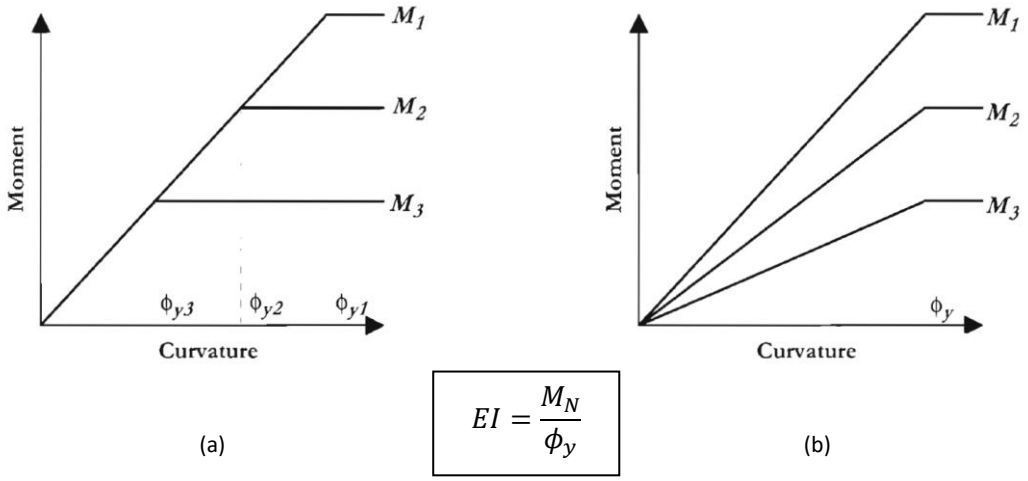

Figure 2.64 – Influence of strength on moment-curvature relationship: (a) design assumption (constant stiffness); (b) realistic conditions (constant yield curvature) (adapted from Priestley *et al,* 2007)

The assumption that the elastic characteristics of a structure are the best indicator of its inelastic performance – as implied by FBD – is, by itself, of doubtful validity. In the cases of RC or masonry structures, the initial elastic stiffness ceases to be valid once yielding occurs, as it degrades due to

crushing of concrete, Bauschinger effect, and damage to crack surfaces. This is illustrated in the idealized force-displacement hysteresis for a RC structure shown in Figure 2.65: the first six continuous arrows represent the first cycle of inelastic response; a second cycle to the same displacement limits is then represented by the following dash-dot arrows. After yielding and moderate inelastic response, the initial stiffness K_i becomes irrelevant, even to the subsequent elastic response. Reloading stiffnesses are substantially lower than the initial value, as are the unloading stiffnesses. It would thus seem obvious that the structural characteristics that represented performance at maximum response might be better predictors of performance at maximum response than the initial values of stiffness and damping (Priestley *et al,* 2007).

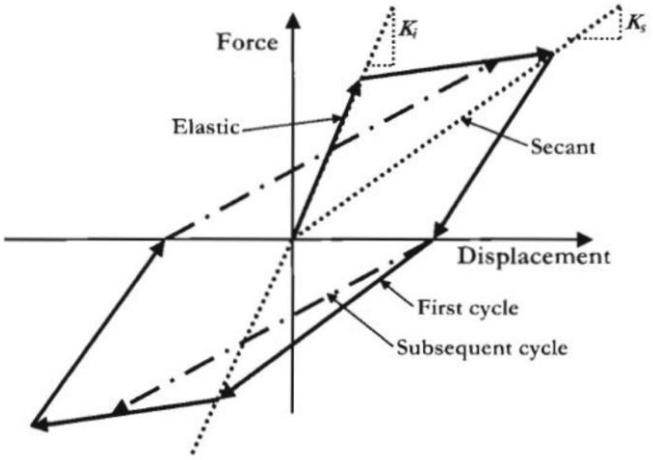

Figure 2.65 – Idealized RC force-displacement hysteretic response, with initial (K_i) and secant (K_s) stiffnesses characterization (adapted from Priestley *et al,* 2007)

Another common assumption in FBD is that increasing the strength of a structure (by reducing the value of the *q*-factor) improves its safety. Referring to Figure 2.61 (above), one observes that an increase in strength V_y causes a reduction of the ductility demand μ, as the yield displacement Δ_y increases while the final displacement Δ_{max} remains unaltered. This reduction of the ductility demand causes a decrease in the associated potential for damage, as it implies a lower demand-to-capacity (*D/C*) ratio in terms of ductility. However, at this point two flaws in this reasoning have already been identified: (i) stiffness is not independent of strength; (ii) the equal displacement approximation is known to be non-conservative for short (or very long) period structures. Priestley *et al* (2007) refer an additional flaw, related to the definition of a unique ductility capacity for each structural type, and numerically demonstrate why the reasoning behind this argument is invalid. They further demonstrate why FBD is not ideally suited to estimate the maximum displacement of structures under seismic demand, which is a serious criticism to the method considering that it is now widely accepted that peak displacements are paramount to determine the level of damage. Despite these criticisms, it should be emphasized that current FBD, when combined with capacity design principles and careful detailing, generally produces safe and satisfactory (new) structures.

As the importance of deformation, rather than strength, in assessing seismic performance has come to be better appreciated, several new methods have been developed to design structures that will achieve, rather than be bounded by, a specified performance limit state under the design-level earthquake. As damage can be directly related to deformation, designing to achieve a specified displacement limit implies designing for a specified risk of damage, which appears more compatible with the above-referred concept of uniform-risk seismic intensity. It thus means that different structures designed to this approach will (ideally) have the same risk of damage, instead of the variable risk associated with current design approaches. Priestley *et al* (2007) refer that, using state-of-the-art detailing / deformation relationships, it is theoretically possible to achieve structures with uniform risk of damage and collapse. For that matter, the way in which stiffness characterization is handled varies between methods. Some adopt the initial pre-yield elastic stiffness K_i – as in conventional FBD – requiring some iterations modifying initial stiffness and strength to achieve the desired displacement. These approaches also rely on existing relationships between elastic and inelastic displacements, such as the above-referred equal displacement or equal energy approximations. Other methods consider the secant stiffness to maximum displacement K_s, requiring little or no iterations, thus being known as "direct displacement-based design" methods. Both stiffness assumptions are illustrated in Figure 2.65 (above) for a typical force-displacement hysteretic response. The way in which hysteretic energy dissipation is handled also varies between methods. Two main types of procedure can be identified: (i) those that use inelastic spectra generated by SDOF analyses of structures of different initial elastic periods, using a specified hysteresis rule and maximum ductility, and (ii) those that use equivalent viscous damping (EVD), provided that the relationships between EVD, ductility, and hysteretic rule have been pre-calibrated by inelastic time-history analyses (this procedure is only appropriate when the secant stiffness K_s is used in the design process). A discussion about the advantages and disadvantages between both procedures can be found in Priestley *et al* (2007).

From among the several DBD methods, the direct displacement-based design (DDBD) approach developed by Priestley *et al* (2007) is thought to be best equipped to address the above-referred deficiencies of conventional FBD methodologies, essentially due to its simplicity, versatility, and suitability to be incorporated in design codes. The fundamental difference from FBD is that it uses a SDOF representation of performance at peak displacement response to characterize the structure, rather than its initial elastic characteristics. This is based on the "substitute structure" approach, pioneered by Gulkan and Sozen (1974) and Shibata and Sozen (1976), that assumes the fundamental vibration mode as dominant. The procedure determines the required strength, at designated plastic hinge locations, to achieve the specified target displacement. It must then be combined with capacity design procedures, to ensure that plastic hinges occur only where intended, and that non-ductile inelastic deformation modes do not develop. These capacity design procedures are calibrated to the DBD approach, thus typically leading to structures that are economically more efficient than those obtained with FBD, as the requirements for DBD are generally less onerous than those for FBD (Priestley *et al,* 2007). The general workflow of the DDBD method is illustrated in Figure 2.66, using the SDOF representation of a frame building as an example. These fundamentals apply, however, to all structural types. The basic formulation of the method is therefore described below, along with the corresponding numerical expressions.

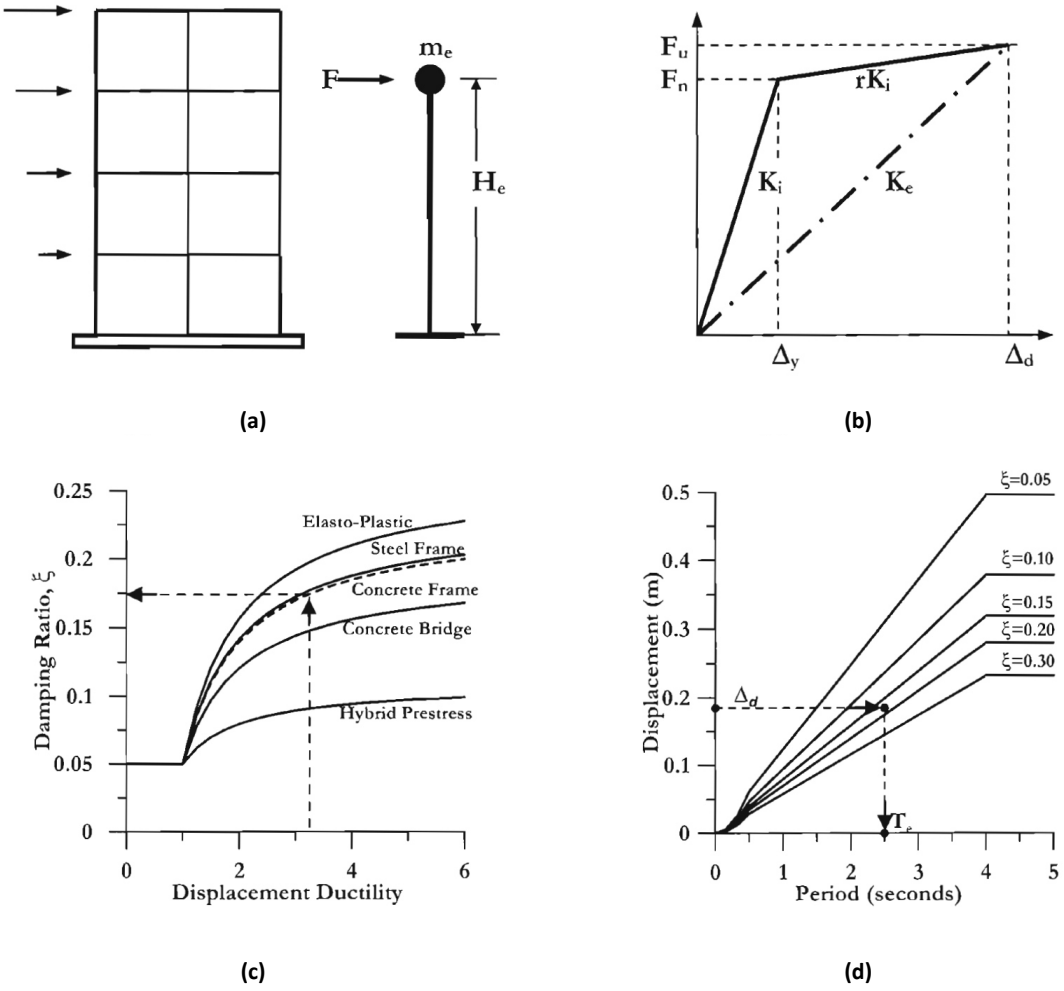

Figure 2.66 – Fundamentals of DDBD: (a) SDOF simulation; (b) effective stiffness K_e; (c) equivalent damping ξ vs. ductility demand; (d) design displacement spectra (adapted from Priestley *et al,* 2007)

Figure 2.66 (b), above, shows the bi-linear envelope of the lateral force-displacement response of the SDOF representation of the frame building, where K_i is the initial elastic stiffness, $r \cdot K_i$ is the post-yielding stiffness, and K_e is the secant stiffness at maximum displacement Δ_d. The EVD ratio ξ (which represents the combined effect of elastic damping and hysteretic energy absorption during inelastic response, as previously discussed in sub-section 2.7.2.1.) is then obtained from curves such as those shown in Figure 2.66 (c), depending on the expected ductility demand $\mu = \Delta_d/\Delta_y$ and on the structural typology under analysis. With the design displacement at maximum response and the corresponding EVD ratio, the effective period T_e at maximum displacement response (measured at the effective height H_e – see Fig. 2.66 (a)) can be read from a set of displacement spectra for different levels of damping such as those shown in Figure 2.66 (d). The secant stiffness K_e of the equivalent SDOF system at maximum displacement is then obtained inverting the normal equation for the period of a SDOF oscillator, as given by Expression (2.56), where m_e is the effective modal mass of the fundamental vibration mode. Finally, the seismic base shear force F_b is quantified using Expression (2.57).

$$K_e = \frac{4 \cdot \pi^2 \cdot m_e}{{T_e}^2} \tag{2.56}$$

$$F_b = K_e \cdot \Delta_d \tag{2.57}$$

The base shear force can now be distributed between the mass elements of the frame building as inertia forces, and structural analysis run to determine the design moments at locations of potential plastic hinges. The design concept is thus very simple. The complexity that exists lies in determining the characteristics of the equivalent SDOF system (effective mass m_e, design displacement Δ_d, EVD ratio ξ), and in developing the design displacement spectra. The design displacement Δ_d depends on the limit state (LS) displacement, or drift, of the most critical member of the frame building and on the assumed displacement shape. The latter is that which corresponds to the inelastic first mode at the design level of seismic excitation. This ensures that changes to the elastic first mode shape, resulting from local changes to member stiffness caused by inelastic action in plastic hinges, are considered at the beginning of the design, which is consistent with characterizing the structure by its secant stiffness to maximum response (nonetheless, the inelastic and elastic first mode shapes can sometimes be very similar). The design displacement Δ_d (generalized coordinate) can thus be obtained with Expression (2.58), where m_i and Δ_i are the masses and displacements of the n floors of the frame building, respectively, while the effective mass m_e is given by Expression (2.59).

$$\Delta_d = \frac{\sum m_i \cdot {\Delta_i}^2}{\sum m_i \cdot \Delta_i} \tag{2.58}$$

$$m_e = \frac{\sum m_i \cdot \Delta_i}{\Delta_d} \tag{2.59}$$

Knowing the LS displacement Δ_c of the most critical member, and the inelastic mode shape δ_i, the floor displacements Δ_i are given by Expression (2.60), where δ_c is the value of the inelastic mode shape at the critical floor. For frame buildings, the LS displacement of the critical member will normally be governed by drift limits at the lower storeys. As for the definition of the inelastic displacement shape, Priestley *et al* (2007) proposed expressions (2.61a) and (2.61b) which, though approximate, were shown to be adequate for the design of frame buildings, provided that capacity design procedures are not overlooked. In expressions (2.61a) and (2.61b), H_i and H_n represent the heights of level i and n (the roof), respectively. For an extensive discussion on the definition of inelastic displacement shapes, for this and other structural typologies, the interested reader is referred to Priestley *et al* (2007) and Sullivan *et al* (2012).

$$\Delta_i = \delta_i \cdot \frac{\Delta_c}{\delta_c} \tag{2.60}$$

$$n \leq 4 \;\Rightarrow\; \delta_i = \frac{H_i}{H_n} \tag{2.61a}$$

$$n > 4 \;\Rightarrow\; \delta_i = \frac{4}{3} \cdot \frac{H_i}{H_n} \cdot \left(1 - \frac{H_i}{4 \cdot H_n}\right) \tag{2.61b}$$

Concerning the EVD ratio ξ, Priestley *et al* (2007) proposed several simplified expressions, based on the structural typology under analysis and on the expected ductility demand $\mu = \Delta_d / \Delta_y$, that can be used to obtain a conservative estimate. Expressions (2.62a) and (2.62b) are those applicable to frame buildings, for a tangent stiffness-proportional elastic damping ratio of 5%. For other formulations and more information about methods for the quantification of EVD ratios, readers are referred to Dwairi *et al* (2007) and Priestley *et al* (2007). The computation of the expected ductility demand μ requires knowing the equivalent SDOF system's yield displacement Δ_y, besides the already known design displacement Δ_d. The above referred Expression (2.58) can be used for that purpose, provided that the computed values of Δ_i correspond to the frame's displacement profile at first significant yielding (which will normally be governed by a lower storey's yield drift). This enables the straightforward application of the expressions given below.

Concrete frame buildings: $$\xi = 0.05 + 0.565 \cdot \left(\frac{\mu - 1}{\mu \cdot \pi}\right) \tag{2.62a}$$

Steel frame buildings: $$\xi = 0.05 + 0.577 \cdot \left(\frac{\mu - 1}{\mu \cdot \pi}\right) \tag{2.62b}$$

The above-described methodology can also be used to address the seismic assessment of existing structures. The basic formulation of the so-called displacement-based seismic assessment (DBA) procedure – which in some ways is the DDBD procedure applied in reverse – was first proposed by Priestley (1997), and later updated by Priestley *et al* (2007). The main challenges (now more complex) continue to be: (i) determining which structural element will first reach the specified performance limit and (ii) defining the corresponding inelastic displacement shape. If the building is of fairly recent construction, then capacity design principles may have been adopted, ensuring that a beam-sway mechanism develops under seismic attack. In this case, the inelastic shape profiles defined above by expressions (2.61a) and (2.61b) can be used. However, for older-structures where capacity design principles were not enforced and soft-storey mechanisms may be prevalent, the use of such beam-sway expressions is no longer valid. In that case, as the displaced shape changes from almost linear at yield to nearly bilinear at LS with high drift of the swayed storey(s), the inelastic shape profile is thus best defined through an adaptive displacement-based pushover analysis, although simplified procedures have been proposed by Priestley *et al* (2007) and others. Figure 2.67 illustrates these two possible LS mechanisms, as well as a possible mixed mechanism that combines column-sway (soft-storey) and beam-column joint sway phenomena, the latter resulting in the inelastic deformation being distributed between the two adjacent floors (rather than concentrated at a single floor as in the simple column-sway mechanism).

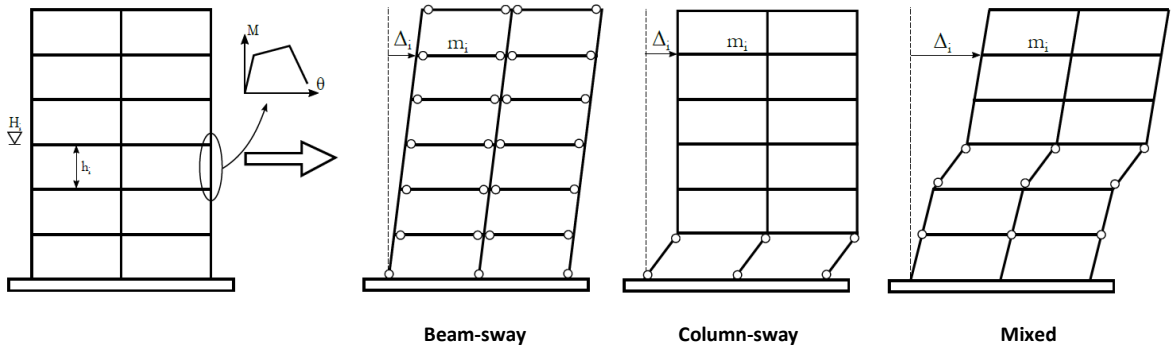

Figure 2.67 – Possible displacement profiles for the seismic assessment of buildings (adapted from O'Reilly, 2016)

Several studies (e.g., Sullivan and Calvi, 2011; Saborio Romano, 2016; O'Reilly, 2016) have applied the DBA methodology to older-type RC frames. The work of O'Reilly (2016), in particular, tested the procedure on a sample of structures, with varying number of storeys and infill typology, and validated it using incremental dynamic analyses' (IDA) results as calibration, while highlighting topics that require further research. The common goal of these studies was to illustrate how it is possible to conduct a detailed assessment without the use of advanced modelling and analysis techniques, such as those discussed in previous sections of this chapter. For that matter, the procedures involved in each step are discussed, with emphasis on how to identify if a column-sway mechanism is to be expected and in which storey it will most likely occur, as well as on establishing the displacement profile. On the latter topic, expressions are proposed to determine a storey's yield drift, according to the identified failure mechanism. More recently, Peng and Guner (2018) developed a computer program thar uses nonlinear FE analysis output and the response spectrum in ASCE 7-10 (2013) code to verify, applying the DBA methodology, whether the performance objectives in FEMA 356 (2000) are satisfied (or not) for a given frame structure. Even though the program was specially written for the output of software platform *VecTor5* (Guner and Vecchio, 2008), the algorithm can easily be adapted to the output of any other nonlinear FE procedure. Further details on the application of the DBA methodology to non-ductile frame buildings can be found in the above-quoted references, their reading being highly recommended due to the included vast amount of valuable information.

The previously referred difficulties that arise when one tries to apply the FBD methodology to hybrid RC-steel systems (see sub-section 2.10.1.) have also motivated several authors (e.g., Sousa and Castro, 2012; Malekpour *et al,* 2013; Mazza and Vulcano, 2015; Ferraioli and Lavino, 2018) to explore the DBD approach when dealing with steel-braced RC structures. For instance, the study performed by Sousa and Castro (2012) attempted to propose a design procedure for the braces, that would explicitly consider the interaction between the two structural systems. Even though the scope of the study is limited due to the reduced number and low-rise of the analysed structures, the obtained results clearly confirm the advantages of the DBD approach. Malekpour *et al* (2013) also investigated a DBD procedure for such structural systems. Frames with 4, 8, and 12 storeys were designed, and their performance evaluated using nonlinear dynamic analysis. However, the proposed procedure relies on the assignment of strength proportions between braces and RC frame members before any analysis can be run, which might not be the best approach when the problem is to design a retrofitting system

for an existing structure. Lastly, Ferraioli and Lavino (2018) proposed a DBD method for the retrofitting of RC buildings using hysteretic dissipative braces, which evolves and improves the procedure proposed by Mazza and Vulcano (2015). It explicitly considers the frame-damper interaction, i.e., the force demands applied to frame members due to damper yielding and strain hardening. It also uses a displacement-based adaptive procedure to carry out the pushover analyses, in an attempt to solve the drawbacks of the fixed load pattern and account for higher modes' contribution and torsion effect in asymmetric buildings. The proposed method was first validated using nonlinear static and dynamic analyses of a numerical example, being afterwards implemented in the case-study of an existing RC school building to assess its applicability in current practice. Once more, the obtained results confirmed the advantages of the DBD approach over traditional methodologies. Nonetheless, the interested reader is referred to the original research papers for full conclusions and details.

2.11. CONCLUDING REMARKS

A general overview of several topics involved in the seismic assessment and retrofitting of existing RC buildings was provided in this chapter. A review of past studies on seismic risk in mainland Portugal and on the characterization of the Portuguese RC building stock, along with a discussion of the typical causes of damage and failure, were also included. The nonlinear modelling of RC frames under cyclic loading was addressed, as well as the applicable analysis methods. The current codes and guidelines were reviewed, with special emphasis on the methodology defined by EC8-3 (2005), the common practice among structural design professionals, and the simplified methods introduced by LNEC Report 81/2019 (Sousa *et al,* 2019). The final part of the chapter was dedicated to the available steel-based retrofitting techniques for RC frames, as well as to the review of past studies on the seismic behaviour and design of RC buildings retrofitted with steel X-braces.

This purpose of this somehow extensive literature review was to provide the interested readers with a reasonable amount of information on such matters. The produced text is quite straightforward but is thought to include the most important and up-to-date references, so the author hopes that it can serve (at least) as a starting point for junior academics and/or designers that wish/need to become involved in the seismic assessment and retrofitting of existing RC buildings. Given the importance of the matter for public safety, and the lack of confidence that most Portuguese designers show towards these procedures, the author believes this to be the main contribution of this chapter.

A final note is made to the need for new design methodologies that are applicable to hybrid structures such as those discussed in the previous sections. The dynamic behaviour of such structures is considerably different from that of pure frame, wall, or steel-braced structures, for which many design recommendations already exist. Those differences are mainly due to the interaction between structural systems, which is not well accounted for in current design practice. The performed studies using the DBD approach have already shown that it can provide solutions that are more consistent than those obtained with FBD methodologies using behaviour factors, so this is a research line that should be followed and expanded.

CHAPTER 2 – LITERATURE REVIEW

2.1. INTRODUCTION 2.1

2.2. EXISTING STUDIES ON SEISMIC RISK IN PORTUGAL 2.3

2.3. CHARACTERIZATION OF THE PORTUGUESE RC BUILDING STOCK 2.9

2.3.1. Geometric properties 2.10

2.3.1.1. Inter-storey height 2.11

2.3.1.2. Column properties 2.11

2.3.1.3. Beam properties 2.12

2.3.1.4. Slab thickness 2.13

2.3.2. Material properties 2.13

2.3.2.1. Concrete properties 2.13

2.3.2.2. Steel properties 2.14

2.3.3. Limitations of the study 2.15

2.4. TYPICAL CAUSES OF DAMAGE AND FAILURE OF NON-DUCTILE RC BUILDINGS 2.15

2.5. NONLINEAR MODELLING OF RC FRAMED STRUCTURES 2.18

2.5.1. Models for beam-column elements 2.19

2.5.2. Finite element formulations for distributed plasticity models 2.27

2.5.3. Material models for RC members under cyclic loading 2.29

2.5.3.1. Steel constitutive laws 2.30

2.5.3.2. Concrete constitutive laws 2.34

2.5.4. Masonry infills 2.38

2.5.4.1. Equivalent strut approach 2.40

2.5.4.2. Element formulation 2.41

2.5.4.3. Hysteretic relationships 2.43

2.5.4.4. Modelling of openings 2.45

2.6. NONLINEAR ANALYSIS METHODS 2.46

2.6.1. Nonlinear static analysis 2.47

2.6.2. Adaptive nonlinear static analysis 2.49

2.6.3. Nonlinear dynamic analysis 2.50

2.7. SEISMIC ASSESSMENT OF EXISTING RC BUILDINGS 2.53

2.7.1. Methodology according to EC8-3 ..... 2.54

2.7.1.1. Performance requirements and compliance criteria 2.55

2.7.1.2. Treatment of uncertainty and confidence factors 2.57
2.7.1.3. Allowed structural analysis methods 2.60
2.7.1.4. Performance evaluation and capacity models 2.61
2.7.2. Seismic demand definition 2.70
2.7.2.1. Target displacement computation for nonlinear static analysis 2.71
2.7.2.2. Selection of accelerograms for nonlinear dynamic analysis 2.79
2.7.3. Common practice among structural design professionals 2.81
2.7.4. Simplified methods introduced by LNEC Report 81/2019 ..... 2.82
2.8. TECHNIQUES USING STEEL ELEMENTS FOR THE SEISMIC RETROFITTING OF RC BUILDINGS 2.88
2.8.1. Retrofitting approaches and strategies 2.89
2.8.2. Traditional retrofitting techniques 2.92
2.8.2.1. Local capacity upgrading using steel plates 2.92
2.8.2.2. Global reduction of demands using concentric steel braces 2.95
2.8.3. Innovative retrofitting techniques 2.98
2.8.3.1. Eccentric braces 2.99
2.8.3.2. Buckling-restrained braces 2.100
2.8.3.3. Metal shear panels 2.102
2.9. SEISMIC BEHAVIOUR OF RC BUILDINGS RETROFITTED WITH CONCENTRIC STEEL BRACES 2.104
2.9.1. Behaviour of steel braces 2.105
2.9.2. Behaviour of RC members 2.107
2.9.3. Interaction between steel braces and RC members 2.108
2.10. METHODOLOGIES FOR THE SEISMIC DESIGN OF CONCENTRIC STEEL-BRACE RETROFITTING SYSTEMS 2.110
2.10.1. Force-based design 2.111
2.10.2. Displacement-based design 2.116
2.11. CONCLUDING REMARKS 2.124

CHAPTER 3

AN APPLICATION OF THE EC8-3 SEISMIC SAFETY ASSESSMENT PROCEDURE

3.1. INTRODUCTION

The RC structure chosen as a case study for this chapter is considered to be representative of the design and construction common practice in southern European countries, such as Italy, Portugal and Greece, until the late 1970's (PRISE Class: RC MR PC – see Figure 2.6). As such, it was designed to withstand only vertical loads. Previous numerical analyses demonstrated that its resistance to horizontal loads, in terms of ultimate limit state, is equivalent to approximately 8% of its weight. Similar analyses in terms of allowable stresses (common practice at the time) led to a lateral resistance of 5% of the structure's weight (Carvalho *et al,* 1999). The reinforcement details were specified according to the available codes and construction practice at that time. Hence, no specific seismic detailing was considered, no preferential inelastic dissipation mechanisms were assumed, and no specific ductility or strength provisions were considered (Varum, 2003). Two full-scale models of this structure (one as a bare frame and another as a frame with brick infilled walls) were tested at the ELSA reaction-wall laboratory (Joint Research Centre (JRC), Ispra, Italy), within the framework of the ICONS research programme (Figure 3.1). Pseudo-dynamic (PsD) testing procedures were used to obtain the experimental seismic response, for increasing intensities of the earthquake input motion. The seismic vulnerability of the structure was thus experimentally evaluated, as well as the influence of the infill walls on the global structural response.

The geometry of the structure, material properties, vertical loading and earthquake input used in the PsD tests are reviewed in the following sections, as well as the available experimental results (Pinto *et al,* 2002; Varum, 2003). Afterwards, the options considered during the development of the numerical models (bare frame and infilled frame) are discussed in light of the state-of-the-art provisions presented in Chapter 2 and their validation is carried out based on the above referred experimental results. The seismic assessment of the bare and infilled structure is then performed according to the provisions of EC8-3 (2005). Nonlinear static and dynamic analyses are carried out and conclusions are drawn from the obtained results. In particular, the local results of the assessment process are compared with the observed damage during the PsD tests and the influence of the infill walls on the seismic assessment results is addressed.

Figure 3.1 – The ICONS frames (Pinto *et al,* 2002)

3.2. CASE STUDY CHARACTERIZATION

3.2.1. Geometry and section detailing

Figure 3.2 shows the general layout of the structure under analysis – a RC four-storey frame with three bays: two of 5.0 *m* span and one of 2.5 *m* span. The inter-storey height is 2.7 *m*. Equal beams (geometry and reinforcement) were considered on all floors, together with a slab of (thickness) 0.15 *m* × (width) 2.0 *m* on each side (Figure 3.5). The cross-section dimensions of the longitudinal beams are (width) 250 *mm* × (height) 500 *mm*, while those of the transversal beams are (width) 200 *mm* × (height) 500 *mm*. Concerning the columns, all but the wider interior one (Column 2) have equal geometric characteristics along the height of the structure. Because Column 2 mobilizes its stronger flexural inertia axis, it plays a dominant role in the seismic response of the frame and will be referred to as "strong column" henceforth. The other columns (1, 3 and 4) will be referred to as "slender columns". The cross-section dimensions of the strong column are (width) 250 *mm* × (height) 600 *mm*, on the first and second storeys, and (width) 250 *mm* × (height) 500 *mm,* on the third and fourth storeys. Columns 1 and 3 cross-section dimensions are (width) 400 *mm* × (height) 200 *mm,* while those of Column 4 are (width) 300 *mm* × (height) 200 *mm.*

The geometric characteristics and reinforcement details of the beams are shown in Figure 3.3. Smooth round steel bars were considered for the longitudinal reinforcement, as it was a common practice fifty years ago. Figure 3.4 shows the columns' geometric dimensions and reinforcement details. The reinforcement splicing, joints and stirrups detailing should be specially noticed, as they are representative of the lack of confinement that is common in non-ductile RC structures built until the late 1970's. For instance, all (four) columns show a longitudinal reinforcement lap-splice (70 *cm*) at the

base of the first and third storeys, which means that a duplication (superposition) of the nominal reinforcement occurs at these locations. Several other deficiencies, regarding the fulfilment of modern seismic code design requirements, have been identified by previous authors (e.g., Griffith, 1999), such as: (i) inadequate transversal reinforcement; (ii) maximum distance between longitudinal bars; (iii) inexistence of transversal reinforcement in the joints; (iv) inadequate bends of the stirrups; (v) no specific mechanism for energy dissipation. For a fully detailed comparison between the reinforcement ratios and details found in this structure and those required by EC2-1-1 (2004) and EC8-1 (2004), the interested reader is referred to the work of Varum (2003).

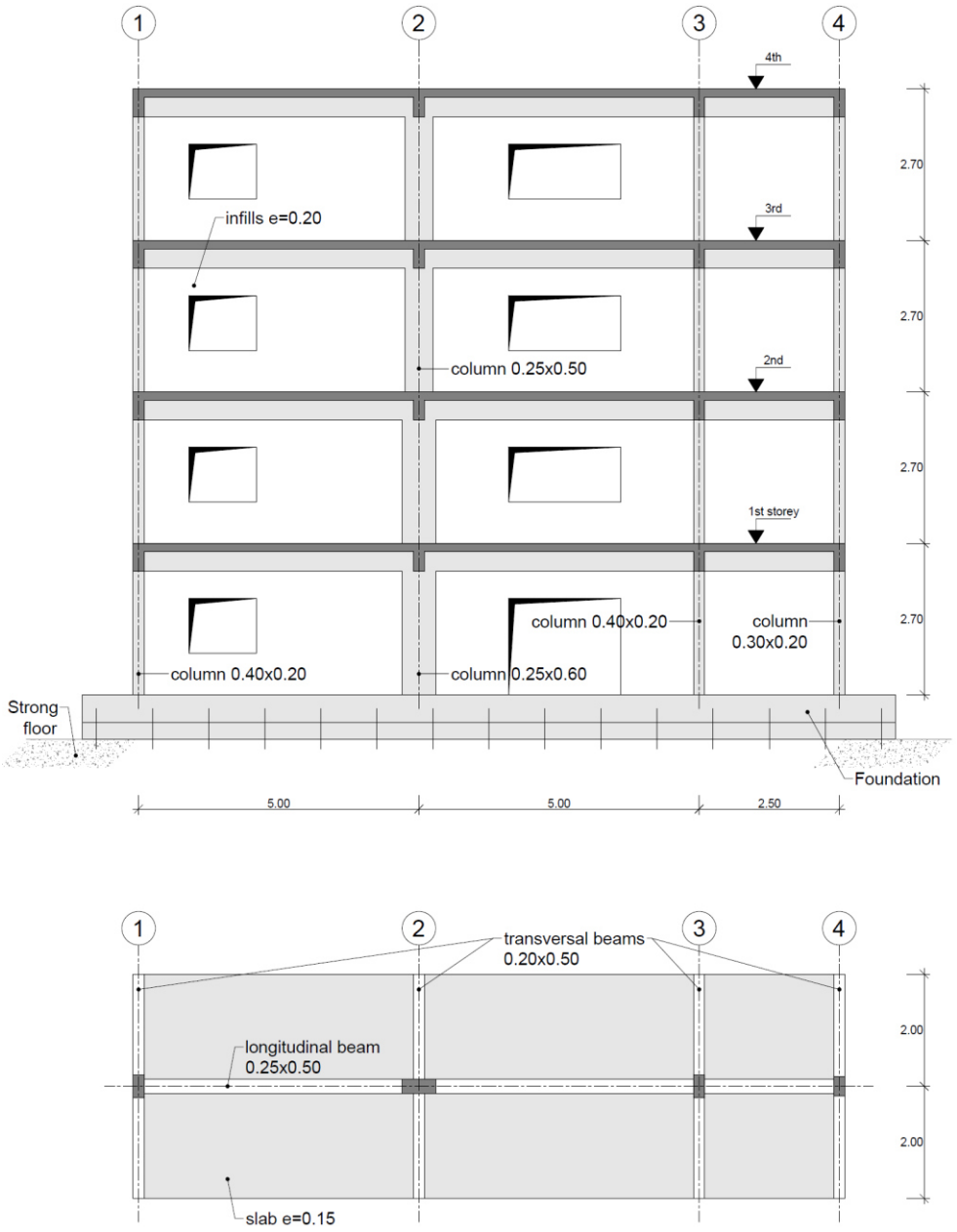

Figure 3.2 – Elevation and plan views of the RC frame (adapted from Pinto *et al,* 2002)

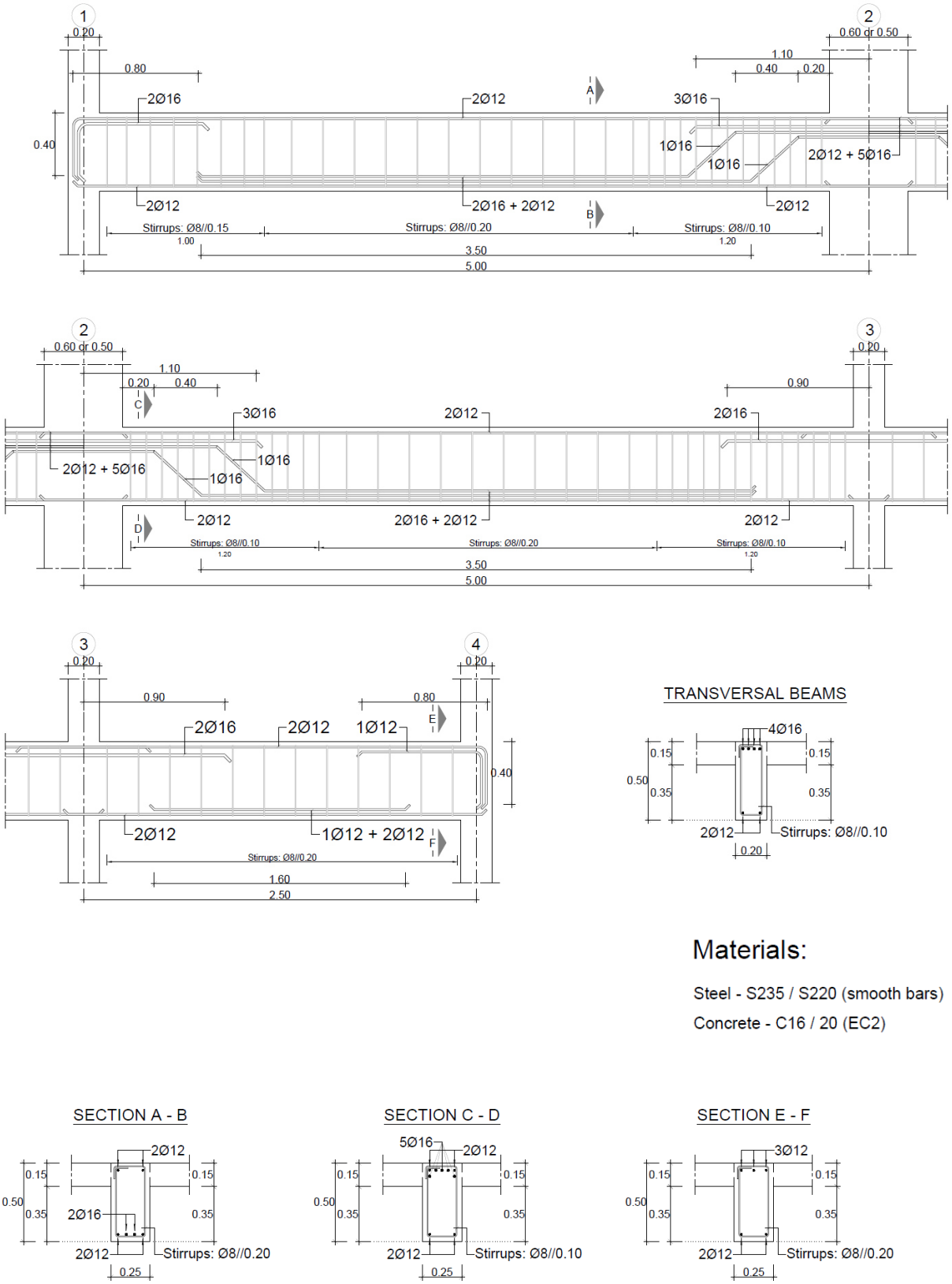

Figure 3.3 – Beam cross-section and reinforcement details (adapted from Pinto *et al,* 2002)

Level	1	2	3	4
4	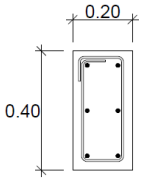	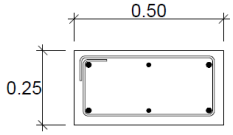	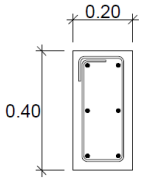	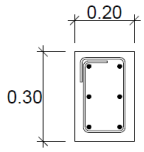
2	6Ø12 stirrups: Ø6//0.15	4Ø16+2Ø12 stirrups: Ø6//0.15	6Ø12 stirrups: Ø6//0.15	6Ø12 stirrups: Ø6//0.15
2	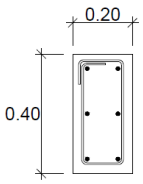	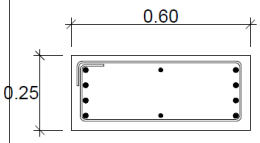	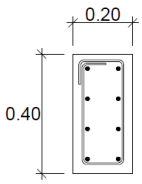	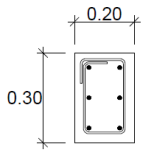
0	6Ø12 stirrups: Ø6//0.15	8Ø16+2Ø12 stirrups: Ø6//0.15	8Ø12 stirrups: Ø6//0.15	6Ø12 stirrups: Ø6//0.15

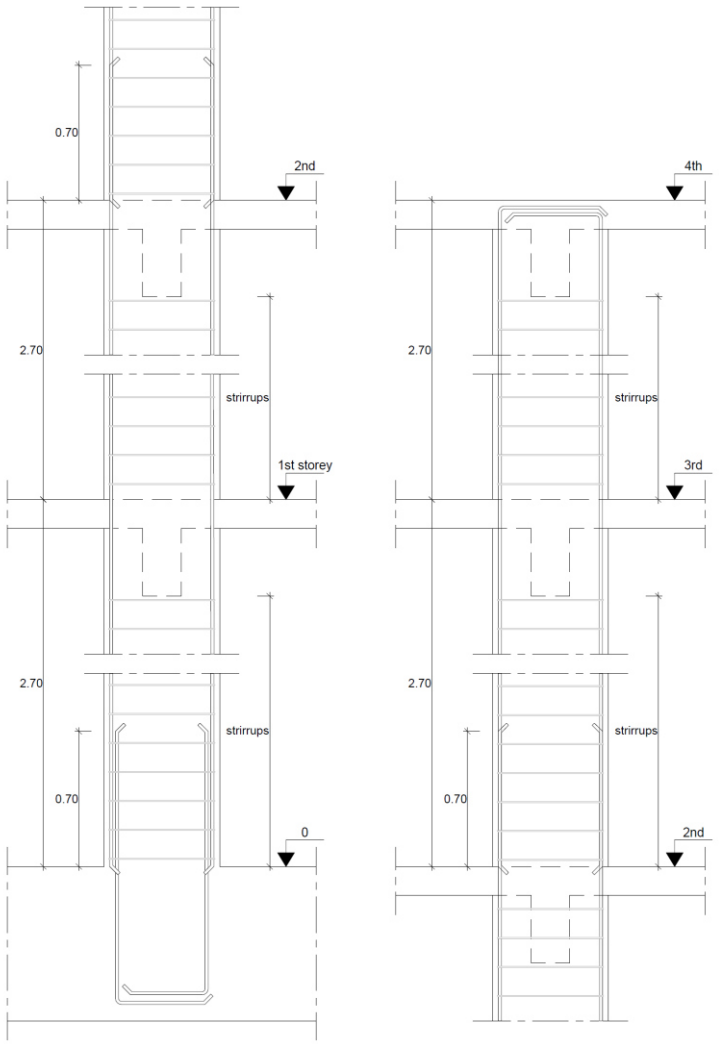

Figure 3.4 – Column cross-section and reinforcement details (adapted from Pinto *et al,* 2002)

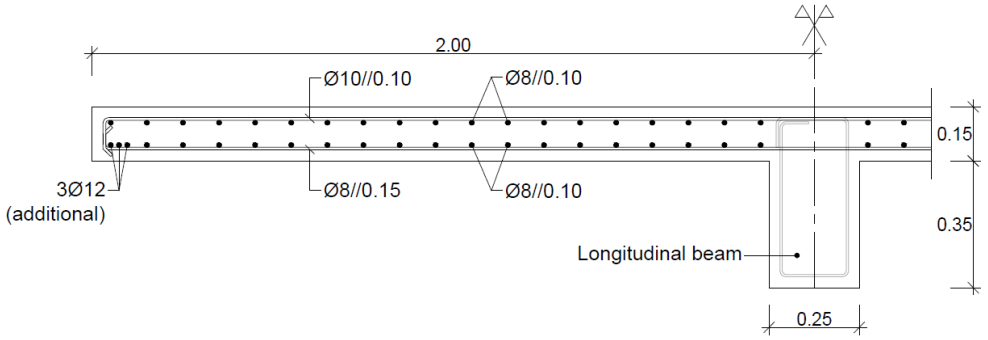

Figure 3.5 – Slab dimensions and reinforcement details (adapted from Pinto *et al,* 2002)

3.2.2. Masonry infill walls

An elevation view of the infilled frame is shown in Figure 3.6, indicating the location and dimensions of the openings on the walls. The latter are non-load bearing and were constructed after the RC frame was concluded. The long external bay infill contains a window opening (1.2 *m* × 1.0 *m*) at each of the four levels. The central bay contains a doorway (2.0 *m* × 1.75 *m*) at the ground level and window openings (2.0 *m* × 1.0 *m*) in each of the upper three levels. The external short bay contains solid infill panels, i.e., without openings (Pinto *et al,* 2002).

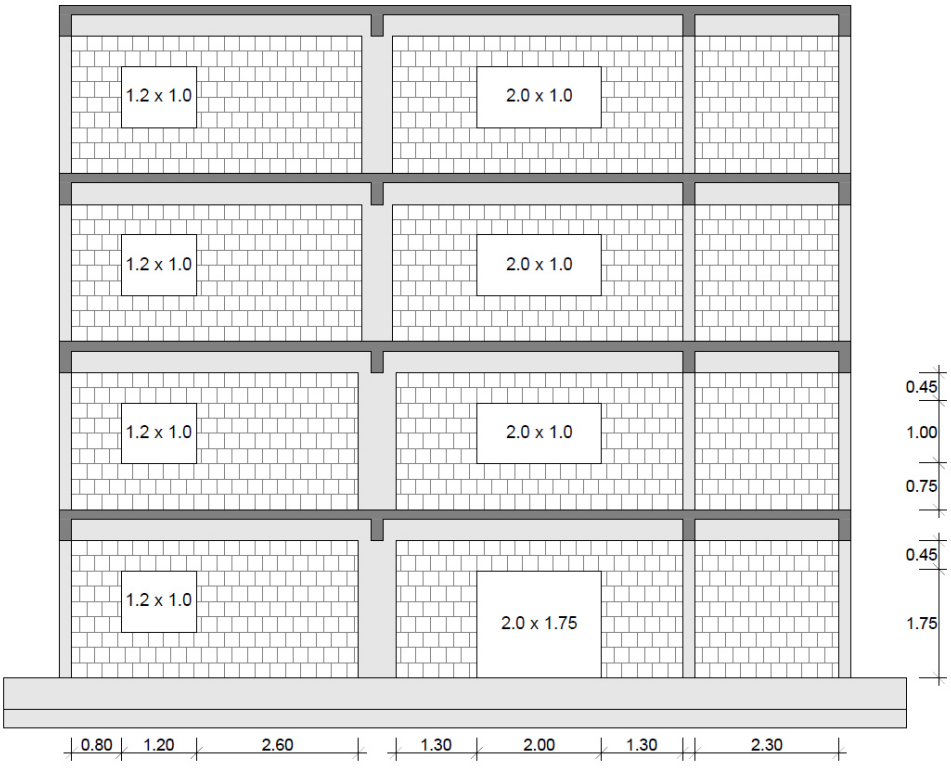

Figure 3.6 – Location and dimensions of the openings on the infill panels (adapted from Pinto *et al,* 2002)

Hollow blocks were used for the construction of the infill walls, as the former are representative of the construction techniques and materials commonly used in Mediterranean countries. These blocks were horizontally perforated, with the following dimensions: (thickness) 0.120 *m* × (base-length) 0.245 *m* × (height) 0.245 *m* (Figure 3.7). The weight of each unit was 42.2 *N*. The infill walls were constructed with the block units bedded on the 0.120 *m* × 0.245 *m* face, with the hollows in the horizontal direction. The mortar joints (vertical and horizontal) were approximately 15 *mm* thick and a plaster coat of the same thickness was applied on both sides of the walls (Figure 3.8). The resulting specific weight, by square meter of wall, was 1.45 *kN*/m^2.

Figure 3.7 – Infill block units (Pinto *et al,* 2002)

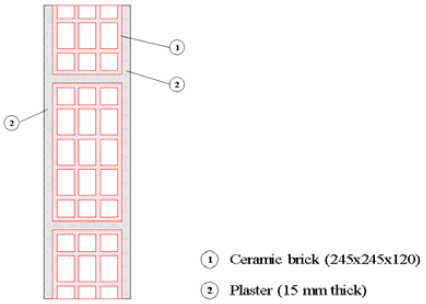

Figure 3.8 – Detail of the infill walls (Pinto *et al,* 2002)

3.2.3. Material properties

The materials considered during the design phase by Carvalho *et al* (1999) were normal weight low strength concrete, class C16/20 (EC2-1-1, 2004), and round smooth reinforcing steel, class Fe B22k (Italian standards). The target was to be as similar as possible to the properties of the materials used in construction practice until the late 1970's, in southern European countries. Afterwards, tests on samples of the materials used in the construction of the frame (steel reinforcement and concrete) were carried out. The full results of the tests can be found in Pinto *et al* (2002) and Varum (2003). The nominal properties of the design concrete are given in Table 3.1, while the average values obtained from the compressive strength tests on concrete reference specimens (cubes with 150 *mm*) are given in Table 3.2. These compression tests on twenty-eight cubes cast during construction led to a mean strength of 16 *MPa,* thus indicating that the concrete was of rather poor quality. A small variance was found within each casting phase, whilst large differences were observed between the various casting phases (Varum, 2003).

Table 3.1 – C16/20 nominal strength values (Varum, 2003)

Compressive ultimate strength (characteristic values - *MPa)*	
Cylindrical strength $f_{ck,cylind}$	Cubic strength $f_{ck,cubic}$
16	20

Table 3.2 – Tests on concrete specimens (average compressive strength) (Varum, 2003)

Specimen group (casting phase)	Date of casting (1999)	Compressive cubic ultimate strength[a] *(MPa)*	Compressive cylindrical ultimate strength[b] *(MPa)*
columns 1st storey	24/02	16.66	13.90
slab/beams 1st floor	17/03	13.24	16.45
columns 2nd storey	22/03	13.78	13.80
slab/beams 2nd floor	06/04	18.10	17.40
columns 3rd storey	08/04	16.50	9.20
slab/beams 3rd floor	20/04	21.63	17.30
columns 4th storey	22/04	13.58	11.00
slab/beams 4th floor	06/05	16.98	20.17

a) Compressive tests on cube specimens carried out on 30/07/1999.
b) Compressive tests on cylindrical core specimens taken in the structure (after the test campaign) on 01/03/2001.

Table 3.3 presents the nominal properties of the reinforcement steel adopted in the frame's construction. The tensile strength tests on steel bar specimens were carried out at the National Civil Engineering Laboratory (LNEC), in Lisbon (Carvalho *et al,* 1999), and the results showed very little variance. The mean mechanical properties of the reinforcement bars were then estimated through a best-fit of experimental diagrams. The obtained values are summarized in Table 3.4. More details about the regression models applied for the development of the best-fit (Figure 3.9) can be found in Carvalho *et al* (1999) and Varum (2003).

Table 3.3 – Steel grade Fe B22k nominal properties (Varum, 2003)

Relevant properties	Characteristic values
Yield stress	$f_{syk} = 215\ MPa$
Ultimate strength	$f_{stuk} = 335 MPa$
Ultimate strain	$\varepsilon_{stuk} = 24.0\,\%$

Table 3.4 – Test on steel specimens (mean mechanical properties) (Varum, 2003)

Mechanical properties	Value
Young modulus – E_m	204.5 *GPa*
Yield stress – f_{sym}	343.6 *MPa*
Hardening strain – ε_{shm}	3.03 *%*
Tangent modulus at beginning of hardening – E_{sh}	2.8 *GPa*
Ultimate strength – f_{sum}	451.5 *MPa*
Ultimate strain – ε_{sum}	22.9 *%*

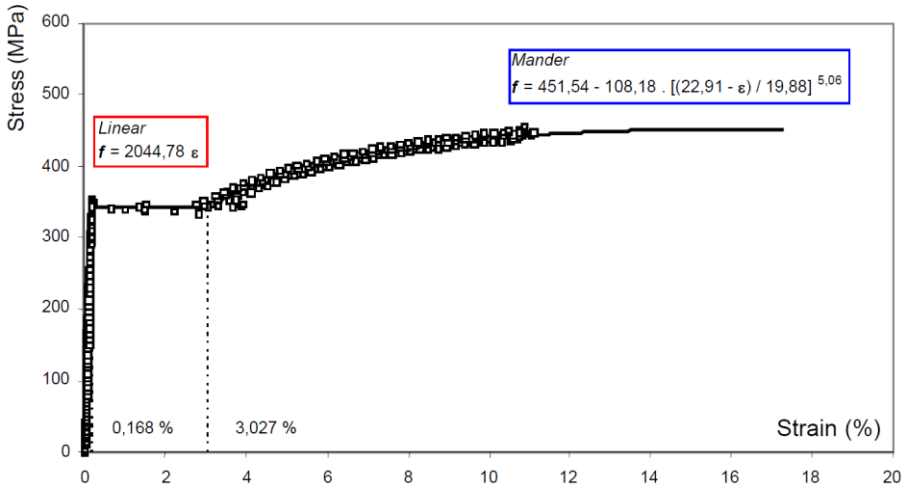

Figure 3.9 – Best-fit of steel constitutive law (Varum, 2003)

The comparison between Tables 3.3 and 3.4 shows that the steel's mechanical properties obtained from tests on specimen bars differ considerably from the nominal values. The steel's strength is significantly higher than expected from the minimum values established in the Italian standards for steel grade Fe B22k. The found values of yield stress and ultimate strength were 45% and 25%, respectively, higher than the nominal values. However, it should be noted that only minimum strength requirements were included in the old codes, which may cause the effective strength of a given steel grade to be much higher than the respective nominal values. Systematic tests of the reinforcement steel in existing buildings would thus be recommendable to achieve a more realistic estimate of its strength (Varum, 2003).

Concerning the masonry infill walls components, tests on mortar specimens and block units were performed at the University of Pavia, Italy, in order to characterize them. Additionally, representative wallets of the infill walls were constructed and tested in compression, in the horizontal, vertical, and diagonal directions. The specimens were constructed using the same materials (block units and mortar) and geometry (joint and plaster thickness) as those of the infill walls. A full description of the performed tests and obtained results can be found in Pinto *et al* (2002). Tables 3.5 and 3.6 summarize below the mean mechanical properties obtained for the masonry walls.

Table 3.5 – Tests on block units and mortar specimens (mean mechanical properties) (Varum, 2003)

Element tested	Test	Symbol	Units	Value
Brick units	Compressive strength (parallel to the bed joints)	$\sigma_c^{\parallel}$	*MPa*	15.36
	Compressive strength (perpendicular to the bed joints)	$\sigma_c^{\perp}$	*MPa*	2.80
Mortar (joints and plaster)	Tensile strength	σ_t	*MPa*	0.59
	Compressive strength	σ_c	*MPa*	1.33

Table 3.6 – Tests on infill specimens (mean mechanical properties) (Varum, 2003)

Element tested	Test	Symbol	Units	Value
Masonry wallets Vertical and horizontal compressive tests (without plaster)	Compressive strength (parallel to the bed joints)	$\sigma_c^{\backslash\backslash}$	*MPa*	1.11
	Compressive strength (perpendicular to the bed joints)	$\sigma_c^{\perp}$	*MPa*	1.10
	Young modulus (parallel to the bed joints)	$E^{\backslash\backslash}$	*GPa*	0.991
	Young modulus (perpendicular to the bed joints)	$E^{\perp}$	*GPa*	1.873
Masonry wallets Diagonal compressive tests (without plaster)	Tensile strength	σ_t	*MPa*	0.233
	Shear modulus	G	*GPa*	0.657
Masonry wallets Diagonal compressive tests (with plaster in both sides)	Tensile strength	σ_t	*MPa*	0.575
	Shear modulus	G	*GPa*	1.171

It is noteworthy that, regardless of the differences between the materials' nominal properties and the test results, the construction of the frames was supervised as to achieve the design specifications in terms of materials, structural geometry, and reinforcement detailing. Therefore, the common uncertainties, that occur in real existing structures, were reduced. Aspects such as variance towards the designed structure in material properties and reinforcement detailing, non-documented structural modifications, trouble finding the original drawings or material degradation make difficult the safety assessment of existing structures. However, in this case, the built frames reproduced the designed structures considerably well.

3.2.4. Vertical loads

The total weight of each cast frame was 101 tonnes, not including the foundation. Figure 3.10 shows the vertical loads defined by Carvalho *et al* (1999) to simulate actions other than the self-weight of the frame elements (columns and longitudinal beams), considering that parallel frames exist every 5.0 *m* (note that the cast frames included only a 4.0 *m* wide slab). The represented values were obtained from the following vertical design loads, considering the referred spacing of the frames (the load distribution applied to the infilled frame is identical to that of the bare frame):

- Weight of slab (150 *mm* thick): 3.75 kN/m^2
- Weight of finishings: 0.75 kN/m^2
- Weight of transverse beams: 2.50 *kN/m*
- Weight of masonry infills: 1.10 kN/m^2 of wall area (infills considered to exist over longitudinal and transverse beams)
- Live load: 1.00 kN/m^2 (quasi-permanent value).

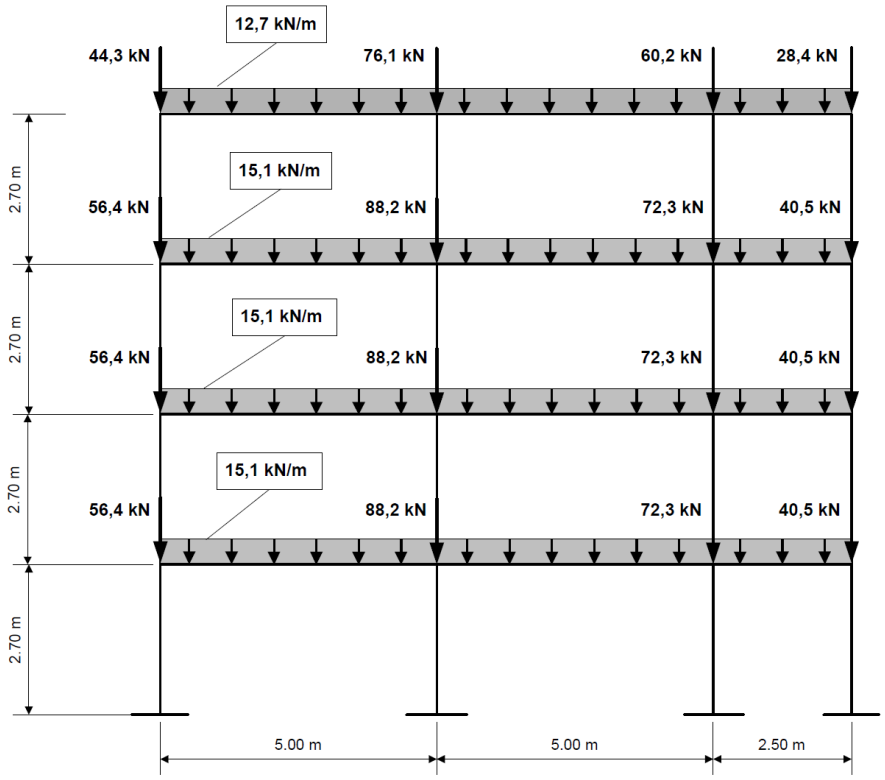

Figure 3.10 – Scheme of vertical static loads (Pinto *et al,* 2002)

3.2.5. Earthquake input used in the PsD tests

The input seismic motions were defined in order to be representative of a moderate-high European seismic hazard scenario (Campos Costa and Pinto, 1999; Carvalho *et al,* 1999). Hazard consistent time series of acceleration (with 15 seconds duration) were artificially generated, yielding a set of twelve uniform hazard response spectra for increasing return periods. The considered time increment to generate the records was 0.01 seconds, leading to input accelerograms with 1500 points. The considered return periods and the corresponding values of peak ground acceleration (PGA) are given in Figure 3.11. The acceleration time-histories used in the PsD tests, corresponding to the 475, 975 and 2000-yrp, are depicted in Figure 3.12. The corresponding 5% damping displacement and pseudo-acceleration linear-elastic response spectra are plotted in Figure 3.13.

The first part of the test campaign focused on the bare frame (BF), which was subjected to two earthquake input signals (475 and 975-yrp). During the 475-yrp earthquake, it performed satisfactorily, showing only minor local damage without significant global consequences. However, during the 975-yrp earthquake, the strong column suffered severe damage at the third level and the test had to be stopped at half-time (7.5 seconds) due to the imminence of collapse (see the following sub-section for experimental results details). As such, no point existed in performing the 2000-yrp earthquake test on the BF. On the other hand, the infilled frame (IN) was subjected to the three consecutive earthquake signals (475, 975 and 2000-yrp). Quasi-linear elastic behaviour was exhibited during the 475-yrp earthquake, while the 975-yrp earthquake inflicted severe damage to the infills, which reached

deformation beyond its peak strength with considerable loss of strength (Varum, 2003). During the 2000-yrp earthquake, the IN reached imminent collapse after only 5 seconds of the input motion. The infills on the first storey reached collapse and the soft-storey mechanism would have formed if the test had not been stopped.

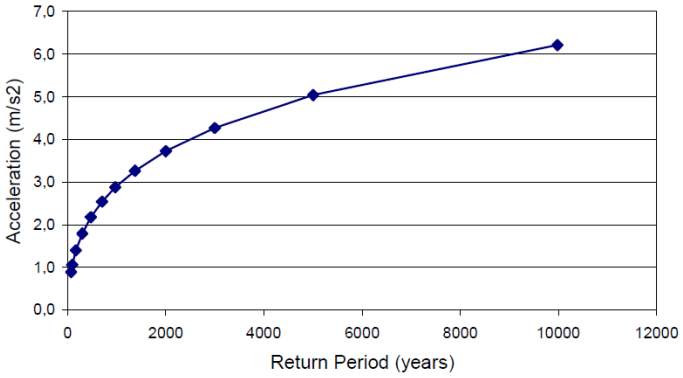

Return period *(years)*	Peak acceleration *(m/s^2)*
73	0.889 (0.09*g*)
100	1.060 (0.11*g*)
170	1.402 (0.14*g*)
300	1.796 (0.18*g*)
475	2.180 (0.22*g*)
700	2.543 (0.26*g*)
975	2.884 (0.29*g*)
1370	3.265 (0.33*g*)
2000	3.728 (0.38*g*)
3000	4.273 (0.44*g*)
5000	5.036 (0.51*g*)
9980	6.213 (0.63*g*)

Figure 3.11 – Seismic hazard curve for the moderate-high European scenario (Varum, 2003)

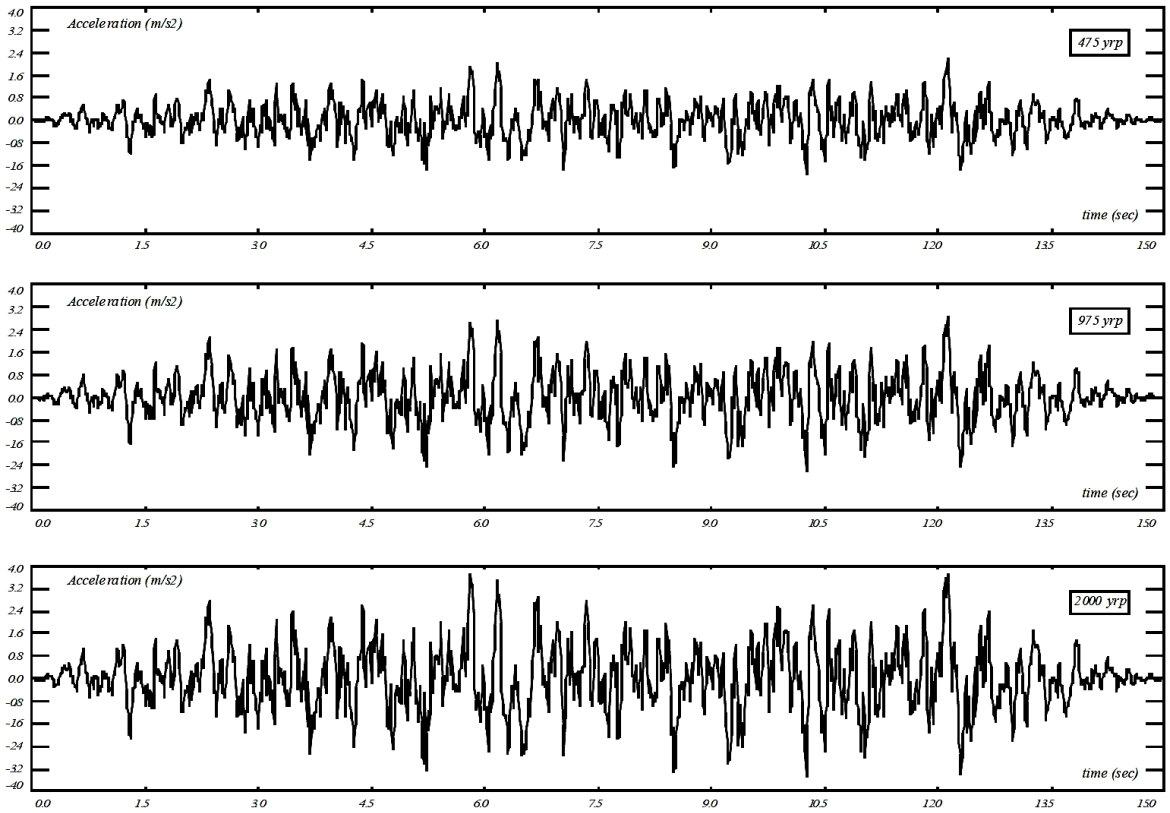

Figure 3.12 – Ground motion acceleration time-histories for 475, 975 and 2000-yrp (Pinto *et al,* 2002)

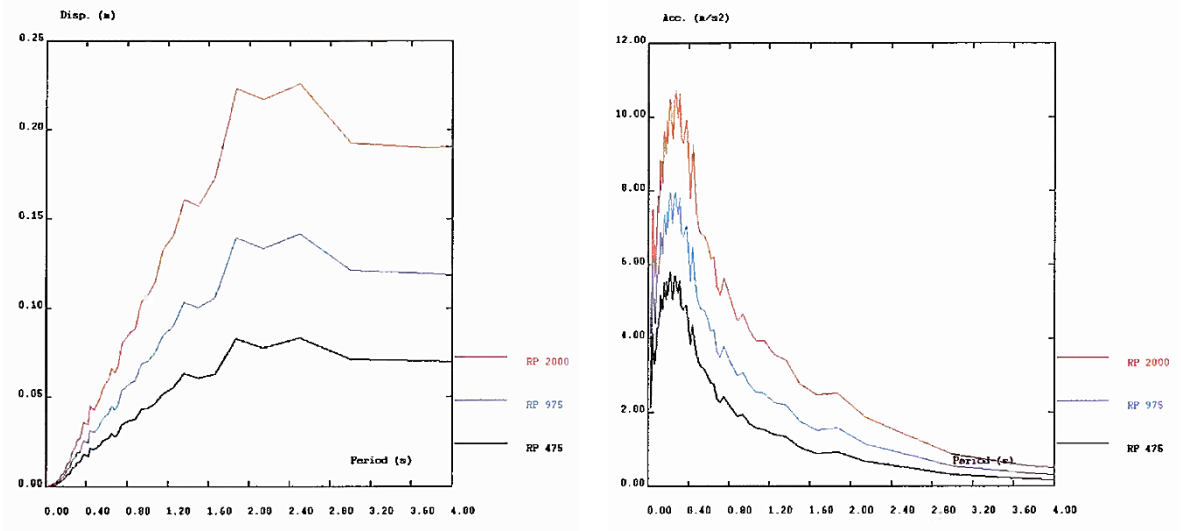

(a) (b)

Figure 3.13 – 5% damping linear-elastic response spectra for 475, 975 and 2000-yrp: (a) displacement; (b) pseudo-acceleration (Pinto *et al,* 2002)

3.2.6. Experimental results

The following sub-sections summarize and discuss the results from the above-described PsD tests. The full record files of the test results were kindly made available by Prof. Humberto Varum. Results are presented and discussed for the bare and infilled frames in terms of modal frequencies identification, storey displacements, drifts, shear and observed damage. Comparison between the most relevant results obtained for the bare and infilled frames is made in the final sub-section, as well as several other concluding remarks.

3.2.6.1. Modal frequencies

In order to provide data for the modal identification of the structure, before and after each test series, a very low intensity earthquake (non-destructive test) was applied, allowing for the excitation of all the vibration modes. This input corresponded to 5% of the intensity associated with the 475-yrp earthquake employed in the PsD tests (0.109 m/s^2 peak acceleration). The frequencies and equivalent viscous damping ratios were obtained applying an identification method to the experimental response of both the bare and infilled frames (Varum, 2003). Unfortunately, it was impossible to carry out the identification of the frequencies of the infilled frame after the PsD tests. Results are thus available only for the original structure (uncracked stiffness). On the other hand, the natural frequencies of the original bare frame were also assessed through modal dynamic tests, carried out with an instrumented (load cell) impact hammer of 5 *kg* mass, which allowed for the validation of the results obtained with the non-destructive tests. The described results are summarized below concerning only the obtained modal frequencies. Regarding results for the equivalent viscous damping ratios, readers are referred to the work of Pinto *et al* (2002) and Varum (2003).

Table 3.7 shows the four modal frequencies of the bare frame, before and after the PsD tests were performed. An eigenfrequency drop of about 20 to 25% is observed for the four vibration modes, as a consequence of the structural damage induced by the applied ground motions. Table 3.8 summarizes the results obtained with the modal dynamic tests for the first three frequencies, showing a good agreement with the non-destructive test results for the original structure. The modal frequencies of the original infilled frame are given in Table 3.9. Comparing the obtained values with those of the original bare frame, one concludes that the presence of the masonry infill panels increases the frequencies approximately four times.

Table 3.7 – Modal frequencies of the BF, before and after the PsD tests (adapted from Varum, 2003)

	f_1 (BF)	f_2 (BF)	f_3 (BF)	f_4 (BF)
Before PsD tests	1.57 *Hz*	4.60 *Hz*	7.58 *Hz*	11.14 *Hz*
After PsD tests	1.19 *Hz*	3.65 *Hz*	5.63 *Hz*	9.06 *Hz*

Table 3.8 – Natural frequencies of the BF evaluated with an impact hammer (adapted from Varum, 2003)

	f_1 (BF-IH)	f_2 (BF-IH)	f_3 (BF-IH)	f_4 (BF-IH)
Before PsD tests	1.57 *Hz*	4.69 *Hz*	7.83 *Hz*	---

Table 3.9 – Modal frequencies of the IN, before the PsD tests (adapted from Varum, 2003)

	f_1 (IN)	f_2 (IN)	f_3 (IN)	f_4 (IN)
Before PsD tests	7.22 *Hz*	20.83 *Hz*	24.93 *Hz*	45.35 *Hz*

3.2.6.2. Storey displacements, drifts, and shear

The time-histories of the BF storey displacements for the 475 and 975-yrp earthquake tests are shown in figures 3.14 and 3.15. The two top-displacement curves are then compared in Figure 3.16. Additional curves for base-shear vs. top-displacement, storey-shear vs. inter-storey drift, maximum inter-storey drift profile, storey-shear profile, relative rotations at critical zones and energy dissipation (among others) can be found in Varum (2003). Table 3.10 collects the maximum values of the characteristic response variables for the BF tests. These outputs show that the deformation demands tend to concentrate on the third storey, for both the 475 and 975-yrp earthquake tests. During the latter, the third storey almost collapsed after 7.5 seconds and the test had to be stopped, as previously referred. If one recalls the previously described geometric and reinforcement details of the strong column, this type of behaviour poses no surprise.

The time-histories of the IN storey displacements for the three PsD tests are depicted in figures 3.17 to 3.19. Similarly to what was done for the BF, the top-displacements curves are then compared in Figure 3.20. The soft-storey mechanism is evident when analysing the data in Figure 3.19 (2000-yrp earthquake test). All storey displacements are shown to be similar, which leads to a much higher inter-storey drift at the first storey than on the other three storeys. The soft-storey mechanism develops from the failure of the infill panels at the first storey and is a direct consequence of the storey softening behaviour characteristics of these infills after failure (Varum, 2003). The maximum values of the

response for the three PsD tests performed on the IN are collected in Table 3.11, in terms of top-displacement, global drift, storey drift and storey shear. If one considers the empirical estimation of masonry strength included in the work of Varum (2003), the maximum values of the inter-storey drifts can be indicative of the behaviour and damage state after each test. The 0.12 % drift reached in the first two storeys during the 475-yrp earthquake test indicates that those infill panels should be reaching their peak strength deformation. Furthermore, the 0.43 % drift reached in the first storey during the 975-yrp earthquake test indicates that the infills should have been severely damaged. The 0.27 % drift at the second storey also indicates serious damage to the infills. Regarding the maximum storey shear values, the fact that a decrease was registered from the 975-yrp to the 2000-yrp earthquake test indicates the degradation of the stiffness and strength properties.

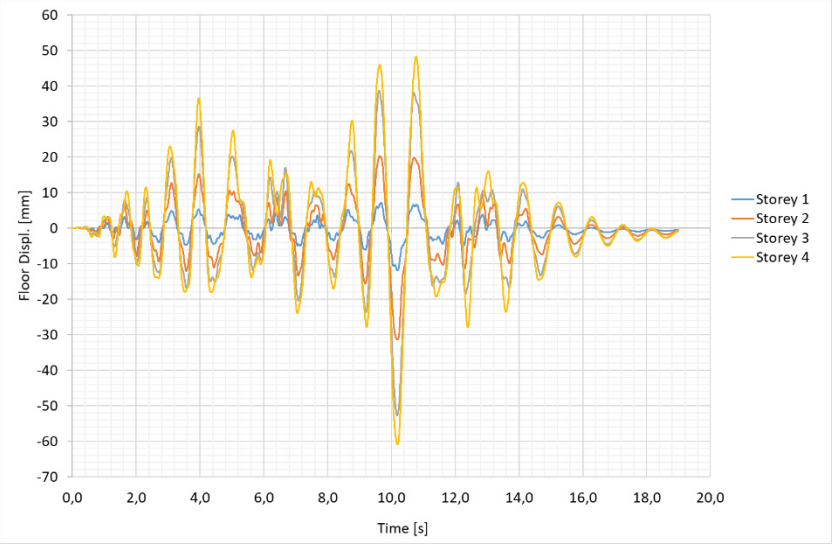

Figure 3.14 – BF storey displacements time-histories for the 475-yrp earthquake (adapted from Varum, 2003)

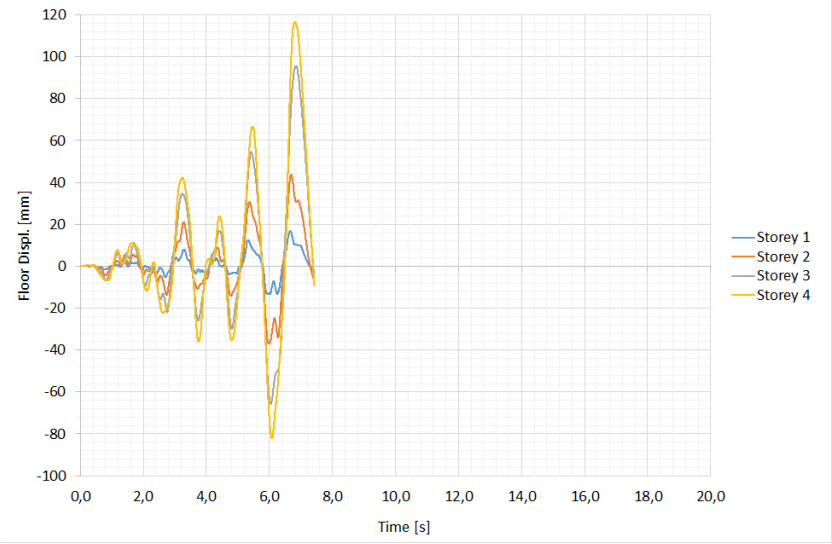

Figure 3.15 – BF storey displacements time-histories for the 975-yrp earthquake (adapted from Varum, 2003)

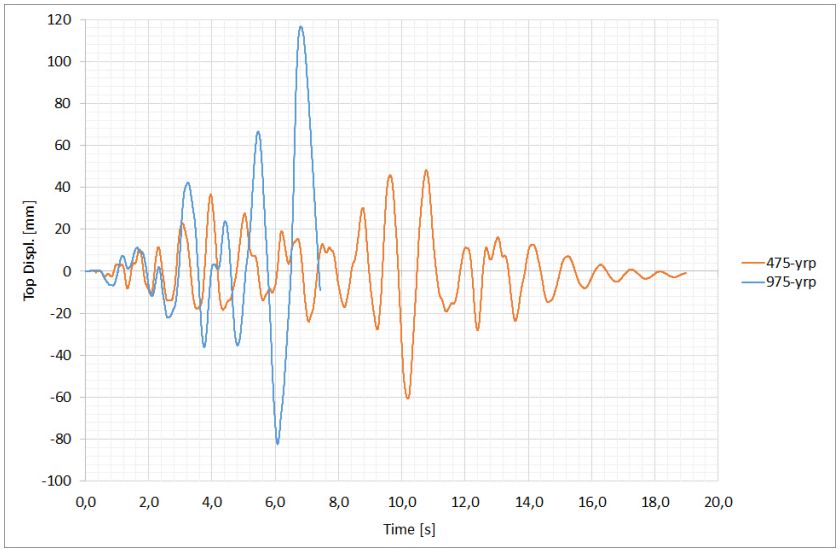

Figure 3.16 – BF top displacement evolution (adapted from Varum, 2003)

Table 3.10 – BF summary of response maximum values (adapted from Varum, 2003)

	Top displacement *(mm)*	**Global drift (%)**
475-yrp	60.8	0.56
975-yrp	116.7	1.08

	Inter-storey drift (%)			
	Storey 1	**Storey 2**	**Storey 3**	**Storey 4**
475-yrp	0.44	0.74	0.80	0.46
975-yrp	0.63	1.03	2.41	0.91

	Storey shear *(kN)*			
	Storey 1	**Storey 2**	**Storey 3**	**Storey 4**
475-yrp	209.0	188.2	139.0	95.8
975-yrp	216.7	202.7	153.9	111.1

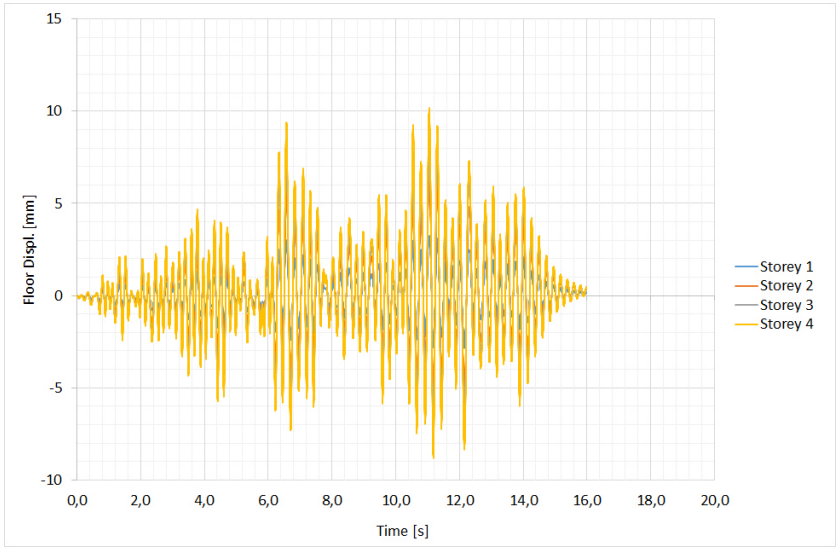

Figure 3.17 – IN storey displacements time-histories for the 475-yrp earthquake (adapted from Varum, 2003)

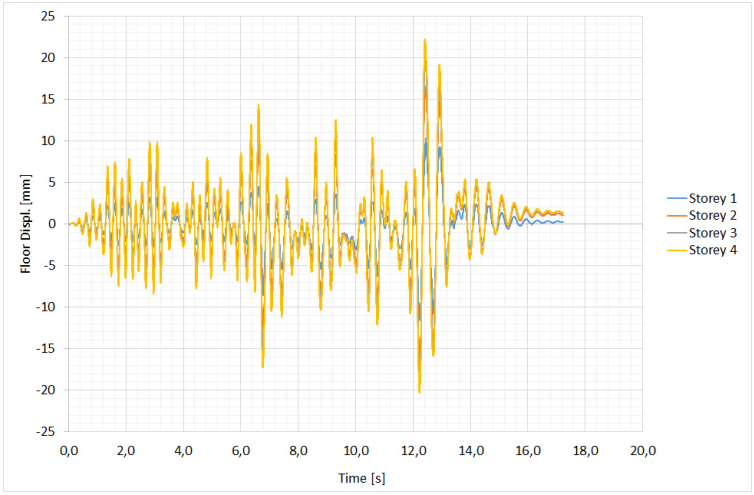

Figure 3.18 – IN storey displacements time-histories for the 975-yrp earthquake (adapted from Varum, 2003)

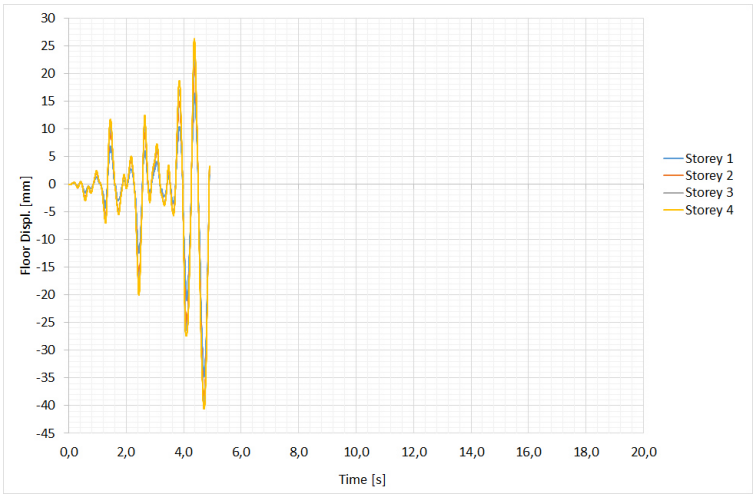

Figure 3.19 – IN storey displacements time-histories for the 2000-yrp earthquake (adapted from Varum, 2003)

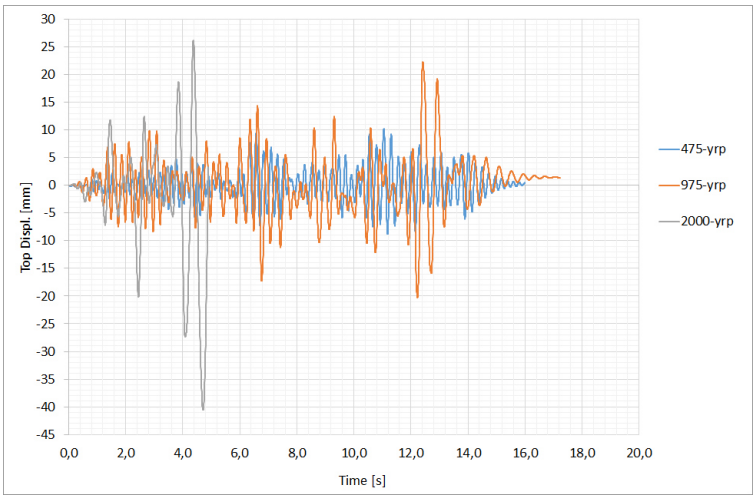

Figure 3.20 – IN top displacement evolution (adapted from Varum, 2003)

Table 3.11 – IN summary of response maximum values (adapted from Varum, 2003)

	Top displacement *(mm)*	Global drift (%)
475-yrp	10.2	0.09
975-yrp	22.3	0.21
2000-yrp	40.6	0.38

	Inter-storey drift (%)			
	Storey 1	**Storey 2**	**Storey 3**	**Storey 4**
475-yrp	0.12	0.12	0.08	0.06
975-yrp	0.43	0.27	0.15	0.11
2000-yrp	1.29	0.22	0.12	0.09

	Storey shear *(kN)*			
	Storey 1	**Storey 2**	**Storey 3**	**Storey 4**
475-yrp	754.0	680.8	512.4	288.4
975-yrp	846.5	749.1	635.5	388.1
2000-yrp	529.2	543.2	446.2	256.5

3.2.6.3. Observed damage

The BF's behaviour was deemed satisfactory for the 475-yrp earthquake test, showing no significant global damage (only minor local damage), as previously referred. On the other hand, as predicted by the numerical pre-test analysis, it sustained extensive damage at the third storey level during the 975-yrp earthquake test. Figure 3.21 shows the damage pattern that was observed after this test was interrupted.

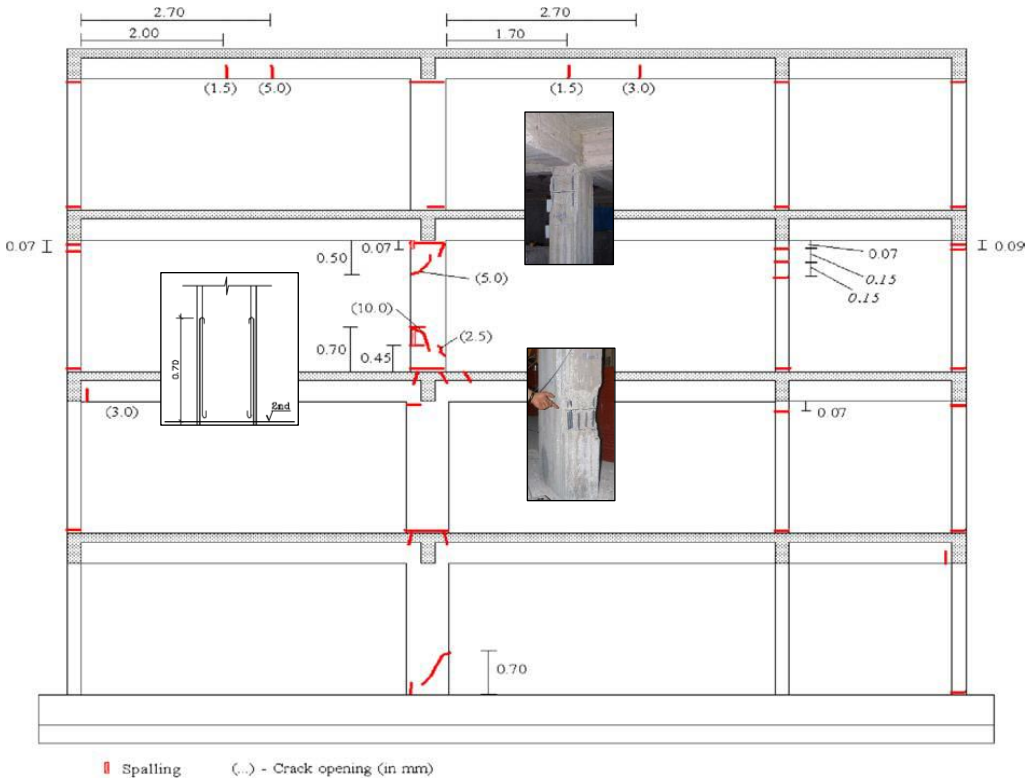

Figure 3.21 – Damage pattern after the BF tests (general layout) (adapted from Varum, 2003)

The pictures on Figure 3.21 show that hinging developed at the top, bottom and rebar lap-splice (70 *cm* from bottom) sections of the strong column, causing the third storey to experience severe deformation. However, only spalling of the concrete cover and yielding of the rebars took place. Neither buckling nor rupture of the rebars occurred. In addition, no stirrups disclosure or rupture occurred, except at the lap-splice zone, where slight yielding / disclosure of stirrups occurred. The sudden reduction of the cross-section's height and reinforcement ratio (plus the consequent lap-splice) contributed to the concentration of damage at this location. Moreover, the spalling of the concrete cover probably indicates the loss of anchorage of the rebars. If one recalls the work of Hassan and Hawkins (1977), the authors concluded (based on experimental tests) that the loss of cover from behind the rebar hooks in buildings surviving an earthquake should be interpreted as a possible loss of anchorage of the reinforcement. This phenomenon is frequently observed in older-type RC buildings that were damaged by earthquakes, as previously referred in Chapter 2.

Regarding the PsD tests performed on the IN, it was subjected to the three consecutive earthquake signals (475, 975 and 2000-yrp). Figure 3.22 shows the damage pattern that was observed once the tests were concluded. A detailed description of the damage observed in each phase can be found in the work of Pinto *et al* (2002) and Varum (2003).

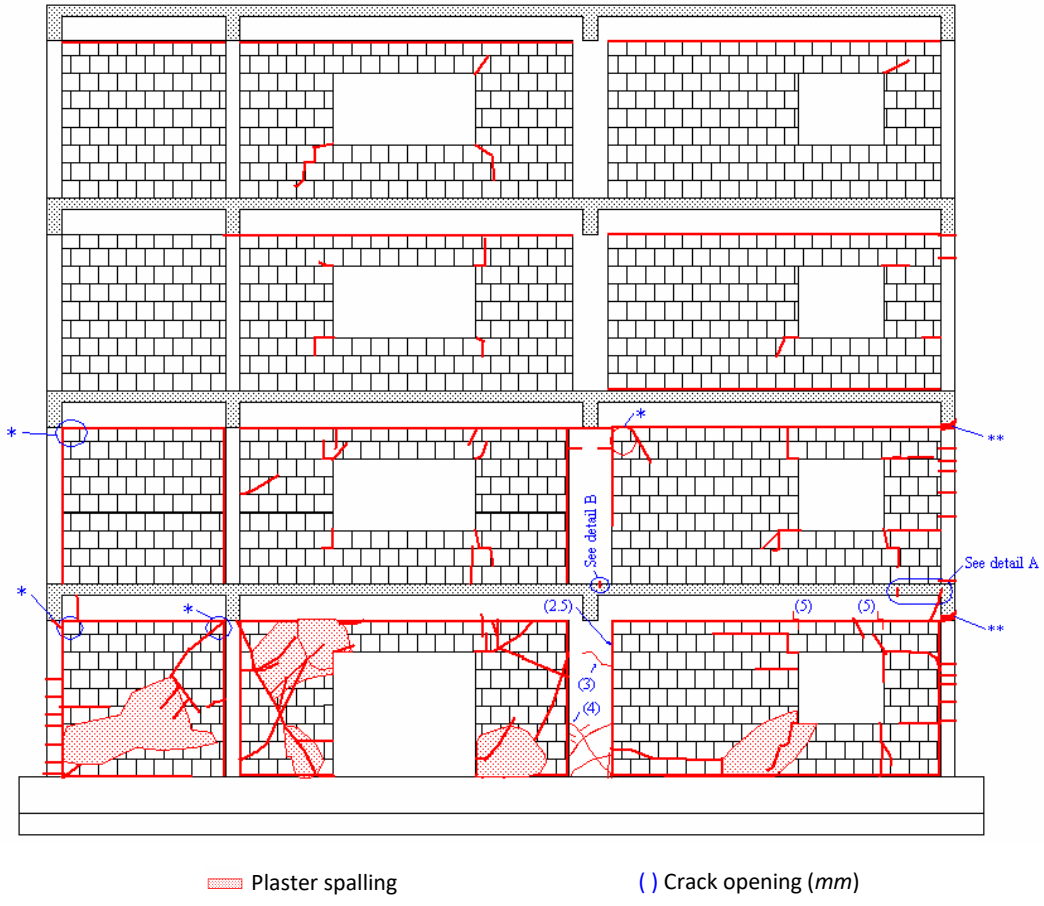

Figure 3.22 – Damage pattern after the IN tests (general layout) (adapted from Varum, 2003)

During the 475-yrp test, overall, the IN behaved quite well. Minor cracking was observed only around the infill openings at the first and second storeys, as well as separation between the infill panels and the surrounding RC members. No significant cracking was observed in any of the RC members. The 975-yrp test, on the other hand, caused a significant amount of damage to the bottom storey's infills (shear cracking became significant), along with some minor damage to the RC beam-column joints and several columns at this level. Smaller amounts of damage in similar locations were noted in the second storey, while no significant damage was observed in the upper two storeys. In summary, at the end of this test, the RC structure was found to be in good condition at all levels, as were the infills at the second, third and fourth storeys. However, the first storey infills were severely damaged (too damaged even to be retrofitted). Given this situation (imminent formation of a soft-storey mechanism at the first storey), the 2000-yrp test was run for only 5 seconds in order to study how gradually the lateral strength dropped off with increasing drift. The damage patterns at the end of this test were essentially more severe versions of what had been observed during the 975-yrp test. What remained from the first storey infills was severely damaged, with the formation of wide diagonal cracks on all three panels. Significant shear cracks (approx. 4 *mm* wide) developed at the bottom section of the strong column along with spalling of the concrete cover. However, the previous cracking patterns on the other RC members showed no significant change. Very little new damage occurred in the upper storeys. The overall structural behaviour was clearly that of a soft-storey structure.

3.2.6.4. Remarks

The results of the tests performed on the BF confirmed the soft-storey mechanism, which was expected to develop during the earthquake response due to the vertical irregularity induced by the sudden reduction in the strong column's cross-section. This structural misconception is common in older-type RC buildings (until the late 1970's) and frequently induces collapse when an earthquake occurs (refer to Chapter 2). In this case, in spite of the very limited damage observed after the 475-yrp earthquake test, the demands for a slightly higher intensity earthquake (1.3 times the maximum acceleration of the 475-yrp record) led to imminent storey failure and consequent collapse of the structure (Varum, 2003). This conclusion is consistent with the high vulnerability which is typical of such structures and further stresses the need for development and validation of adequate, effective, and economic retrofitting solutions and techniques.

Concerning the effect of the masonry infill walls in the seismic response of the structure, conclusions seem clear when comparing the results of the bare and infilled tests. Figure 3.23 shows two diagrams, extracted from the work of Varum (2003), that represent the shear-drift evolution of the first and second storeys for both structures. The infill panels increase substantially the initial stiffness and strength at the storey level and, consequently, the global stiffness and strength of the structure. The maximum strength reached for the first storey infilled frame is about four times the value for the bare structure. However, the brittleness of the infilled structure after reaching its maximum strength should be noticed (i.e., the rapid decrease of strength seen in the first storey diagram). Interesting conclusions can also be drawn if one compares the maximum inter-storey drift profiles (Figure 3.24). The BF tests showed concentration of damage and, consequently, significant inter-storey drift at the third storey.

The presence of infills, however, changed the structural response completely. The concentration of damage at the third storey of the irregular RC frame did not occur during the IN tests. In fact, in this case study, the infill panels prevented the development of an irregular structural response (Varum, 2003).

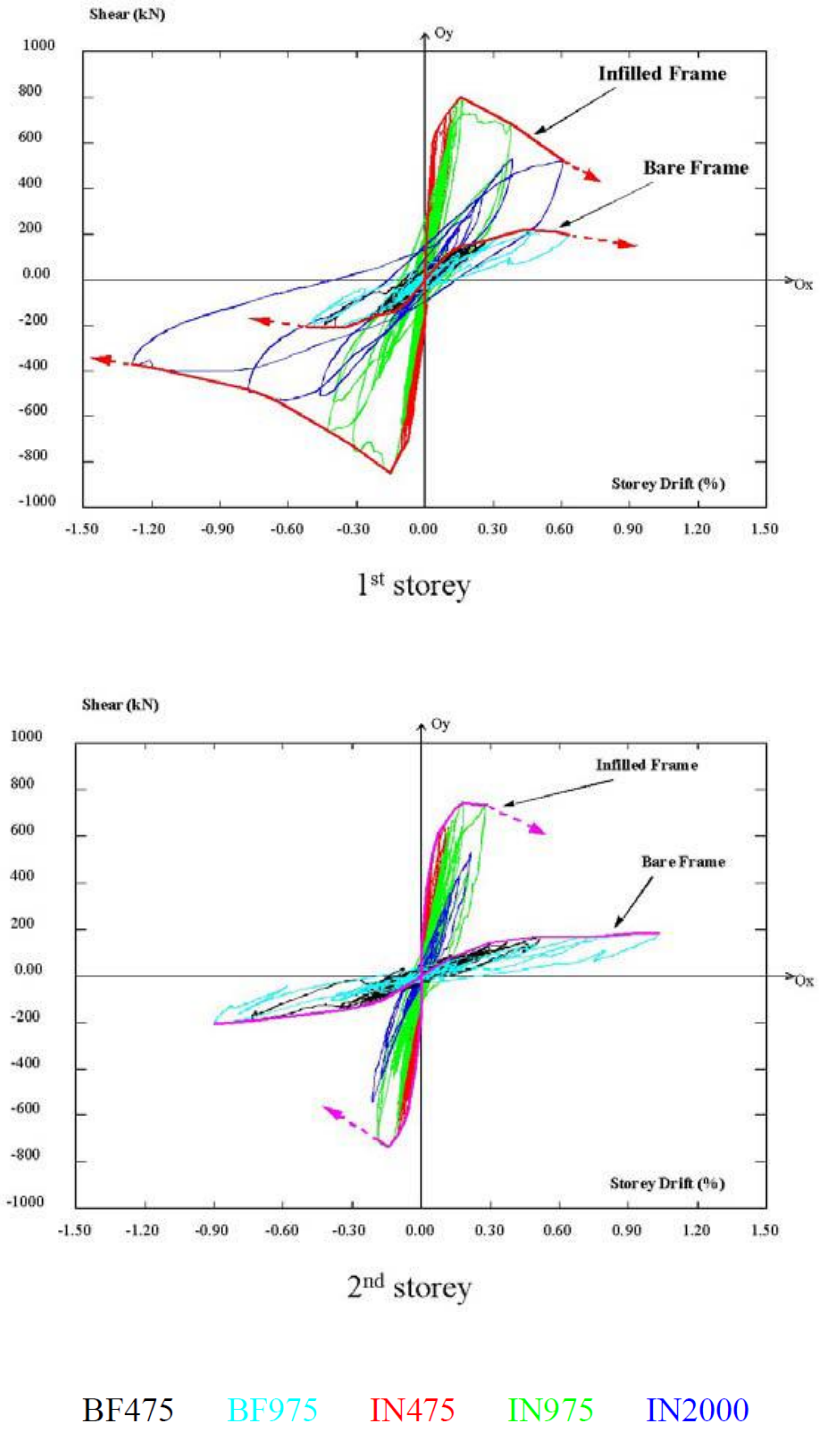

Figure 3.23 – BF and IN tests: 1st and 2nd storey shear vs. inter-storey drift and respective envelope curves (Varum, 2003)

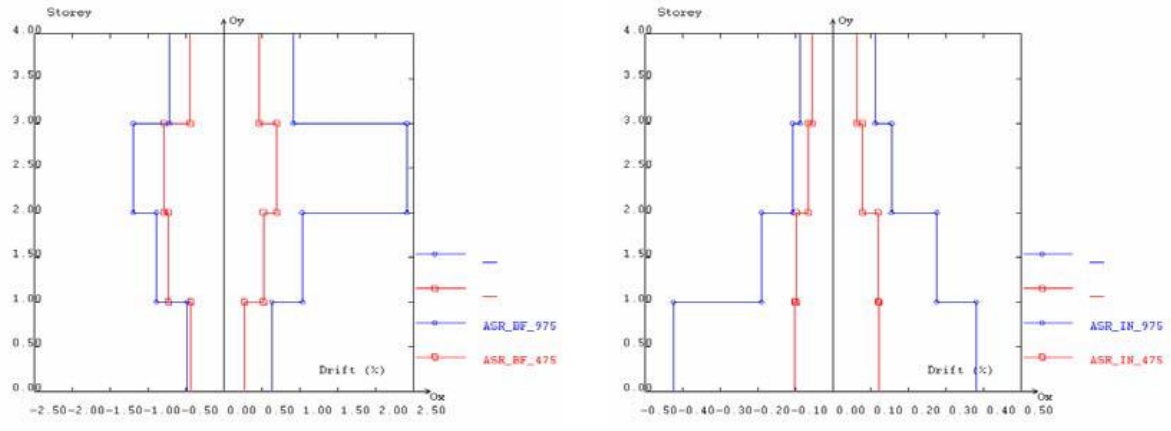

BF tests IN tests

Figure 3.24 – BF and IN tests (475 and 975-yrp): maximum inter-storey drift profiles (Varum, 2003)

3.3. NUMERICAL MODELLING AND STRUCTURAL ANALYSIS

The numerical models of the bare and infilled frames were developed using software platform *SeismoStruct* (Seismosoft, 2018) – a computer program for static and dynamic nonlinear analysis of framed structures developed by Antoniou and Pinho. Figure 3.25, for instance, illustrates the general characteristics of the BF model. Nonlinear dynamic analyses were then run, considering the same earthquake input used in the previously described PsD tests, for the purpose of evaluating the models' capacity to reproduce the structural behaviour of the frames. This procedure was important to build confidence to base further conclusions on the results obtained with such models in situations for which no experimental data are available for comparison. This section thus analyses and discusses the obtained numerical results in light of the available experimental results.

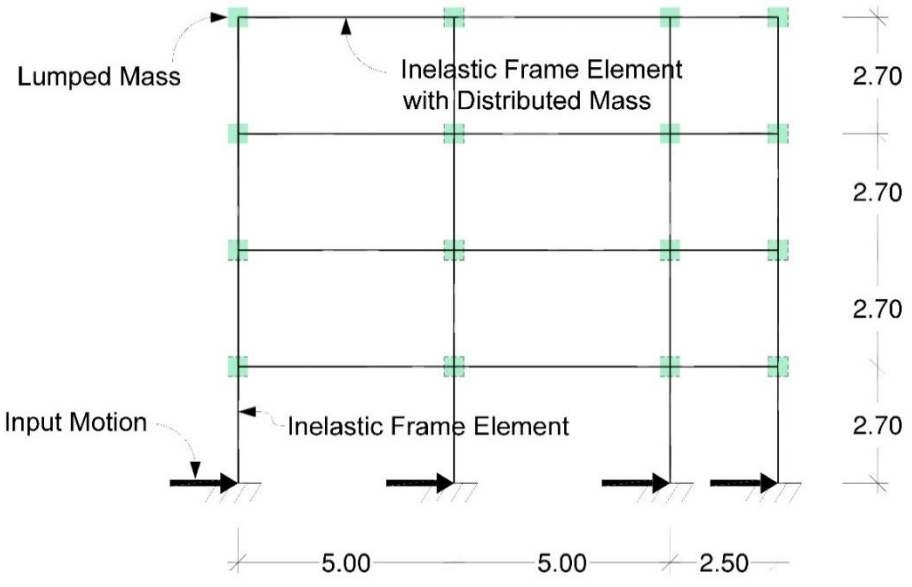

Figure 3.25 – General characteristics of the numerical model developed for the BF

3.3.1. Modelling options

This sub-section describes the options that were taken while developing the numerical models for the bare and infilled frames. The modelling of RC members and masonry infill walls, as well as the applied loads, added masses and considered viscous damping (VD) ratios are discussed based on the work and recommendations of several authors on these matters, as per the literature review carried out in Chapter 2.

3.3.1.1. Modelling of RC members

A distributed plasticity model was considered for both column and beam elements, combined with fibre discretization to represent cross-section behaviour (approx. 200 fibres / section). A force-based FE formulation was used to implement the frame elements, considering five integration sections per element according to the recommendations of Calabrese *et al* (2010). The cross-section dimensions and corresponding reinforcement patterns were defined according to figures 3.3 to 3.5. An effective slab width of 1.05 *m* was considered for the beam elements, according to the slab-participation evaluation that was carried out during the PsD tests. It should, however, be noted that the slab-participation values proposed by EC8-1 (2004) for this case would be significantly higher (approx. 45%), which might tag this as an issue not to overlook when modelling older-type RC structures built with smooth rebars such as this one.

Concerning the constitutive laws defining the cyclic behaviour of the concrete and steel materials, these were chosen among those referred in Chapter 2. The Mander *et al* (1988) model was employed to define the concrete material, with model parameters being set according to the results of the experimental tests described in sub-section 3.2.3. The mean value of the compressive strength was taken for the peak strength of the unconfined concrete and the tensile ultimate strength was assumed to be 1/10 (one tenth) of the corresponding compressive ultimate strength. Due to significant differences of strength found between each casting phase, the columns were divided in two groups with specific parameters: (i) “Columns 1”, including the 1st and 2nd storeys and (ii) “Columns 2”, including the 3rd and 4th storeys. On the other hand, the average strength value of the different casting phases was used for the beams, due to the substantially lower differences. The adopted mechanical properties were, thus, the following:

- Compressive strength:
  - f_c (Columns 1) = 13.85 *MPa*
  - f_c (Columns 2) = 10.10 *MPa*
  - f_c (Beams) = 17.00 *MPa*
- Tensile strength:
  - f_t (Columns 1) = 1.39 *MPa*
  - f_t (Columns 2) = 1.01 *MPa*
  - f_t (Beams) = 1.70 *MPa*
- Modulus of elasticity (initial stiffness):
  - E_c (Columns 1) = 22.80 *GPa*

E_c (Columns 2) = 20.50 *GPa*

E_c (Beams) = 24.40 *GPa*

- Strain at unconfined peak compressive stress: ε_c = 0.0025 *m/m*
- Specific weight: γ_c = 2450 *kg/m³*.

Regarding the steel material's cyclic behaviour, the Menegotto and Pinto (1973) model was employed, combined with the isotropic hardening rules proposed by Filippou *et al* (1983). The model parameters were also defined according to the results of the experimental tests described in sub-section 3.2.3., leading to the following mechanical properties (mean values):

- Modulus of elasticity (initial stiffness): E_s = 204.5 *GPa*
- Yield stress: f_y = 343.6 *MPa*
- Strain hardening parameter: μ = 0.0024
- Specific weight: γ_s = 7850 *kg/m³*.

Concerning the inclusion of bond-slip effects, these were implicitly accounted for in the Menegotto and Pinto (1973) model by following the simplified approach of Caruso *et al* (2018), described in sub-section 2.5.1. Hence, the steel material Young's modulus E_s was reduced to $E_s{}'$, while the yield stress f_y remained unaltered. The reduction factor varied with the return period of the earthquake demand and type of structural member (beam or column). After several runs of the models and subsequent comparisons between experimental and numerical results, the best agreement was found with the following setup: (i) 475-yrp: $E_s' = E_s$ for all members; (ii) 975- and 2000-yrp: $E_s' = 0.50 \cdot E_s$ for columns and $E_s' = E_s$ for beams. Eventually, some refinement could have been achieved by considering different reduction factors per storey or even per column, but the results obtained with the considered constant reduction factor are judged to be of good enough quality. In fact, the differences between experimental and numerical results were notorious for the 975- and 2000-yrp earthquakes, when no bond-slip effect was considered (i.e., $E_s' = E_s$ for all members), thus stressing the importance of not disregarding it for such intensities of the demand. This was not the case for the 475-yrp earthquake, which is coherent with the fact that no evidence of rebars' slippage was observed during the corresponding experimental test, as reported by Pinto *et al* (2002).

Regarding the modelling of shear effects, linear elastic behaviour was considered, uncoupled with the fibre axial stress vs. strain nonlinear constitutive laws. This implies that the nonlinear structural response is not affected by shear failures, which might be seen as a rather optimistic assumption for the modelling of an older-type RC structure with smooth rebars. However, according to the experimental results, shear failure did not occur except at the extremities of the third storey strong column of the BF, at the end of the 975-yrp earthquake. Therefore, the shear capacities of members seemed to be sufficient to allow flexural hinging. This was controlled by performing safety checks during each analysis, with alerts being generated each time a maximum calculated value of shear force reached the shear strength capacity of a member. The testing and implementation in the chosen software platform of one or more of the coupled nonlinear shear models referred in sub-section 2.5.1. is indeed beyond the scope of this work. However, the importance of the topic should not be overlooked when dealing with the seismic assessment of older-type RC buildings.

3.3.1.2. Modelling of masonry infill walls

The nonlinear cyclic model for masonry panels developed by Crisafulli (1997) – briefly presented in sub-section 2.5.4. and implemented in software platform *SeismoStruct* by Blandon (2005) – was considered for the modelling of the masonry infill walls. As previously referred, this model has the advantage of being capable of accounting for the local effects caused by the infill panels in the surrounding frame, without significant increase in the complexity of the analysis. However, it does require the definition of a large number of model-calibrating parameters, in order to fully characterize the nonlinear element. These parameters may be organized in three groups according to their nature: (i) mechanical; (ii) geometrical and (iii) empirical. The mechanical and geometrical parameters define the monotonic behaviour of the strut elements, while the empirical parameters are exclusively associated with the cyclic loading rules. The adopted final values (presented below) were set according to the results of the experimental tests described in sub-section 3.2.3. and/or the recommendations of Crisafulli (1997), Smyrou *et al* (2006), and O'Reilly (2016).

Due to their different characteristics, the infill panels (see Figure 3.6) were divided in four groups with specific parameters: (i) "Full_IN", including all the short panels with no openings; (ii) "Door_IN", including the central long panel with a door opening at the 1st storey; (iii) "LargeW_IN", including the central long panels with large window openings at the 2nd, 3rd and 4th storeys, and (iv) "SmallW_IN", including all the external long panels with small window openings. Table 3.12 summarizes the general dimensions of each panel group:

Table 3.12 – Dimensions of the masonry infill walls according to the defined groups

	Full_IN	**Door_IN**	**LargeW_IN**	**SmallW_IN**
$L\ (m)$	2.50	5.00	5.00	5.00
$H\ (m)$	2.70	2.70	2.70	2.70
$l_w\ (m)$	2.30	4.60	4.60	4.60
$h_w\ (m)$	2.20	2.20	2.20	2.20
$t_w\ (m)$	0.15	0.15	0.15	0.15
$b\ (m)$	0.245	0.245	0.245	0.245
$d\ (m)$	0.245	0.245	0.245	0.245
$d_w\ (m)$	3.18	5.10	5.10	5.10
θ (°)	43.73	25.56	25.56	25.56
$\theta\ (rad)$	0.76318	0.44611	0.44611	0.44611
Openings (m^2)	-	2.00 × 1.75	2.00 × 1.00	1.20 × 1.00

where L is the span of beam between centre line of supporting columns, H is the storey height, l_w is the length of masonry panel between adjacent columns, h_w is the height of masonry panel, t_w is the thickness of masonry infill (12 *cm* thick bricks + 1.5 *cm* of plaster on each side), b and d are, respectively, the height and length of the bricks, d_w is the diagonal length of the masonry panel and θ is the inclination of the diagonal of the masonry panel to the horizontal axis. The sizes of the openings are given as width × height.

The compression / tension cyclic relationship is characterized by six mechanical parameters: (i) initial elastic modulus E_{m0}; (ii) compressive strength for angle θ, $f_{m\theta}$; (iii) tensile strength f_t; (iv) strain at maximum stress ε_m; (v) ultimate strain ε_u and (vi) closing strain ε_{cl}. When no sufficient experimental information exists, the usual approach is to estimate values by applying the empirical expressions and value ranges found in the literature. Along with the experimental test results described in sub-section 3.2.3., the following were used to evaluate the initial elastic modulus E_{m0}:

(Sahlin, 1971; Paulay and Priestley, 1992) $$E_m = 750 \cdot f_m \quad (3.1)$$

(Sinha and Pedreschi, 1983) $$E_m = 1180 \cdot {f_m}^{0.83} \quad (3.2)$$

(Hendry, 1990) $$E_m = 2116 \cdot \sqrt{f_m} \quad (3.3)$$

(Sahlin, 1971; Paulay and Priestley, 1992 and others) $$E_m = 1000 \cdot f_m \quad (3.4)$$

where f_m represents the standard compressive strength of masonry (measured in a vertical compression test) in *MPa*. It is worth noting, however, that these expressions define a secant modulus E_m at a stress level between one-third to two-thirds of the maximum compressive stress, while the initial elastic modulus E_{m0} represents the initial slope of the stress-strain curve. Therefore, the direct use of such values may underestimate the initial stiffness of the infilled frame. Crisafulli (1997) thus recommends, in order to obtain an adequate ascending branch of the strength envelope, that $E_{m0} \geq 2 \cdot f_{m\theta}/\varepsilon_m$. These considerations led to a uniform value of E_{m0} = 2.20 *GPa*, which was used for the four infill panel groups.

The compressive strength for angle θ, $f_{m\theta}$, is the main parameter to control the resistance of the struts. It does not, however, represent the above referred standard compressive strength of masonry, as it depends on the expected failure mode for the panel. Four basic failure modes are considered, each with a corresponding equivalent failure compressive stress: (i) diagonal tension; (ii) sliding shear along horizontal joints (the most common); (iii) crushing of corners in contact with the RC frame and (iv) diagonal compression at the centre of the panel. The expressions described in Decanini *et al* (2004) and O'Reilly (2016) for each failure mode are given below in the same order:

$$\sigma_{w,DT} = \frac{0.6 \cdot f_{ms} + 0.3 \cdot \sigma_v}{\frac{b_w}{d_w}} \quad (3.5)$$

$$\sigma_{w,SH} = \frac{(1.2 \cdot \sin\theta + 0.45 \cdot \cos\theta) \cdot f_{mu} + 0.3 \cdot \sigma_v}{\frac{b_w}{d_w}} \quad (3.6)$$

$$\sigma_{w,CRN} = \frac{1.12 \cdot \sin\theta \cdot \cos\theta}{K_1 \cdot (\lambda H)^{-0.12} + K_2 \cdot (\lambda H)^{0.88}} \cdot f_m \tag{3.7}$$

$$\sigma_{w,DC} = \frac{1.16 \cdot \tan\theta}{K_1 + K_2 \cdot \lambda H} \cdot f_m \tag{3.8}$$

where f_{ms} is the shear strength measured in diagonal compression tests, σ_v is the vertical compression stress due to gravity loads (usually equal to zero, as infill panels are typically not load-bearing), b_w is the equivalent width of the strut, f_{mu} is the sliding resistance of mortar joints measured in triplet tests, λH is a non-dimensional parameter – originally proposed by Stafford Smith (1963) and given below by Expression (3.9) – which expresses the relative stiffness of the infill panel to the RC frame, K_1 and K_2 are two constants, which depend on the value of λH and on the cracking state of the infill panel (i.e. cracked or uncracked), also given below.

$$\lambda H = H \cdot \sqrt[4]{\frac{E_m \cdot t_w \cdot \sin 2\theta}{4 \cdot E_c \cdot I_c \cdot h_w}} \tag{3.9}$$

Cracked panel:

$$\begin{gathered} \lambda H < 3.14 \;\Rightarrow\; K_1 = 1.300;\; K_2 = -0.178 \\ 3.14 \le \lambda H \le 7.85 \;\Rightarrow\; K_1 = 0.707;\; K_2 = 0.010 \\ \lambda H > 7.85 \;\Rightarrow\; K_1 = 0.470;\; K_2 = 0.040 \end{gathered} \tag{3.10}$$

Uncracked panel:

$$\begin{gathered} \lambda H < 3.14 \;\Rightarrow\; K_1 = 1.375;\; K_2 = -0.115 \\ 3.14 \le \lambda H \le 7.85 \;\Rightarrow\; K_1 = 0.748;\; K_2 = 0.085 \\ \lambda H > 7.85 \;\Rightarrow\; K_1 = 0.393;\; K_2 = 0.130 \end{gathered} \tag{3.11}$$

In Expression (3.9), E_c and I_c represent the elastic modulus of concrete and the moment of inertia of the adjacent columns, respectively. It should be kept in mind, though, that the value of I_c significantly decreases after cracking develops in the columns. Consistently, the value of E_m to be used should also correspond to the considered state of the infill panel (cracked or uncracked). Concerning coefficients K_1 and K_2, these were initially introduced by Decanini and Fantin (1986) and later adapted by Bertoldi *et al* (1993). However, as values for when λH < 3.14 in uncracked panel state are not found on these references, those shown in Expression (3.11) are proposed herein by the author. Given all these considerations, the equivalent failure compressive stresses corresponding to each failure mode can be determined, the most likely to occur being defined by the minimum value. The latter should then be taken equal to the panel's $f_{m\theta}$. This process led to values of 1.00 *MPa* and 0.50 *MPa* for the short (Full_IN) and long (Door_IN, LargeW_IN and SmallW_IN) panels, respectively.

The tensile strength f_t represents either the fundamental tensile strength of masonry or the bond strength of the panel-frame interfaces (whichever is smaller). Its consideration brings generality to the model but, as it has no significant influence on the overall response, it can be taken equal to zero in lack of better information. The strain at maximum stress ε_m influences the overall response of the infilled frame through the modification of the secant stiffness of the ascending branch of the stress-strain curve. This parameter usually varies between -0.001 and -0.005 but should be calibrated based on experimental data. The ultimate strain ε_u is a parameter used to control the descending branch of the stress-strain relationship. The adoption of a large value such as $\varepsilon_u = 20 \cdot \varepsilon_m$ ensures a smooth decrease of the strut's compressive stress. Lastly, the closing strain ε_{cl} defines the limit strain at which cracks partially close and compressive stresses can develop. Values ranging between 0 and 0.003 lead to results which agree adequately with experimental data. Alternatively, if a large negative value is adopted (e.g., $\varepsilon_{cl} = \varepsilon_u$), this effect is not considered in the analysis. Table 3.13 shows the final values adopted for these parameters.

Table 3.13 – Final limit strains considered in the calibration of the compression / tension cyclic relationship

	Full_IN	Door_IN	LargeW_IN	SmallW_IN
ε_m	-0.0010	-0.0008	-0.0008	-0.0008
ε_u	-0.0200	-0.0160	-0.0160	-0.0160
ε_{cl}	0.0030	0.0030	0.0030	0.0030

In addition to the above-described mechanical parameters, a set of nine empirical (less intuitive and harder to calibrate) factors is required to complete the characterization of the compression / tension cyclic relationship:

- Unloading stiffness factor (γ_{un}): defines the unloading modulus in proportion to E_{m0}, thus controlling the slope of the unloading branch, modifying the internal cycles but not the envelope;
- Reloading strain factor (α_{re}): predicts the strain at which the reloading curve reaches the strength envelope;
- Inflection strain factor (α_{ch}): predicts the strain at which the reloading curve should feature an inflexion point, thus controlling the loops' "fatness";
- Unloading strain factor (β_a): defines an auxiliary point to determine the plastic deformation after complete unloading;
- Inflection stress factor (β_{ch}): predicts the stress at which the reloading curve should feature an inflexion point;
- Zero stress stiffness factor (γ_{plu}): defines the modulus of the hysteretic curve at zero stress, in proportion to E_{m0}, after complete unloading has occurred;
- Reloading stiffness factor (γ_{plr}): defines the modulus of the reloading curve, in proportion to E_{m0}, after complete unloading has occurred;
- Plastic unloading stiffness factor (e_{x1}): defines the unloading tangent modulus corresponding to the plastic strain, in proportion to E_{m0};

- Repeated cycle strain factor (e_{x2}): defines the strain that the envelope curve should reach after inner cycling, thus representing cumulative damage inside repeated cycles.

Crisafulli (1997) defined the limits for which each parameter has meaning and proposed a range of recommended values based on experimental results. A few years later, Smyrou *et al* (2006) carried out a sensitivity study that seems to show that, when running nonlinear dynamic analyses, only three of these parameters (γ_{un}, α_{ch}, e_{x1}) play significant roles in the energy dissipation capacity of the infill panel (i.e., the remaining parameters are not expected to have a major impact if changed from the proposed default values). Table 3.14 shows the recommended range and final adopted values for these parameters (valid for the four infill panel groups).

Table 3.14 – Empirical parameters: limits recommended by Crisafulli (1997) and final adopted values

	Recommended range	Limits	Adopted value
γ_{un}	1.5 – 2.5	≥ 1	1.70
α_{re}	0.2 – 0.4	≥ 0	0.20
α_{ch}	0.3 – 0.6	0.1 – 0.7	0.70
β_a	1.5 – 2.0	≥ 0	2.00
β_{ch}	0.6 – 0.7	0.5 – 0.9	0.90
γ_{plu}	0.5 – 0.7	0 – 1	1.00
γ_{plr}	1.1 – 1.5	≥ 1	1.10
e_{x1}	1.5 – 2.0	≥ 0	3.00
e_{x2}	1.0 – 1.5	≥ 0	1.00

Concerning the cyclic shear relationship, four parameters need to be defined to fully characterize this response curve: (i) initial shear bond strength τ_0; (ii) friction coefficient μ; (iii) maximum permissible shear stress τ_{max} and (iv) shear stress distribution factor α_s. The values of τ_0 and μ can either be evaluated by direct shear tests or obtained from design specifications. However, whilst the former may lead to an overestimation of values (Wan and Yi, 1986; Riddington and Ghazali, 1988), the latter tend to be over-conservative, so caution is advised when selecting the approach – Crisafulli (1997), for instance, within the proposed modification to the Mann and Müller's (1982) theory, referred the following expressions for reducing values obtained from shear tests:

$$\tau_0{}^* = \frac{\tau_0}{1 + \mu \cdot C_n \cdot \frac{b}{d}} \qquad \mu^* = \frac{\mu}{1 + \mu \cdot C_n \cdot \frac{b}{d}} \tag{3.12}$$

where $\tau_0{}^*$ and μ^* are, respectively, the reduced shear bond strength, the reduced friction coefficient and C_n is a constant that can be taken equal to 1.5 for practical application.

Several researchers (e.g., Hendry, 1990; Paulay and Priestley, 1992) have experimentally determined the initial shear bond strength τ_0, suggesting either relatively narrow value ranges such as 0.3 to 0.6 *MPa,* or broader ones such as 0.1 to 0.7 *MPa* or even 0.1 to 1.5 *MPa*. However, the wide variety of tested materials should be noted. Empirical expressions (dependent on various parameters) have also resulted from these and other research initiatives but should be used with caution given the large number of involved variables. In parallel, the friction coefficient μ has been reported to vary within a range as large as 0.1 to 1.2. However, some of the proposed values are meant for design applications rather than assessment, therefore being conservatively low. Atkinson *et al* (1989) suggested a default range of 0.70 to 0.85 for assessment purposes. These considerations led herein to values of τ_0 equal to 0.25 and 0.30 *MPa* for the modelling of the infill panels with and without openings, respectively, and to a uniform value of μ equal to 0.70.

The maximum permissible shear stress τ_{max} represents an upper limit to the infill panels' shear strength calculation as given by the hysteresis rules proposed by Crisafulli (1997). It is based on experimental and analytical evidence indicating that values provided by such rules become unrealistic when computing medium to high values of compressive stresses at bed joints. Values for τ_{max} can be selected from the shear failure envelope given by the above referred modification of Mann and Müller's (1982) theory, depending on the expected failure mode. However, in the absence of better information, a default range of 0.5 to 1.0 *MPa* can be considered. Concerning the shear stress distribution factor α_s, it is used to take into account the non-uniform distribution of shear stresses along the horizontal section of the infill panels, being defined as the ratio between the maximum and average shear stresses. It usually varies between 1.40 and 1.65, with a proposed default value of 1.50 which will work well for most situations. Values of τ_{max} equal to 0.6 and 1.0 *MPa* were used herein for the modelling of the infill panels with and without openings, respectively, along with a uniform value of α_s equal to 1.50.

Finally, for the characterization of the nonlinear element to be complete, the following parameters are still required: (i) initial strut area A_1; (ii) residual strut area A_2; (iii) strut area reduction strain ε_1; (iv) residual strut area strain ε_2; (v) equivalent contact length h_z; (vi) horizontal offset X_{oi}; (vii) vertical offset Y_{oi} and (viii) shear stiffness factor γ_s. The initial strut area A_1 is defined as the product of the infill panel's thickness t_w by the equivalent width of the strut b_w, the latter typically varying between 10% and 40% of the diagonal length of the panel d_w, as reported by several authors based on experimental data. Numerous empirical expressions have also been proposed – featuring varying degrees of complexity – that can be used to estimate the value of b_w when no sufficient experimental information exists. Expressions (3.13) to (3.17) below are some of the most popular.

(Holmes, 1961) $$b_w = \frac{d_w}{3} \tag{3.13}$$

(Paulay and Priestley, 1992) $$b_w = 0.25 \cdot d_w \tag{3.14}$$

(Mainstone, 1971) $$b_w = 0.16 \cdot (\lambda H)^{-0.3} \cdot d_w \quad (3.15)$$

(Liauw and Kwan, 1984) $$b_w = \frac{0.95 \cdot h_w \cdot \cos\theta}{\sqrt{\lambda H}} \quad (3.16)$$

(Decanini and Fantin, 1986) $$b_w = \left(\frac{K_1}{\lambda H} + K_2\right) \cdot d_w \quad (3.17)$$

From the above referred, Expression (3.17) has the interesting feature of being linked to expressions (3.9), (3.10) and (3.11), thus allowing for the calculation of b_w associated with both the cracked and uncracked states of the infill panel. It should be noted, however, that the values provided by these expressions refer to fully infilled panels. If openings exist in a panel, Smyrou *et al* (2011) suggests reducing the initial strut area A_1 in proportion to the area of the opening in relation to that of the panel, as to consider the expected reduction of the panel's stiffness. In practical terms, this is done by reducing the value of b_w corresponding to the fully infilled panel. The value of the reduction factor will depend on the relative size of the opening to that of the panel, as already said, but also on its location within (e.g., centred vs. near loaded ends of the compressed struts). Engineering judgement and experience are, therefore, of the utmost importance to deal with this matter for which uncertainties are still so predominant.

The residual strut area A_2 is a parameter that accounts for the fact that, due to cracking, the contact length between the frame and the infill panel decreases as the lateral and (consequently) axial displacements increase, thus affecting the area of the equivalent strut. A linear variation as a function of the axial strain is assumed between A_1 and A_2 (Figure 3.26). According to experimental results reported by Decanini and Fantin (1986), cracking induces a decrease of about 20% to 50% of the equivalent width of the strut. Therefore, a default range of about 80% to 50% can be used to define A_2 as a percentage of A_1 in the lack of better information. Concerning the definition of the strut area reduction strain ε_1 and residual strut area strain ε_2, these are parameters for which it is (obviously) difficult to find experimental evidence. Crisafulli (1997) suggests using estimated values of $\varepsilon_m/10$ and $\varepsilon_m/2$, respectively, if no better information is available. Other authors have proposed default value ranges that can also help to determine starting values for these parameters.

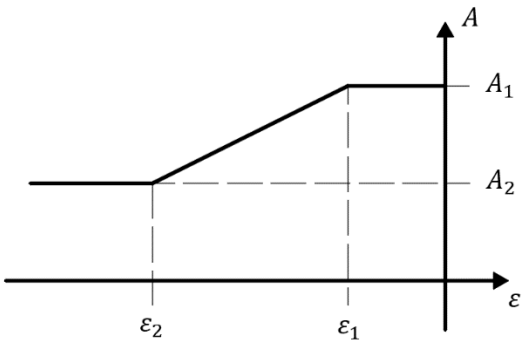

Figure 3.26 – Equivalent strut area variation as a function of the axial strain

The equivalent contact length h_z represents the vertical distance between the compression / tension struts, thus accounting for the actual contact length z between the frame and the infill panel, as defined by Expression (3.18) proposed by Stafford Smith (1966). In Crisafulli's (1997) model, being a double-strut model, h_z is typically taken equal to $z/3$ and introduced as a percentage of the storey's height H. The geometrical definition of the contact length z is shown in Figure 3.27, along with that of several other geometrical parameters that have been referred up to this point. Concerning the horizontal and vertical offsets X_{oi} and Y_{oi}, these are introduced as a percentage of the beam's centreline span L and storey's height H, respectively, and represent the reduction of the latter due to the depth of the frame's members. Lastly, the shear stiffness factor γ_s represents the percentage of the total stiffness of the element to be assigned to the shear spring, thus also affecting the stiffness of the compression / tension struts. A default range of 50% to 75% is suggested by Crisafulli *et al* (2000), to be used in the lack of better information.

(Stafford Smith, 1966)
$$z = \frac{\pi}{2 \cdot \lambda H} \cdot H \tag{3.18}$$

(Crisafulli, 1997)
$$h_z = \frac{z}{3} \tag{3.19}$$

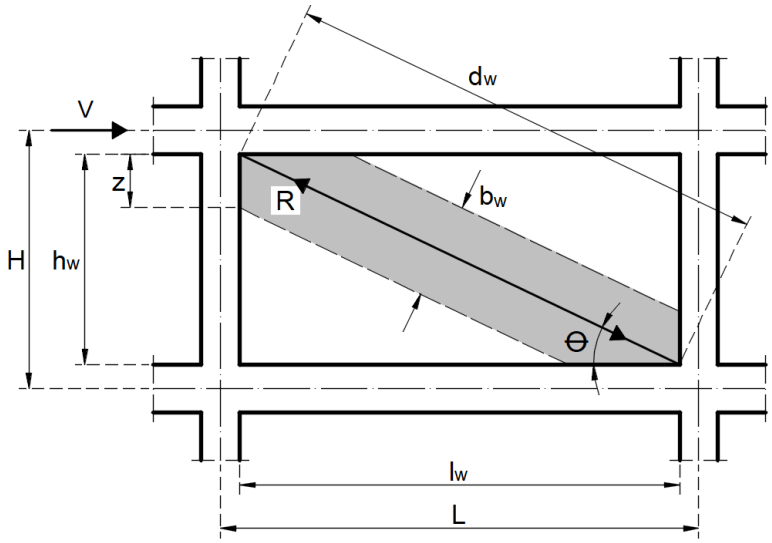

Figure 3.27 – Geometrical properties of the infill panel and surrounding RC frame

Table 3.15 shows the final values adopted herein for the above referred parameters (after several iterations of comparing numerical and experimental results). The values of b_w were estimated with the help of expressions (3.13) to (3.17), thus referring to the equivalent width of the strut of the fully infilled panels (i.e., with no reduction due to the openings). The reduction factors r_{ac} – defining the ratio of the strut areas A_1 of the panels with openings to that of the fully infilled panels – were obtained following the above-mentioned recommendations of Smyrou *et al* (2011) combined with the

information provided by the available experimental results in terms of strength and stiffness of the individual panels. It is worth noting that the values of the equivalent contact length h_z – obtained with expressions (3.9), (3.18) and (3.19) – were also corrected as to somehow consider the effect of the reduction factors r_{ac} on the equivalent width of the struts b_w. Even though no evidence of this procedure was found in the reviewed literature, it made sense to the author and the agreement between numerical and experimental results seemed to be well influenced by it. Concerning the remaining parameters, all were calibrated based on the information provided by the available experimental results, except the horizontal and vertical offsets X_{oi} and Y_{oi} that only depend on the geometry of the panel vs. that of the RC frame elements.

Table 3.15 – Geometrical parameters: final adopted values

	Full_IN	Door_IN	LargeW_IN	SmallW_IN
b_w (m)	1.10	2.60	2.60	2.60
b_w/d_w	0.35	0.51	0.51	0.51
r_{ac} $(\%\ b_w)$	100%	18%	26%	35%
A_1 (m^2)	0.1650	0.0690	0.1006	0.1381
A_2 $(\%\ A_1)$	70%	50%	50%	60%
ε_1	-0.0005	-0.0001	-0.0001	-0.0002
ε_2	-0.0008	-0.0003	-0.0003	-0.0004
h_z $(\%\ H)$	9.40%	3.15%	4.59%	6.30%
X_{oi} $(\%\ L)$	4.00%	6.00%	6.00%	6.00%
Y_{oi} $(\%\ H)$	9.26%	9.26%	9.26%	9.26%
γ_s	70%	40%	40%	60%

3.3.1.3. Loads, masses, and damping

Uniform loads on beams and concentrated loads on beam-column nodes were considered to model the vertical static loading other than the self-weight of the frame's main elements (columns and longitudinal beams). The value and position of each static load, as introduced in the numerical models, are shown in Figure 3.10 (see sub-section 3.2.4.). The earthquake input was modelled using the same 15-seconds artificial accelerograms that were generated for the PsD tests (Figure 3.12 above). Two time-history curves were composed for that purpose: (i) including the 475- and the 975-yrp records, separated by a 35-second interval with no acceleration and (ii) including the 475-, 975- and 2000-yrp records, separated by the same 35-second flat intervals. The first curve was uploaded to the BF model and the second to the IN model, as to reproduce the loading sequences carried out during the experimental tests. Through this methodology, the demands of the 975- and 2000-yrp earthquakes were imposed on a frame model that had already sustained the damage induced by the 475-yrp or by both the 475- and the 975-yrp earthquakes, respectively. Figure 3.18 depicts the time-history curve composed by the three earthquakes, showing the evident increase in terms of demand intensity (it is worth referring that the 35-second flat intervals between records were shortened in the figure as to save space and improve visualization).

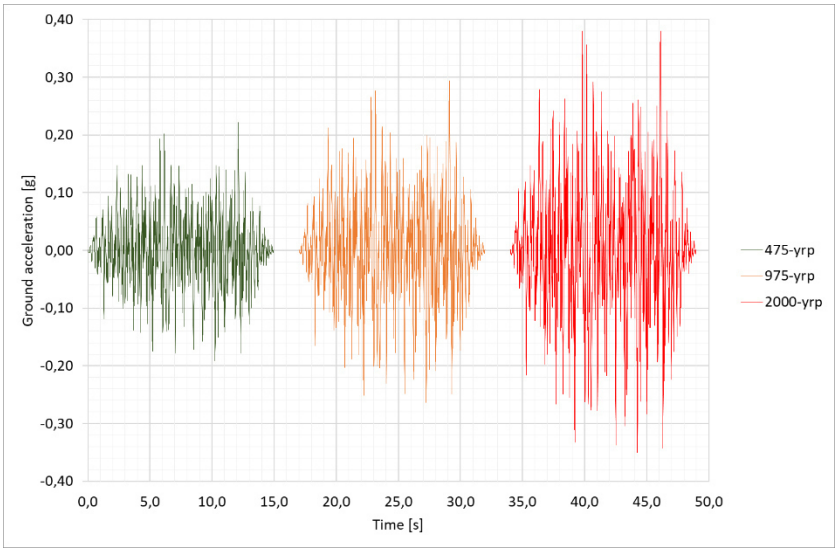

Figure 3.28 – Artificial acceleration time-history composed by the 475-, 975- and 2000-yrp earthquakes

The load-to-mass conversion on the numerical models was done at storey levels in order reproduce well the conditions of the PsD tests. Uniformly distributed floor masses of 45.48 *ton* and 37.49 *ton* were considered for the first three storeys and for the roof storey, respectively. These masses correspond to the weight of the slabs, floor finishing, transversal beams, masonry infill walls and to the quasi-permanent value of the floor's live load. The individual values of the vertical design loads that were converted to mass are given in sub-section 3.2.4. The resulting mass matrix of the structure is obviously diagonal.

Concerning the modelling of damping effects, given that the hysteretic component is implicitly included in the nonlinear model formulation / force-deformation laws describing the post-yield behaviour of inelastic elements under cyclic loading, only the effects of other (non-modelled) energy dissipation mechanisms need to be added as viscous damping (VD). The value to be employed will depend (among other things) on the imposed deformation level, i.e., low deformation levels may justify VD values that are higher than those used in analyses during which buildings are pushed deep into their inelastic range (in the latter case, the contribution of the non-modelled energy dissipation mechanisms is likely to be even smaller). From the available options – discussed in sub-section 2.6.3. – to introduce VD in nonlinear analysis models, the tangent stiffness-proportional damping (TSPD) approach was used herein. The value of the stiffness matrix multiplier α_K was thus defined by Expression (3.20):

$$\alpha_K = \frac{T_1 \cdot \xi_0}{\pi} \tag{3.20}$$

where T_1 is the period of the vibration mode with the highest base shear and ξ_0 is the defined VD ratio (percentage of critical). The TSPD matrix $[C] = \alpha_K \cdot [K]$ was then automatically updated at every load increment during the analyses. The values of ξ_0 introduced in the models varied with the return period

of the earthquake demand and were different for the BF and IN. After several runs and subsequent comparisons between experimental and numerical results, the best agreement was found with the following setup: (i) 475-yrp: $\xi_0\,(BF) = 1.0\%$; $\xi_0\,(IN) = 0.5\%$; (ii) 975-yrp: $\xi_0\,(BF) = 0.5\%$; $\xi_0\,(IN) \approx 0$; (iii) 2000-yrp: $\xi_0\,(IN) \approx 0$. Although some authors claim that this approach may not be totally adequate for vibrations with amplitudes below the elastic limits, these values are judged to reproduce reality fairly well. It is worth referring, though, that the IN model proved to be much more sensitive to slight variations of ξ_0 than the BF model.

3.3.2. Structural analysis results

This sub-section presents and discusses the obtained numerical results in light of the available experimental results (Pinto *et al,* 2002). Modal and nonlinear dynamic analyses were run, and comparisons were established in terms of natural frequencies and vibration mode shapes, as well as of storey displacements, drifts, and base shear. Based on this, conclusions are drawn about the developed models' ability to realistically simulate the structural behaviour of the frames, both in the linear as in the nonlinear ranges.

3.3.2.1. Modal frequencies

The tables below show the frames' experimentally (EXP.) and numerically (NUM.) determined natural frequencies, as well as the numerically determined vibration mode shapes. This comparison in terms of modal parameters allows for the validation of the models in the linear range. The BF model results showed a very good agreement with the experimental frequencies, thus proving to simulate well the elastic behaviour of the bare structure. Concerning the IN model results, a good agreement was also obtained for the first two frequencies, but higher differences were observed for the next. However, it is not clear in the experimental results report if frequencies $f_3(IN)$ and $f_4(IN)$ effectively correspond to the numerically determined vibration mode shapes 3 and 4, which might explain the observed differences (the numerical vibration mode shapes shown below for the IN were determined in direct correspondence with those of the BF).

Table 3.16 – Modal frequencies and vibration mode shapes of the BF: results comparison EXP. vs. NUM.

	MODE 1	MODE 2	MODE 3	MODE 4
	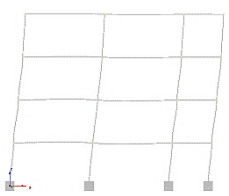	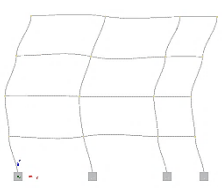	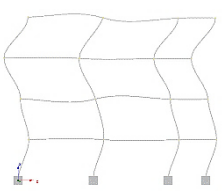	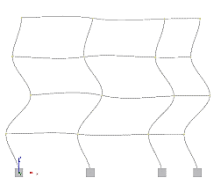
	f_1 (BF)	***f_2 (BF)***	***f_3 (BF)***	***f_4 (BF)***
EXP. (*Hz*)	1.57	4.60	7.58	11.14
NUM. (*Hz*)	1.59	4.67	7.75	10.97

Table 3.17 – Modal frequencies and vibration mode shapes of the IN: results comparison EXP. vs. NUM.

	MODE 1	MODE 2	MODE 3	MODE 4
	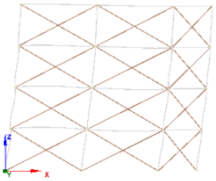	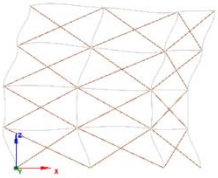	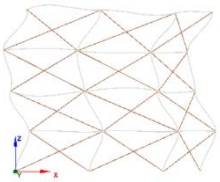	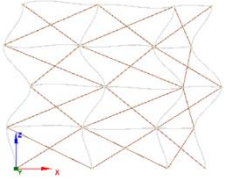
	f_1 (IN)	***f_2 (IN)***	***f_3 (IN)***	***f_4 (IN)***
EXP. (*Hz*)	7.22	20.83	24.93	45.35
NUM. (*Hz*)	7.33	20.92	32.06	38.80

There is one particularity, regarding the final calibration of the Crisafulli (1997) model behind the results given in Table 3.17, that must be pointed out: it included no stiffness reductions due to the openings in the infill panels, i.e., the best agreement with the experimentally determined frequencies was obtained by considering the equivalent width of the struts b_w corresponding to the fully infilled panels (see Table 3.15). This means that unlike for the calibration of the IN model's seismic response, in this case the reduction factors given in Table 3.15 did not help to improve the agreement between experimental and numerical results. In fact, the corresponding natural frequencies $f_1(IN)$ and $f_2(IN)$ were 30% lower than those obtained during the PsD tests. The above referred conclusion was thus reached after several iterations increasing the initial strut area A_1. However, this conclusion should (for now) be stretched no further than the limits of this particular case.

3.3.2.2. Storey displacements, drifts, and shear

The following figures show comparisons between the experimental and numerical time-histories of the BF, for the 475- and 975-yrp earthquakes, in terms of storey displacements (Figures 3.29 to 3.32), drifts (Figures 3.33 to 3.36) and base shear (Figure 3.37). For the case of the 475-yrp earthquake, a good approximation was achieved in terms of all the response variables, although the base shear was slightly underestimated in some cycles. The developed model hence seemed to be able to reproduce well the BF's behaviour when subjected to an earthquake prone to causing only local damage to some structural members (see sub-section 3.2.6.3.). Concerning the 975-yrp earthquake, a good agreement was also obtained and, most importantly, the sudden formation of the soft-storey mechanism at the third storey was captured (see Figure 3.35). It is noteworthy that this was only achieved after the inclusion of the bond-slip effect within the modelling options (see sub-section 3.3.1.1.) and required the testing of several VD ratios (ranging from 1.5% to approx. zero). Despite the slight overestimation of the storeys' displacements, the global approximation was quite satisfactory. Based on these results, the developed numerical model was deemed adequate to simulate the structural behaviour of the BF, even when subjected to an earthquake capable of causing extensive damage to several structural members (see sub-section 3.2.6.3.), thus pushing it to a near-collapse state.

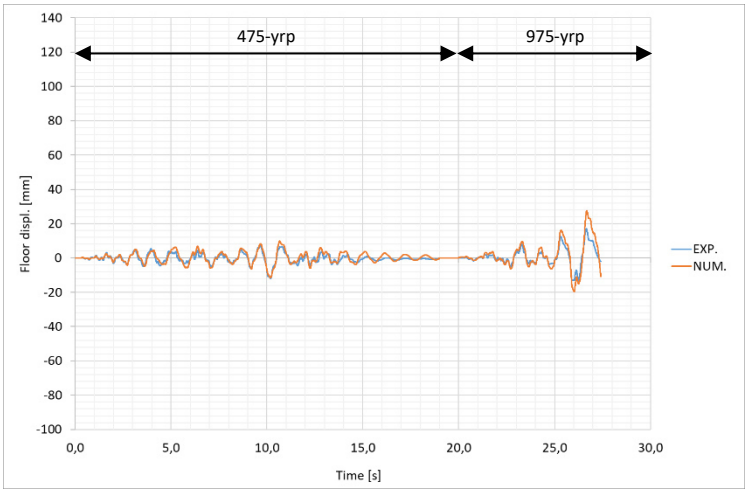

Figure 3.29 – BF storey displacements time-histories: Storey 1

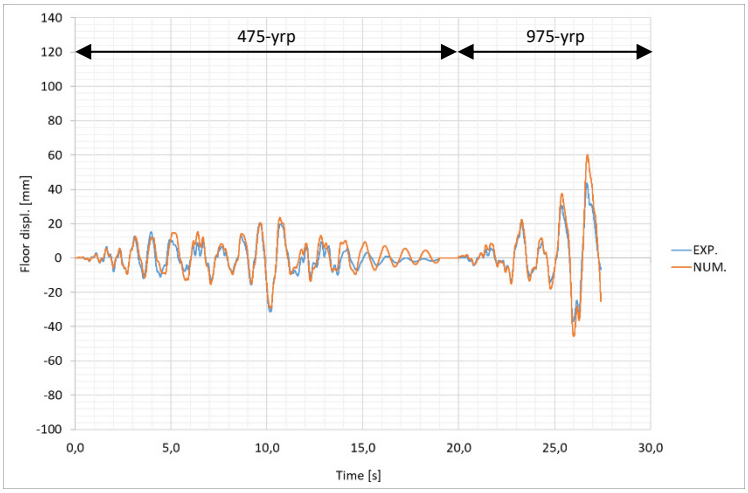

Figure 3.30 – BF storey displacements time-histories: Storey 2

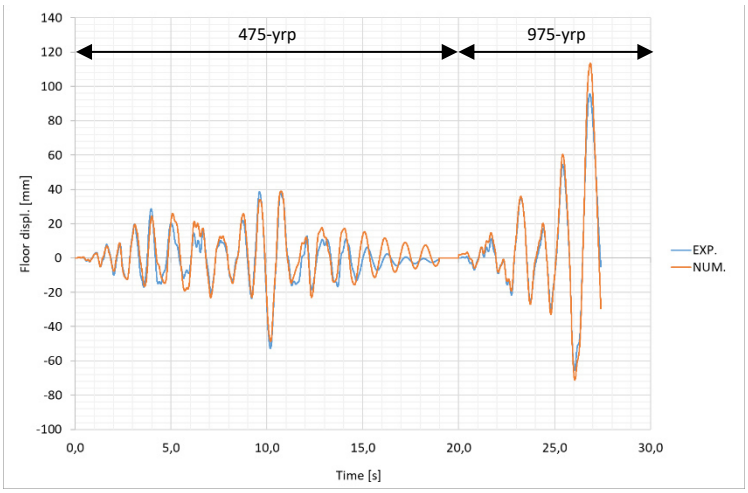

Figure 3.31 – BF storey displacements time-histories: Storey 3

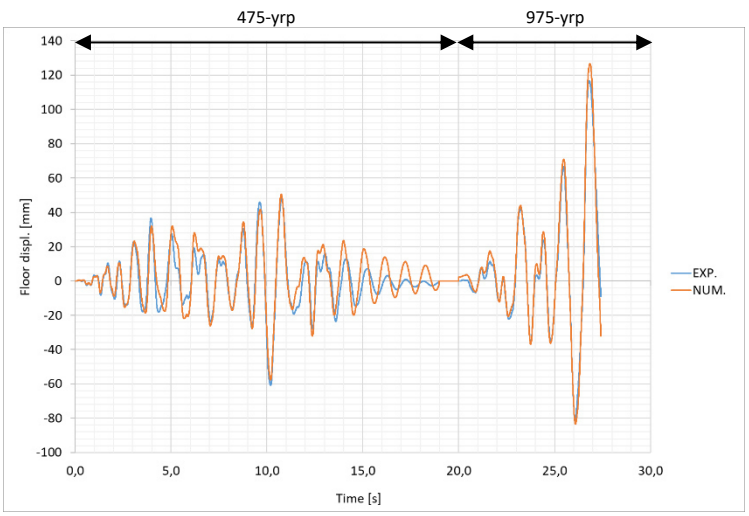

Figure 3.32 – BF storey displacements time-histories: Storey 4

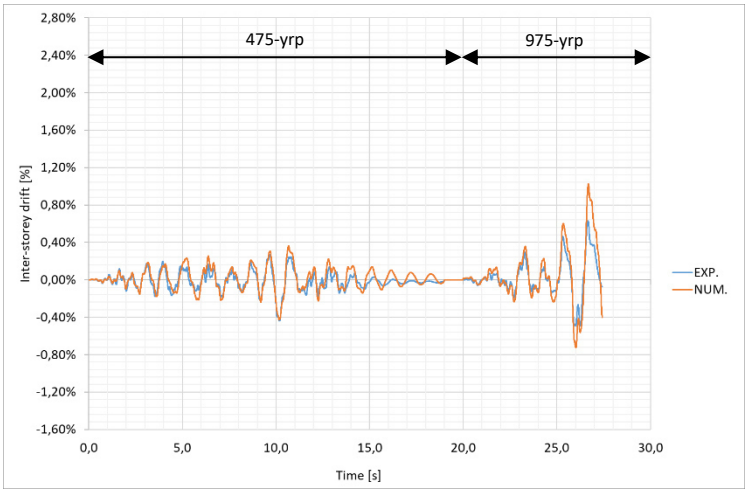

Figure 3.33 – BF inter-storey drifts time-histories: Storey 1

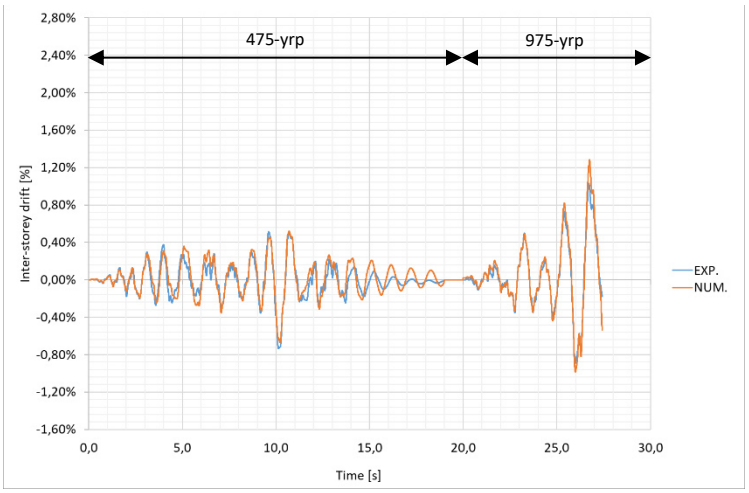

Figure 3.34 – BF inter-storey drifts time-histories: Storey 2

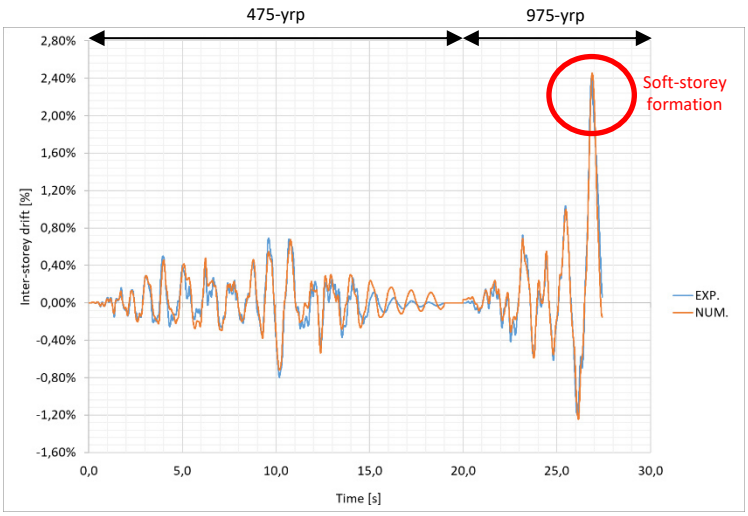

Figure 3.35 – BF inter-storey drifts time-histories: Storey 3

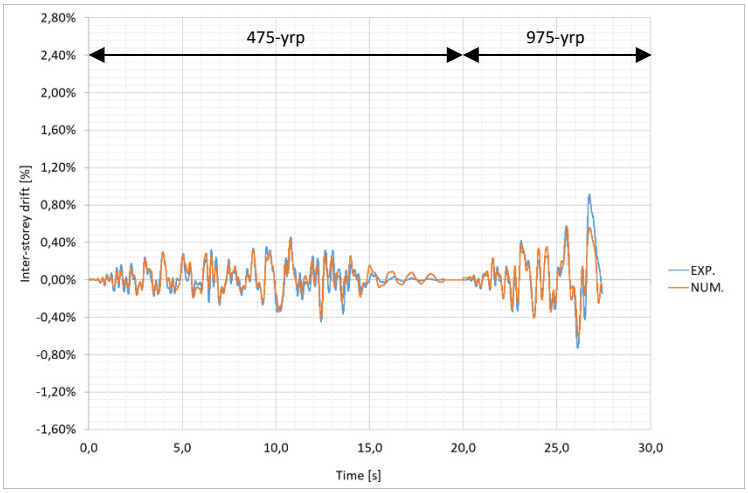

Figure 3.36 – BF inter-storey drifts time-histories: Storey 4

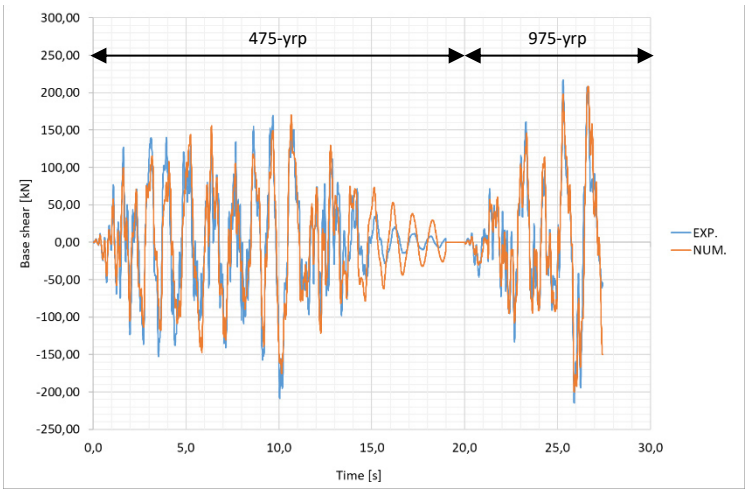

Figure 3.37 – BF base shear time-histories

Similar time-history comparisons are presented below for the IN (Figures 3.38 to 3.46), showing that the numerical model was capable of reproducing the structural response modifications induced by the infill walls. A good agreement between experimental and numerical results was generally obtained for the three earthquakes, despite some underestimation of storey displacements during the initial cycles of the 975-yrp input. More importantly, the formation of the soft-storey mechanism at the first storey during the 2000-yrp earthquake was duly captured (see Figure 3.42). The inclusion of the bond-slip effect within the modelling options was again paramount to achieve this, which is coherent with the reported damage at the bottom section of the strong column near the end of the 2000-yrp test (see sub-section 3.2.6.3.). It is also noteworthy that no concentration of damage was captured at the third storey, hence showing that the infill panels successfully prevented (as expected) the development of that irregular structural response of the RC frame. The developed numerical model was thus deemed robust enough to simulate the structural behaviour of the IN, both when under low intensity seismic inputs and when pushed to a near-collapse state.

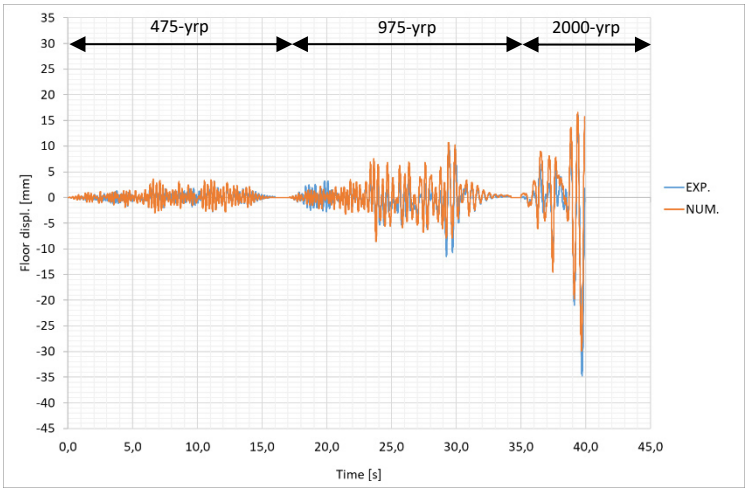

Figure 3.38 – IN storey displacements time-histories: Storey 1

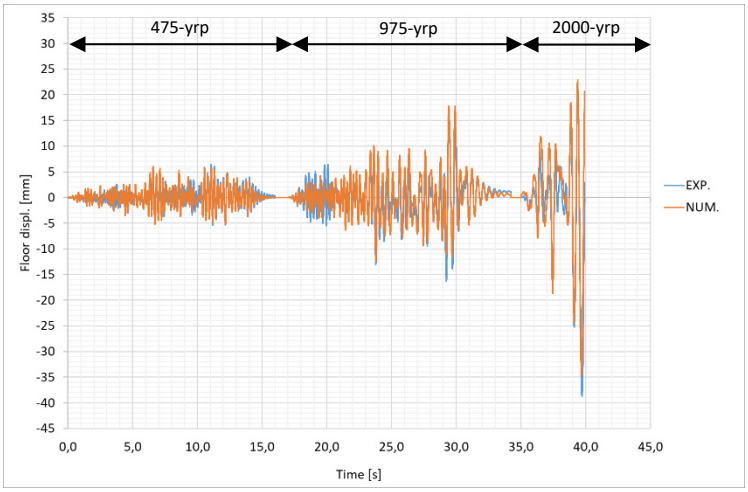

Figure 3.39 – IN storey displacements time-histories: Storey 2

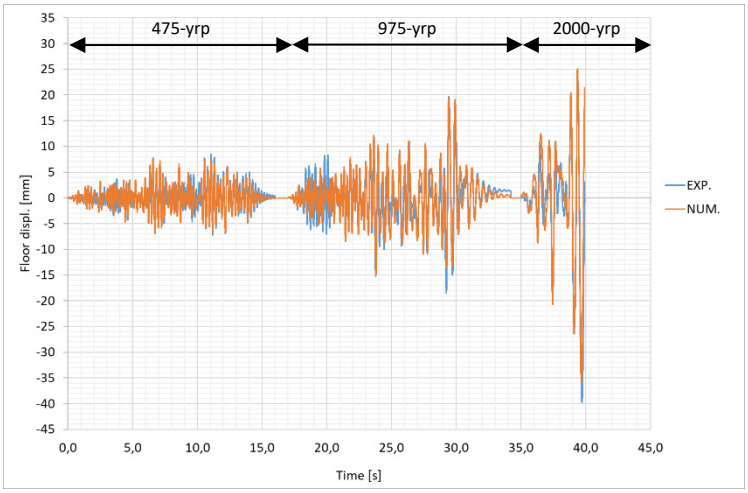

Figure 3.40 – IN storey displacements time-histories: Storey 3

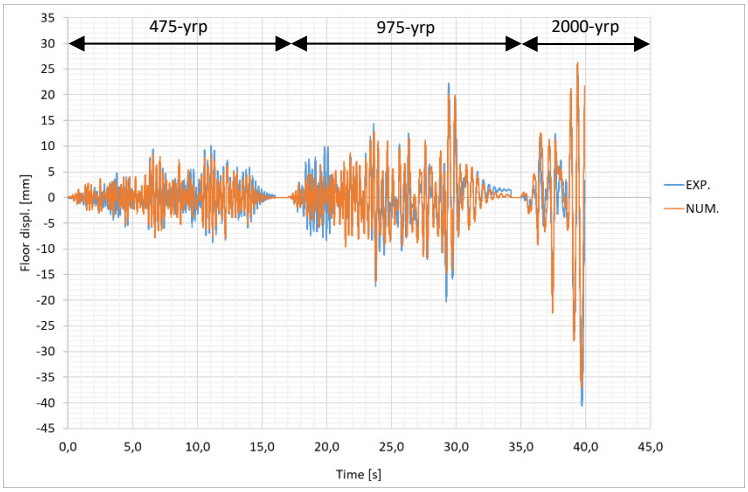

Figure 3.41 – IN storey displacements time-histories: Storey 4

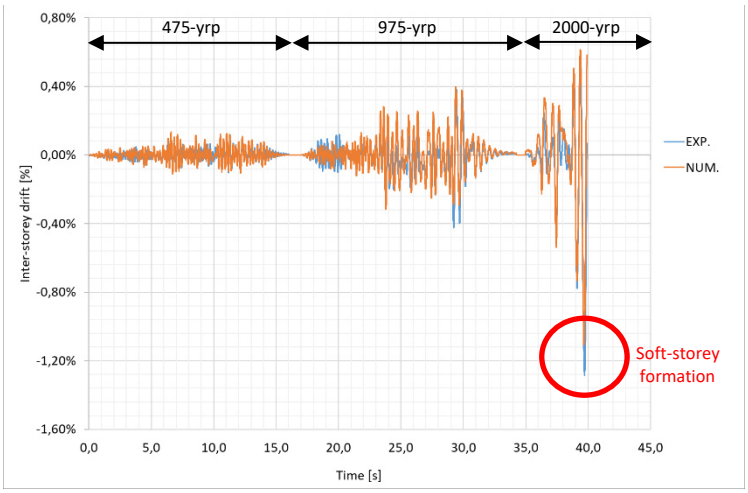

Figure 3.42 – IN inter-storey drifts time-histories: Storey 1

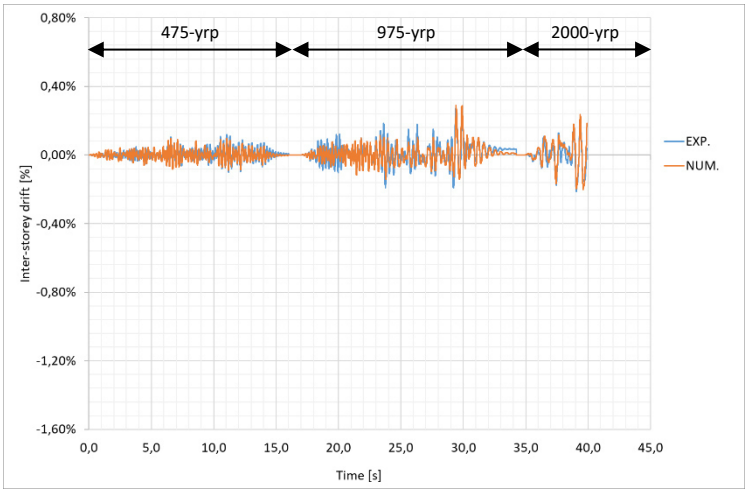

Figure 3.43 – IN inter-storey drifts time-histories: Storey 2

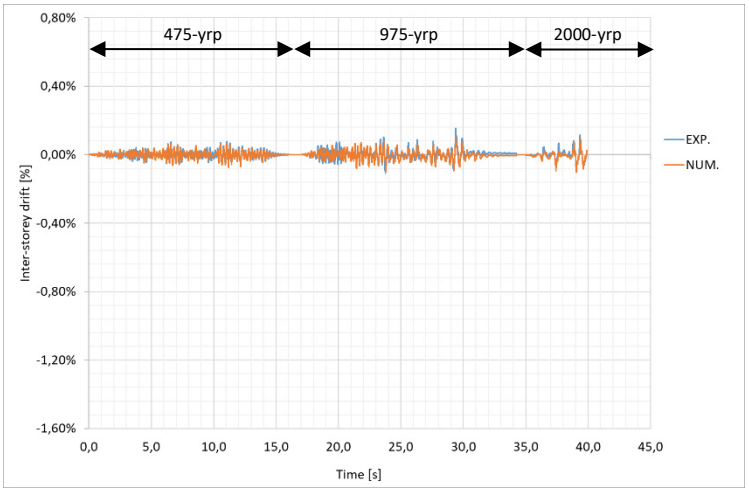

Figure 3.44 – IN inter-storey drifts time-histories: Storey 3

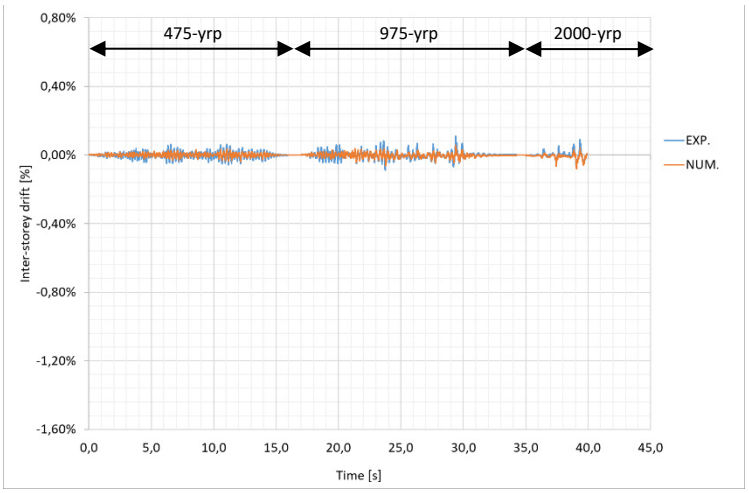

Figure 3.45 – IN inter-storey drifts time-histories: Storey 4

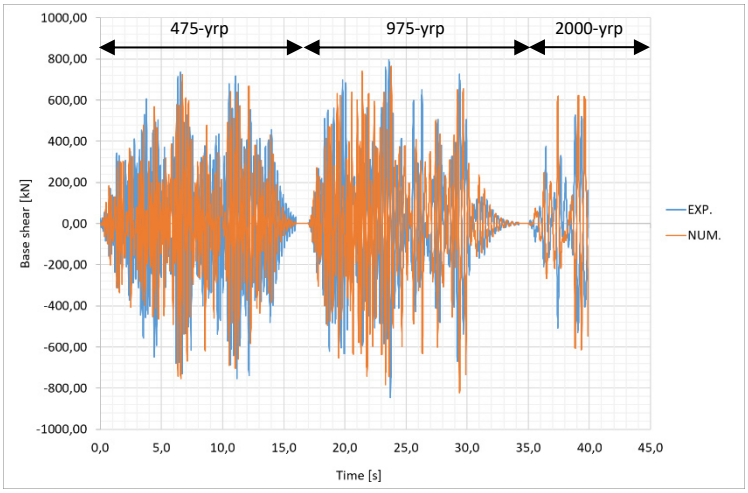

Figure 3.46 – IN base shear time-histories

3.3.2.3. Discussion

The results presented above indicate that the developed numerical models are robust enough to realistically simulate the structural behaviour of the BF and the IN, both in the linear as in the nonlinear ranges. However, the modelling options presented in sub-section 3.3.1. only show the final result of a large number of iterations testing different parameters and comparing the obtained numerical results to the experimental data. Several partial models had to be developed (e.g., single column; single infilled span / storey) and tested under nonlinear static conditions to better understand the effect of some of those parameters on the structural response (this procedure was particularly important to fine-tune the infill panels' modelling). Performing slight setup variations on the global models and testing them under nonlinear dynamic conditions was the last stage of this iterative process, leading to the final setup of parameters referred above and the consequent good agreement between numerical and experimental results.

The results comparison in terms of natural frequencies allowed for the validation of the models in the linear range. The dominance of the first vibration mode was evident, with effective modal mass percentages of 83% and 89%, respectively for the BF and IN. As experimental results were also available for the modal frequencies of the BF after the PsD tests (see Table 3.7 above), additional calculations were carried out to determine the percentage of the uncracked stiffness of RC elements that produced agreeing numerical results. Those shown in Table 3.18 were obtained considering a percentage of 56%, which compares well with the default value of 50% referred in clause 4.3.1 (7) of EC8-1 (2004). Concerning the uncracked stiffness of the IN model, an interesting conclusion was already referred in sub-section 3.3.2.1. as it seemed not to be affected by the presence of openings, i.e., the best agreement with the experimentally determined frequencies was obtained by considering the uncracked stiffness of the fully infilled panels. Given the relative size of some of the openings to that of the panels, and the considerably high stiffness reduction factors that had to be considered for those panels in order to achieve a good approximation between the experimental and numerical seismic responses of the IN, this conclusion was somehow unexpected. However, and even though it

makes sense to the author that the effect of an opening on the initial stiffness of an infill panel might be much smaller than on its cracked stiffness, this matter was pursued no further as it is beyond the scope of this work. Hence, as stated before, for the time being this conclusion should be stretched no further than the limits of the presented case-study.

Table 3.18 – Modal frequencies of the BF after the PsD tests: results comparison EXP. vs. NUM.

	f_1 (BF)	f_2 (BF)	f_3 (BF)	f_4 (BF)
EXP. (*Hz*)	1.19	3.65	5.63	9.06
NUM. (*Hz*) (*)	1.19	3.49	5.80	8.21

(*) Stiffness of RC members = 56% × uncracked stiffness

The BF sustained extensive damage and reached an imminent collapse state during the 975-yrp earthquake test. The significant change in stiffness and strength from the second to the third storey, coupled with the inadequate rebar lap-splice, induced the development of a soft-storey mechanism at the third storey level. As stated before, a good agreement between experimental and numerical results for this earthquake demand was only achieved after the inclusion of the bond-slip effect within the modelling options (this was also required for the IN when testing with the 2000-yrp earthquake, as referred above). Despite the inarguable assets of fibre modelling, the fact that it assumes a perfect bond between reinforcing steel and concrete poses a limitation that cannot be accepted without action when modelling the response of older-type RC structures. Therefore, the enhancement of such models as to include the bond-slip effect through any of the approaches described in sub-section 2.5.1. (or others) should be taken as mandatory if one wants to obtain a realistic description of the cyclic and ultimate behaviour of such RC structures.

The numerical analysis of the IN confirmed that the infill panels protect the RC frame for low and medium intensity input motions but may prompt a soft-storey mechanism in case of their sudden failure and consequent abrupt loss of resistance. However, it should be noted that the IN was able to withstand part of the 2000-yrp earthquake, while the BF reached imminent collapse before the end of the 975-yrp earthquake. This further confirms that infill walls significantly alter the behaviour of RC framed structures and, therefore, should be considered in the assessment and retrofitting of existing structures. The nonlinear cyclic model developed by Crisafulli (1997) provided a satisfactory approach for the modelling of the infill walls, without significant increase in the complexity of the analysis despite the large number of model-calibrating parameters. However, the developed partial models referred above allowed to detect a flaw on its implementation in software platform *SeismoStruct*: within the shear curve programming, in the negative direction of the shear link, the algebraic value of the acting shear force was being checked against the absolute value of the corresponding strength, hence inevitably never reaching it. This induced an unexpected behaviour of the shear link's hysteretic curve and, consequently, of the structure's pushover curve. After careful consideration and developing a comparative model in software platform *OpenSees,* this matter was reported to Prof. Rui Pinho (Seismosoft's Technical Director) and thoroughly discussed. The necessary code correction was then included in a *SeismoStruct 2020* update, released on July 8th.

The final result of the numerical modelling exercise carried out herein and described above was quite satisfactory in terms of the achieved approximation to the experimental results. However, the significant differences found between the results provided by each iteration adjusting parameter setups (specially for the IN model) should be duly noted, because the privilege of knowing what to expect (i.e., having experimental results to compare numerical results with) rarely exists. Data on the real characteristics of buildings that have been subjected to earthquakes is generally difficult to obtain and experimental test campaigns as the one described herein are very expensive. Therefore, when available, experimental results should be extensively used to calibrate the vast number of model parameters and rules required to fully define nonlinear elements. Otherwise, the use of these refined models in the seismic assessment of existing RC structures will invariably lead to unrealistic (and potentially unsafe) results.

3.4. SEISMIC ASSESSMENT PROCEDURE

The seismic assessment of the bare and infilled frames was performed according to the deterministic procedure described in EC8-3 (2005). The performance requirements were defined according to the applicable limit states (LS's). Concerning the treatment of uncertainty, given the available results for the concrete and steel specimen tests, full knowledge conditions corresponding to Knowledge Level 3 (KL3) were assumed to be defined by the materials' mean properties. Nonlinear static and dynamic analyses were carried out to obtain demand values on the designated control sections of the frames' structural members. Member capacities were defined according to the capacity models included in Annex A of EC8-3 (2005) and safety checks were run for both deformation- and strength-controlled mechanisms. This section presents and discusses the obtained results as well as the influence of the infill walls on the overall conclusions of the seismic assessment process.

3.4.1. Seismic demand definition

The base seismic demand for the assessment process was set for zone 1.3 of the Portuguese territory, considering that the frames were located on type B ground, as to be coherent with the moderate-high European seismic hazard scenario that the input seismic motions used in the before described PsD tests were representative of. According to Table NA.I of the Portuguese National Annex (NA) on EC8-1 (2004), the value of the reference peak ground acceleration (PGA) on type A ground a_{gR} and for zone 1.3 is equal to $0.15 \cdot g$. Considering the referred ground type (calculated soil factor $S = 1.29$) and allocating the frames to structural importance class II (importance factor $\gamma_I = 1.00$, associated to a 475-yrp), the design ground acceleration $a_g \cdot S$ results equal to $0.20 \cdot g$. Figure 3.47 shows the comparison between the obtained code-based response acceleration spectrum and the elastic response acceleration spectrum of the 475-yrp PsD test input motion (PGA = $0.22 \cdot g$), both derived considering a viscous damping ratio ξ_0 of 5%. The compatibility between the two was judged to be acceptable enough for the purpose at hand.

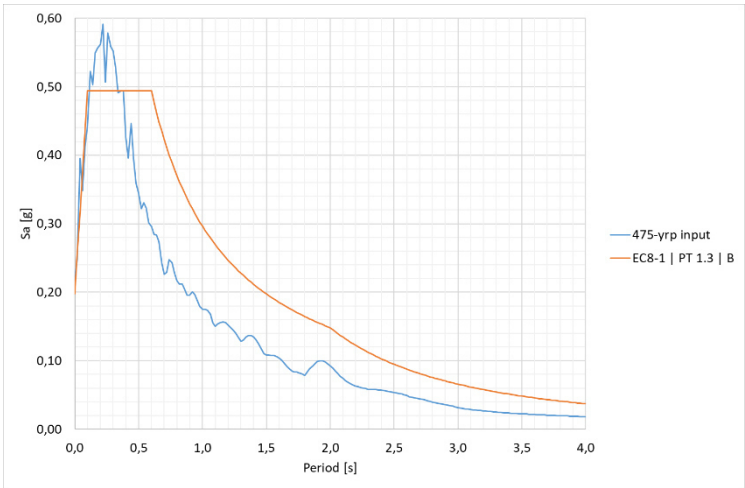

Figure 3.47 – Comparison between the EC8-1 (2004) response acceleration spectrum (zone 1.3 of the Portuguese territory; type B ground; structural importance class II; ξ_0 = 5%) and the elastic response acceleration spectrum of the 475-yrp experimental test input motion (ξ_0 = 5%)

According to the draft version of the Portuguese NA on EC8-3 (2005), different return periods of the seismic demand (i.e., other than a 475-yrp) should be considered during the seismic assessment process, depending on the LS's to be verified. The values of 975, 308 and 73 years are defined for the LS's of Near Collapse (NC), Significant Damage (SD) and Damage Limitation (DL), respectively, as referred in Chapter 2. The reference PGA's on type A ground a_{gR} to be adopted for each LS were thus obtained multiplying the value of a_{gR} associated with the 475-yrp by the coefficients indicated for a type 1 spectrum in Table NA.I of the Portuguese NA on EC8-3 (2005) (also shown in Table 2.9). The assessment ground accelerations on type B ground $a_{gR} \cdot S$ for each LS were then obtained considering the respective soil factor. Table 3.19 shows the obtained values while Figure 3.48 depicts the associated code-based response acceleration spectra. Because the frames were allocated to structural importance class II, only the LS of SD would have to be verified. However, for the purposes of this case-study, the three LS's were considered. Hence, three sets (one per LS) of target displacements were determined to define the performance points for the nonlinear static analysis models, while seven real accelerograms were selected from a database and scaled as to define three different sets of signals, each set being compatible with the demand spectrum of the respective LS. The following sub-sections describe the undergone procedures to obtain these input elements, according to the different methodologies and guidelines presented in Chapter 2.

Table 3.19 – Calculation of the assessment ground accelerations on type B ground for the LS's defined in EC8-3 (2005), based on a 475-yrp reference PGA on type A ground $a_{gR} = 0.15 \cdot g$

Limit state	YRP coefficient	a_{gR}	S	$a_{gR} \cdot S$
NC	1.62	0.25·g	1.18	0.29·g
SD	0.75	0.11·g	1.34	0.15·g
DL	0.29	0.04·g	1.35	0.06·g

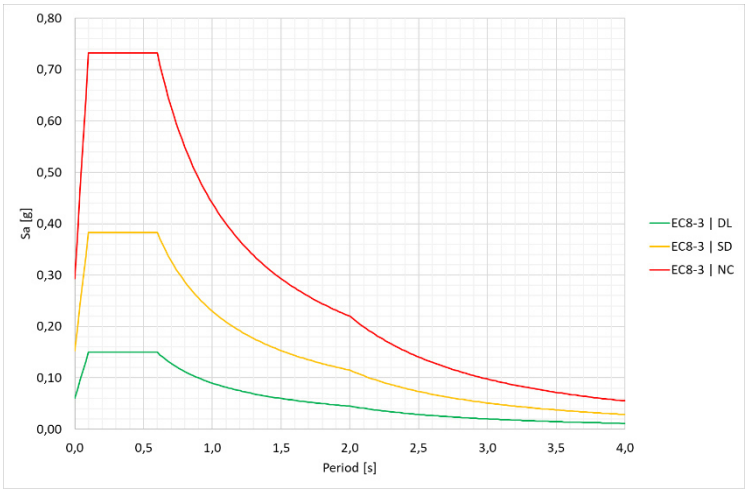

Figure 3.48 – Response acceleration spectra for seismic assessment, according to EC8-3 (2005)

3.4.1.1. Target displacements for nonlinear static analysis

The nonlinear static procedure (NSP) used herein to determine the necessary target displacements is the one currently recommended by EC8-3 (2005), i.e., the "N2 method" presented in Chapter 2 (Fajfar and Fischinger, 1988). As such, the first step was to obtain the capacity curves of both frames, using the two lateral load patterns required by EC8-1 (2004). Table 3.20 shows the calculated initial values of the lateral force vectors. Because the frames are not symmetric about any axis at right angles to the direction of the seismic action, the analysis had to be carried out for both senses of the latter (left-to-right and right-to-left). Afterwards, four target displacement values per LS were determined for each frame. Tables 3.21 and 3.22 show the obtained values, while figures 3.49 and 3.50 plot the performance points (PP's) on the correspondent capacity curves. According to EC8-1 (2004), the chosen target displacement should be the higher value obtained from the pushover curves computed with the considered load patterns. Accordingly, the values obtained with the first mode proportional load pattern were chosen as PP's for the seismic assessment of the frames.

Table 3.20 – Initial values of the lateral load vectors used to obtain the pushover curves of the frames

	Load values F_i *(kN)*				
Load pattern	**1st floor**	**2nd floor**	**3rd floor**	**4th floor**	**Σ F_i *(kN)***
Modal (BF)	0.094	0.222	0.345	0.339	1
Modal (IN)	0.129	0.242	0.326	0.303	1
Uniform	0.260	0.260	0.260	0.220	1

Table 3.21 – Target displacement values d_t for the BF (L-R: left-to-right; R-L: right-to-left)

	d_t *(mm)*			
Limit state	**Modal L-R**	**Modal R-L**	**Uniform L-R**	**Uniform R-L**
NC	157.1	-151.4	139.2	-135.4
SD	82.0	-79.1	72.7	-70.7
DL	32.1	-30.9	28.4	-27.6

Table 3.22 – Target displacement values d_t for the IN (L-R: left-to-right; R-L: right-to-left)

	d_t (mm)			
Limit state	**Modal L-R**	**Modal R-L**	**Uniform L-R**	**Uniform R-L**
NC	16.7	-16.4	15.1	-14.5
SD	7.0	-6.6	6.1	-5.8
DL	2.7	-2.6	2.4	-2.3

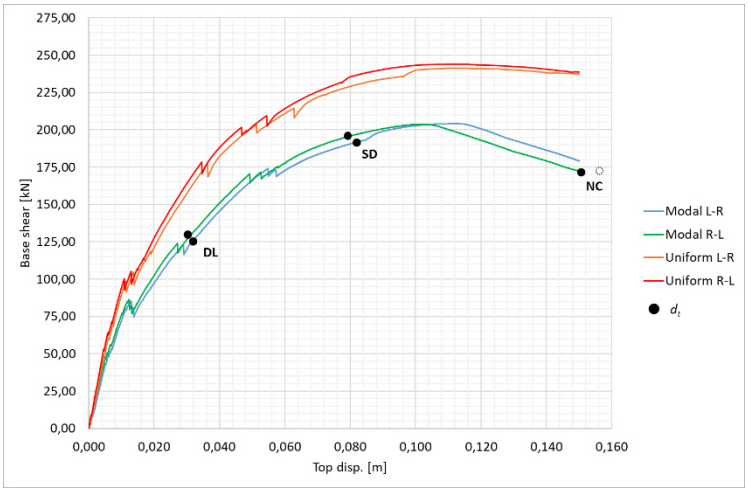

Figure 3.49 – Capacity curves and PP's of the BF: modal and uniform load patterns (L-R: left-to-right; R-L: right-to-left)

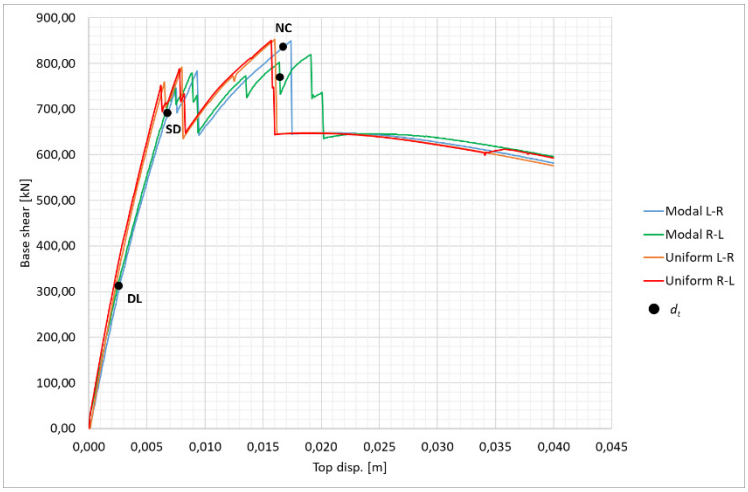

Figure 3.50 – Capacity curves and PP's of the IN: modal and uniform load patterns (L-R: left-to-right; R-L: right-to-left)

The obtained results are coherent with the behaviour of the frames during the experimental tests (see sub-sections 3.2.6.2. and 3.2.6.3.). Given the compatibility between the code-based response acceleration spectra for seismic assessment and the elastic response acceleration spectra for the 475- and 975-yrp experimental test input motions (see comparison below in Figure 3.51), as well as the dominance of the first vibration mode, such agreement was expected and further encouraged the use of pushover analysis to evaluate the performance of the frames.

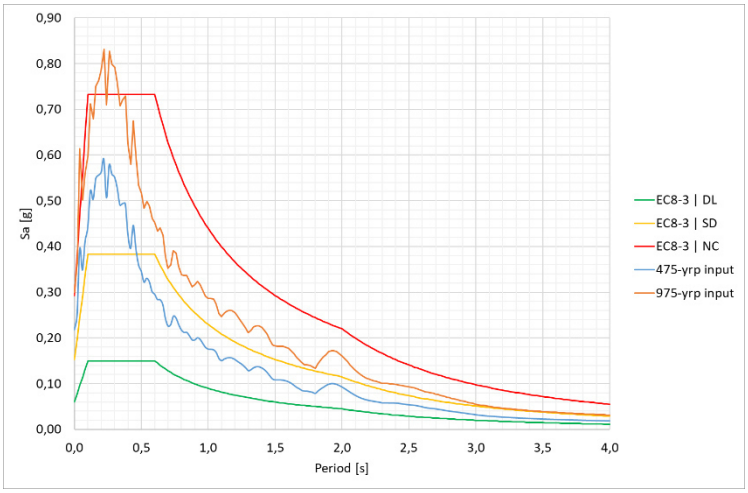

Figure 3.51 – Comparison between the EC8-3 (2005) response acceleration spectra for seismic assessment and the elastic response acceleration spectra of the 475- and 975-yrp experimental test input motions

3.4.1.2. Accelerograms for nonlinear dynamic analysis

The selected ground motion records were obtained from real earthquake events and scaled to meet the spectral matching requirements defined in EC8-3 (2005). The recent recommendations by Araújo *et al* (2016) for the selection and scaling of records were also applied, as well as the SelEQ tool (Macedo and Castro, 2017). Figure 3.52 illustrates the obtained result, showing the individual and average spectra of the seven selected records together with the EC8-1 (2004) target spectrum corresponding to the 475-yrp.

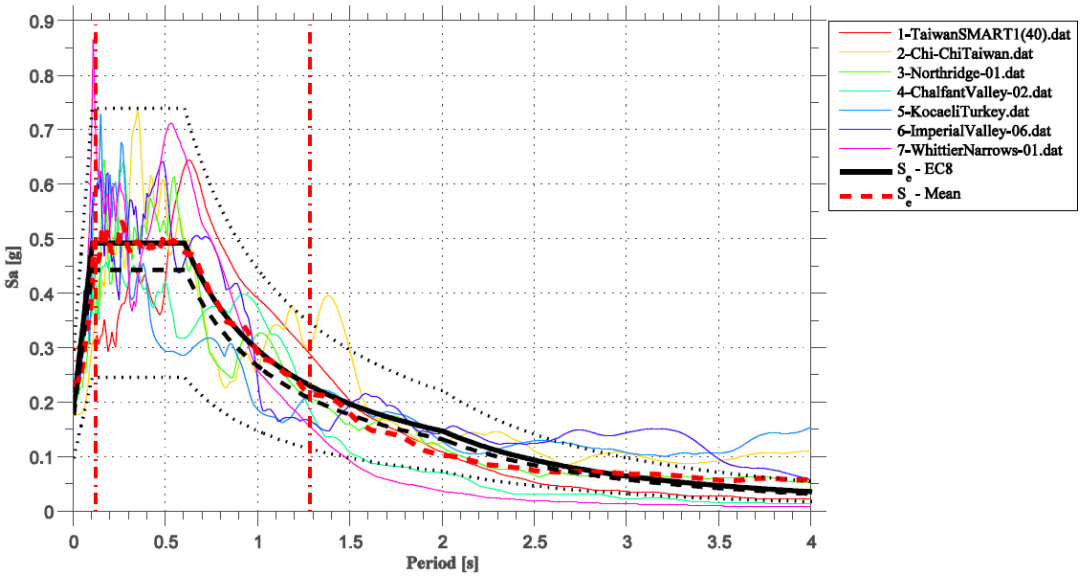

Figure 3.52 – Comparison between the spectra (individual and mean) of the selected records and the EC8-1 (2004) target response acceleration spectrum (zone 1.3 of the Portuguese territory; type B ground; 475-yrp; ξ_0 = 5%)

SelEQ is a software application developed at FEUP that features a wide variety of filtering criteria and incorporates several meta-heuristic algorithms, allowing for the selection of seismic records or groups of seismic records that are compatible with any type of target response spectrum, either obtained from a design code or derived from a probabilistic seismic hazard assessment. Based on the seismological characteristics of the events that define zone 1.3 of the Portuguese territory, magnitudes and epicentral distances higher than 5.5 and 20 *km,* respectively, were considered for the preliminary search. Additionally, an interval of values of the average shear wave velocity $v_{s,30}$ between 360 *m/s* and 800 *m/s* was adopted in agreement with type B ground, as defined in EC8-1 (2004). Moreover, with the aim of reducing the record-to-record variability of the group, an additional criterion was considered which consisted of imposing spectral mismatch limits of ± 50% for each individual record regarding the target spectrum. This process led to the selection of the seven records mentioned above in Figure 3.52 and to the scaling factors shown in the 475-yrp column of Table 3.23. The scaling factors to then match the spectra of the LS's of DL, SD and NC were obtained multiplying the values in the 475-yrp column by factors of 0.30310, 0.77540 and 1.48392, respectively, which are the ratios between the constant acceleration value of each LS spectrum and that of the 475-yrp spectrum. Figures 3.53 to 3.55 show the individual and average spectra of the scaled records set together with its corresponding EC8-3 (2005) target spectrum.

Table 3.23 – Selected records and scaling factors for compatibility with the EC8-3 (2005) LS's

			Scaling factor			
Record	**Time step *(s)***	**N. Steps**	**475-yrp**	**DL**	**SD**	**NC**
R1-TaiwanSMART1(40).dat	0.010	2913	1,17310	0,35556	0,90963	1,74079
R2-Chi-ChiTaiwan.dat	0.005	18000	1,11645	0,33839	0,86570	1,65672
R3-Northridge-01.dat	0.010	2999	1,58148	0,47934	1,22628	2,34679
R4-ChalfantValley-02.dat	0.005	7996	1,21379	0,36790	0,94118	1,80117
R5-KocaeliTurkey.dat	0.005	6000	1,67085	0,50643	1,29558	2,47941
R6-ImperialValley-06.dat	0.010	9992	0,91789	0,27821	0,71173	1,36208
R7-WhittierNarrows-01.dat	0.020	1715	1,26163	0,38240	0,97827	1,87216

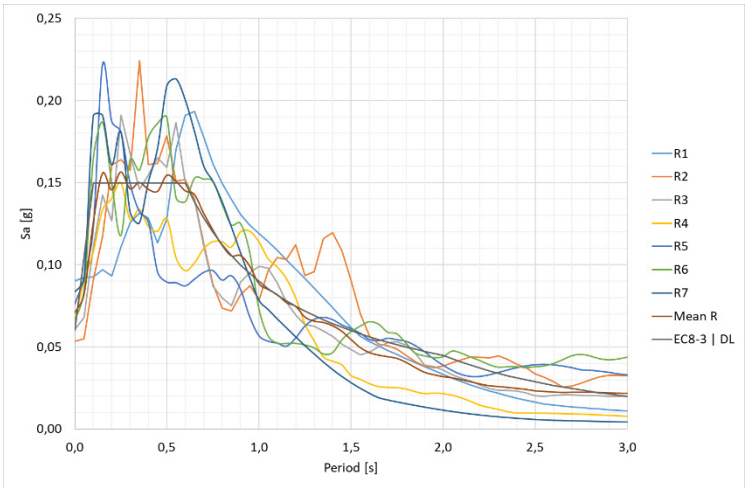

Figure 3.53 – Scaling of the obtained records set for the EC8-3 (2005) LS of DL

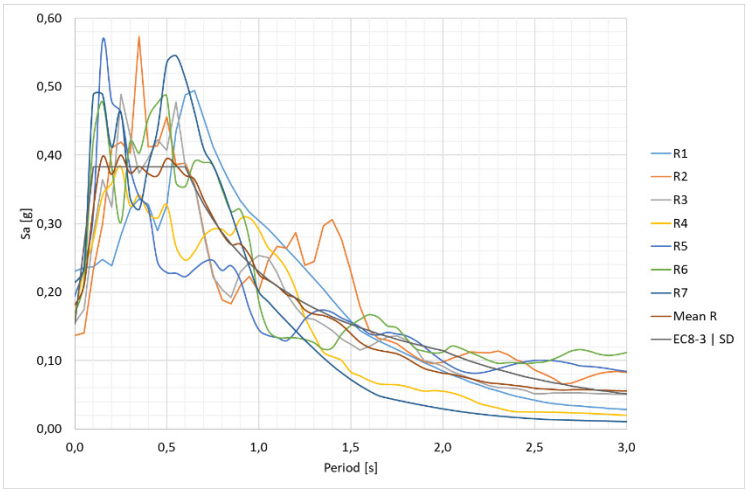

Figure 3.54 – Scaling of the obtained records set for the EC8-3 (2005) LS of SD

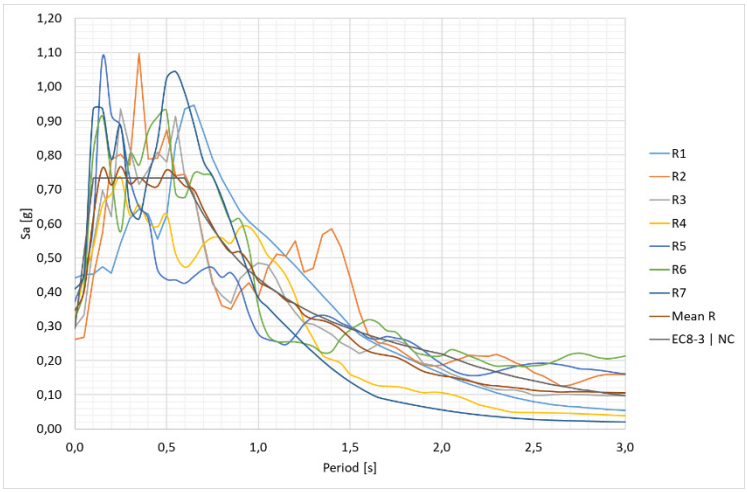

Figure 3.55 – Scaling of the obtained records set for the EC8-3 (2005) LS of NC

3.4.2. Member capacities computation

The capacity models included in Annex A of EC8-3 (2005) were used herein to define the capacity values of the RC structural members. As the nonlinear behaviour is expected to develop at member ends, two control sections (*top* and *bottom* in columns; *left* and *right* in beams) were considered within each member, adding up to 56 control sections. Figure 3.56 shows the numbering of the frame's members that is used henceforth. Capacities were computed for both deformation- and strength-controlled mechanisms (respectively, ductile and brittle), for each considered LS, and the recommendations of several authors (discussed in Chapter 2) were followed as to make the computational process less intensive and time-consuming. A Confidence Factor (CF) equal to 1.00 was considered in all calculations, consistent with the assumed KL3 conditions. The following sub-sections describe the details involved in the computation of the capacities of each of the above referred collapse mechanisms.

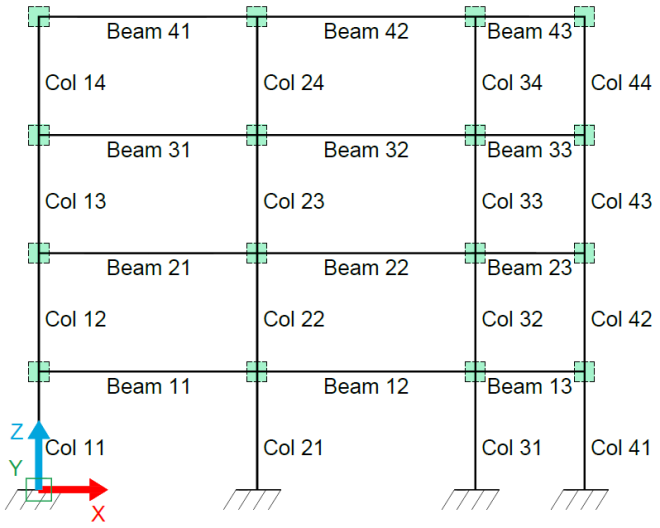

Figure 3.56 – Numbering of the frames' RC structural members

3.4.2.1. Ductile capacities

Member ductile capacities are defined in terms of their admissible chord rotations θ for each LS, respectively θ_{NC}, θ_{SD} and θ_{DL}. For the quantification of θ_{NC}, Expression (2.13) was applied with the approximations proposed by Mpampatsikos *et al* (2008) – see Chapter 2. The corrective factors allowing for rebar lap-splices and/or the use of plain rebars were applied when needed (see clauses A.3.2.2 (3) to (5) in Annex A of EC8-3 (2005)). The values of θ_{SD} were then assumed to be 75% of θ_{NC}, according to clause A.3.2.3 (1) in the same reference. As for the quantification of θ_{DL} $(= \theta_y)$, Expression (2.16a) was applied with the same above-referred approximations. The input values of the yield curvature ϕ_y were estimated with Expression (2.20). In parallel, values of θ_{DL} were also computed by subtracting the results of Expression (2.15) from those of Expression (2.13) (i.e., $\theta_y = \theta_{NC} - {\theta_{NC}}^{pl}$; see Expression (2.15a)), thus eliminating the need for the ϕ_y estimates. The results from both approaches were then compared with the typical value of 0.8% (with an upper limit of 1.0%) referred by Biskinis (2006), the best agreement being found with Expression (2.15a). Lastly, due to the asymmetry of the longitudinal reinforcement on the beams, the θ values were computed for both bending moment signs. Tables 3.24 and 3.25 summarize the obtained results.

Table 3.24 – Chord rotation capacities θ of beams for the EC8-3 (2005) LS's

	θ_{NC} *(mrad)*		θ_{SD} *(mrad)*		θ_{DL} *(mrad)*	
Sections (*)	**Pos. bending**	**Neg. bending**	**Pos. bending**	**Neg. bending**	**Pos. bending**	**Neg. bending**
B11 left	36.27	22.90	27.20	17.17	10.44	8.91
B11 right	42.85	19.98	32.13	14.99	10.75	8.38
B12 left	42.85	19.98	32.13	14.99	10.75	8.38
B12 right	36.82	23.25	27.62	17.44	10.60	9.05
B13 left	28.25	17.83	21.19	13.38	8.13	6.94
B13 right	24.59	20.49	18.44	15.37	7.87	7.38

(*) Capacities are the same for beam sections on the 2nd, 3rd and 4th floors

Table 3.25 – Chord rotation capacities θ of columns for the EC8-3 (2005) LS's

Sections	θ_{NC} (*mrad*)	θ_{SD} (*mrad*)	θ_{DL} (*mrad*)
C11 bot (*)	16.18	12.13	7.51
C11 top	21.11	15.84	7.86
C12 bot	23.20	17.40	8.42
C12 top	23.20	17.40	8.42
C13 bot (*)	17.12	12.84	7.70
C13 top	22.34	16.76	7.93
C14 bot	25.44	19.08	8.70
C14 top	25.44	19.08	8.70
C21 bot (*)	10.61	7.96	4.96
C21 top	13.85	10.39	5.20
C22 bot	15.33	11.50	5.61
C22 top	15.33	11.50	5.61
C23 bot (*)	11.57	8.68	5.28
C23 top	15.10	11.33	5.48
C24 bot	17.87	13.41	6.19
C24 top	17.87	13.41	6.19
C31 bot (*)	13.61	10.21	6.51
C31 top	17.77	13.33	6.90
C32 bot	20.48	15.36	7.68
C32 top	20.48	15.36	7.68
C33 bot (*)	15.33	11.50	7.03
C33 top	20.01	5.01	7.32
C34 bot	24.14	18.11	8.39
C34 top	24.14	18.11	8.39
C41 bot (*)	17.27	12.95	7.93
C41 top	22.54	16.91	8.26
C42 bot	24.35	18.26	8.74
C42 top	24.35	18.26	8.74
C43 bot (*)	17.94	13.45	8.01
C43 top	23.41	17.56	8.22
C44 bot	26.19	19.64	8.91
C44 top	26.19	19.64	8.91

(*) Sections with reinforcement lap-splice

3.4.2.2. Brittle capacities

Member brittle capacities are characterized by the admissible NC shear force V_{NC}, quantified according to expressions (2.22) to (2.24) and subjected to the upper limits imposed by the shear capacity values obtained with the provisions of EC2-1-1 (2004). The recommendations of Mpampatsikos *et al* (2008) and Romão *et al* (2010a) were also followed herein to simplify the computational process, making it less time-consuming. Concerning the evaluation of the sole input parameter $\mu_{\Delta}^{pl} = \left(\theta_{dem} - \theta_y\right)/\theta_y$ ($0 \leq \mu_{\Delta}^{pl} \leq 5$) that remains demand-dependent in spite of the referred approximations (as discussed in Chapter 2), a conservative approach was adopted by making θ_{dem} equal to the chord rotation capacities θ_{NC}, thus eliminating the referred dependency. It should be recalled that, according to clause A.3.3.2 (1) in Annex A of EC8-3 (2005), the verification against the exceedance of the LS's of SD and DL is not required, unless those two are the only LS's to be checked. In the latter case, the respective shear capacity values should also be taken equal to V_{NC}. Tables 3.26 and 3.27 summarize the obtained results. In this case, the differences between the values shown for the positive and negative bending of beams differ not due to the asymmetry of the longitudinal reinforcement but due to different input parameters μ_{Δ}^{pl}.

Table 3.26 – Shear capacities V_{NC} of beams according to EC8-3 (2005)

	V_{NC} (*kN*)	
Sections (*)	**Pos. bending**	**Neg. bending**
B11 left	70.36	73.98
B11 right	103.54	113.22
B12 left	103.54	113.22
B12 right	102.31	107.58
B13 left	67.32	70.74
B13 right	63.47	64.71

(*) Capacities are the same for beam sections on the 2nd, 3rd and 4th floors

Table 3.27 – Shear capacities V_{NC} of columns according to EC8-3 (2005)

Sections	V_{NC} (*kN*)	**Sections**	V_{NC} (*kN*)
C11 bot (*)	30.10	C31 bot (*)	31.66
C11 top	29.65	C31 top	31.22
C12 bot	25.86	C32 bot	31.13
C12 top	25.86	C32 top	31.13
C13 bot (*)	21.93	C33 bot (*)	25.15
C13 top	21.45	C33 top	24.70
C14 bot	17.63	C34 bot	19.17
C14 top	17.63	C34 top	19.17
C21 bot (*)	142.18	C41 bot (*)	24.80
C21 top	142.18	C41 top	24.34
C22 bot	142.18	C42 bot	22.00
C22 top	142.18	C42 top	22.00
C23 bot (*)	88.07	C43 bot (*)	19.44
C23 top	86.48	C43 top	18.95
C24 bot	67.15	C44 bot	16.45
C24 top	67.15	C44 top	16.45

(*) Sections with reinforcement lap-splice

3.4.3. Performance evaluation

The performance evaluation results obtained with two different methods of analysis are presented in the following sub-sections. Results are expressed in terms of demand-to-capacity ratios (D_i/C_i), for each control section i, where a value below or equal to 1.0 represents a safe situation (and an unsafe situation otherwise). The D/C ratios are presented graphically, both for deformation- and strength-controlled mechanisms, to provide a better view of the global scenarios. A discussion of the obtained results concludes the seismic assessment of the bare and infilled frames.

3.4.3.1. Nonlinear static analysis results

The demand values on the control sections of each structural member were obtained from the outputs provided by the numerical models at the target displacements corresponding to each LS, lateral load pattern and seismic action sense. While shear force demands were taken directly, chord rotation demands were computed externally (using the AGM-DR method discussed in Chapter 2), in spite of the latter being internally computed by *SeismoStruct*). Nonetheless, the comparison between both sets of results found a maximum differential of 0.18%, hence demonstrating *SeismoStruct's* internal algorithm for the computation of chord rotation demands to be trustworthy. The D/C ratios presented

below correspond to the most unfavourable results among those obtained with the demand values on each control section. Figures 3.57 and 3.58 refer, respectively, to chord rotations and shear forces on the columns of the BF, while figures 3.59 and 3.60 show the same for the IN. Concerning the beams, the D/C ratios were found to be consistently below 1.0 (typical of older-type structures with no capacity design). Hence, the correspondent graphical representation is deliberately omitted herein to save space. However, it is noteworthy that the computation of the D/C ratios for beams was more laborious than for columns, due to the dependency of the capacities of the former on the signs of the bending moment demands, and the lack of correspondence of the latter with the signs of the chord rotation demands (this lack of sign correspondence might not seem obvious if one thinks only of the effects of the lateral loading but is simply explained by the fact that gravity loads act simultaneously on beam elements).

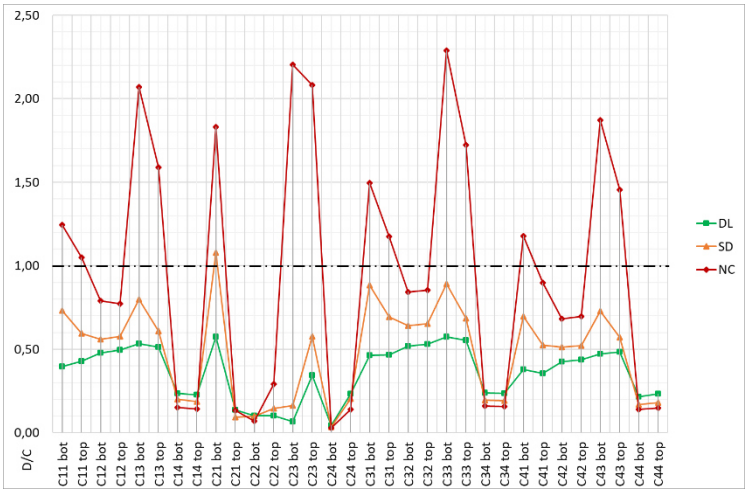

Figure 3.57 – BF: chord rotation D/C ratios on columns (pushover analysis results)

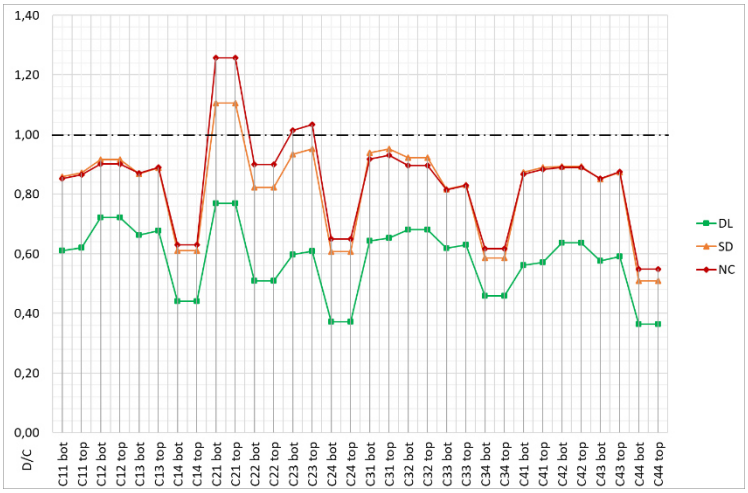

Figure 3.58 – BF: shear force D/C ratios on columns (pushover analysis results)

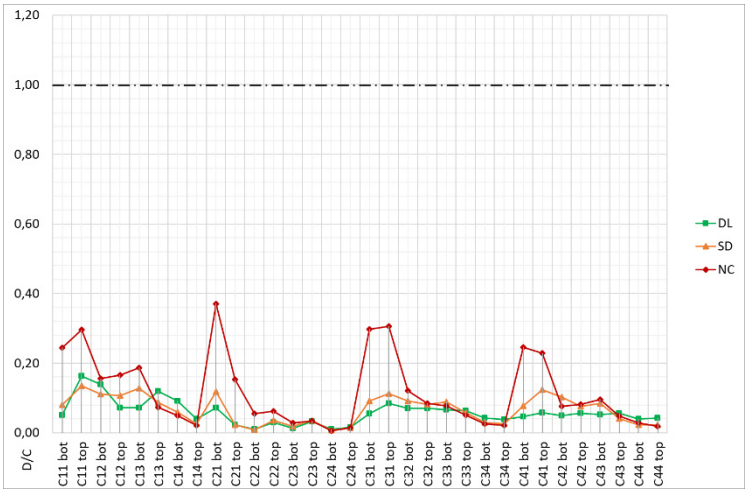

Figure 3.59 – IN: chord rotation D/C ratios on columns (pushover analysis results)

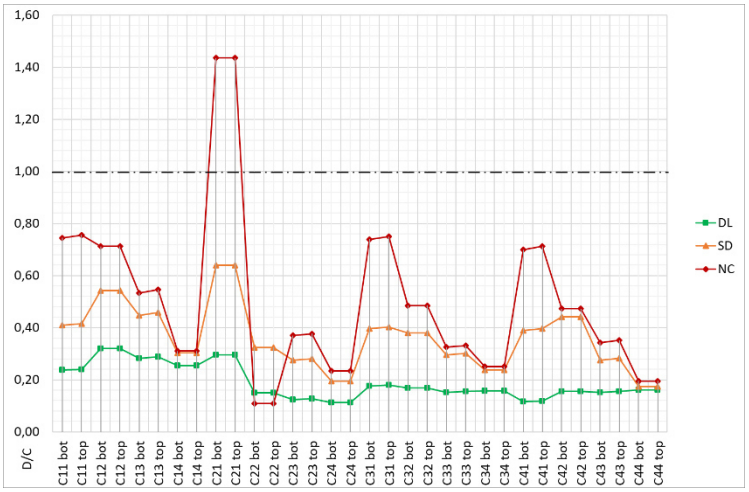

Figure 3.60 – IN: shear force D/C ratios on columns (pushover analysis results)

3.4.3.2. Nonlinear dynamic analysis results

As previously referred, the global seismic demand for the nonlinear dynamic analysis cases was characterized by three sets of seven scaled ground acceleration records, each set being compatible with the demand spectrum of the respective LS. For the computation of the D/C ratios presented below, the demand values on the control sections of each structural member were the mean values over the most unfavourable results obtained within each set of individual records, as required by clause 4.3.3.4.3 (3) of EC8-1 (2004). The capacity values were the same used above in the nonlinear static analysis cases. Figures 3.61 and 3.62 show, respectively, the chord rotation and shear force D/C ratios on the columns of the BF, while figures 3.63 and 3.64 show the same ratios on the columns of the IN. As for the D/C ratios on beams, these were found to be below 1.0 at all times (as expected due to the nonlinear static analyses results), therefore the correspondent graphical representation was again omitted.

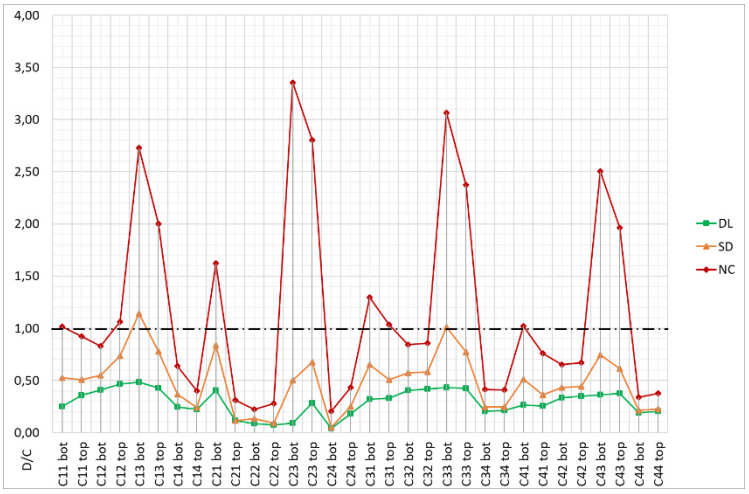

Figure 3.61 – BF: chord rotation D/C ratios on columns (nonlinear dynamic analysis results)

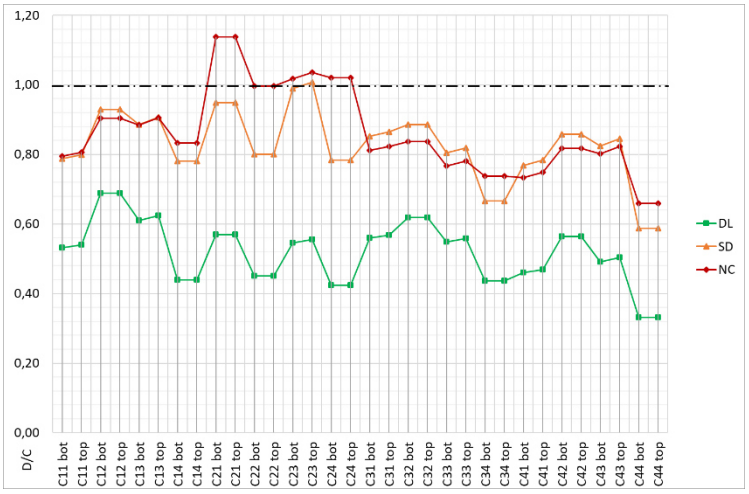

Figure 3.62 – BF: shear force D/C ratios on columns (nonlinear dynamic analysis results)

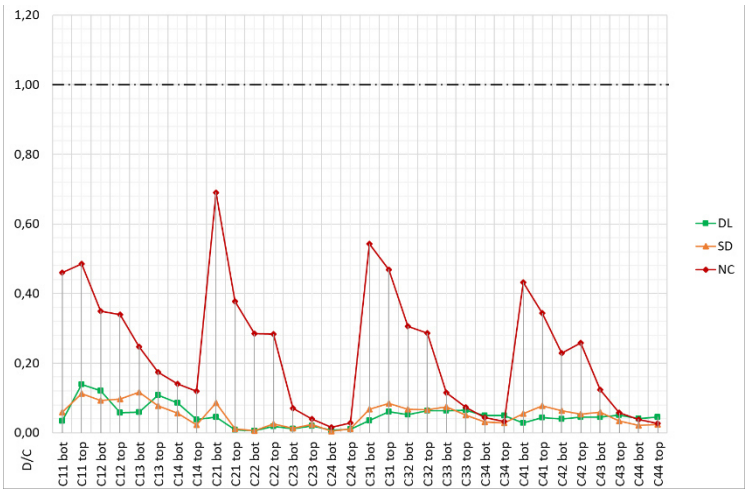

Figure 3.63 – IN: chord rotation D/C ratios on columns (nonlinear dynamic analysis results)

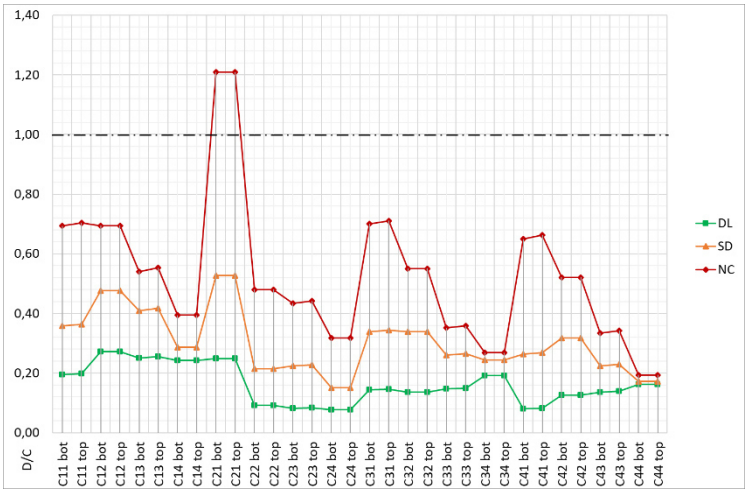

Figure 3.64 – IN: shear force D/C ratios on columns (nonlinear dynamic analysis results)

3.4.3.3. Discussion

Before discussing the results of the seismic assessment process and consequently drawing conclusions about the safety of the frames, it is important to compare the outcomes of the nonlinear static and dynamic analyses. Figures 3.57 to 3.64 (above) allow for the comparison in terms of D/C ratios, while tables 3.28 to 3.30 (below) compare global storey parameters. Given the added complexity of nonlinear dynamic analysis when compared to its static equivalent, the purpose is to verify if similar conclusions are obtained and (eventually) validate the use of pushover analysis as a swift way to evaluate the seismic performance of the frames.

In terms of D/C ratios, similar results were obtained with the two approaches, leading essentially to the same assessment conclusions (i.e., the same control sections were deemed unsafe). For the LS's of DL and SD, pushover analysis results were found to be generally conservative. On the other hand, the NC chord rotation ratios obtained with nonlinear dynamic analysis were found to be higher than those given by pushover analysis, on several control sections. A closer look revealed that this was relevant for the columns located at the storeys which are prone to form soft-storey mechanisms (i.e., the third storey in the case of the BF, and the first storey in the case of the IN). Concerning the NC shear force ratios, no relevant differences were found. The results in terms of global storey parameters also compared well, but some differences are worth referring. Higher parameter values were obtained with pushover analysis for the LS's of DL and SD, for both frames. However, for the LS of NC, the highest floor displacements and inter-storey drifts were given by nonlinear dynamic analysis. Nonetheless, the formation of the above-referred soft-storey mechanisms was well captured by both analysis methods (see inter-storey drift values), which constitutes an important validation of the nonlinear static approach. Concerning the NC base shear values, again no relevant differences were found between the results provided by the two analysis methods. Based on these findings and even though the irregular response of the frames when pushed to a state of near collapse is better captured by the nonlinear dynamic method of analysis, the nonlinear static approach is deemed accurate enough for the purpose of evaluating the seismic performance of the BF and the IN.

Table 3.28 – Floor displacements: nonlinear static (PSHVR) vs. dynamic (NLDA) analyses results

	Floor displacement (*mm*)					
	DL		SD		NC	
BF	PSHVR	NLDA	PSHVR	NLDA	PSHVR	NLDA
Floor 4	32.1	23.6	82.0	71.8	157.1	165.4
Floor 3	27.3	20.3	73.2	62.4	148.2	151.9
Floor 2	17.0	13.2	46.0	38.0	56.7	78.1
Floor 1	6.8	5.3	20.2	16.2	26.4	40.4
	DL		SD		NC	
IN	PSHVR	NLDA	PSHVR	NLDA	PSHVR	NLDA
Floor 4	2.7	1.7	7.0	4.7	16.7	34.4
Floor 3	2.4	1.5	6.3	4.2	15.9	33.2
Floor 2	1.8	1.2	4.7	3.2	13.9	31.5
Floor 1	0.9	0.6	2.5	1.8	10.6	19.2

Table 3.29 – Inter-storey drifts: nonlinear static (PSHVR) vs. dynamic (NLDA) analyses results

	Inter-storey drift (%)					
	DL		SD		NC	
BF	PSHVR	NLDA	PSHVR	NLDA	PSHVR	NLDA
Storey 4	0.18%	0.14%	0.32%	0.41%	0.33%	0.79%
Storey 3	0.38%	0.28%	1.01%	0.94%	3.10%	3.44%
Storey 2	0.38%	0.29%	0.96%	0.81%	1.14%	1.49%
Storey 1	0.25%	0.20%	0.75%	0.60%	0.99%	1.50%
	DL		SD		NC	
IN	PSHVR	NLDA	PSHVR	NLDA	PSHVR	NLDA
Storey 4	0.01%	0.01%	0.03%	0.02%	0.03%	0.05%
Storey 3	0.02%	0.01%	0.06%	0.04%	0.07%	0.09%
Storey 2	0.03%	0.02%	0.08%	0.06%	0.12%	0.49%
Storey 1	0.03%	0.02%	0.09%	0.06%	0.39%	0.71%

Table 3.30 – Base shear: nonlinear static (PSHVR) vs. dynamic (NLDA) analyses results

	Base shear (*kN*)					
	DL		SD		NC	
	PSHVR	NLDA	PSHVR	NLDA	PSHVR	NLDA
BF	126.46	112.45	191.76	185.50	204.05	216.21
IN	316.24	209.49	706.12	529.87	834.56	754.13

Concerning the outcome of the seismic assessment process itself, different conclusions were reached for the BF and for the IN, depending on the LS under evaluation. For the LS of DL, the chord rotation and shear force D/C ratios were found to be below 1.0 on all control sections, thus allowing both frames to be deemed safe. However, it is noteworthy that: (i) the chord-rotation ratios of the BF are typically under 50%, while those of the IN are below 15% and (ii) the shear force ratios of the BF are between 40% and 70%, while those of the IN are below 30%. Next, for the LS of SD, the D/C ratios of the IN continued to be quite low (below 15% and 50% for chord rotation and shear force ratios, respectively), thus allowing it to be deemed safe. On the other hand, the D/C ratios of the BF were

found to be considerably high, both in terms of chord rotation and of shear force, in several control sections (even slightly above 1.0 in three of them). Signs of excessive deformation and shear force effectively started to show for this LS, respectively, on the columns of the third storey and on the strong column (C2) at all storeys. Therefore, in strict terms and mainly due to the potentially excessive shear forces, the BF should not be deemed safe for the LS of SD. Finally, it was for the LS of NC that the most relevant differences were found between the BF and the IN. The chord rotation ratios of the latter, although exhibiting a significant increase on the columns of the first and second storeys, continued to be below 1.0 on all control sections. However, in terms of shear force, the capacity of the strong column was clearly exceeded on the first storey. Regarding the BF, its chord rotation capacities were exceeded on a considerable number of control sections, with D/C ratios above 2.5 being found on the columns of the third storey. In terms of shear force, the capacities of the strong column were exceeded on all storeys. Therefore, even though the scenario for the BF is much worse than for the IN, both frames should be deemed unsafe for the LS of NC.

The conclusions drawn above show that the option to consider (or not) the masonry infill walls in the modelling of existing RC buildings might have significant impact on the outcome of the EC8-3 (2005) seismic assessment process. For this particular case, recalling that structural importance class II only requires the verification of the LS of SD, it would mean the difference between deeming the structure to be perfectly safe and finding it to be borderline unsafe both in terms of deformation- and strength-controlled collapse mechanisms. The latter conclusion would most likely lead to the decision to retrofit the building, with the associated financial investment, as to make it code compliant. Therefore, when low and medium seismic input motions constitute the base demand for the assessment of older-type RC framed buildings, the protection provided to the RC members by the confined masonry infill panels should not be neglected.

A closer look at the results obtained for the LS of NC, combined with the insight provided by the experimental tests, provides additional conclusions about the collapse mechanisms of the frames and the type of retrofitting that would be more adequate. Results for the BF, both in terms of D/C ratios and of global storey parameters, show that deformation tends to concentrate at the third storey, leading to the formation of a soft-storey mechanism (Figure 3.65). They also show that the strong column is the most likely to suffer damage due to excessive shear force, as it absorbs most of the total storey shear (typically more than 70%). Moreover, the chord rotation and shear force ratios on other members are also quite high, indicating that the BF would benefit the most from a global retrofitting solution capable of reducing floor displacements, eliminating the irregular response of the third storey, and increasing the shear capacity of columns. The results for the IN, on the other hand, show a scenario that is quite different. Looking exclusively to the D/C ratios, one could think that the only potentially unsafe situation would be the excessive shear force on the strong column of the first storey, and just recommend a local strengthening solution. However, the inter-storey drift results and the damage by the end of the 975-yrp experimental test show the potential that exists for a soft-storey mechanism in case of sudden failure of the first storey infill panels (Figure 3.66). Therefore, to replace those infill panels by a solution capable of maintaining the storey's deformation under control and increasing the shear capacity of selected columns, while being less vulnerable to abrupt failure, would be a safer retrofitting option.

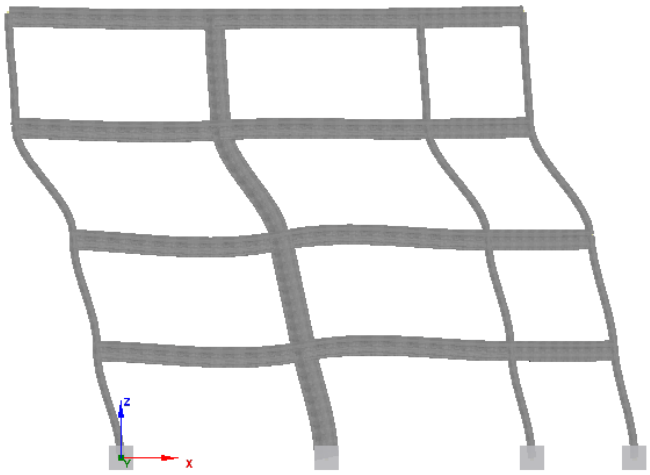

Figure 3.65 – Soft-storey mechanism on the third storey of the BF

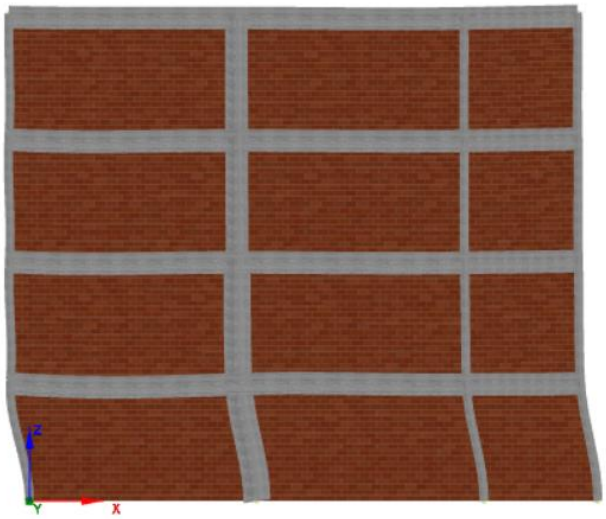

Figure 3.66 – Potential for a soft-storey mechanism on the first storey of the IN (infill panel openings not shown)

3.5. CONCLUDING REMARKS

The seismic behaviour of an older-type RC frame was thoroughly studied during this chapter, with and without considering the effect of its masonry infill walls. Two numerical models were developed according to the state-of-the-art provisions presented in Chapter 2 and their calibration was carried out based on the available experimental results. The seismic assessment of the bare and infilled structure was then performed according to the provisions of EC8-3 (2005), using nonlinear static and dynamic analysis models. The local results of the assessment process were compared with the damage observed during the experimental tests and the influence of the infill walls on the outcome of the seismic assessment process was addressed. Finally, some comments were made on what could be the best retrofitting options to make the structure code compliant.

The discussions and conclusions extracted contribute to the calibration of nonlinear analytical models that adequately reproduce the behaviour of pre-code RC buildings and can, therefore, be extensively used in the seismic assessment of such structures (according to the provisions of EC8-3 (2005) or any other assessment code). The fact that the presented numerical results are supported by the available experimental results is thought to be an advantage of this study, as information on the real properties of buildings that have suffered the effect of earthquakes is seldom difficult to obtain and the cost of large-scale experimental campaigns is quite high. The author thus hopes that the reported findings help other researchers improve their numerical models as well as better interpret the assessment results provided by the EC8-3 (2005) procedure.

A final note regarding the application of these models by structural engineering professionals dealing with seismic assessment problems: severe difficulties should still be expected. Most of them are not acquainted with nonlinear procedures (among other things – see Chapter 2), which impairs their ability to benefit from well-calibrated nonlinear models and related parameters. However, although the author fully agrees that researchers should develop procedures that can be safe and easily applied by professionals, he also firmly believes that this matter will have to retain some of its complexity, under pain of leading to overly simplified procedures that will end up producing assessment results that are too pessimistic, with direct influence on the subsequent decisions. Therefore, it is highly recommended that professionals that wish to be involved in such matters become familiarized with more advanced methods of analysis than their typical design instruments (i.e., linear elastic analysis combined with seismic codes oriented towards the design of new buildings).

CHAPTER 3 – AN APPLICATION OF THE EC8-3 SEISMIC SAFETY ASSESSMENT PROCEDURE

3.1. INTRODUCTION 3.1

3.2. CASE STUDY CHARACTERIZATION 3.2

3.2.1. Geometry and section detailing 3.2

3.2.2. Masonry infill walls 3.6

3.2.3. Material properties 3.7

3.2.4. Vertical loads 3.10

3.2.5. Earthquake input used in the PsD tests 3.11

3.2.6. Experimental results 3.13

3.2.6.1. Modal frequencies 3.13

3.2.6.2. Storey displacements, drifts, and shear 3.14

3.2.6.3. Observed damage 3.18

3.2.6.4. Remarks 3.20

3.3. NUMERICAL MODELLING AND STRUCTURAL ANALYSIS 3.22

3.3.1. Modelling options 3.23

3.3.1.1. Modelling of RC members 3.23

3.3.1.2. Modelling of masonry infill walls 3.25

3.3.1.3. Loads, masses, and damping 3.33

3.3.2. Structural analysis results 3.35

3.3.2.1. Modal frequencies 3.35

3.3.2.2. Storey displacements, drifts, and shear 3.36

3.3.2.3. Discussion 3.43

3.4. SEISMIC ASSESSMENT PROCEDURE 3.45

3.4.1. Seismic demand definition 3.45

3.4.1.1. Target displacements for nonlinear static analysis 3.47

3.4.1.2. Accelerograms for nonlinear dynamic analysis 3.49

3.4.2. Member capacities computation 3.51

3.4.2.1. Ductile capacities 3.52

3.4.2.2. Brittle capacities 3.53

3.4.3. Performance evaluation 3.54

3.4.3.1. Nonlinear static analysis results 3.54

3.4.3.2. Nonlinear dynamic analysis results 3.56

3.4.3.3. Discussion 3.58

3.5. CONCLUDING REMARKS 3.61

CHAPTER 4

ON THE APPLICABILITY OF CONVENTIONAL SEISMIC DESIGN METHODOLOGIES TO HYBRID RC-STEEL SYSTEMS

4.1. INTRODUCTION

Seismic design is currently codified by structural codes and standards of practice using the so-called "force-based design" (FBD). This is mainly due to historical reasons and related to how design is carried out for other actions such as dead and live loads (Priestley *et al,* 2007). This procedure involves the consideration of a behaviour factor (*q*-factor) as a simple mean to account for the nonlinear behaviour of the structure while performing linear static analysis. However, in structures designed according to old seismic codes (or even non-seismic codes), the uncertainties about the nonlinear behaviour are relevant (for instance, the location and ductility capacity of the potentially inelastic regions are not fully known). It is therefore very difficult to define a direct correlation between the real internal forces that develop in structural members during the seismic excitation, and those experienced by an equivalent indefinitely elastic structure. Consequently, several authors (e.g., Mpampatsikos *et al,* 2008) have argued that the force-based seismic assessment of such structures will not yield, in general, satisfactory results.

With the purpose of providing information about the seismic performance of RC buildings strengthened with steel braces, several experimental and analytical studies have been conducted over the last years (as referred in Chapter 2). Unfortunately, only a few (e.g., Maheri and Akbari, 2003; TahamouliRoudsari *et al,* 2017) have resulted in proposals for *q*-factors to be applied in the design process and, moreover, limited confidence should be assigned to them due to the discrepancy between results. In fact, the latter show that the improvement in the seismic behaviour of a RC structure retrofitted with steel braces is not proportional to the corresponding increase in lateral strength, which suggests that the *q*-factor based design process might not be an efficient approach to obtain retrofitted structures with good seismic performance. As such, the nonlinear behaviour of the existing and retrofitted structures should be faced directly, despite the considerable increase in complexity of the assessment and design procedures. However, due to the simplicity and popularity of the *q*-factor approach for the design of new structures, practitioners are more likely to resort to it than to the more complex nonlinear static and dynamic procedures when involved in situations requiring the seismic assessment and strengthening of existing RC buildings.

The application of conventional seismic design methodologies to hybrid RC-steel systems is thus addressed in the following sections. The *q*-factor based EC8-3 (2005) seismic assessment procedure is first reviewed, followed by a case-study application intended to analyse and discuss the difficulties a practitioner will face when assessing the efficiency of a steel-brace retrofitting system designed within the framework of EC8-1 (2004). Afterwards, the obtained retrofitted structure is re-evaluated using nonlinear methods of analysis. The obtained results are discussed in light of the EC8-3 (2005) performance requirements, and conclusions are drawn about the adequacy of the FBD methodology (and associated *q*-factors) to such situations.

4.2. THE *q*-FACTOR APPROACH IN EC8-3

Clause 4.1 (3) on EC8-3 (2005) states that the assessment procedure should be carried out by means of the general analysis methods specified in section 4.3 of EC8-1 (2004), as modified per the former standard to suit the specific problems encountered in the assessment. For a chosen performance requirement, the effects of the seismic action (combined with the other permanent and variable loads) can thus be evaluated by means of linear or nonlinear methods of analysis, depending on the characteristics of the structure under evaluation and the choice of the analyst. Each of these methods involves different levels of complexity, accuracy, computational effort, as well as of requirement for specialized knowledge in the field. The *q*-factor approach – a linear static design method with reduced input seismic action – is prescribed by EC8-1 (2004) as the basic design method and usually referred to as the most conservative.

The seismic action to be adopted when using the *q*-factor approach within the context of EC8-3 (2005) is referred in its clauses 2.2.1 (4) and 4.2 (3). The design spectra for linear analysis are the ones defined in sub-section 3.2.2.5 of EC8-1 (2004), scaled to the values of the design ground acceleration established for the verification of the different limit states (LS's). A default value of q = 1.5 is proposed for RC structures, regardless of structural type. Higher values may eventually be adopted if suitably justified with reference to the local and global available ductility (evaluated according to the relevant provisions of EC8-1, 2004), but this is usually not easy to do. Clause 2.2.2 (3) on EC8-3 (2005) does however refer that the value of q = 1.5 (or a duly justified higher one) corresponds to the fulfilment of the LS of Significant Damage (SD). If the LS under evaluation is that of Near Collapse (NC), that value may be increased by about one-third, although it is also referred that this approach is generally not suitable for checking this LS.

Regarding structural modelling, clause 4.3 (2) of EC8-3 (2005) states that all provisions of sub-sections 4.3.1 and 4.3.2 of EC8-1 (2004) should be applied without modifications. In particular, member stiffness should be simulated according to paragraphs 4.3.1 (6) and 4.3.1 (7). The former states that the effect of cracking should be considered by evaluating the stiffness at the time when the reinforcement starts to yield. The latter states that, unless a more accurate analysis of the cracked elements is performed, their flexural and shear stiffness properties may be taken equal to one-half of those of the uncracked elements. This simplified 50% stiffness reduction is widely used and generally accepted for the design of new structures (as already referred in Chapter 2), but it is difficult to justify for the assessment of existing structures, especially when applied to members that are prone to early

cracking (Pinto and Franchin, 2008). However, within the straightforward context of developing a linear elastic analysis model to be used with the *q*-factor design approach, this simplification is thought to be acceptable enough.

Concerning safety verifications, clauses 2.2.1 (4) to (7) on EC8-3 (2005) state that all structural elements should be verified by checking that demands due to the reduced seismic action do not exceed the corresponding capacities in terms of strength. For the calculation of the latter of ductile or brittle elements, mean value properties of the existing materials should be used as directly obtained from *in-situ* tests and from additional sources of information, appropriately divided by the confidence factors referred in Chapter 2. For new or added materials, nominal properties should be used. In the case of brittle elements, material strengths should be further divided by the partial factor of each material when calculating the corresponding strength capacities. For the verification of the LS's of NC and SD, clauses 2.2.2 (3) and 2.2.3 (3) state that demands shall be based on the reduced seismic action relevant for each LS and capacities evaluated as for non-seismic design situations. On the other hand, for the LS of Damage Limitation (DL), clause 2.2.4 (3) refers that demands and capacities shall be compared in terms of mean inter-storey drift. Two shortcomings can thus be pointed out to the EC8-3 (2005) safety verification procedure when using the *q*-factor design approach: (i) RC member capacities are the same for the LS's of NC and SD (given the installed axial force) and (ii) no limit values are recommended for the inter-storey drifts to be observed when checking for the LS of DL.

The above referred criteria are summarized in Table 4.3 on EC8-3 (2005), including the values of the material properties to be adopted when evaluating the demands and capacities of ductile and brittle elements, for all types of analysis, as well as the criteria that shall be followed for the corresponding safety verifications. However, inconsistencies seem to exist between the contents of Table 4.3 regarding the *q*-factor approach and what is stated in the precedent text: (i) it is said that demands on brittle elements should be determined in accordance with the relevant section of EC8-1 (2004), which appears to be a reference to the capacity design rule (sub-section 5.2.3.3) and related others (no reference to this procedure exists in the before text concerning the *q*-factor approach); (ii) it is said that the mean values of material properties should be divided by both the confidence factor and the material partial factor when calculating the capacities of elements (the before text only applies the material partial factor to the case of the capacities of brittle elements).

4.3. APPLICATION TO A RETROFITTING CASE STUDY

Sub-section 5.1.2 on EC8-3 (2005) states that the selection of the "type, technique, extent and urgency" of the retrofitting intervention should be based on the structural information collected during the assessment of the building. The following aspects should be taken into account: (i) all identified local gross errors should be appropriately remedied; (ii) structural regularity should be improved as much as possible, both in elevation and in plan; (iii) increase in the local ductility supply should be effected where required; (iv) the increase in strength after the intervention should not reduce the available global ductility. The required characteristics of regularity and resistance can be achieved by either the modification of the strength and/or stiffness of an appropriate number of existing components (local modification), or by the introduction of new structural elements (global

modification), as discussed in Chapter 2. The procedure to design the retrofitting system should include the following steps: (a) conceptual design; (b) analysis; (c) verifications. The conceptual design stage should cover the following: (i) selection of techniques and/or materials, as well as of the type and configuration of the intervention; (ii) preliminary estimate of dimensions of additional structural parts; (iii) preliminary estimate of the modified stiffness of the retrofitted elements. Structural analysis should then be performed considering the modified characteristics of the building, and safety verifications should be carried out for existing, modified, and new structural elements. Finally, the description of the expected effect of the retrofitting solution on the structural response of the building should be included in the design documentation. The following sub-sections go through these steps during a case study that tests the approach described in section 4.2.

4.3.1. Structural characterization

The RC structure chosen as a case study for this chapter is the same that was used in Chapter 3 to illustrate the application of the EC8-3 (2005) seismic assessment procedure. The results of the latter for the bare frame (BF) show that, for it to become compliant with the performance requirements of the LS of NC, a global retrofitting intervention is necessary. In order to be effective, the retrofitting system will have to be capable of reducing floor displacements, eliminating the irregular response of the third storey, and reducing the shear demand on columns. A global strengthening intervention using concentric X-diagonal steel braces is proposed herein. Figure 4.1 shows the layout of the bracing system. The diagonals are composed by hot-rolled circular hollow section (CHSH) steel profiles, directly connected to the RC beam-column nodes of the intermediate bay. The connection is thought out to behave as a “nominally pinned joint” (as defined in EC3-1-8, 2005), i.e., capable of transmitting the internal forces without developing significant moments. At the points where the braces cross, no structural connections exist. Additionally, local strengthening of weak RC members will be considered, if necessary, to ensure the success of the intervention.

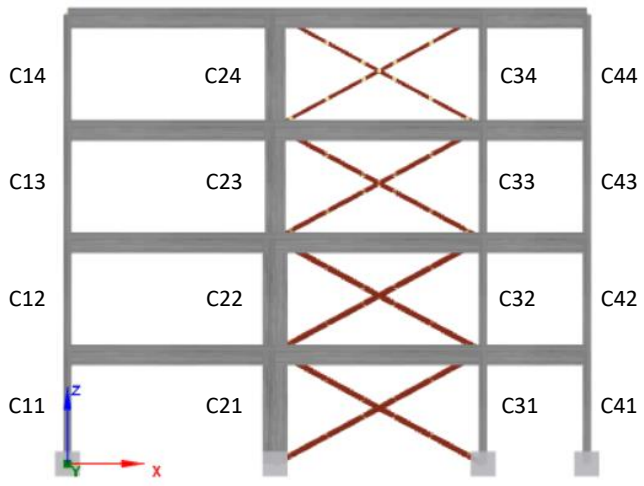

Figure 4.1 – Layout of the proposed retrofitting system for the BF

4.3.2. Design of the retrofitting system

As no specific rules for the design of hybrid RC-steel systems exist in EC8-1 (2004), its provisions concerning steel frames with concentric braces were taken as reference and starting point for the design of the retrofitting system. Beginning with the braces' layout, clause 6.7.1 (2) requires diagonal elements to be placed in such a way that the structure, under load reversals, exhibits similar load deflection characteristics at each storey, in opposite senses of the same braced direction. To that end, the rule provided by clause 6.7.1 (3) should be met at every storey. The geometry shown in Figure 4.1 meets this requirement, so no changes were necessary. A linear elastic analysis model was then developed according to the requirements of sub-section 4.3.1 (on EC8-1, 2004), and the frame was analysed under the effect of its vertical loads combined with the seismic demand defined by the NC elastic response acceleration spectrum (Figures 3.10 and 3.48, respectively, in Chapter 3). The effect of the compressed braces was neglected during the analysis, as required by clause 6.7.2 (2), and behaviour factors *q* corresponding to two different ductility classes (DCL: $q = 1.5$; DCM: $q = 3.0$) were considered to obtain the seismic forces on the retrofitted structure.

Concerning the detailed design of the steel braces, the applicable provisions of sub-section 6.7.3 on EC8-1 (2004) were taken as reference: (i) the non-dimensional slenderness $\bar{\lambda}$, as defined in EC3-1-1 (2005), should be limited to $1.3 < \bar{\lambda} \leq 2.0$; (ii) the yield resistance $N_{pl,Rd}$ of the gross section should be such that $N_{pl,Rd} \geq N_{Ed}$, where N_{Ed} is the design axial force on the tensioned brace; (iii) the maximum overstrength ratio $\Omega_i = N_{pl,Rd,i}/N_{Ed,i}$ over all braces should not differ more than 25% from the minimum value $\Omega = \min(\Omega_i)$. The lower limit to the non-dimensional slenderness $\bar{\lambda}$ is adopted so that, during the pre-buckling stage (when both compression and tension braces are active), the RC frame's columns are not overloaded beyond the action effects obtained from the analysis at the ultimate stage (when only the tension braces are taken as active). Regarding the imposition of a maximum difference of 25% between the overstrength ratios Ω_i, it means to ensure a homogeneous dissipative behaviour of the steel braces. The definition of a retrofitting solution that fulfilled these conditions required an iterative analysis and design procedure, that was carried out considering the two previously referred *q*-factors. Tables 4.1 to 4.3 summarize the obtained results, considering a design yield stress f_y equivalent to that of steel grade S275 (EC3-1-1, 2005).

Table 4.1 – Steel braces design results: *q* = 1.5 (DCL)

						$N_{Ed}\ (kN)$		$\Omega_i = \frac{N_{pl,Rd,i}}{N_{Ed,i}}$	
Storey	**Cross-section**	$L\ (m)$	$f_y\ (MPa)$	$\bar{\lambda}$	$N_{pl,Rd}\ (kN)$	**XX+**	**XX-**	**XX+**	**XX-**
4	CHSH 88.9x3.2	5.68	275.00	2.16	237.05	166.94	169.11	1.42	1.40
3	CHSH 139.7x4.0	5.68	275.00	1.37	470.25	419.19	422.84	1.12	1.11
2	CHSH 139.7x5.0	5.68	275.00	1.37	583.00	564.19	567.67	1.03 = Ω	1.03
1	CHSH 139.7x5.0	5.68	275.00	1.37	583.00	561.51	575.20	1.04	1.01 = Ω

Table 4.2 – Steel braces design results: q = 3.0 (DCM)

						$N_{Ed}\ (kN)$		$\Omega_i = \frac{N_{pl,Rd,i}}{N_{Ed,i}}$	
Storey	**Cross-section**	$L\ (m)$	$f_y\ (MPa)$	$\bar{\lambda}$	$N_{pl,Rd}\ (kN)$	**XX+**	**XX-**	**XX+**	**XX-**
4	CHSH 88.9x3.2	5.68	275.00	2.16	237.05	85.49	89.15	2.77	2.66
3	CHSH 88.9x3.2	5.68	275.00	2.16	237.05	172.61	176.28	1.37	1.34
2	CHSH 114.3x3.2	5.68	275.00	1.67	308.00	238.99	243.48	1.29 = Ω	1.26 = Ω
1	CHSH 114.3x3.2	5.68	275.00	1.67	308.00	222.47	228.35	1.38	1.35

Table 4.3 – Base shear values for the bare (BF) and retrofitted (DCL; DCM) frames

	BF	**DCL**	**DCM**
Fundamental period $T_1\ (sec)$	0.94	0.36	0.45
Spectral corner period $T_c\ (sec)$	0.60	0.60	0.60
NC spectral acceleration $S_{e,NC}\ (T_1)$	0.46768 · g	0.73269 · g	0.73269 · g
Total mass $m\ (ton)$	173.93	173.93	173.93
Elastic base shear $V_e\ (kN)$	683.72	1062.63	1062.63
Behaviour factor q	2.0 (*)	1.5	3.0
Assessment / design base shear $V_b\ (kN)$	341.86	708.42	354.21

(*) q-factor for the seismic assessment of the BF under the LS of NC, as per EC8-3(2005): 2.2.2 (3)

The design axial forces on the tensioned braces, as well as the fundamental period and base shear values shown above, were obtained considering the effective (secant-to-yield) stiffness EI_{eff} of the RC elements equal to one-half of their gross stiffness EI. As referred in section 4.2., this is the default procedure according to clause 4.3.1 (7) on EC8-1 (2004) to consider the effect of cracking when performing seismic design using linear elastic analysis models. Concerning the values of $\bar{\lambda}$ and Ω_i marked in red, those indicate situations for which the design provisions of sub-section 6.7.3 on EC8-1 (2004) were not fulfilled. However, the maximum value of the non-dimensional slenderness is only slightly exceeded, and it is well known that the condition regarding the maximum difference between overstrength ratios is often hard to fulfil on top storeys. Moreover, it is recalled that these are design provisions that apply to concentric-braced steel frames, therefore not being mandatory (just taken as reference) for the design of steel-braced RC structures.

4.3.3. RC member safety checks

For the retrofitting system to be deemed adequate, the RC members must be proven safe by checking that demands due to the reduced seismic action do not exceed their (ductile and brittle) capacities in terms of strength, while duly considering the axial forces induced by the steel braces. As referred in section 4.2., clauses 2.2.2 (3) and 2.2.3 (3) on EC8-3 (2005) state that capacities shall be evaluated as for non-seismic design situations. However, to allow for the possibility that the actual yield strength of

the steel braces is higher than their nominal yield strength f_y, the safety checks were performed herein according to the capacity design rule specified in sub-section 6.7.4 on EC8-1 (2004), adapted to RC members and reproduced below in Expression (4.1):

$$N_{Rd}\,(M_{Ed}) \geq N_{Ed,G} + 1.1 \cdot \gamma_{ov} \cdot \Omega \cdot N_{Ed,E} \tag{4.1}$$

where $N_{Rd}\,(M_{Ed})$ is the design axial resistance of the beam or column according to EC2-1-1 (2004), considering the interaction of the axial resistance with the bending moment M_{Ed}, the latter being defined by its value in the seismic design situation; $N_{Ed,G}$ is the axial force in the beam or column due to the non-seismic actions included in the combination for the seismic design situation; $N_{Ed,E}$ is the axial force in the beam or column due to the design seismic action; $\gamma_{ov} = 1.25$ is the overstrength factor as defined in EC8-1 (2004): 6.1.3 (2); and Ω is the minimum overstrength ratio Ω_i over all steel braces, as already defined above. Additionally, the shear force demands V_{Ed} in the seismic design situation were checked against the shear force capacity values V_{Rd} obtained with the provisions of EC2-1-1 (2004). The material properties used to compute the required ductile and brittle capacities are those referred in sub-section 3.3.1.1. (see Chapter 3).

The results of the safety checks are given below in terms of demand-to-capacity ratios (D_i/C_i) for each control section i, using a graphical representation to provide a better view of the outcome provided by each retrofitting system (a similar process to that adopted in Chapter 3). For comparison purposes, the D/C ratios referring to the seismic assessment of the BF according to the q-factor approach (see data on Table 4.3) are also included. Figures 4.2 and 4.3 thus show, respectively, the NC axial force and NC shear force D/C ratios on the columns of the bare (BF) and retrofitted (DCL; DCM) frames. As for the beams, the D/C ratios were found to be consistently below 1.0, therefore the correspondent graphical representation is deliberately omitted (this was done before in Chapter 3 and will be the default procedure henceforth without further notice).

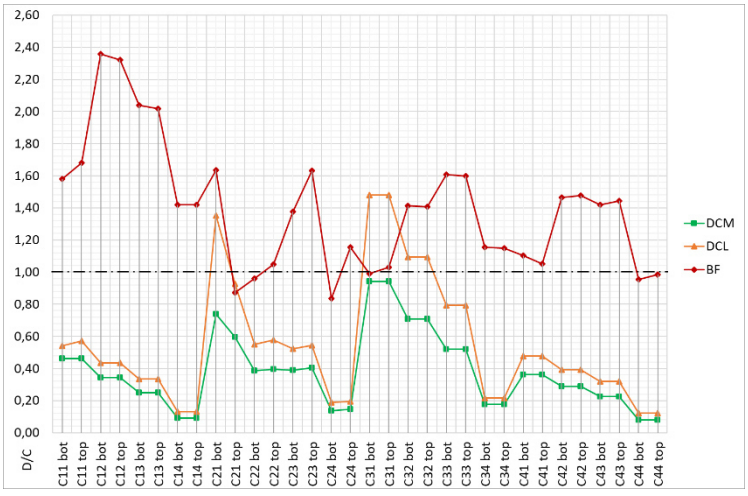

Figure 4.2 – BF, DCL and DCM: NC axial force D/C ratios on columns (q-factor approach results)

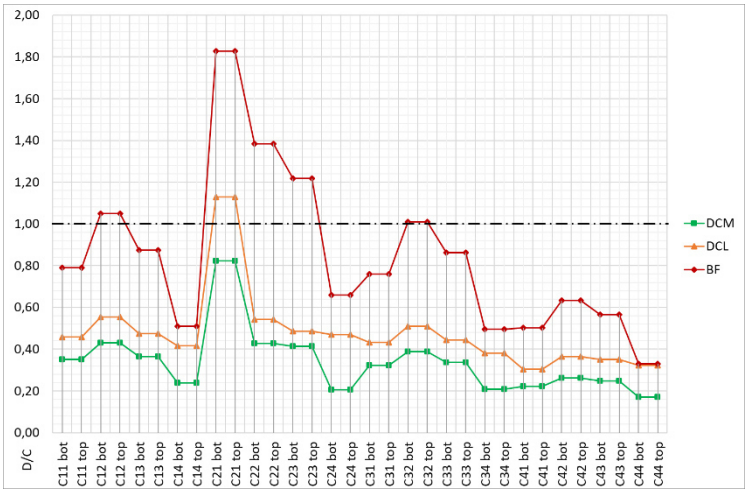

Figure 4.3 – BF, DCL and DCM: NC shear force D/C ratios on columns (q-factor approach results)

The D/C ratios comparison shows the drastic improvement in the seismic behaviour of the frame caused by the inclusion of the steel braces. Even though some control sections remained unsafe when considering the DCL retrofitting system, the global assessment scenario is completely different from that of the BF, which revealed generalized excessive flexural demands and clearly excessive shear demands on the first, second, and third storeys of the strong column (C2) (see Figure 4.1 for structural member numbering). The fact that the axial force D/C ratios on the first storey of column C3 are higher in the DCL than they were in the BF indicates that the global axial force induced by the tensioned steel braces is more than that column can resist. Therefore, the DCL retrofitting system should be deemed inadequate for being too robust. On the other hand, when considering the DCM retrofitting system, both the axial force and shear force D/C ratios were found to be below 1.0 on all control sections, thus allowing the retrofitted frame to be deemed safe for the LS of NC according to the q-factor approach.

4.4. EVALUATION OF THE DESIGNED RETROFITTING SYSTEM

The previous section presented a case-study application of force-based design (FBD) to the global strengthening of an older-type RC building using X-diagonal steel braces. As no specific rules for the design of hybrid RC-steel systems exist in EC8-1 (2004), its provisions concerning steel frames with concentric braces were taken as reference for the design of the retrofitting system. In parallel, to obtain the seismic forces on the retrofitted structure, behaviour factors q corresponding to two different ductility classes were considered. Lastly, to assess the efficiency of the strengthening intervention, the safety of RC members was checked combining the requirements of the q-factor approach on EC8-3 (2005) with the capacity design rule specified in sub-section 6.7.4 on EC8-1 (2004) – adapting it to the case of RC members – to allow for the possibility that the actual yield strength of the steel braces is higher than their nominal yield strength. The outcome of this process was a retrofitted structure that seems to be compliant with the requirements of the LS of NC according to the q-factor approach on EC8-3 (2005). However, due to the several adjustments that were introduced

in the referred code provisions in order to try to adapt them to the structural typology at hand, the performance of the obtained retrofitted structure is evaluated in the following sub-sections using nonlinear static and dynamic methods of analysis. The results are then discussed in light of the applicable EC8-3 (2005) performance requirements for the LS of NC, and conclusions are drawn about the effective seismic safety of the retrofitted structure.

4.4.1. Nonlinear modelling

The numerical model of the retrofitted frame (DCM) was obtained from that of the bare frame (BF) – see sub-section 3.3.1. in Chapter 3 – by adding the necessary elements to simulate the inclusion of the steel braces. The modelling options for the latter were based on the studies by Elghazouli (2003), D'Aniello *et al* (2013), and Karamanci and Lignos (2014). A distributed plasticity model was considered, combined with fibre discretization of the cross-sections (approx. 200 fibres / section), implemented through a force-based FE formulation with five integration sections per element. The connections to the RC frame were modelled using the link elements ("zero-length" elements) available in software platform *SeismoStruct*. This required the definition of nodes at the ends of the steel braces, with the same coordinates as those of the nodes on the RC frame to which the braces connect. The "nominally pinned joint" behaviour referred in sub-section 4.3.1. was obtained by editing the stiffness factor of the corresponding moment-rotation law of the link elements placed between the end nodes of the steel braces and the connecting nodes on the RC frame. Concerning the constitutive law defining the cyclic behaviour of the steel material, the Menegotto and Pinto (1973) model was employed, combined with the isotropic hardening rules proposed by Filippou *et al* (1983), with the following mechanical properties (mean values):

- Modulus of elasticity (initial elastic stiffness): $E_s = 210\ GPa$
- Mean yield stress: $f_{ym} = 1.25 \times f_y(S275) = 343.75\ MPa$
- Strain hardening parameter: $\mu = 0.005$
- Steel specific weight: $\gamma_s = 7850\ kg/m^3$.

While the above-referred modelling aspects are consensual among authors, others are not, like the number of FE's per individual brace, or the brace's initial camber Δ_0. It is, however, widely accepted that the braces should be divided at least in two FE's that are offset (initial camber) at mid-length of the brace, as to trigger flexural buckling (Figure 4.4). Hence, in order to be able to reproduce the buckling response of the braces as close as possible to their expected behaviour, a short parametric study was conducted herein using a single brace auxiliary model.

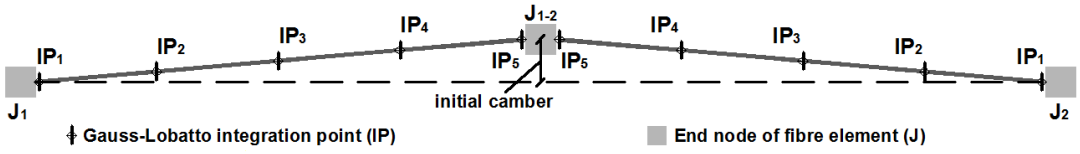

Figure 4.4 – Model of a steel brace with two FE's and bilinear initial camber (adapted from D'Aniello *et al,* 2013)

The single brace was modelled with the same length (L = 5.68 m) and support conditions (nominally pinned) as the braces of the retrofitted structure. Three different cross-sections were considered to obtain values of relative slenderness $\bar{\lambda}$ between 1.5 and 2.5, while the effect of the FE mesh size was considered by varying the number of elements between 2 and 8. Regarding the effect of the initial camber, a bilinear shape was considered with amplitude Δ_0 varying in the range of 0.1% to 0.4% of the brace's total length L. All other modelling options were set as described above. The models were then analysed under monotonically increasing axial displacements, and the response curves – in terms of axial force-axial displacement and axial force-lateral displacement – were plotted against the values of the design buckling loads calculated according to EC3-1-1 (2005). Figures 4.5 to 4.10 below show the obtained response curves, while Table 4.4 shows the relative slenderness $\bar{\lambda}$ and buckling load $N_{b,Rd}$ values of the tested brace cross-sections.

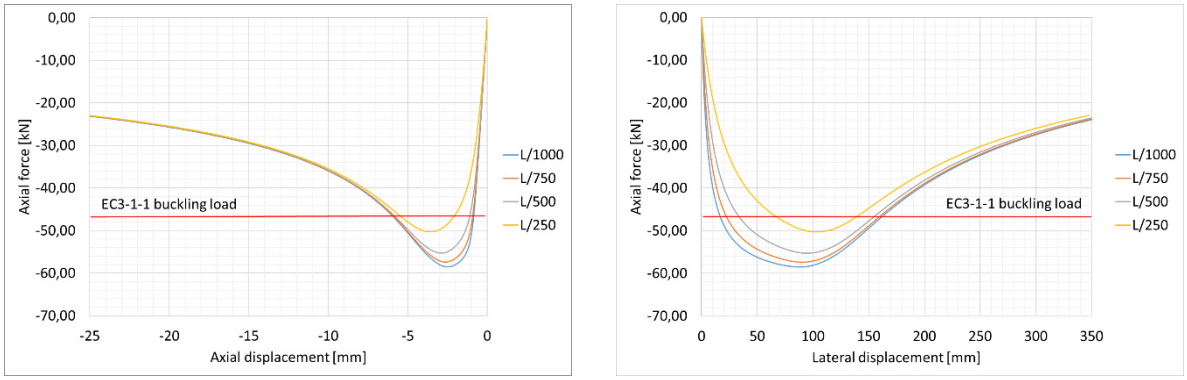

(a) **(b)**

Figure 4.5 – Influence of camber under monotonic loading: CHSH 88.9×3.2 discretized with 2 FE's

(a) axial force vs. axial displacement; (b) axial force vs. lateral displacement

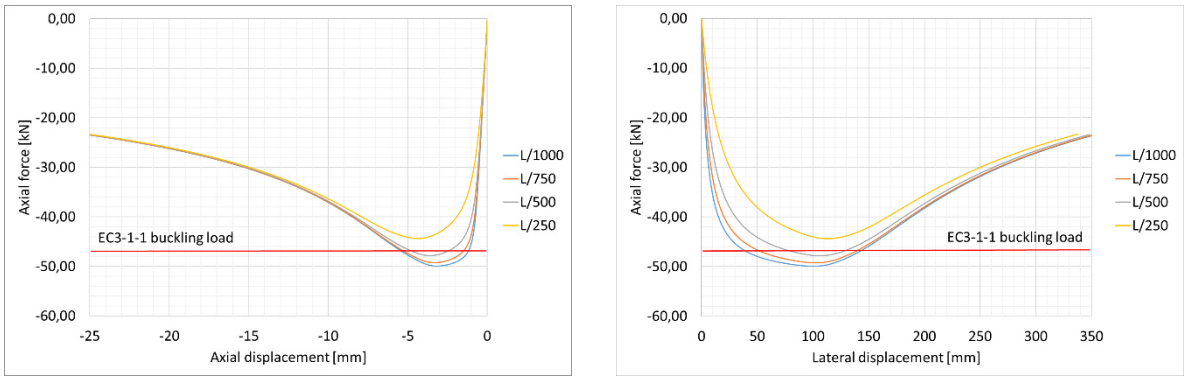

(a) **(b)**

Figure 4.6 – Influence of camber under monotonic loading: CHSH 88.9×3.2 discretized with 8 FE's

(a) axial force vs. axial displacement; (b) axial force vs. lateral displacement

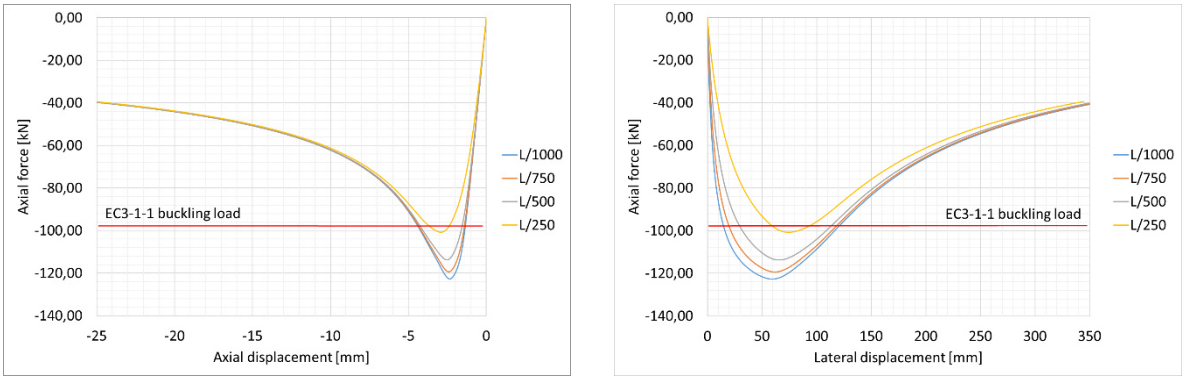

(a) **(b)**

Figure 4.7 – Influence of camber under monotonic loading: CHSH 114.3×3.2 discretized with 2 FE's

(a) axial force vs. axial displacement; (b) axial force vs. lateral displacement

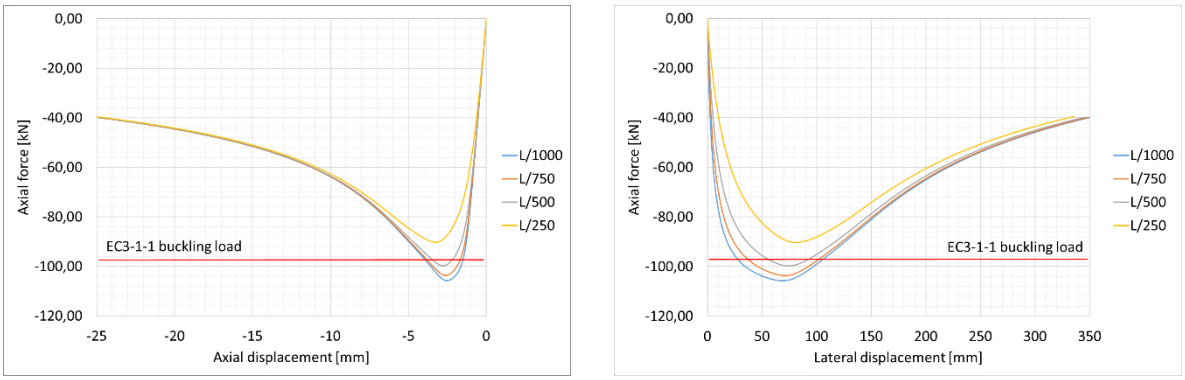

(a) **(b)**

Figure 4.8 – Influence of camber under monotonic loading: CHSH 114.3×3.2 discretized with 8 FE's

(a) axial force vs. axial displacement; (b) axial force vs. lateral displacement

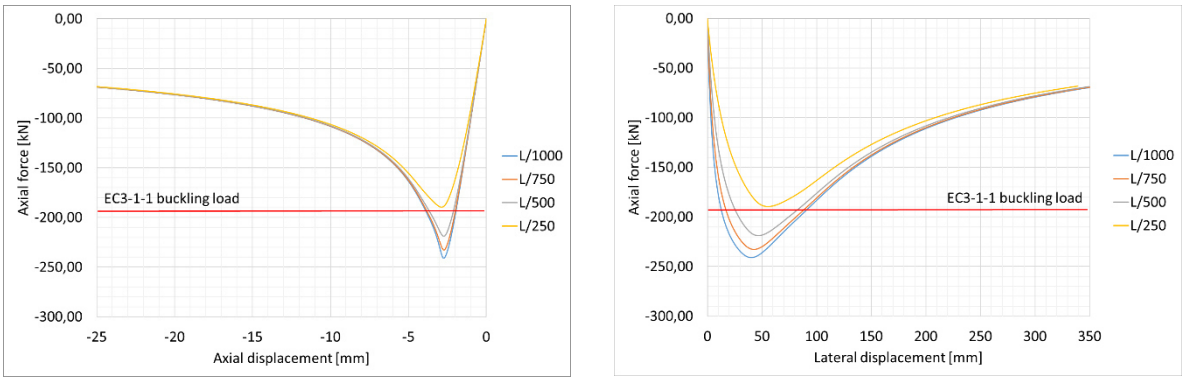

(a) **(b)**

Figure 4.9 – Influence of camber under monotonic loading: CHSH 139.7×3.6 discretized with 2 FE's

(a) axial force vs. axial displacement; (b) axial force vs. lateral displacement

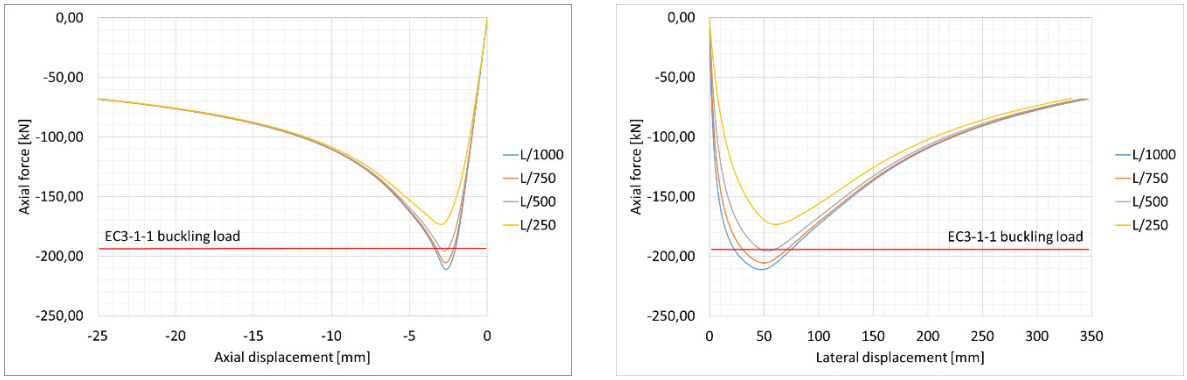

(a) **(b)**

Figure 4.10 – Influence of camber under monotonic loading: CHSH 139.7×3.6 discretized with 8 FE's

(a) axial force vs. axial displacement; (b) axial force vs. lateral displacement

Table 4.4 – Relative slenderness $\bar{\lambda}$ and design buckling loads $N_{b,Rd}$ of the tested braces according to EC3-1-1 (2005)

Cross-section	$L\ (m)$	$f_{ym}\ (MPa)$	$N_{pl,Rd}\ (kN)$	$N_{cr} = \frac{\pi^2 \cdot E \cdot I}{L^2}\ (kN)$	$\bar{\lambda} = \sqrt{\frac{A \cdot f_{ym}}{N_{cr}}}$	$N_{b,Rd}\ (kN)$
CHSH 88.9×3.2	5.68	343.75	296.31	50.88	2.41	46.60
CHSH 114.3×3.2	5.68	343.75	385.00	110.50	1.87	97.08
CHSH 139.7×3.6	5.68	343.75	529.38	229.35	1.52	192.76

The obtained results show that the size of the FE mesh has significant influence on the numerical response of the compressed braces. Using only two FE's, the buckling loads were often higher than the corresponding Euler's critical load, unless for the cases in which the considered camber's amplitude Δ_0 was relatively high (between L/500 and L/250). Moreover, the value of the camber amplitude required to obtain a buckling load close to that given by the provisions of EC3-1-1 (2005) increased with the slenderness of the brace, which did not seem reasonable. Therefore, the 2-FE discretisation was deemed unsatisfactory as a modelling option. On the other hand, the buckling loads obtained with the 8-FE discretisation were always below the corresponding Euler's critical load, regardless of the considered camber amplitude. Moreover, the values obtained with camber amplitudes between L/1000 and L/500 were not significantly different withing each tested slenderness and showed a good agreement with the design buckling loads provided by EC3-1-1 (2005). Therefore, the discretisation using eight FE's and the adoption of an initial camber Δ_0 = L/750 at mid-length were deemed as adequate modelling options to numerically reproduce the buckling response of steel braces as close as possible to their expected behaviour. All the results given in the following sub-sections were thus obtained based on these and on all the other above-referred nonlinear modelling options for RC members and steel braces.

4.4.2. Seismic demand definition

The EC8-3 (2005) response acceleration spectra for the seismic assessment of this case-study were defined in Chapter 3 (see sub-section 3.4.1.), as well as the corresponding target displacements and compatible sets of accelerograms for (respectively) the nonlinear static and dynamic analysis of the bare (BF) and infilled (IN) frames. The same set of accelerograms was used herein to define the NC seismic demand for the retrofitted (DCM) frame (see Table 3.23 and Figure 3.55), but the target displacements had to be recalculated according to the capacity curves of the DCM. The same nonlinear static procedure described in sub-section 3.4.1.1. was thus carried out. Tables 4.5 and 4.6 show, respectively, the initial lateral force vectors and the obtained target displacements, while Figure 4.11 plots the capacity curves and respective NC performance points (PP's) of the DCM together with those previously obtained for the BF (see Figure 3.49). This comparison of the before- and after-retrofitting capacity curves bares evidence of the clear increase in stiffness and strength induced by the steel bracing system, as well as of the significant reduction of the target displacements for the seismic demand scenario under evaluation (as one would expect from a global retrofitting intervention such as this one – refer to Figure 2.39 (a) in Chapter 2).

Table 4.5 – Initial values of the lateral load vectors used to obtain the pushover curves of the retrofitted (DCM) frame

	Load values F_i (kN)				
Load pattern	**1st floor**	**2nd floor**	**3rd floor**	**4th floor**	**Σ F_i (kN)**
Modal	0.110	0.220	0.330	0.340	1
Uniform	0.260	0.260	0.260	0.220	1

Table 4.6 – Target displacement values d_t for the DCM (L-R: left-to-right; R-L: right-to-left)

	d_t (mm)			
Limit state	**Modal L-R**	**Modal R-L**	**Uniform L-R**	**Uniform R-L**
NC	68.8	-61.7	53.0	-49.4

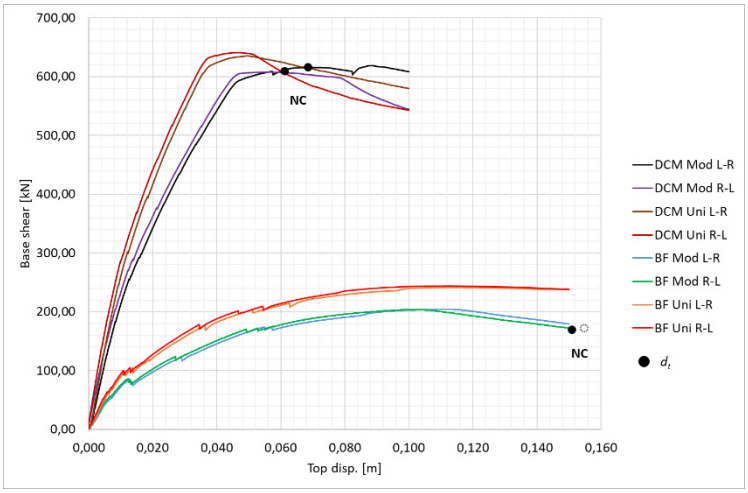

Figure 4.11 – Capacity curves and PP's of the BF and DCM: modal and uniform load patterns

4.4.3. Member capacities computation

The capacity values of this case-study's RC structural members were defined in Chapter 3 (see sub-section 3.4.2.), according to the capacity models included in Annex A of EC8-3 (2005), for deformation- and strength-controlled mechanisms (respectively, ductile and brittle). The recommendations of several authors – discussed in Chapter 2 – were followed to make the computational process less intensive and time-consuming. However, to consider constant the axial force N on columns by using the value due only to gravity loads (Mpampatsikos *et al,* 2008) stops being an admissible simplification when concentric braces are included in the structural system. Instead, a more relevant value of N that varies during the analysis should be used, at least for the columns to which the steel braces are connected. Table 4.7 below illustrates this by comparing the axial forces obtained with the nonlinear static analysis models at the NC target displacements ($N(d_t{}^{NC})$), with those due only to gravity loads (N_G), for the columns of the bare (BF) and retrofitted (DCM) frames (see Figure 4.1 for structural member numbering). Concerning the other recommendations / simplifications adopted in the capacities' calculation process, these are thought to remain admissible.

Table 4.7 – Comparison of axial forces N on columns for the BF and DCM (negative for compression)

Columns	N_G (kN)	$N(d_t{}^{NC})$ (kN)			
		BF		DCM	
		L-R	R-L	L-R	R-L
C11	-330.15	-184.27	-404.59	-198.37	-395.17
C12	-243.28	-151.56	-292.06	-158.36	-284.35
C13	-156.28	-120.19	-181.32	-110.58	-177.82
C14	-69.32	-60.47	-78.76	-50.45	-77.37
C21 (*)	-679.81	-749.24	-741.58	-340.81	-1308.74
C22 (*)	-504.65	-547.55	-540.15	-336.55	-887.61
C23 (*)	-328.63	-341.00	-335.95	-292.22	-500.71
C24 (*)	-152.01	-154.39	-151.63	-158.39	-184.88
C31 (*)	-488.94	-483.60	-440.75	-984.09	-46.95
C32 (*)	-358.16	-354.19	-327.63	-655.47	-151.22
C33 (*)	-230.37	-223.05	-218.52	-353.66	-184.49
C34 (*)	-104.28	-99.85	-98.42	-113.96	-109.64
C41	-207.30	-285.89	-116.29	-333.03	-102.35
C42	-153.96	-204.43	-98.01	-236.37	-71.56
C43	-98.62	-126.81	-75.24	-146.11	-44.54
C44	-42.14	-53.01	-38.92	-60.94	-18.26

(*) Columns to which the steel braces are connected

The admissible NC chord rotations θ_{NC} and shear forces V_{NC} were therefore recomputed, now using the axial forces $N(d_t{}^{NC})$ on the DCM columns as input parameters for the same EC8-3 (2005) expressions applied in Chapter 3. Tables 4.8 and 4.9 summarize the obtained results and compare them with those previously obtained for the BF. However, this strategy is adequate when the corresponding demands on the control sections for performance evaluation are obtained at the same target displacements. On the other hand, when running nonlinear dynamic analysis, the capacity values have to be computed at every time-step t, as a function of the corresponding axial forces $N(t)$, so that they can be compared with the corresponding demand values at each time-step. This procedure makes the

performance evaluation process much more laborious (in terms of computational effort) but ensures that a coherent comparison can be established with the results provided by the nonlinear static analysis models' safety checks. As such, it was adopted herein. The obtained time-dependent capacities (values per time-step of each accelerogram) are not listed below though, for reasons that require no further explaining. Nonetheless, the associated performance evaluation results (demand-to-capacity ratios) are presented in the next sub-section.

Table 4.8 – Chord rotation capacities θ_{NC} of columns, for the BF and the DCM, according to EC8-3 (2005)

Sections	BF	DCM		Sections	BF	DCM	
		L-R	R-L			L-R	R-L
	θ_{NC} (*mrad*)	θ_{NC} (*mrad*)	θ_{NC} (*mrad*)		θ_{NC} (*mrad*)	θ_{NC} (*mrad*)	θ_{NC} (*mrad*)
C11 bot (*)	16.18	18.67	15.07	C31 bot (*)	13.61	7.95	22.01
C11 top	21.11	24.36	19.67	C31 top	17.77	10.37	28.72
C12 bot	23.20	25.45	22.19	C32 bot	20.48	14.83	25.64
C12 top	23.20	25.45	22.19	C32 top	20.48	14.83	25.64
C13 bot (*)	17.12	18.33	16.58	C33 bot (*)	15.33	12.76	16.42
C13 top	22.34	23.92	21.64	C33 top	20.01	16.65	21.42
C14 bot	25.44	26.16	25.13	C34 bot	24.14	23.80	23.95
C14 top	25.44	26.16	25.13	C34 top	24.14	23.80	23.95
C21 bot (*)	10.61	12.91	7.37	C41 bot (*)	17.27	14.40	20.11
C21 top	13.85	16.85	9.62	C41 top	22.54	18.79	26.24
C22 bot	15.33	16.90	12.28	C42 bot	24.35	21.61	27.44
C22 top	15.33	16.90	12.28	C42 top	24.35	21.61	27.44
C23 bot (*)	11.57	11.98	9.82	C43 bot (*)	17.94	16.32	19.97
C23 top	15.10	15.64	12.82	C43 top	23.41	21.30	26.07
C24 bot	17.87	17.77	17.32	C44 bot	26.19	25.23	27.46
C24 top	17.87	17.77	17.32	C44 top	26.19	25.23	27.46

(*) Sections with reinforcement lap-splice

Table 4.9 – Shear capacities V_{NC} of columns, for the BF and the DCM, according to EC8-3 (2005)

Sections	BF	DCM		Sections	BF	DCM	
		L-R	R-L			L-R	R-L
	V_{NC} (kN)	V_{NC} (kN)	V_{NC} (kN)		V_{NC} (kN)	V_{NC} (kN)	V_{NC} (kN)
C11 bot (*)	30.10	24.39	30.16	C31 bot (*)	31.66	31.81	19.29
C11 top	29.65	23.90	29.73	C31 top	31.22	31.48	18.69
C12 bot	25.86	22.15	27.65	C32 bot	31.13	31.31	23.26
C12 top	25.86	22.15	27.65	C32 top	31.13	31.31	23.26
C13 bot (*)	21.93	19.94	22.87	C33 bot (*)	25.15	25.68	23.15
C13 top	21.45	19.44	22.39	C33 top	24.70	25.27	22.69
C14 bot	17.63	16.80	17.98	C34 bot	19.17	19.59	19.40
C14 top	17.63	16.80	17.98	C34 top	19.17	19.59	19.40
C21 bot (*)	142.18	129.66	142.18	C41 bot (*)	24.80	26.62	20.24
C21 top	142.18	126.98	142.18	C41 top	24.34	26.20	19.73
C22 bot	142.18	126.42	142.18	C42 bot	22.00	25.61	18.38
C22 top	142.18	126.42	142.18	C42 top	22.00	25.61	18.38
C23 bot (*)	88.07	84.12	98.78	C43 bot (*)	19.44	21.51	17.08
C23 top	86.48	82.50	97.34	C43 top	18.95	21.05	16.56
C24 bot	67.15	67.85	70.75	C44 bot	16.45	17.28	15.39
C24 top	67.15	67.85	70.75	C44 top	16.45	17.28	15.39

(*) Sections with reinforcement lap-splice

4.4.4. Performance evaluation

The performance evaluation results obtained with the two methods of analysis are given below, in terms of demand-to-capacity ratios (D_i/C_i) for each control section i, using the customary graphical representation. In the case of the nonlinear static (pushover) analysis models, the demand values on structural members were obtained at the NC target displacements corresponding to each lateral load pattern and seismic action sense. The associated D/C ratios presented below thus correspond to the most unfavourable results among those obtained on each control section. On the other hand, the D/C ratios shown for the nonlinear dynamic analysis models are the mean values over the most unfavourable results obtained within the scaled set of ground acceleration records. Figures 4.12 and 4.14 show the chord rotation D/C ratios on the columns of the retrofitted (DCM) frame, while figures 4.13 and 4.15 show the corresponding shear force D/C ratios.

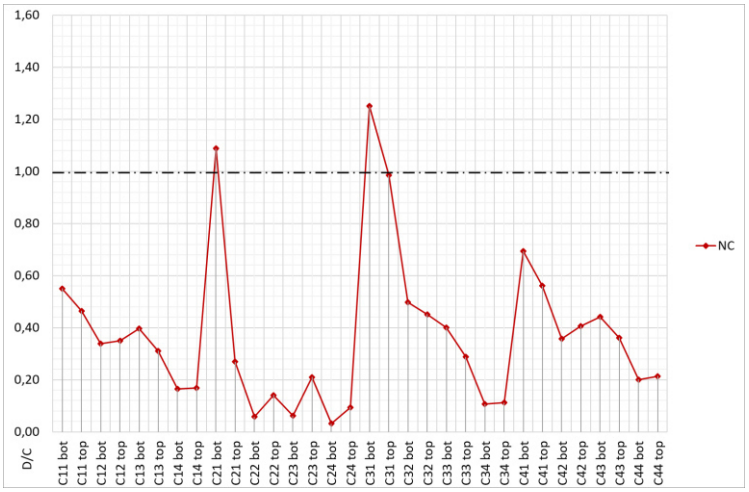

Figure 4.12 – DCM: NC chord rotation D/C ratios on columns (pushover analysis results)

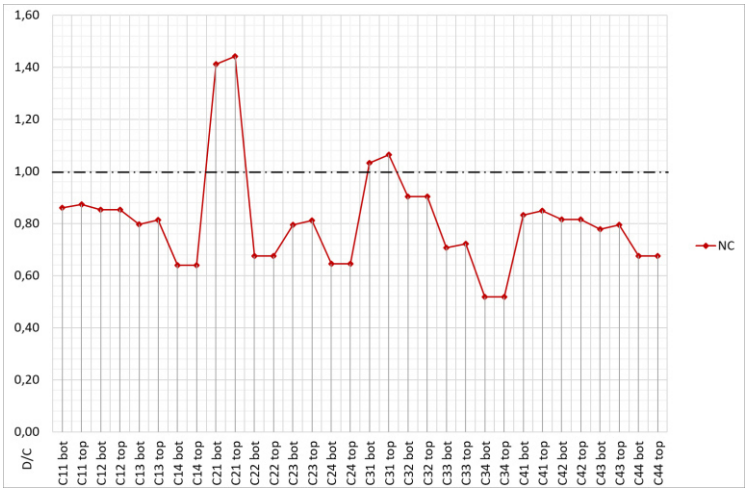

Figure 4.13 – DCM: NC shear force D/C ratios on columns (pushover analysis results)

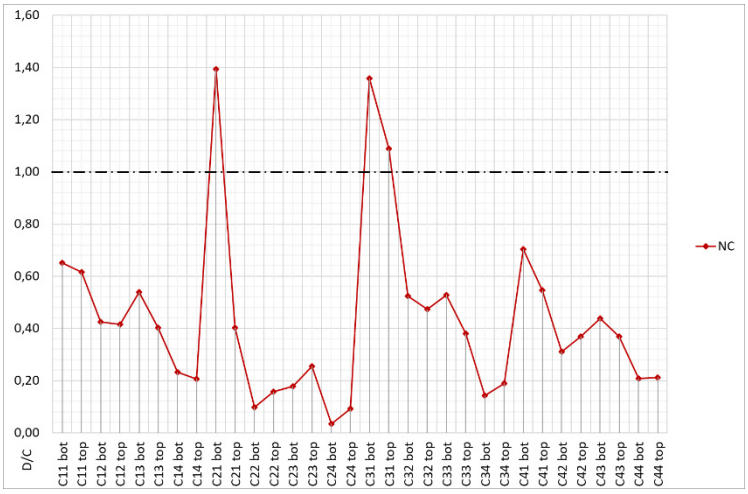

Figure 4.14 – DCM: NC chord rotation D/C ratios on columns (nonlinear dynamic analysis results)

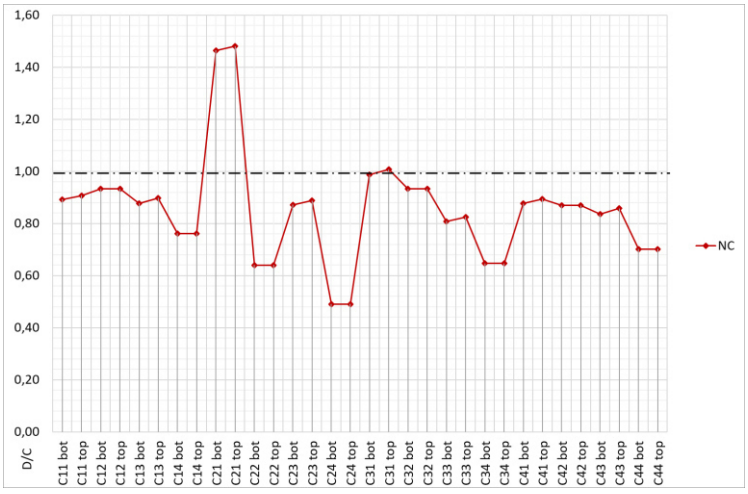

Figure 4.15 – DCM: NC shear force D/C ratios on columns (nonlinear dynamic analysis results)

4.4.5. Discussion

The D/C ratios presented above show a different picture than the one provided by the results given in sub-section 4.3.3. (i.e., the outcome of the q-factor approach). Effectively, values above 1.0 were obtained on two columns (C2 and C3) at the first storey, both for deformation- and strength-controlled collapse mechanisms. This shows that the considered strengthening system is, in fact, unable to reduce the seismic demands on all structural members to values below the corresponding capacities, hence leading to the conclusion that the retrofitted (DCM) frame should, after all, be deemed unsafe for the LS of NC according to EC8-3 (2005). The conclusions were the same regardless of the analysis type (nonlinear static or dynamic), both in terms of D/C ratios and of global storey parameters (see Table 4.10 below). This further encourages the use of the nonlinear static approach as a swift way to evaluate the seismic performance of similarly retrofitted frames and is in line with the conclusions presented on this matter in sub-section 3.4.3.3. (Chapter 3).

Table 4.10 – Global storey parameters: nonlinear static (PSHVR) vs. dynamic (NLDA) analyses results

	Floor Displacement (*mm*)		Inter-storey drift (%)		Base shear (*kN*)	
DCM	**PSHVR**	**NLDA**	**PSHVR**	**NLDA**	**PSHVR**	**NLDA**
Storey 4	68.8	67.7	0.29%	0.32%	-	-
Storey 3	61.0	59.7	0.56%	0.58%	-	-
Storey 2	45.9	45.4	0.73%	0.60%	-	-
Storey 1	26.3	29.8	0.98%	1.10%	615.43	606.55

The alternative retrofitting system (DCL) designed in sub-section 4.3.2. was deemed inadequate for being too robust (i.e., the safety checks performed in sub-section 4.3.3. indicated that excessive axial force had been induced on column C3). In order to confirm this conclusion, the DCL frame was also tested herein under nonlinear static conditions. However, the plot of the capacity curve was interrupted at an early stage, during the L-R pushover, due to convergence difficulties in the numerical model. A closer look at the axial forces installed in the lower RC columns revealed that the capacity of column C31 had been reached, causing this member to collapse (hence the convergence issues). Figure 4.16 shows the *N-M* interaction diagram for column C31, indicating the evolution of the installed forces until the analysis stopped converging. As such, the DCL frame was confirmed to be unsafe for the LS of NC according to EC8-3 (2005).

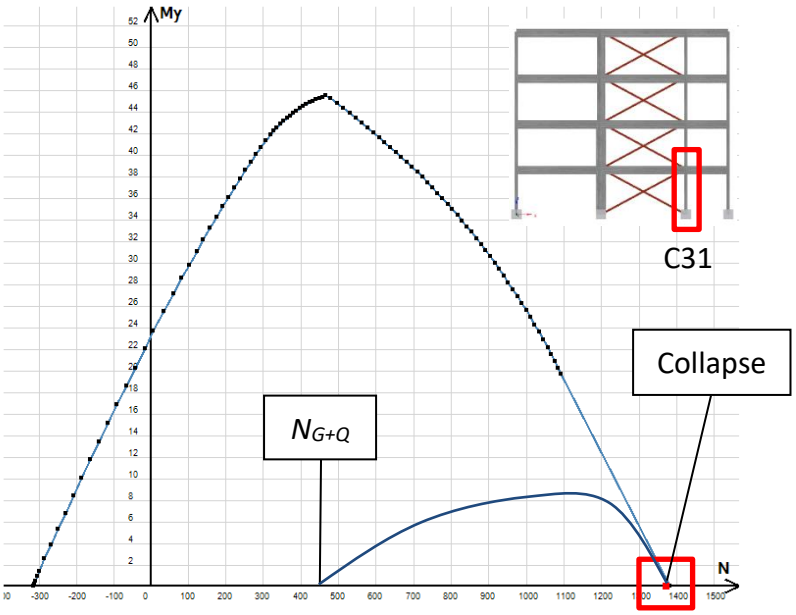

Figure 4.16 – Evolution of the installed forces on column C31 during the L-R pushover analysis

At this point, both bracing systems (DCM and DCL) had been proved unable to make the retrofitted structures fulfil the EC8-3 (2005) performance requirements for the LS of NC, thus raising several questions about the adequacy of the FBD methodology presented in section 4.3, when applied to the design of such hybrid RC-steel structural systems. However, as room seemed to exist between these two retrofitting solutions, an iterative process was carried out to look for an alternative able to comply

with the applicable performance requirements, without being too robust as to induce the premature collapse of the RC columns. Several brace cross-section combinations were then tested, and the associated capacity curves obtained, while the evolution of the axial forces on columns was monitored to detect premature collapse scenarios. New target displacements were determined and evaluated together with the capacity curves, following a deformation control approach. The EC8-3 (2005) seismic assessment procedure was then carried out for the most promising brace combinations, and an acceptable retrofitting solution was finally found. Figure 4.17 plots the capacity curves and corresponding NC performance points (PP's) of the retrofitted (FINAL) frame, together with those previously obtained for the DCM, while figures 4.18 and 4.19 show, respectively, the chord rotation and shear force D/C ratios on the columns of the FINAL frame. The cross-sections of the FINAL bracing system are also indicated in Figure 4.17.

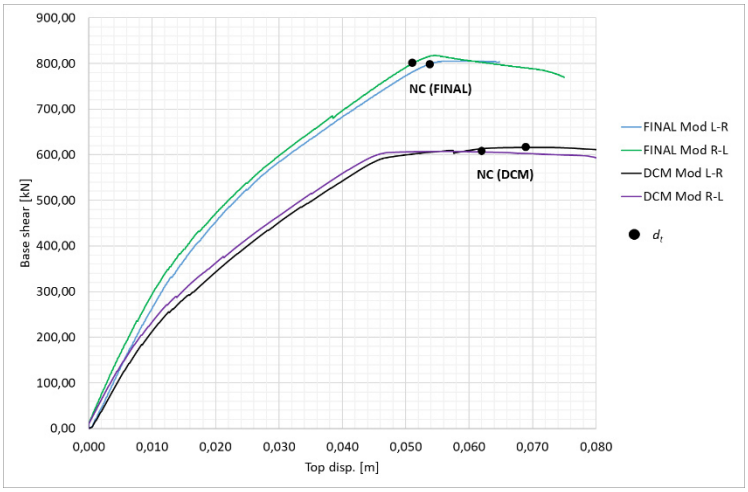

	FINAL
Storey	Cross-section
4	CHSH 88.9x3.2
3	CHSH 114.3x3.6
2	CHSH 139.7x3.6
1	CHSH 139.7x4.0

Figure 4.17 – Capacity curves and PP's of the DCM and FINAL: modal load pattern

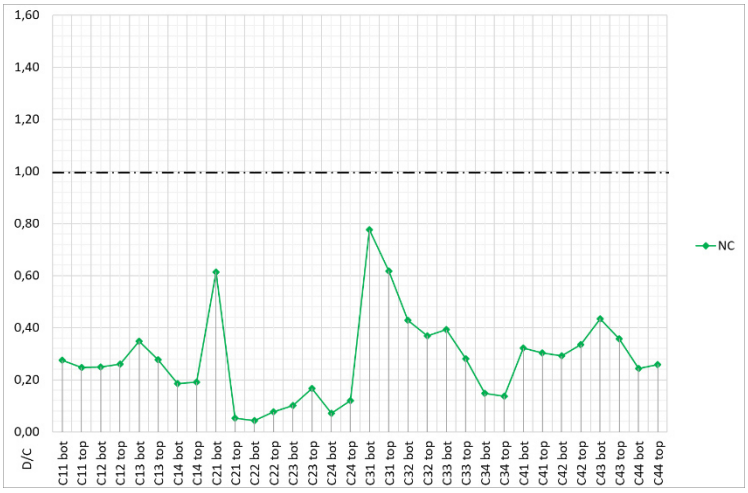

Figure 4.18 – FINAL: NC chord rotation D/C ratios on columns (pushover analysis results)

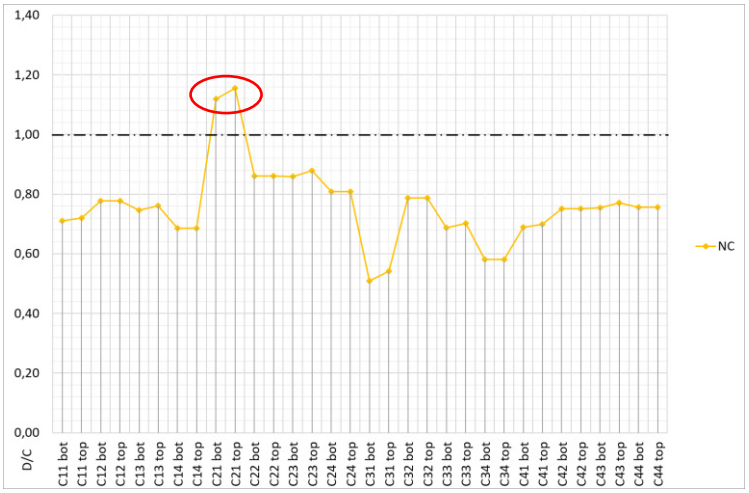

Figure 4.19 – FINAL: NC shear force D/C ratios on columns (pushover analysis results)

The D/C ratios presented above show that no values above 1.0 were obtained for the FINAL solution, except on column C21 (1st storey's strong column) in terms of shear force capacity. In fact, the results obtained during the iterative design process indicate that it is highly unlikely that the shear demand on this column can be reduced to a value below its corresponding capacity only through the action of a global retrofitting system based on concentric steel braces. However, this isolated issue can be efficiently solved through local capacity upgrading (e.g., using steel plates or FRP wrapping), as demonstrated by the Imperial College of London research group during the ICONS research programme (Elnashai and Pinho, 1999). Therefore, provided such an additional local intervention is implemented along the span of column C21, the FINAL bracing system may be deemed adequate to make the frame fulfil the EC8-3 (2005) performance requirements for the LS of NC. Table 4.11 compares key global parameters between the bare (BF) and retrofitted (DCM; FINAL) frames, in order to illustrate the evolution that needed to occur in terms of stiffness (indirectly represented by the fundamental periods) and lateral resistance until a satisfactory design was achieved. The ratio of the NC elastic base shear values to the corresponding assessment base shear values (obtained from the nonlinear analysis models) is also given at the end of Table 4.11.

Table 4.11 – Bare (BF) and retrofitted (DCM; FINAL) frames: comparison of key global parameters

	BF	DCM	FINAL
Fundamental period T_1 (sec) (*)	0.94	0.45	0.40
Spectral corner period T_c (sec)	0.60	0.60	0.60
NC spectral acceleration $S_{e,NC}$ (T_1)	0.46768 · g	0.73269 · g	0.73269 · g
Total mass m (ton)	173.93	173.93	173.93
Elastic base shear V_e (kN)	683.72	1062.63	1062.63
Assessment (PSHVR) base shear V_b (kN)	204.05	615.43	817.15
V_e/V_b	3.35	1.73	1.30

(*) effective (secant-to-yield) stiffness EI_{eff} of RC elements taken as 50% of their gross stiffness EI

Finally, it should be recalled that two behaviour factors *q* corresponding to different ductility classes were considered for the design of the initial retrofitting systems (DCL: $q = 1.5$; DCM: $q = 3.0$), with direct influence over the seismic forces acting on the steel braces. However, the performance evaluation results presented in sub-section 4.4.4., along with the base shear parameters given above in Table 4.11, deem them inadequate for the retrofitting problem at hand. This conclusion further suggests that the FBD methodology might not be an efficient approach to the design of steel-braced retrofitting solutions for RC buildings with inadequate seismic behaviour and begs the need for a more adequate design method.

4.5. CONCLUDING REMARKS

The application of conventional (force-based) seismic design methodologies to hybrid RC-steel systems was addressed during this chapter. The *q*-factor based EC8-3 (2005) seismic assessment procedure was reviewed, and a case-study application was presented to demonstrate the difficulties a practitioner experiences when assessing the efficiency of a steel-brace retrofitting system designed within the framework of EC8-1 (2004). The chosen RC structure was the same used in Chapter 3 to illustrate the EC8-3 (2005) performance-based seismic assessment procedure. The performance of the obtained retrofitted structure was then evaluated using nonlinear methods of analysis. The obtained results were discussed in light of the EC8-3 (2005) performance requirements, and conclusions were drawn about the adequacy of the *q*-factor approach to the design of such structural systems. Finally, some comments were made on how to carry out a better design process.

The conducted study demonstrated that the FBD process gives no guarantees in terms of adequate seismic behaviour of the retrofitted structures. In this case, an adequate strengthening system was eventually found – without the explicit consideration of behaviour factors – but within an extremely laborious seismic assessment iterative process. Further research on this matter is thus needed to develop an effective performance-based design methodology, that takes explicit consideration of the interaction between both structural systems (RC structure and steel braces), namely the influence of the steel braces' resistance on the deformation capacity of the RC members. The author hopes that these findings will help researchers and practitioners become more aware of the likely error associated with the several adjustments that need to be introduced in conventional seismic code provisions in order to try to apply them to a hybrid RC-steel system.

The final note to this chapter is in line with that of the previous one. It is not likely that the above-referred research line will yield performance-based design methodologies that can be efficiently applied within a linear elastic analysis context. Therefore, the author (again) states and expects that professionals involved with the seismic assessment and retrofitting of existing structures pursue the necessary actions to become familiarized with more advanced methods of analysis, under pain of making gross judgement errors and/or becoming obsolete.

CHAPTER 4 – ON THE APPLICABILITY OF CONVENTIONAL SEISMIC DESIGN METHODOLOGIES TO HYBRID RC-STEEL SYSTEMS

4.1. INTRODUCTION 4.1

4.2. THE *Q*-FACTOR APPROACH IN EC8-3 ..... 4.2

4.3. APPLICATION TO A RETROFITTING CASE STUDY 4.3

4.3.1. Structural characterization 4.4

4.3.2. Design of the retrofitting system 4.5

4.3.3. RC member safety checks 4.6

4.4. EVALUATION OF THE DESIGNED RETROFITTING SYSTEM 4.8

4.4.1. Nonlinear modelling 4.9

4.4.2. Seismic demand definition 4.13

4.4.3. Member capacities computation 4.14

4.4.4. Performance evaluation 4.16

4.4.5. Discussion 4.17

4.5. CONCLUDING REMARKS 4.21

CHAPTER 5

A NEW DISPLACEMENT-BASED DESIGN PROCEDURE FOR THE RETROFITTING OF RC BUILDINGS WITH STEEL BRACES

5.1. INTRODUCTION

The merits of employing steel braces to improve the seismic behaviour of existing RC buildings have been demonstrated in the previous chapters of this work. Regarding the available design procedures, Chapter 4 evaluated the adequacy of the conventional (force-based) methodology, demonstrating that the process (with its associated behaviour factors) gives no guarantees in terms of adequate seismic behaviour of the retrofitted structures. This conclusion further stressed the need for the development of alternative design procedures dedicated to this type of hybrid RC-steel systems. Reference to the attempts of several authors to explore the displacement-based design (DBD) approach had already been made in the final sections of Chapter 2, pointing out the advantages of adopting a performance-based design methodology. Nonetheless, the limited scope of those studies (e.g., the low-rise of the analysed structures), as well as the apparent inadequacy of some assumptions to the design of retrofitting systems, called for further developments.

A new displacement-based methodology for the design of concentric steel-brace retrofitting systems for RC framed buildings is thus proposed in this chapter, aimed at obtaining retrofitted structures with better and more predictable seismic performance. This methodology – which follows up on a previously referred study by Sousa and Castro (2012) – relies on deformation control for different levels of seismic intensity, and explicitly considers the interaction between both structural systems (RC structure and steel braces), namely the influence of the steel braces' resistance on the deformation capacity of RC members. In the following sections, the fundamental bases of the procedure are described, followed by the definition of the required primary data, and step-by-step explanation of the design process's general workflow. Afterwards, an application example is carried out for the same RC building studied in the previous chapters. The performance of the obtained retrofitted structure is then addressed, as well as the considered design assumptions and the advantages of the proposed methodology over the traditional design process. Finally, to demonstrate that the procedure is robust enough to be applied systematically by practitioners involved with such matters, it is extensively validated and calibrated using a sample of artificially generated pre-code RC buildings, but the presentation of that study is reserved for Chapter 6.

5.2. BASES OF THE PROCEDURE

The seismic behaviour of RC frames retrofitted with concentric steel braces was thoroughly addressed in Chapter 2 (see section 2.9.), namely that of the two independent structural systems, as well as the interaction between them. Due to the complexity of the latter, it is of prime importance that the design procedure used in the retrofitting process accounts for the response modifications experienced by the structure during lateral excitation. To this end, the proposed methodology is partially based on the equivalent linearization approach adopted by the Capacity Spectrum Method (see sub-section 2.7.2.1. in Chapter 2), as it provides a particularly accurate treatment of the reduction of seismic demand for increasing displacement. Moreover, the combined graphical representation of the global force-displacement capacity curve with the earthquake response spectrum provides a clear picture on how the building responds to the seismic demand, and how a chosen retrofitting technique may impact its response capacity. The proposed methodology then extends the direct displacement-based design (DDBD) approach (see sub-section 2.10.2. in Chapter 2) to steel-braced RC buildings, using it to determine the required lateral strength of the retrofitted structure so that the specified displacement limit can be achieved under the design-level earthquake. In the final steps, a simple capacity design procedure is enforced to obtain the distribution of the braces' strength over the height of the building (i.e., to define the cross-sections of the braces for the upper storeys).

The successful application of a procedure relying on equivalent linearization depends on the assumed lateral displacement shape. As previously referred (in the context of the DDBD approach), the latter should be that which corresponds to the inelastic first mode of the structure at the design level of seismic excitation. This ensures that changes to the elastic first mode shape, resulting from local changes to member stiffness caused by inelastic action in plastic hinges, are considered at the beginning of the design, which is consistent with characterizing the structure by its secant stiffness to maximum response. Approximate expressions proposed by Priestley *et al* (2007) to define displacement shapes for RC framed buildings were referred in Chapter 2. Concerning hybrid RC-steel systems, Pincheira and Jirsa (1995) concluded that such lateral displacement shapes are relatively uniform and storey drifts vary smoothly over the height of the building (even close to collapse, the behaviour of the structure is relatively stable, indicating that the steel braces are able to control damage accumulation over the height of the building). Later on, Sousa (2010) conducted a study using a 1-bay, 3-storey pre-code RC frame retrofitted with steel braces and ran nonlinear dynamic analyses to obtain the deformed shapes at peak displacement response. The obtained results were then plotted against those provided by the above-referred expressions, leading to the conclusion that the steel braces impose higher control of displacements over the height of the building. As the retrofitted structure designed in Chapter 4 has a larger number of storeys and bays than those of the one studied by Sousa (2010) – plus the brace cross-sections' variation along the height of the building – a similar study was conducted herein. The obtained conclusions are essentially the same, but the study was important to build confidence regarding the approach to follow when estimating the lateral displacement shapes within the workflow of the developed design procedure. More important than being very accurate, the critical issue is that the chosen shape should be such that leads to a safe design of the retrofitting system, without being overly conservative. More details on this particular step are given further ahead.

The final purpose of the developed design methodology is thus to obtain a set of steel braces for the RC building under analysis, such that the resulting hybrid system exhibits adequate performance under the design earthquake (meaning that the global deformation demand does not lead to the failure of critical RC elements). From the capacity curve of the original RC structure and a pre-selection of the braces' layout and properties, one can estimate the performance of the retrofitted structure without having to run numerical analyses for several brace configurations. Two other main input parameters to the procedure are the retrofitted structure's yield and design displacements (Δ_y and Δ_d, respectively), which are addressed below in detail. The procedure is thought to be versatile enough to be used in practical applications, while producing reliable solutions and therefore promoting the retrofitting of RC frames with steel braces.

5.3. STEPS OF THE PROCEDURE

The proposed methodology is organized in three main stages: (i) primary data compilation; (ii) design process; (iii) validation process. The first stage defines and organizes data which are required to support the design process carried out in the second stage. The third stage then evaluates the performance of the retrofitted structure, as well as the design assumptions. The following sub-sections thoroughly describe the steps included in each stage.

5.3.1. Primary data compilation

Before the design process of the retrofitting system can be carried out, the following preliminary steps are required to put together a set of fundamental data:

i. Definition of the seismic action for the applicable limit state(s) (LS);
ii. Nonlinear static analysis of the original structure, to obtain the capacity curve;
iii. Evaluation of the critical RC columns' axial force capacity envelope;
iv. Pre-selection of steel brace properties;
v. Selection of the expected inelastic lateral displacement shape δ_i.

The seismic action is represented through the EC8-1 (2004) response acceleration spectrum, derived considering: (i) the seismic hazard of the location in question; (ii) a viscous damping ratio ξ_0 of 5%; (iii) the LS to be verified according to EC8-3 (2005). The spectrum is plotted in ADRS format (S_a vs. S_d), as per the requirements of the Capacity Spectrum Method (CSM), so that it can be used to evaluate the effective seismic demand on the original and retrofitted structures. The capacity curve of the original structure is then obtained through an adaptive displacement-based pushover analysis, as to avoid the drawbacks of using the fixed load pattern. Moreover, as referred in Chapter 2, the inelastic shape profiles of pre-code RC structures are best defined through this procedure, which is fully in line with the performance-based approach adopted herein. At this point, an expedite assessment of the original structure can be carried out using the CSM. Not being able to resist the design earthquake, its capacity curve (converted to ADRS format) will not intersect the demand spectrum derived for the equivalent viscous damping (EVD) ratio corresponding to the structure's maximum displacement ductility ratio μ_Δ. Therefore, a performance point will be impossible to determine.

Evaluating the axial force capacity of the columns located on the frames' bays to be braced is essential to find the allowed additional axial loads that can be induced by the retrofitting system without leading to the premature failure of those RC members. As previously referred in Chapter 2 (see sub-section 2.9.2.), the swiftest way to evaluate this is to plot the axial load-bending moment interaction diagram of each of the affected RC columns, together with the corresponding points representing the initial loading conditions due only to gravity loads. Having done so, a pre-selection of steel brace cross-sections can be carried out, considering material thicknesses $t \geq 3$ *mm* so that the EC3-1-1 (2005) basic design rules for steel structures remain applicable. In terms of limits to the brace members' non-dimensional slenderness $\bar{\lambda}$, values in the range $1.5 < \bar{\lambda} \leq 2.5$ seem to ensure satisfactory results, hence this is the interval proposed herein. The potential increase in the RC columns' axial forces can then be estimated as discussed earlier in Chapter 2 (see sub-sections 2.9.1. and 2.9.3.), based on the steel braces' nominal capacities in tension and compression, helping to narrow down the list of cross-sections that may be used in the design of the retrofitting system. If, by chance, a very limitative situation is encountered already at this point, the option to locally strengthen the columns to which the steel braces will be attached (e.g., using FRP jacketing) should be considered.

Lastly, selecting an inelastic lateral displacement shape for the retrofitted structure is essential to determine the characteristics of the equivalent SDOF system required by the DDBD approach on which the proposed design methodology is based. However, as referred above, the approximation needs only be good enough as to provide a safe design of the steel braces. The results provided by the retrofitted structure designed in this chapter – as well as by those designed in the next – show that, at least for RC frames up to 6 storeys on which an adequately designed retrofitting system has been installed, the actual lateral displacement profiles seem to lie in between the linear shape and that provided by the approximate expression proposed by Priestley *et al* (2007) for RC frame buildings with more than 4 storeys (expression (2.61b) in Chapter 2). Moreover, several tests carried out during the development of the proposed procedure showed that assuming a shape closer to that given by the referred expression provides better design results (i.e., on the safer side), but this conclusion will be discussed further ahead in Chapter 6.

5.3.2. Design process

Having concluded the five preliminary steps described above, the design process of the retrofitting system can now be carried out following the steps below:

vi. Estimation of the yield displacement Δ_y;
vii. Definition of the design displacement Δ_d;
viii. Evaluation of the EVD ratio ξ based on the estimated ductility demand μ_Δ;
ix. Determination of the effective period T_e at maximum displacement response;
x. Determination of the secant stiffness K_e at maximum displacement response;
xi. Quantification of the required lateral strength ${V_b}^{REQ}$ of the retrofitted structure;
xii. Selection of the steel braces for the first storey;
xiii. Selection of the steel braces for the upper storeys.

The global deformed shape of a steel-braced RC frame under lateral loading was already analysed in Chapter 2 with the help of Figure 2.57, the latter being reproduced below as Figure 5.1 for the reader's convenience (blue for tensioned braces; red for compressed braces). Figure 5.2 then plots what could be the capacity curve of this structure, together with the evolution of the axial forces on the tensioned and compressed braces located at the first storey (the plot corresponds to an actual 5-bay, 2-storey RC building retrofitted with hot-rolled circular hollow section (CHSH) steel braces). On this plot, the dashed vertical line marks the displacement d_y that corresponds to the yielding of the tensioned brace (point *A*), which relates well to the onset of the global yielding of the structure (point *B*), as also discussed in Chapter 2 (see sub-section 2.9.3.). Therefore, the main idea underlying step vi. is to estimate the lateral displacement Δ_y at the frame's first floor, which causes the corresponding steel brace to yield in tension. This will be achieved through some simple geometric considerations, based on the deformed shape's components shown in Figure 5.1, and by introducing an approximation that is acceptable given the purpose at hand.

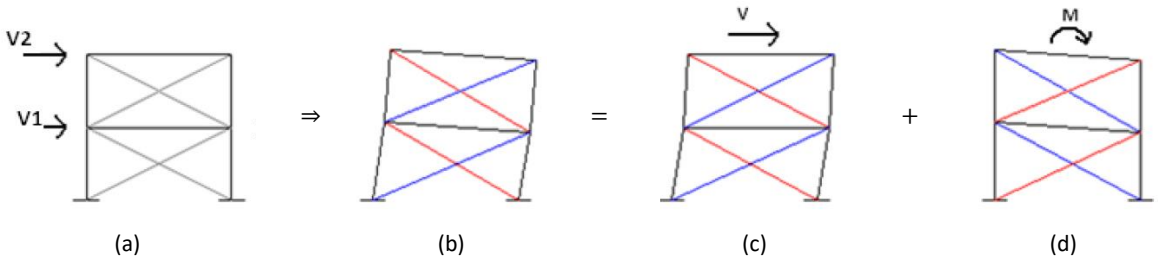

Figure 5.1 – Deformation of a hybrid RC-steel system: (a) undeformed frame with applied lateral loading; (b) deformation due to applied lateral loading; (c) frame distortion due to shear force; (d) frame rotation due to overturning moment (adapted from Sousa, 2010)

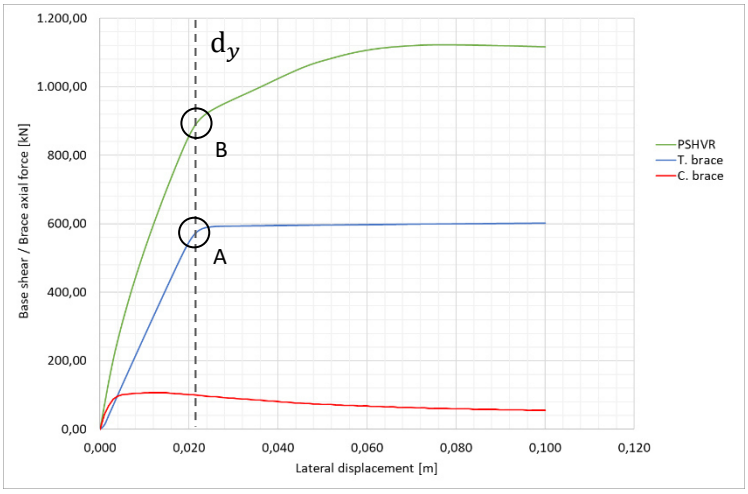

Figure 5.2 – Capacity curve (green) of the hybrid RC-steel system vs. evolution of the axial forces on the tensioned (blue) and compressed (red) steel braces located at the frame's first storey

The geometric parameters of the frame's deformed shape are given in Figure 5.3: B is the bay length; h is the storey height; L_i is the initial length of the braces; L_f is the deformed length of the tensioned brace due to shear force distortion; d_h is the lateral displacement at the first floor; d_v is the axial deformation of the RC columns due to the overturning moment's effect. The initial length L_i is given by Expression (5.1), while the deformed length L_f is provided by Expression (5.2). If one wishes to also consider the axial deformation of the compressed RC column in the calculation of the tensioned brace's deformed length, then Expression (5.3) should be applied instead. However, as the magnitude of the axial deformation is typically much smaller than that of the imposed lateral displacement, the approximation provided by Expression (5.2) will be quite good. In fact, a numerical study carried out by Sousa (2010) demonstrates that, at least for low- and mid-rise structures, the error introduced by this approximation is largely compensated by the simplification it provides.

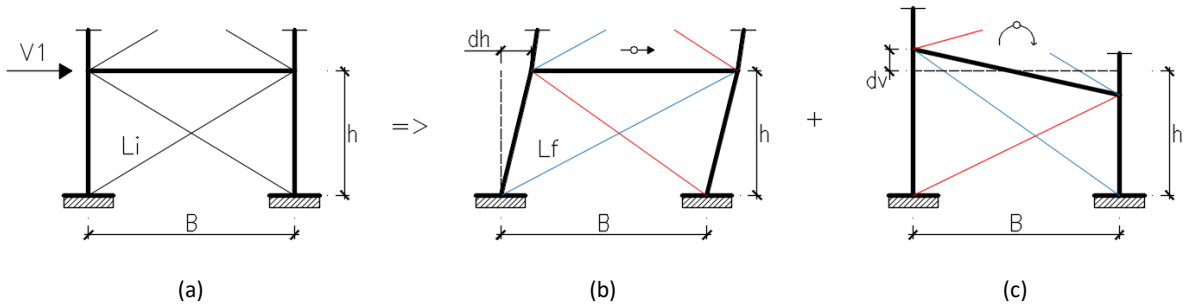

Figure 5.3 – Geometric decomposition of the deformed shape: (a) initial conditions; (b) distortion component due to shear force; (c) rotation component due to overturning moment

$$L_i = \sqrt{B^2 + h^2} \tag{5.1}$$

$$L_f = \sqrt{(B + d_h)^2 + h^2} \tag{5.2}$$

$$L_{f+m} = \sqrt{(B + d_h)^2 + (h + d_v)^2} \tag{5.3}$$

At yielding, the elongation Δ_{yb} of the tensioned brace is given by Expression (5.4), where ε_y is the applicable material yield strain. The corresponding deformed length is then obtained adding Δ_{yb} to the initial length L_i. If in Expression (5.2) the deformed length L_f is made equal to $\left(L_i + \Delta_{yb}\right)$, then the terms can be rearranged to obtain a new expression – Expression (5.5) – that will be used henceforth to estimate the lateral displacement $d_h \left(= \Delta_y\right)$ at the first floor, which causes the tensioned brace to yield. It is noteworthy that the above-referred approximation allows for this estimate to be independent of the strength of the retrofitting system to be installed, therefore contributing to the design procedure's efficiency.

$$\Delta_{yb} = \varepsilon_y \cdot L_i \tag{5.4}$$

$$\Delta_y = \sqrt{\left(L_i + \varepsilon_y \cdot L_i\right)^2 - h^2} - B \tag{5.5}$$

Having determined the yield displacement Δ_y at the first floor of the building, the equivalent SDOF system's yield displacement S_{Δ_y} can be determined using Expression (5.6), where m_i is the mass of the i^{th} storey; δ_i is the selected inelastic lateral displacement shape; and δ_1 is the value of the latter at the first floor. This expression is obtained combining expressions (2.58) and (2.60), both referred in Chapter 2 (see sub-section 2.10.2.).

$$S_{\Delta_y} = \frac{\sum m_i \cdot {\delta_i}^2}{\sum m_i \cdot \delta_i} \cdot \frac{\Delta_y}{\delta_1} \tag{5.6}$$

Past the point of yielding, the design displacement of the hybrid system is governed by the capacity (either shear force or deformation) of the most critical RC member(s), which will typically be among the base columns. Such capacities are determined according to the brittle and ductile failure models proposed in Annex A of EC8-3 (2005), which have already been thoroughly discussed in Chapter 2 (see sub-section 2.7.1.4.). For this purpose, an estimate of the axial loads installed in the columns at the performance point is essential. For those that don't have any steel braces attached to them, the axial forces can be obtained directly from the nonlinear static analysis performed in step ii. For the others, the additional axial loads induced by the bracing system must also be considered. However, at this point the cross-sections of the braces are not known at any of the building's storeys, hence an initial assumption has to be made, for instance, taking the lightest bracing setup provided by the pre-selection that was carried out in step iv. The sum of the vertical components of the forces acting over the height of the structure can then be conservatively evaluated and used to compute the required shear force and deformation capacities, under the assumption that all braces are at their maximum (tensile and compressive) strengths. It is noteworthy that, however important, the accuracy of this first estimate needs not be a major concern, as it is evaluated further ahead and, if need be, iteratively improved until a defined tolerance is achieved.

The design displacement Δ_d at the first floor of the building can now be defined (step vii.) depending on the failure mechanism of the critical RC column(s) at limit state: (i) if governed by deformation capacity, the maximum drift of the first storey (Δ_d/h) is conservatively estimated as being equal to the computed chord rotation capacity θ_{LS} (Mpampatsikos *et al,* 2008); (ii) if governed by shear force capacity, the maximum displacement Δ_d is taken equal to that which causes the column(s)' shear demand to be equal to the computed shear force capacity V_{LS} (this can be easily obtained from the nonlinear static analysis performed in step ii.). The equivalent SDOF system's design displacement S_{Δ_d} is then obtained computing the value of Δ_d in Expression (5.6), instead of that of Δ_y. It should be noted that the results of the seismic assessment of the original structure already indicate which RC columns

may be critical and what might their governing LS mechanisms be. However, due to the changes induced in the capacities by the variation of the axial forces, and the fact that the latter work in opposition (i.e., the increase in a column's axial force will reduce its deformation capacity while enhancing its shear force capacity, and vice-versa), caution is advised. It should also be noted that, when shear force capacities are very limited, relatively low values of Δ_d are usually found, indicating that some local strengthening of the columns will most likely be necessary.

Knowing both the yielding and the design displacements, the estimated ductility demand μ_Δ is given by Expression (5.7). Based on this value, the EVD ratio ξ (which represents the combined effect of elastic damping and hysteretic energy absorption during inelastic response, as previously discussed in sub-sections 2.7.2.1. and 2.10.2.) is then evaluated. For this purpose, as no specific expressions exist for steel-braced RC frames, the one proposed by Priestley *et al* (2007) for concrete frame buildings is adopted herein (Expression (2.62a) in Chapter 2, reproduced below as Expression (5.8) for the reader's convenience). The actual value of ξ for the hybrid structure is expected to fall between the one obtained and that given by the expression proposed by Priestley *et al* (2007) for steel frame buildings (Expression (2.62b) in Chapter 2). Therefore, Expression (5.8) is believed to provide a conservative (yet accurate enough) evaluation of the applicable EVD ratio. Based on this estimate, the response spectrum defined in step i. is scaled down to appropriately represent the nonlinear demand at the design displacement S_{Δ_d}. This procedure requires the calculation of the damping correction factor η, which is a function of ξ. Clause 3.2.2.2 in EC8-1 (2004) proposes a well-known expression for the computation of η. However, a different one – Expression (5.9) – is adopted herein, following the recommendations of Sullivan *et al* (2012). The latter are based on the findings of Pennucci *et al* (2011, 2011a), which state that EVD expressions for nonlinear systems, calibrated using nonlinear dynamic analyses (NLDA), should be used in combination with the spectral damping reduction expression that characterises the records used for the NLDA. As the damping reduction factors for the records used in the development of the EVD expressions proposed by Priestley *et al* (2007) are best described by Expression (5.9), the latter is recommended for structures responding inelastically. This concludes step viii. of the design process.

$$\mu_\Delta = \frac{\Delta_d}{\Delta_y} = \frac{S_{\Delta_d}}{S_{\Delta_y}} \geq 1 \tag{5.7}$$

$$\xi = 0.05 + 0.565 \cdot \left(\frac{\mu_\Delta - 1}{\mu_\Delta \cdot \pi}\right) \tag{5.8}$$

$$\eta = \sqrt{\frac{0.07}{0.02 + \xi}} \tag{5.9}$$

With the value of the design displacement S_{Δ_d}, the effective period T_e at maximum displacement response can easily be read from the reduced demand spectrum. Afterwards, the secant stiffness K_e at maximum displacement response is determined using Expression (5.10), where m_e is the effective

mass of the equivalent SDOF system, given by Expression (5.11). Finally, the required lateral strength ${V_b}^{REQ}$ of the retrofitted structure is quantified using Expression (5.12), which concludes steps ix. to xi. of the design process.

$$K_e = \frac{4 \cdot \pi^2 \cdot m_e}{{T_e}^2} \tag{5.10}$$

$$m_e = \frac{(\sum m_i \cdot \delta_i)^2}{\sum m_i \cdot {\delta_i}^2} \tag{5.11}$$

$${V_b}^{REQ} = K_e \cdot S_{\Delta_d} \tag{5.12}$$

The increment to the original structure's base shear resistance depends solely on the braces located at the first storey, as discussed in Chapter 2 (see sub-section 2.9.3.). Therefore, knowing the base shear force ${V_b}^{BF}$ developed by the RC structure at the design displacement Δ_d (which can be read on the capacity curve obtained in step ii.), the base shear resistance ${V_b}^{BR,REQ}$ required from the first storey braces is determined using Expression (5.13). The respective cross-section can then be selected from the list organized in step iv., considering that ${V_b}^{BR}$ represents the sum of the horizontal components of the first storey braces' tensile and residual post-buckling resistances. For this purpose, the former is taken equal to the corresponding yield strength, while the latter (at Δ_d) is taken approximately equal to 70% of the brace's buckling resistance. The fact that the proposed percentage is substantially higher than that recommended in EC8-1 (2004) for steel frames with concentric braces (30%) is justified by the fact that the ductility demand μ_Δ is typically much lower in steel-braced RC frames, thus allowing for the buckled braces to retain some more of their design resistance. Lastly on step xii., the purpose of the reduction factor 0.85 introduced in Expression (5.13) is to allow for the effect of stiffness modifications induced by the variation of the RC columns' axial forces and, therefore, avoid an eventual underestimation of the strength required from the first storey braces.

$${V_b}^{BR,REQ} = {V_b}^{REQ} - 0.85 \cdot {V_b}^{BF} \leq {V_b}^{BR} \tag{5.13}$$

The last step (xiii.) of the design process is the selection of the cross-sections of the steel braces for the upper storeys. The option to use the same as that of the first storey braces might seem tempting but, besides unnecessary, it would needlessly overload the RC columns to which the braces are attached (particularly in the lower storeys of mid- and high-rise buildings). Hence, the variation of the braces' strength over the height of the building should be considered, based on the expected seismic demand, but ensuring at all times that no situations are created which are prone to the development of soft-storey mechanisms above the first storey. For this purpose, a lateral load pattern F_i is defined (proportional to the storeys' masses m_i and the inelastic displacement shape δ_i), as well as the lateral

overstrength ratio Ω at the first storey (expressions (5.14) and (5.15), respectively). Based on the latter and the required base shear strength ${V_b}^{REQ}$, the required shear strengths ${V_i}^{REQ}$ of the n upper storeys are determined by Expression (5.16). This allows for the calculation of the shear resistances ${V_i}^{BR,REQ}$ required from the upper storeys' braces – Expression (5.17), where ${V_i}^{BF}$ is the shear force developed by the RC structure's i^{th} storey at the design displacement Δ_d – and the respective selection of cross-sections in a similar process to that described for the first storey.

$$F_i = \frac{m_i \cdot \delta_i}{\sum m_j \cdot \delta_j} \tag{5.14}$$

$$\Omega = \frac{{V_b}^{BR} + 0.85 \cdot {V_b}^{BF}}{{V_b}^{REQ}} \geq 1 \tag{5.15}$$

$${V_i}^{REQ} = \Omega \cdot {V_b}^{REQ} \cdot \sum_{j=i}^{n} F_j \tag{5.16}$$

$${V_i}^{BR,REQ} = {V_i}^{REQ} - 0.85 \cdot {V_i}^{BF} \leq {V_i}^{BR} \tag{5.17}$$

At this point, with the full definition of the retrofitting system, one must evaluate the estimate of the axial loads installed in the columns that was used in step vii. for the definition of the design displacement Δ_d at the first floor of the building. This will dictate if the design of the braces was based on an acceptable assumption, or if another iteration of the process should be carried out, this time based on a more educated estimate. The sum of the vertical components of the actual brace forces is thus evaluated under the same assumption referred in step vii., and then compared with the value used in the latter. If the percentual difference falls within the acceptable tolerance (as the estimate is obtained in a rather conservative way, differences up to 25% may be accepted), then the process needs not be repeated and the obtained brace setup advances to its final validation. Otherwise, the design displacement Δ_d should be redefined based on the now obtained estimate, and the design process repeated from step vii.

5.3.3. Validation process

To prove the retrofitted structure's ability to behave adequately under the design earthquake, the ultimate test is to evaluate its performance according to the requirements of EC8-3 (2005), in a similar process to that described in Chapter 4 (see section 4.4.). However, to demonstrate the merits of the devised methodology in predicting seismic behaviour, several other nonlinear analysis results (e.g., ductility demand; base shear strength value and components; RC columns' axial force variations; evolution of brace forces) should be evaluated and compared to the assumptions made during the design process. This procedure will be better illustrated in the case-study application.

5.4. CASE STUDY APPLICATION

The structure chosen as a case study for this chapter is the same used before, in Chapter 3 to illustrate the application of the EC8-3 (2005) seismic assessment procedure, and in Chapter 4 to test the applicability of the *q*-factor approach to the design of concentric steel braces for the seismic retrofitting of pre-code RC structures. The results of the assessment process revealed the need for a global retrofitting intervention to make the frame compliant with the performance requirements of the LS of Near Collapse (NC). An effective retrofitting system was then designed (see sub-section 4.4.5. in Chapter 4), but not through the application of the *q*-factor approach. Far from it, the final design relied on an iterative assessment procedure, combined with the control of inter-storey drifts and the monitoring of axial forces imposed to the columns. Intentionally, no details were given in Chapter 4 concerning the steps of this procedure. At first being extremely laborious (and not particularly well organized), it suffered several changes and improvements until it assumed the shape of the above-presented methodology. As such, even though the performance evaluation results were given then (to demonstrate the existence of a valid retrofitting solution), the details concerning the design procedure were reserved for this chapter. The developed methodology is thus applied herein, showing how it led to the design of the final retrofitting system in a swift and efficient way. The properties of the latter are reproduced below, as Figure 5.4, for the reader's convenience.

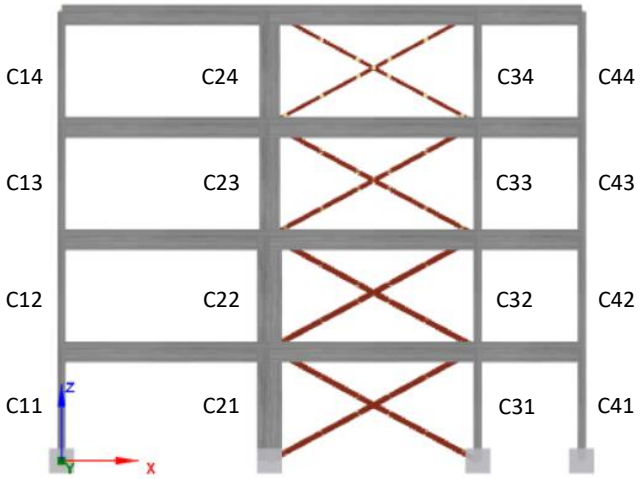

	FINAL
Storey	Cross-section
4	CHSH 88.9x3.2
3	CHSH 114.3x3.6
2	CHSH 139.7x3.6
1	CHSH 139.7x4.0

Figure 5.4 – Layout and cross-sections of the FINAL retrofitting system for the ICONS (bare) frame

5.4.1. Design procedure

The basic seismic action for this case study is defined by the NC elastic response spectrum (see Table 3.19 and Figure 3.48 in Chapter 3). The capacity curves (left-to-right and right-to-left) of the bare frame are also given in Chapter 3 (see Figure 3.49), but those were obtained through conventional force-based pushover analyses. As such, their adaptive displacement-based (ADB) counterparts are depicted below in Figure 5.5 and will be used henceforth. Applying the CSM, the expedite assessment of the bare frame can now be performed. Figure 5.6 shows the above referred elastic spectrum ($\xi_0 = 5\%$),

the over-damped (OD) spectrum derived for the EVD ratio ($\xi = 14.5\%$) corresponding to the structure's maximum ductility demand $\mu_\Delta = d_{max}/d_y$, and the bilinear representation of the left-to-right (L-R) capacity curve, all plotted in ADRS format (the plot for the R-L pushover is similar). As expected from the assessment results given in Chapter 3, no performance point can be determined, hence the original structure is not able to resist the design earthquake.

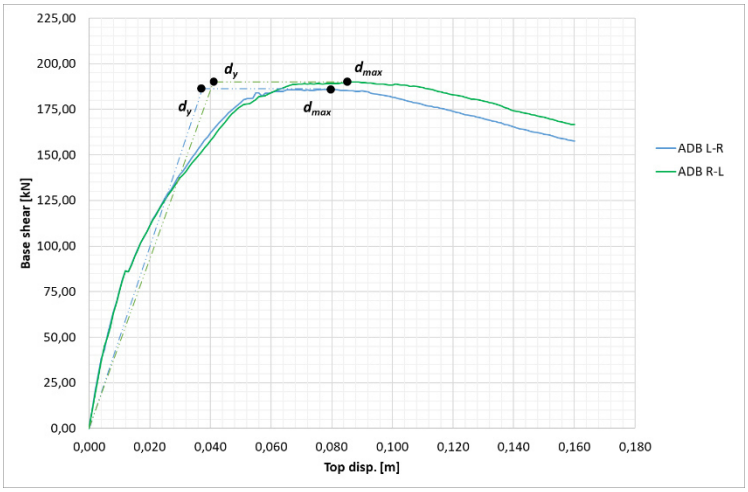

Figure 5.5 – Capacity curves of the original RC structure (L-R: left-to-right; R-L: right-to-left)

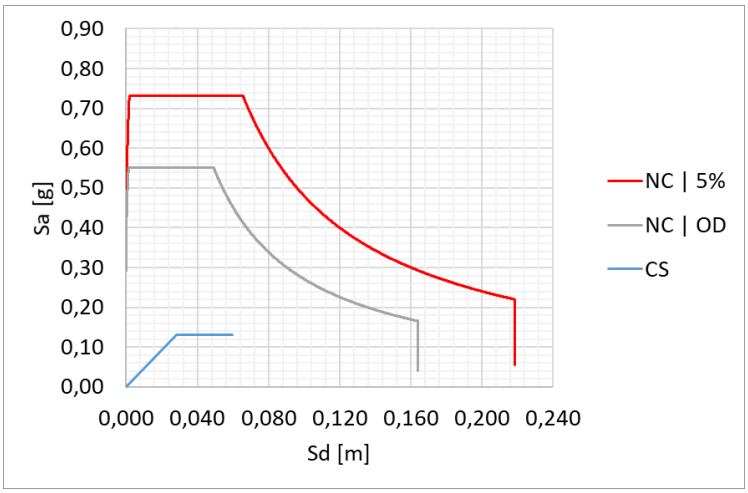

Figure 5.6 – CSM assessment of the original RC structure for the LS of NC

The RC members that are most affected by the additional axial forces induced by the steel braces are columns C31 to C34. Columns C21 to C24 are much more robust that the latter, and those remaining are much less affected (i.e., the variation of their axial forces during the earthquake is similar between bare and retrofitted structures – see sub-section 4.4.3. in Chapter 4). Moreover, column C31 was identified in Chapter 4 as critical, due to its premature failure during the L-R pushover analysis of the frame equipped with the most robust retrofitting solution (see Figure 4.16). Therefore, the axial force

capacity envelope needs only be evaluated for column C31 to find the maximum allowed additional loads that can be induced by the retrofitting system. Figure 5.7 shows the corresponding *N-M* interaction diagram and indicates the axial force N_{G+Q} due only to gravity loads. Examining the limits defined by the curve, one concludes that maximum increments of approximately +900 *kN* / -800 *kN* are allowed in compression / tension, respectively.

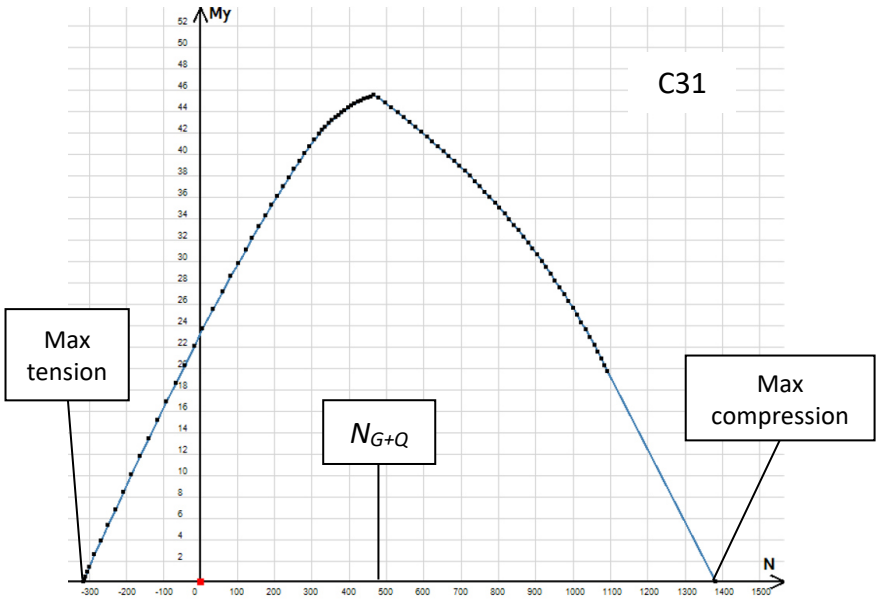

Figure 5.7 – Axial force-bending moment interaction diagram for column C31

The pre-selection of cross-sections for the braces can now be carried out (for this case-study, only hot-rolled circular hollow sections (CHSH) were considered). The steel material mechanical properties are those given in Chapter 4 (see sub-section 4.4.1.). Based on the braces' initial length L_i, the non-dimensional slenderness $\bar{\lambda}$ is determined for all the chosen cross-sections, saving only those in the range $1.5 < \bar{\lambda} \leq 2.5$, as previously referred. Next, the yield and buckling strengths – respectively $N_{pl,Rd}$ and $N_{b,Rd}$ – are determined. With the vertical (V) and horizontal (H) force components of the latter, one respectively evaluates the contribution that each (tensioned or compressed) steel brace can make for: (i) the variation of the columns' axial forces; (ii) the increment to the original structure's base shear resistance. The information provided by the former, combined with the axial force capacity envelope of column C31, leads to the required pre-selection. Table 5.1 provides the detailed results of this process for one example cross-section, while Table 5.2 lists the full pre-selection, but retains only the key results. The information contained in this table is extremely useful throughout the whole design process, as it allows for a quick choice of braces in the final steps of the procedure, as well as for a swift re-evaluation of the solution when an additional iteration is required. However, it is noteworthy that the included vertical and horizontal force components should be taken as maximum values, as they are calculated assuming the tensioned braces have reached their yield strength, and the compressed braces are at their peak buckling strength.

Table 5.1 – Pre-selection of steel braces: detailed results for cross section CHSH 139.7 × 4.0

Cross-section	$A\ (cm^2)$	$I\ (cm^4)$	$B\ (m)$	$h\ (m)$	$L_i\ (m)$	$\alpha = \tan^{-1}\left(\frac{h}{B}\right)$ (°)	$E\ (GPa)$	$f_{ym}\ (MPa)$
CHSH 139.7×4.0	17.10	393.00	5.00	2.70	5.682	28.369	210.00	343.75

$N_{cr} = \frac{\pi^2 \cdot E \cdot I}{{L_i}^2}\ (kN)$	$\bar{\lambda} = \sqrt{\frac{A \cdot f_{ym}}{N_{cr}}}$	$N_{pl,Rd}\ (kN)$	$N_{b,Rd}\ (kN)$	${N_{pl,Rd}}^V\ (kN)$	${N_{b,Rd}}^V\ (kN)$	${N_{pl,Rd}}^H\ (kN)$	${N_{b,Rd}}^H\ (kN)$
252.26	1.53	587.81	212.48	279.30	100.96	517.22	186.96

Table 5.2 – Pre-selection of steel braces: full list of admissible cross-sections

Cross-section	$\bar{\lambda}$	$N_{pl,Rd}\ (kN)$	$N_{b,Rd}\ (kN)$	${N_{pl,Rd}}^V\ (kN)$	${N_{b,Rd}}^V\ (kN)$	${N_{pl,Rd}}^H\ (kN)$	${N_{b,Rd}}^H\ (kN)$
CHSH 139.7×6.0	1.55	866.25	306.07	411.60	145.43	762.22	269.31
CHSH 139.7×5.6	1.54	811.25	287.95	385.46	136.82	713.82	253.37
CHSH 139.7×5.0	1.54	728.75	260.53	346.26	123.79	641.23	229.24
CHSH 139.7×4.0	1.53	587.81	212.48	279.30	100.96	517.22	186.96
CHSH 139.7×3.6	1.52	529.38	192.77	251.53	91.60	465.80	169.62
CHSH 139.7×3.2	1.51	470.94	172.60	223.77	82.01	414.38	151.87
CHSH 114.3 x 6.0	1.91	701.25	170.39	333.20	80.96	617.03	149.93
CHSH 114.3 x 5.6	1.90	656.56	160.63	311.96	76.32	577.71	141.34
CHSH 114.3 x 5.0	1.89	591.25	145.77	280.93	69.26	520.24	128.26
CHSH 114.3 x 4.0	1.88	477.81	119.51	227.03	56.79	420.43	105.16
CHSH 114.3 x 3.6	1.87	429.69	108.64	204.17	51.62	378.08	95.59
CHSH 114.3 x 3.2	1.87	385.00	97.32	182.93	46.24	338.76	85.64
CHSH 88.9 x 6.0	2.49	536.25	79.42	254.80	37.73	471.85	69.88
CHSH 88.9 x 5.0	2.47	453.75	68.18	215.60	32.40	399.26	60.00
CHSH 88.9 x 4.0	2.44	367.81	56.53	174.77	26.86	323.64	49.74
CHSH 88.9 x 3.6	2.42	331.72	51.57	157.62	24.50	291.88	45.38
CHSH 88.9 x 3.2	2.41	296.31	46.44	140.79	22.07	260.73	40.87

Concerning the assumed inelastic lateral displacement shape, this was obtained using the above-referred expression proposed by Priestley *et al* (2007), reproduced below as Expression (5.18) where H_i and H_n represent the heights of level i and n (the roof), respectively. Table 5.3 shows the calculated values for each floor, alongside those of the corresponding linear displacement shape. As previously referred, the actual inelastic displacement profile of the retrofitted structure at peak displacement response is expected to lie in between these two.

$$\delta_i = \frac{4}{3} \cdot \frac{H_i}{H_n} \cdot \left(1 - \frac{H_i}{4 \cdot H_n}\right) \tag{5.18}$$

Table 5.3 – Comparison of the assumed inelastic lateral displacement shape with the corresponding linear shape

	δ_i			
Shape	**1st floor**	**2nd floor**	**3rd floor**	**4th floor**
Assumed	0.313	0.583	0.813	1.000
Linear	0.250	0.500	0.750	1.000

Based on the information given in Table 5.2, the initial estimate ΔN_0 of the axial loads imposed to the critical columns at the performance point can now be obtained, considering a brace setup composed by the lightest pre-selected cross-section (i.e., CHSH 88.9 × 3.2). Assuming that all braces are at their maximum (tensile and compressive) strengths, one obtains $\Delta N_0 = 4 \times 140.79 + 3 \times 22.07 = 629.37\ kN$ (the vertical component of the compressed brace at the first floor is not included, as it is directly transmitted to the column's foundation). As the failure mechanism of the columns at the LS of NC is clearly governed by their deformation capacity (see sub-section 3.4.3. in Chapter 3), the maximum drift of the first storey (Δ_d/h) is conservatively estimated as being equal to the lowest chord rotation capacity θ_{NC} (between columns C21 and C31), the latter being computed based on the updated axial forces $\left(N_{G+Q} + \Delta N_0\right)$. Having defined the design displacement Δ_d, expressions (5.5) to (5.12) can now be applied to obtain all the parameters that are necessary to determine the required lateral strength ${V_b}^{REQ}$ of the retrofitted structure. Table 5.4 summarizes the results.

Table 5.4 – Calculation of the required lateral strength ${V_b}^{REQ}$ (iteration 0)

$\Delta N_0\ (kN)$	${\theta_{NC}}^{C31}\ (rad)$	$\Delta_d\ (mm)$	$S_{\Delta_d}\ (mm)$	$\Delta_y\ (mm)$	$S_{\Delta_y}\ (mm)$	μ_Δ	ξ
629.37	0.00687	18.55	45.03	10.57	25.67	1.754	12.73%

η	$T_e\ (s)$	$m_e\ (ton)$	$K_e\ (kN/m)$	${V_b}^{REQ}\ (kN)$
0.69	0.599	151.75	16696.74	751.78

The base shear resistance ${V_b}^{BR,REQ}$ required from the first storey braces can now be determined using Expression (5.13), thus allowing to select a compatible cross-section from Table 5.2, following the procedure explained in sub-section 5.3.2. Afterwards, the shear resistances ${V_i}^{BR,REQ}$ required from the upper storey braces (2nd, 3rd, and 4th) are determined using expressions (5.14) to (5.17), and the corresponding cross-sections selected in the same way. Tables 5.5 and 5.6 show the calculated parameters and the selected cross-sections.

Table 5.5 – Selection of first storey braces' cross-section (iteration 0)

${V_b}^{REQ}\ (kN)$	${V_b}^{BF}\ (kN)$	${V_b}^{BR,REQ}\ (kN)$	*CHSH 1*	${V_b}^{BR}\ (kN)$	Ω
751.78	185.62	594.00	114.3 x 5.0	610.03	1.02

Table 5.6 – Selection of upper storey braces' cross-section (iteration 0)

Storey (i)	${V_i}^{BR,REQ}\ (kN)$	*CHSH i*	${V_i}^{BR}\ (kN)$
2	534.76	114.3 x 5.0	610.03
3	394.25	114.3 x 3.2	398.71
4	198.55	88.9 x 3.2	289.33

With the full definition of the retrofitting system, the estimate ΔN of the axial loads imposed to the critical columns at the performance point can be updated: $\Delta N = 2 \times 280.93 + 182.93 + 140.79 + 69.26 + 46.24 + 22.07 = 1023.15\ kN$, which is 62.6% above the initial estimate ΔN_0, meaning that the obtained solution cannot be accepted. Even though the updated estimate ΔN exceeds the maximum increment in compression of 900 *kN* calculated for column C31, it still lies within the defined tolerance of 25% referred in sub-section 5.3.2. As such, a new iteration of the design process is carried out, considering $\Delta N_1 = 850\ kN$ (a value close to the limit for column C31), to try to find a compatible retrofitting system. Tables 5.7 to 5.9 give the updated results.

Table 5.7 – Calculation of the required lateral strength $V_b{}^{REQ}$ (iteration 1)

$\Delta N_1\ (kN)$	$\theta_{NC}{}^{C31}\ (rad)$	$\Delta_d\ (mm)$	$S_{\Delta_d}\ (mm)$	$\Delta_y\ (mm)$	$S_{\Delta_y}\ (mm)$	μ_Δ	ξ
850.00	0.00589	15.90	38.63	10.57	25.67	1.505	11.03%

η	$T_e\ (s)$	$m_e\ (ton)$	$K_e\ (kN/m)$	$V_b{}^{REQ}\ (kN)$
0.73	0.538	151.75	20697.64	799.35

Table 5.8 – Selection of first storey braces' cross-section (iteration 1)

$V_b{}^{REQ}\ (kN)$	$V_b{}^{BF}\ (kN)$	$V_b{}^{BR,REQ}\ (kN)$	*CHSH 1*	$V_b{}^{BR}\ (kN)$	Ω
799.35	184.81	642.26	139.7 x 4.0	648.09	1.01

Table 5.9 – Selection of upper storey braces' cross-section (iteration 1)

Storey (i)	$V_i{}^{BR,REQ}\ (kN)$	*CHSH* i	$V_i{}^{BR}\ (kN)$
2	582.03	139.7 x 3.6	584.54
3	441.89	114.3 x 3.6	445.00
4	202.13	88.9 x 3.2	289.33

The estimate ΔN of the axial loads imposed to the critical columns at the performance point can now be updated for this retrofitting system: $\Delta N = 279.30 + 251.53 + 204.17 + 140.79 + 91.60 + 51.62 + 22.07 = 1041.08\ kN$, which is 22.5% above the initial estimate ΔN_1. As the difference falls below the defined tolerance of 25%, the retrofitted structure can move forward to its final validation according to the performance requirements of EC8-3 (2005). Because the obtained solution does in fact correspond to the final retrofitting system shown above in Figure 5.4, the performance evaluation results are already known. Nonetheless, that process is again addressed in the following sub-sections, along with several other aspects regarding the actual seismic behaviour of the retrofitted structure, as all are relevant to the validation of the design process.

5.4.2. Validation

The performance evaluation process of the retrofitted structure using nonlinear static and dynamic methods of analysis is described in Chapter 4 (see section 4.4.), hence there is no need to go through all its details again. Only the key issues are addressed herein. The ADB capacity curves (L-R and R-L) are given in Figure 5.8. Applying the CSM, an expedite assessment is performed. Figure 5.9 shows the elastic demand spectrum ($\xi_0 = 5\%$), the OD demand spectrum derived for the EVD ratio $\xi = 12.2\%$ corresponding to the maximum ductility demand $\mu_\Delta = d_{max}/d_y$, and the bilinear representation of the L-R capacity curve, all plotted in ADRS format. As expected, the inelastic branch of the capacity curve extends through the envelope defined by the demand spectra, indicating that the structure survives the earthquake. The target displacement d_t is then defined by the intersection (Figure 5.10) of the capacity curve with the appropriately damped demand spectrum (i.e., derived for the EVD ratio ξ corresponding to the ductility demand $\mu = d_t/d_y$).

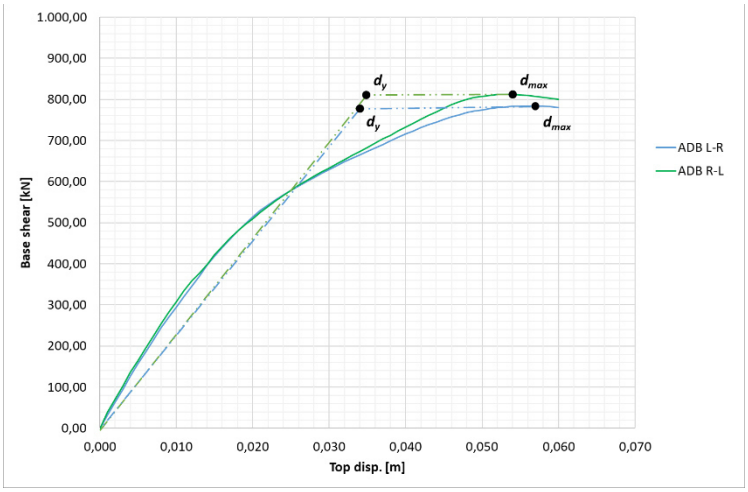

Figure 5.8 – Capacity curves of the retrofitted structure (L-R: left-to-right; R-L: right-to-left)

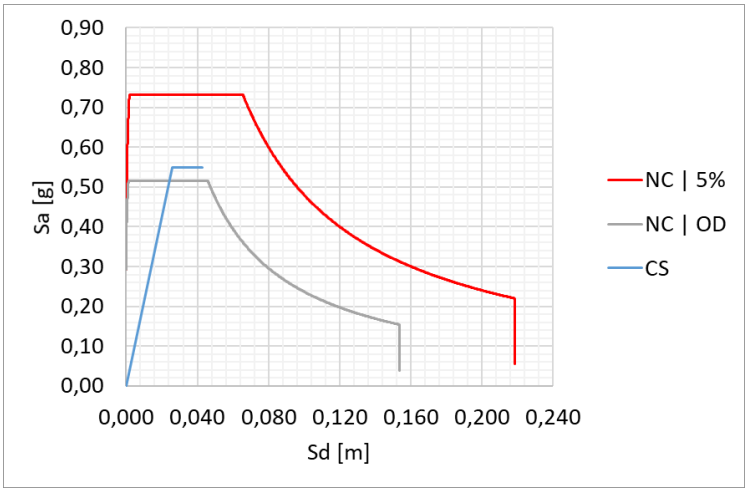

Figure 5.9 – CSM assessment of the retrofitted structure for the LS of NC

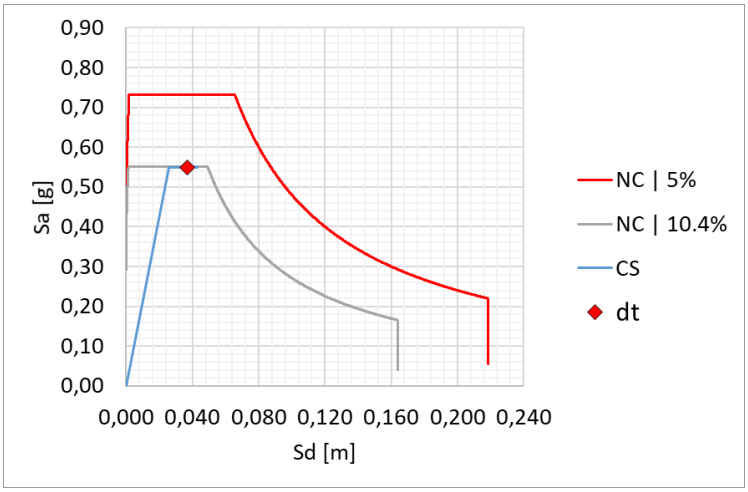

Figure 5.10 – Definition of the L-R performance point of the retrofitted structure for the LS of NC

The L-R target displacement d_t for the LS of NC cannot be read directly on the figure above, as it is plotted in ADRS format. Therefore, it has to be transformed back to floor displacements of the real MDOF system (i.e., the retrofitted structure). Table 5.10 shows those displacements, for both the L-R and R-L pushovers. The RC columns' capacities (chord rotations θ_{NC}; shear forces V_{NC}) at the two performance points are then computed based on the corresponding axial forces $N(d_t)$, according to the procedure described in Chapter 4 (see sub-section 4.4.3.). Combining them with the respective demands, the performance evaluation results (i.e., the demand-to-capacity ratios D_i/C_i) are obtained, corresponding to the most unfavourable values for each control section i. These ratios were given in Chapter 4 (see figures 4.18 and 4.19) but are also reproduced below as figures 5.11 and 5.12, for the reader's convenience. As previously seen, no values above 1.0 were obtained, except for column C21 in terms of shear force. However, as this isolated issue is known to be efficiently solved through (e.g.) FRP wrapping, the designed retrofitting system was deemed adequate to make the frame fulfil the EC8-3 (2005) requirements for the LS of NC. One could argue that another iteration of the design process could have been carried out, based on a lower value of the design displacement Δ_d, in an attempt to limit the shear force on column C21. However, a stronger bracing system would inevitably have been obtained, which would most likely lead to the premature failure of column C31 due to excessive axial force. Moreover, the higher tensile forces induced in column C21 (during the L-R loading) would further reduce its shear force capacity (a step in the wrong direction). The obtained retrofitting solution is therefore believed to be the most efficient for this structure, provided it is combined with the above-referred local strengthening.

Table 5.10 – Target displacement values d_t for the retrofitted structure (L-R: left-to-right; R-L: right-to-left)

	d_t (mm)			
Seismic loading	**1st floor**	**2nd floor**	**3rd floor**	**4th floor (top)**
L-R	12.17	25.98	39.46	49.00
R-L	-10.56	-23.49	-36.46	-46.00

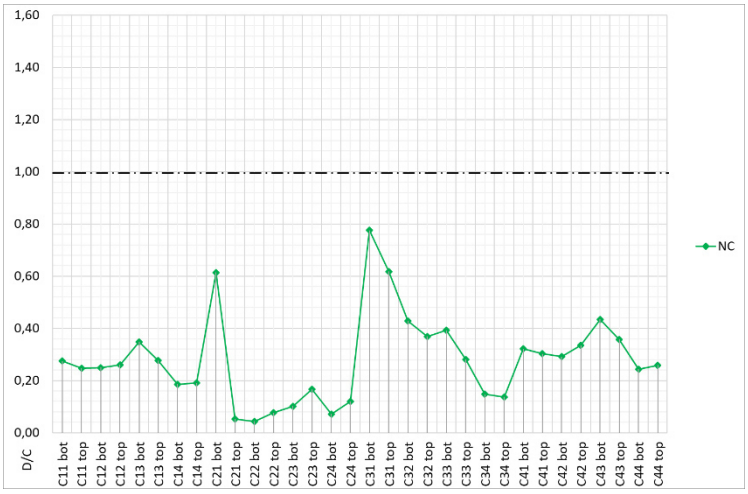

Figure 5.11 – FINAL: NC chord rotation D/C ratios on columns (pushover analysis results)

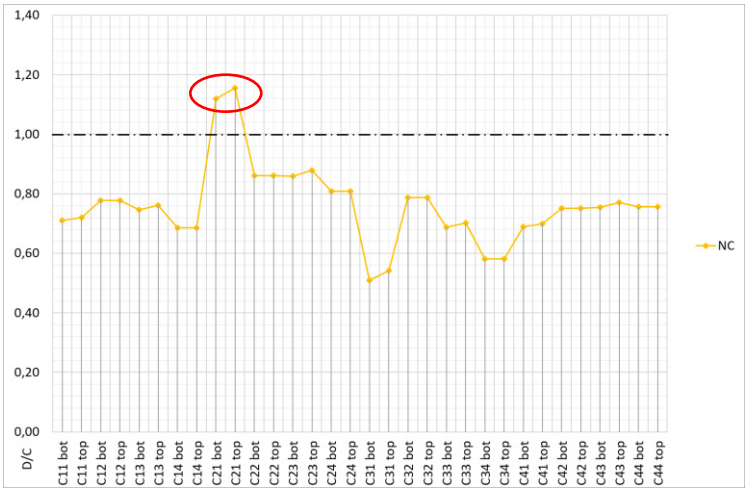

Figure 5.12 – FINAL: NC shear force D/C ratios on columns (pushover analysis results)

5.4.3. Discussion

The performance evaluation results given above show that the proposed design methodology succeeded in providing a set of steel braces that allow the retrofitted structure to behave adequately under the design earthquake. Nonetheless, to also evaluate the merits of the devised procedure in predicting that behaviour, the relevant global parameters are analysed herein and compared to the assumptions made during the design process. In that cause, Figure 5.13 shows the plot of the L-R capacity spectrum along with the representation of the coordinates (S_{Δ_d} ; S_a) of the estimated design point *DP* ($S_{\Delta_d} = 38.63\ mm$ is given in Table 5.7, while $S_a = 0.541 \cdot g$ is the ratio of the estimated base shear resistance V_b to the effective mass m_e). The result confirms that the design point estimated with the proposed methodology is consistent with the global behaviour of the retrofitted structure observed during the pushover analysis. The estimated ductility demand μ_Δ (see Table 5.7) also compares well with that based on the bilinear curve shown below ($\mu_\Delta = 1.66$).

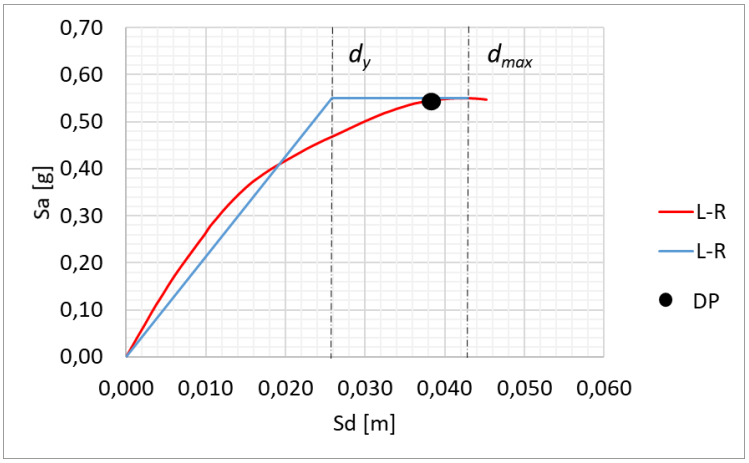

Figure 5.13 – Comparison of the design method's prediction with the L-R capacity spectrum of the retrofitted structure

Concerning the base shear resistance, a maximum value $V_b = 783.81\ kN$ was obtained with the L-R pushover analysis, composed by the contributions of the first storey's RC columns and steel braces, respectively ${V_b}^{RC} = 130.68\ kN$ and ${V_b}^{BR} = 653.13\ kN$. The estimates of the design procedure for these two components are given in Table 5.8. For the steel braces' component, the calculated difference is less than 1%. On the other hand, for the RC columns' component, the reduced estimated value (i.e., affected in Expression (5.13) by the reduction factor 0.85) is still 20% above that given by the pushover analysis. A closer look at the shear forces developed by each of the four columns on the first storey, for the bare and retrofitted frames at the same drift value, reveals no relevant differences in columns C11 and C41 (i.e., those not directly connected to the steel braces), but considerable differences in columns C21 and C31. This reduction in stiffness is anticipated due to the expected variations in the columns' axial forces induced by the steel braces, hence the introduction in Expression (5.13) of the above-referred reduction factor. However, in this particular case, that reduction is unusually high. Evaluating the axial forces at the performance point in columns C21 and C31, one concludes that the latter is close to its compression limit (see Figure 5.7), while the former is significantly reduced to just 7.4% of its value due only to gravity loads. In other words, column C31 is practically in near-collapse state, experiencing inevitable stiffness degradation, while the low compression force on column C21 causes the reduction in its lateral stiffness. This indicates that the designed retrofitting system, although efficient, demands almost too much from the RC columns which are directly affected by it. Therefore, it would be prudent to extend to column C31 the FRP local strengthening referred in the previous sub-section about column C21. Besides the improvement to the shear capacity, enhancement of the concrete confinement would also be obtained, making both columns less vulnerable to the effects of the increased axial forces. The capacity models for RC members with FRP plating and wrapping are described in EC8-3 (2005) – Annex A (see section A.4.4), but this topic will not be developed further herein.

The value of the maximum axial force in column C31 shows that the actual increase $\Delta N = 859.19\ kN$ induced by the retrofitting system is lower than the estimated value. This is due to the fourth storey tensioned brace never reaching its yield strength, and to the first, second, and third storeys

compressed braces being already in post-buckling stage when the structure reaches its maximum lateral displacement. Consequently (and as expected), the sum of the vertical components of brace forces is lower than that given by the design procedure's assumptions, demonstrating the latter to be on the safe side. This distribution of braces forces is coherent with the lateral displacement shape that can be derived from the values given in Table 5.10, which show that the lowest inter-storey drift occurs at the top storey. Figure 5.14 illustrates the obtained displacement shape and compares it to those given above in Table 5.3, demonstrating that it lies between them, as expected. This ensures that the base shear resistance $V_b{}^{BR}$ required from the first storey braces is not underestimated during the design procedure. However, the same might not always be true for the upper storey braces, but this is a matter to be further addressed in Chapter 6.

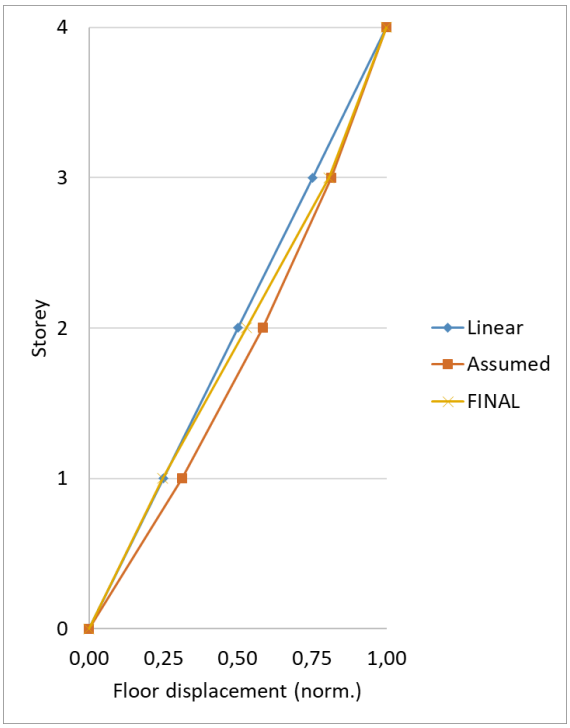

Figure 5.14 – Lateral displacement shapes comparison: Linear; Assumed; FINAL

5.5. CONCLUDING REMARKS

A new displacement-based methodology for the design of concentric steel-brace retrofitting systems for RC framed buildings was proposed in this chapter. The fundamental bases of the procedure were described, as well as the steps of the design workflow. The method was then validated in a case-study application to a structure with insufficient seismic resistance (the same structure that had been addressed in chapters 3 and 4). Afterwards, the performance of the obtained retrofitted structure was evaluated according to the requirements of EC8-3 (2005) using nonlinear static analysis, and the assumptions made during the design process were discussed and validated, with emphasis on the global parameters that define the behaviour of the hybrid system.

This proposal responds to the need pointed out in the end of Chapter 4 concerning the development of an effective performance-based design methodology for hybrid RC-steel structures that explicitly considers the interaction between the two structural systems. The procedure is thought to be intuitive and simple enough to be used in practical applications, with several advantages over the traditional force-based design process. Besides the obvious fact that no behaviour factors are involved (thus eliminating the difficulty in finding an adequate one), it relies on the fundamental knowledge of the seismic behaviour of braced structures to ensure that deformation levels are kept under limits that allow for the fulfilment of the applicable code performance requirements. Despite the introduction of the above-discussed approximations in some of the design steps, the procedure leads to retrofitted structures with adequate and predictable seismic performance, within a swift and simple to follow workflow that can be easily programmed on any platform.

Application examples of this kind of global retrofitting solution in Portugal are almost inexistent, mainly due to the lack of codes providing information about the detailed design process. Further development and improvement of the EC8-3 (2005) provisions are thus necessary. The author hopes that the proposed methodology can contribute to mitigate this lack of guidance, and eventually be considered as an input to a future version of Eurocode 8. However, at this point its use is recommended only for low- and mid-rise RC buildings (Silva (2013) states that only 1.5% of the Portuguese pre-code RC building stock is composed of high-rises, i.e., with seven or more storeys). The application to irregular frames and/or to buildings with RC shear walls should also still be handled with caution, namely concerning the inelastic lateral displacement shapes to be selected, and the percentage of the global seismic force to be carried by the braced frames. Further developments will certainly be attained on these topics in the near future, but already outside the scope of this work.

CHAPTER 5 – A NEW DISPLACEMENT-BASED DESIGN PROCEDURE FOR THE RETROFITTING OF RC BUILDINGS WITH STEEL BRACES

5.1. INTRODUCTION 5.1
5.2. BASES OF THE PROCEDURE 5.2
5.3. STEPS OF THE PROCEDURE 5.3
5.3.1. Primary data compilation 5.3
5.3.2. Design process 5.4
5.3.3. Validation process 5.10
5.4. CASE STUDY APPLICATION 5.11
5.4.1. Design procedure 5.11
5.4.2. Validation 5.17
5.4.3. Discussion 5.19
5.5. CONCLUDING REMARKS 5.21

CHAPTER 6

VALIDATION AND CALIBRATION OF THE PROPOSED DESIGN PROCEDURE

6.1. INTRODUCTION

The previous chapter presented the fundamental bases of the proposed procedure, as well as the steps of the design workflow, and applied it to the retrofitting of the same pre-code RC building that had been used as a case-study in chapters 3 and 4. The performance of the obtained structure was then evaluated according to the requirements of EC8-3 (2005), running nonlinear static analyses, and the assumptions made during the design process were discussed and validated. The method was successful in providing a retrofitted structure with adequate and predictable seismic performance, thus presenting itself as an effective performance-based design tool for hybrid RC-steel systems, without the shortcomings of the traditional force-based design process. However, a single successful application is hardly enough to demonstrate the effectiveness of a design procedure that has the ambition to be used by practitioners in real applications. A more complete set of tests, considering structures with variable size and seismic demand, thus felt mandatory to build confidence on the procedure, and further demonstrate its merits. That is the purpose of the current chapter.

A workplan was thus devised to demonstrate that the proposed design methodology is robust enough to be systematically applied to the retrofitting of Portuguese RC framed buildings, built before the publication of the national seismic code (RSA, 1983). In that cause, a sample of ten tri-dimensional structures with different numbers of spans and storeys was put through the EC8-3 (2005) assessment process, considering four seismic hazard scenarios of growing intensity, which led to eighty numerical models (considering two separate analysis directions). For those deemed unsafe, retrofitting systems were designed according to the proposed methodology. The assessment process was then carried out for the retrofitted structures, and conclusions were drawn concerning the effectiveness of the design procedure and its calibration according to the EC8-3 (2005) performance requirements. The details concerning the definition of the sample of buildings are given in the following sections, as well as those concerning the assessment and retrofitting processes. The obtained results and associated discussions are also presented, giving origin to the final remarks on the method. Due to the large volume of results, the latter are put together in appendices 1 to 6, with just some being shown along the current chapter's text whenever examples are in order.

6.2. SAMPLE DEFINITION

The characterization of the Portuguese RC building stock was addressed in Chapter 2 (see section 2.3.), defining building typologies and probabilistic distributions of the associated geometrical and material properties, citing the works of Silva (2013) and Silva *et al* (2015b), and referring to the data of the 2011 Building Census Survey. Amongst the attributes considered in the latter, Silva (2013) used the year of construction (an indicator of the seismic design philosophy and practice), and the number of storeys, as base for the proposed classification. Six typologies were thus considered: buildings constructed (hence, designed) before the publication of RSA (1983) were categorized as pre-code (PC), whilst those built after were termed post-code (C); regarding the number of storeys, buildings up to three storeys were categorized as low-rise (LR), between four and six storeys as mid-rise (MR), and with seven or more storeys as high-rise (HR). A summary of the RC building stock following these parameters is shown in Figure 2.6, which is reproduced below as Figure 6.1 for the reader's convenience.

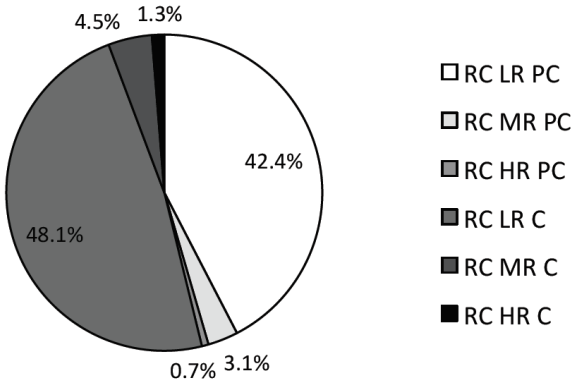

Figure 6.1 – Percentile distribution of residential RC buildings in Portugal according to seismic design philosophy and practice (PC/C) and number of storeys (LR/MR/HR) (adapted from Silva, 2013)

The definition of the sample of artificially generated pre-code RC buildings is bound to the geometrical and mechanical properties given in the above-referred studies. By analysing the percentages shown in Figure 6.1, one concludes that 98.5% of pre-code RC buildings have six or less storeys (i.e., are categorized as low- or mid-rise). As such, only buildings with 2, 3, 4, 5, and 6 storeys were considered herein, with two different regular plans (3×5 and 2×4 spans). This led to the above-referred sample of ten buildings, analysed in two separate directions (referred to as XX and YY, henceforth). The other geometrical properties (i.e., inter-storey height; span length; slab thickness) were defined using the mean values given in Silva *et al* (2015b). The same was done for the required mechanical properties, considering some additional data from Furtado *et al* (2016a). As for the design loads, a mean value $g = 8\ kN/m^2$ was considered for the total dead load (Sousa *et al,* 2019), as well as a residential-type live load $q = 2\ kN/m^2$ (the data of the 2011 Building Census Survey refer that only 0.7% of the RC building stock is of non-residential use). Table 6.1 summarizes the values of the considered properties, as well as the respective sources. The buildings were then designed (without seismic detailing of any kind) to withstand vertical loads only, applying the rules given in the former Portuguese RC design

codes (i.e., RBA, 1935; REBA, 1967; REBAP, 1983), and using the automatic design algorithm developed by Sousa *et al* (2019) (kindly made available by Dr. Romain Sousa). The full definition of the generated sample of synthetic pre-code RC buildings (i.e., the detailed design drawings) can be found in Appendix 1, each under the reference "$nS_y \times x$", where n is the number of storeys, and y and x are, respectively, the number of spans along global axes Y and X.

Table 6.1 – Geometrical and mechanical properties used to define the sample of artificial pre-code RC buildings

Parameter	Variable	Average value	CV (%)	Reference
Dead loads	$g\ (kN/m^2)$	8	12.5	Sousa *et al* (2019)
Live load	$q\ (kN/m^2)$	2	-	
First storey height	$H_1\ (m)$	3.2	10	Silva *et al* (2015b) Furtado *et al* (2016a)
Upper storeys' height	$H_{n>1}\ (m)$	2.8	6	
Span length	$L_{span}\ (m)$	4.4	16	
Slab thickness	$h_{slab}\ (m)$	0.23	24	
Concrete compressive strength	$f_{cm}\ (MPa)$	23.8	49	Silva *et al* (2015b)
Steel yield strength	$f_{ym}\ (MPa)$	440	-	
Longitudinal reinforcement ratio	$\rho_l\ (\%)$	1	40	Furtado *et al* (2016a)

6.3. NUMERICAL MODELLING

The numerical models of the ten pre-code RC buildings were developed using software platform *SeismoStruct* (Seismosoft, 2020). A distributed plasticity model was considered for both column and beam elements, combined with fibre discretization to represent cross-section behaviour (approx. 150 fibres / section). A force-based FE formulation was used, considering five integration sections per element according to the recommendations of Calabrese *et al* (2010). The cross-section dimensions and corresponding reinforcement patterns were defined according to Appendix 1. As for the modelling of the floor slabs, a set of equivalent steel truss elastic elements was used to simulate the slabs' in-plane stiffness K_{slab}, following the same strategy described in Sousa *et al* (2019). This allowed for the calculation of the equivalent struts' cross-section area A_{strut} (making K_{slab} equal to $K_{strut} = (E_s \cdot A_{strut})/L_{strut}$, where E_s is the steel material's modulus of elasticity, and L_{strut} is the length of each truss bar), and enabled an efficient (from the computational point of view) way of simulating the slabs' diaphragm effect.

Concerning the constitutive laws defining the cyclic behaviour of materials, the Mander *et al* (1988) model was employed to define the concrete material, with the following parameters:

- Compressive strength: $f_c = 23.8\ MPa$
- Tensile strength: $f_t \approx 0\ MPa$
- Modulus of elasticity (initial stiffness): $E_c \approx 4700 \cdot \sqrt{f_c} = 22.93\ GPa$
- Strain at unconfined peak compressive stress: $\varepsilon_c = 0.002\ m/m$
- Specific weight: $\gamma_c = 2450\ kg/m^3$.

For the steel material, the Menegotto and Pinto (1973) model was employed, combined with the isotropic hardening rules proposed by Filippou *et al* (1983), with the following parameters:

- Yield strength: $f_y = 440\ MPa$
- Modulus of elasticity (initial stiffness): $E_s = 200\ GPa$
- Strain hardening parameter: $\mu = 0.005$
- Specific weight: $\gamma_s = 7850\ kg/m^3$.

The modelling of vertical static loads other than the self-weight of the frames' main elements (columns and beams) was done applying uniform loads to the beams, and the load-to-mass conversion was then performed at storey levels. Uniformly distributed floor masses of 126.22 *ton* and 232.33 *ton* were considered, for the 2×4 buildings and the 3×5 buildings, respectively. These masses correspond to the slab's self-weight, floor finishing, masonry partition walls, and to the quasi-permanent value of the floor's live load, to simulate the likely combination of loads during the earthquake. This concluded the preparation of the numerical models.

Modal analyses were then carried out to determine the structures' dynamic properties (modal frequencies and vibration mode shapes). The respective capacity curves were obtained afterwards, through adaptive displacement-based pushover analyses, for directions XX and YY. The advantages of this procedure over its conventional force-based counterpart have already been discussed in chapters 2 and 5 (see sub-sections 2.6.2. and 5.3.1., respectively). However, even though the possibility exists in the method to also account for higher-mode effects, only the fundamental vibration mode was considered in each direction. As the buildings under analysis are regular in plan and have limited number of storeys, such effects were rendered irrelevant to characterize the structures' dynamic behaviour. As an example, Figure 6.2 shows two of the developed numerical models. As for the capacity curves (a total of twenty), their graphical representation can be found in Appendix 3.

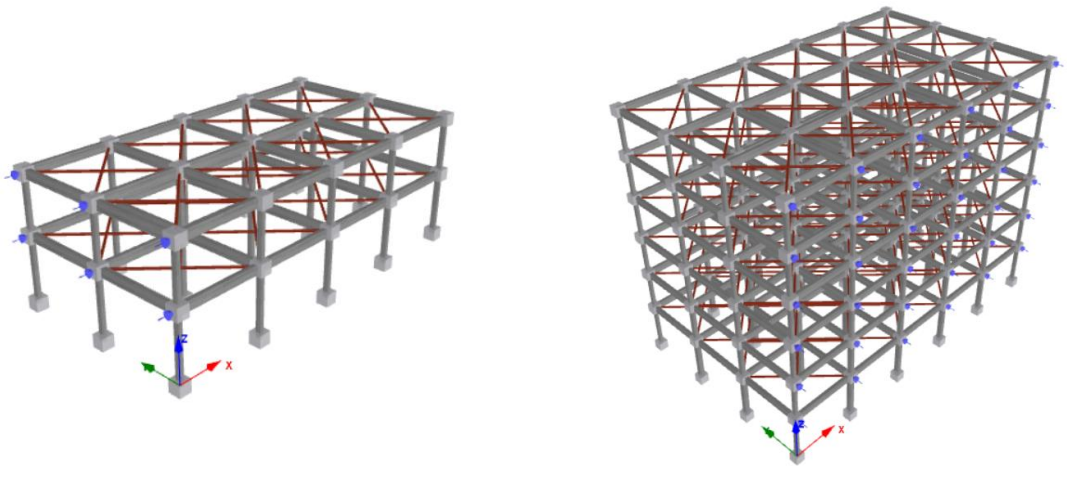

(i) (ii)

Figure 6.2 – Numerical models developed for two of the pre-code RC buildings: (i) 2S_2×4_XX; (ii) 6S_3×5_YY

6.4. SEISMIC ASSESSMENT

The seismic assessment of the pre-code RC buildings was performed according to the deterministic procedure described in EC8-3 (2005), considering four seismic hazard scenarios of growing intensity in mainland Portugal. According to the data of the 2011 Building Census Survey, the buildings were allocated to structural importance class II. As such, the performance requirements were defined according to the limit state (LS) of Significant Damage (SD). Concerning the treatment of uncertainty, normal knowledge conditions were assumed, corresponding to Knowledge Level 2 (KL2). Nonlinear static analyses were carried out to obtain demand values on the designated control sections of the buildings' structural members. The capacities of the latter were defined according to the capacity models included in Annex A of EC8-3 (2005), and safety checks were run for both deformation- and strength-controlled mechanisms. This section presents and discusses the obtained results.

6.4.1. Modal periods

Table 6.2 summarizes the modal analyses' results, concerning the fundamental vibration periods of the pre-code RC buildings, according to directions XX and YY. The corresponding vibration mode shapes are not shown herein as not to take up too much space and (most of all) because nothing out of the ordinary stands out from those results. The only noteworthy fact is the vibration mode shapes of the mid-rise buildings already showing potential for the development of soft-storey mechanisms at some locations, but this too is to be expected when dealing with pre-code structures, due to the absence of capacity design and specific seismic detailing.

Table 6.2 – Fundamental vibration periods of the pre-code RC buildings

	XX	YY		XX	YY
Buildings	$T_1\ (sec)$	$T_1\ (sec)$	**Buildings**	$T_1\ (sec)$	$T_1\ (sec)$
2S_2x4	0.701	0.620	2S_3x5	0.723	0.650
3S_2x4	0.882	0.802	3S_3x5	0.881	0.814
4S_2x4	1.026	0.943	4S_3x5	1.024	0.938
5S_2x4	1.175	1.063	5S_3x5	1.169	1.046
6S_2x4	1.295	1.182	6S_3x5	1.292	1.152

6.4.2. Seismic demand definition

The base seismic demand was set according to the Portuguese National Annex (NA) on EC8-1 (2004), defining four hazard scenarios of increasing intensity (S1, S2, S3, S4), all on type B ground. Most of the possible seismic zone combinations in mainland Portugal were considered, covering the Northern, Central, Lisbon, and West Algarve regions. The underlying ideas behind this strategy were to obtain an overview of the actual need to retrofit these building typologies as their exposure changes within the territory, and also to evaluate the changes in the retrofitting systems' robustness. Table 6.3 generically characterizes the four hazard scenarios.

Table 6.3 – Seismic hazard scenarios for the assessment process

Scenario	Hazard level	EC8-1 seismic zones	Region of mainland Portugal
S1	Very low	1.6 + 2.5	North
S2	Low	1.5 + 2.4	Central
S3	Moderate	1.3 + 2.3	Lisbon
S4	High	1.1 + 2.3	West Algarve

According to the draft version of the Portuguese NA on EC8-3 (2005), a return period of 308 years should be considered to define the reference seismic demand for the LS of SD. As such, the values of the reference peak ground acceleration (PGA) on type A ground a_{gR} are obtained multiplying the values of a_{gR} given in EC8-1 (2004) (associated with a 475-yrp) by the coefficients given in EC8-3 (2005): Table NA.I (reproduced in Chapter 2 as Table 2.9). The assessment ground accelerations on type B ground $a_{gR} \cdot S$ are then obtained applying the soil factor S. Table 6.4 summarizes the obtained values, while figures 6.3 to 6.6 show the code-based response acceleration spectra associated with each hazard scenario, derived considering a viscous damping ratio $\xi_0 = 5\%$.

Table 6.4 – Calculation of the assessment ground accelerations on type B ground for the LS of SD

Scenario	EC8-1 seismic zones	a_{gR} (475-yrp)	YRP coefficient	a_{gR}	S	$a_{gR} \cdot S$
S1	1.6	0.036 · g	0.75	0.027 · g	1.35	0.036 · g
	2.5	0.082 · g	0.84	0.069 · g	1.35	0.092 · g
S2	1.5	0.061 · g	0.75	0.046 · g	1.35	0.062 · g
	2.4	0.112 · g	0.84	0.094 · g	1.35	0.127 · g
S3	1.3	0.153 · g	0.75	0.115 · g	1.34	0.153 · g
	2.3	0.173 · g	0.84	0.146 · g	1.30	0.189 · g
S4	1.1	0.255 · g	0.75	0.191 · g	1.25	0.239 · g
	2.3	0.173 · g	0.84	0.146 · g	1.30	0.189 · g

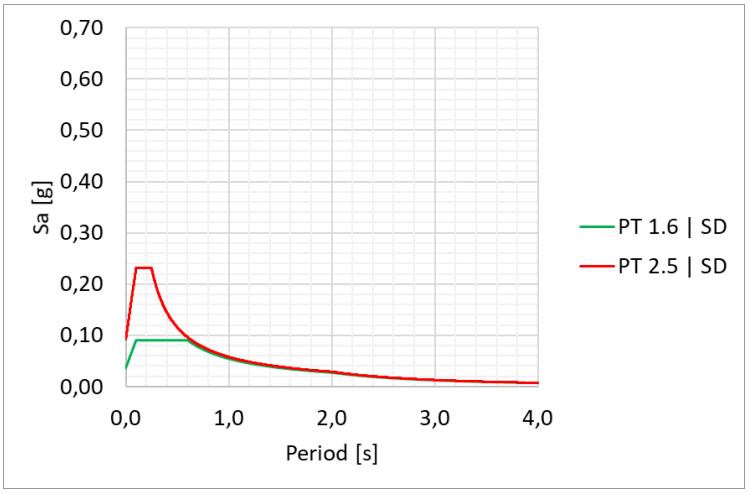

Figure 6.3 – Seismic hazard scenario S1: response acceleration spectra (LS of SD; type B ground; ξ_0 = 5%)

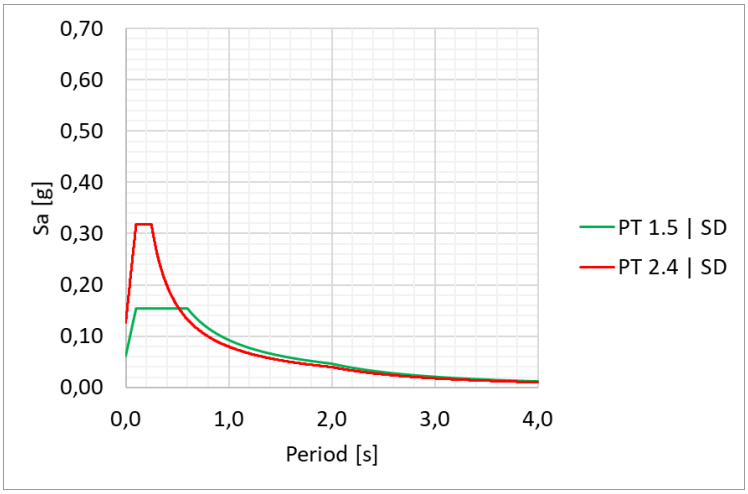

Figure 6.4 – Seismic hazard scenario S2: response acceleration spectra (LS of SD; type B ground; ξ_0 = 5%)

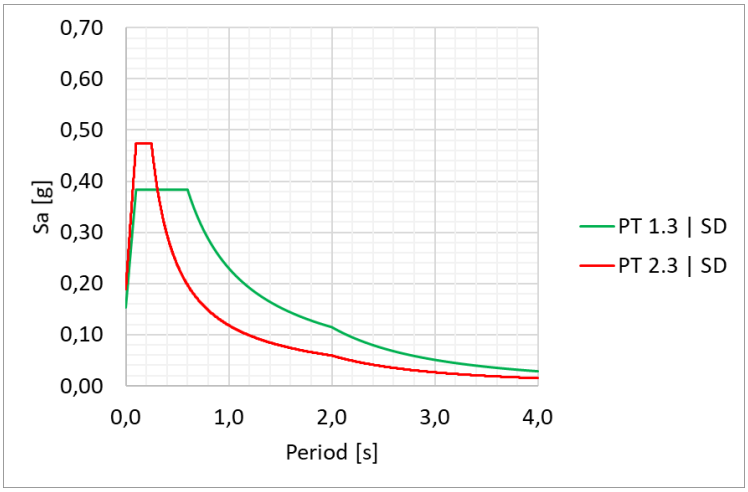

Figure 6.5 – Seismic hazard scenario S3: response acceleration spectra (LS of SD; type B ground; ξ_0 = 5%)

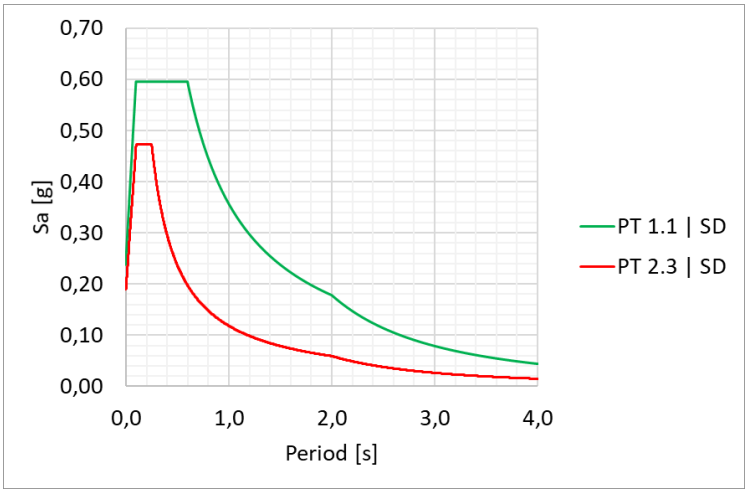

Figure 6.6 – Seismic hazard scenario S4: response acceleration spectra (LS of SD; type B ground; ξ_0 = 5%)

Based on the above-defined demand spectra and on the previously determined capacity curves, the target displacements d_t corresponding to the LS of SD were determined for each of the pre-code RC buildings, according to directions XX and YY, for each hazard scenario. Table 6.5 summarizes the obtained results. The corresponding graphical representation on the capacity curves of each building can be found in Appendix 3.

Table 6.5 – Target displacement values d_t (top displacement) for the pre-code RC buildings

	S1		S2		S3		S4	
Buildings	d_t^{XX} (m)	d_t^{YY} (m)	d_t^{XX} (m)	d_t^{YY} (m)	d_t^{XX} (m)	d_t^{YY} (m)	d_t^{XX} (m)	d_t^{YY} (m)
2S_2x4	0.0177	0.0165	0.0285	0.0265	0.0703	0.0654	0.1095	0.1019
2S_3x5	0.0181	0.0167	0.0291	0.0269	0.0719	0.0664	0.1122	0.1036
3S_2x4	0.0238	0.0220	0.0382	0.0353	0.0947	0.0879	0.1475	0.1370
3S_3x5	0.0241	0.0223	0.0387	0.0358	0.0964	0.0894	0.1502	0.1392
4S_2x4	0.0286	0.0268	0.0460	0.0430	0.1145	0.1073	0.1783	0.1671
4S_3x5	0.0290	0.0268	0.0466	0.0430	0.1157	0.1080	0.1798	0.1677
5S_2x4	0.0335	0.0314	0.0539	0.0505	0.1344	0.1245	0.2093	0.1940
5S_3x5	0.0338	0.0310	0.0543	0.0499	0.1352	0.1243	0.2105	0.1938
6S_2x4	0.0385	0.0367	0.0619	0.0590	0.1530	0.1442	0.2383	0.2247
6S_3x5	0.0388	0.0366	0.0623	0.0589	0.1533	0.1429	0.2386	0.2230

6.4.3. Member capacities computation

The capacities of the buildings' structural members were defined according to the capacity models included in Annex A of EC8-3 (2005), for both deformation- and strength-controlled collapse mechanisms (respectively, ductile and brittle), for the LS of SD. A Confidence Factor (CF) equal to 1.20 was considered in all calculations, consistent with the assumed KL2 conditions, and the recommendations of several authors (see sub-section 2.7.1.4. in Chapter 2) were followed as to make the computational process less intensive and time-consuming. Moreover, following the same strategy described in Sousa *et al* (2019), the member safety checks focused on the columns, hence only those capacities were computed herein.

The ductile capacities of the columns were defined in terms of their admissible chord rotations θ for the LS of SD (θ_{SD}), which are assumed to be 75% of those for the LS of Near Collapse (θ_{NC}), according to clause A.3.2.3 (1) in Annex A of EC8-3 (2005). For the quantification of θ_{NC}, Expression (2.13) was applied – see Chapter 2 – with the approximations proposed by Mpampatsikos *et al* (2008). As for brittle capacities, these were characterized by the admissible shear force V_R, quantified according to expressions (2.22) to (2.24) and subjected to the upper limits imposed by the shear capacity values obtained with the provisions of EC2-1-1 (2004). The recommendations of Mpampatsikos *et al* (2008) and Romão *et al* (2010a) were also followed to simplify the computational process. The obtained values of θ_{SD} and V_R are summarized in Appendix 2, separated by building, column, storey, and seismic demand direction (XX or YY). The numbering of the columns is the same shown in Appendix 1.

6.4.4. Performance evaluation

The performance evaluation results are given in Appendix 3 as demand-to-capacity ratios (D_i/C_i) for each control section i (*bottom* and *top*), for both deformation- and strength-controlled mechanisms, where a value above 1.0 represents an unsafe situation. The results are graphically presented to provide a better view of the global scenarios. The demand values (chord rotations and shear forces) on the columns' control sections were directly obtained from the outputs provided by the numerical models at the target displacements d_t corresponding to the LS of SD. The results are separated by building, hazard scenario, collapse mechanism, and seismic demand direction (XX or YY), adding up to one-hundred and sixty D/C ratio charts.

6.4.5. Discussion

The outcomes of the seismic assessment process led to different conclusions, depending essentially on the hazard scenarios and the buildings' number of storeys. For scenarios S1 and S2, both the chord rotation and the shear force D/C ratios were found to be below 1.0 in all control sections, thus allowing all buildings to be deemed safe for the LS of SD. In detail: (i) for scenario S1, the D/C ratios were typically below 20% and 60%, respectively for chord rotation and shear force; (ii) for scenario S2, these upper limits respectively increased to 30% and 80%. As scenarios S1 and S2 concern the Northern and Central regions of mainland Portugal and cover more than 60% of the territory, this is a very interesting conclusion. Even though the seismic demand spectra were defined considering type B ground conditions at all times, this can be seen as encouraging news concerning the seismic safety of low- and mid-rise pre-code RC buildings located in such regions.

For scenarios S3 and S4 (concerning the Lisbon and West Algarve regions), results pointed in the opposite direction. For scenario S3, the D/C ratios were found to be consistently below 1.0 in terms of chord rotation, but above 1.0 in several control sections in terms of the shear force. The situation found for scenario S4 was generally the same, except for the fact that the low-rise buildings also showed several D/C ratios above 1.0 in terms of chord rotation. All buildings were therefore deemed unsafe for LS of SD when located in hazard scenarios S3 and S4, thus requiring the design of an adequate retrofitting system. These conclusions are coherent with the remarks included in Sousa *et al* (2019) concerning the seismic behaviour of pre-code RC buildings, namely the prevalence of excessive shear force issues over those of chord rotation (at least for the LS of SD), and the potential to develop soft-storey mechanisms due to the several reductions of the columns' cross-sections that typically occur along the height of the buildings (besides, of course, the lack of specific seismic detailing and capacity design principles).

The above-referred prevalence of excessive shear force issues could make one think that a local strengthening strategy – such as FRP column wrapping or other – would be adequate to make the buildings code-compliant for scenarios S3 and S4. However, a closer look at the obtained results reveals that this problem mostly affects columns on the inside of the buildings, rather than those on the outside (i.e., located in the façades), at several storeys. This would make the retrofitting process extremely laborious and disruptive of the buildings' use. Moreover, local strengthening would not be

capable of eliminating the potential for the development of soft-storey mechanisms, hence a more adequate solution needs to be considered. The application of steel braces – on the other hand – will control floor displacements and therefore effectively reduce member demands in terms of shear force and chord rotation, thus adequately addressing the identified problems. Additionally, it will require a much less disruptive installation process, as braces will have to be applied only to the outside frames and (most times) at a single bay per storey. Even though caution is required to control the levels of axial force on columns affected by the braces (additional local FRP wrapping may sometimes be required to address this issue), this will clearly be an adequate solution.

6.5. SEISMIC RETROFITTING

Following up on the above-presented results, the methodology proposed in Chapter 5 was applied herein to design retrofitting systems capable of making the sample buildings code-compliant for scenarios S3 and S4. Each pre-code building thus gave origin to two retrofitted buildings (the design of the bracing system depends on the hazard scenario). The detailed design drawings can be found in Appendix 4, each building under the reference "Si_nS_y × x_RETRO", where n is the number of storeys, y and x are, respectively, the number of spans along global axes Y and X, and i is the number of the seismic hazard scenario (3 or 4). The assessment process was then carried out for the retrofitted buildings, as to evaluate their performance according to the EC8-3 (2005) requirements and thus the effectiveness of the design procedure. The required numerical models were obtained from those of the pre-code buildings by adding elements to simulate the steel braces, with the modelling options for the latter being the same as those considered in Chapter 4 (see sub-section 4.4.1.). The current section gives details on this procedure and discusses the obtained results.

6.5.1. Conceptual design

A global strengthening intervention using concentric X-diagonal steel braces is proposed herein for all of the sample buildings. The diagonals are composed by hot-rolled circular hollow sections (CHSH) steel profiles, directly connected to the RC beam-column nodes of the braced bays. The connections were thought out to behave as "nominally pinned joints" (as defined in EC3-1-8, 2005), i.e., capable of transmitting the internal forces without developing significant moments. At the points where the braces cross, no structural connection exists. When necessary, local strengthening of RC columns (FRP wrapping) was also performed to ensure that the additional axial forces induced by the steel braces do not cause the premature failure of the former structural members. In terms of layout, braces are only applied to the outside frames of the buildings. The initial idea was to brace only one bay per storey at each frame, but it quickly became evident that a larger number of elements would be required when designing retrofitting systems for scenario S4. Figures 6.7 to 6.10 show (as an example) the layouts of braces for the 3-storey buildings (3×5 and 2×4 spans), along global axes X and Y, as required by the seismic demand of scenarios S3 and S4. Incidentally, in these buildings the affected RC columns did not require any local strengthening.

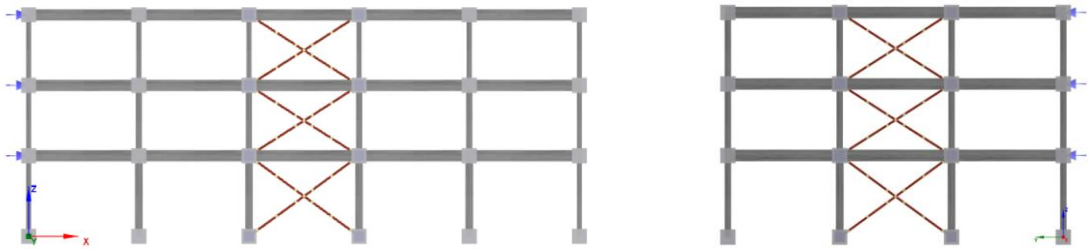

Direction XX Direction YY

Figure 6.7 – Layout of the proposed retrofitting system: S3_3S_3×5_RETRO

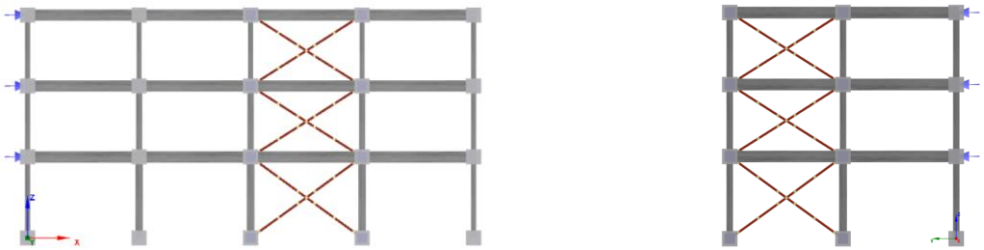

Direction XX Direction YY

Figure 6.8 – Layout of the proposed retrofitting system: S3_3S_2×4_RETRO

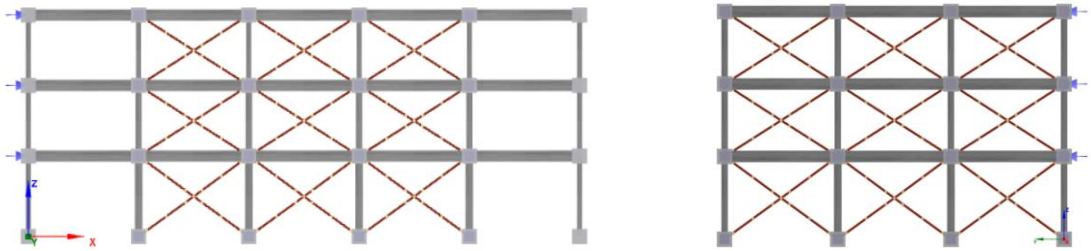

Direction XX Direction YY

Figure 6.9 – Layout of the proposed retrofitting system: S4_3S_3×5_RETRO

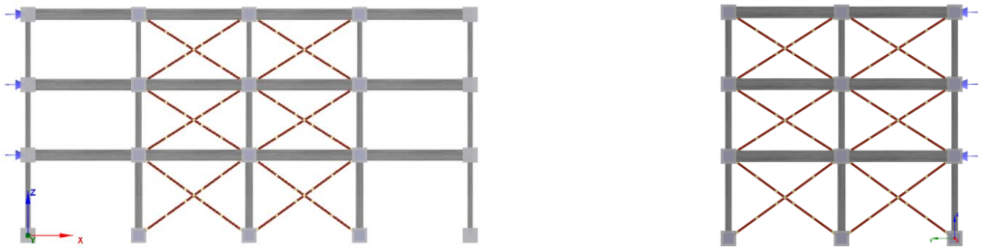

Direction XX Direction YY

Figure 6.10 – Layout of the proposed retrofitting system: S4_3S_2×4_RETRO

6.5.2. Design procedure

The SD elastic response spectra and the capacity curves of the pre-code RC buildings (both required as preliminary data for the design process itself) were already obtained during the seismic assessment process (see figures 6.5 and 6.6, and Appendix 3, respectively). The axial force capacity envelopes of all columns were also evaluated at that stage. Results can be found in Appendix 2. Two tables per building are given in the latter (see tables A2.41 to A2.60), showing axial force capacities, in compression and in tension, for each column at each storey. The corresponding *N-M* interaction diagrams are not included, as it is thought to be redundant information. The pre-selection of cross-sections for the braces was then carried out according to the procedure described in Chapter 5 (see sub-sections 5.3.1. and 5.4.1. for details). However, it is noteworthy that two different pre-selection tables had to be organized herein, due to the height of the first storey being greater than those of the upper storeys (3.20 m vs. 2.80 m, respectively, on all buildings), thus affecting the braces' initial length L_i and all other variables that depend on it. Tables 6.6 and 6.7 summarize the obtained results (all included variables as previously defined in sub-section 5.4.1.). As for the assumed inelastic lateral displacement shapes δ_i of the retrofitted structures, the same approach followed in Chapter 5 was adopted herein, i.e., the expression proposed by Priestley *et al* (2007) (Expression (5.18) in Chapter 5) was applied to all buildings regardless of their height. As previously referred, this option produces better design results (i.e., on the safer side) than those obtained with the linear shape (several trials were run herein considering both). Moreover, the comparison with the final lateral displacement profiles at peak displacement response provided no reasons to change the approach. The assumed lateral displacement shapes δ_i are part of the data compiled in Appendix 5.

Table 6.6 – Pre-selection of steel braces: admissible cross-sections for the first storey

Cross-section	$\bar{\lambda}$	$N_{pl,Rd}$ (kN)	$N_{b,Rd}$ (kN)	$N_{pl,Rd}{}^{V}$ (kN)	$N_{b,Rd}{}^{V}$ (kN)	$N_{pl,Rd}{}^{H}$ (kN)	$N_{b,Rd}{}^{H}$ (kN)
CHSH 139.7×6.0	1.48	866.25	329.65	509.50	193.89	700.57	266.60
CHSH 139.7×5.6	1.48	811.25	310.11	477.15	182.40	656.09	250.79
CHSH 139.7×5.0	1.47	728.75	280.54	428.63	165.00	589.37	226.88
CHSH 139.7×4.0	1.46	587.81	228.74	345.73	134.54	475.39	184.99
CHSH 139.7×3.6	1.46	529.38	207.50	311.36	122.04	428.12	167.81
CHSH 139.7×3.2	1.45	470.94	185.76	276.99	109.26	380.86	150.23
CHSH 114.3 x 6.0	1.83	701.25	184.45	412.46	108.49	567.13	149.17
CHSH 114.3 x 5.6	1.82	656.56	173.87	386.17	102.27	530.99	140.62
CHSH 114.3 x 5.0	1.81	591.25	157.77	347.76	92.80	478.17	127.60
CHSH 114.3 x 4.0	1.80	477.81	129.34	281.04	76.07	386.42	104.60
CHSH 114.3 x 3.6	1.79	429.69	117.56	252.73	69.14	347.50	95.07
CHSH 114.3 x 3.2	1.79	385.00	105.31	226.45	61.94	311.36	85.17
CHSH 88.9 x 6.0	2.38	536.25	86.23	315.41	50.72	433.68	69.74
CHSH 88.9 x 5.0	2.36	453.75	74.03	266.88	43.54	366.96	59.87
CHSH 88.9 x 4.0	2.34	367.81	61.37	216.34	36.10	297.46	49.64
CHSH 88.9 x 3.6	2.32	331.72	55.98	195.11	32.93	268.27	45.27
CHSH 88.9 x 3.2	2.31	296.31	50.41	174.28	29.65	239.64	40.77

Table 6.7 – Pre-selection of steel braces: admissible cross-sections for the upper storeys

Cross-section	$\bar{\lambda}$	$N_{pl,Rd}$ (kN)	$N_{b,Rd}$ (kN)	${N_{pl,Rd}}^{V}$ (kN)	${N_{b,Rd}}^{V}$ (kN)	${N_{pl,Rd}}^{H}$ (kN)	${N_{b,Rd}}^{H}$ (kN)
CHSH 139.7×6.0	1.42	866.25	353.77	465.07	189.93	730.82	298.46
CHSH 139.7×5.6	1.42	811.25	332.76	435.54	178.65	684.42	280.74
CHSH 139.7×5.0	1.41	728.75	300.98	391.25	161.59	614.82	253.93
CHSH 139.7×4.0	1.40	587.81	245.35	315.58	131.72	495.91	206.99
CHSH 139.7×3.6	1.39	529.38	222.53	284.21	119.47	446.61	187.74
CHSH 139.7×3.2	1.39	470.94	199.18	252.83	106.94	397.31	168.04
CHSH 114.3 x 6.0	1.75	701.25	199.07	376.48	106.88	591.62	167.95
CHSH 114.3 x 5.6	1.74	656.56	187.65	352.49	100.74	553.92	158.31
CHSH 114.3 x 5.0	1.74	591.25	170.26	317.43	91.41	498.81	143.64
CHSH 114.3 x 4.0	1.72	477.81	139.55	256.53	74.92	403.11	117.74
CHSH 114.3 x 3.6	1.71	429.69	126.83	230.69	68.09	362.51	107.00
CHSH 114.3 x 3.2	1.71	385.00	113.62	206.70	61.00	324.81	95.85
CHSH 88.9 x 6.0	2.28	536.25	93.38	287.90	50.13	452.41	78.78
CHSH 88.9 x 5.0	2.27	453.75	80.16	243.61	43.04	382.81	67.63
CHSH 88.9 x 4.0	2.24	367.81	66.45	197.47	35.68	310.31	56.06
CHSH 88.9 x 3.6	2.23	331.72	60.61	178.09	32.54	279.86	51.13
CHSH 88.9 x 3.2	2.22	296.31	54.58	159.08	29.30	249.99	46.05

The seismic assessment results given in Appendix 3 show that the failure mechanism of the critical columns at the LS of SD is governed by their shear force capacity. Furthermore, the columns on which the higher D/C ratios occur are typically those located on the inside of the buildings – not on the outside frames where braces will be installed – being therefore less susceptible to strong axial force variations during the earthquake. Consequently, the admissible shear forces V_R on those members can be approximated to those determined in sub-section 6.4.3. (i.e., the shear capacity values before and after the installation of the braces are approximately the same). Hence, the design displacements Δ_d at the first floor of the buildings were defined as those which cause the critical columns' shear demand to come close to the corresponding capacity and obtained from the previously performed nonlinear static analyses. The initial estimate ΔN_0 of the axial loads imposed to the columns by the braces at the performance point was thus not crucial this time, as no updated axial forces ($N_{G+Q} + \Delta N_0$) were required to compute the critical columns' shear capacities after retrofitting. However, this effect obviously exists on the outside frames, and can significantly reduce both the chord rotation and shear force capacities of the affected columns when the limits of their axial force capacity envelopes (both in compression as in tension) start to draw near. Consequently, one had to remain vigilant not to overlook an eventual migration of the problem (i.e., of the critical D/C ratios) to the columns of the outside frames, once the braces are installed. The variation of the axial forces on the columns to which the braces are attached were thus always pre-evaluated (and flagged when excessive), and then used to compute updated capacities for those members during the performance evaluation of the retrofitted structures. Table 6.8 shows (as an example) the results of the design procedure for the 3-storey 3×5 building (scenario S3 and demand direction XX). The calculation tables for the full sample (scenarios S3 and S4, demand directions XX and YY) can be found in Appendix 5.

Table 6.8 – Design procedure result (example): S3_AST1_3S_3×5_XX_RETRO

ASSUMED

STOREY S_i	m_i [ton]	δ_i	F_i [kN]
6	0,00	0,000	0,00
5	0,00	0,000	0,00
4	0,00	0,000	0,00
3	232,33	1,000	0,46
2	232,33	0,754	0,34
1	232,33	0,441	0,20

α1	0,911
PF1	1,245

START	Tens.	Comp.
ΔN_0 [kN]	400,00	650,00

B [m]	h [m]	L_i [m]	E_s [GPa]	f_{ym} [MPa]	ε_y
4,40	3,20	5,441	210,00	343,75	0,001637

1st Storey

Δ_y [m]	Δ_d [m]	μ
0,01101	0,01850	1,681

SDOF

EVD [%]	$S\Delta_d$ [m]	T_e [s]	K_e [kN/m]
12,28%	0,03371	0,844	35185,20

1st Storey

V_b^{REQ} [kN]	V_b^{BF} [kN]	$V_b^{BR,REQ}$ [kN]
1186,19	635,14	646,32

1st Storey

	BR S_1	V_b^{BR} [kN]	V_b [kN]	Ω
	CHSH			
x2	88,9 x 4,0	664,42	1204,28	1,015

ASSUMED

STOREY S_i	DRIFTS [m]	V_i^{BF} [kN]	
6	0,00000		
5	0,00000		
4	-0,04197		
3	0,01032	234,16	x2
2	0,01315	406,19	x2
1	0,01850	635,14	x2

N^{th} Storey

V_i^{REQ} [kN]	$V_i^{BR,REQ}$ [kN]	BR S_i	V_i^{BR} [kN]
0,00	0,00	0	0,00
0,00	0,00	0	0,00
0,00	0,00	0	0,00
548,67	349,64	88,9 x 3,2	564,44
962,45	617,18	88,9 x 3,6	631,30
1186,19	646,32	88,9 x 4,0	664,42

END	Tens.	Comp.
ΔN [kN]	435,12	615,35
	8,78%	-5,33%

SDOF

Sa [g]	0,19336

(All variables as defined for expressions (5.5) to (5.17) in Chapter 5.)

6.5.3. Validation

After assigning the designed cross-sections to their respective brace members in the retrofitted structures' numerical models, the corresponding capacity curves were obtained following the same procedure described in section 6.3. (forty curves in total, as each pre-code building gave origin to two retrofitted buildings, as previously referred). The target displacements d_t corresponding to the LS of SD were then determined based on the demand spectra for scenarios S3 and S4. Table 6.9 summarizes the obtained results. The corresponding graphical representation on the capacity curves of each retrofitted building can be found in Appendix 6.

Table 6.9 – Target displacement values d_t (top displacement) for the retrofitted buildings

	S3			S4	
Buildings	$\boldsymbol{d_t^{XX}\,(m)}$	$\boldsymbol{d_t^{YY}\,(m)}$	**Buildings**	$\boldsymbol{d_t^{XX}\,(m)}$	$\boldsymbol{d_t^{YY}\,(m)}$
S3_2S_2x4_RETRO	0.0273	0.0268	S4_2S_2x4_RETRO	0.0330	0.0318
S3_2S_3x5_RETRO	0.0380	0.0380	S4_2S_3x5_RETRO	0.0303	0.0347
S3_3S_2x4_RETRO	0.0445	0.0475	S4_3S_2x4_RETRO	0.0380	0.0370
S3_3S_3x5_RETRO	0.0505	0.0520	S4_3S_3x5_RETRO	0.0367	0.0370
S3_4S_2x4_RETRO	0.0485	0.0600	S4_4S_2x4_RETRO	0.0520	0.0480
S3_4S_3x5_RETRO	0.0550	0.0580	S4_4S_3x5_RETRO	0.0400	0.0405
S3_5S_2x4_RETRO	0.0565	0.0778	S4_5S_2x4_RETRO (*)	0.0690	0.0700
S3_5S_3x5_RETRO	0.0820	0.0805	S4_5S_3x5_RETRO (*)	0.0620	0.0690
S3_6S_2x4_RETRO	0.0885	0.0912	S4_6S_2x4_RETRO (*)	0.0900	0.0990
S3_6S_3x5_RETRO	0.0995	0.0990	S4_6S_3x5_RETRO (*)	0.0825	0.0830

(*) with CFRP wrapping of braced columns at lower storeys

The performance evaluation results of the retrofitted buildings were analysed, as always, in terms of D/C ratios on the columns' control sections. The demand values (chord rotations and shear forces) were directly obtained from the outputs provided by the numerical models at the above-listed target displacements d_t. As for the capacity values (θ_{SD} and V_R), these were updated considering the corresponding axial forces $N(d_t)$, as previously referred. The obtained D/C ratio charts for all buildings are included in Appendix 6. For scenario S3, no unsafe situations were observed, allowing the designed retrofitting solutions to be accepted as final. For scenario S4, however, the 5- and 6-storey buildings required further action. Two distinct unsafe situations were initially observed: (i) shear force D/C ratios above 1.0 on columns to which braces are attached; (ii) premature collapse of the same type of columns. Both situations were caused by the axial forces induced by the braces (tension or compression, respectively) and expected from the pre-evaluation carried out for those forces during the design stage. In the first situation, the reduced compressive forces on the columns caused shear capacities to drop abruptly, while in the second, the excessive compressive forces caused the columns to collapse before the target displacements could be reached. It thus became clear that these members would require local strengthening to increase their shear and compressive strengths. As such, a CFRP wrapping based solution was designed for the lower storeys. Details are included on the design

drawings in Appendix 4. Updated capacity curves were then obtained from the modified numerical models, the target displacements were adjusted, the new member capacities were computed according to the capacity models described in EC8-3 (2005): A.4.4 for RC members with FRP wrapping, and the final D/C ratios were obtained. No unsafe situations were observed this time, thus allowing the designed retrofitting solutions for scenario S4 to be accepted as final. To be duly noted that the target displacements d_t shown in Table 6.9 (above), as well as the capacity curves and D/C ratio charts in Appendix 6, are the final ones.

6.5.4. Discussion

The performance evaluation results given above show that all buildings were successfully retrofitted and are now expected to behave adequately according to the requirements of EC8-3 (2005) concerning the LS of SD. The proposed design methodology thus provided a swift and efficient way to strengthen the full sample of pre-code RC buildings, while revealing itself to be more versatile and transparent than the traditional force-based design process. The procedure does in fact work well with both types of critical member failure mechanism (deformation or shear force) and provides the user with a clear view (or preview) of what will be the behaviour of the retrofitted structure, which is advantageous over any behaviour factor-based process.

During the validation process, besides obtaining the chord rotation and shear force D/C ratios on the columns' control sections, the relevant global parameters were also evaluated and compared to the assumptions made during the design process, not for the purpose of ruling in favour (or against) the retrofitted structures' code safety, but to check if their behaviour remained coherent at all times with what is described in Chapter 5. In terms of base shear values V_b (and respective components ${V_b}^{RC}$ and ${V_b}^{BR}$), the method's estimates were generally in good agreement with the values provided by the nonlinear static analyses of the retrofitted buildings. The same stands in terms of the axial loads ΔN induced by the braces on the columns to which they are attached, with the method's estimates being on the safe side, as expected. When the values of ΔN became too high for the columns to perform adequately under the design earthquake, then a local strengthening solution was considered to increase their shear and compressive strengths. This allowed for the designed steel braces (i.e., the global retrofitting systems) to develop their full potential. However, already when the limits of the axial force capacity envelopes of the columns start to draw near, a significant reduction of the available global ductility may be observed, and the structures' global behaviour may start to differ from what is expected (i.e., what is shown in Figure 5.2 in Chapter 5). This means that, even when no D/C ratios above 1.0 are found at first, the global behaviour of the retrofitted structure (i.e., the evolution of its capacity curve) should be carefully interpreted to check if the braced columns have become too vulnerable to the effects of the increased axial forces. Looking closely at the results in Appendix 6 and combining them with the respective values of the columns' axial forces, three potential situations are identified in demand direction YY: (i) the 2×4 six-storey building, when in hazard scenario S3; (ii) and (iii) the four-storey buildings, when in hazard scenario S4. As such, it would be beneficial to extend the above-described CFRP wrapping solution to the corner columns of these buildings, as it would stabilize the global behaviour under increasing lateral displacements.

Concerning the inelastic lateral displacement shapes δ_i of the retrofitted structures, the profiles corresponding to each target displacement were plotted against those assumed during the design process. Two examples are shown in Figure 6.11, concerning the three- and six-storey buildings in different hazard scenarios. For these cases, as well as for the others in general, the final shape lies between the linear and assumed shapes (minor differences were identified in the YY direction for the five- and six-storey buildings). As referred in Chapter 5, this ensures that the base shear resistance of first storey braces ${V_b}^{BR}$ is not underestimated during the design process. However, this might not be absolutely true for the upper storey braces (i.e., for ${V_i}^{BR}$), depending on the final shape being closer to the linear or to the assumed shape. Expressions (5.14) to (5.17) (see Chapter 5) apply, within which factors exist that work in opposition (i.e., some contribute to an overestimation of ${V_i}^{BR}$, and others do the opposite). Having said that, at most this may require minor corrections of the upper braces' cross-sections, thus not posing any limitation to the proposed design methodology. Nonetheless, the author is still studying the influence of several factors on the inelastic lateral displacement shapes of pre-code RC framed buildings retrofitted with steel braces and expects that some of the findings may provide inputs to an updated version of this design methodology. Most likely, considerations about the relative lateral stiffness of braces and columns at each storey will be added to the design procedure, for the purpose of achieving even more controlled drift profiles (hence, global collapse mechanisms), but that will fall outside the scope of this thesis.

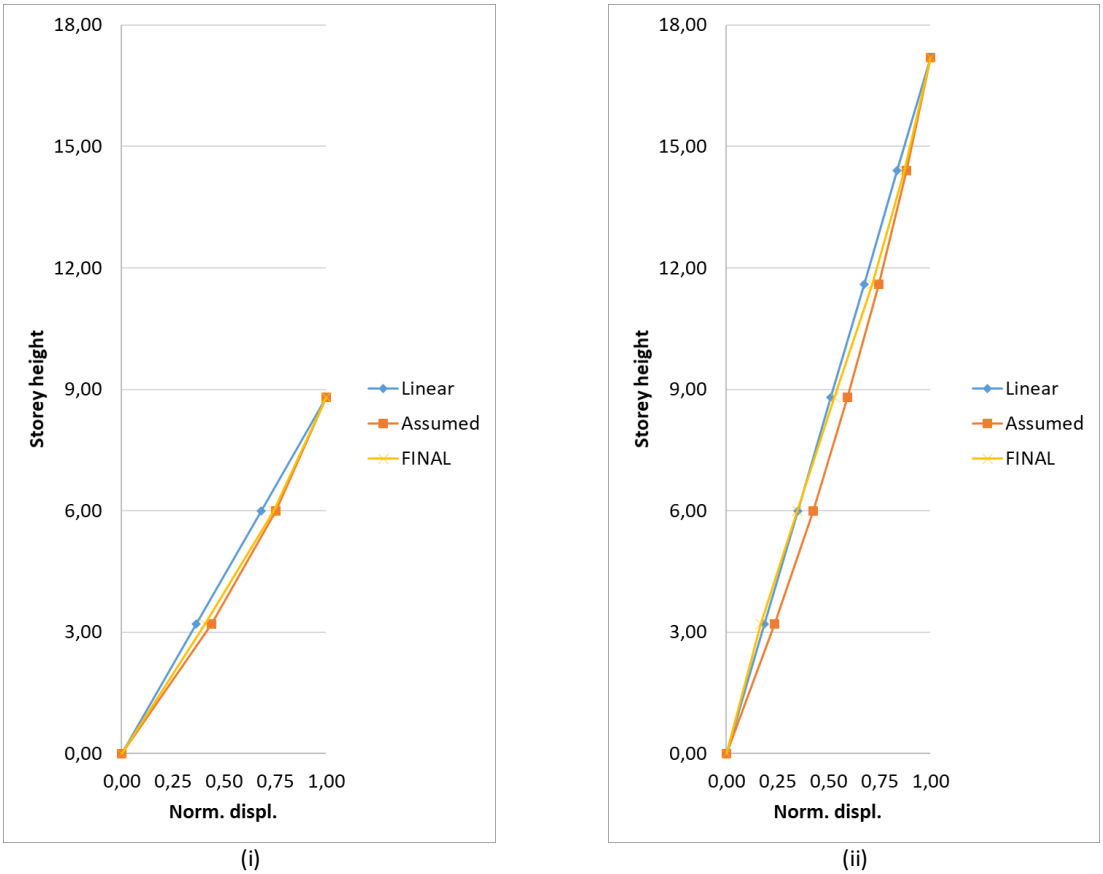

Figure 6.11 – Lateral displacement shapes comparison: (i) S3_3S_3×5_XX_RETRO; (ii) S4_6S_3×5_XX_RETRO

The results discussed above show that the proposed design methodology is robust enough to be systematically applied to the retrofitting of low- and mid-rise pre-code RC buildings which are part of the Portuguese building stock, thus fulfilling this chapter's purpose. In terms of calibration according to the EC8-3 (2005) performance requirements, the procedure proved to be easily adapted to both types of member failure mechanism (deformation- or strength-controlled), hence no adjustments or modifications are required from that point of view. However, the comments made above concerning the potential vulnerability of the braced RC columns to the effects of the increased axial forces suggest the need for an upper limit to the columns' normalized axial forces $\nu = N/(b \cdot h \cdot f_c)$ – where N is the axial force, b is the width of the compression zone, h is the depth of the cross-section, and f_c is the estimated value of the concrete compressive strength – that would help to flag more effectively situations in which the global retrofitting system should be combined with local strengthening of the affected columns. This possibility is currently under evaluation but will surely be included in future updates to the design procedure.

Lastly, tables 6.10 and 6.11 summarize the fundamental vibration periods of the retrofitted buildings, according to directions XX and YY, as to indirectly illustrate the evolution that needed to occur in terms of elastic stiffness for a satisfactory seismic behaviour to be achieved (these results compare directly with those on Table 6.2). For hazard scenario S3, the fundamental periods suffered reductions ranging between 25% and 50%, while for hazard scenario S4 the interval is narrower, with those reductions ranging between 50% and 60%.

Table 6.10 – Fundamental vibration periods of the retrofitted buildings for hazard scenario S3

	XX	YY		XX	YY
Buildings	T_1 (sec)	T_1 (sec)	**Buildings**	T_1 (sec)	T_1 (sec)
S3_2S_2x4_RETRO	0.355	0.345	S3_2S_3x5_RETRO	0.443	0.424
S3_3S_2x4_RETRO	0.473	0.478	S3_3S_3x5_RETRO	0.570	0.521
S3_4S_2x4_RETRO	0.599	0.583	S3_4S_3x5_RETRO	0.661	0.639
S3_5S_2x4_RETRO	0.738	0.715	S3_5S_3x5_RETRO	0.829	0.771
S3_6S_2x4_RETRO	0.838	0.835	S3_6S_3x5_RETRO	0.952	0.879

Table 6.11 – Fundamental vibration periods of the retrofitted buildings for hazard scenario S4

	XX	YY		XX	YY
Buildings	T_1 (sec)	T_1 (sec)	**Buildings**	T_1 (sec)	T_1 (sec)
S4_2S_2x4_RETRO	0.318	0.312	S4_2S_3x5_RETRO	0.348	0.343
S4_3S_2x4_RETRO	0.343	0.342	S4_3S_3x5_RETRO	0.339	0.339
S4_4S_2x4_RETRO	0.409	0.398	S4_4S_3x5_RETRO	0.397	0.400
S4_5S_2x4_RETRO (*)	0.479	0.497	S4_5S_3x5_RETRO (*)	0.490	0.521
S4_6S_2x4_RETRO (*)	0.589	0.622	S4_6S_3x5_RETRO (*)	0.608	0.581

(*) with CFRP wrapping of braced columns at lower storeys

6.6. CONCLUDING REMARKS

In this chapter, the displacement-based design methodology proposed in Chapter 5 was extensively validated and calibrated according to the EC8-3 (2005) performance requirements, using a sample of artificially generated pre-code RC buildings. The before- and after-retrofitting structural performances were evaluated using nonlinear static analysis, the obtained results discussed, and several comments made about the method's robustness. The above-presented conclusions are supported by a large volume of results which can be found in appendices 1 to 6. The purpose of further strengthening the proposed design methodology is therefore successfully achieved.

The contributions of this proposal, as well as its advantages over the traditional force-based design process, have already been summarized in the concluding remarks to Chapter 5. Present limitations and developments in progress have also been referred. Therefore, at this point there is no need to go through them again. The author would, however, like to recall the final notes to chapters 3 and 4, concerning the need for professionals to become familiarized with other (more advanced) methods of analysis than their typical seismic design instruments (i.e., linear elastic analysis combined with behaviour factors and seismic codes oriented towards the design of new buildings). Even though the proposed methodology is simple enough to be applied in practice, it still requires users to be acquainted with nonlinear procedures. The seismic assessment and retrofitting of existing RC structures is a far more complex matter than the seismic design of new RC structures, and any methodology applied within a linear elastic analysis context will produce assessment results that (most likely) are too pessimistic, thus penalizing subsequent decisions. As such, it is the author's firm belief that it's time for professionals to overcome the tendency to remain unchanged and move to upgrading their structural analysis and modelling skills to levels that will allow them not to make gross judgment errors or base their work on results that may not resemble reality in any way.

CHAPTER 6 – VALIDATION AND CALIBRATION OF THE PROPOSED DESIGN PROCEDURE

6.1. INTRODUCTION....6.1
6.2. SAMPLE DEFINITION....6.2
6.3. NUMERICAL MODELLING....6.3
6.4. SEISMIC ASSESSMENT....6.5
6.4.1. Modal periods....6.5
6.4.2. Seismic demand definition....6.5
6.4.3. Member capacities computation....6.8
6.4.4. Performance evaluation....6.9
6.4.5. Discussion....6.9
6.5. SEISMIC RETROFITTING....6.10
6.5.1. Conceptual design....6.10
6.5.2. Design procedure....6.12
6.5.3. Validation....6.15
6.5.4. Discussion....6.16
6.6. CONCLUDING REMARKS....6.19

CHAPTER 7

ON THE EVOLUTION OF THE SEISMIC RISK OF THE STUDIED SAMPLE OF STRUCTURES

7.1. INTRODUCTION

Several applications of the design procedure proposed in this thesis were carried out throughout chapters 5 and 6, showing its merits, testing its robustness, and demonstrating its effectiveness, all in the cause of arguing that it can be systematically used by practitioners who are involved in the seismic assessment and retrofitting of existing RC structures. The effectiveness of the designed retrofitting systems was demonstrated by evaluating the performance of the retrofitted structures according to the requirements of EC8-3 (2005). However, to analyse the evolution of seismic risk between the original conditions and those created by the strengthening interventions, it is necessary to go beyond the verification of code criteria compliance. Fragility functions are required, as well as an exposure model that defines the spatial distribution and economic value of the building typologies under analysis, both of which must then be combined with a seismic hazard model deemed adequate for the locations in question. The purpose of this chapter is to present such a study, using the sample of structures that was defined in Chapter 6, and thus validate the designed retrofitting systems beyond the requirements of the assessment code.

Fragility functions provide the probability of exceeding a set of damage states as function of a ground motion intensity measure (usually ground or building response) and have been recognized in the last decades as a fundamental tool in the process of assessing seismic risk. When combined with a consequence model that relates each damage state with a loss ratio (i.e., the ratio of absolute economic loss to total replacement cost), they generate vulnerability functions, which provide the probabilistic distribution of loss ratio as function of the same intensity measure. Empirical methodologies, based on observed building damage and repair cost data from past earthquakes, have been traditionally used to produce such functions. However, several studies (e.g., Rossetto and Elnashai, 2005) propose the use of analytical methodologies as a way to overcome limitations such as the frequent lack of post-earthquake data. These methodologies can be applied either to a single structure that is believed to be representative of a building class, or to a set of randomly generated buildings, modelled using nonlinear static or dynamic analysis techniques and tested under specific lateral loading patterns or accelerograms. To evaluate how the capacity, fragility, vulnerability, and

risk outputs are influenced by these methodologies, Silva *et al* (2014b) conducted a study comparing static and dynamic approaches and discussed the relative accuracy between them. The results of that study showed similarity between the vulnerability functions obtained through a displacement-based adaptive pushover (DAP) analysis, combined with the N2 method, and those obtained through nonlinear dynamic analysis. This conclusion suggests that nonlinear static procedures may be a valid alternative for the rapid and accurate assessment of seismic vulnerability, which is quite an important finding for large-scale studies. More details can be found in the original research paper, to which readers are strongly referred to.

The fragility functions in this chapter are therefore derived following an analytical methodology based on nonlinear static analyses and procedures. The assessment of seismic risk is then performed using the open-source software *OpenQuake* (Silva *et al,* 2014a). The obtained loss ratios are compared, and the effects of the retrofitting systems obtained with the design procedure proposed in Chapter 5 are analysed and discussed. The detailed framework of the conducted study is presented below. Readers should, however, be aware that no building-to-building variability (i.e., variability of material and geometrical properties within the defined sample) was considered simply because the proposed design procedure is not yet fully automatized, making it thus impracticable (for the time being) to swiftly retrofit what would become a much larger sample of pre-code RC buildings obtained through Monte Carlo simulation. Although the author recognizes that this option may be seen as a limitation of the devised strategy, he also believes it does not compromise the above-referred purpose to validate the designed retrofitting systems beyond the requirements of the assessment code, therefore can be accepted without prejudice.

7.2. FRAMEWORK OF THE STUDY

The considered sample of buildings includes the ten original RC buildings analysed in Chapter 6, plus the two sets of ten correlated retrofitted buildings designed to withstand the seismic demand defined by hazard scenarios S3 and S4 (characterized in Table 6.3). Six building classes were considered within the sample: concerning the number of storeys, the classification proposed by Silva (2013) is followed, i.e., buildings up to three storeys are low-rise (LR), and those between four and six storeys are mid-rise (MR); concerning the structural design approach, original buildings are termed “PC”, while their retrofitted counterparts are termed “R1” and “R2”. This allows results – in terms of structural fragility and seismic risk – to be organized in a way that enables the desired view over the evolution between the original conditions and those created by the strengthening interventions.

The process of deriving the required fragility functions starts with the generation of capacity curves for the original and retrofitted structures. This was accomplished in Chapter 6 through DAP analyses, for the two main directions XX and YY, originating a total of sixty curves (twenty for the original structures, and forty for the retrofitted structures). Each curve is transformed into that of the equivalent SDOF system, and a nonlinear static procedure (the N2 method, in this case) is used to estimate the target displacements for a selected set of ground motion records (the procedure for the selection of records is addressed further ahead). These estimates are then compared with limit state (LS) displacements (the definition of LS’s is also addressed further ahead) to determine, within each building class and per

ground motion record, the number of structures in each damage state. In order to graphically represent these results, an intensity measure of the imposed seismic demand (i.e., of the selected ground motion records) must be chosen. From the available options, the spectral acceleration at the fundamental vibration period $S_a(T_1)$ has been advocated by many authors (e.g., Bommer *et al,* 2002), as it provides good correlation with building damage. It also seemed like the best option for the purpose of this study. However, as each sampled structure has its own fundamental vibration period T_1, the mean value of the latter is considered across each building class (see individual values in Chapter 6, tables 6.2, 6.10, and 6.11). Scatter plots are thus generated (one per building class), relating the spectral acceleration $S_a(T_1)$ of each ground motion record with the respective number (in percentage) of structures that fail under its action. Finally, using least squares regression to fit a lognormal cumulative distribution to the data, the fragility functions are derived.

The seismic risk assessment process is then carried out, starting with the definition of the input components required by the *OpenQuake* engine: (i) the seismic hazard model; (ii) the exposure model; (iii) the vulnerability model. For the hazard model, the seismic ruptures' characteristics are based on the work of Carvalho *et al* (2008a), the ground motion fields are estimated with the ground motion prediction equations (GMPE) proposed by Atkinson and Boore (2006) and Akkar and Bommer (2010), and the amplification effects due to the local site conditions are handled through the approach described in Silva *et al* (2014a). For the spatial distribution of the assets and economic value of their structural components, the ESRM20 exposure model for Portugal (included in the recently developed European Seismic Risk Model (ESRM20) – see Crowley *et al,* 2021) is adopted. As for the structural vulnerability model, the corresponding functions are obtained combining the derived fragility functions with an adequate consequence model (as previously referred). These three components are provided as input to the *OpenQuake* scenario risk calculator, which provides the above-referred loss ratios, per region and building class. Finally, the evolution of seismic risk is analysed comparing the results for the original buildings with those for their retrofitted counterparts. The following sections provide further details on the performed fragility and risk analyses.

7.3. FRAGILITY ANALYSIS

7.3.1. Selection of ground motion records

Several ground motion record selection techniques have been proposed in the last years, ranging from simple procedures based on magnitude, distance, and site conditions, to more complex procedures that consider the spectral shape for each site, the hazard level, and the structural vibration period(s) of interest (Macedo, 2017). In the current study, the recent recommendations by Araújo *et al* (2016) were followed. For each of the site locations corresponding to the above-referred hazard scenarios S3 and S4 (respectively, Lisbon and West Algarve), a set of forty ground motion records was selected and scaled to obtain proper matching between the set's mean spectrum and the EC8-1 (2004) elastic response spectrum. The process was conducted using the *SelEQ* tool (Macedo and Castro, 2017), same as in Chapter 3 (see sub-section 3.4.1.2.). Figure 7.1 shows the individual, median, and mean spectra of the two sets of records, as well as the target response spectrum for each.

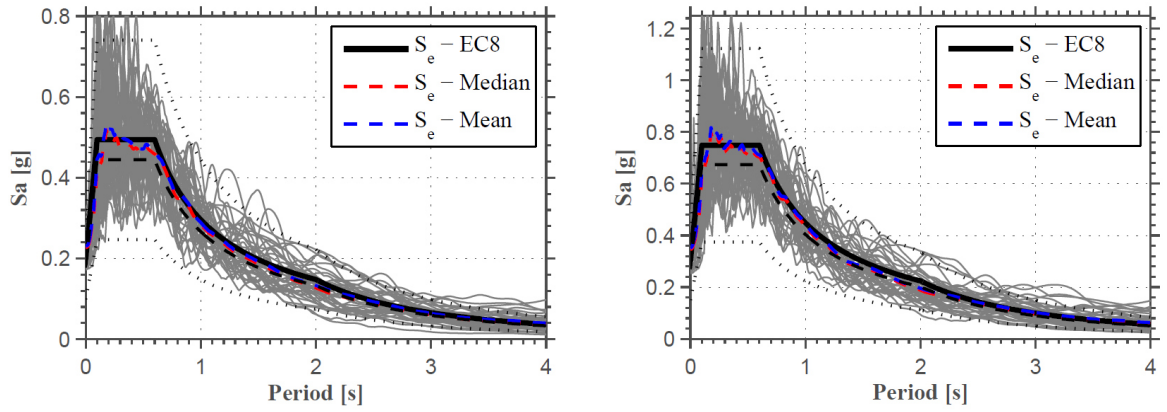

Figure 7.1 – Response spectra of the selected ground motion records and corresponding EC8-1 (2004) target spectrum (475-yrp; $\xi_0 = 5\%$): (a) Lisbon (zone 1.3, type B ground); (b) West Algarve (zone 1.1, type B ground)

The selected ground motion records were obtained from real earthquake events. The seismological criteria for the preliminary search that is first carried out by *SelEQ* were based on the characteristics of the events that define zones 1.3 and 1.1 of the Portuguese territory, according to the country's National Annex (NA) in EC8-1 (2004). Magnitudes and epicentral distances higher than 5.5 and 20 *km*, respectively, were considered accordingly. Additionally, an interval of values between 360 *m/s* and 800 *m/s* was considered for the average shear wave velocity $v_{s,30}$, in agreement with the type B ground as defined in EC8-1 (2004). The preliminary search results were then narrowed down by imposing spectral compatibility between the mean spectrum of the group and each target response spectrum, within the period intervals defined in EC8-1 (2004). In the optimization process, the scaling factors were limited to the interval between 0.5 and 2.0, the mismatch between the mean spectrum of the group and each target spectrum was limited to an interval of ±10%, and the mismatch between each individual record and each target spectrum was limited to an interval of ±50%. This process led to the above-referred two sets of forty records and was carried out with the assistance of Dr. Luís Macedo, one of the developers of the *SelEQ* tool, to whom the author is very grateful.

7.3.2. Definition of limit states

As discussed in Akkar *et al* (2005), there are several options for the engineering demand parameters (EDP) that can be used to allocate buildings to a damage state. These include the maximum roof displacement, inter-storey drift ratio, steel or concrete strain levels, base shear, etc. Each option will naturally lead to different damage distributions, hence different fragility functions. This dependence has been the object of several studies (e.g., Priestley, 1998), to which readers are referred to, but will not be further addressed herein. Damage states, which may be associated with both structural and non-structural components, represent growing levels of installed damage (e.g., none; slight; moderate; extensive; collapse) due to the seismic demand. The transition from a given damage state to the next implies incurring the limit state (LS) separating them, i.e., reaching the adopted EDP's threshold that represents that particular LS. The definition of EDP thresholds corresponding to growing levels of

damage has also been the object of several studies. For instance, Ghobarah (2004) and Sassun *et al* (2015) proposed inter-storey drift ratio limits for different structural systems. These recommendations can be taken as reference. However, for structural systems outside the scope of these proposals, alternatives must be found. Such was the case of a recent study by Sousa *et al* (2021) concerning the derivation of fragility functions for Portuguese RC precast buildings.

Given the purpose of this study, and to maintain coherence with the performance requirements that were adopted in Chapter 6 for the seismic assessment, the same structural LS – Significant Damage (SD) – was considered herein to derive the required fragility functions. According to EC8-3 (2005), it is characterized as follows: "The structure is significantly damaged, with some residual lateral strength and stiffness; vertical elements are capable of sustaining vertical loads; non-structural components are damaged, although partitions and infills have not failed out-of-plane; moderate permanent drifts are present; the structure can sustain after-shocks of moderate intensity; the structure is likely to be uneconomic to repair." As referred in Chapter 6 (see sub-section 6.4.5.), the failure mechanism of the buildings' critical columns at the LS of SD is governed by their shear force capacity. Hence, the inter-storey drift limits used herein to define the LS were those which cause the critical columns' shear demand to come close to the corresponding capacity – which are in fact the same that guided the design of the retrofitting systems. The limit values (Δ_d) for each building and direction are therefore justified in Chapter 6 (see sub-section 6.5.2.) and found in Appendix 5. They range between 0.50% and 0.65%, which compares well with the interval proposed by Ghobarah (2004) for an equivalent damage state of non-ductile RC frames (0.50 % to 0.80%).

7.3.3. Fragility curves

As previously referred, the fragility functions in this chapter were derived using the capacity curves of the original (PC) and retrofitted (R1 and R2) structures and the N2 method to estimate the target displacements for each of the selected ground motion records. The latter were scaled seven times to ensure the full coverage of the capacity curves, leading to 16 800 target displacements (60 curves × 40 records × 7 scale factors) per each set of ground motion records (2 sets of 40). The results were then compared with the above-defined LS displacements (duly transformed into those of the equivalent SDOF systems) to determine, within each of the defined building classes and per ground motion record, the percentage of structures that incurred the LS of SD. Scatter plots relating these percentages with the spectral acceleration $S_a(T_1)$ of each ground motion record were created, and a lognormal cumulative distribution was then fit to the data using least squares regression, providing one fragility function per building class for each set of ground motion records. Figures 7.2 and 7.3 present these results, showing the referred scatter plots for each building class, along with the associated lognormal distributions. The statistical parameters of the latter (i.e., logarithmic means λ and logarithmic standard deviations ζ) are given ahead in Table 7.1. Concerning the correlation between the adjusted curves and the individual data, this was found to be quite acceptable, as the calculated correlation values r^2 are equal or higher than 0.85 on all curves. As for the comparison between results for the original and retrofitted structures, along with the associated discussion, nothing is added at this point as that is the object of the next sub-section.

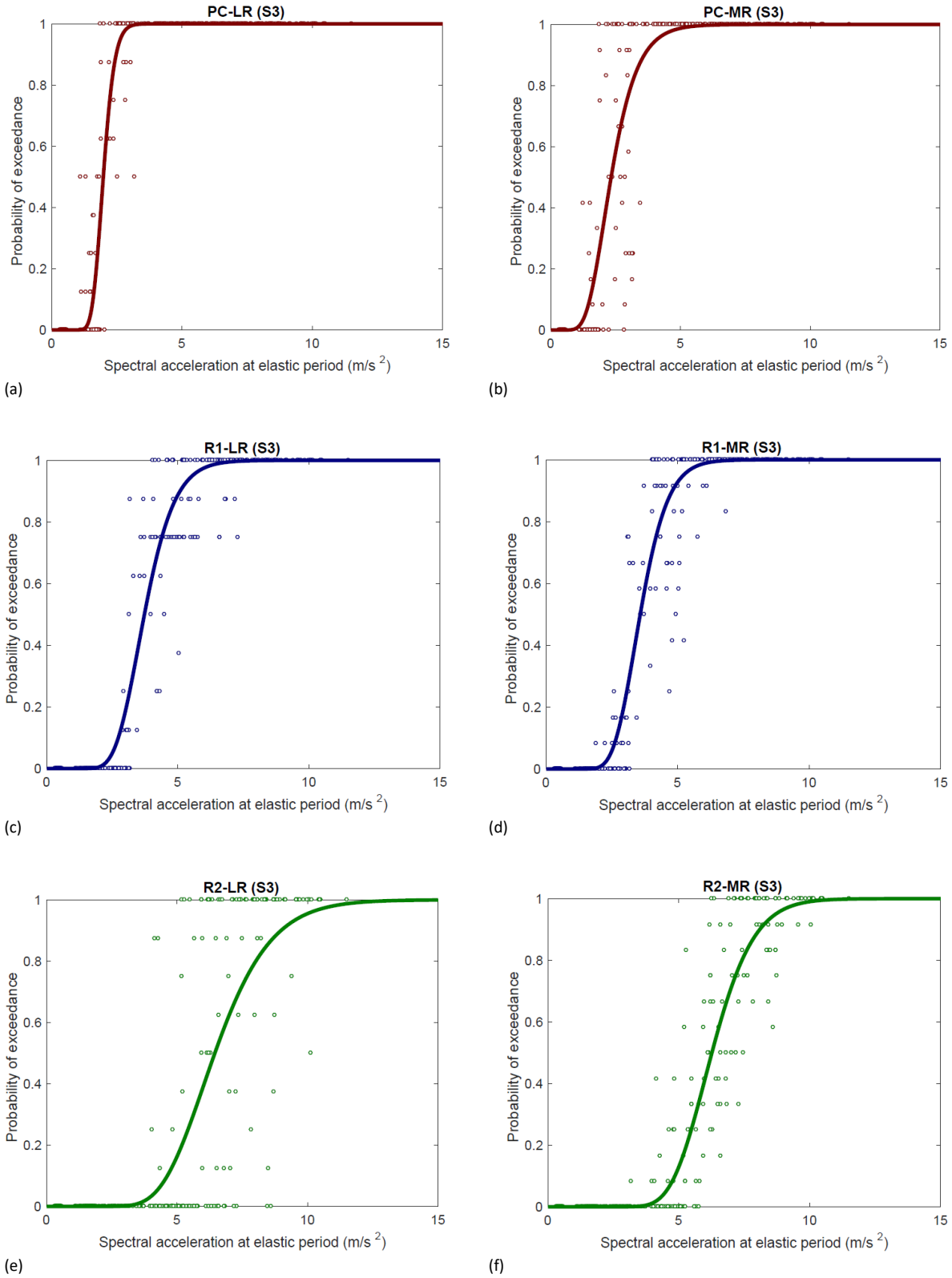

Figure 7.2 – Structural fragility functions for the LS of SD, derived using the ground motion records selected for the Lisbon region (scenario S3), for the defined building classes: (a) Original – Low-rise; (b) Original – Mid-rise; (c) Retrofitted 1 – Low-rise; (d) Retrofitted 1 – Mid-rise; (e) Retrofitted 2 – Low-rise; (f) Retrofitted 2 – Mid-rise.

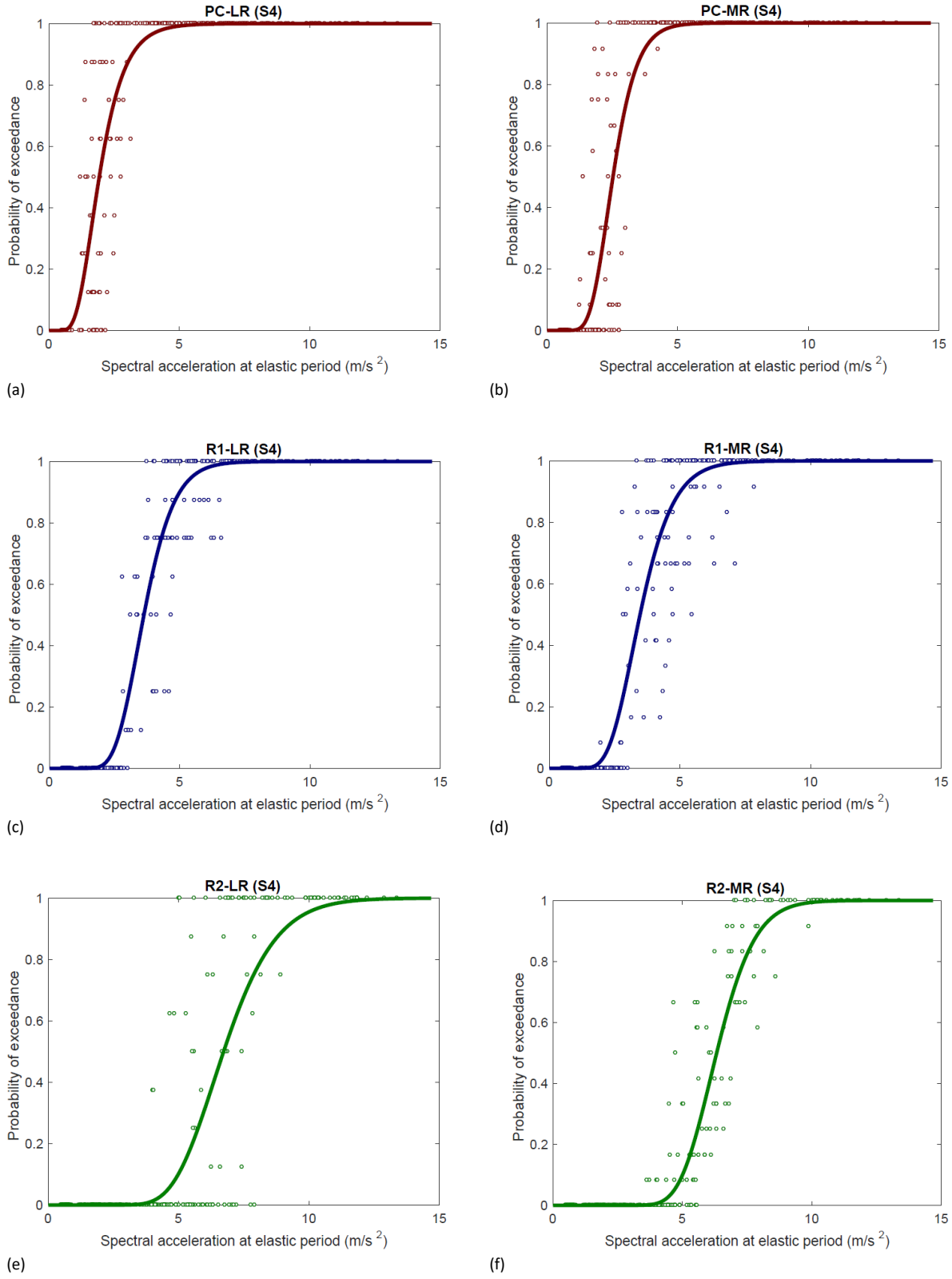

Figure 7.3 – Structural fragility functions for the LS of SD, derived using the ground motion records selected for the West Algarve region (scenario S4), for the defined building classes: (a) Original – Low-rise; (b) Original – Mid-rise; (c) Retrofitted 1 – Low-rise; (d) Retrofitted 1 – Mid-rise; (e) Retrofitted 2 – Low-rise; (f) Retrofitted 2 – Mid-rise.

Table 7.1 – Statistical parameters of the fragility functions (in terms of spectral accelerations at elastic period T_1)

Building Classes		GM records set S3 (Lisbon)		GM records set S4 (West Algarve)	
		$\lambda\ (m/s^2)$	$\zeta\ (m/s^2)$	$\lambda\ (m/s^2)$	$\zeta\ (m/s^2)$
PC	LR	0.68	0.17	0.66	0.39
	MR	0.84	0.34	0.93	0.29
R1	LR	1.32	0.24	1.29	0.25
	MR	1.27	0.23	1.24	0.29
R2	LR	1.86	0.26	1.91	0.23
	MR	1.83	0.20	1.84	0.18

Statistical parameters: λ = logarithmic mean; ζ = logarithmic standard deviation

7.3.4. Discussion

Based on the results presented above, this sub-section analyses the changes that occur in the probability of exceeding the LS of SD after the designed retrofitting systems (R1 or R2) are added to the original (PC) structures. In that cause, figures 7.4 and 7.5 compare the before and after fragility functions, separated according to building class in terms of number of storeys (LR or MR) and to selected ground motion records set (S3 or S4). These comparisons show that, for the same value of spectral acceleration $S_a(T_1)$, the curves for the retrofitted structures always return lower probabilities of exceedance than those for the original structures. Moreover, if one considers the EC8-3 (2005) values of $S_a(T_1)$ for each building class (i.e., those obtained from the response acceleration spectra for the LS of SD – see figures 6.5 and 6.6 in Chapter 6), the probabilities of exceedance for the original structures are quite high, while those for the retrofitted structures stay below 50%. As such, the obtained results confirm the designed retrofitting systems' ability to effectively improve the seismic capacity of the analysed pre-code RC structures and contribute to the reduction of the seismic risk to which such buildings may be exposed.

Concerning the effect of the number of storeys, the comparison between fragility functions for the LR and MR retrofitted buildings shows no significant differences. The graphical similarity between curves is (naturally) confirmed by the statistical parameters λ and ζ given in Table 7.1. The fact that the structural fragility of the retrofitted buildings is not significantly affected by the growing number of storeys is an encouraging finding, as it further goes to show the ability of steel-braced retrofitting systems to stabilize the lateral behaviour of pre-code RC structures. However, given the limited size of the sample considered in this study (see section 7.1 for comments on building-to-building variability), neither generalized conclusions should be drawn, nor should these fragility functions be used for purposes other than those defined within the scope of this chapter. Lastly, concerning the effect of the selected ground motion records set (S3 or S4) on the fragility functions, the similarity between those obtained for each is also noticeable. However, this similarity is not surprising, as the target spectra for both record sets have the same shape, with different peak ground accelerations, thus inevitably leading to similar selections of ground motion records, except for the scale factors. As such and given the considerable number of records in each set, no relevant differences were in fact expected between the two sets of fragility functions (figures 7.2 and 7.3, respectively).

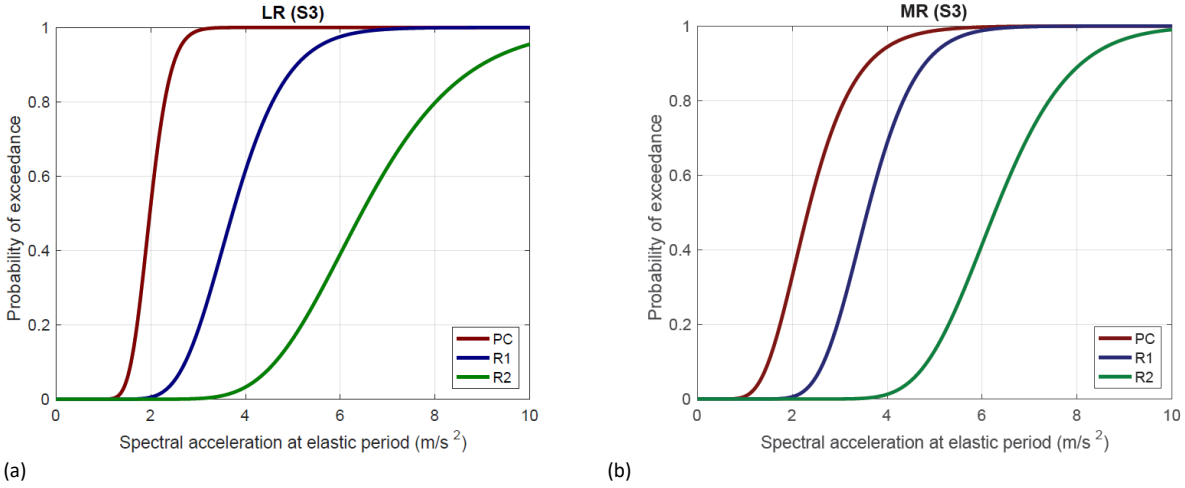

Figure 7.4 – Comparison of structural fragility functions for the LS of SD, derived using the ground motion records selected for the Lisbon region (scenario S3), between original and retrofitted buildings: (a) Low-rise; (b) Mid-rise.

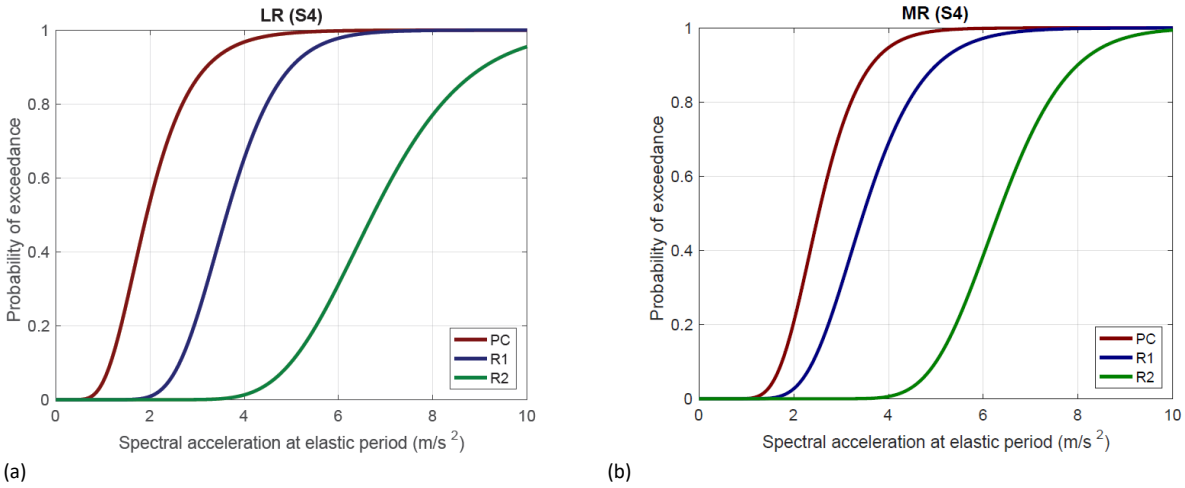

Figure 7.5 – Comparison of structural fragility functions for the LS of SD, derived using the ground motion records selected for the West Algarve region (scenario S4), between original and retrofitted buildings: (a) Low-rise; (b) Mid-rise.

7.4. RISK ANALYSIS

7.4.1. Hazard model

In terms of plate tectonics, Portugal is located at the southwest part of the Eurasian plate, near where the African and North American plates meet (as referred in Chapter 2). Consequently, it may experience offshore seismic events with large to very large magnitude, and onshore events with moderate to large magnitude (Moreira, 1989). Two different earthquake scenarios, representing the country's most relevant seismic sources, were therefore considered in this study for the assessment of potential structural losses: (i) a strong magnitude offshore event, associated with an inter-plate rupture at the Eurasian-African interface; (ii) a moderate onshore event, associated with an intra-plate

rupture at the Tagus Valley fault. The assumed parameters for these two ruptures were based on the work of Carvalho *et al* (2008a) and are summarized in Table 7.2. The surface projections of the hypothesised faults are shown in Figure 7.6, adapted from the work of Silva *et al* (2015c) which considered the same two seismic events.

Table 7.2 – Assumed source parameters for the considered earthquake scenarios

Rupture	Magnitude (M_w)	Center of fault	Strike	Dip	Rake
Offshore	7.6	36.90 N; 9.90 W	20°	24°	90°
Onshore	5.7	38.82 N; 9.05 W	220°	55°	0°

The ground motion fields for the offshore event were calculated using the GMPE proposed by Akkar and Bommer (2010), while those for the onshore event were obtained with the GMPE proposed by Atkinson and Boore (2006). The former are one of the most popular proposals for shallow crustal earthquakes in Europe, while the latter are known to perform reasonably well for close-distance events in mainland Portugal. The selection of an adequate attenuation model for Portugal is challenging due to the lack of ground motion recordings to support the development of specific GMPE or, at least, enable a reliable verification of existing models. However, recommendations on this topic can be found in Vilanova *et al* (2012) and Silva *et al* (2015a). As for the influence of site conditions, the average velocity of seismic shear waves in the top 30 meters layer ($v_{s,30}$) was used to characterize it, following the approach described in Silva *et al* (2014a). One-thousand ground motion fields were generated for each earthquake scenario using the *OpenQuake* engine, thus duly ensuring the propagation of the models' aleatory uncertainty through the loss assessment results. The spatial distribution of the median peak ground acceleration (PGA) is depicted in Figure 7.6.

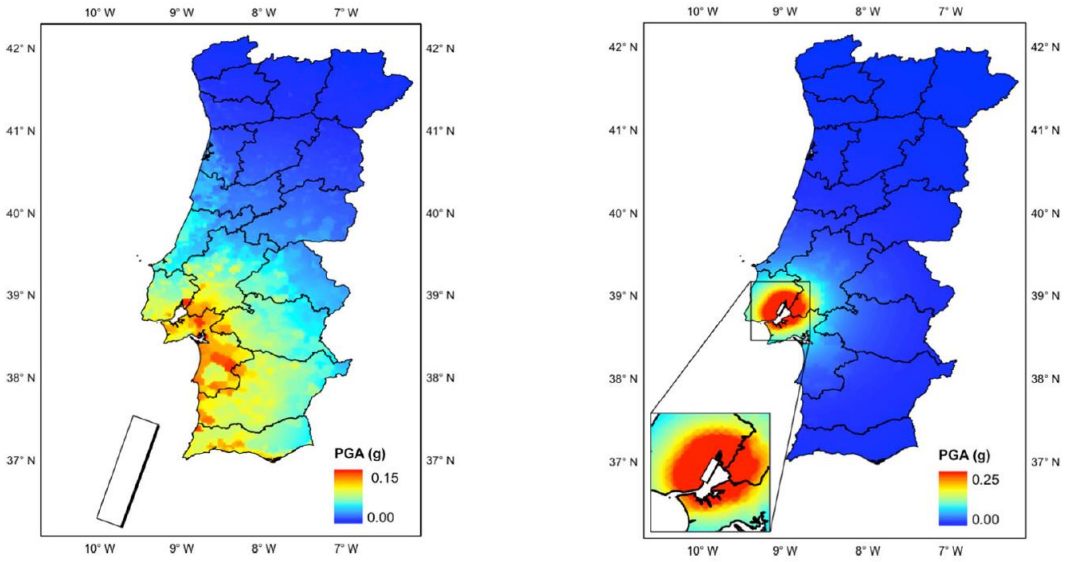

(a) (b)

Figure 7.6 – Median ground motion fields for the offshore (a) and onshore (b) events (adapted from Silva *et al,* 2015c)

7.4.2. Exposure model

The recently developed ESRM20 exposure model for Portugal (see Crawley *et al,* 2021) was adopted in this study to define the spatial distribution and economic value of the assets. According to it, there is a total of 3 353 762 residential (RES) buildings in the mainland territory, adding up to a total replacement cost of 504 074 M€. The number of RC buildings is equal to 1 599 434 (about 47.7% of the total), from which 627 151 were erected before the publication of the RSA (1983) design code and can thus be categorized as pre-code (PC). Within the latter, 573 779 are categorized as low-rise (LR), and 43 973 as mid-rise (MR). In terms of spatial distribution, a significant percentage of the RES buildings on the mainland are located in the Porto, Aveiro, Lisbon, and Setubal districts – for instance, for the RC-PC-LR and -MR building classes, respectively 42.9% and 78.3%. The distribution of the assets included in those two building classes is shown in Figure 7.7.

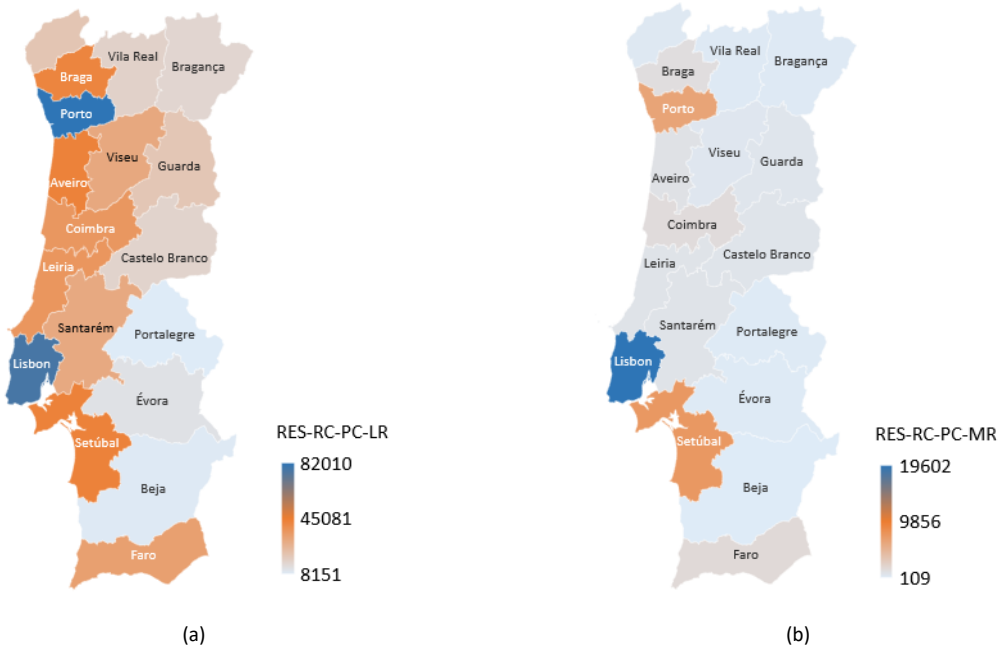

Figure 7.7 – Distribution of the residential pre-code RC buildings in mainland Portugal: (a) low-rise; (b) mid-rise.

The reconstruction costs per square metre included in the exposure model for structural and non-structural components are provided for rural areas, urban areas, and "big cities" (Porto, Lisbon, and Setubal), according to the census data. The values were obtained from expert sources and then validated and calibrated using the data provided in Paprotny *et al* (2020) and COMPASS (2020). The procedure is described in Crawley *et al* (2021). Those costs are assumed to comprise 80% of the total replacement cost, which also includes that of the buildings' contents. Hence, the total replacement cost is divided as follows: 30% for structural; 50% for non-structural; 20% for contents. Filtering the global data to include just the reconstruction cost of structural components for the two building classes considered in this study (i.e., RES-RC-PC-LR and RES-RC-PC-MR), the corresponding economic values for each are, respectively, 20 227 M€ and 10 414 M€.

7.4.3. Vulnerability model

As previously referred, the conversion of fragility functions into vulnerability functions requires the definition of a consequence model that relates each damage state with the expected loss ratio (i.e., the ratio of absolute economic loss to total replacement cost). Several proposals are found in the literature for different regions, building typologies, and definitions of damage states (e.g., Di Pasquale and Goretti, 2001; Kappos *et al,* 2006; Bal *et al,* 2008). The choice of a consequence model has direct impact on the shape of the vulnerability functions, as it defines the contribution of each damage state to the resulting loss ratio per intensity measure level. However, as the fragility functions in this study were derived solely for the LS of SD, the definition of the consequence model came down to defining the loss ratio for a single damage state. As such, based on the characterization given in EC8-3 (2005) for the LS of SD (reproduced in sub-section 7.3.2. for the reader's convenience), a loss ratio of 80% was considered for the buildings' structural components.

The fragility model derived in this study considers the influence of record-to-record variability on structural response, but not that of building-to-building variability (for the previously explained reasons – see section 7.1). However, information regarding that source of aleatory uncertainty is available in the works of Sousa *et al* (2019) and Sanam *et al* (2019) – in which the same statistical properties used herein (see Table 6.1 in Chapter 6) were used to generate and analyse a much larger sample of buildings – and provided by the logarithmic standard deviation of the spectral acceleration for each LS. Hence, combining the latter with those of the above-presented fragility functions through simple quadratic combination (SRSS), the joint effect of the two sources of uncertainty can be obtained, as to ensure its propagation through the results of the loss assessment process. Table 7.3 shows the result of this process, for a logarithmic standard deviation $\zeta_m = 0.33$ accounting for the uncertainty in the buildings' properties. The updated fragility functions were then converted into vulnerability functions, according to the above-defined consequence model. In this process, the percentage of buildings (within each building class) incurring the LS of SD is computed at each level of spectral acceleration and then multiplied by the corresponding loss ratio. Hence, the loss ratio for each level of spectral acceleration is obtained (for each building class), giving origin to the vulnerability functions required as input to the *OpenQuake* scenario risk calculator.

Table 7.3 – Updated statistical parameters of the fragility functions

Building Classes		GM records set S3 (Lisbon)		GM records set S4 (West Algarve)	
		$\lambda\ (m/s^2)$	$\zeta\ (m/s^2)$	$\lambda\ (m/s^2)$	$\zeta\ (m/s^2)$
PC	LR	0.68	0.37	0.66	0.51
	MR	0.84	0.47	0.93	0.44
R1	LR	1.32	0.41	1.29	0.41
	MR	1.27	0.40	1.24	0.44
R2	LR	1.86	0.42	1.91	0.40
	MR	1.83	0.39	1.84	0.38

Statistical parameters: λ = logarithmic mean; ζ = logarithmic standard deviation

7.4.4. Risk assessment

The results of the loss assessment process for the above-defined earthquake scenarios are given below in terms of loss ratios, for the original (PC) and retrofitted (R1 and R2) structures, disaggregated by the country's districts. The presented values correspond to the mean loss ratios over those obtained for each of the 1000 generated ground motion fields. The distribution of the RES-RC-PC buildings in mainland Portugal (i.e., the data behind the maps shown in Figure 7.7) is given in Table 7.4, along with the corresponding reconstruction cost of their structural components. The obtained structural loss ratios are then given in tables 7.5 and 7.6, respectively for the offshore and onshore events (districts with PC loss ratios below 5% were omitted), while figures 7.8 and 7.9 show the corresponding loss ratio maps for the original structures.

Table 7.4 – Distribution and structural value of the residential pre-code RC buildings in mainland Portugal

	Number of buildings			Structural value (M€)		
District	**LR**	**MR**	**TOTAL**	**LR**	**MR**	**TOTAL**
Aveiro	43 328	993	44 321	1289	181	1470
Beja	8709	109	8818	258	20	278
Braga	42 558	1336	43 894	1339	227	1566
Bragança	15 380	267	15 647	424	29	453
Castelo Branco	16 260	760	17 020	488	110	598
Coimbra	36 326	1497	37 823	1098	241	1339
Évora	11 499	189	11 688	363	33	396
Faro	33 415	1688	35 103	1216	395	1611
Guarda	20 450	650	21 100	566	66	632
Leiria	36 751	842	37 593	1140	163	1303
Lisboa	77 196	19 602	96 798	3822	5290	9112
Portalegre	8151	211	8362	239	44	283
Porto	82 010	6398	88 408	3247	1234	4481
Santarém	30 193	861	31 054	925	158	1083
Setúbal	43 419	7437	50 856	1918	2049	3967
Viana do Castelo	20 844	342	21 186	585	54	639
Vila Real	16 736	278	17 014	474	43	517
Viseu	30 554	513	31 067	836	77	913
TOTAL	**573 779**	**43 973**	**617 752**	**20 227**	**10 414**	**30 641**

Table 7.5 – Mean structural loss ratios (%) for the offshore seismic event

	LR			MR		
District	**PC**	**R1**	**R2**	**PC**	**R1**	**R2**
Beja	16.0%	12.6%	1.3%	3.2%	6.6%	0.9%
Castelo Branco	5.0%	1.9%	0.1%	0.4%	1.1%	0.1%
Coimbra	5.2%	2.1%	0.1%	0.5%	1.3%	0.1%
Évora	11.2%	6.4%	0.6%	1.6%	4.8%	0.6%
Faro	22.2%	20.4%	2.5%	5.9%	11.7%	2.0%
Leiria	7.7%	3.9%	0.3%	1.1%	2.4%	0.2%
Lisboa	14.0%	9.7%	0.9%	2.5%	6.1%	0.7%
Portalegre	7.4%	3.7%	0.3%	0.6%	2.3%	0.1%
Santarém	8.6%	4.5%	0.3%	1.0%	2.6%	0.2%
Setúbal	16.2%	12.6%	1.3%	3.1%	8.0%	0.9%

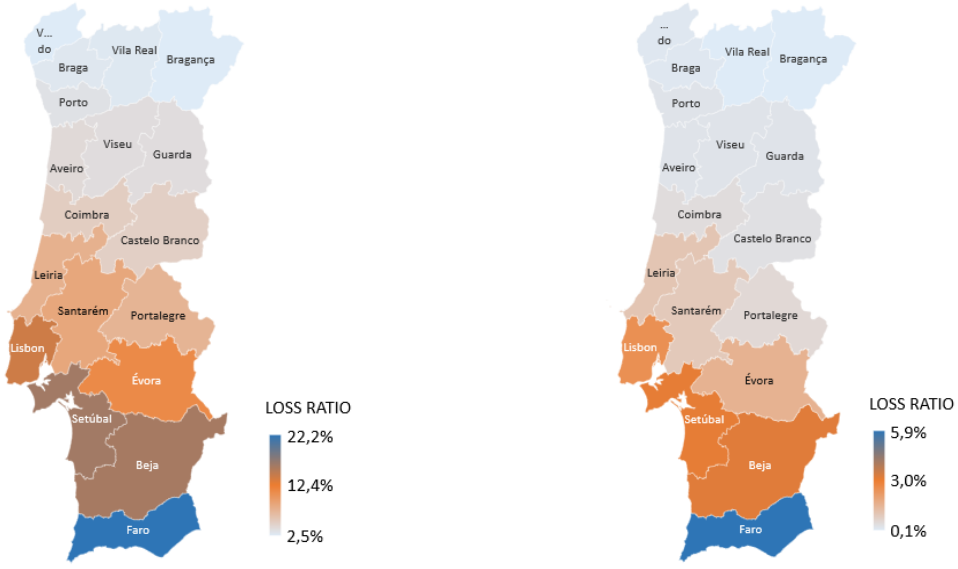

(a) (b)

Figure 7.8 – Distribution of mean structural loss ratios for the offshore seismic event: (a) PC-LR; (b) PC-MR.

Table 7.6 – Mean structural loss ratios (%) for the onshore seismic event

	LR			MR		
District	**PC**	**R1**	**R2**	**PC**	**R1**	**R2**
Lisboa	21.2%	28.0%	4.8%	9.3%	22.0%	4.4%
Setúbal	9.2%	11.0%	2.0%	1.6%	4.8%	1.1%

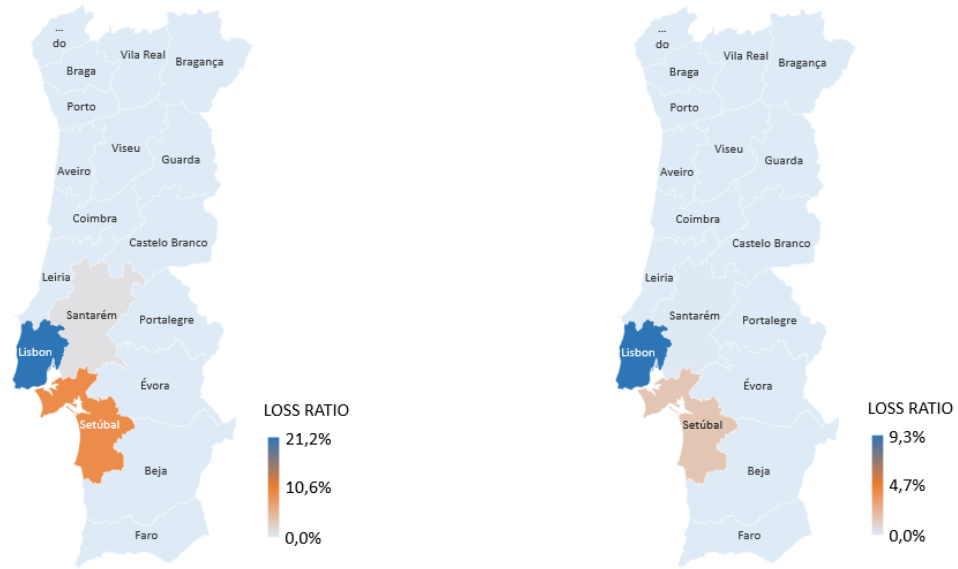

(a) (b)

Figure 7.9 – Distribution of mean structural loss ratios for the onshore seismic event: (a) PC-LR; (b) PC-MR.

7.4.5. Discussion

The outcomes of the loss assessment process led to different conclusions, depending essentially on the seismic rupture (offshore or onshore), number of storeys (LR or MR), and type of retrofitting system (R1 or R2). For the offshore event, the maximum loss ratios for the PC structures were obtained in the Algarve region and consistently decreased moving North. However, significant differences were found between the results for the LR and MR buildings (see Figure 7.8), with the former varying between 2.5% and 22.2%, and the latter between 0.1% and 5.9%. Given the high magnitude of the offshore event, a mean loss ratio of 5.9% in the Algarve region (for instance) seems relatively low and may eventually be explained (at least in part) by some difficulty in obtaining reliable spectral accelerations for higher periods of vibration when using the GMPE proposed by Akkar and Bommer (2010), but this matter will not be further explored herein (the interested reader is referred to Vilanova *et al* (2012) for more details on this effect). As for the onshore event, the maximum loss ratios for the PC structures were obtained in the Lisbon district (21.2% and 9.3% for the LR and MR buildings, respectively), followed by the Setúbal district (9.2% and 1.6%), and with all other returning loss ratio values below 1%, regardless of the number of storeys (see Figure 7.9).

Concerning the effect of the retrofitting systems on the loss assessment process, two different situations were identified within the results for the offshore event: (i) for the LR buildings, consistent reductions were observed in the calculated loss ratios, with those for the R2 systems being the most expressive; (ii) for the MR buildings, the R1 systems seem to consistently increase the calculated loss ratios, while the R2 systems cause the expected reduction. What happens with the R1 systems for the MR buildings, although surprising, is most likely related with the above-mentioned limitations concerning the Akkar and Bommer (2010) GMPE. Considering the vibration periods' strong reduction caused by the retrofitting systems (thus leading to spectral accelerations which are both higher and more realistic), along with the fact that the fragility curves for the PC-MR structures are relatively close to those of the R1-MR structures (see Figure 7.4-b), this situation may be explained. As for the onshore event, while the R1 systems seem to be counter-productive for both the LR and the MR buildings, the R2 systems cause a significant reduction of the calculated loss ratios. The fact that spectral accelerations tend to be strongly amplified by the GMPE in the short period range, in locations close to the seismic rupture, might contribute to explain the situation with the R1 systems. Nonetheless, the question remains about the adequateness of the code spectrum used to define the seismic demand for the Lisbon region during the retrofitting design process (it is recalled that the R2 systems were meant essentially for structures in the Faro district).

To illustrate the evolution between the original conditions (given above in figures 7.8 and 7.9, respectively for the offshore and onshore events) and those created by the strengthening interventions, loss ratio maps were created for the retrofitted structures and are given below in figures 7.10 and 7.11 (in the same order). Being outside the scope of this work, no cost-benefit analysis was carried out to help decide which retrofitting systems should be used (if any). As such, those choices were made imposing a mean loss ratio limit of 5% for the retrofitted structures, being indicated through grey shading above in tables 7.5 and 7.6 (readers should note that no retrofitting systems were applied to structures located in districts with PC loss ratios below 5%). Comparing the before and

after loss ratio maps, the obtained reduction of structural losses is well evident, thus further demonstrating the effectiveness of the retrofitting process carried out in Chapter 6, based on the design methodology proposed in Chapter 5.

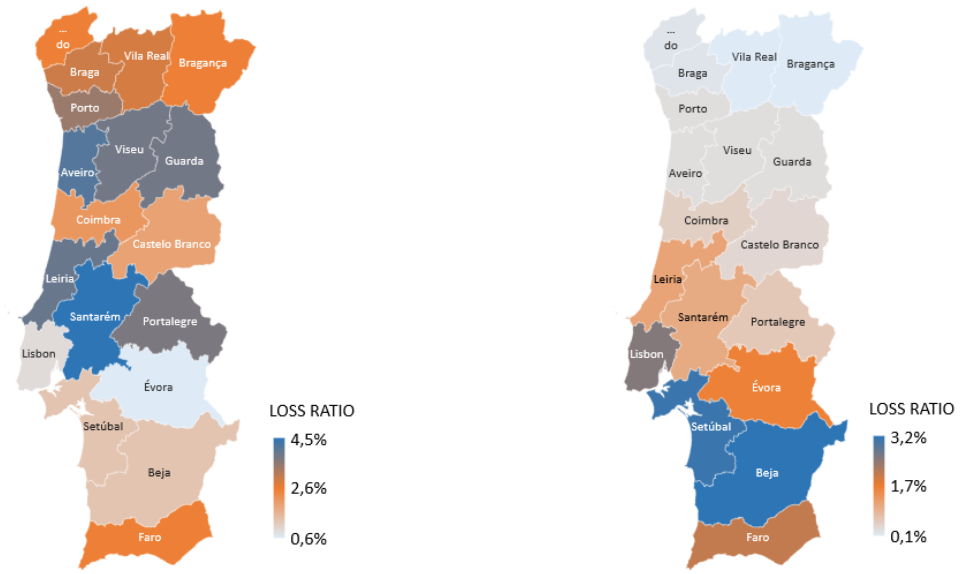

(a) (b)

Figure 7.10 – Distribution of mean structural loss ratios, after retrofitting, for the offshore seismic event: (a) LR; (b) MR.

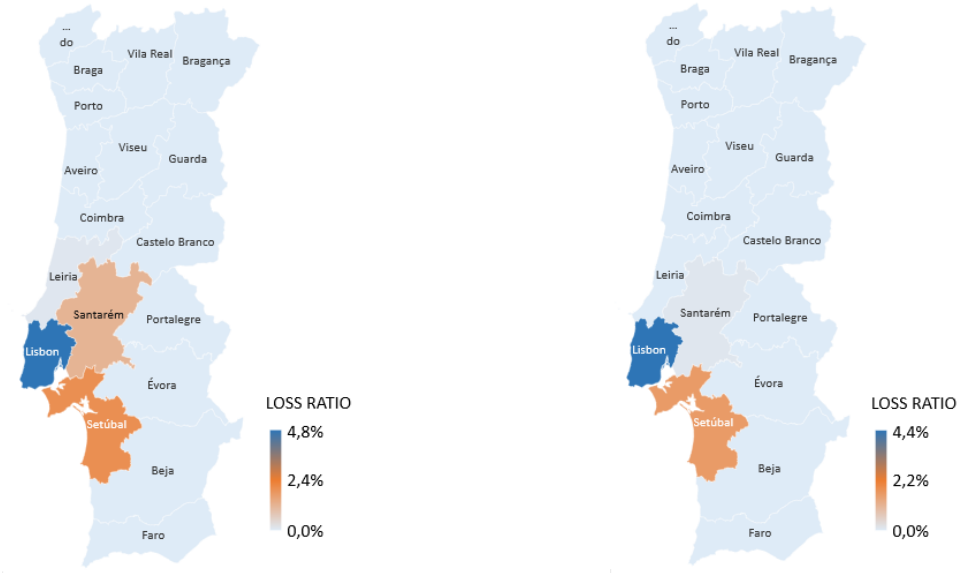

(a) (b)

Figure 7.11 – Distribution of mean structural loss ratios, after retrofitting, for the onshore seismic event: (a) LR; (b) MR.

7.5. CONCLUDING REMARKS

This chapter presented a short seismic risk study of the sample of structures defined in Chapter 6, for the purpose of validating the designed retrofitting systems beyond the requirements of the assessment code. Fragility functions were derived for the before and after retrofitting situations, and the accomplished reduction in the seismic risk to which the structures are exposed was demonstrated through a comparison of loss ratios provided by the *OpenQuake* engine. These conclusions further contribute to validate the design methodology proposed in Chapter 5 and demonstrate it is robust enough to be systematically used by practitioners involved in the seismic assessment and retrofitting of existing RC structures. Moreover, other preliminary conclusions were drawn in parallel (for instance, regarding the behaviour of the GMPE), which will surely contribute to improve the preparation of the more complete seismic risk studies to be carried out in the near future.

Despite the limited size of the studied sample of buildings, the obtained results also provided relevant inputs to the ongoing research project MitRisk, which focus on the development of a cost-benefit analysis platform meant to support the design of retrofitting plans for the most vulnerable types of buildings out of the Portuguese building stock. As such, given the importance of that initiative to the cause of improving seismic safety, this is considered to be the main contribution of this chapter, besides the obvious fulfilment of its purpose within the scope of the thesis.

CHAPTER 7 – ON THE EVOLUTION OF THE SEISMIC RISK OF THE STUDIED SAMPLE OF STRUCTURES

7.1. INTRODUCTION 7.1
7.2. FRAMEWORK OF THE STUDY 7.2
7.3. FRAGILITY ANALYSIS 7.3
7.3.1. Selection of ground motion records 7.3
7.3.2. Definition of limit states 7.4
7.3.3. Fragility curves 7.5
7.3.4. Discussion 7.8
7.4. RISK ANALYSIS 7.9
7.4.1. Hazard model 7.9
7.4.2. Exposure model 7.11
7.4.3. Vulnerability model 7.12
7.4.4. Risk assessment 7.13
7.4.5. Discussion 7.15
7.5. CONCLUDING REMARKS 7.17

CHAPTER 8

CLOSURE

8.1. CONCLUSIONS

The final purpose of this thesis is to contribute to the reduction of the seismic risk to which the Portuguese RC building stock is exposed. Within this context, motivated by the known benefits of using steel braces to reinforce RC framed buildings, as well as by the fact that in Portugal there are almost no application examples, two main objectives were defined in the beginning: (i) to improve knowledge on the seismic behaviour of such retrofitted structures, directly considering the main characteristics of the building classes that exist in the country; (ii) to propose and validate a displacement-based procedure for the design of steel X-brace retrofitting systems. The contributions for the first are included in chapters 2 to 4, while those for the second are given in chapters 5 to 7, defining two well-separated stages of the workplan that was carried out. A short description of the addressed topics is given in the introductory chapter, while detailed discussions of obtained results, as well as dedicated concluding remarks, are found in the end of chapters 2 to 7. Nonetheless, the main contributions and recommendations emerging from the latter are summarized herein.

The extensive literature review included in Chapter 2 is considered to be its main contribution, not only to the above-referred first objective, but also (on a wider scope) to junior academics that wish to become involved in the seismic assessment and retrofitting (using steel elements) of existing RC buildings. A general overview is given of most of the related topics, thoroughly discussing some of the details, and citing a large number of important and up-to-date references. As the produced text is quite straightforward, the author hopes that some professionals will also feel motivated to study it and thus start improving their understanding of the subject. The *status quo* of professional practice is in fact discussed in Chapter 2 (see sub-section 2.7.3.), based on the results of a survey conducted by Araújo and Castro (2017) which led to an unsettling (although not surprising) conclusion: when involved in such matters, most professionals will resort to linear elastic analysis models combined with behaviour factors, codes that prescribe general design and detailing rules, and seismic codes oriented towards the design of new buildings. As this is known to be an inadequate approach to the problem with potential consequences for public safety, it is important that academics keep providing the technical community with updated guidelines which can be systematically applied to professional practice in the cause of reducing the threat to human life posed by seismically vulnerable buildings.

The seismic behaviour of an older-type RC framed structure was thoroughly examined in Chapter 3, with and without considering the effects of its masonry infill walls. Two numerical models (bare and infilled) were developed according to the state-of-the-art provisions presented in Chapter 2, their calibration carried out based on the experimental results of the ICONS research programme, and the seismic assessment of both performed according to the provisions of EC8-3 (2005) using nonlinear static and dynamic analysis models. The included discussions will (hopefully) help other researchers to improve their numerical models of pre-code RC buildings, as well as to better interpret the outcomes provided by the EC8-3 (2005) seismic assessment procedure. In detail, the comparison between numerical and experimental results raised attention for: (i) the effect of varying the amount of viscous damping included in nonlinear dynamic analysis models, and its relationship with the imposed deformation levels; (ii) the importance of including the bond-slip effect when modelling the response of pre-code RC structures (particularly those with plain rebars); (iii) the fact that infill panels may protect RC members from low/medium intensity input motions, but may also prompt soft-storey mechanisms when sudden failures occur; (iv) the significant stiffness reduction that occurs in infill panels when medium/large openings exist. The significant differences between iterations (adjusting calculation parameters) also showed how easily these refined models can provide unrealistic (and potentially unsafe) results when deficiently calibrated, hence extreme caution should be exercised by less experienced analysts. Concerning the conclusions of the seismic assessment process, the following are noteworthy: (v) the results of the nonlinear static analysis models compare well with those of their nonlinear dynamic analysis counterpart; (vi) the member control sections marked as critical are consistent with those identified in the experimental tests; (vii) the option to model (or not) the masonry infill walls significantly influences the overall assessment result. Even though these conclusions add confidence to the EC8-3 (2005) procedure (as well as to the nonlinear static approach as a swift but reliable alternative to dynamic methods), the author recommends that analysts do not become dependent on D/C ratios, but also analyse the evolution of inelastic lateral displacement profiles, as valuable information can be obtained from it.

The application of conventional seismic design methodologies to hybrid RC-steel systems was addressed in Chapter 4, relying on a case-study to first show the difficulties that arise when assessing the efficiency of a retrofitting system designed within the framework of EC8-1 (2004), and then using nonlinear methods of analysis and the requirements of EC8-3 (2005) to evaluate the performance of the retrofitted structure and demonstrate it is not safe. The author hopes that the reported findings will help researchers and practitioners become more aware of the likely error associated with the several adjustments that need to be introduced in conventional seismic code provisions in order to try to apply them to such structural systems. The main conclusions to be retained, and that serve as a prelude to what was done in chapters 5 and 6, are: (i) the conventional (force-based) design process gives no guarantees in terms of adequate behaviour of the retrofitted structures; (ii) to consider the influence of the steel braces' resistance on the deformation capacity of RC members is essential for a (performance-based) design process to be successful. It should be emphasized, however, that despite these criticisms, when combined with capacity design principles and careful (RC or steel) member detailing, the force-based design methodology (and associated q-factors) generally produces safe and satisfactory (new) structures.

Moving on to the second stage of the carried out workplan, chapters 5 and 6 were dedicated to the proposal, validation, and calibration of a new displacement-based method to design concentric steel-brace retrofitting systems for RC framed buildings. The proposed method is thought to be intuitive and simple enough to be used in practical applications, with several advantages over the conventional seismic design process. Besides the obvious fact that no *q*-factors are involved (thus eliminating the difficulty in finding one that is adequate), it relies on knowledge of the fundamental seismic behaviour of braced structures to ensure that deformation levels are kept within limits compatible with the performance requirements of the applicable assessment codes. Despite the introduction of some approximations in its steps, the procedure leads to retrofitted structures with adequate and predictable seismic performance, within a swift and simple to follow workflow that can be easily programmed on any platform. Furthermore, the results presented in Chapter 6 showed that: (i) it is robust enough to be systematically applied to the retrofitting of low- and mid-rise pre-code RC buildings which are part of the Portuguese building stock; (ii) it is easily adapted to both deformation- and strength-controlled member failure mechanisms; (iii) it can be improved to flag more efficiently situations in which the steel braces should be combined with local strengthening of the directly affected RC columns. As such, the author hopes that the proposed methodology can contribute to mitigate the lack of guidance for the detailed design of this kind of global retrofitting solution, which is appointed as the main reason why almost no examples exist in Portugal.

Finally, a step further in the validation of the proposed design methodology (i.e., beyond code criteria compliance) was taken in Chapter 7, using fragility and risk analyses to (once more) demonstrate the effectiveness of the obtained retrofitting systems. Fragility functions were derived for the sample of buildings defined in Chapter 6, before and after retrofitting, and the accomplished reduction in the seismic risk to which the structures are exposed was demonstrated through the comparison of the loss ratios provided by the *OpenQuake* engine. Despite the limited size of the studied sample of buildings, these results provided relevant inputs to the ongoing research project MitRisk and, given the importance of the latter to the cause of improving the seismic safety of the Portuguese building stock, this is considered to be the main contribution of Chapter 7.

At the end of this thesis, the author hopes to have raised awareness about the large number of RC buildings in Portugal at risk of being deficient in terms of seismic resistance. Research in earthquake engineering must therefore continue to focus on the performance evaluation of the existing building stock, as well as on the development of economically attractive retrofitting techniques along with the associated design methodologies. This will allow to efficiently invest money with the purpose of saving lives and money in the event of future earthquakes. The author also hopes to have pointed out that the seismic assessment and retrofitting of existing RC structures is a far more complex matter than the seismic design of new ones, thus requiring procedures that ensure the design will reliably meet a predefined performance level for a given seismic demand (which is the fundamental principle of the performance-based earthquake engineering philosophy). Lastly, the author believes to have justified the title of this thesis by further demonstrating the benefits of using steel braces in the cause of reducing the seismic risk of existing RC buildings. Being a matter of high priority in terms of public safety, may this be a contribute (however small) to the necessary change.

8.2. RECOMMENDATIONS FOR FUTURE DEVELOPMENTS

The course of this (longer than envisioned) research plan raised several questions which were not thoroughly addressed in this thesis, either because they are still under analysis, or their impact on the defined objectives was not paramount. As such, a few comments on the topics that should not be overlooked and/or require further analysis are made below:

- The characterization of the Portuguese RC building stock was addressed in Chapter 2, defining building typologies and probabilistic distributions of the associated geometrical and material properties, citing the works of Silva (2013) and Silva *et al* (2015b), and referring to the data of the 2011 Building Census Survey. Such statistical studies constitute a useful contribution for research in the field of seismic vulnerability assessment and should therefore be updated and expanded whenever possible. The following limitations were pointed out by the authors in the concluding remarks to the referred studies: (i) the size of the analysed sample of buildings needs to be further increased; (ii) results were based on drawings and technical specifications, which might differ from what was actually built; (iii) the investigated building population was exclusively composed of regular moment frames, therefore the influence of stiff elements (e.g., elevator shafts, staircases, or other shear walls) was neglected. An update that would address these limitations, as well as consider the already published results of the 2021 Building Census Survey, would thus be most welcome.
- Fibre modelling assumes a perfect bond between reinforcing steel and concrete, posing a limitation that cannot be accepted without action when modelling the response of older-type RC structures. The enhancement of such models as to include the bond-slip effect is thus mandatory if one wants to obtain a realistic description of the cyclic and ultimate behaviour of such structures. In this work, that effect was implicitly accounted for in the Menegotto and Pinto (1973) model by following the simplified approach of Caruso *et al* (2018), which led to a good agreement with the experimental results. Nonetheless, the further testing of more sophisticated approaches, such as that proposed by Sousa *et al* (2017a), would certainly be most relevant to future updates of software platforms such as *SeismoStruct*, and contribute to stabilize a more detailed approach to the problem.
- The nonlinear modelling of shear effects remains a significant challenge. Many existing buildings in Europe possess column members that are prone to shear failure, which makes the incorporation of shear response an important aspect of modelling. However, currently used in practice software platforms typically neglect these mechanisms by default. The development and implementation of analytical models which can simulate the cyclic behaviour of non-ductile RC columns (while remaining computationally efficient for large-scale applications) is consequently a topic of very active research. Several proposals have been published in the past recent years, as well as some comparative studies pointing out advantages and shortcomings between approaches. However, there is still no consensus on which of the available models is the most efficient. As such, given the importance for the modelling of older-type RC structures, this research topic should be further pursued.
- Despite the refinement of the used nonlinear analysis models (i.e., the explicit modelling of several energy dissipation mechanisms), the comparison between numerical and experimental

results presented in Chapter 3 demonstrated that the best agreement still required some level of viscous damping ξ_0, the value of the latter depending (among other things) on the amplitude of the imposed deformation (this effect was particularly important in the models that included masonry infill panels). As such, and as also referred by Sousa (2015), given the impact that different values of ξ_0 may have on the quality of the results provided by the analysis models, there is an evident need for the development of solutions that minimize (or ideally eliminate) such negative effects (Chopra and McKenna (2016), for instance, seems like a step in the right direction).

- The expression proposed in EC8-3 (2005) for the quantification of the admissible shear force of RC members considers the influence of: (i) concrete strength; (ii) amount of transverse reinforcement; (iii) installed axial load. Priestley *et al* (2007) also proposed an expression based on the same three components, referring it as an approach providing better agreement with experimental results than other methods found in research literature. However, the results provided by both expressions for the concrete strength component differ significantly, with the former being more conservative than the latter. As such, it seems important to (at least) investigate this matter further and evaluate if an update to the EC8-3 (2005) expression might be in order (with beneficial impact on assessment results).

Concerning the performance of the proposed design methodology, despite the results obtained in chapters 5 to 7 being most encouraging, there are certainly limitations to its application and room for improvement in future updates. Such comments have already been made along the method's presentation and validation, but are summarized below for the reader's convenience:

- At this point, the use of the proposed methodology is recommended only for low- and mid-rise RC buildings. The application to irregular frames and/or to buildings with RC shear walls should also still be handled with caution, namely concerning the inelastic lateral displacement shapes to be selected, and the percentage of the global seismic force to be carried by the braced frames.
- The influence of several factors on the inelastic lateral displacement shapes of pre-code RC framed buildings retrofitted with steel braces is still being studied, but it is likely that some of the findings may provide inputs to an updated version of the method. Considerations about the relative lateral stiffness of braces and columns at each storey will most likely be added to the design procedure, for the purpose of achieving even more controlled drift profiles (hence, global collapse mechanisms).
- The procedure proved to be easily adapted to both deformation- and strength-controlled collapse mechanisms. However, the comments made in Chapter 6 concerning the potential vulnerability of the braced RC columns to the effects of the increased axial forces suggest the need for an upper limit to the columns' normalized axial forces, as to help flag more effectively situations in which the global retrofitting system should be combined with local strengthening of the affected columns. This possibility is currently under evaluation but will surely be included in future updates.

Lastly, taking a cue from the seismic risk study presented in Chapter 7, the author would like to point out that further developments are required concerning the identification of the main drivers of vulnerability in RC structures retrofitted with steel braces. The development of fragility functions (reflecting both structural and record-to-record variability) that could be used directly in the assessment of earthquake induced economic losses would surely be an important contribution to further understand the risks in Portugal and, therefore, make better-informed decisions towards the enhancement of public safety. The development of specific GMPE (or at least the reliable verification of the existing attenuation models) also remains a significant challenge due to the lack of ground motion recordings in the country. Nonetheless, further comparative studies should be carried out, now considering the most recently proposed models (e.g., Kotha *et al,* 2020), as to better justify a given selection in future risk studies. All things considered, there is still much to be done in the seismic risk assessment research field (as in so many others).

CHAPTER 8 – CLOSURE

8.1. CONCLUSIONS 8.1

8.2. RECOMMENDATIONS FOR FUTURE DEVELOPMENTS 8.4

REFERENCES

A

Abou-Elfath, H. and Ghobarah, A. (2000). Behaviour of reinforced concrete frames rehabilitated with concentric steel bracing. *Canadian Journal of Civil Engineering,* 27: 433-444;

Aboutaha, R.S., Engelhardt, M.D., Jirsa, J.O. and Kreger, M.E. (1996). Retrofit of concrete columns with inadequate lap splices by the use of rectangular steel jackets. *Earthquake Spectra,* 12 (4): 693-714;

Adam, J.M., Giménez, E., Calderón, P.A. and Ivorra, S. (2008). Experimental study of beam-column joints in axially loaded RC columns strengthened by steel angles and strips. *Steel and Composite Structures,* 8 (4): 329-342;

Addessi, D. and Ciampi, V. (2007). A regularized force-based beam element with a damage-plastic section constitutive law. *International Journal for Numerical Methods in Engineering,* 70 (5): 610-629;

Akkar, S. and Bommer, J. (2010). Empirical equations for the prediction of PGA, PGV, and spectral accelerations in Europe, the Mediterranean region, and the Middle East. *Seismological Research Letters,* 81 (2): 195-206;

Akkar, S., Sucuoglu, H. and Yakut, A. (2005). Displacement-based fragility functions for low- and mid-rise ordinary concrete buildings. *Earthquake Spectra,* 21 (4): 901-927;

Akyuz, S. and Uyan, M. (1992). A study on the concrete steel bars used in Turkey. *Technical Journal Turkish Assembly Civil Engineering,* 35: 497-508 (in Turkish);

Almeida, J.P., Das, S. and Pinho, R. (2012). Adaptive force-based frame element for regularized softening response. *Computers & Structures,* 102-103: 1-13;

Almeida, J.P., Tarquini, D and Beyer, K. (2014). Modelling approaches for inelastic behaviour of RC walls: Multi-level assessment and dependability of results. *Archives of Computational Methods in Engineering;*

Amirsardari, A. (2018). Seismic assessment of reinforced concrete buildings in Australia including the response of gravity frames. Ph.D. thesis. University of Melbourne, Melbourne, Australia;

Antoniou, S., Rovithakis, A. and Pinho, R. (2002). Development and verification of a fully adaptive pushover procedure. *Proceedings of the 12th European Conference on Earthquake Engineering*. London, UK;

Antoniou, S. and Pinho, R. (2004a). Advantages and limitations of adaptive and non-adaptive force-based pushover procedures. *Journal of Earthquake Engineering*, 8 (4): 497-522;

Antoniou, S. and Pinho, R. (2004b). Development and verification of a displacement-based adaptive pushover procedure. *Journal of Earthquake Engineering*, 8 (5): 643-661;

Appleton, J. (2013). *Estruturas de Betão – Volumes 1 e 2*. Alfragide, Portugal: Edições Orion. ISBN 972-8620-21-9 e 972-8620-22-6;

Araújo, M. and Castro, J.M. (2016). On the quantification of local deformation demands and adequacy of linear analysis procedures for the seismic assessment of existing steel buildings to EC8-3. *Bulletin of Earthquake Engineering,* 14 (6): 1613-1642;

Araújo, M. and Castro, J.M. (2017). A critical review of European and American provisions for the seismic assessment of existing steel moment resisting frame buildings. *Journal of Earthquake Engineering*, DOI: 10.1080/13632469.2016.1277568;

Araújo, M., Castro, J.M. and Marques, M. (2015). Vulnerabilidade sísmica e perdas sobre a propriedade do parque industrial edificado em aço para Portugal. *X Congresso de Construção Metálica e Mista.* Coimbra, Portugal (in Portuguese);

Araújo, M., Macedo, L., Marques, M. and Castro, J.M. (2016). Code-based record selection methods for seismic performance assessment of buildings. *Earthquake Engineering & Structural Dynamics*, 45: 129-148;

ARUP (2010). *GB Oxfam Haiti Earthquake Response*. An ARUP Assignment Report;

ASCE 31-03 (2003). *ASCE/SEI Standard ASCE 31-03: Seismic evaluation of existing buildings.* Reston, VA: American Society of Civil Engineers;

ASCE 7-10 (2010). *ASCE/SEI Standard ASCE 7-10: Minimum design loads for buildings and other structures*. Reston, VA: American Society of Civil Engineers;

ASCE 41-06 (2007). *ASCE/SEI Standard ASCE 41-06: Seismic rehabilitation of existing buildings.* Reston, VA: American Society of Civil Engineers;

ASCE 41-13 (2014). *ASCE/SEI Standard ASCE 41-13: Seismic evaluation and retrofit of existing buildings.* Reston, VA: American Society of Civil Engineers;

Asteris, P.G., Chronopoulos, M.P., Chrysostomou, C.Z., Varum, H., Plevris, V., Kyriakides, N. and Silva, V. (2014). Seismic vulnerability assessment of historical masonry structural systems. *Engineering Structures,* 62-63: 118-134;

ATC 40 (1996). *ATC 40 Seismic evaluation and retrofit of concrete buildings.* Redwood City, CA, USA: Applied Technology Council;

ATC 63 (2009). *ATC 63 Quantification of building system performance and response parameters.* Redwood City, CA, USA: Applied Technology Council;

Atkinson, G.M. and Boore, D.M. (2006). Earthquake ground motion prediction equations for eastern North America. *Bulletin of the Seismological Society of America*, 96 (6): 2181-2205;

Atkinson, R.H., Amadei, B.P., Saeb, S. and Sture, S. (1989). Response of masonry bed joints in direct shear. *ASCE Journal of Structural Division,* 115 (9): 2276-2296;

Aykac, S., Kalkan, I., Aykac, B., Karahan, S. and Kayar, S. (2013). Strengthening and repair of reinforced concrete beams using external steel plates. *Journal of Structural Engineering,* 139 (6): 929-939;

B

Badoux, M. and Jirsa, J.O. (1990). Steel bracing of RC frames for seismic retrofitting. *Journal of Structural Engineering,* 116 (1);

Baker, J.W. and Cornell, C.A. (2006). Spectral shape, epsilon and record selection. *Earthquake Engineering & Structural Dynamics*, 35 (9): 1077-1095;

Bae, S., Mieses, A.M. and Bayrak, O. (2005). Inelastic buckling of reinforcing bars. *Journal of Structural Engineering,* 131 (2): 314-321;

Bal, I., Crowley, H., Pinho, R. and Gulay, F. (2008). Detailed assessment of structural characteristics of Turkish RC building stock for loss assessment models. *Soil Dynamics and Earthquake Engineering,* 28 (10-11): 914-932;

Baradaran Shoraka, M. and Elwood, K.J. (2013). Mechanical model for non-ductile reinforced concrete columns. *Journal of Earthquake Engineering,* 17 (7): 937-957;

Barata, M. (2005). The Lisbon earthquake of 1st November 1755 – a historical perspectives approach. *Proceedings of the International Conference 250th Anniversary of the 1755 Lisbon Earthquake*. Lisbon, Portugal;

Baros D. and Anagnostopoulos, S. (2008). An assessment of static nonlinear pushover analyses in 2-D and 3-D applications. *Proceedings of Nonlinear Static Methods for Design / Assessment of 3D Structures.* Lisbon, Portugal;

Bento, R. and Azevedo, J. (2000). Behaviour coefficient assessment for soft storey structures. *Proceedings of the 12th WCEE*. Auckland, New Zealand;

Bento, R., Bhatt, C., Pinho, R. (2010). Using nonlinear static procedures for seismic assessment of the 3D irregular SPEAR building. *Earthquakes and Structures*, 1 (2): 177-195;

Bento, R. and Lopes, M. (2000). Evaluation of the need for weak-beam strong-column design in dual frame-wall structures. *Proceedings of the 12th WCEE*. Auckland, New Zealand;

Bertero, V.V. (1982). State-of-the-art in seismic resistant construction of structures. *Proceedings of the 3rd International Earthquake Microzonation Conference.* Seattle, Washington, USA;

Bertero, V.V., Anderson, J.C., Krawinkler, H. and Miranda, E. (1991). *Design guidelines for ductility and drift limits: Review of state-of-the-practice and state-of-the-art in ductility and drift-based earthquake-resistant design of buildings.* Report No. UCB/EERC-91/15, EERC, University of California, Berkeley, USA;

Bertoldi, S.H., Decanini, L.D. and Gavarini, C. (1993). Telai tamponati soggetti ad azione sismica, un modello semplificato: confronto sperimentale e numerico. *Atti del 6 Convegno Nazionale ANIDIS*. Perugia, Italy;

Beyer, K. and Bommer, J.J. (2007). Selection and scaling of real accelerograms for bi-directional loadings: a review of current practice and code provisions. *Journal of Earthquake Engineering*, 11 (1): 13-45;

Bhatt, C. (2012). Seismic assessment of existing buildings using nonlinear static procedures (NSP's) – a new 3D pushover procedure. Ph.D. Thesis. Technical University of Lisbon, Lisbon, Portugal;

Bhatt, C. and Bento, R. (2012). Comparison of nonlinear static methods for the seismic assessment of plan irregular frame buildings with non-seismic details. *Journal of Earthquake Engineering*, 16: 15-39;

Bianchi, F., Sousa, R. and Pinho, R. (2011). Blind prediction of a full-scale RC bridge column tested under dynamic conditions. *Proceedings of the III ECCOMAS Thematic Conference on Computational Methods in Structural Dynamics and Earthquake Engineering.* Corfu, Greece;

Bilham, R. (2006). Harry Fielding Reid medal citation for Nicholas Ambraseys. *Seismological Research Letters,* 77 (4): 487-489;

Biskinis, D.E. (2006). Deformations of concrete members at yielding and ultimate. Ph.D. thesis. University of Patra, Patra, Greece;

Biskinis, D.E. and Fardis, M.J. (2004). Cyclic strength and deformation capacity of RC members including members retrofitted for earthquake engineering. *Proceedings of the 5th International Ph.D. Symposium in Civil Engineering.* Delft, Balkema, Rotterdam;

Blandon, C. (2005). Implementation of an Infill Masonry Model for Seismic Assessment of Existing Buildings. Individual Study. European School for Advanced Studies in Reduction of Seismic Risk (ROSE School), Pavia, Italy;

Blandon, C. (2012). Sensibility of nonlinear time-history analysis of a RC column using large scale shaking table results as benchmark. *Proceedings of the 15th World Conference on Earthquake Engineering.* Lisbon, Portugal;

Bommer, J.J., Spence, R., Erdik, M., Tabuchi, S., Aydinoglu, N., Booth, E., Re, D.D. and Pterken, D. (2002). Development of an earthquake loss model for Turkish catastrophe insurance. *Journal of Seismology,* 6: 431-446;

Bracci, J.M., Kunnath, S.K., Reinhorn, A.M. (1997). Seismic performance and retrofit evaluation of reinforced concrete structures. *Journal of Structural Engineering*, 123 (1): 3-10;

Bradley, B.A. (2011). Design seismic demands from seismic response analysis: a probability-based approach. *Earthquake Spectra*, 27 (1): 213-224;

Bradley, B.A. (2013). A critical examination of seismic response uncertainty analysis in earthquake engineering. *Earthquake Engineering & Structural Dynamics*, 42 (11): 1717-1729;

BRI (2001a). *Standard for seismic evaluation of existing reinforced concrete buildings*. Tokyo, Japan: Buildings Research Institute, Japan Building Disaster Prevention Association;

BRI (2001b). *Technical manual for seismic evaluation of existing reinforced concrete buildings.* Tokyo, Japan: Buildings Research Institute, Japan Building Disaster Prevention Association;

C

Calabrese, A., Almeida, J.P. and Pinho, R. (2010). Numerical issues in distributed inelasticity modelling of RC frame elements for seismic analysis. *Journal of Earthquake Engineering,* 14 (S1): 38-68;

Calvi, M. and Pinho, R. (2004). *LESSLOSS – A European integrated project on risk mitigation for earthquakes and landslides.* IUSS Press, Pavia, Italy.

Calvi, M., Pinho, R., Magenes, G., Bommer, J., Restrepo-Vélez, L. and Crowley, H. (2006). Development of seismic vulnerability assessment methodologies over the past 30 years. *ISET Journal of Earthquake Technology,* 43 (3): 75-104;

Campos Costa, A., Sousa, M.L., Carvalho, A. and Coelho, E. (2009). Evaluation of seismic risk and mitigation strategies for the existing building stock: application of LNECLoss to the Metropolitan Area of Lisbon. *Bulletin of Earthquake Engineering*, 8: 119-134;

Campos Costa, A. and Pinto, A.V. (1999). *European seismic hazard scenarios – an approach to the definition of input motions for testing and reliability assessment of civil engineering structures.* JRC Special Publication No. X.99.XX. ELSA, JRC Ispra, EC, Italy;

Carrillo, J., Hérnandez-Barrios, H. and Rubiano-Fonseca, A. (2014). Analysis of the earthquake-resistant design approach for buildings in Mexico. *Ingeniería Investigación y Tecnología,* XV (1): 151-162;

Caruso, C.; Bento, R.; Sousa, R. and Correia, A.A. (2018). Modelling strain penetration effects in RC walls with smooth steel bars. *Magazine of Concrete Research,* https://doi.org/10.1680/jmacr.18.00052;

Carvalho, A., Zonno, G., Franceschina. G., Bilé Serra, J. and Campos Costa, A. (2008a). Earthquake shaking scenarios for the metropolitan area of Lisbon. *Soil Dynamics and Earthquake Engineering,* 28 (5): 347-364;

Carvalho, E.C. and Coelho, E. (2001). *Seismic assessment, strengthening and repair of structures*. ECOEST2-ICONS Report no. 2. European Commission – Training and Mobility of Researchers Programme;

Carvalho, E.C., Coelho, E. and Campos Costa, A. (1999). *Preparation of the full-scale tests on reinforced concrete frames: characteristics of the test specimens, materials and testing conditions.* ICONS Report, Innovative Seismic Design Concepts for New and Existing Structures. LNEC, Lisbon, Portugal;

Carvalho, E.C., Coelho, E., Campos Costa, A., Sousa, M. L. and Candeias, P. (2002). Vulnerability evaluation of residential buildings in Portugal. *Proceedings of the 12th European Conference on Earthquake Engineering*. London, United Kingdom;

Carvalho, G., Bento, R. and Bhatt, C. (2013). Nonlinear static and dynamic analyses of reinforced concrete buildings: comparison of different modelling approaches. *Earthquakes and Structures,* 4 (5): 451-470;

Carvalho, J., Dias, R., Pinto, C., Leote, J. and Mendes-Victor, L. (2008b). A soil classification for seismic hazard assessment and mitigation of the Algarve. *Proceedings of the 14th World Conference on Earthquake Engineering.* Beijing, China;

Casarotti, C. and Pinho, R. (2007). An adaptive capacity spectrum method for assessment of bridges subjected to earthquake action. *Bulletin of Earthquake Engineering,* 5 (3): 377-390;

Castellani, A., Scirocco, F. and Boffi, G. (1993). Reinforced concrete columns under cyclic axial compressive forces. *ASCE Journal of Structural Engineering*, 119 (11): 3426-3433;

Castro, J.M., Araújo, M., D'Aniello, M. and Landolfo, R. (2017). Strengthening of RC buildings with steel elements. In A. Costa, A. Arêde and H. Varum (Eds.), *Strengthening and retrofitting of existing structures*. Building Pathology and Rehabilitation, Springer-Verlag Book Series. ISBN 978-981-10-5857-8;

Causevic, M. and Mitrovic, S. (2011). Comparison between non-linear dynamic and static seismic analysis of structures according to European and US provisions. *Bulletin of Earthquake Engineering*, 9 (2): 467-489;

Celarec, D. and Dolšek, M. (2013). Practice-oriented probabilistic seismic performance assessment of infilled frames with consideration of shear failure of columns. *Earthquake Engineering & Structural Dynamics,* 42 (9): 1339-1360;

Charney, F.A. and McNamara, R.J. (2008). A method for computing equivalent viscous damping ratio for structures with added viscous damping. *ASCE Journal of Structural Engineering*, 134 (1): 32-44;

Choffat, P. (1912). Le tremblement de terre du 23 Avril 1909 dans le Ribatejo. *Revista de Obras Públicas e Minas*, Tomo XLIII (in French);

Chopra, A.K. (2001). *Dynamics of Structures: Theory and Applications to Earthquake Engineering, 2nd Edition*. Berkeley, CA, USA: Prentice Hall. ISBN 978-0130869739;

Chopra, A.K. and Goel, R.K. (2002). A modal pushover analysis procedure for estimating seismic demands for buildings. *Earthquake Engineering & Structural Dynamics*, 31: 561-582;

Chopra, A.K. and Goel, R.K. (2004). A modal pushover analysis procedure to estimate seismic demands for unsymmetric- plan buildings. *Earthquake Engineering & Structural Dynamics*, 33: 903-927;

Chopra, A.K. and McKenna, F. (2016). Modelling viscous damping in nonlinear response history analysis of buildings for earthquake excitation. *Earthquake Engineering & Structural Dynamics*, 45(2): 193-211;

Chouw, N., Hao, H. and Goldsworthy, H. (2011). *Some observations of damage in the 22nd February Christchurch earthquake.* Earthquake Reconnaissance Report. Australian Earthquake Engineering Society;

Clifton, C., Bruneau, M., Fussel, A., Leon, R. and MacRae, G. (2011). *Steel building damage from the Christchurch earthquake series of 2010 and 2011.* Technical Report. Royal Commission of Inquiry into Building Failure caused by the Canterbury Earthquakes, Department of Internal Affairs, Christchurch, New Zealand;

Clough, R.W. and Penzien, J. (1993). *Dynamics of Structures: 2nd Edition*. New York, NY, USA: McGraw Hill. ISBN 0-07-011394-7;

Coburn, A. and Spence, R. (2002). *Earthquake Protection, 2nd Edition*. Wiley & Sons. ISBN 978-0-470-84923-1;

Coleman, J. and Spacone, E. (2001a). Localization issues in force-based frame elements. *Journal of Structural Engineering,* 127 (11): 1257-1265;

Coleman, J. and Spacone, E. (2001b). Localization issues in nonlinear frame elements. In P.B. Shing and T. Tanabe (Eds.), *Modelling of inelastic behaviour of RC structures under seismic loads.* ASCE, Reston, VA. ISBN 978-0-7844-0553-6;

Collins, M.P. and Mitchell, D. (1997). *Prestressed Concrete Structures.* New Jersey, USA: Prentice Hall. ISBN 978-0968195802;

COMPASS (2020). *2020 Global Construction Costs Yearbook*. COMPASS International Inc. Available at: https://compassinternational.net/product/global-construction-costs/;

Cosenza, E. and Prota, A. (2006). Experimental behaviour and numerical modelling of smooth steel rebars under compression. *Journal of Earthquake Engineering,* 10 (3): 313-329;

Crisafulli, F.J. (1997). Seismic behaviour of reinforced concrete structures with masonry infills. Ph.D. thesis. University of Canterbury, Canterbury, New Zealand;

Crisafulli, F.J., Carr, A.J. and Park, R. (2000). Analytical modelling of infilled frame structures – a general overview. *Bulletin of the New Zealand Society for Earthquake Engineering,* 33 (1): 30-47;

Crisafulli, F.J. and Carr, A.J. (2007). Proposed macro-model for the analysis of infilled frame structures. *Bulletin of the New Zealand Society of Earthquake Engineering,* 40 (2): 69-77;

Crowley, H., Bommer, J.J., Stafford, P.J. (2008). Recent developments in the treatment of ground motion variability in earthquake loss models. *Journal of Earthquake Engineering,* 12 (1): 71-80;

Crowley, H., Despotaki, V., Rodrigues, D., Silva, V., Toma-Danila, D., Riga, E., Karatzetzou, A., Fotopoulou. S., Zugic, Z., Sousa, L., Ozcebe, S. and Gamba, P. (2020). Exposure model for European seismic risk assessment. *Earthquake Spectra,* 36 (1_suppl): 252-273;

Crowley, H., Dabbeek, J., Despotaki, V., Rodrigues, D., Martins, L., Silva, V., Romão, X., Pereira, N., Weatherill, G. and Danciu, L. (2021). *European Seismic Risk Model (ESRM20).* EFEHR Technical Report 002 V1.0.0, https://doi.org/10.7414/EUC-EFEHR-TR002-ESRM20;

CSI (2016). *Analysis reference manual for SAP2000®, ETABS®, SAFE® and CSiBridge®*. Berkeley, California, USA: Computers and Structures, Inc;

D

D'Aniello, M. (2007). Steel dissipative bracing systems for seismic retrofitting of existing structures: theory and testing. Ph.D. Thesis. Università degli Studi di Napoli Frederico II, Naples, Italy;

D'Aniello, M., Della Corte, G. and Mazzolani, F.M. (2008). Experimental tests of a real building seismically retrofitted by special buckling restrained braces. *Proceedings of the American Institute of Physics* (from Seismic Engineering Conference Commemorating the 1908 Messina and Reggio Calabria Earthquake), 1020 (Part 1-2): 1513-1520;

D'Aniello, M., La Manna Ambrosino, G., Portioli, F. and Landolfo, R. (2003). Modelling aspects of the seismic response of steel concentric braced frames. *Steel and Composite Structures,* 15 (5): 539-566;

De Matteis, G., Formisano, A. and Mazzolani, F.M. (2009). An innovative methodology for seismic retrofitting of of existing RC buildings by metal shear panels. *Earthquake Engineering & Structural Dynamics,* 38 (1): 61-78;

Decanini, L.D. and Fantin, G.E. (1986). Modelos simplificados de la mampostería incluida en pórticos. Características de rigidez y resistencia lateral en estado límite (in Spanish). *Jornadas Argentinas de Ingeniería Estructural.* Buenos Aires, Argentina;

Decanini, L. D., De Sortis, A., Goretti, A., Langenbach, R., Mollaioli, F. and Rasulo, A. (2004]). Performance of Masonry Buildings During the 2002 Molise, Italy, Earthquake. *Earthquake Spectra,* 20 (S1), S191–S220.;

Decanini, L. D., De Sortis, A., Goretti, A., Liberatore, L., Mollaioli, F. and Bazzurro, P. (2004). Performance of Reinforced Concrete Buildings During the 2002 Molise, Italy, Earthquake. *Earthquake Spectra,* 20 (1): S221–S255;

Decanini, L., Mollaioli, F., Mura, A. and Saragoni, R. (2004). Seismic Performance of Masonry Infilled R/C Frames. *Proceedings of the 13th World Conference on Earthquake Engineering.* Vancouver, Canada;

Deierlein, G.G., Reinhorn, A.M. and Wilford, M.R. (2010). *NEHRP Seismic Design Technical Brief No. 4: Nonlinear Structural Analysis for Seismic Design.* Gaithersburg, MD, USA. National Institute of Standards and Technology – U.S. Department of Commerce;

Del Valle, E. (1980). Some lessons from the March 14th earthquake in Mexico City. *Proceedings of the 7th World Conference on Earthquake Engineering.* Istanbul, Turkey;

Delgado, R., Costa, A., Arêde, A., Vila Pouca, N., Guedes, J., Romão, X., Delgado, P. and Rocha, P. (2010). Ongoing research on seismic safety assessment. *Bulletin of Earthquake Engineering*, 8 (1): 181-199;

Della Corte, G., D'Aniello, M. and Landolfo, R. (2013). Analytical and numerical study of plastic overstrength of shear links. *Journal of Constructional Steel Research,* 82: 19-32;

Della Corte, G., D'Aniello, M. and Landolfo, R. (2014). Field testing of all-steel buckling-restrained braces applied to a damaged reinforced concrete building. *Journal of Structural Engineering,* 141 (1): doi.org/10.1061/(ASCE)ST.1943-541X.0001080;

Della Corte, G., Fiorino, L. and Mazzolani, F.M. (2008). Lateral-loading tests on a real RC building including masonry infill panels with and without FRP strengthening. *Journal of Materials in Civil Engineering,* 20 (6): 419-431;

Di Pasquale, G. and Goretti, A. (2001). Vulnerabilità funzionale ed economica degli edifici residenziali colpiti dai recenti eventi sismici italiani. *Proceedings of the 10th National Conference "L'Ingegneria Sismica in Italia".* Potenza-Matera, Italy;

Di Sarno, L. and Manfredi, G. (2009). Design approach for the seismic strengthening of an existing RC building with buckling restrained bracings. In F. Mazzolani, J.M. Ricles and R. Sause (Eds.), *STESSA 2009: Behaviour of steel structures in seismic areas*. Taylor & Francis. ISBN 9780415563260;

Di Sarno, L. and Manfredi, G. (2009). Experimental tests on full scale RC frames retrofitted with buckling restrained bracings. In F. Mazzolani, J.M. Ricles and R. Sause (Eds.), *STESSA 2009: Behaviour of steel structures in seismic areas*. Taylor & Francis. ISBN 9780415563260;

Dolšek, M., Fajfar, P. (2008). The effect of masonry infills on the seismic response of a four-storey reinforced concrete frame — a deterministic assessment. *Engineering Structures,* 30 (7): 1991–2001;

Dwairi, H.M., Kowalsky, M.J. and Nau, J.M. (2007). Equivalent viscous damping in support of direct displacement-based design. *Journal of Earthquake Engineering,* 11 (4): 512-530;

E

Eberhard, M., Baldridge, S., Marshall, J. and Rix, G. (2010). *The M_W 7.0 Haiti Earthquake*. USGS/EERI Advance Reconnaissance Team Report. United States Geological Survey, United States Department of the Interior, USA;

EC2-1-1 (2004). *EN 1992-1-1: 2004. Eurocode 2: Design of concrete structures – Part 1-1: General rules and rules for buildings*. Brussels, Belgium: European Committee for Standardization;

EC3-1-1 (2005). *EN 1993-1-1: 2005. Eurocode 3: Design of steel structures – Part 1-1: General rules and rules for buildings*. Brussels, Belgium: European Committee for Standardization;

EC8-1 (2004). *EN 1998-1: 2004. Eurocode 8: Design of structures for earthquake resistance – Part 1: General rules, seismic actions and rules for buildings*. Brussels, Belgium: European Committee for Standardization;

EC8-3 (2005). *EN 1998-3: 2005. Eurocode 8: Design of structures for earthquake resistance – Part 3: Assessment and retrofitting of buildings*. Brussels, Belgium: European Committee for Standardization;

EERI (2011). *The M 6.3 Christchurch, New Zealand, earthquake of February 22, 2011.* EERI Special Earthquake Report. Earthquake Engineering Research Institute, Oakland, California, USA;

Elnashai, A.S. (2000). Advanced inelastic (pushover) analysis for seismic design and assessment. *The G. Penelis Symposium*. Thessaloniki, Greece;

Elnashai, A., Gencturk, B., Kwon, O.-S., Al Qadi, I., Hashash, Y., Roesler, J., Kim, S., Jeong, S.-H., Dukes, J. and Valdivia, A. (2010). *The Maule (Chile) Earthquake of February 27, 2010: Consequence Assessment and Case Studies*. Mid-America Earthquake (MAE) Center Report Series, CD-Release 10-04;

Elnashai, A. and Pinho, R. (1999). *ICONS Topic 2 – Pseudo-dynamic testing of RC frames – Proposal for selective repair / strengthening of specimen B.* Report Imperial College of London;

Elghazouli, A.Y. (2003). Seismic design procedures for concentrically braced frames. *Structures & Buildings,* 156 (SB4): 381-394;

Elwood, K.J. (2004). Modelling failures in existing reinforced concrete columns. *Canadian Journal of Civil Engineering,* 31 (5): 846-859;

Elwood, K.J. and Moehle, J.P. (2003). Shake table tests and analytical studies on the gravity load collapse of reinforced concrete frames. PEER Report 2003/01. Pacific Earthquake Engineering Research Center, University of California, Berkeley, CA, USA;

Elwood, K.J. and Moehle, J.P. (2008). Dynamic collapse analysis for a reinforced concrete frame sustaining shear and axial failures. *Earthquake Engineering & Structural Dynamics,* 37: 991-1012;

Erdik, M., Aydinoglu, N., Fahjan, Y., Sesetyan, K., Demircioglu, M., Siyahi, B., Durukal, E., Ozbey, C., Biro, Y., Akman, H. and Yuzugullu, O. (2003). Earthquake risk assessment for Istanbul Metropolitan Area. *Earthquake Engineering and Engineering Vibration,* 2(1): 1-23;

Eskandari, R., Vafaei, D., Vafaei, J. and Shemshadian, M.E. (2017). Nonlinear static and dynamic behaviour of reinforced concrete steel-braced frames. *Earthquakes and Structures,* 12 (2): 191-200;

F

Faella, C., Lima, C., Martinelli, E. and Realfonzo, R. (2014). Steel bracing configurations for seismis retrofitting of a reinforced concrete frame. *Structures and Buildings,* 167 (SB1): 64-65;

Fajfar, P. and Dolšek, M. (2008). Seismic performance assessment of infilled reinforced concrete frames. *Proceedings of the International Conference on Earthquake Engineering and Disaster Mitigation.* Jakarta, Indonesia;

Fajfar, P. and Fischinger, M. (1988). N2 – A method for nonlinear seismic analysis of regular buildings. *Proceedings of the Ninth World Conference in Earthquake Engineering*. Tokyo-Kyoto, Japan;

Fajfar, P., Marusic, D. and Perus, I. (2005a). Torsional effects in the pushover-based seismic analysis of buildings. *Journal of Earthquake Engineering*, 9 (6): 831-854;

Fajfar, P., Marusic, D. and Perus, I. (2005b). The extension of the N2 method to asymmetric buildings. *Proceedings of the 4th European workshop on the seismic behaviour of irregular and complex structures*. Thessaloniki, Greece;

Fardis, M. (1998). Seismic assessment and retrofit of RC structures. *Proceedings of the 11th European Conference on Earthquake Engineering – Invited Lectures.* Paris, France;

Fardis, M. (2009). *Seismic design, assessment and retrofitting of concrete buildings*. Patras, Greece: Springer Science+Business Media B.V. ISBN 978-1-4020-9841-3;

Fardis, M. and Biskinis, D.E. (2003). Deformation capacity of RC members, as controlled by flexure or shear. *Proceedings of the Otani Symposium*. Tokyo, Japan;

FEMA 273 (1997). *Guidelines for the seismic rehabilitation of buildings – National Earthquake Hazard Reduction Program.* Washington D.C., USA: Federal Emergency Management Agency;

FEMA 274 (1997). *Commentary for the seismic rehabilitation of buildings – National Earthquake Hazard Reduction Program.* Washington D.C., USA: Federal Emergency Management Agency;

FEMA 310 (1998). *Handbook for the seismic evaluation of buildings – A prestandard – National Earthquake Hazard Reduction Program.* Washington D.C., USA: Federal Emergency Management Agency;

FEMA 356 (2000). *Prestandard and commentary for the seismic rehabilitation of buildings.* Washington D.C., USA: Federal Emergency Management Agency;

FEMA 440 (2005). *Improvement of nonlinear static seismic analysis procedures.* Washington D.C., USA: Federal Emergency Management Agency;

FEMA 547 (2006). *Techniques for the seismic rehabilitation of existing buildings*. Washington D.C., USA: Federal Emergency Management Agency;

FEMA P-58-1 (2018). *Seismic performance assessment of buildings: Volume 1 – Methodology (Second Edition).* Washington D.C., USA: Federal Emergency Management Agency;

FEMA and NIBS (1999). *Earthquake loss estimation methodology – HAZUS 99 Technical Manual.* Federal Emergency Management Agency and National Institute of Buildings Sciences, Washington, D.C., USA;

Fernandes, C., Melo, J., Varum, H. and Costa, A. (2011). Comparative analysis of the cyclic behaviour of beam-column joints with plain and deformed reinforcing bars. *IBRACON Structures and Materials Journal,* 4 (1): 147-172;

Fernandes, C.; Varum, H. and Costa, A. (2007). Concrete-steel bond characterization of RC structural elements built with smooth plain reinforcement bars. *Proceedings of the 2nd Symposium on Connections between Steel and Concrete.* Stuttgart, Germany;

Ferraioli, M. and Lavino, A. (2018). A displacement-based design method for seismic retrofit of RC buildings using dissipative braces. *Mathematical Problems in Engineering,* 2018: 1-28;

Ferraioli, M., Lavino, A. and Mandara, A. (2016). An adaptive capacity spectrum method for estimating seismic response of steel moment-resisting frames. *Ingegneria Sismica,* 33 (1-2): 47-60;

Ferreira, T., Vicente, R., Varum, H., Costa, A. and Mendes da Silva, J. (2013). Seismic vulnerability assessment of the old city centre of Seixal, Portugal. *Bulletin of Earthquake Engineering,* 11 (5): 1753-1773;

fib (2003). *fib Bulletin No. 24: Seismic assessment and retrofit of reinforced concrete buildings*. Lausanne, Switzerland: International Federation for Structural Concrete;

fib (2013). *fib Model Code for Concrete Structures 2010*. Lausanne, Switzerland: Ernst & Sohn. ISBN 978-3-433-03061-5;

Filippou, F.C., Popov, E.P. and Bertero, V.V. (1983). Modelling of RC joints under cyclic excitations. *ASCE Journal of Structural Engineering*, 109 (11): 2666-2684;

Filippou, F.C., Fenves, G.L. (2004). Methods of analysis for earthquake-resistant structures. In Y. Bozorgnia, V.V. Bertero (Eds.), *Earthquake Engineering: From Engineering Seismology to Performance-Based Engineering*. Chapter 6. Boca Raton, FL: CRC Press. ISBN 9780849314391;

Formisano, A. and Mazzolani, F.M. (2015). On the selection of MCDM methods of the optimal system for seismic retrofitting and vertical addition of existing buildings. *Computers and Structures,* 159: 1-13;

Formisano, A., Mazzolani, F.M. and De Matteis, G. (2007). Numerical analysis of slender steel shear panels for assessing design formulas. *International Journal of Structural Stability and Dynamics,* 7 (2): 273-294;

Fragiadakis, M. and Papadrakakis, M. (2008). Modelling, analysis and reliability of seismically excited structures: Computational issues. *International Journal of Computational Methods,* 05 (04): 483-511;

Fragiadakis, M., Pinho, R. and Antoniou, S. (2008). Modelling inelastic buckling of reinforcing bars under earthquake loading. *Computational Structural Dynamics and Earthquake Engineering Structures and Infrastructures,* 2: 363-377;

Franchin, P., Pinto, P.E. and Rajeev, P. (2010). Confidence Factor? *Journal of Earthquake Engineering*, 14 (7): 989-1007;

Freeman, S.A. (1998). The Capacity Spectrum Method as a tool for seismic design. Proceedings of the 11th Conference on Earthquake Engineering. Paris, France;

Freeman, S.A. (2004). Review of the development of the capacity spectrum method. *ISET Journal of Earthquake Technology,* 41 (1): 1-13;

Freeman, S.A., Nicoletti, J.P. and Tyrell, J.V. (1975). Evaluations of existing buildings for seismic risk – a case study of Puget Sound Naval Shipyard, Bremerton, Washington. *Proceedings of the U.S. National Conference on Earthquake Engineering.* Berkeley, USA;

Furtado, A., Costa, A., Arêde, A. and Rodrigues, H. (2016a). Geometric characterization of Portuguese RC buildings with masonry infill walls. *European Journal of Environmental and Civil Engineering,* 20 (4): 396-411;

Furtado, A., Rodrigues, H., Arêde, A. and Varum, H. (2016b). Simplified macro-model for infill masonry walls considering the out-of-plane behaviour. *Earthquake Engineering & Structural Dynamics,* 45: 507-524;

Furtado, A., Rodrigues, H., Varum, H. and Costa, A. (2015). Evaluation of different techniques' efficiency for a soft storey building. *European Journal of Environmental and Civil Engineering,* http://dx.doi.org/10.1080/19648189.2015.1119064;

G

Galanis, P. and Moehle, J.P. (2015). Development of collapse indicators for risk assessment of older-type reinforced concrete buildings. *Earthquake Spectra,* 31 (4): 1991-2006;

Galanis, P., Shin, Y.B. and Moehle, J.P. (2016). Laboratory and computer simulations of reinforced concrete frames with different ductility. *Earthquake Engineering & Structural Dynamics,* 45: 1603-1619;

Garzón-Roca, J., Ruiz-Pinilla, J., Adam, J.M. and Caderón, P.A. (2011). An experimental study on steel-caged RC columns subjected to axial force and bending moment. *Engineering Structures,* 33 (2): 580-590;

Ghannoum, W.M. and Moehle, J.P. (2012a). Rotation-based shear failure model for lightly confined RC columns. *Journal of Structural Engineering,* 138: 1267-1278;

Ghannoum, W.M. and Moehle, J.P. (2012b). Shake-table tests of a concrete frame sustaining column axial failures. *ACI Structural Journal,* 109 (3): 393-402;

Ghobarah, A. (2004). On drift limits associated with different damage levels. *Proceedings of International Workshop on Performance-Based Seismic Design*. Bled, Slovenia;

Giardini, D. (1999). The Global Seismic Hazard Assessment Program (GSHAP) 1992-1999. *Annali di Geofisica,* 42 (6): 957-1230;

Giménez, E., Adam, J.M., Ivorra, S. and Caldéron, P.A. (2009a). Full-scale testing of axially loaded RC columns strengthened by steel angles and strips. *Advance in Structural Engineering,* 12 (2): 169-181;

Giménez, E., Adam, J.M., Ivorra, S. and Caldéron, P.A. (2009b). Influence of strips configuration on the behaviour of axially loaded RC columns strengthened by steel angles and strips. *Materials and Design,* 30 (10): 4103-4111;

Godínez-Domínguez, E.A. and Tena-Colunga, A. (2010). Nonlinear behaviour of code-design reinforced concrete concentric braced frames under lateral loading. *Engineering Structures,* 32: 944-963;

Griffith, M. (1999). *Seismic retrofit of RC frame buildings with masonry infill walls – Literature review and preliminary case study.* JRC Special Publication, Ispra, Italy;

Guedes, J.P. (1997). Seismic behaviour of reinforced concrete bridges. Modelling, numerical analysis and experimental assessment. Ph.D. Thesis. University of Porto, Porto, Portugal;

Gulkan, P. and Sozen, M. (1974). Inelastic response of reinforced concrete structures to earthquake motions. *ACI Journal,* 71 (12): 604-610;

Guner, S. and Vecchio, F.J. (2008). *User's Manual of VecTor5*. Department of Civil Engineering, University of Toronto, Toronto, Canada;

Guner, S. and Vecchio, F.J. (2011). Nonlinear analysis of shear-critical reinforced concrete frames under impact, blast and seismic loads. *Proceedings of the 2nd International Engineering Mechanics and Materials Speciality Conference.* Ottawa, Ontario, Canada;

Guner, S. and Vecchio, F.J. (2010). Pushover analysis of shear-critical frames: formulation. *ACI Structural Journal,* 107 (1): 63-71;

Gupta, B., Kunnath, S.K. (2000). Adaptive spectra-based pushover procedure for seismic evaluation of structures. *Earthquake Spectra*, 16 (2): 367-391;

H

Hall, J.F. (2006). Problems encountered from the use (or misuse) of Rayleigh damping. *Earthquake Engineering & Structural Dynamics*, 35 (5): 525-545;

Hassan, F.M. and Hawkins, N.M. (1977). Anchorage of reinforced bars for seismic forces. *ACI Special Publication,* SP53 (15): 387-416;

Hellesland, J. and Scordelis, A. (1981). Analysis of RC bridge columns under imposed deformations. *Proceedings of the IABSE Colloquium*. Delft, The Netherlands;

Hancock, J., Bommer, J.J., Stafford, P.J. (2008). Numbers of scaled and matched accelerograms required for inelastic dynamic analyses. *Earthquake Engineering & Structural Dynamics*, 37 (14): 1585-1607;

Hendry, A.W. (1990). *Structural Masonry.* London, U.K.: Macmillan Education Ltd. ISBN 978-1-349-14829-5;

Holmes, M. (1961). Steel frames with brickwork and concrete infilling. *Proceedings of the Institution of Civil Engineers,* 19: 473-478;

Hoshikuma, J., Kawashima, K. and Nagaya, K. (1995). A stress-strain model for confined reinforced concrete in bridge piers. *Proceedings of the first Japan-Italy workshop on seismic design of bridges*. Tsukuba, Japan;

I

Iervolino, I. and Cornell, C.A. (2005). Record selection for nonlinear seismic analysis of structures. *Earthquake Spectra*, 21 (3): 685-713;

Iervolino, I., Maddaloni, G. and Cosenza, E. (2008). Eurocode 8 compliant real record sets for seismic analysis of structures. *Journal of Earthquake Engineering*, 12 (1): 54-90;

Ishimura, M., Sadasue, K., Miyauchi, Y., Yokoyama, T., Fujii, T. and Minamo, K. (2012). Seismic performance evaluation for retrofitting steel brace of existing RC buildings with low-strength concrete. *Proceedings of the 15th World Conference on Earthquake Engineering.* Lisbon, Portugal;

J

Jacobsen, L.S. (1930). Steady forced vibrations as influenced by damping. *Transactions ASME,* 52 (APM): 169-181;

Jacobsen, L.S. (1960). Damping in composite structures. *Proceedings of the 2nd World Conference on Earthquake Engineering.* Tokyo and Kyoto, Japan;

Jaiswal, K. and Wald, D.J. (2011). Rapid estimation of the economic consequences of global earthquakes. In US Geological Survey (Ed.), *Large Earthquakes: Estimating Economic Consequences* (1-40). Nova Science Publishers, Inc. ISBN: 978-162100173-7;

Jaiswal, K., Wald, D. and Porter, K. (2010). A global building inventory for earthquake loss estimation and risk management. *Earthquake Spectra*, 26 (3): 731-748;

Jalayer, F., Elefante, L., Iervolino, I. and Manfredi, G. (2011). Knowledge-based performance assessment of existing RC buildings. *Journal of Earthquake Engineering,* 15 (3): 362-389;

Jeon, J., Park, J. and Des Roches, R. (2015). Seismic fragility of lightly reinforced concrete frames with masonry infills. *Earthquake Engineering & Structural Dynamics,* 44 (1: 1783–1803;

K

Kakaletsis, D.J. and Karayannis, C.G. (2008). Influence of masonry strength and openings on infilled RC frames under cyclic loading. *Journal of Earthquake Engineering,* 12 (2): 197-221;

Kappos, A.J. (2013). A pilot application of EC8-3: Reflections and comparisons with the GCSI. *Workshop on the Implementation of the EC8-3: 2005*. Athens, Greece;

Kappos, A.J. and Ellul, F. (2000). Seismic design and performance assessment of masonry infilled RC frames. *Proceedings of the 12th World Conference on Seismic Engineering.* Auckland, New Zealand;

Kappos, A.J. and Konstantinidis, D. (1999). Statistical analysis of confined high strength concrete. *Materials and Structures,* 32 (10): 734-748;

Kappos, A.J., Panagopoulos, G., Panagiotopoulos, C. and Penelis, G. (2006). A hybrid method for the vulnerability assessment of RC and URM buildings. *Bulletin of Earthquake Engineering,* 4 (4): 391-413;

Karamanci, E. and Lignos, D.G. (2014). Computational approach for collapse assessment of concentrically braced frames in seismic regions. *ASCE Journal of Structural Engineering,* 140 (8): A4014019;

Kato, H., Tajiri, S. and Mukai, T. (2010). *Preliminary Reconnaissance Report of the Chile Earthquake 2010*. Building Research Institute, Japan Building Disaster Prevention Association, Tokyo, Japan;

Kawamata, S. and Masaaki, Q. (1980). Strengthening effect of eccentric steel braces to existing reinforced concrete frames. *Proceedings of the 7th World Conference on Earthquake Engineering.* Istanbul, Turkey;

Kent, D.C. and Park, R. (1971). Flexural members with confined concrete. *ASCE Journal of the Structural Division,* 97 (7): 1969-1990;

Kent, D.C. and Park, R. (1973). Cyclic load behaviour of reinforcing steel. *Strain J. British Soc. Strain Meas.,* 9 (3): 98-103;

Kotha, S.R., Weatherill, G., Bindi, D. and Cotton, F. (2020). A regionally adapted ground motion model for shallow crustal earthquakes in Europe. *Bulletin of Earthquake Engineering,* 18 (9): 4091-4125;

Krawinkler, H. (1997). Research issues in performance based seismic engineering. In P. Fajfar and H. Krawinkler (Eds.), *Seismic design methodologies for the next generation of codes, Proceedings of the International Workshop on Seismic Design Methodologies for the Next Generation of Codes.* A.A. Balkema, Rotterdam, The Netherlands. ISBN 978-9054109280;

Krawinkler, H., Median R., Alvi, B. (2003). Seismic drift and ductility demands and their dependence on ground motions. *Engineering Structures*, 25 (5): 637-653;

Kunnath, S. and Erduran, E. (2008). Pushover procedures for seismic assessment of building issues, limitations and future needs. *Proceedings of Nonlinear Static Methods for Design / Assessment of 3D Structures.* Lisbon, Portugal;

Kunnath, S. and Kalkan, E. (2004). Evaluation of seismic deformation demands using nonlinear procedures in multi-storey steel and concrete moment frames. *Journal of Earthquake Technology,* 41 (1): 159-181;

L

Lagomarsino, S. and Giovinazzi, S. (2006). Macroseismic and mechanical models for the vulnerability assessment of current buildings. *Bulletin of Earthquake Engineering*, 4 (4): 413-443;

LeBorgne, M.R. (2012). Modelling the post-shear failure behaviour of reinforced concrete columns. Ph.D. thesis. University of Texas, Austin, Texas, USA;

LeBorgne, M.R. and Ghannoum, W.M. (2014). Calibrated analytical element for lateral-strength degradation of reinforced concrete columns. *Engineering Structures,* 81: 35-48;

Lee, C.S. and Han, S.W. (2018). Computationally effective and accurate simulation of cyclic behaviour of old reinforced concrete columns. *Engineering Structures,* 173: 892-907;

Légeron, F. and Paultre, P. (2005). Damage mechanics modelling of nonlinear seismic behaviour of concrete structures. Journal of Structural Engineering, 131 (6): 946-955;

Leung, C.K.Y. (2001). Delamination failure in concrete beams retrofitted with a bonded plate. *Journal of Materials in Civil Engineering,* 13 (2): 106-113;

Liauw, T.C. and Kwan, K.H. (1984). Nonlinear behaviour of non-integral infilled frames. *Proceedings of the Institution of Civil Engineers,* 63 (Part 2): 641-656;

Lin, P.C., Tsai, K.C., Chang, C.A., Hsiao, Y.Y. and Wu, A.C. (2015). Seismic design and testing of buckling-restrained braces with a thin profile. *Earthquake Engineering & Structural Dynamics,* 45 (3): 339-358;

Longo, A., Montuori, R. and Piluso, V. (2008). Failure mode control of X-braced frames under seismic actions. *Journal of Earthquake Engineering,* 12 (5): 728-759;

Lucco, N. and Bazzurro, P. (2007). Does amplitude scaling of ground motion records result in biased nonlinear drift responses? *Earthquake Engineering & Structural Dynamics*, 36 (13): 1813-1835;

M

Macedo, L. (2017). Performance-based seismic design and assessment of steel moment frame buildings. Ph.D. Thesis. University of Porto, Porto, Portugal;

Macedo, L., Araújo, M. and Castro, J.M. (2013). Assessment and calibration of the harmony search algorithm for earthquake record selection. *Proceedings of the Vienna Congress on Recent Advances in Earthquake Engineering and Structural Dynamics*. Vienna, Austria;

Macedo, L. and Castro, J.M. (2012). Direct displacement-based seismic design of steel moment frames. *Proceedings of the 15th World Conference on Earthquake Engineering.* Lisbon, Portugal;

Macedo, L. and Castro, J.M. (2017). SelEQ: An advanced ground motion record selection and scaling framework. *Advances in Engineering Software,* 114: 32-47;

Madas, P. (1993). Advanced Modelling of Composite Frames Subjected to Earthquake Loading. Ph.D. Thesis. Imperial College – University of London, London, UK;

Madas, P. and Elnashai, A. (1992). A new passive confinement model for the analysis of concrete structures subjected to cyclic and transient dynamic loading. *Earthquake Engineering & Structural Dynamics,* 21 (5): 409-431;

Maheri, M.R. and Akbari, R. (2003). Seismic behaviour factor R for steel X-braced and knee-braced RC buildings. *Engineering Structures,* 25 (12): 1505-1513;

Maheri, M.R. and Hadjipour, A. (2003). Experimental investigation and design of steel brace connection to RC frame. *Engineering Structures,* 25 (13): 1707-1714;

Maheri, M.R., Kousari, R. and Razazan, M. (2003). Pushover tests on steel X-braced and knee-braced RC frames. *Engineering Structures,* 25 (13): 1697-1705;

Maheri, M.R. and Ghaffarzadeh, H. (2008). Connection overstrength in steel-braced RC frames. *Engineering Structures,* 30 (7): 1938-1948;

Maheri, M.R. and Sahebi, A. (1997). Use of steel bracing in reinforced concrete frames. *Engineering Structures,* 19 (12): 1018-1024;

Maheri, M.R. and Yazdani, S. (2016). Design of steel brace connection to an RC frame using uniform force method. *Journal of Constructional Steel Research,* 116: 131-40;

Maheri, M.R. and Yazdani, S. (2016). Seismic performance of different types of connections between steel bracing and RC frames. *Iranian Journal of Science and Technology, Transactions of Civil Engineering,* 40: 287-296;

Mainstone, R.J. (1971). On the stiffnesses and strengths of infilled frames. *Proceedings of the Institution of Civil Engineers,* Supplement IV: 57-90;

Malekpour, S. and Dashti, F. (2013). Application of the direct displacement-based design methodology for different types of RC structural systems. *International Journal of Concrete Structures and Materials,* 7 (2): 135-153;

Malekpour, S., Ghaffarzadeh, H. and Dashti, F. (2013). Direct displacement-based design of steel braced reinforced concrete frames. *Structural Design of Tall and Special Buildings,* 22 (18): 1422-1438;

Mander, J.B., Priestley, M.J.N. and Park, R. (1988). Theoretical stress-strain model for confined concrete. *Journal of Structural Engineering,* 114 (8): 1804-1826;

Manfredi. V. and Masi, A. (2017). Consistency of analysis methods considered in EC8-3 for the seismic assessment of RC existing buildings. *Bulletin of Earthquake Engineering,* 15 (7): 3027-3051;

Mann, W. and Müller, H. (1982). Failure of shear-stresses masonry - an enlarged theory, tests and application to shear walls. *Proceedings of the British Ceramic Society,* 30: 139-149;

Mari, A. and Scordelis, A. (1984). *Nonlinear geometric material and time dependent analysis of three-dimensional reinforced and pre-stressed concrete frames*. SESM Report 82-12. University of California, Berkeley, USA;

Marques, M. (2011). Avaliação probabilística da segurança sísmica de edifícios. Ph.D. Thesis. University of Porto, Porto, Portugal (in Portuguese);

Martinez-Rueda, J.E. and Elnashai, A.S. (1997). Confined concrete model under cyclic load. *Materials and Structures,* 30 (197): 139-147;

Masi, A. (2003). Seismic vulnerability assessment of gravity load design RC frames. *Bulletin of Earthquake Engineering,* 1: 371-395;

Massumi, A. and Absalan, M. (2013). Interaction between bracing system and moment resisting frame in braced RC frames. *Archives of Civil and Mechanical Engineering,* I3: 260-268;

Massumi, A. and Tasnimi, A.A. (2008). Strengthening of low ductile reinforced concrete frames using steel X-bracings with different details. *Proceedings of the 14th World Conference on Earthquake Engineering.* Beijing, China;

Mazza, F. and Vulcano, A. (2015). Displacement-based design procedure of damped braces for the seismic retrofitting of RC framed buildings. *Bulletin of Earthquake Engineering,* 13 (7): 2121-2143;

Mazzolani, F.M. (2008). Innovative metal systems for seismic upgrading of RC structures. *Journal of Constructional Steel Research,* 64 (7-8): 882-895;

Mazzolani, F.M., Della Corte, G. and D'Aniello, M. (2009). Experimental analysis of steel dissipative bracing systems for seismic upgrading. *Journal of Civil Engineering and Management,* 15 (1): 7-19;

McKenna, F.; Fenves, G.L.; Scott, H.M. and Jeremic, B. (2000). *Open System for Earthquake Engineering Simulation (OpenSees).* Pacific Earthquake Engineering Research Center, University of California, Berkeley, CA, USA;

Melo, J., Fernandes, C., Varum, H., Rodrigues, H., Costa, A. and Arêde, A. (2011). Numerical modelling of the cyclic behaviour of RC elements built with plain reinforcing bars. *Engineering Structures,* 33 (2): 273-286;

Mendes-Victor, L.A., Oliveira, C.S., Pais, I., Teves-Costa, P. (1994). Earthquake damage scenarios in Lisbon for disaster preparedness. In B.E. Tucker, M. Erdik, C.N. Hwang (Eds.), *Issues in Urban Earthquake Risk.* NATO ASI Series E, Applied Science, Vol. 271: 265-289. Kluwer Academic Press. ISBN: 978-90-481-4419-8;

Menegotto, M. and Pinto, P. (1973). Method of analysis for cyclically loaded RC plane frames including changes in geometry and non-elastic behaviour of elements under combined normal force and bending. *Proceedings of the IABSE Symposium on the Resistance and Ultimate Deformability of Structures Acted on by Well Defined Repeated Loads*. Zurich, Switzerland;

Moehle, J.P. (1992). Displacement-based design of RC structures subjected to earthquakes. *Earthquake Spectra,* 8 (3): 403-428;

Moehle, J.P. (2000). State of research on seismic retrofit of concrete building structures in the US. *Proceedings of the US-Japan Symposium and Workshop on Seismic Retrofit of Concrete Structures – State of Research and Practice*. USA;

Moehle, J.P. and Mahin, S.A. (1991). Observations on the behaviour of reinforced concrete buildings during earthquakes. In S.K. Ghosh (Ed.), *SP-127: Earthquake-Resistant Concrete Structures – Inelastic Response and Design.* ACI Publication. ISBN 978087031625;

Monti, G. and Nuti, C (1992). Nonlinear cyclic behaviour of reinforcing bars including buckling. *Journal of Structural Engineering,* 118 (12): 3268-3284;

Monti, G. and Spacone, E. (1998). Insertion of bond-slip into RC beam fiber finite elements. *Proceedings of the 11th European Conference on Earthquake Engineering*. Paris, France;

Montuori, R. and Piluso, V. (2009). Reinforced concrete columns strengthened with angles and battens subjected to eccentric load. *Engineering Structures,* 31 (2): 539-550;

Moreira, V. (1989). Seismicity of the Portuguese continental margin. In S. Gregersen, P.W. Basham (Eds.), *Earthquakes at North-Atlantic Passive Margins: Neotectonics and Postglacial Rebound*. Chapter 31: 533-545. Kluwer Academic Publishers. ISBN 978-94-010-7538-1;

Mostafaei, H., Vecchio, F.J. and Kabeyasawa, T. (2009). Deformation capacity of reinforced concrete columns. *ACI Structural Journal,* 106 (2): 187-195;

Mouroux, P. and Le Brun, B.T. (2006). Presentation of RISK-EU Project. *Bulletin of Earthquake Engineering,* 4 (4): 323-339;

Mpampatsikos, V., Nascimbene, R. and Petrini, L. (2008). A critical review of the RC frame existing building assessment procedure according to Eurocode 8 and Italian Seismic Code. *Journal of Earthquake Engineering,* 12 (S1): 52-82;

N

Nagashima, T., Sugano, S., Kimura, H. and Ichikawa, A. (1992). Monotonic axial compression test on ultra-high strength concrete tied columns. *Proceedings of the 10th World Conference on Earthquake Engineering.* Madrid, Spain;

Neuenhofer, A. and Filippou, F. C. (1997). Evaluation of nonlinear frame finite-element models. *Journal of Structural Engineering,* 123 (7): 958–966;

Newmark, N. M. (1959). A Method of Computation for Structural Dynamics. *ASCE Journal of the Engineering Mechanics Division*, 85: 67-94;

NIST (2015). *NIST GCR 15-917-34: Seismic design of steel buckling-restrained braced frames – A guide for practicing engineers.* U.S. Department of Commerce. Gaithersburg, Maryland, USA;

NTC (2008). *Norme Tecniche per le Construzione*. Roma, Italia: Decreto del Ministero delle infrastrutture, Supplemento Ordinario no. 30 alla Gazzetta Ufficiale della Repubblica Italiana no. 29 del 4/02/2008 (in Italian);

NZS 1170.5 (2004). *New Zealand Standard NZS 1170.5: Structural design actions – Part 5: Earthquake actions*. Wellington, New Zealand: New Zealand Standard;

NZSEE (2006). *Assessment and improvement of the structural performance of buildings in earthquake*: *Recommendations of a NZSEE study group on earthquake risk of buildings*. New Zealand: New Zealand Society for Earthquake Engineering;

O

Oehlers, D.J. (1992). Reinforced concrete beams with plates glued to their soffits. *Journal of Structural Engineering,* 188 (8): 2023-2038;

Oliveira, C.S. (2004). The influence of scale on microzonation and impact studies. In A. Ansal (Ed.), *Recent Advances in Earthquake Geotechnical Engineering and Microzonation*. Chapter 2: 27-65. Kluwer Academic Publishers. ISBN 978-1-4020-1827-5;

Oliveira, C.S. (2013). Studies made since early nineteen ninety in Portugal reducing the seismic risk. In C. Adam, R. Heuer, W. Lenhardt and C. Schranz (Eds.), *Proceedings of the Vienna Congress on Recent Advances in Earthquake Engineering and Structural Dynamics 2013 (VEESD 2013).* 28-30. Vienna, Austria.

Oliveira, C.S., Campos Costa, A. and Sousa, M.L. (1997). *Estimativa dos danos causados por sismos no parque habitacional do continente Português – Contribuição para a definição de uma política de seguros*. Report for the Portuguese Association for Insurance Entrepeneurs. Lisbon, Portugal;

Oliveira, C.S., Sousa, M.L. and Campos Costa, A. (1999). Contribuição para a revisão da acção sísmica em Portugal Continental no contexto do Eurocódigo 8. *Proceedings of the 4th National Conference on Earthquake Engineering.* Faro, Portugal (in Portuguese);

Oliveira, C.S., Mota de Sá, F. and Ferreira, M.A. (2005). Application of two different vulnerability methodologies to assess seismic scenarios in Lisbon. *Proceedings of the International Conference 250th Anniversary of the 1755 Lisbon Earthquake*. Lisbon, Portugal;

OPCM 3274 (2003). *Primi elementi in materia di criteri generali per la classificazione sismica del territorio nazionale e di normative tecniche per la construzioni in zona sismica.* Roma, Italia: Ordinanza del Presidente del Consiglio dei Ministri no. 3274/2003, Supplemento Ordinario no. 72 alla Gazetta Ufficiale della Repubblica Italiana no. 105 del 8/5/2003, e successive modifiche ed integrazioni (in Italian);

OPCM 3431 (2005). *Ulteriori modifiche em integrazioni all'Ordinanza no. 3274 del 20/3/2003, recante "Primi elementi in materia di criteri generali per la classificazione sismica del territorio nazionale e di normative tecniche per la construzioni in zona sismica".* Roma, Italia: Ordinanza del Presidente del Consiglio dei Ministri no. 3431/2005, Supplemento Ordinario no. 85 alla Gazetta Ufficiale della Repubblica Italiana no. 107 del 10/5/2005 (in Italian);

O'Reilly, G.J. (2016). Performance-based seismic assessment and retrofit of existing RC frame buildings in Italy. Ph.D. thesis. Scuola Universitaria Superiore IUSS Pavia, Pavia, Italy;

O'Reilly, G.J. and Sullivan, T.J. (2017/2019). Modelling techniques for the seismic assessment of the existing Italian RC frame structures. *Journal of Earthquake Engineering,* 23 (8): 1262-1296;

Osman, A., Rashed, A. and El-Kady, M. (2006). Seismic response of RC frames with concentric steel bracing. *Proceedings of the 8th U.S. National Conference on Earthquake Engineering.* San Francisco, California, USA;

P

P100-3/2008 (2009). *Cod de projectare seismica – Partea A III-A – Prevederi pentru evaluarea seismica a cladirilor existente*. Bucharest, Romania: Ministry of Local Development (in Romanian);

Panagiotakos, T.B. and Fardis, M.N. (2001). A displacement-based seismic design procedure for RC buildings and comparison with EC8. *Earthquake Engineering & Structural Dynamics*, 30 (10): 1439-1462;

Papaioannou, I., Fragiadakis, M. and Papadrakakis, M. (2005). Inelastic analysis of framed structures using the fiber approach. *Proceedings of the 5th GRACM International Congress on Computational Mechanics.* Limassol, Cyprus;

Paprotny, D., Kreibich, H., Morales-Nápoles, O., Terefenko, P. and Schröter, K. (2020). Estimating exposure of residential assets to natural hazards in Europe using open data. *Natural Hazards and Earth Systems Science,* 20: 323-343*;*

Paret, T.F., Sasaki, K.K., Eilbeck, D.H., Freeman, S.A. (1996). Approximate inelastic procedures to identify failure mechanisms from higher mode effects. *Proceedings of the Eleventh World Conference on Earthquake Engineering*. Acapulco, Mexico;

Park, P. and Paulay, T. (1975). *Reinforced Concrete Structures*. Christchurch, New Zealand: John Wiley & Sons;

Paulay, T. and Priestley, M.J.N. (1992). *Seismic Design of Reinforced Concrete and Masonry Buildings*. New York, USA: Wiley. ISBN 978-0471549154;

Pelaez, M.J.A. and Casado, C. (2002). Seismic hazard estimate at the Iberian Peninsula. *Pure Applied Geophysics,* 159 (11-12): 2699-2713;

Peng. C. and Guner, S. (2018). Direct displacement-based seismic assessment of concrete frames. *Computers and Concrete,* 21 (4): 355-365;

Pennucci, D., Sullivan, T.J. and Calvi, G.M. (2011). *Performance-based seismic design of tall RC wall buildings.* Research Report ROSE-2011/02. IUSS Press, Pavia, Italy;

Pennucci, D., Sullivan, T.J. and Calvi, G.M. (2011a). Displacement reduction factors for the design of medium and long period structures. *Journal of Earthquake Engineering,* 15 (S1): 1-29;

Pereira, N. (2019). Assessing the seismic performance of existing reinforced concrete buildings: from standard-based methods to full probabilistic approaches. Ph.D. thesis. University of Porto, Porto, Portugal;

Peres, R. and Castro, J.M. (2010). Comparison of European and American approaches for consideration of P-Δ effects in seismic design. *Proceedings of the 14th European Conference on Earthquake Engineering.* Ohrid, Republic of Macedonia;

Pincheira, J.A. and Jirsa, J.O. (1995). Seismic response of RC frames retrofitted with steel braces or walls. *Journal of Structural Engineering,* 121 (8): 1225-1235;

Pinho. R., Marques, M., Monteiro, R., Casarotti, C. (2008). Using the adaptive capacity spectrum method for seismic assessment of irregular frames. *Proceedings of the 5th European Workshop on the Sesmic Behaviour of Irregular and Complex Structures.* Catania, Italy;

Pinho. R., Marques, M., Monteiro, R., Casarotti, C. and Delgado, R. (2013). Evaluation of nonlinear static procedures in the assessment of building frames. Earthquake Spectra, 29 (4): 1459-1476;

Pinto, A., Varum, H. and Molina, J. (2002). Experimental assessment and retrofit of full-scale models of existing RC frames. *Proceedings of the 12th European Conference on Earthquake Engineering.* London, UK;

Pinto, A., Verzeletti, G., Molina, J., Varum, H., Pinho, R. and Coelho, E. (2002). *Pseudo-dynamic tests on non-seismic resisting RC frames (bare and selective RC frames).* EUR Report 20244 EN. ELSA, JRC Ispra, EC, Italy;

Pinto, P.E. (2005). The Eurocode 8 – Part 3: The new European code for the seismic assessment of existing structures. *Asian Journal of Civil Engineering,* 6 (5): 447-456;

Pinto, P.E. and Franchin, P. (2008). Assessing existing buildings with Eurocode 8 Part 3: a discussion with some proposals. *Background document for the "Eurocodes: Background and applications" workshop*. Brussels, Belgium;

Pinto, P.E. and Franchin, P. (2014). Existing buildings: The new Italian provisions for probabilistic seismic assessment. In Ansal A. (Ed.), *Perspectives on European Earthquake Engineering and Seismology*. Geotechnical, Geological and Earthquake Engineering, Vol. 34. Springer, Cham. ISBN 978-3-319-07117-6;

Pipa, M. (1993). Ductilidade de elementos de betão armado sujeitos a acções cíclicas – Influência das características mecânicas das armaduras. Ph.D. Thesis. Instituto Superior Técnico, Lisbon, Portugal (in Portuguese);

Popov, E.P. and Engelhardt, M.D. (1988). Seismic eccentrically braced frames. *Journal of Constructional Steel Research,* 10: 321-354;

Priestley, M.J.N. (1993). Myths and Fallacies in Earthquake Engineering – Conflicts between Design and Reality. *Proceedings of the Tom Paulay Symposium: Recent Developments in Lateral Force Transfer in Buildings.* La Jolla, CA, USA;

Priestley, M.J.N. (1998). Displacement-based approaches to rational limit states design of new structures. *Proceedings of the 11th European Conference on Earthquake Engineering.* Rotterdam, The Netherlands;

Priestley, M.J.N. (2003). *Myths and Fallacies in Earthquake Engineering, Revisited. The Ninth Mallet Milne Lecture.* Pavia, Italy: IUSS Press. ISBN 978-8873580096;

Priestley, M.J.N. and Grant, D.N. (2005). Viscous damping in seismic design and analysis. *Journal of Earthquake Engineering*, 9 (Special Issue 1): 229-255;

Priestley, M.J.N., Calvi, G.M. and Kowalsky, M.J. (2007). *Displacement-Based Seismic Design of Structures*. Pavia, Italy: IUSS Press. ISBN 88-6198-000-6;

Priestley, M.J.N., Seible, F. and Calvi, G.M. (1996). *Seismic design and retrofit of bridges.* New Jersey, USA: John Wiley & Sons Inc. ISBN 9780471579984;

Proença. J.M. and Sousa Gago, A. (2011). *Seismic Strengthening of School Buildings*. PARQUE ESCOLAR, EPE. ISBN 978-989-96106-7-5;

R

Rahimi, A. and Maheri, M.R. (2018). The effects of retrofitting RC frames by X-bracing on the seismic performance of columns. *Engineering Structures,* 173: 813-830;

Rahimi, A. and Maheri, M.R. (2020). The effects of steel X-brace retrofitting of RC frames on the seismic performance of frames and their elements. *Engineering Structures,* 206: 110149;

Ramberg, W. and Osgood, W.R. (1943). *Technical Note No. 902: Description of stress-strain curves by three parameters*. Washington DC, USA. National Advisory Committee for Aeronautics;

RBA (1935). *Regulamento para o Emprego de Betão Armado.* Lisbon, Portugal: Decreto-Lei n.º 4036 (in Portuguese);

REBA (1967). *Regulamento de Estruturas de Betão Armado.* Lisbon, Portugal: Decreto-Lei n.º 47723 (in Portuguese);

REBAP (1983). *Regulamento de Estruturas de Betão Armado e Pré-Esforçado.* Lisbon, Portugal: Decreto-Lei n.º 349-C/83 (in Portuguese);

RFCS (2013). *Steel Solutions for Seismic Retrofit and Upgrade of Existing Constructions (Steelretro)*. Research Fund for Coal and Steel. ISBN 978-92-79-29046-6;

Riddington, J.R. and Ghazali, M.Z. (1988). Shear strength of masonry walls. *Proceedings of the 8th International Brick and Block Masonry Conference.* Dublin, Ireland;

Rodrigues, H., Arêde, A., Varum, H. and Costa, A. (2012). Experimental evaluation of rectangular reinforced concrete column behaviour under biaxial cyclic loading. *Earthquake Engineering & Structural Dynamics,* 42 (2): 239-259;

Rojas, F., Lew, M. and Naeim, F. (2010). An overview of building codes and standards in Chile at the time of the 27 February 2010 offshore Maule, Chile earthquake. *Structural Design of Tall and Special Buildings,* 19 (8): 853-865;

Romão, X. (2012). Deterministic and probabilistic methods for structural seismic safety assessment. Ph.D. Thesis. University of Porto, Porto, Portugal;

Romão, X., Delgado, R. and Costa, A. (2010b). Practical aspects of demand and capacity evaluation of RC members in the context of EC8-3. *Earthquake Engineering & Structural Dynamics*, 39 (5): 473-499;

Romão, X., Delgado, R. and Costa, A. (2014a). A risk and cost based methodology for the seismic safety assessment of existing buildings. In A.P. Quinn (Ed.), *Earthquakes: Risk Factors, Seismic Effects and Economic Consequences* (79-126). Nova Science Publishers, Inc. ISBN: 978-1-63117-517-6;

Romão, X., Delgado, R. and Costa, A. (2014b). Probabilistic performance analysis of existing buildings under earthquake loading. *Journal of Earthquake Engineering*, 18 (8): 1241–1265;

Romão, X., Delgado, R., Guedes, J. and Costa, A. (2010a). A comparative application of different EC8-3 procedures for the seismic safety assessment of existing structures. *Bulletin of Earthquake Engineering*, 8 (1): 91-118;

Romão, X., Gonçalves, R., Costa, A. and Delgado, R. (2012). Evaluation of the EC8-3 confidence factors for the characterization of concrete strength in existing structures. *Materials and Structures,* 45 (11): 1737-1758;

Romão, X., Guedes, J., Costa, A. and Delgado, R. (2008). Adequacy of the EC8-Part 3 proposed confidence factors for the assessment of existing RC structures. *Proceedings of the 14th World Conference on Earthquake Engineering*. Beijing, China;

Romão, X. and Penna, A. (2017). Code-based procedures for seismic safety assessment and retrofit. In A. Costa, A. Arêde and H. Varum (Eds.), *Strengthening and retrofitting of existing structures*. Building Pathology and Rehabilitation, Springer-Verlag Book Series. ISBN 978-981-10-5857-8;

Rossetto, T. and Elnashai, A. (2005). A new analytical procedure for the derivation of displacement-based vulnerability curves for populations of RC structures. *Engineering Structures,* 27 (3): 397-409;

Rota, M., Penna, A. and Strobbia, C. (2008). Processing Italian damage data to derive typological fragility curves. *Soil Dynamics & Earthquake Engineering,* 28 (10-11): 933-947;

RSA (1983). *Regulamento de Segurança e Acções para Estruturas de Edifícios e Pontes.* Lisbon, Portugal: Decreto-Lei n.º 235/83 (in Portuguese);

RSCCS (1958). *Regulamento de Segurança das Construções contra os Sismos*. Lisbon, Portugal: Decreto-Lei n.º 41658 (in Portuguese);

S

Saborio Romano, D. (2016). Performance-based and simplified displacement-based assessment of infilled RC frame building in L'Aquila, Italy. M.Sc. Thesis. Università degli Studi de Pavia, Pavia, Italy;

Sahlin, S. (1971). *Structural Masonry.* New Jersey, USA: Prentice-Hall Inc. ISBN 978-0138539375;

Said, A. and Nehdi, M. (2008). Rehabilitation of RC frame joints using local steel bracing. *Structure and Infrastructure Engineering,* 4 (6): 431-447;

Salgado, R.A. and Guner, S. (2018). A comparative study on nonlinear models for performance-based earthquake engineering. *Engineering Structures,* 172: 382-391;

Sanam, M., Sousa, R., André, J., Campos Costa, A., Carvalho, A. and Lourenço, P.B. (2019). Updating fragility curves for Portuguese pre-seismic code reinforced concrete buildings. *Proceedings of the 11th National Conference on Seismology and Earthquake Engineering.* Lisbon, Portugal;

Sasani, M., Bertero, V. and Anderson, J. (1999). *Rehabilitation of non-ductile RC frame buildings using encasement plates and energy dissipating devices*. PEER Report 1999/12. Pacific Earthquake Engineering Research Center, University of California, Berkeley, CA, USA;

Sassun, K., Sullivan, T. J., Morandi, P. and Cardone, D. (2015). Characterizing the in-plane seismic performance of infill masonry. *Bulletin of the New Zealand Society for Earthquake Engineering,* 49 (1): 100-117;

Scott, B.D., Park, R. and Priestley, M.J.N. (1982). Stress-strain behaviour of concrete confined by overlapping hoops at low and high strain rates. *ACI Journal,* 79 (1): 13-27;

Scott, M. H. and Fenves, G. L. (2006). Plastic hinge integration methods for force-based beam column elements. *Journal of Structural Engineering,* 132 (2): 244-252;

Scott, M.H. and Hamutçuoglu, O.M. (2008). Numerically consistent regularization of force-based frame elements. *International Journal for Numerical Methods in Engineering,* 76: 1612-1613;

Searer, G.R., Paret, T.F. and Freeman, S.A. (2008). ASCE-31 and ASCE-41: What good are they? *Proceedings of the ASCE Structures Congress.* Vancouver, Canada;

Searer, G.R., Paret, T.F. and Freeman, S.A. (2011). ASCE 31 and 41: Apocalypse now. *Proceedings of the ASCE Structures Congress.* Las Vegas, Nevada, USA;

Segovia, V.A. and Ruiz, S.E. (2017). Direct displacement-based design for buildings with hysteretic dampers, using best combinations of stiffness and strength ratios. *Journal of Earthquake Engineering,* 21 (5): 752-775;

Seismosoft (2018). SeismoStruct 2018 – A computer program for static and dynamic nonlinear analysis of framed structures. Available from http://www.seismosoft.com;

Sextos, A.G., Katsanos, E.I., Manolis, G.D. (2011). EC8-based earthquake record selection procedure evaluation: validation study based on observed damage of an irregular RC building. *Soil Dynamics and Earthquake Engineering*, 31 (4): 583-597;

Sezen, H. and Chowdhury, T. (2009). Hysteretic model for reinforced concrete columns including the effect of shear and axial load failure. *ASCE Journal of Structural Engineering*, 135 (2): 139-146;

Sezen, H. and Moehle, J. (2004). Strength and deformation capacity of reinforced concrete columns with limited ductility. *Proceedings of the 13th World Conference on Earthquake Engineering.* Vancouver, Canada;

Sheikh, S.A. and Uzumeri, S.M. (1982). Analytical model for concrete confined in tied columns. *Journal of the Structural Division,* 108 (ST12): 2703-2722;

Shibata. A. and Sozen, M. (1976). Substitute structure method for seismic design in reinforced concrete. *ASCE Journal of Structural Engineering,* 102 (1): 1-18;

Silva, V. (2013). Development of open models and tools for seismic risk assessment: application to Portugal. Ph.D. Thesis. University of Aveiro, Aveiro, Portugal;

Silva, V., Crowley, H., Varum, H. and Pinho, R. (2015a). Seismic risk assessment for mainland Portugal. *Bulletin of Earthquake Engineering*, 13 (2): 429-457;

Silva, V., Crowley, H., Varum, H., Pinho, R. and Sousa, L. (2015b). Investigation of the characteristics of Portuguese regular moment-frame RC buildings and development of a vulnerability model. *Bulletin of Earthquake Engineering*, 13 (5): 1455-1490;

Silva, V., Crowley, H., Pagani, M., Monelli, D., Pinho, R. (2014a). Development of the OpenQuake engine, the Global Earthquake Model's open-source software for seismic risk assessment. *Natural Hazards*, 72 (3): 1409-1427;

Silva, V., Crowley, H., Varum, H., Pinho, R. and Sousa, R. (2014b). Evaluation of analytical methodologies used to derive vulnerability functions. *Earthquake Engineering & Structural Dynamics*, 43 (2): 181-204;

Silva, V., Marques, M., Castro, J.M. and Varum, H. (2015c). Development and application of a real-time loss estimation framework for Portugal. *Bulletin of Earthquake Engineering*, 13 (9): 2493-2516;

Silva, V. and Paul, N. (2021). Potential impact of earthquakes during the 2020 CoViD-19 pandemic. *Earthquake Spectra,* 37 (1): 73-94;

Sinha, B.P. and Pedreschi, R. (1983). Compressive strength and some elastic properties of brickwork. *International Journal of Masonry Construction,* 3 (1): 19-25;

Siu, W.H. and Su, R.K.L. (2010). Effects of plastic hinges on partial interaction behaviour of bolted side-plated beams. *Journal of Constructional Steel Research,* 66 (5): 622-633;

Smyrou, E. (2006). Implementation and verification of a masonry panel model for nonlinear dynamic analysis of infilled RC frames. M.Sc. Thesis. Università degli Studi de Pavia, Pavia, Italy;

Smyrou, E., Blandon, C., Antoniou, S., Pinho, R. and Crowley, H. (2006). Implementation and verification of a masonry panel model for nonlinear pseudo-dynamic analysis of infilled RC frames. *Proceedings of the 1st European Conference on Earthquake Engineering and Seismology.* Geneva, Switzerland;

Smyrou, E., Blandon, C., Antoniou, S., Pinho, R. and Crisafulli, F. (2011). Implementation and verification of a masonry panel model for nonlinear dynamic analysis of infilled RC frames. *Bulletin of Earthquake Engineering,* 9 (5): 1519-1534;

SNPC (2001). *Estudo do risco sísmico da Área Metropolitana de Lisboa (AML) e concelhos limítrofes*. Report for the Portuguese Civil Protection. Lisbon, Portugal (in Portuguese);

Sousa, M.L. (1996). Modelos probabilísticos para avaliação da casualidade sísmica em Portugal Continental. M.Sc. Thesis. Instituto Superior Técnico, Lisbon, Portugal (in Portuguese);

Sousa, M.L. (2006). Risco sísmico em Portugal continental. Ph.D. Thesis. Instituto Superior Técnico, Lisbon, Portugal (in Portuguese);

Sousa, M.L. and Campos Costa, A. (2009). Ground motion scenarios consistent with probabilistic seismic hazard disaggregation analysis. Application to mainland Portugal. *Bulletin of Earthquake Engineering,* 7 (1): 127-147;

Sousa, M.L. and Campos Costa, A. (2016). Evolution of earthquake losses in Portuguese residential building stock. *Bulletin of Earthquake Engineering*, 14 (7): 2009-2029;

Sousa, M.L., Coelho, E. and Martins, A. (2010). Vulnerabilidade sísmica e danos no parque hoteleiro da região do Algarve. *Proceedings of the 10th National Conference on Earthquake Engineering*. Aveiro, Portugal;

Sousa, R. (2010). A displacement-based design approach for seismic retrofitting of RC frames with steel braces. M.Sc. Thesis. Università degli Studi de Pavia, Pavia, Italy;

Sousa, R. (2015). Development and verification of innovative modelling approaches for the analysis of framed structures subjected to earthquake actions. Ph.D. Thesis. Istituto Universitario di Studi Superiori, Pavia, Italy;

Sousa, R., Almeida, J.P., Correia, A.A. and Pinho, R. (2020). Shake table blind prediction tests: Contributions for improved fibre-based frame modelling. *Journal of Earthquake Engineering,* 24 (9): 1435-1476;

Sousa, R., Batalha, N., Silva, V. and Rodrigues, H. (2021). Seismic fragility functions for Portuguese RC precast buildings. *Bulletin of Earthquake Engineering,* 19: 6573-6590;

Sousa, R., Bianchi, F., Pinho, R. and Nascimbene, R. (2011). Analysis issues on seismic assessment of existing structures. *Proceedings of the III ECCOMAS Thematic Conference on Computational Methods in Structural Dynamics and Earthquake Engineering.* Corfu, Greece;

Sousa, R., Campos Costa, A. and Costa, A. (2019). *Metodologia para a avaliação da segurança sísmica de edifícios existentes baseada em análises de fiabilidade estrutural – Edifícios de betão armado.* LNEC – Proc. 0305/1309/19281. Relatório 81/2019 – DE/NESDE (in Portuguese);

Sousa, R. and Castro, J.M. (2012). Seismic design of RC frames retrofitted with concentric steel braces. In F. Mazzolani and R. Herrera (Eds.), *STESSA 2012: Behaviour of steel structures in seismic areas*. Taylor & Francis. ISBN 9780415621052;

Sousa, R., Correia, A.A., Almeida, J.P. and Pinho, R. (2017a). A fibre-based frame element with explicit consideration of bond-slip effects. *Proceedings of the 16th Word Conference on Earthquake Engineering.* Santiago, Chile;

Sousa, R., Costa, A., Campos Costa, A., Romão, X. and Candeias, P. (2017b). Caracterização do comportamento sísmico de edifícios de betão armado representativos do edificado português sem dimensionamento sísmico sismo-resistente. *Revista Portuguesa de Engenharia de Estruturas,* III (3): 105-114 (in Portuguese);

Spacone, E., Ciampi, V., and Filippou, F. C. (1996). Mixed formulation of nonlinear beam finite element. *Computers & Structures*, 58 (1): 71–83;

Sritharan, S., Priestley, N. and Seible, F. (2000). Nonlinear finite element analyses of concrete bridge joint systems subjected to seismic actions. *Finite Elements in Analysis and Design,* 36 (3-4): 215-233;

Stafford Smith, B. (1963). Lateral stiffness of infilled frames. *ASCE Journal of the Structural Division,* 88 (ST6): 183-199;

Stafford Smith, B. (1966). Behaviour of square infilled frames. *ASCE Journal of the Structural Division,* 92 (ST1): 381-403;

Stewart, J., Javanbarg, M., Di Alessandro, C., Bozorgnia, Y., Abrahamson, N., Boore, D., Campbell, K., Delavaud, E., Erdik, M. and Stafford, P. (2012). *Selection of a global set of ground motion prediction equations.* Technical Report, GEM Foundation, Pavia, Italy;

Stojadinovic, B. and Thewalt, C.R. (1996). Energy balanced hysteresis models. *Proceedings of the Eleventh World Conference on Earthquake Engineering*. Berkeley, CA, USA;

Su, R.K.L., Siu, W.H. and Smith, S.T. (2010). Effects of bolt-plate arrangements on steel plate strengthened reinforced concrete beams. *Engineering Structures,* 32 (6): 1769-1778;

Sullivan, T.J. (2013). Direct displacement-based seismic design of steel eccentrically braced frame structures. *Bulletin of Earthquake Engineering,* 11 (6): 2197-2231;

Sullivan, T.J. and Calvi, G.M. (2011). Considerations for the seismic assessment of buildings using the Direct Displacement-Based Assessment approach. *Atti del 5 Convegno Nazionale ANIDIS*. Bari, Italy;

Sullivan, T.J. and Calvi, G.M. (2013). Towards displacement-based seismic assessment in Europe. *Proceedings of the 2013 New Zealand Society of Earthquake Engineering Conference.* Wellington, New Zealand;

Sullivan, T.J., Priestley, M.J.N. and Calvi, G.M. (2012). *A Model Code for the Displacement-Based Seismic Design of Structures*. Pavia, Italy: IUSS Press. ISBN 978-88-6198-072-3;

T

TahamouliRoudsari, M., Entezari, A., Hadidi, M. and Gandomian, O. (2017). Experimental assessment of retrofitted RC frames with different steel braces. *Structures,* 11: 206-217;

Takeuchi, T., Ozaki, H., Tasui, R. and Sutcu, F. (2013). Out-of-plane stability of buckling-restrained braces including moment transfer capacity. *Earthquake Engineering & Structural Dynamics,* 43 (6): 851-869;

Tanganelli, M., Viti, S., De Stefano, M. and Rinhorn, A.M. (2011). Influence of infill panels on the seismic response of existing RC buildings: a case study. *Proceedings of the 6th European Workshop on the seismic behaviour of irregular and complex structures.* EWICS, Haifa, Israel;

Tankut, T. and Ersoy, U. (1998). Seismic repair/ strengthening of RC structures - METU research and practice. *Proceedings of the 2nd Japan-Turkey Workshop on Earthquake Engineering: Repair & Strengthening of Existing Buildings*. Istanbul, Turkey;

Taucer, F.F., Spacone, E. and Filippou, F.C. (1991). *A fibre beam-column element for seismic response analysis of reinforced concrete structures*. Berkeley, CA, USA. Earthquake Engineering Research Centre – University of California;

Thompson, K.J. and Park, R. (1980). Moment-curvature behaviour of cyclically loaded structural concrete members. *ICE Proceedings*, 69 (2): 317-341;

Tilly, G.P. (1986). *Dynamic behaviour of concrete structures*. Amsterdam, the Netherlands: Elsevier. ISBN 978-0444426246;

Torres Queirós, N., Castro, J.M. and Vila Pouca, N. (2009). Comportamento sísmico de estruturas híbridas aço-betão. *Proceedings of the VI Conference on Steel and Composite Construction.* Lisbon, Portugal (in Portuguese);

Tremblay, R. (2002). Inelastic seismic response of steel bracing members. *Journal of Constructional Steel Research,* 58: 665-701;

V

Valente, M. and Milani, G. (2017). Seismic assessment and retrofitting of an under-designed RC frame through a displacement-based approach. In V. Plevris, G. Kremmyda and Y. Fahjan (Eds.), *Performance-Based Seismic Design of Concrete Structures and Infrastructures.* IGI Global. ISBN 9781522520894;

Vamvatsikos, D. and Cornell, A.C. (2002). Incremental dynamic analysis. *Earthquake Engineering & Structural Dynamics,* 31 (3): 491-514;

Varum, H. (2003). Seismic assessment, strengthening and repair of existing buildings. Ph.D. Thesis. University of Aveiro, Aveiro, Portugal;

Varum, H., Dias Teixeira, F., Marques, P., Pinto, A.V., Bhatti, A.Q. (2013). Performance evaluation of retrofitting strategies for non-seismically designed RC buildings using steel braces. *Bulletin of Earthquake Engineering*, 11 (4): 1129-1156;

Vecchio, F.J. (1990). Reinforced concrete membrane element formulations. *Journal of Structural Engineering,* 116 (3): 730-750;

Vecchio, F.J. and Collins, M.P. (1986). The modified compression-field theory for reinforced concrete elements subjected to shear. *ACI Journal,* 83 (2): 219-231;

Verderame, G.M., Fabbrocino, G. and Manfredi, G. (2008). Seismic response of RC columns with smooth reinforcement. Part 1: Monotonic tests. *Engineering Structures,* 30 (9): 2277-2288;

Vicente, R., Parodi, S., Lagomarsino, S., Varum, H., Mendes Silva, J. (2010). Seismic vulnerability and risk assessment: case study of the historic city centre of Coimbra, Portugal. *Bulletin of Earthquake Engineering,* 9 (4): 1067-1096;

Vilanova, S. and Fonseca, J. (2007). Probabilistic seismic hazard assessment for Portugal. *Bulletin of the Seismological Society of America,* 97 (5): 1702-1717;

Vilanova, S., Fonseca, J. and Oliveira, C. (2012). Ground motion models for seismic hazard assessment in Western Iberia: Constraints from instrumental data and intensity observations. *Bulletin of the Seismological Society of America,* 102 (1): 169-184;

Villani, A., Castro, J.M. and Elghazouli, A.Y. (2009). Improved seismic design procedure for steel moment frames. In F. Mazzolani, J.M. Ricles and R. Sause (Eds.), *STESSA 2009: Behaviour of steel structures in seismic areas*. Taylor & Francis. ISBN 9780415563260;

Villani, A., Guimarães, D.S. and Castro, J.M. (2010). Towards performance-based seismic design of steel moment frames. *Proceedings of the 14th European Conference on Earthquake Engineering*. Ohrid, Macedonia;

W

Wan, Q. and Yi, W. (1986). The shear strength of masonry walls under combined stresses. *Proceedings of the 4th Canadian Masonry Symposium.* University of New Brunswick, Canada;

Wang, L. and Su, R.K.L. (2013). Theoretical and experimental study of plate-strengthened concrete columns under eccentric compression loading. *Journal of Structural Engineering,* 139 (3): 350-359;

Wibowo, A., Wilson, J.L., Lam, N.T.K. and Gad, E.F. (2014). Drift performance of lightly reinforced concrete columns. *Engineering Structures,* 59: 522-535;

Wilson, J.L., Lam, N.T.K. and Gad, E.F. (2015). Hazard identification and behaviour of reinforced concrete framed buildings in regions of lower seismicity. *Proceedings of the 10th Pacific Conference on Earthquake Engineering (PCEE), Building an Earthquake-Resilient Pacific.* Sydney, Australia;

Wilson, E. L. and Penzien, J. (1972). Evaluation of Orthogonal Damping Matrices. *International Journal for Numerical Methods in Engineering*, 4: 5-10;

Woessner, J., Laurentiu, D., Giardini, D., Crowley, H., Cotton, F., Grünthal, G., Valensise, G., Arvidsson, R., Basili, R., Demircioglu, M.B., Hiemer, S., Meletti, C., Musson, R.W., Rovida, A.N., Sesetyan, K. and Stucchi, M. (2015). The 2013 European Seismic Hazard Model: key components and results. *Bulletin of Earthquake Engineering,* 13 (12): 3553-3596;

Wyllie, L. (1983). Seismic strengthening procedures for existing buildings. *Proceedings of the IABSE Symposium on Strengthening of Buildings Structures – Diagnosis and Theory*. Venice, Italy;

Y

Yassin, M.H.M. (1994). Nonlinear analysis of pre-stressed concrete structures under monotonic and cyclic loads. Ph.D. Thesis. University of California, Berkeley, USA;

Yazgan, U. and Dazio, A. (2011a). Simulating maximum and residual displacements of RC structures: I. Accuracy. *Earthquake Spectra.* 27 (4): 1187-1202;

Yazgan, U. and Dazio, A. (2011b). Simulating maximum and residual displacements of RC structures: II. Sensitivity. *Earthquake Spectra.* 27 (4): 1203-1218;

Youssef, M.A., Ghaffarzadeh, H. and Nehdi, M. (2007). Seismic performance of RC frames with concentric internal steel bracing. *Engineering Structures,* 29 (7): 1561-1568;

Z

Zeris, C.A. and Mahin, S.A. (1988). Analysis of reinforced concrete beam-columns under uniaxial excitation. *Journal of Structural Engineering,* 114 (4): 804-820;

Zhao, B. and Taucer, F. (2010). Performance of infrastructure during the May 12, 2008 Wenchuan earthquake in China. *Journal of Earthquake Engineering*, 14 (4): 578-600;

WEB REFERENCES

COMPASS construction cost estimating data publications: https://compassinternational.net/

EPOS-IP research project: http://segal.ubi.pt/epos-ip/

EPOS-SP research project: https://www.epos-eu.org/projects/epos-sp

European Design Codes: https://eurocodes.jrc.ec.europa.eu/

European Seismic Risk Model (ESRM20): http://risk.efehr.org/

ESRM20 maps: https://maps.eu-risk.eucentre.it/

Global Earthquake Model (GEM): https://www.globalquakemodel.org/

OpenQuake: https://platform.openquake.org/

Portuguese Census Survey (2011 and 2021): https://censos.ine.pt/

QGIS: https://www.qgis.org/

RISE research project: http://www.rise-eu.org/

SeismoStruct: https://seismosoft.com/products/seismostruct/

SERA research project: http://www.sera-eu.org/

U.PORTO

FEUP FACULDADE DE ENGENHARIA
UNIVERSIDADE DO PORTO

SEISMIC RISK REDUCTION OF REINFORCED CONCRETE BUILDINGS RETROFITTED WITH STEEL BRACES

RODRIGO ESMERIZ FALCÃO MOREIRA

A thesis submitted to the Faculty of Engineering of the University of Porto, in partial fulfilment of the requirements for the degree of Doctor of Philosophy in Earthquake and Structural Engineering.

APPENDICES

DOCTORAL PROGRAM IN CIVIL ENGINEERING, 2022

FACULTY OF ENGINEERING, UNIVERSITY OF PORTO

Ph.D. Thesis – Doctoral Program in Civil Engineering (PRODEC)

© Rodrigo Esmeriz Falcão Moreira & FEUP, 2022

APPENDIX 1

PRE-CODE RC BUILDINGS – DESIGN DRAWINGS

APPENDIX 1 – PRE-CODE RC BUILDINGS – DESIGN DRAWINGS

BUILDING TYPE 1: 2 storeys, 3×5 spans

Geometry

Details

BUILDING TYPE 2: 3 storeys, 3×5 spans

Id

BUILDING TYPE 3: 4 storeys, 3×5 spans

Id

BUILDING TYPE 4: 5 storeys, 3×5 spans

Id

BUILDING TYPE 5: 6 storeys, 3×5 spans

Id

BUILDING TYPE 6: 2 storeys, 2×4 spans

Id

BUILDING TYPE 7: 3 storeys, 2×4 spans

Id

BUILDING TYPE 8: 4 storeys, 2×4 spans

Id

BUILDING TYPE 9: 5 storeys, 2×4 spans

Id

BUILDING TYPE 10: 6 storeys, 2×4 spans

Id

CONCRETE: fcm = 23.8 MPa
STEEL: fym = 440 MPa
CONCRETE COVER: c = 25 mm

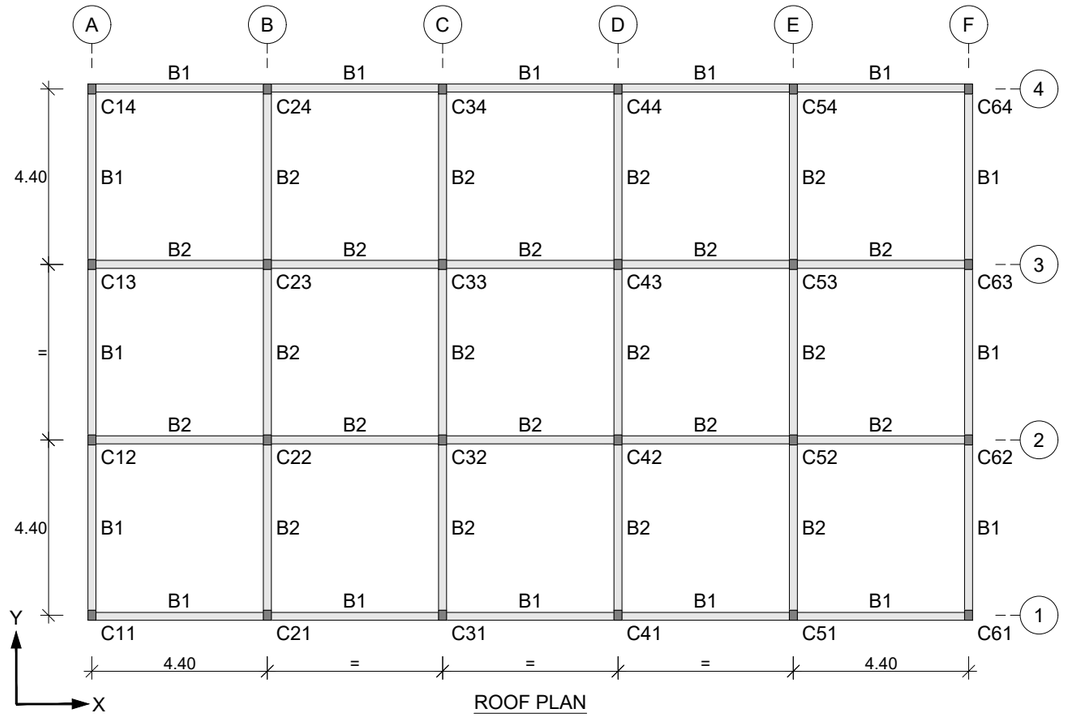

ROOF PLAN

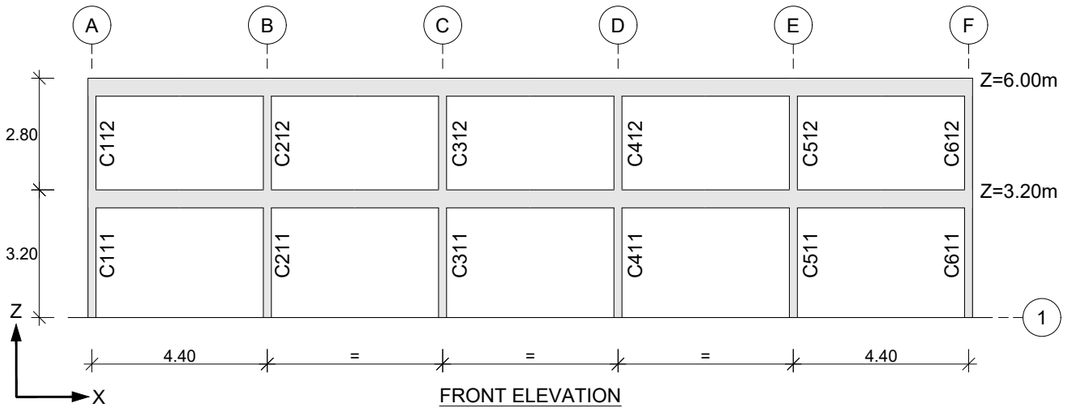

FRONT ELEVATION

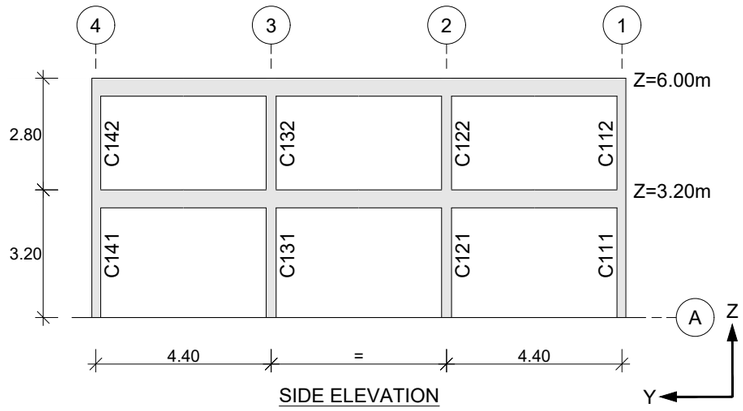

SIDE ELEVATION

2S_3x5	APPENDIX 1
GEOMETRY	A1.1

CONCRETE: fcm = 23.8 MPa
STEEL: fym = 440 MPa
CONCRETE COVER: c = 25 mm

COLUMNS SCHEDULE

	C11 / C61 / C14 / C64	C21 / C31 / C41 / C51 / C12 / C62 / C13 / C63 / C24 / C34 / C44 / C54	C22 / C32 / C42 / C52 / C23 / C33 / C43 / C53
2nd Floor	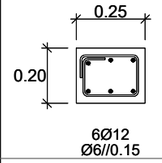	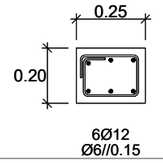	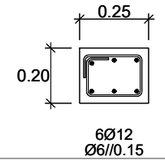
1st Floor	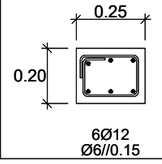	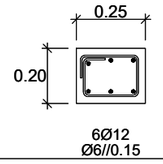	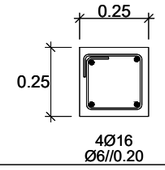
Ground Floor			

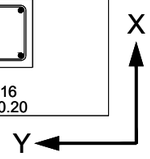

BEAM B1

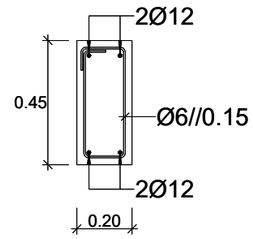

Span and Supports

BEAM B2

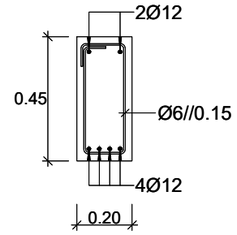

Span

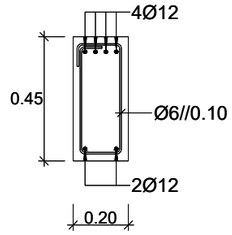

Supports

2S_3x5	APPENDIX 1
DETAILS	A1.2

CONCRETE: fcm = 23.8 MPa
STEEL: fym = 440 MPa
CONCRETE COVER: c = 25 mm

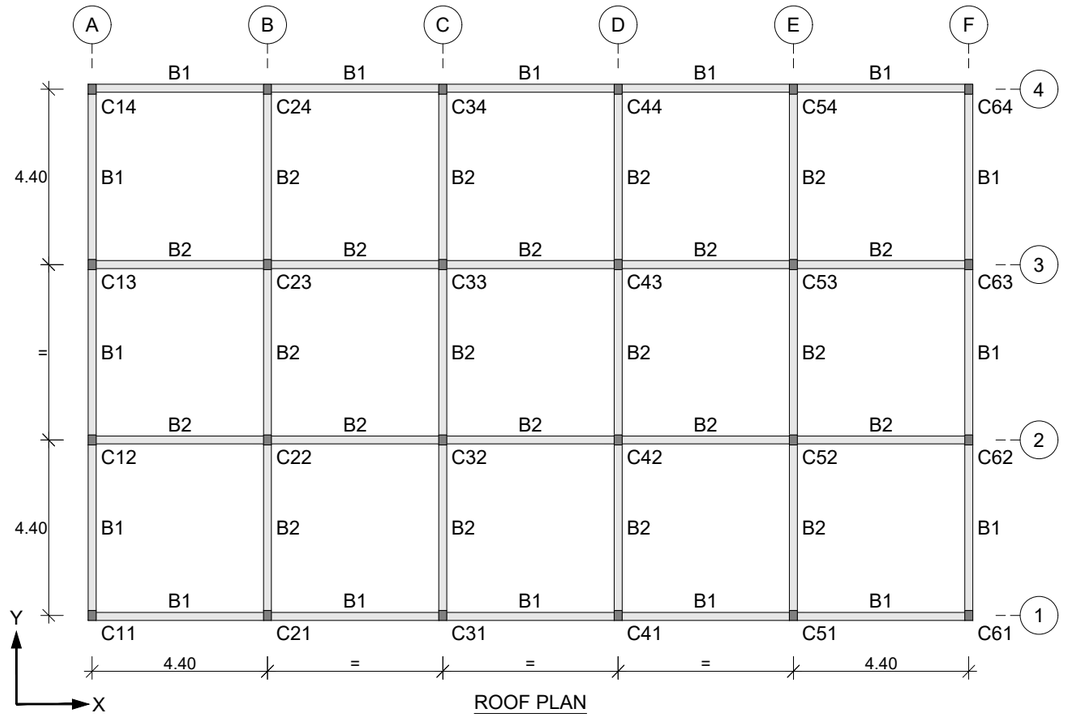

ROOF PLAN

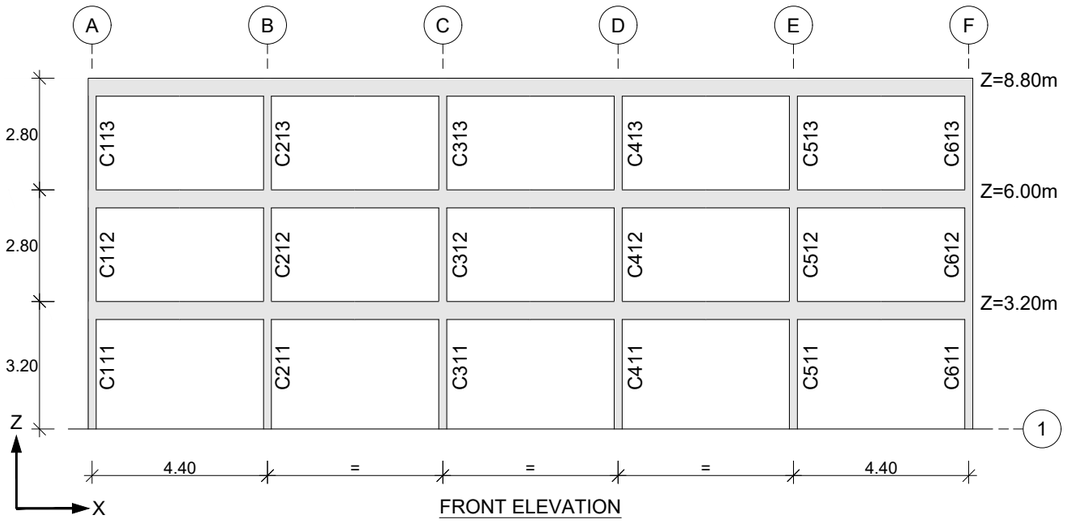

FRONT ELEVATION

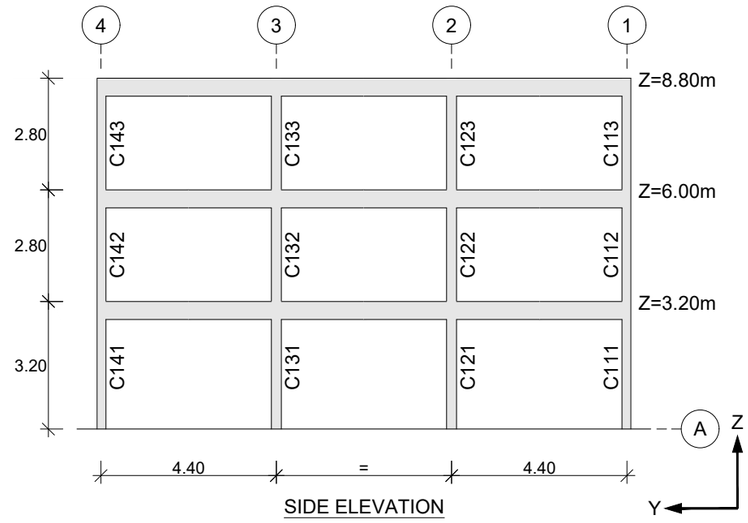

SIDE ELEVATION

3S_3x5	APPENDIX 1
GEOMETRY	A1.3

CONCRETE: fcm = 23.8 MPa
STEEL: fym = 440 MPa
CONCRETE COVER: c = 25 mm

COLUMNS SCHEDULE

	C11 / C61 / C14 / C64	C21 / C31 / C41 / C51 / C12 / C62 / C13 / C63 / C24 / C34 / C44 / C54	C22 / C32 / C42 / C52 / C23 / C33 / C43 / C53
3rd Floor	0.25 / 0.20 — 6Ø12 Ø6//0.15	0.25 / 0.20 — 6Ø12 Ø6//0.15	0.25 / 0.20 — 6Ø12 Ø6//0.15
2nd Floor	0.25 / 0.20 — 6Ø12 Ø6//0.15	0.25 / 0.20 — 6Ø12 Ø6//0.15	0.25 / 0.25 — 4Ø16 Ø6//0.20
1st Floor	0.25 / 0.20 — 6Ø12 Ø6//0.15	0.25 / 0.20 — 6Ø12 Ø6//0.15	0.30 / 0.30 — 8Ø16 Ø6//0.20
Ground Floor			

X
Y

BEAM B1

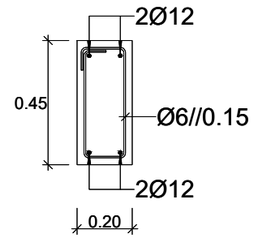

Span and Supports

BEAM B2

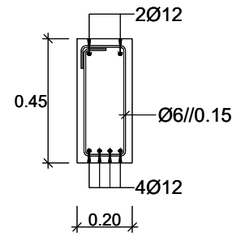

Span

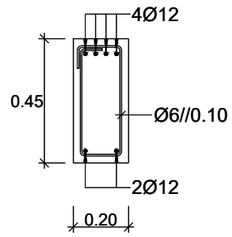

Supports

3S_3x5	APPENDIX 1
DETAILS	A1.4

CONCRETE: fcm = 23.8 MPa
STEEL: fym = 440 MPa
CONCRETE COVER: c = 25 mm

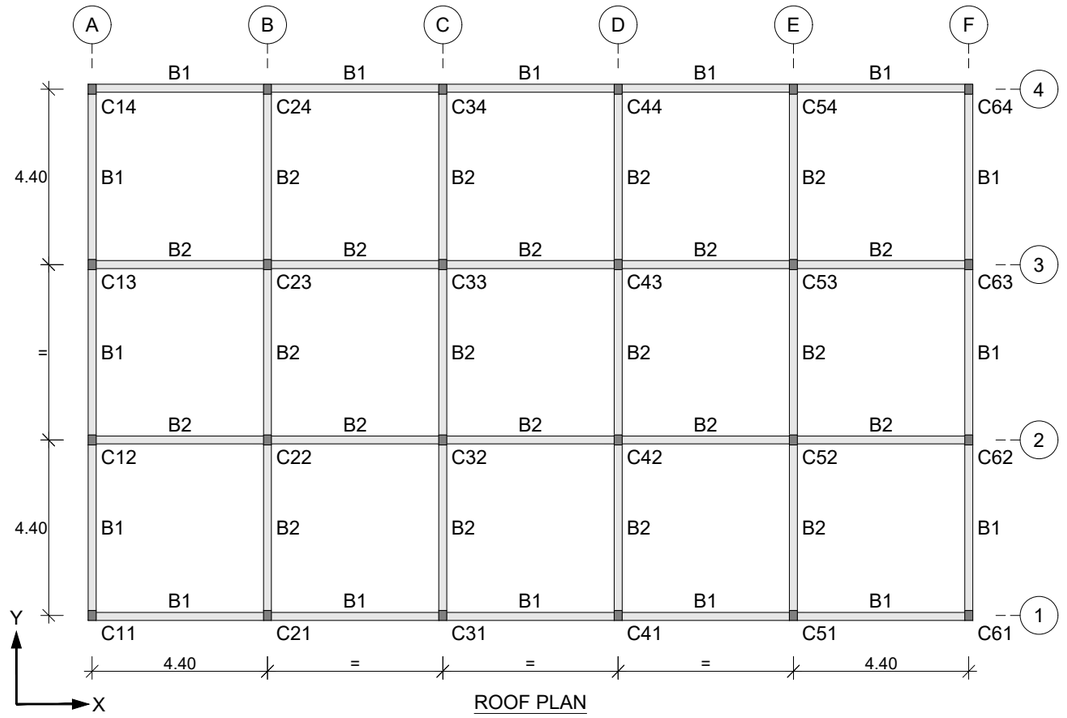

ROOF PLAN

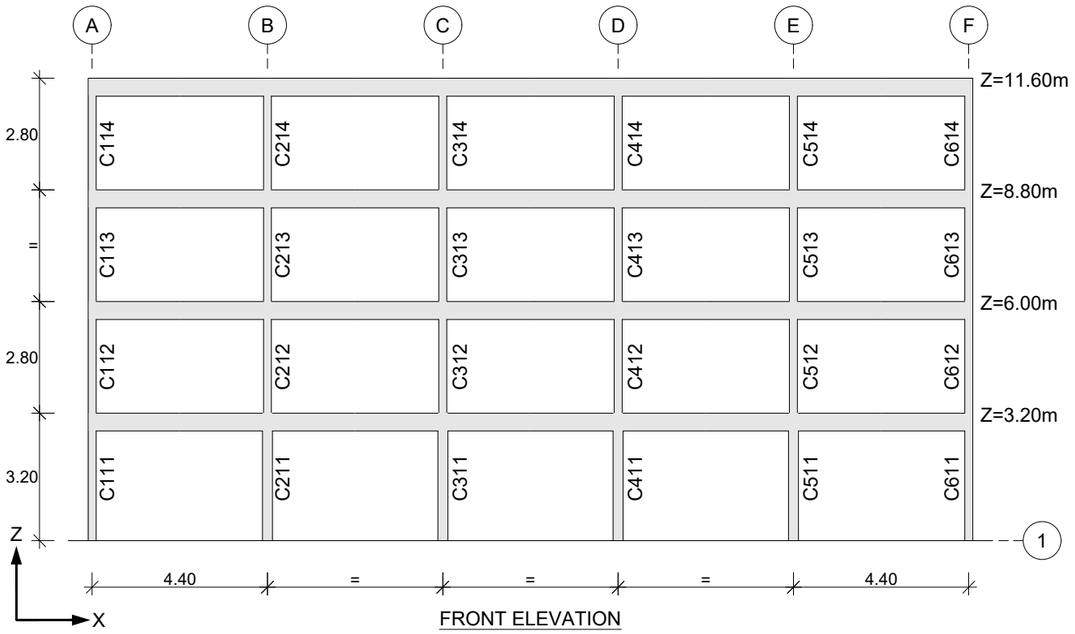

FRONT ELEVATION

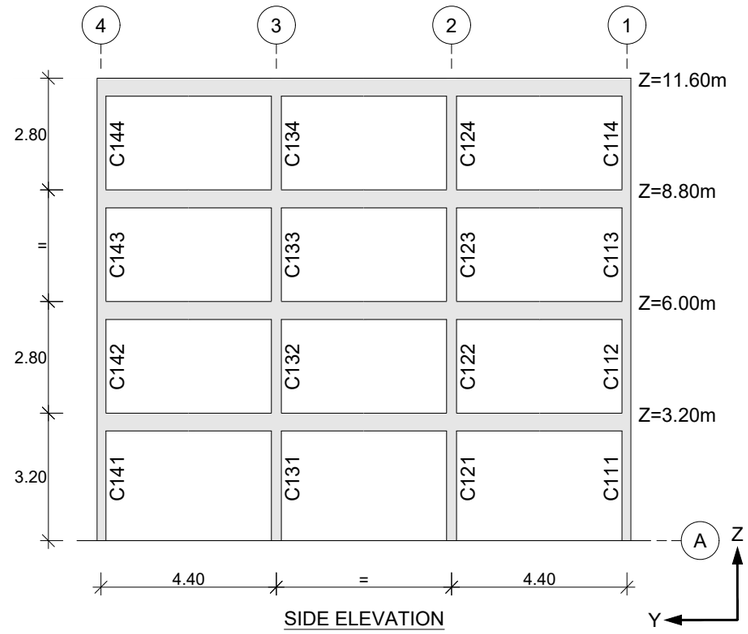

SIDE ELEVATION

4S_3x5	APPENDIX 1
GEOMETRY	A1.5

CONCRETE: fcm = 23.8 MPa
STEEL: fym = 440 MPa
CONCRETE COVER: c = 25 mm

COLUMNS SCHEDULE

	C11 / C61 / C14 / C64	C21 / C31 / C41 / C51 / C12 / C62 / C13 / C63 / C24 / C34 / C44 / C54	C22 / C32 / C42 / C52 / C23 / C33 / C43 / C53
4th Floor	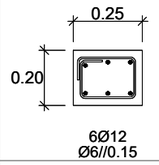	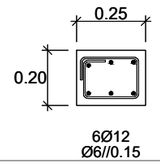	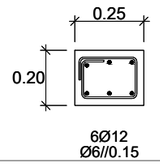
3rd Floor	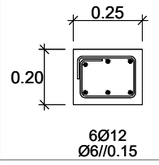	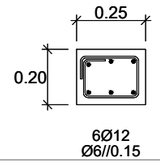	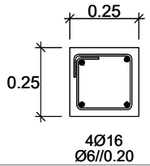
2nd Floor	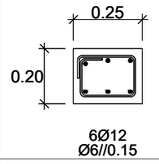	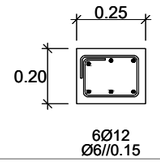	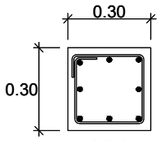
1st Floor	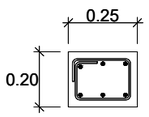	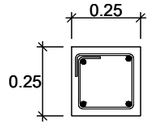	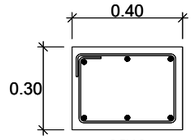
Ground Floor			

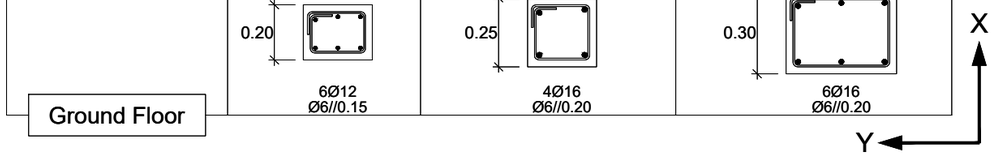

BEAM B1

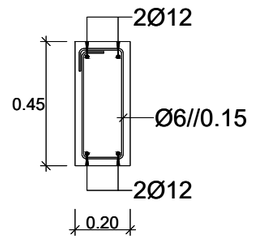

Span and Supports

BEAM B2

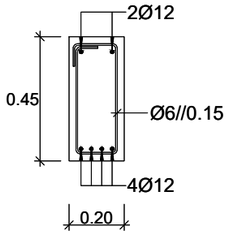

Span

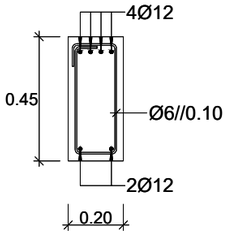

Supports

4S_3x5	APPENDIX 1
DETAILS	A1.6

CONCRETE: fcm = 23.8 MPa
STEEL: fym = 440 MPa
CONCRETE COVER: c = 25 mm

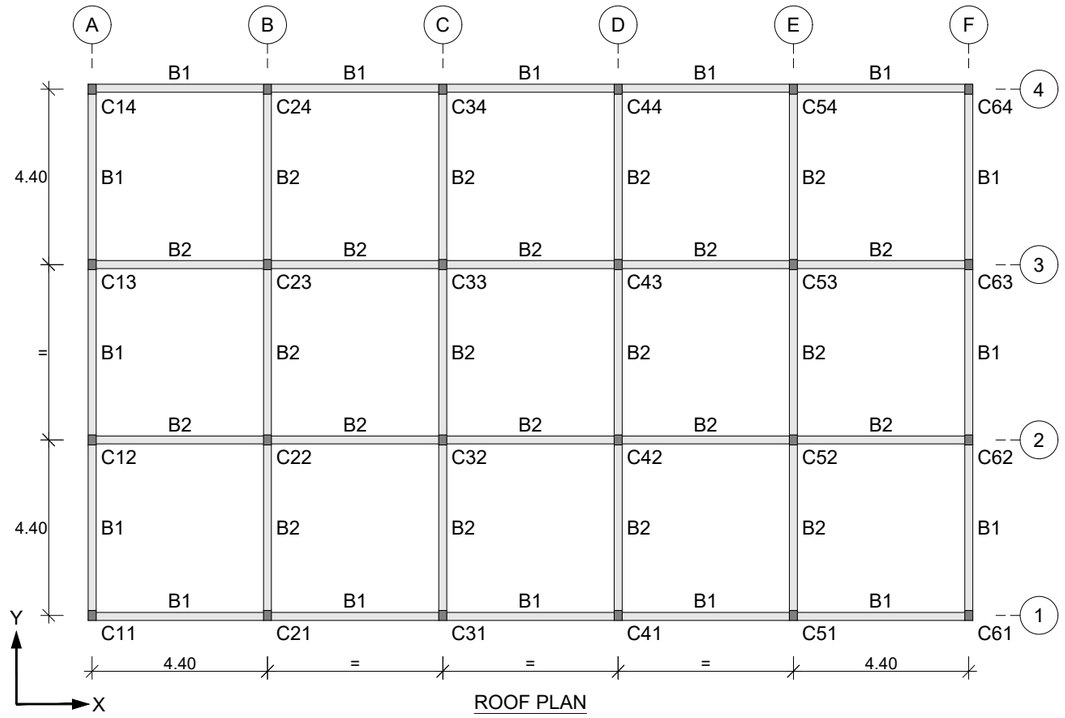

ROOF PLAN

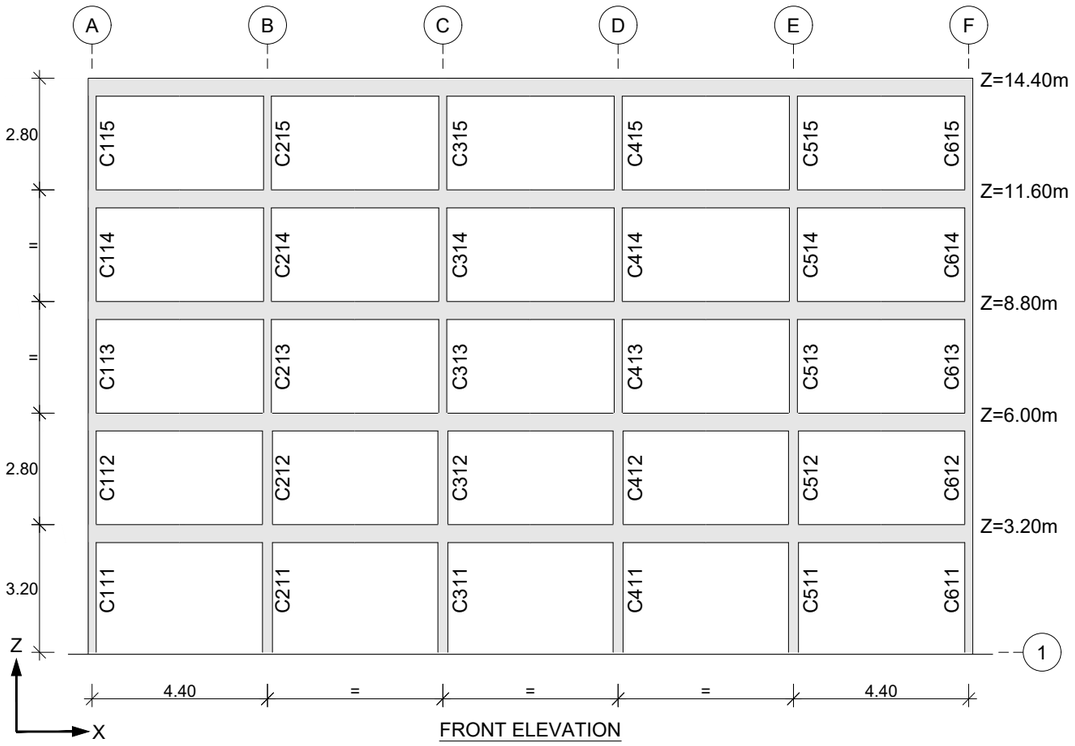

FRONT ELEVATION

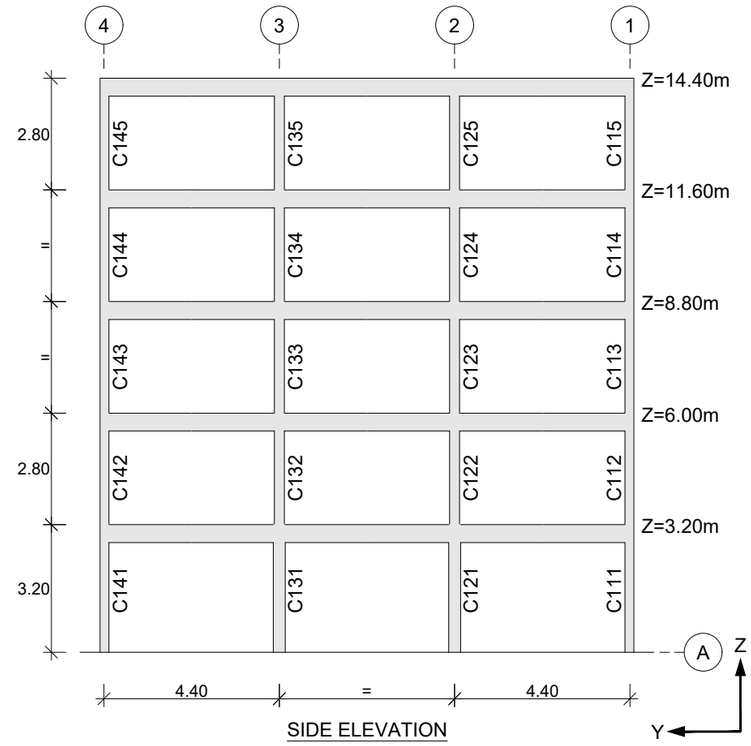

SIDE ELEVATION

5S_3x5	APPENDIX 1
GEOMETRY	A1.7

CONCRETE: fcm = 23.8 MPa
STEEL: fym = 440 MPa
CONCRETE COVER: c = 25 mm

COLUMNS SCHEDULE

	C11 / C61 / C14 / C64	C21 / C31 / C41 / C51 / C12 / C62 / C13 / C63 / C24 / C34 / C44 / C54	C22 / C32 / C42 / C52 / C23 / C33 / C43 / C53
5th Floor	0.25 × 0.20 6Ø12 Ø6//0.15	0.25 × 0.20 6Ø12 Ø6//0.15	0.25 × 0.20 6Ø12 Ø6//0.15
4th Floor	0.25 × 0.20 6Ø12 Ø6//0.15	0.25 × 0.20 6Ø12 Ø6//0.15	0.25 × 0.25 4Ø16 Ø6//0.20
3rd Floor	0.25 × 0.20 6Ø12 Ø6//0.15	0.25 × 0.20 6Ø12 Ø6//0.15	0.30 × 0.30 8Ø16 Ø6//0.20
2nd Floor	0.25 × 0.20 6Ø12 Ø6//0.15	0.25 × 0.25 4Ø16 Ø6//0.20	0.40 × 0.30 6Ø16 Ø6//0.20
1st Floor	0.25 × 0.20 6Ø12 Ø6//0.15	0.30 × 0.25 4Ø16 Ø6//0.20	0.50 × 0.30 8Ø16 Ø6//0.20
Ground Floor			

X
Y

BEAM B1

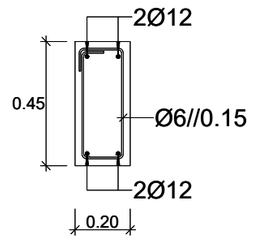

Span and Supports

BEAM B2

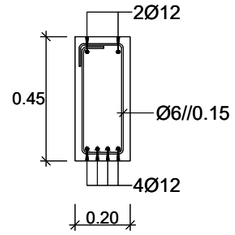

Span

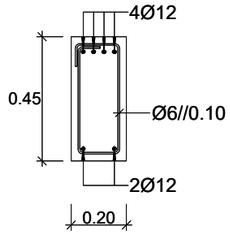

Supports

5S_3x5	APPENDIX 1
DETAILS	A1.8

CONCRETE: fcm = 23.8 MPa
STEEL: fym = 440 MPa
CONCRETE COVER: c = 25 mm

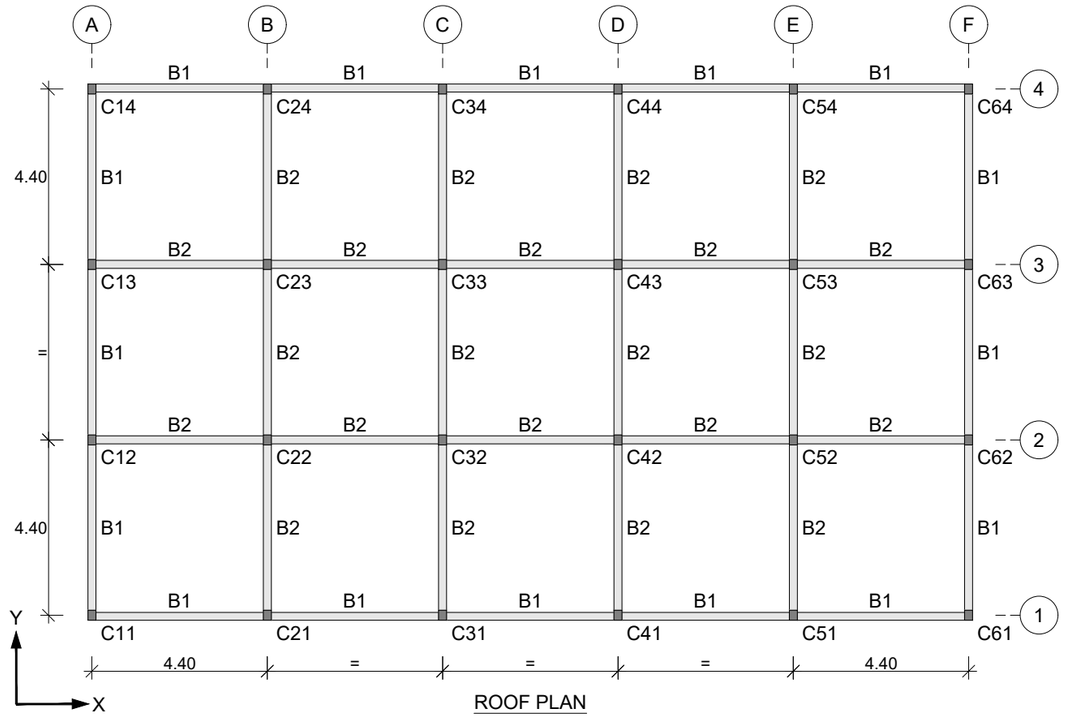

ROOF PLAN

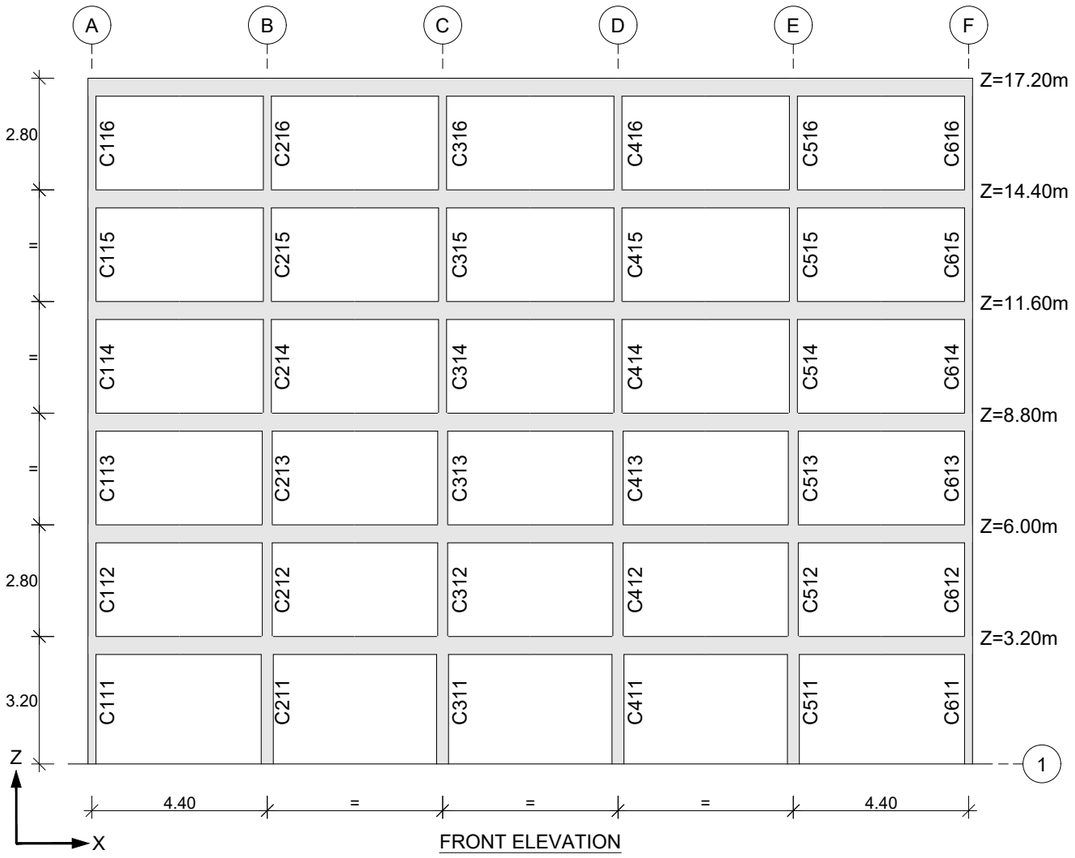

FRONT ELEVATION

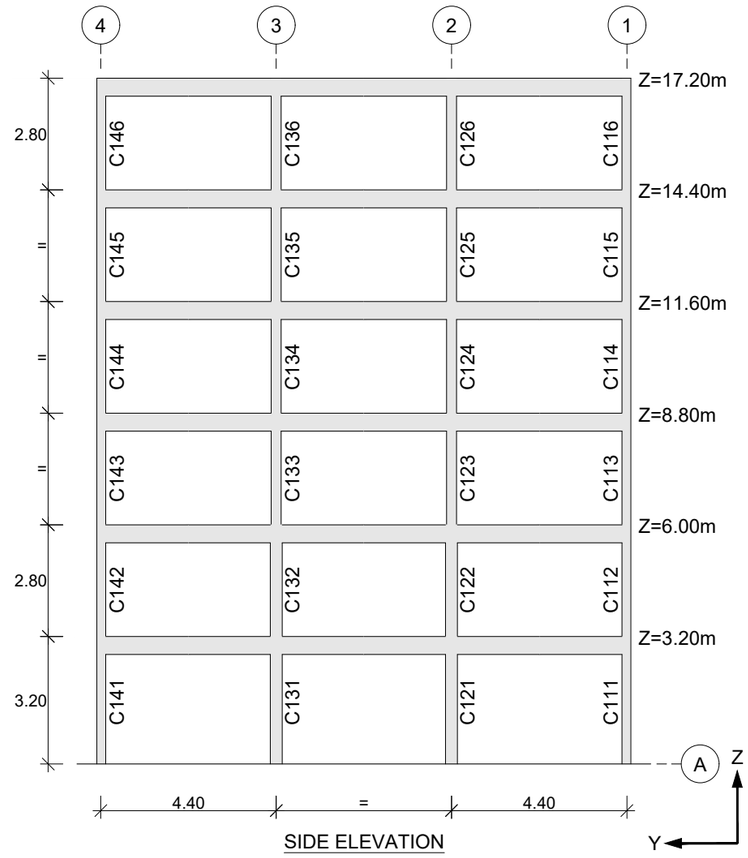

SIDE ELEVATION

6S_3x5	APPENDIX 1
GEOMETRY	A1.9

CONCRETE: fcm = 23.8 MPa
STEEL: fym = 440 MPa
CONCRETE COVER: c = 25 mm

COLUMNS SCHEDULE

	C11 / C61 / C14 / C64	C21 / C31 / C41 / C51 / C12 / C62 / C13 / C63 / C24 / C34 / C44 / C54	C22 / C32 / C42 / C52 / C23 / C33 / C43 / C53
6th Floor	0.25 × 0.20 — 6Ø12 Ø6//0.15	0.25 × 0.20 — 6Ø12 Ø6//0.15	0.25 × 0.20 — 6Ø12 Ø6//0.15
5th Floor	0.25 × 0.20 — 6Ø12 Ø6//0.15	0.25 × 0.20 — 6Ø12 Ø6//0.15	0.25 × 0.25 — 4Ø16 Ø6//0.20
4th Floor	0.25 × 0.20 — 6Ø12 Ø6//0.15	0.25 × 0.20 — 6Ø12 Ø6//0.15	0.30 × 0.30 — 8Ø16 Ø6//0.20
3rd Floor	0.25 × 0.20 — 6Ø12 Ø6//0.15	0.25 × 0.25 — 4Ø16 Ø6//0.20	0.40 × 0.30 — 6Ø16 Ø6//0.20
2nd Floor	0.25 × 0.20 — 6Ø12 Ø6//0.15	0.30 × 0.25 — 4Ø16 Ø6//0.20	0.50 × 0.30 — 8Ø16 Ø6//0.20
1st Floor	0.25 × 0.20 — 6Ø12 Ø6//0.15	0.30 × 0.30 — 8Ø16 Ø6//0.20	0.60 × 0.30 — 6Ø20 Ø6//0.25
Ground Floor			

X
Y

BEAM B1

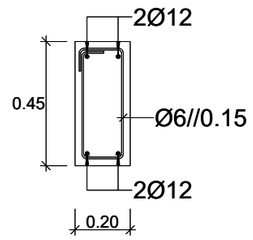

Span and Supports

BEAM B2

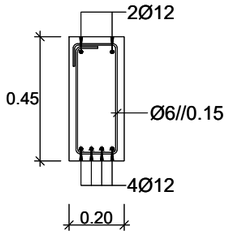

Span

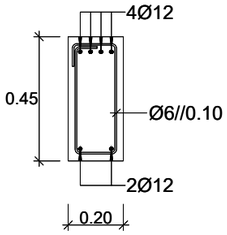

Supports

6S_3x5	APPENDIX 1
DETAILS	A1.10

CONCRETE: fcm = 23.8 MPa
STEEL: fym = 440 MPa
CONCRETE COVER: c = 25 mm

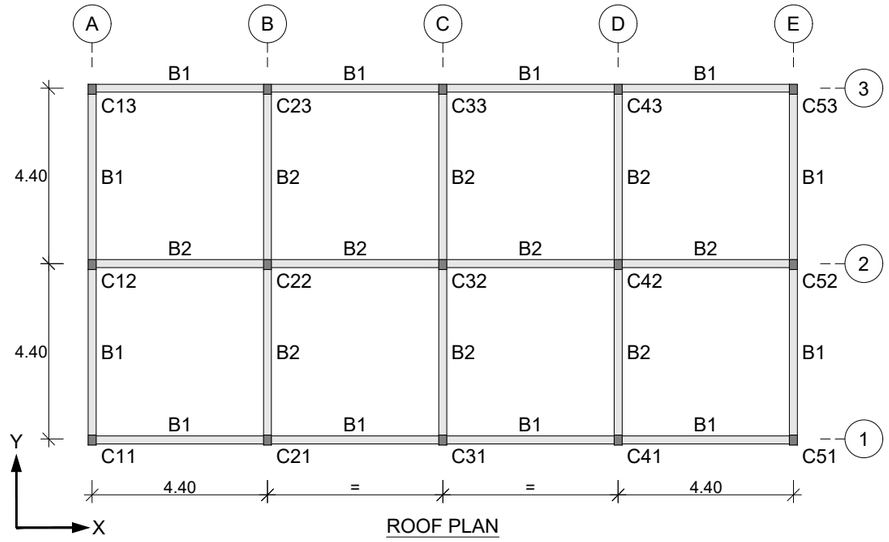

ROOF PLAN

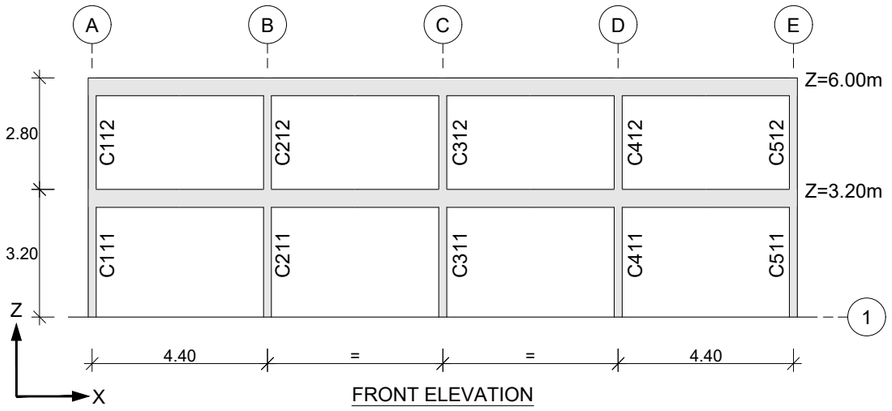

FRONT ELEVATION

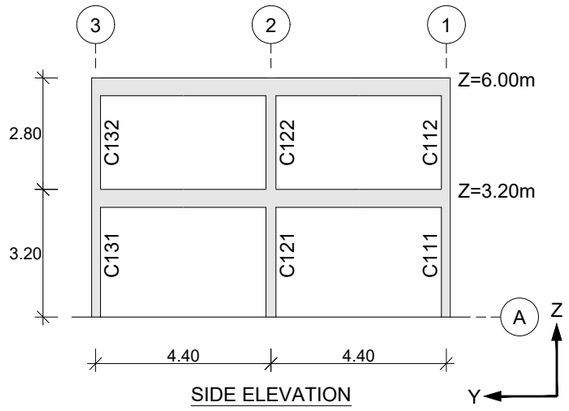

SIDE ELEVATION

2S_2x4	APPENDIX 1
GEOMETRY	A1.11

CONCRETE: fcm = 23.8 MPa
STEEL: fym = 440 MPa
CONCRETE COVER: c = 25 mm

COLUMNS SCHEDULE

	C11 / C13 / C51 / C53	C21 / C31 / C41 / C12 / C52 / C23 / C33 / C43	C22 / C32 / C42
2nd Floor	0.25 × 0.20 — 6Ø12 Ø6//0.15	0.25 × 0.20 — 6Ø12 Ø6//0.15	0.25 × 0.20 — 6Ø12 Ø6//0.15
1st Floor	0.25 × 0.20 — 6Ø12 Ø6//0.15	0.25 × 0.20 — 6Ø12 Ø6//0.15	0.25 × 0.25 — 4Ø16 Ø6//0.20
Ground Floor			

X
Y

BEAM B1

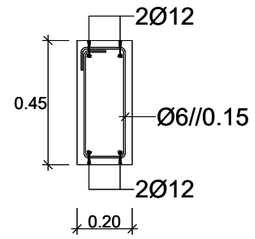

Span and Supports

BEAM B2

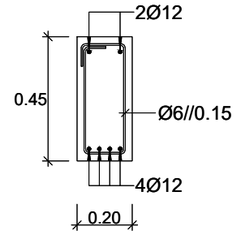

Span

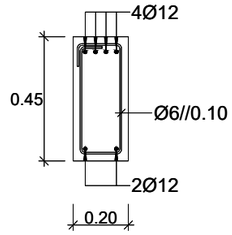

Supports

2S_2x4	APPENDIX 1
DETAILS	A1.12

CONCRETE: fcm = 23.8 MPa
STEEL: fym = 440 MPa
CONCRETE COVER: c = 25 mm

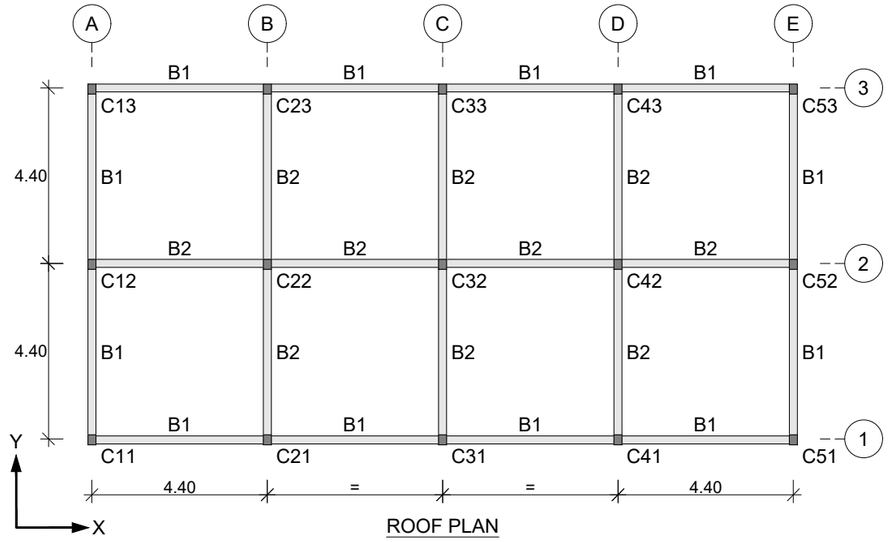

ROOF PLAN

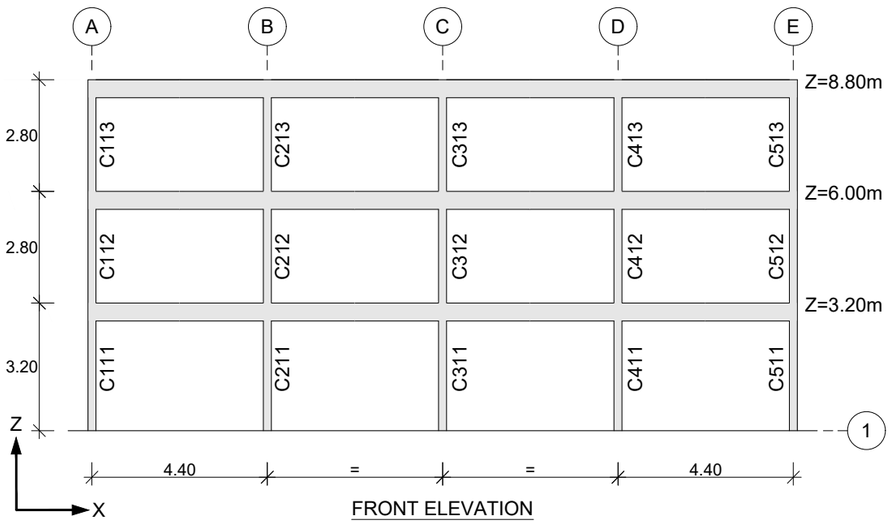

FRONT ELEVATION

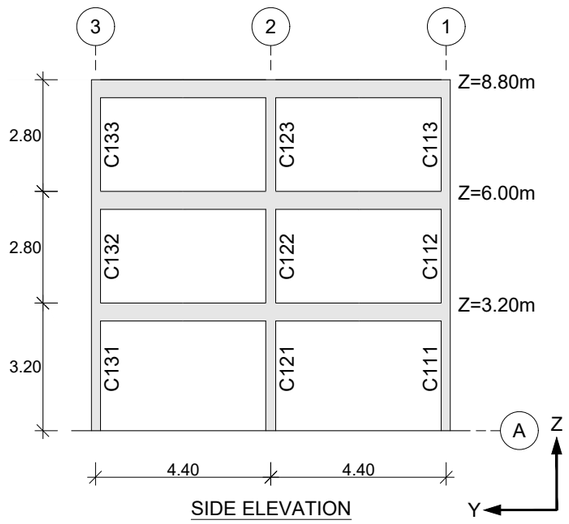

SIDE ELEVATION

3S_2x4	APPENDIX 1
GEOMETRY	A1.13

CONCRETE: fcm = 23.8 MPa
STEEL: fym = 440 MPa
CONCRETE COVER: c = 25 mm

COLUMNS SCHEDULE

	C11 / C13 / C51 / C53	C21 / C31 / C41 / C12 / C52 / C23 / C33 / C43	C22 / C32 / C42
3rd Floor	0.25 × 0.20 — 6Ø12 Ø6//0.15	0.25 × 0.20 — 6Ø12 Ø6//0.15	0.25 × 0.20 — 6Ø12 Ø6//0.15
2nd Floor	0.25 × 0.20 — 6Ø12 Ø6//0.15	0.25 × 0.20 — 6Ø12 Ø6//0.15	0.25 × 0.25 — 4Ø16 Ø6//0.20
1st Floor	0.25 × 0.20 — 6Ø12 Ø6//0.15	0.25 × 0.20 — 6Ø12 Ø6//0.15	0.30 × 0.30 — 8Ø16 Ø6//0.20
Ground Floor			

X
Y

BEAM B1

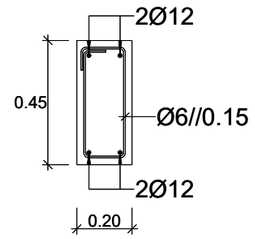

Span and Supports

BEAM B2

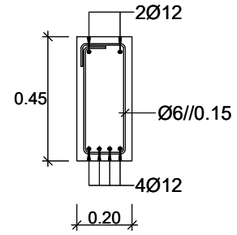

Span

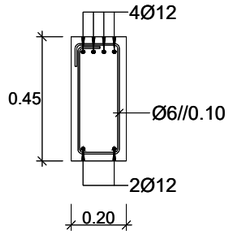

Supports

3S_2x4	APPENDIX 1
DETAILS	A1.14

CONCRETE: fcm = 23.8 MPa
STEEL: fym = 440 MPa
CONCRETE COVER: c = 25 mm

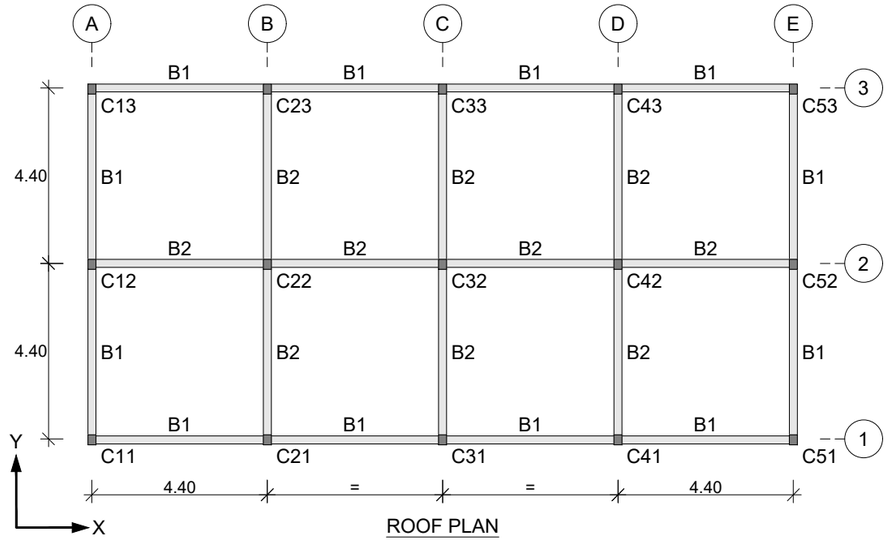

ROOF PLAN

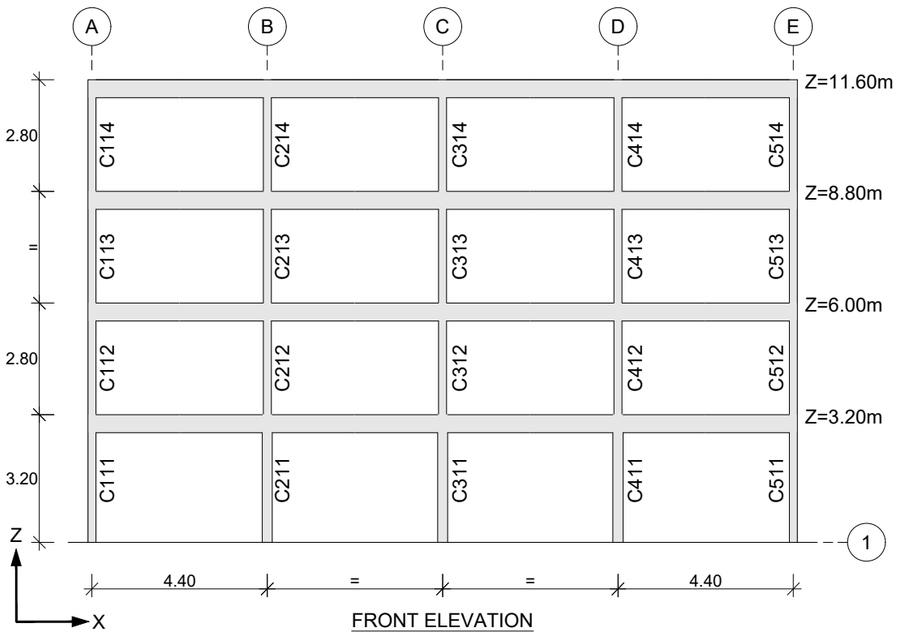

FRONT ELEVATION

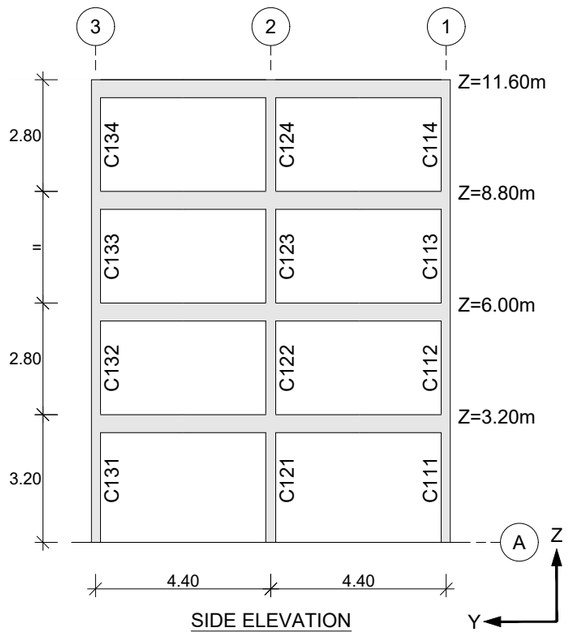

SIDE ELEVATION

4S_2x4	APPENDIX 1
GEOMETRY	A1.15

CONCRETE: fcm = 23.8 MPa
STEEL: fym = 440 MPa
CONCRETE COVER: c = 25 mm

COLUMNS SCHEDULE

	C11 / C13 / C51 / C53	C21 / C31 / C41 / C12 / C52 / C23 / C33 / C43	C22 / C32 / C42
4th Floor	0.25 × 0.20 — 6Ø12 Ø6//0.15	0.25 × 0.20 — 6Ø12 Ø6//0.15	0.25 × 0.20 — 6Ø12 Ø6//0.15
3rd Floor	0.25 × 0.20 — 6Ø12 Ø6//0.15	0.25 × 0.20 — 6Ø12 Ø6//0.15	0.25 × 0.25 — 4Ø16 Ø6//0.20
2nd Floor	0.25 × 0.20 — 6Ø12 Ø6//0.15	0.25 × 0.20 — 6Ø12 Ø6//0.15	0.30 × 0.30 — 8Ø16 Ø6//0.20
1st Floor	0.25 × 0.20 — 6Ø12 Ø6//0.15	0.25 × 0.25 — 4Ø16 Ø6//0.20	0.40 × 0.30 — 6Ø16 Ø6//0.20
Ground Floor			

X
Y

BEAM B1

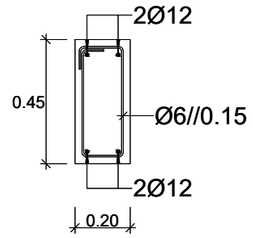

Span and Supports

BEAM B2

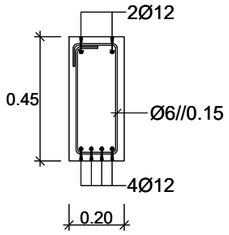

Span

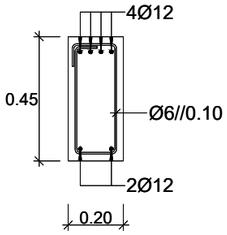

Supports

4S_2x4	APPENDIX 1
DETAILS	A1.16

CONCRETE: fcm = 23.8 MPa
STEEL: fym = 440 MPa
CONCRETE COVER: c = 25 mm

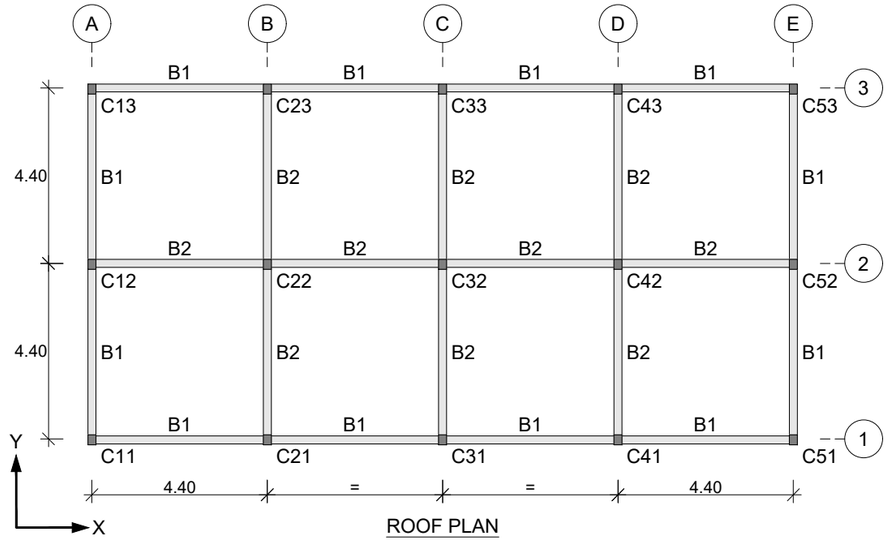

ROOF PLAN

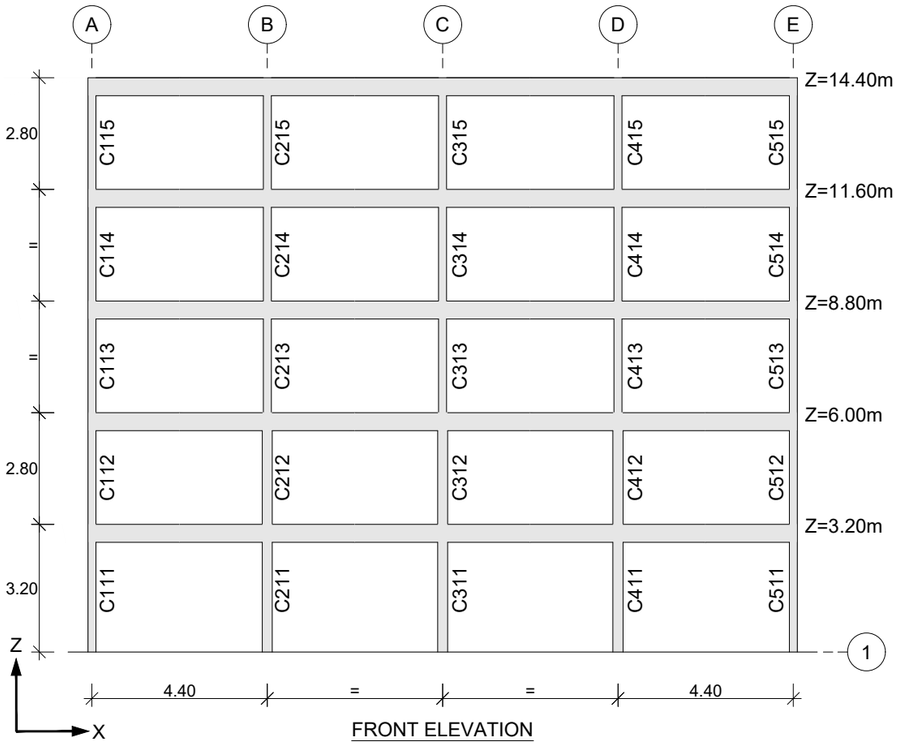

FRONT ELEVATION

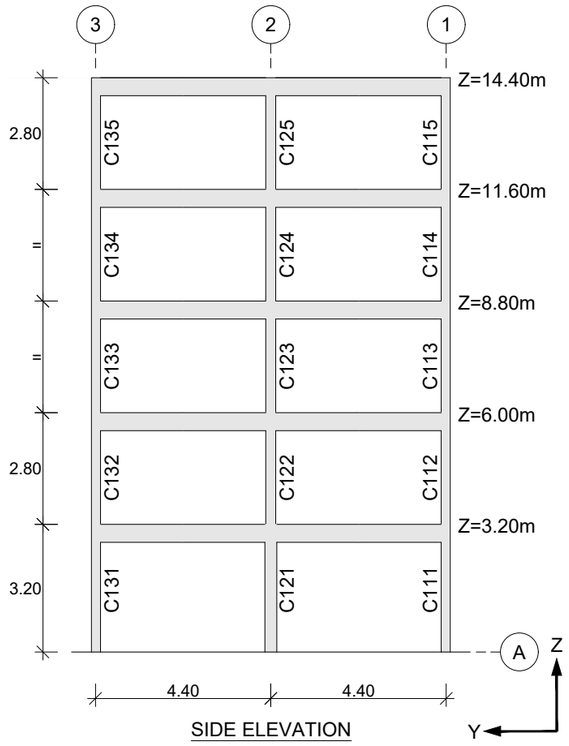

SIDE ELEVATION

5S_2x4	APPENDIX 1
GEOMETRY	A1.17

CONCRETE: fcm = 23.8 MPa
STEEL: fym = 440 MPa
CONCRETE COVER: c = 25 mm

COLUMNS SCHEDULE

	C11 / C13 / C51 / C53	C21 / C31 / C41 / C12 / C52 / C23 / C33 / C43	C22 / C32 / C42
5th Floor	0.25 × 0.20 6Ø12 Ø6//0.15	0.25 × 0.20 6Ø12 Ø6//0.15	0.25 × 0.20 6Ø12 Ø6//0.15
4th Floor	0.25 × 0.20 6Ø12 Ø6//0.15	0.25 × 0.20 6Ø12 Ø6//0.15	0.25 × 0.25 4Ø16 Ø6//0.20
3rd Floor	0.25 × 0.20 6Ø12 Ø6//0.15	0.25 × 0.20 6Ø12 Ø6//0.15	0.30 × 0.30 8Ø16 Ø6//0.20
2nd Floor	0.25 × 0.20 6Ø12 Ø6//0.15	0.25 × 0.25 4Ø16 Ø6//0.20	0.40 × 0.30 6Ø16 Ø6//0.20
1st Floor	0.25 × 0.20 6Ø12 Ø6//0.15	0.30 × 0.25 4Ø16 Ø6//0.20	0.50 × 0.30 8Ø16 Ø6//0.20
Ground Floor			

X
Y

BEAM B1

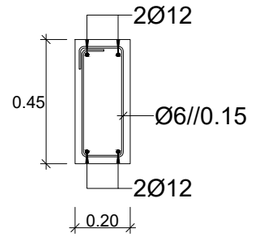

Span and Supports

BEAM B2

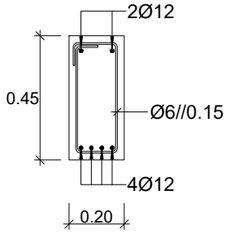

Span

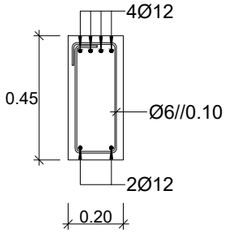

Supports

5S_2x4	APPENDIX 1
DETAILS	A1.18

CONCRETE: fcm = 23.8 MPa
STEEL: fym = 440 MPa
CONCRETE COVER: c = 25 mm

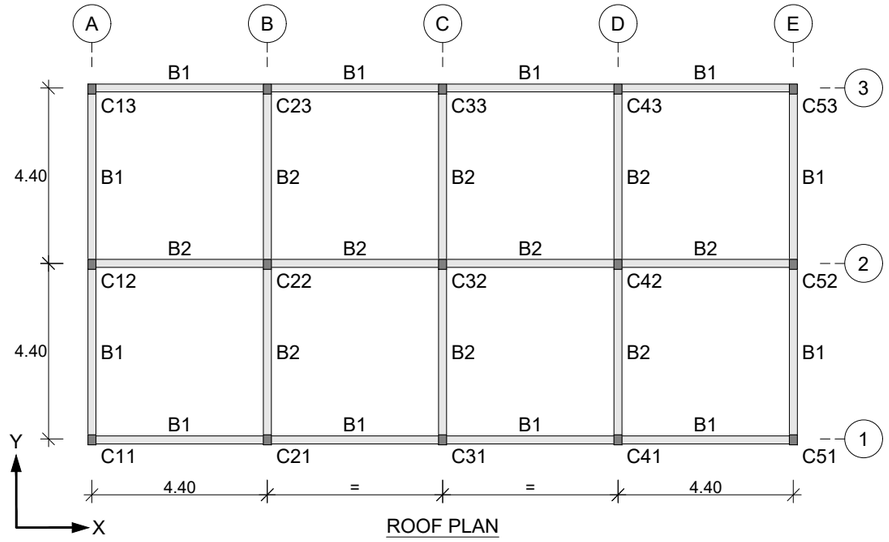

ROOF PLAN

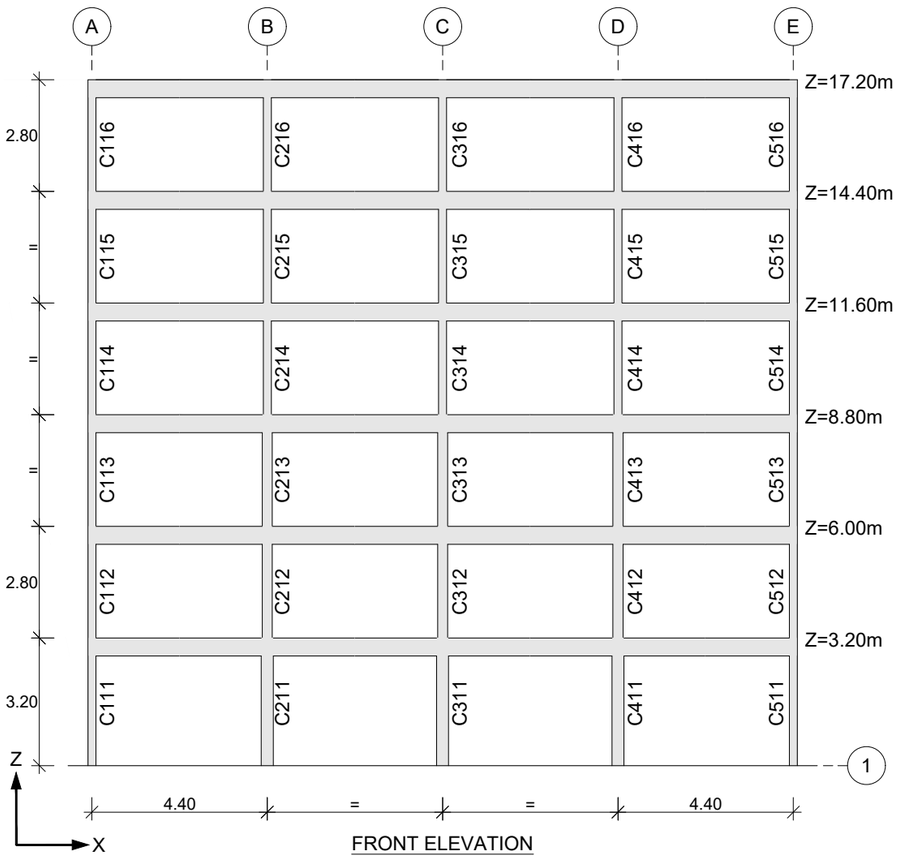

FRONT ELEVATION

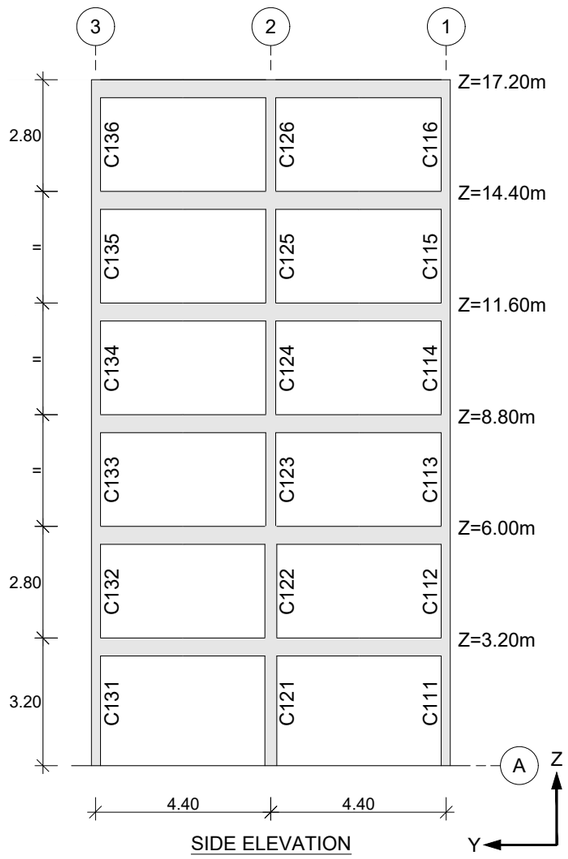

SIDE ELEVATION

6S_2x4	APPENDIX 1
GEOMETRY	A1.19

CONCRETE: fcm = 23.8 MPa
STEEL: fym = 440 MPa
CONCRETE COVER: c = 25 mm

COLUMNS SCHEDULE

	C11 / C13 / C51 / C53	C21 / C31 / C41 / C12 / C52 / C23 / C33 / C43	C22 / C32 / C42
6th Floor	0.25 × 0.20 6Ø12 Ø6//0.15	0.25 × 0.20 6Ø12 Ø6//0.15	0.25 × 0.20 6Ø12 Ø6//0.15
5th Floor	0.25 × 0.20 6Ø12 Ø6//0.15	0.25 × 0.20 6Ø12 Ø6//0.15	0.25 × 0.25 4Ø16 Ø6//0.20
4th Floor	0.25 × 0.20 6Ø12 Ø6//0.15	0.25 × 0.20 6Ø12 Ø6//0.15	0.30 × 0.30 8Ø16 Ø6//0.20
3rd Floor	0.25 × 0.20 6Ø12 Ø6//0.15	0.25 × 0.25 4Ø16 Ø6//0.20	0.40 × 0.30 6Ø16 Ø6//0.20
2nd Floor	0.25 × 0.20 6Ø12 Ø6//0.15	0.30 × 0.25 4Ø16 Ø6//0.20	0.50 × 0.30 8Ø16 Ø6//0.20
1st Floor	0.25 × 0.20 6Ø12 Ø6//0.15	0.30 × 0.30 8Ø16 Ø6//0.20	0.60 × 0.30 6Ø20 Ø6//0.25
Ground Floor			

X
Y

BEAM B1

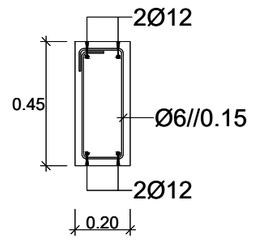

Span and Supports

BEAM B2

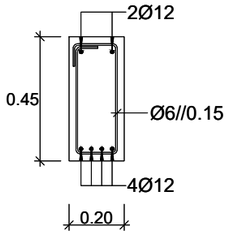

Span

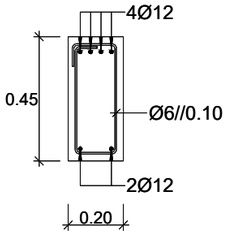

Supports

6S_2x4	APPENDIX 1
DETAILS	A1.20

APPENDIX 2

PRE-CODE RC BUILDINGS – MEMBER CAPACITIES

APPENDIX 2 – PRE-CODE RC BUILDINGS – MEMBER CAPACITIES

BUILDING TYPE 1: 2 storeys, 3×5 spans

Chord rotation capacities θ_{SD} of columns – Direction XX

Shear force capacities V_R of columns – Direction XX

Chord rotation capacities θ_{SD} of columns – Direction YY

Shear force capacities V_R of columns – Direction YY

BUILDING TYPE 2: 3 storeys, 3×5 spans

Id

BUILDING TYPE 3: 4 storeys, 3×5 spans

Id

BUILDING TYPE 4: 5 storeys, 3×5 spans

Id

BUILDING TYPE 5: 6 storeys, 3×5 spans

Id

BUILDING TYPE 6: 2 storeys, 2×4 spans

Id

BUILDING TYPE 7: 3 storeys, 2×4 spans

Id

BUILDING TYPE 8: 4 storeys, 2×4 spans

Id

BUILDING TYPE 9: 5 storeys, 2×4 spans

Id

BUILDING TYPE 10: 6 storeys, 2×4 spans

Id

AXIAL FORCE CAPACITY ENVELOPES

Columns on Building Types 1 to 10

BUILDING TYPE 1: 2 storeys, 3×5 spans

Table A2.1 – Chord rotation capacities θ_{SD} of columns, according to EC8-3 (2005) – Direction XX

Columns	$\boldsymbol{\theta_{SD}\ (rad)}$	
	Storey S1	**Storey S2**
C11	0.02465	0.02478
C21	0.02257	0.02371
C31	0.02257	0.02371
C41	0.02257	0.02371
C51	0.02257	0.02371
C61	0.02465	0.02478
C12	0.02257	0.02371
C22	0.01901	0.02189
C32	0.01901	0.02189
C42	0.01901	0.02189
C52	0.01901	0.02189
C62	0.02257	0.02371
C13	0.02257	0.02371
C23	0.01901	0.02189
C33	0.01901	0.02189
C43	0.01901	0.02189
C53	0.01901	0.02189
C63	0.02257	0.02371
C14	0.02465	0.02478
C24	0.02257	0.02371
C34	0.02257	0.02371
C44	0.02257	0.02371
C54	0.02257	0.02371
C64	0.02465	0.02478

Table A2.2 – Shear force capacities V_R of columns, according to EC8-3 (2005) – Direction XX

Columns	$\boldsymbol{V_R\ (kN)}$	
	Storey S1	**Storey S2**
C11	19.66	18.28
C21	22.37	19.82
C31	22.37	19.82
C41	22.37	19.82
C51	22.37	19.82
C61	19.66	18.28
C12	22.37	19.82
C22	31.29	22.64
C32	31.29	22.64
C42	31.29	22.64
C52	31.29	22.64
C62	22.37	19.82
C13	22.37	19.82
C23	31.29	22.64
C33	31.29	22.64
C43	31.29	22.64
C53	31.29	22.64
C63	22.37	19.82
C14	19.66	18.28
C24	22.37	19.82
C34	22.37	19.82
C44	22.37	19.82
C54	22.37	19.82
C64	19.66	18.28

Table A2.3 – Chord rotation capacities θ_{SD} of columns, according to EC8-3 (2005) – Direction YY

Columns	$\boldsymbol{\theta_{SD}}$ $\boldsymbol{(rad)}$	
	Storey S1	**Storey S2**
C11	0.02286	0.02298
C21	0.02094	0.02199
C31	0.02094	0.02199
C41	0.02094	0.02199
C51	0.02094	0.02199
C61	0.02286	0.02298
C12	0.02094	0.02199
C22	0.01901	0.02030
C32	0.01901	0.02030
C42	0.01901	0.02030
C52	0.01901	0.02030
C62	0.02094	0.02199
C13	0.02094	0.02199
C23	0.01901	0.02030
C33	0.01901	0.02030
C43	0.01901	0.02030
C53	0.01901	0.02030
C63	0.02094	0.02199
C14	0.02286	0.02298
C24	0.02094	0.02199
C34	0.02094	0.02199
C44	0.02094	0.02199
C54	0.02094	0.02199
C64	0.02286	0.02298

Table A2.4 – Shear force capacities V_R of columns, according to EC8-3 (2005) – Direction YY

Columns	$\boldsymbol{V_R}$ $\boldsymbol{(kN)}$	
	Storey S1	**Storey S2**
C11	25.26	23.53
C21	28.65	25.46
C31	28.65	25.46
C41	28.65	25.46
C51	28.65	25.46
C61	25.26	23.53
C12	28.65	25.46
C22	31.29	28.98
C32	31.29	28.98
C42	31.29	28.98
C52	31.29	28.98
C62	28.65	25.46
C13	28.65	25.46
C23	31.29	28.98
C33	31.29	28.98
C43	31.29	28.98
C53	31.29	28.98
C63	28.65	25.46
C14	25.26	23.53
C24	28.65	25.46
C34	28.65	25.46
C44	28.65	25.46
C54	28.65	25.46
C64	25.26	23.53

BUILDING TYPE 2: 3 storeys, 3×5 spans

Table A2.5 – Chord rotation capacities θ_{SD} of columns, according to EC8-3 (2005) – Direction XX

Columns	$\boldsymbol{\theta_{SD}\ (rad)}$		
	Storey S1	**Storey S2**	**Storey S3**
C11	0.02341	0.02352	0.02478
C21	0.02051	0.02154	0.02371
C31	0.02051	0.02154	0.02371
C41	0.02051	0.02154	0.02371
C51	0.02051	0.02154	0.02371
C61	0.02341	0.02352	0.02478
C12	0.02051	0.02154	0.02371
C22	0.01766	0.01814	0.02189
C32	0.01766	0.01814	0.02189
C42	0.01766	0.01814	0.02189
C52	0.01766	0.01814	0.02189
C62	0.02051	0.02154	0.02371
C13	0.02051	0.02154	0.02371
C23	0.01766	0.01814	0.02189
C33	0.01766	0.01814	0.02189
C43	0.01766	0.01814	0.02189
C53	0.01766	0.01814	0.02189
C63	0.02051	0.02154	0.02371
C14	0.02341	0.02352	0.02478
C24	0.02051	0.02154	0.02371
C34	0.02051	0.02154	0.02371
C44	0.02051	0.02154	0.02371
C54	0.02051	0.02154	0.02371
C64	0.02341	0.02352	0.02478

Table A2.6 – Shear force capacities V_R of columns, according to EC8-3 (2005) – Direction XX

Columns	$\boldsymbol{V_R\ (kN)}$		
	Storey S1	**Storey S2**	**Storey S3**
C11	21.25	20.10	18.28
C21	25.32	23.19	19.82
C31	25.32	23.19	19.82
C41	25.32	23.19	19.82
C51	25.32	23.19	19.82
C61	21.25	20.10	18.28
C12	25.32	23.19	19.82
C22	51.78	33.16	22.64
C32	51.78	33.16	22.64
C42	51.78	33.16	22.64
C52	51.78	33.16	22.64
C62	25.32	23.19	19.82
C13	25.32	23.19	19.82
C23	51.78	33.16	22.64
C33	51.78	33.16	22.64
C43	51.78	33.16	22.64
C53	51.78	33.16	22.64
C63	25.32	23.19	19.82
C14	21.25	20.10	18.28
C24	25.32	23.19	19.82
C34	25.32	23.19	19.82
C44	25.32	23.19	19.82
C54	25.32	23.19	19.82
C64	21.25	20.10	18.28

Table A2.7 – Chord rotation capacities θ_{SD} of columns, according to EC8-3 (2005) – Direction YY

Columns	$\boldsymbol{\theta_{SD}\ (rad)}$		
	Storey S1	**Storey S2**	**Storey S3**
C11	0.02171	0.02182	0.02298
C21	0.01902	0.01998	0.02199
C31	0.01902	0.01998	0.02199
C41	0.01902	0.01998	0.02199
C51	0.01902	0.01998	0.02199
C61	0.02171	0.02182	0.02298
C12	0.01902	0.01998	0.02199
C22	0.01766	0.01814	0.02030
C32	0.01766	0.01814	0.02030
C42	0.01766	0.01814	0.02030
C52	0.01766	0.01814	0.02030
C62	0.01902	0.01998	0.02199
C13	0.01902	0.01998	0.02199
C23	0.01766	0.01814	0.02030
C33	0.01766	0.01814	0.02030
C43	0.01766	0.01814	0.02030
C53	0.01766	0.01814	0.02030
C63	0.01902	0.01998	0.02199
C14	0.02171	0.02182	0.02298
C24	0.01902	0.01998	0.02199
C34	0.01902	0.01998	0.02199
C44	0.01902	0.01998	0.02199
C54	0.01902	0.01998	0.02199
C64	0.02171	0.02182	0.02298

Table A2.8 – Shear force capacities V_R of columns, according to EC8-3 (2005) – Direction YY

Columns	$\boldsymbol{V_R\ (kN)}$		
	Storey S1	**Storey S2**	**Storey S3**
C11	27.25	25.82	23.53
C21	32.34	29.67	25.46
C31	32.34	29.67	25.46
C41	32.34	29.67	25.46
C51	32.34	29.67	25.46
C61	27.25	25.82	23.53
C12	32.34	29.67	25.46
C22	51.78	33.16	28.98
C32	51.78	33.16	28.98
C42	51.78	33.16	28.98
C52	51.78	33.16	28.98
C62	32.34	29.67	25.46
C13	32.34	29.67	25.46
C23	51.78	33.16	28.98
C33	51.78	33.16	28.98
C43	51.78	33.16	28.98
C53	51.78	33.16	28.98
C63	32.34	29.67	25.46
C14	27.25	25.82	23.53
C24	32.34	29.67	25.46
C34	32.34	29.67	25.46
C44	32.34	29.67	25.46
C54	32.34	29.67	25.46
C64	27.25	25.82	23.53

BUILDING TYPE 3: 4 storeys, 3×5 spans

Table A2.9 – Chord rotation capacities θ_{SD} of columns, according to EC8-3 (2005) – Direction XX

Columns	$\boldsymbol{\theta_{SD}\ (rad)}$			
	Storey S1	**Storey S2**	**Storey S3**	**Storey S4**
C11	0.02222	0.02234	0.02352	0.02478
C21	0.01853	0.01957	0.02154	0.02371
C31	0.01853	0.01957	0.02154	0.02371
C41	0.01853	0.01957	0.02154	0.02371
C51	0.01853	0.01957	0.02154	0.02371
C61	0.02222	0.02234	0.02352	0.02478
C12	0.01853	0.01957	0.02154	0.02371
C22	0.01762	0.01685	0.01814	0.02189
C32	0.01762	0.01685	0.01814	0.02189
C42	0.01762	0.01685	0.01814	0.02189
C52	0.01762	0.01685	0.01814	0.02189
C62	0.01853	0.01957	0.02154	0.02371
C13	0.01853	0.01957	0.02154	0.02371
C23	0.01762	0.01685	0.01814	0.02189
C33	0.01762	0.01685	0.01814	0.02189
C43	0.01762	0.01685	0.01814	0.02189
C53	0.01762	0.01685	0.01814	0.02189
C63	0.01853	0.01957	0.02154	0.02371
C14	0.02222	0.02234	0.02352	0.02478
C24	0.01853	0.01957	0.02154	0.02371
C34	0.01853	0.01957	0.02154	0.02371
C44	0.01853	0.01957	0.02154	0.02371
C54	0.01853	0.01957	0.02154	0.02371
C64	0.02222	0.02234	0.02352	0.02478

Table A2.10 – Shear force capacities V_R of columns, according to EC8-3 (2005) – Direction XX

Columns	$\boldsymbol{V_R\ (kN)}$			
	Storey S1	**Storey S2**	**Storey S3**	**Storey S4**
C11	22.86	21.91	20.10	18.28
C21	32.49	26.55	23.19	19.82
C31	32.49	26.55	23.19	19.82
C41	32.49	26.55	23.19	19.82
C51	32.49	26.55	23.19	19.82
C61	22.86	21.91	20.10	18.28
C12	32.49	26.55	23.19	19.82
C22	56.48	58.54	33.16	22.64
C32	56.48	58.54	33.16	22.64
C42	56.48	58.54	33.16	22.64
C52	56.48	58.54	33.16	22.64
C62	32.49	26.55	23.19	19.82
C13	32.49	26.55	23.19	19.82
C23	56.48	58.54	33.16	22.64
C33	56.48	58.54	33.16	22.64
C43	56.48	58.54	33.16	22.64
C53	56.48	58.54	33.16	22.64
C63	32.49	26.55	23.19	19.82
C14	22.86	21.91	20.10	18.28
C24	32.49	26.55	23.19	19.82
C34	32.49	26.55	23.19	19.82
C44	32.49	26.55	23.19	19.82
C54	32.49	26.55	23.19	19.82
C64	22.86	21.91	20.10	18.28

Table A2.11 – Chord rotation capacities θ_{SD} of columns, according to EC8-3 (2005) – Direction YY

Columns	$\boldsymbol{\theta_{SD}}$ $\boldsymbol{(rad)}$			
	Storey S1	**Storey S2**	**Storey S3**	**Storey S4**
C11	0.02061	0.02072	0.02182	0.02298
C21	0.01853	0.01815	0.01998	0.02199
C31	0.01853	0.01815	0.01998	0.02199
C41	0.01853	0.01815	0.01998	0.02199
C51	0.01853	0.01815	0.01998	0.02199
C61	0.02061	0.02072	0.02182	0.02298
C12	0.01853	0.01815	0.01998	0.02199
C22	0.01597	0.01685	0.01814	0.02030
C32	0.01597	0.01685	0.01814	0.02030
C42	0.01597	0.01685	0.01814	0.02030
C52	0.01597	0.01685	0.01814	0.02030
C62	0.01853	0.01815	0.01998	0.02199
C13	0.01853	0.01815	0.01998	0.02199
C23	0.01597	0.01685	0.01814	0.02030
C33	0.01597	0.01685	0.01814	0.02030
C43	0.01597	0.01685	0.01814	0.02030
C53	0.01597	0.01685	0.01814	0.02030
C63	0.01853	0.01815	0.01998	0.02199
C14	0.02061	0.02072	0.02182	0.02298
C24	0.01853	0.01815	0.01998	0.02199
C34	0.01853	0.01815	0.01998	0.02199
C44	0.01853	0.01815	0.01998	0.02199
C54	0.01853	0.01815	0.01998	0.02199
C64	0.02061	0.02072	0.02182	0.02298

Table A2.12 – Shear force capacities V_R of columns, according to EC8-3 (2005) – Direction YY

Columns	$\boldsymbol{V_R}$ $\boldsymbol{(kN)}$			
	Storey S1	**Storey S2**	**Storey S3**	**Storey S4**
C11	29.26	28.08	25.82	23.53
C21	32.49	33.88	29.67	25.46
C31	32.49	33.88	29.67	25.46
C41	32.49	33.88	29.67	25.46
C51	32.49	33.88	29.67	25.46
C61	29.26	28.08	25.82	23.53
C12	32.49	33.88	29.67	25.46
C22	82.22	58.54	33.16	28.98
C32	82.22	58.54	33.16	28.98
C42	82.22	58.54	33.16	28.98
C52	82.22	58.54	33.16	28.98
C62	32.49	33.88	29.67	25.46
C13	32.49	33.88	29.67	25.46
C23	82.22	58.54	33.16	28.98
C33	82.22	58.54	33.16	28.98
C43	82.22	58.54	33.16	28.98
C53	82.22	58.54	33.16	28.98
C63	32.49	33.88	29.67	25.46
C14	29.26	28.08	25.82	23.53
C24	32.49	33.88	29.67	25.46
C34	32.49	33.88	29.67	25.46
C44	32.49	33.88	29.67	25.46
C54	32.49	33.88	29.67	25.46
C64	29.26	28.08	25.82	23.53

BUILDING TYPE 4: 5 storeys, 3×5 spans

Table A2.13 – Chord rotation capacities θ_{SD} of columns, according to EC8-3 (2005) – Direction XX

Columns	$\boldsymbol{\theta_{SD}\ (rad)}$				
	Storey S1	**Storey S2**	**Storey S3**	**Storey S4**	**Storey S5**
C11	0.02109	0.02121	0.02234	0.02352	0.02478
C21	0.01829	0.01769	0.01957	0.02154	0.02371
C31	0.01829	0.01769	0.01957	0.02154	0.02371
C41	0.01829	0.01769	0.01957	0.02154	0.02371
C51	0.01829	0.01769	0.01957	0.02154	0.02371
C61	0.02109	0.02121	0.02234	0.02352	0.02478
C12	0.01829	0.01769	0.01957	0.02154	0.02371
C22	0.01758	0.01682	0.01685	0.01814	0.02189
C32	0.01758	0.01682	0.01685	0.01814	0.02189
C42	0.01758	0.01682	0.01685	0.01814	0.02189
C52	0.01758	0.01682	0.01685	0.01814	0.02189
C62	0.01829	0.01769	0.01957	0.02154	0.02371
C13	0.01829	0.01769	0.01957	0.02154	0.02371
C23	0.01758	0.01682	0.01685	0.01814	0.02189
C33	0.01758	0.01682	0.01685	0.01814	0.02189
C43	0.01758	0.01682	0.01685	0.01814	0.02189
C53	0.01758	0.01682	0.01685	0.01814	0.02189
C63	0.01829	0.01769	0.01957	0.02154	0.02371
C14	0.02109	0.02121	0.02234	0.02352	0.02478
C24	0.01829	0.01769	0.01957	0.02154	0.02371
C34	0.01829	0.01769	0.01957	0.02154	0.02371
C44	0.01829	0.01769	0.01957	0.02154	0.02371
C54	0.01829	0.01769	0.01957	0.02154	0.02371
C64	0.02109	0.02121	0.02234	0.02352	0.02478

Table A2.14 – Shear force capacities V_R of columns, according to EC8-3 (2005) – Direction XX

Columns	$\boldsymbol{V_R\ (kN)}$				
	Storey S1	**Storey S2**	**Storey S3**	**Storey S4**	**Storey S5**
C11	24.46	23.74	21.91	20.10	18.28
C21	36.08	34.53	26.55	23.19	19.82
C31	36.08	34.53	26.55	23.19	19.82
C41	36.08	34.53	26.55	23.19	19.82
C51	36.08	34.53	26.55	23.19	19.82
C61	24.46	23.74	21.91	20.10	18.28
C12	36.08	34.53	26.55	23.19	19.82
C22	67.54	63.52	58.54	33.16	22.64
C32	67.54	63.52	58.54	33.16	22.64
C42	67.54	63.52	58.54	33.16	22.64
C52	67.54	63.52	58.54	33.16	22.64
C62	36.08	34.53	26.55	23.19	19.82
C13	36.08	34.53	26.55	23.19	19.82
C23	67.54	63.52	58.54	33.16	22.64
C33	67.54	63.52	58.54	33.16	22.64
C43	67.54	63.52	58.54	33.16	22.64
C53	67.54	63.52	58.54	33.16	22.64
C63	36.08	34.53	26.55	23.19	19.82
C14	24.46	23.74	21.91	20.10	18.28
C24	36.08	34.53	26.55	23.19	19.82
C34	36.08	34.53	26.55	23.19	19.82
C44	36.08	34.53	26.55	23.19	19.82
C54	36.08	34.53	26.55	23.19	19.82
C64	24.46	23.74	21.91	20.10	18.28

Table A2.15 – Chord rotation capacities θ_{SD} of columns, according to EC8-3 (2005) – Direction YY

Columns	$\boldsymbol{\theta_{SD}\ (rad)}$				
	Storey S1	**Storey S2**	**Storey S3**	**Storey S4**	**Storey S5**
C11	0.01956	0.01967	0.02072	0.02182	0.02298
C21	0.01718	0.01769	0.01815	0.01998	0.02199
C31	0.01718	0.01769	0.01815	0.01998	0.02199
C41	0.01718	0.01769	0.01815	0.01998	0.02199
C51	0.01718	0.01769	0.01815	0.01998	0.02199
C61	0.01956	0.01967	0.02072	0.02182	0.02298
C12	0.01718	0.01769	0.01815	0.01998	0.02199
C22	0.01475	0.01524	0.01685	0.01814	0.02030
C32	0.01475	0.01524	0.01685	0.01814	0.02030
C42	0.01475	0.01524	0.01685	0.01814	0.02030
C52	0.01475	0.01524	0.01685	0.01814	0.02030
C62	0.01718	0.01769	0.01815	0.01998	0.02199
C13	0.01718	0.01769	0.01815	0.01998	0.02199
C23	0.01475	0.01524	0.01685	0.01814	0.02030
C33	0.01475	0.01524	0.01685	0.01814	0.02030
C43	0.01475	0.01524	0.01685	0.01814	0.02030
C53	0.01475	0.01524	0.01685	0.01814	0.02030
C63	0.01718	0.01769	0.01815	0.01998	0.02199
C14	0.01956	0.01967	0.02072	0.02182	0.02298
C24	0.01718	0.01769	0.01815	0.01998	0.02199
C34	0.01718	0.01769	0.01815	0.01998	0.02199
C44	0.01718	0.01769	0.01815	0.01998	0.02199
C54	0.01718	0.01769	0.01815	0.01998	0.02199
C64	0.01956	0.01967	0.02072	0.02182	0.02298

Table A2.16 – Shear force capacities V_R of columns, according to EC8-3 (2005) – Direction YY

Columns	$\boldsymbol{V_R\ (kN)}$				
	Storey S1	**Storey S2**	**Storey S3**	**Storey S4**	**Storey S5**
C11	31.27	30.37	28.08	25.82	23.53
C21	43.34	34.53	33.88	29.67	25.46
C31	43.34	34.53	33.88	29.67	25.46
C41	43.34	34.53	33.88	29.67	25.46
C51	43.34	34.53	33.88	29.67	25.46
C61	31.27	30.37	28.08	25.82	23.53
C12	43.34	34.53	33.88	29.67	25.46
C22	127.89	92.17	58.54	33.16	28.98
C32	127.89	92.17	58.54	33.16	28.98
C42	127.89	92.17	58.54	33.16	28.98
C52	127.89	92.17	58.54	33.16	28.98
C62	43.34	34.53	33.88	29.67	25.46
C13	43.34	34.53	33.88	29.67	25.46
C23	127.89	92.17	58.54	33.16	28.98
C33	127.89	92.17	58.54	33.16	28.98
C43	127.89	92.17	58.54	33.16	28.98
C53	127.89	92.17	58.54	33.16	28.98
C63	43.34	34.53	33.88	29.67	25.46
C14	31.27	30.37	28.08	25.82	23.53
C24	43.34	34.53	33.88	29.67	25.46
C34	43.34	34.53	33.88	29.67	25.46
C44	43.34	34.53	33.88	29.67	25.46
C54	43.34	34.53	33.88	29.67	25.46
C64	31.27	30.37	28.08	25.82	23.53

BUILDING TYPE 5: 6 storeys, 3×5 spans

Table A2.17 – Chord rotation capacities θ_{SD} of columns, according to EC8-3 (2005) – Direction XX

Columns	$\boldsymbol{\theta_{SD}\ (rad)}$					
	Storey S1	**Storey S2**	**Storey S3**	**Storey S4**	**Storey S5**	**Storey S6**
C11	0.02002	0.02013	0.02121	0.02234	0.02352	0.02478
C21	0.01719	0.01745	0.01769	0.01957	0.02154	0.02371
C31	0.01719	0.01745	0.01769	0.01957	0.02154	0.02371
C41	0.01719	0.01745	0.01769	0.01957	0.02154	0.02371
C51	0.01719	0.01745	0.01769	0.01957	0.02154	0.02371
C61	0.02002	0.02013	0.02121	0.02234	0.02352	0.02478
C12	0.01719	0.01745	0.01769	0.01957	0.02154	0.02371
C22	0.01753	0.01678	0.01682	0.01685	0.01814	0.02189
C32	0.01753	0.01678	0.01682	0.01685	0.01814	0.02189
C42	0.01753	0.01678	0.01682	0.01685	0.01814	0.02189
C52	0.01753	0.01678	0.01682	0.01685	0.01814	0.02189
C62	0.01719	0.01745	0.01769	0.01957	0.02154	0.02371
C13	0.01719	0.01745	0.01769	0.01957	0.02154	0.02371
C23	0.01753	0.01678	0.01682	0.01685	0.01814	0.02189
C33	0.01753	0.01678	0.01682	0.01685	0.01814	0.02189
C43	0.01753	0.01678	0.01682	0.01685	0.01814	0.02189
C53	0.01753	0.01678	0.01682	0.01685	0.01814	0.02189
C63	0.01719	0.01745	0.01769	0.01957	0.02154	0.02371
C14	0.02002	0.02013	0.02121	0.02234	0.02352	0.02478
C24	0.01719	0.01745	0.01769	0.01957	0.02154	0.02371
C34	0.01719	0.01745	0.01769	0.01957	0.02154	0.02371
C44	0.01719	0.01745	0.01769	0.01957	0.02154	0.02371
C54	0.01719	0.01745	0.01769	0.01957	0.02154	0.02371
C64	0.02002	0.02013	0.02121	0.02234	0.02352	0.02478

Table A2.18 – Shear force capacities V_R of columns, according to EC8-3 (2005) – Direction XX

Columns	$\boldsymbol{V_R\ (kN)}$					
	Storey S1	**Storey S2**	**Storey S3**	**Storey S4**	**Storey S5**	**Storey S6**
C11	26.07	25.57	23.74	21.91	20.10	18.28
C21	54.00	38.63	34.53	26.55	23.19	19.82
C31	54.00	38.63	34.53	26.55	23.19	19.82
C41	54.00	38.63	34.53	26.55	23.19	19.82
C51	54.00	38.63	34.53	26.55	23.19	19.82
C61	26.07	25.57	23.74	21.91	20.10	18.28
C12	54.00	38.63	34.53	26.55	23.19	19.82
C22	74.17	76.56	63.52	58.54	33.16	22.64
C32	74.17	76.56	63.52	58.54	33.16	22.64
C42	74.17	76.56	63.52	58.54	33.16	22.64
C52	74.17	76.56	63.52	58.54	33.16	22.64
C62	54.00	38.63	34.53	26.55	23.19	19.82
C13	54.00	38.63	34.53	26.55	23.19	19.82
C23	74.17	76.56	63.52	58.54	33.16	22.64
C33	74.17	76.56	63.52	58.54	33.16	22.64
C43	74.17	76.56	63.52	58.54	33.16	22.64
C53	74.17	76.56	63.52	58.54	33.16	22.64
C63	54.00	38.63	34.53	26.55	23.19	19.82
C14	26.07	25.57	23.74	21.91	20.10	18.28
C24	54.00	38.63	34.53	26.55	23.19	19.82
C34	54.00	38.63	34.53	26.55	23.19	19.82
C44	54.00	38.63	34.53	26.55	23.19	19.82
C54	54.00	38.63	34.53	26.55	23.19	19.82
C64	26.07	25.57	23.74	21.91	20.10	18.28

Table A2.19 – Chord rotation capacities θ_{SD} of columns, according to EC8-3 (2005) – Direction YY

Columns	$\boldsymbol{\theta_{SD}\ (rad)}$					
	Storey S1	**Storey S2**	**Storey S3**	**Storey S4**	**Storey S5**	**Storey S6**
C11	0.01857	0.01867	0.01967	0.02072	0.02182	0.02298
C21	0.01719	0.01640	0.01769	0.01815	0.01998	0.02199
C31	0.01719	0.01640	0.01769	0.01815	0.01998	0.02199
C41	0.01719	0.01640	0.01769	0.01815	0.01998	0.02199
C51	0.01719	0.01640	0.01769	0.01815	0.01998	0.02199
C61	0.01857	0.01867	0.01967	0.02072	0.02182	0.02298
C12	0.01719	0.01640	0.01769	0.01815	0.01998	0.02199
C22	0.01378	0.01407	0.01524	0.01685	0.01814	0.02030
C32	0.01378	0.01407	0.01524	0.01685	0.01814	0.02030
C42	0.01378	0.01407	0.01524	0.01685	0.01814	0.02030
C52	0.01378	0.01407	0.01524	0.01685	0.01814	0.02030
C62	0.01719	0.01640	0.01769	0.01815	0.01998	0.02199
C13	0.01719	0.01640	0.01769	0.01815	0.01998	0.02199
C23	0.01378	0.01407	0.01524	0.01685	0.01814	0.02030
C33	0.01378	0.01407	0.01524	0.01685	0.01814	0.02030
C43	0.01378	0.01407	0.01524	0.01685	0.01814	0.02030
C53	0.01378	0.01407	0.01524	0.01685	0.01814	0.02030
C63	0.01719	0.01640	0.01769	0.01815	0.01998	0.02199
C14	0.01857	0.01867	0.01967	0.02072	0.02182	0.02298
C24	0.01719	0.01640	0.01769	0.01815	0.01998	0.02199
C34	0.01719	0.01640	0.01769	0.01815	0.01998	0.02199
C44	0.01719	0.01640	0.01769	0.01815	0.01998	0.02199
C54	0.01719	0.01640	0.01769	0.01815	0.01998	0.02199
C64	0.01857	0.01867	0.01967	0.02072	0.02182	0.02298

Table A2.20 – Shear force capacities V_R of columns, according to EC8-3 (2005) – Direction YY

Columns	$\boldsymbol{V_R\ (kN)}$					
	Storey S1	**Storey S2**	**Storey S3**	**Storey S4**	**Storey S5**	**Storey S6**
C11	33.28	32.65	30.37	28.08	25.82	23.53
C21	54.00	48.10	34.53	33.88	29.67	25.46
C31	54.00	48.10	34.53	33.88	29.67	25.46
C41	54.00	48.10	34.53	33.88	29.67	25.46
C51	54.00	48.10	34.53	33.88	29.67	25.46
C61	33.28	32.65	30.37	28.08	25.82	23.53
C12	54.00	48.10	34.53	33.88	29.67	25.46
C22	169.09	141.57	92.17	58.54	33.16	28.98
C32	169.09	141.57	92.17	58.54	33.16	28.98
C42	169.09	141.57	92.17	58.54	33.16	28.98
C52	169.09	141.57	92.17	58.54	33.16	28.98
C62	54.00	48.10	34.53	33.88	29.67	25.46
C13	54.00	48.10	34.53	33.88	29.67	25.46
C23	169.09	141.57	92.17	58.54	33.16	28.98
C33	169.09	141.57	92.17	58.54	33.16	28.98
C43	169.09	141.57	92.17	58.54	33.16	28.98
C53	169.09	141.57	92.17	58.54	33.16	28.98
C63	54.00	48.10	34.53	33.88	29.67	25.46
C14	33.28	32.65	30.37	28.08	25.82	23.53
C24	54.00	48.10	34.53	33.88	29.67	25.46
C34	54.00	48.10	34.53	33.88	29.67	25.46
C44	54.00	48.10	34.53	33.88	29.67	25.46
C54	54.00	48.10	34.53	33.88	29.67	25.46
C64	33.28	32.65	30.37	28.08	25.82	23.53

BUILDING TYPE 6: 2 storeys, 2×4 spans

Table A2.21 – Chord rotation capacities θ_{SD} of columns, according to EC8-3 (2005) – Direction XX

Columns	$\boldsymbol{\theta_{SD}\ (rad)}$	
	Storey S1	**Storey S2**
C11	0.02465	0.02478
C21	0.02257	0.02371
C31	0.02257	0.02371
C41	0.02257	0.02371
C51	0.02465	0.02478
C12	0.02257	0.02371
C22	0.01901	0.02189
C32	0.01901	0.02189
C42	0.01901	0.02189
C52	0.02257	0.02371
C13	0.02465	0.02478
C23	0.02257	0.02371
C33	0.02257	0.02371
C43	0.02257	0.02371
C53	0.02465	0.02478

Table A2.22 – Shear force capacities V_R of columns, according to EC8-3 (2005) – Direction XX

Columns	$\boldsymbol{V_R\ (kN)}$	
	Storey S1	**Storey S2**
C11	19.66	18.28
C21	22.37	19.82
C31	22.37	19.82
C41	22.37	19.82
C51	19.66	18.28
C12	22.37	19.82
C22	31.29	22.64
C32	31.29	22.64
C42	31.29	22.64
C52	22.37	19.82
C13	19.66	18.28
C23	22.37	19.82
C33	22.37	19.82
C43	22.37	19.82
C53	19.66	18.28

Table A2.23 – Chord rotation capacities θ_{SD} of columns, according to EC8-3 (2005) – Direction YY

Columns	$\boldsymbol{\theta_{SD}}$ $\boldsymbol{(rad)}$	
	Storey S1	**Storey S2**
C11	0.02286	0.02298
C21	0.02094	0.02199
C31	0.02094	0.02199
C41	0.02094	0.02199
C51	0.02286	0.02298
C12	0.02094	0.02199
C22	0.01901	0.02030
C32	0.01901	0.02030
C42	0.01901	0.02030
C52	0.02094	0.02199
C13	0.02286	0.02298
C23	0.02094	0.02199
C33	0.02094	0.02199
C43	0.02094	0.02199
C53	0.02286	0.02298

Table A2.24 – Shear force capacities V_R of columns, according to EC8-3 (2005) – Direction YY

Columns	$\boldsymbol{V_R}$ $\boldsymbol{(kN)}$	
	Storey S1	**Storey S2**
C11	25.26	23.53
C21	28.65	25.46
C31	28.65	25.46
C41	28.65	25.46
C51	25.26	23.53
C12	28.65	25.46
C22	31.29	28.98
C32	31.29	28.98
C42	31.29	28.98
C52	28.65	25.46
C13	25.26	23.53
C23	28.65	25.46
C33	28.65	25.46
C43	28.65	25.46
C53	25.26	23.53

BUILDING TYPE 7: 3 storeys, 2×4 spans

Table A2.25 – Chord rotation capacities θ_{SD} of columns, according to EC8-3 (2005) – Direction XX

Columns	$\boldsymbol{\theta_{SD}\ (rad)}$		
	Storey S1	**Storey S2**	**Storey S3**
C11	0.02341	0.02352	0.02478
C21	0.02051	0.02154	0.02371
C31	0.02051	0.02154	0.02371
C41	0.02051	0.02154	0.02371
C51	0.02341	0.02352	0.02478
C12	0.02051	0.02154	0.02371
C22	0.01766	0.01814	0.02189
C32	0.01766	0.01814	0.02189
C42	0.01766	0.01814	0.02189
C52	0.02051	0.02154	0.02371
C13	0.02341	0.02352	0.02478
C23	0.02051	0.02154	0.02371
C33	0.02051	0.02154	0.02371
C43	0.02051	0.02154	0.02371
C53	0.02341	0.02352	0.02478

Table A2.26 – Shear force capacities V_R of columns, according to EC8-3 (2005) – Direction XX

Columns	$\boldsymbol{V_R\ (kN)}$		
	Storey S1	**Storey S2**	**Storey S3**
C11	21.25	20.10	18.28
C21	25.32	23.19	19.82
C31	25.32	23.19	19.82
C41	25.32	23.19	19.82
C51	21.25	20.10	18.28
C12	25.32	23.19	19.82
C22	51.78	33.16	22.64
C32	51.78	33.16	22.64
C42	51.78	33.16	22.64
C52	25.32	23.19	19.82
C13	21.25	20.10	18.28
C23	25.32	23.19	19.82
C33	25.32	23.19	19.82
C43	25.32	23.19	19.82
C53	21.25	20.10	18.28

Table A2.27 – Chord rotation capacities θ_{SD} of columns, according to EC8-3 (2005) – Direction YY

Columns	$\boldsymbol{\theta_{SD}\ (rad)}$		
	Storey S1	**Storey S2**	**Storey S3**
C11	0.02171	0.02182	0.02298
C21	0.01902	0.01998	0.02199
C31	0.01902	0.01998	0.02199
C41	0.01902	0.01998	0.02199
C51	0.02171	0.02182	0.02298
C12	0.01902	0.01998	0.02199
C22	0.01766	0.01814	0.02030
C32	0.01766	0.01814	0.02030
C42	0.01766	0.01814	0.02030
C52	0.01902	0.01998	0.02199
C13	0.02171	0.02182	0.02298
C23	0.01902	0.01998	0.02199
C33	0.01902	0.01998	0.02199
C43	0.01902	0.01998	0.02199
C53	0.02171	0.02182	0.02298

Table A2.28 – Shear force capacities V_R of columns, according to EC8-3 (2005) – Direction YY

Columns	$\boldsymbol{V_R\ (kN)}$		
	Storey S1	**Storey S2**	**Storey S3**
C11	27.25	25.82	23.53
C21	32.34	29.67	25.46
C31	32.34	29.67	25.46
C41	32.34	29.67	25.46
C51	27.25	25.82	23.53
C12	32.34	29.67	25.46
C22	51.78	33.16	28.98
C32	51.78	33.16	28.98
C42	51.78	33.16	28.98
C52	32.34	29.67	25.46
C13	27.25	25.82	23.53
C23	32.34	29.67	25.46
C33	32.34	29.67	25.46
C43	32.34	29.67	25.46
C53	27.25	25.82	23.53

BUILDING TYPE 8: 4 storeys, 2×4 spans

Table A2.29 – Chord rotation capacities θ_{SD} of columns, according to EC8-3 (2005) – Direction XX

Columns	$\boldsymbol{\theta_{SD}\ (rad)}$			
	Storey S1	**Storey S2**	**Storey S3**	**Storey S4**
C11	0.02222	0.02234	0.02352	0.02478
C21	0.01853	0.01957	0.02154	0.02371
C31	0.01853	0.01957	0.02154	0.02371
C41	0.01853	0.01957	0.02154	0.02371
C51	0.02222	0.02234	0.02352	0.02478
C12	0.01853	0.01957	0.02154	0.02371
C22	0.01762	0.01685	0.01814	0.02189
C32	0.01762	0.01685	0.01814	0.02189
C42	0.01762	0.01685	0.01814	0.02189
C52	0.01853	0.01957	0.02154	0.02371
C13	0.02222	0.02234	0.02352	0.02478
C23	0.01853	0.01957	0.02154	0.02371
C33	0.01853	0.01957	0.02154	0.02371
C43	0.01853	0.01957	0.02154	0.02371
C53	0.02222	0.02234	0.02352	0.02478

Table A2.30 – Shear force capacities V_R of columns, according to EC8-3 (2005) – Direction XX

Columns	$\boldsymbol{V_R\ (kN)}$			
	Storey S1	**Storey S2**	**Storey S3**	**Storey S4**
C11	22.86	21.91	20.10	18.28
C21	32.49	26.55	23.19	19.82
C31	32.49	26.55	23.19	19.82
C41	32.49	26.55	23.19	19.82
C51	22.86	21.91	20.10	18.28
C12	32.49	26.55	23.19	19.82
C22	56.48	58.54	33.16	22.64
C32	56.48	58.54	33.16	22.64
C42	56.48	58.54	33.16	22.64
C52	32.49	26.55	23.19	19.82
C13	22.86	21.91	20.10	18.28
C23	32.49	26.55	23.19	19.82
C33	32.49	26.55	23.19	19.82
C43	32.49	26.55	23.19	19.82
C53	22.86	21.91	20.10	18.28

Table A2.31 – Chord rotation capacities θ_{SD} of columns, according to EC8-3 (2005) – Direction YY

Columns	$\boldsymbol{\theta_{SD}}$ $(\boldsymbol{rad})$			
	Storey S1	**Storey S2**	**Storey S3**	**Storey S4**
C11	0.02061	0.02072	0.02182	0.02298
C21	0.01853	0.01815	0.01998	0.02199
C31	0.01853	0.01815	0.01998	0.02199
C41	0.01853	0.01815	0.01998	0.02199
C51	0.02061	0.02072	0.02182	0.02298
C12	0.01853	0.01815	0.01998	0.02199
C22	0.01597	0.01685	0.01814	0.02030
C32	0.01597	0.01685	0.01814	0.02030
C42	0.01597	0.01685	0.01814	0.02030
C52	0.01853	0.01815	0.01998	0.02199
C13	0.02061	0.02072	0.02182	0.02298
C23	0.01853	0.01815	0.01998	0.02199
C33	0.01853	0.01815	0.01998	0.02199
C43	0.01853	0.01815	0.01998	0.02199
C53	0.02061	0.02072	0.02182	0.02298

Table A2.32 – Shear force capacities V_R of columns, according to EC8-3 (2005) – Direction YY

Columns	$\boldsymbol{V_R}$ $(\boldsymbol{kN})$			
	Storey S1	**Storey S2**	**Storey S3**	**Storey S4**
C11	29.26	28.08	25.82	23.53
C21	32.49	33.88	29.67	25.46
C31	32.49	33.88	29.67	25.46
C41	32.49	33.88	29.67	25.46
C51	29.26	28.08	25.82	23.53
C12	32.49	33.88	29.67	25.46
C22	82.22	58.54	33.16	28.98
C32	82.22	58.54	33.16	28.98
C42	82.22	58.54	33.16	28.98
C52	32.49	33.88	29.67	25.46
C13	29.26	28.08	25.82	23.53
C23	32.49	33.88	29.67	25.46
C33	32.49	33.88	29.67	25.46
C43	32.49	33.88	29.67	25.46
C53	29.26	28.08	25.82	23.53

BUILDING TYPE 9: 5 storeys, 2×4 spans

Table A2.33 – Chord rotation capacities θ_{SD} of columns, according to EC8-3 (2005) – Direction XX

Columns	$\boldsymbol{\theta_{SD}\ (rad)}$				
	Storey S1	**Storey S2**	**Storey S3**	**Storey S4**	**Storey S5**
C11	0.02109	0.02121	0.02234	0.02352	0.02478
C21	0.01829	0.01769	0.01957	0.02154	0.02371
C31	0.01829	0.01769	0.01957	0.02154	0.02371
C41	0.01829	0.01769	0.01957	0.02154	0.02371
C51	0.02109	0.02121	0.02234	0.02352	0.02478
C12	0.01829	0.01769	0.01957	0.02154	0.02371
C22	0.01758	0.01682	0.01685	0.01814	0.02189
C32	0.01758	0.01682	0.01685	0.01814	0.02189
C42	0.01758	0.01682	0.01685	0.01814	0.02189
C52	0.01829	0.01769	0.01957	0.02154	0.02371
C13	0.02109	0.02121	0.02234	0.02352	0.02478
C23	0.01829	0.01769	0.01957	0.02154	0.02371
C33	0.01829	0.01769	0.01957	0.02154	0.02371
C43	0.01829	0.01769	0.01957	0.02154	0.02371
C53	0.02109	0.02121	0.02234	0.02352	0.02478

Table A2.34 – Shear force capacities V_R of columns, according to EC8-3 (2005) – Direction XX

Columns	$\boldsymbol{V_R\ (kN)}$				
	Storey S1	**Storey S2**	**Storey S3**	**Storey S4**	**Storey S5**
C11	24.46	23.74	21.91	20.10	18.28
C21	36.08	34.53	26.55	23.19	19.82
C31	36.08	34.53	26.55	23.19	19.82
C41	36.08	34.53	26.55	23.19	19.82
C51	24.46	23.74	21.91	20.10	18.28
C12	36.08	34.53	26.55	23.19	19.82
C22	67.54	63.52	58.54	33.16	22.64
C32	67.54	63.52	58.54	33.16	22.64
C42	67.54	63.52	58.54	33.16	22.64
C52	36.08	34.53	26.55	23.19	19.82
C13	24.46	23.74	21.91	20.10	18.28
C23	36.08	34.53	26.55	23.19	19.82
C33	36.08	34.53	26.55	23.19	19.82
C43	36.08	34.53	26.55	23.19	19.82
C53	24.46	23.74	21.91	20.10	18.28

Table A2.35 – Chord rotation capacities θ_{SD} of columns, according to EC8-3 (2005) – Direction YY

Columns	$\boldsymbol{\theta_{SD}\ (rad)}$				
	Storey S1	**Storey S2**	**Storey S3**	**Storey S4**	**Storey S5**
C11	0.01956	0.01967	0.02072	0.02182	0.02298
C21	0.01718	0.01769	0.01815	0.01998	0.02199
C31	0.01718	0.01769	0.01815	0.01998	0.02199
C41	0.01718	0.01769	0.01815	0.01998	0.02199
C51	0.01956	0.01967	0.02072	0.02182	0.02298
C12	0.01718	0.01769	0.01815	0.01998	0.02199
C22	0.01475	0.01524	0.01685	0.01814	0.02030
C32	0.01475	0.01524	0.01685	0.01814	0.02030
C42	0.01475	0.01524	0.01685	0.01814	0.02030
C52	0.01718	0.01769	0.01815	0.01998	0.02199
C13	0.01956	0.01967	0.02072	0.02182	0.02298
C23	0.01718	0.01769	0.01815	0.01998	0.02199
C33	0.01718	0.01769	0.01815	0.01998	0.02199
C43	0.01718	0.01769	0.01815	0.01998	0.02199
C53	0.01956	0.01967	0.02072	0.02182	0.02298

Table A2.36 – Shear force capacities V_R of columns, according to EC8-3 (2005) – Direction YY

Columns	$\boldsymbol{V_R\ (kN)}$				
	Storey S1	**Storey S2**	**Storey S3**	**Storey S4**	**Storey S5**
C11	31.27	30.37	28.08	25.82	23.53
C21	43.34	34.53	33.88	29.67	25.46
C31	43.34	34.53	33.88	29.67	25.46
C41	43.34	34.53	33.88	29.67	25.46
C51	31.27	30.37	28.08	25.82	23.53
C12	43.34	34.53	33.88	29.67	25.46
C22	127.89	92.17	58.54	33.16	28.98
C32	127.89	92.17	58.54	33.16	28.98
C42	127.89	92.17	58.54	33.16	28.98
C52	43.34	34.53	33.88	29.67	25.46
C13	31.27	30.37	28.08	25.82	23.53
C23	43.34	34.53	33.88	29.67	25.46
C33	43.34	34.53	33.88	29.67	25.46
C43	43.34	34.53	33.88	29.67	25.46
C53	31.27	30.37	28.08	25.82	23.53

BUILDING TYPE 10: 6 storeys, 2×4 spans

Table A2.37 – Chord rotation capacities θ_{SD} of columns, according to EC8-3 (2005) – Direction XX

Columns	$\boldsymbol{\theta_{SD}\ (rad)}$					
	Storey S1	**Storey S2**	**Storey S3**	**Storey S4**	**Storey S5**	**Storey S6**
C11	0.02002	0.02013	0.02121	0.02234	0.02352	0.02478
C21	0.01719	0.01745	0.01769	0.01957	0.02154	0.02371
C31	0.01719	0.01745	0.01769	0.01957	0.02154	0.02371
C41	0.01719	0.01745	0.01769	0.01957	0.02154	0.02371
C51	0.02002	0.02013	0.02121	0.02234	0.02352	0.02478
C12	0.01719	0.01745	0.01769	0.01957	0.02154	0.02371
C22	0.01753	0.01678	0.01682	0.01685	0.01814	0.02189
C32	0.01753	0.01678	0.01682	0.01685	0.01814	0.02189
C42	0.01753	0.01678	0.01682	0.01685	0.01814	0.02189
C52	0.01719	0.01745	0.01769	0.01957	0.02154	0.02371
C13	0.02002	0.02013	0.02121	0.02234	0.02352	0.02478
C23	0.01719	0.01745	0.01769	0.01957	0.02154	0.02371
C33	0.01719	0.01745	0.01769	0.01957	0.02154	0.02371
C43	0.01719	0.01745	0.01769	0.01957	0.02154	0.02371
C53	0.02002	0.02013	0.02121	0.02234	0.02352	0.02478

Table A2.38 – Shear force capacities V_R of columns, according to EC8-3 (2005) – Direction XX

Columns	$\boldsymbol{V_R\ (kN)}$					
	Storey S1	**Storey S2**	**Storey S3**	**Storey S4**	**Storey S5**	**Storey S6**
C11	26.07	25.57	23.74	21.91	20.10	18.28
C21	54.00	38.63	34.53	26.55	23.19	19.82
C31	54.00	38.63	34.53	26.55	23.19	19.82
C41	54.00	38.63	34.53	26.55	23.19	19.82
C51	26.07	25.57	23.74	21.91	20.10	18.28
C12	54.00	38.63	34.53	26.55	23.19	19.82
C22	74.17	76.56	63.52	58.54	33.16	22.64
C32	74.17	76.56	63.52	58.54	33.16	22.64
C42	74.17	76.56	63.52	58.54	33.16	22.64
C52	54.00	38.63	34.53	26.55	23.19	19.82
C13	26.07	25.57	23.74	21.91	20.10	18.28
C23	54.00	38.63	34.53	26.55	23.19	19.82
C33	54.00	38.63	34.53	26.55	23.19	19.82
C43	54.00	38.63	34.53	26.55	23.19	19.82
C53	26.07	25.57	23.74	21.91	20.10	18.28

Table A2.39 – Chord rotation capacities θ_{SD} of columns, according to EC8-3 (2005) – Direction YY

Columns	$\boldsymbol{\theta_{SD}}$ $\boldsymbol{(rad)}$					
	Storey S1	**Storey S2**	**Storey S3**	**Storey S4**	**Storey S5**	**Storey S6**
C11	0.01857	0.01867	0.01967	0.02072	0.02182	0.02298
C21	0.01719	0.01640	0.01769	0.01815	0.01998	0.02199
C31	0.01719	0.01640	0.01769	0.01815	0.01998	0.02199
C41	0.01719	0.01640	0.01769	0.01815	0.01998	0.02199
C51	0.01857	0.01867	0.01967	0.02072	0.02182	0.02298
C12	0.01719	0.01640	0.01769	0.01815	0.01998	0.02199
C22	0.01378	0.01407	0.01524	0.01685	0.01814	0.02030
C32	0.01378	0.01407	0.01524	0.01685	0.01814	0.02030
C42	0.01378	0.01407	0.01524	0.01685	0.01814	0.02030
C52	0.01719	0.01640	0.01769	0.01815	0.01998	0.02199
C13	0.01857	0.01867	0.01967	0.02072	0.02182	0.02298
C23	0.01719	0.01640	0.01769	0.01815	0.01998	0.02199
C33	0.01719	0.01640	0.01769	0.01815	0.01998	0.02199
C43	0.01719	0.01640	0.01769	0.01815	0.01998	0.02199
C53	0.01857	0.01867	0.01967	0.02072	0.02182	0.02298

Table A2.40 – Shear force capacities V_R of columns, according to EC8-3 (2005) – Direction YY

Columns	$\boldsymbol{V_R}$ $\boldsymbol{(kN)}$					
	Storey S1	**Storey S2**	**Storey S3**	**Storey S4**	**Storey S5**	**Storey S6**
C11	33.28	32.65	30.37	28.08	25.82	23.53
C21	54.00	48.10	34.53	33.88	29.67	25.46
C31	54.00	48.10	34.53	33.88	29.67	25.46
C41	54.00	48.10	34.53	33.88	29.67	25.46
C51	33.28	32.65	30.37	28.08	25.82	23.53
C12	54.00	48.10	34.53	33.88	29.67	25.46
C22	169.09	141.57	92.17	58.54	33.16	28.98
C32	169.09	141.57	92.17	58.54	33.16	28.98
C42	169.09	141.57	92.17	58.54	33.16	28.98
C52	54.00	48.10	34.53	33.88	29.67	25.46
C13	33.28	32.65	30.37	28.08	25.82	23.53
C23	54.00	48.10	34.53	33.88	29.67	25.46
C33	54.00	48.10	34.53	33.88	29.67	25.46
C43	54.00	48.10	34.53	33.88	29.67	25.46
C53	33.28	32.65	30.37	28.08	25.82	23.53

AXIAL FORCE CAPACITY ENVELOPE: Building Type 1

Table A2.41 – Axial force capacity in compression N_{comp} of columns

Columns	N_{comp} (kN)	
	Storey S1	**Storey S2**
C11	-1247.83	-1247.83
C21	-1247.83	-1247.83
C31	-1247.83	-1247.83
C41	-1247.83	-1247.83
C51	-1247.83	-1247.83
C61	-1247.83	-1247.83
C12	-1247.83	-1247.83
C22	-1543.73	-1247.83
C32	-1543.73	-1247.83
C42	-1543.73	-1247.83
C52	-1543.73	-1247.83
C62	-1247.83	-1247.83
C13	-1247.83	-1247.83
C23	-1543.73	-1247.83
C33	-1543.73	-1247.83
C43	-1543.73	-1247.83
C53	-1543.73	-1247.83
C63	-1247.83	-1247.83
C14	-1247.83	-1247.83
C24	-1247.83	-1247.83
C34	-1247.83	-1247.83
C44	-1247.83	-1247.83
C54	-1247.83	-1247.83
C64	-1247.83	-1247.83

Table A2.42 – Axial force capacity in tension N_{tens} of columns

Columns	N_{tens} (kN)	
	Storey S1	**Storey S2**
C11	247.83	247.83
C21	247.83	247.83
C31	247.83	247.83
C41	247.83	247.83
C51	247.83	247.83
C61	247.83	247.83
C12	247.83	247.83
C22	293.73	247.83
C32	293.73	247.83
C42	293.73	247.83
C52	293.73	247.83
C62	247.83	247.83
C13	247.83	247.83
C23	293.73	247.83
C33	293.73	247.83
C43	293.73	247.83
C53	293.73	247.83
C63	247.83	247.83
C14	247.83	247.83
C24	247.83	247.83
C34	247.83	247.83
C44	247.83	247.83
C54	247.83	247.83
C64	247.83	247.83

AXIAL FORCE CAPACITY ENVELOPE: Building Type 2

Table A2.43 – Axial force capacity in compression N_{comp} of columns

Columns	N_{comp} (kN)		
	Storey S1	**Storey S2**	**Storey S3**
C11	-1247.83	-1247.83	-1247.83
C21	-1247.83	-1247.83	-1247.83
C31	-1247.83	-1247.83	-1247.83
C41	-1247.83	-1247.83	-1247.83
C51	-1247.83	-1247.83	-1247.83
C61	-1247.83	-1247.83	-1247.83
C12	-1247.83	-1247.83	-1247.83
C22	-2387.45	-1543.73	-1247.83
C32	-2387.45	-1543.73	-1247.83
C42	-2387.45	-1543.73	-1247.83
C52	-2387.45	-1543.73	-1247.83
C62	-1247.83	-1247.83	-1247.83
C13	-1247.83	-1247.83	-1247.83
C23	-2387.45	-1543.73	-1247.83
C33	-2387.45	-1543.73	-1247.83
C43	-2387.45	-1543.73	-1247.83
C53	-2387.45	-1543.73	-1247.83
C63	-1247.83	-1247.83	-1247.83
C14	-1247.83	-1247.83	-1247.83
C24	-1247.83	-1247.83	-1247.83
C34	-1247.83	-1247.83	-1247.83
C44	-1247.83	-1247.83	-1247.83
C54	-1247.83	-1247.83	-1247.83
C64	-1247.83	-1247.83	-1247.83

Table A2.44 – Axial force capacity in tension N_{tens} of columns

Columns	N_{tens} (kN)		
	Storey S1	**Storey S2**	**Storey S3**
C11	247.83	247.83	247.83
C21	247.83	247.83	247.83
C31	247.83	247.83	247.83
C41	247.83	247.83	247.83
C51	247.83	247.83	247.83
C61	247.83	247.83	247.83
C12	247.83	247.83	247.83
C22	587.45	293.73	247.83
C32	587.45	293.73	247.83
C42	587.45	293.73	247.83
C52	587.45	293.73	247.83
C62	247.83	247.83	247.83
C13	247.83	247.83	247.83
C23	587.45	293.73	247.83
C33	587.45	293.73	247.83
C43	587.45	293.73	247.83
C53	587.45	293.73	247.83
C63	247.83	247.83	247.83
C14	247.83	247.83	247.83
C24	247.83	247.83	247.83
C34	247.83	247.83	247.83
C44	247.83	247.83	247.83
C54	247.83	247.83	247.83
C64	247.83	247.83	247.83

AXIAL FORCE CAPACITY ENVELOPE: Building Type 3

Table A2.45 – Axial force capacity in compression N_{comp} of columns

Columns	N_{comp} (kN)			
	Storey S1	**Storey S2**	**Storey S3**	**Storey S4**
C11	-1247.83	-1247.83	-1247.83	-1247.83
C21	-1543.73	-1247.83	-1247.83	-1247.83
C31	-1543.73	-1247.83	-1247.83	-1247.83
C41	-1543.73	-1247.83	-1247.83	-1247.83
C51	-1543.73	-1247.83	-1247.83	-1247.83
C61	-1247.83	-1247.83	-1247.83	-1247.83
C12	-1543.73	-1247.83	-1247.83	-1247.83
C22	-2840.59	-2387.45	-1543.73	-1247.83
C32	-2840.59	-2387.45	-1543.73	-1247.83
C42	-2840.59	-2387.45	-1543.73	-1247.83
C52	-2840.59	-2387.45	-1543.73	-1247.83
C62	-1543.73	-1247.83	-1247.83	-1247.83
C13	-1543.73	-1247.83	-1247.83	-1247.83
C23	-2840.59	-2387.45	-1543.73	-1247.83
C33	-2840.59	-2387.45	-1543.73	-1247.83
C43	-2840.59	-2387.45	-1543.73	-1247.83
C53	-2840.59	-2387.45	-1543.73	-1247.83
C63	-1543.73	-1247.83	-1247.83	-1247.83
C14	-1247.83	-1247.83	-1247.83	-1247.83
C24	-1543.73	-1247.83	-1247.83	-1247.83
C34	-1543.73	-1247.83	-1247.83	-1247.83
C44	-1543.73	-1247.83	-1247.83	-1247.83
C54	-1543.73	-1247.83	-1247.83	-1247.83
C64	-1247.83	-1247.83	-1247.83	-1247.83

Table A2.46 – Axial force capacity in tension N_{tens} of columns

Columns	N_{tens} (kN)			
	Storey S1	**Storey S2**	**Storey S3**	**Storey S4**
C11	247.83	247.83	247.83	247.83
C21	293.73	247.83	247.83	247.83
C31	293.73	247.83	247.83	247.83
C41	293.73	247.83	247.83	247.83
C51	293.73	247.83	247.83	247.83
C61	247.83	247.83	247.83	247.83
C12	293.73	247.83	247.83	247.83
C22	440.59	587.45	293.73	247.83
C32	440.59	587.45	293.73	247.83
C42	440.59	587.45	293.73	247.83
C52	440.59	587.45	293.73	247.83
C62	293.73	247.83	247.83	247.83
C13	293.73	247.83	247.83	247.83
C23	440.59	587.45	293.73	247.83
C33	440.59	587.45	293.73	247.83
C43	440.59	587.45	293.73	247.83
C53	440.59	587.45	293.73	247.83
C63	293.73	247.83	247.83	247.83
C14	247.83	247.83	247.83	247.83
C24	293.73	247.83	247.83	247.83
C34	293.73	247.83	247.83	247.83
C44	293.73	247.83	247.83	247.83
C54	293.73	247.83	247.83	247.83
C64	247.83	247.83	247.83	247.83

AXIAL FORCE CAPACITY ENVELOPE: Building Type 4

Table A2.47 – Axial force capacity in compression N_{comp} of columns

Columns	N_{comp} (kN)				
	Storey S1	**Storey S2**	**Storey S3**	**Storey S4**	**Storey S5**
C11	-1247.83	-1247.83	-1247.83	-1247.83	-1247.83
C21	-1793.73	-1543.73	-1247.83	-1247.83	-1247.83
C31	-1793.73	-1543.73	-1247.83	-1247.83	-1247.83
C41	-1793.73	-1543.73	-1247.83	-1247.83	-1247.83
C51	-1793.73	-1543.73	-1247.83	-1247.83	-1247.83
C61	-1247.83	-1247.83	-1247.83	-1247.83	-1247.83
C12	-1793.73	-1543.73	-1247.83	-1247.83	-1247.83
C22	-3587.45	-2840.59	-2387.45	-1543.73	-1247.83
C32	-3587.45	-2840.59	-2387.45	-1543.73	-1247.83
C42	-3587.45	-2840.59	-2387.45	-1543.73	-1247.83
C52	-3587.45	-2840.59	-2387.45	-1543.73	-1247.83
C62	-1793.73	-1543.73	-1247.83	-1247.83	-1247.83
C13	-1793.73	-1543.73	-1247.83	-1247.83	-1247.83
C23	-3587.45	-2840.59	-2387.45	-1543.73	-1247.83
C33	-3587.45	-2840.59	-2387.45	-1543.73	-1247.83
C43	-3587.45	-2840.59	-2387.45	-1543.73	-1247.83
C53	-3587.45	-2840.59	-2387.45	-1543.73	-1247.83
C63	-1793.73	-1543.73	-1247.83	-1247.83	-1247.83
C14	-1247.83	-1247.83	-1247.83	-1247.83	-1247.83
C24	-1793.73	-1543.73	-1247.83	-1247.83	-1247.83
C34	-1793.73	-1543.73	-1247.83	-1247.83	-1247.83
C44	-1793.73	-1543.73	-1247.83	-1247.83	-1247.83
C54	-1793.73	-1543.73	-1247.83	-1247.83	-1247.83
C64	-1247.83	-1247.83	-1247.83	-1247.83	-1247.83

Table A2.48 – Axial force capacity in tension N_{tens} of columns

Columns	N_{tens} (kN)				
	Storey S1	**Storey S2**	**Storey S3**	**Storey S4**	**Storey S5**
C11	247.83	247.83	247.83	247.83	247.83
C21	293.73	293.73	247.83	247.83	247.83
C31	293.73	293.73	247.83	247.83	247.83
C41	293.73	293.73	247.83	247.83	247.83
C51	293.73	293.73	247.83	247.83	247.83
C61	247.83	247.83	247.83	247.83	247.83
C12	293.73	293.73	247.83	247.83	247.83
C22	587.45	440.59	587.45	293.73	247.83
C32	587.45	440.59	587.45	293.73	247.83
C42	587.45	440.59	587.45	293.73	247.83
C52	587.45	440.59	587.45	293.73	247.83
C62	293.73	293.73	247.83	247.83	247.83
C13	293.73	293.73	247.83	247.83	247.83
C23	587.45	440.59	587.45	293.73	247.83
C33	587.45	440.59	587.45	293.73	247.83
C43	587.45	440.59	587.45	293.73	247.83
C53	587.45	440.59	587.45	293.73	247.83
C63	293.73	293.73	247.83	247.83	247.83
C14	247.83	247.83	247.83	247.83	247.83
C24	293.73	293.73	247.83	247.83	247.83
C34	293.73	293.73	247.83	247.83	247.83
C44	293.73	293.73	247.83	247.83	247.83
C54	293.73	293.73	247.83	247.83	247.83
C64	247.83	247.83	247.83	247.83	247.83

AXIAL FORCE CAPACITY ENVELOPE: Building Type 5

Table A2.49 – Axial force capacity in compression N_{comp} of columns

Columns	N_{comp} (kN)					
	Storey S1	**Storey S2**	**Storey S3**	**Storey S4**	**Storey S5**	**Storey S6**
C11	-1247.83	-1247.83	-1247.83	-1247.83	-1247.83	-1247.83
C21	-2387.45	-1793.73	-1543.73	-1247.83	-1247.83	-1247.83
C31	-2387.45	-1793.73	-1543.73	-1247.83	-1247.83	-1247.83
C41	-2387.45	-1793.73	-1543.73	-1247.83	-1247.83	-1247.83
C51	-2387.45	-1793.73	-1543.73	-1247.83	-1247.83	-1247.83
C61	-1247.83	-1247.83	-1247.83	-1247.83	-1247.83	-1247.83
C12	-2387.45	-1793.73	-1543.73	-1247.83	-1247.83	-1247.83
C22	-4288.42	-3587.45	-2840.59	-2387.45	-1543.73	-1247.83
C32	-4288.42	-3587.45	-2840.59	-2387.45	-1543.73	-1247.83
C42	-4288.42	-3587.45	-2840.59	-2387.45	-1543.73	-1247.83
C52	-4288.42	-3587.45	-2840.59	-2387.45	-1543.73	-1247.83
C62	-2387.45	-1793.73	-1543.73	-1247.83	-1247.83	-1247.83
C13	-2387.45	-1793.73	-1543.73	-1247.83	-1247.83	-1247.83
C23	-4288.42	-3587.45	-2840.59	-2387.45	-1543.73	-1247.83
C33	-4288.42	-3587.45	-2840.59	-2387.45	-1543.73	-1247.83
C43	-4288.42	-3587.45	-2840.59	-2387.45	-1543.73	-1247.83
C53	-4288.42	-3587.45	-2840.59	-2387.45	-1543.73	-1247.83
C63	-2387.45	-1793.73	-1543.73	-1247.83	-1247.83	-1247.83
C14	-1247.83	-1247.83	-1247.83	-1247.83	-1247.83	-1247.83
C24	-2387.45	-1793.73	-1543.73	-1247.83	-1247.83	-1247.83
C34	-2387.45	-1793.73	-1543.73	-1247.83	-1247.83	-1247.83
C44	-2387.45	-1793.73	-1543.73	-1247.83	-1247.83	-1247.83
C54	-2387.45	-1793.73	-1543.73	-1247.83	-1247.83	-1247.83
C64	-1247.83	-1247.83	-1247.83	-1247.83	-1247.83	-1247.83

Table A2.50 – Axial force capacity in tension N_{tens} of columns

Columns	N_{tens} (kN)					
	Storey S1	**Storey S2**	**Storey S3**	**Storey S4**	**Storey S5**	**Storey S6**
C11	247.83	247.83	247.83	247.83	247.83	247.83
C21	587.45	293.73	293.73	247.83	247.83	247.83
C31	587.45	293.73	293.73	247.83	247.83	247.83
C41	587.45	293.73	293.73	247.83	247.83	247.83
C51	587.45	293.73	293.73	247.83	247.83	247.83
C61	247.83	247.83	247.83	247.83	247.83	247.83
C12	587.45	293.73	293.73	247.83	247.83	247.83
C22	688.42	587.45	440.59	587.45	293.73	247.83
C32	688.42	587.45	440.59	587.45	293.73	247.83
C42	688.42	587.45	440.59	587.45	293.73	247.83
C52	688.42	587.45	440.59	587.45	293.73	247.83
C62	587.45	293.73	293.73	247.83	247.83	247.83
C13	587.45	293.73	293.73	247.83	247.83	247.83
C23	688.42	587.45	440.59	587.45	293.73	247.83
C33	688.42	587.45	440.59	587.45	293.73	247.83
C43	688.42	587.45	440.59	587.45	293.73	247.83
C53	688.42	587.45	440.59	587.45	293.73	247.83
C63	587.45	293.73	293.73	247.83	247.83	247.83
C14	247.83	247.83	247.83	247.83	247.83	247.83
C24	587.45	293.73	293.73	247.83	247.83	247.83
C34	587.45	293.73	293.73	247.83	247.83	247.83
C44	587.45	293.73	293.73	247.83	247.83	247.83
C54	587.45	293.73	293.73	247.83	247.83	247.83
C64	247.83	247.83	247.83	247.83	247.83	247.83

AXIAL FORCE CAPACITY ENVELOPE: Building Type 6

Table A2.51 – Axial force capacity in compression N_{comp} of columns

Columns	N_{comp} (kN)	
	Storey S1	**Storey S2**
C11	-1247.83	-1247.83
C21	-1247.83	-1247.83
C31	-1247.83	-1247.83
C41	-1247.83	-1247.83
C51	-1247.83	-1247.83
C12	-1247.83	-1247.83
C22	-1543.73	-1247.83
C32	-1543.73	-1247.83
C42	-1543.73	-1247.83
C52	-1247.83	-1247.83
C13	-1247.83	-1247.83
C23	-1247.83	-1247.83
C33	-1247.83	-1247.83
C43	-1247.83	-1247.83
C53	-1247.83	-1247.83

Table A2.52 – Axial force capacity in tension N_{tens} of columns

Columns	N_{tens} (kN)	
	Storey S1	**Storey S2**
C11	247.83	247.83
C21	247.83	247.83
C31	247.83	247.83
C41	247.83	247.83
C51	247.83	247.83
C12	247.83	247.83
C22	293.73	247.83
C32	293.73	247.83
C42	293.73	247.83
C52	247.83	247.83
C13	247.83	247.83
C23	247.83	247.83
C33	247.83	247.83
C43	247.83	247.83
C53	247.83	247.83

AXIAL FORCE CAPACITY ENVELOPE: Building Type 7

Table A2.53 – Axial force capacity in compression N_{comp} of columns

Columns	N_{comp} (kN)		
	Storey S1	**Storey S2**	**Storey S3**
C11	-1247.83	-1247.83	-1247.83
C21	-1247.83	-1247.83	-1247.83
C31	-1247.83	-1247.83	-1247.83
C41	-1247.83	-1247.83	-1247.83
C51	-1247.83	-1247.83	-1247.83
C12	-1247.83	-1247.83	-1247.83
C22	-2387.45	-1543.73	-1247.83
C32	-2387.45	-1543.73	-1247.83
C42	-2387.45	-1543.73	-1247.83
C52	-1247.83	-1247.83	-1247.83
C13	-1247.83	-1247.83	-1247.83
C23	-1247.83	-1247.83	-1247.83
C33	-1247.83	-1247.83	-1247.83
C43	-1247.83	-1247.83	-1247.83
C53	-1247.83	-1247.83	-1247.83

Table A2.54 – Axial force capacity in tension N_{tens} of columns

Columns	N_{tens} (kN)		
	Storey S1	**Storey S2**	**Storey S3**
C11	247.83	247.83	247.83
C21	247.83	247.83	247.83
C31	247.83	247.83	247.83
C41	247.83	247.83	247.83
C51	247.83	247.83	247.83
C12	247.83	247.83	247.83
C22	587.45	293.73	247.83
C32	587.45	293.73	247.83
C42	587.45	293.73	247.83
C52	247.83	247.83	247.83
C13	247.83	247.83	247.83
C23	247.83	247.83	247.83
C33	247.83	247.83	247.83
C43	247.83	247.83	247.83
C53	247.83	247.83	247.83

AXIAL FORCE CAPACITY ENVELOPE: Building Type 8

Table A2.55 – Axial force capacity in compression N_{comp} of columns

Columns	N_{comp} (kN)			
	Storey S1	**Storey S2**	**Storey S3**	**Storey S4**
C11	-1247.83	-1247.83	-1247.83	-1247.83
C21	-1543.73	-1247.83	-1247.83	-1247.83
C31	-1543.73	-1247.83	-1247.83	-1247.83
C41	-1543.73	-1247.83	-1247.83	-1247.83
C51	-1247.83	-1247.83	-1247.83	-1247.83
C12	-1543.73	-1247.83	-1247.83	-1247.83
C22	-2840.59	-2387.45	-1543.73	-1247.83
C32	-2840.59	-2387.45	-1543.73	-1247.83
C42	-2840.59	-2387.45	-1543.73	-1247.83
C52	-1543.73	-1247.83	-1247.83	-1247.83
C13	-1247.83	-1247.83	-1247.83	-1247.83
C23	-1543.73	-1247.83	-1247.83	-1247.83
C33	-1543.73	-1247.83	-1247.83	-1247.83
C43	-1543.73	-1247.83	-1247.83	-1247.83
C53	-1247.83	-1247.83	-1247.83	-1247.83

Table A2.56 – Axial force capacity in tension N_{tens} of columns

Columns	N_{tens} (kN)			
	Storey S1	**Storey S2**	**Storey S3**	**Storey S4**
C11	247.83	247.83	247.83	247.83
C21	293.73	247.83	247.83	247.83
C31	293.73	247.83	247.83	247.83
C41	293.73	247.83	247.83	247.83
C51	247.83	247.83	247.83	247.83
C12	293.73	247.83	247.83	247.83
C22	440.59	587.45	293.73	247.83
C32	440.59	587.45	293.73	247.83
C42	440.59	587.45	293.73	247.83
C52	293.73	247.83	247.83	247.83
C13	247.83	247.83	247.83	247.83
C23	293.73	247.83	247.83	247.83
C33	293.73	247.83	247.83	247.83
C43	293.73	247.83	247.83	247.83
C53	247.83	247.83	247.83	247.83

AXIAL FORCE CAPACITY ENVELOPE: Building Type 9

Table A2.57 – Axial force capacity in compression N_{comp} of columns

Columns	N_{comp} (kN)				
	Storey S1	**Storey S2**	**Storey S3**	**Storey S4**	**Storey S5**
C11	-1247.83	-1247.83	-1247.83	-1247.83	-1247.83
C21	-1793.73	-1543.73	-1247.83	-1247.83	-1247.83
C31	-1793.73	-1543.73	-1247.83	-1247.83	-1247.83
C41	-1793.73	-1543.73	-1247.83	-1247.83	-1247.83
C51	-1247.83	-1247.83	-1247.83	-1247.83	-1247.83
C12	-1793.73	-1543.73	-1247.83	-1247.83	-1247.83
C22	-3587.45	-2840.59	-2387.45	-1543.73	-1247.83
C32	-3587.45	-2840.59	-2387.45	-1543.73	-1247.83
C42	-3587.45	-2840.59	-2387.45	-1543.73	-1247.83
C52	-1793.73	-1543.73	-1247.83	-1247.83	-1247.83
C13	-1247.83	-1247.83	-1247.83	-1247.83	-1247.83
C23	-1793.73	-1543.73	-1247.83	-1247.83	-1247.83
C33	-1793.73	-1543.73	-1247.83	-1247.83	-1247.83
C43	-1793.73	-1543.73	-1247.83	-1247.83	-1247.83
C53	-1247.83	-1247.83	-1247.83	-1247.83	-1247.83

Table A2.58 – Axial force capacity in tension N_{tens} of columns

Columns	N_{tens} (kN)				
	Storey S1	**Storey S2**	**Storey S3**	**Storey S4**	**Storey S5**
C11	247.83	247.83	247.83	247.83	247.83
C21	293.73	293.73	247.83	247.83	247.83
C31	293.73	293.73	247.83	247.83	247.83
C41	293.73	293.73	247.83	247.83	247.83
C51	247.83	247.83	247.83	247.83	247.83
C12	293.73	293.73	247.83	247.83	247.83
C22	587.45	440.59	587.45	293.73	247.83
C32	587.45	440.59	587.45	293.73	247.83
C42	587.45	440.59	587.45	293.73	247.83
C52	293.73	293.73	247.83	247.83	247.83
C13	247.83	247.83	247.83	247.83	247.83
C23	293.73	293.73	247.83	247.83	247.83
C33	293.73	293.73	247.83	247.83	247.83
C43	293.73	293.73	247.83	247.83	247.83
C53	247.83	247.83	247.83	247.83	247.83

AXIAL FORCE CAPACITY ENVELOPE: Building Type 10

Table A2.59 – Axial force capacity in compression N_{comp} of columns

Columns	N_{comp} (kN)					
	Storey S1	**Storey S2**	**Storey S3**	**Storey S4**	**Storey S5**	**Storey S6**
C11	-1247.83	-1247.83	-1247.83	-1247.83	-1247.83	-1247.83
C21	-2387.45	-1793.73	-1543.73	-1247.83	-1247.83	-1247.83
C31	-2387.45	-1793.73	-1543.73	-1247.83	-1247.83	-1247.83
C41	-2387.45	-1793.73	-1543.73	-1247.83	-1247.83	-1247.83
C51	-1247.83	-1247.83	-1247.83	-1247.83	-1247.83	-1247.83
C12	-2387.45	-1793.73	-1543.73	-1247.83	-1247.83	-1247.83
C22	-4288.42	-3587.45	-2840.59	-2387.45	-1543.73	-1247.83
C32	-4288.42	-3587.45	-2840.59	-2387.45	-1543.73	-1247.83
C42	-4288.42	-3587.45	-2840.59	-2387.45	-1543.73	-1247.83
C52	-2387.45	-1793.73	-1543.73	-1247.83	-1247.83	-1247.83
C13	-1247.83	-1247.83	-1247.83	-1247.83	-1247.83	-1247.83
C23	-2387.45	-1793.73	-1543.73	-1247.83	-1247.83	-1247.83
C33	-2387.45	-1793.73	-1543.73	-1247.83	-1247.83	-1247.83
C43	-2387.45	-1793.73	-1543.73	-1247.83	-1247.83	-1247.83
C53	-1247.83	-1247.83	-1247.83	-1247.83	-1247.83	-1247.83

Table A2.60 – Axial force capacity in tension N_{tens} of columns

Columns	N_{tens} (kN)					
	Storey S1	**Storey S2**	**Storey S3**	**Storey S4**	**Storey S5**	**Storey S6**
C11	247.83	247.83	247.83	247.83	247.83	247.83
C21	587.45	293.73	293.73	247.83	247.83	247.83
C31	587.45	293.73	293.73	247.83	247.83	247.83
C41	587.45	293.73	293.73	247.83	247.83	247.83
C51	247.83	247.83	247.83	247.83	247.83	247.83
C12	587.45	293.73	293.73	247.83	247.83	247.83
C22	688.42	587.45	440.59	587.45	293.73	247.83
C32	688.42	587.45	440.59	587.45	293.73	247.83
C42	688.42	587.45	440.59	587.45	293.73	247.83
C52	587.45	293.73	293.73	247.83	247.83	247.83
C13	247.83	247.83	247.83	247.83	247.83	247.83
C23	587.45	293.73	293.73	247.83	247.83	247.83
C33	587.45	293.73	293.73	247.83	247.83	247.83
C43	587.45	293.73	293.73	247.83	247.83	247.83
C53	247.83	247.83	247.83	247.83	247.83	247.83

APPENDIX 3

PRE-CODE RC BUILDINGS – PERFORMANCE EVALUATION

APPENDIX 3 – PRE-CODE RC BUILDINGS – PERFORMANCE EVALUATION

BUILDING TYPE 1: 2 storeys, 3×5 spans

Seismic hazard scenario 1: PT 1.6 + 2.5 (EC8-1)

Seismic hazard scenario 2: PT 1.5 + 2.4 (EC8-1)

Seismic hazard scenario 3: PT 1.3 + 2.3 (EC8-1)

Seismic hazard scenario 4: PT 1.1 + 2.3 (EC8-1)

BUILDING TYPE 2: 3 storeys, 3×5 spans

Id

BUILDING TYPE 3: 4 storeys, 3×5 spans

Id

BUILDING TYPE 4: 5 storeys, 3×5 spans

Id

BUILDING TYPE 5: 6 storeys, 3×5 spans

Id

BUILDING TYPE 6: 2 storeys, 2×4 spans

Id

BUILDING TYPE 7: 3 storeys, 2×4 spans

Id

BUILDING TYPE 8: 4 storeys, 2×4 spans

Id

BUILDING TYPE 9: 5 storeys, 2×4 spans

Id

BUILDING TYPE 10: 6 storeys, 2×4 spans

Id

BUILDING TYPE 1: 2 storeys, 3×5 spans **| SEISMIC HAZARD SCENARIO 1:** PT 1.6 + 2.5 (EC8-1)

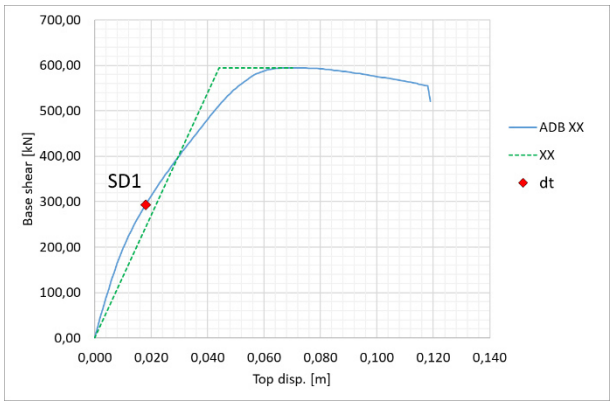

Figure A3.1 – Capacity curve and target displacement d_t, direction XX (S1_AST2_2S_3×5_XX)

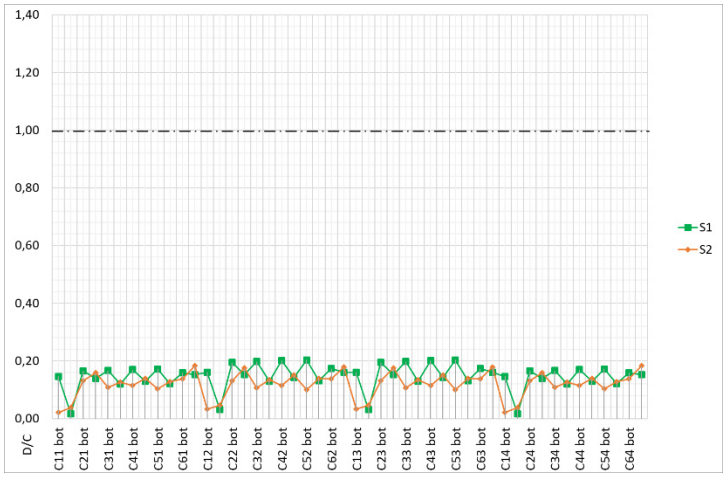

Figure A3.2 – Chord rotation D/C ratios (SD), direction XX (S1_AST2_2S_3×5_XX)

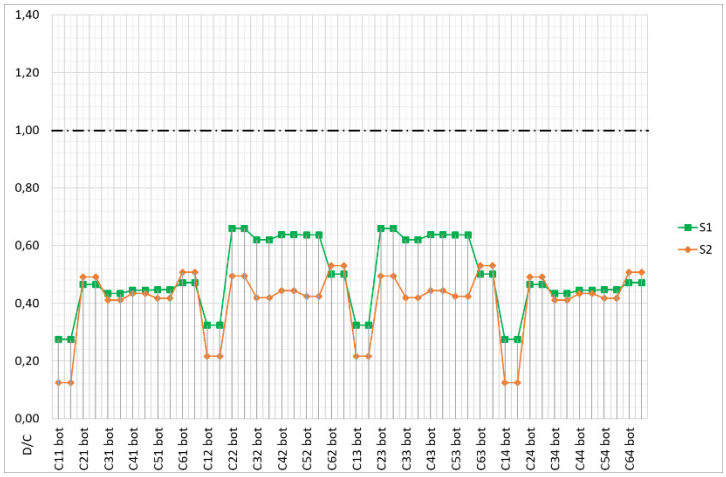

Figure A3.3 – Shear force D/C ratios (SD), direction XX (S1_AST2_2S_3×5_XX)

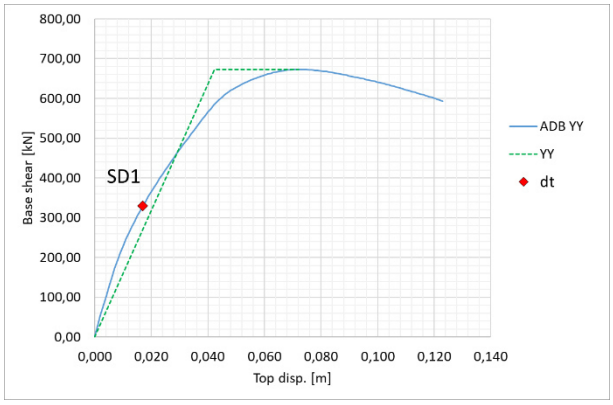

Figure A3.4 – Capacity curve and target displacement d_t, direction YY (S1_AST2_2S_3×5_YY)

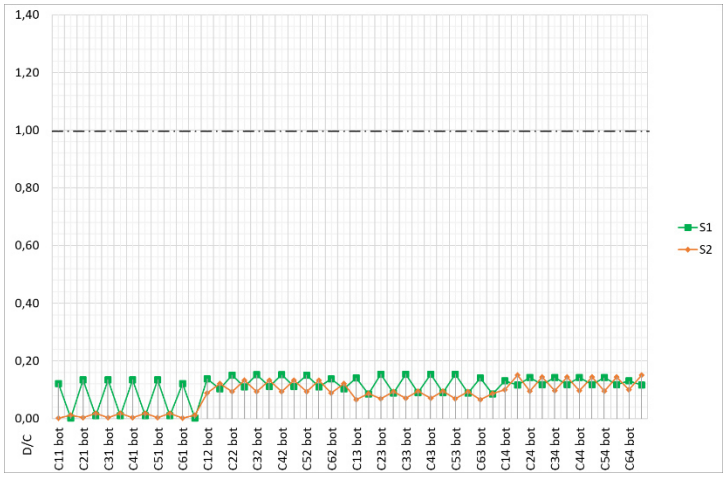

Figure A3.5 – Chord rotation D/C ratios (SD), direction YY (S1_AST2_2S_3×5_YY)

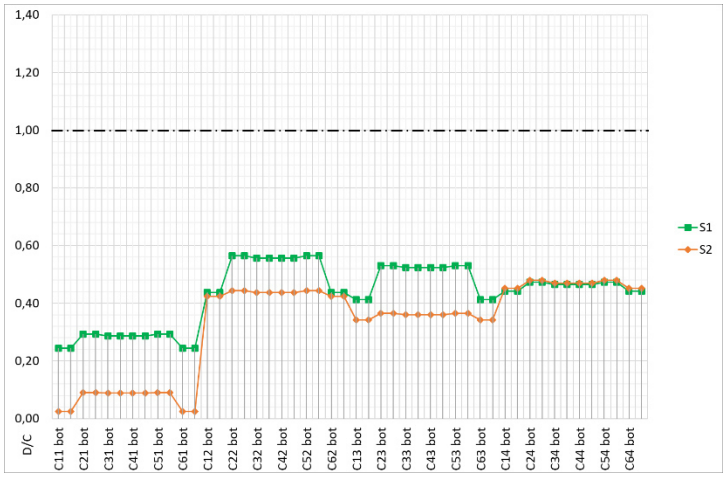

Figure A3.6 – Shear force D/C ratios (SD), direction YY (S1_AST2_2S_3×5_YY)

BUILDING TYPE 1: 2 storeys, 3×5 spans **| SEISMIC HAZARD SCENARIO 2:** PT 1.5 + 2.4 (EC8-1)

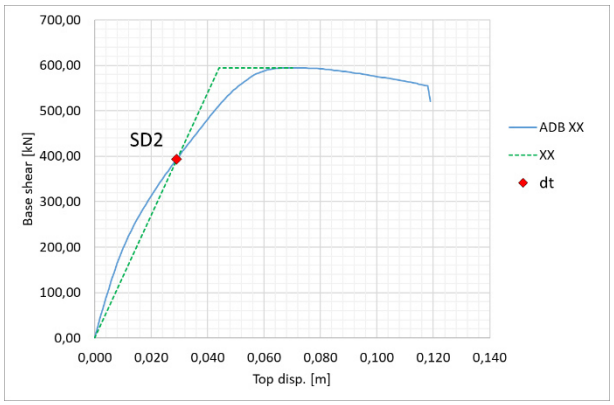

Figure A3.7 – Capacity curve and target displacement d_t, direction XX (S2_AST1_2S_3×5_XX)

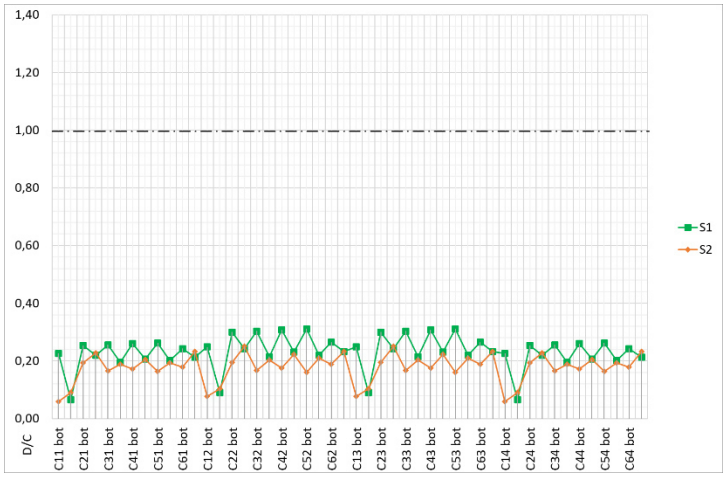

Figure A3.8 – Chord rotation D/C ratios (SD), direction XX (S2_AST1_2S_3×5_XX)

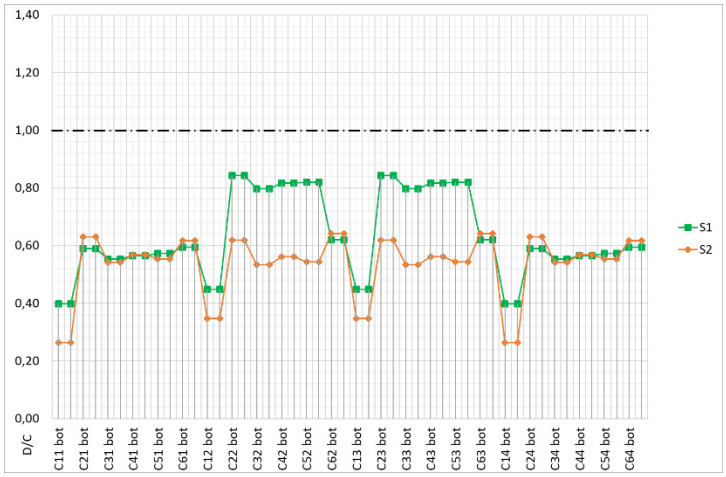

Figure A3.9 – Shear force D/C ratios (SD), direction XX (S2_AST1_2S_3×5_XX)

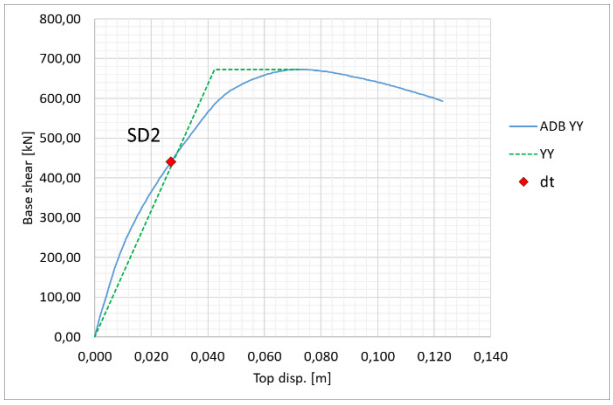

Figure A3.10 – Capacity curve and target displacement d_t, direction YY (S2_AST1_2S_3×5_YY)

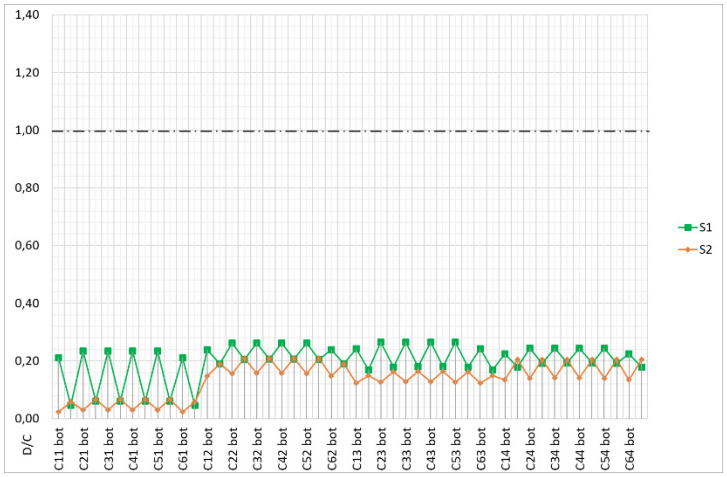

Figure A3.11 – Chord rotation D/C ratios (SD), direction YY (S2_AST1_2S_3×5_YY)

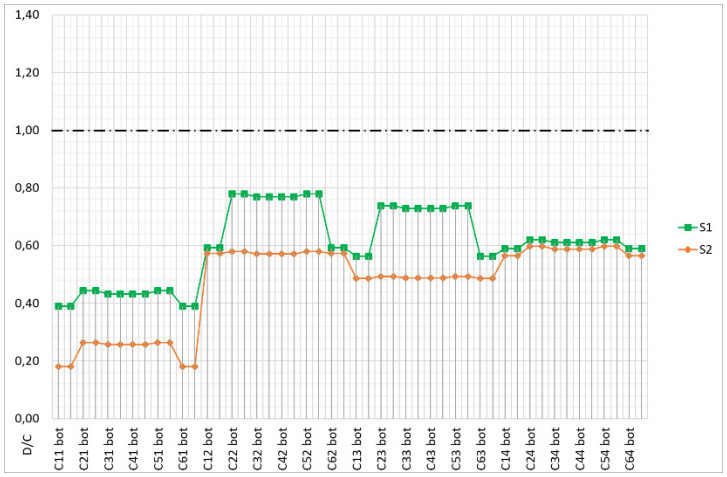

Figure A3.12 – Shear force D/C ratios (SD), direction YY (S2_AST1_2S_3×5_YY)

BUILDING TYPE 1: 2 storeys, 3×5 spans **| SEISMIC HAZARD SCENARIO 3:** PT 1.3 + 2.3 (EC8-1)

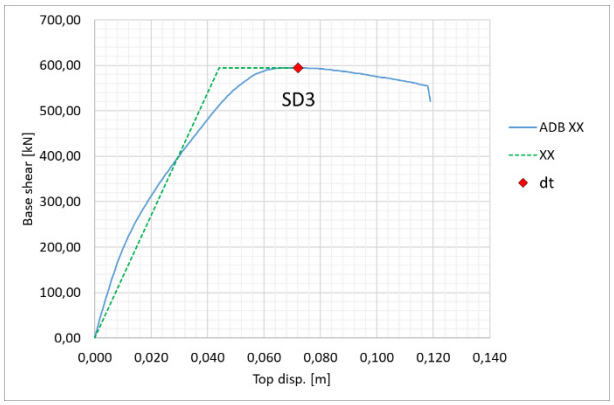

Figure A3.13 – Capacity curve and target displacement d_t, direction XX (S3_AST1_2S_3×5_XX)

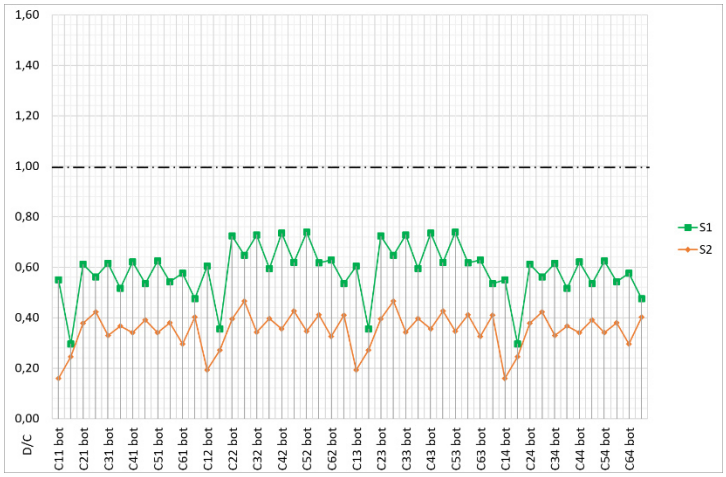

Figure A3.14 – Chord rotation D/C ratios (SD), direction XX (S3_AST1_2S_3×5_XX)

Figure A3.15 – Shear force D/C ratios (SD), direction XX (S3_AST1_2S_3×5_XX)

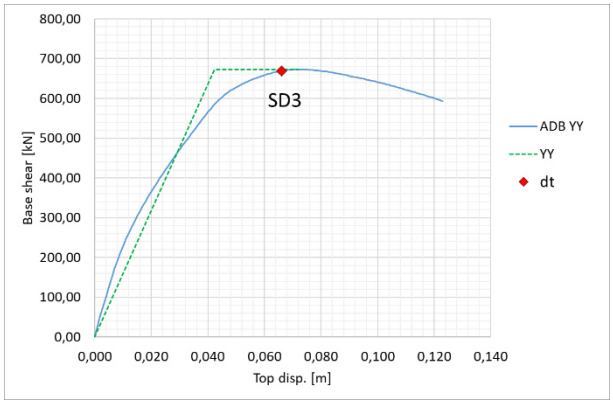

Figure A3.16 – Capacity curve and target displacement d_t, direction YY (S3_AST1_2S_3×5_YY)

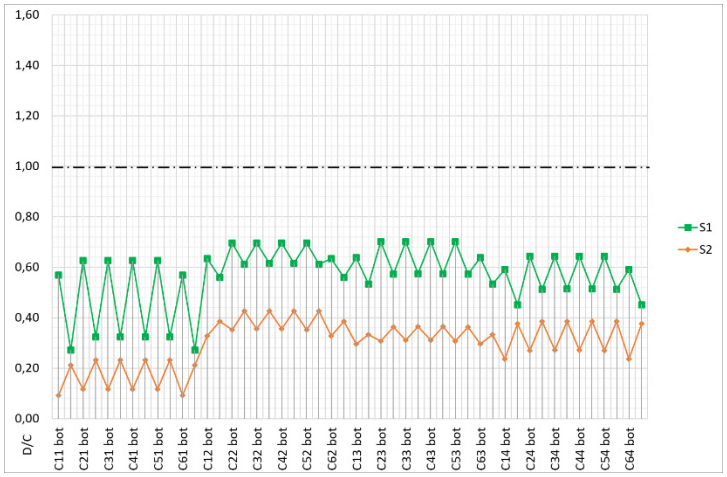

Figure A3.17 – Chord rotation D/C ratios (SD), direction YY (S3_AST1_2S_3×5_YY)

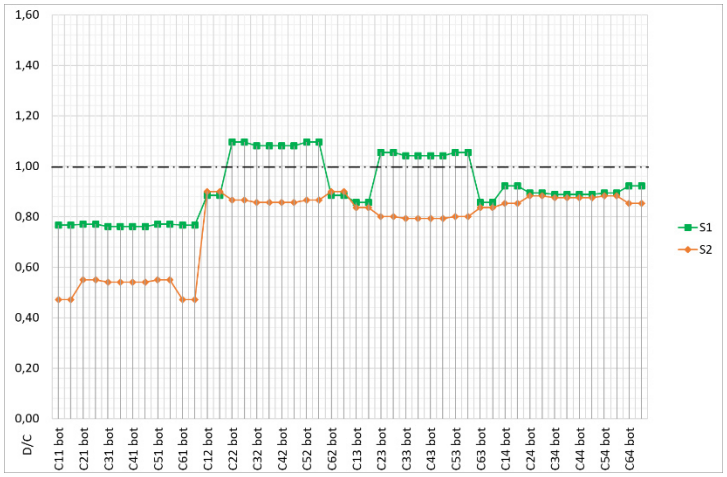

Figure A3.18 – Shear force D/C ratios (SD), direction YY (S3_AST1_2S_3×5_YY)

BUILDING TYPE 1: 2 storeys, 3×5 spans **| SEISMIC HAZARD SCENARIO 4:** PT 1.1 + 2.3 (EC8-1)

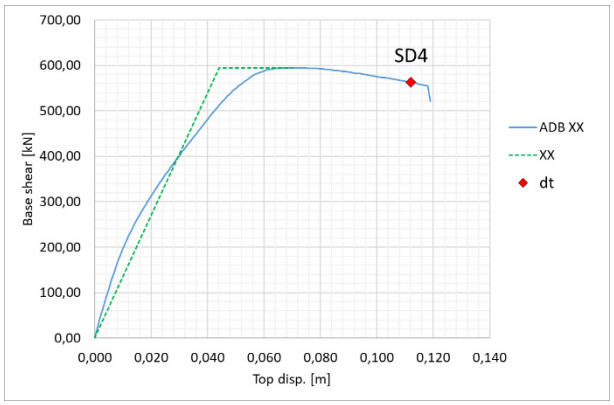

Figure A3.19 – Capacity curve and target displacement d_t, direction XX (S4_AST1_2S_3×5_XX)

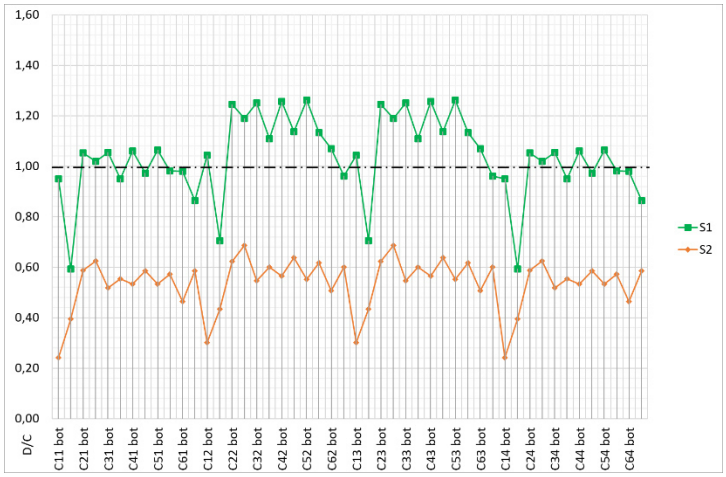

Figure A3.20 – Chord rotation D/C ratios (SD), direction XX (S4_AST1_2S_3×5_XX)

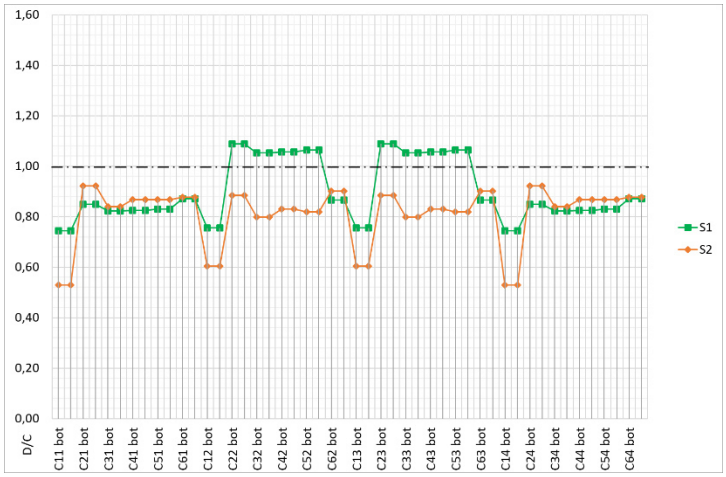

Figure A3.21 – Shear force D/C ratios (SD), direction XX (S4_AST1_2S_3×5_XX)

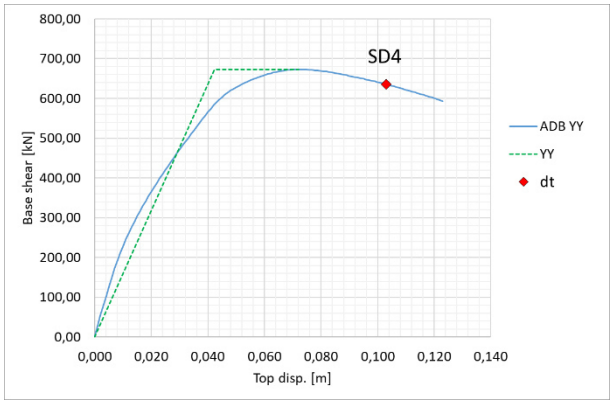

Figure A3.22 – Capacity curve and target displacement d_t, direction YY (S4_AST1_2S_3×5_YY)

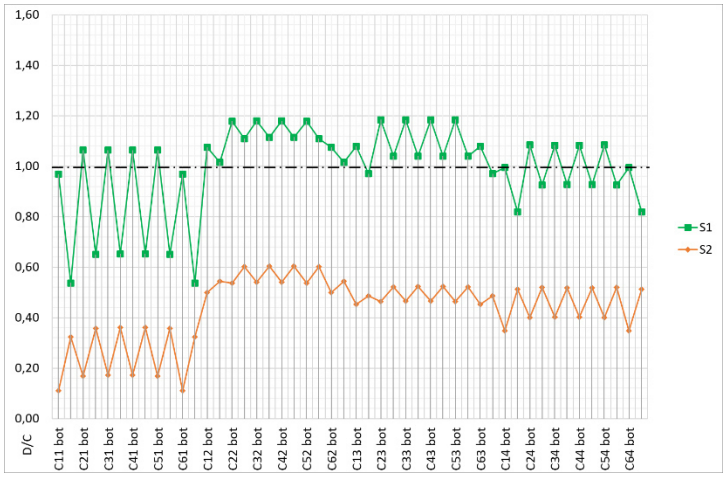

Figure A3.23 – Chord rotation D/C ratios (SD), direction YY (S4_AST1_2S_3×5_YY)

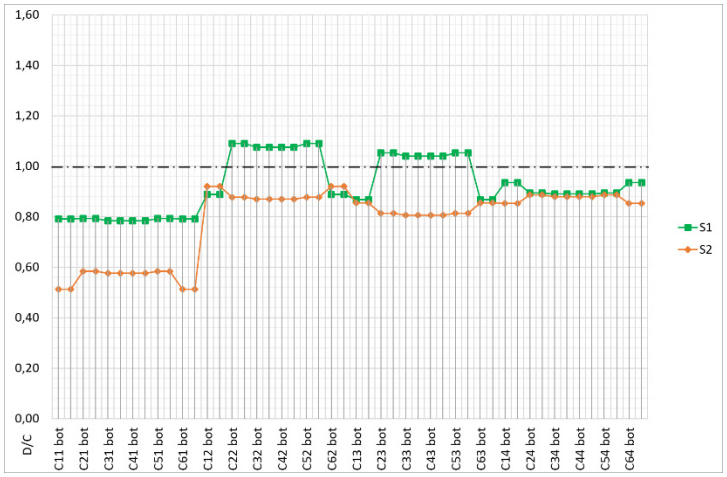

Figure A3.24 – Shear force D/C ratios (SD), direction YY (S4_AST1_2S_3×5_YY)

BUILDING TYPE 2: 3 storeys, 3×5 spans **| SEISMIC HAZARD SCENARIO 1:** PT 1.6 + 2.5 (EC8-1)

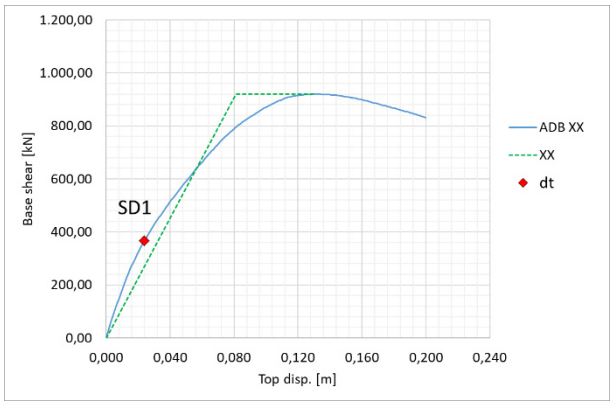

Figure A3.25 – Capacity curve and target displacement d_t, direction XX (S1_AST2_3S_3×5_XX)

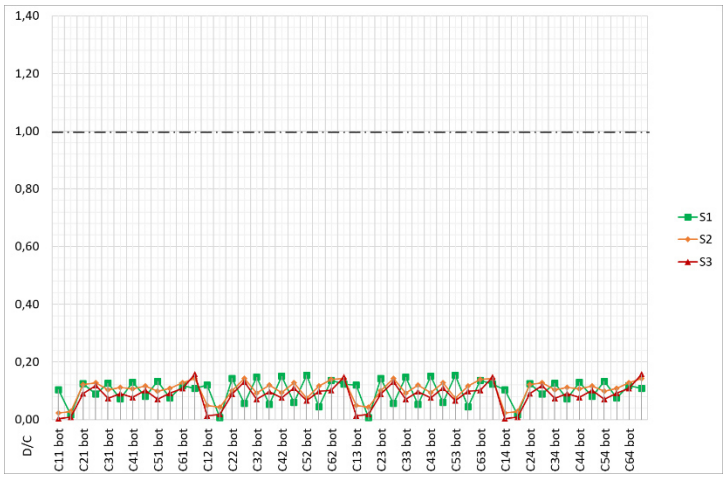

Figure A3.26 – Chord rotation D/C ratios (SD), direction XX (S1_AST2_3S_3×5_XX)

Figure A3.27 – Shear force D/C ratios (SD), direction XX (S1_AST2_3S_3×5_XX)

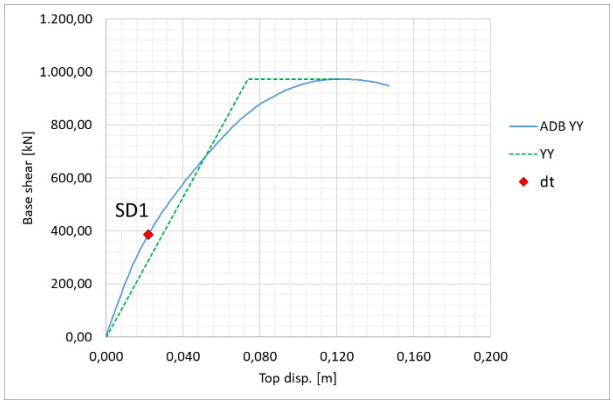

Figure A3.28 – Capacity curve and target displacement d_t, direction YY (S1_AST2_3S_3×5_YY)

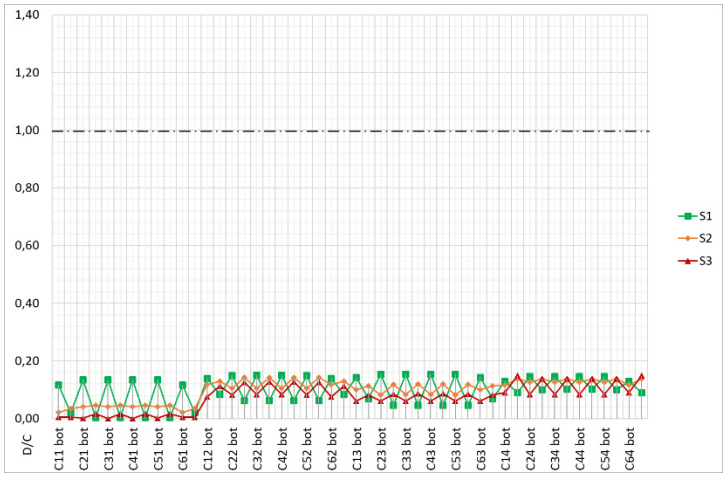

Figure A3.29 – Chord rotation D/C ratios (SD), direction YY (S1_AST2_3S_3×5_YY)

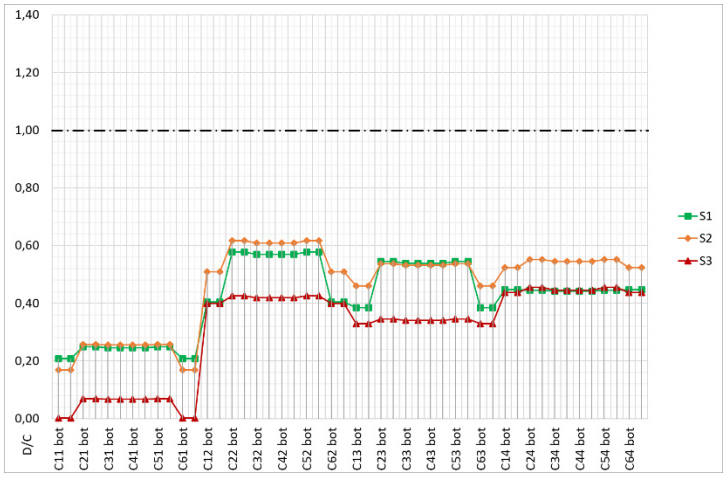

Figure A3.30 – Shear force D/C ratios (SD), direction YY (S1_AST2_3S_3×5_YY)

BUILDING TYPE 2: 3 storeys, 3×5 spans **| SEISMIC HAZARD SCENARIO 2:** PT 1.5 + 2.4 (EC8-1)

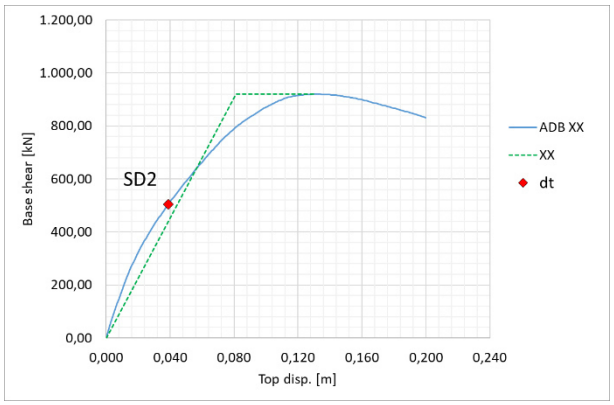

Figure A3.31 – Capacity curve and target displacement d_t, direction XX (S2_AST1_3S_3×5_XX)

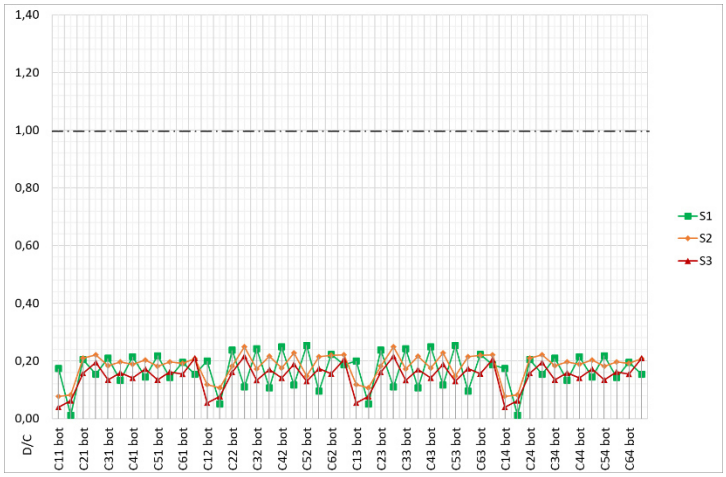

Figure A3.32 – Chord rotation D/C ratios (SD), direction XX (S2_AST1_3S_3×5_XX)

Figure A3.33 – Shear force D/C ratios (SD), direction XX (S2_AST1_3S_3×5_XX)

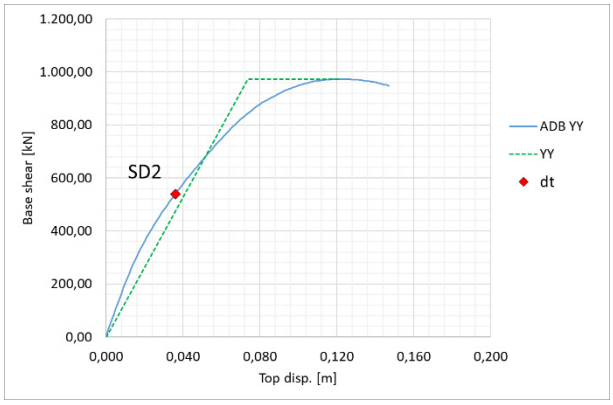

Figure A3.34 – Capacity curve and target displacement d_t, direction YY (S2_AST1_3S_3×5_YY)

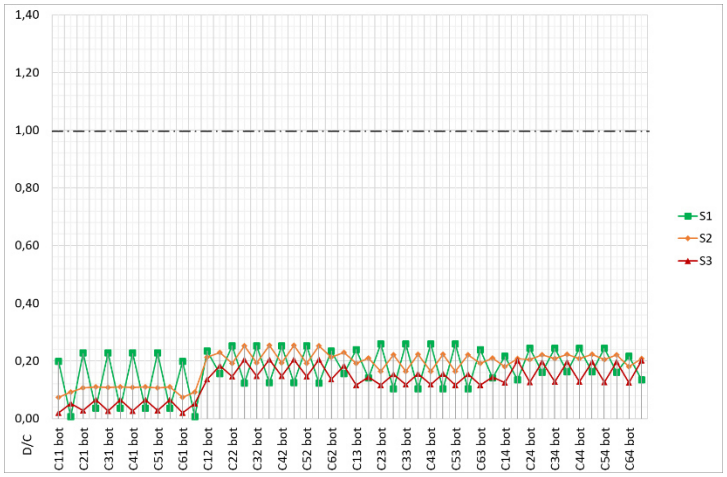

Figure A3.35 – Chord rotation D/C ratios (SD), direction YY (S2_AST1_3S_3×5_YY)

Figure A3.36 – Shear force D/C ratios (SD), direction YY (S2_AST1_3S_3×5_YY)

BUILDING TYPE 2: 3 storeys, 3×5 spans **| SEISMIC HAZARD SCENARIO 3:** PT 1.3 + 2.3 (EC8-1)

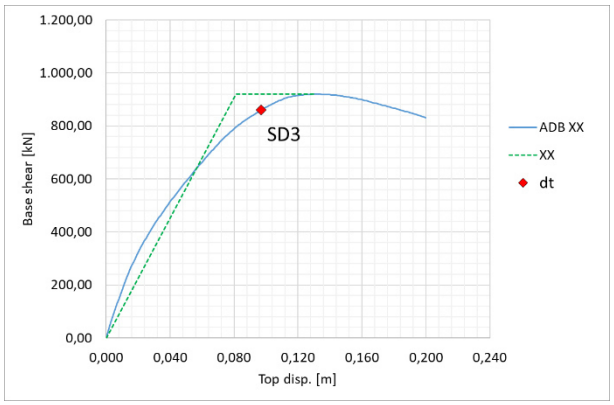

Figure A3.37 – Capacity curve and target displacement d_t, direction XX (S3_AST1_3S_3×5_XX)

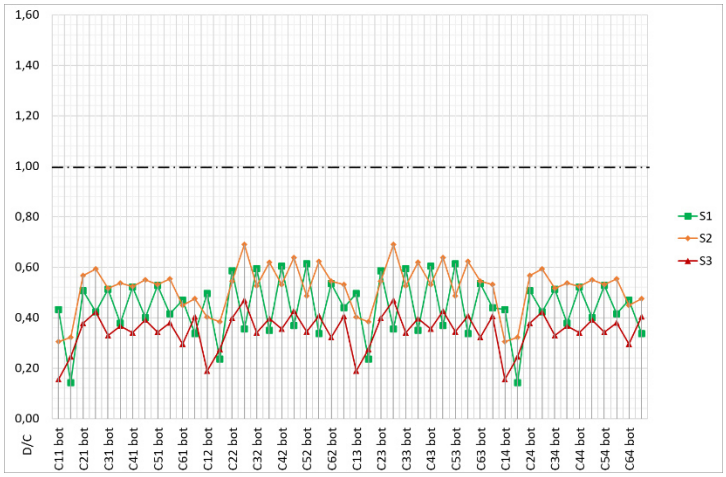

Figure A3.38 – Chord rotation D/C ratios (SD), direction XX (S3_AST1_3S_3×5_XX)

Figure A3.39 – Shear force D/C ratios (SD), direction XX (S3_AST1_3S_3×5_XX)

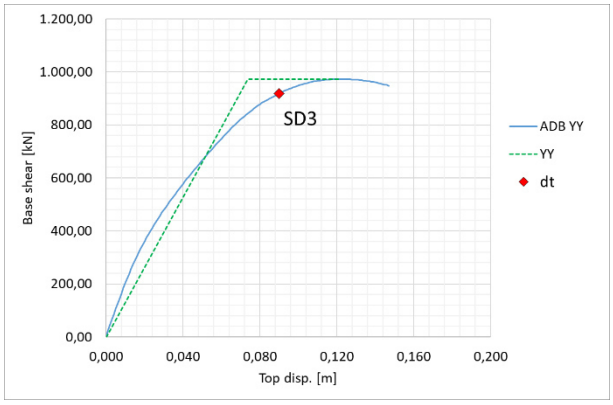

Figure A3.40 – Capacity curve and target displacement d_t, direction YY (S3_AST1_3S_3×5_YY)

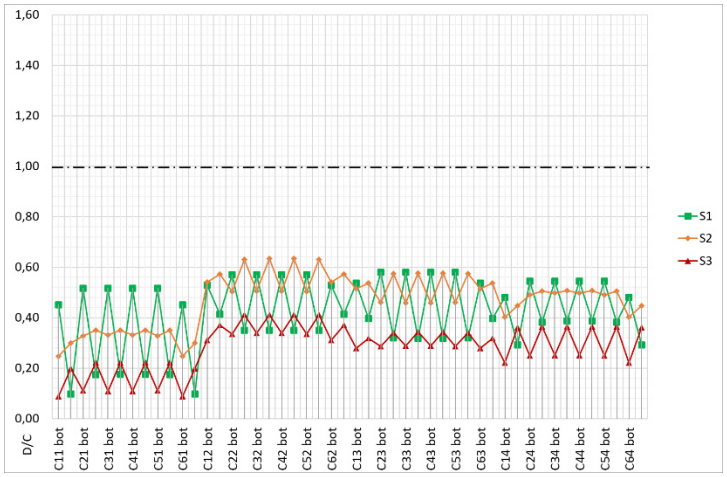

Figure A3.41 – Chord rotation D/C ratios (SD), direction YY (S3_AST1_3S_3×5_YY)

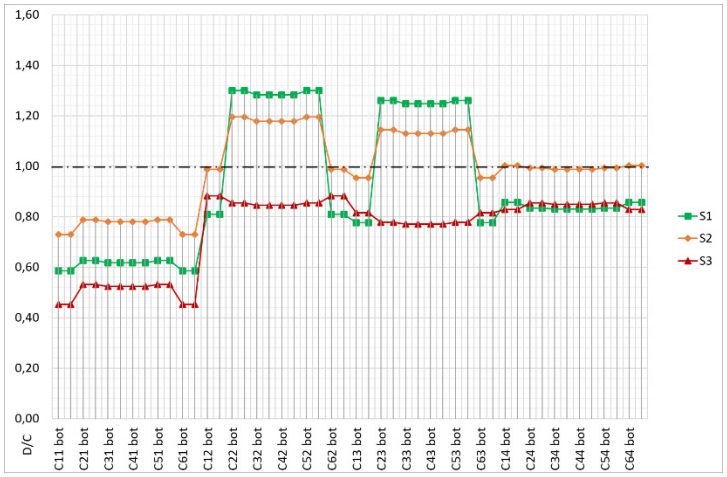

Figure A3.42 – Shear force D/C ratios (SD), direction YY (S3_AST1_3S_3×5_YY)

BUILDING TYPE 2: 3 storeys, 3×5 spans **| SEISMIC HAZARD SCENARIO 4:** PT 1.1 + 2.3 (EC8-1)

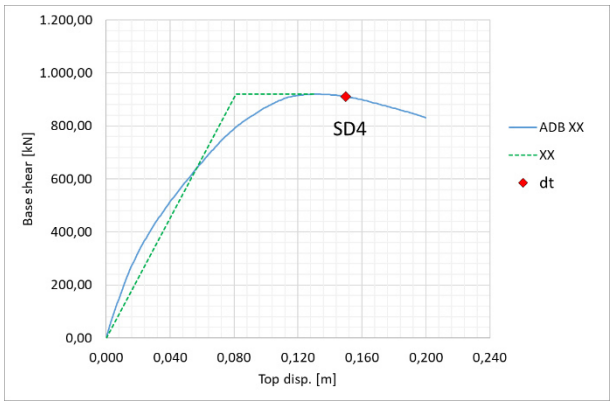

Figure A3.43 – Capacity curve and target displacement d_t, direction XX (S4_AST1_3S_3×5_XX)

Figure A3.44 – Chord rotation D/C ratios (SD), direction XX (S4_AST1_3S_3×5_XX)

Figure A3.45 – Shear force D/C ratios (SD), direction XX (S4_AST1_3S_3×5_XX)

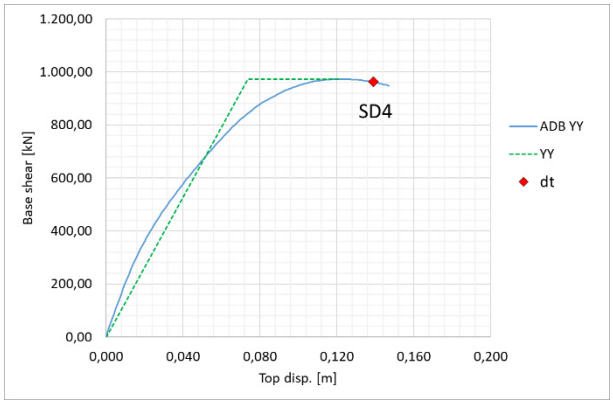

Figure A3.46 – Capacity curve and target displacement d_t, direction YY (S4_AST1_3S_3×5_YY)

Figure A3.47 – Chord rotation D/C ratios (SD), direction YY (S4_AST1_3S_3×5_YY)

Figure A3.48 – Shear force D/C ratios (SD), direction YY (S4_AST1_3S_3×5_YY)

BUILDING TYPE 3: 4 storeys, 3×5 spans **| SEISMIC HAZARD SCENARIO 1:** PT 1.6 + 2.5 (EC8-1)

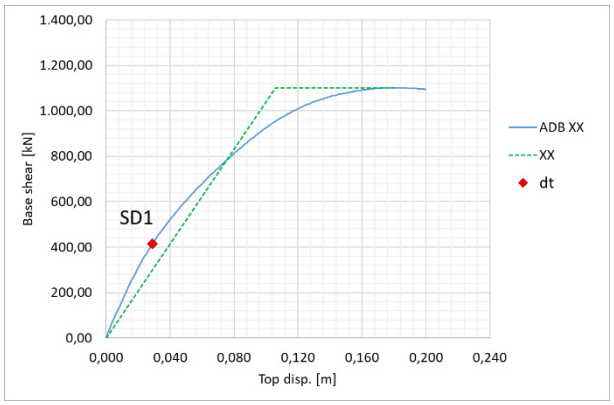

Figure A3.49 – Capacity curve and target displacement d_t, direction XX (S1_AST2_4S_3×5_XX)

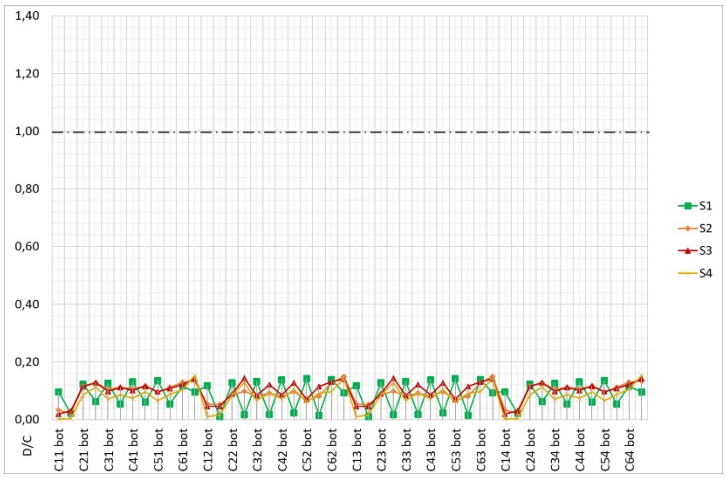

Figure A3.50 – Chord rotation D/C ratios (SD), direction XX (S1_AST2_4S_3×5_XX)

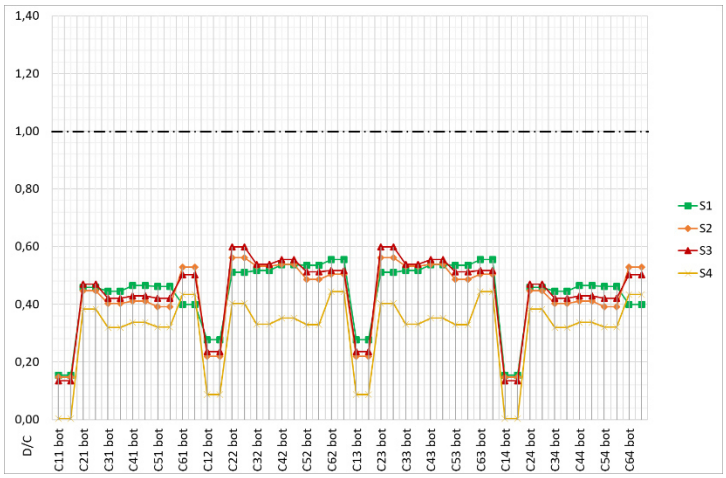

Figure A3.51 – Shear force D/C ratios (SD), direction XX (S1_AST2_4S_3×5_XX)

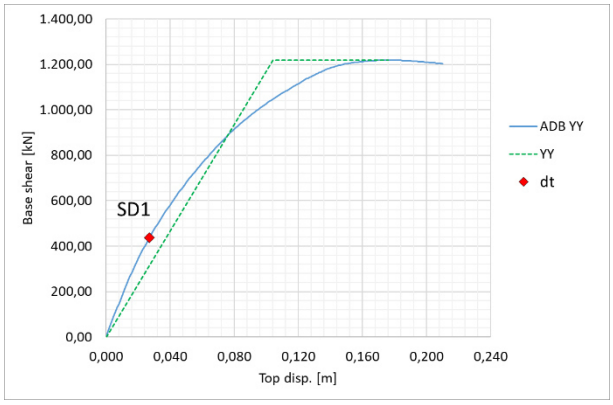

Figure A3.52 – Capacity curve and target displacement d_t, direction YY (S1_AST2_4S_3×5_YY)

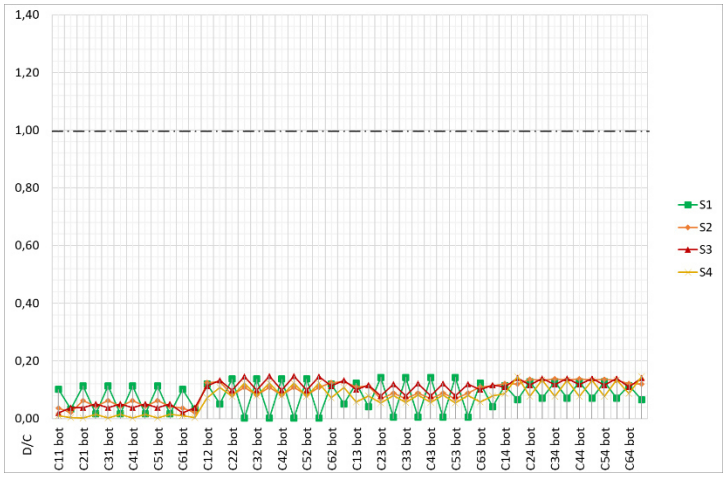

Figure A3.53 – Chord rotation D/C ratios (SD), direction YY (S1_AST2_4S_3×5_YY)

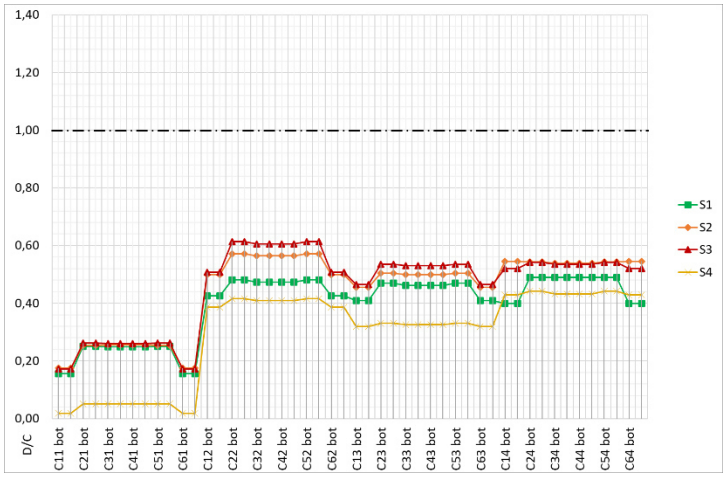

Figure A3.54 – Shear force D/C ratios (SD), direction YY (S1_AST2_4S_3×5_YY)

BUILDING TYPE 3: 4 storeys, 3×5 spans **| SEISMIC HAZARD SCENARIO 2:** PT 1.5 + 2.4 (EC8-1)

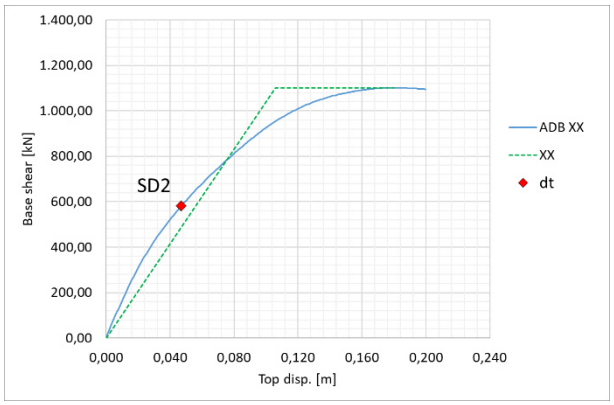

Figure A3.55 – Capacity curve and target displacement d_t, direction XX (S2_AST1_4S_3×5_XX)

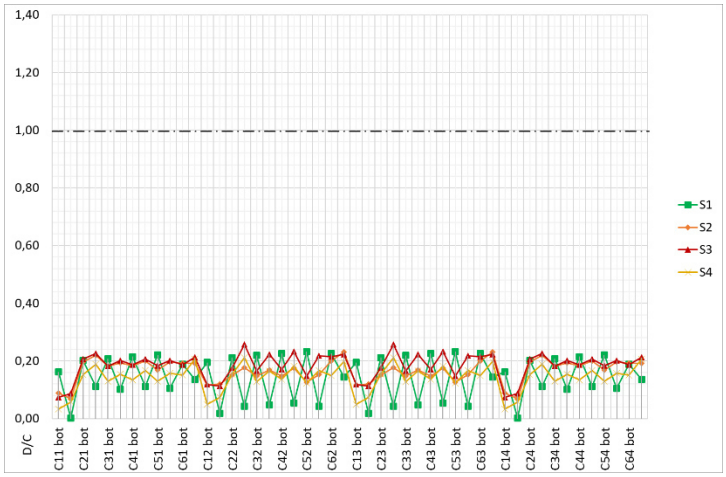

Figure A3.56 – Chord rotation D/C ratios (SD), direction XX (S2_AST1_4S_3×5_XX)

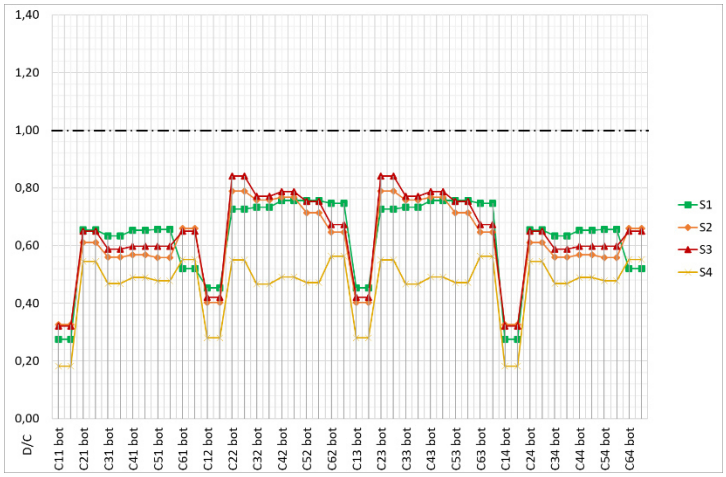

Figure A3.57 – Shear force D/C ratios (SD), direction XX (S2_AST1_4S_3×5_XX)

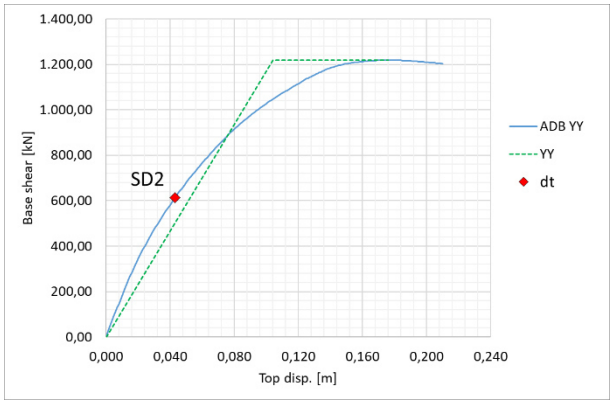

Figure A3.58 – Capacity curve and target displacement d_t, direction YY (S2_AST1_4S_3×5_YY)

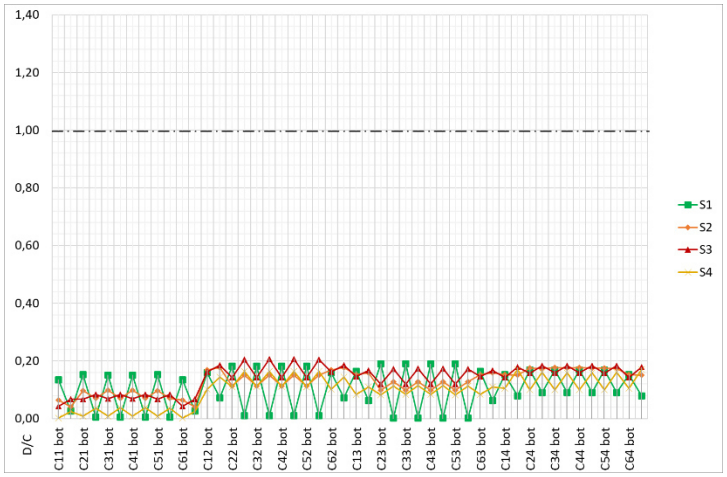

Figure A3.59 – Chord rotation D/C ratios (SD), direction YY (S2_AST1_4S_3×5_YY)

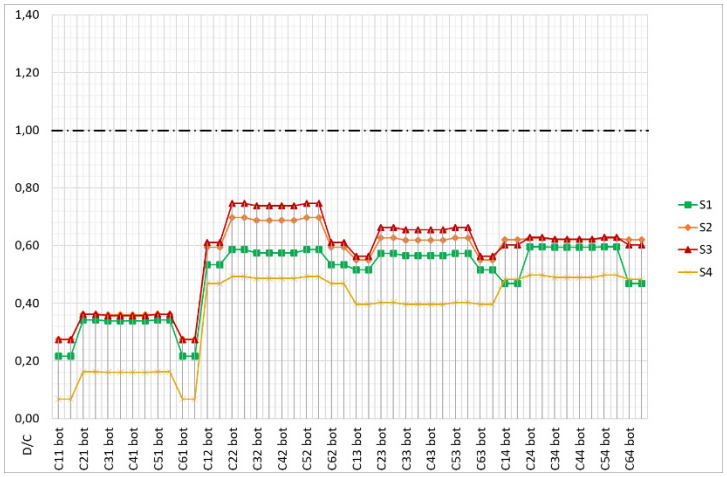

Figure A3.60 – Shear force D/C ratios (SD), direction YY (S2_AST1_4S_3×5_YY)

BUILDING TYPE 3: 4 storeys, 3×5 spans **| SEISMIC HAZARD SCENARIO 3:** PT 1.3 + 2.3 (EC8-1)

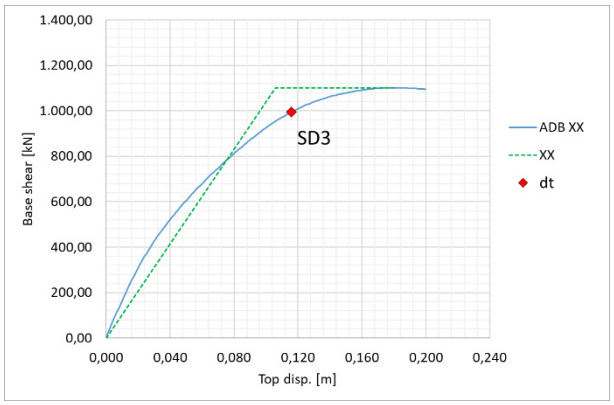

Figure A3.61 – Capacity curve and target displacement d_t, direction XX (S3_AST1_4S_3×5_XX)

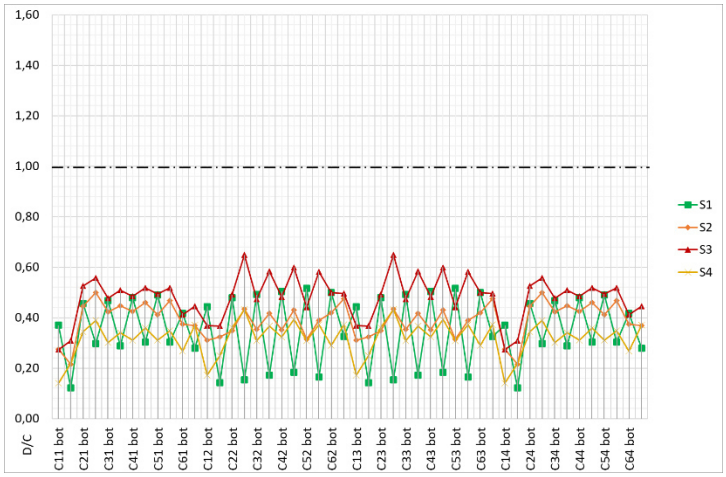

Figure A3.62 – Chord rotation D/C ratios (SD), direction XX (S3_AST1_4S_3×5_XX)

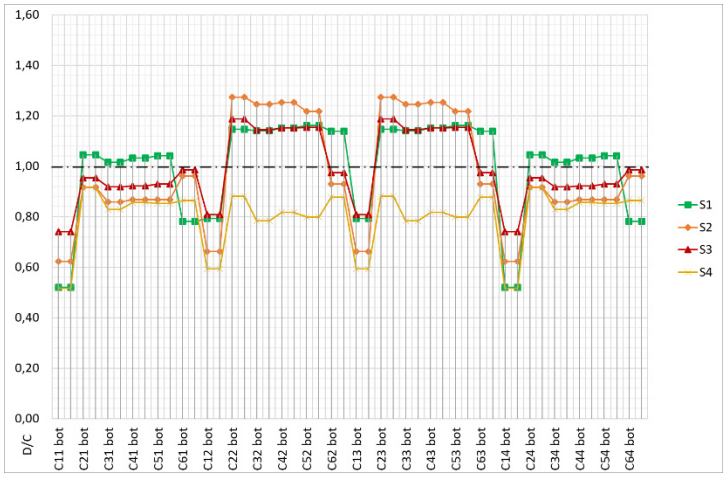

Figure A3.63 – Shear force D/C ratios (SD), direction XX (S3_AST1_4S_3×5_XX)

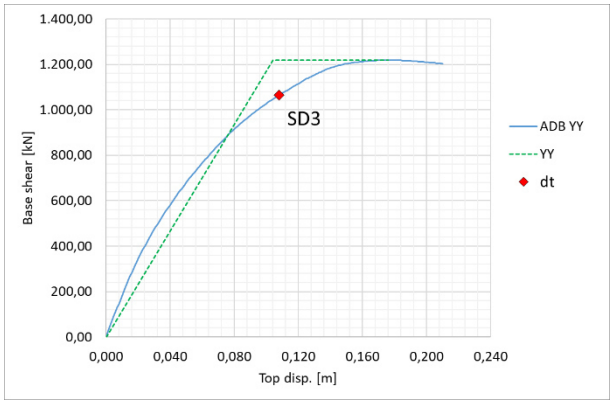

Figure A3.64 – Capacity curve and target displacement d_t, direction YY (S3_AST1_4S_3×5_YY)

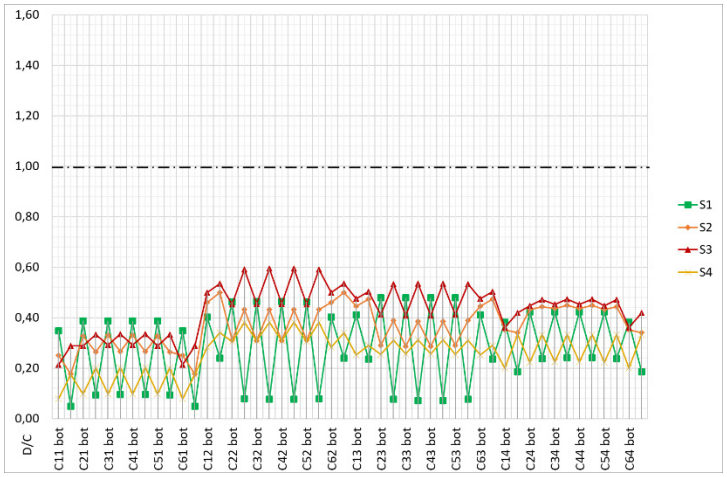

Figure A3.65 – Chord rotation D/C ratios (SD), direction YY (S3_AST1_4S_3×5_YY)

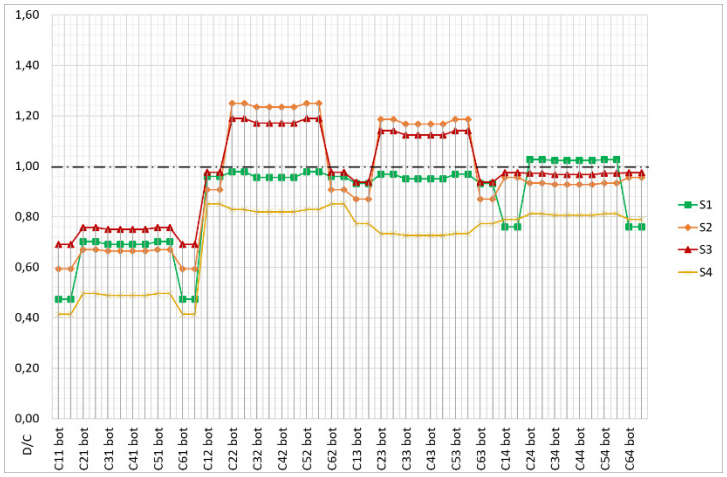

Figure A3.66 – Shear force D/C ratios (SD), direction YY (S3_AST1_4S_3×5_YY)

BUILDING TYPE 3: 4 storeys, 3×5 spans **| SEISMIC HAZARD SCENARIO 4:** PT 1.1 + 2.3 (EC8-1)

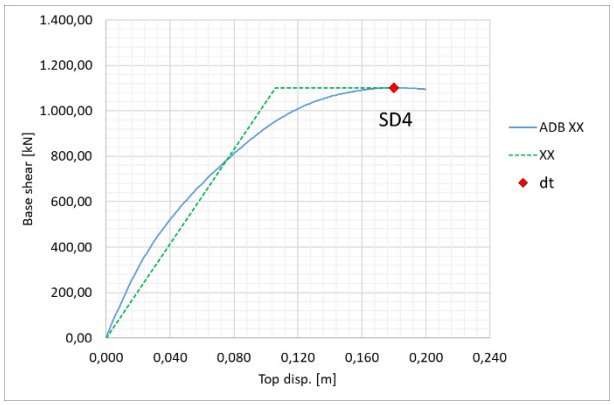

Figure A3.67 – Capacity curve and target displacement d_t, direction XX (S4_AST1_4S_3×5_XX)

Figure A3.68 – Chord rotation D/C ratios (SD), direction XX (S4_AST1_4S_3×5_XX)

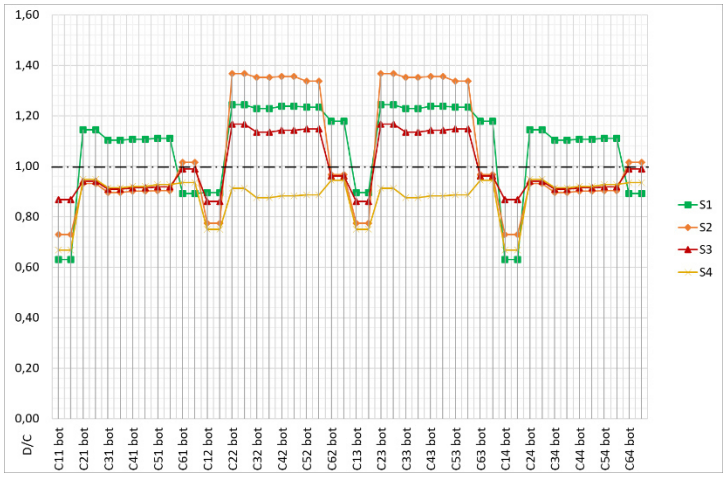

Figure A3.69 – Shear force D/C ratios (SD), direction XX (S4_AST1_4S_3×5_XX)

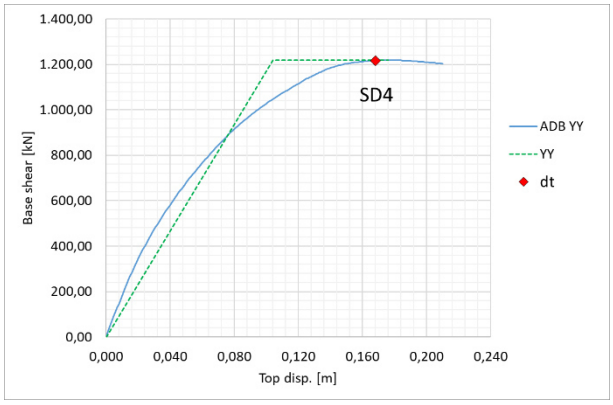

Figure A3.70 – Capacity curve and target displacement d_t, direction YY (S4_AST1_4S_3×5_YY)

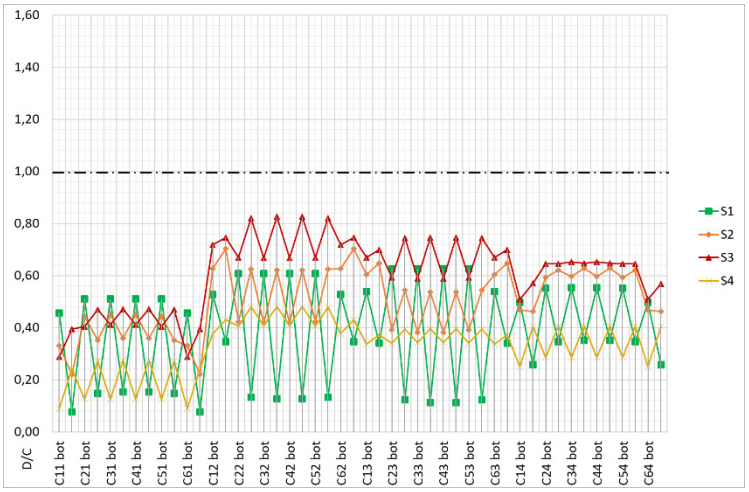

Figure A3.71 – Chord rotation D/C ratios (SD), direction YY (S4_AST1_4S_3×5_YY)

Figure A3.72 – Shear force D/C ratios (SD), direction YY (S4_AST1_4S_3×5_YY)

BUILDING TYPE 4: 5 storeys, 3×5 spans **| SEISMIC HAZARD SCENARIO 1:** PT 1.6 + 2.5 (EC8-1)

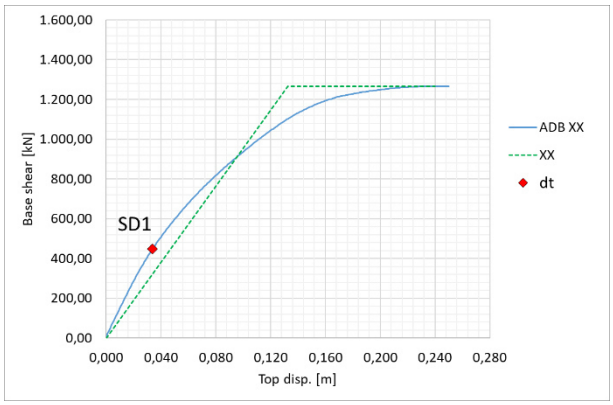

Figure A3.73 – Capacity curve and target displacement d_t, direction XX (S1_AST2_5S_3×5_XX)

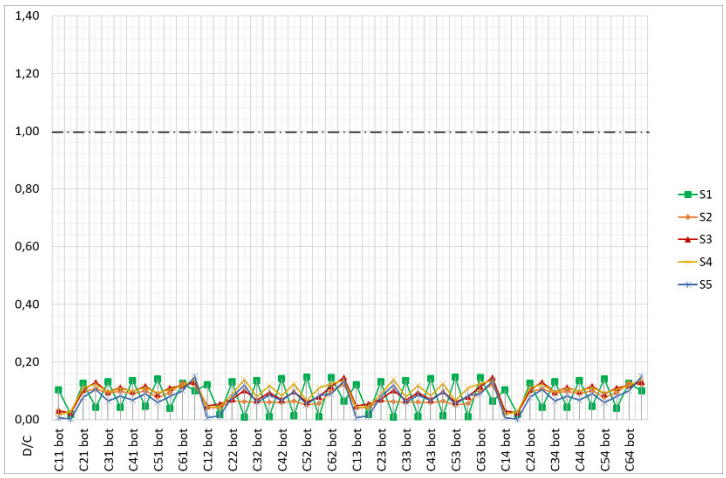

Figure A3.74 – Chord rotation D/C ratios (SD), direction XX (S1_AST2_5S_3×5_XX)

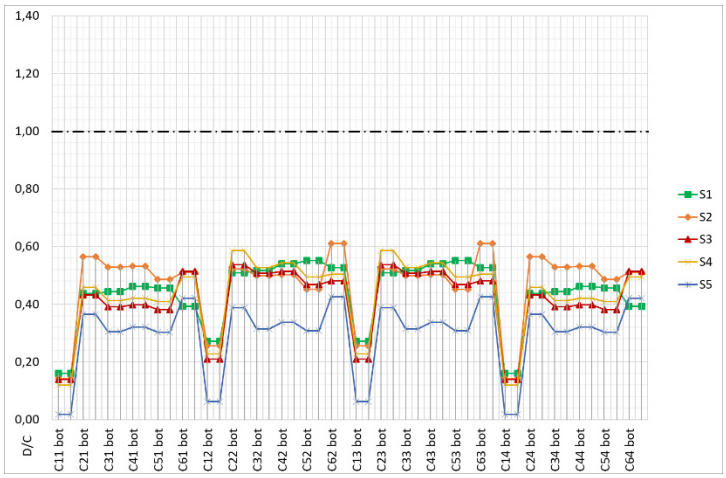

Figure A3.75 – Shear force D/C ratios (SD), direction XX (S1_AST2_5S_3×5_XX)

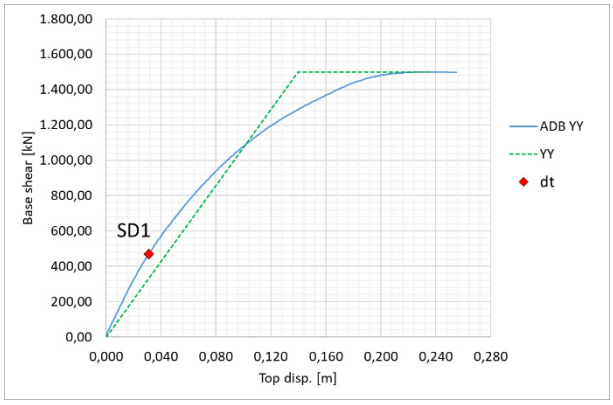

Figure A3.76 – Capacity curve and target displacement d_t, direction YY (S1_AST2_5S_3×5_YY)

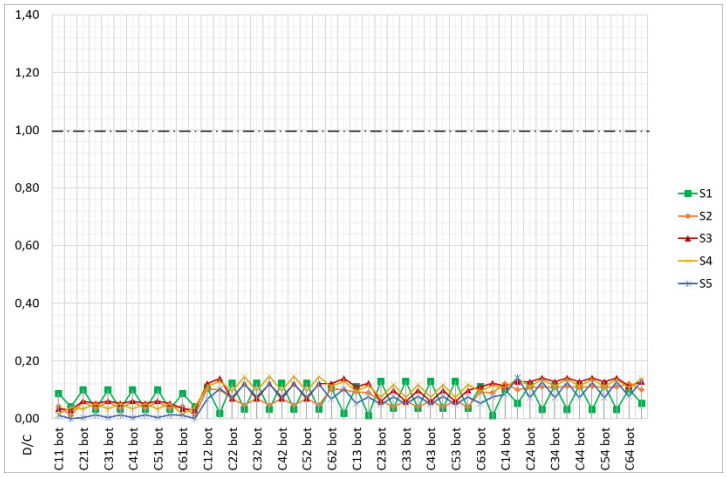

Figure A3.77 – Chord rotation D/C ratios (SD), direction YY (S1_AST2_5S_3×5_YY)

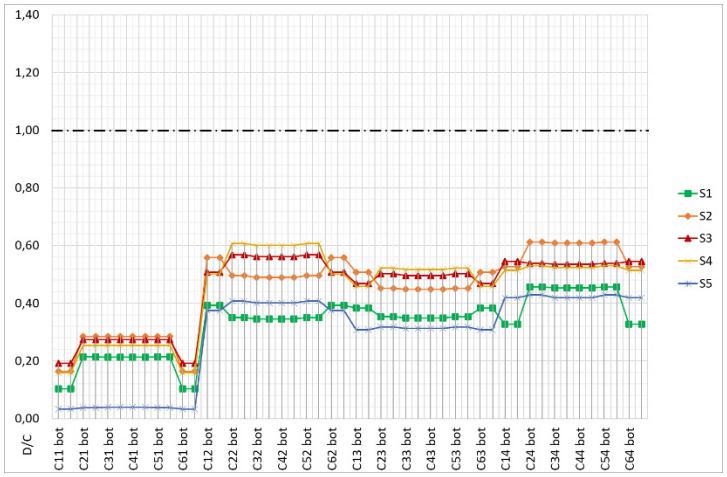

Figure A3.78 – Shear force D/C ratios (SD), direction YY (S1_AST2_5S_3×5_YY)

BUILDING TYPE 4: 5 storeys, 3×5 spans **| SEISMIC HAZARD SCENARIO 2:** PT 1.5 + 2.4 (EC8-1)

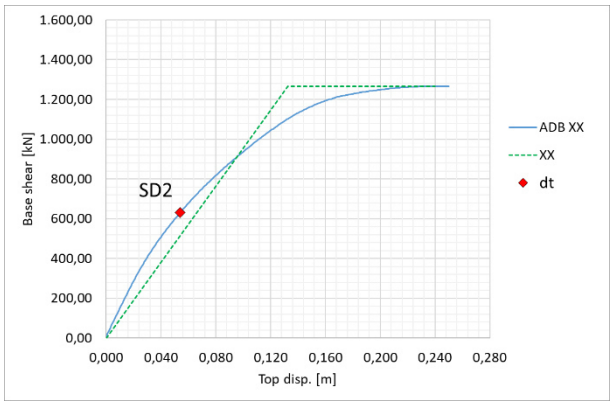

Figure A3.79 – Capacity curve and target displacement d_t, direction XX (S2_AST1_5S_3×5_XX)

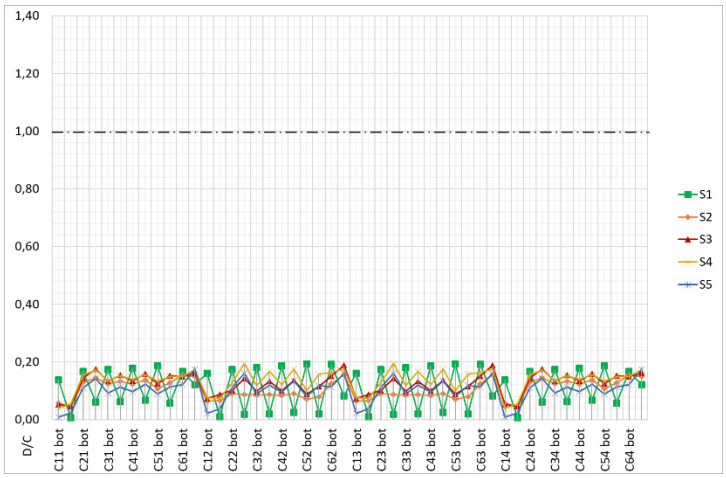

Figure A3.80 – Chord rotation D/C ratios (SD), direction XX (S2_AST1_5S_3×5_XX)

Figure A3.81 – Shear force D/C ratios (SD), direction XX (S2_AST1_5S_3×5_XX)

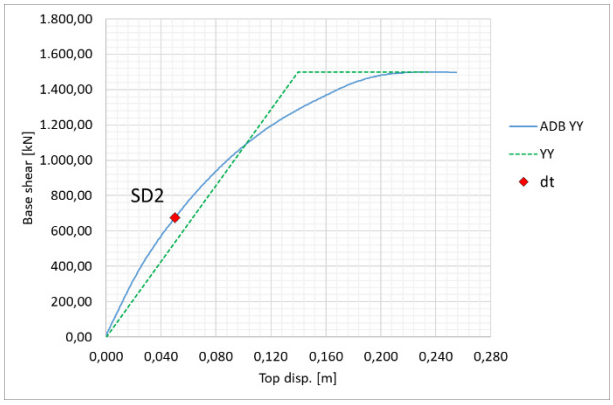

Figure A3.82 – Capacity curve and target displacement d_t, direction YY (S2_AST1_5S_3×5_YY)

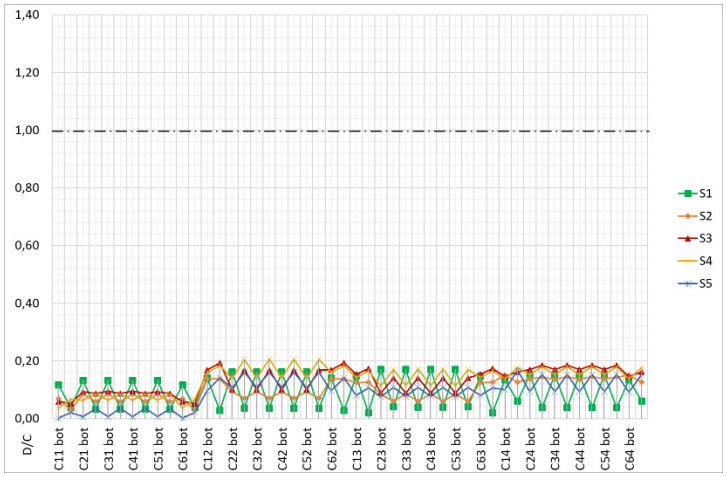

Figure A3.83 – Chord rotation D/C ratios (SD), direction YY (S2_AST1_5S_3×5_YY)

Figure A3.84 – Shear force D/C ratios (SD), direction YY (S2_AST1_5S_3×5_YY)

BUILDING TYPE 4: 5 storeys, 3×5 spans **| SEISMIC HAZARD SCENARIO 3:** PT 1.3 + 2.3 (EC8-1)

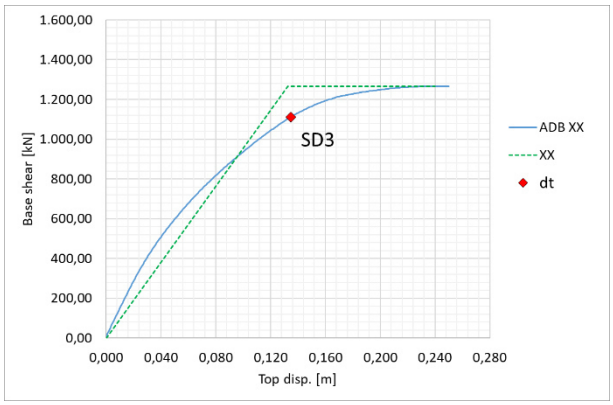

Figure A3.85 – Capacity curve and target displacement d_t, direction XX (S3_AST1_5S_3×5_XX)

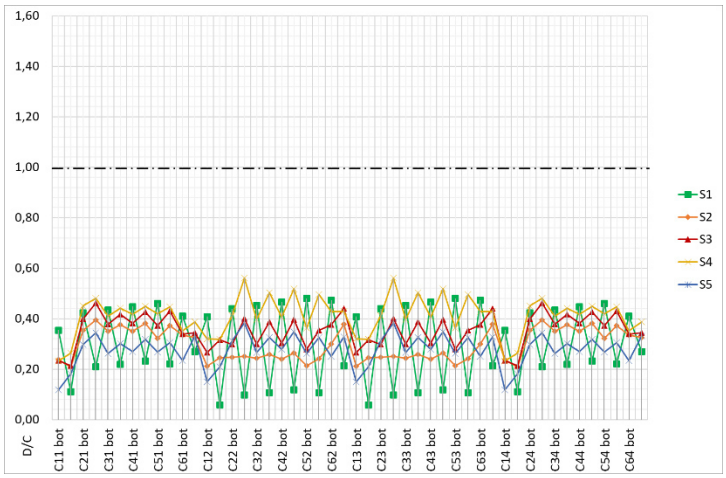

Figure A3.86 – Chord rotation D/C ratios (SD), direction XX (S3_AST1_5S_3×5_XX)

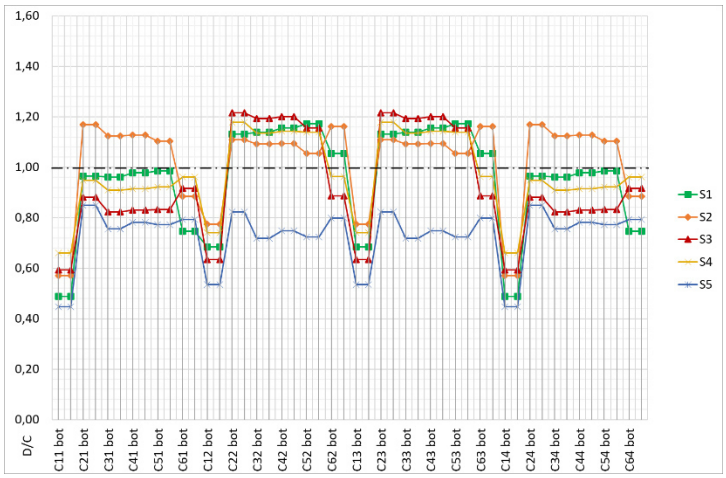

Figure A3.87 – Shear force D/C ratios (SD), direction XX (S3_AST1_5S_3×5_XX)

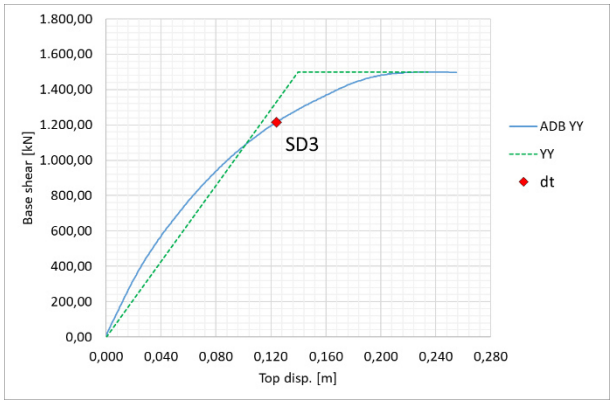

Figure A3.88 – Capacity curve and target displacement d_t, direction YY (S3_AST1_5S_3×5_YY)

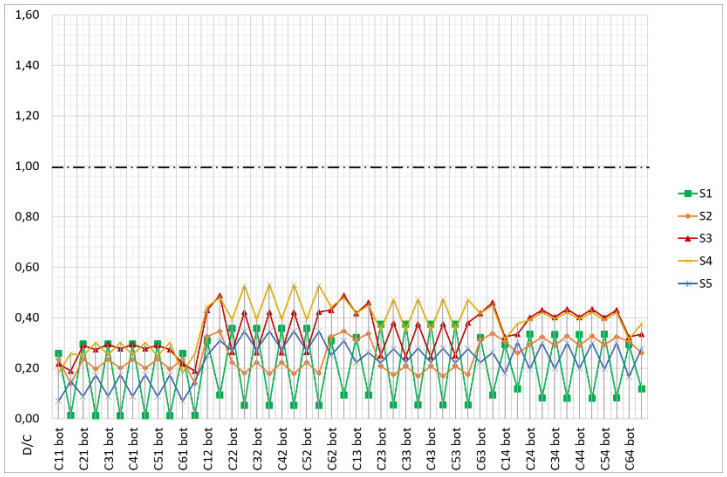

Figure A3.89 – Chord rotation D/C ratios (SD), direction YY (S3_AST1_5S_3×5_YY)

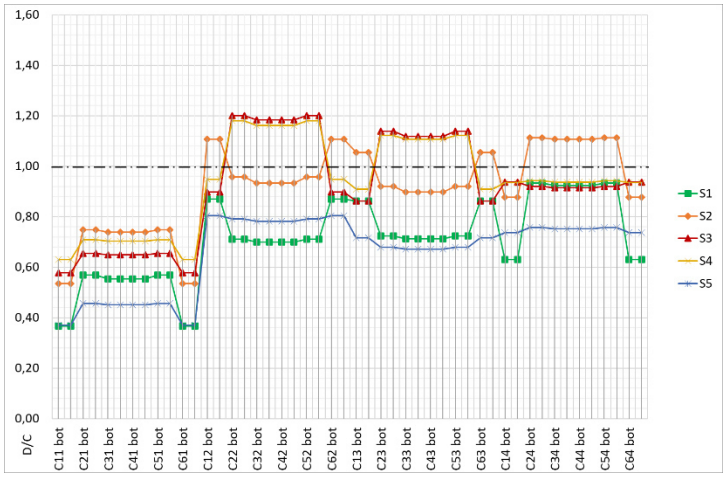

Figure A3.90 – Shear force D/C ratios (SD), direction YY (S3_AST1_5S_3×5_YY)

BUILDING TYPE 4: 5 storeys, 3×5 spans **| SEISMIC HAZARD SCENARIO 4:** PT 1.1 + 2.3 (EC8-1)

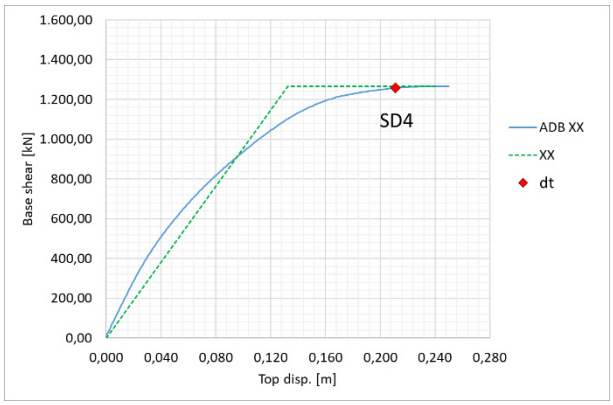

Figure A3.91 – Capacity curve and target displacement d_t, direction XX (S4_AST1_5S_3×5_XX)

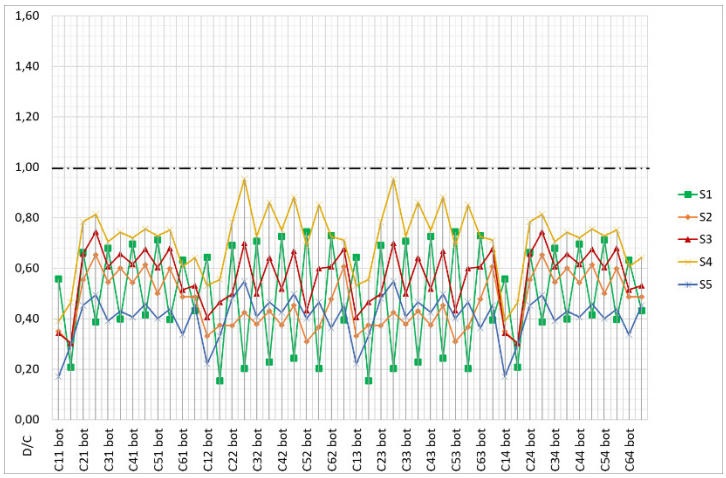

Figure A3.92 – Chord rotation D/C ratios (SD), direction XX (S4_AST1_5S_3×5_XX)

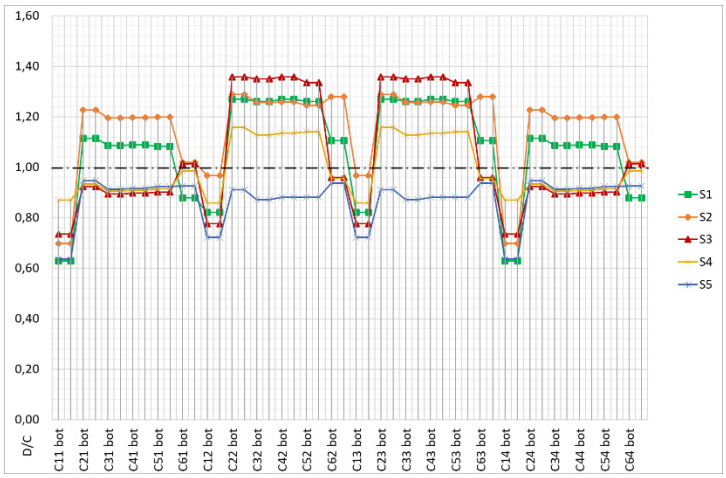

Figure A3.93 – Shear force D/C ratios (SD), direction XX (S4_AST1_5S_3×5_XX)

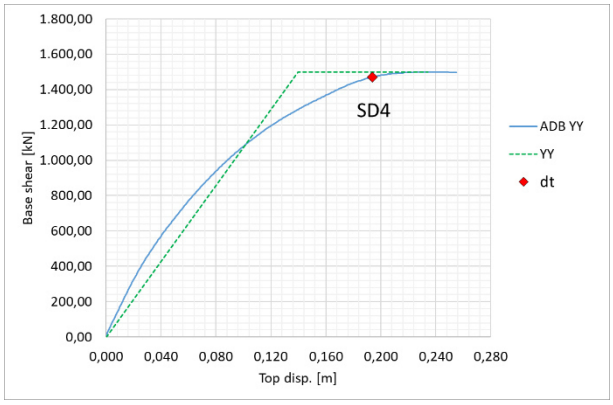

Figure A3.94 – Capacity curve and target displacement d_t, direction YY (S4_AST1_5S_3×5_YY)

Figure A3.95 – Chord rotation D/C ratios (SD), direction YY (S4_AST1_5S_3×5_YY)

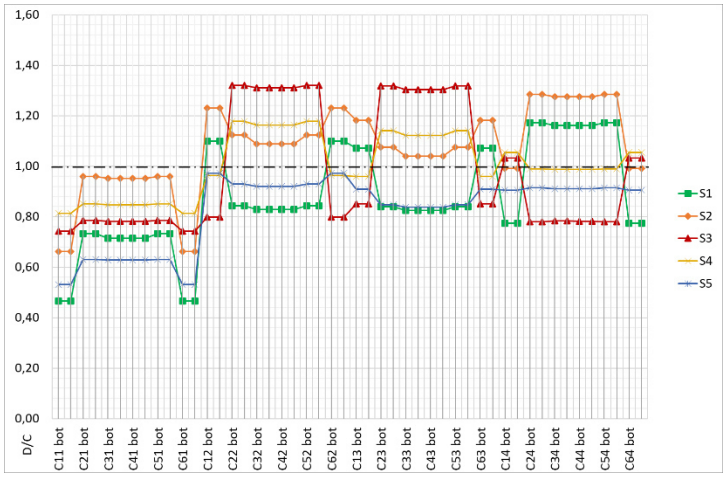

Figure A3.96 – Shear force D/C ratios (SD), direction YY (S4_AST1_5S_3×5_YY)

BUILDING TYPE 5: 6 storeys, 3×5 spans **| SEISMIC HAZARD SCENARIO 1:** PT 1.6 + 2.5 (EC8-1)

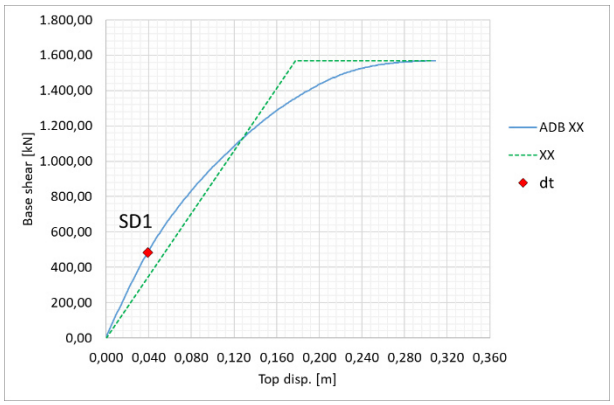

Figure A3.97 – Capacity curve and target displacement d_t, direction XX (S1_AST2_6S_3×5_XX)

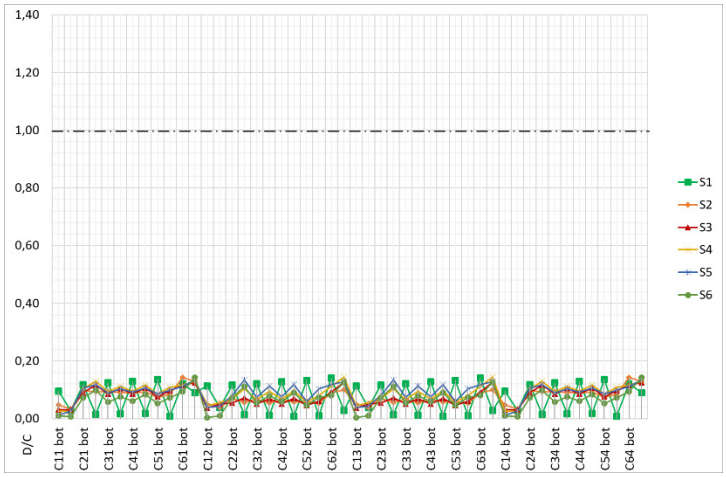

Figure A3.98 – Chord rotation D/C ratios (SD), direction XX (S1_AST2_6S_3×5_XX)

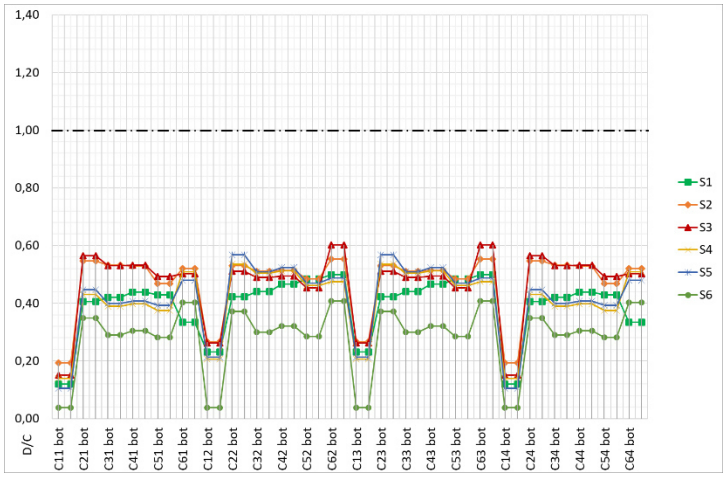

Figure A3.99 – Shear force D/C ratios (SD), direction XX (S1_AST2_6S_3×5_XX)

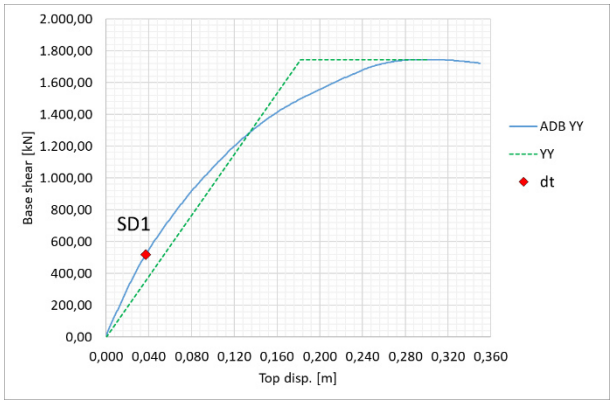

Figure A3.100 – Capacity curve and target displacement d_t, direction YY (S1_AST2_6S_3×5_YY)

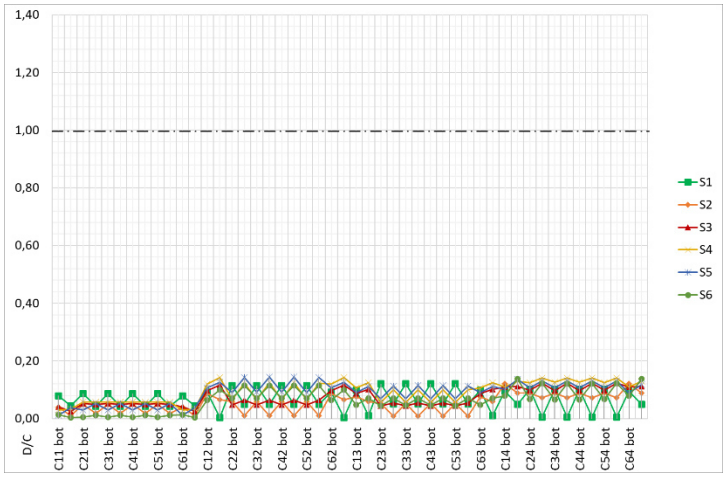

Figure A3.101 – Chord rotation D/C ratios (SD), direction YY (S1_AST2_6S_3×5_YY)

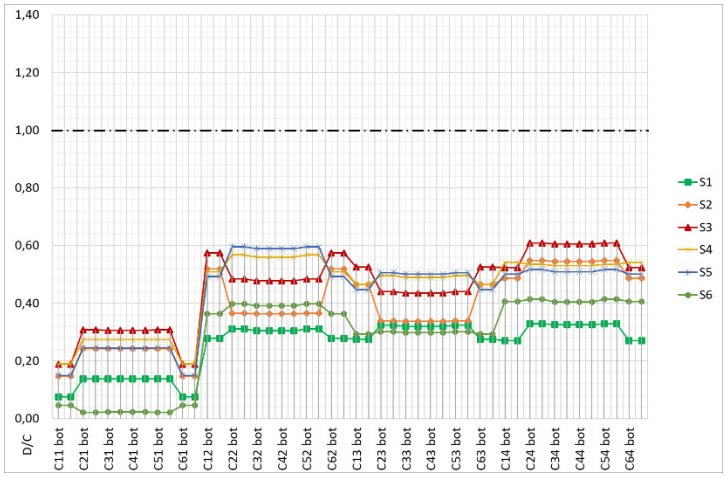

Figure A3.102 – Shear force D/C ratios (SD), direction YY (S1_AST2_6S_3×5_YY)

BUILDING TYPE 5: 6 storeys, 3×5 spans **| SEISMIC HAZARD SCENARIO 2:** PT 1.5 + 2.4 (EC8-1)

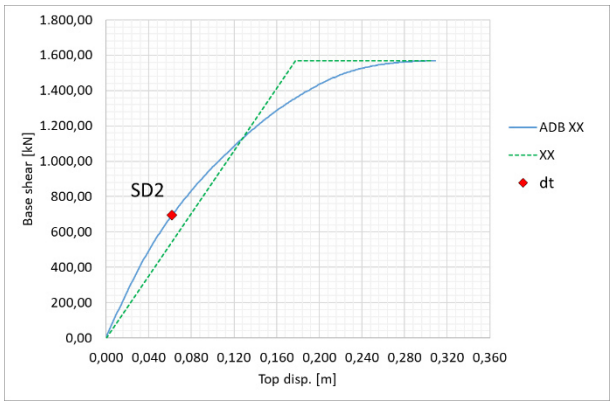

Figure A3.103 – Capacity curve and target displacement d_t, direction XX (S2_AST1_6S_3×5_XX)

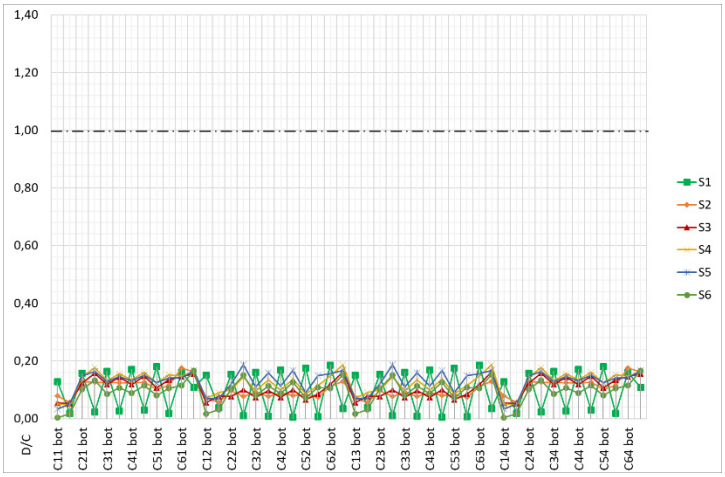

Figure A3.104 – Chord rotation D/C ratios (SD), direction XX (S2_AST1_6S_3×5_XX)

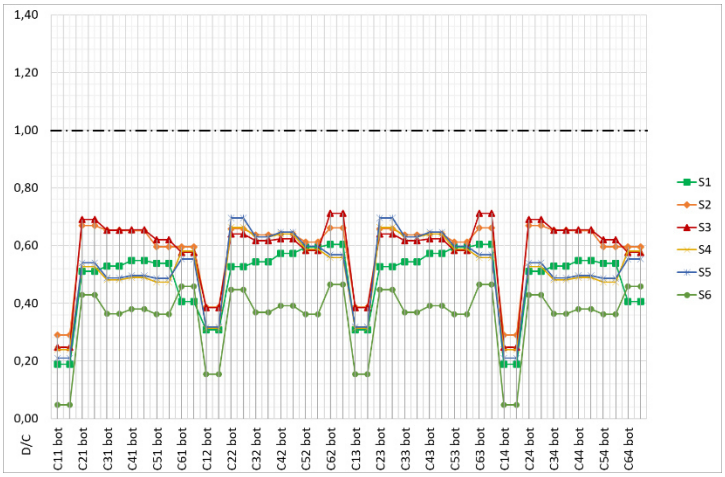

Figure A3.105 – Shear force D/C ratios (SD), direction XX (S2_AST1_6S_3×5_XX)

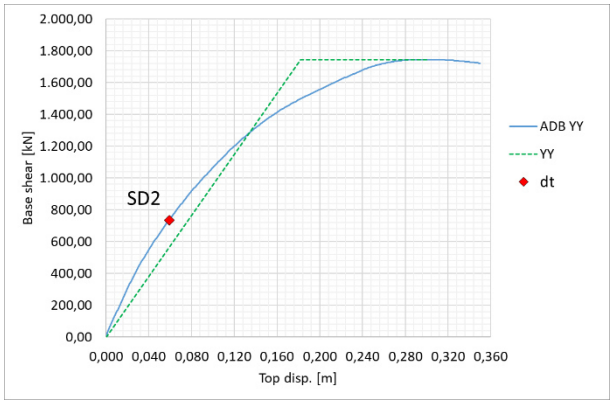

Figure A3.106 – Capacity curve and target displacement d_t, direction YY (S2_AST1_6S_3×5_YY)

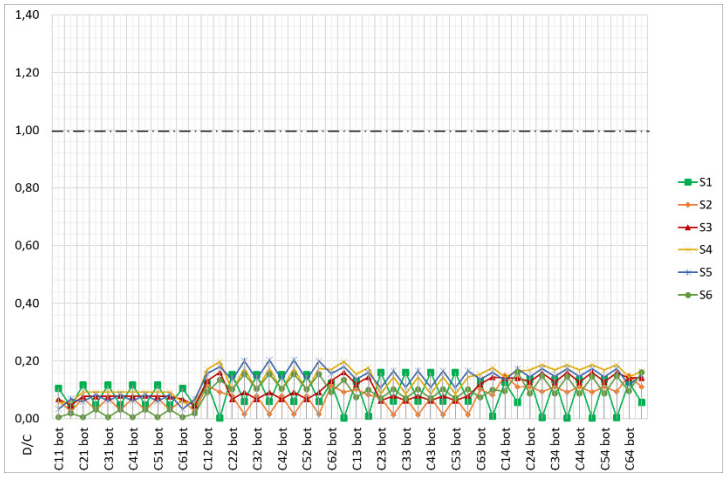

Figure A3.107 – Chord rotation D/C ratios (SD), direction YY (S2_AST1_6S_3×5_YY)

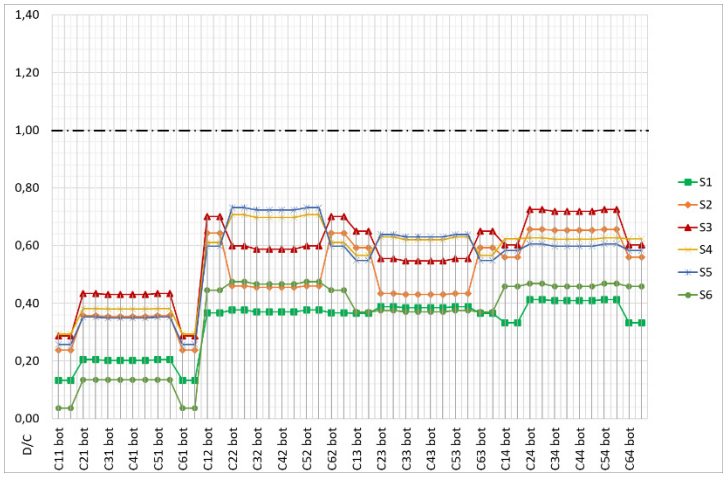

Figure A3.108 – Shear force D/C ratios (SD), direction YY (S2_AST1_6S_3×5_YY)

BUILDING TYPE 5: 6 storeys, 3×5 spans **| SEISMIC HAZARD SCENARIO 3:** PT 1.3 + 2.3 (EC8-1)

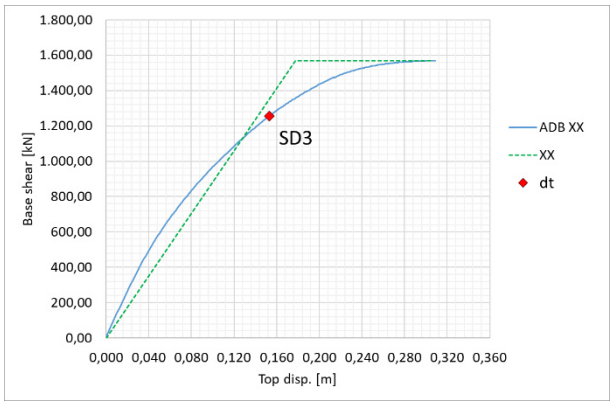

Figure A3.109 – Capacity curve and target displacement d_t, direction XX (S3_AST1_6S_3×5_XX)

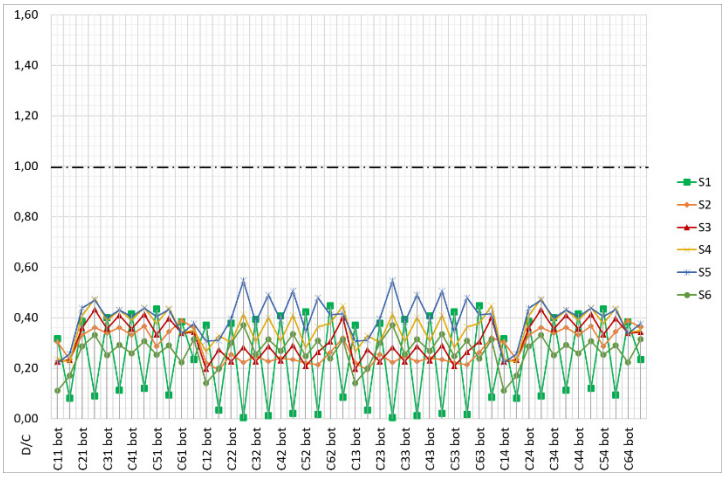

Figure A3.110 – Chord rotation D/C ratios (SD), direction XX (S3_AST1_6S_3×5_XX)

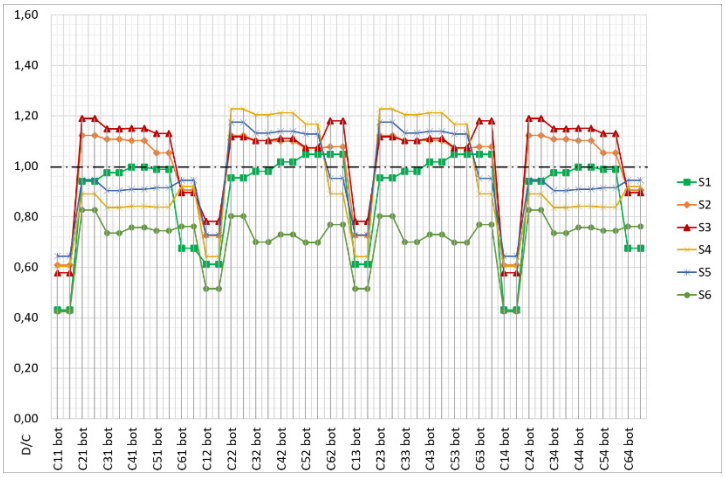

Figure A3.111 – Shear force D/C ratios (SD), direction XX (S3_AST1_6S_3×5_XX)

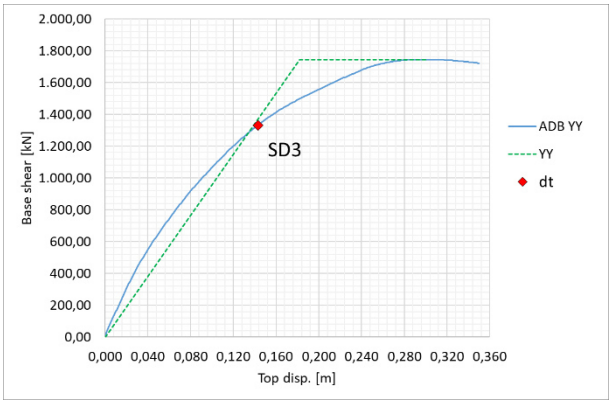

Figure A3.112 – Capacity curve and target displacement d_t, direction YY (S3_AST1_6S_3×5_YY)

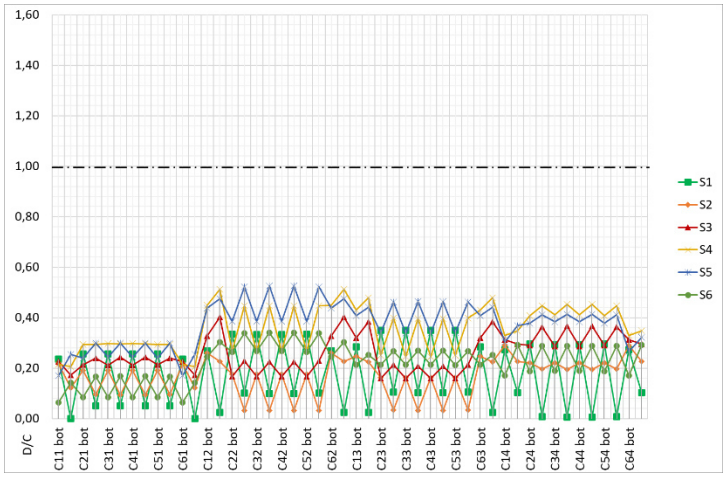

Figure A3.113 – Chord rotation D/C ratios (SD), direction YY (S3_AST1_6S_3×5_YY)

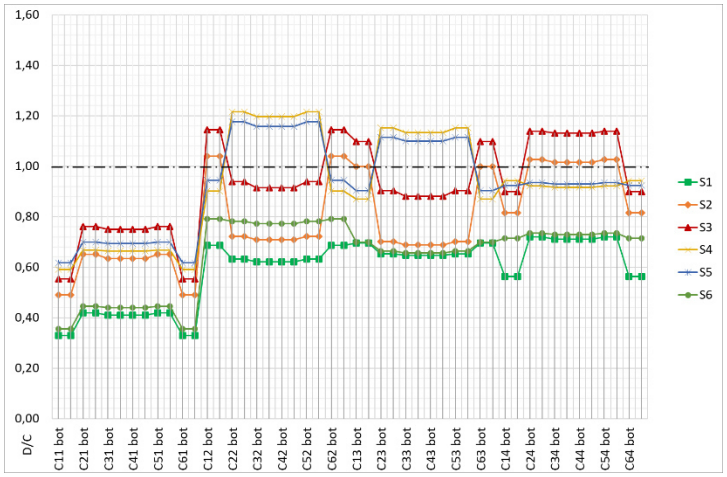

Figure A3.114 – Shear force D/C ratios (SD), direction YY (S3_AST1_6S_3×5_YY)

BUILDING TYPE 5: 6 storeys, 3×5 spans **| SEISMIC HAZARD SCENARIO 4:** PT 1.1 + 2.3 (EC8-1)

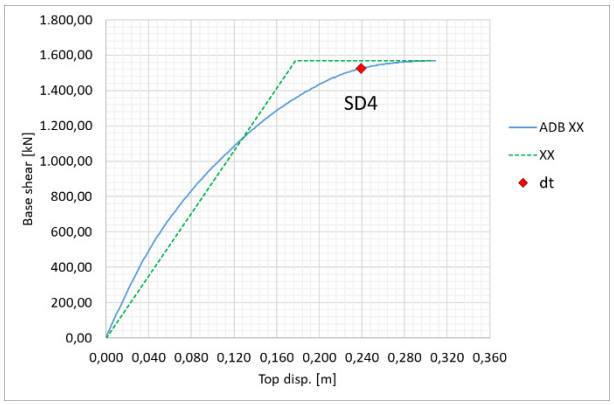

Figure A3.115 – Capacity curve and target displacement d_t, direction XX (S4_AST1_6S_3×5_XX)

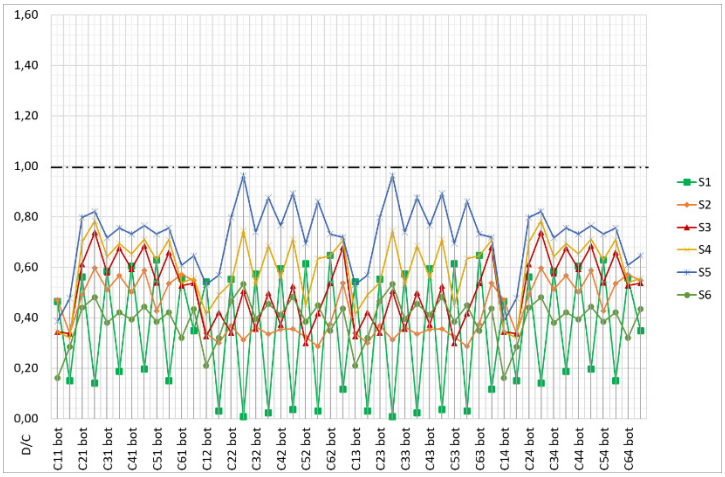

Figure A3.116 – Chord rotation D/C ratios (SD), direction XX (S4_AST1_6S_3×5_XX)

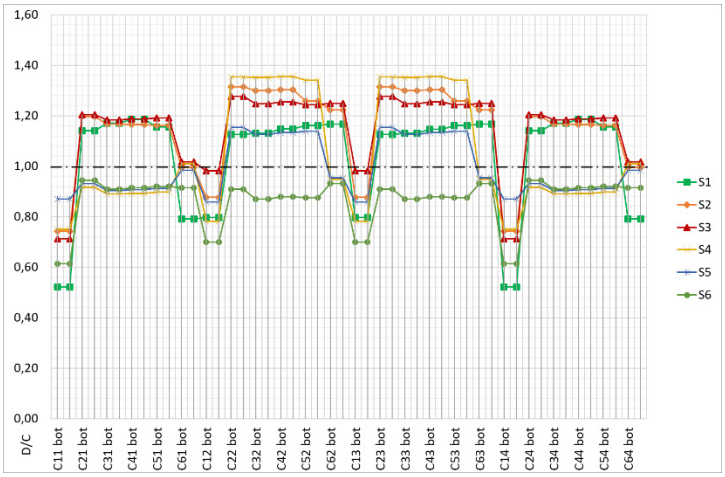

Figure A3.117 – Shear force D/C ratios (SD), direction XX (S4_AST1_6S_3×5_XX)

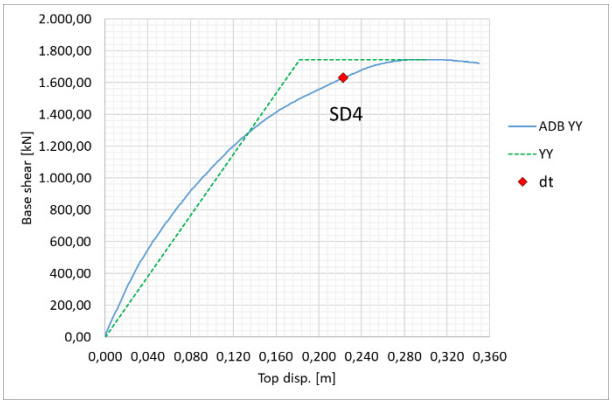

Figure A3.118 – Capacity curve and target displacement d_t, direction YY (S4_AST1_6S_3×5_YY)

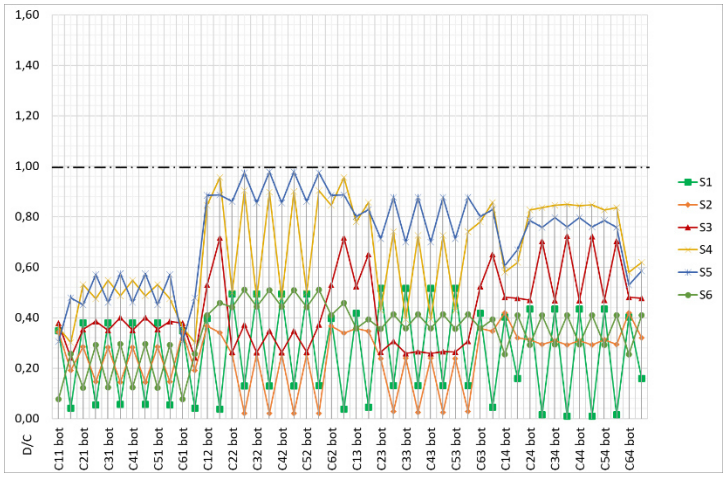

Figure A3.119 – Chord rotation D/C ratios (SD), direction YY (S4_AST1_6S_3×5_YY)

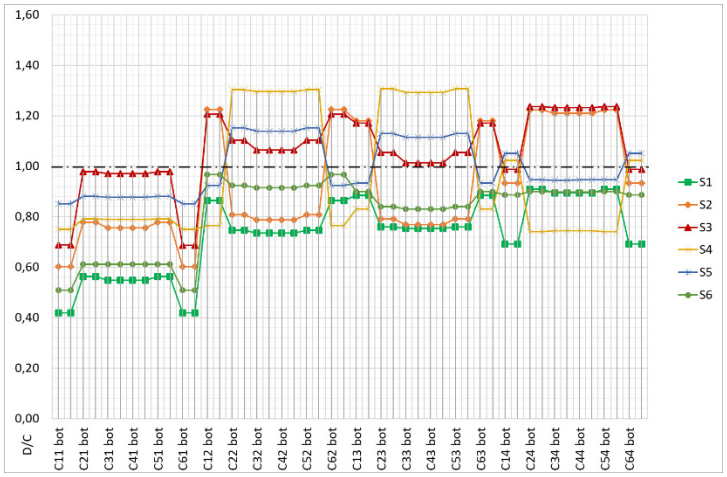

Figure A3.120 – Shear force D/C ratios (SD), direction YY (S4_AST1_6S_3×5_YY)

BUILDING TYPE 6: 2 storeys, 2×4 spans **| SEISMIC HAZARD SCENARIO 1:** PT 1.6 + 2.5 (EC8-1)

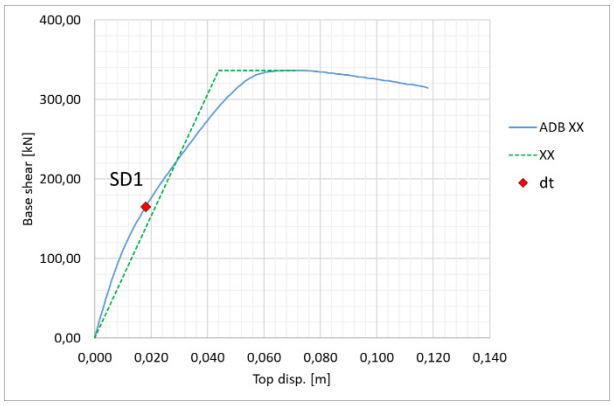

Figure A3.121 – Capacity curve and target displacement d_t, direction XX (S1_AST2_2S_2×4_XX)

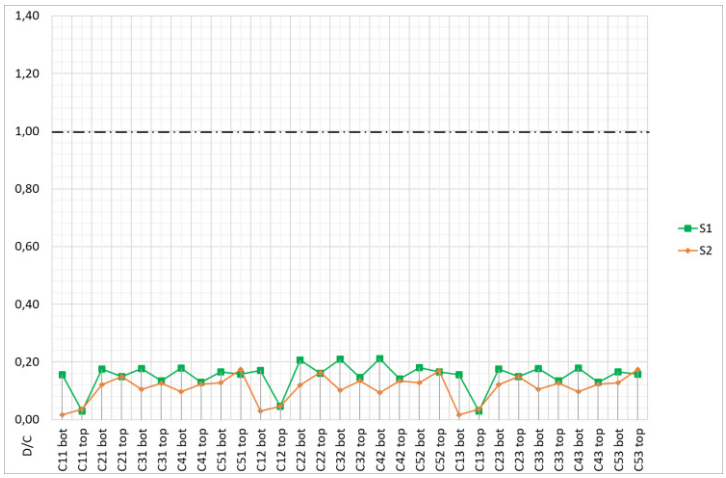

Figure A3.122 – Chord rotation D/C ratios (SD), direction XX (S1_AST2_2S_2×4_XX)

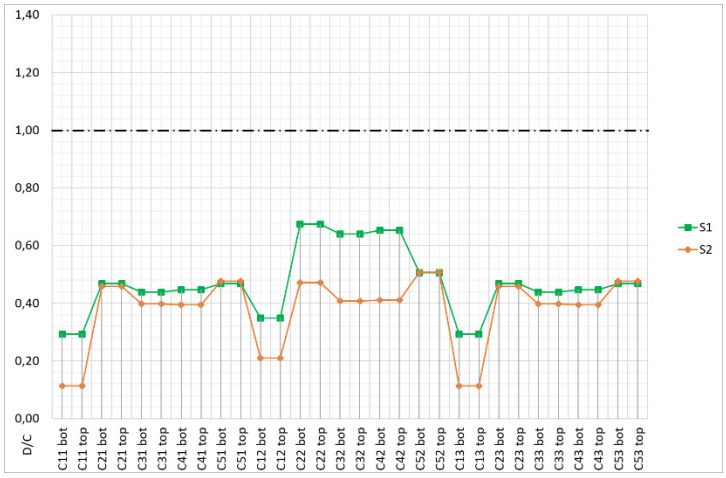

Figure A3.123 – Shear force D/C ratios (SD), direction XX (S1_AST2_2S_2×4_XX)

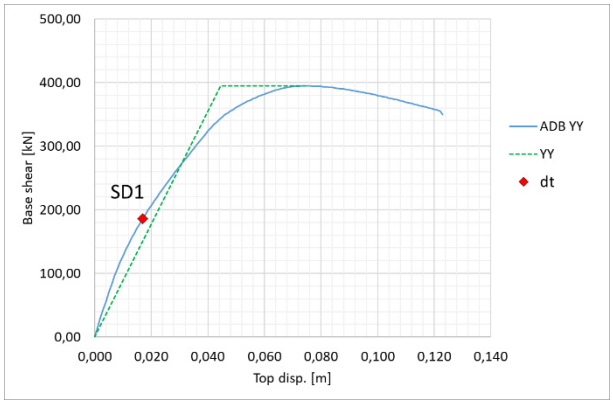

Figure A3.124 – Capacity curve and target displacement d_t, direction YY (S1_AST2_2S_2×4_YY)

Figure A3.125 – Chord rotation D/C ratios (SD), direction YY (S1_AST2_2S_2×4_YY)

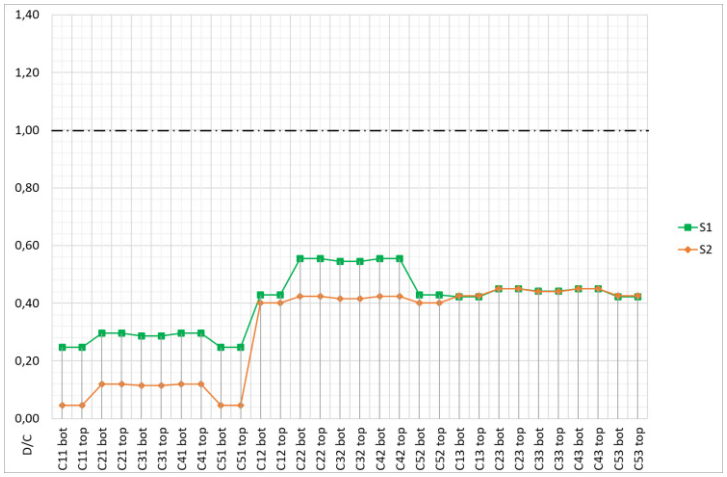

Figure A3.126 – Shear force D/C ratios (SD), direction YY (S1_AST2_2S_2×4_YY)

BUILDING TYPE 6: 2 storeys, 2×4 spans **| SEISMIC HAZARD SCENARIO 2:** PT 1.5 + 2.4 (EC8-1)

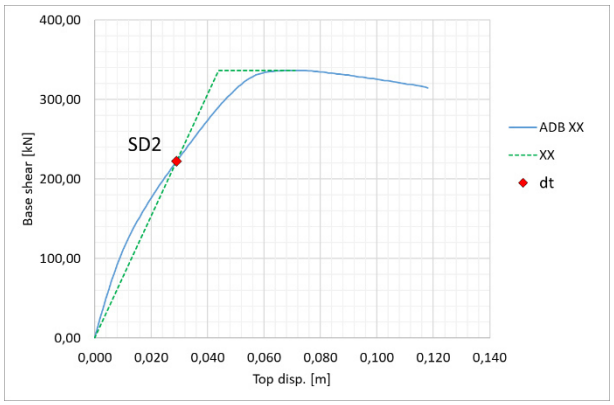

Figure A3.127 – Capacity curve and target displacement d_t, direction XX (S2_AST1_2S_2×4_XX)

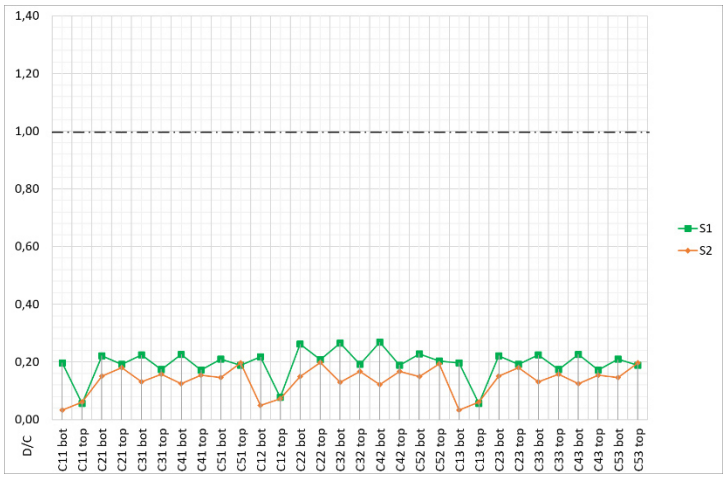

Figure A3.128 – Chord rotation D/C ratios (SD), direction XX (S2_AST1_2S_2×4_XX)

Figure A3.129 – Shear force D/C ratios (SD), direction XX (S2_AST1_2S_2×4_XX)

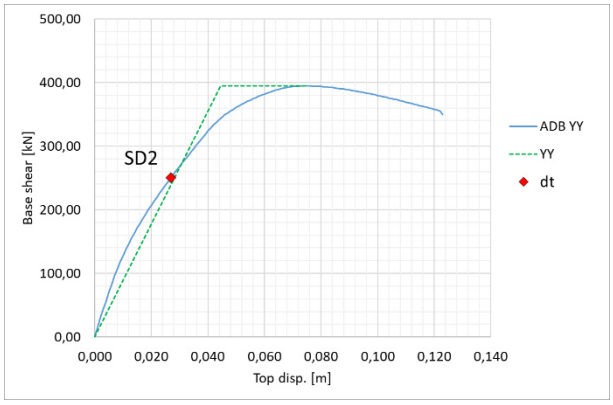

Figure A3.130 – Capacity curve and target displacement d_t, direction YY (S2_AST1_2S_2×4_YY)

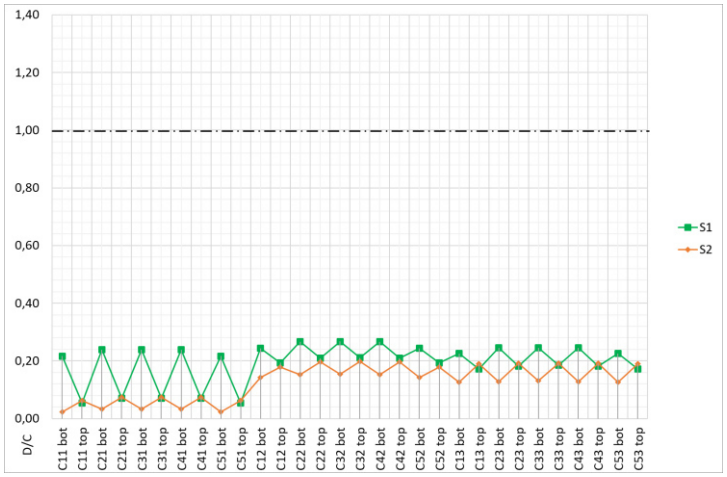

Figure A3.131 – Chord rotation D/C ratios (SD), direction YY (S2_AST1_2S_2×4_YY)

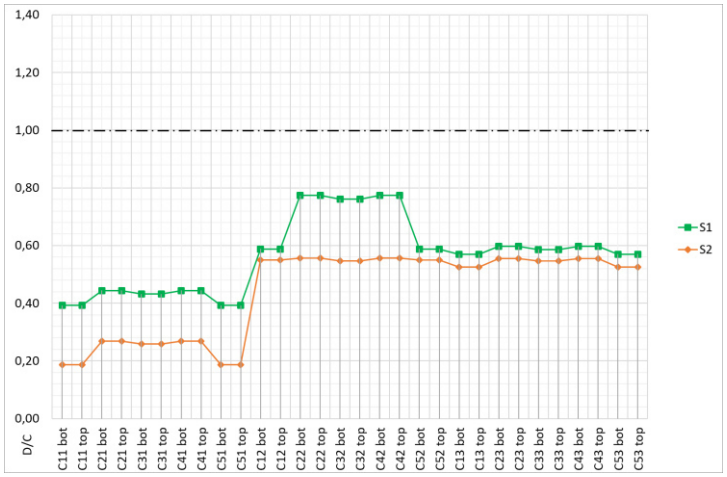

Figure A3.132 – Shear force D/C ratios (SD), direction YY (S2_AST1_2S_2×4_YY)

BUILDING TYPE 6: 2 storeys, 2×4 spans **| SEISMIC HAZARD SCENARIO 3:** PT 1.3 + 2.3 (EC8-1)

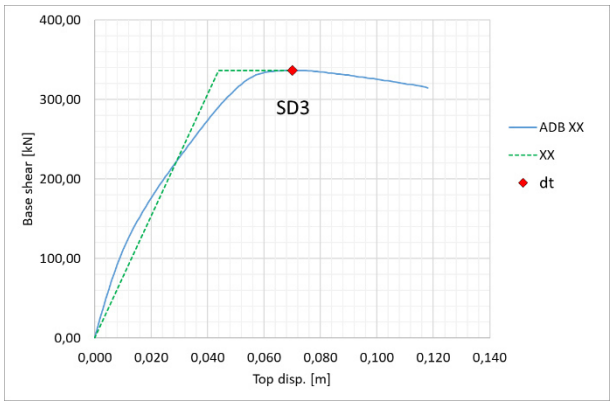

Figure A3.133 – Capacity curve and target displacement d_t, direction XX (S3_AST1_2S_2×4_XX)

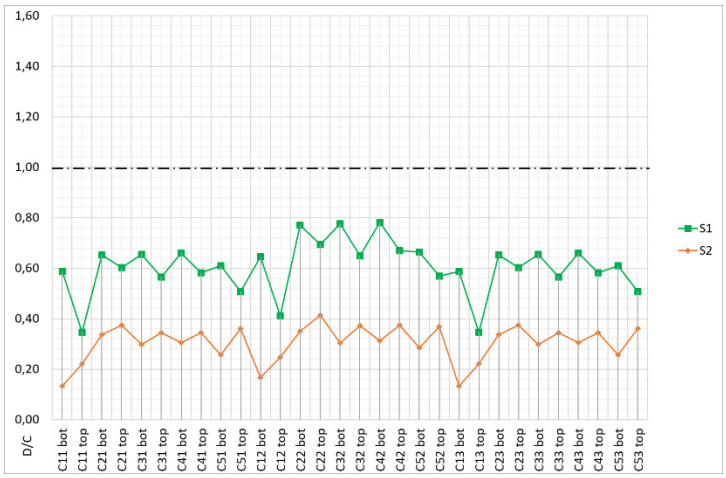

Figure A3.134 – Chord rotation D/C ratios (SD), direction XX (S3_AST1_2S_2×4_XX)

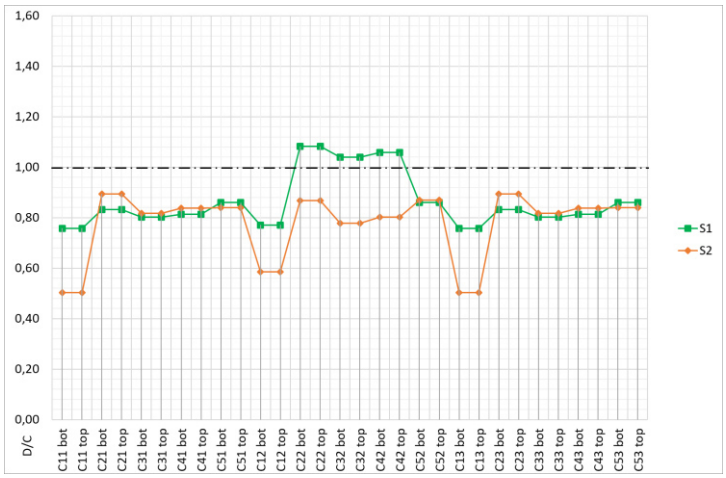

Figure A3.135 – Shear force D/C ratios (SD), direction XX (S3_AST1_2S_2×4_XX)

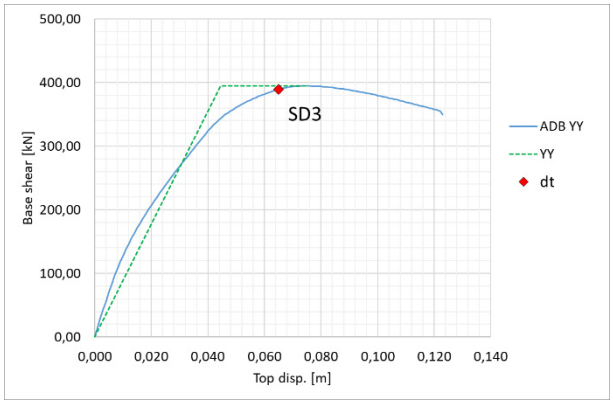

Figure A3.136 – Capacity curve and target displacement d_t, direction YY (S3_AST1_2S_2×4_YY)

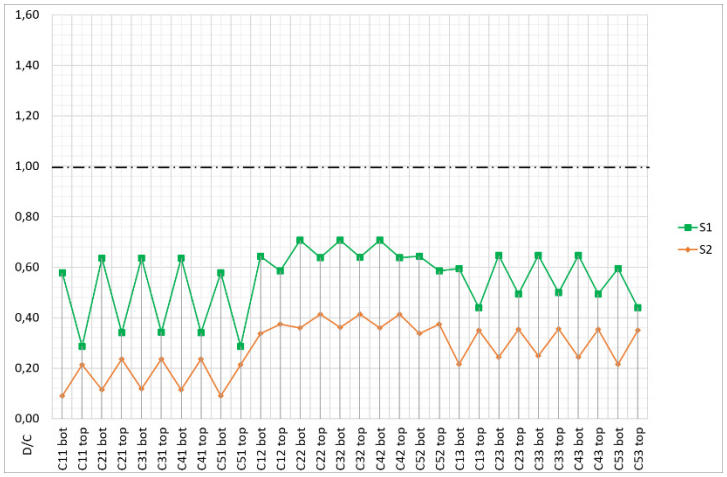

Figure A3.137 – Chord rotation D/C ratios (SD), direction YY (S3_AST1_2S_2×4_YY)

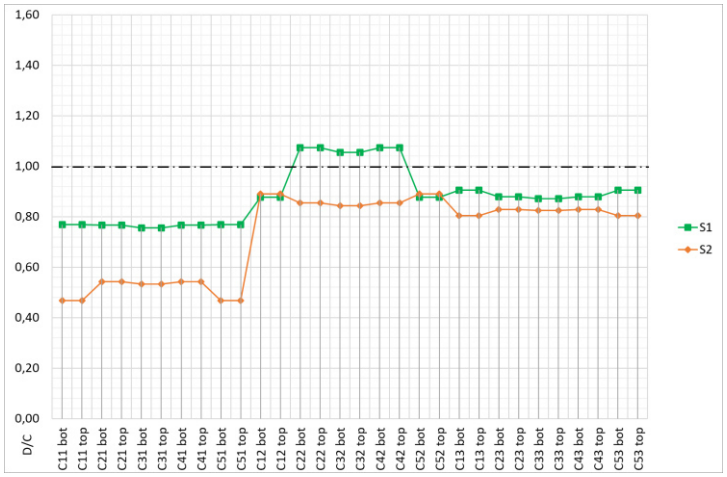

Figure A3.138 – Shear force D/C ratios (SD), direction YY (S3_AST1_2S_2×4_YY)

BUILDING TYPE 6: 2 storeys, 2×4 spans **| SEISMIC HAZARD SCENARIO 4:** PT 1.1 + 2.3 (EC8-1)

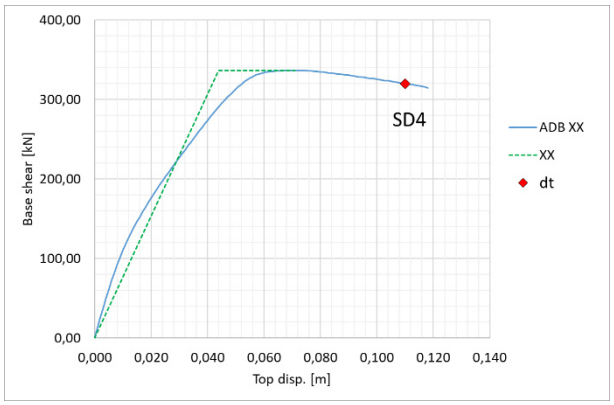

Figure A3.139 – Capacity curve and target displacement d_t, direction XX (S4_AST1_2S_2×4_XX)

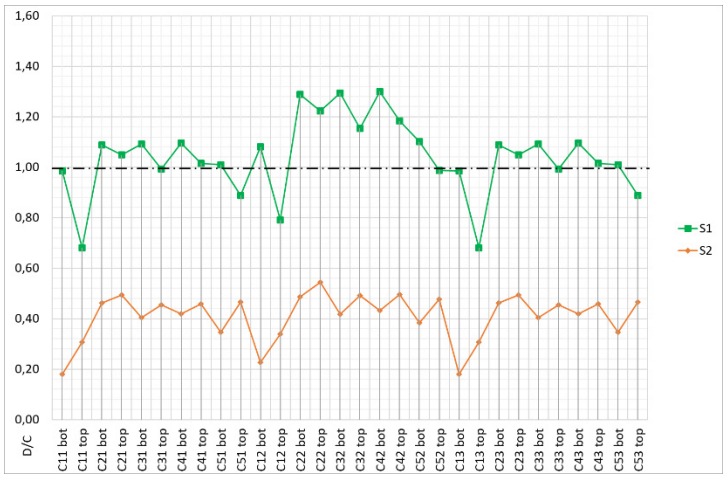

Figure A3.140 – Chord rotation D/C ratios (SD), direction XX (S4_AST1_2S_2×4_XX)

Figure A3.141 – Shear force D/C ratios (SD), direction XX (S4_AST1_2S_2×4_XX)

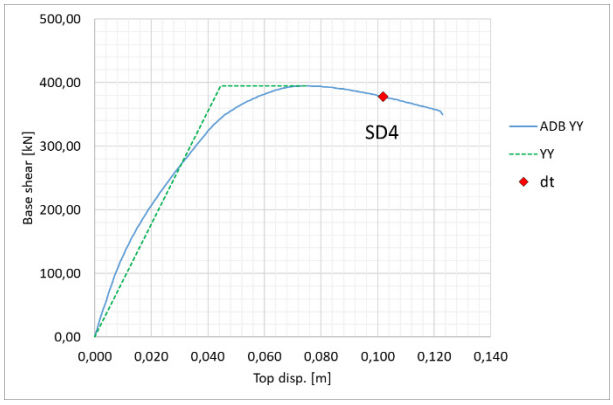

Figure A3.142 – Capacity curve and target displacement d_t, direction YY (S4_AST1_2S_2×4_YY)

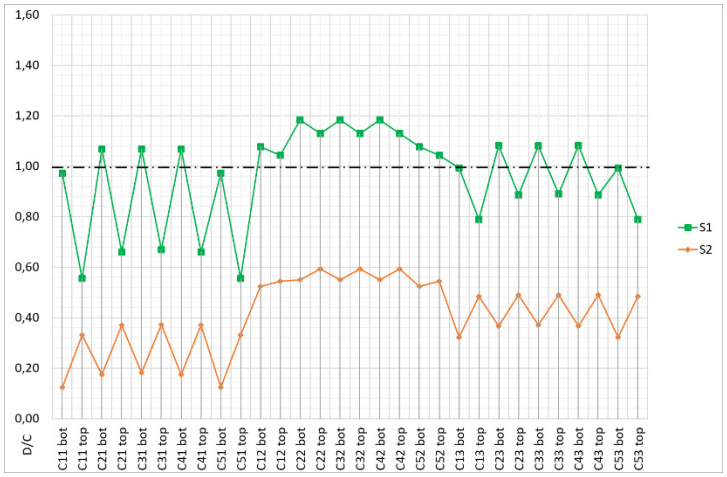

Figure A3.143 – Chord rotation D/C ratios (SD), direction YY (S4_AST1_2S_2×4_YY)

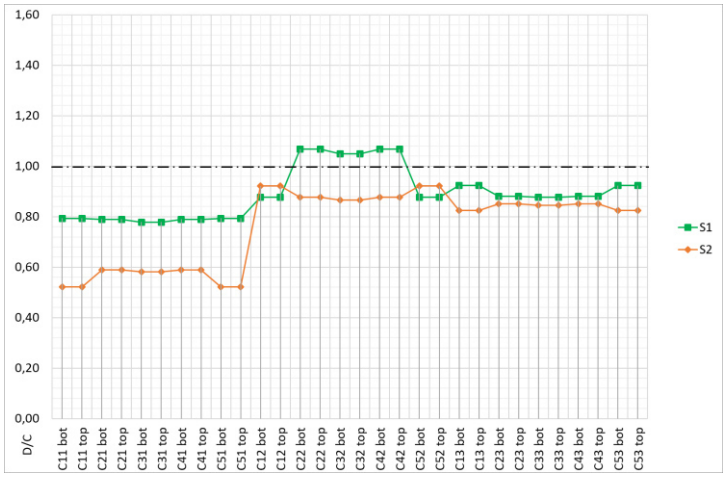

Figure A3.144 – Shear force D/C ratios (SD), direction YY (S4_AST1_2S_2×4_YY)

BUILDING TYPE 7: 3 storeys, 2×4 spans **| SEISMIC HAZARD SCENARIO 1:** PT 1.6 + 2.5 (EC8-1)

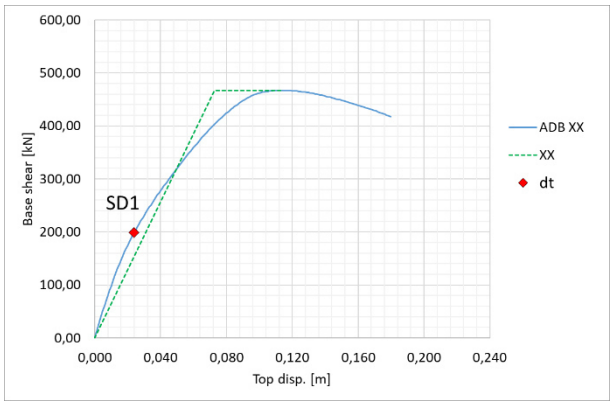

Figure A3.145 – Capacity curve and target displacement d_t, direction XX (S1_AST2_3S_2×4_XX)

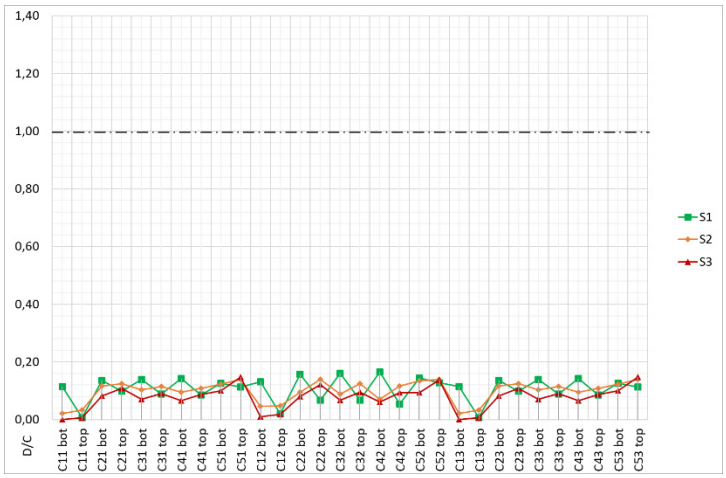

Figure A3.146 – Chord rotation D/C ratios (SD), direction XX (S1_AST2_3S_2×4_XX)

Figure A3.147 – Shear force D/C ratios (SD), direction XX (S1_AST2_3S_2×4_XX)

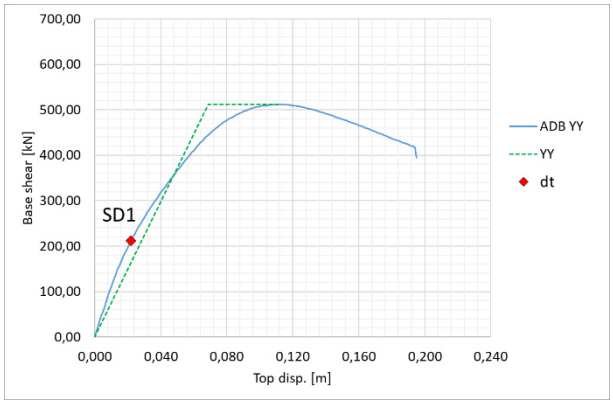

Figure A3.148 – Capacity curve and target displacement d_t, direction YY (S1_AST2_3S_2×4_YY)

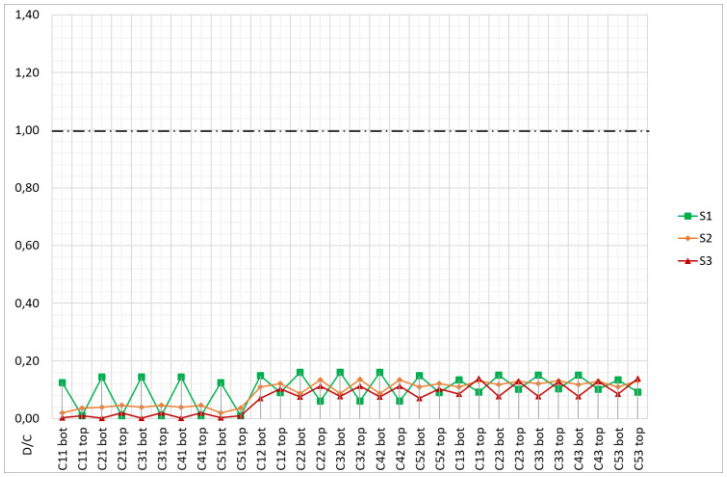

Figure A3.149 – Chord rotation D/C ratios (SD), direction YY (S1_AST2_3S_2×4_YY)

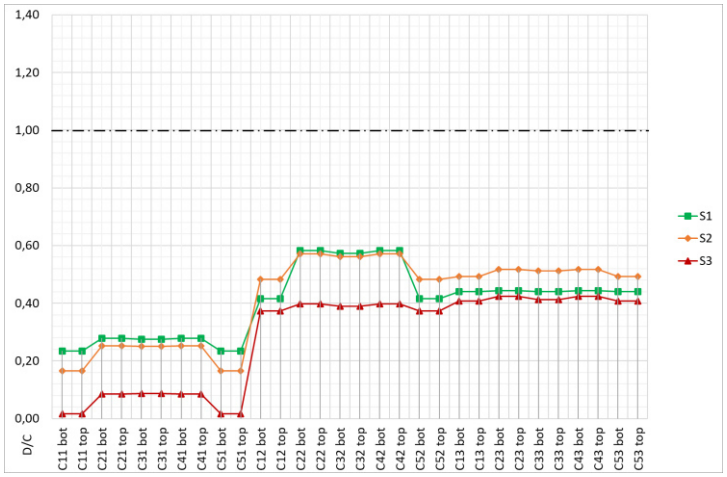

Figure A3.150 – Shear force D/C ratios (SD), direction YY (S1_AST2_3S_2×4_YY)

BUILDING TYPE 7: 3 storeys, 2×4 spans **| SEISMIC HAZARD SCENARIO 2:** PT 1.5 + 2.4 (EC8-1)

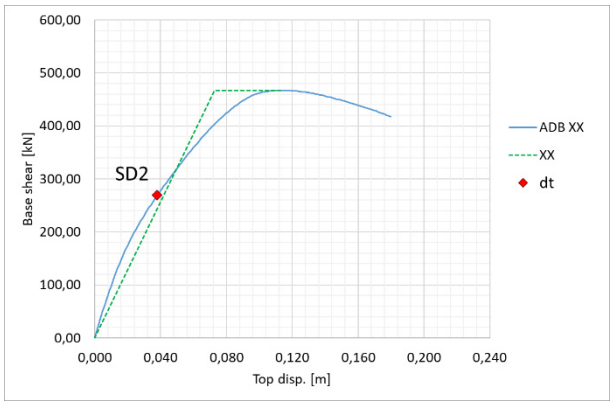

Figure A3.151 – Capacity curve and target displacement d_t, direction XX (S2_AST1_3S_2×4_XX)

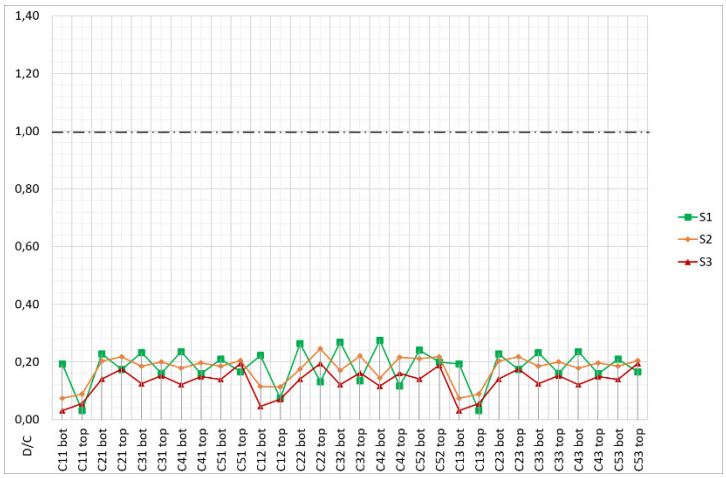

Figure A3.152 – Chord rotation D/C ratios (SD), direction XX (S2_AST1_3S_2×4_XX)

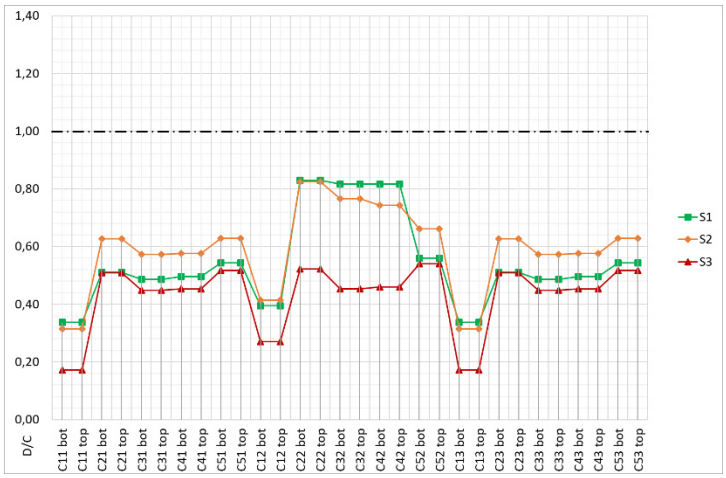

Figure A3.153 – Shear force D/C ratios (SD), direction XX (S2_AST1_3S_2×4_XX)

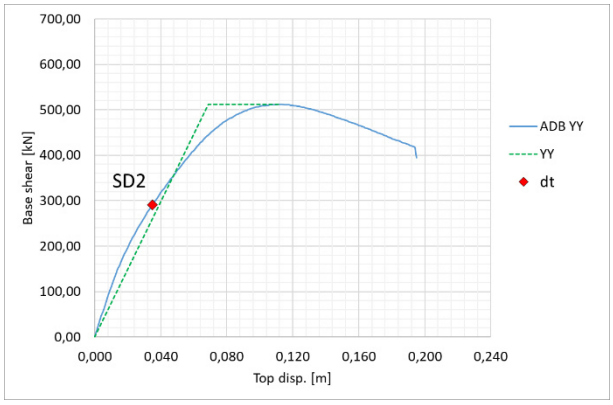

Figure A3.154 – Capacity curve and target displacement d_t, direction YY (S2_AST1_3S_2×4_YY)

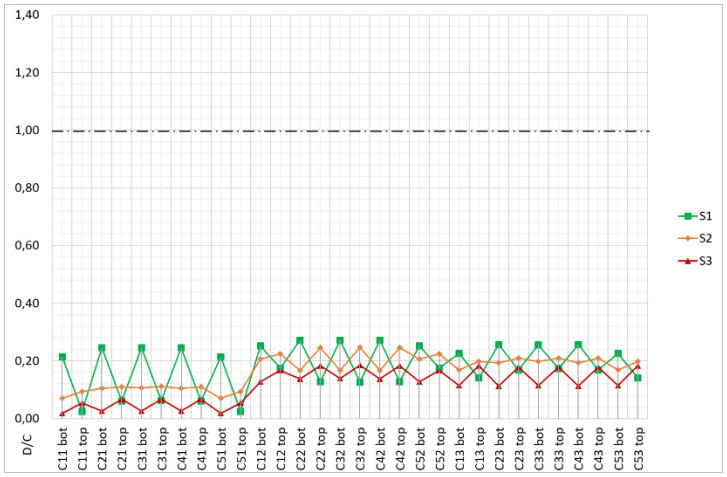

Figure A3.155 – Chord rotation D/C ratios (SD), direction YY (S2_AST1_3S_2×4_YY)

Figure A3.156 – Shear force D/C ratios (SD), direction YY (S2_AST1_3S_2×4_YY)

BUILDING TYPE 7: 3 storeys, 2×4 spans **| SEISMIC HAZARD SCENARIO 3:** PT 1.3 + 2.3 (EC8-1)

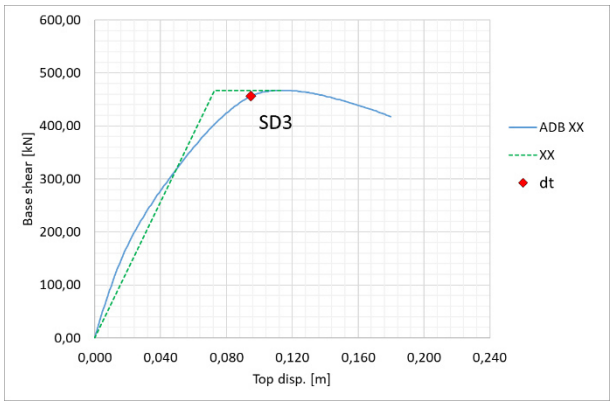

Figure A3.157 – Capacity curve and target displacement d_t, direction XX (S3_AST1_3S_2×4_XX)

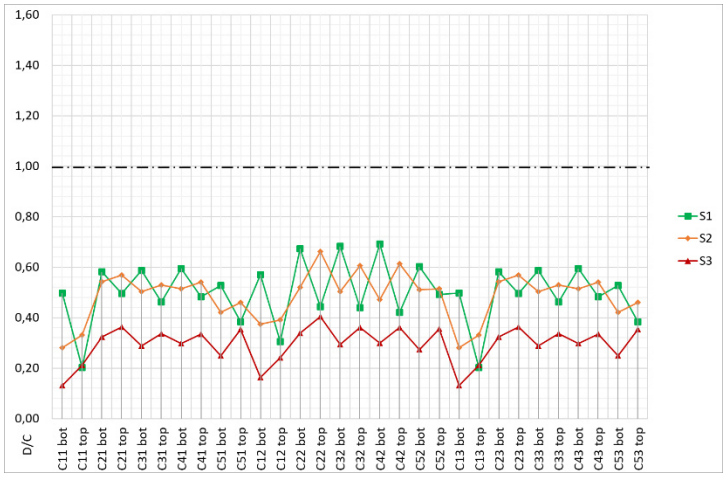

Figure A3.158 – Chord rotation D/C ratios (SD), direction XX (S3_AST1_3S_2×4_XX)

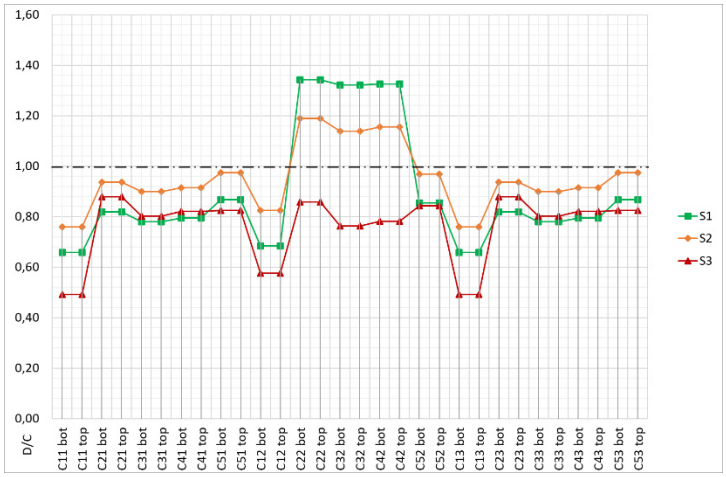

Figure A3.159 – Shear force D/C ratios (SD), direction XX (S3_AST1_3S_2×4_XX)

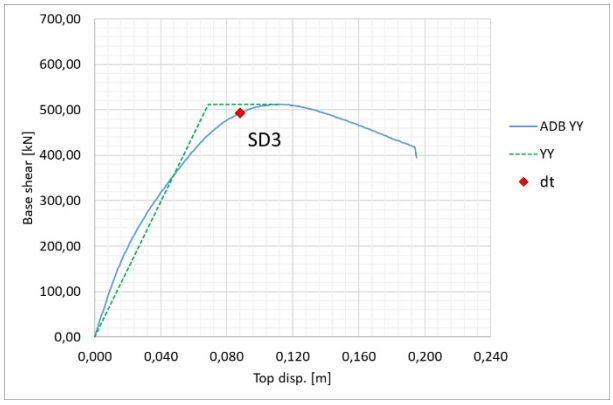

Figure A3.160 – Capacity curve and target displacement d_t, direction YY (S3_AST1_3S_2×4_YY)

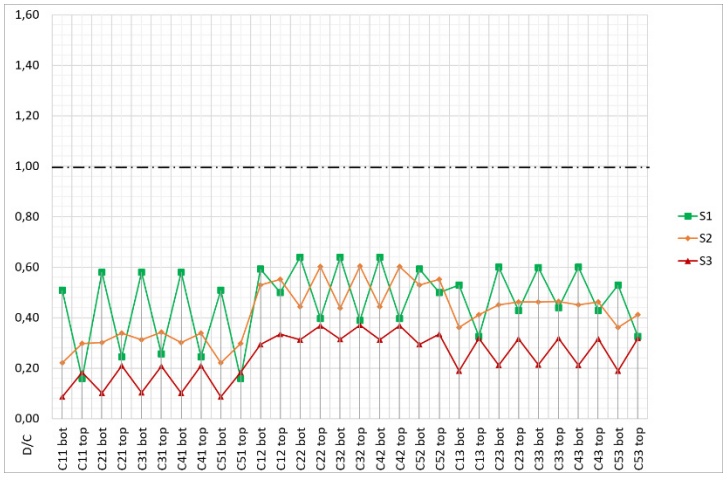

Figure A3.161 – Chord rotation D/C ratios (SD), direction YY (S3_AST1_3S_2×4_YY)

Figure A3.162 – Shear force D/C ratios (SD), direction YY (S3_AST1_3S_2×4_YY)

BUILDING TYPE 7: 3 storeys, 2×4 spans **| SEISMIC HAZARD SCENARIO 4:** PT 1.1 + 2.3 (EC8-1)

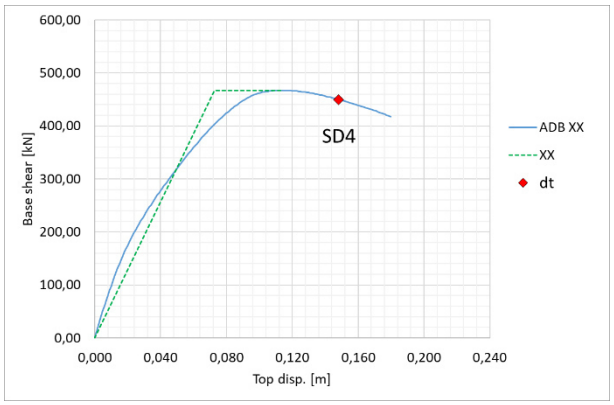

Figure A3.163 – Capacity curve and target displacement d_t, direction XX (S4_AST1_3S_2×4_XX)

Figure A3.164 – Chord rotation D/C ratios (SD), direction XX (S4_AST1_3S_2×4_XX)

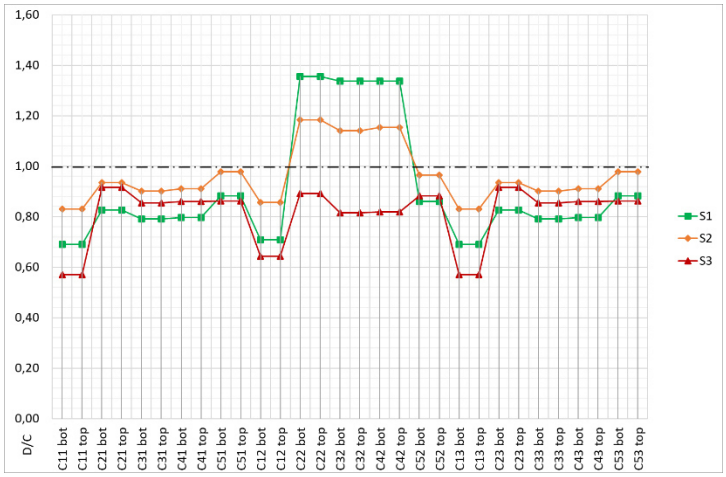

Figure A3.165 – Shear force D/C ratios (SD), direction XX (S4_AST1_3S_2×4_XX)

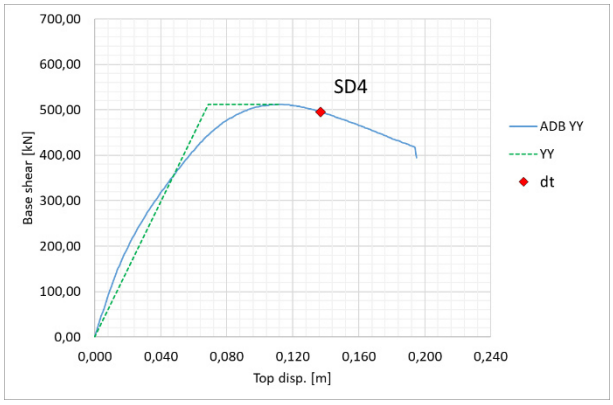

Figure A3.166 – Capacity curve and target displacement d_t, direction YY (S4_AST1_3S_2×4_YY)

Figure A3.167 – Chord rotation D/C ratios (SD), direction YY (S4_AST1_3S_2×4_YY)

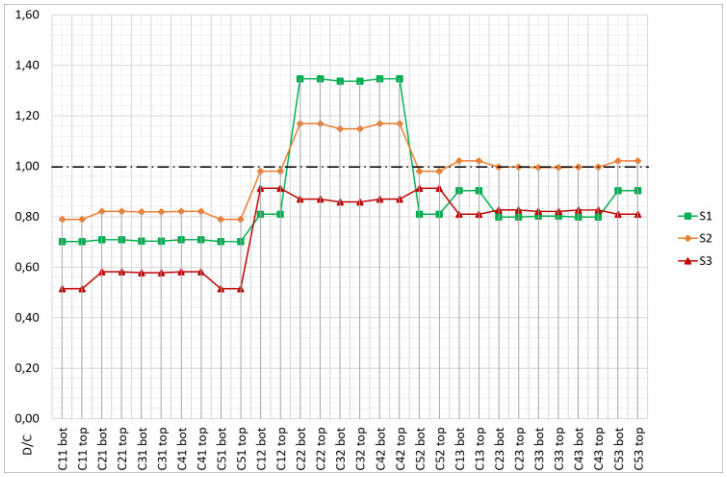

Figure A3.168 – Shear force D/C ratios (SD), direction YY (S4_AST1_3S_2×4_YY)

BUILDING TYPE 8: 4 storeys, 2×4 spans **| SEISMIC HAZARD SCENARIO 1:** PT 1.6 + 2.5 (EC8-1)

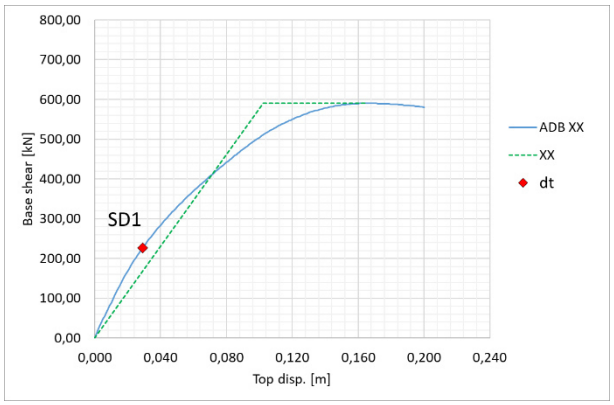

Figure A3.169 – Capacity curve and target displacement d_t, direction XX (S1_AST2_4S_2×4_XX)

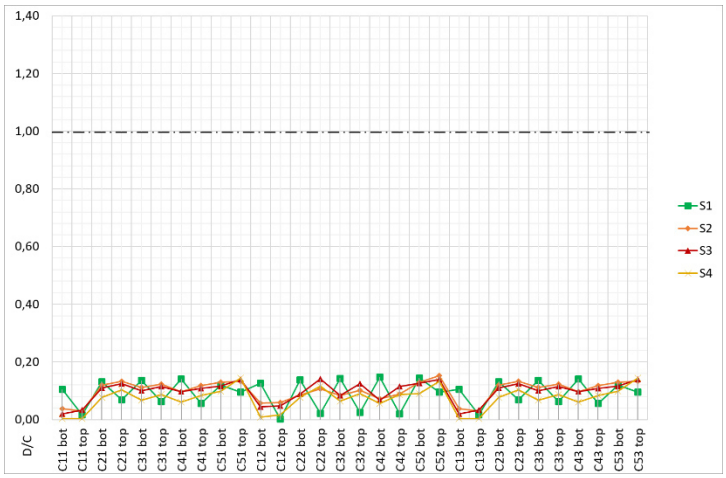

Figure A3.170 – Chord rotation D/C ratios (SD), direction XX (S1_AST2_4S_2×4_XX)

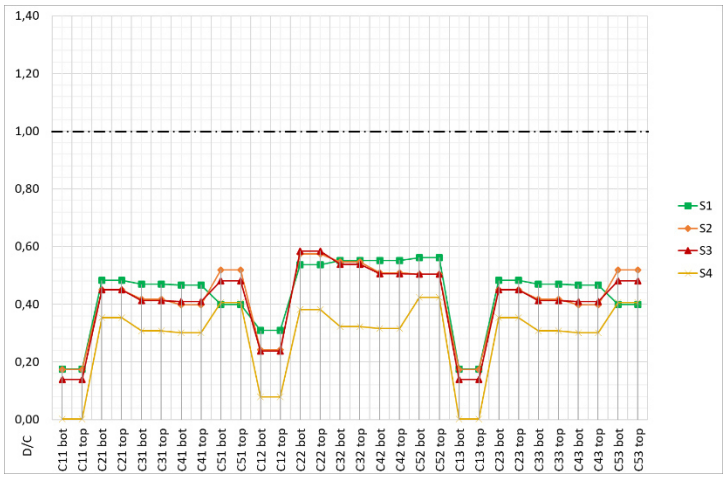

Figure A3.171 – Shear force D/C ratios (SD), direction XX (S1_AST2_4S_2×4_XX)

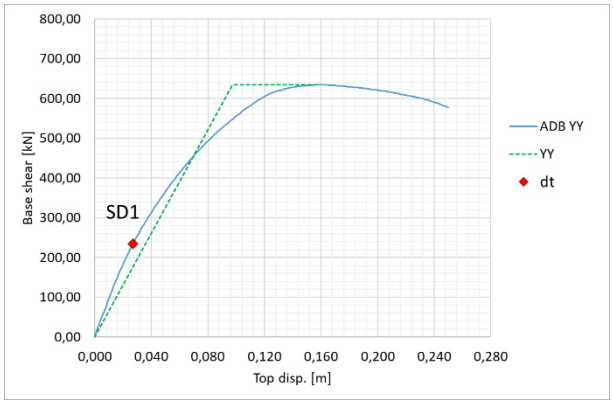

Figure A3.172 – Capacity curve and target displacement d_t, direction YY (S1_AST2_4S_2×4_YY)

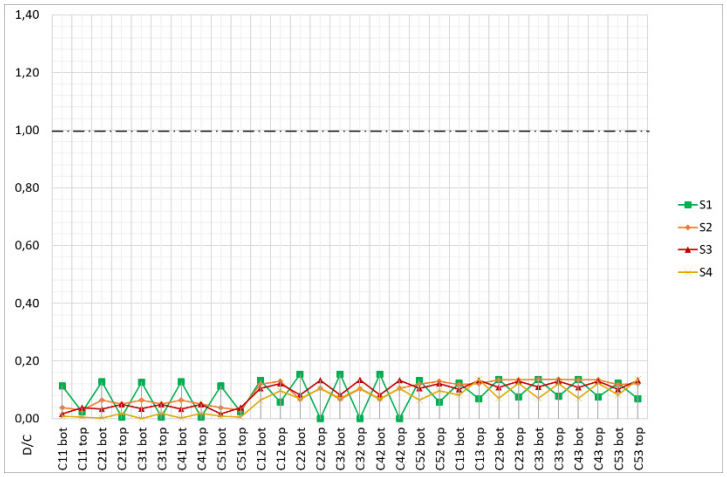

Figure A3.173 – Chord rotation D/C ratios (SD), direction YY (S1_AST2_4S_2×4_YY)

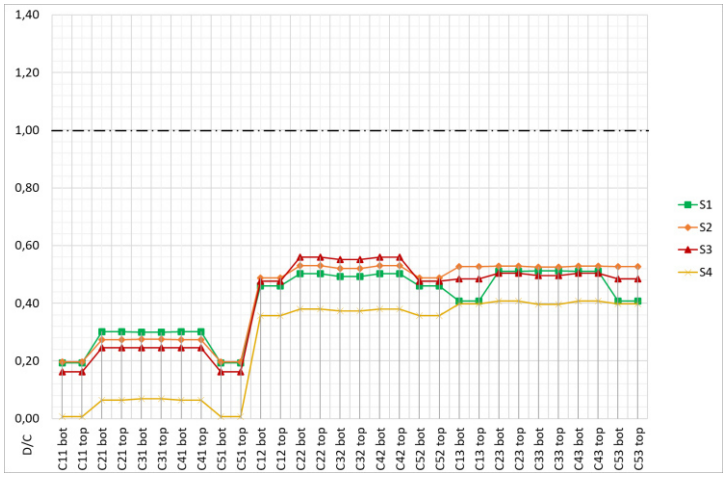

Figure A3.174 – Shear force D/C ratios (SD), direction YY (S1_AST2_4S_2×4_YY)

BUILDING TYPE 8: 4 storeys, 2×4 spans **| SEISMIC HAZARD SCENARIO 2:** PT 1.5 + 2.4 (EC8-1)

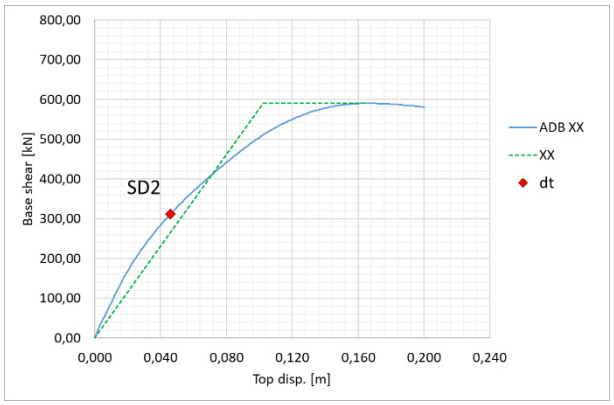

Figure A3.175 – Capacity curve and target displacement d_t, direction XX (S2_AST1_4S_2×4_XX)

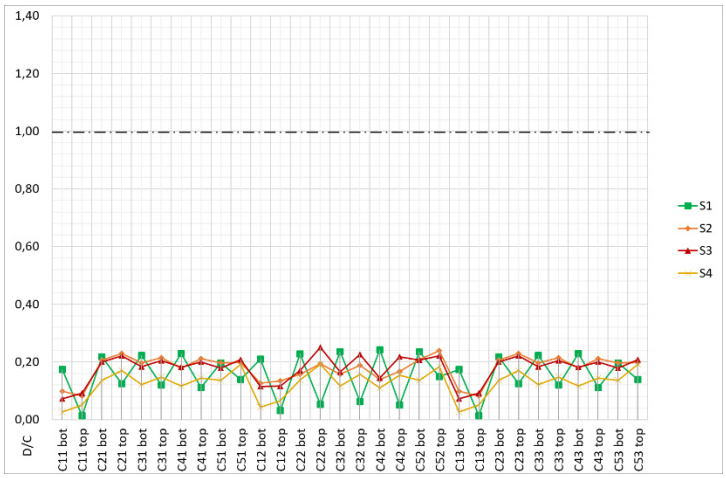

Figure A3.176 – Chord rotation D/C ratios (SD), direction XX (S2_AST1_4S_2×4_XX)

Figure A3.177 – Shear force D/C ratios (SD), direction XX (S2_AST1_4S_2×4_XX)

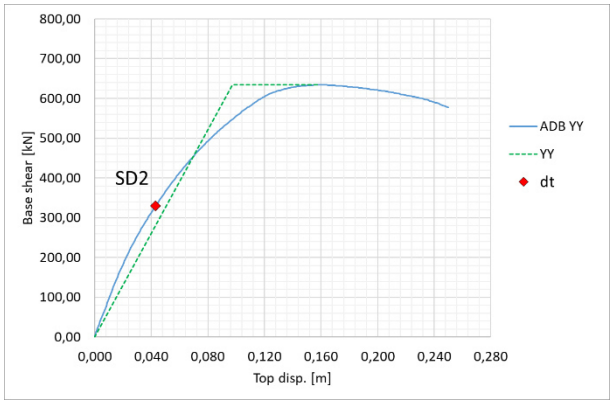

Figure A3.178 – Capacity curve and target displacement d_t, direction YY (S2_AST1_4S_2×4_YY)

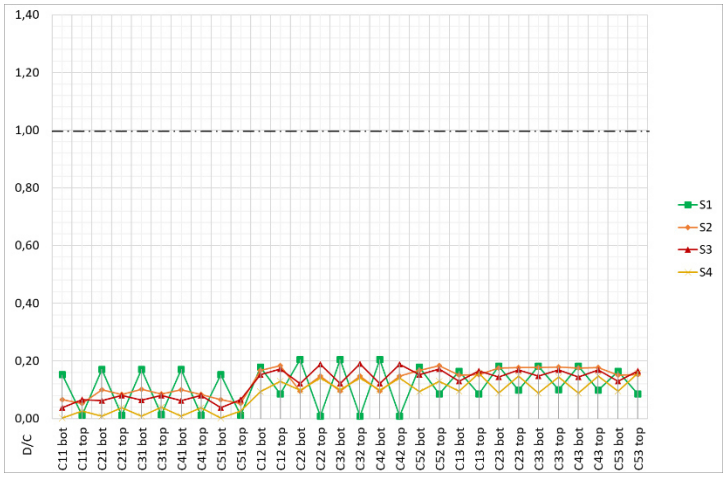

Figure A3.179 – Chord rotation D/C ratios (SD), direction YY (S2_AST1_4S_2×4_YY)

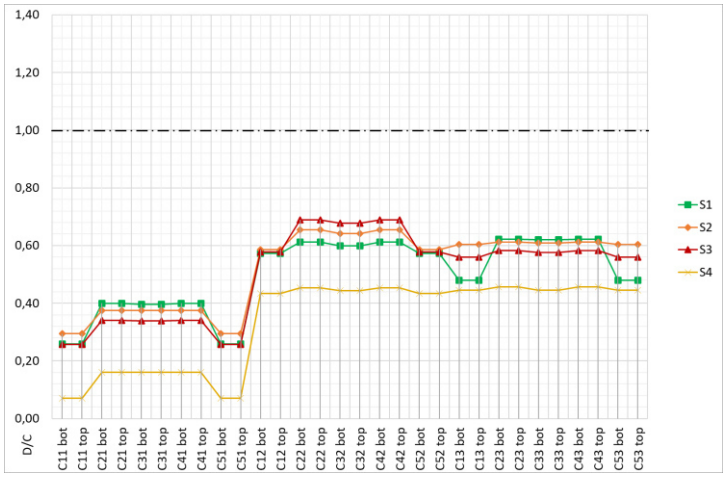

Figure A3.180 – Shear force D/C ratios (SD), direction YY (S2_AST1_4S_2×4_YY)

BUILDING TYPE 8: 4 storeys, 2×4 spans **| SEISMIC HAZARD SCENARIO 3:** PT 1.3 + 2.3 (EC8-1)

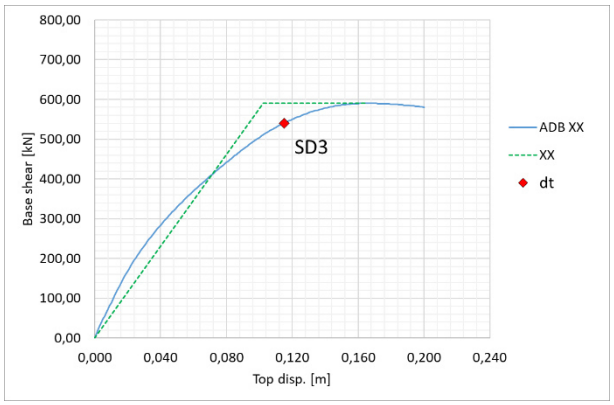

Figure A3.181 – Capacity curve and target displacement d_t, direction XX (S3_AST1_4S_2×4_XX)

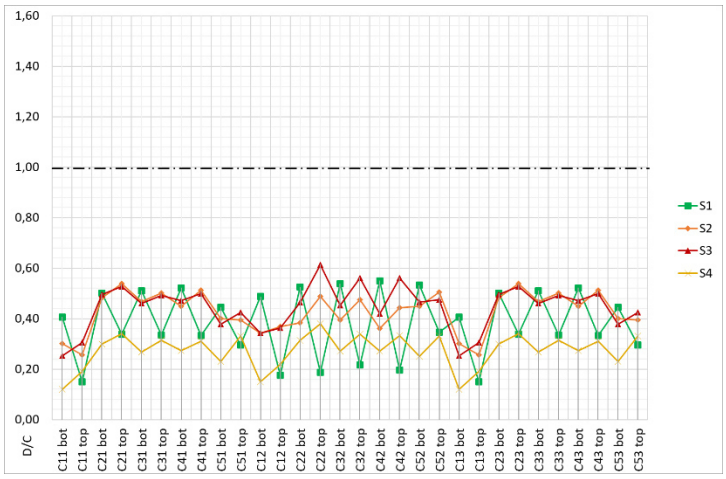

Figure A3.182 – Chord rotation D/C ratios (SD), direction XX (S3_AST1_4S_2×4_XX)

Figure A3.183 – Shear force D/C ratios (SD), direction XX (S3_AST1_4S_2×4_XX)

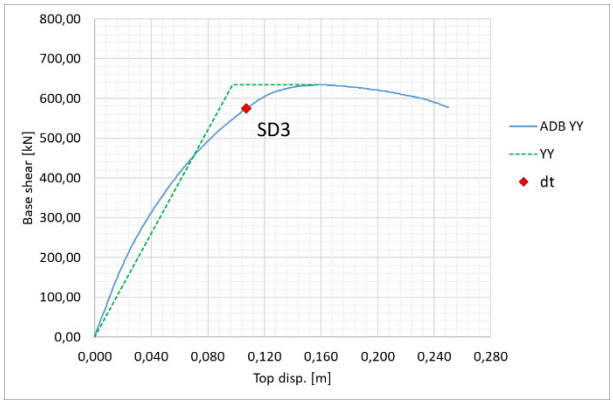

Figure A3.184 – Capacity curve and target displacement d_t, direction YY (S3_AST1_4S_2×4_YY)

Figure A3.185 – Chord rotation D/C ratios (SD), direction YY (S3_AST1_4S_2×4_YY)

Figure A3.186 – Shear force D/C ratios (SD), direction YY (S3_AST1_4S_2×4_YY)

BUILDING TYPE 8: 4 storeys, 2×4 spans **| SEISMIC HAZARD SCENARIO 4:** PT 1.1 + 2.3 (EC8-1)

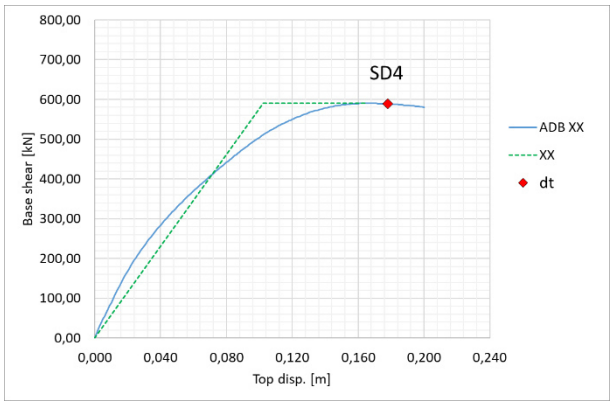

Figure A3.187 – Capacity curve and target displacement d_t, direction XX (S4_AST1_4S_2×4_XX)

Figure A3.188 – Chord rotation D/C ratios (SD), direction XX (S4_AST1_4S_2×4_XX)

Figure A3.189 – Shear force D/C ratios (SD), direction XX (S4_AST1_4S_2×4_XX)

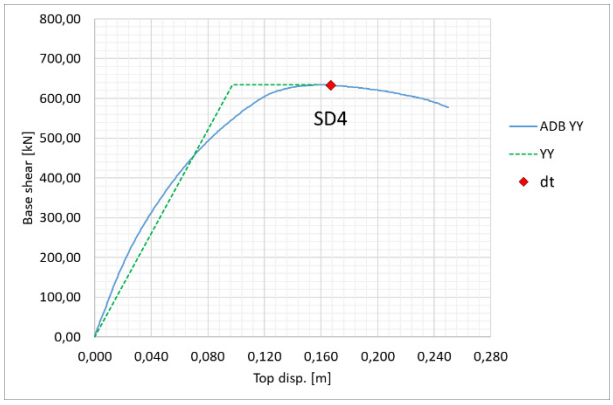

Figure A3.190 – Capacity curve and target displacement d_t, direction YY (S4_AST1_4S_2×4_YY)

Figure A3.191 – Chord rotation D/C ratios (SD), direction YY (S4_AST1_4S_2×4_YY)

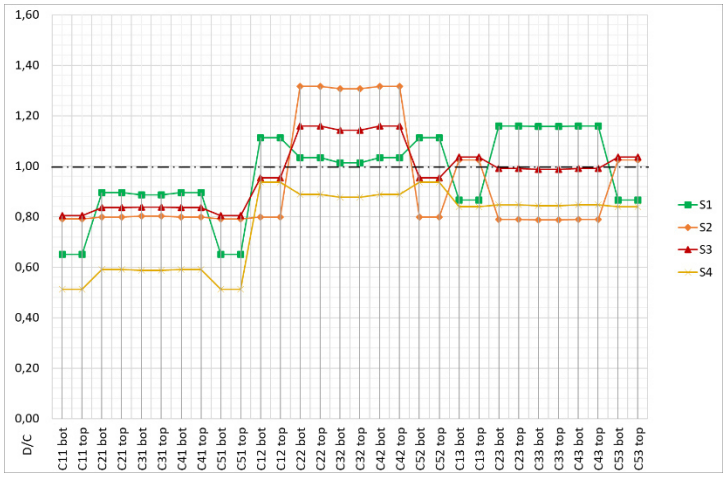

Figure A3.192 – Shear force D/C ratios (SD), direction YY (S4_AST1_4S_2×4_YY)

BUILDING TYPE 9: 5 storeys, 2×4 spans **| SEISMIC HAZARD SCENARIO 1:** PT 1.6 + 2.5 (EC8-1)

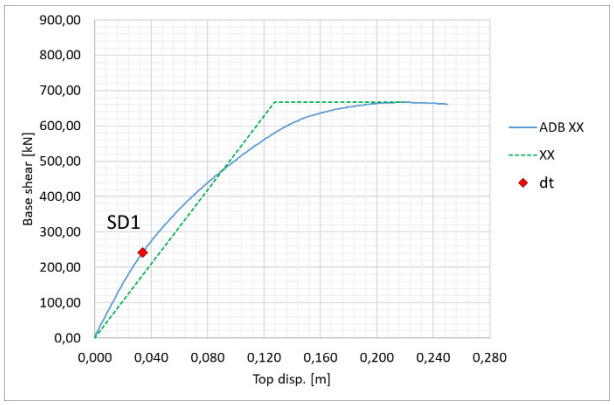

Figure A3.193 – Capacity curve and target displacement d_t, direction XX (S1_AST2_5S_2×4_XX)

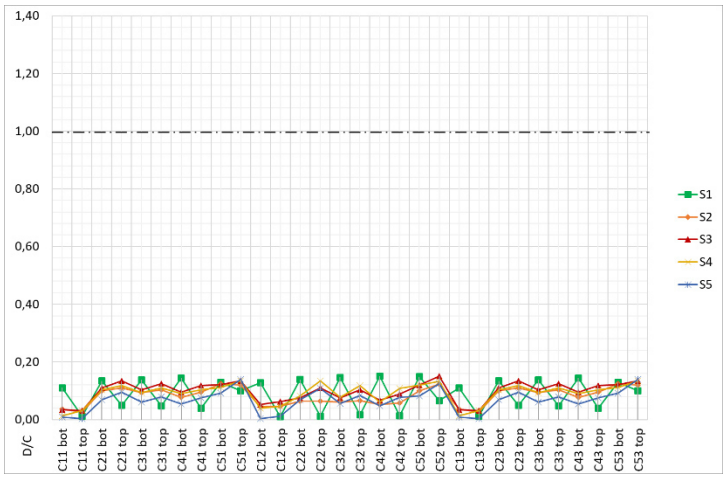

Figure A3.194 – Chord rotation D/C ratios (SD), direction XX (S1_AST2_5S_2×4_XX)

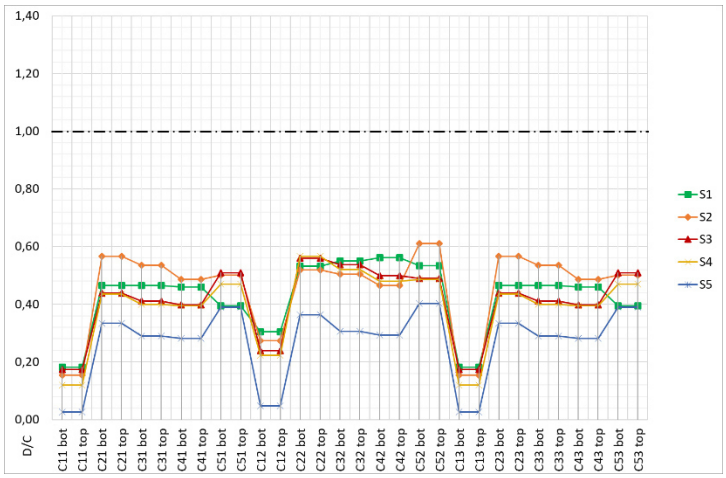

Figure A3.195 – Shear force D/C ratios (SD), direction XX (S1_AST2_5S_2×4_XX)

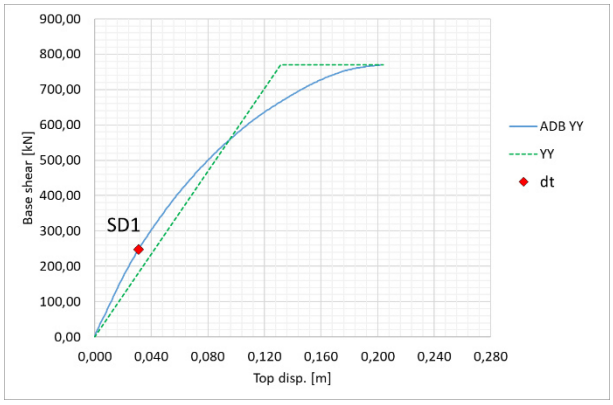

Figure A3.196 – Capacity curve and target displacement d_t, direction YY (S1_AST2_5S_2×4_YY)

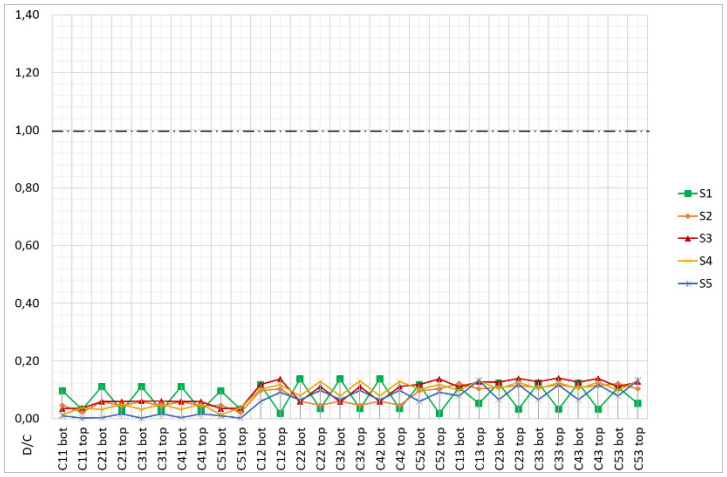

Figure A3.197 – Chord rotation D/C ratios (SD), direction YY (S1_AST2_5S_2×4_YY)

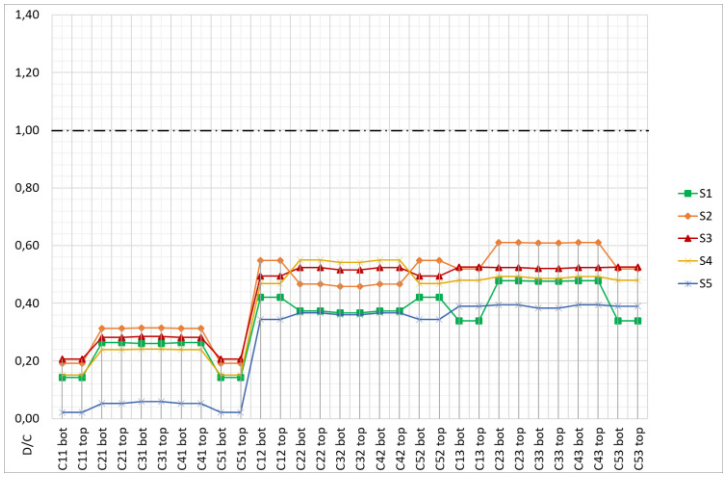

Figure A3.198 – Shear force D/C ratios (SD), direction YY (S1_AST2_5S_2×4_YY)

BUILDING TYPE 9: 5 storeys, 2×4 spans **| SEISMIC HAZARD SCENARIO 2:** PT 1.5 + 2.4 (EC8-1)

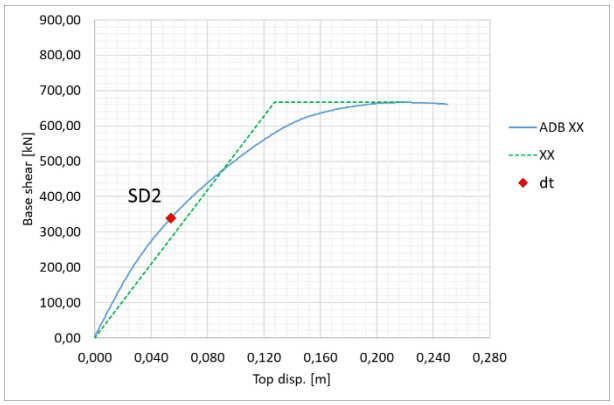

Figure A3.199 – Capacity curve and target displacement d_t, direction XX (S2_AST1_5S_2×4_XX)

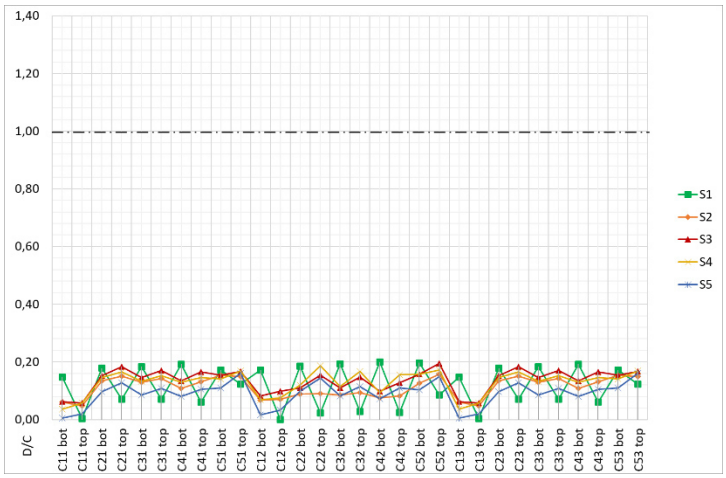

Figure A3.200 – Chord rotation D/C ratios (SD), direction XX (S2_AST1_5S_2×4_XX)

Figure A3.201 – Shear force D/C ratios (SD), direction XX (S2_AST1_5S_2×4_XX)

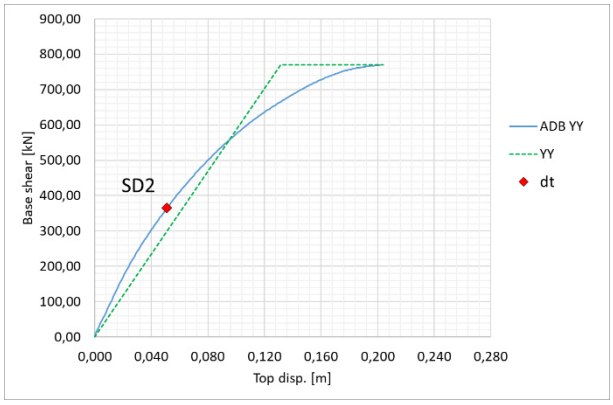

Figure A3.202 – Capacity curve and target displacement d_t, direction YY (S2_AST1_5S_2×4_YY)

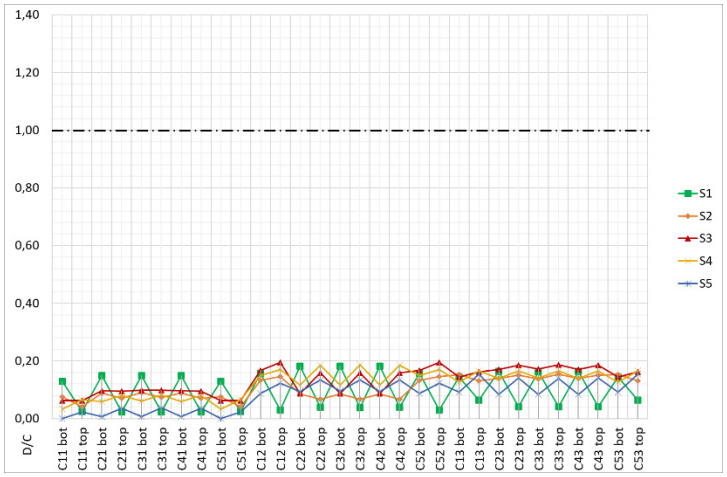

Figure A3.203 – Chord rotation D/C ratios (SD), direction YY (S2_AST1_5S_2×4_YY)

Figure A3.204 – Shear force D/C ratios (SD), direction YY (S2_AST1_5S_2×4_YY)

BUILDING TYPE 9: 5 storeys, 2×4 spans **| SEISMIC HAZARD SCENARIO 3:** PT 1.3 + 2.3 (EC8-1)

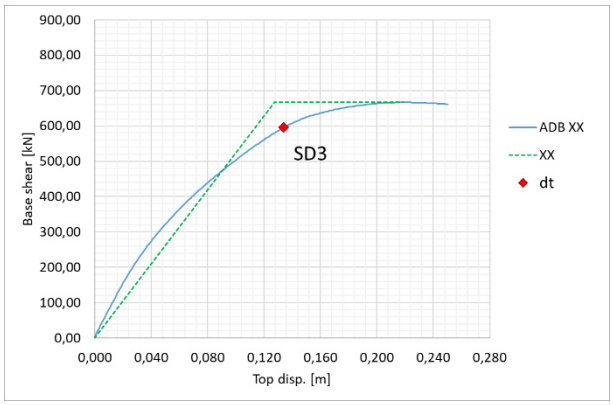

Figure A3.205 – Capacity curve and target displacement d_t, direction XX (S3_AST1_5S_2×4_XX)

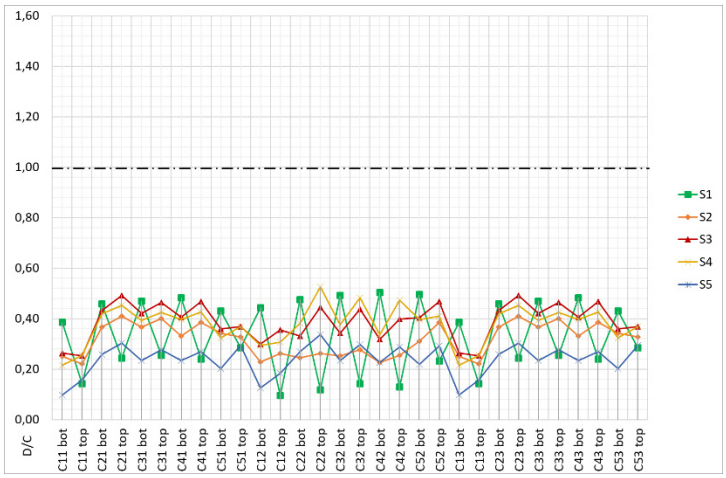

Figure A3.206 – Chord rotation D/C ratios (SD), direction XX (S3_AST1_5S_2×4_XX)

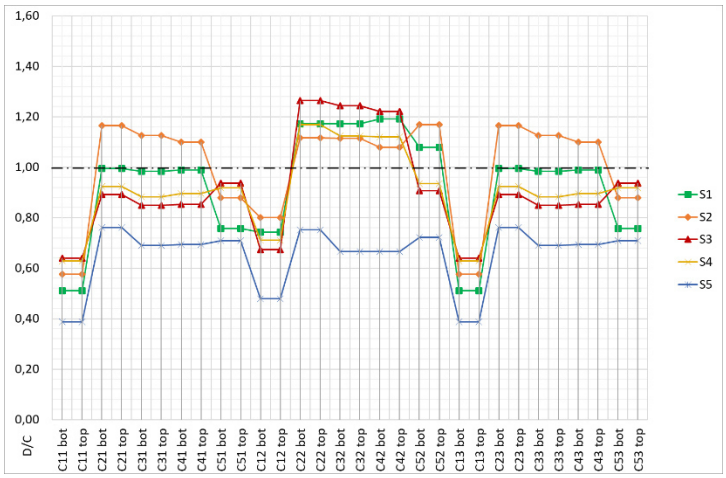

Figure A3.207 – Shear force D/C ratios (SD), direction XX (S3_AST1_5S_2×4_XX)

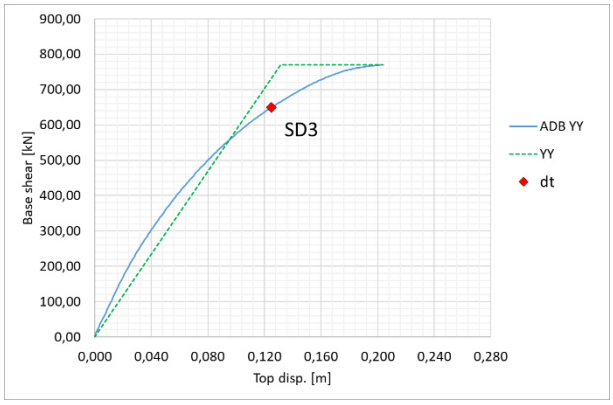

Figure A3.208 – Capacity curve and target displacement d_t, direction YY (S3_AST1_5S_2×4_YY)

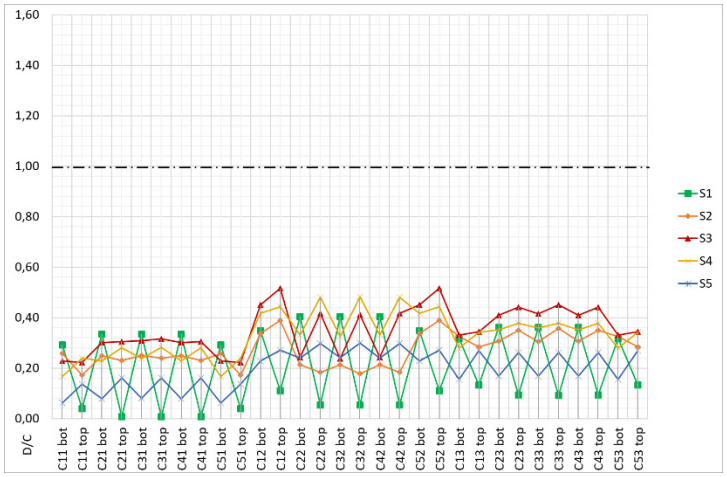

Figure A3.209 – Chord rotation D/C ratios (SD), direction YY (S3_AST1_5S_2×4_YY)

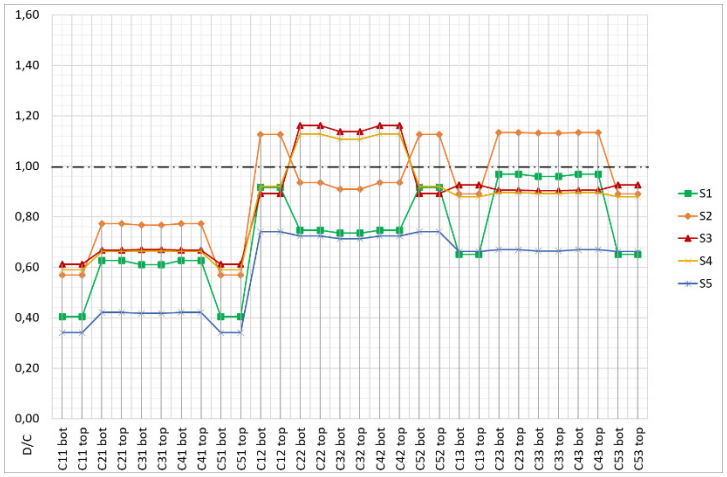

Figure A3.210 – Shear force D/C ratios (SD), direction YY (S3_AST1_5S_2×4_YY)

BUILDING TYPE 9: 5 storeys, 2×4 spans **| SEISMIC HAZARD SCENARIO 4:** PT 1.1 + 2.3 (EC8-1)

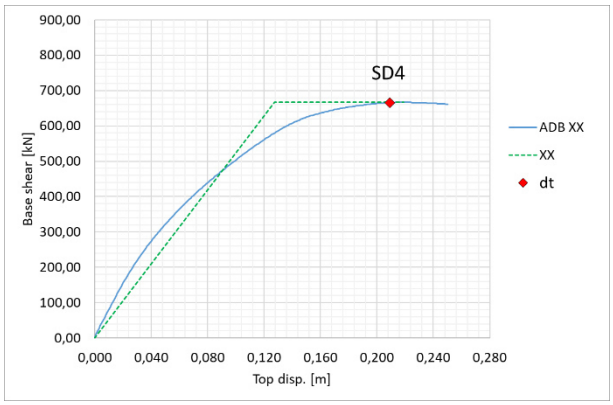

Figure A3.211 – Capacity curve and target displacement d_t, direction XX (S4_AST1_5S_2×4_XX)

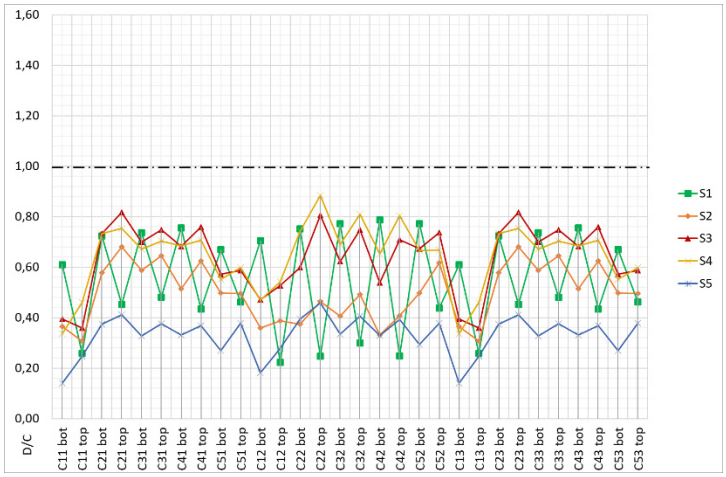

Figure A3.212 – Chord rotation D/C ratios (SD), direction XX (S4_AST1_5S_2×4_XX)

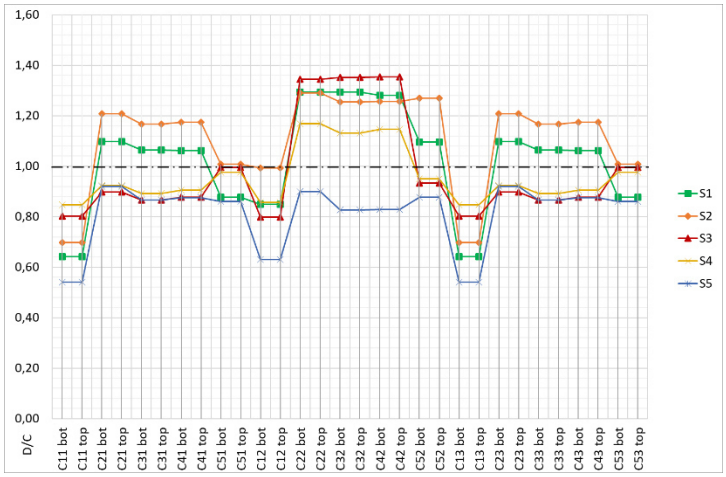

Figure A3.213 – Shear force D/C ratios (SD), direction XX (S4_AST1_5S_2×4_XX)

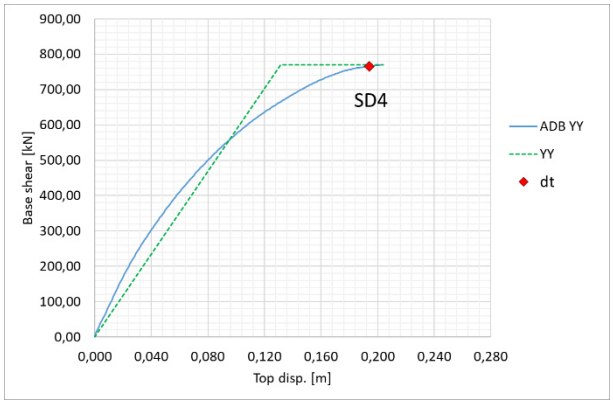

Figure A3.214 – Capacity curve and target displacement d_t, direction YY (S4_AST1_5S_2×4_YY)

Figure A3.215 – Chord rotation D/C ratios (SD), direction YY (S4_AST1_5S_2×4_YY)

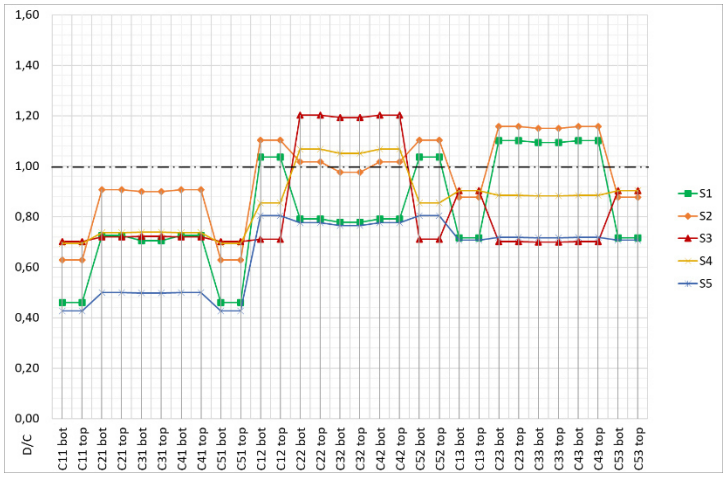

Figure A3.216 – Shear force D/C ratios (SD), direction YY (S4_AST1_5S_2×4_YY)

BUILDING TYPE 10: 6 storeys, 2×4 spans **| SEISMIC HAZARD SCENARIO 1:** PT 1.6 + 2.5 (EC8-1)

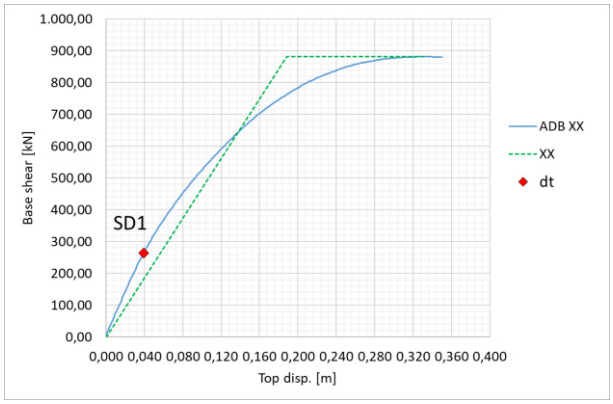

Figure A3.217 – Capacity curve and target displacement d_t, direction XX (S1_AST2_6S_2×4_XX)

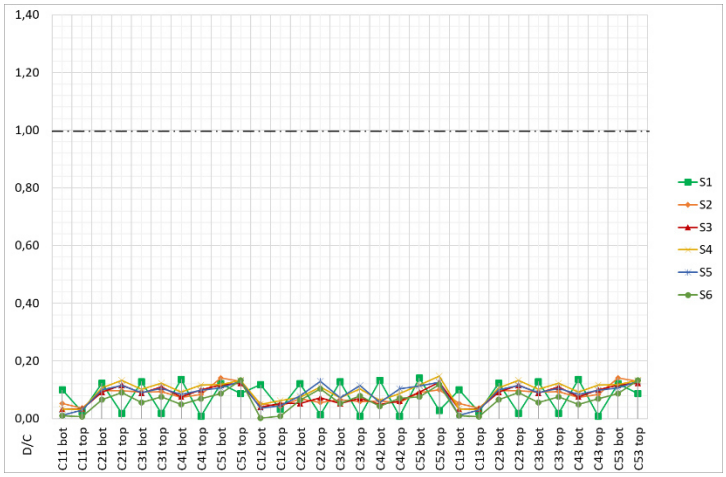

Figure A3.218 – Chord rotation D/C ratios (SD), direction XX (S1_AST2_6S_2×4_XX)

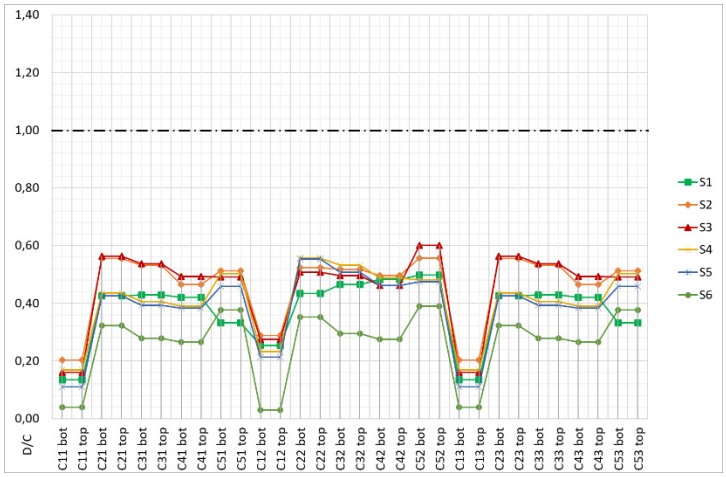

Figure A3.219 – Shear force D/C ratios (SD), direction XX (S1_AST2_6S_2×4_XX)

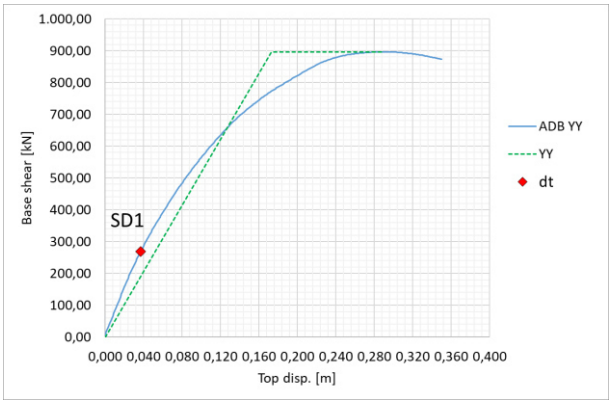

Figure A3.220 – Capacity curve and target displacement d_t, direction YY (S1_AST2_6S_2×4_YY)

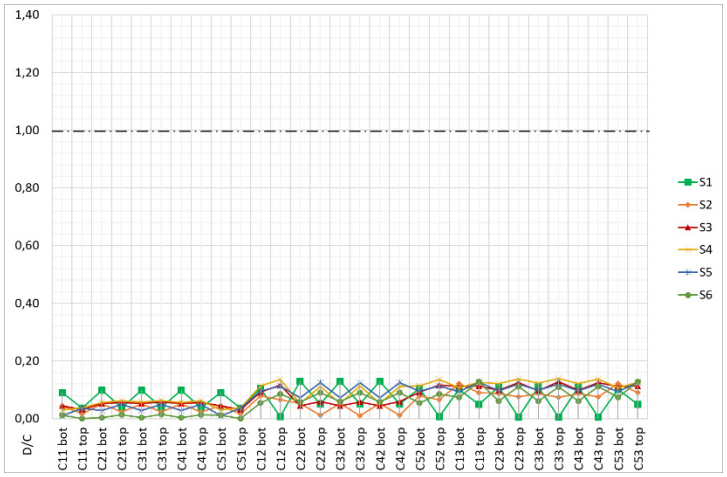

Figure A3.221 – Chord rotation D/C ratios (SD), direction YY (S1_AST2_6S_2×4_YY)

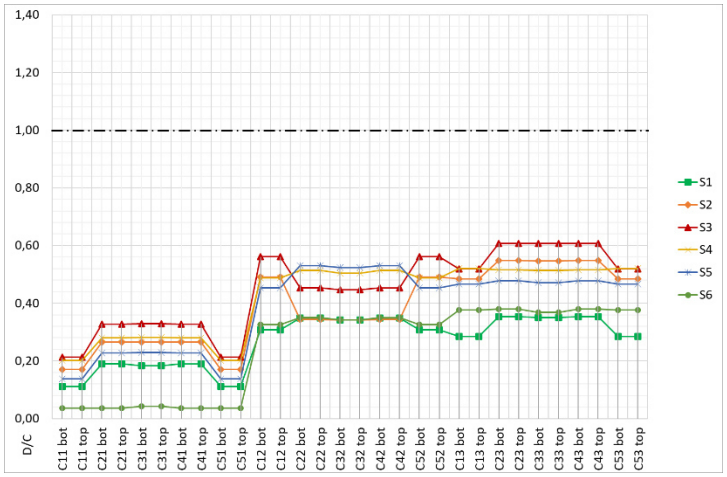

Figure A3.222 – Shear force D/C ratios (SD), direction YY (S1_AST2_6S_2×4_YY)

BUILDING TYPE 10: 6 storeys, 2×4 spans **| SEISMIC HAZARD SCENARIO 2:** PT 1.5 + 2.4 (EC8-1)

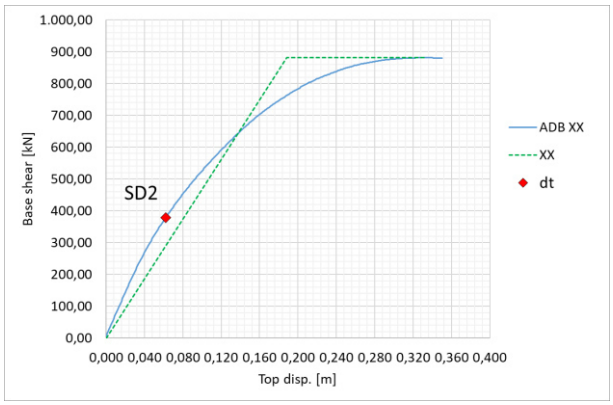

Figure A3.223 – Capacity curve and target displacement d_t, direction XX (S2_AST1_6S_2×4_XX)

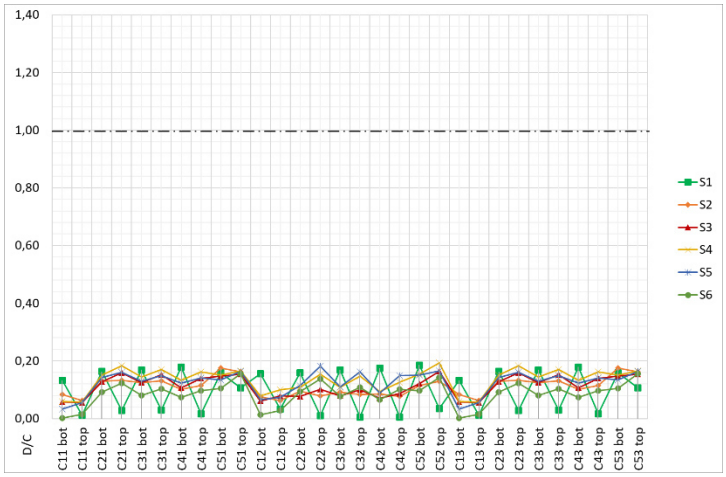

Figure A3.224 – Chord rotation D/C ratios (SD), direction XX (S2_AST1_6S_2×4_XX)

Figure A3.225 – Shear force D/C ratios (SD), direction XX (S2_AST1_6S_2×4_XX)

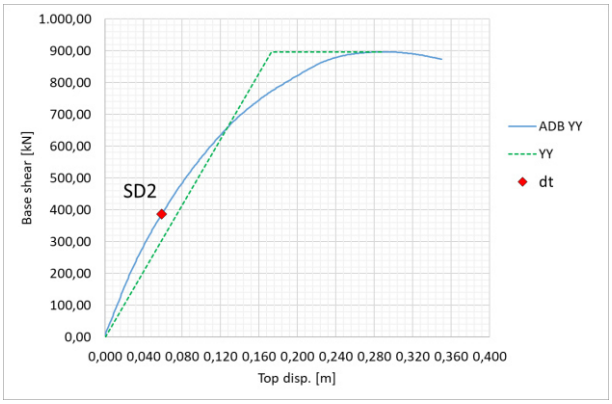

Figure A3.226 – Capacity curve and target displacement d_t, direction YY (S2_AST1_6S_2×4_YY)

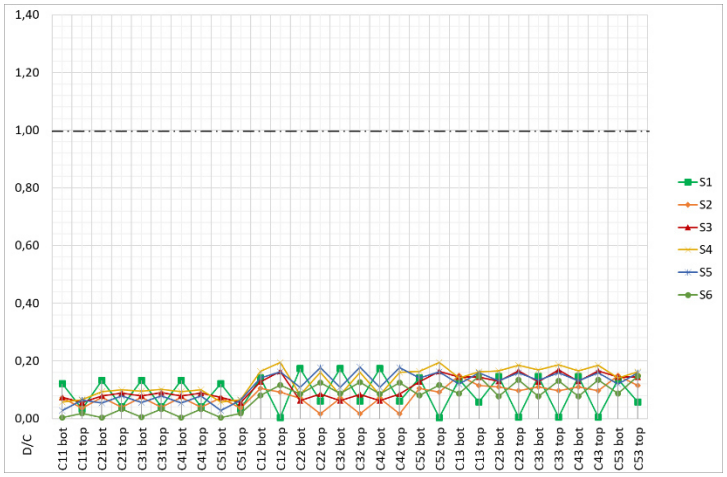

Figure A3.227 – Chord rotation D/C ratios (SD), direction YY (S2_AST1_6S_2×4_YY)

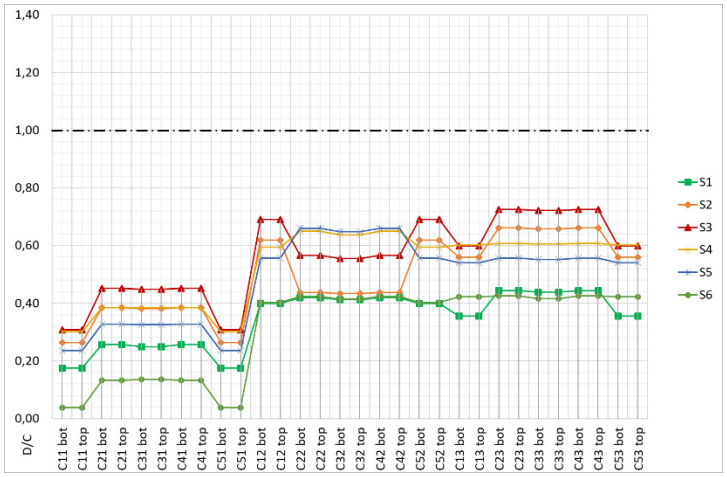

Figure A3.228 – Shear force D/C ratios (SD), direction YY (S2_AST1_6S_2×4_YY)

BUILDING TYPE 10: 6 storeys, 2×4 spans **| SEISMIC HAZARD SCENARIO 3:** PT 1.3 + 2.3 (EC8-1)

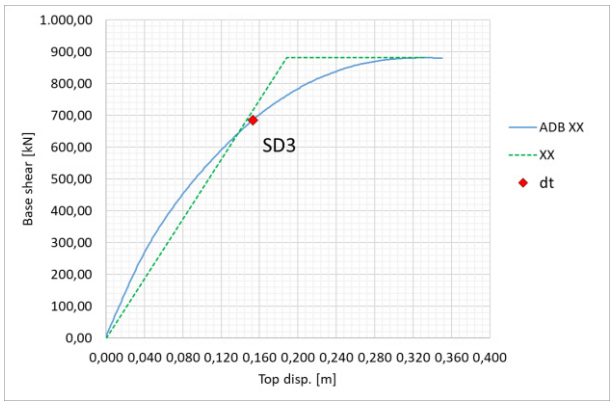

Figure A3.229 – Capacity curve and target displacement d_t, direction XX (S3_AST1_6S_2×4_XX)

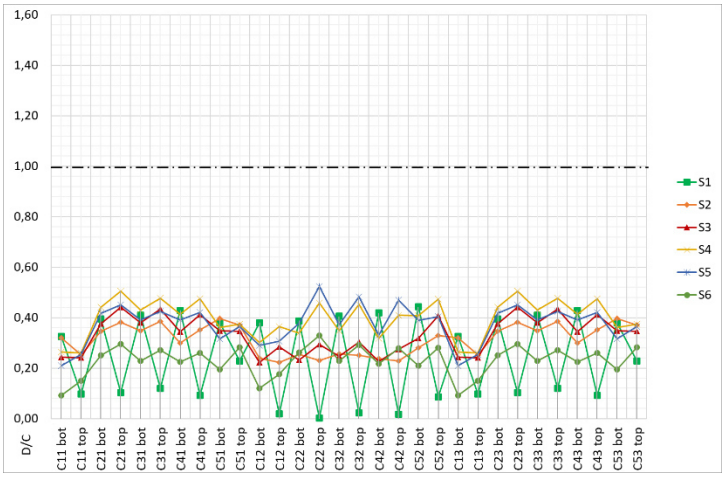

Figure A3.230 – Chord rotation D/C ratios (SD), direction XX (S3_AST1_6S_2×4_XX)

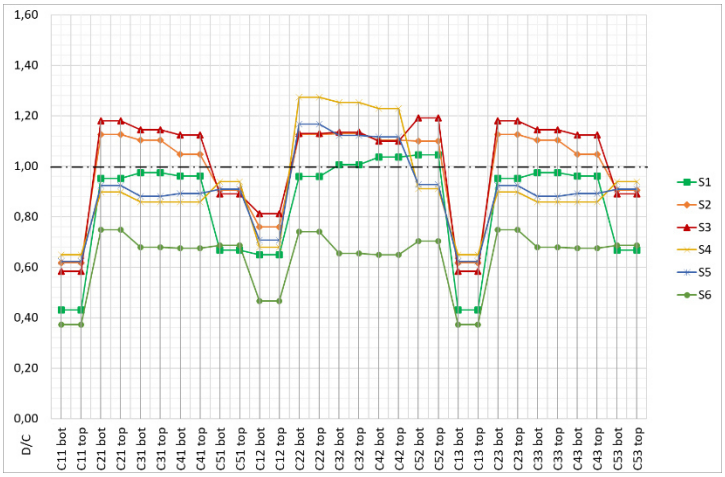

Figure A3.231 – Shear force D/C ratios (SD), direction XX (S3_AST1_6S_2×4_XX)

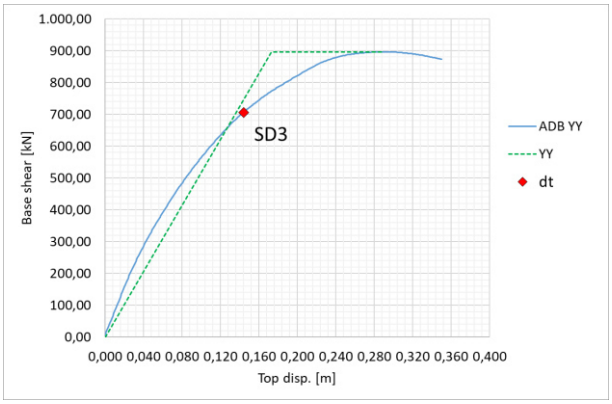

Figure A3.232 – Capacity curve and target displacement d_t, direction YY (S3_AST1_6S_2×4_YY)

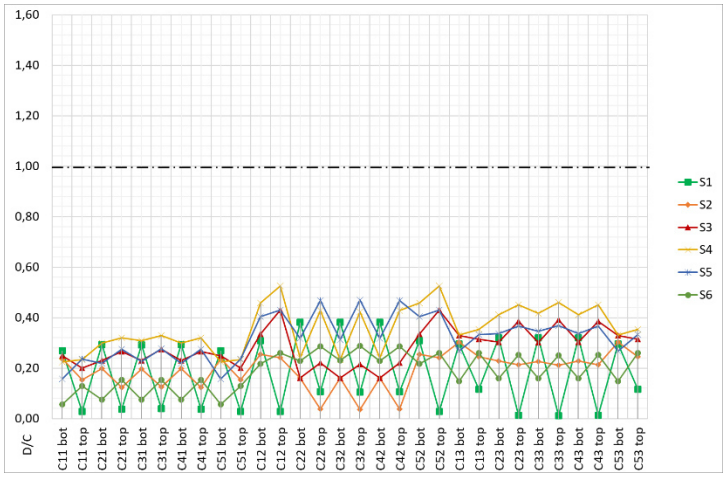

Figure A3.233 – Chord rotation D/C ratios (SD), direction YY (S3_AST1_6S_2×4_YY)

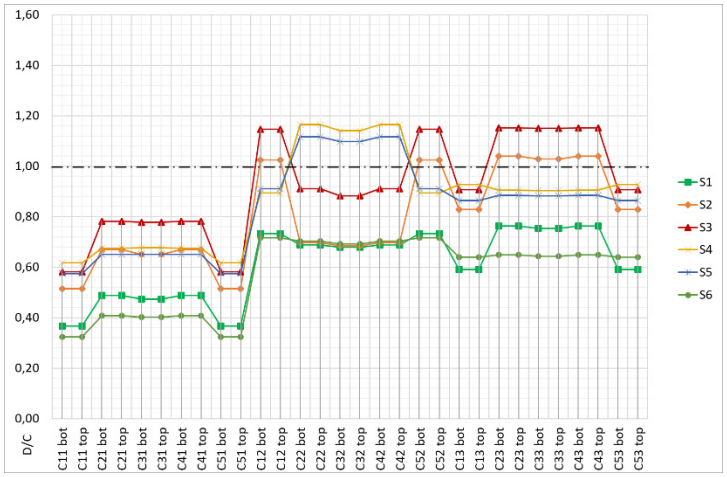

Figure A3.234 – Shear force D/C ratios (SD), direction YY (S3_AST1_6S_2×4_YY)

BUILDING TYPE 10: 6 storeys, 2×4 spans **| SEISMIC HAZARD SCENARIO 4:** PT 1.1 + 2.3 (EC8-1)

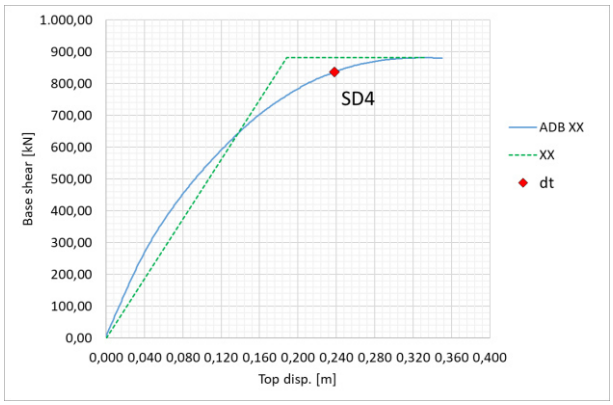

Figure A3.235 – Capacity curve and target displacement d_t, direction XX (S4_AST1_6S_2×4_XX)

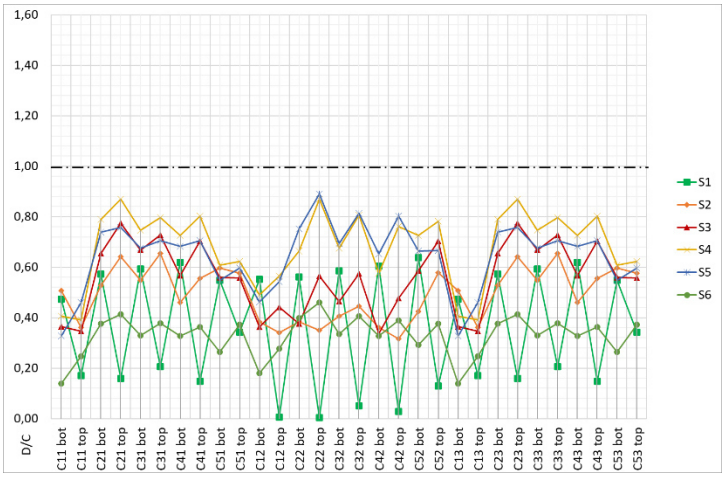

Figure A3.236 – Chord rotation D/C ratios (SD), direction XX (S4_AST1_6S_2×4_XX)

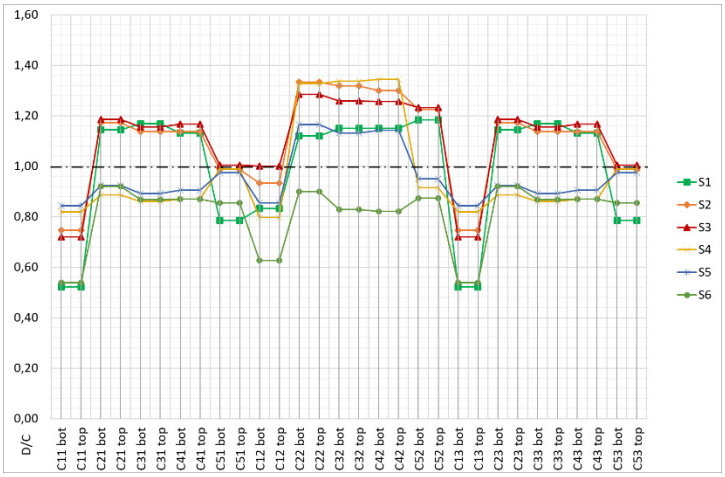

Figure A3.237 – Shear force D/C ratios (SD), direction XX (S4_AST1_6S_2×4_XX)

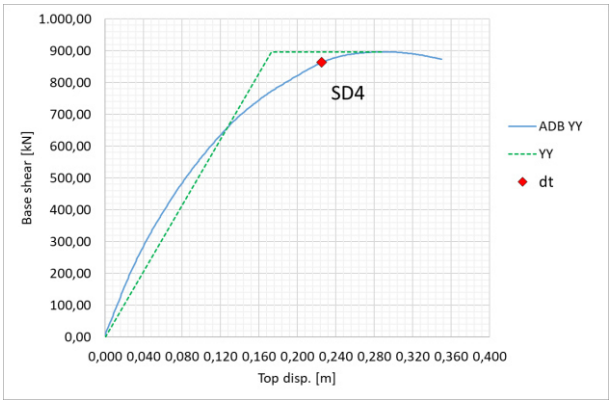

Figure A3.238 – Capacity curve and target displacement d_t, direction YY (S4_AST1_6S_2×4_YY)

Figure A3.239 – Chord rotation D/C ratios (SD), direction YY (S4_AST1_6S_2×4_YY)

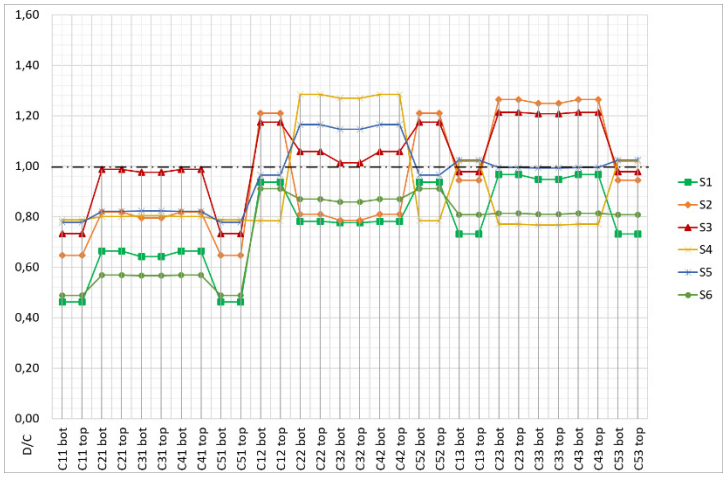

Figure A3.240 – Shear force D/C ratios (SD), direction YY (S4_AST1_6S_2×4_YY)

APPENDIX 4

RETROFITTED BUILDINGS – DESIGN DRAWINGS

APPENDIX 4 – RETROFITTED BUILDINGS – DESIGN DRAWINGS

BUILDING TYPE 1: 2 storeys, 3×5 spans

Seismic hazard scenario 3: PT 1.3 + 2.3 (EC8-1)

Geometry

Details

Seismic hazard scenario 4: PT 1.1 + 2.3 (EC8-1)

Geometry

Details

BUILDING TYPE 2: 3 storeys, 3×5 spans

Id

BUILDING TYPE 3: 4 storeys, 3×5 spans

Id

BUILDING TYPE 4: 5 storeys, 3×5 spans

Id

BUILDING TYPE 5: 6 storeys, 3×5 spans

Id

BUILDING TYPE 6: 2 storeys, 2×4 spans

Id

BUILDING TYPE 7: 3 storeys, 2×4 spans

Id

BUILDING TYPE 8: 4 storeys, 2×4 spans

Id

BUILDING TYPE 9: 5 storeys, 2×4 spans

Id

BUILDING TYPE 10: 6 storeys, 2×4 spans

Id

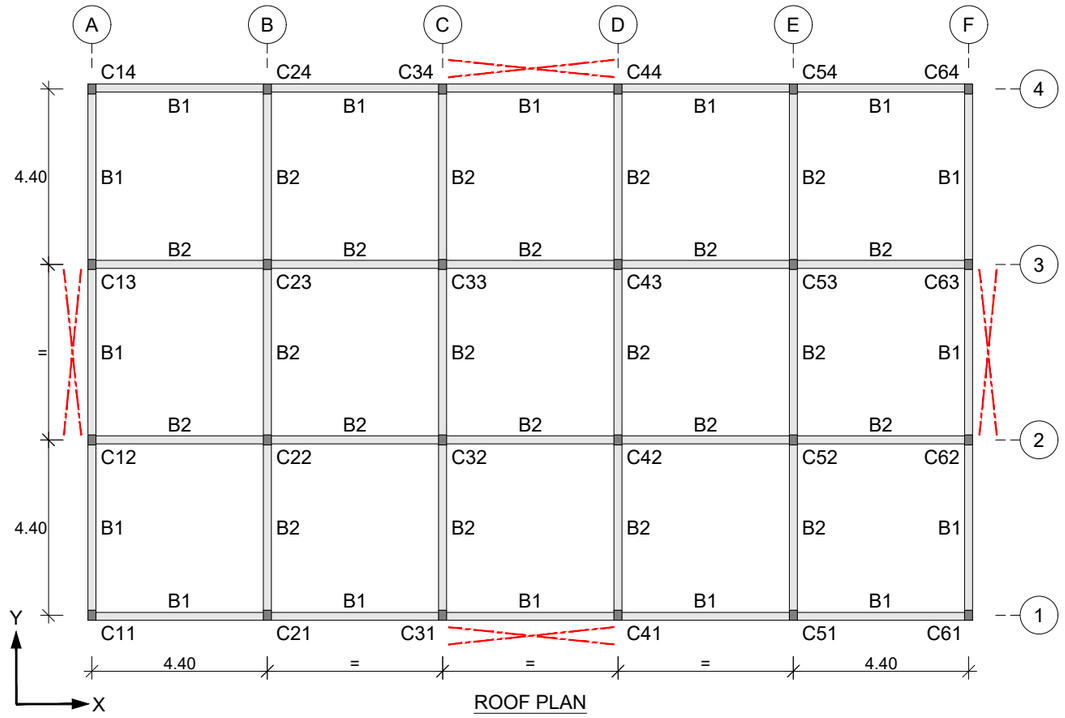

ROOF PLAN

KEY:

- Steel Braces

CONCRETE: fcm = 23.8 MPa
STEEL: fym = 440 MPa
CONCRETE COVER: c = 25 mm
STEEL BRACES: fym = 275 MPa

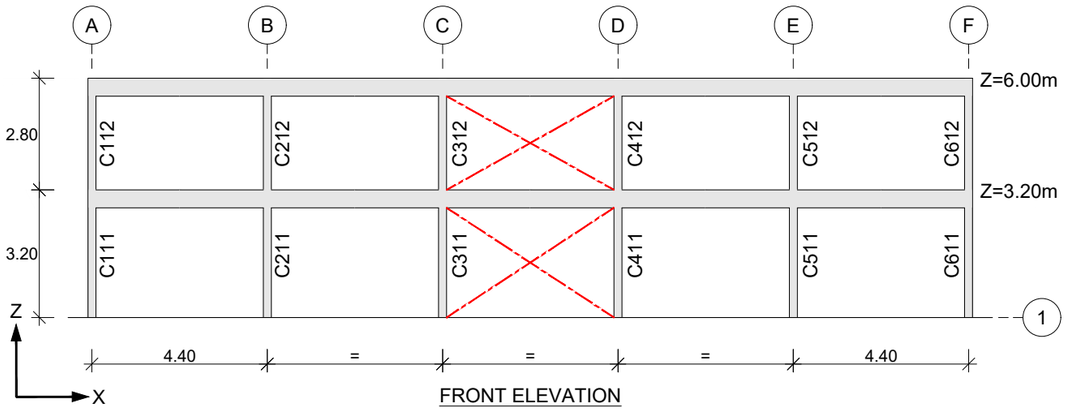

FRONT ELEVATION

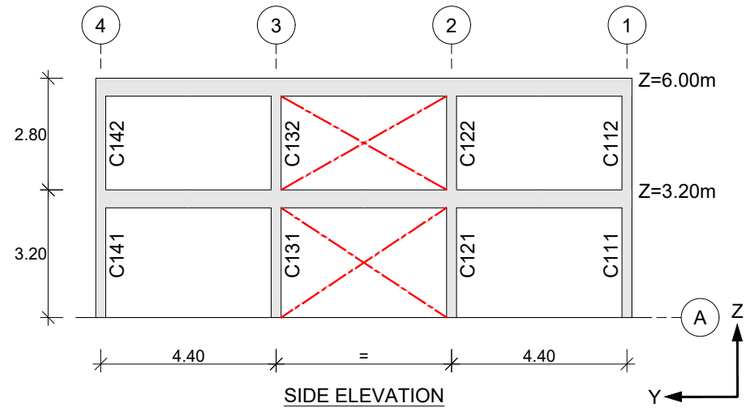

SIDE ELEVATION

S3_2S_3x5_RETRO	APPENDIX 4
GEOMETRY	A4.1

CONCRETE: fcm = 23.8 MPa
STEEL: fym = 440 MPa
CONCRETE COVER: c = 25 mm
STEEL BRACES: fym = 275 MPa

COLUMNS SCHEDULE

	C11 / C61 / C14 / C64	C21 / C31 / C41 / C51 / C12 / C62 / C13 / C63 / C24 / C34 / C44 / C54	C22 / C32 / C42 / C52 / C23 / C33 / C43 / C53
2nd Floor	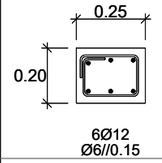	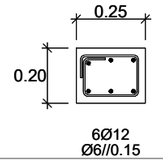	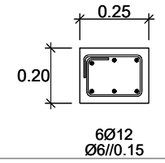
1st Floor	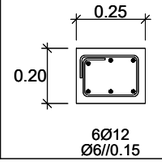	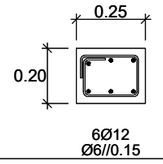	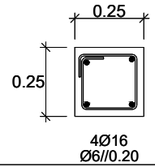
Ground Floor			

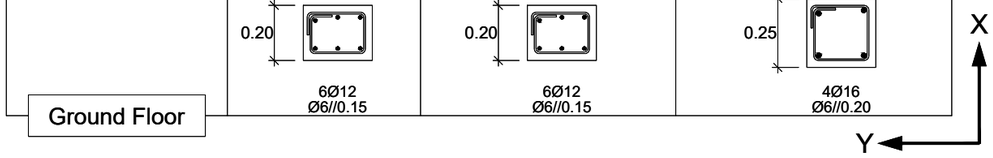

BEAM B1

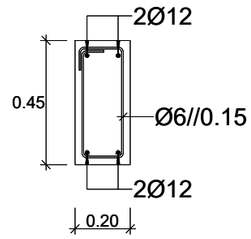

Span and Supports

BEAM B2

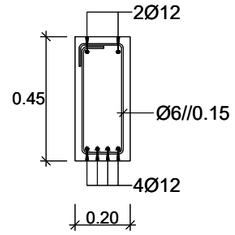

Span

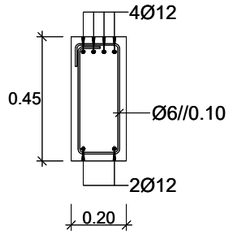

Supports

STEEL BRACES

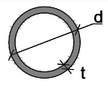

CHSH dxt (mm)

STOREY	STEEL BRACES	
	DIRECTION XX	DIRECTION YY
2nd	CHSH 88.9x3.2	CHSH 88.9x3.2
1st	CHSH 88.9x3.2	CHSH 88.9x3.2

S3_2S_3x5_RETRO	APPENDIX 4
DETAILS	A4.2

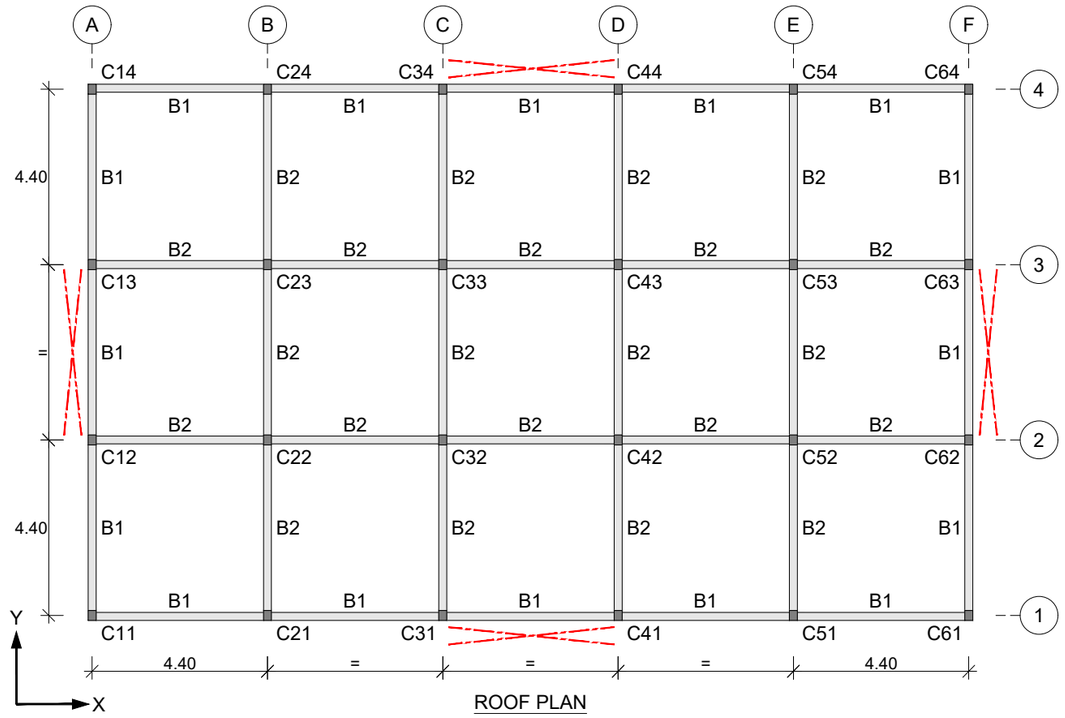

ROOF PLAN

KEY:

- Steel Braces

CONCRETE: fcm = 23.8 MPa
STEEL: fym = 440 MPa
CONCRETE COVER: c = 25 mm
STEEL BRACES: fym = 275 MPa

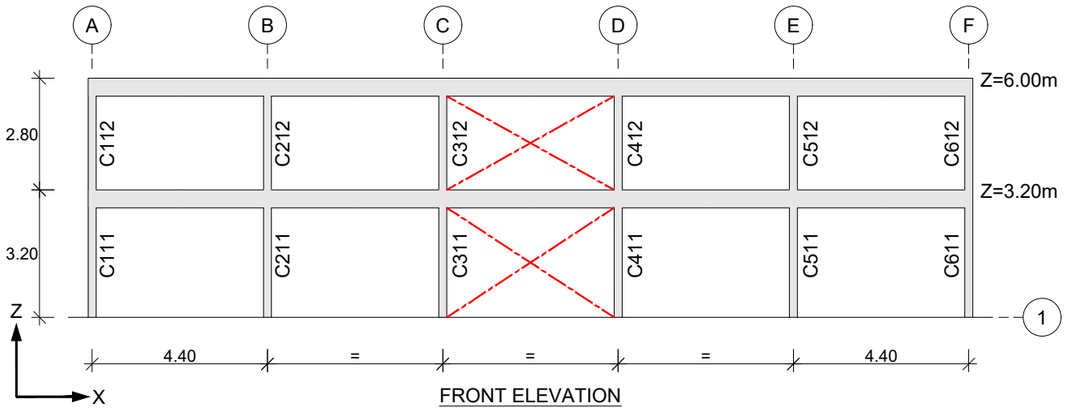

FRONT ELEVATION

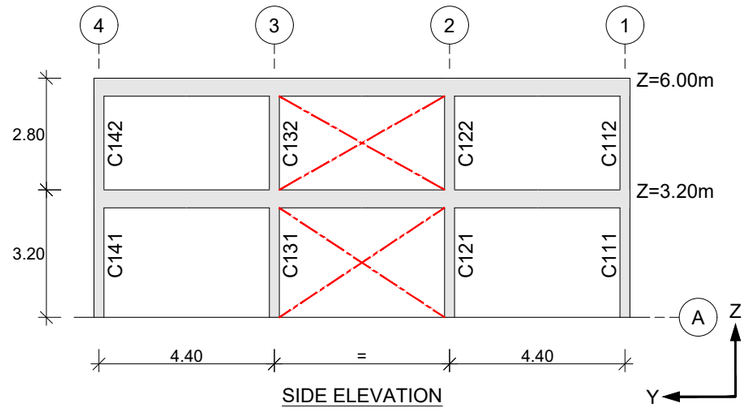

SIDE ELEVATION

S4_2S_3x5_RETRO	APPENDIX 4
GEOMETRY	A4.3

CONCRETE: fcm = 23.8 MPa
STEEL: fym = 440 MPa
CONCRETE COVER: c = 25 mm
STEEL BRACES: fym = 275 MPa

COLUMNS SCHEDULE

	C11 / C61 / C14 / C64	C21 / C31 / C41 / C51 / C12 / C62 / C13 / C63 / C24 / C34 / C44 / C54	C22 / C32 / C42 / C52 / C23 / C33 / C43 / C53
2nd Floor	0.25 × 0.20 6Ø12 Ø6//0.15	0.25 × 0.20 6Ø12 Ø6//0.15	0.25 × 0.20 6Ø12 Ø6//0.15
1st Floor	0.25 × 0.20 6Ø12 Ø6//0.15	0.25 × 0.20 6Ø12 Ø6//0.15	0.25 × 0.25 4Ø16 Ø6//0.20
Ground Floor			

X
Y

BEAM B1

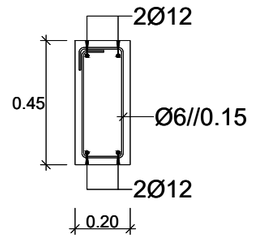

Span and Supports

BEAM B2

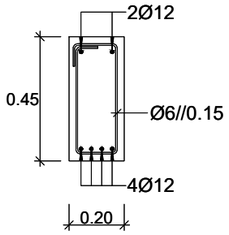

Span

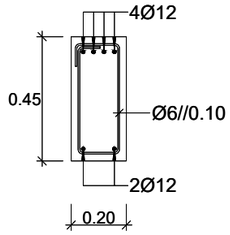

Supports

STEEL BRACES

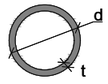

CHSH dxt (mm)

STOREY	STEEL BRACES	
	DIRECTION XX	DIRECTION YY
2nd	CHSH 139.7x3.2	CHSH 114.3x3.6
1st	CHSH 139.7x5.0	CHSH 114.3x6.0

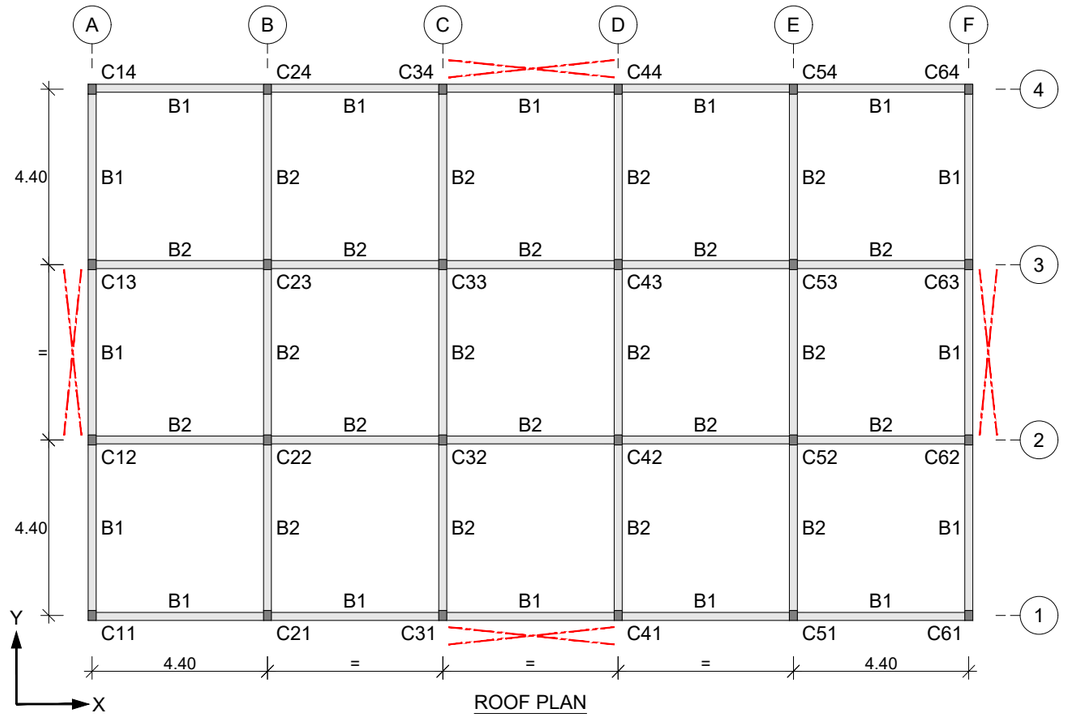

ROOF PLAN

KEY:

- Steel Braces

CONCRETE: fcm = 23.8 MPa
STEEL: fym = 440 MPa
CONCRETE COVER: c = 25 mm
STEEL BRACES: fym = 275 MPa

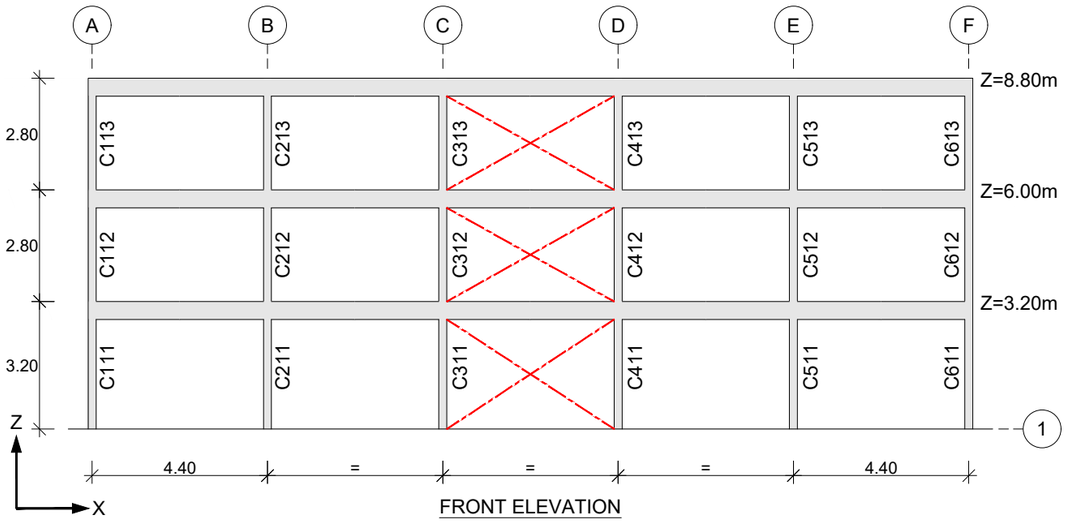

FRONT ELEVATION

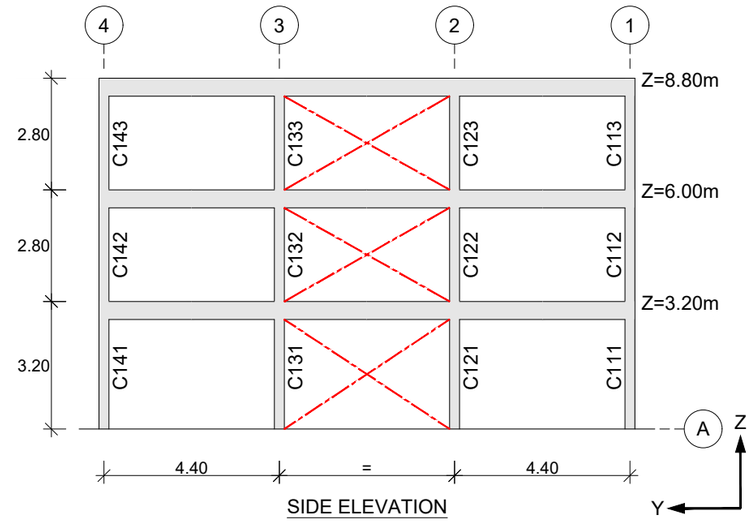

SIDE ELEVATION

S3_3S_3x5_RETRO	APPENDIX 4
GEOMETRY	A4.5

CONCRETE: fcm = 23.8 MPa
STEEL: fym = 440 MPa
CONCRETE COVER: c = 25 mm
STEEL BRACES: fym = 275 MPa

COLUMNS SCHEDULE

	C11 / C61 / C14 / C64	C21 / C31 / C41 / C51 / C12 / C62 / C13 / C63 / C24 / C34 / C44 / C54	C22 / C32 / C42 / C52 / C23 / C33 / C43 / C53
3rd Floor	0.25 / 0.20 — 6Ø12 Ø6//0.15	0.25 / 0.20 — 6Ø12 Ø6//0.15	0.25 / 0.20 — 6Ø12 Ø6//0.15
2nd Floor	0.25 / 0.20 — 6Ø12 Ø6//0.15	0.25 / 0.20 — 6Ø12 Ø6//0.15	0.25 / 0.25 — 4Ø16 Ø6//0.20
1st Floor	0.25 / 0.20 — 6Ø12 Ø6//0.15	0.25 / 0.20 — 6Ø12 Ø6//0.15	0.30 / 0.30 — 8Ø16 Ø6//0.20
Ground Floor			

X
Y

BEAM B1

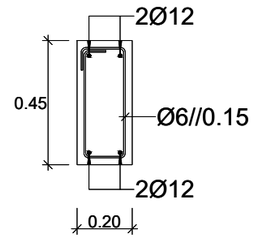

Span and Supports

BEAM B2

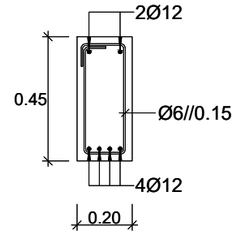

Span

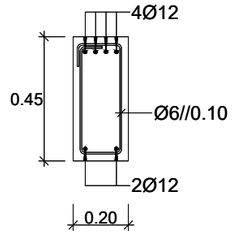

Supports

STEEL BRACES

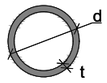

CHSH dxt (mm)

STOREY	STEEL BRACES	
	DIRECTION XX	DIRECTION YY
3rd	CHSH 88.9x3.2	CHSH 88.9x3.2
2nd	CHSH 88.9x3.6	CHSH 88.9x5.0
1st	CHSH 88.9x4.0	CHSH 88.9x5.0

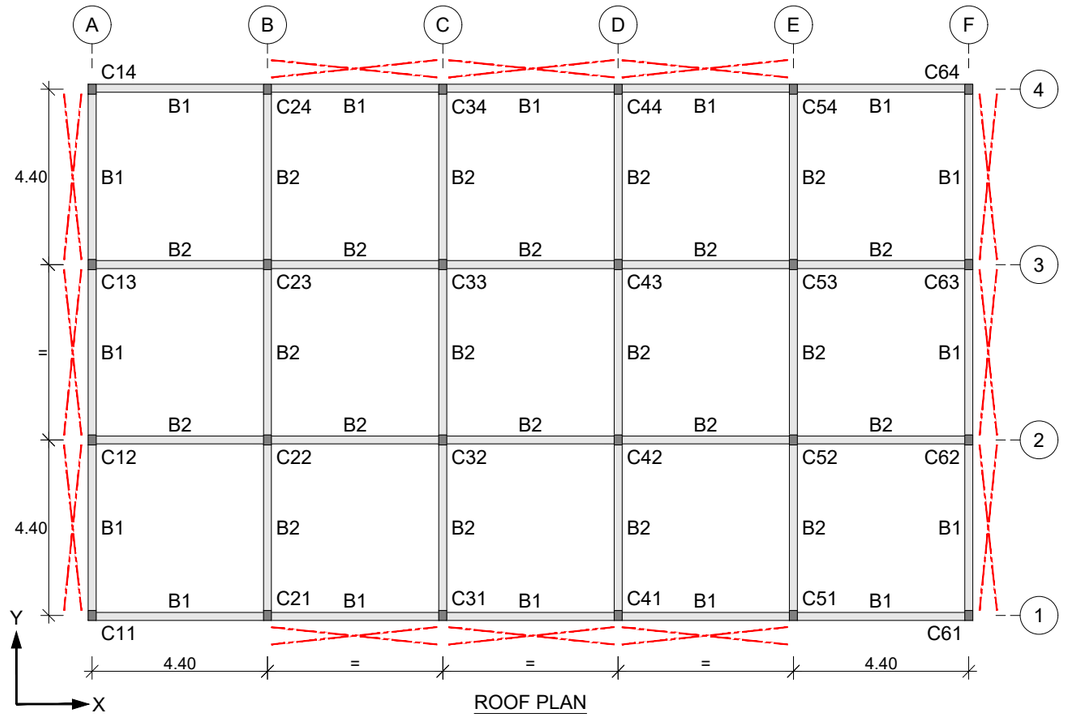

ROOF PLAN

KEY:

- Steel Braces

CONCRETE: fcm = 23.8 MPa
STEEL: fym = 440 MPa
CONCRETE COVER: c = 25 mm
STEEL BRACES: fym = 275 MPa

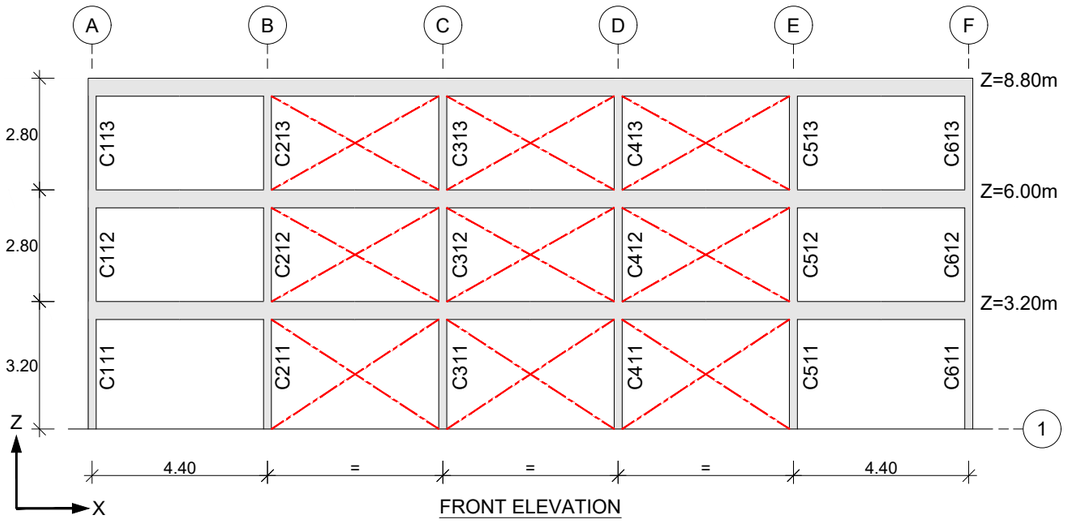

FRONT ELEVATION

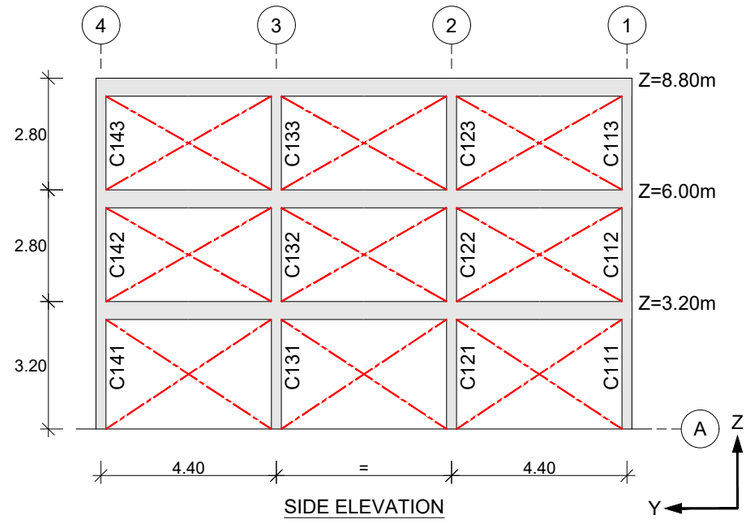

SIDE ELEVATION

S4_3S_3x5_RETRO	APPENDIX 4
GEOMETRY	A4.7

CONCRETE: fcm = 23.8 MPa
STEEL: fym = 440 MPa
CONCRETE COVER: c = 25 mm
STEEL BRACES: fym = 275 MPa

COLUMNS SCHEDULE

	C11 / C61 / C14 / C64	C21 / C31 / C41 / C51 / C12 / C62 / C13 / C63 / C24 / C34 / C44 / C54	C22 / C32 / C42 / C52 / C23 / C33 / C43 / C53
3rd Floor	0.25 × 0.20 — 6Ø12 Ø6//0.15	0.25 × 0.20 — 6Ø12 Ø6//0.15	0.25 × 0.20 — 6Ø12 Ø6//0.15
2nd Floor	0.25 × 0.20 — 6Ø12 Ø6//0.15	0.25 × 0.20 — 6Ø12 Ø6//0.15	0.25 × 0.25 — 4Ø16 Ø6//0.20
1st Floor	0.25 × 0.20 — 6Ø12 Ø6//0.15	0.25 × 0.20 — 6Ø12 Ø6//0.15	0.30 × 0.30 — 8Ø16 Ø6//0.20
Ground Floor			

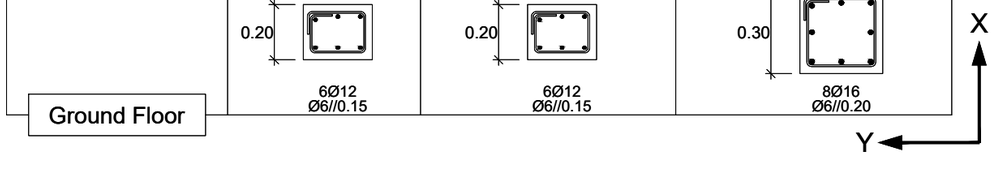

BEAM B1

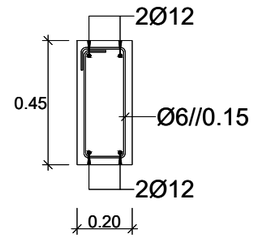

Span and Supports

BEAM B2

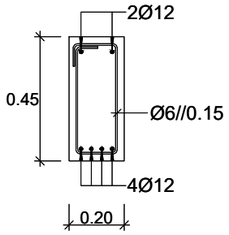

Span

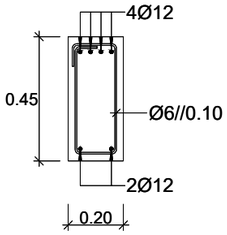

Supports

STEEL BRACES

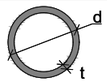

CHSH dxt (mm)

STOREY	STEEL BRACES	
	DIRECTION XX	DIRECTION YY
3rd	CHSH 88.9x3.2	CHSH 88.9x3.2
2nd	CHSH 88.9x5.0	CHSH 88.9x5.0
1st	CHSH 88.9x5.0	CHSH 88.9x5.0

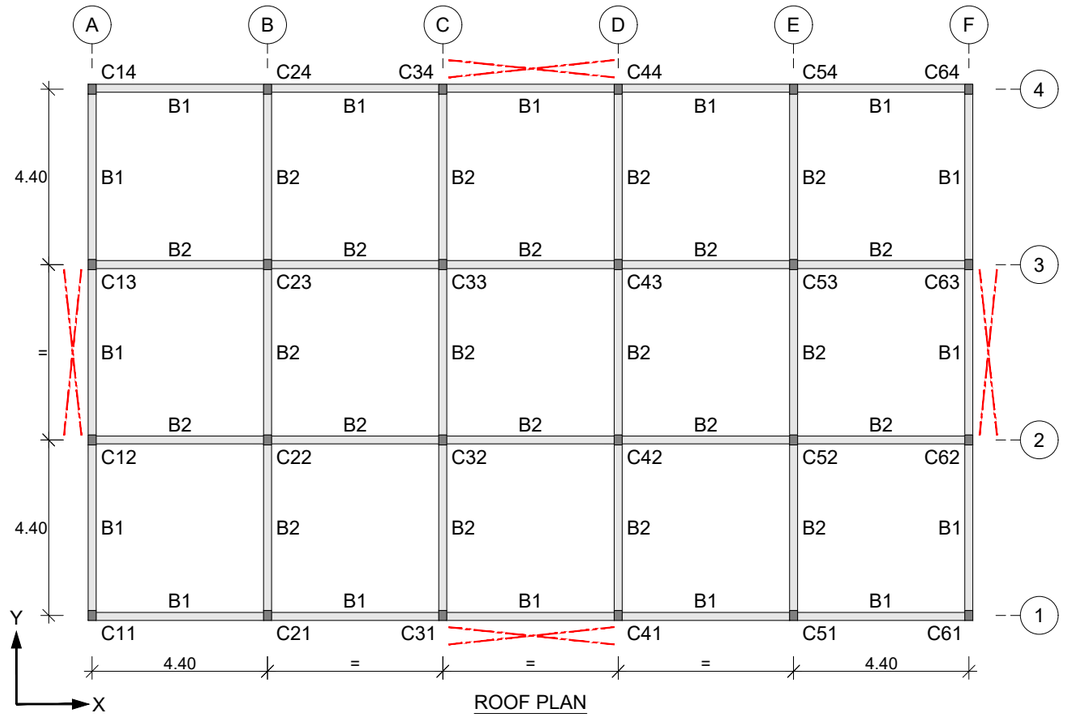

ROOF PLAN

KEY:

- Steel Braces

CONCRETE: fcm = 23.8 MPa
STEEL: fym = 440 MPa
CONCRETE COVER: c = 25 mm
STEEL BRACES: fym = 275 MPa

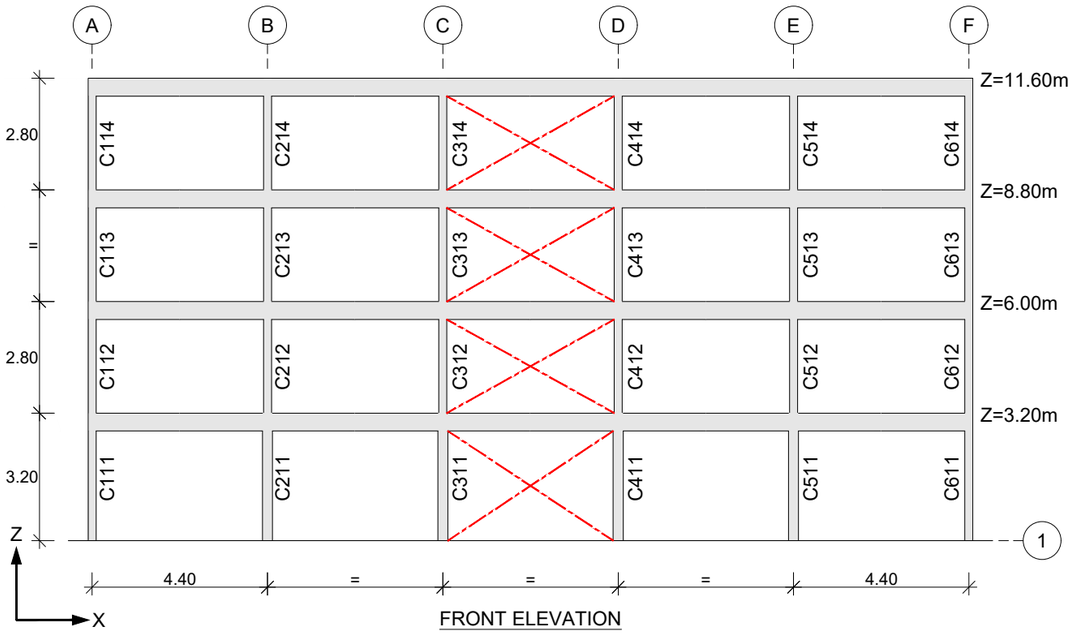

FRONT ELEVATION

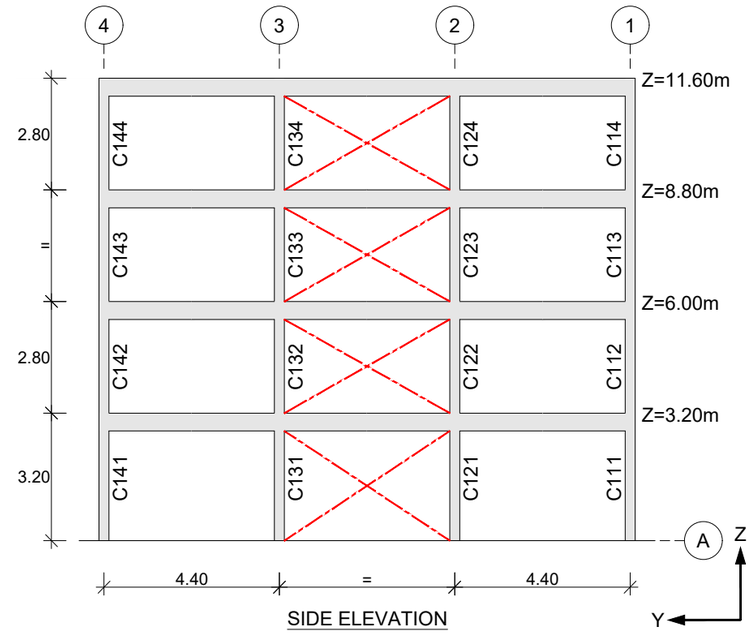

SIDE ELEVATION

S3_4S_3x5_RETRO	APPENDIX 4
GEOMETRY	A4.9

CONCRETE: fcm = 23.8 MPa
STEEL: fym = 440 MPa
CONCRETE COVER: c = 25 mm
STEEL BRACES: fym = 275 MPa

COLUMNS SCHEDULE

	C11 / C61 / C14 / C64	C21 / C31 / C41 / C51 / C12 / C62 / C13 / C63 / C24 / C34 / C44 / C54	C22 / C32 / C42 / C52 / C23 / C33 / C43 / C53
4th Floor	0.25 / 0.20 — 6Ø12 Ø6//0.15	0.25 / 0.20 — 6Ø12 Ø6//0.15	0.25 / 0.20 — 6Ø12 Ø6//0.15
3rd Floor	0.25 / 0.20 — 6Ø12 Ø6//0.15	0.25 / 0.20 — 6Ø12 Ø6//0.15	0.25 / 0.25 — 4Ø16 Ø6//0.20
2nd Floor	0.25 / 0.20 — 6Ø12 Ø6//0.15	0.25 / 0.20 — 6Ø12 Ø6//0.15	0.30 / 0.30 — 8Ø16 Ø6//0.20
1st Floor	0.25 / 0.20 — 6Ø12 Ø6//0.15	0.25 / 0.25 — 4Ø16 Ø6//0.20	0.40 / 0.30 — 6Ø16 Ø6//0.20
Ground Floor			

X
Y

BEAM B1

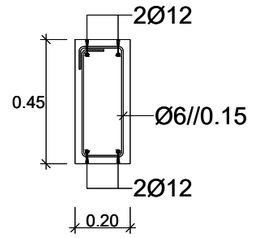

Span and Supports

BEAM B2

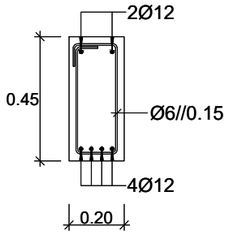

Span

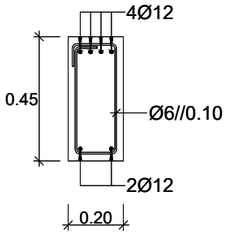

Supports

STEEL BRACES

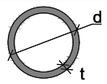

CHSH dxt (mm)

STOREY	STEEL BRACES	
	DIRECTION XX	DIRECTION YY
4th	CHSH 88.9x3.2	CHSH 88.9x3.2
3rd	CHSH 88.9x5.0	CHSH 114.3x4.0
2nd	CHSH 114.3x5.0	CHSH 114.3x5.0
1st	CHSH 114.3x5.0	CHSH 114.3x5.0

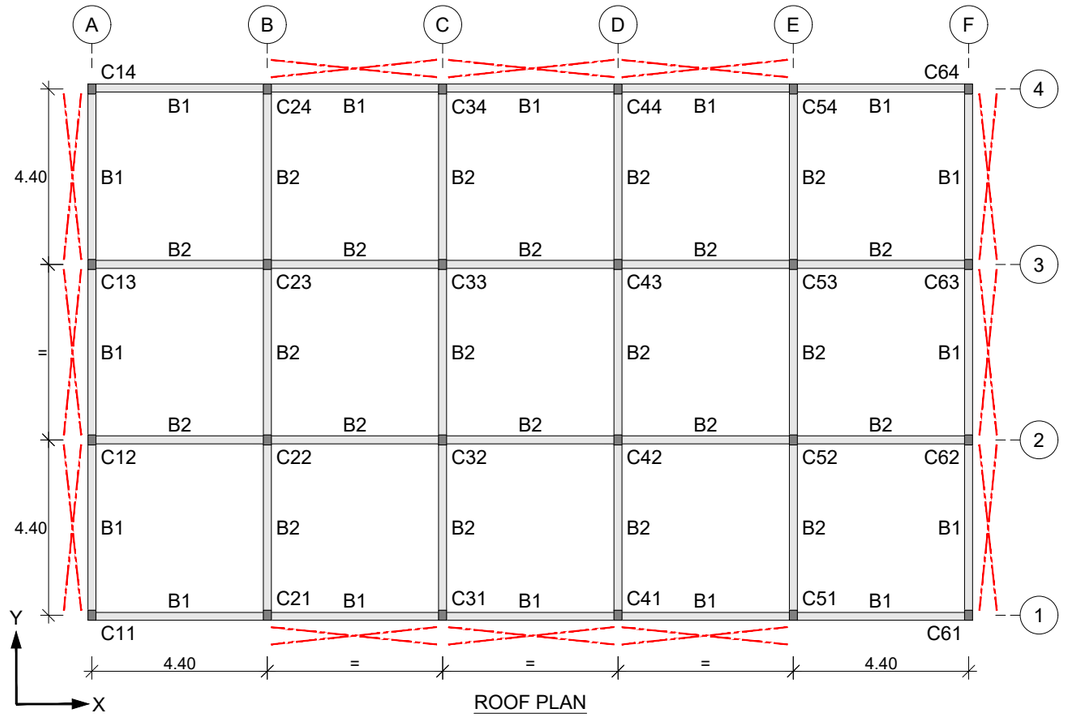

ROOF PLAN

KEY:

- Steel Braces

CONCRETE: fcm = 23.8 MPa
STEEL: fym = 440 MPa
CONCRETE COVER: c = 25 mm
STEEL BRACES: fym = 275 MPa

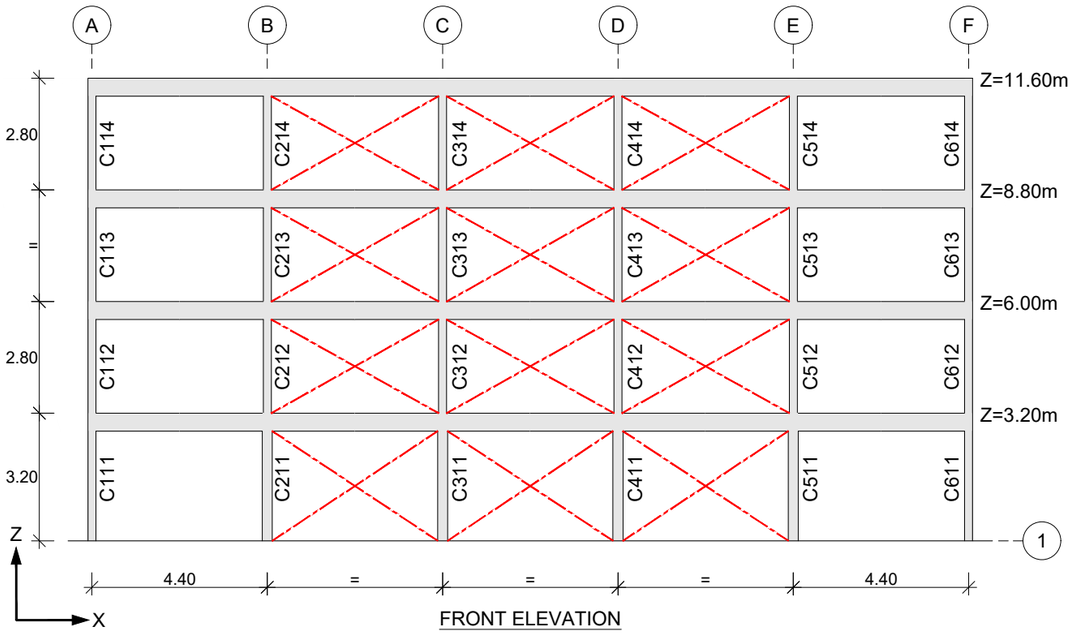

FRONT ELEVATION

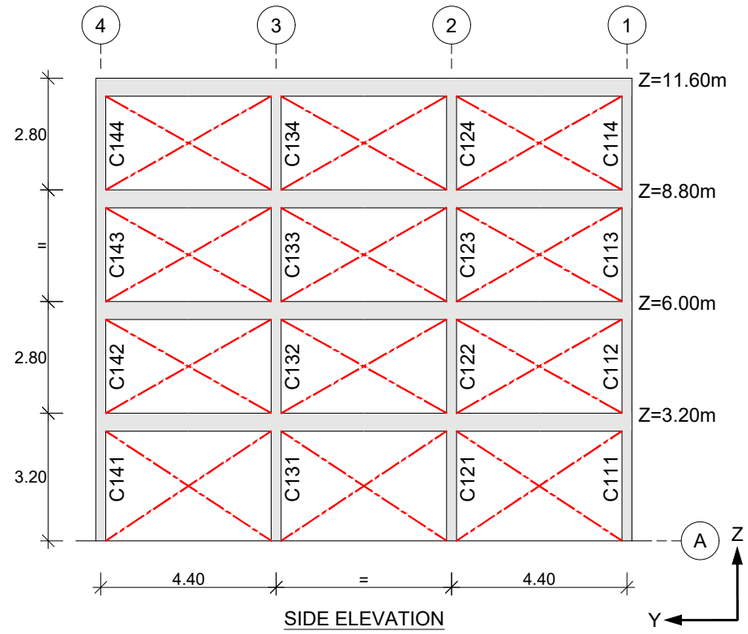

SIDE ELEVATION

S4_4S_3x5_RETRO	APPENDIX 4
GEOMETRY	A4.11

CONCRETE: fcm = 23.8 MPa
STEEL: fym = 440 MPa
CONCRETE COVER: c = 25 mm
STEEL BRACES: fym = 275 MPa

COLUMNS SCHEDULE

	C11 / C61 / C14 / C64	C21 / C31 / C41 / C51 / C12 / C62 / C13 / C63 / C24 / C34 / C44 / C54	C22 / C32 / C42 / C52 / C23 / C33 / C43 / C53
4th Floor	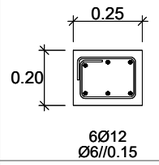	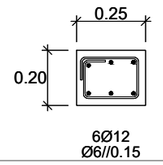	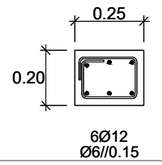
3rd Floor	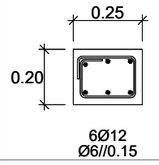	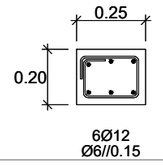	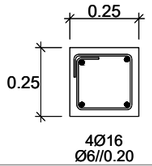
2nd Floor	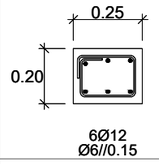	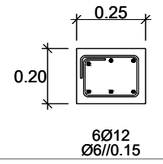	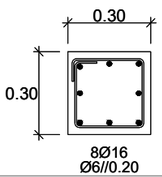
1st Floor	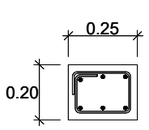	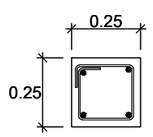	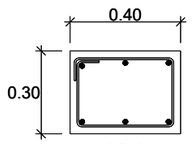
Ground Floor			

X
Y

BEAM B1

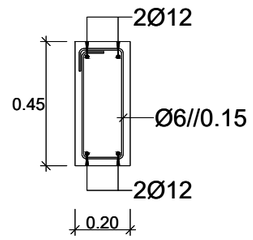

Span and Supports

BEAM B2

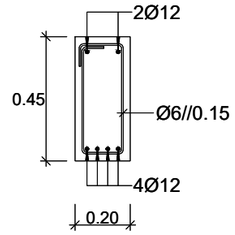

Span

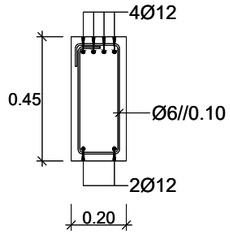

Supports

STEEL BRACES

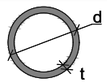

CHSH dxt (mm)

STOREY	STEEL BRACES	
	DIRECTION XX	DIRECTION YY
4th	CHSH 88.9x3.2	CHSH 88.9x3.2
3rd	CHSH 88.9x5.0	CHSH 88.9x5.0
2nd	CHSH 114.3x5.0	CHSH 114.3x5.0
1st	CHSH 114.3x5.0	CHSH 114.3x5.0

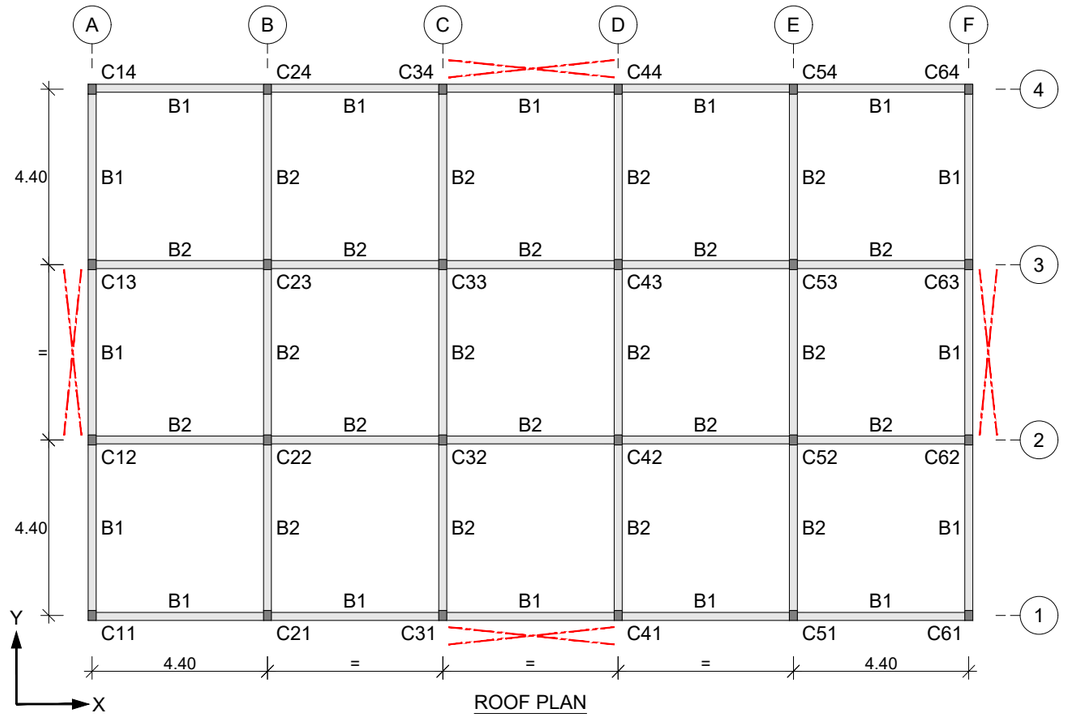

ROOF PLAN

KEY:

- Steel Braces

CONCRETE: fcm = 23.8 MPa
STEEL: fym = 440 MPa
CONCRETE COVER: c = 25 mm
STEEL BRACES: fym = 275 MPa

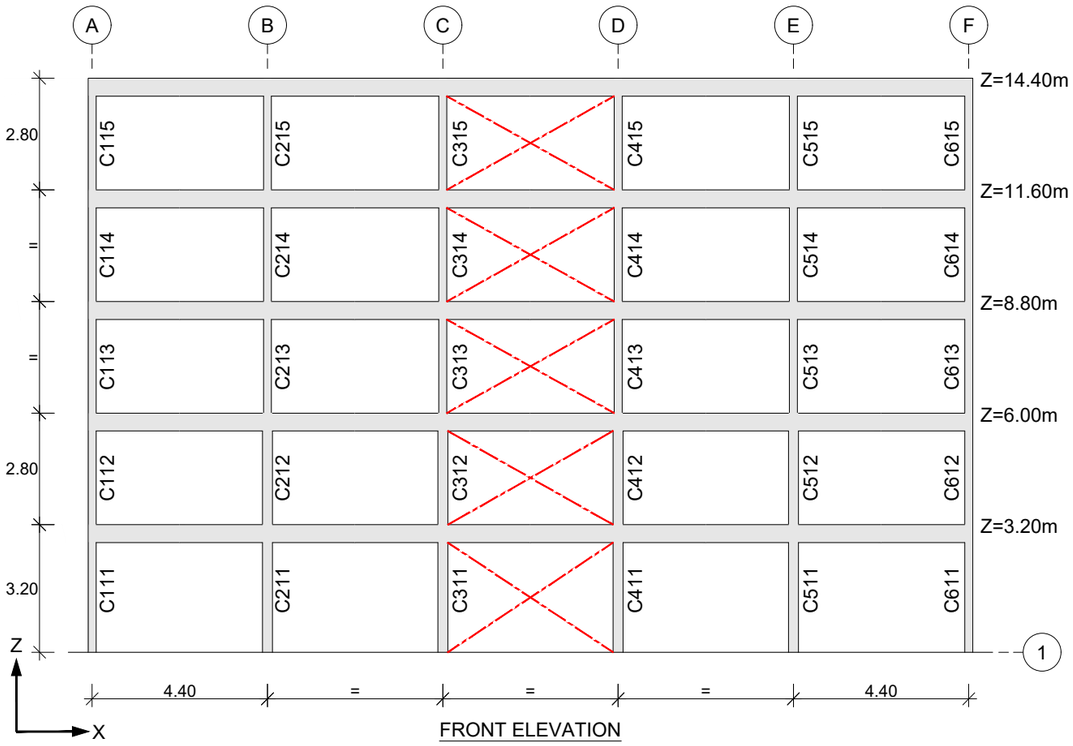

FRONT ELEVATION

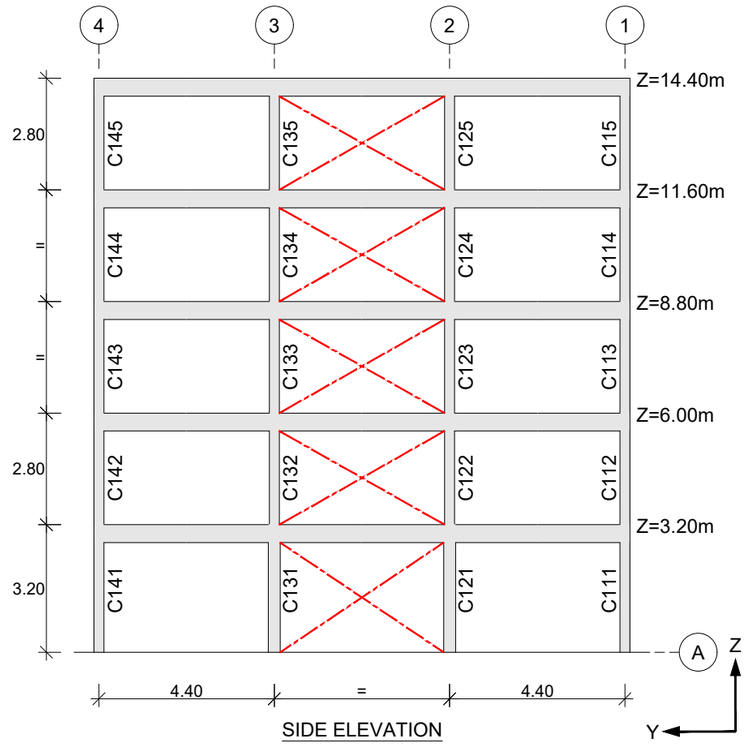

SIDE ELEVATION

S3_5S_3x5_RETRO	APPENDIX 4
GEOMETRY	A4.13

CONCRETE: fcm = 23.8 MPa
STEEL: fym = 440 MPa
CONCRETE COVER: c = 25 mm
STEEL BRACES: fym = 275 MPa

COLUMNS SCHEDULE

	C11 / C61 / C14 / C64	C21 / C31 / C41 / C51 / C12 / C62 / C13 / C63 / C24 / C34 / C44 / C54	C22 / C32 / C42 / C52 / C23 / C33 / C43 / C53
5th Floor	0.25 × 0.20 6Ø12 Ø6//0.15	0.25 × 0.20 6Ø12 Ø6//0.15	0.25 × 0.20 6Ø12 Ø6//0.15
4th Floor	0.25 × 0.20 6Ø12 Ø6//0.15	0.25 × 0.20 6Ø12 Ø6//0.15	0.25 × 0.25 4Ø16 Ø6//0.20
3rd Floor	0.25 × 0.20 6Ø12 Ø6//0.15	0.25 × 0.20 6Ø12 Ø6//0.15	0.30 × 0.30 8Ø16 Ø6//0.20
2nd Floor	0.25 × 0.20 6Ø12 Ø6//0.15	0.25 × 0.25 4Ø16 Ø6//0.20	0.40 × 0.30 6Ø16 Ø6//0.20
1st Floor	0.25 × 0.20 6Ø12 Ø6//0.15	0.30 × 0.25 4Ø16 Ø6//0.20	0.50 × 0.30 8Ø16 Ø6//0.20
Ground Floor			

X
Y

BEAM B1

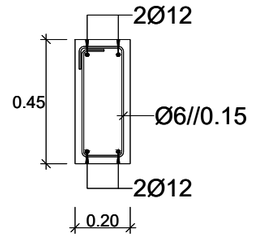

Span and Supports

BEAM B2

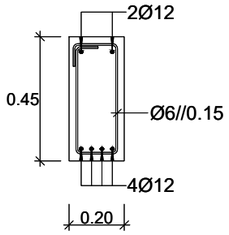

Span

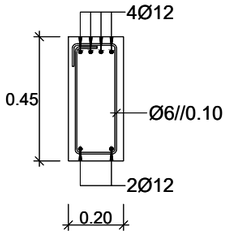

Supports

STEEL BRACES

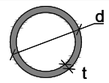

CHSH dxt (mm)

STOREY	STEEL BRACES	
	DIRECTION XX	DIRECTION YY
5th	CHSH 88.9x3.2	CHSH 88.9x3.2
4th	CHSH 88.9x3.6	CHSH 88.9x3.6
3rd	CHSH 88.9x5.0	CHSH 88.9x5.0
2nd	CHSH 88.9x5.0	CHSH 88.9x5.0
1st	CHSH 88.9x5.0	CHSH 88.9x3.6

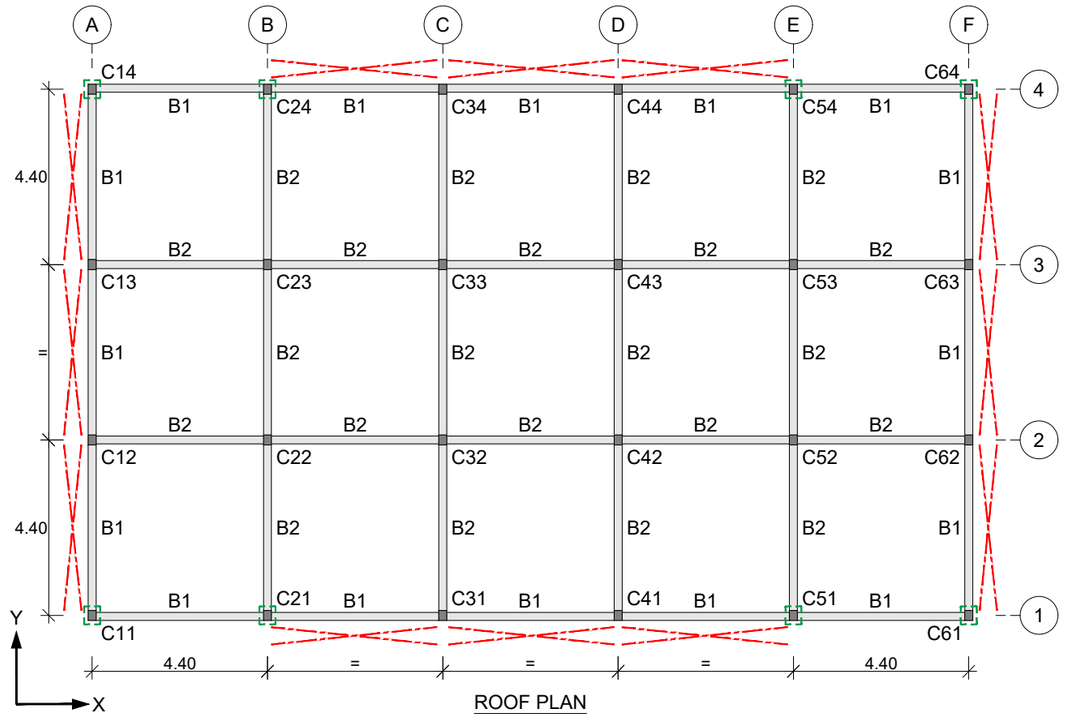

ROOF PLAN

KEY:

- Steel Braces
- Columns with FRP wrapping

CONCRETE: fcm = 23.8 MPa
STEEL: fym = 440 MPa
CONCRETE COVER: c = 25 mm
STEEL BRACES: fym = 275 MPa

FRP SHEET:
SikaWrap-230 C
N = 3
R = 30mm

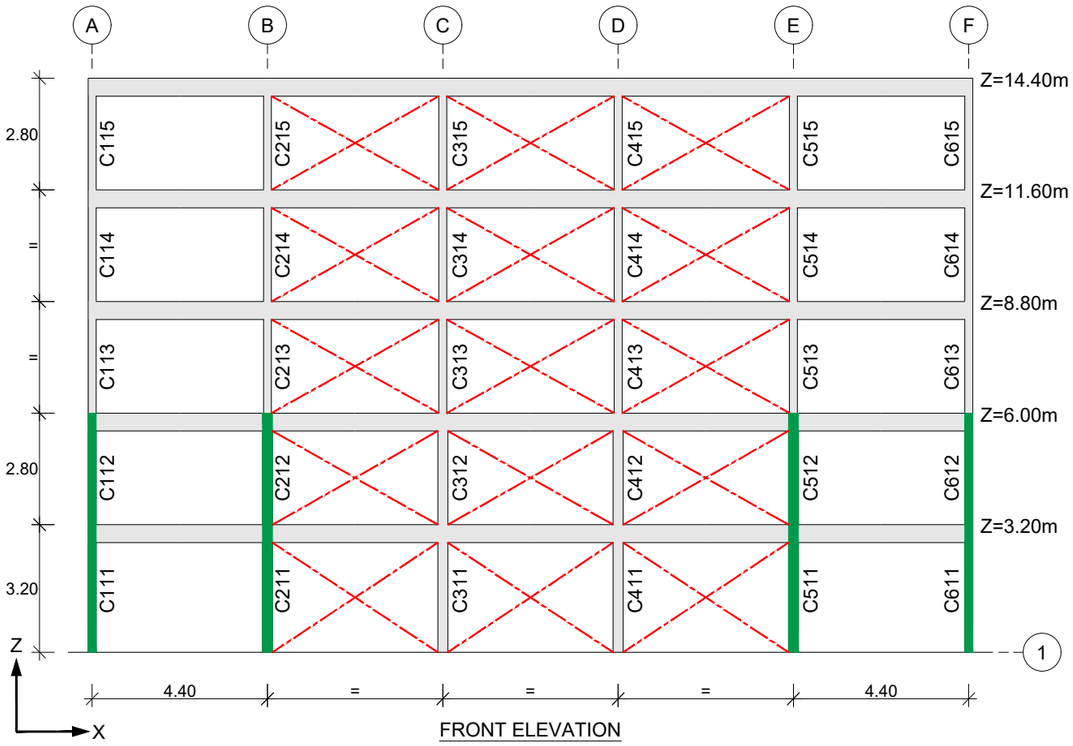

FRONT ELEVATION

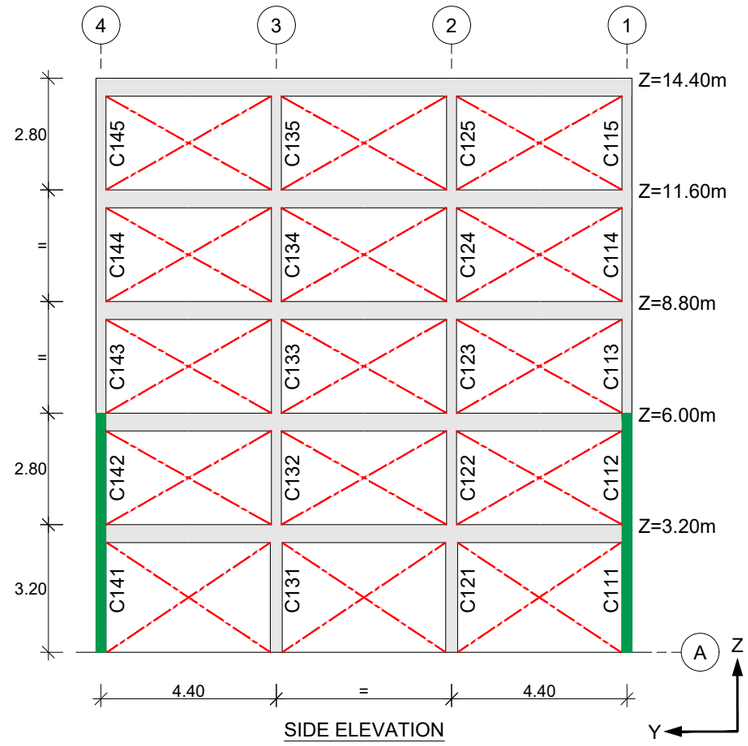

SIDE ELEVATION

S4_5S_3x5_RETRO	APPENDIX 4
GEOMETRY	A4.15

COLUMNS SCHEDULE

	C11 / C61 / C14 / C64	C31 / C41 / C12 / C62 / C13 / C63 / C34 / C44	C22 / C32 / C42 / C52 / C23 / C33 / C43 / C53	C21 / C51 / C24 / C54
5th Floor	0.25 / 0.20 / 6Ø12 Ø6//0.15	0.25 / 0.20 / 6Ø12 Ø6//0.15	0.25 / 0.20 / 6Ø12 Ø6//0.15	0.25 / 0.20 / 6Ø12 Ø6//0.15
4th Floor	0.25 / 0.20 / 6Ø12 Ø6//0.15	0.25 / 0.20 / 6Ø12 Ø6//0.15	0.25 / 0.25 / 4Ø16 Ø6//0.20	0.25 / 0.20 / 6Ø12 Ø6//0.15
3rd Floor	0.25 / 0.20 / 6Ø12 Ø6//0.15	0.25 / 0.20 / 6Ø12 Ø6//0.15	0.30 / 0.30 / 8Ø16 Ø6//0.20	0.25 / 0.20 / 6Ø12 Ø6//0.15
2nd Floor	0.25 / 0.20 / 6Ø12 Ø6//0.15 FRP	0.25 / 0.25 / 4Ø16 Ø6//0.20 FRP	0.40 / 0.30 / 6Ø16 Ø6//0.20	0.25 / 0.25 / 4Ø16 Ø6//0.20 FRP
1st Floor	0.25 / 0.20 / 6Ø12 Ø6//0.15 FRP	0.30 / 0.25 / 4Ø16 Ø6//0.20	0.50 / 0.30 / 8Ø16 Ø6//0.20	0.30 / 0.25 / 4Ø16 Ø6//0.20 FRP
Ground Floor				

X

Y

CONCRETE: fcm = 23.8 MPa
STEEL: fym = 440 MPa
CONCRETE COVER: c = 25 mm
STEEL BRACES: fym = 275 MPa

FRP SHEET:
SikaWrap-230 C
N = 3
R = 30mm

BEAM B1

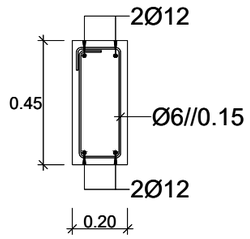

Span and Supports

BEAM B2

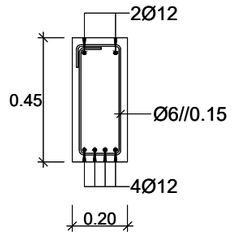

Span

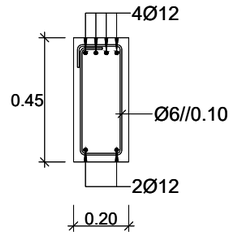

Supports

STEEL BRACES

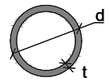

CHSH dxt (mm)

STOREY	STEEL BRACES	
	DIRECTION XX	DIRECTION YY
5th	CHSH 88.9x3.2	CHSH 88.9x3.2
4th	CHSH 88.9x4.0	CHSH 88.9x3.6
3rd	CHSH 114.3x4.0	CHSH 114.3x3.6
2nd	CHSH 114.3x5.0	CHSH 114.3x4.0
1st	CHSH 114.3x5.0	CHSH 114.3x4.0

S4_5S_3x5_RETRO	APPENDIX 4
DETAILS	A4.16

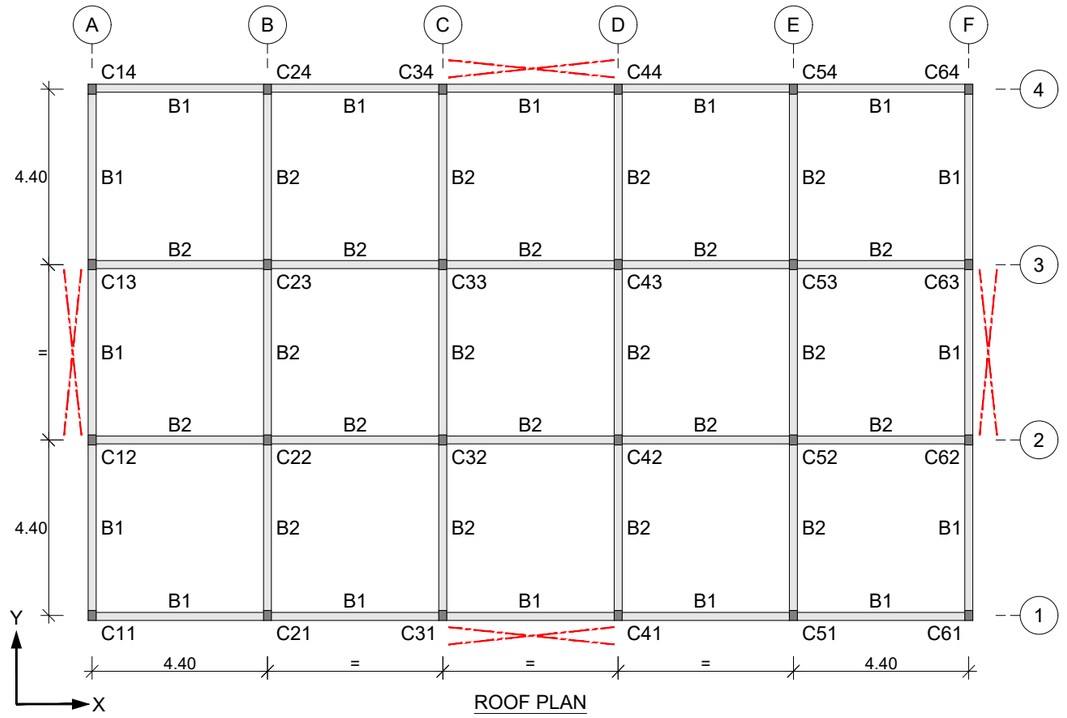

ROOF PLAN

KEY:

- Steel Braces

CONCRETE: fcm = 23.8 MPa
STEEL: fym = 440 MPa
CONCRETE COVER: c = 25 mm
STEEL BRACES: fym = 275 MPa

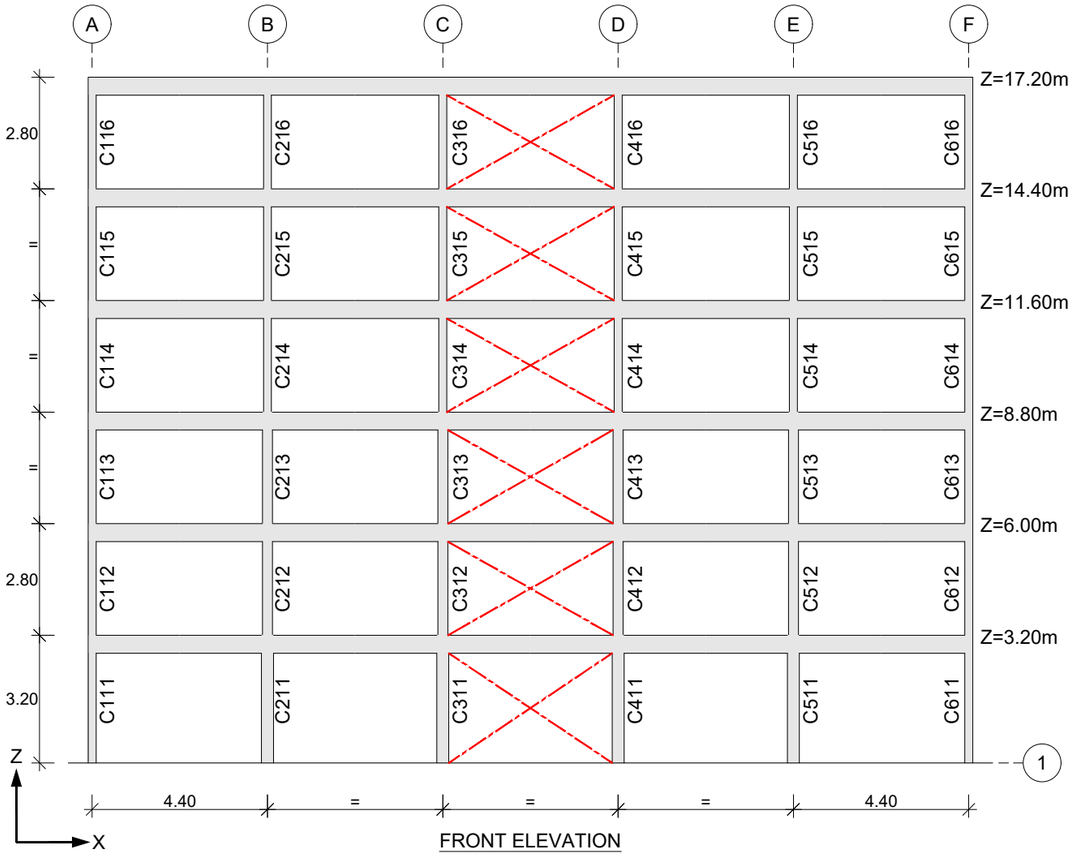

FRONT ELEVATION

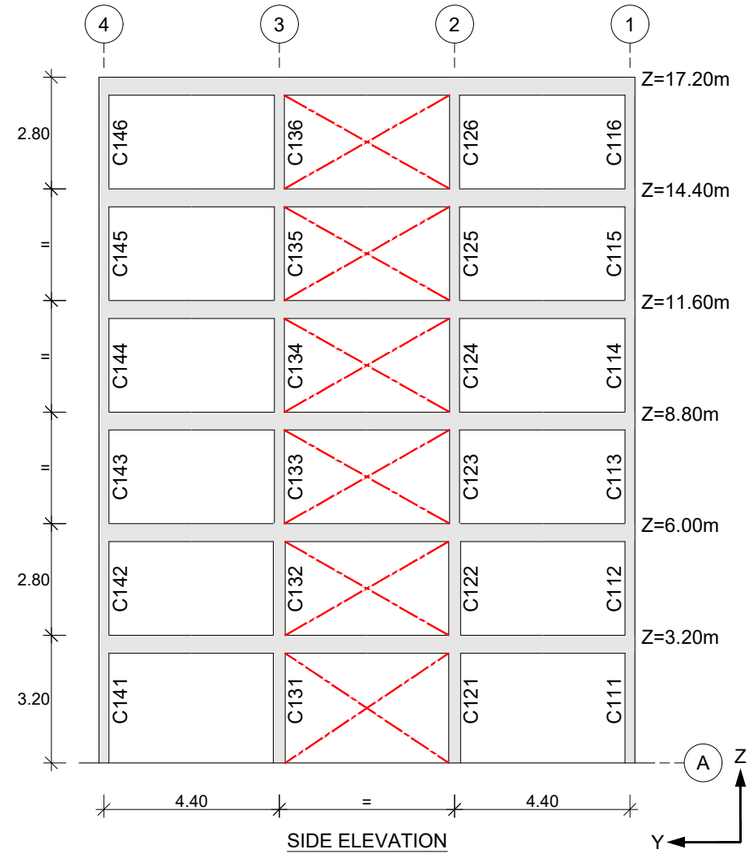

SIDE ELEVATION

S3_6S_3x5_RETRO	APPENDIX 4
GEOMETRY	A4.17

CONCRETE: fcm = 23.8 MPa
STEEL: fym = 440 MPa
CONCRETE COVER: c = 25 mm
STEEL BRACES: fym = 275 MPa

COLUMNS SCHEDULE

	C11 / C61 / C14 / C64	C21 / C31 / C41 / C51 / C12 / C62 / C13 / C63 / C24 / C34 / C44 / C54	C22 / C32 / C42 / C52 / C23 / C33 / C43 / C53
6th Floor	0.25 × 0.20 — 6Ø12 Ø6//0.15	0.25 × 0.20 — 6Ø12 Ø6//0.15	0.25 × 0.20 — 6Ø12 Ø6//0.15
5th Floor	0.25 × 0.20 — 6Ø12 Ø6//0.15	0.25 × 0.20 — 6Ø12 Ø6//0.15	0.25 × 0.25 — 4Ø16 Ø6//0.20
4th Floor	0.25 × 0.20 — 6Ø12 Ø6//0.15	0.25 × 0.20 — 6Ø12 Ø6//0.15	0.30 × 0.30 — 8Ø16 Ø6//0.20
3rd Floor	0.25 × 0.20 — 6Ø12 Ø6//0.15	0.25 × 0.25 — 4Ø16 Ø6//0.20	0.40 × 0.30 — 6Ø16 Ø6//0.20
2nd Floor	0.25 × 0.20 — 6Ø12 Ø6//0.15	0.30 × 0.25 — 4Ø16 Ø6//0.20	0.50 × 0.30 — 8Ø16 Ø6//0.20
1st Floor	0.25 × 0.20 — 6Ø12 Ø6//0.15	0.30 × 0.30 — 8Ø16 Ø6//0.20	0.60 × 0.30 — 6Ø20 Ø6//0.25
Ground Floor			

X
Y

BEAM B1

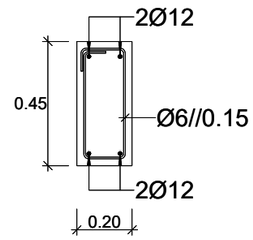

Span and Supports

BEAM B2

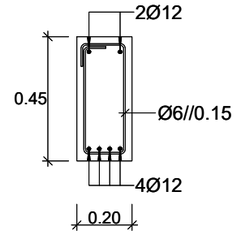

Span

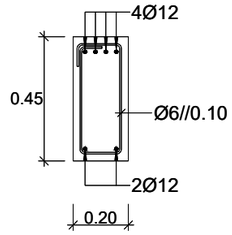

Supports

STEEL BRACES

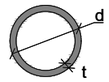

CHSH dxt (mm)

STOREY	STEEL BRACES	
	DIRECTION XX	DIRECTION YY
6th	CHSH 88.9x3.2	CHSH 88.9x3.2
5th	CHSH 88.9x3.2	CHSH 88.9x3.2
4th	CHSH 88.9x4.0	CHSH 88.9x5.0
3rd	CHSH 88.9x5.0	CHSH 88.9x5.0
2nd	CHSH 88.9x5.0	CHSH 88.9x5.0
1st	CHSH 88.9x3.6	CHSH 88.9x3.2

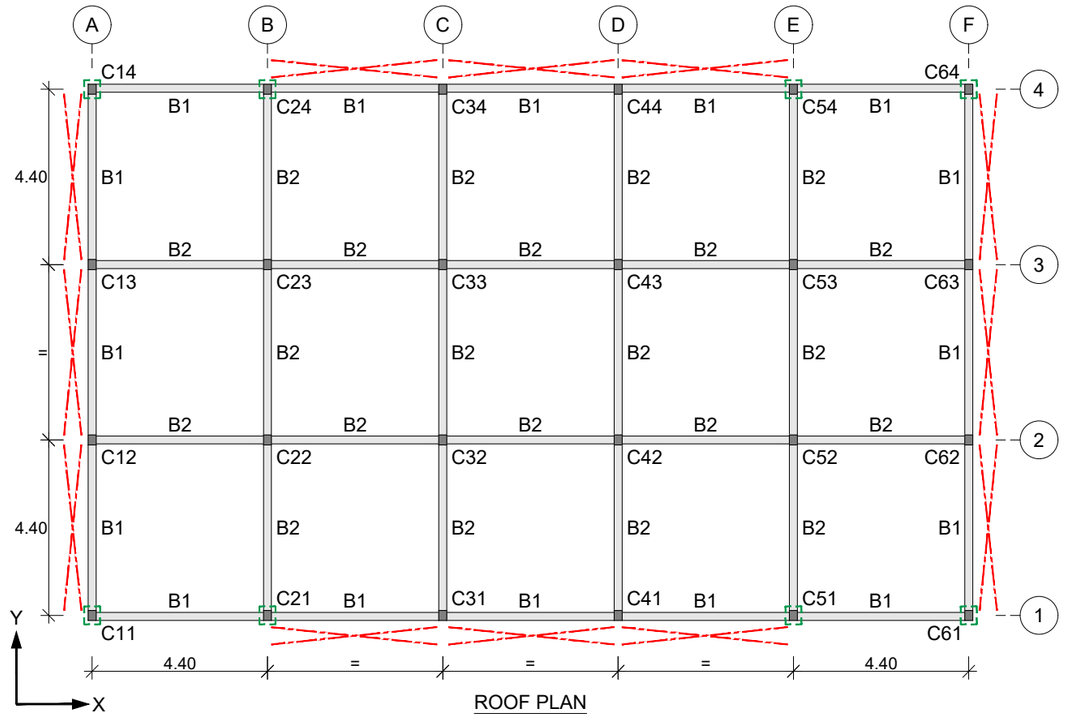

ROOF PLAN

KEY:

- Steel Braces
- Columns with FRP wrapping

CONCRETE: fcm = 23.8 MPa
STEEL: fym = 440 MPa
CONCRETE COVER: c = 25 mm
STEEL BRACES: fym = 275 MPa

FRP SHEET:
SikaWrap-230 C
N = 3
R = 30mm

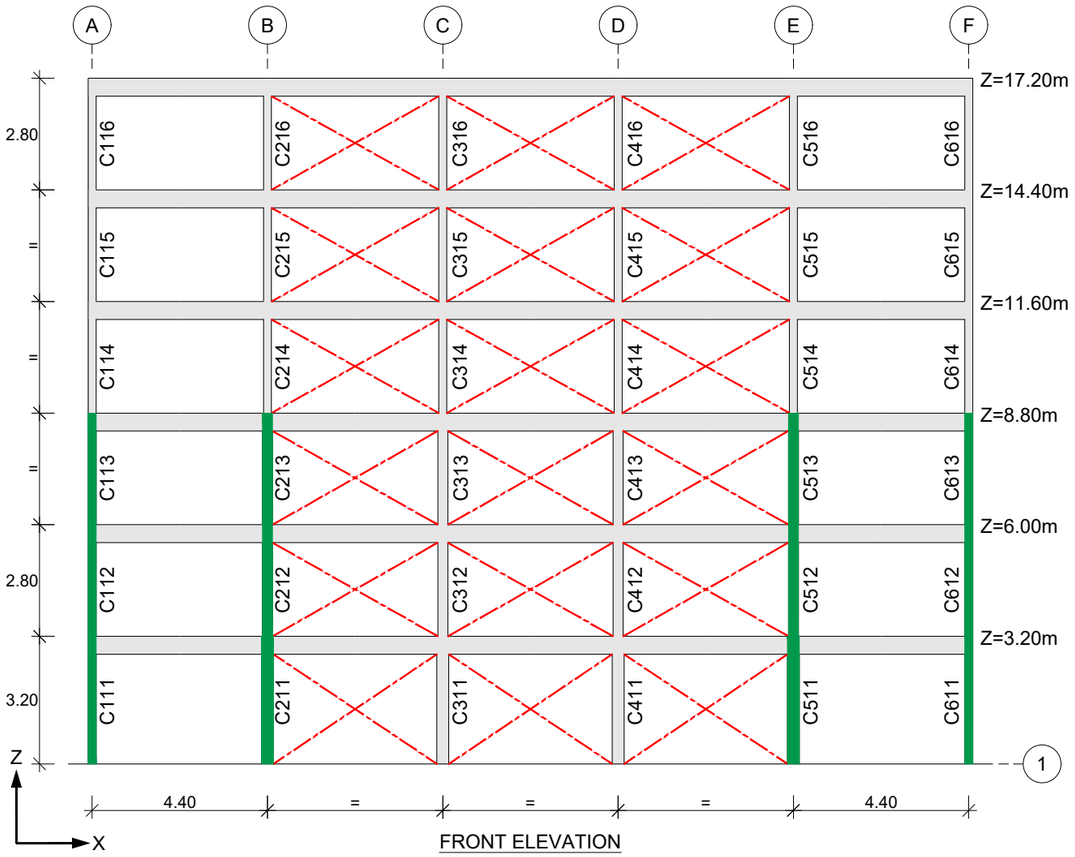

FRONT ELEVATION

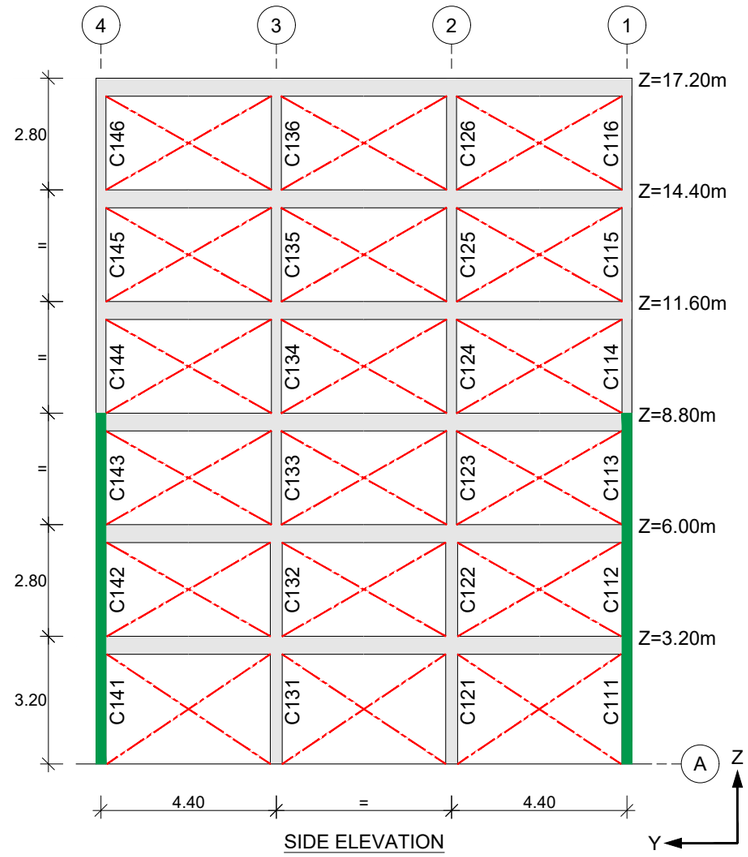

SIDE ELEVATION

S4_6S_3x5_RETRO	APPENDIX 4
GEOMETRY	A4.19

COLUMNS SCHEDULE

	C11 / C61 / C14 / C64	C31 / C41 / C12 / C62 / C13 / C63 / C34 / C44	C22 / C32 / C42 / C52 / C23 / C33 / C43 / C53	C21 / C51 / C24 / C54
6th Floor	0.25 / 0.20 / 6Ø12 Ø6//0.15	0.25 / 0.20 / 6Ø12 Ø6//0.15	0.25 / 0.20 / 6Ø12 Ø6//0.15	0.25 / 0.20 / 6Ø12 Ø6//0.15
5th Floor	0.25 / 0.20 / 6Ø12 Ø6//0.15	0.25 / 0.20 / 6Ø12 Ø6//0.15	0.25 / 0.25 / 4Ø16 Ø6//0.20	0.25 / 0.20 / 6Ø12 Ø6//0.15
4th Floor	0.25 / 0.20 / 6Ø12 Ø6//0.15	0.25 / 0.20 / 6Ø12 Ø6//0.15	0.30 / 0.30 / 8Ø16 Ø6//0.20	0.25 / 0.20 / 6Ø12 Ø6//0.15
3rd Floor	0.25 / 0.20 / 6Ø12 Ø6//0.15 FRP	0.25 / 0.25 / 4Ø16 Ø6//0.20	0.40 / 0.30 / 6Ø16 Ø6//0.20	0.25 / 0.25 / 4Ø16 Ø6//0.20 FRP
2nd Floor	0.25 / 0.20 / 6Ø12 Ø6//0.15 FRP	0.30 / 0.25 / 4Ø16 Ø6//0.20	0.50 / 0.30 / 8Ø16 Ø6//0.20	0.30 / 0.25 / 4Ø16 Ø6//0.20 FRP
1st Floor	0.25 / 0.20 / 6Ø12 Ø6//0.15 FRP	0.30 / 0.30 / 8Ø16 Ø6//0.20	0.60 / 0.30 / 6Ø20 Ø6//0.25	0.30 / 0.30 / 8Ø16 Ø6//0.20 FRP
Ground Floor				

X

Y

CONCRETE: fcm = 23.8 MPa
STEEL: fym = 440 MPa
CONCRETE COVER: c = 25 mm
STEEL BRACES: fym = 275 MPa

FRP SHEET:
SikaWrap-230 C
N = 3
R = 30mm

BEAM B1

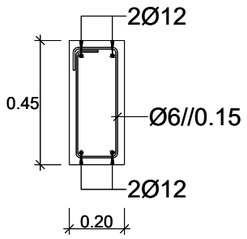

Span and Supports

BEAM B2

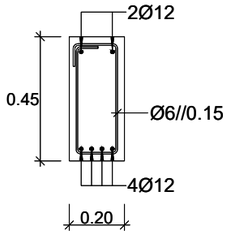

Span

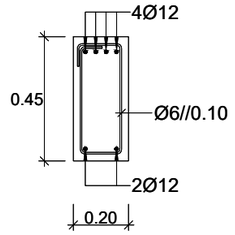

Supports

STEEL BRACES

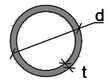

CHSH dxt (mm)

STOREY	STEEL BRACES	
	DIRECTION XX	DIRECTION YY
6th	CHSH 88.9x3.2	CHSH 88.9x3.2
5th	CHSH 88.9x3.6	CHSH 88.9x4.0
4th	CHSH 114.3x3.2	CHSH 88.9x6.0
3rd	CHSH 114.3x3.6	CHSH 114.3x5.0
2nd	CHSH 114.3x4.0	CHSH 114.3x5.0
1st	CHSH 114.3x4.0	CHSH 114.3x5.0

S4_6S_3x5_RETRO	APPENDIX 4
DETAILS	A4.20

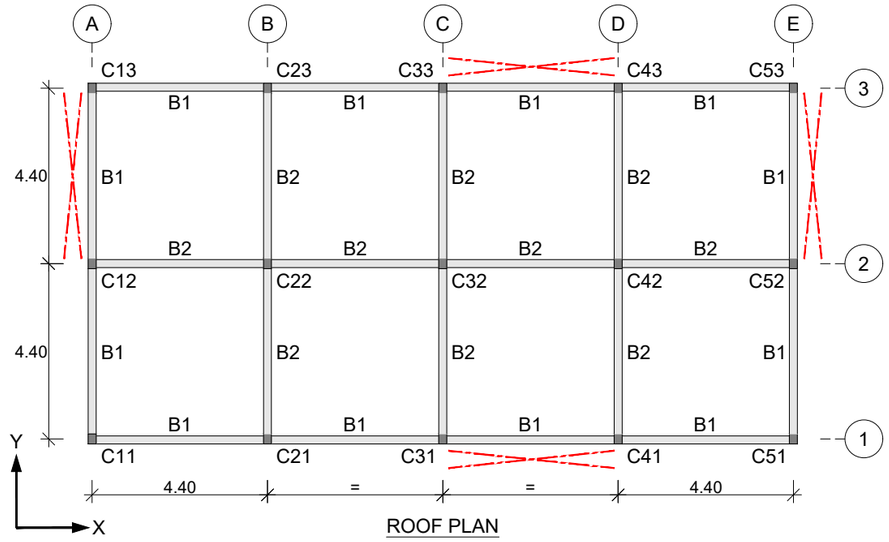

ROOF PLAN

KEY:

- Steel Braces

CONCRETE: fcm = 23.8 MPa
STEEL: fym = 440 MPa
CONCRETE COVER: c = 25 mm
STEEL BRACES: fym = 275 MPa

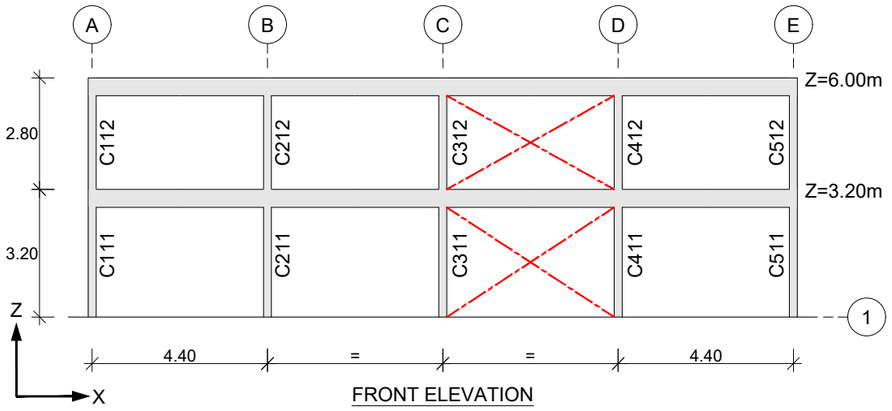

FRONT ELEVATION

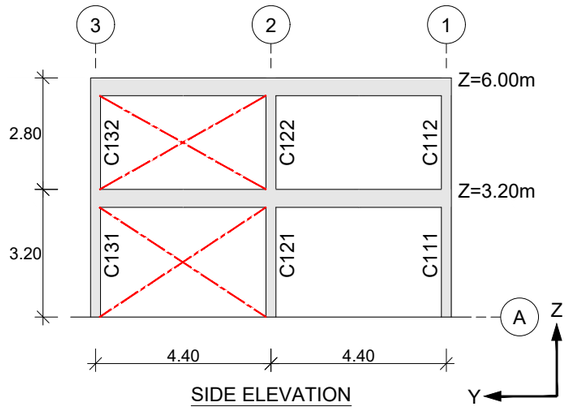

SIDE ELEVATION

S3_2S_2x4_RETRO	APPENDIX 4
GEOMETRY	A4.21

CONCRETE: fcm = 23.8 MPa
STEEL: fym = 440 MPa
CONCRETE COVER: c = 25 mm
STEEL BRACES: fym = 275 MPa

COLUMNS SCHEDULE

	C11 / C13 / C51 / C53	C21 / C31 / C41 / C12 / C52 / C23 / C33 / C43	C22 / C32 / C42
2nd Floor	0.25 / 0.20 — 6Ø12 Ø6//0.15	0.25 / 0.20 — 6Ø12 Ø6//0.15	0.25 / 0.20 — 6Ø12 Ø6//0.15
1st Floor	0.25 / 0.20 — 6Ø12 Ø6//0.15	0.25 / 0.20 — 6Ø12 Ø6//0.15	0.25 / 0.25 — 4Ø16 Ø6//0.20
Ground Floor			

X
Y

BEAM B1

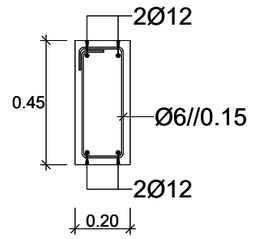

Span and Supports

BEAM B2

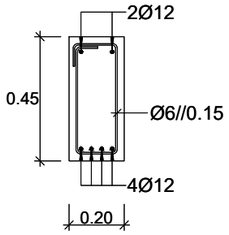

Span

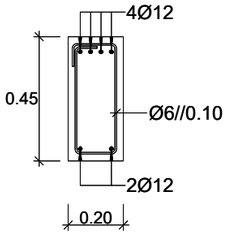

Supports

STEEL BRACES

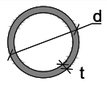

CHSH dxt (mm)

STOREY	STEEL BRACES	
	DIRECTION XX	DIRECTION YY
2nd	CHSH 88.9x3.2	CHSH 88.9x3.2
1st	CHSH 88.9x3.2	CHSH 88.9x3.2

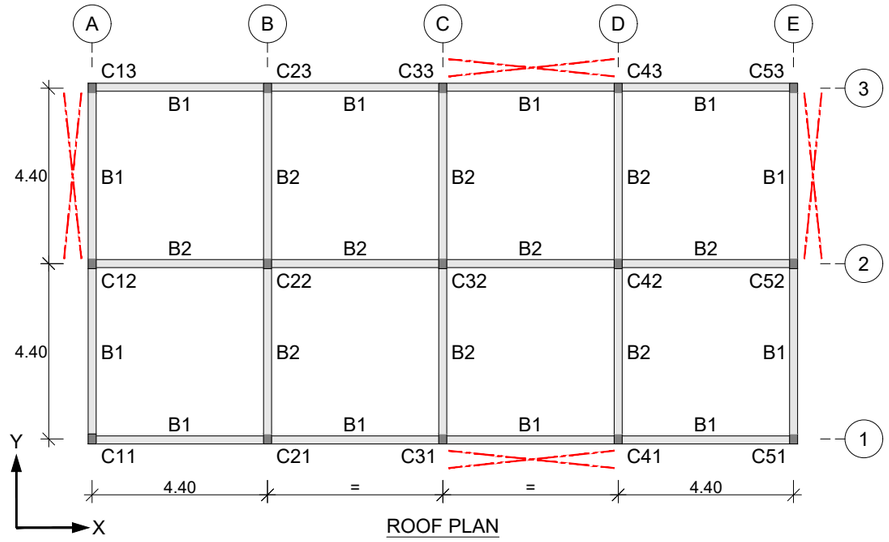

ROOF PLAN

KEY:

- Steel Braces

CONCRETE: fcm = 23.8 MPa
STEEL: fym = 440 MPa
CONCRETE COVER: c = 25 mm
STEEL BRACES: fym = 275 MPa

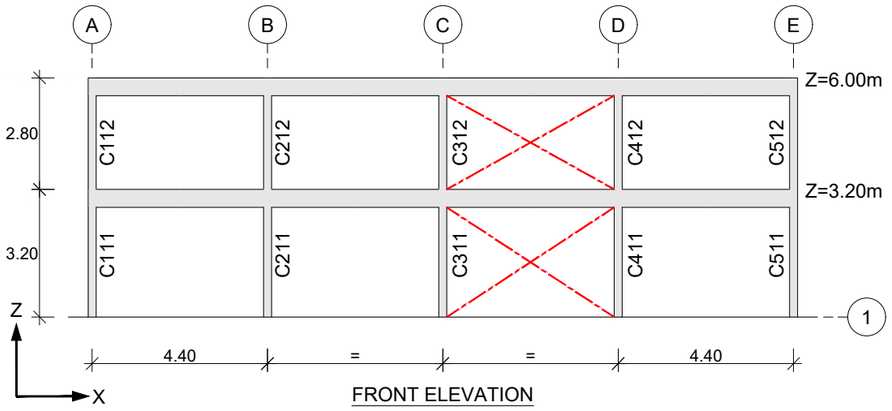

FRONT ELEVATION

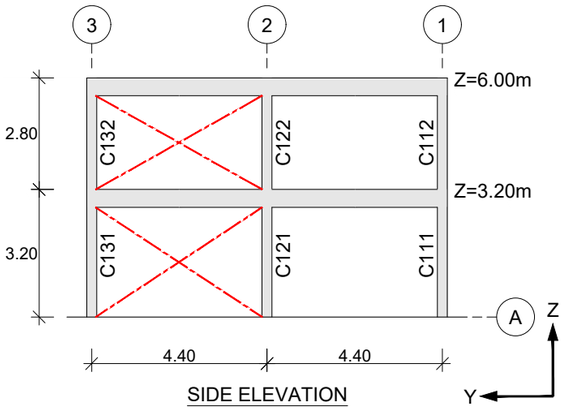

SIDE ELEVATION

S4_2S_2x4_RETRO	APPENDIX 4
GEOMETRY	A4.23

CONCRETE: fcm = 23.8 MPa
STEEL: fym = 440 MPa
CONCRETE COVER: c = 25 mm
STEEL BRACES: fym = 275 MPa

COLUMNS SCHEDULE

	C11 / C13 / C51 / C53	C21 / C31 / C41 / C12 / C52 / C23 / C33 / C43	C22 / C32 / C42
2nd Floor	0.25 / 0.20 — 6Ø12 Ø6//0.15	0.25 / 0.20 — 6Ø12 Ø6//0.15	0.25 / 0.20 — 6Ø12 Ø6//0.15
1st Floor	0.25 / 0.20 — 6Ø12 Ø6//0.15	0.25 / 0.20 — 6Ø12 Ø6//0.15	0.25 / 0.25 — 4Ø16 Ø6//0.20
Ground Floor			

X
Y

BEAM B1

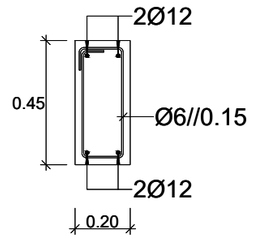

Span and Supports

BEAM B2

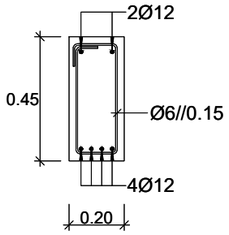

Span

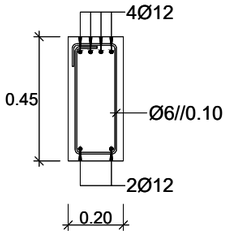

Supports

STEEL BRACES

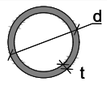

CHSH dxt (mm)

STOREY	STEEL BRACES	
	DIRECTION XX	DIRECTION YY
2nd	CHSH 88.9x3.2	CHSH 88.9x3.2
1st	CHSH 88.9x5.0	CHSH 88.9x5.0

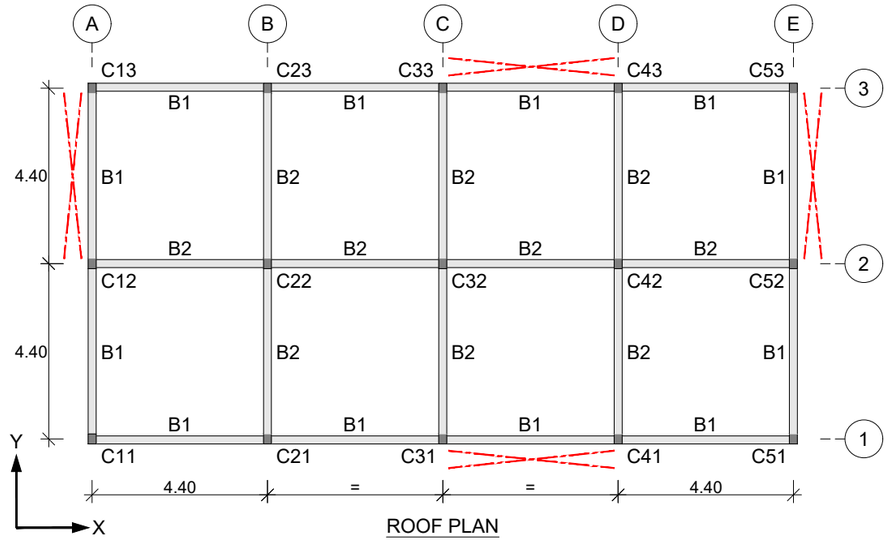

ROOF PLAN

KEY:

- Steel Braces

CONCRETE: fcm = 23.8 MPa
STEEL: fym = 440 MPa
CONCRETE COVER: c = 25 mm
STEEL BRACES: fym = 275 MPa

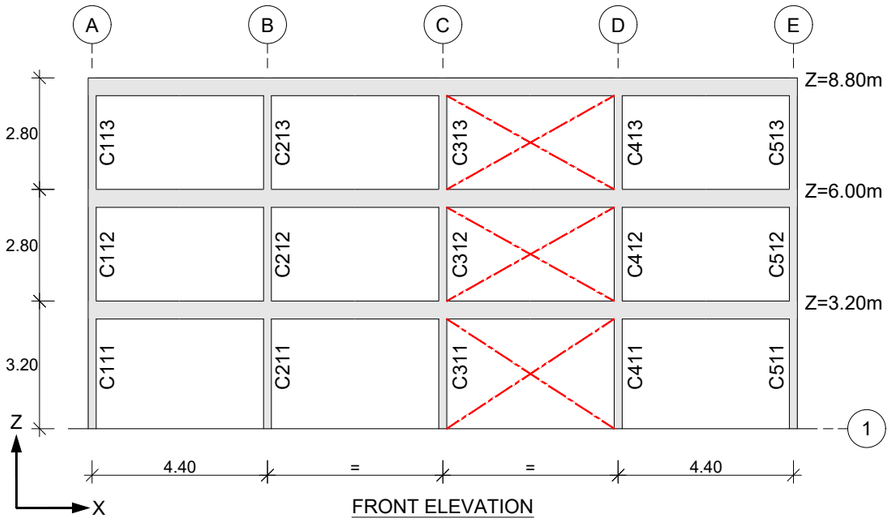

FRONT ELEVATION

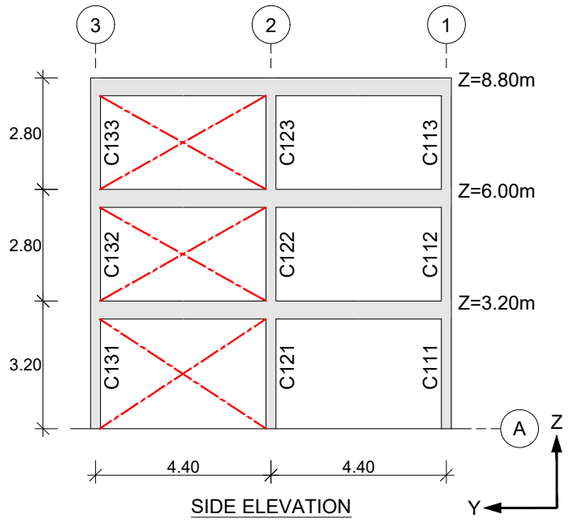

SIDE ELEVATION

S3_3S_2x4_RETRO	APPENDIX 4
GEOMETRY	A4.25

CONCRETE: fcm = 23.8 MPa
STEEL: fym = 440 MPa
CONCRETE COVER: c = 25 mm
STEEL BRACES: fym = 275 MPa

COLUMNS SCHEDULE

	C11 / C13 / C51 / C53	C21 / C31 / C41 / C12 / C52 / C23 / C33 / C43	C22 / C32 / C42
3rd Floor	0.25 × 0.20 — 6Ø12 Ø6//0.15	0.25 × 0.20 — 6Ø12 Ø6//0.15	0.25 × 0.20 — 6Ø12 Ø6//0.15
2nd Floor	0.25 × 0.20 — 6Ø12 Ø6//0.15	0.25 × 0.20 — 6Ø12 Ø6//0.15	0.25 × 0.25 — 4Ø16 Ø6//0.20
1st Floor	0.25 × 0.20 — 6Ø12 Ø6//0.15	0.25 × 0.20 — 6Ø12 Ø6//0.15	0.30 × 0.30 — 8Ø16 Ø6//0.20
Ground Floor			

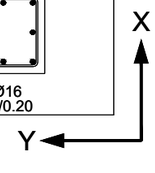

BEAM B1

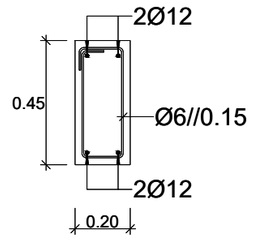

Span and Supports

BEAM B2

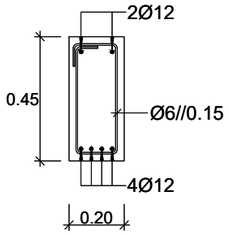

Span

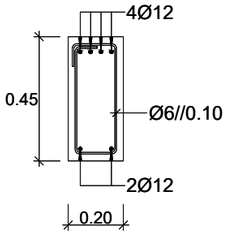

Supports

STEEL BRACES

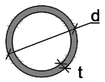

CHSH dxt (mm)

STOREY	STEEL BRACES	
	DIRECTION XX	DIRECTION YY
3rd	CHSH 88.9x3.2	CHSH 88.9x3.2
2nd	CHSH 88.9x3.6	CHSH 88.9x3.2
1st	CHSH 88.9x3.6	CHSH 88.9x3.2

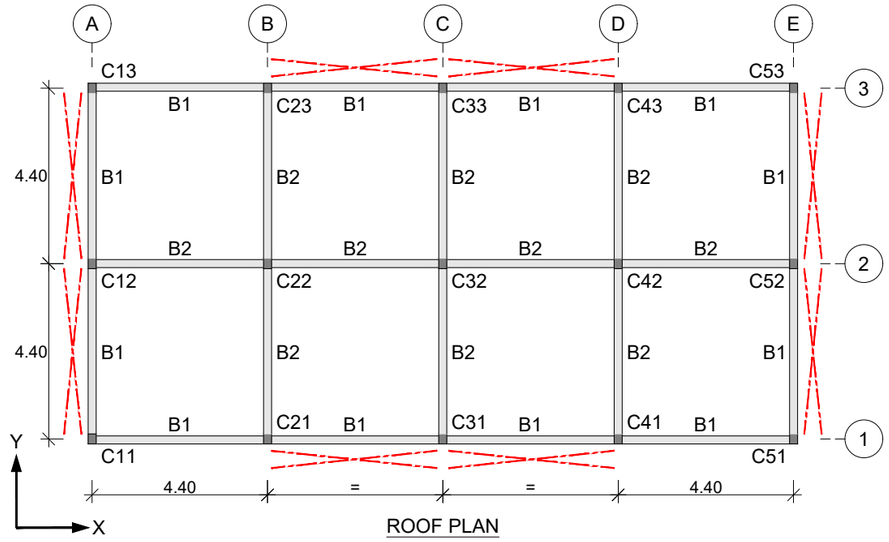

ROOF PLAN

KEY:

- Steel Braces

CONCRETE: fcm = 23.8 MPa
STEEL: fym = 440 MPa
CONCRETE COVER: c = 25 mm
STEEL BRACES: fym = 275 MPa

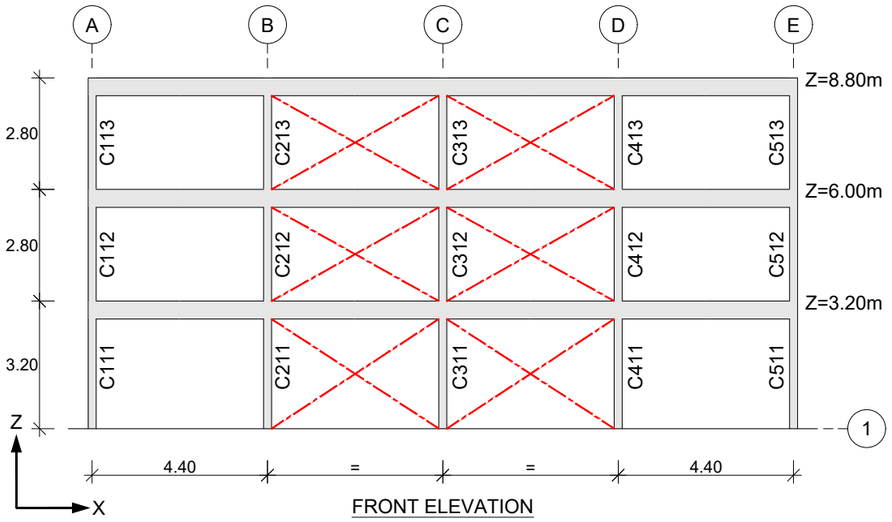

FRONT ELEVATION

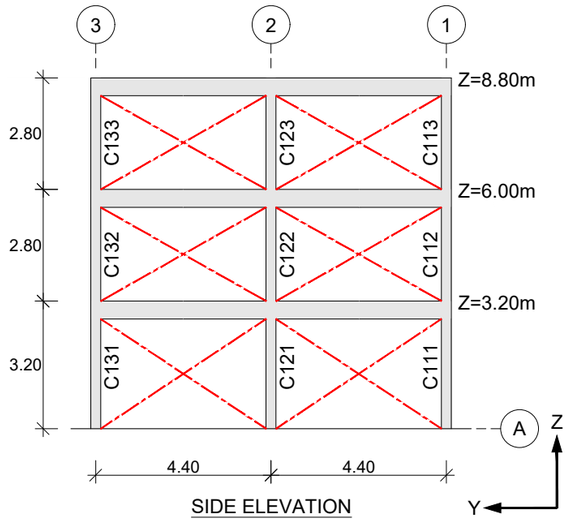

SIDE ELEVATION

S4_3S_2x4_RETRO	APPENDIX 4
GEOMETRY	A4.27

CONCRETE: fcm = 23.8 MPa
STEEL: fym = 440 MPa
CONCRETE COVER: c = 25 mm
STEEL BRACES: fym = 275 MPa

COLUMNS SCHEDULE

	C11 / C13 / C51 / C53	C21 / C31 / C41 / C12 / C52 / C23 / C33 / C43	C22 / C32 / C42
3rd Floor	0.25 / 0.20 — 6Ø12 Ø6//0.15	0.25 / 0.20 — 6Ø12 Ø6//0.15	0.25 / 0.20 — 6Ø12 Ø6//0.15
2nd Floor	0.25 / 0.20 — 6Ø12 Ø6//0.15	0.25 / 0.20 — 6Ø12 Ø6//0.15	0.25 / 0.25 — 4Ø16 Ø6//0.20
1st Floor	0.25 / 0.20 — 6Ø12 Ø6//0.15	0.25 / 0.20 — 6Ø12 Ø6//0.15	0.30 / 0.30 — 8Ø16 Ø6//0.20
Ground Floor			

X
Y

BEAM B1

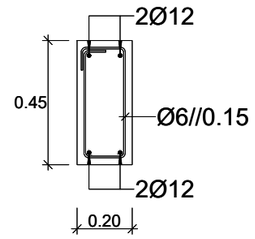

Span and Supports

BEAM B2

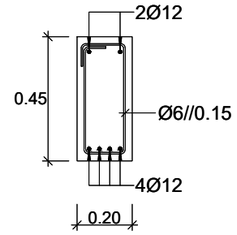

Span

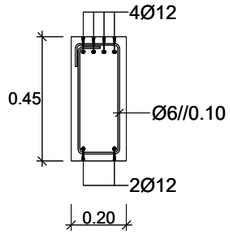

Supports

STEEL BRACES

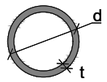

CHSH dxt (mm)

STOREY	STEEL BRACES	
	DIRECTION XX	DIRECTION YY
3rd	CHSH 88.9x3.2	CHSH 88.9x3.2
2nd	CHSH 88.9x3.6	CHSH 88.9x3.6
1st	CHSH 88.9x4.0	CHSH 88.9x4.0

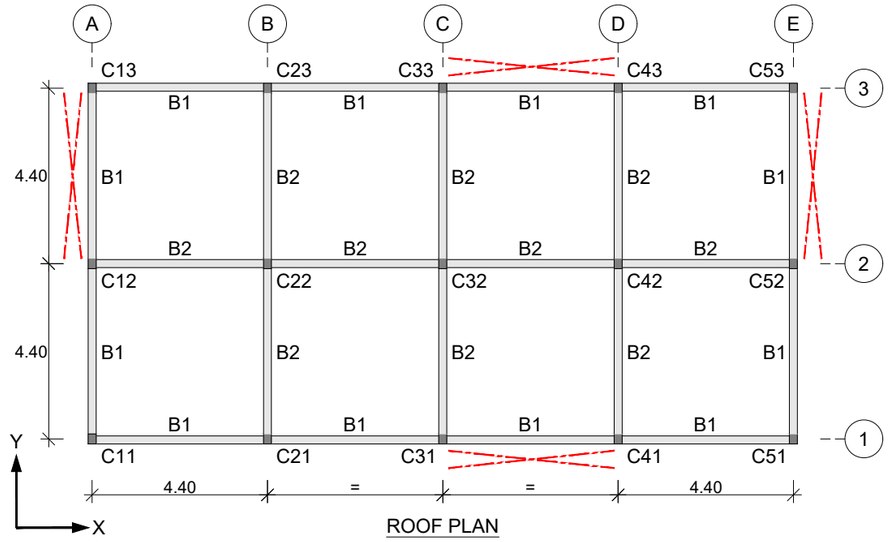

ROOF PLAN

KEY:

- Steel Braces

CONCRETE: fcm = 23.8 MPa
STEEL: fym = 440 MPa
CONCRETE COVER: c = 25 mm
STEEL BRACES: fym = 275 MPa

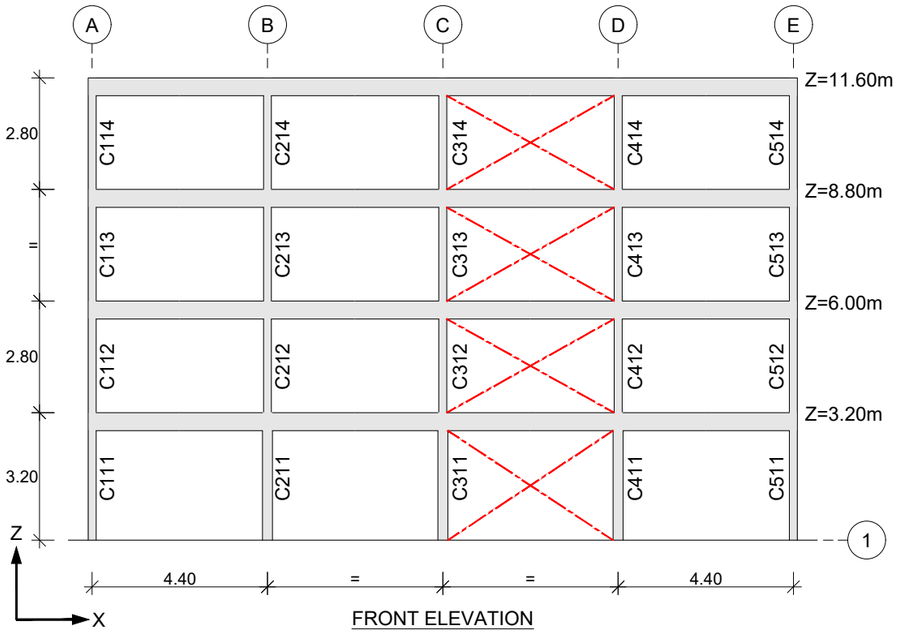

FRONT ELEVATION

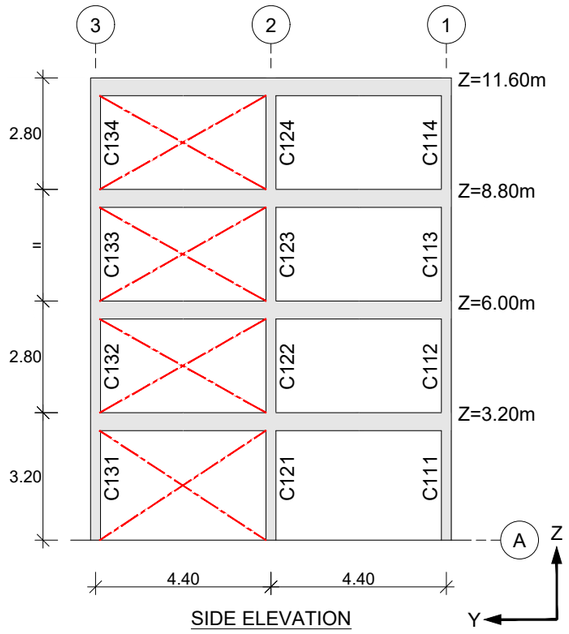

SIDE ELEVATION

S3_4S_2x4_RETRO	APPENDIX 4
GEOMETRY	A4.29

CONCRETE: fcm = 23.8 MPa
STEEL: fym = 440 MPa
CONCRETE COVER: c = 25 mm
STEEL BRACES: fym = 275 MPa

COLUMNS SCHEDULE

	C11 / C13 / C51 / C53	C21 / C31 / C41 / C12 / C52 / C23 / C33 / C43	C22 / C32 / C42
4th Floor	0.25 × 0.20 — 6Ø12 Ø6//0.15	0.25 × 0.20 — 6Ø12 Ø6//0.15	0.25 × 0.20 — 6Ø12 Ø6//0.15
3rd Floor	0.25 × 0.20 — 6Ø12 Ø6//0.15	0.25 × 0.20 — 6Ø12 Ø6//0.15	0.25 × 0.25 — 4Ø16 Ø6//0.20
2nd Floor	0.25 × 0.20 — 6Ø12 Ø6//0.15	0.25 × 0.20 — 6Ø12 Ø6//0.15	0.30 × 0.30 — 8Ø16 Ø6//0.20
1st Floor	0.25 × 0.20 — 6Ø12 Ø6//0.15	0.25 × 0.25 — 4Ø16 Ø6//0.20	0.40 × 0.30 — 6Ø16 Ø6//0.20
Ground Floor			

X
Y

BEAM B1

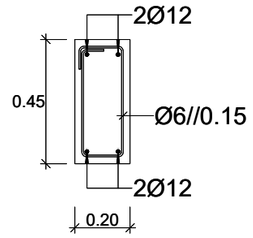

Span and Supports

BEAM B2

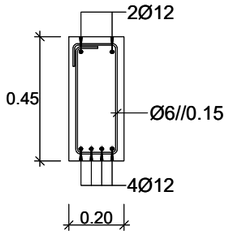

Span

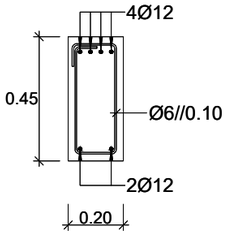

Supports

STEEL BRACES

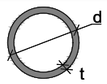

CHSH dxt (mm)

STOREY	STEEL BRACES	
	DIRECTION XX	DIRECTION YY
4th	CHSH 88.9x3.2	CHSH 88.9x3.2
3rd	CHSH 88.9x3.2	CHSH 88.9x3.2
2nd	CHSH 88.9x3.6	CHSH 88.9x4.0
1st	CHSH 88.9x3.6	CHSH 88.9x4.0

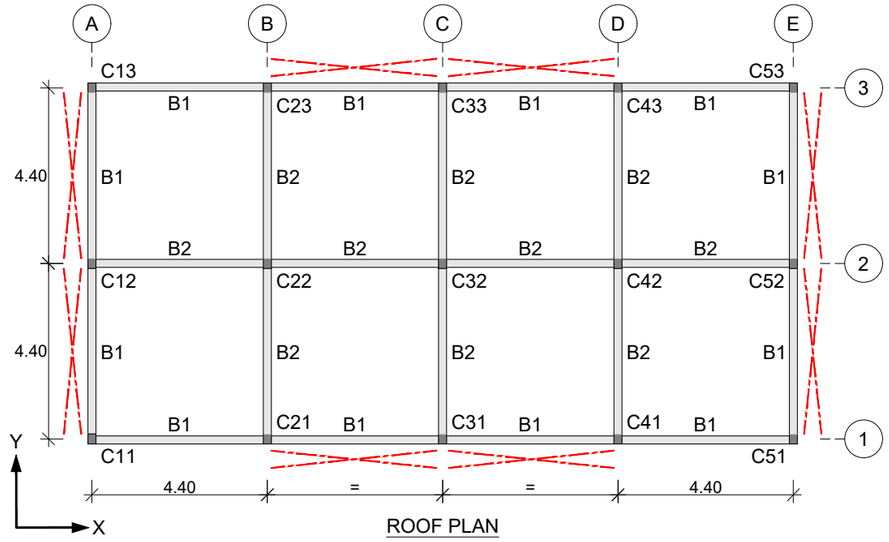

ROOF PLAN

KEY:

- Steel Braces

CONCRETE: fcm = 23.8 MPa
STEEL: fym = 440 MPa
CONCRETE COVER: c = 25 mm
STEEL BRACES: fym = 275 MPa

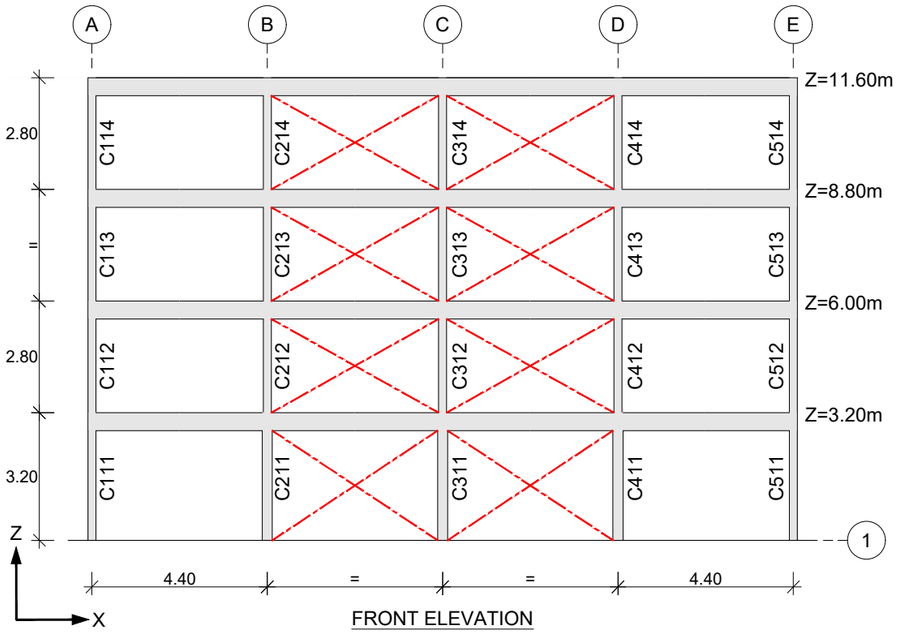

FRONT ELEVATION

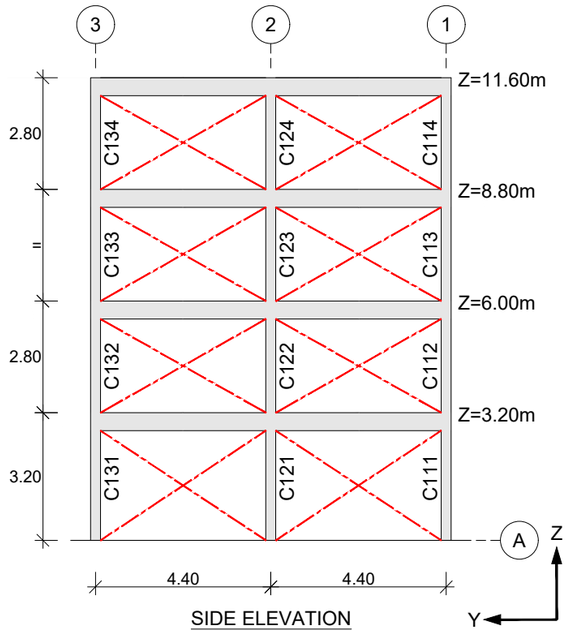

SIDE ELEVATION

S4_4S_2x4_RETRO	APPENDIX 4
GEOMETRY	A4.31

CONCRETE: fcm = 23.8 MPa
STEEL: fym = 440 MPa
CONCRETE COVER: c = 25 mm
STEEL BRACES: fym = 275 MPa

COLUMNS SCHEDULE

	C11 / C13 / C51 / C53	C21 / C31 / C41 / C12 / C52 / C23 / C33 / C43	C22 / C32 / C42
4th Floor	0.25 × 0.20 — 6Ø12 Ø6//0.15	0.25 × 0.20 — 6Ø12 Ø6//0.15	0.25 × 0.20 — 6Ø12 Ø6//0.15
3rd Floor	0.25 × 0.20 — 6Ø12 Ø6//0.15	0.25 × 0.20 — 6Ø12 Ø6//0.15	0.25 × 0.25 — 4Ø16 Ø6//0.20
2nd Floor	0.25 × 0.20 — 6Ø12 Ø6//0.15	0.25 × 0.20 — 6Ø12 Ø6//0.15	0.30 × 0.30 — 8Ø16 Ø6//0.20
1st Floor	0.25 × 0.20 — 6Ø12 Ø6//0.15	0.25 × 0.25 — 4Ø16 Ø6//0.20	0.40 × 0.30 — 6Ø16 Ø6//0.20
Ground Floor			

X
Y

BEAM B1

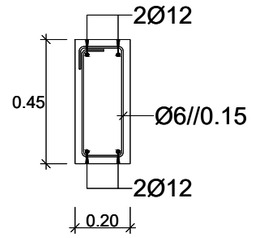

Span and Supports

BEAM B2

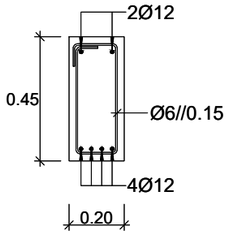

Span

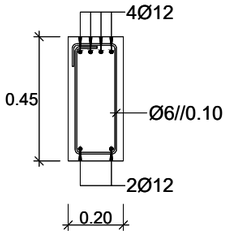

Supports

STEEL BRACES

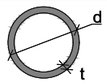

CHSH dxt (mm)

STOREY	STEEL BRACES	
	DIRECTION XX	DIRECTION YY
4th	CHSH 88.9x3.2	CHSH 88.9x3.2
3rd	CHSH 88.9x3.6	CHSH 88.9x4.0
2nd	CHSH 88.9x5.0	CHSH 88.9x6.0
1st	CHSH 88.9x5.0	CHSH 88.9x6.0

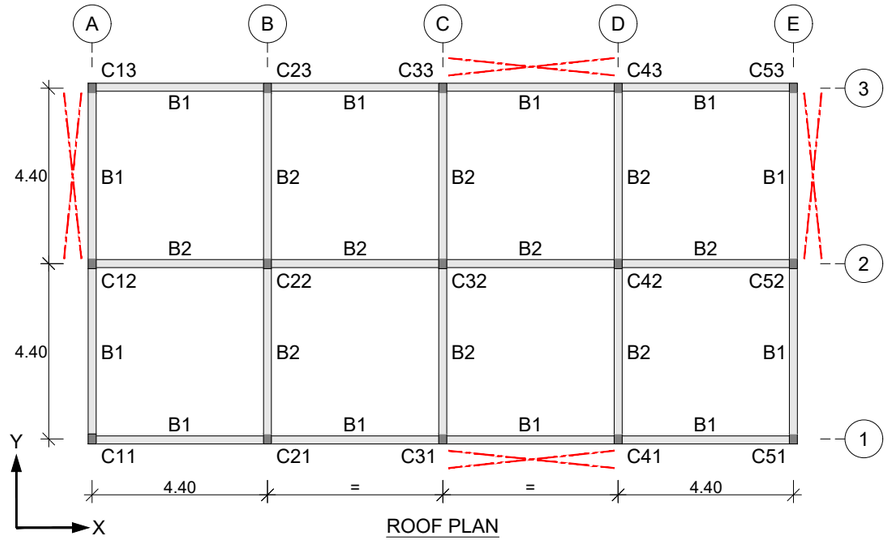

ROOF PLAN

KEY:

- Steel Braces

CONCRETE: fcm = 23.8 MPa
STEEL: fym = 440 MPa
CONCRETE COVER: c = 25 mm
STEEL BRACES: fym = 275 MPa

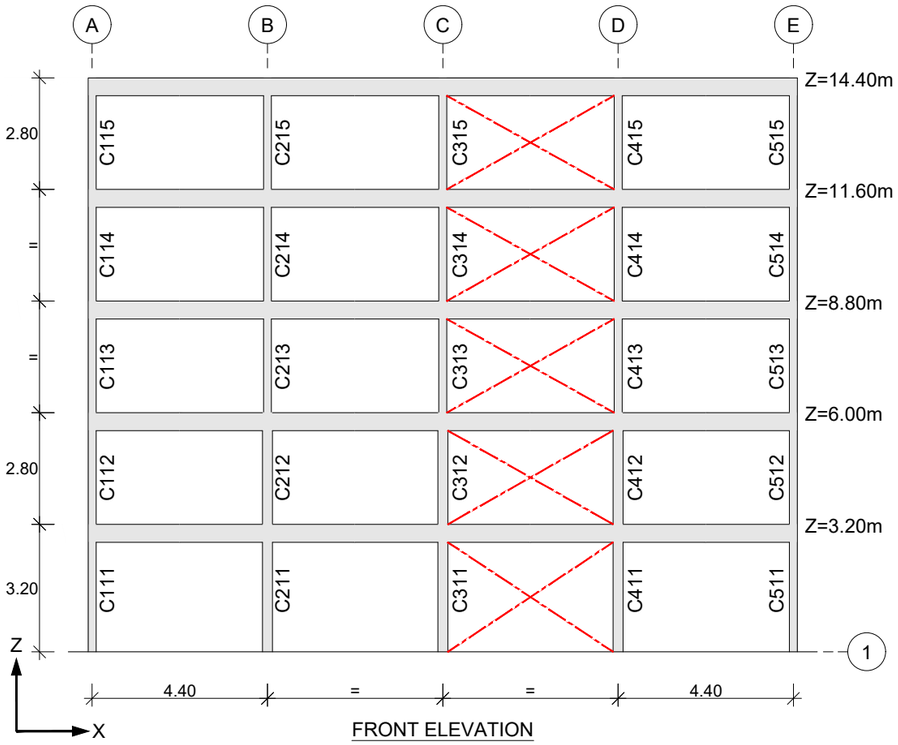

FRONT ELEVATION

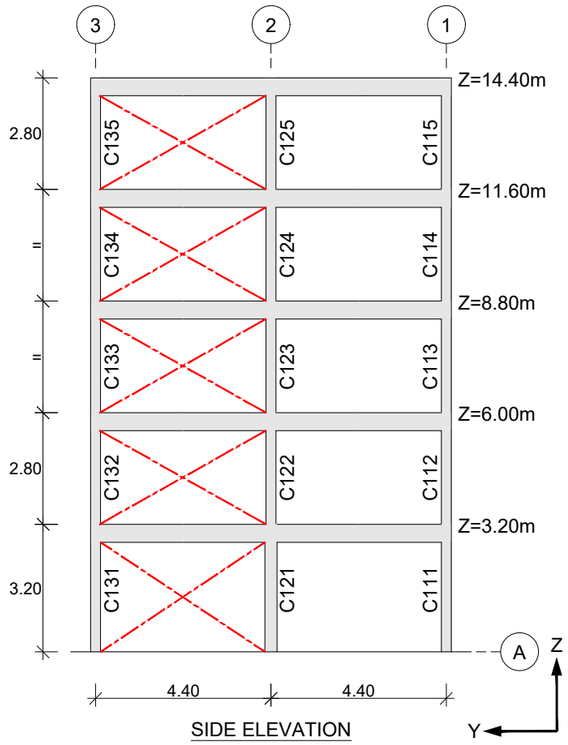

SIDE ELEVATION

S3_5S_2x4_RETRO	APPENDIX 4
GEOMETRY	A4.33

CONCRETE: fcm = 23.8 MPa
STEEL: fym = 440 MPa
CONCRETE COVER: c = 25 mm
STEEL BRACES: fym = 275 MPa

COLUMNS SCHEDULE

	C11 / C13 / C51 / C53	C21 / C31 / C41 / C12 / C52 / C23 / C33 / C43	C22 / C32 / C42
5th Floor	0.25 × 0.20 6Ø12 Ø6//0.15	0.25 × 0.20 6Ø12 Ø6//0.15	0.25 × 0.20 6Ø12 Ø6//0.15
4th Floor	0.25 × 0.20 6Ø12 Ø6//0.15	0.25 × 0.20 6Ø12 Ø6//0.15	0.25 × 0.25 4Ø16 Ø6//0.20
3rd Floor	0.25 × 0.20 6Ø12 Ø6//0.15	0.25 × 0.20 6Ø12 Ø6//0.15	0.30 × 0.30 8Ø16 Ø6//0.20
2nd Floor	0.25 × 0.20 6Ø12 Ø6//0.15	0.25 × 0.25 4Ø16 Ø6//0.20	0.40 × 0.30 6Ø16 Ø6//0.20
1st Floor	0.25 × 0.20 6Ø12 Ø6//0.15	0.30 × 0.25 4Ø16 Ø6//0.20	0.50 × 0.30 8Ø16 Ø6//0.20
Ground Floor			

X
Y

BEAM B1

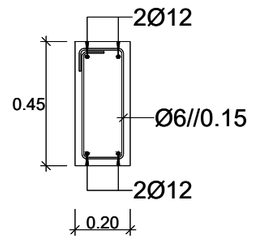

Span and Supports

BEAM B2

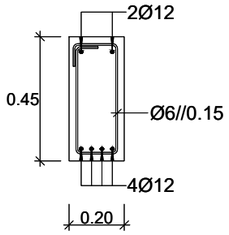

Span

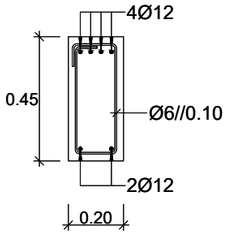

Supports

STEEL BRACES

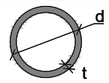

CHSH dxt (mm)

STOREY	STEEL BRACES	
	DIRECTION XX	DIRECTION YY
5th	CHSH 88.9x3.2	CHSH 88.9x3.2
4th	CHSH 88.9x3.2	CHSH 88.9x3.2
3rd	CHSH 88.9x3.2	CHSH 88.9x3.6
2nd	CHSH 88.9x3.2	CHSH 88.9x4.0
1st	CHSH 88.9x3.2	CHSH 88.9x3.2

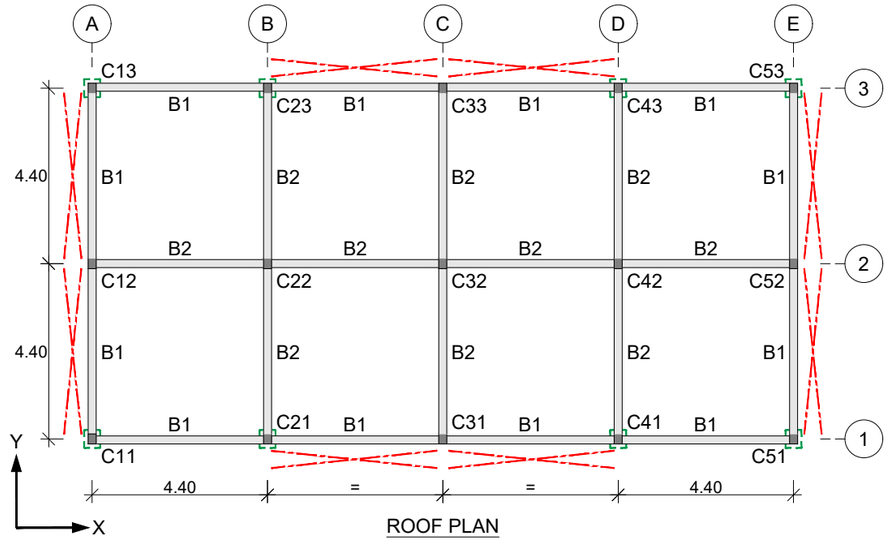

ROOF PLAN

KEY:

- Steel Braces

- Columns with FRP wrapping

CONCRETE: fcm = 23.8 MPa
STEEL: fym = 440 MPa
CONCRETE COVER: c = 25 mm
STEEL BRACES: fym = 275 MPa

FRP SHEET:
SikaWrap-230 C
N = 3
R = 30mm

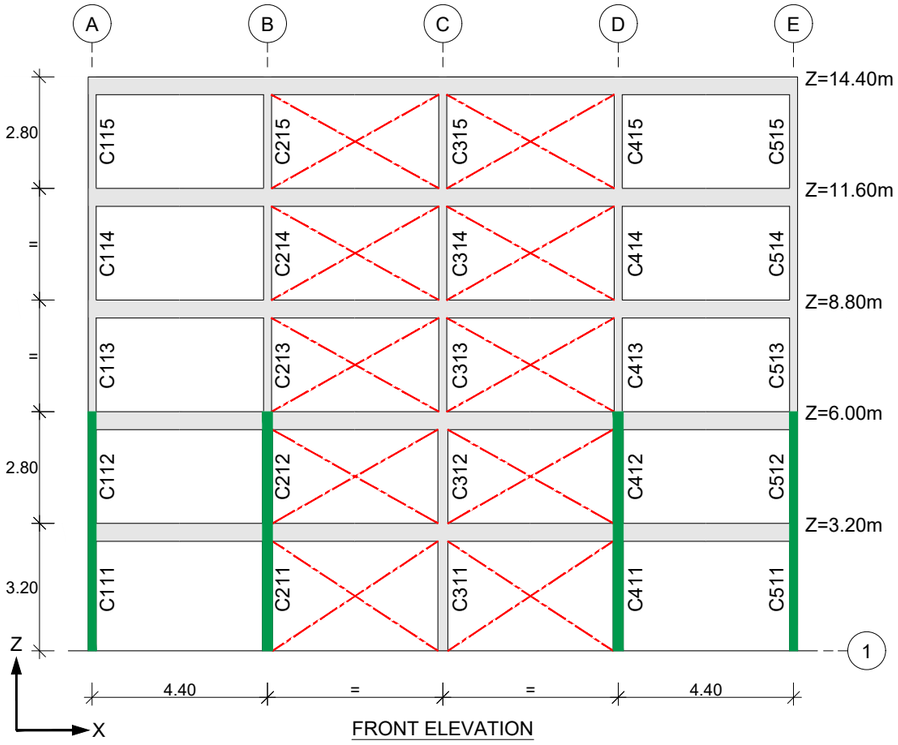

FRONT ELEVATION

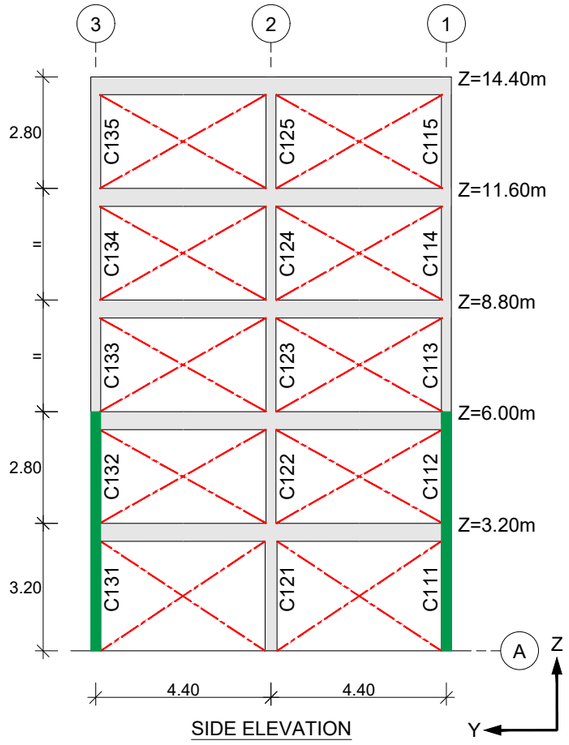

SIDE ELEVATION

S4_5S_2x4_RETRO	APPENDIX 4
GEOMETRY	A4.35

COLUMNS SCHEDULE

	C11 / C13 / C51 / C53	C31 / C12 / C52 / C33	C22 / C32 / C42	C21 / C41 / C23 / C43
5th Floor	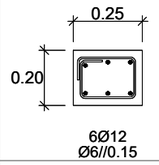	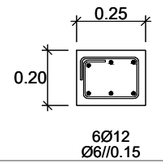	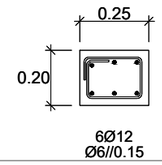	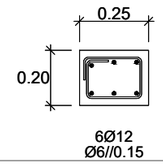
4th Floor	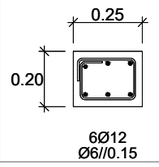	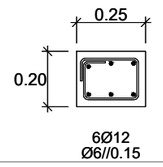	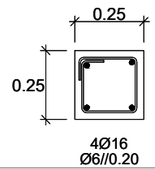	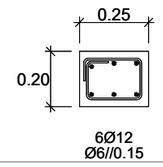
3rd Floor	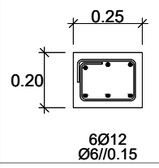	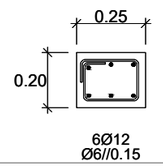	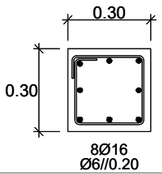	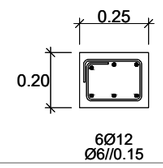
2nd Floor	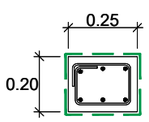	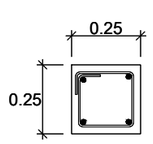	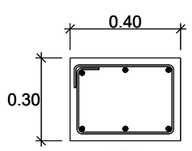	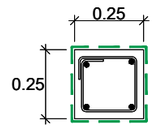
1st Floor	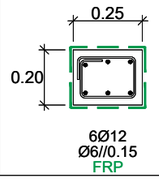	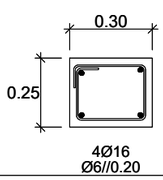	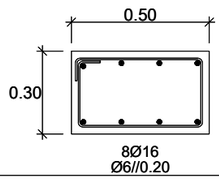	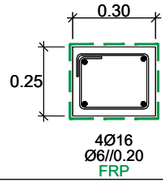
Ground Floor				

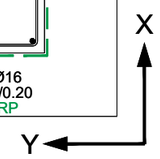

CONCRETE: fcm = 23.8 MPa
STEEL: fym = 440 MPa
CONCRETE COVER: c = 25 mm
STEEL BRACES: fym = 275 MPa

FRP SHEET:
SikaWrap-230 C
N = 3
R = 30mm

BEAM B1

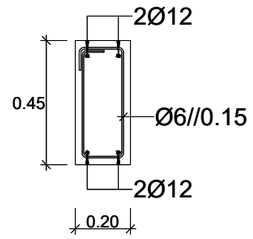

Span and Supports

BEAM B2

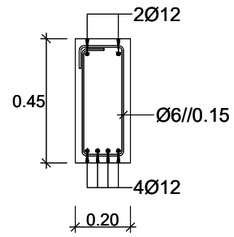

Span

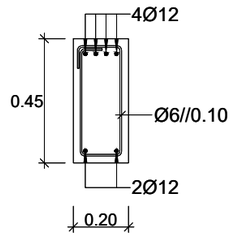

Supports

STEEL BRACES

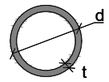

CHSH dxt (mm)

STOREY	STEEL BRACES	
	DIRECTION XX	DIRECTION YY
5th	CHSH 88.9x3.2	CHSH 88.9x3.2
4th	CHSH 88.9x3.6	CHSH 88.9x3.6
3rd	CHSH 88.9x5.0	CHSH 88.9x5.0
2nd	CHSH 88.9x6.0	CHSH 88.9x6.0
1st	CHSH 88.9x6.0	CHSH 88.9x6.0

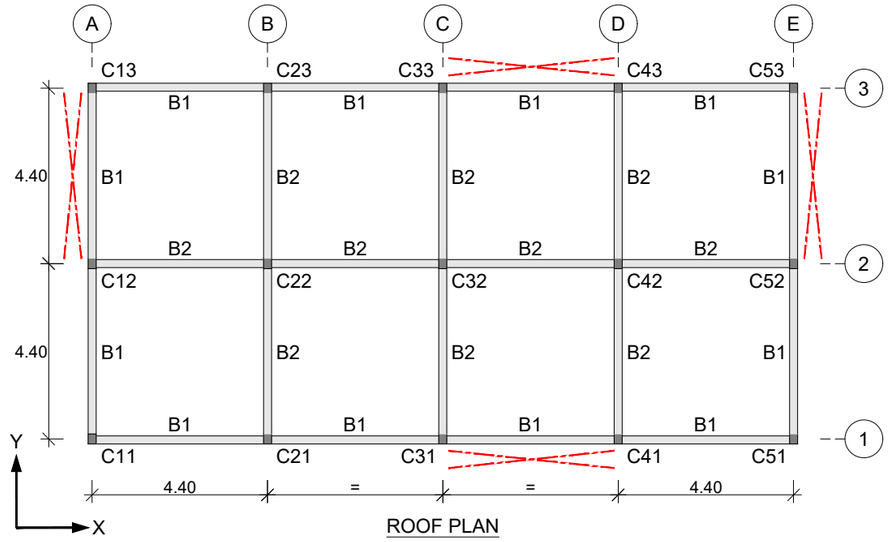

ROOF PLAN

KEY:

- Steel Braces

CONCRETE: fcm = 23.8 MPa
STEEL: fym = 440 MPa
CONCRETE COVER: c = 25 mm
STEEL BRACES: fym = 275 MPa

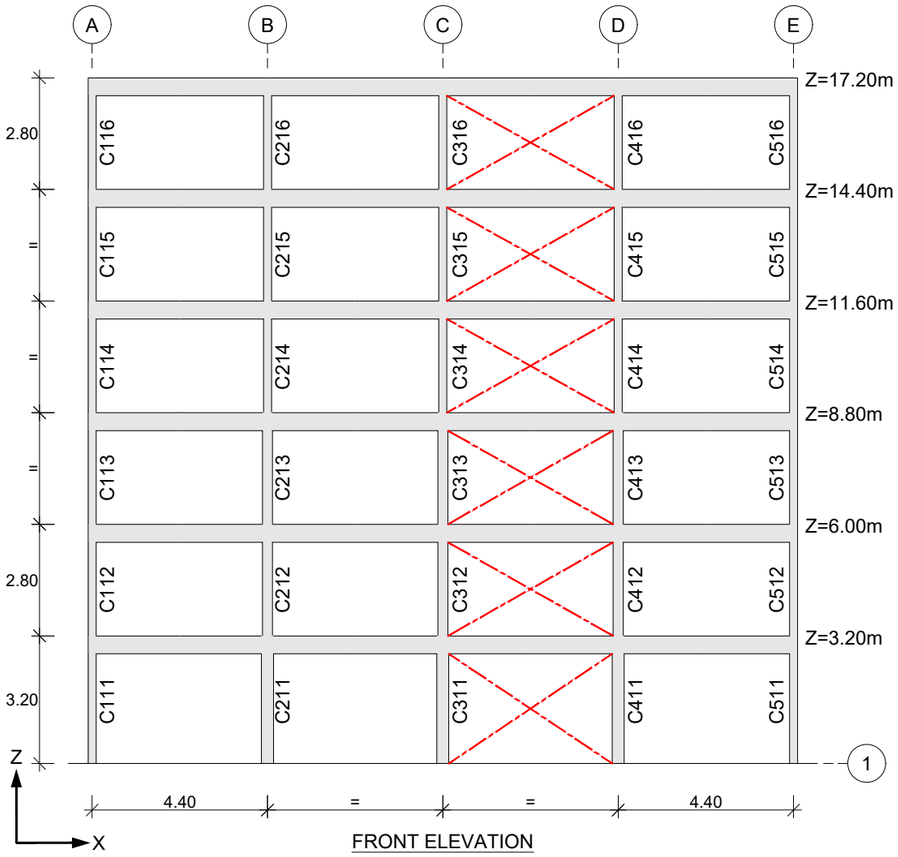

FRONT ELEVATION

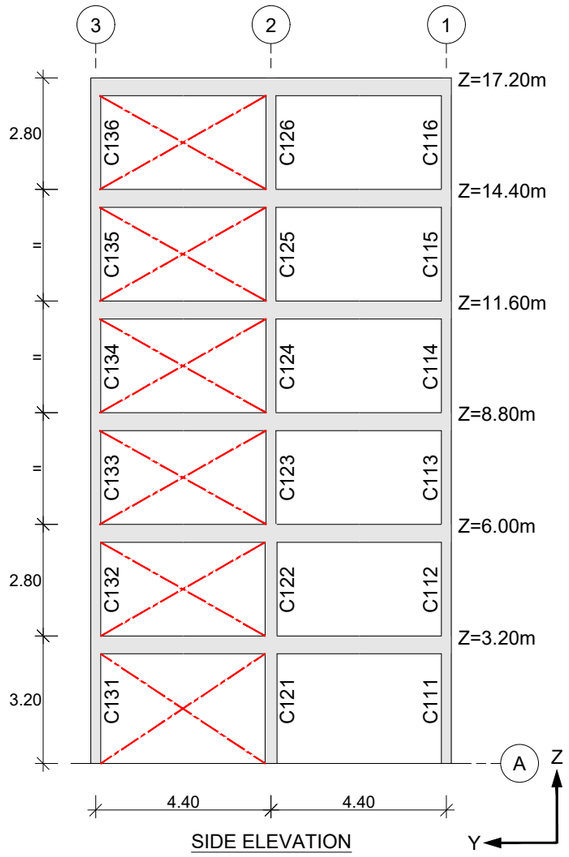

SIDE ELEVATION

S3_6S_2x4_RETRO	APPENDIX 4
GEOMETRY	A4.37

CONCRETE: fcm = 23.8 MPa
STEEL: fym = 440 MPa
CONCRETE COVER: c = 25 mm
STEEL BRACES: fym = 275 MPa

COLUMNS SCHEDULE

	C11 / C13 / C51 / C53	C21 / C31 / C41 / C12 / C52 / C23 / C33 / C43	C22 / C32 / C42
6th Floor	0.25 / 0.20 — 6Ø12 Ø6//0.15	0.25 / 0.20 — 6Ø12 Ø6//0.15	0.25 / 0.20 — 6Ø12 Ø6//0.15
5th Floor	0.25 / 0.20 — 6Ø12 Ø6//0.15	0.25 / 0.20 — 6Ø12 Ø6//0.15	0.25 / 0.25 — 4Ø16 Ø6//0.20
4th Floor	0.25 / 0.20 — 6Ø12 Ø6//0.15	0.25 / 0.20 — 6Ø12 Ø6//0.15	0.30 / 0.30 — 8Ø16 Ø6//0.20
3rd Floor	0.25 / 0.20 — 6Ø12 Ø6//0.15	0.25 / 0.25 — 4Ø16 Ø6//0.20	0.40 / 0.30 — 6Ø16 Ø6//0.20
2nd Floor	0.25 / 0.20 — 6Ø12 Ø6//0.15	0.30 / 0.25 — 4Ø16 Ø6//0.20	0.50 / 0.30 — 8Ø16 Ø6//0.20
1st Floor	0.25 / 0.20 — 6Ø12 Ø6//0.15	0.30 / 0.30 — 8Ø16 Ø6//0.20	0.60 / 0.30 — 6Ø20 Ø6//0.25
Ground Floor			

X
Y

BEAM B1

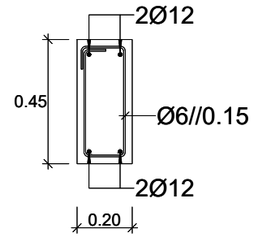

Span and Supports

BEAM B2

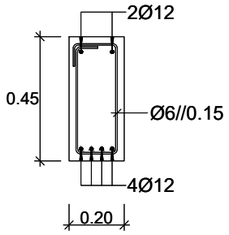

Span

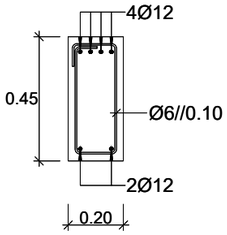

Supports

STEEL BRACES

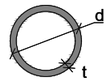

CHSH dxt (mm)

STOREY	STEEL BRACES	
	DIRECTION XX	DIRECTION YY
6th	CHSH 88.9x3.2	CHSH 88.9x3.2
5th	CHSH 88.9x3.2	CHSH 88.9x3.2
4th	CHSH 88.9x3.2	CHSH 88.9x3.6
3rd	CHSH 88.9x3.6	CHSH 88.9x4.0
2nd	CHSH 88.9x4.0	CHSH 88.9x4.0
1st	CHSH 88.9x3.2	CHSH 88.9x3.2

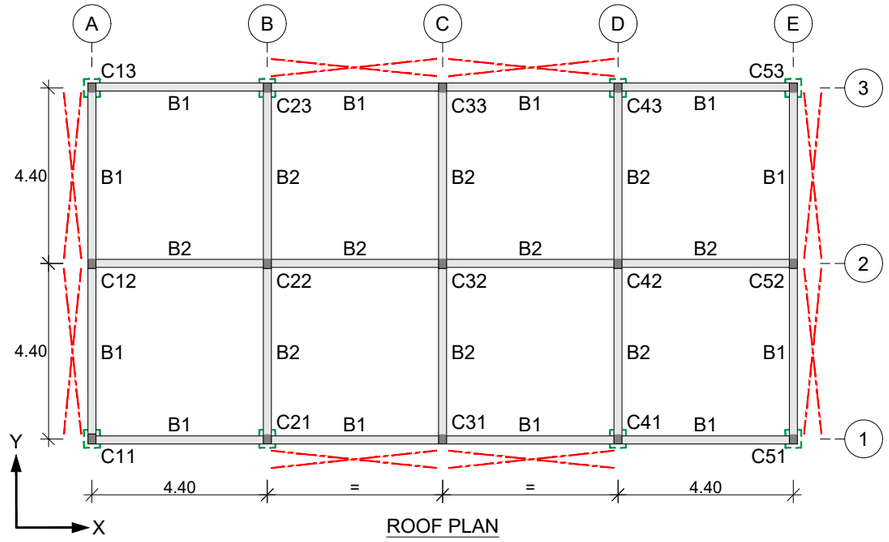

ROOF PLAN

KEY:

- Steel Braces
- Columns with FRP wrapping

CONCRETE: fcm = 23.8 MPa
STEEL: fym = 440 MPa
CONCRETE COVER: c = 25 mm
STEEL BRACES: fym = 275 MPa

FRP SHEET:
SikaWrap-230 C
N = 3
R = 30mm

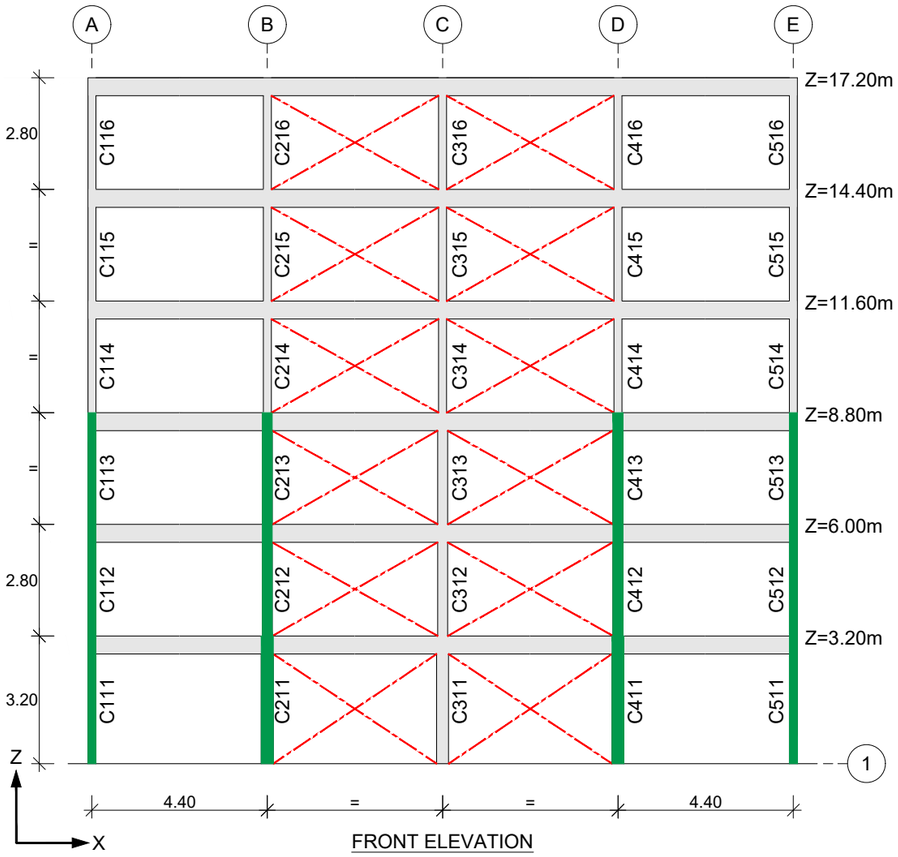

FRONT ELEVATION

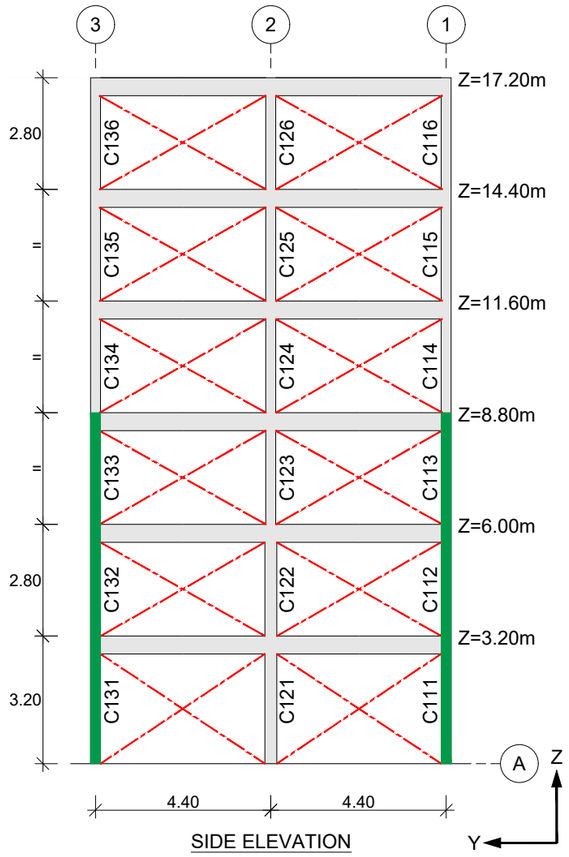

SIDE ELEVATION

S4_6S_2x4_RETRO	APPENDIX 4
GEOMETRY	A4.39

COLUMNS SCHEDULE

	C11 / C13 / C51 / C53	C31 / C12 / C52 / C33	C22 / C32 / C42	C21 / C41 / C23 / C43
6th Floor	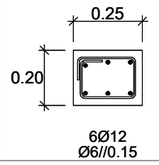	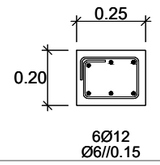	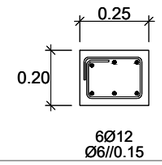	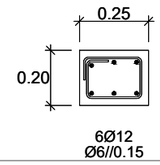
5th Floor	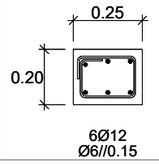	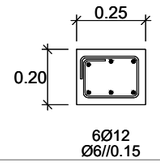	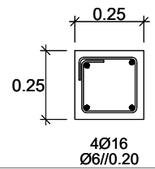	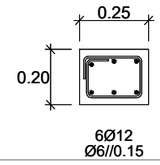
4th Floor	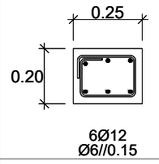	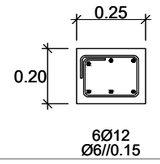	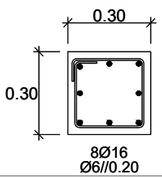	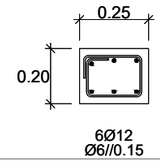
3rd Floor	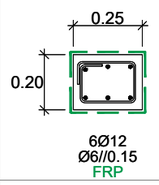	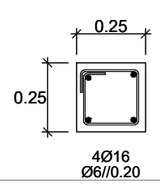	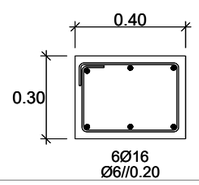	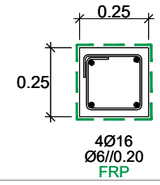
2nd Floor	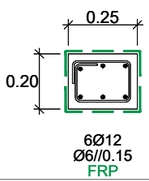	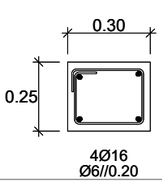	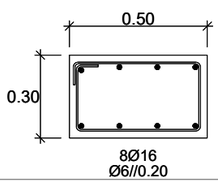	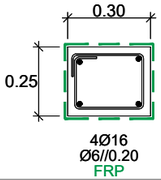
1st Floor	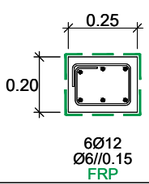	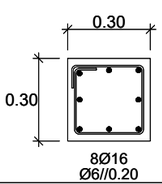	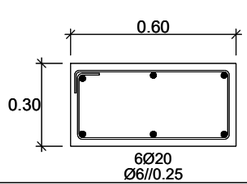	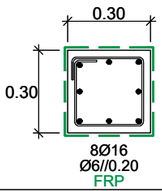
Ground Floor				

CONCRETE: fcm = 23.8 MPa
STEEL: fym = 440 MPa
CONCRETE COVER: c = 25 mm
STEEL BRACES: fym = 275 MPa

FRP SHEET:
SikaWrap-230 C
N = 3
R = 30mm

BEAM B1

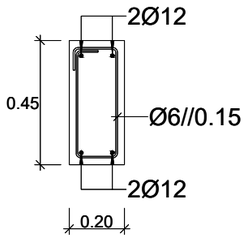

Span and Supports

BEAM B2

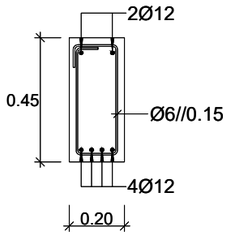

Span

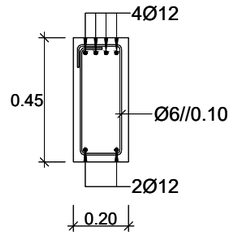

Supports

STEEL BRACES

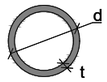

CHSH dxt (mm)

STOREY	STEEL BRACES	
	DIRECTION XX	DIRECTION YY
6th	CHSH 88.9x3.2	CHSH 88.9x3.2
5th	CHSH 88.9x3.2	CHSH 88.9x3.2
4th	CHSH 88.9x3.6	CHSH 88.9x4.0
3rd	CHSH 88.9x5.0	CHSH 88.9x5.0
2nd	CHSH 88.9x5.0	CHSH 88.9x5.0
1st	CHSH 88.9x5.0	CHSH 88.9x5.0

APPENDIX 5

RETROFITTED BUILDINGS – DESIGN PROCEDURE

APPENDIX 5 – RETROFITTED BUILDINGS – DESIGN PROCEDURE

BUILDING TYPE 1: 2 storeys, 3×5 spans

Seismic hazard scenario 3: PT 1.3 + 2.3 (EC8-1)

Seismic hazard scenario 4: PT 1.1 + 2.3 (EC8-1)

BUILDING TYPE 2: 3 storeys, 3×5 spans

Id

BUILDING TYPE 3: 4 storeys, 3×5 spans

Id

BUILDING TYPE 4: 5 storeys, 3×5 spans

Id

BUILDING TYPE 5: 6 storeys, 3×5 spans

Id

BUILDING TYPE 6: 2 storeys, 2×4 spans

Id

BUILDING TYPE 7: 3 storeys, 2×4 spans

Id

BUILDING TYPE 8: 4 storeys, 2×4 spans

Id

BUILDING TYPE 9: 5 storeys, 2×4 spans

Id

BUILDING TYPE 10: 6 storeys, 2×4 spans

Id

BUILDING TYPE 1: 2 storeys, 3×5 spans **| SEISMIC HAZARD SCENARIO 3:** PT 1.3 + 2.3 (EC8-1)

Table A5.1 – Design procedure result – Direction XX (S3_AST1_2S_3×5_XX_RETRO)

ASSUMED

STOREY S_i	m_i [ton]	δ_i
6	0,00	0,000
5	0,00	0,000
4	0,00	0,000
3	0,00	0,000
2	232,33	1,000
1	232,33	0,616

F_i [kN]
0,00
0,00
0,00
0,00
0,62
0,38

α1	0,947
PF1	1,171

START	Tens.	Comp.
ΔN_0 [kN]	200,00	350,00

B [m]	h [m]	L_i [m]
4,40	3,20	5,441

E_s [GPa]	f_{ym} [MPa]	ε_y
210,00	343,75	0,001637

1st Storey

Δ_y [m]	Δ_d [m]	μ
0,01101	0,02100	1,908

SDOF

EVD [%]	$S\Delta_d$ [m]	T_e [s]	K_e [kN/m]
13,56%	0,02909	0,760	30064,71

1st Storey

V_b^{REQ} [kN]	V_b^{BF} [kN]	$V_b^{BR,REQ}$ [kN]
874,56	450,29	491,81

1st Storey

BR S_1	V_b^{BR} [kN]	V_b [kN]	Ω
CHSH 88,9 x 3,2	536,36	919,11	1,051

ASSUMED

STOREY S_i	DRIFTS [m]	V_i^{BF} [kN]		Nth Storey V_i^{REQ} [kN]	$V_i^{BR,REQ}$ [kN]	BR S_i	V_i^{BR} [kN]
6	0,00000			0,00	0,00	0	0,00
5	0,00000			0,00	0,00	0	0,00
4	0,00000			0,00	0,00	0	0,00
3	-0,03407			0,00	0,00	0	0,00
2	0,01307	281,23	x2	568,65	329,60	88,9 x 3,2	564,44
1	0,02100	450,29	x2	874,56	491,81	88,9 x 3,2	536,36

END	Tens.	Comp.
ΔN [kN]	218,04	362,67
	9,02%	3,62%

SDOF

Sa [g]	0,21300

Table A5.2 – Design procedure result – Direction YY (S3_AST1_2S_3×5_YY_RETRO)

	ASSUMED	
STOREY S_i	**m_i [ton]**	**δ_i**
6	0,00	0,000
5	0,00	0,000
4	0,00	0,000
3	0,00	0,000
2	232,33	1,000
1	232,33	0,616

F_i [kN]
0,00
0,00
0,00
0,00
0,62
0,38

α1	0,947
PF1	1,171

	START	Tens.	Comp.
ΔN_0 [kN]		200,00	350,00

B [m]	**h [m]**	**L_i [m]**
4,40	3,20	5,441

E_s [GPa]	**f_{ym} [MPa]**	**ε_y**
210,00	343,75	0,001637

1st Storey			SDOF			
Δ_y [m]	**Δ_d [m]**	**μ**	**EVD [%]**	**$S\Delta_d$ [m]**	**T_e [s]**	**K_e [kN/m]**
0,01101	0,02100	1,908	13,56%	0,02909	0,760	30064,71

1st Storey				1st Storey			
V_b^{REQ} [kN]	**V_b^{BF} [kN]**	**$V_b^{BR,REQ}$ [kN]**		**BR S_1**	**V_b^{BR} [kN]**	**V_b [kN]**	**Ω**
				CHSH			
874,56	519,44	433,03	x2	88,9 x 3,2	536,36	977,88	1,118

	ASSUMED			Nth Storey			
STOREY S_i	**DRIFTS [m]**	**V_i^{BF} [kN]**		**V_i^{REQ} [kN]**	**$V_i^{BR,REQ}$ [kN]**	**BR S_i**	**V_i^{BR} [kN]**
6	0,00000			0,00	0,00	0	0,00
5	0,00000			0,00	0,00	0	0,00
4	0,00000			0,00	0,00	0	0,00
3	-0,03407			0,00	0,00	0	0,00
2	0,01307	343,19	x2	605,02	313,30	88,9 x 3,2	564,44
1	0,02100	519,44	x2	874,56	433,03	88,9 x 3,2	536,36

END	Tens.	Comp.
ΔN [kN]	218,04	362,67
	9,02%	3,62%

SDOF	
Sa [g]	0,22662

BUILDING TYPE 1: 2 storeys, 3×5 spans **| SEISMIC HAZARD SCENARIO 4:** PT 1.1 + 2.3 (EC8-1)

Table A5.3 – Design procedure result – Direction XX (S4_AST1_2S_3×5_XX_RETRO)

ASSUMED

STOREY S_i	m_i [ton]	δ_i
6	0,00	0,000
5	0,00	0,000
4	0,00	0,000
3	0,00	0,000
2	232,33	1,000
1	232,33	0,616

F_i [kN]
0,00
0,00
0,00
0,00
0,62
0,38

α1	0,947
PF1	1,171

START	Tens.	Comp.
ΔN_0 [kN]	525,00	750,00

B [m]	h [m]	L_i [m]
4,40	3,20	5,441

E_s [GPa]	f_{ym} [MPa]	ε_y
210,00	343,75	0,001637

1st Storey

Δ_y [m]	Δ_d [m]	μ
0,01101	0,02100	1,908

SDOF

EVD [%]	$S\Delta_d$ [m]	T_e [s]	K_e [kN/m]
13,56%	0,02909	0,541	59332,09

1st Storey

V_b^{REQ} [kN]	V_b^{BF} [kN]	$V_b^{BR,REQ}$ [kN]
1725,92	450,29	1343,18

1st Storey

	BR S_1	V_b^{BR} [kN]	V_b [kN]	Ω
x2	CHSH 139,7 x 5,0	1496,36	1879,11	1,089

ASSUMED

STOREY S_i	DRIFTS [m]	V_i^{BF} [kN]
6	0,00000	
5	0,00000	
4	0,00000	
3	-0,03407	
2	0,01307	281,23 x2
1	0,02100	450,29 x2

Nth Storey

V_i^{REQ} [kN]	$V_i^{BR,REQ}$ [kN]	BR S_i	V_i^{BR} [kN]
0,00	0,00	0	0,00
0,00	0,00	0	0,00
0,00	0,00	0	0,00
0,00	0,00	0	0,00
1162,60	923,56	139,7 x 3,2	1029,89
1725,92	1343,18	139,7 x 5,0	1496,36

END	Tens.	Comp.
ΔN [kN]	524,78	788,40
	-0,04%	5,12%

SDOF

Sa [g]	0,43547

Table A5.4 – Design procedure result – Direction YY (S4_AST1_2S_3×5_YY_RETRO)

	ASSUMED	
STOREY S_i	**m_i [ton]**	**δ_i**
6	0,00	0,000
5	0,00	0,000
4	0,00	0,000
3	0,00	0,000
2	232,33	1,000
1	232,33	0,616

F_i [kN]
0,00
0,00
0,00
0,00
0,62
0,38

α1	0,947
PF1	1,171

	START	**Tens.**	**Comp.**
ΔN_0 [kN]		450,00	700,00

B [m]	**h [m]**	**L_i [m]**
4,40	3,20	5,441

E_s [GPa]	**f_{ym} [MPa]**	**ε_y**
210,00	343,75	0,001637

1st Storey			**SDOF**			
Δ_y [m]	**Δ_d [m]**	**μ**	**EVD [%]**	**$S\Delta_d$ [m]**	**T_e [s]**	**K_e [kN/m]**
0,01101	0,02100	1,908	13,56%	0,02909	0,541	59332,09

1st Storey				**1st Storey**			
V_b^{REQ} [kN]	**V_b^{BF} [kN]**	**$V_b^{BR,REQ}$ [kN]**		**BR S_1**	**V_b^{BR} [kN]**	**V_b [kN]**	**Ω**
				CHSH			
1725,92	519,44	1284,40	x2	114,3 x 6,0	1343,09	1784,61	1,034

	ASSUMED			**Nth Storey**			
STOREY S_i	**DRIFTS [m]**	**V_i^{BF} [kN]**		**V_i^{REQ} [kN]**	**$V_i^{BR,REQ}$ [kN]**	**BR S_i**	**V_i^{BR} [kN]**
6	0,00000			0,00	0,00	0	0,00
5	0,00000			0,00	0,00	0	0,00
4	0,00000			0,00	0,00	0	0,00
3	-0,03407			0,00	0,00	0	0,00
2	0,01307	343,19	x2	1104,14	812,42	114,3 x 3,6	874,82
1	0,02100	519,44	x2	1725,92	1284,40	114,3 x 6,0	1343,09

END	**Tens.**	**Comp.**
ΔN [kN]	407,26	711,23
	-9,50%	1,60%

SDOF	
Sa [g]	0,41357

BUILDING TYPE 2: 3 storeys, 3×5 spans **| SEISMIC HAZARD SCENARIO 3:** PT 1.3 + 2.3 (EC8-1)

Table A5.5 – Design procedure result – Direction XX (S3_AST1_3S_3×5_XX_RETRO)

ASSUMED

STOREY S_i	m_i [ton]	δ_i
6	0,00	0,000
5	0,00	0,000
4	0,00	0,000
3	232,33	1,000
2	232,33	0,754
1	232,33	0,441

F_i [kN]
0,00
0,00
0,00
0,46
0,34
0,20

α1	0,911
PF1	1,245

START	Tens.	Comp.
ΔN_0 [kN]	400,00	650,00

B [m]	h [m]	L_i [m]
4,40	3,20	5,441

E_s [GPa]	f_{ym} [MPa]	ε_y
210,00	343,75	0,001637

1st Storey

Δ_y [m]	Δ_d [m]	μ
0,01101	0,01850	1,681

SDOF

EVD [%]	$S\Delta_d$ [m]	T_e [s]	K_e [kN/m]
12,28%	0,03371	0,844	35185,20

1st Storey

V_b^{REQ} [kN]	V_b^{BF} [kN]	$V_b^{BR,REQ}$ [kN]
1186,19	635,14	646,32

1st Storey

	BR S_1	V_b^{BR} [kN]	V_b [kN]	Ω
x2	CHSH 88,9 x 4,0	664,42	1204,28	1,015

ASSUMED

STOREY S_i	DRIFTS [m]	V_i^{BF} [kN]	
6	0,00000		
5	0,00000		
4	-0,04197		
3	0,01032	234,16	x2
2	0,01315	406,19	x2
1	0,01850	635,14	x2

Nth Storey

V_i^{REQ} [kN]	$V_i^{BR,REQ}$ [kN]	BR S_i	V_i^{BR} [kN]
0,00	0,00	0	0,00
0,00	0,00	0	0,00
0,00	0,00	0	0,00
548,67	349,64	88,9 x 3,2	564,44
962,45	617,18	88,9 x 3,6	631,30
1186,19	646,32	88,9 x 4,0	664,42

END	Tens.	Comp.
ΔN [kN]	435,12	615,35
	8,78%	-5,33%

SDOF	
Sa [g]	0,19336

Table A5.6 – Design procedure result – Direction YY (S3_AST1_3S_3×5_YY_RETRO)

	ASSUMED	
STOREY S_i	**m_i [ton]**	**δ_i**
6	0,00	0,000
5	0,00	0,000
4	0,00	0,000
3	232,33	1,000
2	232,33	0,754
1	232,33	0,441

F_i [kN]
0,00
0,00
0,00
0,46
0,34
0,20

α1	0,911
PF1	1,245

	START	**Tens.**	**Comp.**
ΔN_0 [kN]		500,00	700,00

B [m]	**h [m]**	**L_i [m]**
4,40	3,20	5,441

E_s [GPa]	**f_{ym} [MPa]**	**ε_y**
210,00	343,75	0,001637

1st Storey			**SDOF**			
Δ_y [m]	**Δ_d [m]**	**μ**	**EVD [%]**	**$S\Delta_d$ [m]**	**T_e [s]**	**K_e [kN/m]**
0,01101	0,01750	1,590	11,67%	0,03189	0,781	41090,63

1st Storey				**1st Storey**			
V_b^{REQ} [kN]	**V_b^{BF} [kN]**	**$V_b^{BR,REQ}$ [kN]**		**BR S_1**	**V_b^{BR} [kN]**	**V_b [kN]**	**Ω**
				CHSH			
1310,40	674,94	736,70	x2	88,9 x 5,0	817,75	1391,45	1,062

	ASSUMED			**Nth Storey**			
STOREY S_i	**DRIFTS [m]**	**V_i^{BF} [kN]**		**V_i^{REQ} [kN]**	**$V_i^{BR,REQ}$ [kN]**	**BR S_i**	**V_i^{BR} [kN]**
6	0,00000			0,00	0,00	0	0,00
5	0,00000			0,00	0,00	0	0,00
4	-0,03970			0,00	0,00	0	0,00
3	0,00976	277,43	x2	633,94	398,13	88,9 x 3,2	564,44
2	0,01244	429,18	x2	1112,02	747,22	88,9 x 5,0	860,31
1	0,01750	674,94	x2	1310,40	736,70	88,9 x 5,0	817,75

END	**Tens.**	**Comp.**
ΔN [kN]	518,57	741,91
	3,71%	5,99%

SDOF	
Sa [g]	0,22341

BUILDING TYPE 2: 3 storeys, 3×5 spans **| SEISMIC HAZARD SCENARIO 4:** PT 1.1 + 2.3 (EC8-1)

Table A5.7 – Design procedure result – Direction XX (S4_AST1_3S_3×5_XX_RETRO)

ASSUMED

STOREY S_i	m_i [ton]	δ_i
6	0,00	0,000
5	0,00	0,000
4	0,00	0,000
3	232,33	1,000
2	232,33	0,754
1	232,33	0,441

F_i [kN]
0,00
0,00
0,00
0,46
0,34
0,20

α1	0,911
PF1	1,245

START	Tens.	Comp.
ΔN_0 [kN]	500,00	750,00

B [m]	h [m]	L_i [m]
4,40	3,20	5,441

E_s [GPa]	f_{ym} [MPa]	ε_y
210,00	343,75	0,001637

1st Storey

Δ_y [m]	Δ_d [m]	μ
0,01101	0,01850	1,681

SDOF

EVD [%]	$S\Delta_d$ [m]	T_e [s]	K_e [kN/m]
12,28%	0,03371	0,570	77142,76

1st Storey

V_b^{REQ} [kN]	V_b^{BF} [kN]	$V_b^{BR,REQ}$ [kN]
2600,69	635,14	2060,82

1st Storey

	BR S_1	V_b^{BR} [kN]	V_b [kN]	Ω
x6	CHSH 88,9 x 5,0	2453,24	2993,11	1,151

ASSUMED

STOREY S_i	DRIFTS [m]	V_i^{BF} [kN]		V_i^{REQ} [kN]	$V_i^{BR,REQ}$ [kN]	BR S_i	V_i^{BR} [kN]
6	0,00000			0,00	0,00	0	0,00
5	0,00000			0,00	0,00	0	0,00
4	-0,04197			0,00	0,00	0	0,00
3	0,01032	234,16	x6	1363,66	1164,63	88,9 x 3,2	1693,33
2	0,01315	406,19	x6	2392,04	2046,78	88,9 x 5,0	2580,92
1	0,01850	635,14	x6	2600,69	2060,82	88,9 x 5,0	2453,24

Nth Storey

END	Tens.	Comp.
ΔN [kN]	518,57	741,91
	3,71%	-1,08%

SDOF

Sa [g]	0,48058

Table A5.8 – Design procedure result – Direction YY (S4_AST1_3S_3×5_YY_RETRO)

	ASSUMED	
STOREY S_i	**m_i [ton]**	**δ_i**
6	0,00	0,000
5	0,00	0,000
4	0,00	0,000
3	232,33	1,000
2	232,33	0,754
1	232,33	0,441

F_i [kN]
0,00
0,00
0,00
0,46
0,34
0,20

α1	0,911
PF1	1,245

	START	**Tens.**	**Comp.**
ΔN_0 [kN]		500,00	750,00

B [m]	**h [m]**	**L_i [m]**
4,40	3,20	5,441

E_s [GPa]	**f_{ym} [MPa]**	**ε_y**
210,00	343,75	0,001637

1st Storey			**SDOF**			
Δ_y [m]	**Δ_d [m]**	**μ**	**EVD [%]**	**$S\Delta_d$ [m]**	**T_e [s]**	**K_e [kN/m]**
0,01101	0,01750	1,590	11,67%	0,03189	0,548	83461,04

1st Storey				**1st Storey**			
V_b^{REQ} [kN]	**V_b^{BF} [kN]**	**$V_b^{BR,REQ}$ [kN]**		**BR S_1**	**V_b^{BR} [kN]**	**V_b [kN]**	**Ω**
				CHSH			
2661,61	674,94	2087,91	x6	88,9 x 5,0	2453,24	3026,94	1,137

	ASSUMED			**N[th] Storey**			
STOREY S_i	**DRIFTS [m]**	**V_i^{BF} [kN]**		**V_i^{REQ} [kN]**	**$V_i^{BR,REQ}$ [kN]**	**BR S_i**	**V_i^{BR} [kN]**
6	0,00000			0,00	0,00	0	0,00
5	0,00000			0,00	0,00	0	0,00
4	-0,03970			0,00	0,00	0	0,00
3	0,00976	277,43	x6	1379,08	1143,26	88,9 x 3,2	1693,33
2	0,01244	429,18	x6	2419,08	2054,28	88,9 x 5,0	2580,92
1	0,01750	674,94	x6	2661,61	2087,91	88,9 x 5,0	2453,24

END	**Tens.**	**Comp.**
ΔN [kN]	518,57	741,91
	3,71%	-1,08%

SDOF	
Sa [g]	0,48601

BUILDING TYPE 3: 4 storeys, 3×5 spans **| SEISMIC HAZARD SCENARIO 3:** PT 1.3 + 2.3 (EC8-1)

Table A5.9 – Design procedure result – Direction XX (S3_AST1_4S_3×5_XX_RETRO)

ASSUMED

STOREY S_i	m_i [ton]	δ_i
6	0,00	0,000
5	0,00	0,000
4	232,33	1,000
3	232,33	0,820
2	232,33	0,600
1	232,33	0,342

F_i [kN]
0,00
0,00
0,36
0,30
0,22
0,12

α1	0,888
PF1	1,285

START	Tens.	Comp.
ΔN_0 [kN]	950,00	1150,00

B [m]	h [m]	L_i [m]
4,40	3,20	5,441

E_s [GPa]	f_{ym} [MPa]	ε_y
210,00	343,75	0,001637

1st Storey

Δ_y [m]	Δ_d [m]	μ
0,01101	0,01600	1,454

SDOF

EVD [%]	$S\Delta_d$ [m]	T_e [s]	K_e [kN/m]
10,61%	0,03636	0,855	44544,01

1st Storey

V_b^{REQ} [kN]	V_b^{BF} [kN]	$V_b^{BR,REQ}$ [kN]
1619,47	747,33	984,24

1st Storey

	BR S_1	V_b^{BR} [kN]	V_b [kN]	Ω
x2	CHSH 114,3 x 5,0	1134,97	1770,20	1,093

ASSUMED

STOREY S_i	DRIFTS [m]	V_i^{BF} [kN]	
6	0,00000		
5	-0,04672		
4	0,00843	204,20	x2
3	0,01024	448,90	x2
2	0,01206	523,95	x2
1	0,01600	747,33	x2

Nth Storey

V_i^{REQ} [kN]	$V_i^{BR,REQ}$ [kN]	BR S_i	V_i^{BR} [kN]
0,00	0,00	0	0,00
0,00	0,00	0	0,00
640,78	467,21	88,9 x 3,2	564,44
1165,99	784,43	88,9 x 5,0	860,31
1550,76	1105,41	114,3 x 5,0	1198,73
1619,47	984,24	114,3 x 5,0	1134,97

END	Tens.	Comp.
ΔN [kN]	976,66	1231,62
	2,81%	7,10%

SDOF

Sa [g]	0,21877

Table A5.10 – Design procedure result – Direction YY (S3_AST1_4S_3×5_YY_RETRO)

	ASSUMED	
STOREY S_i	**m_i [ton]**	**δ_i**
6	0,00	0,000
5	0,00	0,000
4	232,33	1,000
3	232,33	0,820
2	232,33	0,600
1	232,33	0,342

F_i [kN]
0,00
0,00
0,36
0,30
0,22
0,12

α1	0,888
PF1	1,285

	START	Tens.	Comp.
ΔN_0 [kN]		950,00	1200,00

B [m]	**h [m]**	**L_i [m]**
4,40	3,20	5,441

E_s [GPa]	**f_{ym} [MPa]**	**ε_y**
210,00	343,75	0,001637

1st Storey			SDOF			
Δ_y [m]	**Δ_d [m]**	**μ**	**EVD [%]**	**$S\Delta_d$ [m]**	**T_e [s]**	**K_e [kN/m]**
0,01101	0,01600	1,454	10,61%	0,03636	0,855	44544,01

1st Storey				1st Storey			
V_b^{REQ} [kN]	**V_b^{BF} [kN]**	**$V_b^{BR,REQ}$ [kN]**		**BR S_1**	**V_b^{BR} [kN]**	**V_b [kN]**	**Ω**
				CHSH			
1619,47	873,46	877,02	x2	114,3 x 5,0	1134,97	1877,41	1,159

	ASSUMED			Nth Storey			
STOREY S_i	**DRIFTS [m]**	**V_i^{BF} [kN]**		**V_i^{REQ} [kN]**	**$V_i^{BR,REQ}$ [kN]**	**BR S_i**	**V_i^{BR} [kN]**
6	0,00000			0,00	0,00	0	0,00
5	-0,04672			0,00	0,00	0	0,00
4	0,00843	246,16	x2	679,58	470,35	88,9 x 3,2	564,44
3	0,01024	378,95	x2	1236,61	914,50	114,3 x 4,0	971,05
2	0,01206	565,11	x2	1644,68	1164,34	114,3 x 5,0	1198,73
1	0,01600	873,46	x2	1619,47	877,02	114,3 x 5,0	1134,97

END	Tens.	Comp.
ΔN [kN]	1021,47	1276,43
	7,52%	6,37%

SDOF	
Sa [g]	0,23202

BUILDING TYPE 3: 4 storeys, 3×5 spans **| SEISMIC HAZARD SCENARIO 4:** PT 1.1 + 2.3 (EC8-1)

Table A5.11 – Design procedure result – Direction XX (S4_AST1_4S_3×5_XX_RETRO)

ASSUMED

STOREY S_i	m_i [ton]	δ_i
6	0,00	0,000
5	0,00	0,000
4	232,33	1,000
3	232,33	0,820
2	232,33	0,600
1	232,33	0,342

F_i [kN]
0,00
0,00
0,36
0,30
0,22
0,12

α1	0,888
PF1	1,285

START	Tens.	Comp.
ΔN_0 [kN]	950,00	1150,00

B [m]	h [m]	L_i [m]
4,40	3,20	5,441

E_s [GPa]	f_{ym} [MPa]	ε_y
210,00	343,75	0,001637

1st Storey

Δ_y [m]	Δ_d [m]	μ
0,01101	0,01600	1,454

SDOF

EVD [%]	$S\Delta_d$ [m]	T_e [s]	K_e [kN/m]
10,61%	0,03636	0,574	98832,03

1st Storey

V_b^{REQ} [kN]	V_b^{BF} [kN]	$V_b^{BR,REQ}$ [kN]
3593,19	747,33	2957,96

1st Storey

	BR S_1	V_b^{BR} [kN]	V_b [kN]	Ω
x6	CHSH 114,3 x 5,0	3404,90	4040,13	1,124

ASSUMED

STOREY S_i	DRIFTS [m]	V_i^{BF} [kN]
6	0,00000	
5	-0,04672	
4	0,00843	204,20
3	0,01024	448,90
2	0,01206	523,95
1	0,01600	747,33

Nth Storey

	V_i^{REQ} [kN]	$V_i^{BR,REQ}$ [kN]	BR S_i	V_i^{BR} [kN]
	0,00	0,00	0	0,00
	0,00	0,00	0	0,00
x6	1462,44	1288,87	88,9 x 3,2	1693,33
x6	2661,15	2279,59	88,9 x 5,0	2580,92
x6	3539,31	3093,96	114,3 x 5,0	3596,18
x6	3593,19	2957,96	114,3 x 5,0	3404,90

END	Tens.	Comp.
ΔN [kN]	976,66	1231,62
	2,81%	7,10%

SDOF

Sa [g]	0,49930

Table A5.12 – Design procedure result – Direction YY (S4_AST1_4S_3×5_YY_RETRO)

	ASSUMED	
STOREY S_i	**m_i [ton]**	**δ_i**
6	0,00	0,000
5	0,00	0,000
4	232,33	1,000
3	232,33	0,820
2	232,33	0,600
1	232,33	0,342

F_i [kN]
0,00
0,00
0,36
0,30
0,22
0,12

α1	0,888
PF1	1,285

	START	**Tens.**	**Comp.**
ΔN_0 [kN]		950,00	1150,00

B [m]	**h [m]**	**L_i [m]**
4,40	3,20	5,441

E_s [GPa]	**f_{ym} [MPa]**	**ε_y**
210,00	343,75	0,001637

1st Storey			**SDOF**			
Δ_y [m]	**Δ_d [m]**	**μ**	**EVD [%]**	**$S\Delta_d$ [m]**	**T_e [s]**	**K_e [kN/m]**
0,01101	0,01600	1,454	10,61%	0,03636	0,574	98832,03

1st Storey				**1st Storey**			
V_b^{REQ} [kN]	**V_b^{BF} [kN]**	**$V_b^{BR,REQ}$ [kN]**		**BR S_1**	**V_b^{BR} [kN]**	**V_b [kN]**	**Ω**
				CHSH			
3593,19	873,46	2850,75	x6	114,3 x 5,0	3404,90	4147,34	1,154

	ASSUMED			**Nth Storey**			
STOREY S_i	**DRIFTS [m]**	**V_i^{BF} [kN]**		**V_i^{REQ} [kN]**	**$V_i^{BR,REQ}$ [kN]**	**BR S_i**	**V_i^{BR} [kN]**
6	0,00000			0,00	0,00	0	0,00
5	-0,04672			0,00	0,00	0	0,00
4	0,00843	246,16	x6	1501,25	1292,02	88,9 x 3,2	1693,33
3	0,01024	378,95	x6	2731,77	2409,66	88,9 x 5,0	2580,92
2	0,01206	565,11	x6	3633,23	3152,89	114,3 x 5,0	3596,18
1	0,01600	873,46	x6	3593,19	2850,75	114,3 x 5,0	3404,90

END	**Tens.**	**Comp.**
ΔN [kN]	976,66	1231,62
	2,81%	7,10%

SDOF	
Sa [g]	0,51255

BUILDING TYPE 4: 5 storeys, 3×5 spans **| SEISMIC HAZARD SCENARIO 3:** PT 1.3 + 2.3 (EC8-1)

Table A5.13 – Design procedure result – Direction XX (S3_AST1_5S_3×5_XX_RETRO)

ASSUMED

STOREY S_i	m_i [ton]	δ_i
6	0,00	0,000
5	232,33	1,000
4	232,33	0,858
3	232,33	0,690
2	232,33	0,498
1	232,33	0,280

F_i [kN]
0,00
0,30
0,26
0,21
0,15
0,08

α1	0,871
PF1	1,310

START	Tens.	Comp.
ΔN_0 [kN]	950,00	1150,00

B [m]	h [m]	L_i [m]
4,40	3,20	5,441

E_s [GPa]	f_{ym} [MPa]	ε_y
210,00	343,75	0,001637

1st Storey

Δ_y [m]	Δ_d [m]	μ
0,01101	0,01700	1,544

SDOF

EVD [%]	$S\Delta_d$ [m]	T_e [s]	K_e [kN/m]
11,34%	0,04637	1,122	31745,18

1st Storey

V_b^{REQ} [kN]	V_b^{BF} [kN]	$V_b^{BR,REQ}$ [kN]
1471,97	890,55	715,00

1st Storey

	BR S_1	V_b^{BR} [kN]	V_b [kN]	Ω
x2	CHSH 88,9 x 5,0	817,75	1574,71	1,070

ASSUMED

STOREY S_i	DRIFTS [m]	V_i^{BF} [kN]		V_i^{REQ} [kN]	$V_i^{BR,REQ}$ [kN]	BR S_i	V_i^{BR} [kN]
6	-0,06075			0,00	0,00	0	0,00
5	0,00864	205,57	x2	473,51	298,78	88,9 x 3,2	564,44
4	0,01017	340,53	x2	879,67	590,22	88,9 x 3,6	631,30
3	0,01170	502,61	x2	1206,55	779,33	88,9 x 5,0	860,31
2	0,01323	688,71	x2	1442,21	856,81	88,9 x 5,0	860,31
1	0,01700	890,55	x2	1471,97	715,00	88,9 x 5,0	817,75

Nth Storey

END	Tens.	Comp.
ΔN [kN]	1015,85	1239,19
	6,93%	7,76%

SDOF

Sa [g]	0,15857

Table A5.14 – Design procedure result – Direction YY (S3_AST1_5S_3×5_YY_RETRO)

	ASSUMED	
STOREY S_i	**m_i [ton]**	**δ_i**
6	0,00	0,000
5	232,33	1,000
4	232,33	0,858
3	232,33	0,690
2	232,33	0,498
1	232,33	0,280

F_i [kN]
0,00
0,30
0,26
0,21
0,15
0,08

α1	0,871
PF1	1,310

	START	Tens.	Comp.
ΔN_0 [kN]		950,00	1150,00

B [m]	**h [m]**	**L_i [m]**
4,40	3,20	5,441

E_s [GPa]	**f_{ym} [MPa]**	**ε_y**
210,00	343,75	0,001637

1st Storey			SDOF			
Δ_y [m]	**Δ_d [m]**	**μ**	**EVD [%]**	**$S\Delta_d$ [m]**	**T_e [s]**	**K_e [kN/m]**
0,01101	0,01700	1,544	11,34%	0,04637	1,122	31745,18

1st Storey				1st Storey			
V_b^{REQ} [kN]	**V_b^{BF} [kN]**	**$V_b^{BR,REQ}$ [kN]**		**BR S_1**	**V_b^{BR} [kN]**	**V_b [kN]**	**Ω**
				CHSH			
1471,97	1200,42	451,61	x2	88,9 x 3,6	599,93	1620,29	1,101

	ASSUMED			Nth Storey			
STOREY S_i	**DRIFTS [m]**	**V_i^{BF} [kN]**		**V_i^{REQ} [kN]**	**$V_i^{BR,REQ}$ [kN]**	**BR S_i**	**V_i^{BR} [kN]**
6	-0,06075			0,00	0,00	0	0,00
5	0,00864	248,75	x2	487,21	275,78	88,9 x 3,2	564,44
4	0,01017	370,23	x2	905,13	590,43	88,9 x 3,6	631,30
3	0,01170	538,25	x2	1241,47	783,96	88,9 x 5,0	860,31
2	0,01323	784,84	x2	1483,95	816,83	88,9 x 5,0	860,31
1	0,01700	1200,42	x2	1471,97	451,61	88,9 x 3,6	599,93

END	Tens.	Comp.
ΔN [kN]	1005,23	1167,42
	5,81%	1,51%

SDOF	
Sa [g]	0,16316

BUILDING TYPE 4: 5 storeys, 3×5 spans **| SEISMIC HAZARD SCENARIO 4:** PT 1.1 + 2.3 (EC8-1)

Table A5.15 – Design procedure result – Direction XX (S4_AST1_5S_3×5_XX_RETRO)

ASSUMED

STOREY S_i	m_i [ton]	δ_i
6	0,00	0,000
5	232,33	1,000
4	232,33	0,858
3	232,33	0,690
2	232,33	0,498
1	232,33	0,280

F_i [kN]
0,00
0,30
0,26
0,21
0,15
0,08

α1	0,871
PF1	1,310

START	Tens.	Comp.
ΔN_0 [kN]	1200,00	1500,00

B [m]	h [m]	L_i [m]
4,40	3,20	5,441

E_s [GPa]	f_{ym} [MPa]	ε_y
210,00	343,75	0,001637

1st Storey

Δ_y [m]	Δ_d [m]	μ
0,01101	0,01700	1,544

SDOF

EVD [%]	$S\Delta_d$ [m]	T_e [s]	K_e [kN/m]
11,34%	0,04637	0,720	77090,09

1st Storey

V_b^{REQ} [kN]	V_b^{BF} [kN]	$V_b^{BR,REQ}$ [kN]
3574,53	890,55	2817,56

1st Storey

	BR S_1	V_b^{BR} [kN]	V_b [kN]	Ω
x6	CHSH 114,3 x 5,0	3404,90	4161,86	1,164

ASSUMED

STOREY S_i	DRIFTS [m]	V_i^{BF} [kN]		V_i^{REQ} [kN]	$V_i^{BR,REQ}$ [kN]	BR S_i	V_i^{BR} [kN]
6	-0,06075			0,00	0,00	0	0,00
5	0,00864	205,57	x6	1251,46	1076,72	88,9 x 3,2	1693,33
4	0,01017	340,53	x6	2324,91	2035,46	88,9 x 4,0	2097,32
3	0,01170	502,61	x6	3188,83	2761,61	114,3 x 4,0	2913,16
2	0,01323	688,71	x6	3811,66	3226,26	114,3 x 5,0	3596,18
1	0,01700	890,55	x6	3574,53	2817,56	114,3 x 5,0	3404,90

Nth Storey

END	Tens.	Comp.
ΔN [kN]	1254,61	1509,57
	4,55%	0,64%

SDOF

Sa [g]	0,41910

Table A5.16 – Design procedure result – Direction YY (S4_AST1_5S_3×5_YY_RETRO)

ASSUMED		
STOREY S_i	**m_i [ton]**	**δ_i**
6	0,00	0,000
5	232,33	1,000
4	232,33	0,858
3	232,33	0,690
2	232,33	0,498
1	232,33	0,280

F_i [kN]
0,00
0,30
0,26
0,21
0,15
0,08

α1	0,871
PF1	1,310

START	**Tens.**	**Comp.**
ΔN_0 [kN]	1100,00	1400,00

B [m]	**h [m]**	**L_i [m]**
4,40	3,20	5,441

E_s [GPa]	**f_{ym} [MPa]**	**ε_y**
210,00	343,75	0,001637

1st Storey		
Δ_y [m]	**Δ_d [m]**	**μ**
0,01101	0,01700	1,544

SDOF			
EVD [%]	**SΔ_d [m]**	**T_e [s]**	**K_e [kN/m]**
11,34%	0,04637	0,720	77090,09

1st Storey		
V_b^{REQ} [kN]	**V_b^{BF} [kN]**	**$V_b^{BR,REQ}$ [kN]**
3574,53	1200,42	2554,17

1st Storey				
	BR S_1	**V_b^{BR} [kN]**	**V_b [kN]**	**Ω**
x6	CHSH 114,3 x 4,0	2757,87	3778,22	1,057

ASSUMED				**N[th] Storey**			
STOREY S_i	**DRIFTS [m]**	**V_i^{BF} [kN]**		**V_i^{REQ} [kN]**	**$V_i^{BR,REQ}$ [kN]**	**BR S_i**	**V_i^{BR} [kN]**
6	-0,06075			0,00	0,00	0	0,00
5	0,00864	248,75	x6	1136,10	924,66	88,9 x 3,2	1693,33
4	0,01017	370,23	x6	2110,60	1795,91	88,9 x 3,6	1893,91
3	0,01170	538,25	x6	2894,89	2437,37	114,3 x 3,6	2624,46
2	0,01323	784,84	x6	3460,30	2793,19	114,3 x 4,0	2913,16
1	0,01700	1200,42	x6	3574,53	2554,17	114,3 x 4,0	2757,87

END	**Tens.**	**Comp.**
ΔN [kN]	1105,32	1310,28
	0,48%	-6,41%

SDOF	
Sa [g]	0,38047

BUILDING TYPE 5: 6 storeys, 3×5 spans **| SEISMIC HAZARD SCENARIO 3:** PT 1.3 + 2.3 (EC8-1)

Table A5.17 – Design procedure result – Direction XX (S3_AST1_6S_3×5_XX_RETRO)

ASSUMED

STOREY S_i	m_i [ton]	δ_i	F_i [kN]
6	232,33	1,000	0,26
5	232,33	0,883	0,23
4	232,33	0,748	0,19
3	232,33	0,595	0,15
2	232,33	0,425	0,11
1	232,33	0,237	0,06

α1	0,860
PF1	1,327

START	Tens.	Comp.
ΔN_0 [kN]	1150,00	1450,00

B [m]	h [m]	L_i [m]	E_s [GPa]	f_{ym} [MPa]	ε_y
4,40	3,20	5,441	210,00	343,75	0,001637

1st Storey

Δ_y [m]	Δ_d [m]	μ
0,01101	0,01700	1,544

SDOF

EVD [%]	$S\Delta_d$ [m]	T_e [s]	K_e [kN/m]
11,34%	0,05415	1,309	27609,70

1st Storey

V_b^{REQ} [kN]	V_b^{BF} [kN]	$V_b^{BR,REQ}$ [kN]
1495,17	1101,91	558,54

1st Storey

	BR S_1	V_b^{BR} [kN]	V_b [kN]	Ω
x2	CHSH 88,9 x 3,6	599,93	1536,55	1,028

ASSUMED

STOREY S_i	DRIFTS [m]	V_i^{BF} [kN]		Nth Storey V_i^{REQ} [kN]	$V_i^{BR,REQ}$ [kN]	BR S_i	V_i^{BR} [kN]
6	0,00844	199,99	x2	395,38	225,39	88,9 x 3,2	564,44
5	0,00971	324,17	x2	744,36	468,82	88,9 x 3,2	564,44
4	0,01097	480,12	x2	1039,95	631,85	88,9 x 4,0	699,11
3	0,01224	640,12	x2	1275,17	731,07	88,9 x 5,0	860,31
2	0,01351	771,59	x2	1443,04	787,18	88,9 x 5,0	860,31
1	0,01700	1101,91	x2	1495,17	558,54	88,9 x 3,6	599,93

END	Tens.	Comp.
ΔN [kN]	1216,13	1378,32
	5,75%	-4,94%

SDOF

Sa [g]	0,13071

Table A5.18 – Design procedure result – Direction YY (S3_AST1_6S_3×5_YY_RETRO)

	ASSUMED	
STOREY S_i	**m_i [ton]**	**δ_i**
6	232,33	1,000
5	232,33	0,883
4	232,33	0,748
3	232,33	0,595
2	232,33	0,425
1	232,33	0,237

F_i [kN]
0,26
0,23
0,19
0,15
0,11
0,06

α1	0,860
PF1	1,327

	START	**Tens.**	**Comp.**
ΔN_0 [kN]		1200,00	1450,00

B [m]	**h [m]**	**L_i [m]**
4,40	3,20	5,441

E_s [GPa]	**f_{ym} [MPa]**	**ε_y**
210,00	343,75	0,001637

1st Storey			**SDOF**			
Δ_y [m]	**Δ_d [m]**	**μ**	**EVD [%]**	**$S\Delta_d$ [m]**	**T_e [s]**	**K_e [kN/m]**
0,01101	0,01600	1,454	10,61%	0,05097	1,199	32908,08

1st Storey				**1st Storey**			
V_b^{REQ} [kN]	**V_b^{BF} [kN]**	**$V_b^{BR,REQ}$ [kN]**		**BR S_1**	**V_b^{BR} [kN]**	**V_b [kN]**	**Ω**
				CHSH			
1677,26	1390,63	495,23	x2	88,9 x 3,2	536,36	1718,39	1,025

	ASSUMED			**Nth Storey**			
STOREY S_i	**DRIFTS [m]**	**V_i^{BF} [kN]**		**V_i^{REQ} [kN]**	**$V_i^{BR,REQ}$ [kN]**	**BR S_i**	**V_i^{BR} [kN]**
6	0,00794	231,64	x2	442,17	245,28	88,9 x 3,2	564,44
5	0,00913	341,45	x2	832,45	542,22	88,9 x 3,2	564,44
4	0,01033	482,96	x2	1163,03	752,51	88,9 x 5,0	860,31
3	0,01152	678,43	x2	1426,08	849,42	88,9 x 5,0	860,31
2	0,01272	944,22	x2	1613,81	811,22	88,9 x 5,0	860,31
1	0,01600	1390,63	x2	1677,26	495,23	88,9 x 3,2	536,36

END	**Tens.**	**Comp.**
ΔN [kN]	1266,36	1410,99
	5,53%	-2,69%

SDOF	
Sa [g]	0,14617

BUILDING TYPE 5: 6 storeys, 3×5 spans **| SEISMIC HAZARD SCENARIO 4:** PT 1.1 + 2.3 (EC8-1)

Table A5.19 – Design procedure result – Direction XX (S4_AST1_6S_3×5_XX_RETRO)

ASSUMED

STOREY S_i	m_i [ton]	δ_i
6	232,33	1,000
5	232,33	0,883
4	232,33	0,748
3	232,33	0,595
2	232,33	0,425
1	232,33	0,237

F_i [kN]
0,26
0,23
0,19
0,15
0,11
0,06

α1	0,860
PF1	1,327

START	Tens.	Comp.
ΔN_0 [kN]	1300,00	1500,00

B [m]	h [m]	L_i [m]
4,40	3,20	5,441

E_s [GPa]	f_{ym} [MPa]	ε_y
210,00	343,75	0,001637

1st Storey

Δ_y [m]	Δ_d [m]	μ
0,01101	0,01700	1,544

SDOF

EVD [%]	$S\Delta_d$ [m]	T_e [s]	K_e [kN/m]
11,34%	0,05415	0,841	66888,12

1st Storey

V_b^{REQ} [kN]	V_b^{BF} [kN]	$V_b^{BR,REQ}$ [kN]
3622,23	1101,91	2685,61

1st Storey

	BR S_1	V_b^{BR} [kN]	V_b [kN]	Ω
x6	CHSH 114,3 x 4,0	2757,87	3694,49	1,020

ASSUMED

STOREY S_i	DRIFTS [m]	V_i^{BF} [kN]		N^{th} Storey V_i^{REQ} [kN]	$V_i^{BR,REQ}$ [kN]	BR S_i	V_i^{BR} [kN]
6	0,00844	199,99	x6	950,66	780,67	88,9 x 3,2	1693,33
5	0,00971	324,17	x6	1789,75	1514,20	88,9 x 3,6	1893,91
4	0,01097	480,12	x6	2500,47	2092,37	114,3 x 3,2	2351,45
3	0,01224	640,12	x6	3066,03	2521,93	114,3 x 3,6	2624,46
2	0,01351	771,59	x6	3469,64	2813,79	114,3 x 4,0	2913,16
1	0,01700	1101,91	x6	3622,23	2685,61	114,3 x 4,0	2757,87

END	Tens.	Comp.
ΔN [kN]	1373,01	1577,98
	5,62%	5,20%

SDOF

Sa [g]	0,31427

Table A5.20 – Design procedure result – Direction YY (S4_AST1_6S_3×5_YY_RETRO)

ASSUMED

STOREY S_i	m_i [ton]	δ_i
6	232,33	1,000
5	232,33	0,883
4	232,33	0,748
3	232,33	0,595
2	232,33	0,425
1	232,33	0,237

F_i [kN]
0,26
0,23
0,19
0,15
0,11
0,06

α1	0,860
PF1	1,327

START	Tens.	Comp.
ΔN_0 [kN]	1550,00	1900,00

B [m]	h [m]	L_i [m]
4,40	3,20	5,441

E_s [GPa]	f_{ym} [MPa]	ε_y
210,00	343,75	0,001637

1st Storey

Δ_y [m]	Δ_d [m]	μ
0,01101	0,01600	1,454

SDOF

EVD [%]	$S\Delta_d$ [m]	T_e [s]	K_e [kN/m]
10,61%	0,05097	0,770	79792,03

1st Storey

V_b^{REQ} [kN]	V_b^{BF} [kN]	$V_b^{BR,REQ}$ [kN]
4066,85	1390,59	2884,85

1st Storey

	BR S_1	V_b^{BR} [kN]	V_b [kN]	Ω
x6	CHSH 114,3 x 5,0	3404,90	4586,90	1,128

ASSUMED

STOREY S_i	DRIFTS [m]	V_i^{BF} [kN]
6	0,00794	231,64
5	0,00913	341,45
4	0,01033	482,96
3	0,01152	678,43
2	0,01272	944,22
1	0,01600	1390,59

N^th Storey

	V_i^{REQ} [kN]	$V_i^{BR,REQ}$ [kN]	BR S_i	V_i^{BR} [kN]
x6	1180,29	983,40	88,9 x 3,2	1693,33
x6	2222,06	1931,83	88,9 x 4,0	2097,32
x6	3104,46	2693,94	88,9 x 6,0	3045,36
x6	3806,63	3229,97	114,3 x 5,0	3596,18
x6	4307,73	3505,14	114,3 x 5,0	3596,18
x6	4066,85	2884,85	114,3 x 5,0	3404,90

END	Tens.	Comp.
ΔN [kN]	1670,03	1924,99
	7,74%	1,32%

SDOF	
Sa [g]	0,39018

BUILDING TYPE 6: 2 storeys, 2×4 spans **| SEISMIC HAZARD SCENARIO 3:** PT 1.3 + 2.3 (EC8-1)

Table A5.21 – Design procedure result – Direction XX (S3_AST1_2S_2×4_XX_RETRO)

	ASSUMED			
STOREY S_i	**m_i [ton]**	**δ_i**		**F_i [kN]**
6	0,00	0,000		0,00
5	0,00	0,000		0,00
4	0,00	0,000		0,00
3	0,00	0,000		0,00
2	126,22	1,000		0,62
1	126,22	0,616		0,38

			START	Tens.	Comp.
α1	0,947		**ΔN_0 [kN]**	200,00	350,00
PF1	1,171				

B [m]	**h [m]**	**L_i [m]**		**E_s [GPa]**	**f_{ym} [MPa]**	**ε_y**
4,40	3,20	5,441		210,00	343,75	0,001637

1st Storey				SDOF			
Δ_y [m]	**Δ_d [m]**	**μ**		**EVD [%]**	**SΔ_d [m]**	**T_e [s]**	**K_e [kN/m]**
0,01101	0,02000	1,817		13,09%	0,02770	0,713	18557,87

1st Storey				1st Storey			
V_b^{REQ} [kN]	**V_b^{BF} [kN]**	**$V_b^{BR,REQ}$ [kN]**		**BR S_1**	**V_b^{BR} [kN]**	**V_b [kN]**	**Ω**
				CHSH			
514,13	246,19	304,87	x2	88,9 x 3,2	536,36	745,62	1,450

	ASSUMED			Nth Storey			
STOREY S_i	**DRIFTS [m]**	**V_i^{BF} [kN]**		**V_i^{REQ} [kN]**	**$V_i^{BR,REQ}$ [kN]**	**BR S_i**	**V_i^{BR} [kN]**
6	0,00000			0,00	0,00	0	0,00
5	0,00000			0,00	0,00	0	0,00
4	0,00000			0,00	0,00	0	0,00
3	-0,03245			0,00	0,00	0	0,00
2	0,01245	157,78	x2	461,31	327,20	88,9 x 3,2	564,44
1	0,02000	246,19	x2	514,13	304,87	88,9 x 3,2	536,36

END	Tens.	Comp.		SDOF	
ΔN [kN]	218,04	362,67		**Sa [g]**	0,31805
	9,02%	3,62%			

Table A5.22 – Design procedure result – Direction YY (S3_AST1_2S_2×4_YY_RETRO)

	ASSUMED	
STOREY S_i	**m_i [ton]**	**δ_i**
6	0,00	0,000
5	0,00	0,000
4	0,00	0,000
3	0,00	0,000
2	126,22	1,000
1	126,22	0,616

F_i [kN]
0,00
0,00
0,00
0,00
0,62
0,38

α1	0,947
PF1	1,171

	START	**Tens.**	**Comp.**
ΔN_0 [kN]	200,00	350,00

B [m]	**h [m]**	**L_i [m]**
4,40	3,20	5,441

E_s [GPa]	**f_{ym} [MPa]**	**ε_y**
210,00	343,75	0,001637

1st Storey			**SDOF**			
Δ_y [m]	**Δ_d [m]**	**μ**	**EVD [%]**	**SΔ_d [m]**	**T_e [s]**	**K_e [kN/m]**
0,01101	0,02000	1,817	13,09%	0,02770	0,713	18557,87

1st Storey				**1st Storey**			
V_b^{REQ} [kN]	**V_b^{BF} [kN]**	**$V_b^{BR,REQ}$ [kN]**		**BR S_1**	**V_b^{BR} [kN]**	**V_b [kN]**	**Ω**
				CHSH			
514,13	290,99	266,79	x2	88,9 x 3,2	536,36	783,70	1,524

	ASSUMED			**Nth Storey**			
STOREY S_i	**DRIFTS [m]**	**V_i^{BF} [kN]**		**V_i^{REQ} [kN]**	**$V_i^{BR,REQ}$ [kN]**	**BR S_i**	**V_i^{BR} [kN]**
6	0,00000			0,00	0,00	0	0,00
5	0,00000			0,00	0,00	0	0,00
4	0,00000			0,00	0,00	0	0,00
3	-0,03245			0,00	0,00	0	0,00
2	0,01245	189,76	x2	484,87	323,58	88,9 x 3,2	564,44
1	0,02000	290,99	x2	514,13	266,79	88,9 x 3,2	536,36

END	**Tens.**	**Comp.**
ΔN [kN]	218,04	362,67
	9,02%	3,62%

SDOF	
Sa [g]	0,33430

BUILDING TYPE 6: 2 storeys, 2×4 spans **| SEISMIC HAZARD SCENARIO 4:** PT 1.1 + 2.3 (EC8-1)

Table A5.23 – Design procedure result – Direction XX (S4_AST1_2S_2×4_XX_RETRO)

ASSUMED

STOREY S_i	m_i [ton]	δ_i
6	0,00	0,000
5	0,00	0,000
4	0,00	0,000
3	0,00	0,000
2	126,22	1,000
1	126,22	0,616

F_i [kN]
0,00
0,00
0,00
0,00
0,62
0,38

α1	0,947
PF1	1,171

START	Tens.	Comp.
ΔN_0 [kN]	250,00	450,00

B [m]	h [m]	L_i [m]
4,40	3,20	5,441

E_s [GPa]	f_{ym} [MPa]	ε_y
210,00	343,75	0,001637

1st Storey

Δ_y [m]	Δ_d [m]	μ
0,01101	0,02000	1,817

SDOF

EVD [%]	$S\Delta_d$ [m]	T_e [s]	K_e [kN/m]
13,09%	0,02770	0,524	34359,32

1st Storey

V_b^{REQ} [kN]	V_b^{BF} [kN]	$V_b^{BR,REQ}$ [kN]
951,89	246,19	742,63

1st Storey

	BR S_1	V_b^{BR} [kN]	V_b [kN]	Ω
x2	CHSH 88,9 x 5,0	817,75	1027,01	1,079

ASSUMED

STOREY S_i	DRIFTS [m]	V_i^{BF} [kN]
6	0,00000	
5	0,00000	
4	0,00000	
3	-0,03245	
2	0,01245	157,78
1	0,02000	246,19

Nth Storey

	V_i^{REQ} [kN]	$V_i^{BR,REQ}$ [kN]	BR S_i	V_i^{BR} [kN]
	0,00	0,00	0	0,00
	0,00	0,00	0	0,00
	0,00	0,00	0	0,00
	0,00	0,00	0	0,00
x2	635,41	501,30	88,9 x 3,2	564,44
x2	951,89	742,63	88,9 x 5,0	817,75

END	Tens.	Comp.
ΔN [kN]	231,93	455,27
	-7,23%	1,17%

SDOF

Sa [g]	0,43808

Table A5.24 – Design procedure result – Direction YY (S4_AST1_2S_2×4_YY_RETRO)

	ASSUMED	
STOREY S_i	**m_i [ton]**	**δ_i**
6	0,00	0,000
5	0,00	0,000
4	0,00	0,000
3	0,00	0,000
2	126,22	1,000
1	126,22	0,616

F_i [kN]
0,00
0,00
0,00
0,00
0,62
0,38

α1	0,947
PF1	1,171

	START	**Tens.**	**Comp.**
ΔN_0 [kN]	200,00	450,00

B [m]	**h [m]**	**L_i [m]**
4,40	3,20	5,441

E_s [GPa]	**f_{ym} [MPa]**	**ε_y**
210,00	343,75	0,001637

1st Storey		
Δ_y [m]	**Δ_d [m]**	**μ**
0,01101	0,02000	1,817

SDOF			
EVD [%]	**SΔ_d [m]**	**T_e [s]**	**K_e [kN/m]**
13,09%	0,02770	0,524	34359,32

1st Storey			
V_b^{REQ} [kN]	**V_b^{BF} [kN]**	**$V_b^{BR,REQ}$ [kN]**	
951,89	290,99	704,55	x2

1st Storey			
BR S_1	**V_b^{BR} [kN]**	**V_b [kN]**	**Ω**
CHSH 88,9 x 5,0	817,75	1065,09	1,119

	ASSUMED			**Nth Storey**			
STOREY S_i	**DRIFTS [m]**	**V_i^{BF} [kN]**		**V_i^{REQ} [kN]**	**$V_i^{BR,REQ}$ [kN]**	**BR S_i**	**V_i^{BR} [kN]**
6	0,00000			0,00	0,00	0	0,00
5	0,00000			0,00	0,00	0	0,00
4	0,00000			0,00	0,00	0	0,00
3	-0,03245			0,00	0,00	0	0,00
2	0,01245	189,76	x2	658,97	497,67	88,9 x 3,2	564,44
1	0,02000	290,99	x2	951,89	704,55	88,9 x 5,0	817,75

END	**Tens.**	**Comp.**
ΔN [kN]	231,93	455,27
	15,96%	1,17%

SDOF	
Sa [g]	0,45433

BUILDING TYPE 7: 3 storeys, 2×4 spans **| SEISMIC HAZARD SCENARIO 3:** PT 1.3 + 2.3 (EC8-1)

Table A5.25 – Design procedure result – Direction XX (S3_AST1_3S_2×4_XX_RETRO)

ASSUMED

STOREY S_i	m_i [ton]	δ_i
6	0,00	0,000
5	0,00	0,000
4	0,00	0,000
3	126,22	1,000
2	126,22	0,754
1	126,22	0,441

F_i [kN]
0,00
0,00
0,00
0,46
0,34
0,20

α1	0,911
PF1	1,245

START	Tens.	Comp.
ΔN_0 [kN]	400,00	600,00

B [m]	h [m]	L_i [m]
4,40	3,20	5,441

E_s [GPa]	f_{ym} [MPa]	ε_y
210,00	343,75	0,001637

1st Storey

Δ_y [m]	Δ_d [m]	μ
0,01101	0,01700	1,544

SDOF

EVD [%]	$S\Delta_d$ [m]	T_e [s]	K_e [kN/m]
11,34%	0,03098	0,749	24271,92

1st Storey

V_b^{REQ} [kN]	V_b^{BF} [kN]	$V_b^{BR,REQ}$ [kN]
751,93	307,70	490,38

1st Storey

	BR S_1	V_b^{BR} [kN]	V_b [kN]	Ω
x2	CHSH 88,9 x 3,6	599,93	861,47	1,146

ASSUMED

STOREY S_i	DRIFTS [m]	V_i^{BF} [kN]	
6	0,00000		
5	0,00000		
4	-0,03857		
3	0,00948	129,49	x2
2	0,01209	209,54	x2
1	0,01700	307,70	x2

Nth Storey

V_i^{REQ} [kN]	$V_i^{BR,REQ}$ [kN]	BR S_i	V_i^{BR} [kN]
0,00	0,00	0	0,00
0,00	0,00	0	0,00
0,00	0,00	0	0,00
392,49	282,42	88,9 x 3,2	564,44
688,48	510,37	88,9 x 3,6	631,30
751,93	490,38	88,9 x 3,6	599,93

END	Tens.	Comp.
ΔN [kN]	431,94	594,13
	7,99%	-0,98%

SDOF

Sa [g]	0,25460

Table A5.26 – Design procedure result – Direction YY (S3_AST1_3S_2×4_YY_RETRO)

	ASSUMED	
STOREY S_i	**m_i [ton]**	**δ_i**
6	0,00	0,000
5	0,00	0,000
4	0,00	0,000
3	126,22	1,000
2	126,22	0,754
1	126,22	0,441

F_i [kN]
0,00
0,00
0,00
0,46
0,34
0,20

α1	0,911
PF1	1,245

	START	**Tens.**	**Comp.**
ΔN_0 [kN]		400,00	550,00

B [m]	**h [m]**	**L_i [m]**
4,40	3,20	5,441

E_s [GPa]	**f_{ym} [MPa]**	**ε_y**
210,00	343,75	0,001637

1st Storey			**SDOF**			
Δ_y [m]	**Δ_d [m]**	**μ**	**EVD [%]**	**$S\Delta_d$ [m]**	**T_e [s]**	**K_e [kN/m]**
0,01101	0,01700	1,544	11,34%	0,03098	0,749	24271,92

1st Storey				**1st Storey**			
V_b^{REQ} [kN]	**V_b^{BF} [kN]**	**$V_b^{BR,REQ}$ [kN]**		**BR S_1**	**V_b^{BR} [kN]**	**V_b [kN]**	**Ω**
				CHSH			
751,93	346,92	457,04	x2	88,9 x 3,2	536,36	831,24	1,105

	ASSUMED			**Nth Storey**			
STOREY S_i	**DRIFTS [m]**	**V_i^{BF} [kN]**		**V_i^{REQ} [kN]**	**$V_i^{BR,REQ}$ [kN]**	**BR S_i**	**V_i^{BR} [kN]**
6	0,00000			0,00	0,00	0	0,00
5	0,00000			0,00	0,00	0	0,00
4	-0,03857			0,00	0,00	0	0,00
3	0,00948	152,65	x2	378,71	248,96	88,9 x 3,2	564,44
2	0,01209	237,85	x2	664,31	462,14	88,9 x 3,2	564,44
1	0,01700	346,92	x2	751,93	457,04	88,9 x 3,2	536,36

END	**Tens.**	**Comp.**
ΔN [kN]	406,43	551,06
	1,61%	0,19%

SDOF	
Sa [g]	0,24567

BUILDING TYPE 7: 3 storeys, 2×4 spans **| SEISMIC HAZARD SCENARIO 4:** PT 1.1 + 2.3 (EC8-1)

Table A5.27 – Design procedure result – Direction XX (S4_AST1_3S_2×4_XX_RETRO)

ASSUMED

STOREY S_i	m_i [ton]	δ_i
6	0,00	0,000
5	0,00	0,000
4	0,00	0,000
3	126,22	1,000
2	126,22	0,754
1	126,22	0,441

F_i [kN]
0,00
0,00
0,00
0,46
0,34
0,20

α1	0,911
PF1	1,245

START	Tens.	Comp.
ΔN_0 [kN]	400,00	600,00

B [m]	h [m]	L_i [m]
4,40	3,20	5,441

E_s [GPa]	f_{ym} [MPa]	ε_y
210,00	343,75	0,001637

1st Storey

Δ_y [m]	Δ_d [m]	μ
0,01101	0,01700	1,544

SDOF

EVD [%]	$S\Delta_d$ [m]	T_e [s]	K_e [kN/m]
11,34%	0,03098	0,537	47219,26

1st Storey

V_b^{REQ} [kN]	V_b^{BF} [kN]	$V_b^{BR,REQ}$ [kN]
1462,82	307,70	1201,27

1st Storey

	BR S_1	V_b^{BR} [kN]	V_b [kN]	Ω
x4	CHSH 88,9 x 4,0	1328,83	1590,38	1,087

ASSUMED

STOREY S_i	DRIFTS [m]	V_i^{BF} [kN]
6	0,00000	
5	0,00000	
4	-0,03857	
3	0,00948	129,49 x4
2	0,01209	209,54 x4
1	0,01700	307,70 x4

Nth Storey

V_i^{REQ} [kN]	$V_i^{BR,REQ}$ [kN]	BR S_i	V_i^{BR} [kN]
0,00	0,00	0	0,00
0,00	0,00	0	0,00
0,00	0,00	0	0,00
724,58	614,51	88,9 x 3,2	1128,88
1271,00	1092,89	88,9 x 3,6	1262,61
1462,82	1201,27	88,9 x 4,0	1328,83

END	Tens.	Comp.
ΔN [kN]	435,12	615,35
	8,78%	2,56%

SDOF

Sa [g]	0,47003

Table A5.28 – Design procedure result – Direction YY (S4_AST1_3S_2×4_YY_RETRO)

	ASSUMED	
STOREY S_i	**m_i [ton]**	**δ_i**
6	0,00	0,000
5	0,00	0,000
4	0,00	0,000
3	126,22	1,000
2	126,22	0,754
1	126,22	0,441

F_i [kN]
0,00
0,00
0,00
0,46
0,34
0,20

α1	0,911
PF1	1,245

	START	Tens.	Comp.
ΔN_0 [kN]		400,00	600,00

B [m]	**h [m]**	**L_i [m]**
4,40	3,20	5,441

E_s [GPa]	**f_{ym} [MPa]**	**ε_y**
210,00	343,75	0,001637

1st Storey		
Δ_y [m]	**Δ_d [m]**	**μ**
0,01101	0,01700	1,544

SDOF			
EVD [%]	**$S\Delta_d$ [m]**	**T_e [s]**	**K_e [kN/m]**
11,34%	0,03098	0,537	47219,26

1st Storey				1st Storey			
V_b^{REQ} [kN]	**V_b^{BF} [kN]**	**$V_b^{BR,REQ}$ [kN]**		**BR S_1**	**V_b^{BR} [kN]**	**V_b [kN]**	**Ω**
				CHSH			
1462,82	346,92	1167,94	x4	88,9 x 4,0	1328,83	1623,71	1,110

	ASSUMED			Nth Storey			
STOREY S_i	**DRIFTS [m]**	**V_i^{BF} [kN]**		**V_i^{REQ} [kN]**	**$V_i^{BR,REQ}$ [kN]**	**BR S_i**	**V_i^{BR} [kN]**
6	0,00000			0,00	0,00	0	0,00
5	0,00000			0,00	0,00	0	0,00
4	-0,03857			0,00	0,00	0	0,00
3	0,00948	152,65	x4	739,77	610,01	88,9 x 3,2	1128,88
2	0,01209	237,85	x4	1297,65	1095,47	88,9 x 3,6	1262,61
1	0,01700	346,92	x4	1462,82	1167,94	88,9 x 4,0	1328,83

END	Tens.	Comp.
ΔN [kN]	435,12	615,35
	8,78%	2,56%

SDOF	
Sa [g]	0,47988

BUILDING TYPE 8: 4 storeys, 2×4 spans **| SEISMIC HAZARD SCENARIO 3:** PT 1.3 + 2.3 (EC8-1)

Table A5.29 – Design procedure result – Direction XX (S3_AST1_4S_2×4_XX_RETRO)

ASSUMED

STOREY S_i	m_i [ton]	δ_i
6	0,00	0,000
5	0,00	0,000
4	126,22	1,000
3	126,22	0,820
2	126,22	0,600
1	126,22	0,342

F_i [kN]
0,00
0,00
0,36
0,30
0,22
0,12

α1	0,888
PF1	1,285

START	Tens.	Comp.
ΔN_0 [kN]	600,00	750,00

B [m]	h [m]	L_i [m]
4,40	3,20	5,441

E_s [GPa]	f_{ym} [MPa]	ε_y
210,00	343,75	0,001637

1st Storey

Δ_y [m]	Δ_d [m]	μ
0,01101	0,01600	1,454

SDOF

EVD [%]	$S\Delta_d$ [m]	T_e [s]	K_e [kN/m]
10,61%	0,03636	0,855	24199,82

1st Storey

V_b^{REQ} [kN]	V_b^{BF} [kN]	$V_b^{BR,REQ}$ [kN]
879,82	399,39	540,34

1st Storey

BR S_1	V_b^{BR} [kN]	V_b [kN]	Ω
CHSH			
88,9 x 3,6	599,93	939,41	1,068

x2

ASSUMED

STOREY S_i	DRIFTS [m]	V_i^{BF} [kN]
6	0,00000	
5	-0,04672	
4	0,00843	117,24
3	0,01024	185,10
2	0,01206	269,47
1	0,01600	399,39

Nth Storey

V_i^{REQ} [kN]	$V_i^{BR,REQ}$ [kN]	BR S_i	V_i^{BR} [kN]
0,00	0,00	0	0,00
0,00	0,00	0	0,00
340,05	240,39	88,9 x 3,2	564,44
618,77	461,44	88,9 x 3,2	564,44
822,96	593,91	88,9 x 3,6	631,30
879,82	540,34	88,9 x 3,6	599,93

x2 x2 x2 x2

END	Tens.	Comp.
ΔN [kN]	620,33	782,51
	3,39%	4,33%

SDOF

Sa [g]	0,21370

Table A5.30 – Design procedure result – Direction YY (S3_AST1_4S_2×4_YY_RETRO)

	ASSUMED	
STOREY S_i	**m_i [ton]**	**δ_i**
6	0,00	0,000
5	0,00	0,000
4	126,22	1,000
3	126,22	0,820
2	126,22	0,600
1	126,22	0,342

F_i [kN]
0,00
0,00
0,36
0,30
0,22
0,12

α1	0,888
PF1	1,285

	START	Tens.	Comp.
ΔN_0 [kN]		650,00	850,00

B [m]	**h [m]**	**L_i [m]**
4,40	3,20	5,441

E_s [GPa]	**f_{ym} [MPa]**	**ε_y**
210,00	343,75	0,001637

1st Storey			SDOF			
Δ_y [m]	**Δ_d [m]**	**μ**	**EVD [%]**	**$S\Delta_d$ [m]**	**T_e [s]**	**K_e [kN/m]**
0,01101	0,01500	1,363	9,79%	0,03408	0,775	29453,78

1st Storey				1st Storey			
V_b^{REQ} [kN]	**V_b^{BF} [kN]**	**$V_b^{BR,REQ}$ [kN]**		**BR S_1**	**V_b^{BR} [kN]**	**V_b [kN]**	**Ω**
				CHSH			
1003,91	430,63	637,87	x2	88,9 x 4,0	664,42	1030,45	1,026

	ASSUMED			Nth Storey			
STOREY S_i	**DRIFTS [m]**	**V_i^{BF} [kN]**		**V_i^{REQ} [kN]**	**$V_i^{BR,REQ}$ [kN]**	**BR S_i**	**V_i^{BR} [kN]**
6	0,00000			0,00	0,00	0	0,00
5	-0,04380			0,00	0,00	0	0,00
4	0,00790	133,11	x2	373,00	259,86	88,9 x 3,2	564,44
3	0,00960	200,33	x2	678,74	508,46	88,9 x 3,2	564,44
2	0,01130	283,92	x2	902,72	661,38	88,9 x 4,0	699,11
1	0,01500	430,63	x2	1003,91	637,87	88,9 x 4,0	664,42

END	Tens.	Comp.
ΔN [kN]	646,02	826,26
	-0,61%	-2,79%

SDOF	
Sa [g]	0,23441

BUILDING TYPE 8: 4 storeys, 2×4 spans **| SEISMIC HAZARD SCENARIO 4:** PT 1.1 + 2.3 (EC8-1)

Table A5.31 – Design procedure result – Direction XX (S4_AST1_4S_2×4_XX_RETRO)

ASSUMED

STOREY S_i	m_i [ton]	δ_i
6	0,00	0,000
5	0,00	0,000
4	126,22	1,000
3	126,22	0,820
2	126,22	0,600
1	126,22	0,342

F_i [kN]
0,00
0,00
0,36
0,30
0,22
0,12

α1	0,888
PF1	1,285

START	Tens.	Comp.
ΔN_0 [kN]	700,00	950,00

B [m]	h [m]	L_i [m]
4,40	3,20	5,441

E_s [GPa]	f_{ym} [MPa]	ε_y
210,00	343,75	0,001637

1st Storey

Δ_y [m]	Δ_d [m]	μ
0,01101	0,01600	1,454

SDOF

EVD [%]	$S\Delta_d$ [m]	T_e [s]	K_e [kN/m]
10,61%	0,03636	0,574	53693,36

1st Storey

V_b^{REQ} [kN]	V_b^{BF} [kN]	$V_b^{BR,REQ}$ [kN]
1952,10	399,39	1612,62

1st Storey

	BR S_1	V_b^{BR} [kN]	V_b [kN]	Ω
x4	CHSH 88,9 x 5,0	1635,49	1974,97	1,012

ASSUMED

STOREY S_i	DRIFTS [m]	V_i^{BF} [kN]	
6	0,00000		
5	-0,04672		
4	0,00843	117,24	x4
3	0,01024	185,10	x4
2	0,01206	269,47	x4
1	0,01600	399,39	x4

Nth Storey

V_i^{REQ} [kN]	$V_i^{BR,REQ}$ [kN]	BR S_i	V_i^{BR} [kN]
0,00	0,00	0	0,00
0,00	0,00	0	0,00
714,90	615,25	88,9 x 3,2	1128,88
1300,88	1143,54	88,9 x 3,6	1262,61
1730,16	1501,11	88,9 x 5,0	1720,61
1952,10	1612,62	88,9 x 5,0	1635,49

END	Tens.	Comp.
ΔN [kN]	729,20	952,55
	4,17%	0,27%

SDOF

Sa [g]	0,44927

Table A5.32 – Design procedure result – Direction YY (S4_AST1_4S_2×4_YY_RETRO)

	ASSUMED	
STOREY S_i	**m_i [ton]**	**δ_i**
6	0,00	0,000
5	0,00	0,000
4	126,22	1,000
3	126,22	0,820
2	126,22	0,600
1	126,22	0,342

F_i [kN]
0,00
0,00
0,36
0,30
0,22
0,12

α1	0,888
PF1	1,285

	START	**Tens.**	**Comp.**
ΔN_0 [kN]		750,00	1000,00

B [m]	**h [m]**	**L_i [m]**
4,40	3,20	5,441

E_s [GPa]	**f_{ym} [MPa]**	**ε_y**
210,00	343,75	0,001637

1st Storey			**SDOF**			
Δ_y [m]	**Δ_d [m]**	**μ**	**EVD [%]**	**$S\Delta_d$ [m]**	**T_e [s]**	**K_e [kN/m]**
0,01101	0,01500	1,363	9,79%	0,03408	0,546	59341,58

1st Storey				**1st Storey**			
V_b^{REQ} [kN]	**V_b^{BF} [kN]**	**$V_b^{BR,REQ}$ [kN]**		**BR S_1**	**V_b^{BR} [kN]**	**V_b [kN]**	**Ω**
				CHSH			
2022,61	430,63	1656,58	x4	88,9 x 6,0	1930,00	2296,04	1,135

	ASSUMED			**Nth Storey**			
STOREY S_i	**DRIFTS [m]**	**V_i^{BF} [kN]**		**V_i^{REQ} [kN]**	**$V_i^{BR,REQ}$ [kN]**	**BR S_i**	**V_i^{BR} [kN]**
6	0,00000			0,00	0,00	0	0,00
5	-0,04380			0,00	0,00	0	0,00
4	0,00790	133,11	x4	831,12	717,98	88,9 x 3,2	1128,88
3	0,00960	200,33	x4	1512,35	1342,07	88,9 x 4,0	1398,21
2	0,01130	283,92	x4	2011,42	1770,09	88,9 x 6,0	2030,24
1	0,01500	430,63	x4	2022,61	1656,58	88,9 x 6,0	1930,00

END	**Tens.**	**Comp.**
ΔN [kN]	810,28	1074,97
	8,04%	7,50%

SDOF	
Sa [g]	0,52231

BUILDING TYPE 9: 5 storeys, 2×4 spans **| SEISMIC HAZARD SCENARIO 3:** PT 1.3 + 2.3 (EC8-1)

Table A5.33 – Design procedure result – Direction XX (S3_AST1_5S_2×4_XX_RETRO)

ASSUMED

STOREY S_i	m_i [ton]	δ_i
6	0,00	0,000
5	126,22	1,000
4	126,22	0,858
3	126,22	0,690
2	126,22	0,498
1	126,22	0,280

F_i [kN]
0,00
0,30
0,26
0,21
0,15
0,08

α1	0,871
PF1	1,310

START	Tens.	Comp.
ΔN_0 [kN]	800,00	1000,00

B [m]	h [m]	L_i [m]
4,40	3,20	5,441

E_s [GPa]	f_{ym} [MPa]	ε_y
210,00	343,75	0,001637

1st Storey

Δ_y [m]	Δ_d [m]	μ
0,01101	0,01600	1,454

SDOF

EVD [%]	$S\Delta_d$ [m]	T_e [s]	K_e [kN/m]
10,61%	0,04364	1,026	20624,89

1st Storey

V_b^{REQ} [kN]	V_b^{BF} [kN]	$V_b^{BR,REQ}$ [kN]
900,08	452,68	515,31

1st Storey

	BR S_1	V_b^{BR} [kN]	V_b [kN]	Ω
x2	CHSH 88,9 x 3,2	536,36	921,14	1,023

ASSUMED

STOREY S_i	DRIFTS [m]	V_i^{BF} [kN]		V_i^{REQ} [kN]	$V_i^{BR,REQ}$ [kN]	BR S_i	V_i^{BR} [kN]
6	-0,05718			0,00	0,00	0	0,00
5	0,00813	112,86	x2	276,98	181,05	88,9 x 3,2	564,44
4	0,00957	175,38	x2	514,57	365,50	88,9 x 3,2	564,44
3	0,01101	247,07	x2	705,78	495,77	88,9 x 3,2	564,44
2	0,01246	353,26	x2	843,63	543,36	88,9 x 3,2	564,44
1	0,01600	452,68	x2	900,08	515,31	88,9 x 3,2	536,36

Nth Storey

END	Tens.	Comp.
ΔN [kN]	783,20	927,83
	-2,10%	-7,22%

SDOF

Sa [g]	0,17074

Table A5.34 – Design procedure result – Direction YY (S3_AST1_5S_2×4_YY_RETRO)

ASSUMED

STOREY S_i	m_i [ton]	δ_i
6	0,00	0,000
5	126,22	1,000
4	126,22	0,858
3	126,22	0,690
2	126,22	0,498
1	126,22	0,280

F_i [kN]
0,00
0,30
0,26
0,21
0,15
0,08

α1	0,871
PF1	1,310

START	Tens.	Comp.
ΔN_0 [kN]	800,00	1000,00

B [m]	h [m]	L_i [m]
4,40	3,20	5,441

E_s [GPa]	f_{ym} [MPa]	ε_y
210,00	343,75	0,001637

1st Storey

Δ_y [m]	Δ_d [m]	μ
0,01101	0,01600	1,454

SDOF

EVD [%]	$S\Delta_d$ [m]	T_e [s]	K_e [kN/m]
10,61%	0,04364	1,026	20624,89

1st Storey

V_b^{REQ} [kN]	V_b^{BF} [kN]	$V_b^{BR,REQ}$ [kN]
900,08	591,19	397,57

1st Storey

	BR S_1	V_b^{BR} [kN]	V_b [kN]	Ω
x2	CHSH 88,9 x 3,2	536,36	1038,87	1,154

ASSUMED

STOREY S_i	DRIFTS [m]	V_i^{BF} [kN]	
6	-0,05718		
5	0,00813	133,28	x2
4	0,00957	194,46	x2
3	0,01101	267,37	x2
2	0,01246	378,94	x2
1	0,01600	591,19	x2

Nth Storey

V_i^{REQ} [kN]	$V_i^{BR,REQ}$ [kN]	BR S_i	V_i^{BR} [kN]
0,00	0,00	0	0,00
312,38	199,10	88,9 x 3,2	564,44
580,34	415,05	88,9 x 3,2	564,44
795,98	568,72	88,9 x 3,6	631,30
951,45	629,35	88,9 x 4,0	699,11
900,08	397,57	88,9 x 3,2	536,36

END	Tens.	Comp.
ΔN [kN]	850,20	994,83
	6,28%	-0,52%

SDOF	
Sa [g]	0,19256

BUILDING TYPE 9: 5 storeys, 2×4 spans **| SEISMIC HAZARD SCENARIO 4:** PT 1.1 + 2.3 (EC8-1)

Table A5.35 – Design procedure result – Direction XX (S4_AST1_5S_2×4_XX_RETRO)

ASSUMED

STOREY S_i	m_i [ton]	δ_i
6	0,00	0,000
5	126,22	1,000
4	126,22	0,858
3	126,22	0,690
2	126,22	0,498
1	126,22	0,280

F_i [kN]
0,00
0,30
0,26
0,21
0,15
0,08

α1	0,871
PF1	1,310

START	Tens.	Comp.
ΔN_0 [kN]	1000,00	1350,00

B [m]	h [m]	L_i [m]
4,40	3,20	5,441

E_s [GPa]	f_{ym} [MPa]	ε_y
210,00	343,75	0,001637

1st Storey

Δ_y [m]	Δ_d [m]	μ
0,01101	0,01600	1,454

SDOF

EVD [%]	$S\Delta_d$ [m]	T_e [s]	K_e [kN/m]
10,61%	0,04364	0,659	49993,74

1st Storey

V_b^{REQ} [kN]	V_b^{BF} [kN]	$V_b^{BR,REQ}$ [kN]
2181,76	452,68	1796,98

1st Storey

	BR S_1	V_b^{BR} [kN]	V_b [kN]	Ω
x4	CHSH 88,9 x 6,0	1930,00	2314,78	1,061

ASSUMED

STOREY S_i	DRIFTS [m]	V_i^{BF} [kN]	
6	-0,05718		
5	0,00813	112,86	x4
4	0,00957	175,38	x4
3	0,01101	247,07	x4
2	0,01246	353,26	x4
1	0,01600	452,68	x4

N^{th} Storey

V_i^{REQ} [kN]	$V_i^{BR,REQ}$ [kN]	BR S_i	V_i^{BR} [kN]
0,00	0,00	0	0,00
696,05	600,11	88,9 x 3,2	1128,88
1293,09	1144,02	88,9 x 3,6	1262,61
1773,59	1563,58	88,9 x 5,0	1720,61
2120,00	1819,73	88,9 x 6,0	2030,24
2181,76	1796,98	88,9 x 6,0	1930,00

END	Tens.	Comp.
ΔN [kN]	1074,41	1339,10
	7,44%	-0,81%

SDOF

Sa [g]	0,42906

Table A5.36 – Design procedure result – Direction YY (S4_AST1_5S_2×4_YY_RETRO)

	ASSUMED	
STOREY S_i	**m_i [ton]**	**δ_i**
6	0,00	0,000
5	126,22	1,000
4	126,22	0,858
3	126,22	0,690
2	126,22	0,498
1	126,22	0,280

F_i [kN]
0,00
0,30
0,26
0,21
0,15
0,08

α1	0,871
PF1	1,310

	START	**Tens.**	**Comp.**
ΔN_0 [kN]		1000,00	1350,00

B [m]	**h [m]**	**L_i [m]**
4,40	3,20	5,441

E_s [GPa]	**f_{ym} [MPa]**	**ε_y**
210,00	343,75	0,001637

1st Storey			**SDOF**			
Δ_y [m]	**Δ_d [m]**	**μ**	**EVD [%]**	**$S\Delta_d$ [m]**	**T_e [s]**	**K_e [kN/m]**
0,01101	0,01600	1,454	10,61%	0,04364	0,659	49993,74

1st Storey				**1st Storey**			
V_b^{REQ} [kN]	**V_b^{BF} [kN]**	**$V_b^{BR,REQ}$ [kN]**		**BR S_1**	**V_b^{BR} [kN]**	**V_b [kN]**	**Ω**
				CHSH			
2181,76	591,19	1679,25	x4	88,9 x 6,0	1930,00	2432,51	1,115

	ASSUMED			**N^th Storey**			
STOREY S_i	**DRIFTS [m]**	**V_i^{BF} [kN]**		**V_i^{REQ} [kN]**	**$V_i^{BR,REQ}$ [kN]**	**BR S_i**	**V_i^{BR} [kN]**
6	-0,05718			0,00	0,00	0	0,00
5	0,00813	133,28	x4	731,45	618,16	88,9 x 3,2	1128,88
4	0,00957	194,46	x4	1358,86	1193,57	88,9 x 3,6	1262,61
3	0,01101	267,37	x4	1863,80	1636,53	88,9 x 5,0	1720,61
2	0,01246	378,94	x4	2227,83	1905,73	88,9 x 6,0	2030,24
1	0,01600	591,19	x4	2181,76	1679,25	88,9 x 6,0	1930,00

END	**Tens.**	**Comp.**
ΔN [kN]	1074,41	1339,10
	7,44%	-0,81%

SDOF	
Sa [g]	0,45088

BUILDING TYPE 10: 6 storeys, 2×4 spans **| SEISMIC HAZARD SCENARIO 3:** PT 1.3 + 2.3 (EC8-1)

Table A5.37 – Design procedure result – Direction XX (S3_AST1_6S_2×4_XX_RETRO)

ASSUMED

STOREY S_i	m_i [ton]	δ_i
6	126,22	1,000
5	126,22	0,883
4	126,22	0,748
3	126,22	0,595
2	126,22	0,425
1	126,22	0,237

F_i [kN]
0,26
0,23
0,19
0,15
0,11
0,06

α1	0,860
PF1	1,327

START	Tens.	Comp.
ΔN_0 [kN]	1000,00	1200,00

B [m]	h [m]	L_i [m]
4,40	3,20	5,441

E_s [GPa]	f_{ym} [MPa]	ε_y
210,00	343,75	0,001637

1st Storey

Δ_y [m]	Δ_d [m]	μ
0,01101	0,01650	1,499

SDOF

EVD [%]	$S\Delta_d$ [m]	T_e [s]	K_e [kN/m]
10,99%	0,05256	1,254	16344,39

1st Storey

V_b^{REQ} [kN]	V_b^{BF} [kN]	$V_b^{BR,REQ}$ [kN]
859,08	593,83	354,32

1st Storey

	BR S_1	V_b^{BR} [kN]	V_b [kN]	Ω
x2	CHSH 88,9 x 3,2	536,36	1041,11	1,212

ASSUMED

STOREY S_i	DRIFTS [m]	V_i^{BF} [kN]
6	0,00819	114,21
5	0,00942	173,61
4	0,01065	241,42
3	0,01188	335,33
2	0,01312	400,05
1	0,01650	593,83

N^{th} Storey

	V_i^{REQ} [kN]	$V_i^{BR,REQ}$ [kN]	BR S_i	V_i^{BR} [kN]
x2	267,90	170,82	88,9 x 3,2	564,44
x2	504,35	356,79	88,9 x 3,2	564,44
x2	704,64	499,43	88,9 x 3,2	564,44
x2	864,01	578,98	88,9 x 3,6	631,30
x2	977,75	637,71	88,9 x 4,0	699,11
x2	859,08	354,32	88,9 x 3,2	536,36

END	Tens.	Comp.
ΔN [kN]	1038,59	1183,22
	3,86%	-1,40%

SDOF

Sa [g]	
	0,16301

Table A5.38 – Design procedure result – Direction YY (S3_AST1_6S_2×4_YY_RETRO)

ASSUMED

STOREY S_i	m_i [ton]	δ_i
6	126,22	1,000
5	126,22	0,883
4	126,22	0,748
3	126,22	0,595
2	126,22	0,425
1	126,22	0,237

F_i [kN]
0,26
0,23
0,19
0,15
0,11
0,06

α1	0,860
PF1	1,327

START	Tens.	Comp.
ΔN_0 [kN]	1000,00	1250,00

B [m]	h [m]	L_i [m]
4,40	3,20	5,441

E_s [GPa]	f_{ym} [MPa]	ε_y
210,00	343,75	0,001637

1st Storey

Δ_y [m]	Δ_d [m]	μ
0,01101	0,01600	1,454

SDOF

EVD [%]	$S\Delta_d$ [m]	T_e [s]	K_e [kN/m]
10,61%	0,05097	1,199	17878,27

1st Storey

V_b^{REQ} [kN]	V_b^{BF} [kN]	$V_b^{BR,REQ}$ [kN]
911,22	698,47	317,52

1st Storey

	BR S_1	V_b^{BR} [kN]	V_b [kN]	Ω
x2	CHSH 88,9 x 3,2	536,36	1130,06	1,240

ASSUMED

Nth Storey

STOREY S_i	DRIFTS [m]	V_i^{BF} [kN]		V_i^{REQ} [kN]	$V_i^{BR,REQ}$ [kN]	BR S_i	V_i^{BR} [kN]
6	0,00794	130,28	x2	290,78	180,05	88,9 x 3,2	564,44
5	0,00913	188,78	x2	547,44	386,98	88,9 x 3,2	564,44
4	0,01033	252,69	x2	764,83	550,05	88,9 x 3,6	631,30
3	0,01152	345,36	x2	937,83	644,27	88,9 x 4,0	699,11
2	0,01272	470,50	x2	1061,28	661,36	88,9 x 4,0	699,11
1	0,01600	698,47	x2	911,22	317,52	88,9 x 3,2	536,36

END	Tens.	Comp.
ΔN [kN]	1083,35	1227,98
	8,33%	-1,76%

SDOF

Sa [g]	0,17694

BUILDING TYPE 10: 6 storeys, 2×4 spans **| SEISMIC HAZARD SCENARIO 4:** PT 1.1 + 2.3 (EC8-1)

Table A5.39 – Design procedure result – Direction XX (S4_AST1_6S_2×4_XX_RETRO)

	ASSUMED	
STOREY S_i	**m_i [ton]**	**δ_i**
6	126,22	1,000
5	126,22	0,883
4	126,22	0,748
3	126,22	0,595
2	126,22	0,425
1	126,22	0,237

F_i [kN]
0,26
0,23
0,19
0,15
0,11
0,06

α1	0,860
PF1	1,327

	START	Tens.	Comp.
	ΔN_0 [kN]	1150,00	1450,00

B [m]	**h [m]**	**L_i [m]**
4,40	3,20	5,441

E_s [GPa]	**f_{ym} [MPa]**	**ε_y**
210,00	343,75	0,001637

1st Storey

Δ_y [m]	**Δ_d [m]**	**μ**
0,01101	0,01650	1,499

SDOF

EVD [%]	**$S\Delta_d$ [m]**	**T_e [s]**	**K_e [kN/m]**
10,99%	0,05256	0,805	39661,77

1st Storey

V_b^{REQ} [kN]	**V_b^{BF} [kN]**	**$V_b^{BR,REQ}$ [kN]**
2084,66	593,83	1579,90

1st Storey

	BR S_1	**V_b^{BR} [kN]**	**V_b [kN]**	**Ω**
	CHSH			
x4	88,9 x 5,0	1635,49	2140,25	1,027

	ASSUMED			**Nth Storey**			
STOREY S_i	**DRIFTS [m]**	**V_i^{BF} [kN]**		**V_i^{REQ} [kN]**	**$V_i^{BR,REQ}$ [kN]**	**BR S_i**	**V_i^{BR} [kN]**
6	0,00819	114,21	x4	550,72	453,65	88,9 x 3,2	564,44
5	0,00942	173,61	x4	1036,81	889,25	88,9 x 3,2	1128,88
4	0,01065	241,42	x4	1448,54	1243,34	88,9 x 3,6	1262,61
3	0,01188	335,33	x4	1776,18	1491,15	88,9 x 5,0	1720,61
2	0,01312	400,05	x4	2009,99	1669,95	88,9 x 5,0	1720,61
1	0,01650	593,83	x4	2084,66	1579,90	88,9 x 5,0	1635,49

END	Tens.	Comp.
ΔN [kN]	1204,24	1427,58
	4,72%	-1,55%

SDOF	
Sa [g]	0,33511

Table A5.40 – Design procedure result – Direction YY (S4_AST1_6S_2×4_YY_RETRO)

	ASSUMED	
STOREY S_i	**m_i [ton]**	**δ_i**
6	126,22	1,000
5	126,22	0,883
4	126,22	0,748
3	126,22	0,595
2	126,22	0,425
1	126,22	0,237

F_i [kN]
0,26
0,23
0,19
0,15
0,11
0,06

α1	0,860
PF1	1,327

	START	Tens.	Comp.
ΔN_0 [kN]		1150,00	1450,00

B [m]	**h [m]**	**L_i [m]**
4,40	3,20	5,441

E_s [GPa]	**f_{ym} [MPa]**	**ε_y**
210,00	343,75	0,001637

1st Storey			SDOF			
Δ_y [m]	**Δ_d [m]**	**μ**	**EVD [%]**	**$S\Delta_d$ [m]**	**T_e [s]**	**K_e [kN/m]**
0,01101	0,01600	1,454	10,61%	0,05097	0,769	43462,15

1st Storey				1st Storey			
V_b^{REQ} [kN]	**V_b^{BF} [kN]**	**$V_b^{BR,REQ}$ [kN]**		**BR S_1**	**V_b^{BR} [kN]**	**V_b [kN]**	**Ω**
				CHSH			
2215,18	698,47	1621,48	x4	88,9 x 5,0	1635,49	2229,19	1,006

	ASSUMED			Nth Storey			
STOREY S_i	**DRIFTS [m]**	**V_i^{BF} [kN]**		**V_i^{REQ} [kN]**	**$V_i^{BR,REQ}$ [kN]**	**BR S_i**	**V_i^{BR} [kN]**
6	0,00794	130,28	x4	573,61	462,87	88,9 x 3,2	564,44
5	0,00913	188,78	x4	1079,90	919,44	88,9 x 3,2	1128,88
4	0,01033	252,69	x4	1508,74	1293,95	88,9 x 4,0	1398,21
3	0,01152	345,36	x4	1849,99	1556,43	88,9 x 5,0	1720,61
2	0,01272	470,50	x4	2093,52	1693,59	88,9 x 5,0	1720,61
1	0,01600	698,47	x4	2215,18	1621,48	88,9 x 5,0	1635,49

END	Tens.	Comp.
ΔN [kN]	1226,75	1450,09
	6,67%	0,01%

SDOF	
Sa [g]	0,34904

APPENDIX 6

RETROFITTED BUILDINGS – PERFORMANCE EVALUATION

APPENDIX 6 – RETROFITTED BUILDINGS – PERFORMANCE EVALUATION

BUILDING TYPE 1: 2 storeys, 3×5 spans

Seismic hazard scenario 3: PT 1.3 + 2.3 (EC8-1)

Seismic hazard scenario 4: PT 1.1 + 2.3 (EC8-1)

BUILDING TYPE 2: 3 storeys, 3×5 spans

Id

BUILDING TYPE 3: 4 storeys, 3×5 spans

Id

BUILDING TYPE 4: 5 storeys, 3×5 spans

Id

BUILDING TYPE 5: 6 storeys, 3×5 spans

Id

BUILDING TYPE 6: 2 storeys, 2×4 spans

Id

BUILDING TYPE 7: 3 storeys, 2×4 spans

Id

BUILDING TYPE 8: 4 storeys, 2×4 spans

Id

BUILDING TYPE 9: 5 storeys, 2×4 spans

Id

BUILDING TYPE 10: 6 storeys, 2×4 spans

Id

BUILDING TYPE 1: 2 storeys, 3×5 spans **| SEISMIC HAZARD SCENARIO 3:** PT 1.3 + 2.3 (EC8-1)

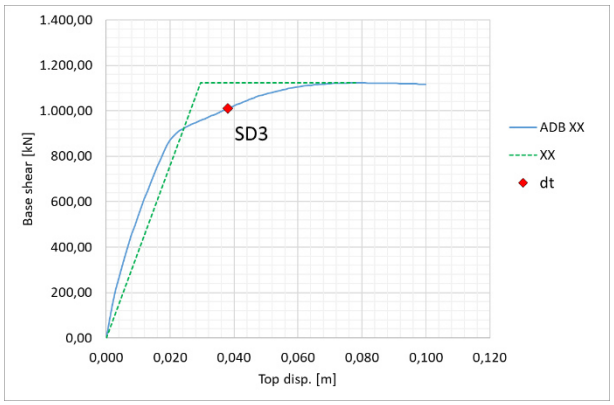

Figure A6.1 – Capacity curve and target displacement d_t, direction XX (S3_AST1_2S_3×5_XX_RETRO)

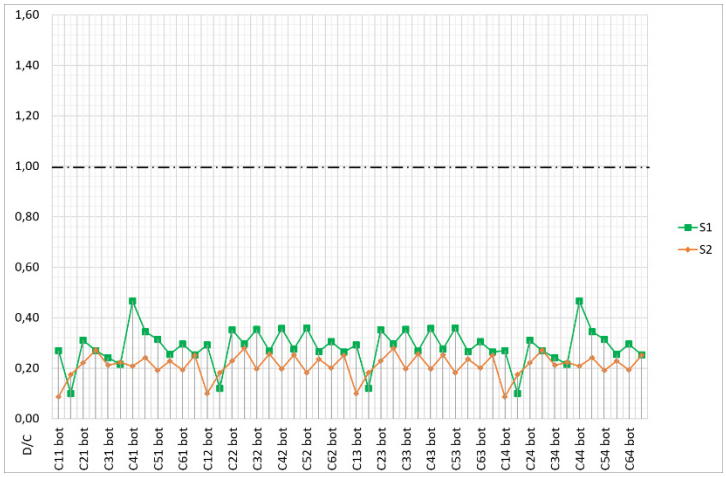

Figure A6.2 – Chord rotation D/C ratios (SD), direction XX (S3_AST1_2S_3×5_XX_RETRO)

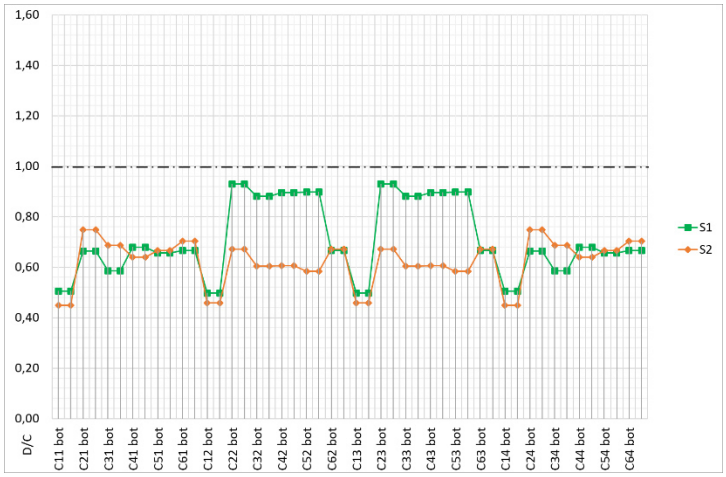

Figure A6.3 – Shear force D/C ratios (SD), direction XX (S3_AST1_2S_3×5_XX_RETRO)

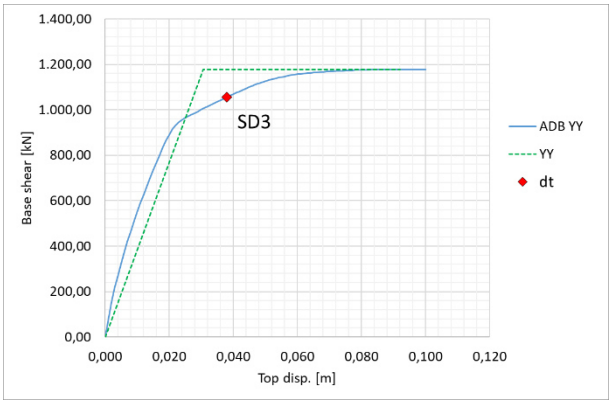

Figure A6.4 – Capacity curve and target displacement d_t, direction YY (S3_AST1_2S_3×5_YY_RETRO)

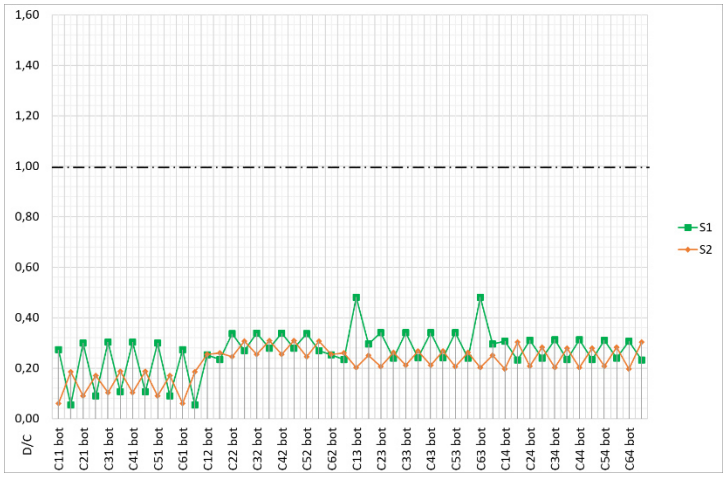

Figure A6.5 – Chord rotation D/C ratios (SD), direction YY (S3_AST1_2S_3×5_YY_RETRO)

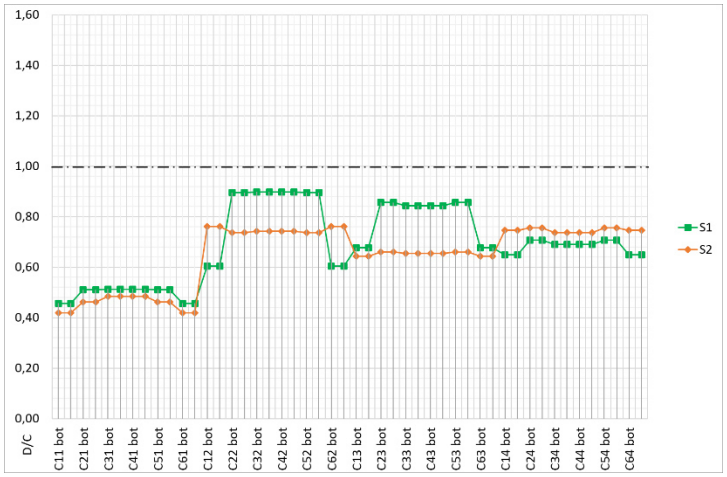

Figure A6.6 – Shear force D/C ratios (SD), direction YY (S3_AST1_2S_3×5_YY_RETRO)

BUILDING TYPE 1: 2 storeys, 3×5 spans **| SEISMIC HAZARD SCENARIO 4:** PT 1.1 + 2.3 (EC8-1)

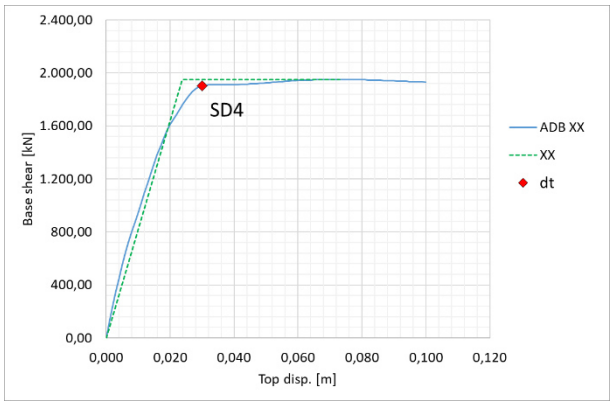

Figure A6.7 – Capacity curve and target displacement d_t, direction XX (S4_AST1_2S_3×5_XX_RETRO)

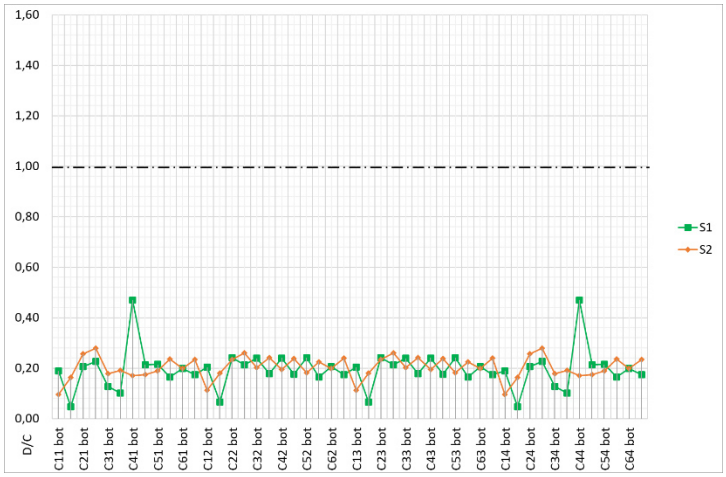

Figure A6.8 – Chord rotation D/C ratios (SD), direction XX (S4_AST1_2S_3×5_XX_RETRO)

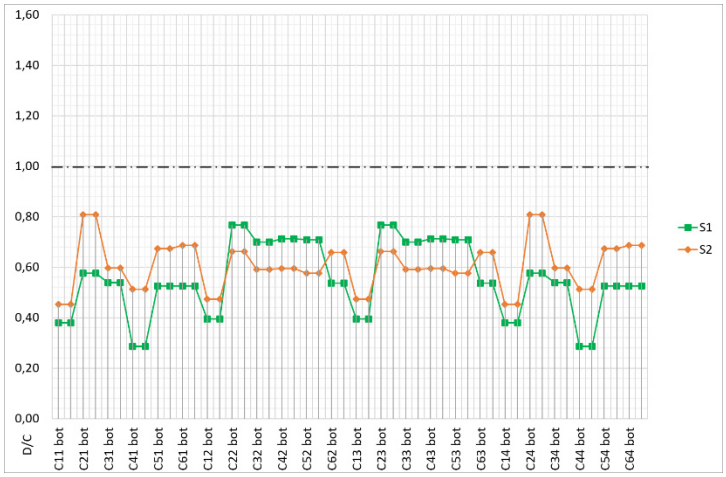

Figure A6.9 – Shear force D/C ratios (SD), direction XX (S4_AST1_2S_3×5_XX_RETRO)

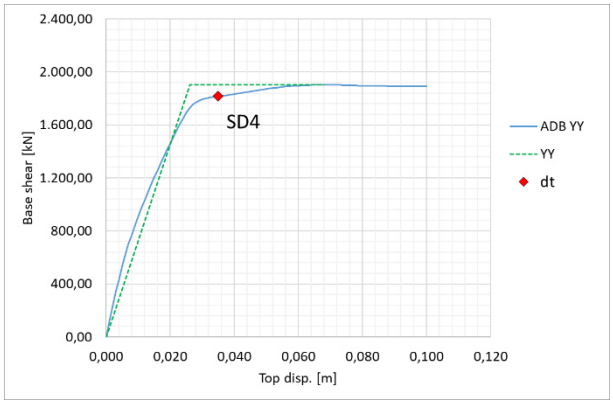

Figure A6.10 – Capacity curve and target displacement d_t, direction YY (S4_AST1_2S_3×5_YY_RETRO)

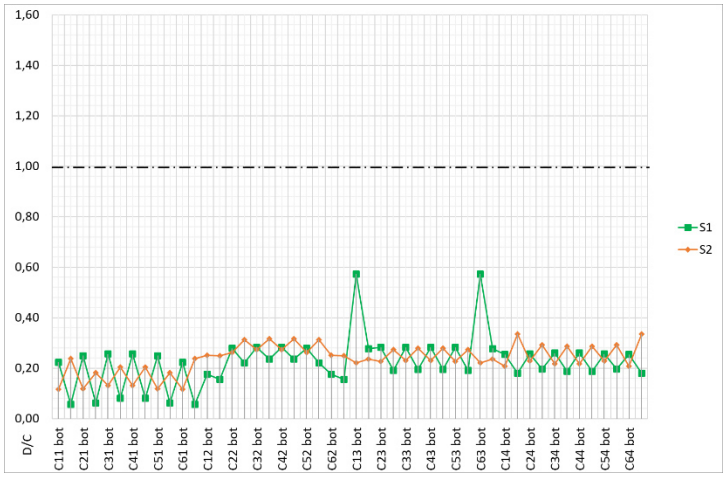

Figure A6.11 – Chord rotation D/C ratios (SD), direction YY (S4_AST1_2S_3×5_YY_RETRO)

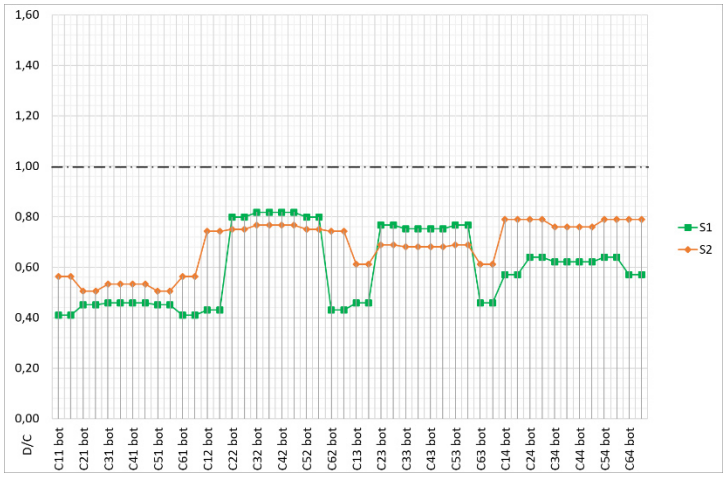

Figure A6.12 – Shear force D/C ratios (SD), direction YY (S4_AST1_2S_3×5_YY_RETRO)

BUILDING TYPE 2: 3 storeys, 3×5 spans **| SEISMIC HAZARD SCENARIO 3:** PT 1.3 + 2.3 (EC8-1)

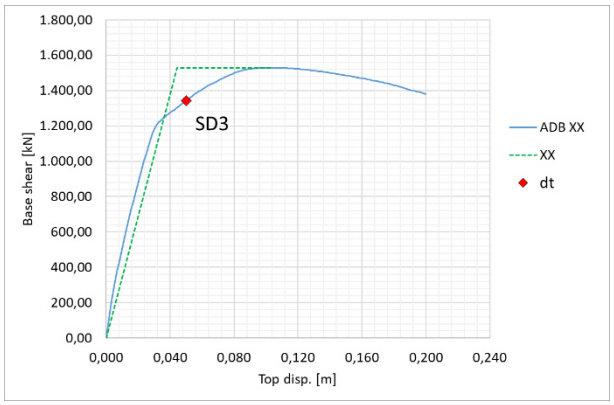

Figure A6.13 – Capacity curve and target displacement d_t, direction XX (S3_AST1_3S_3×5_XX_RETRO)

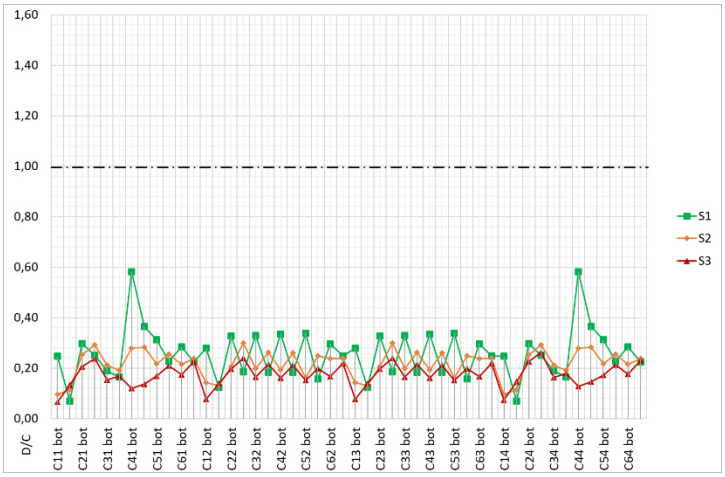

Figure A6.14 – Chord rotation D/C ratios (SD), direction XX (S3_AST1_3S_3×5_XX_RETRO)

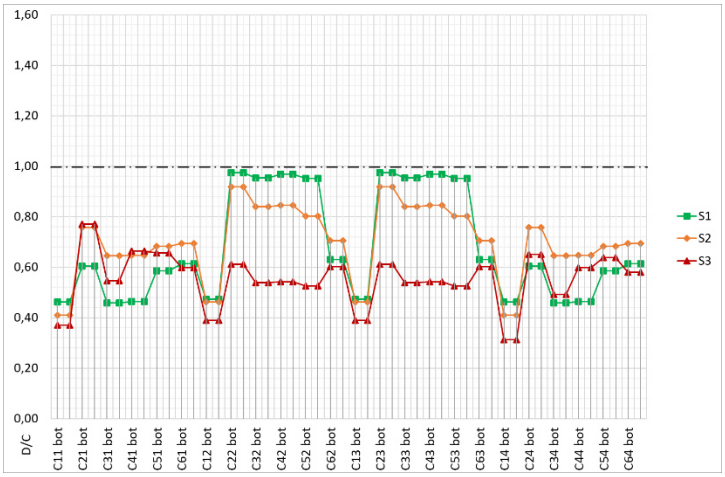

Figure A6.15 – Shear force D/C ratios (SD), direction XX (S3_AST1_3S_3×5_XX_RETRO)

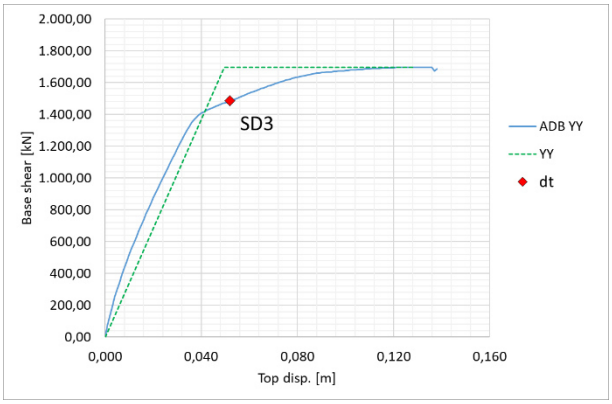

Figure A6.16 – Capacity curve and target displacement d_t, direction YY (S3_AST1_3S_3×5_YY_RETRO)

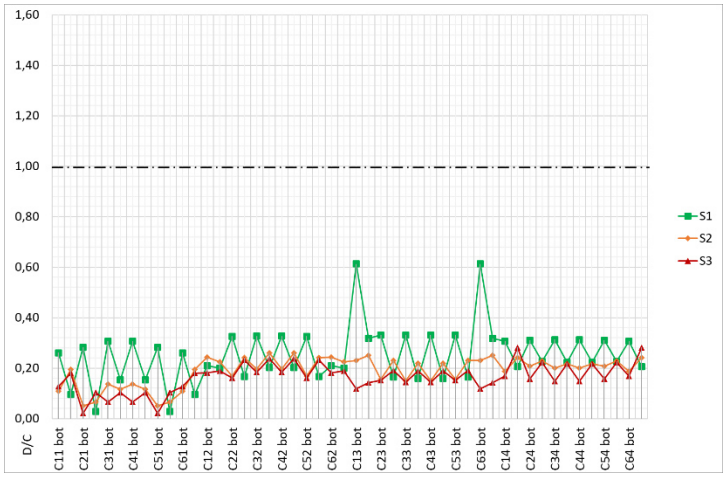

Figure A6.17 – Chord rotation D/C ratios (SD), direction YY (S3_AST1_3S_3×5_YY_RETRO)

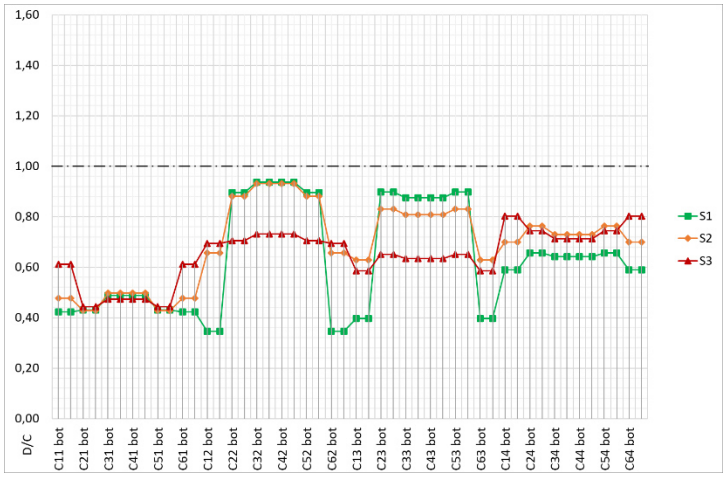

Figure A6.18 – Shear force D/C ratios (SD), direction YY (S3_AST1_3S_3×5_YY_RETRO)

BUILDING TYPE 2: 3 storeys, 3×5 spans **| SEISMIC HAZARD SCENARIO 4:** PT 1.1 + 2.3 (EC8-1)

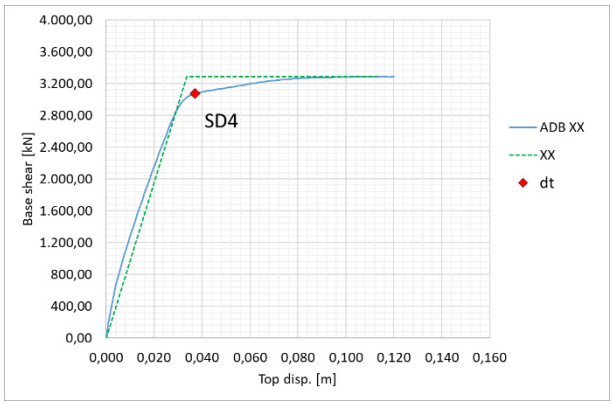

Figure A6.19 – Capacity curve and target displacement d_t, direction XX (S4_AST1_3S_3×5_XX_RETRO)

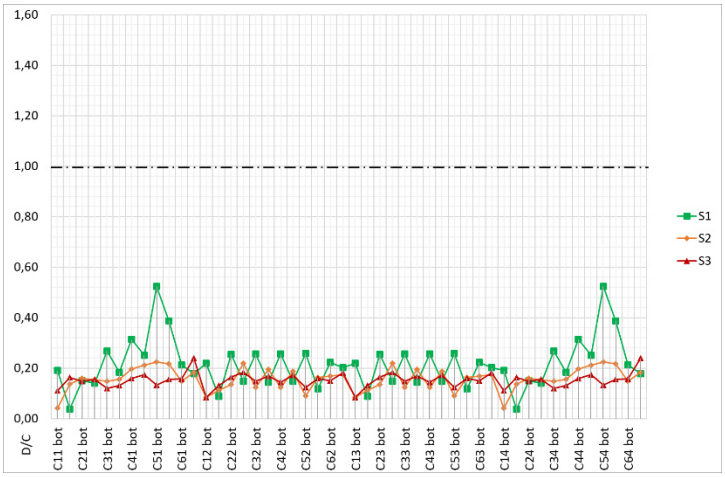

Figure A6.20 – Chord rotation D/C ratios (SD), direction XX (S4_AST1_3S_3×5_XX_RETRO)

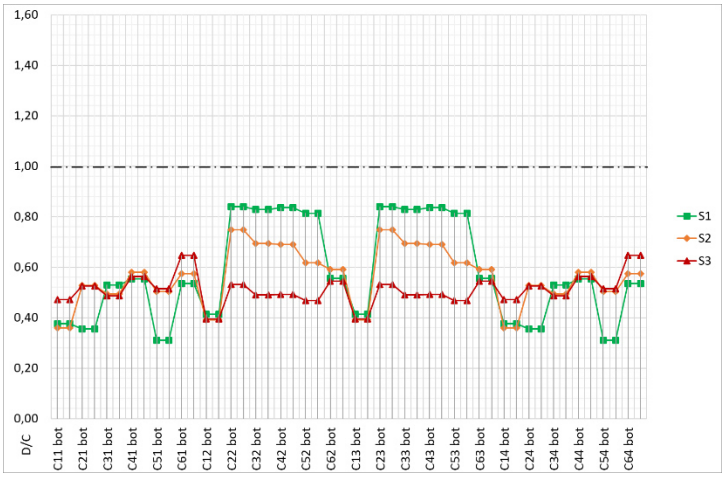

Figure A6.21 – Shear force D/C ratios (SD), direction XX (S4_AST1_3S_3×5_XX_RETRO)

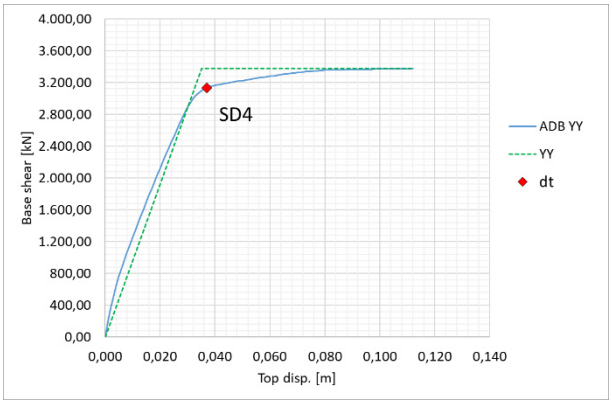

Figure A6.22 – Capacity curve and target displacement d_t, direction YY (S4_AST1_3S_3×5_YY_RETRO)

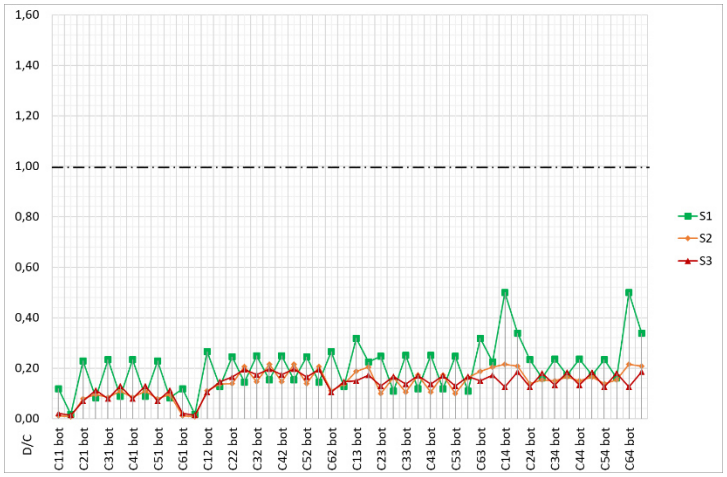

Figure A6.23 – Chord rotation D/C ratios (SD), direction YY (S4_AST1_3S_3×5_YY_RETRO)

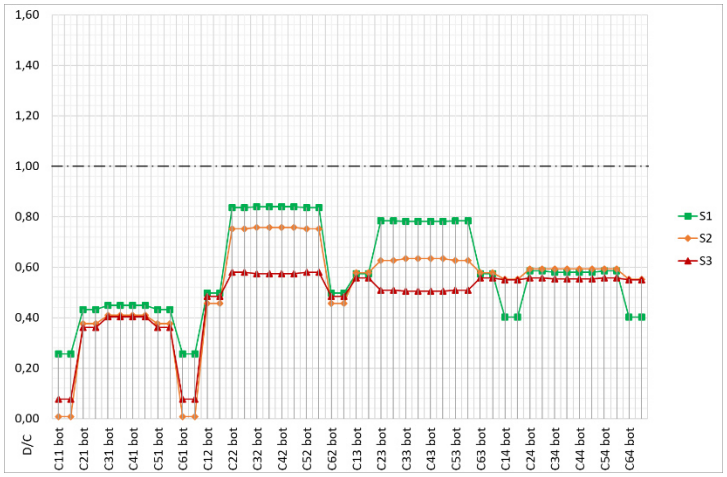

Figure A6.24 – Shear force D/C ratios (SD), direction YY (S4_AST1_3S_3×5_YY_RETRO)

BUILDING TYPE 3: 4 storeys, 3×5 spans **| SEISMIC HAZARD SCENARIO 3:** PT 1.3 + 2.3 (EC8-1)

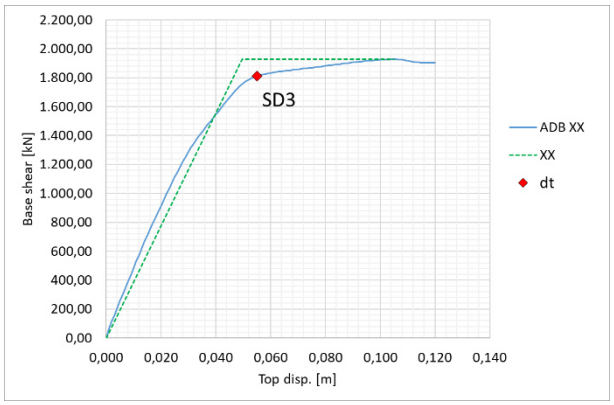

Figure A6.25 – Capacity curve and target displacement d_t, direction XX (S3_AST1_4S_3×5_XX_RETRO)

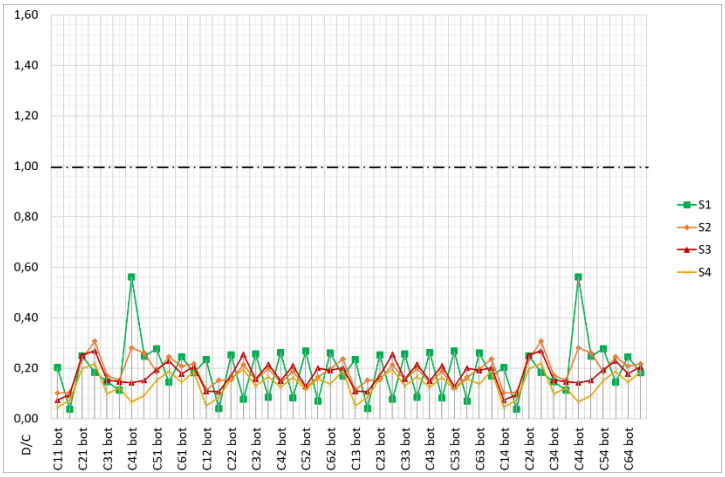

Figure A6.26 – Chord rotation D/C ratios (SD), direction XX (S3_AST1_4S_3×5_XX_RETRO)

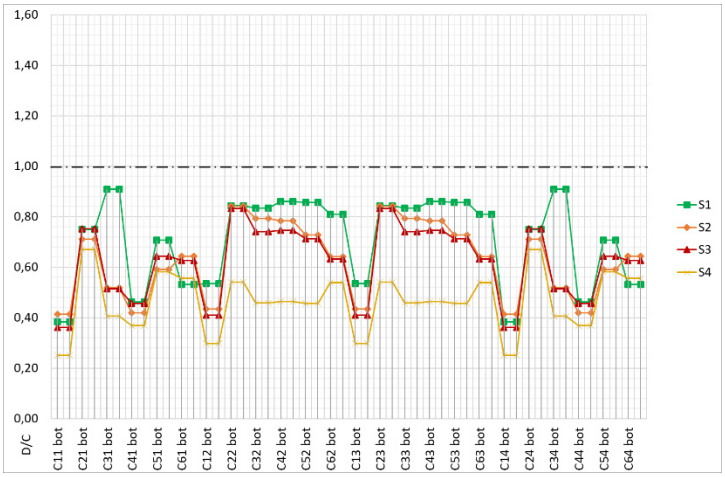

Figure A6.27 – Shear force D/C ratios (SD), direction XX (S3_AST1_4S_3×5_XX_RETRO)

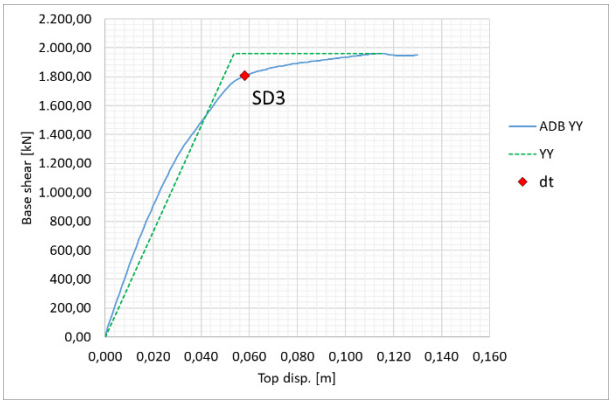

Figure A6.28 – Capacity curve and target displacement d_t, direction YY (S3_AST1_4S_3×5_YY_RETRO)

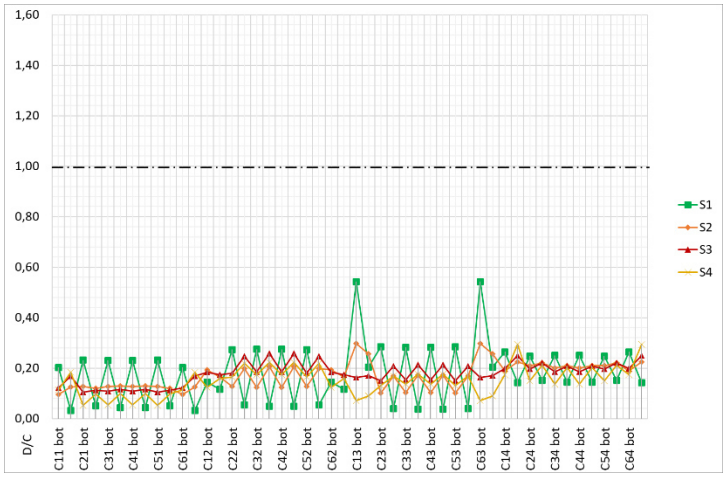

Figure A6.29 – Chord rotation D/C ratios (SD), direction YY (S3_AST1_4S_3×5_YY_RETRO)

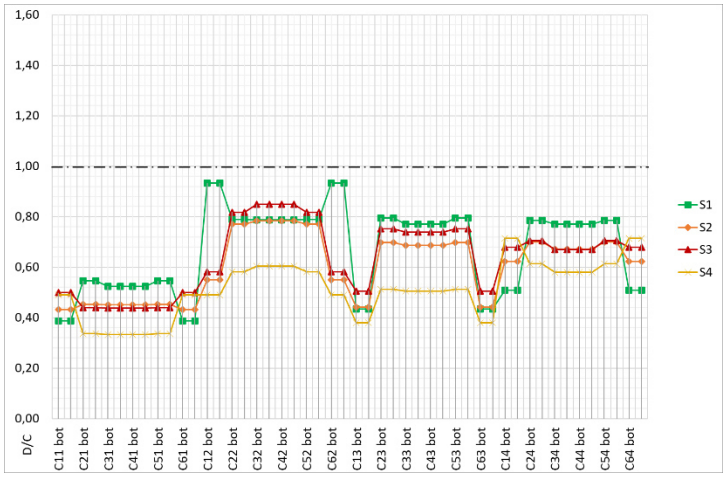

Figure A6.30 – Shear force D/C ratios (SD), direction YY (S3_AST1_4S_3×5_YY_RETRO)

BUILDING TYPE 3: 4 storeys, 3×5 spans **| SEISMIC HAZARD SCENARIO 4:** PT 1.1 + 2.3 (EC8-1)

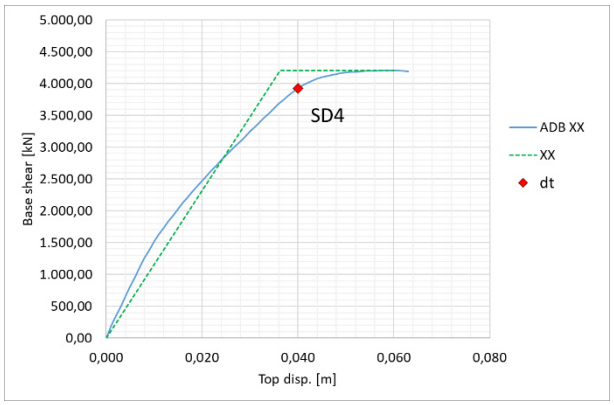

Figure A6.31 – Capacity curve and target displacement d_t, direction XX (S4_AST1_4S_3×5_XX_RETRO)

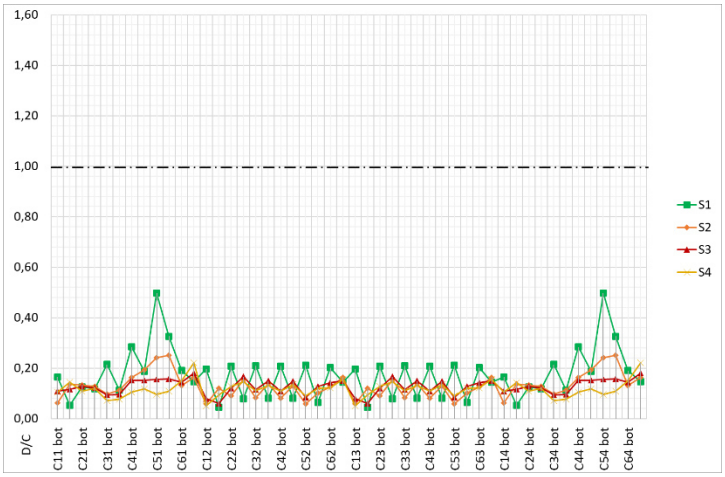

Figure A6.32 – Chord rotation D/C ratios (SD), direction XX (S4_AST1_4S_3×5_XX_RETRO)

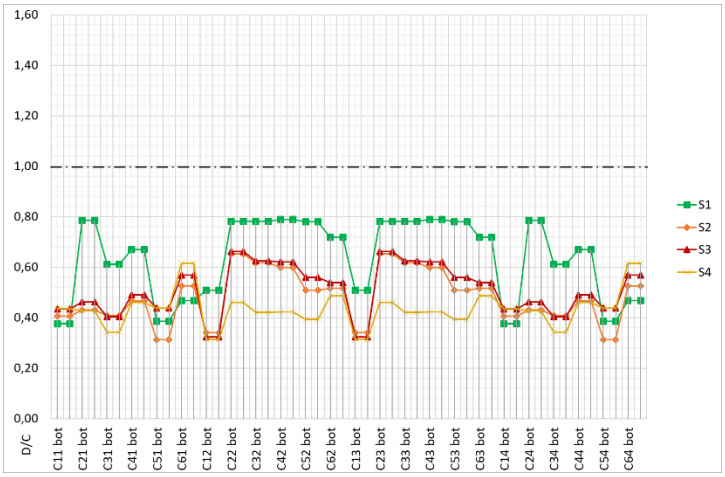

Figure A6.33 – Shear force D/C ratios (SD), direction XX (S4_AST1_4S_3×5_XX_RETRO)

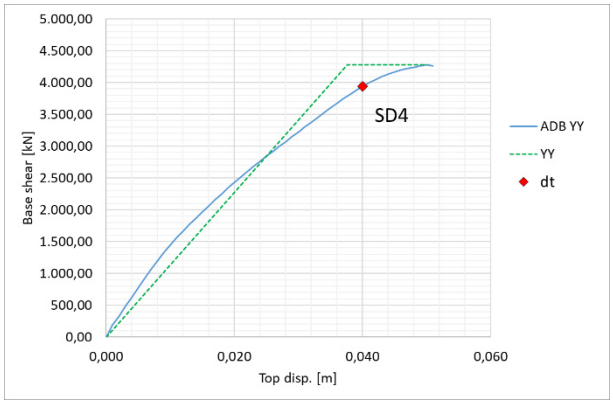

Figure A6.34 – Capacity curve and target displacement d_t, direction YY (S4_AST1_4S_3×5_YY_RETRO)

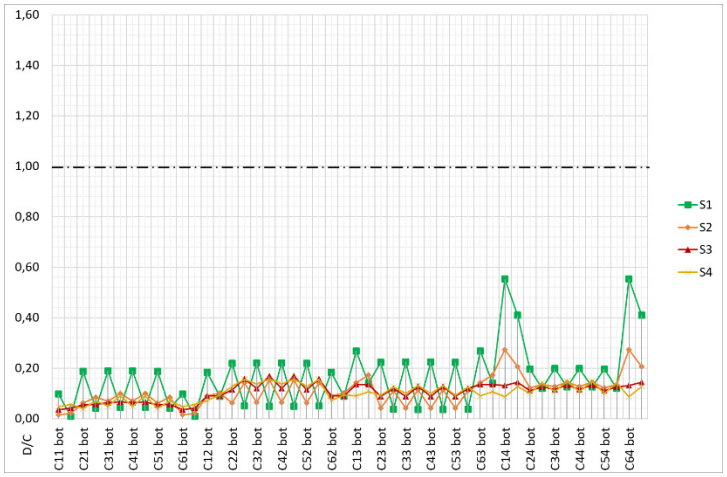

Figure A6.35 – Chord rotation D/C ratios (SD), direction YY (S4_AST1_4S_3×5_YY_RETRO)

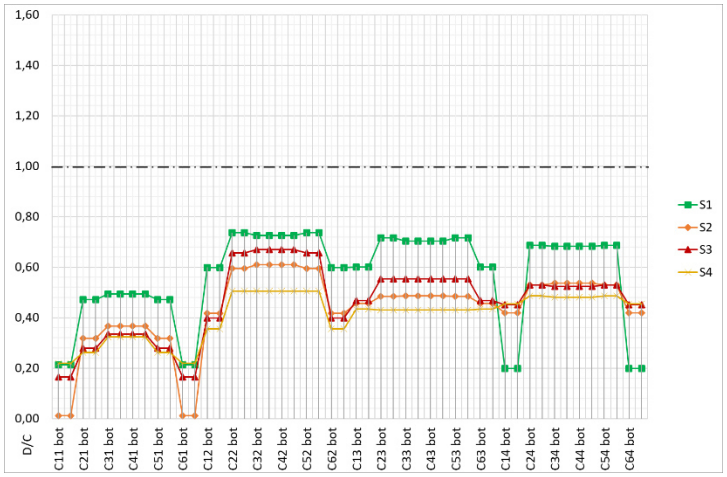

Figure A6.36 – Shear force D/C ratios (SD), direction YY (S4_AST1_4S_3×5_YY_RETRO)

BUILDING TYPE 4: 5 storeys, 3×5 spans **| SEISMIC HAZARD SCENARIO 3:** PT 1.3 + 2.3 (EC8-1)

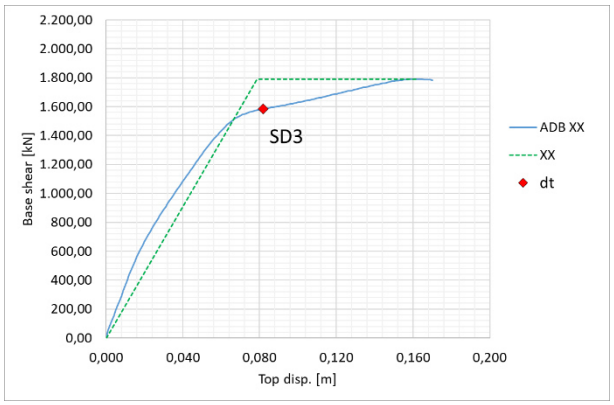

Figure A6.37 – Capacity curve and target displacement d_t, direction XX (S3_AST1_5S_3×5_XX_RETRO)

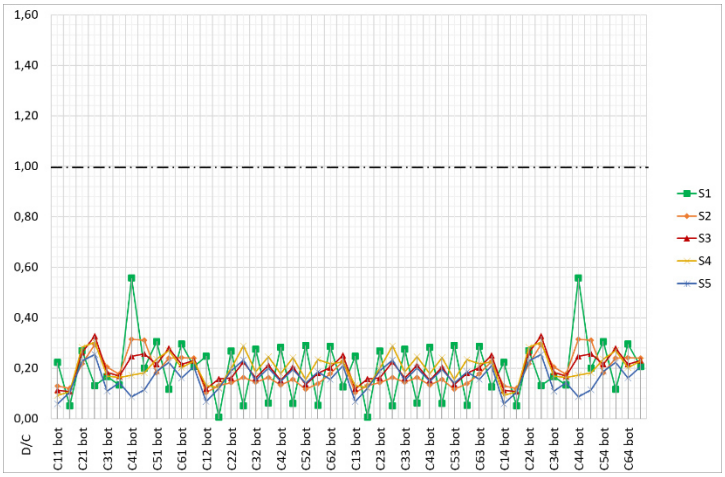

Figure A6.38 – Chord rotation D/C ratios (SD), direction XX (S3_AST1_5S_3×5_XX_RETRO)

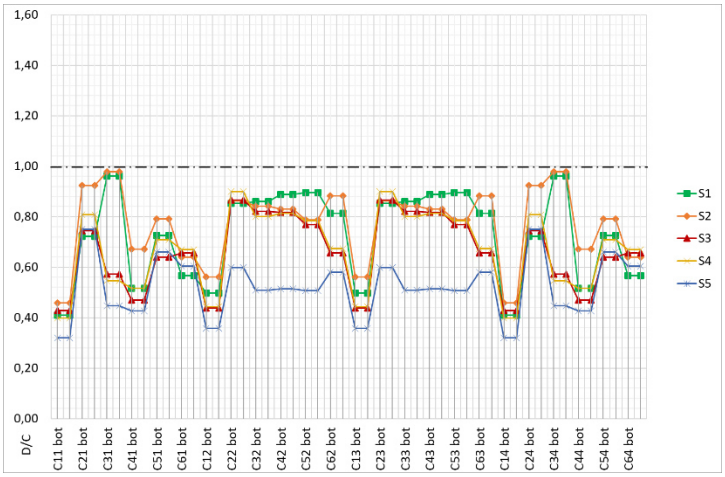

Figure A6.39 – Shear force D/C ratios (SD), direction XX (S3_AST1_5S_3×5_XX_RETRO)

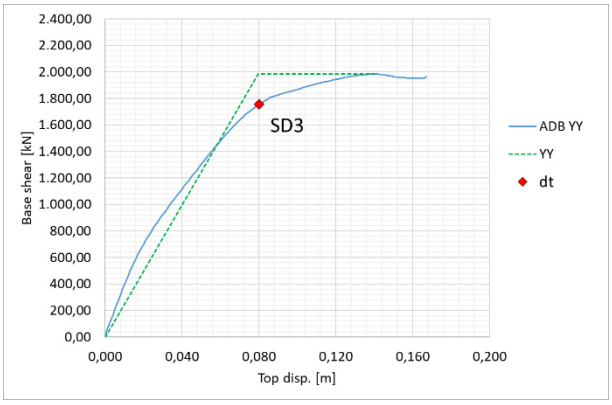

Figure A6.40 – Capacity curve and target displacement d_t, direction YY (S3_AST1_5S_3×5_YY_RETRO)

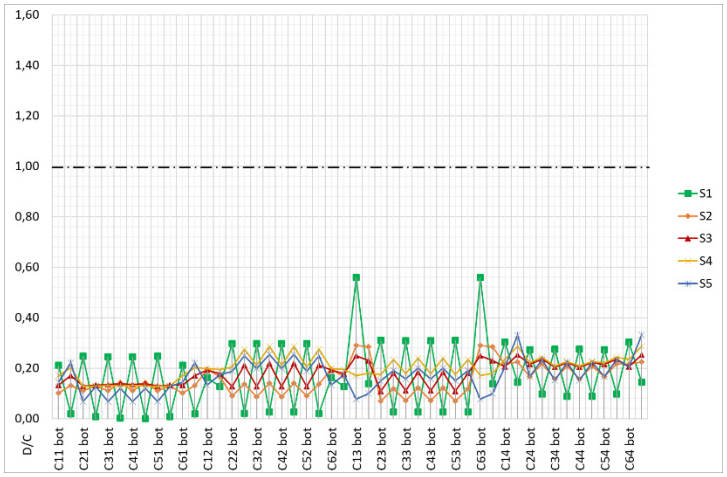

Figure A6.41 – Chord rotation D/C ratios (SD), direction YY (S3_AST1_5S_3×5_YY_RETRO)

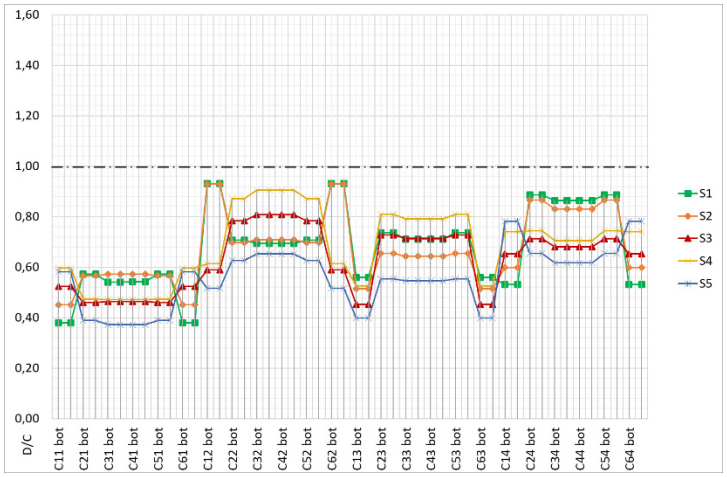

Figure A6.42 – Shear force D/C ratios (SD), direction YY (S3_AST1_5S_3×5_YY_RETRO)

BUILDING TYPE 4: 5 storeys, 3×5 spans **| SEISMIC HAZARD SCENARIO 4:** PT 1.1 + 2.3 (EC8-1)

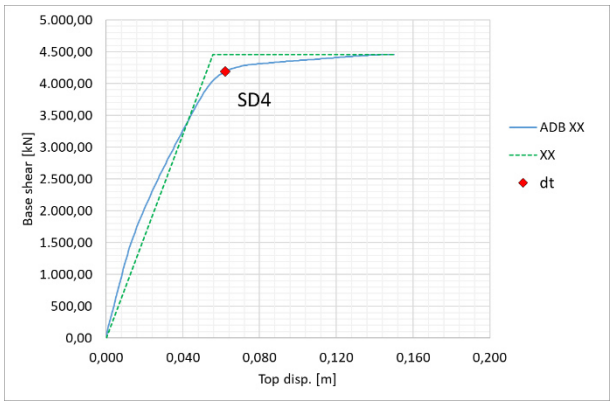

Figure A6.43 – Capacity curve and target displacement d_t, direction XX (S4_AST1_5S_3×5_XX_RETRO)

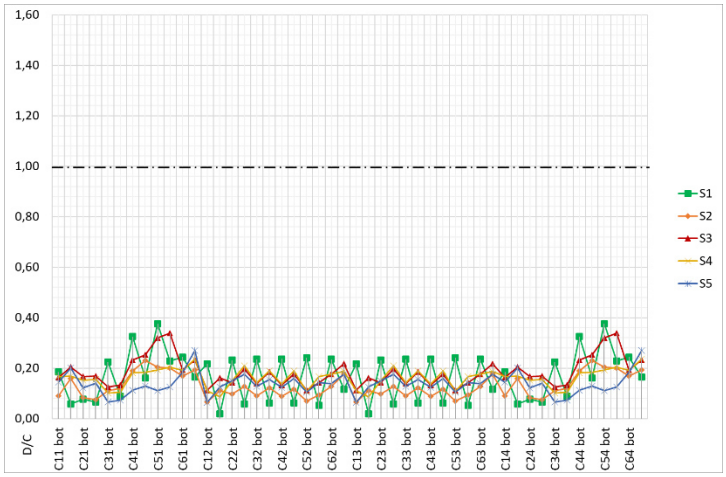

Figure A6.44 – Chord rotation D/C ratios (SD), direction XX (S4_AST1_5S_3×5_XX_RETRO)

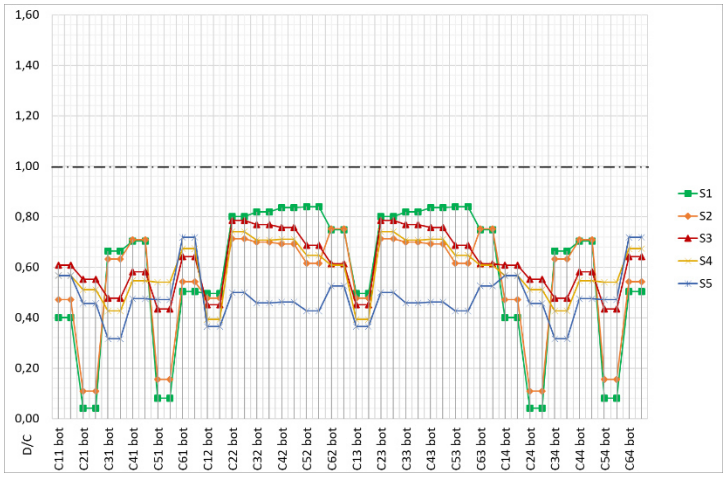

Figure A6.45 – Shear force D/C ratios (SD), direction XX (S4_AST1_5S_3×5_XX_RETRO)

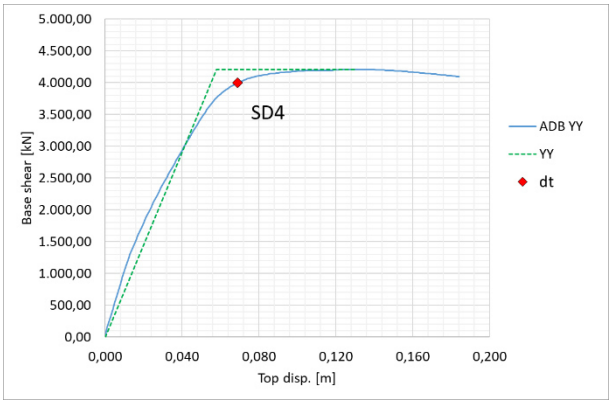

Figure A6.46 – Capacity curve and target displacement d_t, direction YY (S4_AST1_5S_3×5_YY_RETRO)

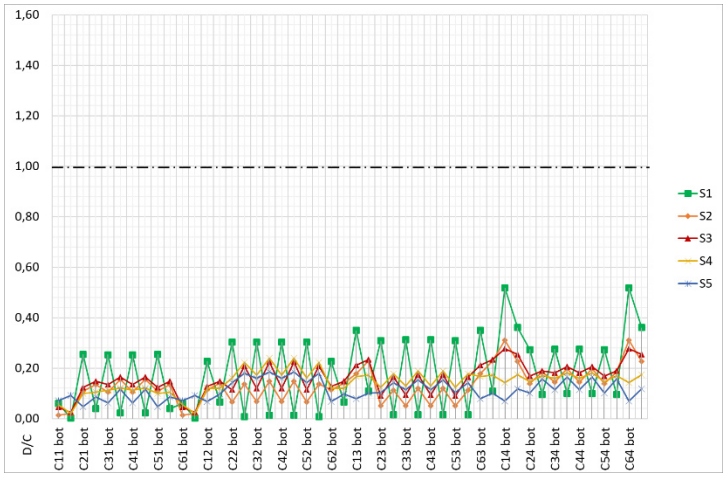

Figure A6.47 – Chord rotation D/C ratios (SD), direction YY (S4_AST1_5S_3×5_YY_RETRO)

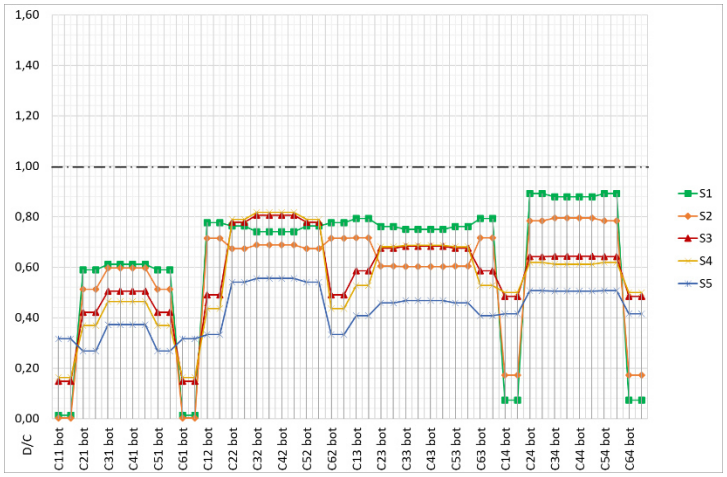

Figure A6.48 – Shear force D/C ratios (SD), direction YY (S4_AST1_5S_3×5_YY_RETRO)

BUILDING TYPE 5: 6 storeys, 3×5 spans **| SEISMIC HAZARD SCENARIO 3:** PT 1.3 + 2.3 (EC8-1)

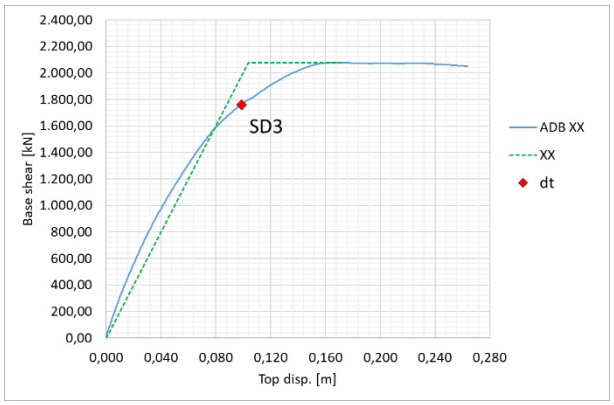

Figure A6.49 – Capacity curve and target displacement d_t, direction XX (S3_AST1_6S_3×5_XX_RETRO)

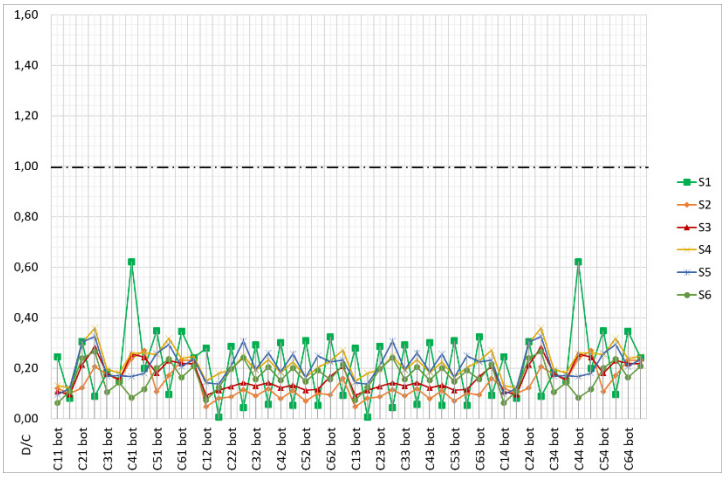

Figure A6.50 – Chord rotation D/C ratios (SD), direction XX (S3_AST1_6S_3×5_XX_RETRO)

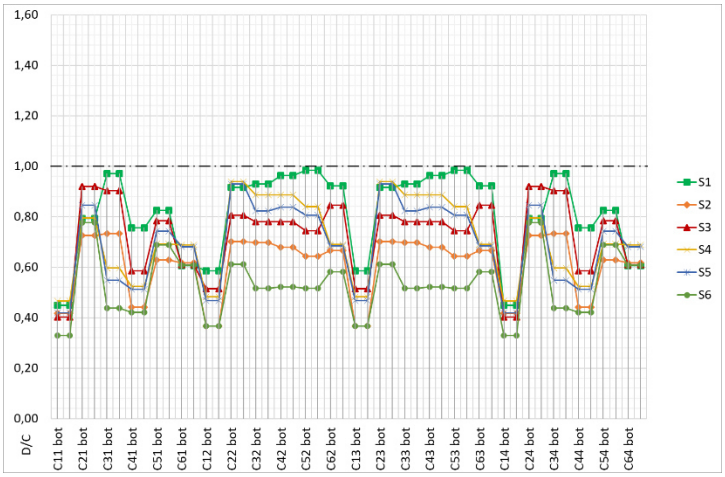

Figure A6.51 – Shear force D/C ratios (SD), direction XX (S3_AST1_6S_3×5_XX_RETRO)

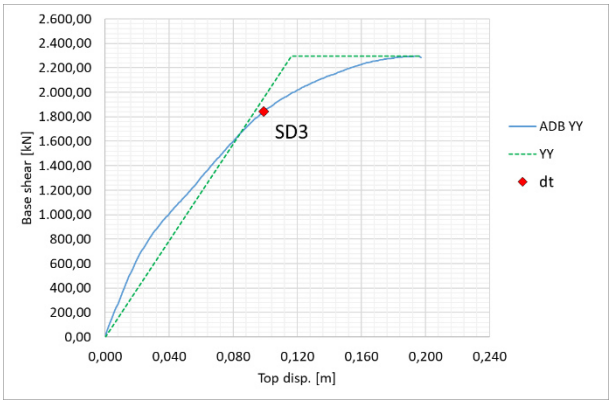

Figure A6.52 – Capacity curve and target displacement d_t, direction YY (S3_AST1_6S_3×5_YY_RETRO)

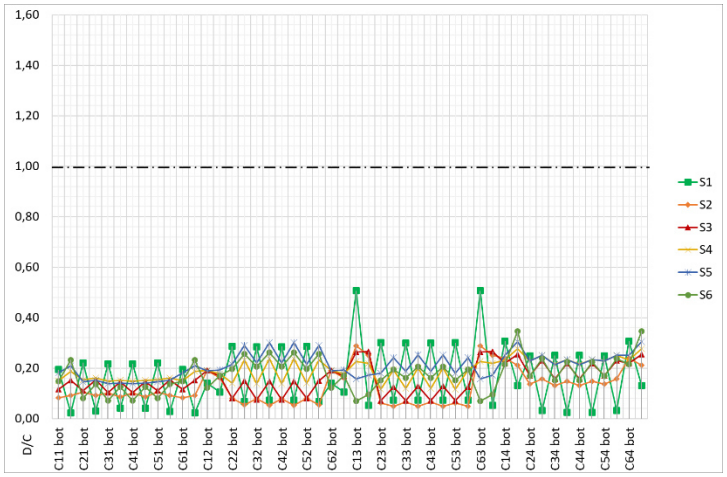

Figure A6.53 – Chord rotation D/C ratios (SD), direction YY (S3_AST1_6S_3×5_YY_RETRO)

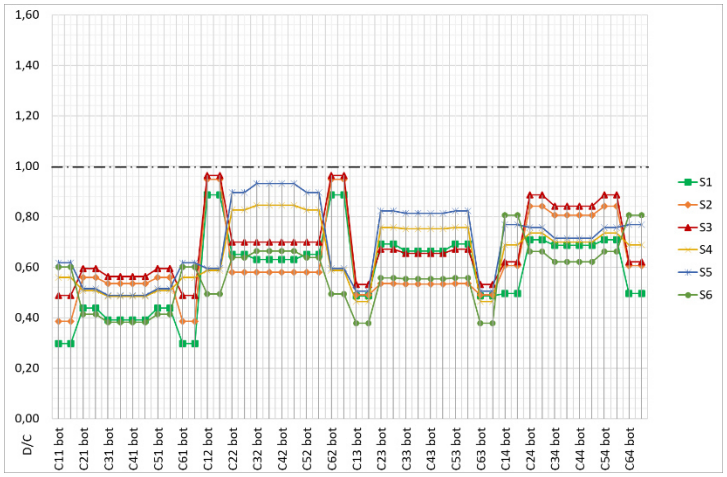

Figure A6.54 – Shear force D/C ratios (SD), direction YY (S3_AST1_6S_3×5_YY_RETRO)

BUILDING TYPE 5: 6 storeys, 3×5 spans **| SEISMIC HAZARD SCENARIO 4:** PT 1.1 + 2.3 (EC8-1)

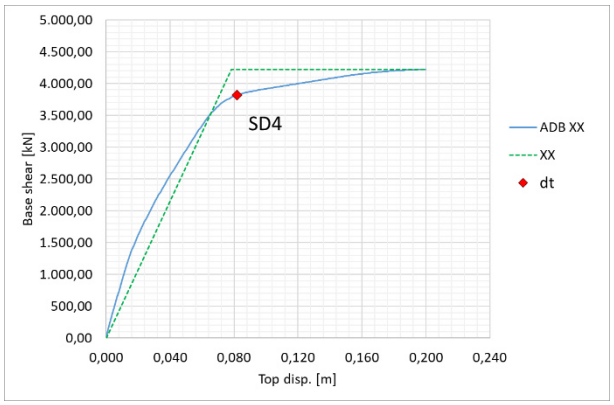

Figure A6.55 – Capacity curve and target displacement d_t, direction XX (S4_AST1_6S_3×5_XX_RETRO)

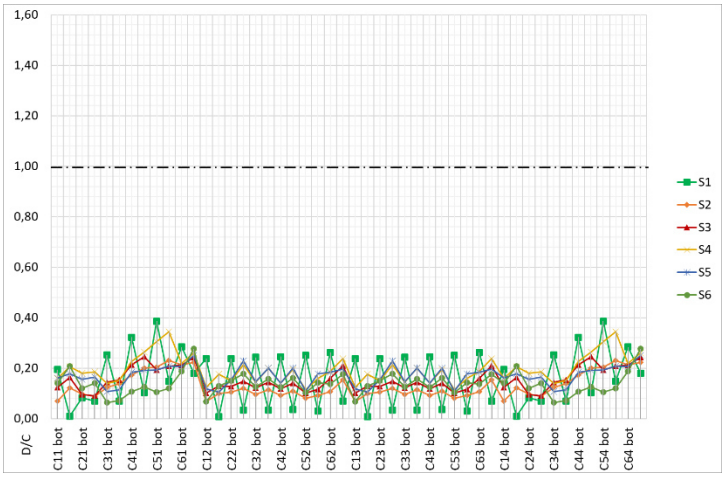

Figure A6.56 – Chord rotation D/C ratios (SD), direction XX (S4_AST1_6S_3×5_XX_RETRO)

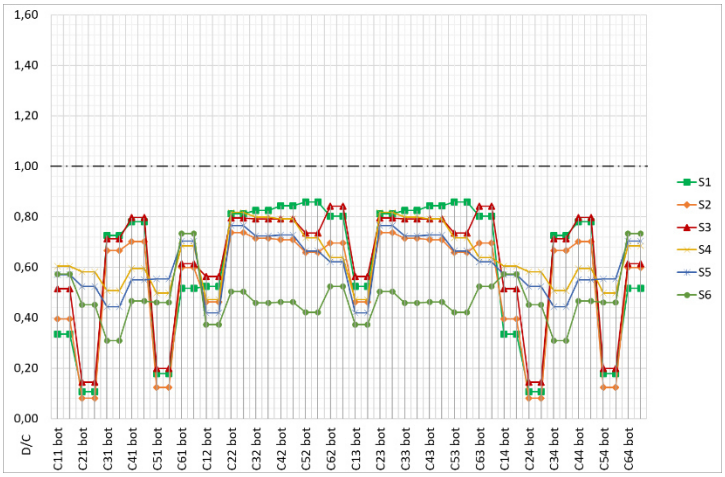

Figure A6.57 – Shear force D/C ratios (SD), direction XX (S4_AST1_6S_3×5_XX_RETRO)

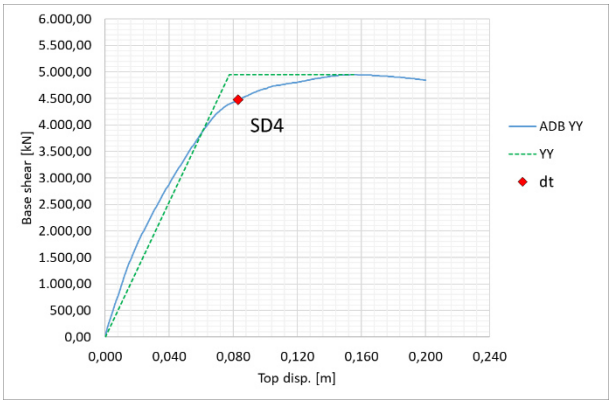

Figure A6.58 – Capacity curve and target displacement d_t, direction YY (S4_AST1_6S_3×5_YY_RETRO)

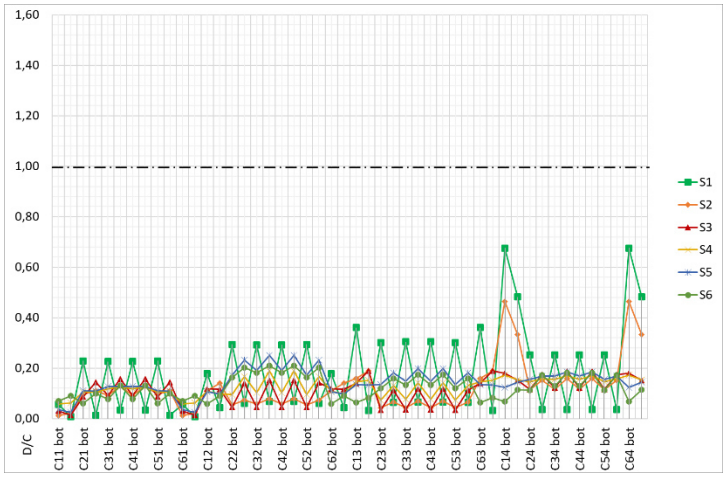

Figure A6.59 – Chord rotation D/C ratios (SD), direction YY (S4_AST1_6S_3×5_YY_RETRO)

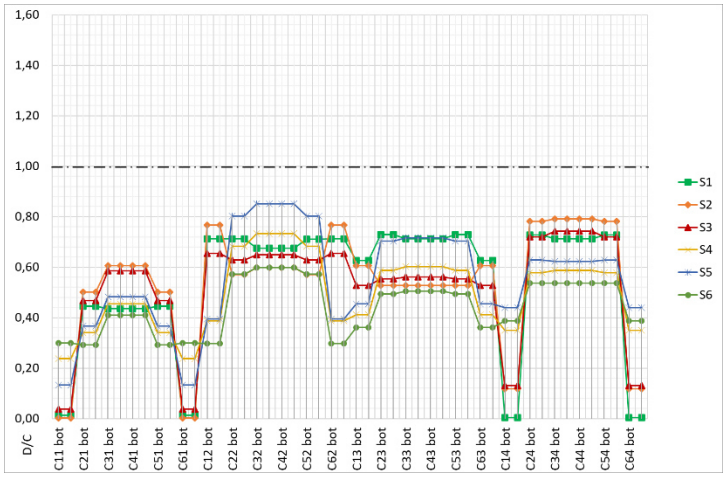

Figure A6.60 – Shear force D/C ratios (SD), direction YY (S4_AST1_6S_3×5_YY_RETRO)

BUILDING TYPE 6: 2 storeys, 2×4 spans **| SEISMIC HAZARD SCENARIO 3:** PT 1.3 + 2.3 (EC8-1)

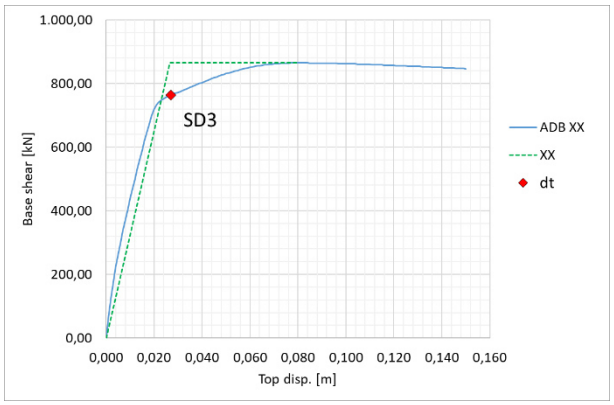

Figure A6.61 – Capacity curve and target displacement d_t, direction XX (S3_AST1_2S_2×4_XX_RETRO)

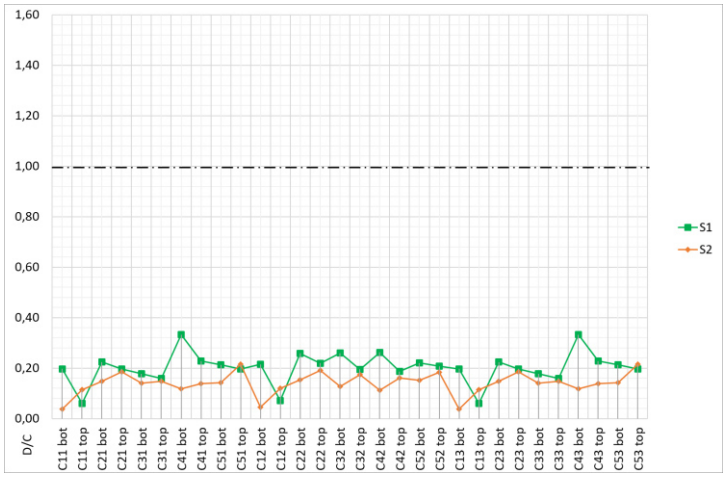

Figure A6.62 – Chord rotation D/C ratios (SD), direction XX (S3_AST1_2S_2×4_XX_RETRO)

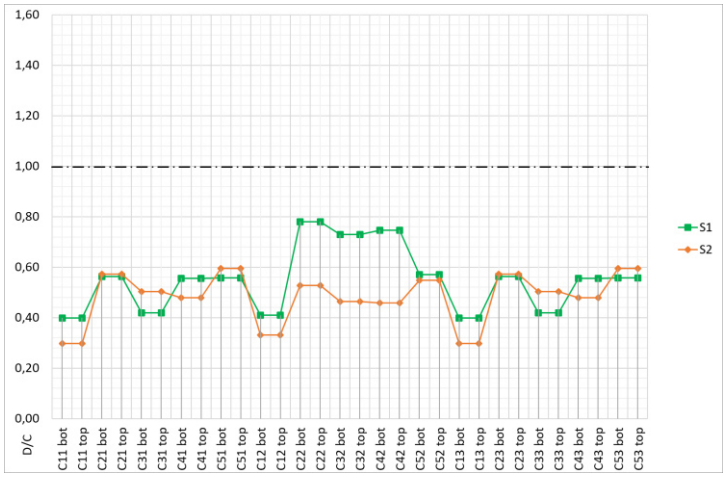

Figure A6.63 – Shear force D/C ratios (SD), direction XX (S3_AST1_2S_2×4_XX_RETRO)

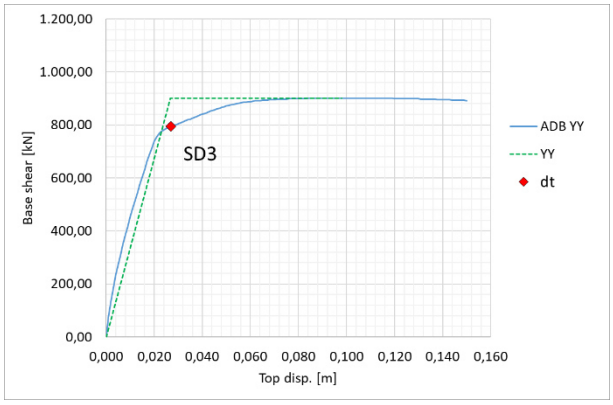

Figure A6.64 – Capacity curve and target displacement d_t, direction YY (S3_AST1_2S_2×4_YY_RETRO)

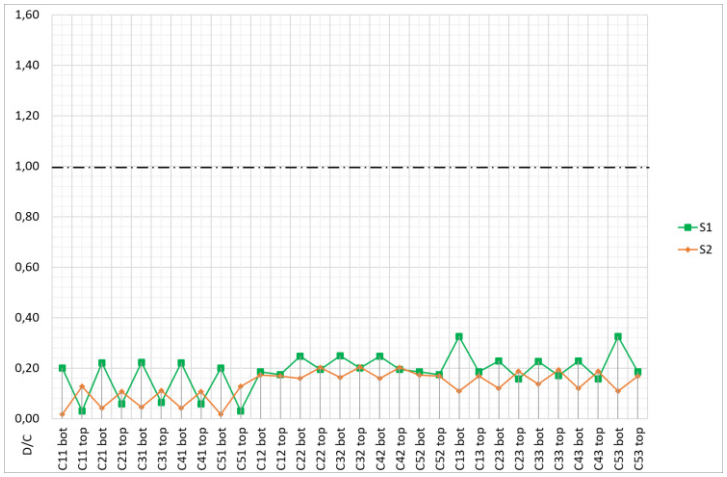

Figure A6.65 – Chord rotation D/C ratios (SD), direction YY (S3_AST1_2S_2×4_YY_RETRO)

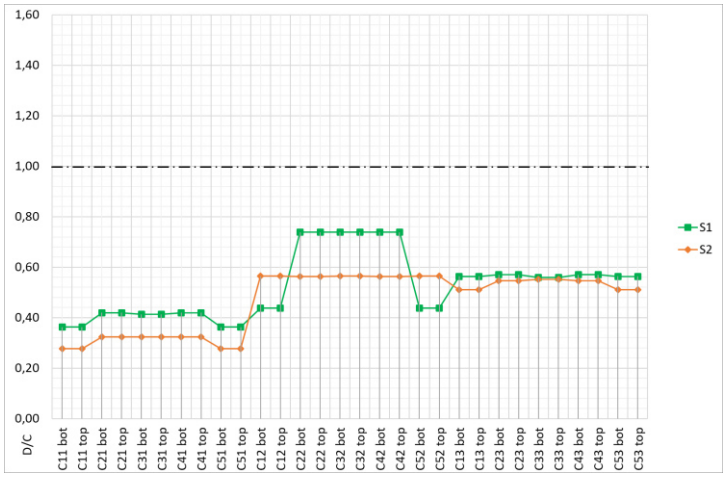

Figure A6.66 – Shear force D/C ratios (SD), direction YY (S3_AST1_2S_2×4_YY_RETRO)

BUILDING TYPE 6: 2 storeys, 2×4 spans **| SEISMIC HAZARD SCENARIO 4:** PT 1.1 + 2.3 (EC8-1)

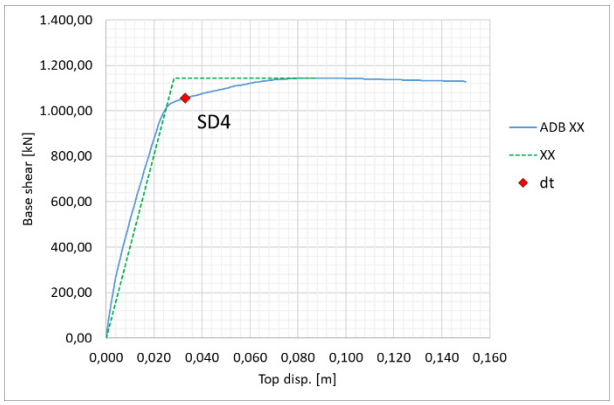

Figure A6.67 – Capacity curve and target displacement d_t, direction XX (S4_AST1_2S_2×4_XX_RETRO)

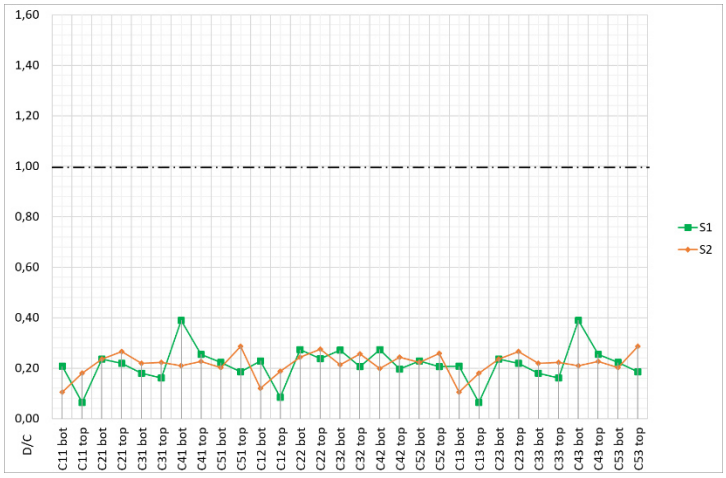

Figure A6.68 – Chord rotation D/C ratios (SD), direction XX (S4_AST1_2S_2×4_XX_RETRO)

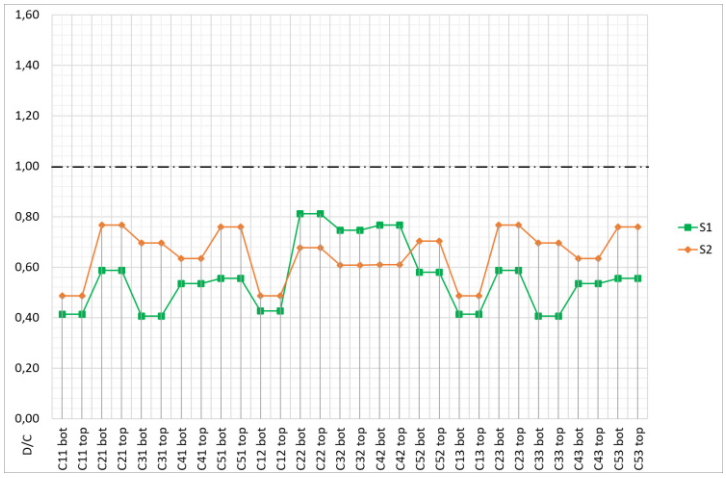

Figure A6.69 – Shear force D/C ratios (SD), direction XX (S4_AST1_2S_2×4_XX_RETRO)

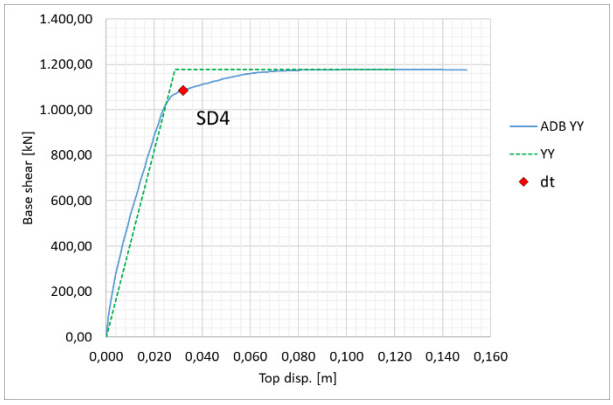

Figure A6.70 – Capacity curve and target displacement d_t, direction YY (S4_AST1_2S_2×4_YY_RETRO)

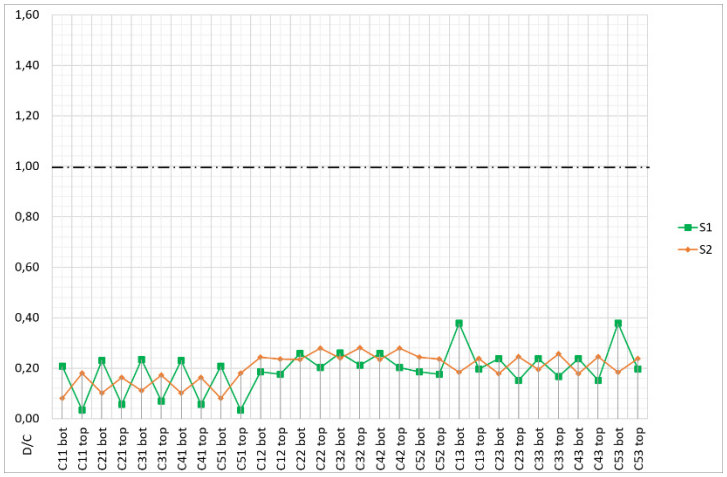

Figure A6.71 – Chord rotation D/C ratios (SD), direction YY (S4_AST1_2S_2×4_YY_RETRO)

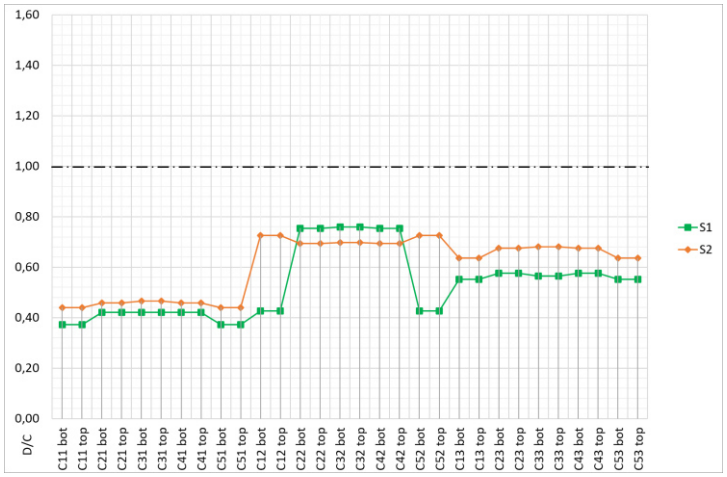

Figure A6.72 – Shear force D/C ratios (SD), direction YY (S4_AST1_2S_2×4_YY_RETRO)

BUILDING TYPE 7: 3 storeys, 2×4 spans **| SEISMIC HAZARD SCENARIO 3:** PT 1.3 + 2.3 (EC8-1)

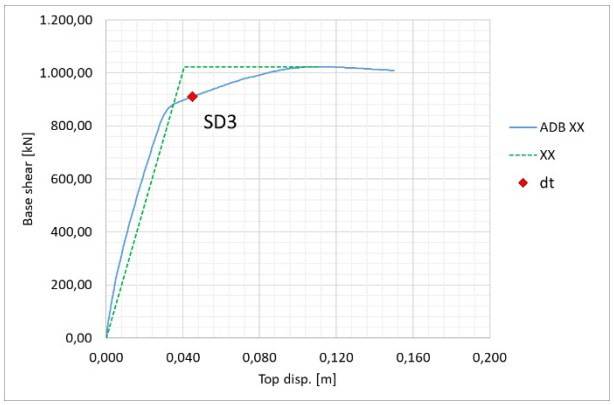

Figure A6.73 – Capacity curve and target displacement d_t, direction XX (S3_AST1_3S_2×4_XX_RETRO)

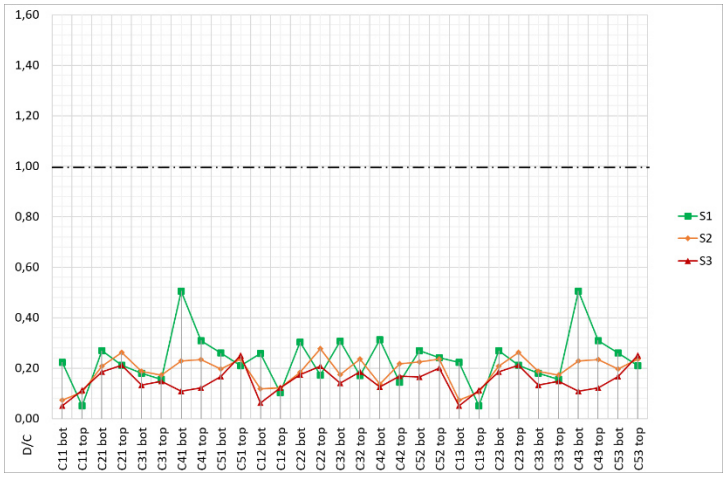

Figure A6.74 – Chord rotation D/C ratios (SD), direction XX (S3_AST1_3S_2×4_XX_RETRO)

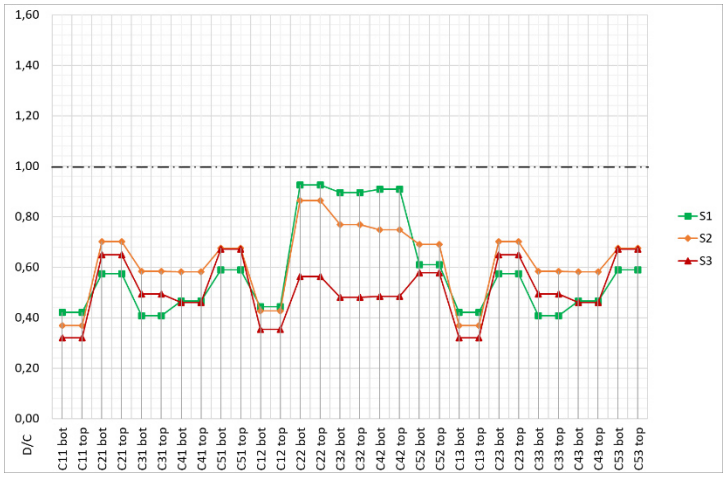

Figure A6.75 – Shear force D/C ratios (SD), direction XX (S3_AST1_3S_2×4_XX_RETRO)

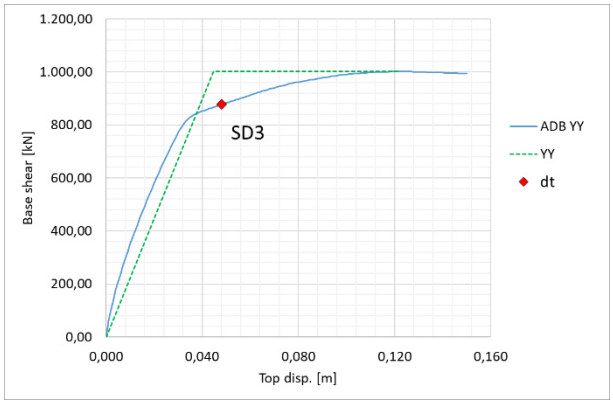

Figure A6.76 – Capacity curve and target displacement d_t, direction YY (S3_AST1_3S_2×4_YY_RETRO)

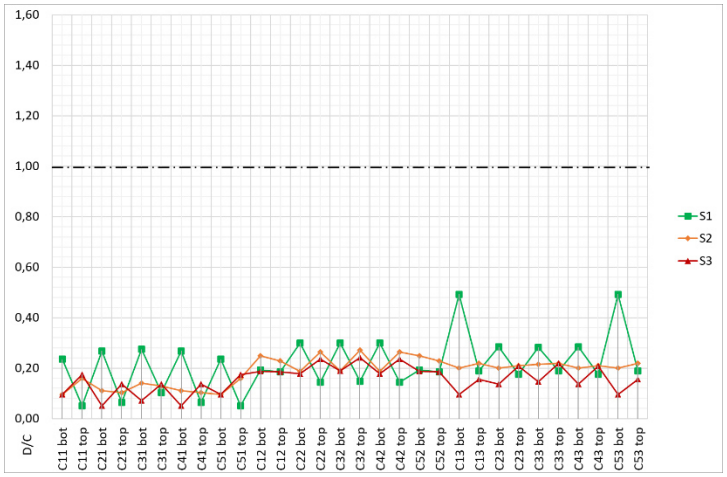

Figure A6.77 – Chord rotation D/C ratios (SD), direction YY (S3_AST1_3S_2×4_YY_RETRO)

Figure A6.78 – Shear force D/C ratios (SD), direction YY (S3_AST1_3S_2×4_YY_RETRO)

BUILDING TYPE 7: 3 storeys, 2×4 spans **| SEISMIC HAZARD SCENARIO 4:** PT 1.1 + 2.3 (EC8-1)

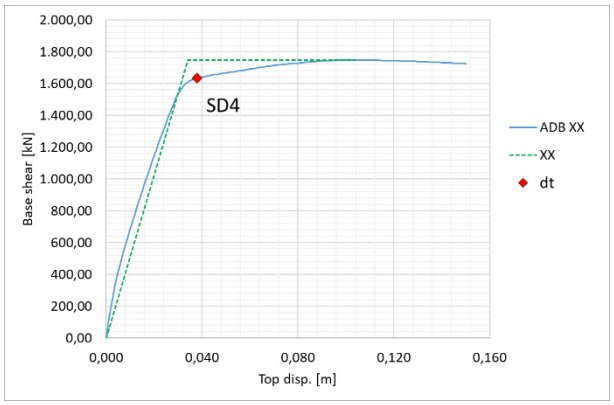

Figure A6.79 – Capacity curve and target displacement d_t, direction XX (S4_AST1_3S_2×4_XX_RETRO)

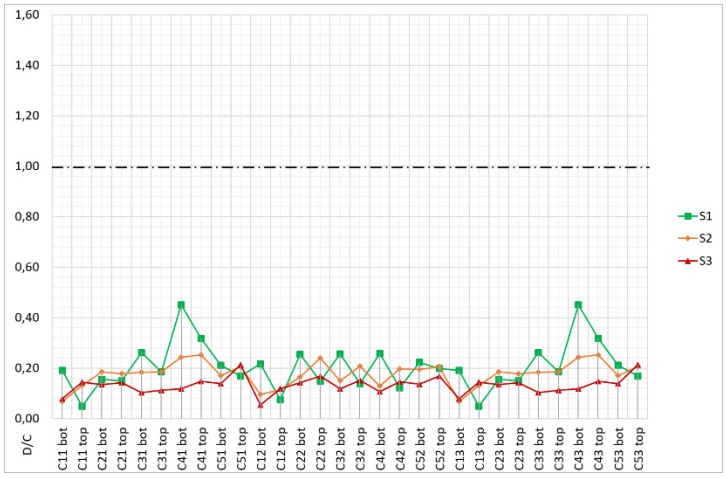

Figure A6.80 – Chord rotation D/C ratios (SD), direction XX (S4_AST1_3S_2×4_XX_RETRO)

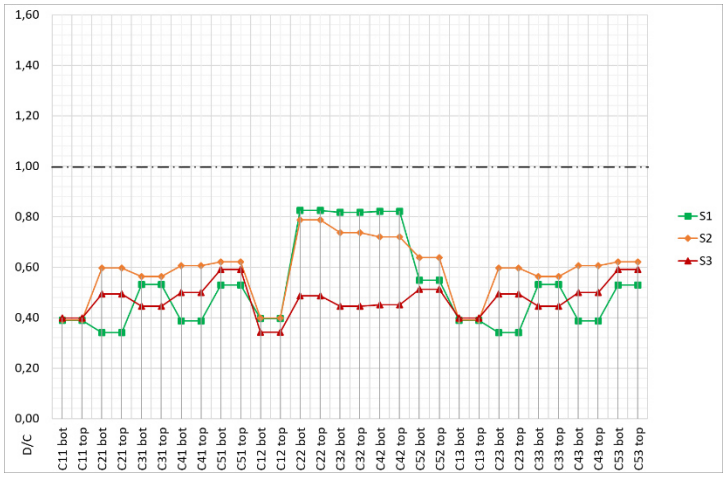

Figure A6.81 – Shear force D/C ratios (SD), direction XX (S4_AST1_3S_2×4_XX_RETRO)

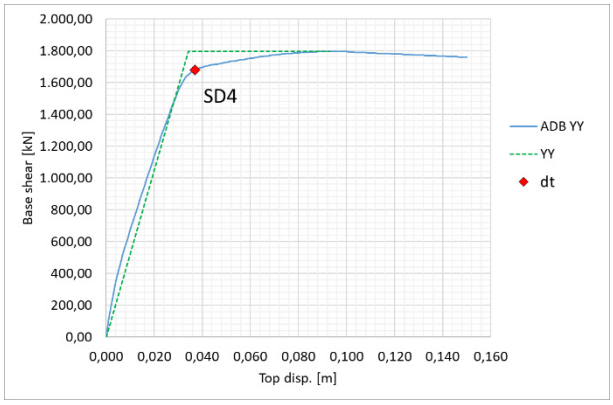

Figure A6.82 – Capacity curve and target displacement d_t, direction YY (S4_AST1_3S_2×4_YY_RETRO)

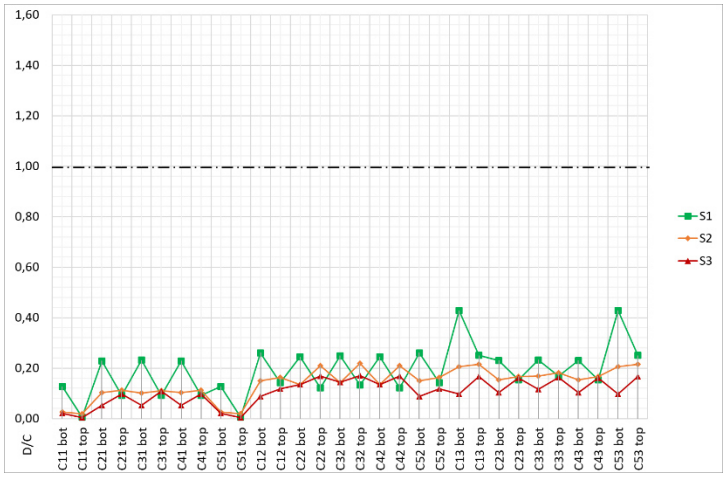

Figure A6.83 – Chord rotation D/C ratios (SD), direction YY (S4_AST1_3S_2×4_YY_RETRO)

Figure A6.84 – Shear force D/C ratios (SD), direction YY (S4_AST1_3S_2×4_YY_RETRO)

BUILDING TYPE 8: 4 storeys, 2×4 spans **| SEISMIC HAZARD SCENARIO 3:** PT 1.3 + 2.3 (EC8-1)

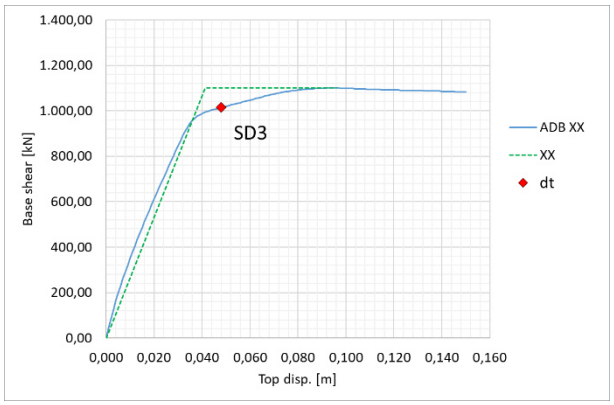

Figure A6.85 – Capacity curve and target displacement d_t, direction XX (S3_AST1_4S_2×4_XX_RETRO)

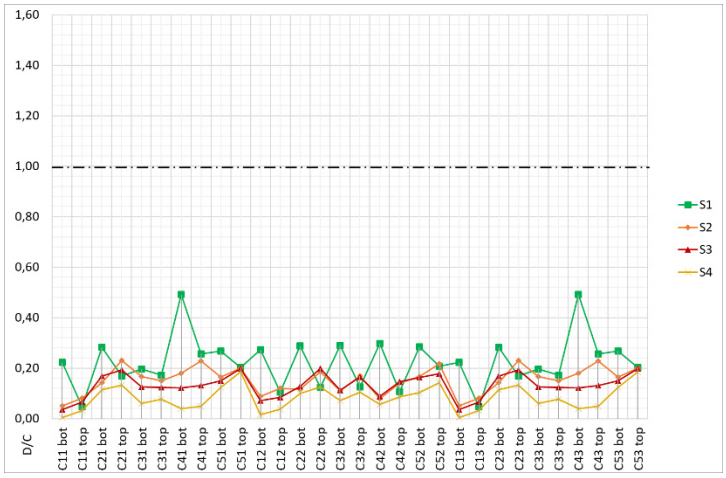

Figure A6.86 – Chord rotation D/C ratios (SD), direction XX (S3_AST1_4S_2×4_XX_RETRO)

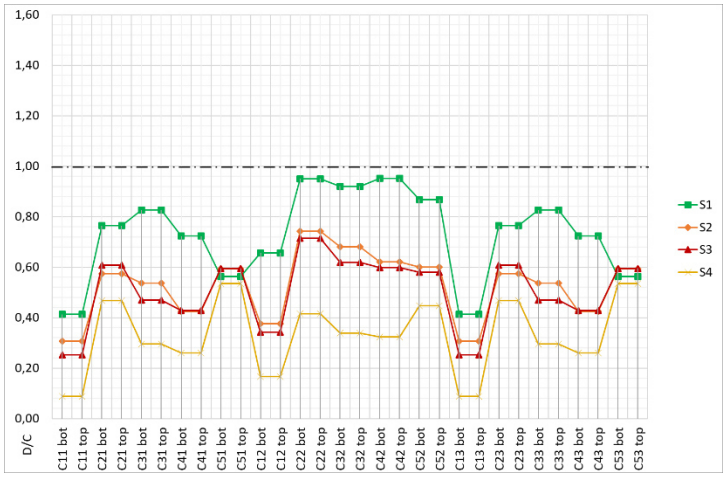

Figure A6.87 – Shear force D/C ratios (SD), direction XX (S3_AST1_4S_2×4_XX_RETRO)

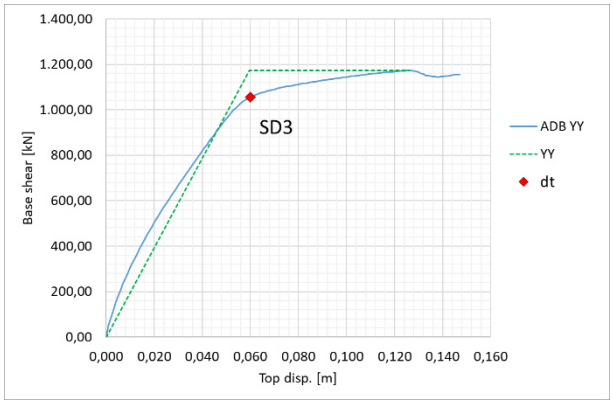

Figure A6.88 – Capacity curve and target displacement d_t, direction YY (S3_AST1_4S_2×4_YY_RETRO)

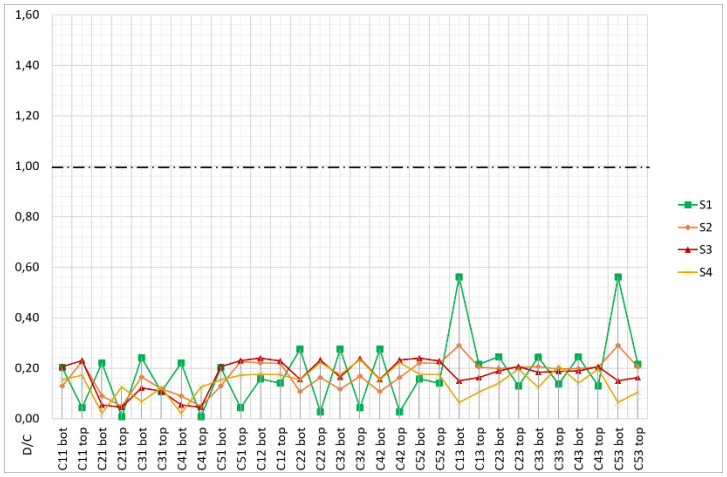

Figure A6.89 – Chord rotation D/C ratios (SD), direction YY (S3_AST1_4S_2×4_YY_RETRO)

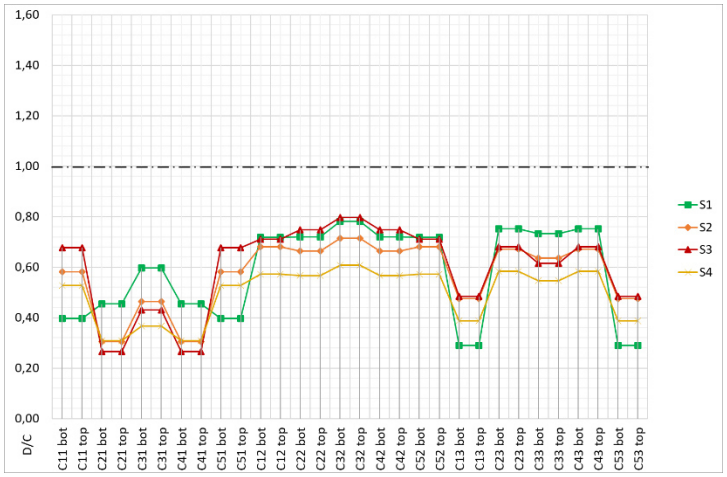

Figure A6.90 – Shear force D/C ratios (SD), direction YY (S3_AST1_4S_2×4_YY_RETRO)

BUILDING TYPE 8: 4 storeys, 2×4 spans **| SEISMIC HAZARD SCENARIO 4:** PT 1.1 + 2.3 (EC8-1)

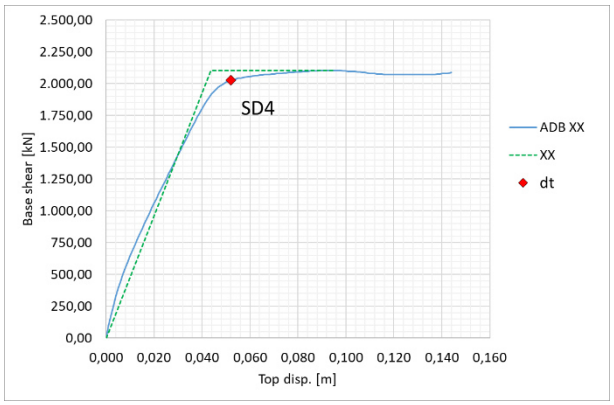

Figure A6.91 – Capacity curve and target displacement d_t, direction XX (S4_AST1_4S_2×4_XX_RETRO)

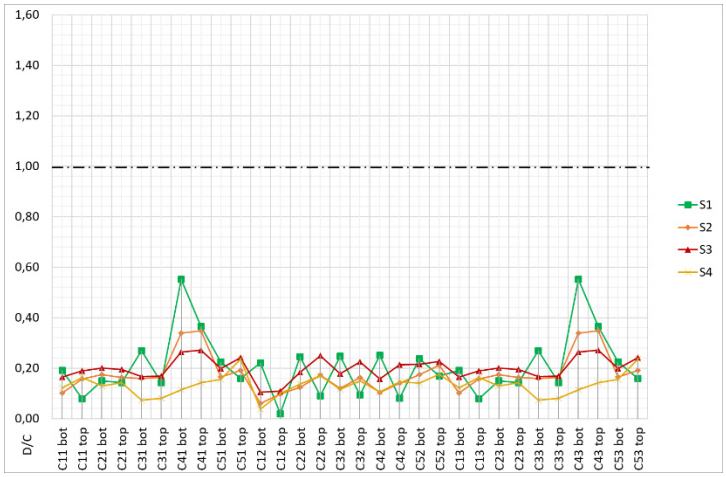

Figure A6.92 – Chord rotation D/C ratios (SD), direction XX (S4_AST1_4S_2×4_XX_RETRO)

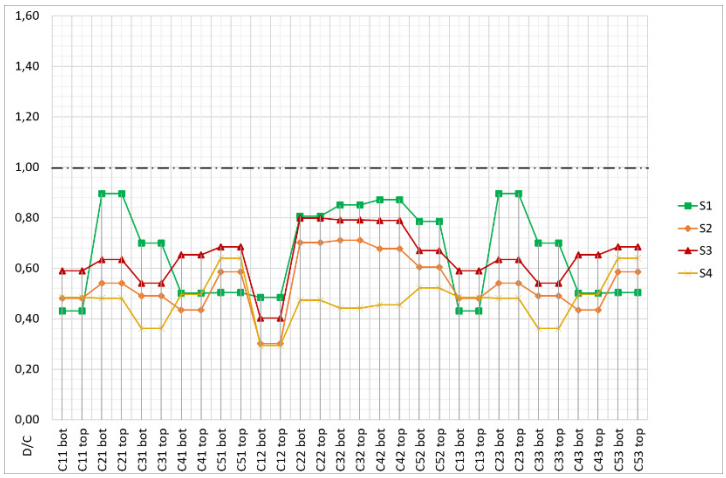

Figure A6.93 – Shear force D/C ratios (SD), direction XX (S4_AST1_4S_2×4_XX_RETRO)

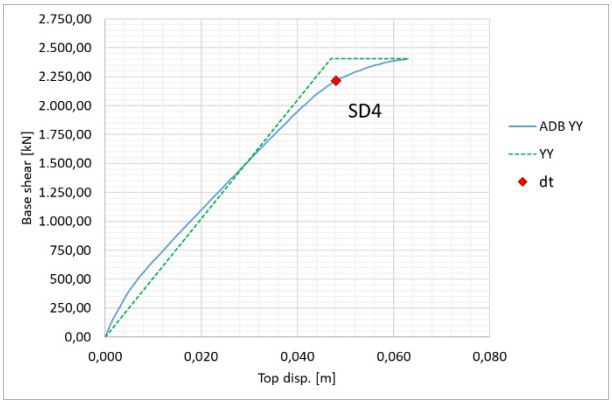

Figure A6.94 – Capacity curve and target displacement d_t, direction YY (S4_AST1_4S_2×4_YY_RETRO)

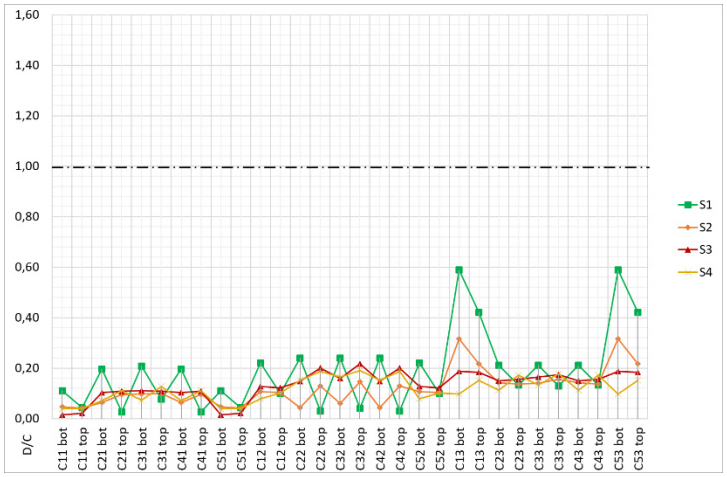

Figure A6.95 – Chord rotation D/C ratios (SD), direction YY (S4_AST1_4S_2×4_YY_RETRO)

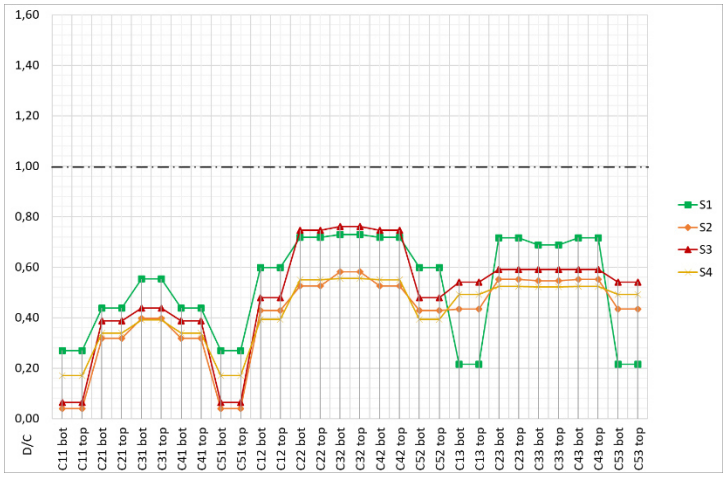

Figure A6.96 – Shear force D/C ratios (SD), direction YY (S4_AST1_4S_2×4_YY_RETRO)

BUILDING TYPE 9: 5 storeys, 2×4 spans **| SEISMIC HAZARD SCENARIO 3:** PT 1.3 + 2.3 (EC8-1)

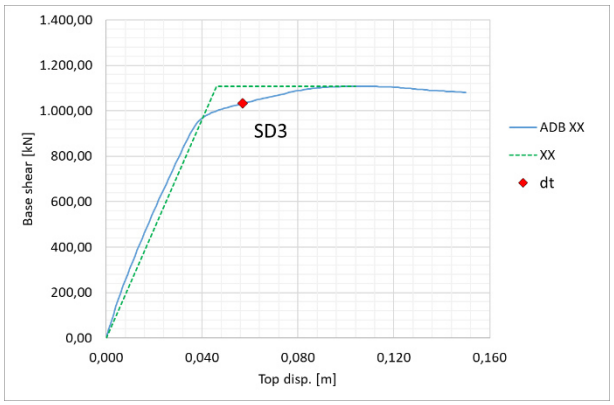

Figure A6.97 – Capacity curve and target displacement d_t, direction XX (S3_AST1_5S_2×4_XX_RETRO)

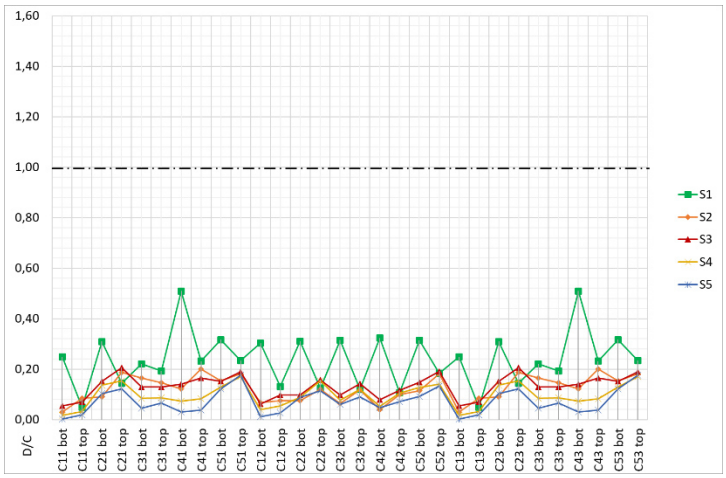

Figure A6.98 – Chord rotation D/C ratios (SD), direction XX (S3_AST1_5S_2×4_XX_RETRO)

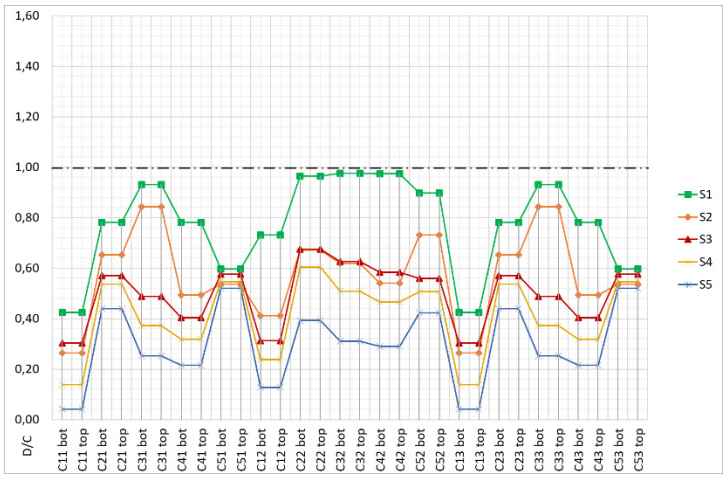

Figure A6.99 – Shear force D/C ratios (SD), direction XX (S3_AST1_5S_2×4_XX_RETRO)

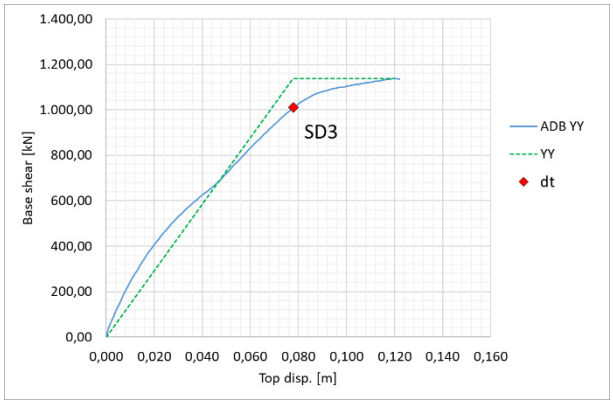

Figure A6.100 – Capacity curve and target displacement d_t, direction YY (S3_AST1_5S_2×4_YY_RETRO)

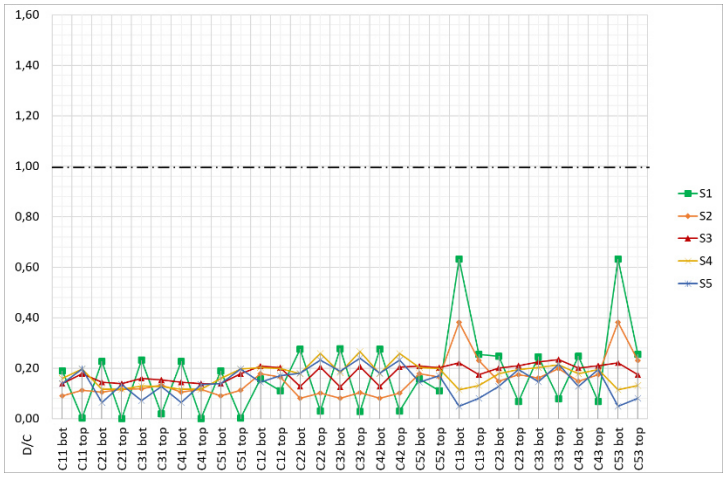

Figure A6.101 – Chord rotation D/C ratios (SD), direction YY (S3_AST1_5S_2×4_YY_RETRO)

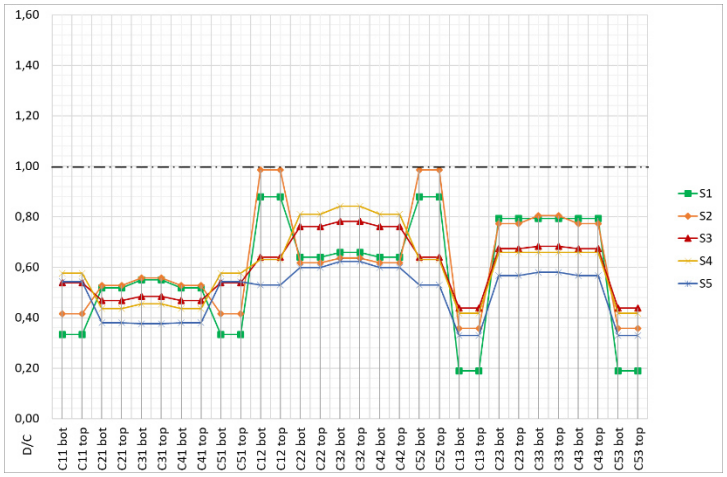

Figure A6.102 – Shear force D/C ratios (SD), direction YY (S3_AST1_5S_2×4_YY_RETRO)

BUILDING TYPE 9: 5 storeys, 2×4 spans **| SEISMIC HAZARD SCENARIO 4:** PT 1.1 + 2.3 (EC8-1)

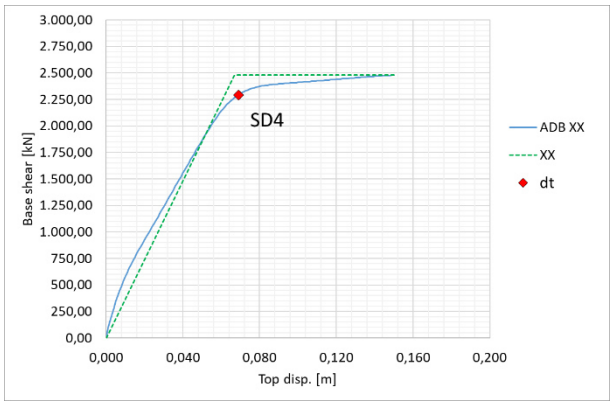

Figure A6.103 – Capacity curve and target displacement d_t, direction XX (S4_AST1_5S_2×4_XX_RETRO)

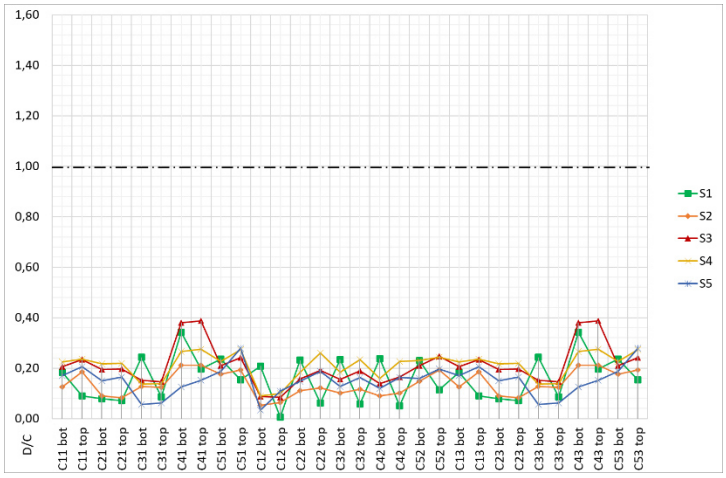

Figure A6.104 – Chord rotation D/C ratios (SD), direction XX (S4_AST1_5S_2×4_XX_RETRO)

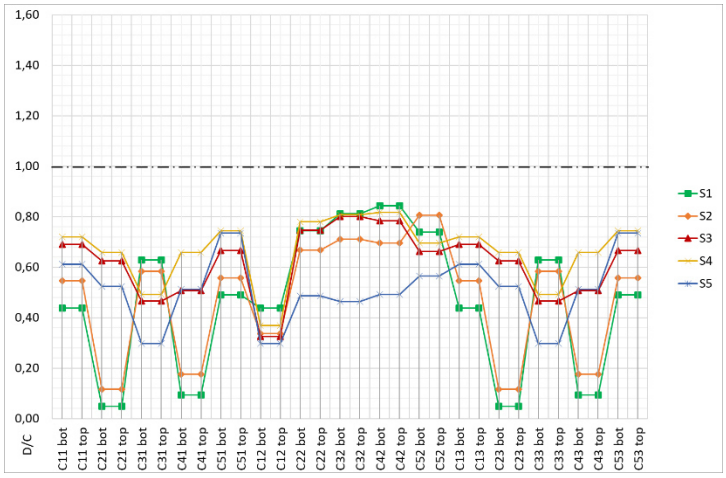

Figure A6.105 – Shear force D/C ratios (SD), direction XX (S4_AST1_5S_2×4_XX_RETRO)

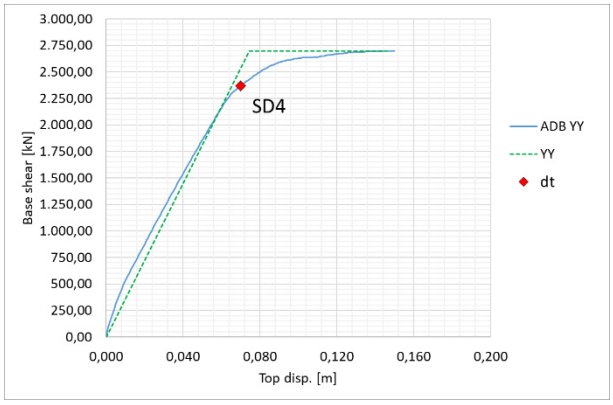

Figure A6.106 – Capacity curve and target displacement d_t, direction YY (S4_AST1_5S_2×4_YY_RETRO)

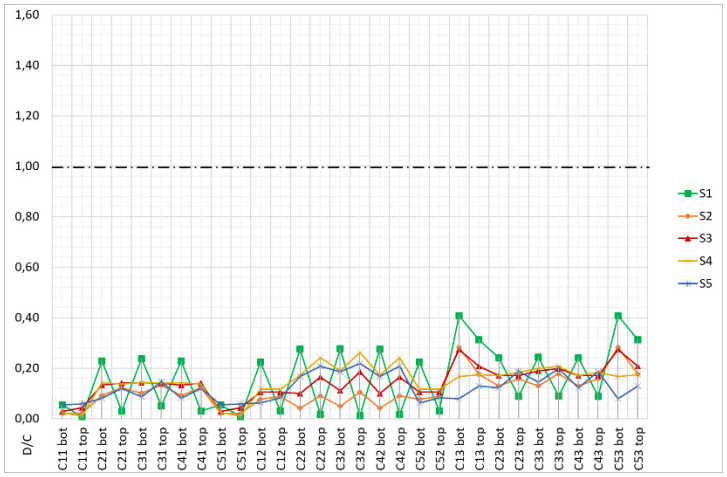

Figure A6.107 – Chord rotation D/C ratios (SD), direction YY (S4_AST1_5S_2×4_YY_RETRO)

Figure A6.108 – Shear force D/C ratios (SD), direction YY (S4_AST1_5S_2×4_YY_RETRO)

BUILDING TYPE 10: 6 storeys, 2×4 spans **| SEISMIC HAZARD SCENARIO 3:** PT 1.3 + 2.3 (EC8-1)

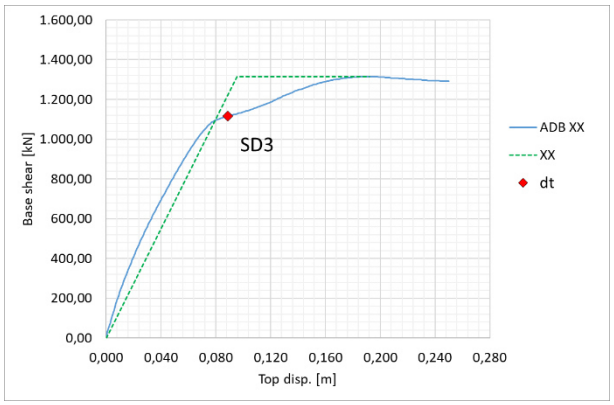

Figure A6.109 – Capacity curve and target displacement d_t, direction XX (S3_AST1_6S_2×4_XX_RETRO)

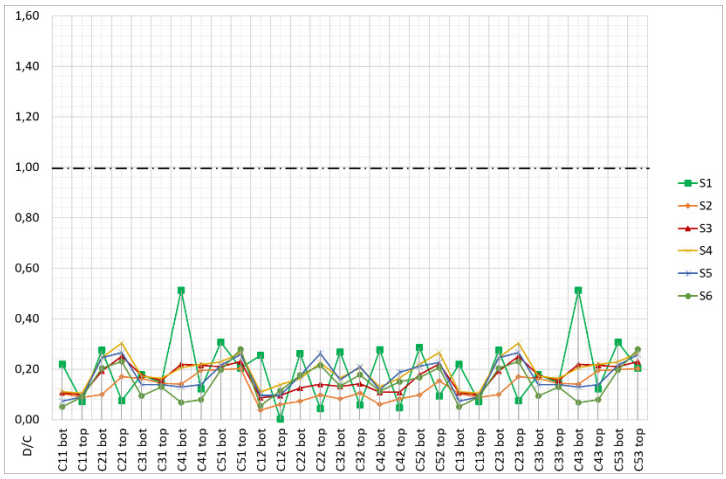

Figure A6.110 – Chord rotation D/C ratios (SD), direction XX (S3_AST1_6S_2×4_XX_RETRO)

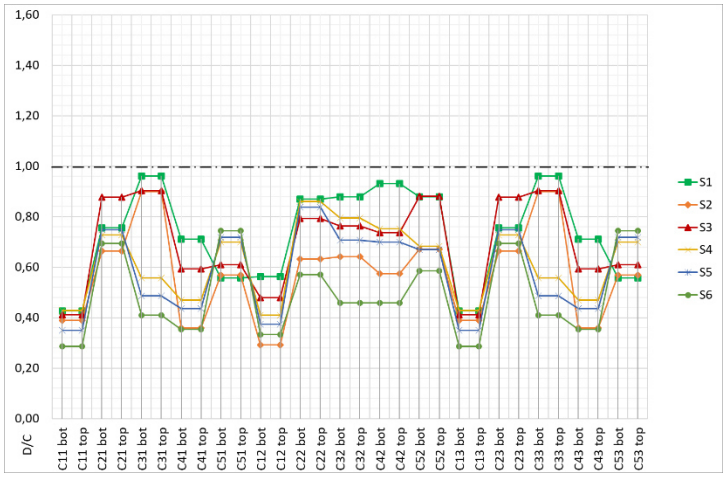

Figure A6.111 – Shear force D/C ratios (SD), direction XX (S3_AST1_6S_2×4_XX_RETRO)

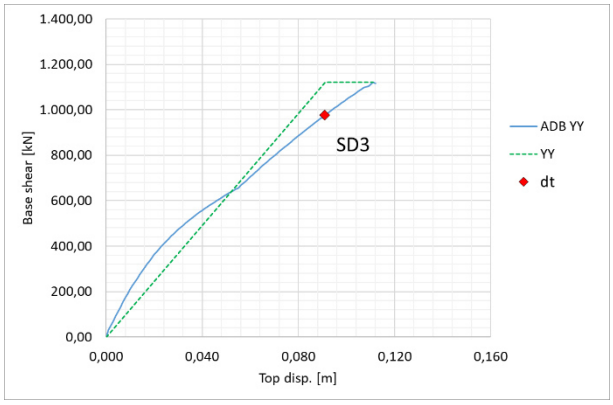

Figure A6.112 – Capacity curve and target displacement d_t, direction YY (S3_AST1_6S_2×4_YY_RETRO)

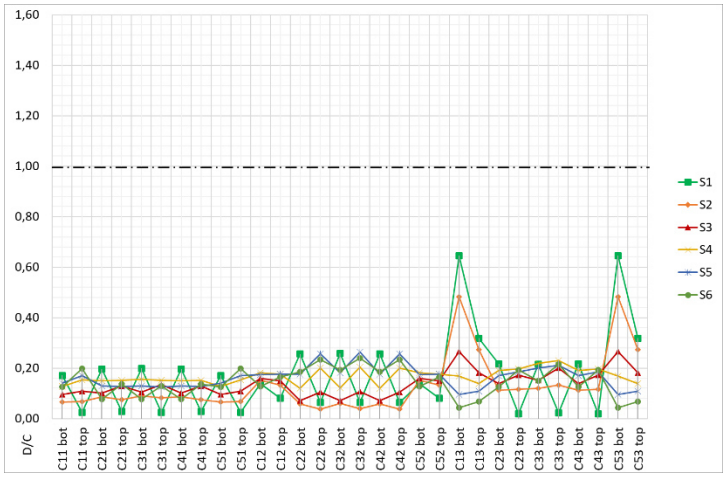

Figure A6.113 – Chord rotation D/C ratios (SD), direction YY (S3_AST1_6S_2×4_YY_RETRO)

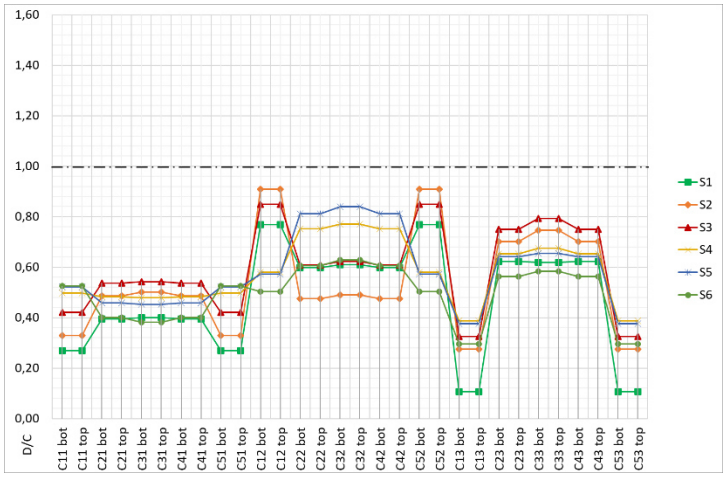

Figure A6.114 – Shear force D/C ratios (SD), direction YY (S3_AST1_6S_2×4_YY_RETRO)

BUILDING TYPE 10: 6 storeys, 2×4 spans **| SEISMIC HAZARD SCENARIO 4:** PT 1.1 + 2.3 (EC8-1)

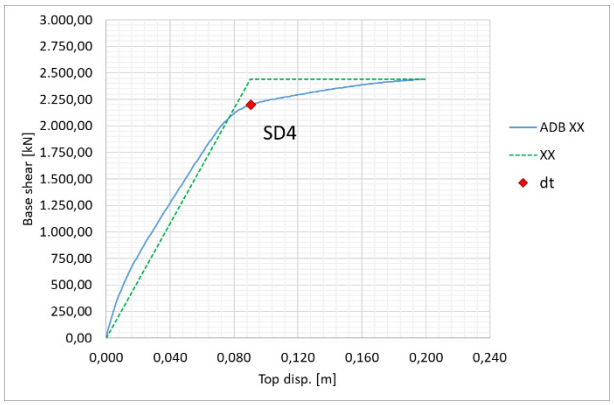

Figure A6.115 – Capacity curve and target displacement d_t, direction XX (S4_AST1_6S_2×4_XX_RETRO)

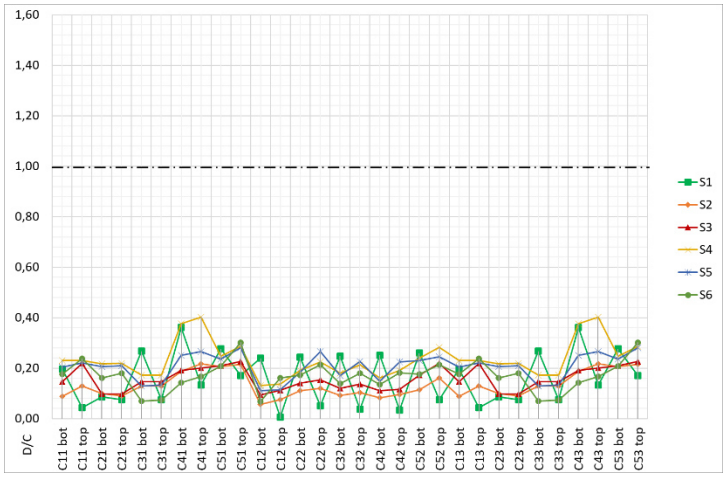

Figure A6.116 – Chord rotation D/C ratios (SD), direction XX (S4_AST1_6S_2×4_XX_RETRO)

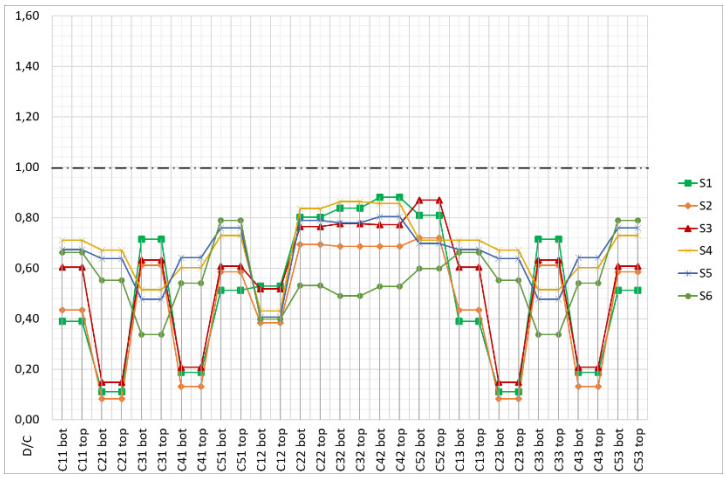

Figure A6.117 – Shear force D/C ratios (SD), direction XX (S4_AST1_6S_2×4_XX_RETRO)

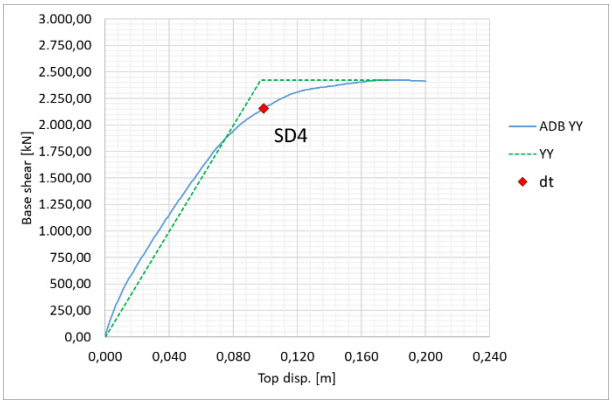

Figure A6.118 – Capacity curve and target displacement d_t, direction YY (S4_AST1_6S_2×4_YY_RETRO)

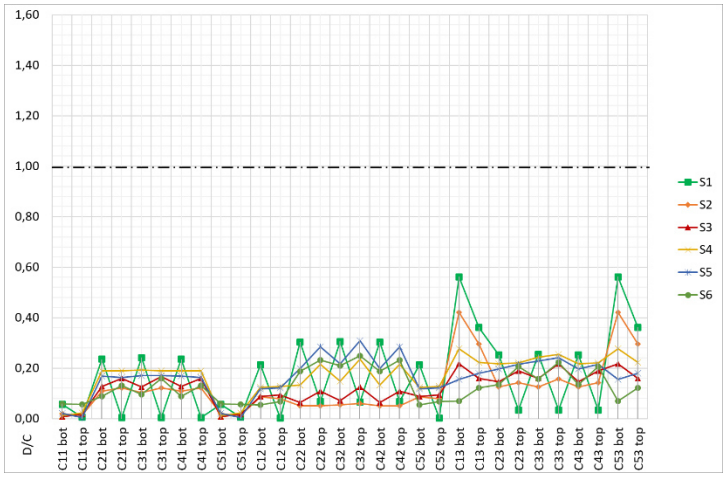

Figure A6.119 – Chord rotation D/C ratios (SD), direction YY (S4_AST1_6S_2×4_YY_RETRO)

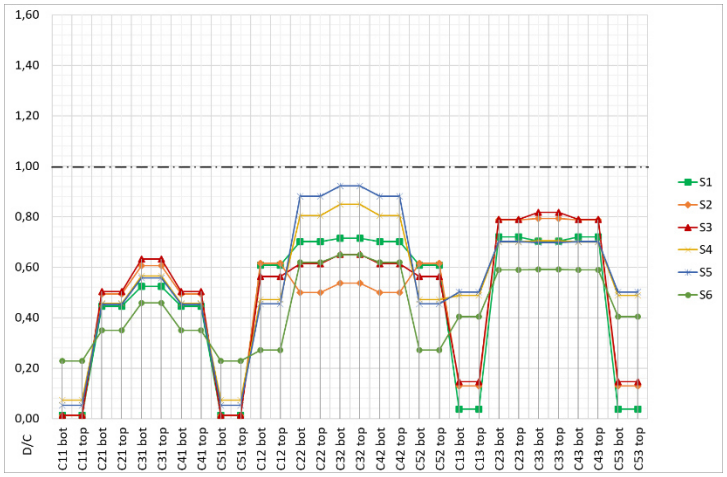

Figure A6.120 – Shear force D/C ratios (SD), direction YY (S4_AST1_6S_2×4_YY_RETRO)

APPENDIX 7

GROUND MOTION RECORD SETS

APPENDIX 7 – GROUND MOTION RECORD SETS

Selection of 40 ground motion records for the Lisbon Region (hazard scenario S3)

Selection of 40 ground motion records for the West Algarve Region (hazard scenario S4)

Table A7.1 – Ground motion records for the Lisbon Region (1/2)

Event	Year	M_w	Epicentral distance [*km*]	Hypocenter distance [*km*]	Campbell distance [*km*]	Closest distance to fault rupture [*km*]	Joyner-Boore distance [*km*]	$V_{s,30}$ [*m/s*]	Lowest useable freq, [Hz]	Rake angle [°]	PGA [*g*]
Imperial Valley-02	1940	6,95	12,99	15,69	7,51	6,09	6,09	213,40	0,25	180,00	0,31
Imperial Valley-02	1940	6,95	12,99	15,69	7,51	6,09	6,09 2	13,40	0,25	180,00	0,21
Kern County	1952	7,36	43,49	46,21	38,89	38,89	38,42	385,40	0,06	61,00	0,16
Kern County	1952	7,36	43,49	46,21	38,89	38,89	38,42	385,40	0,06	61,00	0,18
Coyote Lake	1979	5,74	23,24	24,58	19,70	19,70	19,46	370,80	0,25	176,00	0,11
Imperial Valley-06	1979	6,53	43,15	44,29	10,57	10,42	8,54	208,70	0,13	180,00	0,22
Imperial Valley-06	1979	6,53	24,82	26,74	16,06	15,19	15,19	659,60	0,13	180,00	0,16
Imperial Valley-06	1979	6,53	33,73	35,17	22,54	22,03	22,03	274,50	0,06	180,00	0,35
Imperial Valley-06	1979	6,53	31,99	33,50	18,85	17,94	17,94	196,90	0,13	180,00	0,14
Irpinia, Italy-01	1980	6,90	22,65	24,56	10,76	8,18	8,14	1000,00	0,13	-90,00	0,14
Coalinga-01	1983	6,36	37,97	38,25	29,38	29,38	28,00	376,10	0,25	90,00	0,12
Morgan Hill	1984	6,19	38,20	39,13	13,35	13,02	13,01	349,90	0,13	180,00	0,20
Taiwan SMART1(40)	1986	6,32	65,48	67,36	-	-	-	274,50	0,25	100,00	0,18
N. Palm Springs	1986	6,06	21,14	23,83	10,84	10,84	10,08	207,50	0,25	150,00	0,16
Superstition Hills-02	1987	6,54	29,91	31,24	17,37	17,03	17,03	208,70	0,16	180,00	0,16
Superstition Hills-02	1987	6,54	19,28	21,27	18,79	18,48	18,48	207,50	0,19	180,00	0,12
Loma Prieta	1989	6,93	30,78	35,40	20,34	20,34	19,97	597,10	0,13	140,00	0,15
Loma Prieta	1989	6,93	54,54	57,27	39,51	39,51	39,32	367,60	0,25	140,00	0,12
Loma Prieta	1989	6,93	20,13	26,66	14,69	14,69	14,18	671,80	0,06	140,00	0,23
Loma Prieta	1989	6,93	27,23	32,35	8,50	8,50	7,58	370,80	0,13	140,00	0,51

Table A7.1 – Ground motion records for the Lisbon Region (2/2)

Event	Year	M_w	Epicentral distance [*km*]	Hypocenter distance [*km*]	Campbell distance [*km*]	Closest distance to fault rupture [*km*]	Joyner-Boore distance [*km*]	$V_{s,30}$ [*m/s*]	Lowest useable freq, [Hz]	Rake angle [°]	PGA [*g*]
Landers	1992	7,28	27,33	28,21	21,98	21,78	21,78	345,40	0,07	180,00	0,17
Landers	1992	7,28	59,68	60,09	54,34	54,25	54,25	345,40	0,10	180,00	0,10
Northridge-01	1994	6,69	48,32	51,40	40,34	40,34	34,78	234,90	0,10	103,00	0,12
Northridge-01	1994	6,69	48,32	51,40	40,34	40,34	34,78	234,90	0,10	103,00	0,12
Northridge-01	1994	6,69	17,95	25,07	22,50	22,50	12,92	416,60	0,12	103,00	0,19
Northridge-01	1994	6,69	23,61	29,39	24,03	24,03	19,73	316,50	0,20	103,00	0,23
Northridge-01	1994	6,69	31,73	36,24	31,33	31,33	27,82	270,20	0,20	103,00	0,19
Northridge-01	1994	6,69	32,72	37,11	31,48	31,48	28,82	376,10	0,20	103,00	0,13
Northridge-01	1994	6,69	32,72	37,11	31,48	31,48	28,82	376,10	0,20	103,00	0,18
Northridge-01	1994	6,69	29,59	34,38	29,74	29,74	25,60	405,20	0,16	103,00	0,16
Northridge-01	1994	6,69	19,55	26,24	23,60	23,60	14,55	392,20	0,12	103,00	0,25
Northridge-01	1994	6,69	22,45	28,47	26,45	26,45	17,28	336,20	0,14	103,00	0,37
Northridge-01	1994	6,69	24,13	29,81	13,35	13,35	12,38	446,00	0,06	103,00	0,13
Chi-Chi, Taiwan	1999	7,62	55,23	55,80	25,88	24,11	24,11	442,20	0,05	55,00	0,18
Chi-Chi, Taiwan	1999	7,62	68,78	69,24	37,92	37,48	37,48	272,60	0,05	55,00	0,14
Chi-Chi, Taiwan	1999	7,62	69,29	69,75	49,15	49,15	44,89	473,90	0,03	55,00	0,12
Hector Mine	1999	7,13	47,97	50,20	43,05	43,05	41,82	271,40	0,08	179,00	0,15
Chi-Chi, Taiwan-03	1999	6,20	31,85	32,79	24,38	24,38	23,44	542,60	0,10	80,00	0,14
Chi-Chi, Taiwan-04	1999	6,20	50,36	53,48	50,14	50,04	50,02	228,70	0,25	15,00	0,10
Chi-Chi, Taiwan-06	1999	6,30	58,32	60,47	41,58	41,58	40,36	473,90	0,25	100,00	0,16

Table A7.2 – Ground motion records for the West Algarve Region (1/2)

Event	Year	M_w	Epicentral distance [*km*]	Hypocenter distance [*km*]	Campbell distance [*km*]	Closest distance to fault rupture [*km*]	Joyner-Boore distance [*km*]	$V_{s,30}$ [*m/s*]	Lowest useable freq, [Hz]	Rake angle [°]	PGA [*g*]
Imperial Valley-02	1940	6,95	12,99	15,69	7,51	6,09	6,09	213,40	0,25	180,00	0,21
Imperial Valley-02	1940	6,95	12,99	15,69	7,51	6,09	6,09	213,40	0,25	180,00	0,31
Kern County	1952	7,36	43,49	46,21	38,89	38,89	38,42	385,40	0,06	61,00	0,16
Kern County	1952	7,36	43,49	46,21	38,89	38,89	38,42	385,40	0,06	61,00	0,18
Imperial Valley-06	1979	6,53	33,73	35,17	22,54	22,03	22,03	274,50	0,06	180,00	0,24
Imperial Valley-06	1979	6,53	27,13	28,90	7,38	7,05	4,90	208,90	0,13	180,00	0,49
Imperial Valley-06	1979	6,53	24,82	26,74	16,06	15,19	15,19	659,60	0,13	180,00	0,16
Imperial Valley-06	1979	6,53	43,15	44,29	10,57	10,42	8,54	208,70	0,13	180,00	0,22
Irpinia, Italy-02	1980	6,20	11,97	13,87	10,55	8,83	8,81	600,00	0,25	-90,00	0,16
Coalinga-01	1983	6,36	55,67	55,86	44,72	44,72	43,83	184,80	0,25	90,00	0,11
Coalinga-01	1983	6,36	37,97	38,25	29,38	29,38	28,00	376,10	0,25	90,00	0,12
Morgan Hill	1984	6,19	38,20	39,13	13,35	13,02	13,01	349,90	0,13	180,00	0,20
Taiwan SMART1(40)	1986	6,32	65,48	67,36	-	-	-	274,50	0,25	100,00	0,18
Superstition Hills-02	1987	6,54	29,91	31,24	17,37	17,03	17,03	208,70	0,16	180,00	0,16
Superstition Hills-02	1987	6,54	35,83	36,94	18,52	18,20	18,20	192,10	0,13	180,00	0,36
Superstition Hills-02	1987	6,54	19,28	21,27	18,79	18,48	18,48	207,50	0,19	180,00	0,12
Loma Prieta	1989	6,93	55,16	57,86	39,85	39,85	39,66	284,80	0,13	140,00	0,19
Loma Prieta	1989	6,93	54,54	57,27	39,51	39,51	39,32	367,60	0,25	140,00	0,12
Loma Prieta	1989	6,93	20,13	26,66	14,69	14,69	14,18	671,80	0,06	140,00	0,23
Loma Prieta	1989	6,93	18,46	25,42	3,88	3,88	0,00	477,70	0,13	140,00	0,59

Table A7.2 – Ground motion records for the West Algarve Region (2/2)

Event	Year	M_w	Epicentral distance [*km*]	Hypocenter distance [*km*]	Campbell distance [*km*]	Closest distance to fault rupture [*km*]	Joyner-Boore distance [*km*]	$V_{s,30}$ [*m/s*]	Lowest useable freq, [Hz]	Rake angle [°]	PGA [*g*]
Loma Prieta	1989	6,93	35,47	39,54	18,33	18,33	17,92	663,30	0,25	140,00	0,13
Loma Prieta	1989	6,93	30,78	35,40	20,34	20,34	19,97	597,10	0,13	140,00	0,15
Landers	1992	7,28	75,20	75,53	69,27	69,21	69,21	271,40	0,10	180,00	0,15
Landers	1992	7,28	27,33	28,21	21,98	21,78	21,78	345,40	0,07	180,00	0,17
Northridge-01	1994	6,69	24,13	29,81	13,35	13,35	12,38	446,00	0,06	103,00	0,13
Northridge-01	1994	6,69	29,59	34,38	29,74	29,74	25,60	405,20	0,16	103,00	0,16
Northridge-01	1994	6,69	19,55	26,24	23,60	23,60	14,55	392,20	0,12	103,00	0,25
Northridge-01	1994	6,69	20,22	26,74	23,41	23,41	15,54	278,00	0,14	103,00	0,22
Northridge-01	1994	6,69	48,32	51,40	40,34	40,34	34,78	234,90	0,10	103,00	0,12
Northridge-01	1994	6,69	25,44	30,88	28,30	28,30	20,36	234,90	0,25	103,00	0,32
Northridge-01	1994	6,69	17,95	25,07	22,50	22,50	12,92	416,60	0,12	103,00	0,19
Northridge-01	1994	6,69	31,73	36,24	31,33	31,33	27,82	270,20	0,20	103,00	0,10
Northridge-01	1994	6,69	31,73	36,24	31,33	31,33	27,82	270,20	0,20	103,00	0,19
Kobe, Japan	1995	6,90	45,97	49,33	28,49	19,15	19,14	256,00	0,13	180,00	0,21
Chi-Chi, Taiwan	1999	7,62	55,23	55,80	25,88	24,11	24,11	442,20	0,05	55,00	0,18
Chi-Chi, Taiwan	1999	7,62	68,78	69,24	37,92	37,48	37,48	272,60	0,05	55,00	0,14
Chi-Chi, Taiwan	1999	7,62	38,91	39,73	9,45	3,78	3,78	487,30	0,03	55,00	0,29
Hector Mine	1999	7,13	47,97	50,20	43,05	43,05	41,82	271,40	0,08	179,00	0,15
Chi-Chi, Taiwan-04	1999	6,20	38,91	42,87	38,25	38,14	38,11	442,20	0,25	15,00	0,12
Chi-Chi, Taiwan-06	1999	6,30	58,32	60,47	41,58	41,58	40,36	473,90	0,25	100,00	0,16